UNCLASSIFIED

AD NUMBER

AD037466

NEW LIMITATION CHANGE

TO

Approved for public release, distribution unlimited

FROM

Distribution authorized to U.S. Gov't. agencies and their contractors; Administrative/Operational use; 30 Sep 1950. Other requests shall be referred to Office of Naval Research, Arlington VA. 22217-0000

AUTHORITY

ONR ltr, 4 Sep 2003

THIS PAGE IS UNCLASSIFIED

...s Technical Information Agency

...ly, you are requested to return this copy WHEN IT HAS SERVED ... it may be made available to other requesters. Your cooperation

37466

...T OR OTHER DRAWINGS, SPECIFICATIONS OR OTHER DATA ... OTHER THAN IN CONNECTION WITH A DEFINITELY RELATED ...ENT OPERATION, THE U. S. GOVERNMENT THEREBY INCURS ...ANY OBLIGATION WHATSOEVER; AND THE FACT THAT THE ...FORMULATED, FURNISHED, OR IN ANY WAY SUPPLIED THE ...CATIONS, OR OTHER DATA IS NOT TO BE REGARDED BY ...WISE AS IN ANY MANNER LICENSING THE HOLDER OR ANY OTHER ...N, OR CONVEYING ANY RIGHTS OR PERMISSION TO MANUFACTURE, ...TED INVENTION THAT MAY IN ANY WAY BE RELATED THERETO.

Reproduced by

...MENT SERVICE CENTER

...TT BUILDING, DAYTON, 2 OHIO

Reproduced From Best Available Copy

CLASSIFIED

UNDERWATER EXPLOSION RESEARCH

A COMPENDIUM OF BRITISH AND AMERICAN REPORTS

1950

OFFICE OF NAVAL RESEARCH ★ DEPARTMENT OF THE NAVY

British Crown Copyright reserved. Reproduced with the permission of the Controller of His Britannic Majesty's Stationery Office.

Bibliography

Most of the papers in this volume contain references to further work, some of which may be included within this Compendium. Properly qualified persons may obtain additional references or material on application to the following establishments:

1. Secretary, Undex Sub-Panel
   Naval Construction Research Establishment
   Rosyth
   Fife
   Scotland

2. Chief of Naval Research
   c/o Navy Research Section
   Library of Congress
   Washington 25, D. C.

3. The Director
   David W. Taylor Model Basin
   Carderock, Maryland

4. The Commander
   U.S. Naval Ordnance Laboratory
   White Oak, Maryland

PREFACE

During the recent war there arose on both sides of the Atlantic among research workers in the field of underwater explosions the feeling that some of the problems posed by the conditions of undersea warfare had already presented themselves in the past and that various attempts had been made to solve them. Many of the records, however, had been lost or effectively hidden except for what had crept into open publications and consequently a whole new literature had to be developed at considerable cost in both time and money, encompassing both old and new problems. A corollary of this experience has been the firm conviction that this new literature should not suffer a similar fate. The idea of the joint publication of American and British research in the field of underwater explosions took form in the latter part of 1946 and the idea was further explored with the Bureau of Ordnance and the Bureau of Ships, United States Navy Department and with the British Admiralty. The Office of Naval Research, Navy Department, in its capacity of disseminator of scientific information undertook to sponsor the publication and has eventually seen the project through to its present form.

The Compendium has three major purposes: first, to give a greater availability to many papers which otherwise would exist in a very small number of copies, and to preserve and revive certain rare items, the scarcity of which was due to wartime shortages rather than to any deficiencies in the papers themselves; second, to present a representative summary of original source material and to display the scope of this material in a manner which might make it of more universal interest to schools and colleges as a branch of applied science; and third, to stimulate interest in this field for the general benefit of the sciences of Naval Architecture and Naval Ordnance and to provide those working in these fields with ready reference material on many of the important problems which they must face in their work.

The scheme of the Compendium is as follows: All of the papers selected, which represent between 10 and 20 percent of the total quantity of material known to exist, have been divided into three volumes. The first volume is devoted to the primary underwater shock wave, the second to the hydrodynamical effects falling under incompressible theory including the oscillations and behaviour of the gas globe formed by the explosion products, and the third to the effects of all of these phenomena on structures and to the measurement and calculation of the resulting damage. Three papers have been selected with the object of summarizing the knowledge over the field within the scope of the Compendium; these papers, which are placed in the first volume, serve to introduce the subject both in general terms, and also with some mathematical detail.

The allocation of the original papers to the different volumes has, in a few cases, not been obvious and the editors must assume full responsibility for any arbitrary assignments. A far greater responsibility of the editors has lain in the selection of the papers and in this, various considerations have had a voice.

Many of the older papers have been included for their historical interest. Some papers have been used to provide suitable introductory or background material. Most of the other papers have been included intact and represent the opinions of the authors at the time of writing. A few of the papers have been reworked and consist of new material incorporated into the older original papers, or consist of a summary of several progress reports which were too repetitive for economical inclusion without condensation. Papers which have been rewritten are so marked with the new date affixed. In general, selections have been made in an effort to give the best review of the entire subject in order to convey the most, and the best information within the space limitations imposed by the exigencies of publication, and within the scope permitted by considerations of security. Both these features prevent this compilation from being exhaustive, and the latter feature prevents many successful workers in this field from receiving recognition here.

The editors believe that this Compendium is a new venture in international co-operation and hope that this effort may prove useful in pointing the way for other similar joint enterprises which may be considered desirable.

It is our desire to acknowledge the continued interest of Dr. A. T. Waterman, Deputy Chief, Office of Naval Research, Navy Department, without whose help these volumes could not

have been produced, to thank Mr. Martin Jansson of the Technical Information Division, Office of Naval Research, and his capable staff for their painstaking and careful work in preparing the material for reproduction. We also acknowledge the guidance afforded by the British Undex Panel, particularly Dr. A. R. Bryant and Dr. E. N. Fox (a former member), the assistance of Mr. T. Aves of the Department of Research Programmes & Planning and Miss E. Lord of the Department of Physical Research in the preparation of the British contribution, and to thank Dr. T. L. Brownyard of the Bureau of Ordnance Navy Department for his help in some of the correspondence and in some of the problems of security clearance.

G. K. Hartmann
Chief, Explosive Research Department
U.S. Naval Ordnance Laboratory

E. G. Hill
Department of Physical Research
Admiralty

TABLE OF CONTENTS

VOLUME II

THE GAS GLOBE

	Page
Preface	v
SUMMARY PAPERS	
REPORT ON THE THEORETICAL SHAPE OF THE PRESSURE-TIME CURVE AND ON THE GROWTH OF THE GAS-BUBBLE (B)* S. Butterworth, Admiralty Research Laboratory	1
UNDERWATER EXPLOSIONS. TIME INTERVAL BETWEEN SUCCESSIVE EXPLOSIONS (B) H. F. Willis, H. M. Anti-Submarine Experimental Establishment	13
THEORY OF THE PULSATIONS OF THE GAS BUBBLE PRODUCED BY AN UNDERWATER EXPLOSION (A)* Conyers Herring, Bell Telephone Laboratories, Murray Hill, N. J.	35
THEORY OF PULSATIONS	
VERTICAL MOTION OF A SPHERICAL BUBBLE AND THE PRESSURE SURROUNDING IT (B) G. I. Taylor, Cambridge University	131
ON THE CHANGING FORM OF A NEARLY SPHERICAL SUBMARINE BUBBLE (B) W. G. Penney and A. T. Price, Imperial College of Science and Technology, London	145
THE BEHAVIOUR OF AN UNDERWATER EXPLOSION BUBBLE (B) A. R. Bryant, Road Research Laboratory, London	163
RADIAL MOTION OF WATER SURROUNDING A SPHERE OF GAS IN RELATION TO PRESSURE WAVES (A) E. H. Kennard, David W. Taylor Model Basin	183
THE MOTION AND SHAPE OF THE HOLLOW PRODUCED BY AN EXPLOSION IN A LIQUID (B) G. I. Taylor and R. M. Davies, Cambridge University	227
STUDIES ON THE GAS BUBBLE RESULTING FROM UNDERWATER EXPLOSIONS: ON THE BEST LOCATION OF A MINE NEAR THE SEA BED (A) M. Shiffman and B. Friedman, Institute for Mathematics and Mechanics, New York University	247
THE BEHAVIOUR OF AN UNDERWATER EXPLOSION BUBBLE FURTHER APPROXIMATIONS (B) A. R. Bryant, Road Research Laboratory, London	321
THEORY OF UNDERWATER EXPLOSION BUBBLES (A) B. Friedman, Institute for Mathematics and Mechanics, New York University	329

* (A) American Contribution
(B) British Contribution

TABLE OF CONTENTS (Continued)

Page

THEORY OF MIGRATION

MIGRATION OF UNDERWATER GAS GLOBES DUE TO GRAVITY AND NEIGHBORING SURFACES (A)
E. H. Kennard, David W. Taylor Model Basin 377

THE RATE OF RISE OF LARGE VOLUMES OF GAS IN WATER (B)
G. I. Taylor and R. M. Davies, Cambridge University 415

A SIMPLIFIED THEORY OF THE EFFECT OF SURFACES ON THE MOTION OF AN EXPLOSION BUBBLE (B)
A. R. Bryant, Road Research Laboratory, London 431

THE RATE OF RISE OF LARGE VOLUMES OF GAS IN WATER (B)
H. N. V. Temperley and Ll. G. Chambers, Admiralty Undex Works, Rosyth, Scotland 437

THE ATTRACTION OF AN UNDERWATER EXPLOSION BUBBLE TO A RIGID DISC (B)
A. R. Bryant, Road Research Laboratory, London 445

THE EFFECT OF AN ADJACENT DEFORMING TARGET UPON THE BUBBLE DUE TO A SUBMARINE EXPLOSION (B)
Ll. G. Chambers, Admiralty Undex Works, Rosyth, Scotland 455

PRESSURE PULSES

THE PRESSURES PRODUCED BY EXPLOSIONS UNDERWATER OF SMALL CHARGES NEAR A RIGID BOTTOM (B)
G. Charlesworth, Road Research Laboratory, London 465

SECONDARY PRESSURE PULSES DUE TO GAS GLOBE OSCILLATION IN UNDERWATER EXPLOSIONS. I. EXPERIMENTAL DATA (A)
A. B. Arons, J. P. Slifko, and A. Carter, Underwater Explosives Research Laboratory, Woods Hole Oceanographic Institution 475

SECONDARY PRESSURE PULSES DUE TO GAS GLOBE OSCILLATION IN UNDERWATER EXPLOSIONS. II. SELECTION OF ADIABATIC PARAMETERS IN THE THEORY OF OSCILLATION (A)
A. B. Arons, Stevens Institute of Technology, Hoboken, N. J. 481

THE THEORETICAL SHAPE OF THE PRESSURE PULSE PRODUCED BY AN UNDERWATER EXPLOSION BUBBLE (B)
A. R. Bryant and Ll. G. Chambers, Naval Construction Research Establishment, Rosyth, Scotland 487

EXPERIMENTAL TECHNIQUES AND MEASUREMENTS

THE OSCILLATION OF THE GAS-BUBBLE FORMED BY A DETONATOR EXPLODING UNDERWATER. DETAILED COMPARISON OF THEORY WITH EXPERIMENT (B)
H. N. V. Temperley, Admiralty Undex Works, Rosyth, Scotland 497

* (A) American Contribution
(B) British Contribution

TABLE OF CONTENTS (Continued)

Page

EXPERIMENTAL TECHNIQUES AND MEASUREMENTS (Continued)

PHOTOGRAPHIC MEASUREMENTS OF THE SIZE, SHAPE AND MOVEMENT OF THE BUBBLE PRODUCED BY 1-CWT. CHARGES OF POLAR AMMON GELIGNITE DETONATED UNDERWATER AT A DEPTH OF 3 FEET (B)
A. R. Bryant, Road Research Laboratory, London 505

A TECHNIQUE FOR MULTIFLASH PHOTOGRAPHY OF UNDERWATER EXPLOSION PHENOMENA (B)
A. R. Bryant and K. J. Bobin, Road Research Laboratory, London 525

PHOTOGRAPHIC MEASUREMENTS OF THE ATTRACTION OF AN UNDERWATER EXPLOSION BUBBLE TO A BOX MODEL TARGET (B)
A. R. Bryant, Road Research Laboratory, London 539

MEASUREMENT OF BUBBLE PULSE PHENOMENA, III. RADIUS AND PERIOD STUDIES (A)
E. Swift, Jr. and J. C. Decius, Underwater Explosives Research Laboratory, Woods Hole Oceanographic Institution 553

SURFACE PHENOMENA: DOMES AND PLUMES

ANALYSIS OF THE SPRAY DOME (B)
G. W. Walker, Mine Design Department, Admiralty 601

A METHOD OF DETERMINING THE DEPTH OF UNDERWATER EXPLOSIONS (B)
R. A. Shaw, Marine Aircraft Experimental Establishment, Scotland 611

A FURTHER INVESTIGATION INTO THE DOME ANALYSIS METHOD OF DETERMINING THE DEPTH OF UNDERWATER EXPLOSIONS (B)
R. A. Shaw, Marine Aircraft Experimental Establishment, Scotland 621

THE RELATION BETWEEN THE APPEARANCE OF THE PLUMES AND THE GAS GLOBE BEHAVIOR IN UNDERWATER EXPLOSIONS (A)
G. K. Hartmann, Naval Ordnance Laboratory 631

THE DETERMINATION OF PEAK PRESSURE OF AN UNDERWATER EXPLOSION FROM A STUDY OF THE INITIAL DOME VELOCITY (A)
D. A. Wilson, B. A. Cotter, and R. S. Price, Underwater Explosives Research Laboratory, Woods Hole Oceanographic Institution 637

SURFACE PHENOMENA: GRAVITY WAVES

GRAVITY WAVES PRODUCED BY SURFACE AND UNDERWATER EXPLOSIONS (B)
W. G. Penney, Imperial College of Science and Technology, London 679

SURFACE WAVES PRODUCED BY FIRING UNDERWATER 32-LB. CHARGES OF POLAR AMMON GELIGNITE AT VARIOUS DEPTHS (B)
G. Charlesworth, Road Research Laboratory, London 695

* (A) American Contribution
(B) British Contribution

Page

SURFACE PHENOMENA: GRAVITY WAVES (Continued)

SURFACE WAVES PRODUCED BY UNDERWATER EXPLOSIONS COMPARISON OF THE THEORY OF W. G. PENNEY WITH EXPERIMENTAL RESULTS FOR A 32-LB. CHARGE (B)
A. R. Bryant, Road Research Laboratory, London 701

SURFACE WAVES FROM AN UNDERWATER EXPLOSION (A)
J. G. Kirkwood, Cornell University, N. Y., and
R. J. Seeger, Naval Ordnance Laboratory 707

* (A) American Contribution
(B) British Contribution

REPORT ON THE THEORETICAL SHAPE OF THE PRESSURE-TIME CURVE AND ON THE GROWTH OF THE GAS-BUBBLE

S. Butterworth
Admiralty Research Laboratory

British Contribution

August 1923

REPORT ON THE THEORETICAL SHAPE OF THE PRESSURE-TIME CURVE AND ON THE GROWTH OF THE GAS-BUBBLE

S. Butterworth

August 1923

* * * * * * * * * *

Summary.

Lamb's theory of under water explosions is shown to give a pressure-time curve in very fair agreement with that obtained by experiment, provided that the two gas-constants are appropriately chosen. An attempt is made to estimate the effect of the compressibility of water by assuming that outside a sphere of radius 3.7 times that of the original charge the water has its normal compressibility and within this radius is incompressible, the incompressible core being introduced to cover that region for which the pressures are too great for the usual acoustic equations to apply.

It is found that, for an explosion in which a given quantity of energy is released, the initial gas pressure for this case must be of the order 360 tons per square inch to account for the experimental pressure-time curve, whereas the incompressible theory gives only 60 tons per square inch for this pressure. The theory thus indicates that the maximum pressure may diminish with distance very rapidly in the immediate vicinity of the charge. Lamb's theory is extended to include the effect of a constant external hydrostatic pressure, the result being that the bubble tends to oscillate in size the time of oscillation being of the order of one second for a 100 lb. charge. In deep water this may result in a succession pulses which would, however, diminish rapidly in amplitude.

The only theory which has so far been published in regard to the shape of the pressure-time curve due to an underwater explosion is that due to Lamb*. Lamb assumes that the water may be regarded as incompressible and that the products of detonation during expansion follow the law PV^{γ} = constant where γ remains invariable throughout the expansion. He takes the case of spherical symmetry and works out the form of the pressure-time curve for the values $\gamma = 1$ and $\gamma = 4/3$. For the latter case his result is given in the following formulae. Let R_o be the initial radius of the sphere containing the products of detonation and R the radius after time t. Let P_o be the initial pressure in the sphere R_o. Then if ρ be the density of the surrounding incompressible fluid and $\beta = R/R_o$ the relation between β and t is

$$\frac{t}{R_o} = \frac{2}{15}\sqrt{\frac{\rho}{2P_o}}\,(\beta - 1)^{\frac{1}{2}}\,(3\beta^2 + 4\beta + 8) \qquad (1)$$

Also if p is the pressure at a time t at a point distant r from the centre of the bubble

$$\frac{p}{R_o} = \frac{R_o}{r\beta^2} - \left[\frac{R_o}{r}\right]^4 (\beta - 1) \qquad (2)$$

Formulae (1) and (2) can be used to calculate the pressure-time curve when P_o, R_o, ρ are known. It should be noted that (2) will hold only so long as r is greater than R so that there are no negative values of p.

This formula may be compared with experimental results if we can assign a value to P_o. Two methods suggest themselves. First if w is the energy released by the detonation of one gram.

of the .....

* Phil. Mag. January, 1923.

of the explosive, then by thermodynamics

$$P_o = (\gamma - 1) w\delta \qquad (3)$$

where δ is the density of the explosive.

For T.N.T. $w = 3.88 \times 10^{10}$ ergs per gram.

$$\delta = 1.2$$

so that with $\gamma = 4/3$

$$P_o = 1.55 \times 10^{10} \text{ dynes/sq.cm.} = 100 \text{ tons/square inch.}$$

Alternatively equation (2) shows that maximum pressure P_{max} at distance r is related to P_o by

$$P_o R_o = P_{max} r \qquad (4)$$

so that if P_{max} is determined experimentally we can estimate P_o. Now for 100 lbs. T.N.T. at 40 feet the piezo-electric method gives $P_{max} = 1.02$ tons/square inch and since $R_o = 0.7$ foot

$$P_o = 58 \text{ tons/square inch.}$$

Taking the latter estimate the following Table is calculated from equations (1) and (2).

TABLE 1.

Theoretical course of pressure-time curve for 100 lbs. T.N.T. at 40 feet.

β	=	1.00	1.02	1.05	1.1	1.2	1.3	1.4
p/P_{max}	=	1.000	0.961	0.904	0.826	0.694	0.592	0.510
10^4 t (seconds)	=	0	0.45	0.72	1.06	1.60	2.10	2.58
β	=	1.5	1.6	1.7	1.8	1.9	2.0	2.5
p/P_{max}	=	0.444	0.391	0.346	0.309	0.277	0.250	0.160
$10^4 t$	=	3.06	3.58	4.10	4.70	5.25	5.85	9.42

These values are compared with those obtained by the piezo-electric method in Figure 1 in which A represents the theoretical curve and B the experimental curve.

It is seen that apart from the finite time required to reach the maximum pressure there is very fair agreement between the theoretical and experimental curves.

As regards other weights of charge, formula (2) (with $\beta = 1$) shows that the maximum pressure at a given distance varies as the linear dimension R_o, that is as the cube root of the weights. This is in agreement with the experimental results at any rate so long as the weight exceeds 100 lbs. The law of distance for maximum pressure should theoretically by $P_{max}\, r$ = constant. This law is found to hold experimentally throughout the range for which the piezo-electric records have been obtained but observations with Hilliar crusher gauges at small distances show a tendency for P_{max} to be greater than this law would give.

If r is so large that the second term in (2) may be neglected, the theoretical shape of the curve is the same at all distances. If we include the second term there is a somewhat more rapid fall of pressure near to the charge. The experimental evidence from the piezo-electric gauges is not sufficiently precise to test the constancy of shape.

In .....

In spite of the agreement between the incompressible theory and observation as illustrated in Figure 1 it is important to attempt to find the effect of the finite compressibility of the water before we can conclude that it is safe to extrapolate by the inverse distance law to obtain the pressures in the immediate neighbourhood of the charge. Lamb has stated that a complete solution including compressibility appears hopeless. We know, however, that if we choose a distance sufficiently large the ordinary laws for propagation of sound will hold and that the compressibility of water diminishes for very high pressures. The following procedure should therefore give us results nearer the truth than if complete incompressibility is assumed. Suppose the gas bubble surrounded by an incompressible envelope so large that outside it the ordinary laws for the propagation of sound may be taken to hold and let us attempt to find the form of the pressure wave thrown off from this system. If a is the radius of the boundary between the incompressible and compressible region, then at a point $r > a$ the velocity potential is given by

$$\phi = F\left(t - \frac{r-a}{c}\right)/r \tag{5}$$

the equation of pressure is

$$p + \tfrac{1}{2}\rho u^2 = -\rho \frac{d\phi}{dt} = -\rho F'/r \tag{6}$$

and the velocity is

$$u = \frac{d\phi}{dr} = -\frac{F'}{cr} - \frac{F}{r^2} \tag{7}$$

In these equations c is the velocity of sound in water and ρ the normal density.

Within the region $r < a$ since incompressibility is assumed

$$\phi = \chi(t)/r + \psi(t)/a \tag{5a}$$

$$p + \tfrac{1}{2}\rho u^2 = -\rho \chi'(t)/r - \rho \psi'(t)/a \tag{6a}$$

$$u = -\chi(t)/r^2 \tag{7a}$$

The function ψ is possible since there is no restriction to a pressure variation independent of r. ψ must be zero in the outer region as p and u vanish at infinity.

Since p and u are continuous at $r = a$,

$$F' = \chi' + \psi', \quad F'a/c + F = \chi,$$

$$\text{or} \quad \psi = F - \chi = -F'a/c \tag{8}$$

By (6) and (8) since u^2 is negligible when $r > a$ the pressure at a may be written

$$p = \rho c \psi/a^2 \tag{9}$$

so that the function ψ gives the form of the pressure-time curve in the outer medium.

To determine these functions we must form the energy equation from the assumed law of expansion of the gas bubble. Let the bubble have initial radius R_0 and radius R at time t so that by (7a)

$$\frac{dR}{dt} = -\frac{\chi}{R^2} \tag{10}$$

To form the energy equation the work done by the bubble in expanding from R_0 to R must be equated to the energy stored in the medium between R_0 and a together with the energy that has escaped from the surface a. The energy escaping from a

$$= 4\pi a^2 \int_0^t u\,(p + \tfrac{1}{2}\rho u^2)\,dt$$

$$= 4\pi\frac{\rho}{a}\int_0^t (\chi' + \psi')\,\chi\,dt$$

$$= 4\pi\frac{\rho}{a}\left(\tfrac{1}{2}\chi^2 + \int_0^t \psi'\,\chi\,dt\right) \qquad (11)$$

The energy stores between R and a is kinetic and is equal to

$$2\pi\rho\int_R^a r^2u^2dr = 2\pi\rho\chi^2\int_R^a \frac{dr}{r^2} = 2\pi\rho\chi^2\left(\frac{1}{R}-\frac{1}{a}\right) \qquad (12)$$

The work done by the bubble

$$= \int PdV = \frac{4\pi P_o R_o^3}{3n}\left\{1-\left(\frac{R_o}{R}\right)^{3n}\right\} \qquad (13)$$

the law of expansion being PV^{n+1} = constant.

Equating (13) to (11) and (12)

$$\frac{2P_o}{3n\rho}R_o^3\left\{1-\left(\frac{R_o}{R}\right)^{3n}\right\} = \frac{\chi^2}{R}+\frac{2}{a}\int_0^t \chi\psi'\,dt \qquad (14)$$

This equation together with

$$\psi' + \frac{c}{a}\psi + \chi' = 0 \qquad (15)$$

obtained from (8)

and $$R' + \frac{\chi}{c} = 0 \qquad (16)$$

give three first order equations to determine χ, ψ, R. When ψ is known the required pressure follows from (9).

If we choose as our units of length and time, for length the initial radius R_o of the bubble and for time the time required to traverse $2R_o$ with the velocity of sound, equations (14), (15), (16), may be written

$$\left.\begin{aligned}\left(\frac{A}{R^{3n+1}}+\frac{\chi^2}{R}\right)\delta R - \frac{2\chi}{R}\delta\chi - \frac{2\chi}{a}\delta\psi &= 0\\ \delta\psi + \delta\chi + \frac{2\psi}{a}\delta t &= 0\\ \delta R + \chi\,\delta t/R^2 &= 0\end{aligned}\right\} \qquad (17)$$

in which $A = 8P_o/\rho c^2$ (18)

so that .....

so that

$$\left.\begin{aligned} \delta\chi &= -\left(\frac{A}{R^{3n+3}} + \frac{\chi^2}{R^4} - \frac{4\psi}{a^2}\right)\delta t \Big/ \left(\frac{2}{R} - \frac{2}{a}\right) \\ \delta\psi &= -\delta\chi - 2\psi\,\delta t/a \\ \delta R &= -\chi\,\delta t/R^2 \end{aligned}\right\} \qquad (19)$$

In this form if we know χ, ψ, R at a given instant we can calculate $\delta\chi$, $\delta\psi$, δR and therefore determine χ, ψ, R at a future instant. In particular when $t = 0$, $\chi = \psi = 0$, $R = 1$ so that we can step out from the initial conditions and calculate the curve of ψ. It may be remarked that if we put a equal to infinity in (14), then (14) and (15) may be used to develop the incompressible theory. The results obtained in this way agree with those of Lamb.

Using the above method the results of Table II have been obtained.

The values of A,n chosen in the three cases tabulated are such that the total energy content of the gas bubble is the same in all cases, so that the numbers illustrate the effect merely of the alteration of the mode of delivery of a given total energy.

They correspond respectively to --

P_o = 72, 216, 360 tons/square inch

with γ = 4/3, 2, 8/3 (see Footnote).

The incompressible region in all cases is taken to be included within a sphere of radius 3.7 R_o. The pressure-time curves are plotted in Figure 2 and it is immediately seen that the effect of endowing the external region with the ordinary compressibility of water has been to alter very profoundly the shape of the pressure-time curve.

The curve A for $\gamma = 4/3$ was that which on the incompressible theory was found to fit the facts most closely. On this assumption it now --

TABLE II .....

Footnote: The large values of γ indicated are not physically impossible as at very high pressures, it is probable that we are working on a very steep portion of the adiabatic curve for the gas so that the value of γ in the assumed law PV^{γ} = constant is not the ratio of the specific heats of the gas but a value which fits the slope of the relevant portion of the adiabatic curve.

TABLE II.

Values of χ, ψ, R. a = 3.7

A =	3.8			11.4			19.0		
3n =	1			3			5		
t	χ	ψ	R	χ	ψ	R	$-\chi$	ψ	R
0.00	0	0	1	0	0	1	0	0	1
0.02	0.05	0.05	1.00	0.16	0.16	1.00	0.26	0.26	1.00
0.04	0.10	0.10	1.00	0.31	0.31	1.00	0.52	0.52	1.00
0.06	0.16	0.15	1.00	0.46	0.46	1.01	0.78	0.77	1.01
0.08	0.21	0.20	1.01	0.62	0.61	1.02	1.03	1.01	1.03
0.10	0.26	0.25	1.01	0.76	0.74	1.03	1.26	1.22	1.05
0.15	0.38	0.37	1.02	1.11	1.07	1.07	1.77	1.70	1.11
0.20	0.51	0.47	1.04	1.43	1.35	1.12	2.17	2.05	1.18
0.25	0.63	0.59	1.06	1.70	1.59	1.17	2.47	2.29	1.26
0.30	0.74	0.69	1.09	1.93	1.78	1.23	2.70	2.46	1.33
0.35	0.86	0.78	1.12	2.13	1.93	1.30	2.88	2.58	1.41
0.40	0.96	0.87	1.16	2.30	2.05	1.36	3.03	2.66	1.48
0.45	1.06	0.95	1.19	2.45	2.14	1.42	3.15	2.70	1.55
0.50	1.16	1.02	1.23	2.58	2.21	1.48	3.25	2.73	1.62
0.55	1.25	1.08	1.27	2.69	2.26	1.54	3.33	2.74	1.69
0.60	1.33	1.13	1.31	2.77	2.30	1.60	3.40	2.73	1.75
0.65	1.41	1.18	1.35	2.88	2.32	1.65	3.45	2.71	1.80
0.70	1.48	1.23	1.38	2.96	2.33	1.70	3.50	2.69	1.86
0.75	1.55	1.26	1.42	3.03	2.33	1.75	3.54	2.65	1.91
0.80	1.62	1.30	1.46	3.09	2.32	1.80	3.57	2.60	1.96
0.85	1.68	1.32	1.50	3.14	2.31	1.85	3.59	2.55	2.00
0.90	1.74	1.34	1.54	3.18	2.29	1.90	3.60	2.49	2.05
0.95	1.80	1.37	1.57	3.22	2.26	1.94	3.61	2.43	2.09
1.00	1.85	1.38	1.61	3.25	2.23	1.98	3.61	2.37	2.13
1.1	1.94	1.40	1.68	3.30	2.16	2.07	3.60	2.23	2.21
1.2	2.03	1.41	1.75	3.33	2.07	2.14	3.58	2.09	2.29
1.3	2.10	1.40	1.82	3.34	1.97	2.22	3.54	1.94	2.36
1.4	2.16	1.39	1.88	3.33	1.86	2.28	3.50	1.79	2.42
1.5	2.21	1.37	1.94	3.31	1.74	2.35	3.45	1.64	2.48

Table continued .....

t	$-\chi$	ψ	R	$-\chi$	ψ	R	$-\chi$	ψ	R
1.6	2.26	1.34	2.00	3.28	1.62	2.41	3.39	1.50	2.54
1.7	2.29	1.30	2.06	3.24	1.50	2.47	3.33	1.36	2.59
1.8	2.32	1.26	2.11	3.20	1.38	2.52	3.27	1.23	2.64
1.9	2.34	1.21	2.16	3.16	1.27	2.57	3.21	1.10	2.68
2.0	2.36	1.16	2.21	3.12	1.16	2.62	3.16	0.99	2.73
2.2	2.39	1.06	2.31	3.03	0.94	2.71	3.06	0.78	2.82
2.4	2.40	0.96	2.40	2.95	0.76	2.79	2.95	0.60	2.89
2.6	2.40	0.86	2.48	2.89	0.62	2.87	2.89	0.47	2.96
2.8	2.40	0.77	2.56	2.84	0.50	2.94	2.85	0.37	3.03
3.0	2.40	0.69	2.64	2.81	0.42	3.01	2.83	0.31	3.09
3.2	2.40	0.60	2.70				2.83	0.27	3.15
3.4	2.40	0.54	2.77				2.84	0.25	3.21
3.6	2.40	0.48	2.83				2.85	0.23	3.26

gives a pressure less than half the observed pressure and its rate of rise and fall are much slower than is actually the case. Of the three it is that curve corresponding to P_o = 360 tons per square inch which fits the observations most closely.

In view of the enormous change that the partial introduction of compressibility has brought about it is seen that we cannot rely upon the incompressible theory either to estimate the properties of the gas or to extrapolate the experimental results to deduce the pressures near the charge. The indications are that the initial gas pressure may be much larger than 60 tons per square inch, the value of γ being correspondingly increased so as to satisfy total energy considerations. If we measure the areas of the pressure-time curves of Figure 2 for the first 10^{-3} second we obtain the following results:-

$$P_o = 72,\ 216,\ 350 \text{ tons/square inch}$$

$$\int p\,dt = 0.720,\ 0.938,\ 0.958$$

While the pieze-electric curve gives for the same interval 0.932 lb.-second-units.

When phenomena involving integral pressure are being studied the effect of the rate of energy delivery will not be so marked as in the case of those which depend on maximum pressure. The present investigation shows, however, that measurements of the pressure-wave ought to be made as near the charge as possible before we can estimate damage at small distances.

Returning now to the case of incompressibility it must be noted that the rate of growth of the gas bubble given by equation (i) will only hold if the pressure at infinity is zero. According to the formula the size of the bubble continues to increase indefinitely.

If we postulate a finite pressure at infinity a modification occurs which limits the maximum size of the bubble and suggests certain interesting phenomena. Let the pressure at infinity be Q. Then the work done by the bubble during expansion from R_o to R has to supply an amount of work equal to $\frac{4}{3}\pi Q (R^3 - R_o^3)$ in addition to imparting kinetic energy to the fluid.

Hence .....

Hence by (12), (13), (16), we have when $3n = 1$ and $\alpha = \infty$

$$4\pi P_0 R_0^3 \left[1 - \frac{R_0}{R}\right] - \frac{4}{3}\pi Q (R^3 - R_0^3) = \frac{2\pi\rho\chi^2}{R} = 2\pi\rho R^3 \left(\frac{dR}{dt}\right)^2$$

Putting $R = \beta R_0$

$$\left[\frac{d\beta}{dt}\right]^2 = \frac{2P_0}{\rho R_0^2}\left\{1 - \frac{1}{\beta} - \frac{Q}{3P_0}(\beta^3 - 1)\right\}\Big/\beta^3 \qquad (20)$$

The bubble ceases to grow when

$$Q/3P_0 = (\beta - 1)/(\beta^4 - \beta)$$

or since Q is small compared with P_0, β is large and approximately equal to $(3P_0/Q)^{1/3}$.

Thus if $Q = 2$ atmospheres (which will be the case for an explosion at a depth of about 30 feet) and $P_0 = 9000$ atmospheres, $\beta = 2.4$. Thus if the incompressible theory held rigidly the bubble would oscillate perpetually between the radii R_0 and $2.4\,R_0$. In the actual case energy will be dissipated partly as a pressure wave and partly in the form of heat, but the tendency to oscillate should not be entirely absent. The varied form of the surface effects as the bubble breaks the surface may be accounted for by the variation in size and internal pressure. The spout-like form of the surface upheaval which occasionally is observed is what we should expect from a high-pressure, small-volume bubble. The occasional spout like form of the surface upheaval is referred to by Hilliar, and he quotes a case of two shots of 40 lbs. 40/60 amatol at a depth of 16 feet in which the upheaval reached a height of nearly 200 feet while in similar shots the upheaval only reached a height of 80 feet. The comparative rareness of its occurrence is in accord with time considerations which we now proceed to investigation.

By equation (20)

$$\frac{t}{R_0}\sqrt{\frac{2P_0}{\rho}} = \int_1^\beta \frac{\beta^2\,d\beta}{(\beta-1)^{\frac{1}{2}}\{1 - \beta(\beta^2 + \beta + 1)/\beta_0^3\}^{\frac{1}{2}}}$$

where β_0^3 is written for $3P_0/Q$ since β_0 is large.

The term involving β_0^3 will only be of importance when β is large and then $\beta^2 + \beta + 1 = \beta^2$. Hence

$$\frac{t}{R_0}\sqrt{\frac{2P_0}{\rho}} = \beta_0^{3/2}\int_1^\beta \frac{\beta^2 d\beta}{(\beta-1)^{\frac{1}{2}}(\beta_0^3 - \beta^3)^{\frac{1}{2}}} \qquad (21)$$

The integrand in (21) is infinite when $\beta = 1$, $\beta = \beta_0$ and imaginary when $\beta > \beta_0$.

If we write for the integral $I_1 + I_2 + I_3$ where

$$I_1 = \frac{1}{(\beta_0^3 - 1)^{\frac{1}{2}}}\int_1^\beta \frac{\beta^2\,d\beta}{(\beta-1)^{\frac{1}{2}}} = 2(\beta-1)^{\frac{1}{2}}(3\beta^2 + 4\beta + 8)/15(\beta_0^3 - 1)^{\frac{1}{2}} \qquad (22)$$

$$I_2 = \frac{1}{(\beta_0 - 1)^{\frac{1}{2}}}\int_1^\beta \frac{\beta^2\,d\beta}{(\beta_0^3 - \beta^3)^{\frac{1}{2}}} = 2\{(\beta_0^3 - 1)^{\frac{1}{2}} - (\beta_0^3 - \beta^3)^{\frac{1}{2}}\}/3(\beta_0 - 1)^{\frac{1}{2}} \qquad (23)$$

$$I_3 = \int_1^\beta \beta^3\,d\beta\left\{\frac{1}{(\beta-1)^{\frac{1}{2}}(\beta_0^3 - \beta^3)^{\frac{1}{2}}} - \frac{1}{(\beta-1)^{\frac{1}{2}}(\beta_0^3 - 1)^{\frac{1}{2}}} - \frac{1}{(\beta_0 - 1)^{\frac{1}{2}}(\beta_0^3 - \beta^3)^{\frac{1}{2}}}\right\} \qquad (24)$$

then .....

then I_3 is real and finite throughout the range of integration and may therefore be evaluated by any approximate method. Now for the case $\beta_0 = 24$ the expression in $\{\}$ in equation (24) is nearly constant. In fact it never differs by more than 3% from -1.72×10^{-3} throughout its while range. Hence to this accuracy we may write $I_3 = -0.57 \times 10^{-3}(\beta^3 - 1)$ when $\beta_0 = 24$. Calculating I_1, I_2, I_3 from these formulae and using in (21), we find that the time required for the bubble to reach its maximum radius is given by $t = 2170\sqrt{\frac{\rho}{p}}$ R_0. In the case of 100 lb. charge of T.N.T. with $P_0 = 9000$ atmospheres $R_0 = 0.7$ foot, $t = 0.0$ second, so that if the incompressible theory held rigidly the bubble would r' to its original state in one second and a series of expl. ions at intervals of one second would be heard. As a matter of fact two reports are often hea. but observers generally attribute the second report to the breaking of the surface b, the bubble. In Figure 3, curve A gives the charge of radius of bubble with time according to equation (1) and curve B shows the modified course as calculated from the above data. Curve B is one half of a periodic curve and shows that during the greater proportion of its existence the bubble is of large volume and low pressure thus accounting for the scarcity of spout-like upheavals mentioned in the last section.

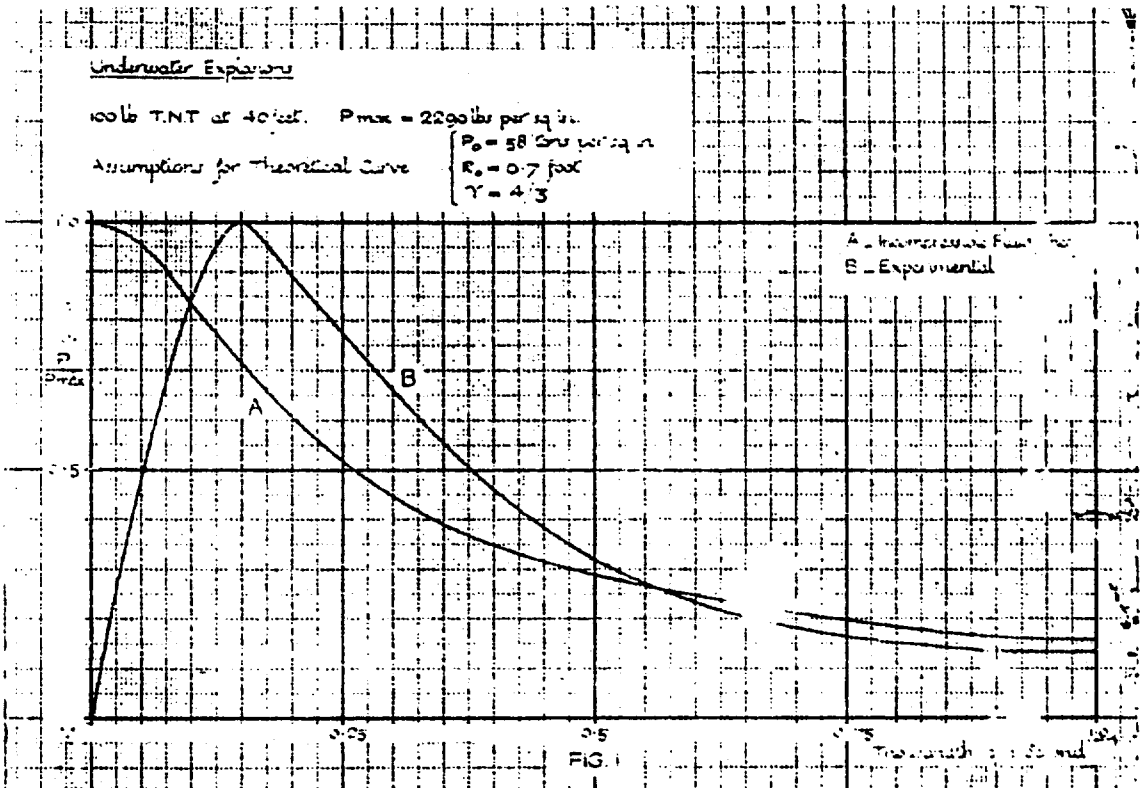
Underwater Explosions
100 lb T.N.T at 40 feet. Pmax = 2290 lbs per sq in.
Assumptions for Theoretical Curve
P_o = 58 Tons per sq in
R_o = 0.7 foot
γ = 4/3
A – Theoretical
B – Experimental
P / Pmax
A
B
0·25
0·5
0·75
1·0
Thousandths of a second

FIG. 1

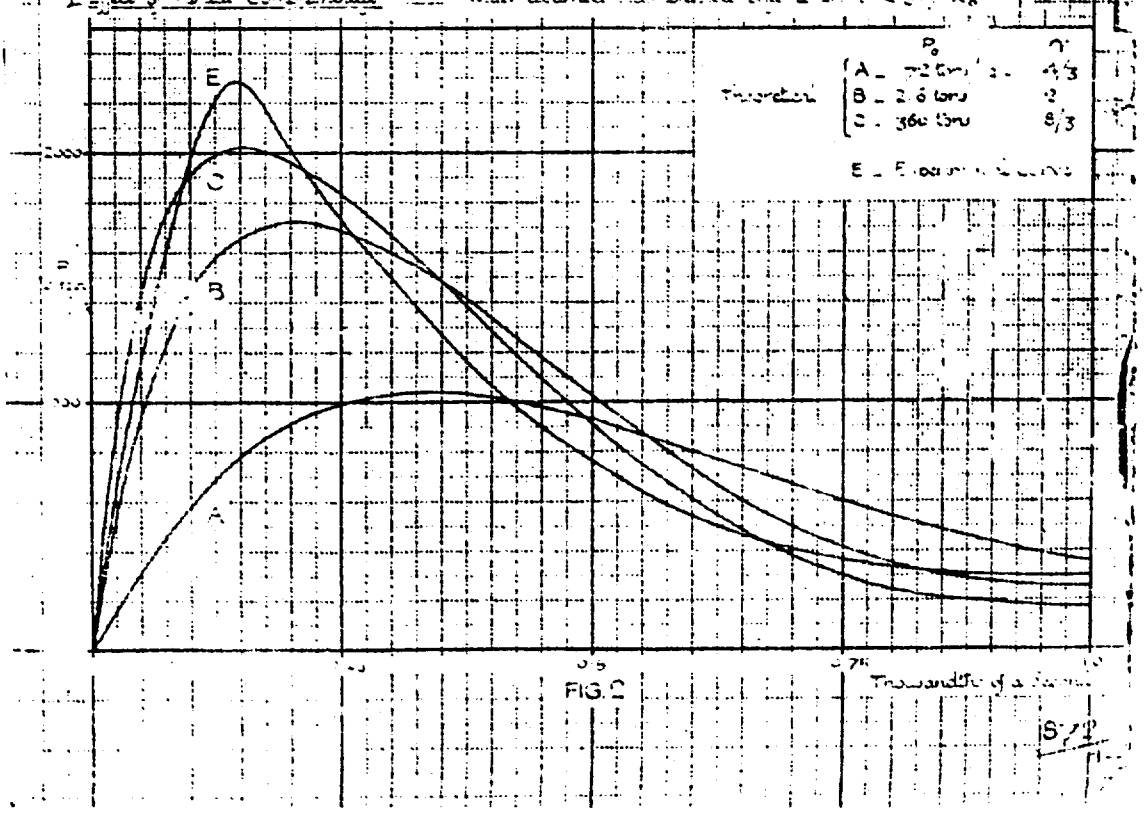
Effect of Partial Compressibility
Theoretical
A – P_o = 2 Tons, γ = 4/3
B – P_o = 2.6 Tons, γ = 2
C – P_o = 360 Tons, γ = 8/3
E – Experimental Curve
E
C
B
A
2000
1000
0·5
0·75
1·0
Thousandths of a second

FIG. 2

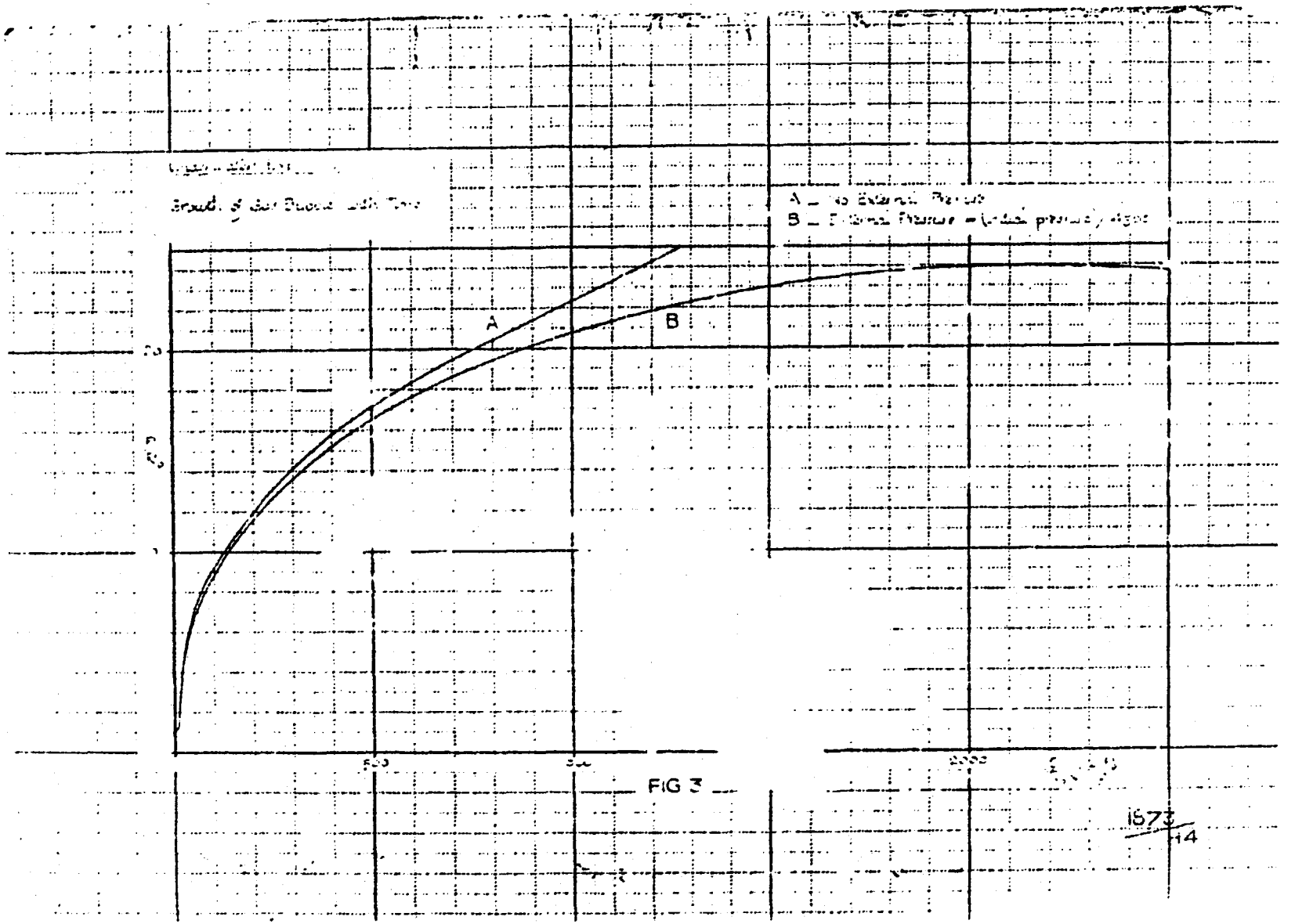

FIG 3

1573
14

UNDERWATER EXPLOSIONS
TIME INTERVAL BETWEEN SUCCESSIVE EXPLOSION

H. F. Willis
H. M. Anti-Submarine Experimental Establishment

British Contribution

February 1941

UNDERWATER EXPLOSIONS.
TIME INTERVAL BETWEEN SUCCESSIVE EXPLOSIONS

H. F. Willis

February 1941

* * * * * * * * *

Introduction.

It has frequently been observed that an underwater explosion is followed after a short time by a second explosion. The time interval may be of the order of a few seconds for large depth charges, whereas for small detonators it is about 20 milliseconds. It is the purpose of this note to submit an explanation of this phenomenon, to calculate the magnitudes of the effects to be expected, and to compare these with available experimental data.

Description of main experimental results.

Little information appears to be available concerning large explosions, but a fair amount of work has been done in connection with small detonators. In these experiments, detonators have been fired at some distance from a 2½" flat-response quartz receiver, and the resulting voltages amplified and spread out on a C.R.O.

Figure 1 shows a typical C.R.O. photograph. Figure 2 shows the same thing using greater amplification. Both photographs show evidence of a number of explosions which become progressively weaker. The time interval between them is not constant but diminishes slowly with each explosion. The first explosion differs from the rest in that it shows an instantaneous rise in pressure up to its peak value. In all subsequent explosions the pressure increase is more gradual and for the later explosions the pulses have a nearly symmetrical appearance. Between each pair of pulses there is evidence of a small rarefaction which extends over the major part of the interval. This is particularly noticeable in the case of the later explosions shown in Figure 2.

Assumptions made in calculations.

In the following calculations a natural explanation of all these characteristics results from a consideration of what happens to the gaseous products of an explosion as they expand outwards from the instant of the explosion. The following assumptions are made:-

(I) that the explosion takes place in an infinitely short time. Actually, for the type of detonator studied, the time interval is of the order of 2 microseconds. Subsequent consideration shows that there is little change in the size of the bubble in this time interval, so that little error is involved in treating the explosion as instantaneous.

(II) that the gaseous products do not dissolve in the water to any appreciable extent during the short period concerned.

(III) that the gaseous products at all times assume the form of a spherical bubble, and behave as a permanent gas.

(Iv) that, to a first approximation, the water can be treated as an incompressible fluid. The extent to which this is justified is later considered in the light of the results obtained. The assumption implies that there is no loss of energy by acoustic radiation.

(v) that there is no dissipation of energy by thermal conduction across the face of the bubble.

Suggested explanation of phenomenon.

With these assumptions it is now possible to see in a general way what happens after the explosion. At the instant of explosion a certain amount of gas is instantaneously generated at

high .....

high pressure and temperature. This immediately begins to force outwards the water in contact with it, a motion which is communicated to a lesser extent to all parts of the surrounding fluid. The potential energy initially possessed by the gas bubble by virtue of its pressure is thus gradually communicated to the water in the form of kinetic energy. By reason of the inertia of the water, this motion overshoots the point at which the pressure in the bubble is equal to the external pressure of the liquid. The bubble thereafter becomes rarefied, and its radial motion is slowed up and brought to rest. The external pressure now compresses the rarefied bubble. Again the equilibrium configuration is overshot, and since by hypothesis there has been no loss of energy to the system by radiation or dissipation, it follows that the bubble comes to rest at the same pressure and volume as at the moment of the explosion. The physical aspects of the explosion are therefore reproduced, and theoretically this process goes on repeatedly, with undiminished amplitude. In practice, of course, energy is lost by acoustic radiation and by dissipation, and this causes a progressive diminution of the amplitudes of the successive pulses.

The fact that the C.R.O. records show a series of compressional pulses with only small rarefactions is readily explained. The peak pressure of the bubble is of the order of 4000 atmospheres. The maximum degree of rarefaction of the bubble that can occur is equal to the external pressure of the sea (say 1 atmosphere). Thus although compressions alternate with rarefactions the magnitude of the latter are small in comparison with the former.

The fact that the C.R.O. traces show the successive compressions as isolated peaks, separated by long regions where the amplitude appears to be zero, results from the high degree of asymmetry of the vibrational properties of a bubble when the pressure variations are excessively high. In such cases the vibrations no longer show the sinusoidal character of a bubble vibrating with small amplitude. Immediately after the explosion the high pressure causes a very rapid expansion of the bubble. This, in conjunction with the smallness of the bubble, results in a rapid drop in pressure which soon becomes immeasurably small in comparison with the peak value. The bubble, however, moves relatively slowly when its size is greater, so that the major part of the time interval between two successive compressions is taken up by the bubble in moving at pressures which are insignificant compared with the peak value.

Mathematical development.

The foregoing description of the expanding bubble is now formulated mathematically.

The gaseous products of the explosion form a bubble of radius r_0 and pressure p_0, the radius and pressure at any subsequent time t being r(t) and p(t), or simply r, p. The external pressure of the sea is P. It is required in the first instance to determine the variation of p and r with t. This is most easily obtained by writing down the energy equation for the system, which is got as follows:-

Potential Energy.

This is simply the work done by the bubble when it expands from radius r to infinity,

i.e. $$V(r) = \int_r^\infty (p - P)\, 4\pi r^2\, dr \qquad (1)$$

Kinetic Energy.

This is the energy associated with the water by reason of its radial motion. By the conditions of continuity of the medium and spherical symmetry, the radial velocity at a point distant y from the centre of the bubble is $\frac{r^2}{y^2} \cdot \frac{dr}{dt}$

The total K.E. of the medium is therefore

$$K = \int_r^\infty \frac{1}{2} \cdot \rho\, (4\pi y^2\, dy) \cdot \left[\frac{r^2}{y^2} \frac{dr}{dt}\right]^2 = 2\pi \rho r^3 \dot{r}^2 \qquad (2)$$

The .....

The total energy of the system is therefore

$$V + K = 2\pi\rho r^3 \dot{r}^2 + \int_r^\infty (p - P)\, 4\pi r^2\, dr = A \qquad \text{(a constant).}$$

The value of A is determined from the fact that at the commencement of the motion when $r = r_0$, $\dot{r} = 0$ so that

$$A = \int_{r_0}^\infty (p - P)\, 4\pi r^2\, dr$$

and using this value, the energy equation becomes

$$r^3 \dot{r}^2 = \frac{2}{\rho} \int_{r_0}^r [\, p - P\,]\, r^2\, dr \qquad (3)$$

This equation can be integrated when the nature of the dependence of p on r is known. It is assumed that an adiabatic law is obeyed: this of course is implied by our previous assumption that no heat is conducted across the surface of the bubble.

The adiabatic law, $pv^\gamma = \text{const.}$, gives

$$pr^{3\gamma} = p_0 r_0^{3\gamma} \qquad (4)$$

Using this relation, equation (3) becomes

$$r^3 \dot{r}^2 = \frac{2}{\rho} \int_{r_0}^r \left[p_0 \left(\frac{r_0}{r}\right)^{3\gamma} - P \right] r^2\, dr$$

This integrates directly and gives

$$\frac{dr}{dt} = \sqrt{\frac{2\, p_0}{3\,(\gamma - 1)\,\rho}}\ \frac{1}{x^2}\ \sqrt{(1 + \alpha)\, x - \alpha\, x^4 - x^{-3\gamma + 4}} \qquad (5)$$

where

$$x = r/r_0$$

$$\alpha = (\gamma - 1)\, P/p_0$$

This result can now be written

$$t = r_0 \sqrt{\frac{3\,(\gamma - 1)}{2}\ \frac{\rho}{p_0}} \int_1^{r/r_0} \frac{x^2\, dx}{\sqrt{(1 + \alpha)\, x - \alpha\, x^4 - x^{-3\gamma + 4}}} \qquad (6)$$

This equation gives the relationship between r and t and specifies the radial motion of the bubble subsequent to the explosion. The pressure inside the bubble at any instant is furnished by equation (6) in conjunction with (4).

Pressure variations inside the bubble.

In order to simplify further calculations, a definite value is now given to γ. For the type of detonators studied experimentally a value $\gamma = 1.3$ is quoted by the makers. The value $\gamma = 4/3$ is particularly convenient mathematically, and is near enough to 1.3, and has therefore been taken.

Equation .....

Equation (6) now becomes

$$t = r_0 \sqrt{\frac{\rho}{2 p_0}} \int_1^{r/r_0} \frac{x^2\,dx}{\sqrt{(1+\alpha)\,x - \alpha\,x^4 - 1}} \quad \text{with } \alpha = p/3\,p_0 \qquad (7)$$

The evaluation of this integral is not possible by ordinary methods. Even graphical methods run into difficulties on account of the singularities of the integrand. However, a sufficiently accurate method is available on account of the smallness of α. For the small detonators, α has a value of about 10^{-4}, and over the early part of the region of integration it therefore plays little part. The value of the integrand, in fact, differs from $\sqrt{\frac{x^2}{x-1}}$ by less than 1% up to the point $x = 5$. The same therefore applies to the integral, the integrand being always positive. But when x varies from $x = 1$ to $x = 5$ the internal pressure of the bubble drops from its initial value p_0 to $\frac{p_0}{5^4} = \frac{p_0}{625}$. This variation in pressure is probably larger than one is likely to be interested in, the pressures at subsequent points being of little significance. Hence for practical purposes the pressure variations in the early stages correspond to

$$t = r_0 \sqrt{\frac{\rho}{2 p_0}} \int_1^{r/r_0} \frac{x^2\,dx}{\sqrt{x-1}}$$

$$= r_0 \sqrt{\frac{2\rho}{p_0}} \left\{ \left(\frac{r}{r_0} - 1\right)^{1/2} + \frac{2}{3}\left(\frac{r}{r_0} - 1\right)^{3/2} + \frac{1}{5}\left(\frac{r}{r_0} - 1\right)^{5/2} \right\} \qquad (8)$$

or, expressing this in terms of the internal pressure p,

$$t = r_0 \sqrt{\frac{2\rho}{p_0}} \left\{ \left[\left(\frac{p_0}{p}\right)^{1/4} - 1\right]^{1/2} + \frac{2}{3}\left[\left(\frac{p_0}{p}\right)^{1/4} - 1\right]^{3/2} + \frac{1}{5}\left[\left(\frac{p_0}{p}\right)^{1/4} - 1\right]^{5/2} \right\} \qquad (9)$$

Time intervals between pulses.

Equation (9) cannot be used to determine the time interval T between successive pulses. To determine this it is necessary to revert to the general formula (7) and to carry out the integration over a complete cycle. In this formula the denominator of the integrand

$$(1+\alpha)\,x - \alpha\,x^4 - 1$$

becomes zero for two positive values of x. One of those values is $x = 1$. The other is a large number, which is denoted by x_1. The physical significance of these zeros is that they correspond to the turning points of the vibrations of the bubble. When $x = 1$ the bubble is in its highest state of compression and when $x = x_1$ it is in its highest state of rarefaction. Furthermore, the motion during compression corresponds completely with the motion during expansion, except for sign. Hence, if the integral of equation (7) is evaluated between the limits $x = 1$ and $x = x_1$ the result will be $t = T/2$. Hence

$$T = r_0 \sqrt{\frac{2\rho}{p_0}} \int_1^{x_1} \frac{x^2\,dx}{\sqrt{(1+\alpha)\,x - \alpha\,x^4 - 1}} \qquad (10)$$

where x_1 is the larger positive root of

$$(1+\alpha)\,x - \alpha\,x^4 - 1 = 0.$$

The approximate evaluation of (10) is again possible by reason of the smallness of α. Details of this evaluation are given in Appendix 2. The result is

$$T = r_0 \sqrt{\frac{2\rho}{p_0}} \cdot \frac{2I}{3} \cdot \alpha^{-5/6} \qquad (11)$$

where .....

where $$I = \int_0^{\pi/2} \sin^{2/3}\theta \, d\theta = 1.12$$

substituting for α this becomes

$$T = \frac{2\sqrt{2}\,I}{3^{1/6}} \rho^{1/2} r_0 p_0^{1/3} p^{-5/6} \qquad (12)$$

It may be shown that the error involved in the derivation of this relation is of the order $\alpha^{1/3}$, i.e. about 1/20 for the detonators studied.

Equation (12) was derived on the assumption that $\gamma = 4/3$. The corresponding formula when γ has any value may be shown to be

$$T = I \left(\frac{8}{3}\right)^{1/2} (\gamma - 1)^{-1/3} \rho^{1/2} r_0 p_0^{1/3} p^{-5/6} \qquad (12a)$$

Equation (12a) can be expressed in alternative and more convenient forms as follows.

The equation of state for the gas in the bubble gives

$$m R \theta_0 = p_0 v_0 = \frac{4\pi}{3} r_0^3 p_0 \qquad (13)$$

where m = quantity of gas in gm. molecules

R = universal gas constant = 8.3×10^7 ergs.

θ_0 = initial gas temperature on absolute scale.

By virtue of (13) the term $r_0 p_0^{1/3}$ can be eliminated from (12a) with the result

$$T = \left\{\frac{32}{3\pi^2 (\gamma - 1)^2}\right\}^{1/6} I \rho^{1/2} (m R \theta_0)^{1/3} p^{-5/6} \qquad (12b)$$

T can alternatively be expressed in terms of the initial potential energy of the bubble W_0. For W_0 is the work done by the bubble in expanding and is

$$W_0 = \int_{v_0}^{\infty} p\,dv = p_0 v_0^{\gamma} \int \frac{dv}{v^{\gamma}} = \frac{p_0 v_0}{\gamma - 1}$$

$$= \frac{4\pi}{3(\gamma - 1)} \cdot r_0^3 p_0 \qquad (14)$$

Eliminating $r_0 p_0^{1/3}$ between (14) and (12a)

$$T = I \left(\frac{32}{3\pi^2}\right)^{1/6} \rho^{1/2} W_0^{1/3} p^{-5/6} \qquad (12c)$$

From equation (12c) the following conclusions are drawn.

(1) T is proportional to $W_0^{1/3}$. Since, for a given detonator, the successive pulses in practice become weaker, so that the potential energy W_0 at the stages of maximum compression becomes less and less, it follows that T should decrease slowly with each successive pulse. This agrees with the facts described earlier.

(2) In the case of the initial pulse W_0 may be identified with the total energy of the explosion. The interval between the first and second pulses is therefore proportional to the cube root of the heat value of the charge, irrespective of the nature of this charge.

(3) .....

(3) T varies inversely with the 5/6 power of the total external pressure. Shorter time intervals are therefore to be expected if a charge is fired at any appreciable depth in the sea.

Pressure variations outside the bubble.

Equation (9) shows how the pressure inside the bubble varies with time. This variation is not readily measured. What is frequently measured is the form of the pressure pulse at a distant point outside the bubble. The form of this pulse is not the same as that of the internal pressure, and the nature of the difference is now considered.

At any instant, t, the expanding bubble functions as a source whose strength S is equal to the rate at which water is being forced outwards, i.e.

$$S = \frac{d}{dt}\left(\frac{4\pi}{3} r^3\right) \tag{15}$$

The velocity potential, χ, at a point distant a from the bubble is, by the usual formula,

$$\chi = \frac{S}{4\pi a} = \frac{1}{4\pi a} \frac{d}{dt}\left(\frac{4\pi}{3} r^3\right) = \frac{1}{a} \frac{d}{dt}\left(\frac{r^3}{3}\right) \tag{16}$$

No retarded potential is here involved as the medium is assumed incompressible, and the velocity of sound is therefore infinite. The pressure at the point a is, therefore, by the usual hydrodynamic formula

$$\Pi = \rho \frac{\partial \chi}{\partial t} + \frac{1}{2} \rho v^2$$

where v is the radial velocity at a

$$= \frac{\rho}{a} \frac{d^2}{dt^2}\left(\frac{r^3}{3}\right) + \frac{1}{2} \rho \left[\frac{r^2 \dot{r}}{a^2}\right]^2 \tag{17}$$

The second term on the right hand side varies inversely with a^4, and therefore rapidly becomes negligible in comparison with the first term which varies inversely with a. Equation (17) therefore simplifies in practice to

$$\Pi = \frac{\rho}{a} \frac{d^2}{dt^2}\left(\frac{r^3}{3}\right) \tag{18}$$

This equation, together with the solution for r furnished by equation (8), specifies the values of Π for any time t. This, however, is not a convenient solution, and a more useful result can be obtained in the following way:-

Equation (18) can be written

$$r^2 \ddot{r} + 2 r \dot{r}^2 = \frac{a \Pi}{\rho} \tag{19}$$

Differentiation of the energy equation (3) gives

$$r^2 \ddot{r} + \frac{3}{2} r \dot{r}^2 = \frac{r}{\rho} (p - P) \tag{20}$$

Subtraction of (20) from (19) gives

$$\Pi = \frac{r}{a} \left\{ (p - P) + \frac{1}{2} \rho \dot{r}^2 \right\} \tag{21}$$

Substituting in (21) the value for $\dot{r}$ given by (5), and taking $\gamma = 4/3$ gives

$$\Pi = \frac{r}{a} \left\{ p - P + \frac{p_0}{4} \left[(1 + \alpha) x - \alpha x^4 - 1 \right] \right\} \tag{22}$$

But ....

But

$$\rho = \frac{\rho_0}{x^3} \quad \text{from (4)}$$

$$x = \frac{r}{r_0}, \quad P = 3\rho_0 \alpha \quad \text{from (5)}$$

Inserting these values in (22)

$$\Pi = p_0 \frac{r_0^3}{ar^2} \{ (1+\alpha) - 4\alpha x^3 \} \tag{23}$$

In the early stage of the motion, which is now considered, the terms α and αx^3 can be neglected in comparison with unity, and then

$$\Pi = p_0 \frac{r_0^3}{ar^2} \tag{24}$$

This is a more useful formula than (18).

The peak value Π_0 of the external pressure corresponds to $r = r_0$, and is

$$\Pi_0 = p_0 \left(\frac{r_0}{a}\right) \tag{25}$$

Equation (24) can now be written as

$$\Pi = \Pi_0 \left(\frac{r_0}{r}\right)^2 \tag{26}$$

so that, using equation (8)

$$t = r_0 \sqrt{\frac{2\rho}{p_0}} \left\{ \left[\left(\frac{\Pi_0}{\Pi} \right)^{1/2} - 1 \right]^{1/2} + \frac{2}{3} \left[\left(\frac{\Pi_0}{\Pi} \right)^{1/2} - 1 \right]^{3/2} + \frac{1}{5} \left[\left(\frac{\Pi_0}{\Pi} \right)^{1/2} - 1 \right]^{5/2} \right\} \tag{27}$$

which shows how Π varies with t in the early stages.

The maximum amplitude of the rarefaction at a distant point is deducible from the more accurate equation (23). From formula (10) it appears that the maximum expansion of the bubble corresponds to $x = x_1$, where x_1 is the larger positive root of

$$(1+\alpha) x - \alpha x^4 - 1 = 0$$

and is approximately $x_1 = \alpha^{-1/3}$ when α is very small. The corresponding value of Π is given by equation (23) as

$$\Pi_{min} = -\frac{3 p_0 r_0^3}{a r^2}$$

this variation being superposed upon the existing pressure P. Substituting in the above $r = x_1 r_0 = r_0 \alpha^{-1/3}$

$$\Pi_{min} = \frac{3 p_0 r_0}{a} \alpha^{2/3}$$

$$= -3\Pi_0 \alpha^{2/3} \quad \text{(from 25).}$$

The maximum amplitude of the rarefaction is therefore a fraction $3\alpha^{2/3}$ of the initial positive pressure pulse.

Comparison .....

Comparison with experiment.

Experiments made with small 1 gm. detonators have enabled the foregoing theoretical results to be tested in various ways.

(a) Shape of pulses.

Detailed calculations of the form of the external pressure pulses have been made, and on the basis of the results the appearance of the first two pulses has been sketched in Figure 3. In these calculations, equation (27) was used in order to obtain the form of the pulses down to a pressure amplitude of $\Pi_o/100$, a separate estimation of the maximum rarefaction being made.

Figure 1 shows a typical C.R.O. record of a detonator explosion. The receiver employed was a small 2½" quartz hydrophone calculated to have a principal resonance at about 400 kc/s. and aimed to have a flat response at lower frequencies. The receiver was used in conjunction with an amplifier having a high input impedance (10 - 20 megohms) and wide band frequency response (10 c/s to 100 Kc/s). The deflections on the C.R.O. records are proportional to the voltage variations across the receiver and therefore, for a perfect receiver, proportional to the pressure variations Π in the water.

In a general way the appearance of the C.R.O. trace agrees with that calculated, as regards the sharpness and isolated character of the pulses. There is one difference, however; on the C.R.O. record the initial pressure rise is followed after a very short time by a small sharp negative pulse. This effect is more apparent in Figure 2 where more amplification has been used. Here it appears that the negative peak is only associated with the first few explosions; it is absent from later explosions where the pressure variations appear to accord more nearly with theory. This effect may be due to the failure of the receiver to respond reliably to the very high frequencies which would be associated with the initial explosions.

(b) Amplitude of initial pressure pulse.

Equation (25) enables the peak pressure amplitude Π_o at any external point to be calculated. In Appendix I the following data are derived for the detonators

$$p_o = 3700 \text{ atm.} \qquad r_o = 0.62 \text{ cms.}$$

Substituting these in equation (25), absolute values are got for the pressure amplitudes: it is calculated, for example, that the pressure at a distance of 10 feet rises to 7.5 atmospheres. Experimentally, a value of about 3 atmospheres is obtained at the same range. Accurate agreement is here not to be expected, for the calculated value is very materially dependent upon p_o and r_o, reliable values for which are not available.

(c) The time interval T between the first and second pulses.

Equation (12b) has been used in order to get a theoretical value for T. Taking, for example, the case when a detonator is fired at a depth of 15 feet below the surface of the sea, the total pressure P at this depth is found to be

$$P = 1.45 \text{ atm.} = 1.45\ 10^6 \text{ dynes/cm}^2$$

In addition, the makers specify for their detonators

$$\theta_o = 3000^\circ \text{ C} = 3273^\circ \text{ K.}$$

$$m = 0.0136 \text{ corresponding to } 300 \text{ ccs. of gas} \quad \text{(Appendix I).}$$

$$\gamma = 1.30.$$

Using also the known values

$$R = 8.3\ 10^7 \text{ ergs/gm. molecule.}$$

$$I = 1.12.$$

formula .....

formula (12b) now gives

$$T = 18.6 \text{ milliseconds}$$

The corresponding value obtained by direct measurement is

$$T = 17 \text{ milliseconds}$$

By the same method the interval T can be calculated for the case of a depth charge. For this purpose equation (12c) is more convenient. Consider for example the case of a 300 lb. charge of T.N.T. The heat value of T.N.T. is given as 1040 calories/gm., from which the total energy W_0 of the entire charge is found to be $5.9\ 10^{15}$ ergs. At a depth of (say) 30 feet P = 1.9 atm. = $1.9\ 10^6$ dynes/cm^2. Equation (12c) then gives

$$T = 1.2 \text{ seconds.}$$

An experimental value

$$T = 0.6 \text{ seconds}$$

has been quoted for a 300 lb. mine exploding at a depth of 30 feet.

(d) Variation of T with pressure P_0.

As already pointed out, the dependence of T upon P expressed by equation (12b) implies that T should vary with the depth at which a charge is fired. Values of T for the detonators have been worked out for various depths up to 300 feet just as in the example worked out above for 15 feet. The resulting values define the continuous curve drawn in Figure 5. To test these values, direct measurements of T were carried out at sea down to a depth of 245 feet. These experimental values are set out in Table 1 and are marked by the circles in Figure 5. These values lie close to the theoretical curve, showing that equation (12b) gives a reliable figure for the absolute value of T under external pressures P ranging from 1 to 8 atmospheres.

Theoretically T should vary inversely with $P^{5/6}$. To test the accuracy with which the index 5/6 is operative the experimental values for T and P have been plotted on a logarithmic scale in Figure 6. A straight line of slope -5/6 has been drawn passing through these points. For purpose of comparison lines with slopes $-2/3$ and -1 have also been indicated. It is evident that the experimental values discriminate quite sharply in favour of the index $-5/6$.

(e) Time intervals between successive pulses.

As was mentioned earlier, it is found experimentally that the time intervals between successive pulses get shorter and shorter, and this effect is in qualitative agreement with theory. It is now possible to make quantitative comparison.

Equation (12a) shows that the time interval between the first and second pulses is proportional to $r_0\, \rho_0^{1/3}$ where r_0 and ρ_0 refer to the initial values of r and ρ at the first explosion. For a given mass of gas, by virtue of equation (4), r_0 is proportional to $\rho_0^{-1/4}$ (assuming $\gamma = 4/3$) so that T depends on the initial pressure of the gas according to the relation

$$T \propto \rho_0^{1/12}$$

But from equations (4) and (25)

$$\rho_0 \propto \Pi_0^{4/3}$$

ρ_0 being the internal and Π_0 the external pressure, so that

$$T \propto \Pi_0^{1/9}$$

This is strictly accurate only if the vibrations are undamped, Π_0 being then the same for the first and second pulses. For a damped train of pulses it is not quite legitimate to apply this formula to the pressure amplitude for the first pulse; it is more accurate to regard the first half of the

period .....

period as being determined by the pressure Π_1 of the first pulse and the second half as determined by the value Π_2 for the second pulse. The time interval can then be taken to be proportional to $(\Pi_1^{1/9} + \Pi_2^{1/9})$. In practice little difference is involved, otherwise equation (12a) would require correction for damping. The above result can be generalised for any two consecutive pulses of a train arising from a single detonator. If Π_n, Π_{n+1} are the amplitudes of the nth, (n + 1)th pulses and $T_{n, n+1}$ the time interval between them, then

$$T_{n, n+1} \propto (\Pi_n^{1/9} + \Pi_{n+1}^{1/9}) \qquad (31)$$

This relation has been tested against experimental figures. Relative values of Π_n appropriate to successive pulses have been measured off from the C.R.O. records. This cannot be done satisfactorily from one single photograph because Π_n decreases too rapidly with n to allow of accurate measurement over a number of pulses. However, a series of photographs were taken in which the amplification was progressively increased. These enabled mean values to be given to the ratios Π_n/Π_{n+1} from various pairs of consecutive pulses. In this way it was found that the pressure amplitudes of the first five pulses were in the ratio

$$\Pi_1 : \Pi_2 : \Pi_3 : \Pi_4 : \Pi_5$$

$$= 45 : 30 : 6 : 2 : 1$$

From equation (31) the corresponding time intervals are calculated to be in the ratio

$$T_{12} : T_{23} : T_{34} : T_{45}$$

$$= 1.45 : 1.29 : 1.12 : 1.00$$

The corresponding values got by direct measurement from Figure 2 are

$$= 1.67 : 1.23 : 1.10 : 1.00$$

Agreement is considered satisfactory in view of the fact that complete reliance cannot be placed in the amplitudes of the pulses shown in Figure 2. The initial pulses are richer than the late ones in high frequency sound of the order of several hundred Kc/s., and the receiver and amplifier do not necessarily reproduce them in true proportion to the others. This would affect the calculation of T_{12} more than the other intervals.

Considerations of the assumptions made.

The foregoing results have been derived on the basis of certain assumptions. These assumptions are now considered in the light of the results obtained

(a) The compressibility of the water.

It is legitimate to treat the water as an incompressible fluid only in so far as the radial velocity of the bubble is small compared with that of sound in water. From equation (8) it may be shown that the maximum radial velocity of the bubble occurs when $\frac{r}{r_0} = \frac{4}{3}$, and that this maximum velocity is

$$\frac{3}{16}\sqrt{\frac{6\,p_0}{\rho}}$$

For the small detonators this amounts to $2.7\ 10^4$ cms/second. The velocity of sound is $15\ 10^4$ cms/second, so that the radial velocity is at most 1/6 that of sound. The assumption of incompressibility is therefore quite reasonable as a first approximation when it is remembered that this maximum velocity is operative for only a relatively short part of the expansion.

(b) The finite duration of the explosion.

It was assumed that the explosion took place instantaneously, whereas in fact for the detonators it lasts about 2 micro seconds. Assuming an instantaneous explosion, the expansion which takes place in the first 2 μ seconds is now considered. Equation (8), for small values of t, can

be .....

be written

$$\frac{r}{r_o} = 1 + \frac{1}{2} t^2 \frac{p_o}{\rho r_o^2}$$

Inserting actual values it is found that, after 2 μ seconds

$$\frac{r}{r_o} = 1.018.$$

There is thus very little expansion in this time interval, so that it makes little difference whether the explosion occurs at the beginning of this interval or is distributed over it.

(c) The radiation of acoustic energy.

It was earlier assumed that there was no radiation of sonic energy. Taking the solution obtained on this assumption as a first approximation, it is now possible to calculate what energy is actually radiated when account is taken of the finite speed of sound, c.

The instantaneous flux of sonic energy per unit area per unit time at a range a is $\frac{\Pi^2}{\rho c}$. Substituting for Π from equation (24) this becomes $\frac{p_o^2 r_o^6}{\rho c a^2 r^4}$. Integrating over the surface of a sphere of radius a, the rate of emission of energy from the bubble becomes

$$\frac{dW}{dt} = \frac{4\pi p_o^2 r_o^6}{\rho c r^4} = \frac{4\pi p_o^2 r_o^2}{\rho c} \frac{1}{x^4}$$

The energy emitted in the course of the first pulse is therefore

$$W = \frac{4\pi p_o^2 r_o^2}{\rho c} \int_{x=1}^{x=x_1} \frac{dt}{x^4} \qquad (28)$$

where x_1 has the same significance as in equation (10).

Putting $\frac{r}{r_o} = x$ in equation (8) and differentiating, gives

$$dt = r_o \sqrt{\frac{\rho}{2 p_o}} \frac{x^2 dx}{\sqrt{x-1}}$$

and substituting this in (28) gives

$$W = 2\pi\sqrt{2} \frac{r_o^3 p_o^{3/2}}{c \rho^{1/2}} \int_1^{x_1} \frac{dx}{x^2\sqrt{x-1}} \qquad (29)$$

In equation (29) the major part of the integral arises from values of x near to unity. This fact justifies the use of equation (8) over the range of integration x = 1 to x = x_1 for equation (8) is valid only over the initial part of this interval (x = 1 to x = 5). The error introduced on this account is extremely small, and for the same reason it is quite legitimate, and more convenient to write the limits of integration in (29) as x = 1 to x = ∞. Then

$$W = 2\pi\sqrt{2} \frac{r_o^3 p_o^{3/2}}{c \rho^{1/2}} \int_1^{\infty} \frac{dx}{x^2\sqrt{x-1}}$$

$$= \pi^2\sqrt{2} \frac{r_o^3 p_o^{3/2}}{c \rho^{1/2}} \qquad (30)$$

This is now to be compared with the total energy W_o available at the moment of the explosion. Taking $\gamma = 4/3$, this latter by virtue of equation (14) is $\frac{4}{3}\pi r_o^3 p_o$, so that the fraction of the

initial .....

initial energy radiated in the first pulse is

$$\frac{W}{W_0} = \frac{\pi}{2\sqrt{2}} \frac{1}{c} \sqrt{\frac{p_0}{\rho}} \qquad (35)$$

For the small detonators this works out to be 0.43.

The appreciable magnitude of this figure implies a considerable degree of damping of vibrations. This fact will affect to some extent the accuracy of the expressions obtained for $p(t)$ and $\Pi(t)$. The deviations arising will be cumulative and will not impair greatly the validity of the formulae in the earlier stages of the explosion. The errors will be [illegible] range of validity of these formulae. The effect on the formulae for Π will be quite small with this the fact that the period of any simple harmonic vibratory system is little affected by quite heavy damping).

Formula (32) shows that the damping increases with p_0, so that the amplitude of the pulse should become relatively less. It is possible, therefore, that if p_0 is made large the second pulse may be too weak to be noticed in comparison.

Appendix [illegible]

APPENDIX I.

Detonator Figures.

The following is the information furnished by the makers concerning the detonators used. The amount of explosive used is 1 gm., part of which is lead azide. The volume of gas formed, at N.T.P., is 300 ccs. The initial temperature θ_0 is 3000° C (= 3273° K). The effective value of γ is 1.3.

The value of p_0 is not given, but, since the initial volume v_0 is known, it may be deduced from the equation of state (13). In this equation m is readily determined, for one gm. molecule of any gas at N.T.P. occupies 22 litres, so that the 300 ccs. of gas resulting from the explosion correspond to a value

$$m = \frac{300}{22000} = 0.0136.$$

The value of v_0 is not given, but is estimated to be about 1 cc. Inserting these values in (13) gives

$$p_0 = 3700 \times 10^6 \text{ dynes/cm}^2.$$

The accuracy of this value depends on the accuracy with which v_0 is known.

The total mechanical energy of the detonator explosion is, from equation (14), $\frac{p_0 v_0}{\gamma - 1}$.

By reason of equation (13) this can be written $\frac{m R \theta_0}{\gamma - 1}$. On substituting the values for m, θ_0 and γ already quoted, a figure of 1200 Joules is obtained for the energy of the detonator.

Appendix II .....

APPENDIX II.

Evaluation of the integral for T.

This integral is

$$K(\alpha) = \int_1^{x_1} \frac{x^2\,dx}{\sqrt{(1+\alpha)\,x - \alpha\,x^4 - 1}}$$

where x_1 is the larger positive root of

$$(1+\alpha)\,x - \alpha\,x^4 - 1 = 0$$

The integral defines a function of α. The asymptotic form of this function as $\alpha \to 0$ is now calculated.

When $\alpha \to 0$ the value of x_1 approaches $\alpha^{-1/3}$. A number x_2 is now chosen which is of a lower order than x_1, but still large compared with unity. This can always be done, and such a number would be $x_2 = \alpha^{-q}$ where q is positive and less than 1/3. Then $K(\alpha)$ may be written in the form

$$K(\alpha) = \int_1^{x_2} \frac{x^2\,dx}{\sqrt{(1+\alpha)\,x - \alpha\,x^4 - 1}} + \int_{x_2}^{x_1} \frac{x^2\,dx}{\sqrt{(1+\alpha)\,x - \alpha\,x^4 - 1}} \qquad (33)$$

This is now compared with the function

$$K_1(\alpha) = \int_1^{x_2} \frac{x^2\,dx}{\sqrt{x-1}} + \int_{x_2}^{\alpha^{-1/3}} \frac{x^2\,dx}{\sqrt{x - \alpha\,x^4}} \qquad (34)$$

It can be shown that, by virtue of the choice of x_2, the relative differences between corresponding terms of (33) and (34) get less and less as $\alpha \to 0$. Hence the limiting forms of both $K(\alpha)$ and $K_1(\alpha)$ are the same.

The integration of the expression for $K_1(\alpha)$ can be carried out. Putting $\sin^2\theta = \alpha\,x^3$ in the second integral, the result is

$$K_1(\alpha) = 2\{(x_2-1)^{1/2} + \tfrac{2}{3}(x_2-1)^{3/2} + \tfrac{1}{5}(x_2-1)^{5/2}\} + \tfrac{2}{3}\alpha^{-5/6}\int_{\sin^{-1}(\alpha x_2^3)^{1/2}}^{\pi/2} \sin^{2/3}\theta\,d\theta.$$

But since $x_2 \gg 1$ it is possible to write x_2 for $(x_2 - 1)$ in the first term. Then

$$K_1(\alpha) = 2\{x_2^{1/2} + \tfrac{2}{3}x_2^{3/2} + \tfrac{1}{5}x_2^{5/2}\} + \tfrac{2}{3}\alpha^{-5/6}\left\{\int_0^{\pi/2} \sin^{2/3}\theta\,d\theta - \int_0^{\sin^{-1}(\alpha x_2^3)^{1/2}} \sin^{2/3}\theta\,d\theta\right\} \qquad (35)$$

But since $x_2 \ll \alpha^{-1/3}$, $(\alpha x_2^3)^{1/2} \ll 1$ so that the last integral on the right hand side simplifies to

$$\int_0^{(\alpha x_2^3)^{1/2}} \theta^{2/3}\,d\theta = \tfrac{3}{5}(\alpha x_2^3)^{5/6}$$

Putting .....

Putting this result in (35)

$$K_1(\alpha) = 2\left\{x_2^{1/2} + \frac{2}{3}x_2^{3/2}\right\} + \frac{2I}{3}\alpha^{-5/6} \qquad (36)$$

where

$$I = \int_0^{\pi/2} \sin^{2/3}\theta \, d\theta \doteq 1.12$$

But if x_2 is assumed to have the value α^{-q} then

$$\frac{x_2^{3/2}}{\alpha^{-5/6}} = \alpha^{5/6-3q/2}$$

and since $q < 1/3$ this is a positive power of α, whose value accordingly tends to zero as $\alpha \to 0$. Thus the first term of (36) finally becomes negligible in comparison with the second, which accordingly represents the limiting form of $K_1(\alpha)$. Hence

$$K(\alpha) \to K_1(\alpha) \to \frac{2I}{3}\alpha^{-5/6} \quad \text{as} \quad \alpha \to 0.$$

When α is not infinitesimally small, $K(\alpha)$ will differ from its limiting form. It has been estimated that the relative error involved is of the order $\alpha^{1/3}$.

Table I .....

28

TABLE 1.

Theoretical and observed values of T for various depths at which detonators are fired.

Depth (in feet) at which detonator is fired	Total external pressure P (in atmospheres)	Calculated values of T (in milli-seconds)	Observed values of T (in milliseconds)
3	1.09	23.5	23.5, 24.1
25	1.75	15.0	15.2, 16.5, 14.9
45	2.35	12.4	11.4, 11.7
65	2.95	10.3	10.6, 9.2, 9.3
85	3.55	8.75	8.9
105	4.15	7.76	8.4, 7.2
125	4.75	6.93	6.9
145	5.35	6.25	6.4, 6.8
165	5.95	5.73	5.7
185	6.55	5.28	5.5, 5.7
205	7.15	4.92	5.0
225	7.75	4.60	4.8, 5.0
245	8.35	4.33	4.2

FIG. I

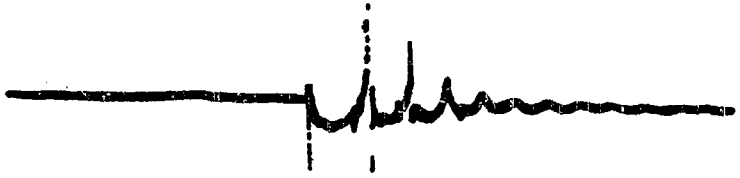

FIG. II

100 Cycles/Sec.

FIGURE 3.

CALCULATED FORM OF FIRST TWO PRESSURE PULSES FROM DETONATOR EXPLOSIONS

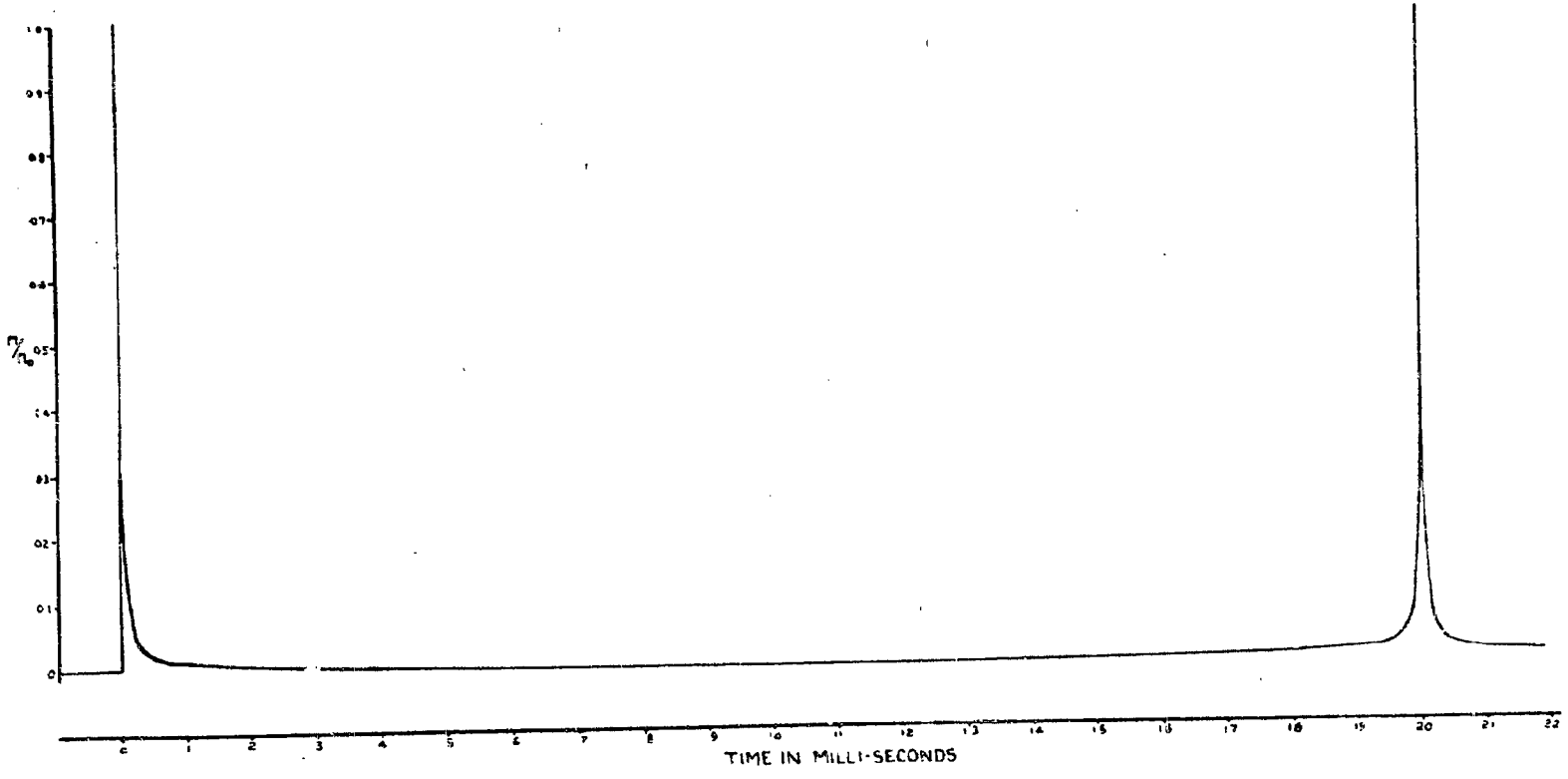

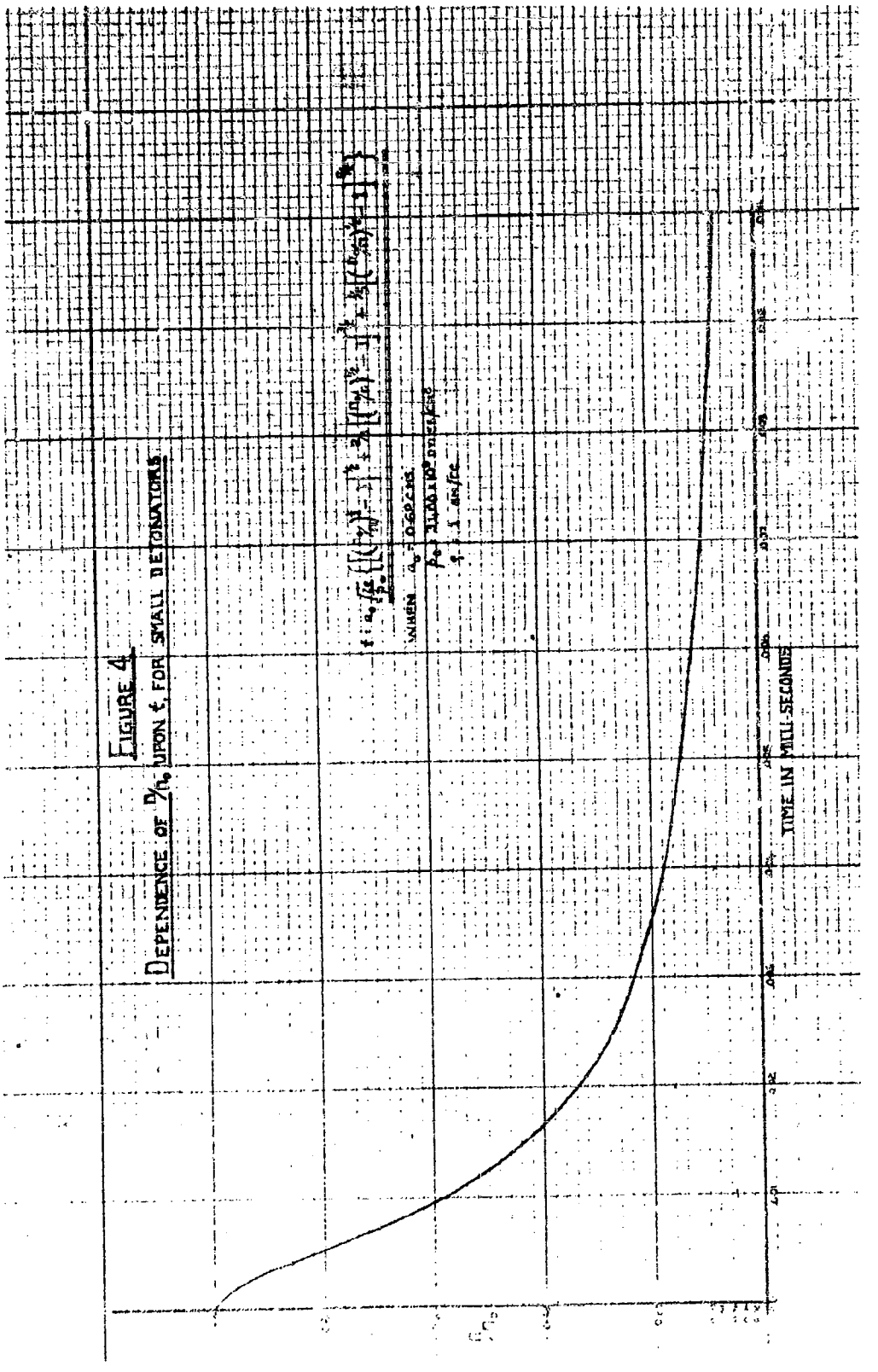

FIGURE 4

DEPENDENCE OF P/P_0 UPON t, FOR SMALL DETONATIONS

FIGURE 5

VARIATION OF INTERVAL T WITH DEPTH AT WHICH DETONATOR IS FIRED

CONTINUOUS CURVE REPRESENTS THEORETICAL VALUES
CIRCLES REPRESENT OBSERVED VALUES

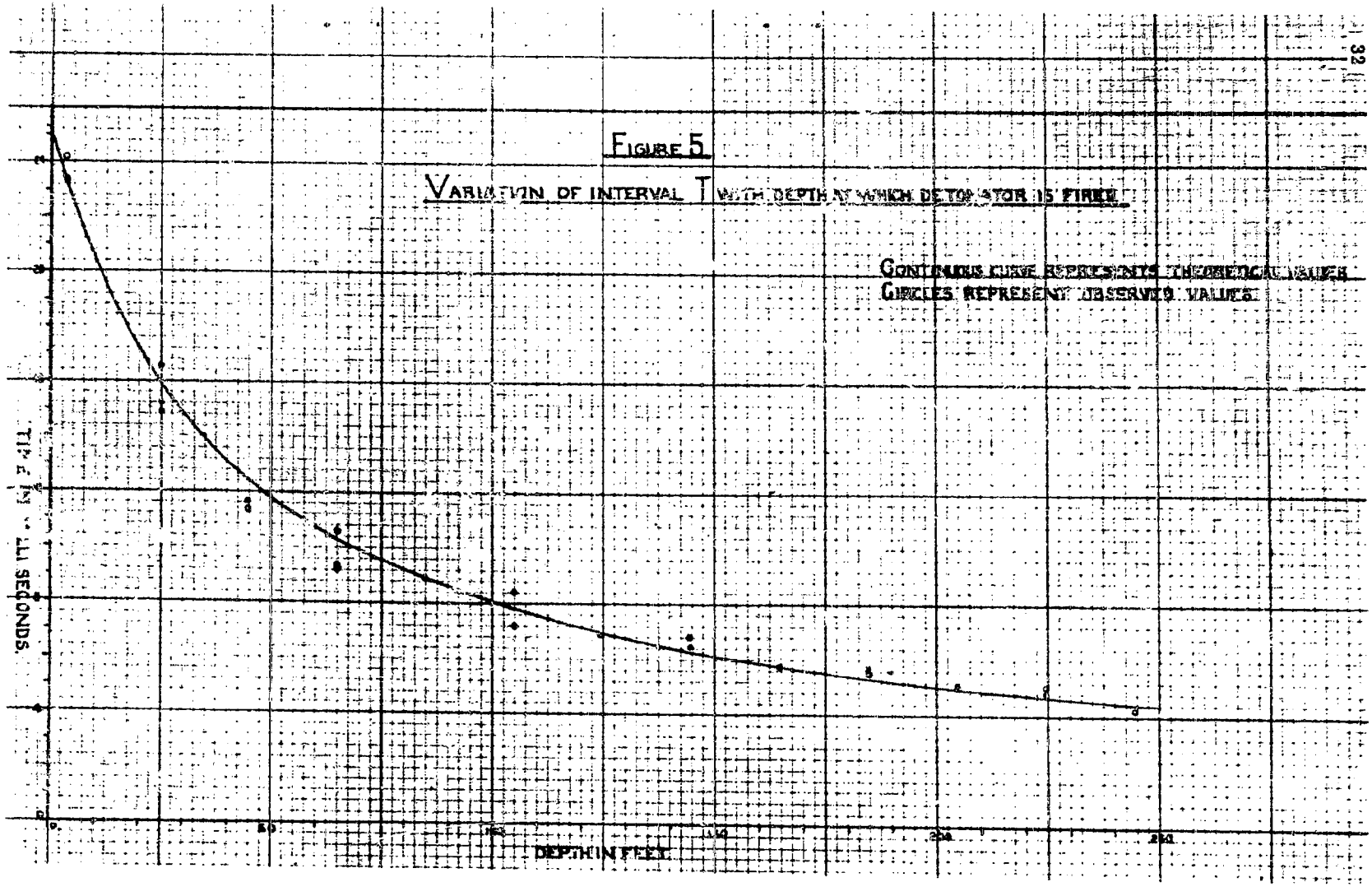

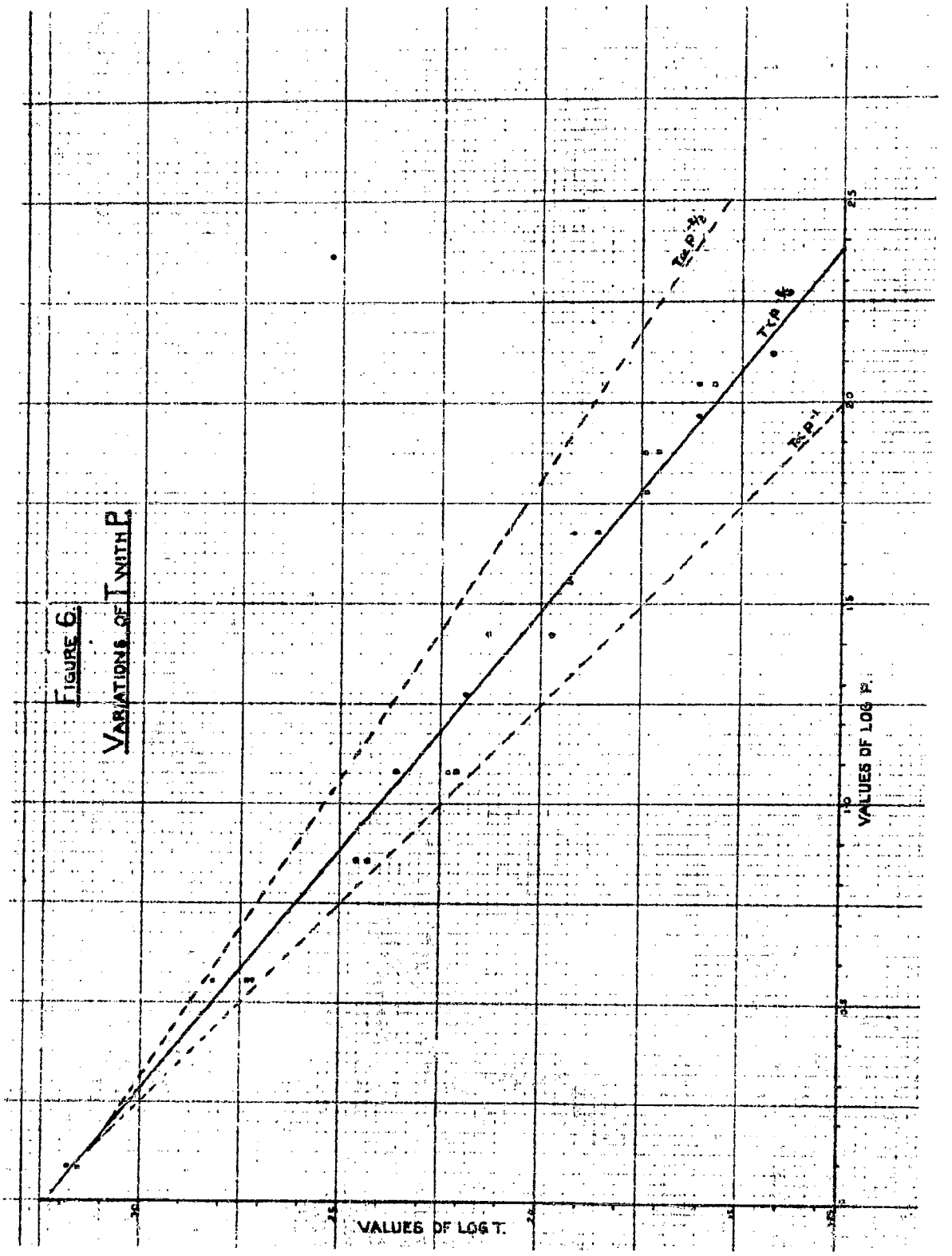

FIGURE 6.
VARIATIONS OF T WITH P.

THEORY OF THE PULSATIONS OF THE GAS BUBBLE PRODUCED BY AN UNDERWATER EXPLOSION

Conyers Herring
Bell Telephone Laboratories, Murray Hill, N. J.

American Contribution

1949

Most of the work on which this paper is based was done in 1941 for the Columbia University Division of National Defense Research, and appeared as a report in October 1941 with the NDRC number C4-sr20-010. In the present paper this report has been revised so as to omit material no longer of interest and to include additional material presented by the author at the Washington Meeting of the American Physical Society in the spring of 1947.

THEORY OF THE PULSATIONS OF THE GAS BUBBLE PRODUCED BY AN UNDERWATER EXPLOSION

by

Conyers Herring

CONTENTS

1. Introduction	1
2. Homology Rules	6
3. Non-Compressive Theory with Spherical Symmetry	9
4. Acoustic Radiation by a Spherically Symmetrical Bubble	16
5. Migration of a Shperical Bubble	22
6. Departures from Spherical Shape	32
7. The Energy Balance	35
Appendix 1 : Pulsations of a Bubble in an Incompressible Fluid	39
Appendix 2 : Pulsations of a Bubble in a Fluid of Finite Compressibility	44
Appendix 3 : Calculations of the Rate of Radiation of Energy	54
Appendix 4 : Effect of Gravity	59
Appendix 5 : Effect of Proximity to a Free or to a Rigid Surface	64
Appendix 6 : Pressure Distribution in Non-Compressive Radial Motion	79
Appendix 7 : Effect of the Inertia of the Gas on the Pressure Pulse	82
Appendix 8 : Resume of Ramsauer's Experiments	84

NOTATION

A	strength of a simple source
A_0, A_1, etc.	coefficients in expansion of velocity - potential
a	radius of bubble
$\bar{a}$	time average of a
a_1	radius at which gas pressure equals p_∞.
a_{max}, a_{min}, a_{mean}	maximum and minimum radius, and average of these.
B_x (m, n)	Incomplete beta function
B_1, etc.	coefficients in expansion of velocity - potential.
C_1, etc.	coefficients in expansion of velocity - potential
c	velocity of sound in water
c_g	velocity of sound in gas in bubble
D	distance of receiver from bubble
E	field strength in equivalent electrostatic problem
e	charge of bubble in equivalent electrostatic problem
F	defined by eq. (9), Appendix 2.
$\mathcal{F}$	potential energy of gas in bubble
g	acceleration of gravity
h	distance of center of bubble from plane free or rigid surface.
K	thermal conductivity
L	length of a cylinder; any characteristic length
ℓ	order of spherical harmonic

$\vec{M}$	momentum
$\vec{n}$	unit outward normal
P_ℓ	Legendre polynomial
p	pressure
p_o, p_1, etc.	coefficients in expansion of pressure (Appendices 4 and 5)
$\bar{p}$	pressure of gas under static conditions
p_∞	pressure of water at a great distance from bubble, at same depth as center of bubble.
p_{im}	pressure due to image (Appendix 5)
Q	total energy released by explosion
q_1, q_2	masses of explosive
R	perturbed bubble radius (Appendices 4 and 5)
R_1, $R_1^{(\ell)}$, etc.	coefficients in spherical harmonic expansion of radius vector of bubble.
r	distance from initial center of bubble.
$\vec{r}$	radius vector
T	period of a pulsation
T_o	period calculated from simplest theory
T_s	period for small oscillations
t	time
t_m	time of maximum size of the bubble
V	volume or molar volume
v	velocity
W	total energy of the pulsating motion
x, x_1	$a^{5/2}$, $a_1^{5/2}$ (Appendix 1)

x	a/a_{min} (Appendix 3) ; distance (Appendix 5)
y, y_1	a/a_{max}, a_1/a_{max}
z	variable of integration (Appendix 1); cartesian coordinate (Appendices 4 and 5)
β	defined by eq. (5), Appendix 3
Γ	gamma function
γ	ratio of specific heats, or quantity playing same role in equation of state.
δ	Dirac delta function
η	viscosity
θ	polar angle (Section 6 and Appendices 4 and 5); temperature (Section 7)
ξ	radius of a cylinder
Π	unspecified function
ρ	density of water
ρ_g	density of water at a great distance from bubble
ρ_∞	density of gas in bubble
σ	divergence of velocity
$d\tau$	element of volume
Υ	unspecified function
Φ	defined by eq. (14) or (15), Appendix 2
ϕ	velocity - potential
ϕ_0, ϕ_1, etc.	coefficients in expansion of velocity - potential

1. INTRODUCTION

During the last generation or two it has been noticed from time to time by different observers that when a charge of explosive is set off under water, the sound received by a hydrophone some distance away consists of a number of sharp "pokes", which decrease gradually in amplitude and become more and more closely spaced in time. The intervals between the pokes are greater the greater the charge of explosive and the smaller the depth of the charge below the surface; at shallow to moderate depths the intervals which have been observed range from one or a few hundredths of a second for detonating caps to around one second for charges of several hundred pounds of explosive. It has been convincingly shown by Willis[1] that the periodic phenomenon involved is one of radial pulsations of the gas bubble produced by the explosion. Further investigations of this pulsation phenomenon have shown that its interest is not limited to the field of the acoustics of explosive sound: it appears essential to a detailed understanding of the "plumes" of water thrown up over an underwater explosion; in some cases it may have an important effect on the damage inflicted by an underwater explosion on neighboring structures; it may provide a useful research tool in the experimental study of explosions and other problems in hydrodynamics. Moreover, bubbles formed by explosions are not the only ones which may be made to undergo radial pulsations of large amplitude: an example is the collapse of cavitation

---

[1] See the article by Willis in this Volume.

bubbles after application of a positive pressure; another example is the observation by M. Ewing and his associates at the Woods Hole Oceanographic Institution that multiple shocks are heard by a microphone placed near a submerged pipe with a diaphragm at one end which is burst by water at high pressure inside the pipe.[2] Although this article and the others in this volume are concerned primarily with explosion bubbles, and although additional factors such as surface tension may have to be invoked in applying the theory to tiny bubbles[3], it is worth bearing in mind that similar principles govern a variety of widely different phenomena.

The essential features of the pulsation phenomenon arise from the fact that an explosion creates a cavity filled with high pressure gas, which pushes the water out radially against the opposing external hydrostatic pressure. The high velocity thus imparted to the water causes it to overshoot the equilibrium radius at which internal and external pressures are equal, and when the external pressure finally succeeds in bringing the expansion to a halt a contraction sets in, which again overshoots and recompresses the gas to a high pressure. This sort of oscillation may be repeated a number of times, until the original energy has become dissipated in one way or another. At each compression

- -

[2]Private communication from Dr. Ewing.

[3]See for example R. S. Silver, Engineering 154, 501 (1942).

the high pressure developed gives rise to an acoustic impulse which can be heard at a distance. These features of the phenomenon will be discussed in detail in Sections 3 and 4 of the text, the former dealing with the spherically symmetrical pulsations of a bubble in an incompressible fluid, the latter with the effect of the finite compressibility of the water, which gives rise to acoustic radiation. Mathematical details are given in Appendix 1 and in Appendices 2 and 3, respectively.

In actual experiments with explosion bubbles there are always asymmetrical influences which prevent the motion of the water from conforming exactly with the spherically symmetrical theory just mentioned. The most interesting features of the pulsation phenomenon are, in fact, those which are associated with asymmetries in the motion, and many of the papers contained in this Volume are devoted to these features. If the only asymmetrical influence is the pressure gradient due to gravity, the bubble will rise; it turns out that the velocity of rise increases enormously during the contracted stages, and that appreciable departures from spherical shape may also occur in these stages. An additional "migration effect" can be caused by proximity of the bubble to a rigid body or to a free surface: roughly described, a rigid surface attracts a pulsating bubble while a free surface repels it; these effects may sometimes be more intense than that due to gravity. The importance of both kinds of asymmetry in the motion is obvious, since the position and characteristics of the bubble at the time of its minimum volume will greatly influence the

damage which the high pressure accompanying this stage is capable of doing to neighboring structures; moreover, the form of the plumes sent up by the explosion will obviously depend on the way the bubble is moving when it breaks the surface. A theoretical discussion of the migration effects due to gravity and to neighboring surfaces is given in Section 5, with mathematical details in Appendices 4 and 5, respectively. The mathematical methods used here, and those used in most of the other theoretical papers of this volume dealing with the migration effect, have not been elaborated far enough to provide a quantitative calculation of the extent of the departures of the bubble from spherical shape. However, some qualitative comments on these departures are given in Section 6.

Experiments on the various aspects of the pulsation phenomenon have usually shown a quite satisfactory agreement with the predictions of the theory. A notable exception has to do with the apparent loss of energy between successive pulsations, a loss which occurs in the brief time when the radius of the bubble is near its minimum. It has been established[4] that some as yet unelucidated mechanism of dissipation does away with an amount of energy of the same order as the known energy loss from acoustic radiation. Some brief speculations on this topic are given in Section 7.

- -

[4]A. B. Arons, J. P. Slifko, and A. Carter, J. Acous. Soc. Am. 20,271 (1948); A. B. Arons and D. R. Yennie, Rev. Mod. Phys. 20,519 (1948), also Volume I of this Compendium.

No introduction to the subject of bubble pulsations can be complete without mention of several early papers, theoretical ones by Lamb and by Rayleigh[5], and an experimental one by Ramsauer[6], which preceded the work of Butterworth and Willis presented elsewhere in this Volume. Rayleigh was concerned with the collapse of cavitation bubbles, while Lamb and Ramsauer studied only the expanding phase of the motion, and make no mention of the phenomenon of successive pulsations; however, their work contains the essential ideas of the theory of Section 3 and has other interesting features as well. A brief account of Ramsauer's work is given in Appendix 8.

---

[5] H. Lamb, Phil. Mag. 45,257(1923); Lord Rayleigh, Phil. Mag. 34,94 (1917).

[6] C. Ramsauer, Ann. d. Physik 72,265 (1923).

44

2. HOMOLOGY RULES

Before undertaking a detailed study of bubble motion it is worth while to mention a few very general conclusions which can be drawn directly from the basic equations governing the motion. The motion is completely determined by:

(a) the three Hugoniot equations at the advancing front of the shock wave generated by the explosion[7];

(b) the Euler equations and the equation of continuity for the water inside the shock front;

(c) similar equations for the motion of the explosion products inside the bubble;

(d) the equations of state of the water and the explosion products.

In the stages before the detonation is complete, equations of the Hugoniot type at the advancing detonation front must also be included. Now if it is legitimate to assume

(i) that there is no body-force term in the Euler equations - i.e., that gravity may be neglected - and

(ii) that the pressure in the explosion products is a unique function of the density, independent of the rate of change of density,

then all the equations (a) to (d) will be unchanged if all distances and times are changed by the same constant factor, pressures being left unchanged. This means that if (i) and (ii) can

---

[7] See Volume I of this Compendium.

be assumed, the pressure and velocity distributions produced by different amounts of the same explosive are identical if referred to units of distance and time which are proportional to the linear dimensions of the charges. Mathematically expressed, if a mass q_1 of a given explosive produces the pressure and velocity distributions

$$p = \Pi(\vec{r},t) \quad , \quad v = \Psi(\vec{r},t)$$

(t to be measured from the start of the explosion), then a mass q_2 of the same substance produces the distributions

$$p = \Pi\left[\vec{r}\left(\frac{q_1}{q_2}\right)^{1/3}, t\left(\frac{q_1}{q_2}\right)^{1/3}\right], \quad v = \Psi\left[\vec{r}\left(\frac{q_1}{q_2}\right)^{1/3}, t\left(\frac{q_1}{q_2}\right)^{1/3}\right] \quad (1)$$

Strictly speaking, it must also be specified that the initial shape of the explosive be the same in the two cases, and that the behavior of surrounding obstacles or surfaces, if any are present, can also be scaled. This rule has long been known and applied to characteristics of shock waves; it is equally applicable to bubble pulsations, provided (i) and (ii) hold.

Another homology rule which is approximately valid for bubble pulsations results from the fact, which will be demonstrated in the next section, that over most of the cycle the motion approximates fairly closely to the motion which would be executed in an incompressible fluid by a bubble with no gas inside it at all.

Of the equations enumerated above, only those enumerated under (b) are needed to determine the latter motion. In the absence of gravity these equations are invariant under any scale changes for pressures, lengths and times which satisfy $p_1/p_2 = (L_1/L_2)^2/(t_1/t_2)^2$. In this approximation explosion bubbles from all sizes of charge at all depths execute homologous motions. Taylor[8] has shown that if gravity is not neglected, this homology rule does not completely disappear, but reduces to a homology over one degree of freedom instead of two.

Departures from the scaling law (1) can be produced by irreversible processes taking place inside the bubble, and departures from both types of scaling law may be expected if turbulence becomes serious in the water. Failures of scaling, if properly interpreted, may thus be of considerable significance in detecting the presence of irreversible phenomena.

---

[8] See the article by Taylor immediately following this one in this Volume.

3. NON-COMPRESSIVE THEORY WITH SPHERICAL SYMMETRY

Let us consider now the simplest possible model of the motion of the bubble, by assuming the water incompressible and the motion spherically symmetrical. This model, simple though it is, turns out to be capable of giving a fairly satisfactory account of the radius-time curve under most conditions. It is not surprising that it does so, in view of the following facts:

(a) The shock wave advances so much faster than the boundary of the bubble that, before an appreciable part of the first pulsation period has elapsed, the motion of the water has become fairly clearly separated into a shock wave region and a "bubble region", between which the water is relatively quiescent, as shown in Fig. 1 (b).* This empirical fact is accounted for by theoretical calculations on the form of the shock wave.[9]

(b) In the "bubble region" the pressure is never large enough to change the density of water by more than a few percent.

(c) With the possible exception of times very close to the minimum of the contraction, the pressure in the

---

[9] See the articles by Kirkwood and Brinkley and by Temperley and Craig in Volume I of this Compendium.

*Refer to the end of this article for all referenced figures.

gas bubble (and therefore that in the water) changes by only a very small fraction of its value in the time required for an acoustic wave to be propagated through a distance of the order of the radius of the bubble. This ensures that the flow in the bubble region will keep in phase with the motion of the boundary of the bubble.

(d) In many cases, though not all, the unilateral migration of the bubble in its first period, due to gravity or other influences, is of fairly small magnitude compared with the maximum radius of the bubble, and the bubble remains fairly accurately spherical in shape. As will be shown later, this is the case when the size of the explosive charge is sufficiently small in comparison with the external hydrostatic pressure.

The more refined theories to be considered later in this article will explain the validity and limitations of the simple theory in a more quantitative way.

We shall therefore assume for the present that the water moves radially outward or inward in such manner that the amounts of water crossing any two concentric spheres in a given time are always the same; if the motion is spherically symmetrical this means that the variation of velocity v with radius r is given by

$$v = \left(\frac{a^2}{r^2}\right) \frac{da}{dt} \tag{2}$$

where a(t) is the radius of the bubble. Under our assumptions the total energy, which is constant, equals the kinetic energy of the water, plus the potential energy of the compressed gas, plus the potential energy due to expansion against the pressure p_∞ of the water far from the bubble. The kinetic energy is

$$\int_a^\infty \tfrac{1}{2}\rho v^2 \cdot 4\pi r^2 dr = 2\pi\rho a^3\left(\frac{da}{dt}\right)^2 \tag{3}$$

The work done against p_∞ is, to within an additive constant

$$\frac{4\pi a^3}{3} \quad p_\infty \tag{4}$$

Denoting the potential energy of the gas for the present merely by G, the energy equation is

$$2\pi\rho a^3 \frac{(da)^2}{(dt)} + \frac{4\pi a^3}{3} p_\infty + G(a) = W \tag{5}$$

where W is constant in time. This equation can be solved for $\frac{da}{dt}$ and integrated to get the motion. The term G(a) complicates the integration considerably; fortunately however it can be shown that for the first pulse or two the calculated period is very little altered by setting G = 0. The reason for this is that G is appreciable only in stages of the motion when the bubble is small, and these stages occupy only a small fraction of a period. A rough estimate of the error introduced by ignoring G can be obtained from Appendix 1. For the later pulsations the amplitude of the motion is much less, and eventually the

pulsations can be regarded as small oscillations in the neighborhood of the radius at which the gas pressure equals the surrounding hydrostatic pressure. For these small oscillations G is essential, but the calculation of the period is simplified by the assumption of small amplitudes.

In Appendix 1 it is shown that when G = 0 in (5), the period of the motion is

$$T_0 \approx 1.135\, \rho^{\frac{1}{3}} p_\infty^{-5/6} W^{1/3} \qquad (6)$$

This formula has been derived by Willis[10] and others. Of course, the comparison of this formula with observation is not complete unless a definite value can be inserted for W. From the discussion given above it is clear that W will be appreciably less than the total energy released by the explosion. Theoretical calculations reported in Volume I of this Compendium agree with observation[11] in assigning to the first pulsation of the bubble a value of W of the order of half the chemical energy Q released by the explosive, the remaining energy being distributed in comparable proportions between energy carried off to appreciable distances by the shock wave and energy dissipated as heat by irreversible processes at the shock front in the very early stages of its motion. A convenient

---

[10] See the article by Willis in this Volume.

[11] See the article by Arons and Yennie in Volume I of this Compendium, or Rev. Mod. Phys. 20, 519 (1948).

alternative to deriving W from Q is to derive it from the maximum radius a_{max} of the bubble, if measurements of this quantity are available. If $G(a_{max})$ is neglected[12], $W = (4\pi/3)\, a_{max}^3\, p_\infty$, and so (6) becomes

$$T_o = 1.829\, \rho^{\frac{1}{2}}\, p_\infty^{-\frac{1}{2}}\, a_{max} \qquad (7)$$

The corresponding expression for the period of small oscillations about the equilibrium radius a_1 is, according to Appendix 1,

$$T_s = \frac{2\pi}{\sqrt{3\gamma}}\, \rho^{\frac{1}{2}}\, p_\infty^{-\frac{1}{2}}\, a_1 \qquad (8)$$

where γ is the ratio of the specific heats of the gas. For $\gamma = 1.3$, (8) becomes

$$3.18\, \rho^{\frac{1}{2}}\, p_\infty^{-\frac{1}{2}}\, a_1$$

Willis[13] has shown that (6) does in fact describe the periods of oscillation of the bubbles produced by charges of various sizes at various depths. With a suitable choice of

---

[12] The rather indirect experimental determination of $G(a_{max})$ reported in reference 11 gives a value of the order of $0.2W$ at the maximum of the first pulsation, presumably at 500 feet depth; however, this value is open to suspicion since it is 50% higher than the value obtained in a similar way for the second pulsation, whereas it should be smaller. Thus the correct $G(a_{max})$ might be as small as $0.1W$ at this depth; at the surface, where p_∞ is 16 times smaller, a_{max}^3 will be roughly 16 times larger, and $G(a_{max})/W$ will be smaller by a factor $16^{1-\gamma} \approx \frac{1}{2}$, if we use Arons' value of 1.25 for the effective ratio of specific heats γ.

[13] See the article by Willis in this Volume.

W/Q , constant for a given type of explosive, (6) can be made to give results correct to within a fraction of a percent, an accuracy comparable to the degree of reproducibility of experiments. However, the value of W which one must use in (6) to get the best fit to a given range of experimental data will of course differ a little from the correct value of the energy of the motion, because of the slight effect of gas pressure on the period. More refined comparisons of theory and experiment than those given by Willis have been made subsequently, and are reported elsewhere in this Volume.

A rough idea of the error involved in neglecting gas pressure may be conveyed by quoting the results which one obtains by substituting into the theoretical calculations of period made by Shiffman and Friedman[14] the empirical value 1.25 obtained by Arons[15] for the adiabatic exponent in the equation $pV^{\gamma} = \text{const.}$ and the value obtained by Arons for the energy of the first pulsation. This gives a period which is lower than that given by (6) by less than a percent, if W is interpreted as including the total energy of the gas relative to infinite adiabatic expansion; the ratio of T to a_{max} is greater than that given by (7) by an amount which varies from about 4% at sea level to about 9% at 500 feet depth.

Fig. 2 shows a comparison of an observed radius-time curve with the curve calculated in Appendix 1 by integration of (5) with G = 0 . The observed points were taken by Ewing and Crary from a motion picture taken by Edgerton in 1941 of a

---

[14] See the article by Friedman in this Volume.

[15] A. B. Arons, J. Acous. Soc. Am. 20, 277 (1948).

bubble produced by a detonating cap a foot below the surface; they refer to the first oscillation. The constant W has been chosen to make the theoretical maximum radius agree with the observed one; the times of maximum size have also been made to coincide. The agreement is reasonably good; however, the comparison is not capable of indicating just how accurate the simple theory is, because of the deviations due to the presence of the free surface, deviations which will be discussed at length in Section 5 .

In the present approximation the shape of the theoretical curve is independent of the size and depth of the explosion, there being only the single adjustable parameter a_{max}. Thus the curve of Fig. 2 is applicable to all explosions, if the horizontal and vertical scales are expanded or contracted in proportion to a_{max}.

As the successive pulsations of a given bubble decrease in amplitude because of acoustic radiation and other dissipative processes, the periods will shorten and approach the value (8). If the bubble can be made to remain reasonably spherical until the amplitude of oscillation has become small, measurements of a_1 or T_s , or both, may provide a check on the equation of state of the explosion products.

It is interesting to speculate that the use of propellent charges, which give no shock wave, might result in values of W/Q approaching unity, with correspondingly more violent bubble pulsations.

4. ACOUSTIC RADIATION BY A SPHERICALLY SYMMETRICAL BUBBLE

An exact calculation of the motion of a pulsating gas bubble in a compressible fluid would be very difficult: Lamb[16] has derived a partial differential equation governing the variation of velocity with radius and time for the spherically symmetrical case, but this equation is complicated and would be very difficult to solve. Fortunately, however, the effect of the finite compressibility of water on the motion of the bubble produced by an explosion amounts, except in the very early stages represented by Fig. 1 (a), only to a small to moderate correction to the simple theory of the preceding section. It is therefore possible to work out the details of the motion, as affected by the finite compressibility, by an iterative process of successive approximations, taking the non-compressive motion as the zeroth approximation. One way of doing this is carried through in Appendix 2. This method involves transforming the equations of motion of the boundary of the bubble into a form in which the correction for compressibility is represented by a radial integral whose integrand decreases very rapidly with increasing distance from the center of the bubble; in this form but little error is made if the non-compressive approximation to the integrand is used. The result is a differential equation -- Eq. (19) or (20) of Appendix 2 -- for the time variation of the radius

---

[16] H. Lamb, Phil. Mag. 45, 257 (1923).

a of the bubble. This equation is similar to that which would be obtained by differentiating Eq. (5) above with respect to time, but contains several additional terms, of which the most important is one proportional to $a^3(da/dt)[dp(a)/dt]/\rho c$, where c is the velocity of sound in water. As this expression is intrinsically negative, one might be tempted to interpret it as the instantaneous rate of loss of energy by acoustic radiation. This is not quite correct, however, although it gives the correct total loss of energy over the whole interval when a is small. For the fact that the term just written is proportional to the time rate of change of the left of (5) does not imply that it is proportional, with a suitable constant time lag, to the rate of reception of acoustic energy at a distance.

The equations of Appendix 2 are therefore directly applicable only to the calculation of the total energy of a pulse and to the calculation of how the time variation of a is affected by compressibility. It is easy to show from these equations that the effect of the finite compressibility of water on the curve of a against t is negligible when a is more than a few times its minimum value; details are given in Appendix 3. Near the minimum the effect may theoretically be either small or large, depending on the equation of state of the gas in the bubble. Recent experiments[17] have shown that

---

[17] A. B. Arons, J. P. Slifko, and A. Carter, J. Acous. Soc. Am. 20, 271 (1948); A. B. Arons and D. R. Yennie, Rev. Mod. Phys. 20, 519 (1948), also Volume I of this Compendium.

with common explosives the total acoustic loss of energy during the first contracted stage is never more than a fraction ($\sim$25%) of the total energy W of the pulsation, so that the correction to the motion is small to moderate. It might therefore be supposed that the radius-time curve could be fairly accurately calculated by the methods of Appendix 2. However, this does not seem to be the case: the energy loss between the first pulsation and the second is found experimentally[17] to be much greater than the observed acoustic energy in the first bubble pulse, indicating that some dissipative mechanism is acting which has not been taken into account in the present theory. As an adequate discussion of this question of energy balance requires a knowledge of the effects to be expected from migration and asymmetry of the bubble, further remarks on this point will be postponed until Section 7.

Let us now consider the way in which the pressure in the acoustic pulse radiated by the bubble varies with time. This is most conveniently computed in the way suggested by Willis[18]: if a value r_1 of r can be found which is small enough so that the relative change of pressure in time r_1/c is small, and which is at the same time large enough so that the linear approximation of acoustic theory is valid for $r \geqslant r_1$, then the acoustic impulse received at any large distance r should have an amplitude given approximately by

---

[18] See the article by Willis in this Volume.

$$p(r,t) - p_\infty = (r_1/r)\left[p(r_1, t-r/c) - p_\infty\right] \qquad (9)$$

The quantity in brackets can be computed by using non-compressive theory for the motion inside r_1. The well-known equation which relates pressure to velocity for irrotational motion of an incompressible fluid is

$$p - p_\infty = \rho \frac{\partial \phi}{\partial t} - \frac{\rho}{2} v^2 \qquad (10)$$

where ϕ is the velocity potential and $v = -\nabla\phi$ is the velocity. This expression should give a fairly reliable value for the pressure at all distances from the bubble. Inside r_1 we may substitute the non-compressive approximations to v and ϕ, viz.,

$$v = \frac{a^2}{r^2}\frac{da}{dt} \quad , \qquad \phi = \frac{a^2}{r}\frac{da}{dt} \quad ;$$

it is then easily shown(Appendix 6) that (10) reduces to

$$p - p_\infty = \frac{a}{r}\left[p(a) - p_\infty + \frac{\rho}{2}\left(\frac{da}{dt}\right)^2\left(1 - \frac{a^3}{r^3}\right)\right] \qquad (11)$$

The maximum of (11) will occur at the time when a is a minimum, if the gas behaves at all like a perfect gas. It is easy to see that the pressure given by (11) at the minimum of the first contraction, where a_{min} is of the order of twice the initial radius of the explosive, cannot be more than a fraction of the pressure produced at the same point when the original shock wave crosses it. By (9) this implies that the peak pressure in the bubble pulse is at most a fraction of that in the shock

wave; experiments give a ratio of about one fifth[19].

The situation is quite different, however, with regard to the impulse of pressure. Assume for simplicity that r is several times a_{max}; the second term on the right of (10) will then at all times be negligible compared with the first, and we have

$$\int_{t_1}^{t_2} (p - p_\infty)\, dt \approx \rho\phi\Big]_{t_1}^{t_2} = \frac{\rho}{r}\left[a^2 \frac{da}{dt}\right]_{t_1}^{t_2} \qquad (12)$$

This will be valid regardless of whether or not r is small enough for the non-compressive approximation to be valid at r at times near the minimum of the contraction; it is only necessary that the non-compressive approximation be valid at t_1 and t_2. Now $\left|a^2 da/dt\right|$ has its maximum value, as shown in Appendix 6, when $a = 2^{-2/3} a_{max}$, i.e., when the bubble is still fairly large. If we take t_1 and t_2 to be the times when a has this value in the contracting and expanding phases respectively, (12) will give the maximum impulse of pressure due to the non-compressive motion. Expressing $\frac{da}{dt}$ in terms of more convenient quantities, the maximum impulse (12) can be reduced to

$$\text{maximum impulse of pressure} = \frac{2^{1/6} a_{max}^2}{r}\sqrt{\rho\, p_\infty}$$

$$= \frac{0.34 T^2}{r}\, p_\infty^{3/2} \rho^{-1/2} \qquad (13)$$

This turns out to be of the order of six or eight times the impulse measured in the shock wave by the time the pressure

---

[19] A. B. Arons and D. R. Yennie, Rev. Mod. Phys. 20, 519 (1948), also Volume I, this Compendium.

has dropped to $1/e^2$ o
be expected to be 20%
of the second pulsat
prediction is in app

In 1941, wh
done, some of the e
from small explosi
some workers suggested that
of the gas in the bubble during
others regarded it as a spurious
tical analysis made at that time,
indicated that the former hypothe
subsequent experiments [19] have sho
symmetrical conditions the pressur e curve for the bubble pulse has a smooth bell-shaped form.

It must be emphasized that all the formulas of the present section and Appendices 2, 3, and 6 have been derived only for a pulsation in which the motion is spherically symmetrical, although generalization to other cases is not difficult. In most actual explosions gravity and proximity to surface, bottom, or objects will introduce asymmetrical influences. As will be shown in the next two sections, these influences have an effect on the motion, which, though it may be slight when the bubble is large, is greatly enhanced in the contracted stages. Taylor[20] and others have shown that these effects can greatly modify the acoustic pulse given out in the contracted stages. In certain cases, however, it is possible to balance the asymmetrical influence of surface and bottom against that of gravity, and in such cases the theories discussed in the present section should be applicable.

---

[20] See the article by Taylor in this Volume.

5. MIGRATION OF A SPHERICAL BUBBLE

The motion pictures from which Fig. 2 was constructed showed the migration effect mentioned in the introduction: the center of the gas bubble was observed to rise slightly up to the time of maximum size and later to sink rapidly, with periodic fluctuations, through a distance of several inches. Only after the pulsations had practically ceased did the bubble rise again. The explanation of this phenomenon, interestingly enough, appeared automatically as a by-product of an attempt to understand the deviations of the points of Figure 2 from the theoretical curve, in a way which will now be described.

It will be noticed that the theoretical curve is too broad, and that there seems to be a slight asymmetry in the experimental curve. Now the theory from which the curve was constructed has disregarded a number of factors, of which the most important are:

(i) The gas pressure (responsible for the term G in §)) has been disregarded.

(ii) The water has been assumed incompressible, so that the damping effect of acoustic radiation has been ignored.

(iii) The bubble has been assumed spherically symmetrical.

(iv) The explosion has been assumed to take place in an infinite body of water. In the photographs

represented in Fig. 2 the cap was only 12 inches from the surface, and was so close to a slanting steel plate beneath it that the bubble almost touched the plate at the time of its maximum size.

The correction to the simple theory necessitated by (i) is estimated in Appendix 1, and that necessitated by (ii) in Section 4 and Appendices 2 and 3. These quantitative calculations show that, as one would expect, the corrections from factors (i) and (ii) are negligible when a is near a_{max}, and tend anyway to broaden the curve in time, as compared with the simple theory. The correction from (iii) can hardly be appreciable in the neighborhood of the maximum radius, since the bubble is observed to be very nicely spherical at this stage. There remains the factor (iv). The effect on the motion of proximity to a free surface can easily be predicted qualitatively. The water between the bubble and the surface can be more easily given a radial acceleration when the surface is near than when it is distant. Consequently the stream lines tend to bend toward the surface, with the result that for a given a and $\frac{da}{dt}$, the kinetic energy of the water is less than the value (3) which applies in the absence of a free surface. The potential energy is of course the same function of a and γ_0 as in the absence of a surface. Thus the effect of the surface is like decreasing the inertia of a simple oscillator without changing the spring constant, and so it decreases the period. In Appendix 5 this effect is worked

out quantitatively by the method of images, and it is shown that when the center of the bubble is a distance h below the surface, the period $T(h)$ is related to the period $T(\infty)$ in the absence of a surface (but for the same p_∞) by

$$T(h) = T(\infty)\left(1 - \frac{\bar{a}}{4h}\right) + O\left(\frac{1}{h^2}\right) \qquad (14)$$

where $\bar{a}$ is the time average of a over a complete period. Near the maximum, the radius-time curve is contracted in the time direction by the factor $\left[1 - \frac{a_{max}}{4h} + O\left(\frac{1}{h^2}\right)\right]$ as compared with the curve for $h = \infty$.

The theory of Appendix 5 also predicts that when the explosion takes place at distance h from a plane rigid surface the period will be longer than in the absence of such a surface: quantitatively

$$T(h) = T(\infty)\left(1 + \frac{\bar{a}}{4h}\right) + O\left(\frac{1}{h^2}\right) \qquad (15)$$

The qualitative explanation follows the pattern outlined above for a free surface. The stream lines avoid the rigid surface, so that for given a, $\frac{da}{dt}$, the kinetic energy is greater than in the absence of the surface. Thus the effective inertia of the water is increased and the period lengthened. The formula (15) is

an asymptotic one which should be a good approximation when h is two or three times a_{max}. A clue as to how T varies for smaller values of h is provided by considering the case $h = 0$. The motion of the water for this case must be the same as the motion to one side of an imaginary plane drawn through the center of the bubble produced by the explosion in free water of double the charge used. Since T is proportional to the cube root of the charge,

$$T(0) = T(\infty) \sqrt[3]{2} \tag{16}$$

When free and rigid surfaces are simultaneously present in the neighborhood of the bubble, the effect on the period, though calculable, is not simply the sum of the effects due to the various surfaces separately. For example, it is shown in Appendix 5 that when the explosion takes place halfway between the surface and a horizontal rigid bottom, and at distance h from either, the effects of surface and bottom do not cancel each other; instead we have

$$T = T(\infty)\left(1 - \frac{\bar{a} \log 2}{4h}\right)$$

Similar calculations can be made when a free and a rigid surface intersect at an angle. In general, when both kinds of surface are present the effect of the free surface tends to predominate.

A quantitative check of this theory by means of the curvature of the a vs. t curve of Fig. 2 at its maximum seems out of the question, since the distances involved are not very accurately known, and since flow of water around the sides of the steel plate and even bending of the plate may have been quite appreciable. The factor $(1 - \frac{a_{max}}{4h})$, which would describe the narrowing of the curve near the maximum due to the surface effect in the absence of a steel plate, has the value 0.86. This figure is only slightly less than the ratio of the curvatures of the observed and theoretical curves in Fig. 2; apparently therefore the steel plate had a surprisingly slight effect, or else the measurements of radius were falsified by bending of the mirror with which the photographs were taken, or by distortion of the surface. A similar situation exists with regard to the period. The experimental errors just mentioned could not falsify the observed period, but they could affect the calculated period, which is proportional to a_{max}. The period calculated from (7) is $T_o(\infty) = .0297$ sec., assuming normal atmospheric pressure and fresh water ($\rho = 1.00$). If only the free surface were present, (14) would modify this to $T_o(h) = .026_8$. The observed period is $T = .028_0$, and the difference between this and $T_o(h)$ could be amply accounted for by the effect of gas pressure alone, without radiation damping or any effect of the steel plate.

The complete theory of the motion in the presence of a free or rigid surface, as worked out in Appendix 5, predicts that

the bubble, besides being sucked back and forth periodically by its image, should be continually repelled from a free surface and attracted to a rigid one. In the case of the bubble of Fig. 2, the repulsion from the free surface was actually great enough to make the bubble sink. As the mathematical details of the theory are rather involved, only a rather loose picture of the mechanisms involved will be given in the present section; moreover, it will be advantageous to discuss first the simpler theory of the migration due to gravity alone. This theory, which is worked out in detail in Appendix 4, can be described by saying that the bubble has associated with it a vertical momentum equal to its velocity of rise times $(2\pi/3)\rho a^3$, and that the time rate of change of this momentum equals the buoyant force $(4\pi/3)\rho a^3$. This gives

$$\text{velocity of rise due to gravity} = \frac{2g}{a^3}\int_0^t a^3\,dt \qquad (17)$$

Note that the velocity of rise becomes enormously accelerated during the contraction, when a becomes small while the integral remains large. Although Appendix 4 assumes gravity to be a small perturbation, so that its conclusions are rigorously valid only when the velocity of rise is small. Taylor[21] has shown that the effect of this rise on the motion can be calculated, to a fair approximation, by assuming that the bubble is constrained to remain spherical, so that (17) becomes valid at all times.

---

[21] See the article by Taylor in this Volume.

The migration due to a neighboring free or rigid surface can be explained with similar concepts. The image of the bubble in the surface affects conditions in the neighborhood of the real bubble in two ways: it gives to the water there a velocity normal to the surface, and it creates a pressure gradient in this direction. As is shown at the close of Appendix 5, the migration can be calculated, correctly to the second order in $1/h$, by a simple momentum argument. To begin with, the pressure gradient due to the image will impel the bubble in the direction of lower pressure, just as the buoyancy of the bubble does when the pressure gradient is due to gravity. The normal momentum due to this effect can therefore be obtained by integrating the product of the image pressure gradient by the volume of the bubble, and the corresponding normal velocity can be computed. The sum of this velocity and the velocity field of the image, evaluated at the position of the center of the bubble, turns out to give the correct value of the velocity of migration normal to the surface, to order $1/h^2$, as determined by the more rigorous calculation given earlier in Appendix 5. This velocity is

$$\frac{dh}{dt} = -\frac{3a^2}{4h^2}\frac{da}{dt} + \frac{3}{2h^2a^3}\int_o^t a^4 \left(\frac{da}{dt}\right)^2 dt \qquad (18)$$

for a bubble at a distance h from a free surface; if the free surface is replaced by a rigid one, the sign of dh/dt is reversed.

It will be noticed that (18) consists of a periodic term and a monotonic one, the latter corresponding to repulsion from a free surface and attraction to a rigid one. This can be understood qualitatively from the fact that the pressure gradient due to the image is most effective, in imparting normal momentum to the bubble, when the bubble is large. At this time the image pressure gradient is toward a free surface or away from a rigid surface. The predominant motion is in the direction opposite to this pressure gradient. Just as in the case of the rise due to gravity, the velocity of migration due to the surface contains a term proportional to the reciprocal of the volume of the bubble, which becomes extremely large in the contracted stages.

In making comparisons of theoretical and observed migration rates, one must usually deal with cases where both gravity and boundary surfaces are present. To the order of approximation used in Appendices 4 and 5, the velocities (17) and (18) can merely be added in such cases. The relative importance of the migration effects (17) and (18) as compared with the rest of the motion can be measured by a ratio such as $(dh/dt)/(da/dt)$. For (18) this ratio at any stage is essentially a function of h/a_{max}, and is practically independent of p_∞ or the size of the explosion. For (17), however, the corresponding ratio is proportional to $\rho g a_{max}/p_\infty$, so that the gravity rise is more important the larger the explosion or the smaller p_∞.

For the experiments of Ramsauer mentioned in the introduction and described in Appendix 8, the combined effects of

surface and bottom would never be more than a fraction of (17). If we set $t = \frac{1}{2} T$ in (17) and use the simple theory of Appendix 1 for the variation of a with t, the right of (13) becomes

$$(\text{velocity of rise at } a = a_{max}) = 0.62\ gT$$

We may, therefore, expect the distance risen by this time to be very roughly $0.15\ gT^2 = 0.5\ \frac{\rho g a_{max}^2}{p_\infty}$; if we set $a_{max} =$ 150 cm. corresponding to a typical one of Ramsauer's measurements, we find the distance risen to be only a little under the figure 10% of a_{max} which he reported. By way of contrast, the distance which the Edgerton bubble would have risen by the time of the first maximum, due to gravity alone, is only a little over a millimeter, or less than 1% of a_{max}.

The slight asymmetry of the experimental points in Fig. 2 about the maximum is hard to account for theoretically. It is shown in Appendix 2 that the chief effect of the finite compressibility of the water is to produce a radiation of energy, and in Appendix 3 that only a negligible radiation of energy occurs during the time when a is greater than say $a_{max/3}$. The calculations of Appendices 4 and 5 show that, to the first approximation, neither gravity nor proximity to the surface can produce an asymmetry. Moreover, the surface waves produced by the expansion of the bubble could not travel an appreciable distance before the contraction sets in. A retardation of the

contraction could of course be produced by the gradual burning of some constituent of the cap which did not explode, but an improbably large amount of such material would be required to produce an appreciable effect while the bubble is large. During the later stages of the contraction the measurements of the radius may have been systematically too large, since the bubble grew an opaque "beard". Near the maximum, however, the only explanation of the asymmetry would seem to be the distortion of the pictures by disturbance of the water surface or bending of the mirror, as already mentioned.

6. DEPARTURES FROM SPHERICAL SHAPE

In the analysis of Appendices 4 and 5, which has just been discussed, the effects of gravity and of nearby surfaces are treated as small perturbations on the motion. As is shown in these appendices, the perturbed motion is in first approximation merely a superposition of radial and translatory motions, without any change in the spherical shape of the bubble. Moreover, Taylor[22] has shown that the observed motion of bubbles can be approximately calculated, even when the migration is large, by a theory in which the bubble is constrained to be spherical at all times. However, it is clear that in higher approximations departures from sphericity will occur, and photographs taken during the later war years[23] do in fact show that in the contracted stages the bubble becomes flattened in a plane, normal to its direction of migration, and sometimes develops a mushroom-like shape. As this flattening has a significant effect on the rate of migration and on the intensity of the pressure pulse, some theoretical study has been devoted to it[24]. The present section

---

[22] See the article by Taylor in this volume.

[23] See the article "Motion and Shape of the Hollow Produced by an Explosion in Liquid" by Taylor and Davies in this volume.

[24] See for example the article of Penney and Price in this volume.

will be devoted to some qualitative comments on the physical causes of this flattening and of finer-scale departures from sphericity.

An easy way to see why a rapidly moving bubble must become flattened is to consider the non-uniformity in the distribution of pressure over the surface of a bubble which is constrained to remain spherical. In Taylor's approximation, where the bubble, though constrained to be spherical, is free to expand or contract and to move up and down, it is clear that the average pressure over the surface of the bubble will equal the gas pressure and that the first moment of the pressure will be zero. It is not hard to show further that the second moment of the pressure, i.e., the coefficient of the second order spherical harmonic in the expansion of the pressure at the surface of the bubble, must in this approximation be the same as for a uniformly moving rigid sphere whose size and translational velocity are the same as the instantaneous values for the bubble. This can be verified from Taylor's explicit expression for the pressure[25], in which the only terms in $\cos^2 \theta$ or $\sin^2 \theta$ are simply proportional to the square of the velocity of migration, independent of radial velocity and acceleration. Now it is well known that in the steady motion of a rigid sphere through an incompressible frictionless fluid the pressure is higher at the front and rear stagnation points than

---

[25]See the article by Taylor in this volume.

at the sides where the fluid moves tangentially to the sphere. It is therefore to be expected that an explosion bubble will flatten if Taylor's constraint of sphericity is replaced by the boundary condition that the pressure be constant over the boundary.

Small-scale distortions of the surface of the bubble tend to become greatly exaggerated during the contracted stages. This is illustrated by the fact that near the minimum radius bubbles usually present a decidedly prickly appearance. The phenomenon can be understood mathematically in terms of the treatment given by Penney and Price[26] for the motion of a bubble departing slightly from spherical shape. Qualitatively, the cause seems to be that illustrated in Fig. 3. Here the top curve may be taken to represent a small portion of the surface of the bubble, as distorted by some accidental ripples. This surface is of course a contour of constant pressure. As we go away from the surface into the water (down in the figure) the contours of constant pressure must become smoother, as shown. This means that the pressure gradient must be numerically greater at the "troughs" of the ripples in the figure than at the crests. If the pressure is higher in the bubble than a short distance outside it, as is the case in the contracted stages, the troughs will be accelerated downward much more than the crests, and the amplitude of the riples will increase. If on the other hand the pressure gradient is in the opposite direction, as it is when the bubble is large, the troughs will be accelerated upward relatively to the crests, and the ripples will be leveled out.

---

[26] See the article by Penney and Price in this volume.

7. THE ENERGY BALANCE

It has already been mentioned in Section 4 above that the energy lost between successive pulsations seems to be considerably greater than the acoustic energy radiated. This is illustrated in Fig. 4, which shows, on a smaller scale, the successive pulsations of the same bubble as Fig. 2 . The energies of the first two pulsations are roughly proportional to the cubes of the maximum radii, hence are in about the ratio 1:0.31 . As a check, the kinetic energies shortly before and shortly after the first minimum appear to be in about the same ratio. Although no acoustic measurements of the bubble pulse were made for this explosion, it seems quite certain from other cases in which such measurements have been taken[27] that nowhere near 70% of the energy of the first oscillation could have been radiated acoustically. Several processes may be considered in an effort to find a cause for this additional dissipation:

(1) Turbulence. It has been noticed that for some cases, where the bubble is migrating rapidly the non-acoustic dissipation of energy is of the same order of magnitude as that which would be expected for the dissipation in the turbulent wake of a uniformly moving solid sphere of the same size and velocity as the bubble at its minimum, in a time of the same order as the duration of the contracted stage. Since the Reynolds number for such cases may be of the order

---

[27] See for example A. B. Arons and D. R. Yennie, Rev. Mod. Phys. 20, 519 (1948), also Volume I of this Compendium.

of 10^7, it is certainly worth while to examine seriously the possibility of turbulent dissipation. However, there are two considerations which make it seem unlikely that this is the principal cause of the energy loss. In the first place, there is to the author's knowledge no evidence that the disappearance of energy is significantly less serious for bubbles which do not migrate than for bubbles which migrate rapidly; since one expects turbulence to be much less serious for a stationary bubble, a large energy disappearance for such cases would probably have to be attributed to other mechanisms. In the second place, it is questionable whether turbulence could develop quickly enough to produce a steady-state rate of dissipation in the very short time covered by the contracted stage. For there are no solid boundaries to help start the turbulence, and a calculation of the stresses due to viscosity in the velocity field of Taylor's theory shows these stresses to be negligible in comparison with the hydrostatic pressure.

(ii) Cavitation. It is just possible that the pressure a short distance above a rising bubble may be low enough to produce a cavitation. However, even if this should occur for a rising bubble it would not explain the energy loss of a stationary bubble.

(iii) Transfer of heat from the compressed gas to the water. Loss of energy through thermal conduction can easily be shown to be negligible if the motion of the gas in the bubble is non-turbulent. If an appreciable portion of the energy of the gas is to be lost by conduction, the drop in temperature between center and boundary of the bubble must be distributed over an appreciable fraction of the radius a. In such a case the

flow of heat outward in one period has the order of magnitude

$$4\pi \int_0^T a^2 . \frac{K \Delta\theta}{a} dt \qquad (19)$$

where K is the thermal conductivity of the gas and $\Delta\theta$ the difference in temperature between the center of the bubble and the water at the boundary. The ratio of (19) to Q or W becomes smaller the larger the explosion. However, it is easily verified that (19) is entirely negligible as compared with the total energy Q or W, even for the smallest explosions. It seems unlikely that there can be any appreciable departure from adiabatic conditions, even when convection inside the bubble is taken into account.

(iv) A lag in the achievement of thermal equilibrium in the gas as it is compressed. If such a lag is present the work done by the water in compressing the gas will be greater than the work given up by the gas in re-expanding, and the difference will be manifested as an irreversible heating of the gas. It is not unlikely that such an effect exists , especially since soot particles and possibly water droplets may be present in the gas. However, if this is the predominant cause of the energy loss, the unbalance in the energy equation ought to depend strongly on the scale of the explosion. For the dissipation due to the lag in equilibrium should become very small when the duration of the contracted stage becomes either very short or very long compared with the time required to establish thermal equilibrium in the gas. To the best of the author's knowledge, no such dependence on scale has been noticed; however, there is not a very wide range of charge sizes for which accurate .

measurements of bubble sizes and acoustic pressures have been made.

APPENDIX 1. PULSATIONS OF A BUBBLE IN AN INCOMPRESSIBLE FLUID

We have to integrate the energy equation (5) of Section 3. This equation is

$$2\pi\rho a^3\left(\frac{da}{dt}\right)^2 + \frac{4\pi a^3}{3} p_\infty + G(a) = W \qquad (1)$$

Consider first the case where the potential energy G of the gas is neglected. Solving (1) for dt and integrating we have for the expanding phase

$$t_m - t = \int_a^{a_{max}} \frac{a^{3/2}\, da}{\sqrt{\frac{W}{2\pi\rho} - \frac{2}{3}\frac{p_\infty}{\rho} a^3}} \qquad (2)$$

where t_m is the time of maximum size. (It is convenient to choose the maximum as origin because the approximations of this simplified theory are most nearly fulfilled near the maximum.) Putting

$$y = \frac{a}{a_{max}} = a\sqrt[3]{\frac{4\pi}{3}\frac{p_\infty}{W}} \qquad (3)$$

we have from (2)

$$t_m - t = 3^{5/6} 2^{-7/6} \pi^{-1/3} \rho^{1/2} p_\infty^{-5/6} W^{1/3} \int_y^1 \frac{y^{3/2}\, dy}{\sqrt{1 - y^3}} \qquad (4)$$

The most convenient way to evaluate the integral for values of the lower limit different from zero is to transform it into an incomplete beta function. If we set

$$z = \tfrac{1}{2} - \tfrac{1}{2}\sqrt{1 - y^3} \qquad (5)$$

we have $y^3 = 4z(1-z)$

$$dz = \frac{3}{4}\frac{y^2\, dy}{\sqrt{1 - y^3}} \qquad \text{so that}$$

$$\int_y^1 \frac{y^{3/2}\,dy}{\sqrt{1-y^3}} = \frac{2}{3}\int_z^{\frac{1}{2}} z^{-1/6}(1-z)^{-1/6}\,dz$$

$$= \frac{2}{3}\left[B_{\frac{1}{2}}\left(\frac{5}{6},\frac{5}{6}\right) - B_z\left(\frac{5}{6},\frac{5}{6}\right)\right] \qquad (6)$$

where $B_x(m,n) = \int_0^x x^{m-1}(1-x)^{n-1}\,dx$ is the incomplete beta function. Now in the range from 0 to 1/2 the factor $(1-z)^{-1/6}$ varies quite slowly, and it can be quite satisfactorily approximated over the range of integration by a parabola. By this means the curve shown in Fig. 2 was constructed. The radius-time curve is thus

$$t_m - t = \sqrt{\frac{8}{3\pi^2}}\,\rho^{1/2}p_\infty^{-5/6}\,W^{1/3}\left[B_{\frac{1}{2}} - B_z\right] \qquad (7)$$

where z is given by (5) and (3) and B_z is to be read from Fig. 5 .

The period is obtained in the present approximation by setting z = 0 in (7) and multiplying by two. We have

$$2B_{\frac{1}{2}}\left(\frac{5}{6},\frac{5}{6}\right) = B_1\left(\frac{5}{6},\frac{5}{6}\right) = \frac{\left[\Gamma\left(\frac{5}{6}\right)\right]^2}{\Gamma\left(\frac{5}{3}\right)},$$

so the period is

$$T_0 = 1.135\,\rho^{1/2}p_\infty^{-5/6}\,W^{1/3} \qquad (8)$$

Let us now consider the other extreme, that of small oscillations about the equilibrium radius a_1 . If the pressure-volume relation for the gas is

$$pa^{3\gamma} = p_\infty a_1^{3\gamma} \qquad (9)$$

Where γ is the ratio of the specific heats, we may set

$$G = \int_V^\infty p \, dV = \frac{pV}{\gamma - 1} = \frac{4\pi}{3(\gamma-1)} p_\infty \left(\frac{a_1}{a}\right)^{3\gamma} a^3 \qquad (10)$$

If we set $x = a^{5/2}$, the kinetic energy term of (1) is

$$\frac{8\pi\rho}{25}\left(\frac{dx}{dt}\right)^2 \qquad (11)$$

If we expand the potential energy terms in powers of $(x - x_1)$, where $x_1 = a_1^{5/2}$, we find

$$\text{Potential energy} = \text{constant} + \frac{24}{25}\pi\gamma p_\infty x_1^{-4/5}(x-x_1)^2 + \cdots \qquad (12)$$

From (11) and (12) the limiting period for small oscillations comes out as

$$T_s = 2\pi\sqrt{\frac{8\pi\rho/25}{24\pi\gamma p_\infty x^{-4/5}/25}} = \frac{2\pi}{\sqrt{3\gamma}} \rho^{1/2} p_\infty^{-1/2} a_1 \qquad (13)$$

No detailed calculation of the period for intermediate cases will be attempted here. The order of magnitude of the deviation from (8) caused by gas pressure can, however, be estimated as follows. Since in (13) the radius a_1 is the mean of the maximum and minimum radii for the small oscillations, it is tempting to rewrite (8) in terms of the mean of the two radii a_{max} and 0. If this is done by putting

$$a_{mean} = \frac{1}{2} a_{max}, \quad \frac{4}{3}\pi a_{max}^3 p_\infty = W,$$

and if in (13) we take $\gamma = 1.4$ to get a numerical value, we find from (8) and (13) respectively

$$T_o = 1.829\,\rho^{1/2} p_\infty^{-1/2} a_{max} \qquad (14)$$

$$= 3.66\,\rho^{1/2} p_\infty^{-1/2} a_{mean} \qquad (14a)$$

$$T_s = 3.07\,\rho^{1/2} p_\infty^{-1/2} a, \qquad (15)$$

Thus, the coefficient of the mean radius in the expression for the period varies only slightly from infinitely large to infinitely small amplitudes. A numerical calculation made by Professor Kennard gives the result that for $\gamma = 1.4$, $a_{max} = 5.9\, a_{min} = 2.07\, a$, ,

$$T = 3.30\,\rho^{1/2} p_\infty^{-1/2} a_{mean} = 1.93\,\rho^{1/2} p_\infty^{-1/2} a_{max}$$

Thus, for large amplitudes (14) gives a better approximation to T than (14a), while for small amplitudes the reverse is the case.

A calculation of the form of the a vs. t curve taking account of gas pressure could be made as follows. For small a and reasonably large amplitudes, the second term of (1) could be neglected or treated as a small correction; the integral for t could then be reduced to an incomplete beta function with indices involving γ. For large values of a, the term G(a) could be regarded as a small correction, and another tractable integral obtained. It is hardly worth while to carry out the calculations for small a, however, since when the amplitude of motion is large the a vs. t curve in this region will be influenced by dissipation (see Sections 4 and 7). The calculations for large a will be briefly sketched here, in order to show that the effect of gas pressure on the outer parts of the

motion is slight. The correct refinement of (2) is

$$t_m - t = \int_a^{a_{max}} \frac{a^{3/2}\, da}{\sqrt{\frac{W}{2\pi\rho} - \frac{G}{2\pi\rho}(a_{max}) - \frac{2}{3}\frac{p_\infty}{\rho}a^3 - \frac{G(a)}{2\pi\rho} + \frac{G(a_{max})}{2\pi\rho}}} \qquad (16)$$

We may treat the last two terms under the radical as small compared with the remaining ones and so replace the integrand by the first two terms of its expansion in powers of these. Setting $W - G(a_{max}) = \frac{4\pi}{3} p_\infty a_{max}^3$ we have, on making the same substitutions as before,

$$t_m - t = a_{max}\sqrt{\frac{3\rho}{2p_\infty}}\left[\int_y^1 \frac{y^{3/2}\, dy}{\sqrt{1-y^3}} + \frac{y_1^{3\gamma}}{2(\gamma-1)}\int_y^1 \frac{y^{3/2}}{\sqrt{1-y^3}}\left(\frac{y^{3-3\gamma}-1}{1-y^3}\right) dy\right] \qquad (17)$$

where $y_1 = a_1/a_{max}$. The first term in the brackets would give the motion as previously calculated. The second can be evaluated with sufficient accuracy for values of y near 1 by setting

$$\frac{y^{3-3\gamma}-1}{1-y^3} = (\gamma-1) + \frac{\gamma(\gamma-1)}{2}(1-y^3)^2 \ldots.$$

and then introducing the variable z defined by (5). The details will be omitted here, since we shall only need the order of magnitude of the ratio of the second term of (17) to the first when y is near 1. This ratio is asymptotically $y_1^{3\gamma}/2$, which is small for the value of y_1 (~ 0.4) which characterizes the first pulsation.

It should be remembered that $\frac{da}{dt}$ becomes large almost instantaneously after the detonation, so that the influence of gas pressure does not increase the time taken by the first expansion in the way that it increases the time of the ensuing contraction.

APPENDIX 2 PULSATIONS OF A BUBBLE IN A FLUID OF FINITE COMPRESSIBILITY

In this discussion we shall start from the equation of motion of a viscous fluid, although it will turn out that the effect of viscosity on the pulsation of a spherically symmetrical bubble is negligible. The Stokes-Navier equation is

$$\frac{\partial \vec{v}}{\partial t} + \vec{v} \cdot \nabla \vec{v} - \frac{\eta}{3\rho} \nabla \nabla \cdot \vec{v} - \frac{\eta}{\rho} \nabla^2 \vec{v} = - \frac{\nabla p}{\rho} \qquad (1)$$

where the symbols have the meanings explained on the notation sheet. For spherically symmetrical motion we have for the radial components of the various terms

$$\vec{v} \cdot \nabla \vec{v} \quad : \quad \frac{\partial}{\partial r} \left(\tfrac{1}{2} v^2 \right)$$

$$\nabla \nabla \cdot \vec{v} \quad : \quad \frac{\partial}{\partial r} \left[\frac{1}{r^2} \frac{\partial}{\partial r} \left(r^2 v \right) \right]$$

$$\nabla^2 \vec{v} \quad : \quad \frac{\partial^2 v}{\partial r^2} + \frac{2}{r} \frac{\partial v}{\partial r} - \frac{2v}{r^2}$$

and so (1) becomes

$$\frac{\partial v}{\partial t} + \frac{\partial}{\partial r} \left(\tfrac{1}{2} v^2 \right) - \frac{4\eta}{3\rho} \frac{\partial}{\partial r} \left(\frac{\partial v}{\partial r} + \frac{2v}{r} \right) = - \frac{1}{\rho} \frac{\partial p}{\partial r} \qquad (2)$$

Let us integrate this equation on r, at a given instant of time, from the surface of the bubble to infinity. The order of magnitude of the effect of the viscosity term is not likely to be much influenced by assuming that $\frac{\eta}{\rho}$ is constant for all stages of compression; this simplifying assumption will therefore be made, since this term will

turn out to be negligible anyway. It will be convenient to separate the integrated equation into terms characteristic of incompressible motion and terms involving $\nabla\cdot\vec{v} = \frac{1}{r^2}\frac{\partial}{\partial r}(r^2 v) = \sigma$, say. Accordingly, we note that

$$\int_a^\infty \frac{\partial v}{\partial t}\,dr = \int_a^\infty \frac{\partial}{\partial t}(r^2 v)\,d(-1/r) = r\frac{\partial v}{\partial t}\Big]_\infty^a + \int_a^\infty r\frac{\partial \sigma}{\partial t}\,dr$$

$$\frac{d^2 a}{dt^2} = \left[\frac{\partial v}{\partial t} + v\frac{\partial v}{\partial r}\right]_{r=a}$$

The integrated equation (2) now becomes

$$a\frac{d^2 a}{dt^2} - a\frac{da}{dt}\cdot\left(\frac{\partial v}{\partial r}\right)_{r=a} + \int_a^\infty r\frac{\partial \sigma}{\partial t}\,dr - \frac{1}{2}\left(\frac{da}{dt}\right)^2$$

$$+ \frac{4\eta}{3\rho}\left(\frac{\partial v}{\partial r} + \frac{2v}{r}\right)_{r=a} = -\int_{r=a}^{r=\infty}\frac{dp}{\rho},$$

or finally,

$$a\frac{d^2 a}{dt^2} + \frac{3}{2}\left(\frac{da}{dt}\right)^2 - a\frac{da}{dt}\sigma(a) + \int_a^\infty r\frac{\partial \sigma}{\partial t}\,dr + \frac{4\eta}{3\rho}\sigma(a)$$

$$= -\int_{r=a}^{r=\infty}\frac{dp}{\rho} \qquad (3)$$

This equation should be valid even for rather early stages of the motion, when the shock wave front has advanced only a few times the initial bubble radius. This is because the starting equation (1) is valid right through the shock

wave front. In the interpretation of the right side of (3) we should remember that, strictly speaking, p is not quite the same function of ρ in the shock wave front that it is elsewhere, because heat is being generated in this region by irreversible processes. In practice we may ignore this complication, however, as the extra pressure due to this heating is negligible. If this is done, the right side of (3) will be a known function of the pressure at $r = a$. Moreover, we have

$$\sigma(a) = -\left.\frac{d \log \rho}{dt}\right]_{r=a} = -\left.\frac{1}{c^2 \rho}\frac{dp}{dt}\right]_{r=a} \qquad (4)$$

where $c = \left(\frac{dp}{d\rho}\right)^{\frac{1}{2}}$ is the velocity of sound in water. Thus, if we assume that the pressure is uniform throughout the bubble, so that p(a) is a known function corresponding to an adiabatic law, (3) will become an ordinary differential equation for a(t), except for the term $\int_a^\infty r \frac{\partial \sigma}{\partial t}\, dr$. We shall now try to transform this term.

An inspection of (3) shows that the only terms which can be responsible for a dissipation of energy are the last two on the left, since all the others are unchanged when the sign of $\frac{da}{dt}$ is changed. The first of these must account for the energy radiated away in the form of sound. A hint on how to evaluate this term is provided by considering the special case in which the amplitude of the motion is small enough so that the ordinary acoustical theory can be used. In such a case σ will obey the wave equation and, since only outgoing

waves satisfy our boundary conditions, we may write

$$r\sigma(r,t) = f(t - \frac{r}{c}) , \tag{5}$$

where c is the velocity of sound in water. We then have

$$\int_a^\infty r \frac{\partial \sigma}{\partial t} dr = -c \int_a^\infty \frac{\partial (r\sigma)}{\partial r} dr = ca\sigma(a) \tag{6}$$

For the large amplitudes with which we are chiefly concerned the acoustical theory on which (5) is based is of course invalid. It will be shown below, however, that for large amplitudes of motion the integral on the left of (6) can be represented by the same term, $ca\sigma(a)$, plus other terms of lesser importance.

Let us start by taking the divergence of the Euler equation (i.e., of equation (1) without the viscosity terms) and then differentiate with respect to time. The result is

$$\frac{\partial^2 \sigma}{\partial t^2} + \frac{1}{2}\nabla^2 \frac{\partial (v^2)}{\partial t} = -\nabla^2\left(\frac{1}{\rho}\frac{\partial p}{\partial t}\right) \tag{7}$$

Now $$\frac{\partial p}{\partial t} = \frac{dp}{d\rho}\frac{\partial \rho}{\partial t} = c^2\left[-\rho\sigma - \vec{v}\cdot\nabla\rho\right]$$

For simplicity it will be assumed that c is not appreciably changed under the compressions to be encountered, so that it can be treated as a constant in the differentiation. This approximation is only bad at the start of the first pulse, a stage which we have already excluded from the present treatment because at this stage the pressure cannot be assumed constant throughout the gas bubble. For constant

c, (7) becomes

$$\frac{\partial^2\sigma}{\partial t^2} - c^2\nabla^2\sigma = \nabla^2\left[c^2\vec{v}\cdot\nabla\log\rho - \vec{v}\cdot\frac{\partial\vec{v}}{\partial t}\right] \qquad (8)$$

i.e., in the present case of spherical symmetry

$$\frac{\partial^2(r\sigma)}{\partial t} - c^2\frac{\partial^2(r\sigma)}{\partial r^2} = F(r,t)\ , \text{ say.} \qquad (9)$$

Let us multiply the equation (9) by an arbitrary function $\delta\left[t+\frac{(r-r_1)}{c}\right]$ and integrate on t from $-\infty$ to 0 and on r from r_0 to ∞, where $r_0 < r_1$. (The function δ will play the role of the "Dirac delta function" used in quantum mechanics.)

On integrating by parts and taking σ and F as vanishing at $t = -\infty$ or at $r = \infty$, we obtain

$$\int_{r_0}^{\infty}\int_{-\infty}^{0} r\sigma\left(\frac{\partial^2\delta}{\partial t^2} - c^2\frac{\partial^2\delta}{\partial r^2}\right)dtdr + \int_{r_0}^{\infty}\left[\frac{\partial(r\sigma)}{\partial t}\delta\right]_{t=0}dr - \int_{r_0}^{\infty}\left[r\sigma\frac{\partial\delta}{\partial t}\right]_{t=0}dr$$

$$+\int_{-\infty}^{0} c^2\left[\frac{\partial(r\sigma)}{\partial r}\delta\right]_{r=r_0}dt - \int_{-\infty}^{0} c^2\left[r\sigma\frac{\partial\delta}{\partial r}\right]_{r=r_0}dt = \int_{r_0}^{\infty}\int_{-\infty}^{0} F\delta\,dtdr \qquad (10)$$

But $\frac{\partial^2\delta}{\partial t^2} - c^2\frac{\partial^2\delta}{\partial r^2} = 0$, and

in the third integral on the left we can use $\frac{\partial\delta}{\partial t} = c\frac{\partial\delta}{\partial r}$,

so that (10) becomes

$$\int_{r_0}^{\infty}\left[\frac{\partial(r\sigma)}{\partial t} + \frac{c\,\partial(r\sigma)}{\partial r}\right]_{t=0}\delta\left(\frac{r-r_1}{c}\right)dr + cr_0\sigma(r_0,0)\,\delta\left(\frac{r_0-r_1}{c}\right)$$

$$+\int_{-\infty}^{0} c^2\left[\frac{\partial(r\sigma)}{\partial r}\delta - r\sigma\frac{\partial\delta}{\partial r}\right]_{r=r_0}dt = \int_{r_0}^{\infty}\int_{-\infty}^{0} F\delta\,dtdr \qquad (11)$$

Now let us specify that $\delta(x)$ be different from zero only in a very narrow range about $x = 0$, and that $\int_{-\infty}^{\infty}\delta(x)dx = 1$. As we make $\delta(x)$ narrower and narrower the last two terms on the left of (11) will eventually vanish, while the rest of the equation approaches

$$c\left[\frac{\partial(r\sigma)}{\partial t} + c\,\frac{\partial(r\sigma)}{\partial r}\right]_{\substack{t=0\\ r=r_1}} = c\int_{-\infty}^{0} F\,(r_1 - ct, t)dt \qquad (12)$$

Integrating (12) on r_1 gives now, for $t = 0$

$$\int_a^{\infty}\frac{\partial(r_1\sigma)}{\partial t}\,dr_1 = ca\sigma(a) + \int_a^{\infty}\int_{-\infty}^{0} F\,(r_1 - ct, t)\,dt dr_1 \qquad (13)$$

The double integral on the right represents the correction to (6) necessitated by the fact that the amplitude of motion is large. It can be approximately evaluated by inserting for F a function obtained from the non-compressive approximation. We have from (8) and (9)

$$F = r\nabla^2\Phi = \frac{\partial^2(r\Phi)}{\partial r^2} \qquad (14)$$

where

$$\Phi = \vec{v}\cdot\left[c^2\nabla\log\rho - \frac{\partial\vec{v}}{\partial t}\right]$$

Now

$$c^2\nabla\log\rho = \frac{c^2}{\rho}\frac{d\rho}{dp}\nabla p = \frac{1}{\rho}\nabla p$$

$$= -\frac{\partial\vec{v}}{\partial t} - \vec{v}\cdot\nabla\vec{v}$$

so we have

$$\Phi = -2v\frac{\partial v}{\partial t} - v^2\frac{\partial v}{\partial r} \qquad (15)$$

Since v in the non-compressive approximation varies inversely as r^2, Φ will die off very rapidly as we go away from the bubble, and the chief contribution to the double integral in (13) will come from values of $(r_1 - ct)$ very close to a. Therefore, there can hardly be a very large error introduced by using the non-compressive approximation to v in the evaluation of this integral. Also, we may note that if $\frac{da}{dt} \ll c$, most of the variation in F during the integration on t is due to the change in the argument $(r_1 - ct)$, and very little to the change in the argument t. Thus, we may set

$$F(r_1 - ct, t) \approx F(r_1 - ct, 0) + t\,\dot{F}(r_1 - ct, 0) \qquad (16)$$

and gauge the adequacy of the approximation by the smallness of the effect of the second term. We have

$$\int_a^\infty \int_{-\infty}^{\infty} F(r_1 - ct, t)\,dt\,dr_1 \approx \int_a^\infty \int_{r_1}^{\infty} F(r,0)\,\frac{dr}{c}\,dr_1 + \int_a^\infty \int_{r_1}^{\infty} \left(\frac{r_1 - r}{c}\right) \dot{F}(r,0)\,\frac{dr}{c}\,dr_1$$

$$= \frac{1}{c}\int_a^\infty (r-a)\,F(r,0)\,dr - \frac{1}{2c^2}\int_a^\infty (r-a)^2\,\dot{F}(r,0)\,dr \qquad (17)$$

Using (14) the first of these integrals becomes just $\frac{a}{c}\Phi(a,0)$. The second can be evaluated using (14) and (15) with the non-compressive approximation to v. The details of this will not be given here and we shall merely state the result. It is that the effect on the motion of the second term of (17) is rather less than that of the first during the first contraction of the bubble. Both terms are largest for the stages near that of minimum radius, although the

first vanishes at this radius. The effect of the second term may be larger than that of the first just after the explosion takes place, but the present analysis is prevented by other reasons from applying to these stages. The larger the radius of the bubble, the smaller the effect of the second term compared with the first: a numerical calculation gives a value of about .05 for the ratio of the second term to the first when $\frac{a}{a_{max}} = \frac{1}{3}$. Since the first term itself is not very important, we shall drop the second term and write (17) as

$$\int_a \int_{-\infty}^{\infty} \frac{F(r_1 - ct, t)}{r_1} \, dt \, dr_1 \approx \frac{a}{c} \Phi(a,0)$$

$$= \frac{a}{c}\left\{ -\frac{1}{a^4}\frac{d}{dt}\left[a^4\left(\frac{da}{dt}\right)^2\right] + \frac{2}{a}\left(\frac{da}{dt}\right)^3 \right\} = -\frac{1}{ca}\frac{d}{dt}\left[a^2\left(\frac{da}{dt}\right)^2\right] \qquad (18)$$

We are now ready to solve (3) by using (18), (13), and (4). The last term on the left of (3) can now be seen to be entirely negligible, since the principal part of the correction to the non-compressive approximation is the term $ca\sigma(a)$ in (13): we have in fact, in c.g.s. units, $\frac{4\eta}{3\rho} \sim 10^{-2}$ while $ca \sim 10^{5}$ to 10^{7}. We thus write (3)

$$a\frac{d^2a}{dt^2} + \frac{3}{2}\left(\frac{da}{dt}\right)^2 - \frac{1}{ca}\frac{d}{dt}\left[a^2\left(\frac{da}{dt}\right)^2\right] = -\int_{r=a}^{r=\infty} \frac{dp}{\rho} + \frac{a}{\rho c}\frac{dp(a)}{dt}\left(1 - \frac{\frac{da}{dt}}{c}\right) \qquad (19)$$

Now the left side of (19) is

$$\frac{1}{2a^2}\frac{d}{da}\left[a^3\left(\frac{da}{dt}\right)^2 - \frac{4}{3}\frac{a^3}{c}\left(\frac{da}{dt}\right)^3\right]$$

while on the right we have

$$\int_{r=a}^{r=\infty} \frac{dp}{\rho} = \frac{p(a) - p_\infty}{\rho_\infty} - \frac{[p(a) - p_\infty]^2}{2 c^2 \rho_\infty} + \ldots .$$

where ρ_∞ is the density at infinity. The second term is negligible for all stages of the motion except those immediately following the explosion, so we may write (19) in integrated form as

$$a^3 \left(\frac{da}{dt}\right)^2 \left(1 - \frac{4}{3}\frac{\frac{da}{dt}}{c}\right) = \int_{a_{max}}^{a} \left[\frac{p(a) - p_\infty}{\rho_\infty} + \frac{a}{\rho c}\frac{dp(a)}{dt}\left(1 - \frac{\frac{da}{dt}}{c}\right)\right] \cdot 2a^2\, da \quad (20)$$

The equation (20) is the extension of the energy equation (5) of Section 3, to which it reduces as $c \to \infty$.

The factor $\left(1 - \frac{4}{3}\frac{\frac{da}{dt}}{c}\right)$ on the left of (20) has merely the effect of making the curve of a against t asymmetrical (i.e., of making the contraction slower than the expansion), without however producing any dissipation of energy. Since $\frac{da}{dt} \ll c$ for all those stages of the motion which we are considering here, this factor is rather unimportant. The dissipation of energy arises from the term in $\frac{dp}{dt}$ on the right. For we have

$$\int_{a_{max}}^{a} \frac{2a^3}{\rho c}\frac{dp(a)}{dt}\, da = \frac{2}{\rho c}\int_{a=a_{max}}^{a=a} a^3 \left(\frac{da}{dt}\right)^2 \frac{dp(a)}{da}\, dt \quad (21)$$

Since $\frac{dp}{da} < 0$, this term is negative and becomes ever greater in magnitude in the course of time. The effect of this dissipation on the motion is discussed briefly in

Appendix 3, where it is shown that only a negligible amount of energy is radiated when the bubble is large, but that at the first contraction an appreciable radiation of energy may take place.

Before concluding, it should be mentioned that the preceding analysis disposes of an objection which may be raised against the simple theory of Appendix 1. The objection is that for a certain range of depths the pressure jump at the shock wave remains greater than p_∞ for a large part of the period of the first pulsation. It is therefore not immediately obvious that the motion of the bubble will be the same in the actual case as in the non-compressive approximation, for which the pressure-radius curve of Figure 1 would be replaced by a monotonic curve with asymptote p_∞.

APPENDIX 3 CALCULATIONS OF THE RATE OF RADIATION OF ENERGY

In this Appendix the rate of radiation of energy from the pulsating bubble will be calculated on the assumption that the rate of energy loss is so small that it has a negligible effect on the course of the motion. This assumption will turn out to be somewhat rough near the first minimum or two, but the calculations here will at least indicate the order of magnitude of the energy loss. Our starting point will be equation (20) of Appendix 2. As explained there, it is a fairly good approximation to neglect the $\frac{da}{dt}/c$ on both sides, so we write the equation as

$$2\pi\rho a^3\left(\frac{da}{dt}\right)^2 = \int_{a_{max}}^{a}\left(p(a) - p_\infty\right) 4\pi a^2 da = \frac{4\pi}{c}\int_{a_{max}}^{a}\frac{dp}{da}\frac{da}{dt}\,a^3 da \quad (1)$$

The left of (1) differs only by an additive constant from the left of equation (5) of Section 3 of the text: it thus represents the kinetic and potential energy which would be present for the motion of a bubble in an incompressible

fluid with the same a and $\frac{da}{dt}$. There cannot be much error involved in assuming that the amount of energy radiated during the contracted stage is equal to the total change in the right of (1) during this stage.

The right of (1) will be evaluated by inserting the value of $\frac{da}{dt}$ which would obtain if there were no dissipation. We shall consider three extreme cases:

(i) Small vibrations about the equilibrium radius a_1. This case provides a check on the starting formula (1), which should yield the same result as the usual acoustical theory for a simple source.

(ii) Near the maximum radius for vibrations of any amplitude.

(iii) Near the minimum radius, for vibrations of large amplitude.

In all three cases we shall assume for simplicity that the pressure-volume relation is

$$pa^{3\gamma} = p_\infty a_1^{3\gamma} \quad \text{or} \quad = p_{max} a_{min}^{3\gamma} \tag{2}$$

(i) From (1) and (2) the energy dissipated in one cycle is

$$-\frac{4\pi}{c}\oint \frac{dp}{da}\left(\frac{da}{dt}\right)^2 a^3\,dt = \frac{12\pi\gamma p_\infty}{c}\oint \left(\frac{a_1}{a}\right)^{3\gamma}\left(\frac{da}{dt}\right)^2 a^2\,dt$$

which in the limit of very small oscillations is

$$\frac{6\pi\gamma p_\infty}{c} a_1^{2\gamma}\left(\frac{da}{dt}\right)^{2}_{max} T_s$$

where T_s is the period. At the same time the total energy is

$$2\pi\rho a_1^3\left(\frac{da}{dt}\right)^2_{max} \tag{3}$$

so that the fraction of this energy lost per cycle is

$$\frac{3p_\infty T_s}{\rho c a_1} = 2\pi\sqrt{3\gamma}\ \frac{\sqrt{\frac{p_\infty}{\rho}}}{c} \tag{4}$$

by (13) of Appendix 1. In the usual acoustical theory the energy radiated by a simple source in one period is

$$\frac{\pi}{2}\ \frac{\rho}{c}\ \frac{A^2}{T_s^2}\ \cdot T_s$$

where $A = 4\pi a_1^2 \left(\frac{da}{dt}\right)_{max}$ is the "strength" of the source. The ratio of this to (3) is easily verified, by using (13) of Appendix 1, to be the same as (4). For p_∞ = 1 atmosphere, $\gamma = 1.4$, $c = 1.5 \times 10^5$ cm/sec, (4) comes out to be .086.

(ii) In the neighborhood of the maximum radius let

$$(a_{max}-a) \sim \beta t^2 \tag{5}$$

where the time t=0 is taken as the time of maximum radius. The negative of the right of (1) is then asymptotically

$$\frac{12\pi\gamma p_\infty}{c}\left(\frac{a_1}{a_{max}}\right)^{3\gamma} a_{max}^2 \int_0^t (2\beta t)^2\, dt$$

$$= \frac{16\pi\gamma p_\infty}{c}\left(\frac{a_1}{a_{max}}\right)^{3\gamma} a_{max}^2\ \frac{(a_{max}-a)^2}{t} \tag{6}$$

The kinetic energy is

$$2\pi\rho\, a^3\left(\frac{da}{dt}\right)^2 \sim 8\pi\rho\, a_{max}^3 \left(\frac{a_{max}-a}{t}\right)^2 \tag{7}$$

and the ratio of (6) to (7) is

$$\frac{2\gamma p_\infty}{\rho c}\left(\frac{a_1}{a_{max}}\right)^{3\gamma}\frac{t}{a_{max}} = 3.66\gamma\frac{\sqrt{\frac{p_\infty}{\rho}}}{c}\left(\frac{a_1}{a_{max}}\right)^{3\gamma}\frac{t}{T_0} \tag{8}$$

by (14) of Appendix 1. The quantity (8) represents the fractional change in $\left(\frac{da}{dt}\right)^2$ produced by the dissipation, as compared with the ideal motion of Appendix 1. This change is negligible in the neighborhood of the maximum radius, since for $\gamma = 1.4$, $p_\infty = 1$ atmosphere, $c = 1.5 \times 10^5$ cm/sec, $\frac{a_i}{a_{max}} = \frac{1}{3}$, (8) reduces to $3.4 \times 10^{-4} \frac{t}{T_o}$.

(iii) For large amplitudes of motion we may ignore p_∞ in the neighborhood of the minimum radius, and thus obtain from equation (1) of Appendix 1

$$\frac{da}{dt} = \frac{\sqrt{W - G}}{\sqrt{2\pi\rho a^3}} \tag{9}$$

where $$G = W\left(\frac{a_{min}}{a}\right)^{3\gamma - 3} \tag{10}$$

Using this and (2), the right of (1) becomes

$$\frac{12\pi\gamma p_{max} a_{min}^{3/2}}{c}\sqrt{\frac{W}{2\pi\rho}}\int x^{\frac{1}{2}-3\gamma}\sqrt{1 - x^{3-3\gamma}}\,dx \tag{11}$$

where $x = \frac{a}{a_{min}}$. We want to find out how much energy is radiated away during the entire portion of a cycle when the radius of the bubble is small (we have seen that the radiation is negligible at other times). To do this let us take the limits of the integral in (11) to be 1 and ∞ (the exact value of the upper limit is unimportant) and multiply by two. The resulting integral can be expressed in terms of gamma functions, and dividing (11) by W we have finally

$$\text{Fraction of total energy radiated} = \frac{4\gamma\sqrt{2\pi}}{(\gamma-1)} \cdot \frac{\Gamma(3/2)\Gamma\left(\frac{2\gamma-1}{2\gamma-2}\right)}{\Gamma\left(\frac{5\gamma-4}{2\gamma-2}\right)} \frac{p_{max}\, a_{min}^{3/2}}{c\sqrt{W\rho}} \qquad (12)$$

If we set

$$W = \frac{4\pi}{3} \frac{a_{min}^3\, p_{max}}{(\gamma-1)} ,$$

(12) takes the more convenient form

$$\text{Fraction radiated} = 6\gamma\sqrt{\frac{2}{3(\gamma-1)}} \frac{\Gamma(3/2)\Gamma\left(\frac{2\gamma-1}{2\gamma-2}\right)}{\Gamma\left(\frac{5\gamma-4}{2\gamma-2}\right)} \frac{\sqrt{\frac{p_{max}}{\rho}}}{c} \qquad (13)$$

The coefficient of $\sqrt{\frac{p_{max}}{\rho}}/c$ has the values

γ	Coefficient
1.2	1.6
1.6	3.0
2.0	3.8

It must be remembered, of course, that (13) will not be exactly correct even for a spherically symmetrical motion, because we have ignored the modification of the motion produced by the radiation and by other dissipative mechanisms. When asymmetrical influences are present, the radiated energy may be very much less, as Taylor[28] has shown, because the bubble will not shrink to so small a radius.

---

[28] See the article by Taylor in this Volume.

APPENDIX 4 EFFECT OF GRAVITY

Whenever the radius of the pulsating bubble is small enough compared with the height of the column of water necessary to produce pressure p_∞, we may expect the effect of gravity on the pulsations to be small. Accordingly let us expand the velocity potential ϕ and the shape of the bubble in powers of g. Choosing the initial position of the center of the bubble as origin of coordinates, we may denote the radial distance to a point on the boundary of the bubble by $R(\theta)$, where $\theta = \frac{z}{r}$ is the angle with the vertical. We thus set

$$\phi(\vec{r},t) = \phi_0 + g\phi_1 + \cdots \quad (1)$$

$$p(\vec{r},t) = p_0 + gp_1 + \cdots \quad (2)$$

$$R(\theta,t) = a(t) + gR_1(\theta,t) + \cdots \quad (3)$$

Taking p_∞ to be the pressure at infinity in the plane $z = 0$, the equation of motion is

$$\frac{\partial \phi}{\partial t} - \frac{1}{2}(\nabla\phi)^2 = \frac{p - p_\infty}{\rho} + gz \quad (4)$$

and the first order part of this is

$$\frac{\partial \phi_1}{\partial t} - \frac{\partial \phi_0}{\partial r}\frac{\partial \phi_1}{\partial r} = \frac{p_1}{\rho} + z \quad (5)$$

To integrate this we must use three additional relations:

(1) Since $\nabla^2\phi_1 = 0$, the expansion of ϕ_1 in spherical harmonics must have the form

$$\phi_1 = \frac{A_1}{r} + \frac{B_1\cos\theta}{r^2} + \frac{C_1 P_2(\cos\theta)}{r^3} \cdots \quad (6)$$

provided there are no obstacles or free surfaces nearby.

(ii) The boundary condition which p_1 must satisfy is determined by the fact that $p(R)$ is a fixed function of the volume V of the bubble, independent of g. Thus, to the first order in g

$$p(R,t) = p_0(a,t) + gR_1\left[\frac{\partial p_0}{\partial r}\right]_{r=a} + gp_1(a,t)$$

$$= p_0(a,t) + g\left(\frac{\partial V}{\partial g}\right)_t \frac{dp_0(a,t)}{dV}$$

from which

$$p_1(a,\theta,t_1) = -\left[\frac{\partial p_0}{\partial r}\right]_{r=a} R_1 + \frac{1}{4\pi a^2}\left(\frac{\partial V}{\partial g}\right)_t \frac{dp_0(a,t)}{da} \qquad (7)$$

(iii) Since

$$\frac{dR}{dt} = -\left(\frac{\partial \phi}{\partial r}\right)_{r=R}$$

we have

$$\frac{dR_1}{dt} = \frac{A_0}{a^2}\left(-2\,\frac{R_1}{a}\right) + \frac{A_1}{a^2} + \frac{2B_1\cos\theta}{a^3} + \cdots\cdots$$

$$= -\frac{2}{a}\frac{da}{dt}R_1 + \frac{A_1}{a^2} + \frac{2B_1\cos\theta}{a^3} + \cdots\cdots \qquad (8)$$

The procedure is now to substitute (6) and (7) in (5), and to use (8) to express A_1, B_1, ... in terms of the coefficients in the spherical harmonic expansion of R_1. If we let

$$R_1 = \sum_{\ell=0}^{\infty} R_1^{(\ell)}(t)\, P_\ell(\cos\theta) \qquad (9)$$

the differential equation which results for $R_l^{(\ell)}$ will be homogeneous when $\ell > 1$, so that the solution which satisfies

$$R_l^{(\ell)} = 0, \quad \frac{dR_l^{(\ell)}}{dt} = 0 \quad \text{at } t = 0 \text{ (start of motion)} \tag{10}$$

will be simply $R_l^{(\ell)} = 0$. The same will be true when $\ell = 0$, since the second term on the right of (7) is proportional to $R_l^{(0)}$. Thus we have only the equation for $\ell = 1$ to consider: this equation is

$$\frac{1}{a^2}\frac{dB_1}{dt} - \frac{da}{dt}\cdot\frac{2B_1}{a^3} = -\left(\frac{\partial p_a}{\partial r}\right)_{r=a}\frac{R_1^{(1)}}{\rho} + a$$

or, using (8) and the relation $\left(\frac{\partial p_a}{\partial r}\right)_{r=a} = -\rho\frac{d^2a}{dt^2}$,

$$\frac{a}{2}\frac{d^2R_1^{(1)}}{dt^2} + \frac{3}{2}\frac{da}{dt}\frac{dR_1^{(1)}}{dt} = a \tag{11}$$

This integrates to

$$\frac{dR_1^{(1)}}{dt} = \frac{2}{a^3}\int_0^t a^3\,dt \tag{12}$$

The equation

$$R = a + gR_1^{(1)}\cos\theta$$

means that to the first order in g the bubble is displaced upward by the amount $gR_1^{(1)}$, without change of size or shape. If one is interested only in the relation (12), a much simpler derivation can be given. Consider the momentum of the water contained in a large vertical cylinder of radius $\overline{\xi}$ and length $L \gg \xi$, with center at the origin. This momentum is

$$\vec{M} = \rho\iiint \vec{v}\,d\tau = \rho\iint_{\text{bubble}} \vec{n}\phi\,dS - \rho\iint_{\text{cylinder}} \vec{n}\phi\,dS$$

where $\vec{n}$ is the outward normal in each case. As $L \to \infty$, the second surface integral goes to zero. If we take the origin of coordinates at the instantaneous center of the bubble, the evaluation of the first surface integral is simplified: we have $R_1 = 0$ at the given instant, so that to the first order in ε

$$\lim_{L\to\infty} M_z = \rho \iint \frac{\varepsilon B_1}{a^2} \cos^2\theta \, dS = \frac{4\pi}{3} \rho \varepsilon B_1$$

$$= \frac{1}{2} \cdot \frac{4\pi}{3} a^3 \rho \varepsilon \frac{dR_1^{(1)}}{dt} \qquad (13)$$

by (8). Now the time rate of change of M_z is equal to the total gravity force acting on the water in the cylinder, plus the total pressure force on the ends, plus the momentum entering across the surface. In the limit $L \to \infty$ the last contribution vanishes, and the first two give

$$\lim_{L\to\infty} \frac{dM_z}{dt} = \frac{4\pi}{3} a^3 \rho \varepsilon \qquad (14)$$

Equating (13) to the time integral of (14) gives (12).

At the maximum of the first expansion the value of $\frac{dR_1^{(1)}}{dt}$ can be obtained by substituting the value of $\frac{da}{dt}$ from Appendix 1 into (12): disregarding gas pressure, the result turns out to be

$$\varepsilon \left[\frac{dR_1^{(1)}}{dt}\right]_{a=a_{max}} = 0.62 \; \varepsilon g T_0 \qquad (15)$$

The value of $\varepsilon R_1^{(1)}$ at this stage is obtained, as to order of magnitude at least, by multiplying half of (15) by $T_0/2$.

The rise of the bubble during the first expansion is thus proportional to T^2, and the ratio of the distance risen to a_{max} proportional to T. The rise is therefore negligible for small explosions, but considerable for large ones.

A conspicuous feature of (12) is that the rise is enormously accelerated during the contracting stage, because of the a^3 in the denominator. This is an illustration of the general instability of the contracting stage. Even for rather small explosions, the velocity of rise will probably become so great during the contraction that the approximation of treating the gravity correction as small will break down. It is certain, however, that a very rapid vertical acceleration will take place, which will tend to create turbulence much sooner than it would be created in the absence of gravity.

APPENDIX 5 EFFECT OF PROXIMITY TO A FREE OR TO A RIGID SURFACE

Let the center of the gas bubble at the start of the motion be a distance h beneath the free surface of the water, or alternatively a distance h from a plane rigid surface. The water will be treated as incompressible, and gravity will be neglected, since it is easy to show that the first-order effects of the surface and of gravity are additive. We shall be interested in two effects due to the presence of the surface, namely, the change in period and the rising or sinking of the bubble. The complete theory, which is similar to that of Appendix 4, is rather complicated; however, the calculation of the effect on the period can be made quite simply, and this will be given first.

The boundary condition which must be satisfied at a free surface is that the pressure p must be constant over the surface. This means that the velocity potential ϕ must satisfy

$$\frac{\partial \phi}{\partial t} - \frac{1}{2} (\nabla \phi)^2 = 0 \qquad (1)$$

on the surface. Since ϕ is of order $1/r$, where r is the distance from the center of the bubble, the ratio of the second term of (1) to the first will be of order $1/h^3$ as $h \to \infty$. It is not hard to show that this ratio is quite small when h is even a few times a_{max}, so that it will be good enough for our purposes to replace (1) by the condition

$$\phi = 0 \qquad \text{on the free surface} \tag{2a}$$

Alternatively, we must have

$$\vec{n} \cdot \nabla\phi = 0 \qquad \text{on the rigid surface} \tag{2b}$$

where $\vec{n}$ is the unit normal to the surface. It will be convenient to picture ϕ as the electrostatic potential due to a charge (and, if necessary, a set of multipoles) located at the initial center of the bubble, in the presence of (a) a grounded conducting plane, or (b) a plane boundary of a medium of dielectric constant zero. The total "charge" of the bubble is

$$e = -\frac{1}{4\pi} \iint_{\substack{\text{bubble} \\ \text{surface}}} \vec{n} \cdot \nabla\phi \, dS = \frac{1}{4\pi} \frac{dV}{dt} \tag{3}$$

where V is the volume of the bubble. As is well known, the field due to the charges induced on the plane in case (a) is the same as that produced by an oppositely charged mirror image of the charged bubble: the lines of force (stream lines in the hydrodynamical problem) accordingly look as shown in Figure 6 (a). Similarly in case (b) the field produced by the polarized dielectric is the same as that produced by an image with the same sign of charge, and the lines of force are as shown in Figure 6 (b). Now the kinetic energy of the hydrodynamical problem is

$$\iiint_{\substack{\text{entire} \\ \text{fluid}}} \frac{\rho}{2} (\nabla\phi)^2 \, d\tau.$$

which differs only by a constant factor from the electrostatic energy

$$\frac{1}{8\pi}\iiint (\nabla\phi)^2 \, d\tau$$

of the electrical problem. The change in the latter when the bubble is brought from infinity to a distance h from the plane is equal to the work done in this operation. If h is a few times larger than the radius a of the bubble, the field E acting on the bubble, due to its image, when it is a distance x from the plane, can be taken as $\pm e^2/4x^2$, with the upper sign in case (a), the lower in case (b). The work done, therefore, is

$$\mp \int_{-\infty}^{-h} \frac{e^2}{4x^2}\, dx = \mp \frac{e^2}{4h} \qquad (4)$$

Any redistribution of charge (normal velocity) on the surface of the bubble, and any alteration in the shape of the bubble, due to its proximity to the surface, will give a contribution to this work which is of higher order in 1/h, and negligible if h is several times a. The work (4) is to be compared with the electrostatic energy $e^2/2a$ of the bubble when it is spherical and at an infinite distance from the plane. Thus, to the first order in 1/h we have for given V, $\frac{dV}{dt}$,

$$\text{Kinetic energy in presence of surface} = (1 \mp \frac{a}{2h}) \times \left(\text{Kinetic energy in absence of surface}\right) \quad (5)$$

where the upper sign is to be used for a free surface, the lower sign for a rigid surface.

The motion of the bubble in the presence of the surface is accordingly given to the first order by multiplying the first term of (1) of Appendix 1 by the factor $(1 \mp \frac{a}{2h})$, and integrating the resulting equation. This equation may be written simply

$$(1 \mp \frac{R}{2h}) \left(\frac{dR}{dt}\right)^2 = f(R) \quad (6)$$

(R is used rather than a for the radius of the bubble, since it will be convenient to use a(t) for the radius in the absence of perturbing influences.) The form of the function f(R) cannot depend on h, since both the total energy, and the form of the potential energy function, are independent of h.

If we set

$$R(t) = a(t) + \frac{1}{h} R_1(t) + \frac{1}{h^2} R_2(t) + \ldots . \qquad (7)$$

the first order part of (6) is just

$$\mp \frac{a}{2}\left(\frac{da}{dt}\right)^2 + 2\,\frac{da}{dt}\,\frac{dR_1}{dt} = \frac{df}{dR} R_1 = \frac{R_1}{\frac{da}{dt}} \cdot 2\,\frac{da}{dt}\,\frac{d^2a}{dt^2}$$

$$= 2 R_1 \frac{d^2a}{dt^2} \qquad (8)$$

Since $R_1 = 0$ at the start of the motion, which we take at $t = 0$, the solution of (8) is

$$R_1 = \mp \frac{1}{4}\,\frac{da}{dt} \int_0^t a\, dt \qquad (9)$$

Now $R_1/h\,\frac{da}{dt}$ is simply the time interval by which the curve of R against t lags behind the curve of a against t for a fixed radius. The value of this quantity after one complete cycle represents the amount by which the period is shortened because of the surface. Thus, we have to the first order in 1/h

$$T(h) = T(\infty)\left(1 \mp \frac{\bar{a}}{4h}\right) \qquad (10)$$

where $\bar{a}$ is the time average of a, and where the upper sign is for a free surface, the lower for a rigid one.

When there are two or more plane surfaces near the bubble, their effects on the motion are not simply additive, even in the first order. In some cases the combined effect can be calculated rather easily by the image methods of electrostatics already used. For example, consider a

bubble halfway between the surface and a horizontal rigid bottom. The field between these two planes in the equivalent electrostatic problem is that of the original charge e and an infinite set of images, as shown in Fig. 7. The two nearest images give equal and opposite contributions to the potential at the bubble, and thus cancel; however, the next two images both have charge $-e$, so give a negative contribution. The potential at the bubble due to the infinite set of images comes out to be $-\frac{e}{2h}\log 2$, which differs

only by the factor log 2 = 0.69 from the value $-\frac{a}{2h}$ which we would have if the bubble were a distance h from the surface in infinitely deep water. Thus for this case

$$T = T(\infty)\left(1 - \frac{\bar{a}\log 2}{4h}\right)$$

If, on the other hand, the bubble were between two parallel infinite rigid surfaces, its kinetic energy when expanding or contracting would be infinite; for this case $T = \infty$ in the non-compressive approximation.

In the discussion so far, nc account has been taken of any displacement of the center of the bubble, or of any deviation from spherical shape, due to the proximity of the surface. Following the ideas used in Appendix 4, let us set

$$\phi(\vec{r},t) = \phi_0 + \frac{1}{h}\phi_1 + \frac{1}{h^2}\phi_2 \cdots \quad (11)$$

$$p(\vec{r},t) = p_0 + \frac{1}{h}p_1 + \frac{1}{h^2}p_2 \cdots \quad (12)$$

$$R(\theta,t) = a(t) + \frac{1}{h}R_1 + \frac{1}{h^2}R_2 \cdots \quad (13)$$

where R is the distance from the origin (taken at the initial position of the center of the bubble) to the boundary of the bubble in a direction making angle θ with the z axis, which we shall draw from the origin toward the surface and normal to the latter. The equation of motion is

$$\frac{\partial\phi}{\partial t} - \frac{1}{2}(\nabla\phi)^2 = \frac{p - p_\infty}{\rho} \quad (14)$$

and the first and second order parts of this are

$$\frac{\partial \phi_1}{\partial t} - \frac{\partial \phi_0}{\partial r}\frac{\partial \phi_1}{\partial r} = \frac{p_1}{\rho} \tag{15}$$

$$\frac{\partial \phi_2}{\partial t} - \frac{\partial \phi_0}{\partial r}\frac{\partial \phi_2}{\partial r} - \frac{1}{2}(\nabla \phi_1)^2 = \frac{p_2}{\rho} \tag{16}$$

As in Appendix 4, we use three additional relations to integrate these:

(i) Since $\nabla^2 \phi_n = 0$, the expansion of ϕ_n in spherical harmonics must have the form

$$\phi_n = \phi'_n + \phi''_n = \frac{A'_n}{r} + A''_n + \left(\frac{B'_n}{r^2} + B''_n r\right)\cos\theta$$

$$+ \left(\frac{C'_n}{r^3} + C''_n r^2\right) P_2(\cos\theta) + \ldots\ldots \tag{17}$$

where the terms in A''_n, B''_n, C''_n, ... represent the field produced by the image of the bubble in the surface. The potential ϕ'' at the origin due to this image is $\mp \frac{e}{2h}$, correct to the second order in $1/h$, where e is given by (3) and where the upper sign is for a free surface, the lower for a rigid one. Similarly, the gradient of the image potential at the origin is, to the second order in $1/h$

$$\left(\frac{\partial \phi''}{\partial z}\right)_0 = \mp \frac{e}{4h^2}$$

and, in general, the k^{th} derivative of ϕ'' at the origin is of order h^{-k-1}. Thus, we have

$$A_1'' = \mp \frac{a^2}{2} \frac{da}{dt}, \quad B_1'' = C_1'' = \cdots\cdots = 0 \tag{18}$$

$$A_2'' = 0, \quad B_2'' = \mp \frac{a^2}{4} \frac{da}{dt}, \quad C_2'' = \cdots\cdots = 0 \tag{19}$$

(ii) To order $1/h^2$, the pressure at the boundary of the bubble is

$$p(R,t) = p_0(a,t) + (R_1/h + R_2/h^2) \frac{\partial p_0}{\partial r} + \frac{R_1^2}{2h^2} \frac{\partial^2 p_0}{\partial r^2} + p_1(a,t)/h + \frac{R_1}{h^2} \frac{\partial p_1}{\partial r} + p_2/h^2 \tag{20}$$

Also, to the first order in $1/h$,

$$p(R,t) = p_0(a,t) + 4\tau a^2 \frac{R_1^{(0)}}{h} \frac{dp_0}{dV} = p_0 + \frac{R_1^{(0)}}{h \frac{da}{dt}} \frac{dp_0}{dt} \tag{21}$$

where $R_1^{(0)}$ is the spherical average of R_1. Since at the boundary of the bubble

$$\frac{dp_0}{dt} = \frac{\partial p_0}{\partial t} + \frac{da}{dt} \frac{\partial p_0}{\partial r},$$

(20) and (21) give

$$p_1(a, \theta, t) = \frac{R_1^{(0)}}{\frac{da}{dt}} \left[\frac{\partial p_0}{\partial t} \right]_{r=a} \tag{22}$$

Into this we may insert p_0 from (14) which is,

since $\phi_0 = \frac{a^2}{r}\frac{da}{dt}$,

$$\frac{p_0}{\rho} = \frac{p_\infty}{\rho} + \frac{1}{r}\frac{d}{dt}\left[a^2\frac{da}{dt}\right] - \frac{1}{2r^4}\left[a^2\frac{da}{dt}\right]^2 \qquad (23)$$

We shall not be interested in the spherically symmetrical part of p_2; if we anticipate the result to be proved below that R_1 is spherically symmetrical and remember that $p(R,t)$ is constant over the surface of the bubble, we have from (20)

$$p_2(a,\theta,t) = -R_2\left[\frac{\partial p_0}{\partial r}\right]_{r=a} + \begin{matrix}\text{spherically}\\ \text{symmetrical}\\ \text{terms}\end{matrix} \qquad (24)$$

(iii) In the equation $\frac{dR}{dt} = -\left(\frac{\partial\phi}{\partial r}\right)_{r=R}$ let us insert

$$R_n = \sum_{\ell=0}^{\infty} R_n^{(\ell)} P_\ell(\cos\theta) \qquad (25)$$

We obtain, as in Appendix 4,

$$\left.\begin{aligned}\frac{dR_1^{(0)}}{dt} &= -\frac{2}{a}\frac{da}{dt}R_1^{(0)} + \frac{A_1'}{a^2}\\ \frac{dR_1^{(1)}}{dt} &= -\frac{2}{a}\frac{da}{dt}R_1^{(1)} + \left(\frac{2B_1'}{a^3} - B_1''\right)\end{aligned}\right\} \qquad (26)$$

$$\frac{dR_2^{(1)}}{dt} = -\frac{2}{a}\frac{da}{dt}R_2^{(1)} + \left(\frac{2B_2'}{a^3} - B_2''\right) \qquad (27)$$

To obtain the differential equations for the $R_1^{(\ell)}$, we first insert (18) into (26) and solve these equations for A_1', B_1', etc. In this way the expression (17) for ϕ, can

be evaluated in terms of the $R_1^{(\ell)}$, $\frac{dR_1^{(\ell)}}{dt}$, a, and $\frac{da}{dt}$. If this is now inserted into (15) and the right of (15) expressed in terms of $R_1^{(0)}$, and of a and its derivatives, by (22) and (23), a set of second order differential equations for the $R_1^{(\ell)}(t)$ result. All the equations will be homogeneous except that for $\ell=0$; since at $t=0$, $R_1=\frac{dR_1}{dt}=0$, this means that

$$R_1^{(\ell)}=0 \qquad \text{for } \ell>0 \tag{28}$$

For $\ell=0$ we obtain the equation

$$a\frac{da}{dt}\frac{d^2R_1^{(0)}}{dt^2}+3\left(\frac{da}{dt}\right)^2\frac{dR_1^{(0)}}{dt}-\left(3\frac{da}{dt}\frac{d^2a}{dt^2}+a\frac{d^3a}{dt^3}\right)R_1^{(0)}$$

$$=\pm\left[a\left(\frac{da}{dt}\right)^3+\frac{a^2}{2}\frac{da}{dt}\frac{d^2a}{dt^2}\right] \tag{29}$$

It can be verified that (8) is an integral of (29), so that the solution (9) obtained by the simpler method is checked. Another check on (29) is obtained by noting that the left side reduces to zero if we set $R_1^{(0)}=\frac{da}{dt}$, corresponding to a shift in the starting time.

The same procedure can be used to get the differential equations for the $R_2^{(\ell)}$, using (19), (27), (17), (16), and (24). For $\ell>1$ the resulting equation is homogeneous, so

$$R_2^{(\ell)}=0 \qquad \text{for } \ell>1 \tag{30}$$

For $\ell=1$ we have on collecting the terms

$$a\frac{d^2R_2^{(1)}}{dt^2}+3\frac{da}{dt}\frac{dR_2^{(1)}}{dt}=\pm\left[\frac{9}{4}a^2\left(\frac{da}{dt}\right)^2+\frac{3}{4}a^3\frac{d^2a}{dt^2}\right] \tag{31}$$

i.e.,

$$\frac{1}{a^2}\frac{d}{dt}\left(a^3\frac{dR_2^{(1)}}{dt}\right) = \pm\frac{3}{4}\frac{d}{dt}\left(a^3\frac{da}{dt}\right)$$

which when integrated by parts gives

$$\frac{dR_2^{(1)}}{dt} = \pm\frac{3}{4}a^2\frac{da}{dt} \mp \frac{3}{2a^3}\int_0^t a^4\left(\frac{da}{dt}\right)^2 dt \qquad (32)$$

$$R_2^{(1)} = \pm\frac{1}{4}\left[a^3(t) - a^3(0)\right] \mp \frac{3}{2}\int_0^t \frac{dt'}{a^3}\int_0^{t'} a^4\left(\frac{da}{dt''}\right)^2 dt'' \qquad (33)$$

We conclude that as far as the second order in $1/h$, the effect of the surface is to change the period of the motion (first order) and to shift the center of the bubble a distance $R_2^{(1)}/h^2$ toward the surface. This latter displacement consists of a periodic part and a monotonic part. The periodic part represents a sucking of the bubble back and forth by its image: the velocity at the origin due to the image is $\pm e/4h^2 = \pm a^2\frac{da}{dt}/4h^2$; the first term of (32) is three times this because the bubble acquires a dipole moment just sufficient to keep the pressure constant over its surface. The monotonic second term of (32) is negligible compared to the first in the limit of small velocities, although not for the velocities encountered in explosions. This term, like (12) of Appendix 4, contains a^3 in the denominator, and thus illustrates the instability of deviations from spherical symmetry during the contraction. The ratio of the monotonic part of the velocity $\frac{1}{h^2}\frac{dR_2^{(1)}}{dt}$, due to the surface, to the gravity term $g\frac{dR_1^{(1)}}{dt}$ of

Appendix 4, is

$$\left|\frac{\text{surface term}}{\text{gravity term}}\right| = \frac{3}{4}\,\frac{\int_0^t a^4\left(\frac{da}{dt}\right)^2 dt}{gh^3\int_0^t a^3\,dt}$$

The integrals can be evaluated for $t = T$, by the methods of Appendix 1, in the approximation which neglects gas pressure. The results are

$$\int_0^{T_0} a^4\left(\frac{da}{dt}\right)^2 dt = 0.30\sqrt{\frac{p_\infty}{\rho}}\,a_{max}^5 \qquad (34)$$

$$\int_0^{T_0} a^3\,dt = 1.14\sqrt{\frac{\rho}{p_\infty}}\,a_{max}^4 \qquad (35)$$

so that the ratio is

$$\left|\frac{\text{surface term}}{\text{gravity term}}\right| = 0.20\,\frac{p_\infty}{\rho gh}\cdot\frac{a_{max}}{h} \qquad (36)$$

For small explosions in shallow water or close to a rigid surface this ratio can become appreciably greater than one, so that the bubble can, for example, sink instead of rise. It must be remembered of course that when h is as small as two or three times a_{max} the rate of drift given by (32) becomes so large during the contraction that it can by no means be regarded as a small correction to the motion. However, (32) should give the drift fairly well over the greater part of the first period, so the qualitative conclusion that a bubble will rise or sink in a given experiment is probably safe.

In conclusion, it will be shown that the $R_2^{(1)}$ satisfying (31) can be represented as a sum of the displacement due to the pressure gradient produced by the image, and the mass motion produced by the image. The pressure gradient due to the image is

$$\frac{\partial p_{im}}{\partial z} = \mp \frac{a}{4h^2}\left[p(a) - p_\infty + \frac{\rho}{2}\left(\frac{da}{dt}\right)^2\right] + o\left(\frac{1}{h^3}\right) \tag{37}$$

Equating the time rate of change of the normal momentum (compare (13) and (14) of Appendix 4) to the buoyant effect of this pressure gradient would give a value z_p for the coordinate of the bubble in the z-direction, satisfying

$$\frac{d}{dt}\left[\frac{2\pi\rho a^3}{3}\frac{dz_p}{dt}\right] = -\frac{4\pi a^3}{3}\frac{\partial p_{im}}{\partial z} \tag{38}$$

In combining this with (37) we may eliminate p(a) by the differentiated energy equation (5) of the text--i.e., by Eq. (19) of Appendix 2 with c set equal to infinity -- viz.,

$$p(a) - p_\infty = \rho\left[a\frac{d^2a}{dt^2} + \frac{3}{2}\left(\frac{da}{dt}\right)^2\right]$$

The result is, to order $1/h^2$,

$$\frac{d}{dt}\left[a^3\frac{dz_p}{dt}\right] = \pm\frac{a^4}{2h^2}\left[a\frac{d^2a}{dt^2} + 2\left(\frac{da}{dt}\right)^2\right] \tag{39}$$

Now as was stated above in the paragraph following Eq. (33), the velocity field due to the image would, in the absence of the bubble itself, cause a velocity of motion dz_v/dt in the z-coordinate of the water at the position of

the bubble center, where

$$\frac{dz_v}{dt} = \pm \frac{a^2}{4h^2} \frac{da}{dt} + O(\tfrac{1}{h}3) \quad ,$$

whence, to order $1/h^2$,

$$\frac{d}{dt}\left[a^3 \frac{dz_v}{dt}\right] = \pm \frac{a^4}{4h^2} \left[a \frac{d^2a}{dt^2} + 5\left(\frac{da}{dt}\right)^2\right] \tag{40}$$

Adding (39) and (40) gives

$$\frac{1}{a^2} \frac{d}{dt} \left[a^3 \frac{d}{dt} (z_p + z_v)\right] = \pm \frac{1}{h^2} \left[\tfrac{3}{4} a^3 \frac{d^2a}{dt^2} + \frac{9}{4} a^2 \left(\frac{da}{dt}\right)^2\right] \tag{41}$$

Comparison of (31) and (41) shows that to this accuracy $(z_p + z_v)$ satisfies the same differential equation as $R_2^{(1)}/h^2$.

APPENDIX 6 PRESSURE DISTRIBUTION IN NON-COMPRESSIVE RADIAL MOTION

The Euler equation for radial flow is

$$\frac{dv}{dt} = \frac{\partial v}{\partial t} + v\frac{\partial v}{\partial r} = -\frac{1}{\rho}\frac{\partial p}{\partial r} \tag{1}$$

Integrating this from r to infinity and writing

$$\phi = \int_r^\infty v\,dr \quad \text{so that } v = -\frac{\partial \phi}{\partial r} \tag{2}$$

we find, assuming ρ constant

$$p - p_\infty = \rho\frac{\partial \phi}{\partial t} - \frac{\rho}{2}v^2 \tag{3}$$

For non-compressive motion outside a bubble of radius a we have

$$v = \frac{a^2}{r^2}\frac{da}{dt} \tag{4}$$

so that

$$\phi = \frac{a^2}{r}\frac{da}{dt} \tag{5}$$

Substituting (4) and (5) into (3) gives

$$p - p_\infty = \frac{\rho a^2}{r}\frac{d^2a}{dt^2} + \frac{2\rho a}{r}\left(\frac{da}{dt}\right)^2 - \frac{\rho a^4}{2r^4}\left(\frac{da}{dt}\right)^2 \tag{6}$$

Setting $r = a$ gives

$$p(a) - p_\infty = \rho a\frac{d^2a}{dt^2} + \frac{3\rho}{2}\left(\frac{da}{dt}\right)^2 \tag{7}$$

and solving (7) for $\frac{d^2a}{dt^2}$ and inserting in (6) gives finally

$$p(r) - p_\infty = \frac{a}{r}\left[p(a) - p_\infty + \frac{\rho}{2}\left(\frac{da}{dt}\right)^2\left(1 - \frac{a^3}{r^3}\right)\right] \tag{8}$$

It is obvious that the maximum value of (8) will occur when a is less than the radius at which $\frac{da}{dt}$ is a maximum, but it is not immediately obvious that (8) is a maximum when a is a minimum, since in this region increasing a decreases p(a) but increases $\frac{da}{dt}$. However, if we assume p(a) to follow an adiabatic law $pa^{3\gamma}$ = constant and neglect the p_∞ term in equation (1) of Appendix 1, we have

$$\frac{\rho}{2}\left(\frac{da}{dt}\right)^2 = \frac{W}{4\pi a^3}\left[1 - \left(\frac{a_{min}}{a}\right)^{3\gamma-3}\right] \tag{9}$$

$$W = G(a_{min}) = \frac{4\pi}{3}\,\frac{p(a_{min})\,a_{min}^3}{(\gamma-1)} \tag{10}$$

If (9) and (10) are assumed it can be verified that (8) increases with decreasing a all the way down to a_{min}, whenever $\gamma > 1$, as is always the case for perfect gases.

If r is large enough so that the last term of (3) can be neglected we have

$$\int_{t_1}^{t_2} (p - p_\infty)\,dt \approx \frac{\rho}{r}\left[a^2\frac{da}{dt}\right]_{t_1}^{t_2} \tag{11}$$

The maximum of (11) will come when t_1 and t_2 are two times for which $\left|a^2\frac{da}{dt}\right|$ is a maximum, in the expanding and contracting stages respectively. From equation (1) of Appendix 1 we have, neglecting G,

$$a^4\left(\frac{da}{dt}\right)^2 = \frac{Wa}{2\pi\rho} - \frac{2}{3}\,\frac{p_\infty}{\rho}\,a^4 \tag{12}$$

This is a maximum when

$$\frac{W}{2\pi\rho} = \frac{2}{3}\frac{p_\infty}{\rho} a_{max}^3 = \frac{8}{3}\frac{p_\infty}{\rho} a^3$$

i.e., when $a = 2^{-2/3} a_{max}$ (13)

This maximum value of (12) is

$$\frac{2}{3}\frac{p_\infty}{\rho} a_{max}^4 (2^{-2/3} - 2^{-1/3}) = 2^{-5/3}\frac{p_\infty}{\rho} a_{max}^4$$

Insertion of this into (11) gives

$$\text{maximum impulse of pressure} = 2^{1/6} a_{max}^2 \sqrt{\rho p_\infty} \quad (14)$$

APPENDIX 7 EFFECT OF THE INERTIA OF THE GAS ON THE PRESSURE PULSE

It seems unlikely that oscillations of the gas in the bubble, i.e., non-uniformity of the pressure in the bubble due to the inertia of the gas, can cause any appreciable wiggles in the pressure pulse emitted during the contracted stages. The reasons are as follows:

(i) The pressure gradient at the outer edge of the gas there is

$$\left(\frac{\partial p}{\partial r}\right)_{r=a} = \rho_g \frac{d^2a}{dt^2} \qquad (1)$$

where ρ_g is the density of the gas. The equation of motion of the gas can apparently be satisfied by a velocity distribution approximating a uniform contraction or expansion combined with a pressure distribution which is roughly parabolic in r with the slope (1) at the boundary. For such a distribution it is easy to calculate the fractional deviation of $p(a)$ from the pressure $\bar{p}$ which the gas would have under static conditions at the same volume: the result is

$$p(a) \approx \bar{p}\left[1 - \frac{\rho_g a}{5\bar{p}} \frac{d^2a}{dt^2}\right] \qquad (2)$$

At the minimum radius, for example,

$$a \frac{d^2a}{dt^2} \approx \frac{p(a)}{\rho} \qquad \text{(eq. (19), Appendix 2)}$$

so the second term in the brackets is essentially $\frac{\rho_g}{5\rho}$, which is negligible at all times after the initial stages of the explosion. Thus a motion is possible for which gas inertia is negligible, although it may not be the motion which actually occurs.

(ii) We might suppose the gas to oscillate in one of its normal modes, with an amplitude that increases as the radius gets smaller. Now the lowest normal mode of a sphere of gas has the period[29] (for small amplitudes) $1.40a/c_g$, where c_g is the velocity of sound in the gas. Near the minimum radius the gas is hot, so that c_g is high, and the period of the gas oscillation is rather small even on the scale of the a vs. t curve at this stage. We may, therefore, expect the efficiency of the water in exciting such an oscillation to be small.

(iii) If the amplitude of such a normal mode of vibration is to increase greatly as the bubble contracts, the normal mode cannot lose much of its energy to the water in a period. But if little energy is lost in this way the effect of the gas oscillations on the sound received at a distance in the water will be small.

---

[29] Lord Rayleigh, Theory of Sound, #331.

APPENDIX 8 RESUME OF RAMSAUER'S EXPERIMENTS[30]

In the experiments of Ramsauer mentioned in the introduction, the objective was to obtain measurements of the radius-time curve for the first expansion of the bubble. Ramsauer worked with charges of one or two kilograms of guncotton at depths up to 9 meters, at a place where the total depth of water was 12 meters. The charge was suspended near a submerged iron framework which carried a number of rigid electrodes. Electrolytic currents flowed to each of these electrodes from a single electrode some distance away. When the expanding gas bubble from the explosion reached any particular electrode, that electrode became isolated from the water and the current in the circuit to which it was connected ceased. Measurement of the time of cessation of the current in the circuit of each electrode thus gave a point on the radius-time curve of the bubble. Only the expanding phase of the motion was studied, and the difficulty of supporting electrodes rigidly close to the explosion prevented measurements from being taken at less than about a quarter of the maximum radius.

Ramsauer found the variation of a_{max} with depth and charge of explosive to agree nicely with the prediction $W = \frac{4}{3}\pi\rho_\infty a_{max}^3$ of the simple theory, with $W = 0.41Q$. This is in fair agreement with values of W/Q found in recent work for other high explosives. He also attempted to check the energy equation (5) by using his measured values of $\frac{da}{dt}$ and some calculated

---

[30] C. Ramsauer, Ann. d. Physik 72, 265 (1923)

values of the gas energy G(a); however, his measurements of velocity are not very accurate, and the assumptions from which he obtained the equation of state of the gas may be considerably in error. Plotting the left side of (5) as a function of a he drew the conclusion that about four-fifths of the quantity (Q-W) represented acoustical energy radiated in the stages $a < \frac{a_{max}}{8}$ while one-fifth represented dissipation due to viscosity and thermal conduction in the later stages of the expansion. Very little weight can be given to this, however, because of the uncertainty in both the kinetic and potential energies. Ramsauer also concluded that the temperature of the gas at the end of the expansion was 160° C., so that none of the water formed by the explosion could condense. This conclusion of course rests on the validity of Ramsauer's assumptions regarding the equation of state of the explosion products.

Ramsauer noticed that at maximum size the bubble extended about 10% farther, measured from the initial center of the explosive, in the horizontal direction than in the downward direction. This rising of the gas bubble is to be expected, of course, and is in approximate quantitative agreement with the theory of Section 5 and Appendix 4. Another incidental effect was observed which if real is a little puzzling: a_{max} seemed to be slightly decreased by placing an equal volume of air in the tube which contained the guncotton.

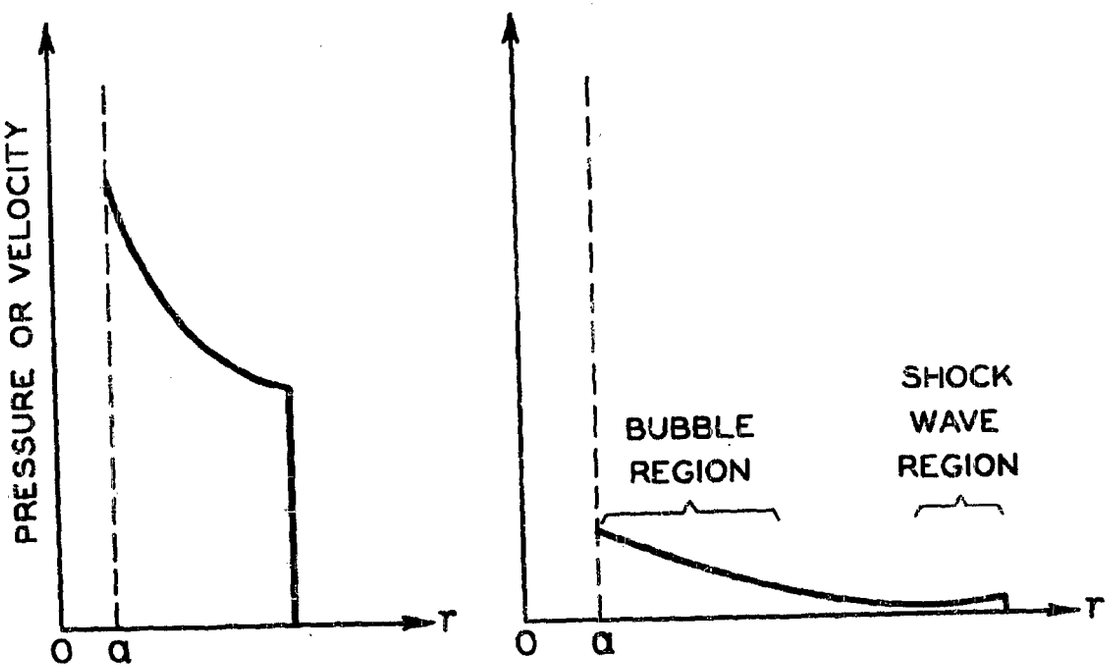

(a) EARLY STAGE (b) LATER STAGE

Fig. 1. Separation of the disturbance produced by an underwater explosion into a bubble region and a shock wave region.

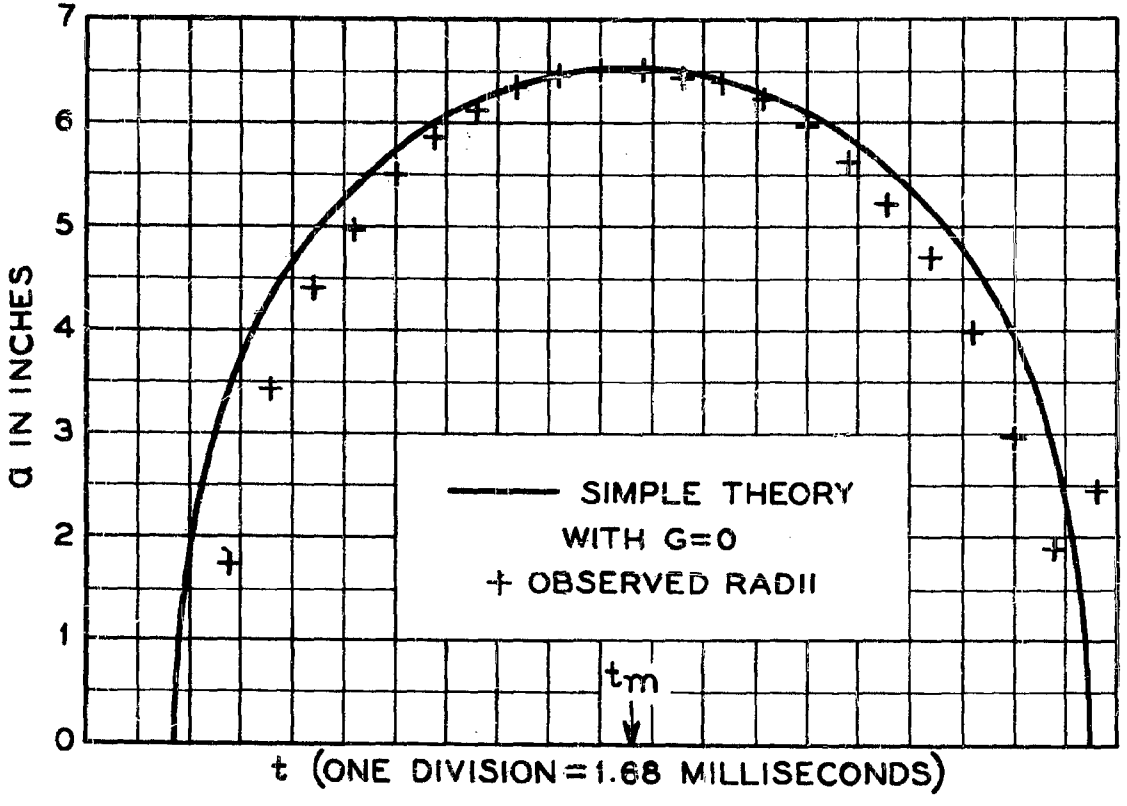

Fig. 2. Observed radius-time curve for the first pulsation of the bubble produced bya detonating cap at one foot depth, and the theoretical curve computed from Eq. (7) of Appendix 1 .

Fig. 3. Contours of constant pressure beneath a ripply surface which is undergoing a normal acceleration.

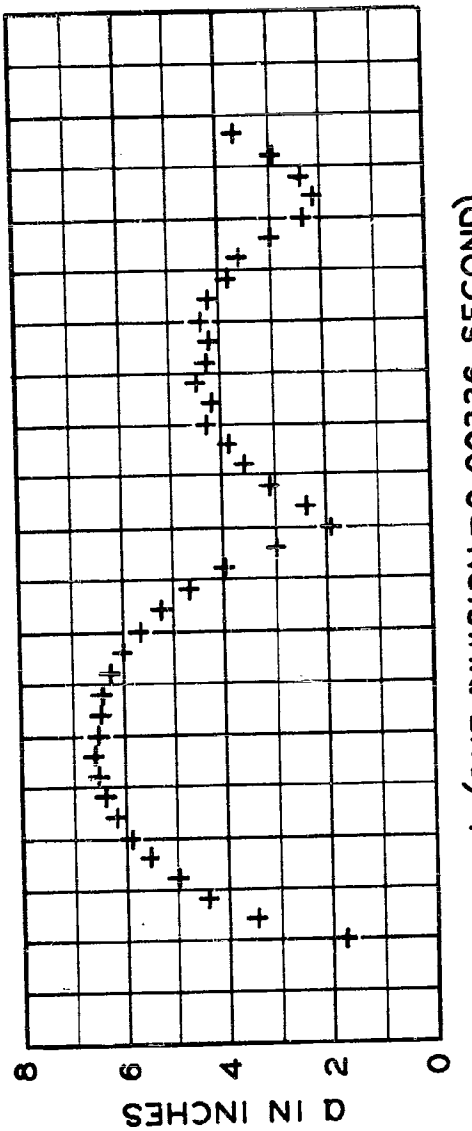

Fig. 4. Radius-time curve for the first two pulsations of the bubble of Fig. 2, showing loss of energy at the first contraction.

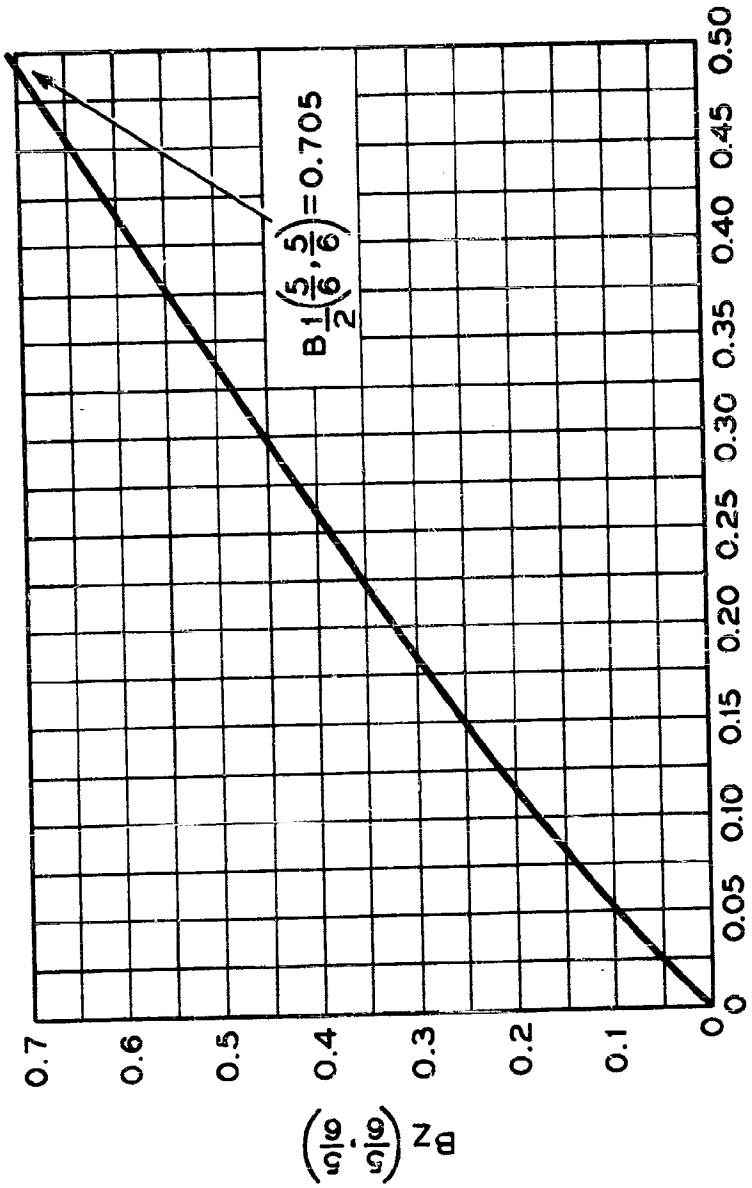

Fig. 5. Plot of the incomplete beta function $B_z\left(\frac{5}{6},\frac{5}{6}\right)$.

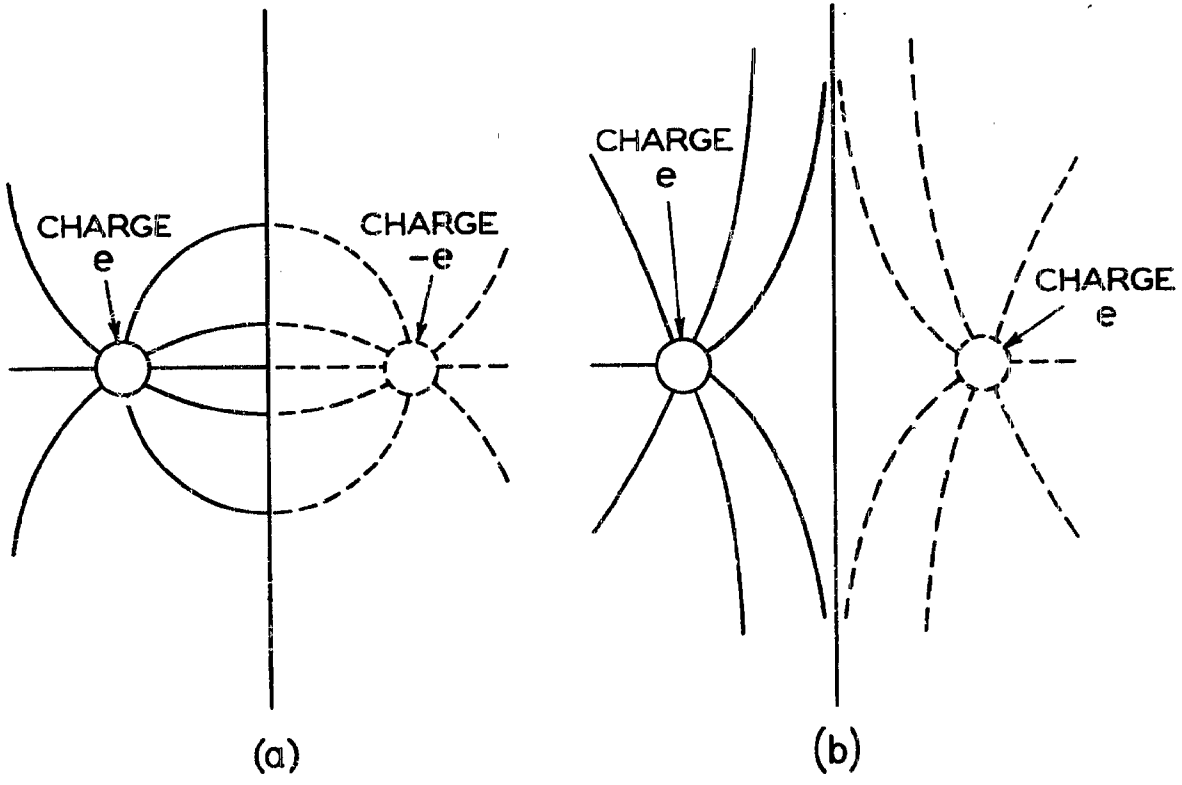

Fig. 6. Electrostatic analogues for:(a) a bubble near a free surface; and (b) a bubble near a rigid surface. The surface is represented in each case by a vertical line. The curved lines represent stream lines in the hydrodynamical case, lines of force in the electrostatic case.

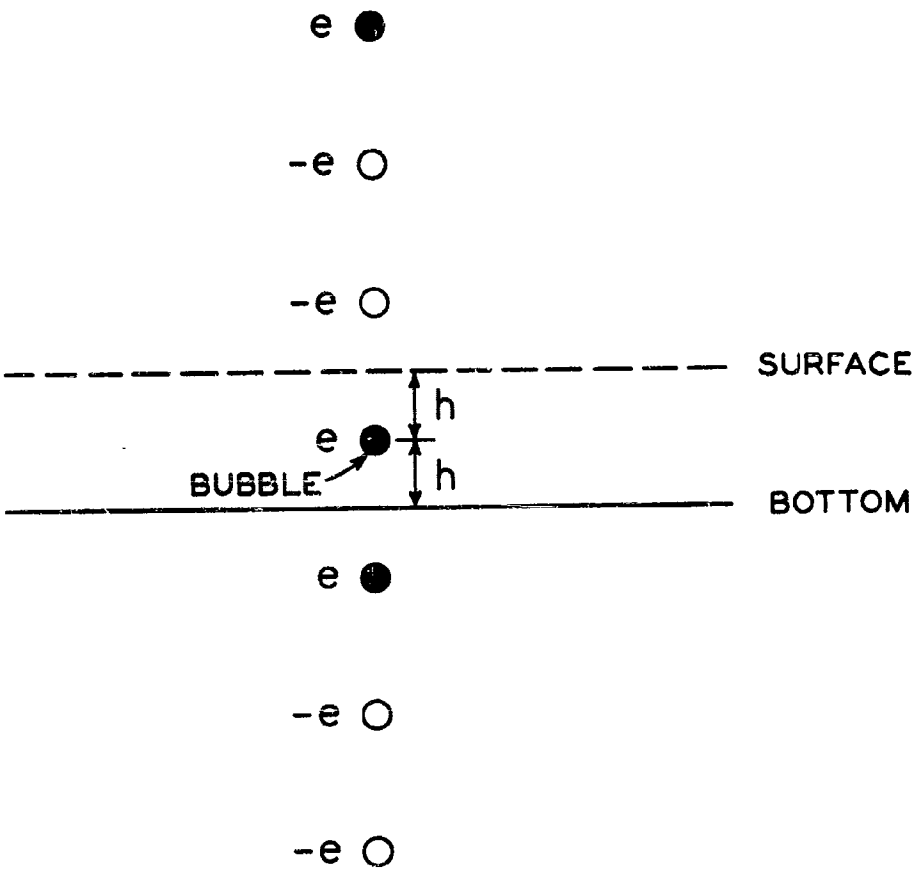

Fig. 7. Part of the infinite series of images required for the calculation of the flow about a bubble placed midway between a free surface and a rigid bottom.

VERTICAL MOTION OF A SPHERICAL BUBBLE AND THE PRESSURE SURROUNDING IT

G. I. Taylor
Cambridge University

British Contribution

August 1942

VERTICAL MOTION OF A SPHERICAL BUBBLE AND THE PRESSURE SURROUNDING IT

G. I. Taylor

August 1942

* * * * * * * * *

Summary.

The upward motion of the spherical hollow which is formed in water by an explosion is discussed on the assumption that the spherical form is preserved. During the expanding stage the buoyancy of the hollow gives a large amount of vertical momentum to the surrounding water. During the contracting stage this momentum is concentrated round a rapidly diminishing volume. An intense concentration of vertical momentum is thus produced in the neighbourhood of the vertical line through the charge. The pressure at points above the charge and near this line rises to considerable values owing to two causes:-

(a) When the hollow is near its greatest contraction at the end of its first oscillation its centre is nearer to points vertically above the seat of the explosion than it was at the time of the explosion (but further from points on the level of the explosion).

(b) The pressure due to the combination of vertical motion and expansion on the second expansion is in certain circumstances large.

For comparison with observation, the maximum displacements to be expected in a rectangular plate 6 feet x 4 feet x 0.173 inches attacked by 4.65 lb. of T.N.T. placed (a) 14 feet below the plate; (b) 14 feet away horizontally are calculated. They are found to be 4.3 and 1.5 inches respectively. The observed displacements were 4.35 and 1.15 inches.

Though complete dynamical similarity is not possible when charges of varying sizes are exploded under water, yet in certain circumstances dynamical similarity should be very nearly attained. It is shown, however, that there are large ranges of depth and charge weight which could not be explored even approximately by model experiments unless the experimental apparatus were so constructed that the atmospherical pressure above the water surface could be reduced.

The radial motion of the water near the seat of an explosion has been studied by many writers. Recently Conyers Herring* has analysed the small change in shape which the expanding spherical hollow suffers owing to the varying hydrostatic pressure in the water due to gravity. He showed that during the period when this effect is small it merely displaces the sphere vertically without changing its shape. This vertical motion may be regarded as being due to the vertical momentum given to the fluid surrounding the spherical hollow by the floating power of the hollow. The momentum associated with a spherical hollow of radius a moving with velocity $-\frac{dz}{dt}$ is $-\frac{1}{2}(\frac{4}{3}\pi\rho a^3)\frac{dz}{dt}$, z being the depth of its centre and ρ the density of water. The rate at which upward momentum is communicated by the floating power of the hollow is $\frac{4}{3}\pi\rho a^3 g$, so that

$$a^3 g = -\tfrac{1}{2}\frac{d}{dt}\left(a^3\frac{dz}{dt}\right)$$

$$\text{or} \qquad -\frac{dz}{dt} = \frac{2g}{a^3}\int a^3 dt \qquad (1)$$

Starting with a very small at t = 0, the time of the explosion, it will be seen that during the early stages while a is increasing rapidly $-dz/dt$ is less than $2gt$, i.e. the hollow moves upwards more slowly than it would if a were constant. On the other hand, during the period while the hollow is large $\int a^3 dt$ acquires a considerable magnitude so that when the bubble contracts,

and .....

and a becomes small, $\int a^3 dt$ becomes much larger than $a^3 t$ so that $-dz/dt$ becomes large compared with $2gt$. Thus the centre of the bubble will be displaced upwards at a rate which rapidly increases as a diminishes, in fact the analysis by which Conyers Herring showed that the hollow is displaced upwards rapidly ceases to apply. Herring describes this rapid increase in displacement as an "illustration of the general instability of the contracting stage".

Though instability would probably prevent the hollow from remaining approximately spherical during the contracting stage, yet photographs of the bubble from the explosion of a detonator by Edgerton[4] have given measurable radii over rather more than 2 complete pulsations, so that the hollow appears to remain sufficiently coherent for this time to pulsate as though it were spherical.

This experimental result encourages one to pursue the subject further and to calculate what the motion would be if the bubble were constrained to be spherical by some kind of constraint which absorbs no energy and no inertia. (1) is still applicable. The other equation which must be satisfied is that which ensures constancy of energy. The kinetic energy of the water surrounding a sphere of radius a is

$$2\pi\rho a^3 \left[\frac{da}{dt}\right]^2 + \frac{1}{3}\pi\rho a^3 \left[\frac{dz}{dt}\right]^2,$$

(no terms containing the product $\frac{da}{dt} \cdot \frac{dz}{dt}$ appear)

so that the equation of energy is

$$\frac{4}{3}\pi\rho a^3 (g z) + 2\pi\rho a^3 \left[\frac{da}{dt}\right]^2 + \frac{1}{3}\pi\rho a^3 \left[\frac{dz}{dt}\right]^2 = W - G(a) \qquad (2)$$

where $g\rho z$ is the pressure at the level z so that z is measured from a point 33 feet above the sea surface, W is the total energy associated with the motion and G(a) is the work which the gas would do on the walls of the bubble if expanded adiabatically from radius a to infinity.

Reduction to non-dimensional form.

For convenience of calculation (2) may be reduced to non-dimensional form by means of the length L which is defined by

$$L = \left\{\frac{W}{g\rho}\right\}^{\frac{1}{3}} \qquad (3)$$

Setting $a = a'L$, $z = z'L$ $\qquad t = t'\sqrt{\frac{L}{g}}$ $\qquad (4)$

a', z' and t' are non-dimensional and (2) and (1) can be written

$$\left[\frac{da'}{dt'}\right]^2 = \frac{1}{2\pi a'^3}\left\{1 - \frac{G(a)}{W}\right\} - \frac{1}{6}\left[\frac{dz'}{dt'}\right]^2 - \frac{2}{3}z' \qquad (5)$$

$$-\frac{dz'}{dt'} = \frac{2}{a'^3}\int_0^{t'} a'^3 dt' \qquad (6)$$

It will be seen that if G(a) could be neglected compared with W, (5) would be non-dimensional so that the complete range of solutions of (5) and (6) would only involve the one variable parameter which is introduced during integration, namely z'_0, the value of z' at the level of the explosion. For this reason it is necessary to estimate the value of $G(a)/W$.

Value of G(a)/W.

The ratio G(a)/W can be calculated from the adiabatic relationship for the gaseous products of the explosion. Using the adiabatic relationship calculated by H. Jones and Miller for T.N.T. it is found that below a pressure of about 300 atmospheres the gases expand according to the law

$$pv^{1.25} = \text{constant} = (1.725 \times 10^6)(839.3)^{1.25} = 7.830 \times 10^9 \qquad (7)$$

where .....

where v is the volume of 1 gramme of the products of combustion.

By definition

$$G(a) = M\int_v^\infty p\,dv = M\frac{pv}{\gamma-1} \quad (\text{if } pv^\gamma = \text{constant})$$

$$= \frac{Mpv}{0.25} = M\left\{\frac{7.83\times10^9}{0.25}\right\}v^{-0.25} \qquad (8)$$

where M is the mass of explosive.

Since $Mv = \frac{4}{3}\pi a^3$ (8) may be written in the form

$$G(a) = 2.189\times10^{10}\,M\left[\frac{M}{a^3}\right]^{0.25} \qquad (9)$$

The measurements of the period of the first vibration of bubbles formed by T.N.T. explosions show that $W = 0.5Q$ approximately, where Q is the total energy released, which for T.N.T. may be taken as 880 cal. per gam. Thus

$$W = M(0.5\times880\times4.2\times10^7) = 1.85\times10^{10}M \qquad (10)$$

Thus $$\frac{G(a)}{W} = 1.183\left[\frac{M}{a^3}\right]^{0.25} \qquad (11)$$

The corresponding formula for p is $p = 1.308\times10^9\left[\frac{M}{a^3}\right]^{1.25}$ dynes/sq.cm. (12)

G(a)/W may be expressed in terms of p only; thus eliminating M/a^3 from (11) and (12)

$$\frac{G(a)}{W} = 1.183\left\{\frac{p}{1.308\times10^9}\right\}^{1/5} = 0.0177\,p^{1/5}$$ where p is expressed in dynes/sq.cm.

or $$\frac{G(a)}{W} = 0.281\,p^{1/5}$$ where p is expressed in atmospheres. (13)

The exponent 1/5 is merely the value of $\frac{\gamma-1}{\gamma}$ when $\gamma = 1.25$.

Conditions under which G(a)/W may be neglected.

It is clear from (13) that it is only when p is considerably less than atmospheric pressure that G(a)/W could be neglected. When the bubble is formed at moderate depths the pressure is less than atmospheric pressure over a great part of the period of oscillation. It is during this period that the greater part of the upward momentum associated with the rise of the bubble is acquired. It is useful, therefore, to solve (5) neglecting G(a)/W when one is concerned with the vertical motion. It is necessary, however, to remember the limitations involved in making this simplification. The results will certainly be very inaccurate near the point of minimum radius, but they serve to bring out certain points which are important in considering whether it is possible to make model experiments to explore the motion of the bubble.

Calculation neglecting G(a)/W.

For purposes of calculation (5) may conveniently be written in the form

$$\left[\frac{da'}{dt'}\right]^2 = \frac{1}{2\pi a'^3} - \frac{1}{6}\left[\frac{dz'}{dt'}\right]^2 - \frac{2}{3}(z'-z'_0) - \frac{2}{3}z'_0 \qquad (14)$$

where z'_0 is the value of z' at the depth of the explosion. This equation, together with (6), can be integrated step-by-step for any given value of z'_0. In the early states when the bubble

is .....

is small the first term in (14) is much greater than the others so that (14) may be integrated approximately giving

$$t' = \frac{2}{5}\sqrt{2\pi}\,a'^{5/2} = 1.0025\,a'^{5/2} \qquad (15)$$

Substituting for a' (6) becomes

$$-\frac{dz'}{dt'} = \frac{2}{t'^{6/5}}\int_0^{t'} t'^{6/5}\,dt' = \frac{10}{11}\,t' \qquad (16)$$

which may be integrated to

$$z'_0 - z' = \frac{5}{11}\,t'^2_1 \qquad (17)$$

$z'_0 = 2.0$

Using (16) and (17) up to t' = 0 05 and subsequently solving (14) and (6), step-by-step, the results for $z'_0 = 2.0$ are shown in Figure 1. The radius of the bubble, the height of its centre and the level of its highest point are shown.

It will be seen that the bubble at first rises slowly but that its centre jumps rapidly through a height about equal to twice its maximum radius during the short period while its radius is only half the maximum radius.

The minimum radius is given by a' = 0.211. This seems strange, because if the vertical motion is neglected the approximation in which G(a)/W is also neglected implies that the bubble collapses completely into a point; there is, in fact, no gas pressure to prevent this collapse. When the vertical motion is taken into account the collapse is (theoretically) prevented by the fact that at a certain minimum radius the whole energy is concentrated in the flow due to the rapid vertical motion of the spherical hollow.

Similarity on varying scales.

Since Figure 1 is non-dimensional it is possible to assign to it any desired linear scale. The scale is, in fact, determined only by W and for any given explosive this appears to be proportional to M. Thus for T.N.T. the unit length is, from (3) and (10),

$$L = \left[\frac{W}{g\rho}\right]^{\frac{1}{3}} = \left[\frac{1.85 \times 10^{10}}{g\rho}\right]^{\frac{1}{3}} M^{\frac{1}{3}} = 65.91\,M^{\frac{1}{3}} \qquad (18)$$

when M is expressed in gm. of explosive and L is in cm.

The depth below a point 33 feet above the sea is in this case 2L. Thus Figure 1 represents a single series of explosions in which $\left\{\frac{\text{depth of water + 33 feet}}{(\text{charge diameter})^{\frac{1}{3}}}\right\}$ is fixed.

A set of scales of depth and the corresponding positions of the sea surface in relation to the explosive are shown at the side of Figure 1. Scales are given for M = 2200 lb., 300 lb., 10 lb., and 1 oz. It will be seen that the level of the sea surface is well clear of the bubble through the greater part of the motion for M = 2200 lb. at 103 feet and 300 lb. at 50 feet depth and that these two explosions might therefore be expected to give similar pressure distributions. The 30 lb. charge at 14 feet would give a similar bubble during the greater part of its expansion, but near its greatest expansion it would be above the surface and similarity would break down. It is evidently impossible to place a charge of less than 30 lb. in water so as to give a regime which is similar to that produced by the two larger charges. On the other hand, if it were possible to reduce the atmospheric pressure to less than 33 feet of water, small-scale models could be made; moreover by using the correct pressure a model experiment could be carried out which would represent either of the large explosions. Thus if a 1 oz. charge were exploded at a depth of 10.0 - 2.4 = 7.6 feet below the surface of water and the air pressure above the water surface were reduced to that of 2.4 feet of water, the resulting bubble would (in the present approximation) be

similar .....

similar to that of 2200 lb. exploding at 103 feet. Similarly a 1 oz. charge exploding at a depth of 10.0 - 4.0 = 6.0 feet below the surface would be similar to a 300 lb. charge at 50 feet if the atmospheric pressure above the 1 oz. charge were reduced to 4.0 feet of water.

Conditions when the bubble is near its point of greatest contraction.

The approximation in which G(a) is neglected in comparison with W does not give useful results near the point of minimum radius. To investigate phenomena which depend on conditions near this point it is necessary to use (5) instead of (14). The calculation must then refer to one charge and one depth only, though it is still convenient to use the non-dimensional form (5). As an example a charge of 4.65 lb. exploded at depth of 20 feet is chosen, because in an experiment made under these conditions effects were produced which might be attributed to the effect of gravity. In this case the value of L is 445 cm. or 14.6 feet, and $z'_0 = \frac{33 + 20}{14.6} = 3.62$, and $t' = 1.47t$ when t is expressed in seconds.

For convenience in calculation (11) may be expressed in terms of a' and L by the formula

$$\frac{G(a)}{W} = 0.0177\, L^{0.25}\, a'^{-0.75} \qquad (19)$$

and when L = 445 cm., this gives

$$\frac{G(a)}{W} = 0.0815\, a'^{-0.75} \qquad (20)$$

Figure 2 shows the radius and depth of the centre at time t after the explosion. In the experiment above a box containing an air-backed plate was placed at a depth of 6 feet, 14 feet above the charge. This is shown in Figure 2.

Effect of vertical motion on maximum pressure.

When the effect of compressibility and of vertical motion is neglected the maximum pressure in the bubble occurs when G(a) = W and from (11) this will be found to correspond with

$$\frac{M}{a^3} = (1.183)^{-4} = 0.51 \quad \text{and}$$

$$p = 1.308 \times 10^9\, (0.51)^{1.25} = 5.63 \times 10^8 = 563 \text{ atmos.} \qquad (21)$$

when $M = 4.65$ lb. $= 2100$ gm.

$$a^3 = \frac{M}{0.51} = 4130 \quad \text{so that } a = 16.0 \text{ cm.}$$

and $$a' = \frac{16.0}{445} = 0.036 \qquad (22)$$

It will be seen that the effect of the vertical motion is to prevent the high pressure associated with this very small radius from being formed. Thus in Figure 2 the minimum radius will be seen to be a' = 0.120, which is 3.3 times as great as that which would occur in the absence of gravity. The pressure corresponding with a = (0.120)(445) = 53.4 cm. is only 5.0 atmos., so that this effect on gravity is to reduce the maximum pressure in this case in the ratio 100:1.

The amount of energy radiated in the form of a compressibility wave during the period of greatest compression depends on the p_{max}, the greatest pressure. Conyers Herring and Willis have developed formulae giving for the proportion of W which is radiated the formula

$$F = \text{Fraction radiated} = A\sqrt{\frac{p_{max}}{\rho}}\Big/ c \qquad (23)$$

where A depends only on γ and c is the velocity of sound in water. For $\gamma = 1.25$, A = 1.87, so that (23) would give as the fraction radiated

$$F = \frac{1.87\sqrt{5.63 \times 10^8}}{1.44 \times 10^5} = 0.31 \qquad (24)$$

If .....

if the effect of gravity is neglected,

$$\text{or} \qquad F = \frac{1.87\sqrt{5.9 \times 10^6}}{1.44 \times 10^5} = 0.03 \qquad (25)$$

according to the calculations illustrated in Figure 2.

If the same charge had been exploded at a greater depth the bubble would not have expanded to so great a radius; it would therefore not have risen so much and F would have been greater. It would be interesting to repeat the calculation for the same charge for a range of depths, i.e. of values of z'_0.

Pressure distribution.

The pressure in an incompressible fluid due to the motion of an expanding or contracting sphere when the centre moves with velocity U in a straight line is obtained from Bernoulli's equation. The velocity potential ϕ is

$$\phi = \frac{a^2\dot{a}}{r} + \frac{1}{2}\frac{Ua^3}{r^2}\cos\theta$$

where θ is the angle between the radius vector r and the direction of motion, $\dot{a}$ written for da/dt. ϕ referred to axes which move with velocity U so that the pressure is given by

$$\frac{p}{\rho} - gz = \frac{\partial\phi}{\partial t} - U\frac{\partial\phi}{\partial x} - \frac{1}{2}(u^2 + v^2) \qquad (26)$$

where u and v are the velocity components referred to fixed axes and $\partial\phi/\partial t$ is the time rate of variation of ϕ at a point which is fixed relative to the centre of the sphere and therefore moves with velocity U. $\partial\phi/\partial x$ is the space rate of change of ϕ in the direction of U. The velocity components u and v are radial and tangential, so that

$$u = -\frac{\partial\phi}{\partial r} = \frac{a^2\dot{a}}{r^2} + \frac{Ua^3}{r^3}\cos\theta \qquad (27)$$

$$v = -\frac{1}{r}\frac{\partial\phi}{\partial\theta} = \frac{1}{2}\frac{a^3}{r^3}U\sin\theta \qquad (28)$$

and $$-\frac{\partial\phi}{\partial x} = u\cos\theta - v\sin\theta = \frac{a^2\dot{a}}{r^2}\cos\theta + \frac{Ua^3}{r^3}\left(\cos^2\theta - \tfrac{1}{2}\sin^2\theta\right)$$

The complete expression for pressure is therefore

$$\frac{p}{\rho} - gz = \frac{2a\dot{a}^2 + a^2\ddot{a}}{r} + \frac{1}{2}\frac{a^2}{r^2}(a\dot{U} + 5\dot{a}U)\cos\theta + \frac{a^3}{r^3}U^2\left(\cos^2\theta - \tfrac{1}{2}\sin^2\theta\right)$$
$$- \left[\frac{1}{2}\frac{a^4}{r^4}\dot{a}^2 + \frac{a^5}{r^5}\dot{a}U\cos\theta + \frac{1}{2}\frac{a^6}{r^6}U^2\left(\cos^2\theta + \tfrac{1}{4}\sin^2\theta\right)\right] \qquad (29)$$

This may be expressed in terms of the non-dimensional variables defined in (3) and (4).

$$\frac{p}{g\rho L} - z' = \frac{2a'\dot{a}'^2 + a'^2\ddot{a}'}{r'} + \frac{1}{2}\frac{a'^2}{r'^2}(a'\dot{U}' + 5\dot{a}'U')\cos\theta + \frac{a'^3U'^2}{r'^3}\left(\cos\theta - \tfrac{1}{2}\sin^2\theta\right)$$
$$- \left[\frac{1}{2}\left(\frac{a'}{r'}\right)^4\dot{a}'^2 + \left(\frac{a'}{r'}\right)^5\dot{a}'U'\cos\theta + \frac{1}{2}\left(\frac{a'}{r'}\right)^6U'^2\left(\cos^2\theta + \tfrac{1}{4}\sin^2\theta\right)\right] \qquad (30)$$

where $U' = -\frac{dz'}{dt'} = \frac{U}{\sqrt{gL}}$, $\dot{a}'$ is $\frac{da'}{dt'}$, and $\dot{U}'$ is $\frac{dU'}{dt'}$ or $-\frac{d^2z'}{dt'^2}$.

(30) is now expressed in a form suitable for computation.

Pressure .....

Pressure at fixed point vertically above an explosion.

In some experiments carried out recently, in which a rectangular air-backed steel plate 0.173 inches thick and 6 feet x 4 feet sides was used, it was found that a charge of 4.65 lb. fired at a distance of 14 feet vertically below the plate (which was then horizontal) produced a displacement whose maximum value was 4.35 inches. A similar plate held vertically was dished so that the maximum displacement was only 1.15 inches when the charge was fired at the same distance (14 feet) but in the same horizontal plane as the plate. This very large difference cannot be accounted for by considerations based on the pressure waves which have been measured by piezo-electric gauges, for no great differences have been detected in the pressure waves at points over a sphere centred on the explosive.

It was to account for these experimental results that the present investigation was made and the values of charge weight and depth used were taken to correspond with those of the experiment. The expression (30) for calculating pressure contains some quantities which were not needed in calculating the radius and vertical velocity of the bubble. The accelerations "$\ddot{a}$" and $\dot{U}'$ have to be calculated. This was done graphically, plotting the values of $\ddot{a}'$ and $\dot{U}'$ against t'. The initial (non-dimensional) height of the plate above the charge was 0.97 (i.e. 14 feet/L). At each value of t' values of a', $\dot{a}'$, $\ddot{a}'$, U', $\dot{U}'$ and r' (= 0.97 - a') were tabulated for a range of values near the time when the bubble was reaching its minimum diameter (i.e. at t' = 0.408).

Setting these in the expression (30) the following values were calculated:-

TABLE 1.

t'	0.380	0.400	0.405	0.407 to 0.409 (mean value)	0.411	0.416	0.426	0.432	0.440
t (seconds)	0.268	0.272	0.275		0.280	0.283	0.290	0.293	0.299
$p_{(plate)}$ (atmospheres) (i.e. 10^6 dynes/ sq.cm.)	0.7	1.8	3.4	12	10.5	9.1	6.2	4.1	2.6

These values are shown graphically in Figure 3.

Comparison with pressure during the early stages of the expansion of the bubble.

The maximum pressure in the pressure wave is known from piezo gauge measurements. An empirical expression representing approximately by results of these pressure measurements is

$$p = p_0 e^{-nt}$$

where

$$p_0 = 4.6 \times 10^9 M^{1/3}/r$$

$$n = 7.5 \times 10^4 M^{-1/3} \qquad (31)$$

p_0 being expressed in dynes/sq.cm., M mass in gm. of T.N.T., r distance in cm. from the charge. For a charge of 4.65 lb. $n = 5.86 \times 10^3$ seconds and $p_0 = 138.5 \times 10^6 = 138$ atmos. at a distance r = 14 feet = 426 cm. This pressure is very much larger than the maximum pressure calculated for the later pressure rise illustrated in Figure 3, but its duration is so small that it is difficult to show it in a diagram of the scale of Figure 3. The attempt is made, however, on the left hand side of the figure. The pressure falls to 10 atmos. in time given by $e^{-5.8 \times 10^3 t} = \frac{10}{138} = .072$, i.e. in time 0.5 milliseconds. If this exponential fall in pressure were continued it would fall to $\frac{1}{10}$ of an atmosphere in a little over a millisecond. In fact this does not happen, the pressure

falls .....

falls rapidly till it is, say $\frac{1}{10}$th or $\frac{1}{20}$th of its maximum value and then falls comparatively very slowly. This gradual decay of pressure is shown in most piezo gauge records and was particularly noticeable in Hillar's early measurements. It must evidently be associated with the motion of the water round the expanding bubble and can be treated as associated with radial flow of an incompressible liquid.

In the early stages when the bubble has not risen appreciably under the action of gravity, the formulae derived by neglecting $\dot{u}$, $\dot{U}$ and the variation in z in (5) may be used. If $G(a)/W$ is neglected, i.e. if it is assumed that the whole kinetic energy is given to the bubble at the instant of the explosion and the work done by the subsequent expansion of the gases is neglected, the equations are then those used by Rayleigh in discussing the collapse of a spherical cavity and by Ramsauer and others. In the early stages of such an expansion, i.e. in a time after the explosion which is small compared with the period of the first expansion and contraction of the bubble, the term $2/3\ z'$ in (5) may be neglected compared with $(da'/dt')^2$. (5) then assumes the form $a'^{3/2}\dot{a} = 1/\sqrt{2\pi}$. Inserting this value in (30) the leading term (i.e. the term which is greater than all the others except close to the bubble) is

$$\frac{p}{g\rho L} - z' = \frac{1}{r'}\frac{d}{dt'}(a'^2\dot{a}') = \frac{1}{r'}\frac{d}{dt'}\left[\frac{a'^{1/2}}{\sqrt{2\pi}}\right] = \frac{1}{2\sqrt{2\pi}}\frac{a'^{-1/2}\dot{a}'}{r'} = \frac{1}{4\pi r' a'^2} \qquad (32)$$

In terms of t' this becomes (see (15))

$$\frac{p}{g\rho L} - z' = \frac{1}{4\pi r'}\left[\frac{2\sqrt{2\pi}}{5}\right]^{4/5} t'^{-4/5} = 0.0798\, t'^{-4/5} r'^{-1} \qquad (33)$$

Restoring the dimensions (33) becomes

$$p - p_z = 0.0798\, g^{3/5} \rho L^{12/5} t^{-4/5} r^{-1} \qquad (34)$$

where p_z is the pressure at the depth of the explosion.

Putting $g = 981$, $g^{3/5} = 62.37$, $\rho = 1$, (34) becomes

$$p - p_z = 4.98\, L^{12/5} t^{-4/5} r^{-1} \qquad (35)$$

In the case corresponding with W = 4.66 lb. T.N.T. where L = 445 cm., $L^{12/5} = 2.265 \times 10^6$ so that (35) becomes

$$p - p_z = 1.131 \times 10^7\, t^{-4/5} r^{-1} \qquad (36)$$

At r = 14 feet = 426 cm. this is $p - p_z = 2.655 \times 10^4\, t^{-4/5}$. At time t = 0.005 seconds $t^{-4/5} = 69.5$ so that $p - p_z = 1.85 \times 10^6 = 1.85$ atmos.; at time t = 0.010, $p - p_z = 1.07$ atmos.

A better approximation is found by extending the solution of (5) back step-by-step towards the time when the bubble is small, using the expression (11) for taking account of the gas pressure. The pressure is then given by (30) but it is found that the vertical motion may be neglected so that the simplified expression

$$\frac{p}{\rho} - gz = \frac{2a\dot{a}^2 + a^2\ddot{a}}{r} - \frac{1}{2}\frac{a^4\dot{a}^2}{r^4} \qquad (37)$$

may be used. When this calculation is carried out it is found that the minimum radius a_0 is attained at a time which is actually earlier than the origin of time used in the step-by-step calculations already described. This is because in starting the calculations the conditions at the beginning of the explosion were not required, all that was required was a knowledge of the energy W. The way in which this energy was communicated to the water to give it radial motion was immaterial so far as the motion during the first contraction was concerned. When, however, it is desired to calculate the pressure round the bubble in its early stages the exact instant of explosion has to be determined, because otherwise it is not possible to get any idea of the way in which the shock wave pulse is related to the subsequent pressure distribution due to radial expansion. This question is a difficult one in any case. If the water were truly incompressible the pressure would jump to its maximum value instantaneously at the moment of explosion. Actually the compressibility delays the first rise in

pressure .....

pressure at distance r from the explosion till a time which is approximately r/c seconds after the explosion, c being the velocity of sound in water. Till some better method is discovered a fairly good approximation can be made by imagining that at time r/c after the explosion the pressure pulse arrives at radius r and that the pressure jumps to p_0 and then falls according to the empirical law (31) till it reaches the pressure which would exist at that time and radius if the water had been incompressible. The subsequent pressure is then calculated by the methods described above.

This proposed method is shown in Figure 3, where the pressure pulse and the subsequent slow fall due to the radial flow are both shown on the correct scale for a radius r = 14 feet from the charge. It will be seen that the two curves cross. It is assumed that the actual pressure distribution is simply determined by whichever is the greater of the two. This method, though necessarily inaccurate near the time when the two curves cut, is possibly not far from the truth over the main part of the range. The virtual parts of the curves where the shock wave pressure is small compared with that due to the radial flow and vice versa are shown dotted in Figure 3.

The results of using the step-by-step process and calculating pressure from (30) are shown in Figure 3. This calculation must be regarded as provisional and liable to modification when better methods have been developed. It is included here in order to show the order of magnitude of the pressures to be expected at 14 feet from the 4.65 lb. charge after the pressure pulse has passed.

Effect of calculated pressure on plate rigidly held at its edges.

Pressure wave.

The effect of the pressure wave of the form $p = p_0 e^{-nt}$ on a steel plate which is free or elastically supported has been discussed in my note "The pressure and impulse of submarine explosion waves on plates". It depends on a non-dimensional number $\epsilon = \rho c/mn$, where m is the mass of the plate per sq.cm., c the velocity of sound in water, ρ the density of water. For plates of thickness 0.173 inches $m = .173 \times 2.54 \times 7.8 = 3.43$. For a charge of 4.65 lb. T.N.T. $n = 5.86 \times 10^{-3}$ and $c = 1.44 \times 10^5$ cm./second so that $\epsilon = 7.2$.

In the above mentioned report the case where water will not sustain tension is worked out. It is found that with the above values of ϵ and n the plate will part from the water after time

$$t = \frac{1}{n(\epsilon - 1)} \ln \epsilon = 5.5 \times 10^{-5} \text{ seconds} \qquad (38)$$

and that its velocity will then be

$$\dot{\xi} = \frac{2p_0}{mn} \epsilon^{-\frac{\epsilon}{\epsilon - 1}} = \frac{2(1.385 \times 10^8)}{(3.43)(5.86 \times 10^{-3})} \; 7.2^{-1.161} = 1.38 \times 10^3 \text{ cm./second} \qquad (39)$$

The kinetic energy per c.c. of the plate is then

$$\tfrac{1}{2} \rho_{\text{steel}} \dot{\xi}^2 = \tfrac{1}{2} (7.83)(1.38)^2 \times 10^6 = 7.45 \times 10^6 \text{ ergs/c.c.} \qquad (40)$$

If the water can sustain some tension at the surface of the plate this energy would be reduced. If the water could sustain internal tension though not at the surface of the plate, no further energy would be communicated to the plate. If, however, the water could sustain no internal tension, drops would be projected from the water on to the plate and further energy might be communicated to it.

Dishing of plate.

The time during which the high pressure (initially 2 x 138.5 = 277 atmos.) is acting on the plate is short compared with the time taken by the plate to come to rest in its displaced position under the action of plastic and elastic stresses. For this reason the dynamics of the plate can be treated separately from that of the water on the assumption that a velocity of 1.38×10^3 cm./second is instantaneously given to the plate. In an analysis in which I hope to publish shortly the dishing

of a .....

of a rectangular plastic plate under uniform pressure, p, acting on one side, is studied. Though the distribution of the plastic strain in the plane of the plate is not uniform the plate behaves, so far as displacement normal to the surface is concerned, like a soap film or membrane with uniform tension. This uniform tension is related to the yield stress measured in a tensile test by a factor which differs according to whether v. Mises' or Mohr's theory of plasticity is used and varies slightly with the ratio of length to breadth of the plate, but with a plate for which length/breadth = 3/2 v. Mises' theory gives a result which is 1.8 per cent too small and Mohr's 4.8 per cent too big as compared with a rough theory which simply assumes that the plate behaves like a membrane stretched to uniform tension Pd in all directions, where P is the yield point of the steel and d the thickness of the plate.

Using this theory for a plate whose dimensions are 2b x 4/3b (b is 3 feet in the particular plate to which we are now applying the analysis) I find the following formulae:-

$$\text{Maximum displacement} \quad h = 0.179 \frac{pb^2}{Pd} \tag{41}$$

$$\text{Mean displacement} \quad \bar{y} = 0.0870 \frac{pb^2}{Pd} \tag{42}$$

$$\text{so that} \quad \bar{y}/h = 0.485 \tag{43}$$

The energy absorbed by the plate during its displacement is

$$E_p = [\ 3.76\ P(\bar{y})^2\ d/b^2\ ] \qquad \text{(area of plate)}$$

so that work done on unit volume of the material of the plate is

$$W_p = 5.76\ \bar{y}^2\ P/b^2 \tag{44}$$

Time taken for displacement to reach maximum.

The vibrations of a membrane stretched with tension Pd on a rectangular frame of dimensions $2b_1$ and $2b_2$ have been studied by Rayleigh who showed that the period of the fundamental is

$$4\sqrt{\frac{\rho_s}{P}}\sqrt{\frac{b_1^2\ b_2^2}{b_1^2 + b_2^2}}$$

where ρs is the density of the membrane. A plastic sheet is like a membrane during the time when it reaches its maximum displacement it only recovers by the amount of elastic recovery which is in the case here considered small compared with the plastic displacement. Thus a possible movement of a plastic sheet is identical with the first $\frac{1}{4}$-period of the analogous elastic membrane. Thus if the plastic sheet is given initially the normal velocity distribution corresponding with the fundamental period it will come to rest in time

$$\tau = \sqrt{\frac{\rho_s}{P}\left[\frac{b_1^2 + b_2^2}{b_1^2\ b_1^2}\right]} \tag{45}$$

In the case of a plate 6 feet x 4 feet and density 7.8 this time of displacement τ is

$$\left.\begin{aligned} \tau &= 2.07 \times 10^{-3} \text{ seconds} \quad \text{if P is 30 tons/square inch} \\ \text{or} \quad \tau &= 2.54 \times 10^{-3} \text{ seconds} \quad \text{if P is 20 tons/square inch} \end{aligned}\right\} \tag{46}$$

This time τ is marked on Figure 3 so that the relationship between it and the durations of the pressures may be understood. It will be seen that τ is very long compared with the duration of the pressure wave but that the duration of the long continued pressure associated with the expansion and vertical motion of the bubble is longer than τ.

This is convenient for it necessarily implies that it is justifiable to use the method of the report "The pressure and impulse of submarine explosion waves on plates" in discussing the

displacement .....

displacement due to the pressure wave. The pressures due to the succeeding bubble expansion can, so far as their effect on the plate is concerned, probably be considered as though applied statically, though this is not quite certain because the pressure due to the first contraction of the bubble does rise in time less than τ.

Comparison of calculated and observed displacements.

The average energy absorbed by the plate per unit volume must be equal to the average kinetic energy per unit volume given to it by the pressure wave. From (44), (43) and (40) therefore,

$$5.76\ (0.485)^2\ h^2P/b^2 = 7.45 \times 10^6 \text{ ergs/c.c.}$$

Using P = 20 tons/square inch = 3.09×10^9 dynes/sq.cm. and b = 3 feet = 91.4 cm., I find

$$h^2 = 14.6 \text{ sq.cm.} \quad \text{or} \quad h = 3.8 \text{ cm.} = 1.5 \text{ m.} \tag{47}$$

The observed value for the plate in the experiment was 1.15 inches and for a similar plate but with R.D.X./T.N.T. as explosive it was 1.41 inches (48)

In the case of these two experiments the plate was set vertically with the explosive at the same level. The bubble might be expected to break surface before again contracting in both cases so that the subsequent pressure due to the contraction and second expansion would not be expected to appear in any case, but even if the plate and explosive were at such a depth that it would occur, it would not produce an effect comparable with that which occurs between t = 0.275 seconds and t = 0.30 seconds when the plate is placed horizontally 14 feet above the explosive.

The effect of a static pressure applied to the air-backed plate is according to (41) to produce a maximum displacement

$$h = 0.179\ \frac{pb^2}{Pd} = \frac{0.179(36 \times 2.54)^2 \rho}{20(1.54 \times 10^9)(0.173 \times 2.54)} = 1.104 \times 10^{-6}\ \rho \text{ cm.}$$

where P is taken as 20 tons/square inch and d = 0.173 inches. Thus the plate would be dished 1.104 cm. per atmos. of applied pressure.

Since the plate has already been dished to 3.8 cm. by the pressure wave, it will be seen from Figure 3 that the pressure due to the kinetic wave which follows immediately after the pressure wave and which has a maximum pressure of about 2 atmos. cannot increase the dishing and is therefore ineffective in doing further damage to the plate.

Plates, which were placed in a horizontal position 14 feet above the charge, were, according to the present analysis, subjected to a long continued pressure which was calculated to begin at about t = 0.275 seconds, rise rapidly to a sharp peak, drop to about 11 atmos. and then fall off gradually till at about t = 0.30 or 0.31 seconds it is again only one or two atmospheres.

The conditions determining the thickness and intensity of the pulse at t = 0.278 seconds (when the bubble reaches its minimum value) are not likely to be in fact as they are described in the theory, because the bubble in collapsing will probably be far from spherical. It may well be, however, that the large and long-continued pressure which occurs between t = 0.278 and t = 0.30 seconds, i.e. during the second expansion, will be produced in the actual explosion because there is a strong tendency for the bubble to become spherical while expanding°. It will be seen in Figure 3 that a pressure of 9.4 atmos. is maintained for a duration of τ = 2.54 milliseconds. Thus the maximum displacement of the plate is likely to be at least equal to

$$h = (1.104 \times 10.0) = 11 \text{ cm.} = 4.3 \text{ inches}$$

The observed maximum displacement was

$$h = 4.35 \text{ inches}$$

This close agreement is almost certainly purely accidental.

The .....

The observed maximum deflection with R.D.X./T.N.T. was 5.46 inches, but the plate was at 13 feet instead of 14 feet and R.D.X./T.N.T. is a more powerful explosive than T.N.T. alone.

References.

* U.S. Report No. C4 - sr 20-010, "The theory of the pulsations of the gas bubble produced by an underwater explosion".

6 U.S. Report "A photographic study of underwater explosions"

4 Conyers Herring

* Photographs by Edgerton. U.S. Report.

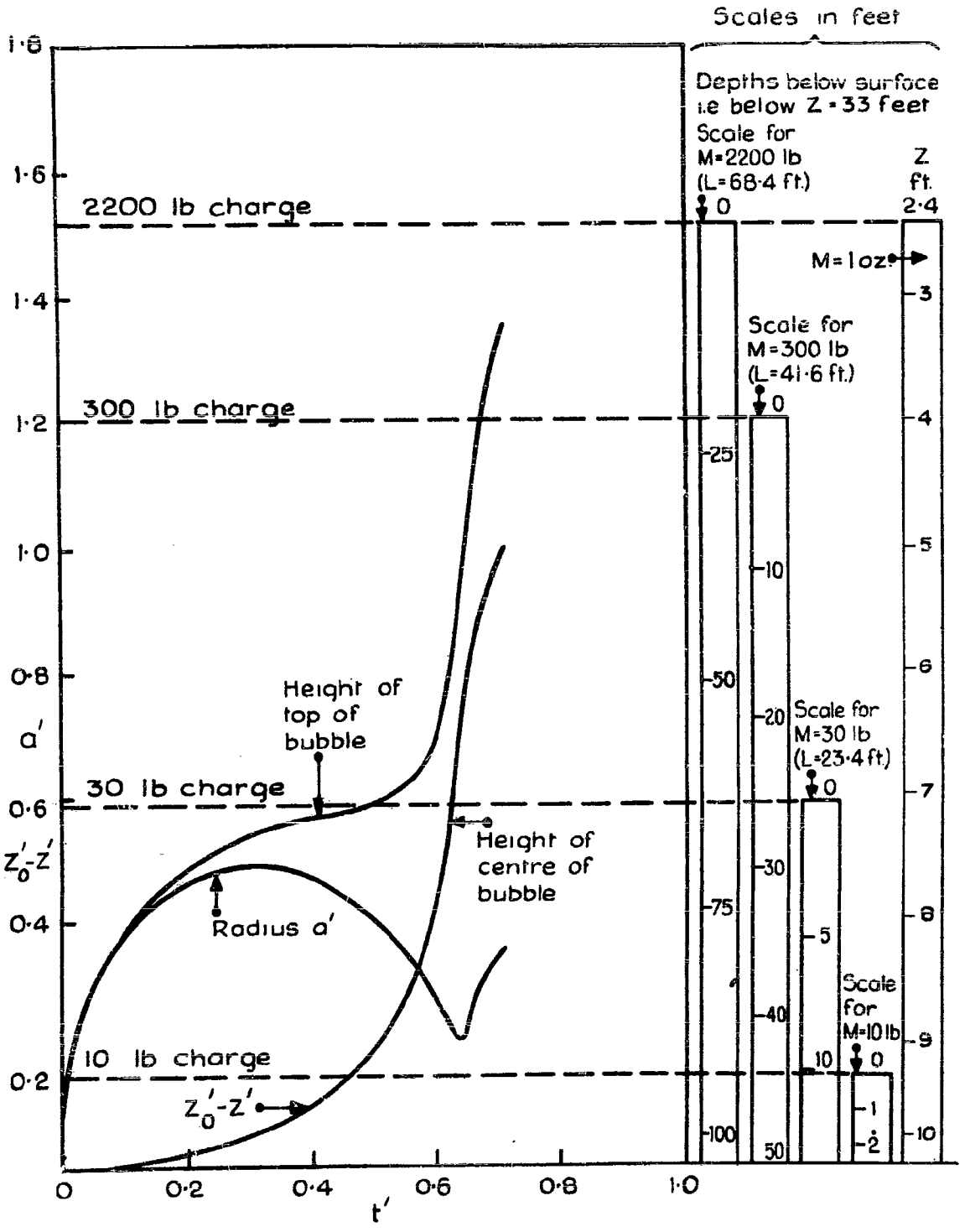

Fig. 1.

Calculations for $Z_0' = 2$

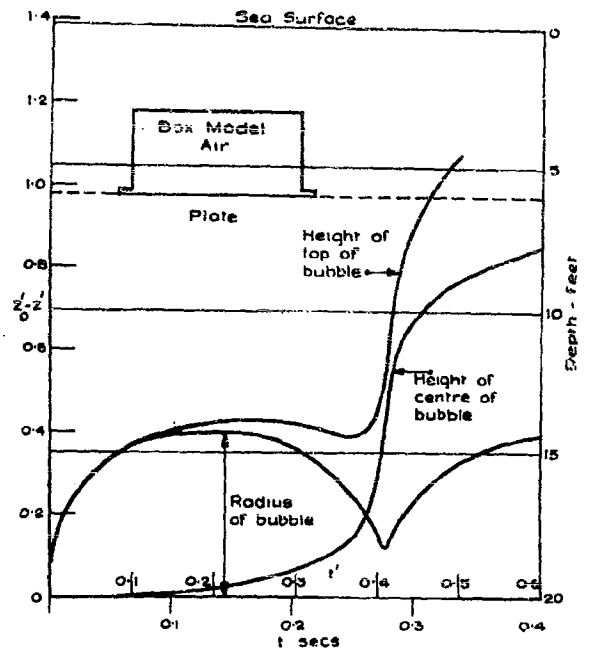

Fig. 2.

Calculations for case of 4·65 lb T.N.T. fired at depth of 20 feet.

$Z_0' = 3{\cdot}62$ L = 445 cm = 14·6 feet.

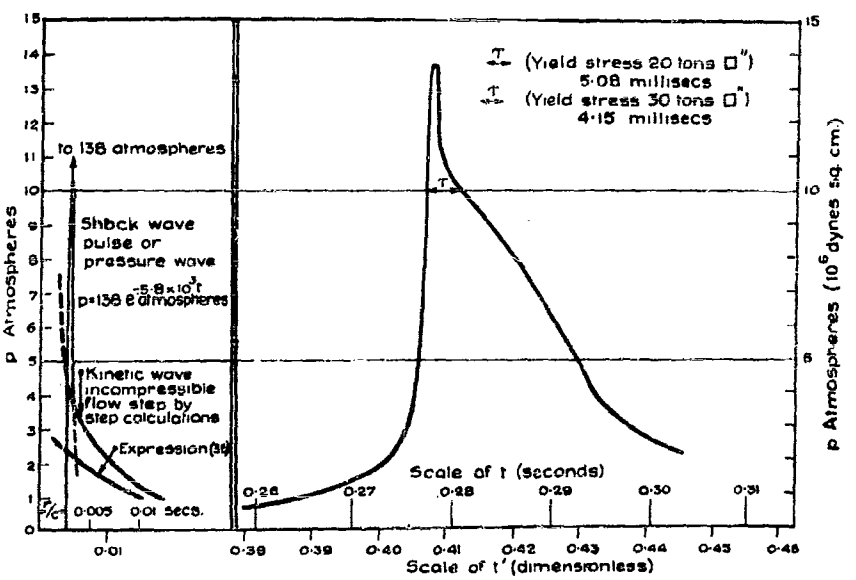

Fig. 3.

Pressure at 14 feet above 4·65 lb T.N.T.

ON THE CHANGING FORM OF A NEARLY SPHERICAL SUBMARINE BUBBLE

W. G. Penney and A. T. Price
Imperial College of Science and Technology, London

British Contribution

October 1942

ON THE CHANGING FORM OF A NEARLY SPHERICAL SUBMARINE BUBBLE

W. G. Penney and A. T. Price

October 1942

* * * * * * * *

Introduction.

When an explosive charge is detonated under water the resulting bubble, as it grows in size, rapidly approaches a spherical form. The degree of stability of this spherical form is a matter of some interest, especially in view of the fact that the bubble may contract again, as both photographic and acoustic observations show. In the case of small charges several pulsations may occur, and there is evidence of at least one complete oscillation being possible with a large charge. On the other hand, for a very deep explosion, where no dome or plume appears, what finally reaches the surface is not a gas bubble but an emulsion of gas and water; this suggests that the bubble has departed so greatly from the spherical form that it has entirely broken up and disintegrated.

The mathematical calculation of the changing form of the bubble would present considerable difficulty even if there were no uncertain factors in the problem. A start can, however, be made by considering the case of small deviations from the spherical form, and investigating the tendency of these to increase or decrease as time proceeds. In the calculations which will now be described, a first order perturbation theory is developed for a nearly spherical bubble expanding or pulsating in an infinite incompressible fluid. The radius vector from the centre of the bubble to its surface is expressed as a constant plus the sum of spherical harmonic components of different orders n, the coefficient of each component varying with the time. Thus the departure from accurate sphericity at any moment is measured by the magnitudes of these harmonic components.

Each harmonic component of order n is found to contain a quasi-periodic time-factor of the form $C_1 e^{\lambda_n t} f_n(t) + C_2 e^{-\lambda_n t} f_n(-t)$, where $f_n(t)$ is a periodic function having the same period T as that of the pulsation of the bubble, λ_n is a certain (complex) constant, and C_1 and C_2 are arbitrary constants determined by the initial conditions. The order of magnitude of the function $f_n(t)$ at any moment is roughly proportional to the reciprocal of the radius of the bubble; consequently, in the case of large pulsations, i.e. intense explosions, the non-sphericity is greatest when the bubble is small. Also, in virtue of the exponential factor $e^{\lambda_n t}$ (λ_n contains in general both real and imaginary parts), the non-sphericity at any stage, say at the minimum size, increases with each pulsation, indicating that the spherical form is ultimately unstable.

The harmonics of high order are found to increase exponentially at first, and then oscillate in magnitude. The higher the order n, the greater is the initial magnification. Hence any needle shape imperfections on the charge will become highly magnified as the charge explodes. This may be the explanation of the prickly appearance sometimes observed in photographs of the early stages of submarine explosions.

The conclusions which can be drawn from these calculations are, however, restricted by the general condition that the perturbation must be small and it is clearly desirable to extend them so as to avoid this restriction.

Basic assumptions.

Taking the mean centre of the bubble at time $t = 0$ as origin, and assuming that the departure from sphericity is small for all times to be considered, we write the radius vector R to the surface of the bubble in the form

$$R = a(t) + \sum_{n=1}^{\infty} b_n(t)\, S_n(\theta, \phi), \quad \Sigma \mid b_n \mid \qquad (a < \epsilon) \qquad (1)$$

where S_n is a surface spherical harmonic of degree n, and ϵ is a small quantity of first order. S_n may be supposed analysed into zonal and tesseral harmonics in the form

S_n .....

$$S_n = \sum_{m=0}^{n} C_{m,n} P_{m,n}(\theta) \cos(m\phi + \gamma_{m,n}) \qquad (2)$$

but it should be noted that the time factor $b_n(t)$ depends only on the degree n of the harmonic, and not on m.

The volume of the bubble is the integral of $R^3/3$ over a unit sphere, which to the first order is equal to $4\pi a^3/3$, in virtue of the orthogonal properties of the harmonics S_n.

We assume that the bubble is filled with an almost massless perfectly elastic gas; pressure waves in this gas are neglected, so that the pressure p at any instant is uniform throughout the bubble. Assuming the usual adiabatic relation between pressure and volume, we have

$$p\, a^{3\gamma} = P\, a_0^{3\gamma} \qquad (3)$$

where P is the pressure and a_0 the mean radius at time t = 0.

The motion of the surrounding fluid, since it is generated from rest by pressure, will possess a velocity potential ϕ, say. Assuming the fluid is incompressible, this potential satisfies Laplace's equation and is therefore expressible in the form

$$\phi = r^{-1} A(t) + \sum_{n=1}^{\infty} r^{-n-1} B_n(t) S_n(\theta, \phi) \qquad (4)$$

We shall assume that the surface harmonics S_n in (4) are identical with the corresponding harmonics in (1), and that the time factors $B_n(t)$ in (4) are of the same order of smallness as the b_n's in (1). These assumptions are justified by the consistency of the subsequent analysis.

The leading term on the right of (4) is separated from the others because it corresponds to the case when the bubble is accurately spherical, for which the solution is known.

Spherical harmonics of negative degree only are taken in the expression for ϕ, because the velocity, and therefore also ϕ, vanishes at infinity.

The pressure in the fluid is given by the hydrodynamical equation

$$\frac{p}{\rho} = \dot{\phi} + \Omega - \frac{1}{2} (\text{grad}\,\phi)^2 + F(t) \qquad (5)$$

where Ω is the potential of the extraneous forces, limited in our case to gravity, so that $\Omega = -gz$.

The arbitrary function F(t) is determined in the present case by the conditions at infinity. Taking the pressure at infinity at the original level of the bubble to be constant and equal to Q, we have, since ϕ tends to zero,

$$F(t) = Q/\rho \qquad (6)$$

Substituting for ϕ from (4) into (5), and retaining terms up to the first order, then gives for the pressure p in the fluid at distance r from the origin,

$$\frac{p - Q}{\rho} - \Omega = \frac{\dot{A}}{r} - \frac{1}{2}\frac{A^2}{r^4} + \Sigma \left\{ \frac{\dot{B}_n}{r^{n+1}} - \frac{(n+1)\, A\, B_n}{r^{n+4}} \right\} S_n \qquad (7)$$

Boundary conditions.

The conditions to be satisfied by the velocity and the pressure at infinity have already been considered. We now investigate the conditions to be satisfied at the surface of the bubble.

The condition to be satisfied by the velocity is that its normal component at the surface shall be equal to the normal component of the velocity of the surface as determined by the expression (1) for R. These normal components are, to the first order of small quantities, equal to the corresponding radial components, and hence, to this order of approximation.

$$\dot{R} = \ldots\ldots$$

$$\dot{R} = -[\partial\phi/\partial r]_{r=R},$$

that is

$$\dot{a} + \Sigma \dot{b}_n S_n = A a^{-2}(1 - 2a^{-1}\Sigma b_n S_n) + a^{-n-2}\Sigma (n+1) B_n S_n \qquad (8)$$

on retaining the terms as far as the first order only.

Since (8) is true over a complete sphere, we have on equating coefficients of the corresponding harmonics

$$\dot{a} = a^{-2} A; \quad \dot{b}_n = -2a^{-3} A b_n + (n+1) a^{-n-2} B_n \qquad (9)$$

or, solving for A and B_n,

$$A = a^2\dot{a}; \quad B_n = (a^{n+2}\dot{b}_n + 2a^{n+1}\dot{a} b_n)/(n+1) \qquad (10)$$

The remaining boundary condition is that the pressure is continuous across the surface of the bubble. This requires that the values of p as given by (3) and (7) shall be equal when r = R. Substituting from (3) and (1) in (7), and using (10), we find, to the first order,

$$\{P(a_0/a)^{3\gamma} - Q\}/\rho + ga S_1 = a\ddot{a} + \tfrac{3}{2}\dot{a}^2 + \Sigma \frac{1}{n+1}\{(1-n)\ddot{a} b_n + 3\dot{a}\dot{b}_n + a\ddot{b}_n\} S_n \qquad (11)$$

The differential equations for a(t) and $b_n(t)$

Since the spherical harmonic expansion on the right of (11) is the expansion of a constant over a complete sphere, we have

$$a\ddot{a} + \tfrac{3}{2}\dot{a}^2 = (P a_0^{3\gamma} - Q a^{3\gamma})/\rho a^{3\gamma}, \qquad (12)$$

$$3\dot{a}\dot{b}_1 + a\ddot{b}_1 = 2ga \qquad (13)$$

and $$(1-n)\ddot{a} b_n + 3\dot{a}\dot{b}_n + a\ddot{b}_n = 0, \quad n \geq 2. \qquad (14)$$

Equation (12) agrees with the known result when the bubble is accurately spherical, and it may be solved to give a(t) in terms of P, Q, ρ and γ. Substituting this value in (14), we obtain the differential equation to determine $b_n(t)$. Equation (13) integrates immediately

$$b_1 = 2g\int_0^t \frac{dt}{a^3}\int_0^t a^3 dt + \int_0^t \frac{\dot{b}_1(0)\{a(0)\}^3}{a^3}\,dt \qquad (14a)$$

The first part of this expression is Herring's formula (4) for the rise of the bubble due to gravity; the second part represents the effect of an initial velocity.

Except for the case when Q = 0, the solution of (12) makes a(t) a periodic function of t, i.e. the bubble pulsates. Consequently the equation (14) for b_n is one in which the coefficients are periodic functions, the period (T, say) being equal to that of the pulsation of the bubble. From Floquet's theory of such equations, it is known that the general solution is ordinarily of the form

$$b_n = C_1 e^{\lambda t} f(t) + C_2 e^{-\lambda t} f(-t) \qquad (15)$$

where C_1 and C_2 are arbitrary constants, and f(t) is a periodic function of period T. The constants λ and the function f(t) are determined by the periodic coefficients of the equation.

When, however, the equation possesses a periodic solution, say g(t) (corresponding to $\lambda = 0$) the general solution is not of the form (15); the second solution $g_2(t)$ is not periodic but satisfies a functional equation of the type

$$g_2(t+T) = g_2(t) + T g_1(t).$$

An example of this occurs in the present calculations for the case n = 1.

When .....

When λ is purely imaginary, b_n will be the product of two periodic functions of different periods; if it is not purely imaginary, b_n will ultimately increase to large values. Actually λ is found to be small and purely imaginary for small pulsations of the bubble, i.e. when P is nearly equal to Q. For other values of P/Q it is complex, except when $n = 1$, when it is zero. Hence in general the perturbation is unstable.

The calculation of the mean radius a(t) of the bubble.

Before proceeding with the solution of (14) for b_n, it is convenient to consider the function a(t) which determines the coefficients appearing in (14).

Writing

$$\alpha = a/a_0, \quad x = c_0 t/a_0 \text{ where } c_0^2 = \gamma P/\rho \tag{16}$$

the equation (12) has a first integral of the form

$$\left[\frac{\dot{a}}{c_0}\right]^2 = \left[\frac{d\alpha}{dx}\right]^2 = \frac{2}{3(\gamma-1)}\left\{\alpha^{-3} - \alpha^{-3\gamma} + \frac{(\gamma-1)}{\gamma} Q\,(\alpha^{-3} - 1)\right\} \tag{17}$$

and a further integration gives

$$x = \sqrt{\left(\frac{3(\gamma-1)}{2}\right)} \int_1^{\alpha} \frac{d\alpha}{\sqrt{\{\alpha^{-3} - \alpha^{-3\gamma} + (\gamma-1)\,P^{-1}Q(\alpha^{-3}-1)\}}} \tag{18}$$

Values of this integral for a small range of α have been given by Lamb(1) for the case $Q = 0$ and $\gamma = 4/3$. In this case the motion is not, of course, periodic but α continually increases with t(or x).

When Q is not zero, α is periodic; i.e. the bubble pulsates. The period T_x, measured in terms of x, is equal to twice the interval in x between the two singularities of the integrand in (18). One of these is at $\alpha = 1$, and the other is at $\alpha = \alpha_m$, say, where α_m is the ratio of the maximum radius to the minimum radius.

The evaluation of the integral in (18), when P/Q is large, has been discussed by Butterworth(2) Willis(3), and Herring(4), but their methods and formulae are only applicable to the accurate determination of α as a function of t when α is near unity, and to the determination of α/α_m as a function of $(T-t)$ when α is near α_m. Their results are in fact equivalent to first approximations to the integral between 1 and α near the singularity $\alpha = 1$, and to the integral between α and α_m near the singularity $\alpha = \alpha_m$.

An extension of these reults, which enables a(t) to be determined with any desired accuracy over the whole period, is readily obtained. The analysis is greatly simplifed when $\gamma = 4/3$, and as this is probably a fair approximation to the actual case, only this value of γ will be considered. Most of the investigations referred to above have also dealt only with this value of γ.

When $\gamma = 4/3$, the expression (18) can be written in the factorised form

$$\sqrt{\frac{P}{\rho}}\frac{t}{a_0} = x = \frac{1}{\sqrt{2}} \int_1^{\alpha} \frac{\alpha^2\,d\alpha}{\sqrt{(\alpha-1)}\sqrt{\{1-Q\,(\alpha+\alpha^2+\alpha^3)/(3P)\}}} \tag{19}$$

from which it will be seen that α_m is the positive root of

$$\alpha^3 + \alpha^2 + \alpha = 3P/Q. \tag{20}$$

Since $P > Q$, this root is greater than unity, and for large P/Q, its value is approximately $(3P/Q)^{1/3}$. An expression for the root in the form of a power series, suitable for all $P/Q > 1$, can be obtained by a simple iteration method; this gives

$$\alpha_m = \alpha_1\left\{1 - \frac{1}{3\alpha_1} - \frac{2}{9\alpha_1^2} + \frac{8}{27\alpha_1^3} - \cdots\cdots\right\} \tag{21}$$

where .....

where

$$a_1^3 = 3P/Q \qquad (22)$$

Since $Q(a + a^2 + a^3)/3P$ is less than unity for $a < a_m$, we can expand the second factor in the denominator of the integrand in (19), and obtain

$$x = \sqrt{\tfrac{1}{2}} \int_1^a \sqrt{\frac{a^2}{(a-1)}} \left\{ 1 - \frac{1}{2a_1^3}(a + a^2 + a^3) + \frac{3}{8a_1^6}(a + a^2 + a^3)^2 + \ldots \right\} da \qquad (23)$$

When $Q \to 0$, $a_1 \to \infty$ and the above reduces to the first term, which is Lamb's result. In the general case it will be seen that x can be evaluated in terms of integrals of the type

$$\int_1^a \sqrt{\frac{a^q\, da}{(a-1)}} = 2(a-1)^{1/2} P_q(a-1),$$

where

$$P_q(z) = 1 + \tfrac{1}{3}qz + \frac{1}{3.2!}q(q-1)z^2 + \ldots + \frac{1}{2q+1}z^q \qquad (24)$$

The series for x obtained in this way is convergent when $1 \leqslant a < a_m$, and is useful for calculation over the greater part of this range. When $a = a_m$ the series is divergent, and to obtain values of x in this neighbourhood we first consider

$$x_m - x = \sqrt{\tfrac{1}{2}} \int_a^{a_m} \frac{da}{\sqrt{\{a^{-3} - a^{-4} + a_1^3(a^{-3} - 1)\}}},$$

which, on putting $y = a/a_m$, reduces to

$$x_m - x = \sqrt{\tfrac{1}{2}} \int_{a/a_m}^1 \frac{a_1^{3/2} a_m\, da}{\sqrt{\{(1 + a_1^3)a_m^{-3} - y^{-3} - a_1^3 a_m^{-4} y^{-1}\}}}$$

On taking out a factor $\sqrt{(1 - y^3)}$ from the denominator and expanding the remaining factor by the binomial theorem, we obtain

$$x_m - x = \sqrt{\tfrac{1}{2}}\, a_1^{3/2} a_m \int_{a/a_m}^1 \frac{y^{3/2}}{\sqrt{(1-y^3)}} \left\{ 1 + \tfrac{1}{2} a_1^3 a_m^{-4} \frac{1}{y + y^2 + y^3} + \ldots \right\} dy \qquad (25)$$

which is equivalent to the result obtained by Herring, and may be evaluated in terms of the incomplete beta-functions. Now both the expressions (23) and (25) are found sufficiently convergent for calculation over a common range of values for a. Hence by taking a suitable value of a, say $a = a'$, in this range, x_m may be calculated from the sum of the two expressions (23) and (25); x can then be found from $x = x_m - (x_m - x)$ for other values of $a > a'$.

The above formulae are especially useful when P/Q is large or moderate. If P is nearly equal to Q the pulsation should reduce to a simple harmonic one of small amplitude. On writing

$$P = Q(1 + \epsilon), \quad a_m = 1 + \xi_m, \quad \epsilon \text{ small} \qquad (26)$$

it is easily seen from (20) that $\xi_m = \tfrac{1}{2}\epsilon$. Substituting $(1 + \xi)$ for a in (19), and neglecting terms beyond the first order, we obtain

$$x = \tfrac{1}{2} \int_0^{\xi} \frac{d\xi}{\sqrt{\{(\tfrac{\epsilon}{4})^2 - (\xi - \tfrac{\epsilon}{4})^2\}}} = \tfrac{1}{2}\left\{ \sin^{-1}\left(\frac{4\xi}{\epsilon} - 1 \right) + \frac{\pi}{2} \right\}$$

so that

$$a = 1 + \xi = 1 + \frac{\epsilon}{4}(1 - \cos 2x). \qquad (27)$$

it will .....

It will be seen from this expression and from (26) that for small pulsations, the period is $\pi a_0 \sqrt{(\rho/P)}$.

The equation for $b_n(t)$.

The equation (14) for b_n is reduced to the normal form by writing

$$y = a^{3/2} b_n, \tag{28}$$

which gives

$$\ddot{y} = \left\{ (n + \tfrac{1}{2}) \frac{\ddot{a}}{a} + \frac{3}{4}\left(\frac{\dot{a}}{a}\right)^2 \right\} y.$$

Substituting for $\ddot{a}$ from (12), and for a from (17) with $\gamma = 4/3$, we obtain

$$\frac{d^2y}{dx^2} = \left(\frac{a_0}{c_0}\right)^2 \ddot{y} = F(x)y, \tag{29}$$

where

$$F(x) = (4n + \tfrac{1}{2})\,\alpha^{-6} - 3n\,(1 + \tfrac{Q}{3P})\,\alpha^{-5} - \frac{Q}{2P}\,\alpha^{-2} \tag{30}$$

The following properties of this function are easily verified.

(i) $F(x)$ is periodic in x, the period being the same as that of α, and therefore ranging from π for small α_m to approximately $\alpha_m^{5/2}$ for large α_m.

(ii) $F(0) = (n + \tfrac{1}{2})\,(1 - Q/P)$.

(iii) $F(\pi/2) = (n + \tfrac{1}{2})\,(\alpha_m^{-6} - Q\,\alpha_m^{-2}/P)$. Hence, when the bubble reaches its maximum size, $F(x)$ is negative. When P/Q is large, its value is approximately $-3(n + \tfrac{1}{2})\,\alpha_m^{-5}$.

(iv) $F(x)$ is zero for only one value of α between 1 and α_m. When P/Q is large, this value of α is approximately $(8n + 1)/6n$ and thus lies between the narrow limits $1\frac{1}{3}$ and $1\frac{1}{2}$ for all n.

(v) $F(x)$ has maxima when $\alpha = 1$ and $\alpha = \alpha_m$, and has a minimum when

$$\tfrac{9}{4}\alpha^4 + 5n\,(1 + \tfrac{3}{5})\,\alpha - (8n + 1) = 0.$$

For large P/Q, this minimum occurs approximately when $\alpha = (8n + 1)/5n$, and its value is approximately $-\frac{n}{2}\left(\frac{5n}{(8n+1)}\right)^5$

(vi) In the case of small pulsations, on substituting from (27) in (30) and neglecting terms beyond the first order, we have

$$F(x) = (n + \tfrac{1}{2})\,\epsilon \cos 2x. \tag{31}$$

Most of the above properties are shown diagrammatically in Figure 1, which refers to the two extreme cases, P/Q large and $P/Q = 1 + \epsilon$, ϵ small. As P/Q decreases from large values the two minima shown in the figures move together, eventually obliterating the maximum at $\alpha = \alpha_m$ and tending to the simple cosine function (31) for small pulsations.

Solution for n = 1. Motion of bubble in absence of extraneous forces.

The first harmonic term $b_1(t)S_1$ in (1) simply represents a displacement of the bubble, without change of form and of amount $b_1(t)$ along the axis of the harmonic. Hence the solution when $n = 1$ gives the motion of the bubble in the absence of extraneous forces.

The solution in this case is easy, and does not require the preceding analysis. We have from (13) with $g = 0$, (compare also 14a)

$$\dot{b}_1 = \dot{b}_1(0)/a^3, \tag{32}$$

which .....

which shows that the velocity of the centre of the bubble varies inversely as the cube of the radius of the bubble, and therefore increases greatly as the bubble contracts. The motion is in fact the same as that of a particle, whose mass is variable and proportional to the volume of the bubble.

If we write

$$\beta_n = b_n(t)/b\ (0) \tag{33}$$

and regard β_n as a function of α, we obtain from (32) and (17)

$$\frac{d\beta_1}{d\alpha} = \frac{C}{\alpha^3\sqrt{(\alpha^{-3} - \alpha^{-3\gamma} + (\gamma - 1)\, P^{-1} Q\, (\alpha^{-3} - 1))}} \tag{34}$$

where

$$C = \frac{b_1\ (0)}{b_1\ (0)}\ \frac{a(0)}{c_0}\sqrt{\frac{3\ (\gamma - 1)}{2}} \tag{35}$$

Hence

$$\beta_1(\alpha) = 1 + C\int_1^{\alpha} \frac{d\alpha}{\alpha^3\sqrt{(\alpha^{-3} - \alpha^{-3\gamma} + (\gamma - 1)\, P^{-1} Q\, (\alpha^{-3} - 1))}} \tag{36}$$

and β_1 is therefore an inverse-periodic function of α.

When $\gamma = 4/3$, the integral may be evaluated in exactly the same way as the integral in (18) for x. For values of α near unity, we find an expansion in powers of Q/P of the form

$$\beta_1(\alpha) = 1 + C\left[2\tan^{-1}\sqrt{(\alpha - 1)} + 3QP^{-1}\sqrt{(\alpha - 1)}\left\{1 + \tfrac{4}{5}(\alpha - 1) + \tfrac{1}{15}(\alpha - 1)^2\right\} + \ldots\right] \tag{37}$$

while from α near α_m

$$\beta_1(\alpha) = \beta_m(\alpha) + \frac{C\,2\sqrt{3}}{\alpha_m}\sqrt{(\alpha_m - \alpha)} \tag{38}$$

The graph of $\beta - 1$ as a function of α is shown in Figure 2, for the case when $P/Q = 10^4$, and corresponding to any initial velocity. When the initial velocity is zero the curve shrinks up to the straight line $\beta = 1$, corresponding to the obvious fact that the centre of the bubble will remain in any displaced position unless it is given an initial velocity.

Nature of the solution for large n.

An interesting question, but one difficult to answer satisfactorily without mechanical aid such as the differential analyser, is that of finding numerical solutions of (2 9) for large n. What in fact one would like to know is whether initial small irregularities on the surface become bigger or die out as the motion proceeds. There seems no doubt that any irregularity limited initially to a small solid angle is unstable, and that the instability increases rapidly as the initial solid angle decreases. Perhaps the prickly appearance of the bubble in Edgerton's photographs is a manifestation of instability of the type now under discussion; at least there seems no more probable alternative. It may be noted, however, that the photographs do not show any pits, but only needles, whereas the theory in its present form indicates both equally. There is clearly a close formal similarity between the instability of very small irregularities on the surface of the bubble and ripples on the free surface of water, as the pressure wave strikes. A theory of the magnification of these ripples has been developed by G.I. Taylor.

The function F(x) as defined by (30) has as its dominant terms, when n is large,

$$F(x) = n(4\alpha^{-6} - 3\alpha^{-5})$$

so that (29) becomes

$$\frac{d^2\gamma}{dx^2} = n\gamma(4\alpha^{-6} - 3\alpha^{-5}).$$

The .....

The coefficient of y on R.H.S. is positive in the range $1 < \alpha < 4/3$, and is negative for $\alpha > 4/3$. Hence for large n, y increases exponentially in the range $1 < \alpha < 4/3$, and thereafter oscillates. The interval between successive zeros, as n is varied, decreases like $2/\sqrt{n}$. The ratio of the maximum value of y and the value of y at $\alpha = 1$ is of the same order of magnitude as

$$\chi = \exp\{\sqrt{n} \int_0^{x_0} \sqrt{(4\alpha^{-6} - 3\alpha^{-5})}\, dx\},$$

where x_0 is the value of x at the zero of the integrand. Replacing the integrand by an approximate expression, obtained from

$$\alpha = 1 + z$$

$$x = (1 + 2z/3 + z^2/5)\sqrt{(2z)} \qquad \text{(Lamb's substitution)}$$

it will be found that

$$\chi = \exp\{4\sqrt{n/9}\}.$$

If n = 10 the magnification χ is 4.09; if n = 100, χ is 85; and if n = 1000, χ is 1,300,000.

Solution for small pulsations of the bubble.

The solution of (39) in a simple form can be obtained for any value of n in the case of small pulsations. Although this theory is clearly not applicable to real bubbles because surface tension, which would now be relatively important, is neglected, we give the theory because it may indicate some features of the more general motion.

From (26), (29) and (31), the equation to determine y is now

$$\frac{d^2y}{dx^2} = (n + \tfrac{1}{2})\,\epsilon \cos 2x \qquad (39)$$

which is a degenerate form of Mathieu's equation. Since ϵ is small, we seek an approximate solution in the form

$$y = A + Bx + \epsilon f(x).$$

On substituting in the equation and retaining only first order terms we find

$$f(x) = -\tfrac{1}{4}(n + \tfrac{1}{2})\{(A + Bx)\cos x + B \sin 2x\},$$

so that

$$y = (A + Bx)\{1 - \tfrac{1}{4}(n + \tfrac{1}{2})\,\epsilon \cos 2x\} + \tfrac{1}{4}(n + \tfrac{1}{2})\,\epsilon\, B \sin 2x \qquad (40)$$

Since $y = a^{3/2} b_n$, $\beta_n = \text{const. } y\alpha^{-3/2}$, where α is given by (27); hence β_n can be reduced to the form

$$\beta_n = (A' + B'x)\{1 - \tfrac{1}{4}(n - 1)\,\epsilon \cos 2x\} + \tfrac{1}{4}(n + \tfrac{1}{2})\,\epsilon\, B' \sin 2x \qquad (41)$$

This result may be checked when n = 1 from our previous calculation. We have

$$\beta_1 = \beta(1)\,\alpha^{-3} = \beta(1)\{1 - \tfrac{3}{4}\epsilon(1 - \cos 2x)\},$$

which on integration gives

$$\beta = 1 + \text{const.}\{(1 - \tfrac{3}{4}\epsilon)\,x + \tfrac{3}{4}\epsilon \sin 2x\},$$

which agrees with (40) when n = 1.

At any value of α, a measure of the non-sphericity associated with the harmonic S_n is afforded by the ratio b_n/a; this divided by its initial value is equal to β_n/α, which is found from (41) by dividing by α, as given by (27); this gives

$$\frac{\beta_n}{\alpha} \ldots\ldots$$

$$\frac{\beta_n}{\alpha} = (A' + B'x)\left\{1 - \tfrac{1}{4}(n-2)\epsilon\cos 2x\right\} + \tfrac{1}{4}(n+\tfrac{1}{2})\epsilon B'\sin 2x \qquad (42)$$

Hence the perturbation associated with S_n may be regarded as a small oscillation of period T, about a mean value which is continually increasing with t (or x). When $n = 2$, the amplitude of this small oscillation is constant, but when $n > 2$ the amplitude also increases with t. The greater the value of n, the greater is the amplitude of this oscillation. This is illustrated in Figure 9, where the graphs of β_2/α and β_4/α for two pulsations of the bubble are shown.

When β_n is initially zero, the constant B' in (41) is zero, and the perturbation is simple harmonic, the amplitude being proportional to $(n-2)$.

The solution of the equation (39) can also be obtained in the form (15). Adopting Hill's method of solving Mathieu's equation, we seek a solution of (39) in the form

$$y = e^{\lambda x}\sum_{r=-\infty}^{\infty} c_r e^{2ri x},$$

in which one coefficient, say c_0, is arbitrary.

Substituting in (39) and equating coefficients of like powers of e^{ix} to zero, we have

$$(\lambda + 2ri)^2 c_r - \tfrac{1}{2}(n+\tfrac{1}{2})\epsilon(c_{r-1} + c_{r+1}) = 0,$$

for all positive and negative integral values of r.

Eliminating the c's gives an infinite continuant equated to zero to determine λ. This continuant is a limiting form of Hill's determinant (Whittaker and Watson, Modern Analysis, 1920, p.415) and on neglecting terms of order higher than the first, we find

$$\lambda = \pm i\theta/\sqrt{2} \quad \text{where} \quad \theta = \tfrac{1}{2}(n+\tfrac{1}{2})\epsilon,$$

and $c_1 = c_{-1} = -\frac{1}{4}\theta c_0$, $c_2 = c_{-2} = \ldots = O(\epsilon^2)$.

This leads to a real solution of the form

$$\frac{\beta_n}{\alpha} = \left[A'' \cos\frac{\theta x}{\sqrt{2}} + B'' \sin\frac{\theta x}{\sqrt{2}}\right]\left\{1 - \tfrac{1}{4}(n-2)\epsilon\cos 2x\right\} \qquad (43)$$

For small x this agrees with the result (41) provided $B'/B'' = \theta/\sqrt{2}$, a small quantity of the first order. The apparent difference in the two results for other values of x is due to the fact that they are both approximations to the first order in ϵ, and it is possible for the ratio of the arbitrary constants to have any order of smallness. Thus if A''/B'' is assumed to be of the first order in ϵ, a further term in ϵ^2 would be required to be retained in the coefficient of e^{2ix} in the above solution, to ensure that all the terms retained are of the same order. This would give a term corresponding to the sin 2x term in (41).

Without going further into these refinements, it will be seen from (43) that, provided the condition that $\beta_n/(\alpha - 1)$ remains small is not violated, the perturbation can be regarded as a quasi-periodic variation of period T in which both the mean value and the amplitude have a slow periodic variation of period $\frac{8\sqrt{2}}{(2n+1)\epsilon}T$.

Solution for the general case.

In the general case where Q/P has any value < 1, and n is any positive integer, it is convenient to derive an equation for β in terms of α, and solve this instead of dealing with the equation (29) directly. This method is somewhat analogous to Lindemann's treatment of Mathieu's equation.

Since a is periodic in t, b_n will be a multi-valued function of a with branch points at $a = a_0$ and $a = a_m$. Denote the value of b_n in the half-period $\frac{s-1}{2}T < t < \frac{s}{2}T$ by $b_{n,s}$, which is then a single-valued function of a. Thus $b_{n,1}$ is the value of b_n during the first expansion, $b_{n,2}$ the value during the first contraction and so on.

Considering .....

Considering any half-period, and changing the independent variable in (14) to a, we obtain

$$\frac{d^2 b_{n,s}}{da^2} + \left[\frac{\ddot{a}}{a^2} + \frac{3}{a}\right] \frac{db_{n,s}}{da} + (1-n)\frac{\ddot{a}}{a^2}\, b_{n,s} = 0 \qquad (44)$$

Putting

$$b_{n,s} = b(0)\, \beta_{n,s} \qquad (45)$$

and using (17), this equation becomes

$$\frac{d^2\beta}{d\alpha^2} + \frac{1}{\alpha}\left\{ f(\alpha) + \frac{3}{2}\right\} \frac{d\beta}{d\alpha} - (n-1)\frac{1}{\alpha^2}\left\{ f(\alpha) - \frac{3}{2}\right\} \beta \qquad (46)$$

where the suffix (n,s) is omitted from β for the present, and

$$f(\alpha) = \frac{3(\gamma-1)}{2}\, \frac{\alpha^{-3\gamma} - \sigma}{\alpha^{-3} - \alpha^{-3\gamma} + \sigma(\gamma-1)(\alpha^{-3}-1)} \qquad (47)$$

$$\sigma = Q/P. \qquad (48)$$

When $\gamma = 4/3$, the equation (46) reduces to

$$\alpha^2\left\{ -\tfrac{1}{3}\sigma\alpha^4 + (1+\tfrac{1}{3}\sigma)\alpha - 1\right\} \frac{d^2\beta}{d\alpha^2} + \alpha\left\{ -\sigma\alpha^4 + (\tfrac{3}{2}+\tfrac{1}{2}\sigma)\alpha - 1\right\}\frac{d\beta}{d\alpha}$$

$$+ (n-1)\left\{ (\tfrac{3}{2}+\tfrac{1}{2}\sigma)\alpha - 2\right\} \beta = 0 \qquad (49)$$

The general solution of this equation is required for the range $1 < \alpha < \alpha_m$. It may be noted that when $\sigma = 0$ the equation reduces to a Lamé equation, and can be transformed to Legendre's equation for $P_r^m(\eta)$ by the substitution $\eta = \sqrt{(1-\alpha)}$, but m, r and η are all complex or imaginary.

The equation has regular singularities at the origin and at infinity, and also at the four zeros of

$$-\tfrac{1}{3}\sigma\alpha^4 + (1+\tfrac{1}{3}\sigma)\alpha - 1,$$

i.e. at

$$\alpha = 1,\ \alpha_m,\ -\tfrac{1}{2}(\alpha_m + \tfrac{1}{\alpha_m}) \pm i(\alpha_m^2 + 1).$$

At the four latter singularities the indicial equation is the same, viz.

$$2\mu(\mu-1) + \mu = 0,$$

so that the exponents relative to any one of these singularities is 0 or $\frac{1}{2}$.

Hence two fundamental solutions of (49) can be obtained in the forms

$$\left.\begin{aligned} \beta &= A_0 g_1(z) \equiv A_0 + A_1 z + A_2 z^2 + \ldots\ldots \\ \beta &= A_{1/2} z^{1/2} J_1(z) \equiv A_{1/2} z^{1/2} + A_{3/2} z^{3/2} + \ldots\ldots \end{aligned}\right\} \qquad (50)$$

where $z = \alpha - \alpha_i$, and α_i is any one of the above four singularities.

By considering the positions of the singularities in the complex plane, it can be seen that the series expressions (50) relative to $\alpha = 1$ (i.e. with $z = \alpha - 1$) are convergent for $z < 1$, i.e. for $\alpha < 2$, and the series with $z = \alpha - \alpha_m$ are convergent for $z < \alpha_m - 1$, i.e. for the whole range (except for $\alpha = 1$) over which the solution is required.

The .....

The recurrence relation between the coefficients in (50) is found to be

$$(r+1)(2r+1)\,k\,A_{r+1} = \{-4mr^2 + (n-1)\,l\}\,A_r + \{-(r-1)(2r-1)\,p + (n-1)(9+3\sigma)\}\,A_{r-1}$$

$$-(r-2)(r-1)\,30\sigma k^2 A_{r-2} - (r-3)(2r-3)\,6\sigma k\,A_{r-3} - 2(r-4)(r-2)\,\sigma A_{r-4}, \qquad (51)$$

where $k = 1$ or α_m as the case may be, and

$$\left.\begin{array}{lccc} & \underline{k=1} & & \underline{k=\alpha_m} \\ l = 3(2\sigma k^4 - (3+\sigma)\,k + 2) & = & 3(\sigma-1) & = 3(3\alpha_m + \sigma\alpha_m - 4) \\ m = \tfrac{1}{4}(30\sigma k^4 - (18+6\sigma)\,k + 6) & = & \tfrac{1}{4}(2\sigma-1) & = 2l+3 \\ p = 20\sigma k^3 - 3 - \sigma & = & 20\sigma - 3 & = 20\sigma\alpha_m^3 - 3 - \sigma \end{array}\right\} \qquad (52)$$

By taking r any positive integer (including zero) in (51) and taking $B_{-r} = 0$ for $r > 0$, we obtain the coefficients of the first series in (50), and by taking r equal to half an odd integer we obtain the coefficients of the second series.

It will be noted that the approximations to β near $\alpha = 1$ and near $\alpha = \alpha_m$ are respectively

$$\beta = A_0\{1 + (n-1)(\alpha-1)\} + A_{1/2}\sqrt{(\alpha-1)} \qquad (53)$$

$$\beta = A'_0\left\{1 - \frac{n-1}{\alpha_m}(\alpha_m - \alpha)\right\} + A'_{1/2}\sqrt{(\alpha_m - \alpha)} \qquad (54)$$

In the numerical case worked out (corresponding to $\alpha_m = 30.732$) it was found that the above series were only suitable for calculation in the regions $\alpha = 1$ to 1.5 when $z = \alpha - 1$, and $\alpha = 10$ to 30.75 when $z = \alpha_m - \alpha$. Hence to supplement these series, the Taylor expansion

$$\beta = C_0 + C_1 z + C_2 z^2 + \ldots\ldots, \quad z = \alpha - k \qquad (55)$$

of the solution, relative to any ordinary point $z = k$, was obtained. The recurrence relation for the coefficients of this expansion is

$$(r+2)(r+1)(+hk^2)\,C_{r+2} = (r+1)(2r+1)(-lk)\,C_{r+1} + \{-4mr^2 + (n-1)\,q\}\,C_r$$

$$+ (r-1)(2r-1)(-p) + (n-1)(9+3\sigma)\,C_{r-1} + (r-2)(r-1)(-30\sigma k^2)\,C_{r-2}$$

$$+ (r-3)(2r-3)(-6\sigma k)\,C_{r-3} + (r-4)(r-2)(-2\sigma)\,C_{r-4} \qquad (56)$$

where

$$\left.\begin{array}{l} h = 2\sigma k^4 - (6+2\sigma)\,k + 6 \\ q = (9+3\sigma)\,k - 12 \end{array}\right\} \qquad (57)$$

and l, m and p are given in (52).

The relation between $\beta_{n,s}$ and $\beta_{n,s+1}$.

The above expressions give $\beta_{n,s}$ as a function of α (with two arbitrary constants) over any half-period. If s is odd, $\beta_{n,s}$ corresponds to an expanding phase, and $\beta_{n,s+1}$ to the succeeding contracting phase. To obtain the relation between these β's we have the conditions that β and $\dot\beta$ are continuous at $\alpha = \alpha_m$. The value of $\dot\beta$ is given by

$$\dot\beta = \frac{d\beta}{d\alpha}\dot\alpha = \pm\frac{d\beta}{d\alpha}\,\frac{c_0\sqrt{2}}{a_0}\sqrt{\{\alpha^{-3} - \alpha^{-4} - \tfrac{1}{3}\sigma(\alpha^{-3} - 1)\}} \qquad (58)$$

$$= \pm\frac{d\beta}{d\alpha}\sqrt{(\alpha_m - \alpha)}\,\phi(\alpha), \text{ say,}$$

and the positive or negative value must be taken according as we are considering an expanding or contracting phase.

Hence .....

Hence, if when s is odd, we write

$$\beta_{n,s} = B_{0,s}\, g_m(z) + B_{1/2,s} \sqrt{(\alpha_m - \alpha)}\; j_m(z), \quad z = \alpha - \alpha_m \tag{59}$$

$$\beta_{n,s+1} = B_{0,s+1}\, g_m(z) + B_{1/2,s+1} \sqrt{(\alpha_m - \alpha)}\; j_m(z),$$

where $g_m(z)$ and $j_m(z)$ correspond to the two fundamental solutions in (50), the continuity of β at $\alpha = \alpha_m$ requires

$$B_{0,s} = B_{0,s+1} \tag{60}$$

Also

$$\frac{d\beta_{n,s}}{d\alpha} = B_{0,s}\, g'_m(z) + B_{1/2,s} \left\{ \sqrt{(\alpha_m - \alpha)}\; j'_m(z) - \frac{1}{2\sqrt{(\alpha_m - \alpha)}}\, j_m(z) \right\}$$

and therefore

$$\beta_{n,s} \to -\tfrac{1}{2} B_{1/2,s}\, j_m(z)\, \phi(\alpha) \qquad \text{as } \alpha \to \alpha_m.$$

Similarly

$$\beta_{n,s+1} \to +\tfrac{1}{2} B_{1/2,s+1}\, j_m(z)\, \phi(\alpha) \quad \text{as } \alpha \to \alpha_m,$$

so that the continuity of β at $\alpha = \alpha_m$ requires

$$B_{1/2,s} = -B_{1/2,s+1} \tag{61}$$

In the same way the continuity of β and $\dot{\beta}$ at $\alpha = 1$ determines the relation between $\beta_{n,s}$ and $\beta_{n,s+1}$ when s is even. Writing

$$\left.\begin{aligned} \beta_{n,s} &= A_{0,s}\, g_1(z) + A_{1/2,s} \sqrt{(\alpha - 1)}\; j_1(z), \quad z = \alpha - 1 \\ \beta_{n,s+1} &= A_{0,s+1}\, g_1(z) + A_{1/2,s+1} \sqrt{(\alpha - 1)}\; j_1(z) \end{aligned}\right\} \tag{62}$$

we find

$$A_{0,s} = A_{0,s+1} \tag{63}$$

and

$$A_{1/2,s} = -A_{1/2,s+1} \tag{64}$$

The solution when $P/Q = 10^4$, $n = 2$

The case when P/Q is large is of most interest in connection with underwater explosions, and the above result has therefore been evaluated for the second harmonic term, with $P/Q = 10^4$. The second harmonic S_2 includes (among others) the deviation which deforms a sphere into a prolate or oblate spheroid. It will be assumed that this deformation exists at the instant of the explosion, and that its velocity is initially zero.

When $P/Q = 10^4$, the value of the maximum radius is found to be

$$\alpha_m = 30.73, \tag{65}$$

and the period of pulsation of the bubble is

$$T = 0.056\, a_0 \quad (T \text{ in sec. and } a_0 \text{ in cm.}) \tag{66}$$

These values are of the same order as those observed for T.N.T. and similar explosives.

When .....

When P/Q is much greater than 10^3, the compressibility of the water will be important during the (short) time that α is near to 1, and will give rise to a radiation of acoustic energy and a consequent decay of the pulsations. This effect is ignored in the present calculations. Nevertheless the result may be expected to indicate what happens during the greater part of a pulsation and particularly when $\alpha > 2$, for when α has reached 2, the pressur will have fallen to a value of order 10^3Q or less.

The method adopted in the calculations was to determine first two fundamental solutions of equation (49) for $\beta_{2,5}$ as a function of α, using the expansions (50) and (54). These solutions, denoted respectively by g_1 and $\sqrt{(\alpha - 1)}\, j_1$, were chosen to satisfy the conditions,

$$g_1 = 1, \quad \frac{dg_1}{d\alpha} = 0 \qquad \text{at } \alpha = 1 \qquad (67)$$

$$\sqrt{(\alpha - 1)}\, j_1 = 0, \quad \frac{dj_1}{d\alpha} = 1 \qquad \text{at } \alpha = 1 \qquad (68)$$

and thus correspond to the expansions given in (50) when $\alpha_1 = 1$, and $A_0 = 1$, $A_{1/2} = 1$. Their values were determined from (50) for the range $\alpha = 1$ to $\alpha = 1.5$. These solutions were then extended by analytic continuation over the range $\alpha = 1.5$ to $\alpha = 10$ by means of Taylor expansions of the form (54) relative to the points $k = 2$ and 6. For the remainder of the range, $\alpha = 10$ to $\alpha = \alpha_m$, the solutions were continued by means of the expansions (50) with $z = \alpha - \alpha_m$. The various expansions used have certain common regions, where their convergence is sufficiently rapid for calculation, so that a number of checks on the results could be made. The values of g_1 and $\sqrt{(\alpha - 1)}\, j_1$ found in this way are given in Table I.

TABLE I.

α	g_1	$\sqrt{(\alpha-1)}\, j_1$	α	g_1	$\sqrt{(\alpha-1)}\, j_1$	g_m	$\sqrt{(\alpha_m-\alpha)}\, j_m$
1.0	1.000	0	4.0	.824	.678		
1.1	1.089	.315	6.0	.406	.456		
1.2	1.164	.441	8.0	.109	.268		
1.5	1.309	.667	9.0	−.004	.189	−.860	4.47
1.6	1.337	.716	10.0	−.103	.117	−.671	4.64
1.7	1.351	.762	$\alpha_m - 15$	−.426	−.156	+.112	4.37
1.8	1.353	.778	$\alpha_m - 10$	−.536	−.282	.528	3.49
1.9	1.347	.796	$\alpha_m - 4$	−.551	−.358	.851	2.01
2.0	1.334	.808	$\alpha_m - 1$	−.516	−.373	.966	1.011
2.1	1.316	.815	$\alpha_m - .5$	−.498	−.371	.983	0.711
2.2	1.294	.818	$\alpha_m - .1$	−.469	−.366	.997	0.317
2.3	1.269	.818	α_m	−.443	−.358	1.000	0
2.4	1.241	.815	(=30.73)				
2.5	1.212	.810					
3.0	1.080	.779					

Apart from the variable α, the functions g_1 and j_1 depend on two parameters, σ (=Q/P) and n. As far as σ is concerned, the values of g_1 and j_1 given in the table are unaffected up to $\alpha = 2$ by taking any value of σ not greater than 10^{-4}, and they are not affected by more than about 1% up to $\alpha = 6$. Increasing σ to 10^{-3} does not change the values up to $\alpha = 3$ by more than about 1%. Consequently the early part of Table I will give a fair approximation to the solution of equation (49) for values of α from 1 to 3 (and possibly as far as 6), for any value of P/Q likely to arise in connection with explosions. On the other hand, altering n has a great effect on the values of g_1 and j_1, as is obvious from the approximate expressions (58) for β near $\alpha = 1$.

The determination of β during a contracting phase, following the known variation during the preceding expanding phase, is determined, as shown above, by expressing β in terms of the two fundamental solutions g_m and $\sqrt{(\alpha_m - \alpha)}\, j_m$. Hence the values of these solutions from $\alpha = 9$ to $\alpha = \alpha_m$ were also calculated and are shown in Table I.

The relation between the two pairs of fundamental solutions in Table I is found to be

$$g_1 = \cdots\cdots$$

$$\left.\begin{aligned} g_1 &= -.4434\, g_m - .08625\sqrt{(\alpha_m - \alpha)}\; j_m \\ (\alpha - 1)\, j_1 &= -.3583\, g_m - .02661\sqrt{(\alpha_m - \alpha)}\; j_m \end{aligned}\right\} \qquad (69)$$

The relation between the pairs of arbitrary constants appearing in the alternative expressions for β is obtained immediately from (69), for if

$$\beta(\alpha) = B_0\, g_m + B_{1/2}\sqrt{(\alpha_m - \alpha)}\; j_m = A_0\, g_1 + A_{1/2}\sqrt{(\alpha - 1)}\; j_1,$$

and g_1 and j_1 are expressed in terms of g_m and j_m by (69) we have, on comparing coefficients of g_m and j_m in the resulting identity,

$$\left.\begin{aligned} B_0 &= -.4434\, A_0 - .3583\, A_{1/2} \\ B_{1/2} &= -.08625\, A_0 - .0266\, A_{1/2} \end{aligned}\right\} \qquad (70)$$

Conversely

$$\left.\begin{aligned} A_0 &= 1.393\, B_0 - 18.76\, B_{1/2} \\ A_{1/2} &= -4.516\, B_0 + 23.22\, B_{1/2} \end{aligned}\right\} \qquad (71)$$

Since the initial velocity of the deviation is zero, we have

$$\beta_{2,1} = 1, \quad \dot{\beta}_{2,1} = 0 \text{ when } \alpha = 1.$$

Now if

$$\beta_{2,1} = A_0\, g_1 + A_{1/2}\sqrt{(\alpha - 1)}\; j_1,$$

then

$$\beta_{2,1} = \left\{ A_0\, g'_1 + A_{1/2}\left[\frac{1}{2\sqrt{(\alpha - 1)}}\; j_1 + \sqrt{(\alpha - 1)}\; j'_1\right]\right\}\dot{\alpha}$$

$$\to \tfrac{1}{2} A_{1/2}\frac{c_0}{a_0}\sqrt{(2 - 2\sigma)} \quad \text{as } \alpha \to 1.$$

Hence the above conditions require

$$A_0 = 1 \quad \text{and} \quad A_{1/2} = 0,$$

that is, the value of β during the first expansion is given by g_1 in Table I.

The coefficients B_0, $B_{1/2}$ in the alternative expression for $\beta_{2,1}$ are obtainable from (70), and the coefficients in the corresponding expression for $\beta_{2,2}$ are thus obtained by simply changing the sign of $B_{1/2}$ as in (61). The coefficients for the succeeding expanding and contracting phases are then obtained by successive applications of equations (58) – (61) and (70), (71). Their values for the first two pulsations of the bubble are given in Table II.

TABLE II.

Expansion	Contraction	A_0	$A_{1/2}$	B_0	$B_{1/2}$
$\beta_{2,1}$	–	1.000	0	– .4434	– .08625
–	$\beta_{2,2}$	– 2.237	+ 4.006	– .4434	+ .08625
$\beta_{2,3}$	–	– 2.237	– 4.006	+2.427	+ .2994
–	$\beta_{2,4}$	+ 8.997	–17.910	+2.427	– .2994

It will be seen that the values of A_0 correspond to the successive values of β at $\alpha = 1$, and the values of B_0 to the successive values of β at $\alpha = \alpha_m$.

The .....

The graph of β as a function of α during the first two pulsations is easily constructed from Tables I and II. This is shown in Figure 4. It will be seen that the variation of β during the second pulsation is generally of a similar nature to that during the first pulsation, but the sign is changed and the amplitude is increased.

When β is regarded as a function of t, it should be expressible in the form (15). It is easily verified that for any function of this form

$$\cosh \lambda T = \tfrac{1}{2} [\beta (t + 2T) + \beta (t)] / \beta (t + T),$$

so that λ is determined by any 3 values of β separated by intervals of T. Taking the values of 0, T and 2T as given by A_0 in Table II, we find

$$\cosh \lambda T = -2.06,$$

whence $$e^{\lambda T} = -3.95, \quad \text{or} \quad \lambda = (1.38 + 1\pi)/T. \qquad (72)$$

This shows that eventually (if the pulsations could continue) the perturbation β increases four-fold in absolute magnitude and changes sign during each complete pulsation. In this sense, therefore, the perturbation is unstable.

At any value of α the departure of the bubble from sphericity is measured, not by β, but by β/α. This implies that the non-sphericity greatly decreases during the expansion. At the end of the first expansion we have $\beta/\alpha = -.443/30.7 = -.015$, or about 1.5% of its value initially, and of opposite sign.

When β/α is regarded as a function of t, it decreases very rapidly at first, due to the rapid initial increase of α. It remains small and changes very slowly during the relatively long period that the bubble is large, but it increases very rapidly (in absolute value) when the bubble approaches its minimum again. These changes are illustrated in Figure 5, which shows β/α as a function of t during the first two pulsations. It is evident from this figure that any small disturbance of the bubble when it is large (e.g. due to gravity) would lead to very great changes in its shape when it contracts again.

References.

(1) Lamb, Phil. Mag., 45, 257, 1923.

(2) Butterworth, "Report on the theoretical shape of the pressure time curve and on the growth of the gas-bubble", 1923.

(3) Willis, "Underwater explosions. Time interval between successive explosions", 1941.

(4) Herring, C4 - Sr 20 - 010, N.D.R.C., 1941.

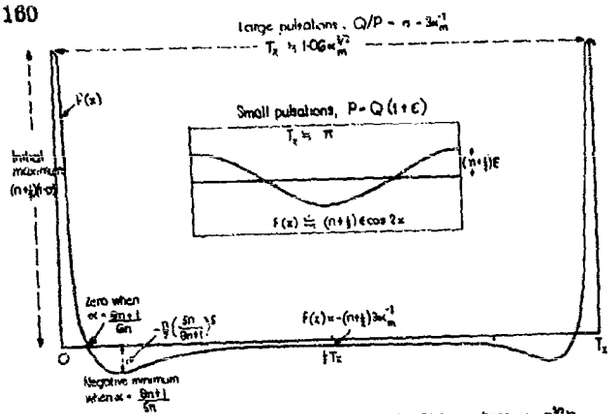

FIG · 1 · The function $F(x)$ in the equation $\psi'' = F(x)\psi$, where $\psi = a^{3/2}b$, $x = \sqrt{(P/\rho)}\,t/a_0$.

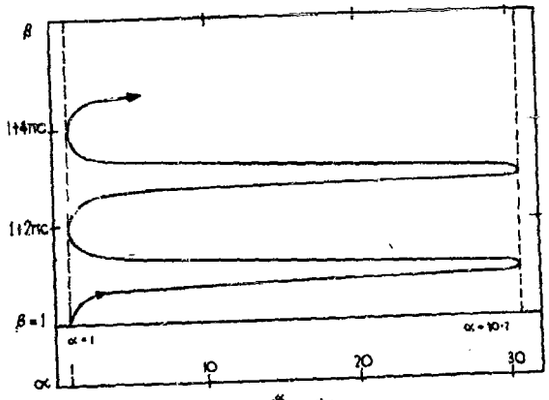

$$\beta_1 = 1 + C\int_1^{\alpha} \frac{d\alpha}{\alpha\sqrt{[\alpha^{-1} + \frac{1}{3}P^{-1}Q(\alpha-\alpha^4)]}}$$

$$\beta_1 = C c_0 \sqrt{2}\,\alpha^{-3}$$

When $\beta_1(0) = 0$, curve shrinks to straight line $\beta = 1$

FIG · 2 · Graph of β_n when $n = 1$, $P/Q = 10^4$, giving (small) displacement of centre of bubble as a function of α

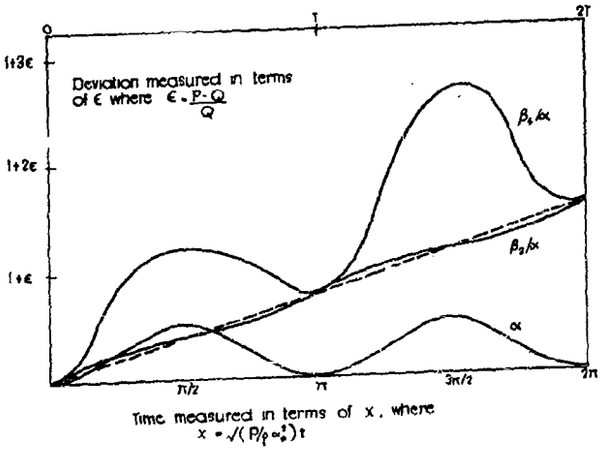

Time measured in terms of x, where $x = \sqrt{(P/\rho\alpha_0^3)}\,t$

FIG · 3 · The deviations from sphericity expressed by the second and fourth harmonic terms in the case of small pulsations.

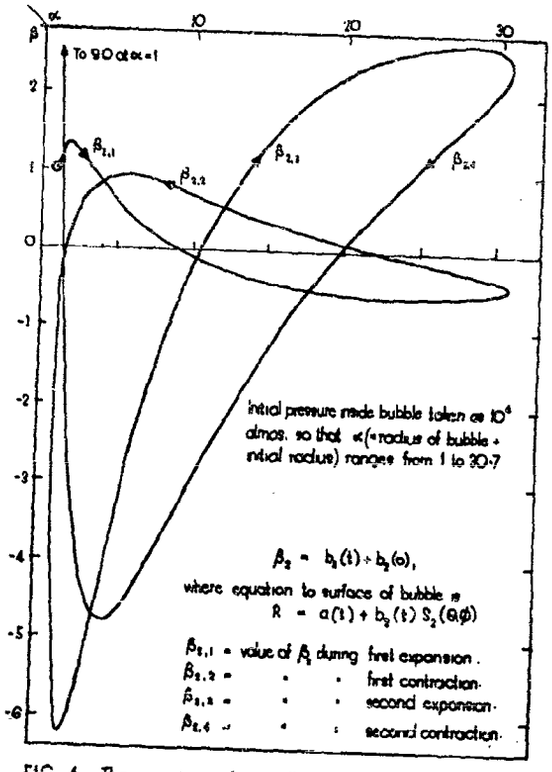

FIG. 4. The variation of a small second harmonic perturbation of the shape of the bubble during two pulsations.

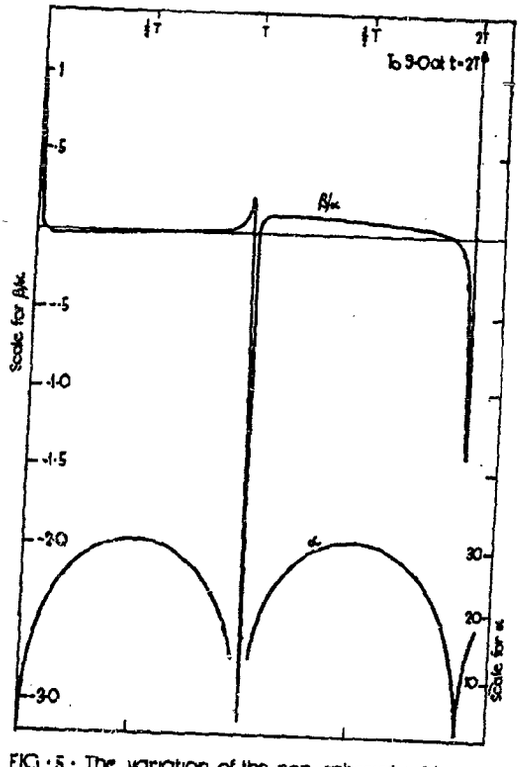

FIG. 5. The variation of the non-sphericity β/α as a function of t over two pulsations.

THE BEHAVIOUR OF AN UNDERWATER EXPLOSION BUBBLE

Approximations based on the theory of
Professor G. I. Taylor

A. R. Bryant
Road Research Laboratory, London

British Contribution

December 1942

THE BEHAVIOUR OF AN UNDERWATER EXPLOSION BUBBLE

Approximations based on the theory of
Professor G. I. Taylor.

A. R. Bryant

December 1942.

* * * * * * * * *

Summary

Approximate solutions are presented for the equations of motion of the gas bubble produced by an underwater explosion, as given by Professor G. I. Taylor. The equations enable the most important features of the bubble motion to be computed approximately with comparatively little labour. In addition graphs are given which are based upon the approximations, and which enable most of the quantities to be read directly as functions of the depth for various charge weights. The effect produced on the bubble motion by changing the charge weight or the depth of the charge may be easily seen from these approximations, which should assist in an appreciation of the relations which arise when the scale of an experiment is changed.

Introduction.

Professor G. I. Taylor has treated the radial expansion and vertical motion of the bubble of gas formed when a charge is detonated in water*. He has developed equations which require to be integrated step by step numerically and has shown that exact scaling for different charge weights is not possible, so that the numerical integration must be repeated for different values of the charge weight and the depth. The following note puts forward approximate solutions to these equations which enable most of the important features of the bubble motion to be computed with comparatively little labour. In order that these equations may be readily available they have been listed at the beginning of the note, with an explanation of the symbols used, but with their derivation omitted. Although the numerical constants for T.N.T. have been employed throughout, the methods of approximation used are applicable to any explosive.

As in the Report "Vertical motion of a spherical bubble and the pressure surrounding it", free or rigid surfaces have been assumed remote enough to cause no disturbance to the motion. Their perturbing effect as given by Conyers Herring is discussed in an Appendix.

The non-dimensional form of the Equations.

The basic equations of motion of the bubble are used in the non-dimensional form given by Professor Taylor. In the list of formulae below, and in their subsequent derivation, some of the equations are best left in this form. To convert to real quantities all non-dimensional lengths must be multiplied by the length scale factor L, and all non-domensional times multiplied by $\sqrt{\frac{L}{g}}$, g being the acceleration due to gravity. For T.N.T. the value of L is given by

$$L \text{ (feet)} = 10\, M^{\frac{1}{3}} \qquad (1)$$

where M is the charge weight in lbs. L is plotted against charge weight in Figure 1.

To avoid confusion non-dimensional quantities will be denoted by small letters, while capital letters will be used for dimensional quantities (with the exception of the symbols g, and ρ the density of water). Non-dimensional equations will be labelled as such.

Part I .....

* Vertical motion of a spherical bubble and the pressure surrounding it. G.I. Taylor.

PART I.

Summary of Approximation Formulae.

Two non-dimensional variables define the size, position and motion of the bubble at any time t, viz:- the radius of the bubble a and the depth z of the centre of the bubble measured from a point 33 feet above sea level.

A parameter c appears in the equations, in their non-dimensional forms, which is related to the potential energy in the gas; the value of c for T.N.T. is given by:-

$$c = 0.075\, W^{\frac{1}{16}} \qquad (2)$$

where W is in lbs.

The period of the first oscillation – T (seconds)

$$T = \frac{4.32\, W^{\frac{1}{3}}}{Z_o^{\frac{5}{6}}} \qquad (3)$$

where Z_o is the depth of the charge in feet below a point 33 feet above sea level.

W is the charge weight in lbs.

The period is the time taken for the bubble to expand and contract again to its minimum radius.

At a distance d non-dimensional units from a free or rigid surface the period T is altered to T' where

$$\frac{T'}{T} = \left(1 \mp \frac{0.21\, a_m}{d}\right) \quad \text{(R.R.S. non-dimensional)} \qquad (3a)$$

where the upper sign is for a free surface, the lower for a rigid surface, and a_m is the maximum radius (see equation (4)).

The maximum radius of the bubble – a_m

$$a_m^3 = \frac{3}{4\pi z_o}\left(1 - c\, a_m^{-\frac{1}{2}}\right) \quad \text{(non-dimensional)} \qquad (4)$$

z_o being the non-dimensional depth of the charge at detonation; a_m is plotted in Figure 2 against z_o.

The vertical momentum constant – m.

The non-dimensional constant m is involved in several equations and is given by:

$$m = \frac{0.7\, a_m^3}{z_o^{\frac{5}{6}}} \quad \text{(non-dimensional)} \qquad (5)$$

At a distance d non-dimensional units below a free surface or above a rigid surface the vertical momentum constant is changed to m' where

$$m' = m\left(1 - 0.52\, \frac{a_m^3\, z_o^{\frac{5}{3}}}{d^2}\right) \quad \text{(non-dimensional)} \qquad (5a)$$

This value of m' must be used in all subsequent equations involving m if the surface effect is appreciable in the case considered.

The .....

The total vertical momentum of the water surrounding the bubble.

During the period when the bubble is near its minimum radius at the end of the first oscillation the vertical momentum of the water is approximately constant and equal to

$$1481\ L^{\frac{7}{2}}\ m \quad \text{lbs.feet/second.} \tag{6}$$

where L is the scale factor in feet and m is non-dimensional.

The minimum radius of the bubble - a_1

$$a_1^3\ (1 - c a_1^{-\frac{3}{2}}) = \frac{4\pi}{3} m^2 \quad \text{(non-dimensional)} \tag{7}$$

Equation (7) must be solved graphically. Using equations (5) and (4), a_1 has been plotted in Figure 3 against the non-dimensional depth z_0.

The pressure wave emitted by the collapsing and expanding bubble.

During the period when the bubble is near its minimum radius a pressure pulse is radiated outwards with the velocity of sound. For points not too near the bubble the peak pressure P_m (lb./square inch), the total positive impulse I (lb.-second/square inch) and the duration of the positive pressure pulse D (second) are given by the following formulae:-

$$\frac{RP_m}{0.434\ L^2} = \frac{3}{4\pi\ a_1^2}\ (1 - \tfrac{3}{4} c a_1^{-\frac{3}{2}}) \quad \text{(R.H.S. non-dimensional)} \tag{8}$$

where R is the distance in feet from the point to the centre of the bubble.

The right-hand side of equation (8) is plotted against a_1, in Figure 4 for a number of charge weights. Using Figure 3, P_m may be tabulated for various charge weights and depths and is given as a function of the depth in Figure 5.

$$\text{The Impulse} \quad I = \frac{15.1\ M^{\frac{2}{3}}}{R\ z_0^{\frac{1}{6}}} \tag{9}$$

The impulse I is plotted in Figure 6 against charge weight M.

$$\left.\begin{aligned} \text{The duration} \quad D &= 0.218\ T \\ \text{or } D &= \frac{0.944\ M^{\frac{1}{3}}}{z_0^{\frac{5}{6}}} \end{aligned}\right\} \tag{10}$$

The maximum vertical velocity of the bubble - U_m feet/second.

$$\frac{U_m}{11.31\ L^{\frac{1}{2}}} = \frac{m}{a_1^3} \quad \text{(R.H.S. non-dimensional)} \tag{11}$$

U_m is plotted against the depth in Figure 7.

The rise of the bubble at the end of the first oscillation - h.

At the point where the bubble is at its minimum radius it has risen a distance h (non-dimensional) above the point where the charge was detonated

$$h = \frac{1.19}{z_0^{\frac{5}{6}}} \quad \text{(non-dimensional)} \tag{12}$$

The rise h is plotted against z_0 in Figure 8.

At a .....

At a distance d non-dimensional units below a free surface or above a rigid surface the rise h is altered to h' where

$$h' = h\left(1 - \frac{1}{3}\,\frac{a_m^3 z_0}{d^3}\right) \qquad \text{(non-dimensional)} \qquad (12a)$$

Agreement of approximations with exact solutions.

Recently the full numerical integration of Taylor's equations has been carried out for a few depths and charge weights, covering the range of non-dimensional depths from 1 to 4, and charge weights from 2 to 400 lbs. Comparison of the above approximations with these figures, and with some unpublished figures for a 1-oz. charge at 6 feet depth shows that the agreement over the whole range is satisfactory. The period of the motion and the maximum and minimum radii agree within 1 to 5 per cent, the maximum vertical velocity and the rise of the bubble within 5 to 10 per cent, and the peak pressure within 7 to 20 per cent.

PART II.

Derivation of the Approximate Solutions.

Taylor's equations of motion of the bubble, when expressed in their non-dimensional form, are (1):

$$\left.\begin{aligned} \left(\frac{da}{dt}\right)^2 &= \frac{1}{2\pi a^3}\left(1 - \frac{Ga}{W}\right) - \frac{1}{6}\left(\frac{dz}{dt}\right)^2 - \frac{2}{3}z \\ -\frac{dz}{dt} &= \frac{2}{a^3}\int_0^t a^3\,dt \end{aligned}\right\} \text{(non-dimensional)} \quad (13)$$

W is the total energy of the motion, Ga the potential energy of the gas in the bubble at radius a. For T.N.T. Taylor expresses the potential energy term (2)

$$\left.\begin{aligned} \frac{Ga}{W} &= ca^{-3} \\ \text{where } c &= 0.075\,M^{\frac{1}{3.6}} \end{aligned}\right\} \qquad (14)$$

During the numerical integration of equations (13) by a step by step process it is noticed that at different stages of the motion some of the terms in the equations either remain sensibly constant or become negligible in comparison with the remaining terms. The following approximations arise from these observations.

The maximum radius of the bubble - a_m

During the first half period of the bubble the vertical motion remains small, so that in equation (13) the term $\frac{2}{3}z$ remains substantially equal to $\frac{2}{3}z_0$ (the initial depth), while the $\frac{1}{6}\left(\frac{dz}{dt}\right)^2$ term is negligible. The maximum radius of the bubble is obtained by setting $\frac{da}{dt} = 0$ in equation (13) simplified by these assumptions

$$a_m^3 = \frac{3}{4\pi z_0}\left(1 - ca_m^{-3}\right) \qquad \text{(non-dimensional)} \qquad (4)$$

The .....

(1) "Vertical motion of a spherical bubble and the pressure surrounding it". Equations 5 and 6. Taylor distinguishes all non-dimensional quantities by dashes, which are omitted for convenience.

(2) Above report. Equation 19. The exponent 3 is strictly true only for T.N.T.

The period of the oscillation T

In the step by step integration of (13) it is observed that the time T taken by the bubble to reach its minimum radius at the end of the first oscillation is within a few per cent of twice the time taken to reach the maximum radius. It is also found that omission of the term $\frac{Ga}{W}$ in integrating (13) causes very little difference in the time taken to reach the maximum radius, although the actual value of the maximum radius is quite considerably altered. The value of the non-dimensional half-period $\frac{t_M}{2}$ is accordingly obtained from

$$\frac{t_M}{2} = \int dt = \int \frac{da}{\sqrt{\frac{1}{2}\left(\frac{1}{a^3} - \frac{2}{3}z_0\right)}} \quad \text{(non-dimensional)} \qquad (15)$$

where the integral on the right is taken from a = c to the maximum value of a. The value of this integral has been given by Lamb (1) and Conyers Herring (2). The result, expressed in the non-dimensional variables used in this note is:

$$t_M = \frac{1.135}{z_0^{\frac{5}{6}}} \quad \text{(non-dimensional)} \qquad (16)$$

This value of the period (3), converted into real units, is

$$T = \frac{4.32\, M^{\frac{1}{3}}}{z_0^{\frac{5}{6}}} \qquad (3)$$

The vertical momentum constant - m

In the step by step integration of equation (13) it is found that the non-dimensional quantity $\int a^3 dt$ becomes substantially constant when the bubble has contracted to about a half of its maximum radius, and remains constant up to and beyond the time when the bubble radius is a minimum. This constant value may be put equal to m, and is proportional to the vertical momentum of the water surrounding the contracted bubble. It can be shown that the vertical momentum in lbs.feet/second units is given by

$$\text{Vertical momentum} = 1481\, L^{\frac{7}{2}}\, m \text{ lbs.feet/second} \qquad (6)$$

A knowledge of the value of m enables several quantities associated with the motion of the bubble to be calculated, so that an approximation to m is desirable. It is clear that the value of m depends mainly on the radius time-curve when the bubble radius is large. An approximate evaluation of m may be made if it be assumed that the effect of altering either the depth z_0 or the charge weight (i.e. the parameter c) is mainly to alter the maximum radius and the period of the motion, without appreciably altering the shape of the radius time curve, at least in that portion when the radius is large and the vertical momentum is mainly acquired. This is equivalent to assuming that the radius time curves could be superposed in this region if the length and time scales were adjusted to make the maximum radius and period agree. Mathematically, this assumption is that in the equation:

$$\left(\frac{a}{a_m}\right)^3 = f\left(\frac{t}{t_M}\right) \quad \text{(non-dimensional)} \qquad (17)$$

for $o < t < \frac{1}{2}t_M$

the function $f\left(\frac{t}{t_M}\right)$ is independent of depth and charge weight.

The .....

(1) Hydrodynamics. H. Lamb, p.114.

(2) Theory of the Pulsations of the Gas Bubble Produced by an Underwater Explosion. Conyers Herring.

(3) The period may be expressed in a form valid for any explosive. If λ be the energy of the motion in calories per gram of explosive, M the weight of the charge in lbs. (3) becomes

$$T \text{ (seconds)} = \frac{0.567\, M^{\frac{1}{3}}\, \lambda^{\frac{1}{3}}}{z_0^{\frac{5}{6}}} \qquad (3a)$$

This expression enables λ to be calculated from experimental measurements of the period T.

The final justification of this assumption is that the results to which it leads are in reasonable agreement with the exact solution of equation (13). Hence

$$m = \int_0^{t_M} a^3\,dt = t_M a_m^3 \int_0^{\frac{t}{t_M}} f\left(\frac{t}{t_M}\right) d\left(\frac{t}{t_M}\right)$$

$$\therefore m = k a_m^3 t_M$$

or using (16)
$$m = \frac{k' a_m^3}{z_o^{\frac{5}{6}}} \qquad \text{(non-dimensional)} \qquad (18)$$

The constant k' may be obtained from any one step by step solution of the equation of motion of the bubble (13), and its value is about 0.70, leading to equation (5)

$$m = \frac{0.70\, a_m^3}{z_o^{\frac{5}{6}}} \qquad \text{(non-dimensional)} \qquad (5)$$

The minimum radius – a_1

In the neighbourhood of the minimum radius the term $\frac{2}{3}z$ in equation (13) is negligible, but the term $\frac{1}{6}\left(\frac{dz}{dt}\right)^2$ must be included. As shown in the last section $\frac{dz}{dt}$ may be written (when a is near the minimum radius)

$$-\frac{dz}{dt} = \frac{2m}{a^3} \qquad \text{(non-dimensional)} \qquad (19a)$$

and the equation of motion of the bubble becomes:

$$\frac{da}{dt} = \sqrt{\frac{1}{2\pi a^3}\left(1 - ca^{-\frac{1}{2}}\right) - \frac{2}{3}\frac{m^2}{a^6}} \qquad \text{(non-dimensional)} \qquad (19b)$$

The minimum radius a_1 is given by setting $\frac{da}{dt} = 0$, yielding

$$a_1^3\left(1 - ca_1^{-\frac{1}{2}}\right) = \frac{4\pi m^2}{3} \qquad \text{(non-dimensional)} \qquad (7)$$

The pressure wave produced by the collapsing bubble.

During the period when the radius of the bubble is near its minimum value, pressures are set up in the immediate neighbourhood of the bubble which give rise to a pressure pulse propagated outward with the velocity of sound. Taylor has discussed the pressure distribution close to the bubble, neglecting the compressibility of the water, and gives the following equation (1). If P is the pressure (in lbs./square inch above the normal hydrostatic pressure at the same depth) at a point distant r (non-dimensional units) from the bubble, and if θ is the angle between the radius vector v and the vertical, then

$$\frac{1}{\rho}\frac{\partial p}{\partial r} = \frac{1}{r}\frac{d}{dt}\left(a^2\dot{a}\right) + \frac{1}{2}\frac{a^2}{r^2}\left(a\dot{u} + 5\dot{a}u\right)\cos\theta + \frac{a^3u^2}{r^3}\left(\cos\theta - \frac{1}{2}\sin^2\theta\right)$$

$$- \left[\frac{1}{2}\left(\frac{a}{r}\right)^4\dot{a}^2 + \left(\frac{a}{r}\right)^5 \dot{a}u\cos\theta + \frac{1}{2}\left(\frac{a}{r}\right)^6 u^2\left(\cos^2\theta + \frac{1}{4}\sin^2\theta\right)\right] \qquad (20)$$

(R.H.S. non-dimensional)

where $\dot{a} = \frac{da}{dt}$, $\dot{u} = \frac{du}{dt}$, and u is the vertical velocity in non-dimensional units.

In this .....

(1) "Vertical motion of a spherical bubble and the pressure surrounding it". Equation (30). Taylor's notation has been modified to conform with the rest of this note.

In this expression for the pressure the first term is the most important and will determine the pressure at points not too near the bubble. Considering here only this leading term, the pressure at a point R feet from the bubble centre becomes

$$\frac{144RP}{\rho L^2} = \frac{d}{dt}\left(a^2 \dot{a}\right) \qquad \text{(R.H.S. non-dimensional)} \qquad (20a)$$

Since the simplified equations of motion (19) are valid near the time of the minimum radius, when the pressure disturbance is mainly produced, (20a) may be evaluated to give:

$$\frac{144RP}{\rho L^2} = \frac{1}{4\pi a^3} - \frac{c}{16\pi a^{\frac{11}{3}}} + \frac{2}{3}\frac{m^2}{a^5} \qquad \text{(R.H.S. non-dimensional)} \qquad (21)$$

The maximum value of the pressure Pm is obtained by inserting in (21) the value of the minimum radius a_1 given by (7); hence

$$\frac{RPm}{0.434\, L^2} = \frac{3}{4\pi a_1^2}\left(1 - \tfrac{2}{3}ca_1^{-\frac{1}{3}}\right) \qquad \text{(R.H.S. non-dimensional)} \qquad (8)$$

It may be remarked that in a similar way all the other terms in (20) may be evaluated as functions of the radius a alone, using equations (19) and their value at the minimum radius computed.

When the radius is a minimum, $\dot{a}$ and $\dot{u}$ vanish while $u = -\frac{dz}{dt}$ is given by (19a). Inserting the value a_1 for the minimum radius, and converting to real units, the maximum vertical velocity U_m (feet/second) is

$$\frac{U_m}{11.31L^{\frac{1}{2}}} = \frac{m}{a_1^{\frac{7}{2}}} \qquad \text{(R.H.S. non-dimensional)} \qquad (11)$$

Owing to the rise of the bubble points situated some distance vertically above the charge may be quite close to the bubble when it is near its minimum radius, and the peak value of the pressure would then require the computation of further terms in (20).

The total positive impulse in the pressure wave is got by integrating (20a) with respect to time between the two times for which $a^2\frac{da}{dt}$ is a maximum (1). Conyers Herring has obtained the value of this impulse using an equation of motion which is identical with (13) with the vertical velocity and the gas energy term ca^{-2} neglected. Since the value of the impulse depends only on the maximum value of $a^2\frac{dt}{dt}$, which occurs when the bubble is comparatively large, Herring's neglect of the two above mentioned factors will not cause much error. Herring's value of the total positive impulse (lbs.second/square inch units) may be converted into the following useful form, if the simple approximation $a_m^3 = \frac{3}{4\pi z_0}$ be used:

$$= \frac{15.1\, M^{\frac{2}{3}}}{RZ_0^{\frac{1}{6}}} \qquad (9)$$

where R is the distance in feet from the bubble centre.

It can be shown that the duration D of this positive pulse is a constant fraction of the period T. Since the times when $a^2\frac{da}{dt}$ is a maximum occur when the radius is large, the approximation involved in equation (17) may be used. Differentiating (17) twice with respect to time, and using in equation (20a),

$$\frac{144RP}{\rho L^2} = \frac{d}{dt}\left(a^2\frac{da}{dt}\right) = \frac{a_m^3}{3t_w^2} f''\left(\frac{t}{t_w}\right) \qquad \text{(R.H.S. non-dimensional)} \qquad (22)$$

The .....

(1) The assumption is made that the expansion taking place at the beginning of the second oscillation is similar to the contraction taking place at the end of the first oscillation.

The pressure P can only be zero when $f''(\frac{t}{T_N})$ is zero, i.e. at fixed values of $\frac{t}{T_N}$. Hence the duration of the positive pulse must be a constant fraction of the total period T. Using the proportionality factor obtained from the full step by step calculation for 1 oz. of T.N.T. at 6 feet depth yields equation (10) for the duration D

$$D = 0.218T \qquad (10)$$

The shape of the pressure wave.

Equation (21) giving the pressure as a function of bubble radius and the constant m cannot be used directly to plot a pressure-time curve. A rough idea of the shape of any given pressure-time curve may, however, be obtained for any case by calculating from these equations the "shape factor" $\frac{2I}{P_m D}$. This is equal to the ratio of the area under the pressure-time curve to the area of a triangular wave form having the same peak pressure and duration. The factor thus gives a measure of the "hollowness" of the pressure-time curve.

Values of P_m, I, D and this "shape factor" for a few charge weights and depths have been given in Table 1 to demonstrate the effect of these variables on the "shape factor". In order to visualize the meaning of a particular value of the "shape factor" a few imaginary pressure wave forms have been sketched in Figure 9 and their "shape factors" computed. The curve labelled "0.24" has been drawn to resemble closely the actual pressure-time curve calculated for 1 oz. of T.N.T. at 6 feet depth.

TABLE 1.

PEAK PRESSURE, DURATION, IMPULSE AND SHAPE FACTOR.

(Pressures and impulses multiplied by the numerical value of the distance in feet from the point considered to the bubble centre)

Charge weight	Depth below sea level (feet)	Peak pressure P_m (lbs/sq.in.) x distance R (feet)	Duration D (seconds)	Impulse I (lbs.sec./sq.in) x distance R (feet)	"Shape Factor" $\frac{2I}{P_m D}$
800 lbs.	150	11,450	0.113	548	0.84
"	100	7,090	0.148	578	1.10
"	80	5,350	0.169	594	1.32
256 lbs.	150	10,600	0.078	256	0.62
"	100	6,000	0.101	270	0.78
"	50	2,950	0.151	292	1.31
16 lbs.	80	4,130	0.046	43	0.46
"	50	2,750	0.060	46	0.56
"	30	1,800	0.075	48	0.70
1 lbs.	40	1,750	0.026	7.4	0.32
"	20	1,160	0.034	7.8	0.39
"	10	830	0.041	8.0	0.47
1 oz.	6	580	0.018	1.3	0.24

The .....

The rise of the bubble - h.

An important quantity concerned with the motion of the bubble is the rise at the end of the first oscillation, since this determines the position of the bubble when the peak pressure in the wave is omitted. None of the above methods of approximation enables this quantity to be estimated. Inspection of the full calculations published for four depths, and of the unpublished calculations for a 1 oz. charge at 6 feet show that the rise h due to gravity is given by the following empirical formula with an error not exceeding 10 per cent over the range of non-dimensional depths from $z_0 = 2$ to $z_0 = 9$

$$h = 1.05\, t_M \qquad \text{(non-dimensional)}$$

Using equation (16) this becomes

$$h = \frac{1.19}{z_0^{\frac{5}{6}}} \qquad \text{(non-dimensional)} \qquad (12)$$

This rise of the bubble has been calculated on the assumption that all free or rigid surfaces are remote enough to exert no disturbing effect on the motion. Its value is plotted in Figure 8. The correction for the proximity of a surface is dealt with in the Appendix.

Appendix .....

APPENDIX

Effect of the Proximity of a Free or Rigid Surface.

Conyers Herring has shown that if the charge is exploded at distance d (non-dimensional units) from an infinite free or rigid surface the bubble acquires a velocity v towards that surface, given by

$$v = \mp \frac{2}{a^3} \int_0^t \frac{3}{4d^2} \cdot a^4 \left(\frac{da}{dt}\right)^2 dt \qquad \text{(non-dimensional)} \qquad (23)$$

where the upper sign is taken for a free surface, the lower for a rigid surface. Since usually the two most important surfaces are horizontal (e.g. the sea surface and the sea-bed) this velocity may be added to the term $-\frac{dz}{dt}$ in equation (13) for the motion, i e. the gravity term. Its effect on the minimum radius, the peak vertical velocity and the peak pressure in the bubble collapse pressure wave may be allowed for by re-defining the momentum constant m which determines them (see e.g. equations (7), (8) and (11)). Hence if m' is the vertical momentum constant for a charge detonated d non-dimensional units below the sea surface or above the sea-bed, then

$$m' = \int_0^t a^3 \left[1 - \frac{3}{4d^2} a \left(\frac{da}{dt}\right)^2\right] dt \qquad \text{(non-dimensional)} \qquad (24)$$

Using the method which led to the approximate value of m (equations (18) and (5)) gives

$$m' = m \left(1 - 0.52 \frac{a_m^3 z_o^3}{d^2}\right) \qquad \text{(non-dimensional)} \qquad (5a)$$

where the constant 0.52 is determined from one full step by step solution of the equations of motion of the bubble (13).

As regards the effect of the surface on the rise of the bubble Conyers Herring gives a simple approximation which may be expressed in the following way:-

Rise of the bubble at end of first oscillation, in proximity to the sea's surface or the sea bed

$$h' = h\left(1 - \frac{1}{5} \frac{a_m z_o}{d^2}\right) \qquad \text{(non-dimensional)} \qquad (12a)$$

where h is the rise in the absence of the surface effect (see equation (12)).

Finally Herring has shown that the presence of a surface alters the period of the motion, so that if T' is the period in proximity to a surface, and T is the value given by equation (3),

$$T' = T \left(1 \mp \frac{\bar{a}}{4d}\right) \qquad (25)$$

where $\bar{a}$ is the average value of the bubble radius (non-dimensional) over a complete oscillation the upper sign refers to a free surface, the lower to a rigid one. Using the assumptions involved in computing the vertical momentum constant m (page 6), $\bar{a}$ is a constant fraction of the maximum radius a_m, so that (28) may be written

$$T' = T \left(1 \mp 0.21 \frac{a_m}{d}\right) \qquad (3a)$$

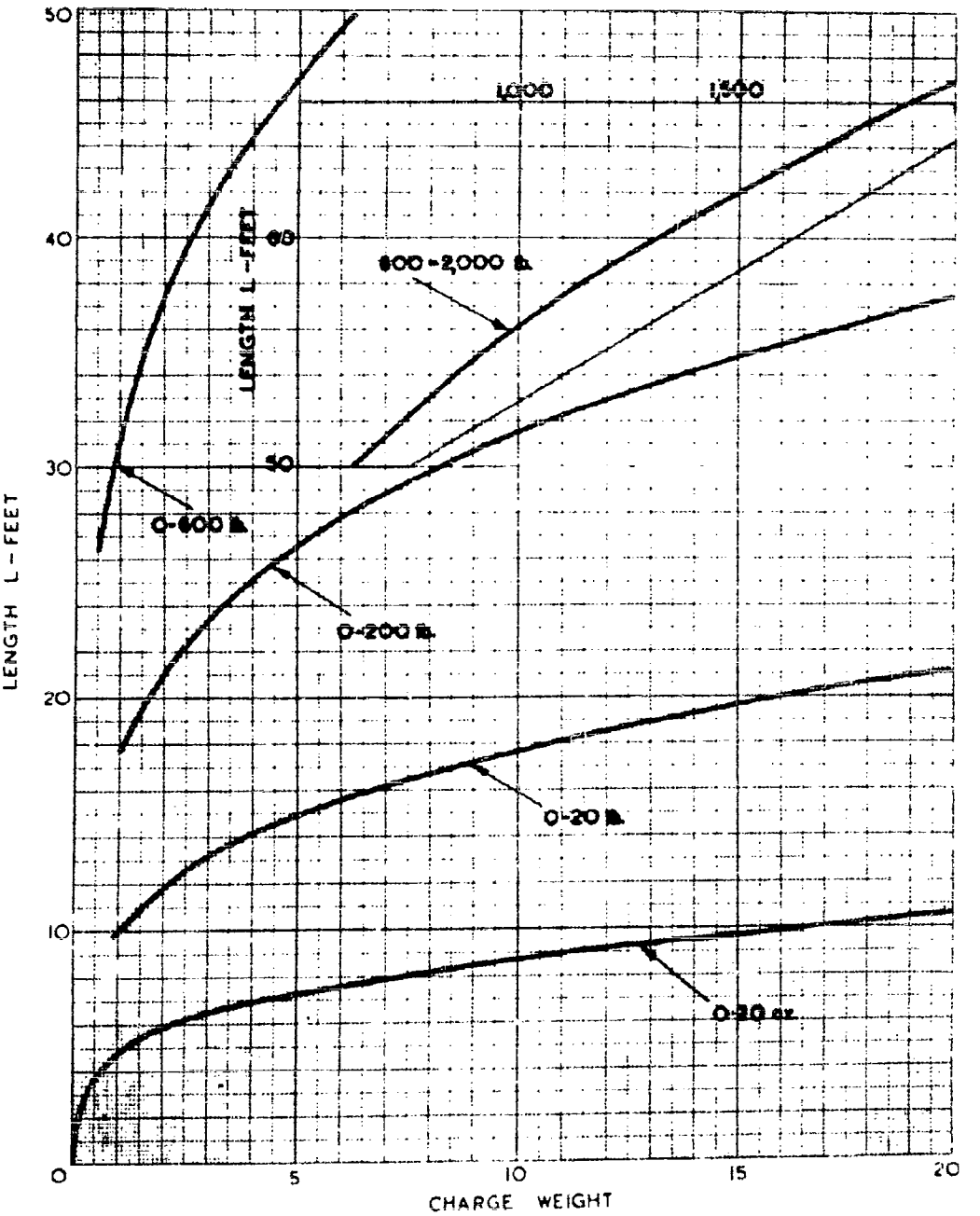

FIG 1 LENGTH SCALE FACTOR $L = \left(\frac{W}{qp}\right)^{\frac{1}{4}}$

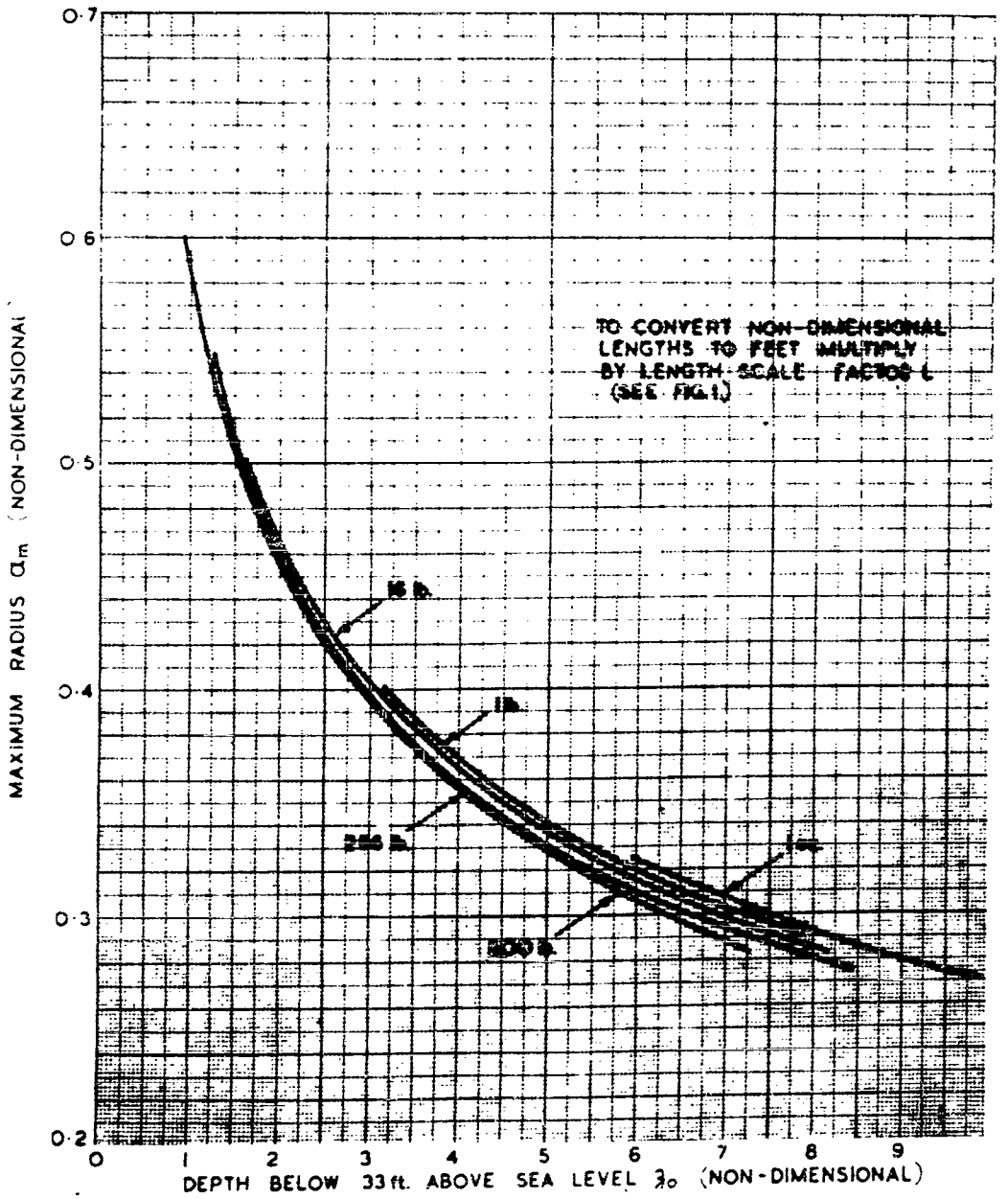

FIG. 2 MAXIMUM RADIUS OF BUBBLE

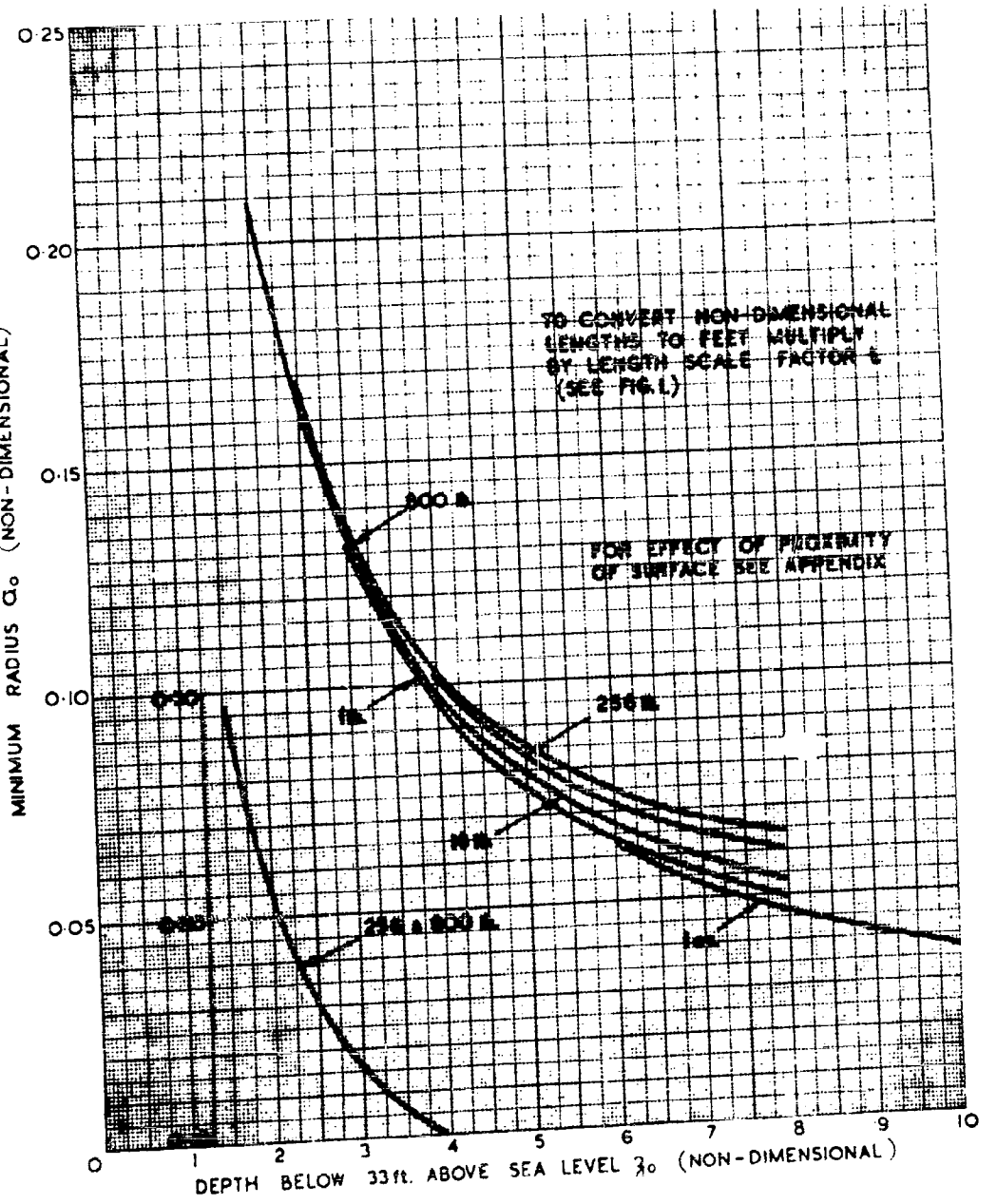

FIG. 3 MINIMUM RADIUS OF BUBBLE
(when remote from free or rigid surfaces)

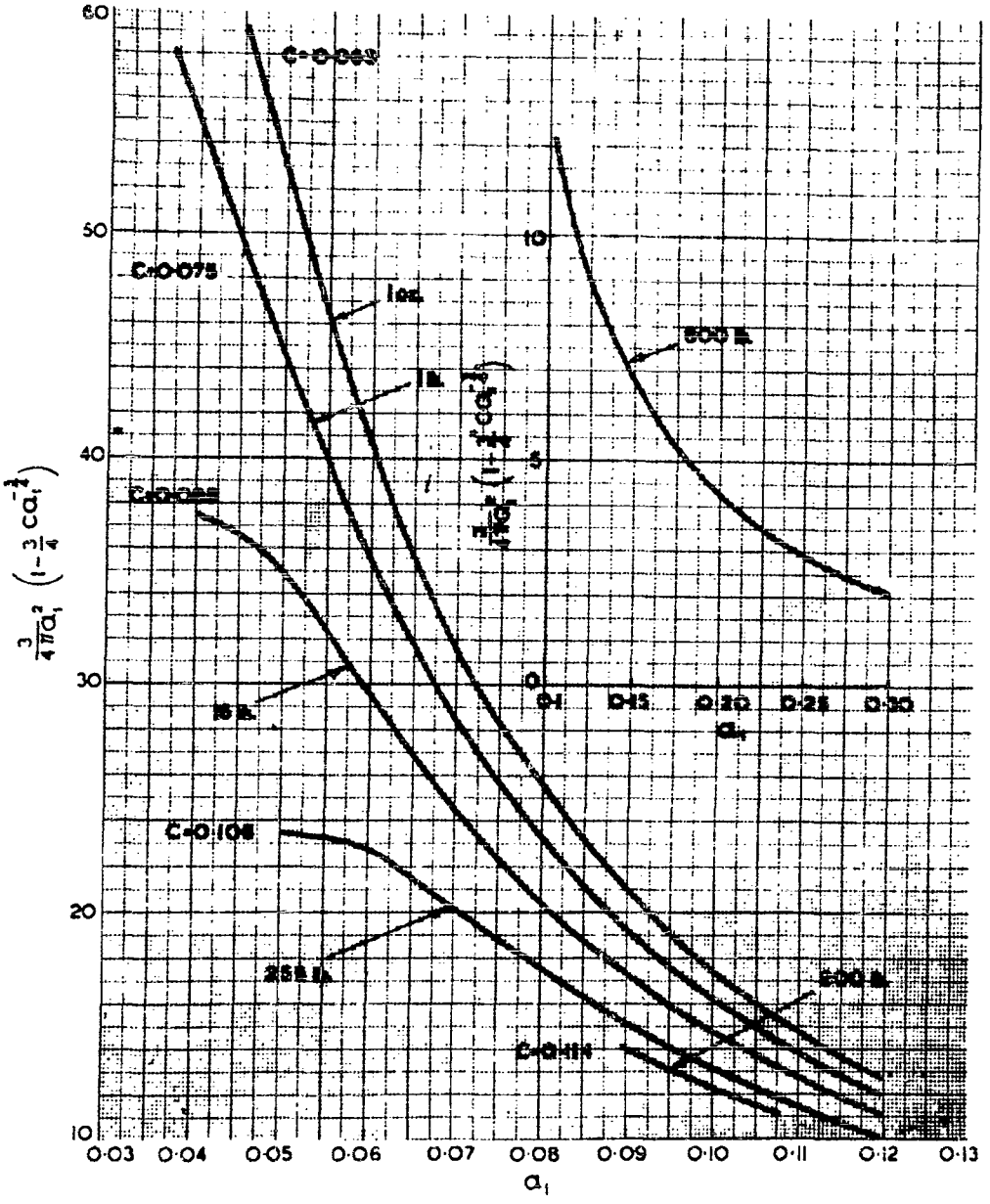
C=0·063
C=0·075
C=0·088
C=0·108
C=0·141
1 sq.
1 sq.
500 sq.
25 sq.
250 sq.
500 sq.
60
50
40
30
20
10
0·03
0·04
0·05
0·06
0·07
0·08
0·09
0·10
0·11
0·12
0·13
0·15
0·20
0·25
0·30
α_1
$\frac{3}{4\pi\alpha_1^2}\left(1-\frac{3}{4}C\alpha_1^{-\frac{1}{2}}\right)$

FIG. 4.

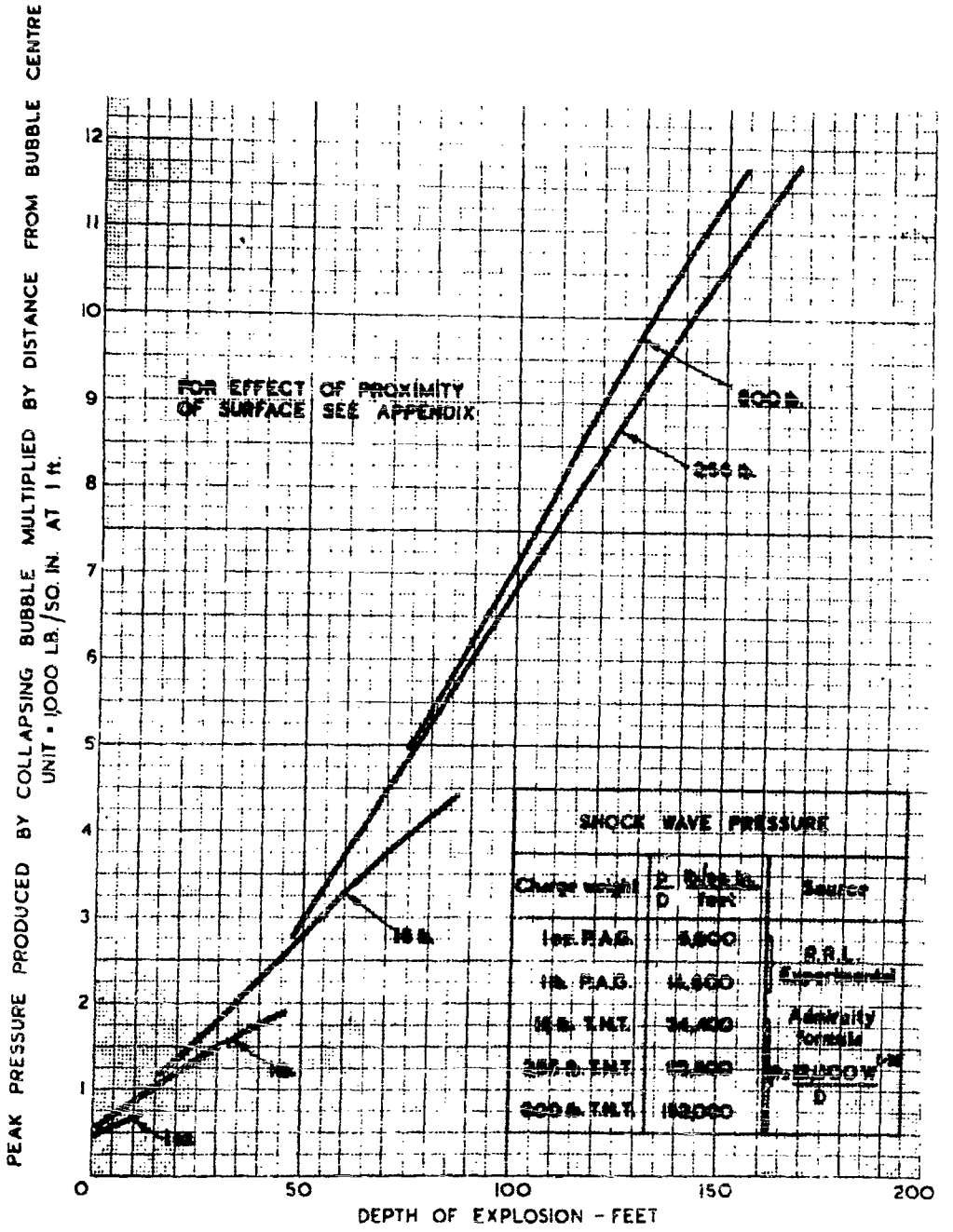

FIG. 5. PEAK PRESSURE FROM FIRST BUBBLE COLLAPSE
(When remote from free or rigid surface)

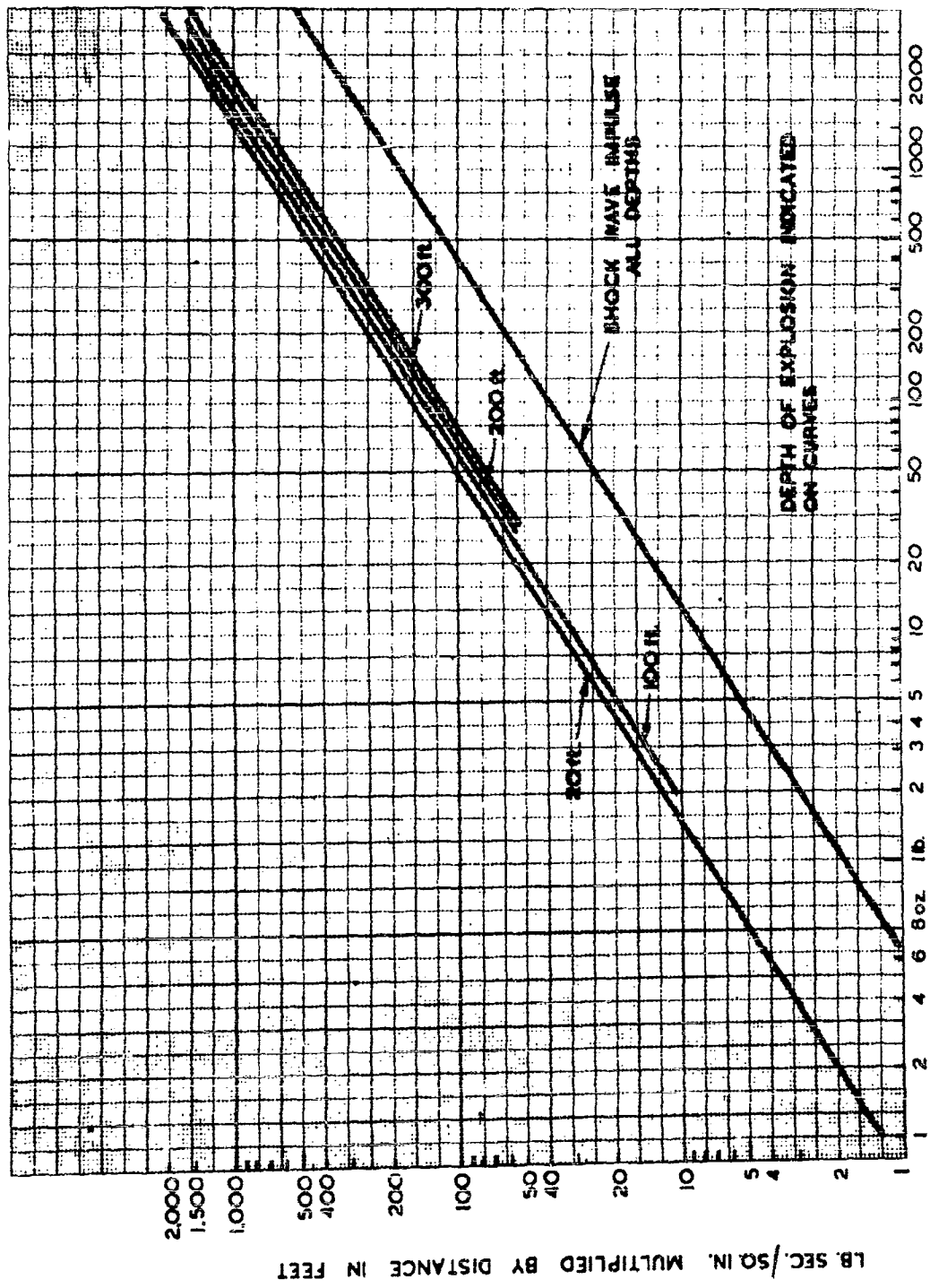

FIG. 8. IMPULSE IN FIRST BUBBLE COLLAPSE PRESSURE WAVE

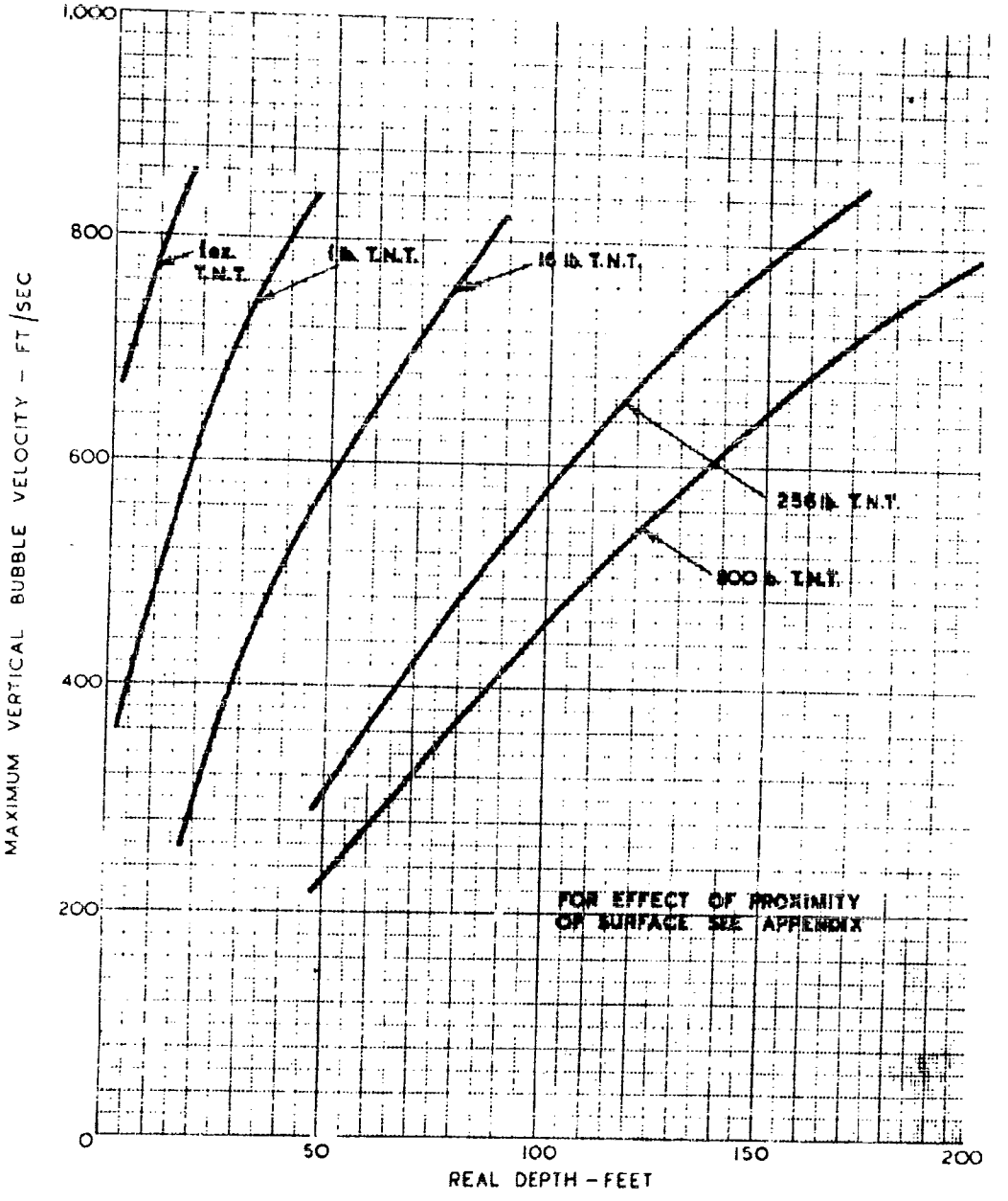

FIG. 7. VERTICAL VELOCITY OF BUBBLE AT MINIMUM RADIUS
(When remote from free or rigid surface)

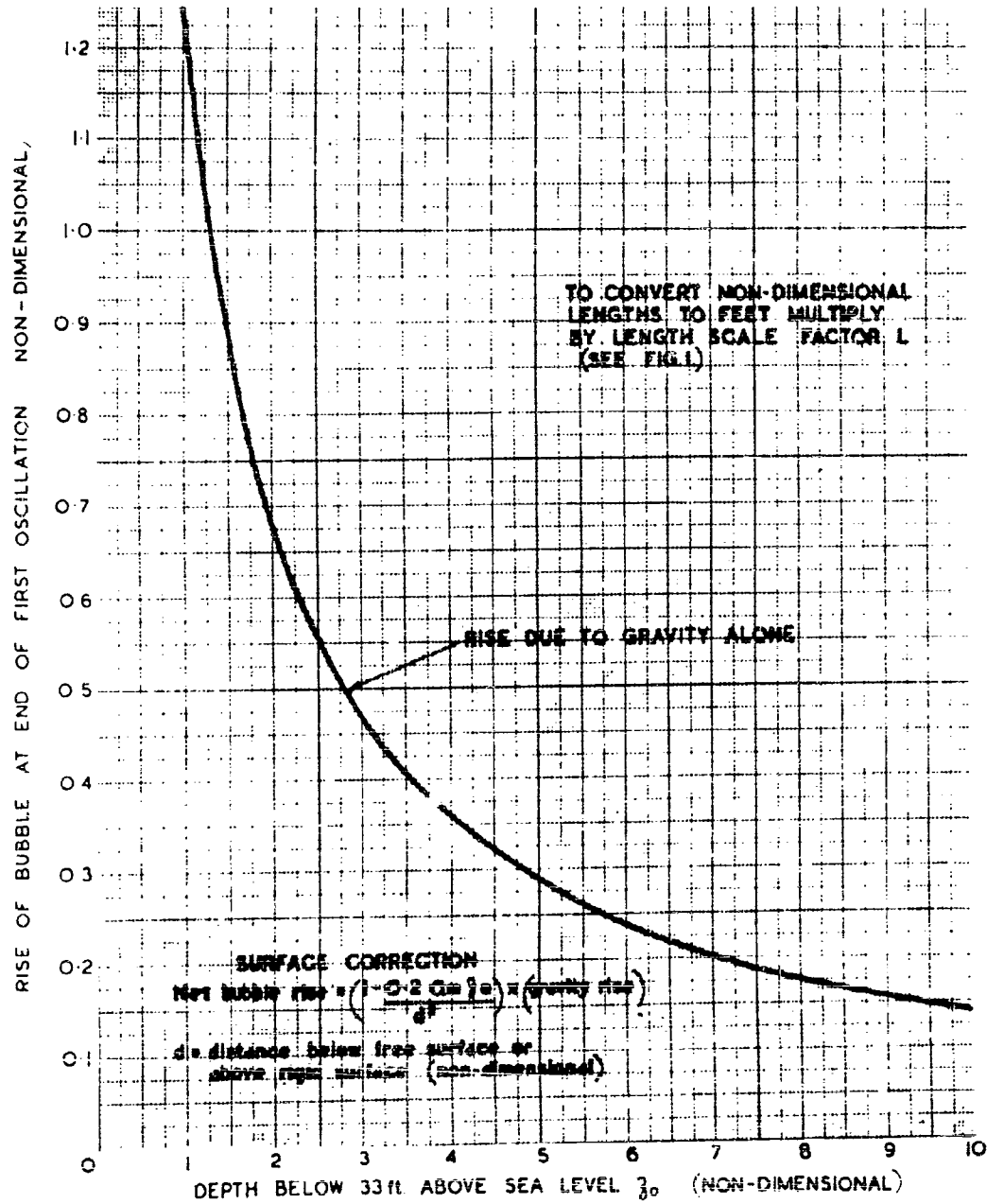

FIG 8. RISE OF BUBBLE AT END OF FIRST OSCILLATION

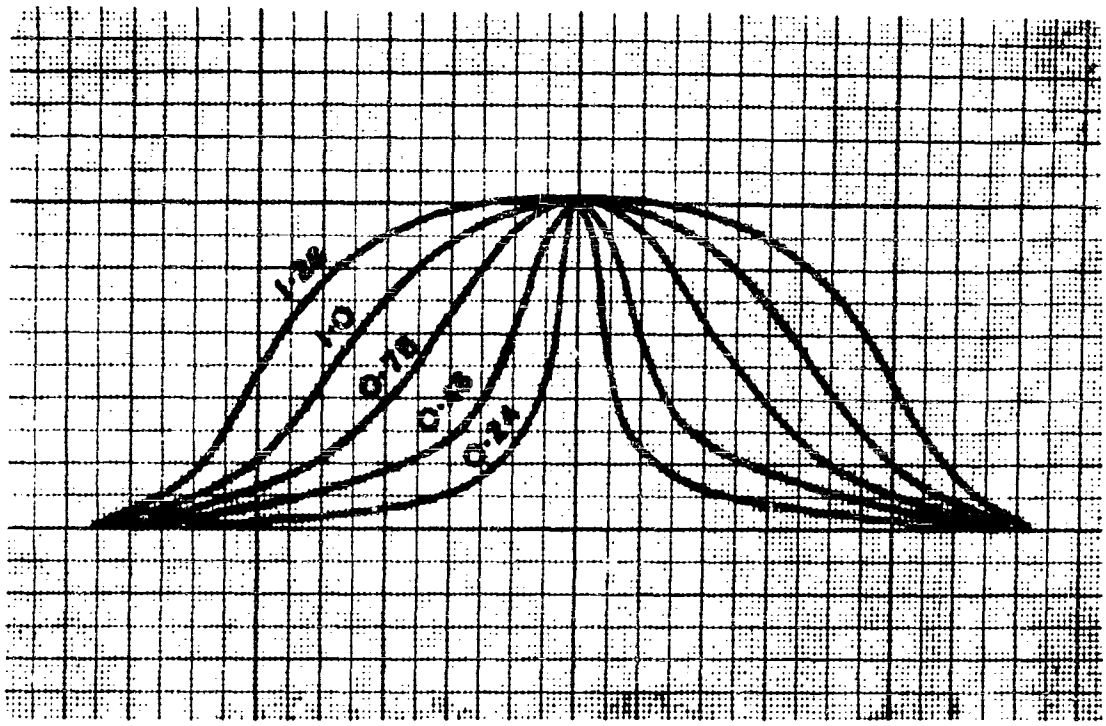

FIG. 9. IMAGINARY PRESSURE - TIME CURVES WITH VARIOUS "SHAPE FACTORS"

RADIAL MOTION OF WATER SURROUNDING A SPHERE OF GAS IN RELATION TO PRESSURE WAVES

E. H. Kennard
David W. Taylor Model Basin

American Contribution

September 1943

NOTATION

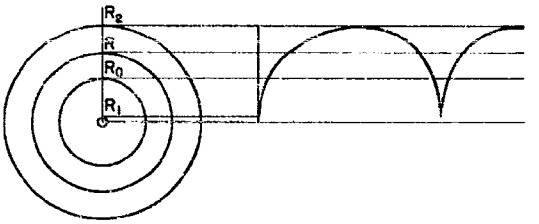

R	Radius of the spherical cavity
R_1 or R_{min}	Value at the peak of compression
R_0	Value at the point where the gas pressure equals the external pressure p_0
R_2 or R_{max}	Value at the limit of the first expansion
V	Volume of the cavity = $4\pi R^3/3$
γ	Ratio of specific heat at constant pressure to that at constant volume = 1.4 for air, or 1.3 for TNT gas
ρ	Mass density, ordinarily in dynamical or ips units
r	Radial distance from the center of the bubble to a station in the water
t	Symbol for time in general
T	Period or duration of the motion from minimum to minimum of R
T_0	Value of T when R does not depart widely from R_0
p	Symbol for pressure in general
p_A	Any pressure expressed in atmospheres
p_0	Hydrostatic pressure; the pressure on the cavity before the explosion, or the pressure in the water at a great distance from the charge
p_g	Pressure in the gas, assumed to be uniform
p_{max}	Value at the peak of compression
v	Symbol for particle velocity, zero at great distance from the charge
v_g	Velocity of the gas, equal to that in the water at the boundary
c	Velocity of sound in homogeneous water
c'	Speed of sound in water containing bubbles
Ω	The whole energy radiated in one cycle of pulsation, concentrated in the phase of peak pressure
E	Energy of oscillation, represented by the kinetic energy when $R = R_0$, also by the work done against p_0 (less the small work of the gas) in expanding from R_0 to R_2
I	Impulse or time-integral of a pressure
f	Fraction of the space occupied by bubbles in water

N	$= c\sqrt{3}/\omega_0 R_0$; N^2 represents the ratio of the adiabatic volume elasticity of water to that of the gas in the bubbles when under hydrostatic pressure
β	Extinction coefficient (the amplitude of a pressure wave decreases by a factor $e^{-2\pi\beta}$, where e is the Napierian base, in going a distance equal to one wave length as measured in homogeneous water)
ω	Frequency times 2π of sinusoidal waves
ω_0	Frequency times 2π for free small oscillations of a bubble
K	Coefficient of reflection

PERSONNEL

This report was written by Professor E.H. Kennard; the necessary numerical integrations and the plotting of certain figures were done by S. Pines.

DIGEST

This paper summarizes, and in the Appendix derives the main formulas concerned with the radial expansion and compression of spherical gas-filled cavities in water. The principal needs for these formulas are twofold, in connection with the pulsating motion of the gas globe resulting from an underwater explosion, and in connection with the behavior of bubbles of gas suspended in the water when subjected to changes in external pressure.

A sphere of gas in water under hydrostatic pressure, not subject to the action of gravity, is capable of oscillating radially with preservation of its spherical form. The period of oscillation at small amplitude is

$$T_0 = \frac{R_0}{124}\,\frac{1}{\sqrt{p_A}} \qquad [2b]$$

when T_0 is in seconds and R_0 in inches. As the amplitude increases the pulsation is slower, and the variation within moderate limits is shown in Figure 1. At large amplitudes the formula becomes

$$T = \frac{R_{max}}{217}\,\frac{1}{\sqrt{p_A}} \qquad [4b]$$

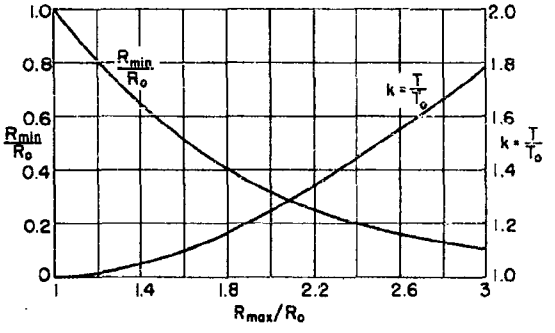

Figure 1 - Curves referring to Undamped Oscillations of a Bubble or Globe of Gas under Water

R_0 is the radius when the gas pressure equals the hydrostatic pressure, R_{max} is the maximum radius, R_{min} is the minimum radius, T_0 is the period of very small oscillations, T is the period of oscillation having given value of R_{max}/R_o. The curves are drawn for $\gamma = 4/3$, but γ makes little difference.

The pulsation of the cavity may be described as a cyclic variation of R/R_0, and examples of this are given in Figure 2. These show the main features of the motion, including the increase of intensity of the pressure peak and the lengthening of the period at greater amplitudes. The values of R_{min}/R_0 at different values of R_{max}/R_0 are shown also in Figure 1.

The pressure in the water is equal to that in the gas at the boundary between them, to the static pressure p_0 at a great distance, and at intermediate positions is affected by the flow as shown in Equation [7b], page 6; its peak value is given by the formula

$$p_{max} = p_0\,\frac{R_{min}}{r}\left[\left(\frac{R_0}{R_{min}}\right)^4 - 1\right] + p_0 \qquad [8b]$$

---

* This digest is a condensation of the text of the report, containing a description of all essential features and giving the principal results. It is prepared and included for the benefit of those who cannot spare the time to read the whole report.

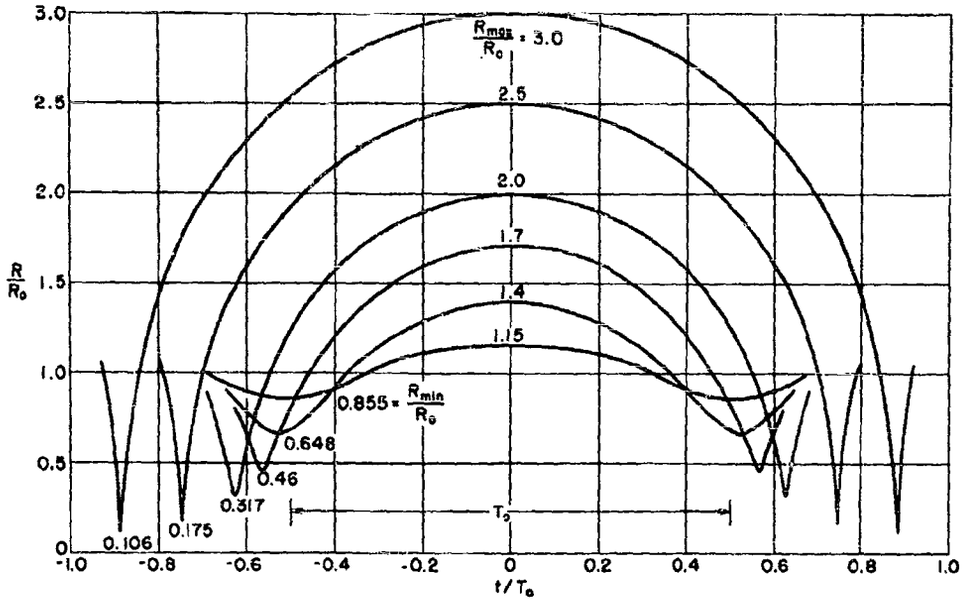

Figure 2 - Calculated Time-Displacement Curves for Undamped Oscillation of a Bubble or Globe of Gas under Water

R = radius t = time

R_0 = radius when in equilibrium T_0 = period of very small oscillations

The time relations of pressure variation are also studied in the report, and the conclusion is reached that though the peak of first compression is lower than the initial pressure peak, it is still high enough to give rise to a wave of compression in the water. Since this first compression peak is broader than the initial shock wave, it may carry with it an impulse exceeding that of the high-pressure part of the primary pressure wave.

The calculations discussed in this report deal mainly with the hydrodynamic phenomena in an incompressible fluid; however, at each pressure peak the compressibility of the water enters to play a part, and energy is radiated in a shock wave. Especial interest attaches to the quantity of energy lost in this way because it acts in structural targets in a different way from that associated with the slower motion of pulsation. No valid measurement of the energy in the shock wave is yet available, and in particular its value relative to that of the energy of oscillation E is still a matter of opinion.

The analysis thus applied to the pulsations of large gas globes resulting from explosions also explains the curious effect known to be caused by the presence of small bubbles suspended in water traversed by a shock wave. It is shown that these may serve as radiating sources of new shock waves

Figure 8a - Before the Explosion

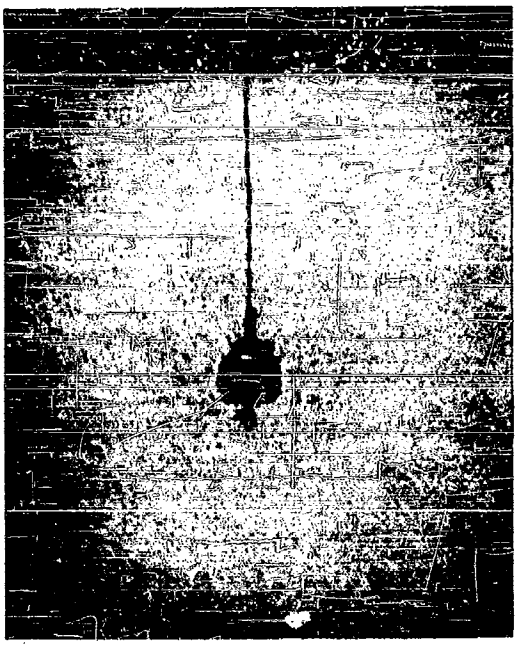

Figure 8b - After the Explosion

Figure 8 - Photographs showing a Shock Wave forming in Bubbly Water

which in turn cause a layer of bubbles to behave as a dispersive absorbing medium. The layer thus reflects an acoustic wave in somewhat the same way and for somewhat the same reason as a layer of molecules reflects light.

The only case yet amenable to full analytical treatment is a weak sinusoidal wave traversing a field containing many bubbles in each cubic wave length. The alteration in the speed of sound caused by the presence of the bubbles is shown to be proportional to the fraction of the whole space occupied by the bubbles, and, in a rather intricate way, on the ratio of the frequency of the wave to that of the bubbles; see Equation [21], page 18. The symbols used in this development are separately listed on page 18.

It is found that even a small concentration of bubbles may produce a surprisingly large reflection coefficient, and where the frequency of the wave is near that of the bubbles, not over, say, three times as great, reflection is nearly total. At much higher wave frequencies the reflection falls away to near zero.

It is thought that results similar in a qualitative sense will hold in the case of an incident shock wave, except for the unknown results of cavitation.

TABLE OF CONTENTS

	Page
ABSTRACT	1
INTRODUCTION	1
PERIOD OF OSCILLATION	2
TIME-DISPLACEMENT CURVES	4
PRESSURE IN THE WATER	5
RADIATION OF ENERGY	9
A PRESSURE WAVE AND A GAS BUBBLE	11
SLOWLY VARYING PRESSURE	12
IMPULSIVE PRESSURE	14
THE GENERAL CASE	15
A PRESSURE WAVE INCIDENT ON BUBBLY WATER	15
WEAK SINUSOIDAL WAVES IN FINE-GRAINED BUBBLY WATER	17
REFERENCES	23

APPENDIX

MATHEMATICAL THEORY OF RADIAL MOTION
AROUND GAS SPHERES IN WATER

THE RADIAL MOTION	24
PRESSURE IN THE WATER	26
RADIATION OF ENERGY	28
BUBBLE UNDER VARIABLE EXTERNAL PRESSURE	30
EFFECT OF MANY SMALL BUBBLES ON LONG PLANE SINUSOIDAL WAVES OF A SMALL AMPLITUDE	31
COEFFICIENT OF REFLECTION	36
SCATTERING BY A SINGLE BUBBLE	37

RADIAL MOTION OF WATER SURROUNDING A SPHERE* OF GAS IN RELATION TO PRESSURE WAVES

ABSTRACT

In the study of explosive pressure waves, the theory of a sphere of gas expanding or contracting under water is needed in two connections - in discussing the motion of the gas globe produced by the explosive itself, and in considering the effect of bubbles in the water upon the propagation of pressure waves. The relevant analytical formulas are collected here and discussed. Their deduction is given in an appendix.

The following topics are treated:

1. the period and form of the radial oscillations of a gas globe, and the pressure and impulse thereby generated in the water;

2. the effect of a pressure wave upon a single gas bubble;

3. the inverse effect of a layer of bubbles in water upon an incident wave of pressure, which is partially to reflect or scatter the incident wave, and to make the transmitted wave weaker but of longer duration;

4. an exact treatment for the analytically simple case of weak waves of pressure incident upon water containing bubbles of relatively small size;

5. scattering by a single bubble.

INTRODUCTION

In the study of explosive pressure waves, the theory of the expansion and contraction of a sphere of gas under water enters at two points: First, in considering the motion of the gas globe produced by the explosive, which results in secondary impulses of pressure; and second, in considering the effect of bubbles of gas in the water upon an incident pressure wave. Therefore it is proposed to collect and extend the relevant analytical formulas pertaining to such motion. Only radial motion will be considered here; effects due to gravity or to the presence of obstacles will be reserved for discussion elsewhere. Furthermore, the assumption will usually be made that compression of the water surrounding the gas globe can be neglected.

The relevant mathematical analysis has for the most part already been published (1) (2) (3),** but it will all be included for convenience in an appendix.

---

* In this report a distinction is made between the *gas globe* formed by the bulk of the gaseous products of an underwater explosion, and *gas bubbles*. The word *sphere* applies to either or both.

** Numbers in parentheses indicate references on page 23 of this report.

PERIOD OF OSCILLATION

A sphere of gas in water under hydrostatic pressure p_0, not subject to the action of gravity, is capable of oscillating radially with preservation of its spherical form. Let the gas be assumed to follow the adiabatic law, pV^γ = constant, an assumption that appears to hold well in practical cases. Then, for a small amplitude of oscillation, the period is given by Equation [34] or

$$T_0 = 2\pi R_0 \sqrt{\frac{\rho}{3\gamma p_0}} \qquad [1]$$

where R_0 is the radius of the sphere when in equilibrium under hydrostatic pressure p_0 (atmospheric pressure included), ρ is the density of water, and γ is the ratio of the specific heat of the gas under constant pressure to its specific heat under constant volume. For air, $\gamma = 1.4$ and the formula can be written

$$T_0 = \frac{R_0}{129} \frac{1}{\sqrt{p_A}} \text{ second} \qquad [2a]$$

where p_A is the pressure in atmospheres,* and R_0 is in inches. For the gas globe from an exploded charge, $\gamma = 1.3$ more nearly, and

$$T_0 = \frac{R_0}{124} \frac{1}{\sqrt{p_A}} \text{ second} \qquad [2b]$$

In sea water T_0 would be 1.3 per cent greater at the same R_0 and p_A.

The value of R_0 for gas globes from charges exploded under water is uncertain. Perhaps $R_0 = R_{max}/2.6$ is not far from the truth, where R_{max} is the maximum radius. A fair estimate for tetryl is

$$R_{max} = 49\left(\frac{W}{p_A}\right)^{\frac{1}{3}} \text{ inches}$$

where W is the weight of the charge in pounds and p_A is the hydrostatic pressure in atmospheres; the value for TNT should not be greatly different. With this value of R_0, Equation [2b] becomes

$$T_0 = 0.15 \frac{W^{\frac{1}{3}}}{p_A^{\frac{5}{6}}} \qquad [2c]$$

With increasing amplitude the period increases; it may be written

$$T = kT_0 \qquad [3]$$

where k is a dimensionless factor. In Figure 1 the factor k or T/T_0 is plotted against R_{max}/R_0. In the same figure there is shown, for convenience, the

* The period under one atmosphere is thus $R_0/129$ second.

ratio of the minimum radius, R_{min}, to R_0. The values of k were obtained by numerical integration of Equation [35] for several values of C; R_{max}/R_0 and R_{min}/R_0 were found as values of x_1 and x_2 from Equation [36]. The value $\gamma = 4/3$ was used, in order to simplify the calculation; a somewhat different value would give nearly the same curve.

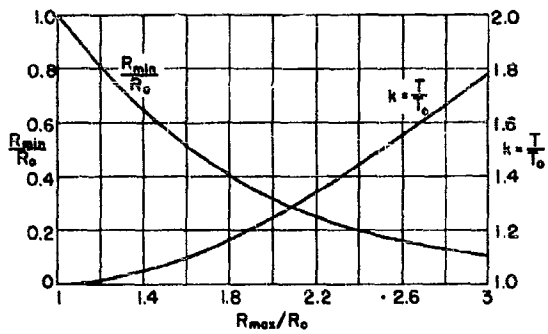

Figure 1 - Curves referring to Undamped Oscillations of a Bubble or Globe of Gas under Water

R_0 is the radius when the gas pressure equals the hydrostatic pressure, R_{max} is the maximum radius, R_{min} is the minimum radius, T_0 is the period of very small oscillations, T is the period of oscillation having given value of R_{max}/R_0. The curves are drawn for $\gamma = 4/3$, but γ makes little difference.

For large amplitudes, perhaps where R_{max}/R_0 is greater than 2.25, the formula given in Equation [22] on page 48 of TMB Report 480 (4) may be used

$$T = 1.83\, R_{max} \sqrt{\frac{\rho}{p_0}} \qquad [4a]$$

For a gas globe or bubble in water this may be written

$$T = \frac{R_{max}}{217} \frac{1}{\sqrt{p_A}} \text{ second} \qquad [4b]$$

where p_A is the hydrostatic pressure in atmospheres and R_{max} is in inches. For a given mass of gas, $R_{max} \propto 1/p_A^{\frac{1}{3}}$, hence T is proportional to $1/p_A^{\frac{5}{6}}$. In sea water, 217 is replaced in Equation [4b] by 214. If use is made of the value just given for R_{max}, Equation [4b] becomes

$$T = 0.23 \frac{W^{\frac{1}{3}}}{p_A^{\frac{5}{6}}} \qquad [4c]$$

These latter formulas may be used to estimate the time of collapse of a bubble under suddenly applied steady pressure. If R_{max} represents the initial radius of the bubble and p_0 or p_A the suddenly applied pressure, the time of collapse is $T/2$. The estimate should be of high accuracy if the ratio of pressure increase exceeds 2.25^4 or about 25.

If the amplitude R_{max}/R_0 is very large, compressibility of the water will play an important part. The direct effect of compressibility on the period will be small, since the high-pressure phase of the motion occupies only a very small part of the total period; but a loss of energy occurs by acoustic radiation during the time of intense contraction, so that each outward swing is less in amplitude than the preceding inward swing. The period

between two minimum radii should then be given quite accurately by the formulas if the intervening maximum radius is used, whereas the interval of time between two successive maxima should be the average of the periods as given by the formulas for the two successive maximum radii.

The formulas for the period have been derived from hydrodynamical theory but appear to have been confirmed satisfactorily by observation. No allowance has been made for the effect of the displacement of a gas globe due to gravity, but this effect should be large only under extreme conditions.

TIME-DISPLACEMENT CURVES

A number of curves are drawn in Figure 2 which show for several amplitudes, the value of R/R_0 during an oscillation as a function of the time. The unit for time is the period of small oscillation, T_0; thus the curves are valid for any value of R_0. They refer to the case $\gamma = 4/3$, which is the easiest to calculate. For air, however, the curves would differ so little that it is not worth while to attempt to illustrate the difference. The curves were constructed by integrating Equation [32] numerically. As with the period, no allowance has been made for gravitational displacement of a gas globe.

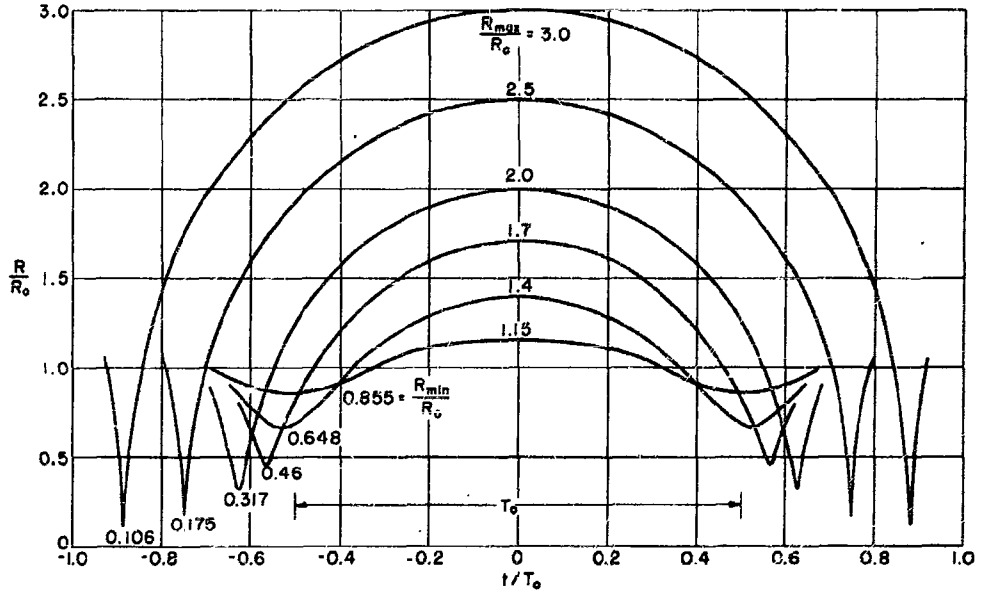

Figure 2 - Calculated Time-Displacement Curves for Undamped Oscillation of a Bubble or Globe of Gas under Water

R = radius t = time

R_0 = radius when in equilibrium T_0 = period of very small oscillations

The maximum radius R_{max} and the minimum radius R_{min} are connected by the equation

$$\frac{R_0}{R_{min}} + \frac{1}{3}\left(\frac{R_{min}}{R_0}\right)^3 = \frac{1}{3}\left(\frac{R_{max}}{R_0}\right)^3 + \frac{R_0}{R_{max}} \qquad [5a]$$

which for large amplitudes can be shortened approximately to

$$\frac{R_0}{R_{min}} = \frac{1}{3}\left(\frac{R_{max}}{R_0}\right)^3 + \frac{R_0}{R_{max}} \qquad [5b]$$

see Equation [30], with $\gamma = 4/3$.

It is noteworthy that, as the amplitude increases, the time-displacement curve, which approximates to a sine curve at small amplitudes, becomes more and more pointed near the minimum radius. Thus the sphere spends very little time at radii below the equilibrium radius R_0 when the amplitude is large. This effect arises physically from the diminution in the area across which the inrushing water is moving; because of this diminution the water has a strong tendency to increase in velocity, and hence the gas meets great difficulty in stopping the motion.

The curves are calculated on the assumption of incompressible water. For this reason the incoming and outgoing motions as shown in Figure 2 are similar. When the minimum radius becomes extremely small relatively to R_0, however, compression of the water begins to play a role, as already stated; consequently, the amplitudes of successive oscillations will progressively decrease. Each loop of the actual curve, extending from one minimum to the next will be very nearly the same as it would be, at the same maximum radius, for incompressible water.

PRESSURE IN THE WATER

Let the pressure in the water at great distances be the hydrostatic pressure p_0; and let gravity be assumed not to act. At the surface of the sphere of gas, the pressure in the water must be that of the gas or

$$p_g = \left(\frac{R_0}{R}\right)^{3\gamma} p_0 \qquad [6]$$

by Equation [26], where R is the instantaneous radius of the sphere. At any other point, at a distance r from the center of the sphere, the pressure, if the motion is non-compressive, is found to be

$$p = \frac{R}{r}\left(p_g + \frac{1}{2}\rho v_g^2 - p_0\right) - \frac{1}{2}\rho v^2 + p_0 \qquad [7a]$$

or, for $\gamma = 4/3$,

$$p = p_0 \frac{R}{r}\left\{\left[\left(\frac{R_0}{R_1}\right)^4 + \frac{1}{3}\right]\left(\frac{R_1}{R}\right)^3 - \frac{4}{3}\right\} - \frac{1}{2}\rho v^2 + p_0 \qquad [7b]$$

where $R_1 = R_{min}$, the minimum radius, v is the particle velocity at the point in question, and v_s is the velocity of the surface of the sphere, which is also equal to dR/dt; see Equations [38] and [39a]. At considerable distances the Bernouilli term $1/2\,\rho v^2$ may be dropped.

The maximum pressure at any point occurs at the instant at which the radius of the sphere is a minimum, without any time delay, in the approximation in which compression of the water is neglected. At this instant both v_s and v vanish; hence, from Equations [6] and [7a], the maximum pressure is

$$p_{max} = \frac{R_{min}}{r}(p_s - p_0) + p_0$$

or

$$p_{max} = p_0 \frac{R_{min}}{r}\left[\left(\frac{R_0}{R_{min}}\right)^{3\gamma} - 1\right] + p_0 \qquad [8a]$$

where R_{min} is the minimum radius of the bubble. For $\gamma = 4/3$,

$$p_{max} = p_0 \frac{R_{min}}{r}\left[\left(\frac{R_0}{R_{min}}\right)^4 - 1\right] + p_0 \qquad [8b]$$

These formulas should be applicable to the pressure in the water that is associated with the oscillations of explosive gas globes. As an example, if $R_{max}/R_0 = 2.6$, which appears to represent fairly well the first outswing for a Number 8 detonator when $p_0 = 15$ pounds per square inch, and when R_{max} is about 5 inches, then $R_{min}/R_0 = 0.16$, and at a distance $r = 18$ inches from the center of the explosion

$$p_{max} - p_0 = 15\,\frac{0.31}{18}\left[\left(\frac{1}{0.16}\right)^4 - 1\right] = 400 \text{ pounds per square inch}$$

However, the pressure varies extremely rapidly near its maximum value when the amplitude of oscillation is large. Thus a concentrated pulse of pressure is emitted during the phase of extreme contraction of the globe, whereas during most of the time the increment of pressure due to the motion is small. In Equations [43] and [37] the following formulas are obtained connecting the pressure p at a distance r from the center with the radius R of the sphere of gas and the time t, in the neighborhood of the time t_1 at which $R = R_1 = R_{min}$, when $\gamma = 4/3$:

$$p = (p_{max} - p_0)\left(\frac{R_1}{R}\right)^2 - \frac{1}{2}\rho v^2 + p_0 \qquad [9]$$

$$t - t_1 = \frac{\sqrt{2}}{15\pi} T_0 \left(\frac{R_1}{R_0}\right)^3 \sqrt{\frac{R}{R_1} - 1} \left[8 + 4\frac{R}{R_1} + 3\left(\frac{R}{R_1}\right)^2\right] \qquad [10a]$$

For the first contraction of an explosive gas globe, these formulas should hold well at least up to $R = R_0/2$, and the error in Equation [9] should not exceed 5 per cent. The significance of Equation [10a] may appear more clearly if it is written

$$t - t_1 = G\left(\frac{R_{min}}{R_0}\right)^3 T_0 \qquad [10b]$$

in terms of a dimensionless factor G. For a decrease of the pressure to half of its maximum value, $G = 0.4$; for a decrease to one quarter, $G = 0.8$. In the example just described, referring to a Number 8 detonator, where $R_{max}/R_0 = 2.6$, $T_0 = 1/65$ second, $R_{min}/R_0 = 0.16$, and the two values of $t - t_1$ are about 0.025 and 0.05 millisecond, respectively, the pressure curve is symmetrical about its maximum, and the entire time taken from $p = p_{max}/4$ through p_{max} and back to $p_{max}/4$ is about 0.1 millisecond. These results indicate that the pressure pulse emitted during the first compression peak should be broader than the primary pulse due to the explosion itself, in which the pressure should decrease to a quarter of its initial maximum in less than 0.02 millisecond. For 1 ounce of TNT or tetryl, the time from $p_{max}/4$ to $p_{max}/4$ in the pulse due to the first compression peak might be 0.4 millisecond; for 300 pounds at a depth of 50 feet, 5 milliseconds.

The total impulse or $\int p\,dt$ in the second pulse, on the other hand, may be relatively large. The impulse from the time t_1 of minimum radius up to any other time t, when the term $\rho v^2/2$ is negligible, is found to be, for $\gamma = 4/3$,

$$I = \frac{\sqrt{2}}{\pi} p_0 T_0 \frac{R_0}{r} \left\{\left[\frac{R_0}{R_{1,2}} + \frac{1}{3}\left(\frac{R_{1,2}}{R_0}\right)^3\right]\frac{R}{R_0} - \frac{1}{3}\left(\frac{R}{R_0}\right)^4 - 1\right\}^{\frac{1}{2}} \qquad [11]$$

where $R_{1,2}$ may be taken to stand either in both places for $R_1 = R$, the minimum radius, or in both places for $R_2 = R_{max}$, the maximum radius; see Equation [44a].

If, in Equation [11], $R_{1,2} = R_{max}$ and also $R = R_{max}$, then $I = 0$. This shows that the impulse during a complete swing is zero, the negative part cancels the positive part. The negative impulse arises from extremely small negative pressures, however, and is for this reason unimportant. The positive part may be obtained separately as the maximum value of I as given by Equation [11]. The positive impulse emitted during an entire compression and re-expansion when $\gamma = 4/3$ is thus found to be

$$2I_+ = \frac{2\sqrt{2}}{\pi} p_0 T_0 \frac{R_0}{r}\left\{\left(\frac{3}{4}\right)^{\frac{4}{3}}\left[\frac{R_0}{R_1} + \frac{1}{3}\left(\frac{R_1}{R_0}\right)^3\right]^{\frac{4}{3}} - 1\right\}^{\frac{1}{2}} \qquad [12]$$

see Equation [45].

In the example of a Number 8 detonator, where $R_0 = 2$ inches, $R_2/R_0 = 2.6$, $R_1/R_0 = 0.16$, $T_0 = 0.015$ second, $p_0 = 15$ pounds per square inch, at $r = 18$ inches from the center of the detonator, Equation [12] gives, for the total positive impulse due to the first compression and re-expansion, 0.059 pound-second per square inch. The part of this that arises from the central peak, in which the pressure exceeds a quarter of the maximum pressure, as found by substituting $R = 2R_1$ in Equation [11] and multiplying I by 2, is about 0.024 pound-second per square inch. This accounts for rather less than half of the total. Even so, it probably exceeds the impulse due to the high-pressure part of the primary pressure-wave, which should not exceed 0.02 pound-second per square inch.

In Figure 3 the pressure p is shown as a function of the time t, for a contraction from a maximum radius $R_2 = 2.5\,R_0$ and a subsequent re-expansion. The ordinates represent values of p/p_{max}; the maximum pressure p_{max} is given by Equation [8b]. The abscissa represents t/T, where T is the period of oscillation of the gas globe. Part of the curve is repeated on an expanded scale. The curve is independent of the quantity of the gas, which determines the value of R_0.

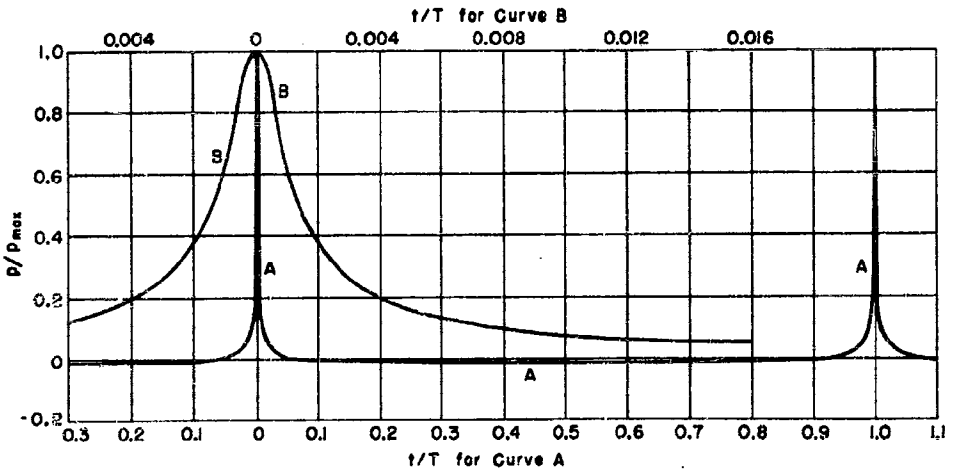

Figure 3 - Curve showing the Calculated Pressure p developed in the Water during the Oscillation of a Bubble or Gas Globe under Water, in Terms of the Maximum Pressure p_{max}

Acoustic radiation of energy is ignored. Time t is plotted in terms of the period of oscillation T. Part of the curve is repeated on an enlarged time scale.

In this discussion no account has been taken of the effects of acoustic radiation of energy. This radiation will cause each expansion to be somewhat less energetic than the preceding contraction, so that the emitted pressure and impulse will be somewhat less. No attempt will be made here to develop a more accurate theory of this phenomenon, but the total radiation of energy associated with compressibility in the water can be estimated roughly.

RADIATION OF ENERGY

At considerable distances from the center of the gas sphere, where ρv^2 is negligible, the pressure as given by Equation [7a] or [7b] falls off with increasing r according to the same law that holds for spherical waves. This observation leads to the surmise that moderate compression of the water will not greatly alter the magnitude of the pressure p at any distant point but will introduce the following features as characteristics of spherical waves in contrast to non-compressive motion:

1. a time lag corresponding to the finite speed of propagation of sound waves, and

2. a component $p/\rho c$ in the particle velocity, added to the velocity as derived from non-compressive theory.

This surmise is confirmed for small amplitudes of oscillation by acoustic theory.

In order to form a rough estimate of the energy radiated, therefore, the pressure as derived from non-compressive theory may be combined with the acoustic formula for the energy that is carried off to infinity, in spite of the fact that a strict use of non-compressive theory leads to no loss of energy to infinity at all. In acoustic theory, the emission of radiation results from the component $p/\rho c$ in the particle velocity and amounts to $p^2/\rho c$ per unit area per second. Hence, to find the total amount of radiation, it is only necessary to integrate $p^2/\rho c$ twice, first over a large spherical surface drawn about the gas sphere, and then with respect to the time. Furthermore, the pressure falls so rapidly from its maximum value that the emission of energy occurs almost entirely while the pressure is in the neighborhood of its maximum, or while the sphere is near its minimum radius; hence a good approximate value can be obtained by using an approximate value for the pressure that holds near its maximum.

The amount of energy radiated per cycle by a sphere of gas for which $\gamma = 4/3$ is thus found to be, in the notation already employed,

$$\Omega = 2\sqrt{2}\,\pi^3 \frac{p_0 R_0^4}{c T_0} \left(\frac{R_0}{R_{min}}\right)^3 \qquad [14]$$

where c denotes the velocity of sound in water; see Equation [48]. To make this formula approximately correct, the amplitude of oscillation must be large enough to make the peak of emitted pressure a sharp one, but not so large that great compression of the water occurs; the range of its validity may be something like

$$\frac{1}{7} < \frac{R_{min}}{R_0} < \frac{1}{2}, \quad 1.6 < \frac{R_{max}}{R_0} < 2.75$$

A more interesting quantity is the dimensionless ratio of the energy emitted in a cycle to the total energy of vibration, E. The excess energy that is present as a result of the oscillatory motion is the same as the kinetic energy of the water at the instant at which $R = R_0$, since, if this energy were suddenly removed at that instant, the sphere would remain in equilibrium. As the gas expands to maximum radius, this kinetic energy is expended in doing work against the difference between the hydrostatic pressure and the pressure of the gas, and the latter work is readily calculated.* In this way the energy of vibration is found to be

$$E = 4\pi p_0 R_0^3 \left[\frac{R_0}{R_1} + \frac{1}{3}\left(\frac{R_1}{R_0}\right)^3 - \frac{4}{3}\right] = 4\pi p_0 R_0^3 \left[\frac{R_0}{R_2} + \frac{1}{3}\left(\frac{R_2}{R_0}\right)^3 - \frac{4}{3}\right] \quad [15]$$

provided $\gamma = 4/3$; compare Equation [49a]. Thus for the first cycle

$$\frac{\mathcal{Q}}{E} = \frac{\frac{\pi^2}{\sqrt{2}} \frac{R_0}{cT_0}\left(\frac{R_0}{R_1}\right)^3}{\frac{R_0}{R_1} + \frac{1}{3}\left(\frac{R_1}{R_0}\right)^3 - \frac{4}{3}} \quad [16]$$

or, after inserting $c = 4810 \times 12$ inches per second and using Equation [2b],

$$\frac{\mathcal{Q}}{E} = \frac{\frac{1}{66}\sqrt{p_A}\left(\frac{R_0}{R_{min}}\right)^3}{\frac{R_0}{R_{min}} + \frac{1}{3}\left(\frac{R_{min}}{R_0}\right)^3 - \frac{4}{3}} \quad [16a]$$

where p_A is the hydrostatic pressure measured in atmospheres.

Measurements of the radiated energy are not available, but a comparison may be made between the calculated loss by radiation and the total observed loss of oscillatory energy, which is easily found from the progressive decrease in the maximum radius for successive oscillations. From Equation [15], the change in energy is

* The water is driven, so to speak, by two springs, the gas inside and the hydrostatic pressure outside. As it oscillates, one spring loses energy while the other gains energy; the excess of the gain by one spring over the loss by the other, as the radius changes from its equilibrium value R_0 to a value R, represents the potential energy of vibration.

$$\Delta E = 4\pi p_0 R_0^3 \Delta\left[\frac{R_0}{R_2} + \frac{1}{3}\left(\frac{R_2}{R_0}\right)^3\right] \qquad [17]$$

or, if the relatively small term R_0/R_2 is dropped,

$$\Delta E = \Delta\left(\frac{4}{3}\pi p_0 R_2^3\right) \qquad [17a]$$

This last formula represents the change in the energy as approximately equal to the change in the work required to produce the cavity of maximum size, which can be calculated without making any assumption concerning the equilibrium size of the gas globe.

For the gas globe formed by Number 8 detonators exploded just far enough under the surface of the water to avoid blowing through, an average value for the first expansion, as inferred from the periods of oscillation, seems to be about $R_{max}/R_0 = 2.6$. This corresponds, by Equation [5a], to $R_0/R_{min} = 6.2$. For this case, by Equation [16a], $Q/E = \frac{6.2^3}{4.9} \times \frac{1}{66} = 0.74$. The observed decrease in energy during the first contraction, calculated in the manner just described, is about 40 per cent.

The discrepancy between 0.74 and 0.40 is in the right direction and may well be due to compression of the water. At minimum radius, Equation [6] makes p_s equal to $6.2^4 = 1500$ atmospheres, which would compress the water by about 7 per cent. An attempt to estimate the amount of compressional energy that would exist in the water leads, however, to a divergent integral, which merely indicates that the non-compressive approximation to p is inadequate for the purpose. It is clear, however, that, if the gas at minimum radius absorbs only part of the energy of motion, its minimum radius will be greater than it has been calculated to be on the assumption that the gas takes up the whole energy, and the pressure peak will accordingly be lower and will result in a considerably smaller radiant emission of energy. Thus the true value of Q/E may easily be 0.40 instead of 0.74.

The estimate of the radiated energy has been based, as have all of the preceding formulas, upon the assumption of perfectly symmetrical radial motion. Further losses of the energy of the radial motion may result in actual cases from turbulence caused by departures from radial symmetry, or from conversion of the oscillatory energy into energy of translation due to gravity or to the proximity of obstacles.

A PRESSURE WAVE AND A GAS BUBBLE

It is of special interest to investigate the propagation of explosive pressure waves through water containing bubbles of air, since a screen of bubbles has been proposed as a protective device. Let it be assumed that

the wave begins with a very steep front behind which the pressure falls off, and that the bubbles ahead of the wave are in equilibrium under hydrostatic pressure. The behavior of a bubble under such a wave will vary according to circumstances. Special cases of this phenomenon will now be considered.

SLOWLY VARYING PRESSURE

Suppose the pressure falls off slowly as compared with the time of contraction of the bubble under the maximum pressure in the wave. This should be the case when the shock wave from a large charge enters water containing small bubbles. In this case the pressure on the bubble is practically steady during the process of compression.

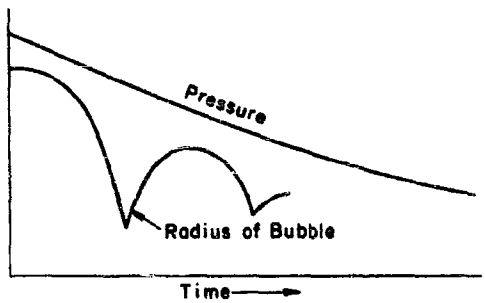

Figure 4 - Curve illustrating Behavior of a Bubble under a Slowly Varying Pressure Wave

Estimates of the rapidity of heat exchange between the gas in the bubble and the water indicate that the gas should follow the adiabatic law, $pV^{\gamma} =$ constant. Since $V \propto R^3$, the new equilibrium radius R under pressure p will be

$$R = \left(\frac{p_0}{p}\right)^{\frac{1}{3\gamma}} R_0 \qquad [18]$$

where R_0 is the radius under hydrostatic pressure p_0. For air, $\gamma = 1.4$ and

$$R = \left(\frac{p_0}{p}\right)^{\frac{1}{4.2}} R_0 \qquad [18a]$$

Thus the equilibrium radius changes but slowly in comparison with the pressure. If $p/p_0 = 200$, corresponding to a rise of pressure from atmospheric to 3000 pounds per square inch, $R/R_0 = 1/3.5$; if $p/p_0 = 400$, corresponding to 6000 pounds per square inch, $R/R_0 = 1/4.2$.

The time required for a bubble of initial radius R_0 to contract when the pressure is suddenly raised to a high value and then held steady may be estimated as half of T as given by Equation [4a] or [4b] with R_{max} replaced by R_0. For bubbles in water,

$$\frac{1}{2} T = \frac{0.0023 R_0}{\sqrt{p_A}} \qquad [19]$$

where R_0 is in inches and p_A is the applied pressure in atmospheres. Thus, even if R_0 is as large as 0.1 inch and the pressure no greater than 150 pounds per square inch, so that $p_A = 10$, the bubble collapses in less than

1/12 millisecond, which is a short time relative to the duration of the pressure wave from a large charge. If R_0 = 0.1 inch and p = 1000 pounds or p_A = 67, $T/2$ is less than 1/30 millisecond, which is a short time even for the wave from a pound of explosive. Smaller bubbles will collapse more quickly in proportion to their smaller radius.

In collapsing, the bubble will overshoot its new position of equilibrium under the increased pressure, and will then re-expand. If the bubble lost no energy, and if the pressure remained constant, then the bubble would actually expand to its initial size, after which it would collapse again; it would, in fact, execute undamped oscillations about its equilibrium radius under the increased pressure. The bubble would be analogous to a mass on the end of a spring; if, when the mass is at rest, a constant force suddenly begins to act on it, the mass oscillates about a new position of equilibrium and, in doing so, returns periodically to its initial position.

The period of the oscillations will be much shorter, however, than those which the same bubble would execute under normal pressure. Under a pressure of 1000 pounds per square inch, for example, the equilibrium radius is reduced from its value under one atmosphere in the ratio $\left(\frac{14.7}{1000}\right)^{\frac{1}{4.2}} = \frac{1}{2.7}$. The period of oscillation, which is proportional by Equation [1] both to $p_0^{-\frac{1}{2}}$ and to the equilibrium radius, would then be $2.7 \left(\frac{1000}{14.7}\right)^{\frac{1}{2}}$ = 22 times less than under one atmosphere. Under 3000 pounds per square inch, the period would be 50 times less than under one atmosphere, for the same relative amplitude of oscillation.

Compression of the water cannot be ignored in these cases. Calculation of the pressure in the bubble when at its minimum radius gives fantastically high values. This means that, because of compression of the water, the minimum radius will actually be several times larger, and the maximum pressure many times smaller, than the values derived from non-compressive theory. Furthermore, it is certain that much of the kinetic energy acquired by the bubble as it contracts will be radiated away during the phase of extreme compression. The oscillations of the bubble about its new equilibrium radius will thus be highly damped.

An upper limit can easily be set to the amount of energy that can be radiated away by such a bubble in collapsing. The total work done by the applied pressure as the bubble collapses is equal to the product of the pressure into the change of volume of the bubble. With any explosive wave of consequence, however, the final volume is relatively small. For example, even if p is only 300 pounds per square inch as against an initial pressure p_0 = 15, from the relation $pV^\gamma = p_0V_0^\gamma$ the ratio of the corresponding volumes

is, for air, $V/V_0 = (p_0/p)^{1/\gamma} = (p_0/p)^{1/1.4} = 1/8.5$. Hence, the work can be calculated from the initial volume only and is nearly equal to

$$W = \frac{4}{3}\pi p R_0^3$$

where R_0 is the initial radius.

It may now be asserted that the radiated energy cannot exceed W. It may well be almost equal to W, however. For the part of W that is spent in compressing the gas is approximately, or exactly if $\gamma = 4/3$, equal to

$$4\pi p_0 \frac{R_0^4}{R} - 4\pi p_0 R_0^3 = 4\pi p_0 R_0^3\left(\frac{R_0}{R} - 1\right) = 4\pi p R_0^3\left[\left(\frac{p_0}{p}\right)^{\frac{3}{4}} - \frac{p_0}{p}\right]$$

by Equation [27a]. This is less than $W/5$ if p is greater than $20\,p_0$. Loss of energy due to friction should also be small, unless departures from symmetry cause appreciable turbulence.

After the bubble has settled into its new position of equilibrium, it may contract somewhat further as it loses heat of compression, and as the gas dissolves in the water. If the pressure slowly decreases, the bubble will re-expand without executing marked oscillations.

IMPULSIVE PRESSURE

At the opposite extreme from the case of steady pressure stands the impulsive case. Let the pressure be applied suddenly and let it disappear again before the bubble has had time to change appreciably in size. Then the bubble will begin contracting at a certain inward radial velocity v_0. If compressibility of the water can be neglected, the analysis gives

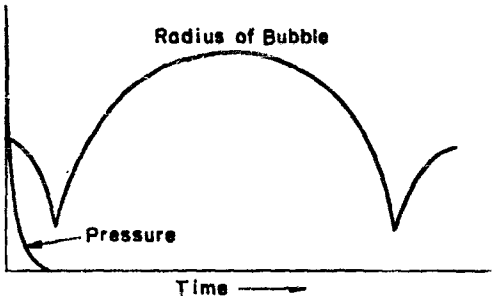

Figure 5 - Curve illustrating Behavior of a Bubble under a Pressure Wave of Very Short Duration

$$v_0 = -\frac{I}{\rho R_0} \qquad [20]$$

where ρ is the density of water and $I = \int p\,dt$, the applied impulse; see Equation [51]. If I is in pound-seconds per square inch and R_0 in inches,

$$v_0 = -10{,}700\,\frac{I}{R_0} \text{ inches per second} \qquad [20a]$$

It is clear from this formula that enormous velocities are easily produced, while the inertia effect on the bubble motion is relatively small. From a Number 8 detonator at 18 inches, for example, the shock-wave impulse

may be about 0.013 pound-second, so that, even if R_0 is as large as 0.1 inch, v_0 according to Equation [20a] equals 1400 inches per second. Moving at this velocity, the bubble would shrink to nothing in 1/14 millisecond. Since the duration of the shock wave scarcely exceeds 1/50 millisecond, the value obtained for v_0 and for the time of collapse should be roughly correct.

For heavier charges, however, this analysis ceases to apply. Thus for the same bubble at a distance of 18 inches from 1 ounce of TNT or tetryl, I = 0.2 pound-second and v_0 = 21,000 inches per second; at this velocity the bubble would collapse in 1/210 millisecond, whereas the shock wave lasts perhaps 1/10 millisecond. In such cases a better estimate of the time of collapse is obtained from Equation [19]. If in this equation R_0 = 0.1 inch, p_A = 4000/14.7, representing a peak pressure of 4000 pounds per square inch, the value $T/2$ = 1/72 millisecond is obtained for the time of collapse. Even this latter value is probably considerably in error, but it serves to confirm the conclusion that the bubble will collapse long before the shock wave has disappeared.

After collapsing, the bubble will re-expand. If the time of collapse exceeds the duration of the shock wave, so that the expansion occurs under the original low pressure, the bubble may overshoot its original size. The time required to reach the original dimensions may be of the same order as the time of collapse; for the shortening of the time that results from the loss of energy by radiation will be offset somewhat by a lengthening due to the fact that the expansion occurs against a lower pressure.

THE GENERAL CASE

Between the two simple cases of relatively steady pressure and of impulsive action there lies an intermediate range in which analytical treatment is laborious. Qualitatively, light can be thrown upon these situations with the aid of estimates based on the formulas pertaining to the simple extremes, but quantitative results can be obtained only by numerical integration.

The foregoing discussion of the effect of a pressure wave on a single bubble may now be followed by consideration of cases involving more than one bubble.

A PRESSURE WAVE INCIDENT ON BUBBLY WATER

A problem of great interest is that of a plane wave of pressure entering at normal incidence a layer of water containing bubbles of air or other gas.

The principal *qualitative* features of the effect of the bubbles upon the pressure wave are easily inferred.

The bubbles make the water effectively much more compressible, hence the velocity of propagation will be greatly reduced. An isolated pulse of pressure may, for this reason, be retarded in its passage through the bubbly water.

Furthermore, if there is a definite boundary between the homogeneous and the bubbly water, partial reflection of the wave may be expected at the boundary. The reflection may, however, be reduced in amount by the occurrence of cavitation at the boundary of the layer of bubbly water. The wave reflected from the first surface of this layer will necessarily be one of tension, since the bubbles reduce the acoustic impedance of the water. If the water cannot stand the requisite tension, cavitation will occur in the homogeneous water, and in this case the reflected tension wave will be partly or wholly absent. A layer of cavitated water should then advance against the bubbly water, and subsequently move back again; the impact of this layer against other water may give rise to a secondary reflected wave of positive pressure.

It would be expected that high-pressure waves would be less effectively reflected than low-pressure waves. For, if the pressure is great enough to cause the bubbles to collapse almost completely, further increase of pressure will not cause materially greater amplitude of motion of the bubbles, so that the reflecting action cannot increase in proportion to the incident pressure.

Additional complications, perhaps resembling resonance effects, may result from the inertia of the water surrounding the bubbles. Furthermore, loss of energy due to scattering of the wave by the oscillating bubbles, or to other causes, will result in a weakening of the wave.

Because of these effects, the bubbly water will behave as a dispersive, absorbing medium. The dispersive action, signifying that the various harmonic components of the wave travel at different speeds, will cause the wave to increase in length as it passes through the bubbly layer. If the duration of the wave is short enough relative to the time of vibration of the bubbles, the lengthening may be so great that it is best described as a reemission of pressure by the compressed bubbles as they expand again.

The wave of pressure that emerges on the far side of the layer of bubbles will thus be likely to be weaker but of longer duration than the original incident wave. There are, furthermore, other effects that lengthen the transmitted wave. Repeated reflections from the boundaries of the layer may occur. A single entering pulse may thus emerge as a series of repeated pulses of rapidly diminishing amplitude, which will blend together more or less completely into a transmitted wave of increased length.

Then, finally, there are the wavelets scattered in all directions by the bubbles. In part, effects of these scattered wavelets have already been taken into account, for they actually constitute the physical mechanism by which the incident wave is weakened and partly reflected. But the scattered wavelets will also appear independently as an additional wave of pressure scattered in all directions. In a similar way the waves of light scattered by the molecules of the atmosphere, which, on the one hand, cause a refraction and a weakening of the sun's rays, also appear independently as the blue light that comes from the sky. Scattered wavelets coming from more and more distant parts of the bubbly layer may prolong the transmitted wave as observed in regions beyond the layer.

The ***momentum*** carried by the waves, on the other hand, should be reduced only if a reflected wave of tension occurs. Such a reflected wave may carry back a large part of the incident momentum. If, however, the reflection is prevented by the occurrence of cavitation, all of the incident momentum must appear somehow in the transmitted wave.

The transmitted momentum might, as a matter of fact, exceed the incident momentum. In such a case the conservation of momentum might be preserved in either of two ways. Partial reflection from the farther side of the bubbly layer, occurring in the medium of lesser acoustic impedance, may cause momentum reversed in direction to be carried back toward the source of the waves. Or, momentum of the same sort may be carried back by the rear halves of wavelets scattered off in all directions.

Several features corresponding to those just described have been observed in experiments at the David W. Taylor Model Basin, which are to be described in other reports.

The *quantitative* treatment of these phenomena, unfortunately, encounters great difficulty, as does any problem in highly non-linear wave motion. The analysis can be effected readily, in fact, only for the extremely simple case of very weak waves of sinusoidal form, passing through water that contains many bubbles in each cubic wave length. After this case has been solved, a weak wave of arbitrary form can be treated, if desired, by means of Fourier analysis. Although devoid of direct bearing on the topic of explosion waves, the analytical results for weak waves may be suggestive enough to be quoted here. Their deduction is given in the Appendix.

WEAK SINUSOIDAL WAVES IN FINE-GRAINED BUBBLY WATER

Let the following assumptions be made:

1. The pressure is so weak that linear acoustic theory can be applied. This implies that the bubbles change size only slightly as the waves pass.

2. The spacing of the bubbles is large relatively to their own diameter, but yet small relative to the wave length of the waves in the bubbly water. Let

c be the speed of sound in homogeneous water,

c' be the speed of sound in the bubbly water,

β be the extinction coefficient, with the significance that the amplitude of the pressure decreases by a factor $e^{-2\pi\beta}$ as the wave traverses in the bubbly water a distance equal to its wave length in homogeneous water,

f be the fraction of space occupied by the gas in the bubbles,

R_0 be the equilibrium radius of the bubbles, assumed the same for all,

$\omega = 2\pi/T$, where T is the period of the waves,

$\omega_0 = 2\pi/T_0$, where T_0 is the natural period of small radial oscillation of a bubble,

$N = \frac{\sqrt{3}\,c}{\omega_0 R_0}$. Here N^2 represents the ratio of ρc^2, the volume elasticity of water, to γp_0, the volume elasticity of the gas contained in the bubbles.

Then, according to Equations [66] and [67], the analytical treatment yields the equations:

$$\frac{c^2}{c'^2} - \beta^2 = 1 + fN^2 \frac{1 - \frac{\omega^2}{\omega_0^2}}{\left(1 - \frac{\omega^2}{\omega_0^2}\right)^2 + \frac{3}{N^2}\frac{\omega^6}{\omega_0^6}} \qquad [21]$$

$$2\beta \frac{c}{c'} = \sqrt{3}\, fN \frac{\frac{\omega^3}{\omega_0^3}}{\left(1 - \frac{\omega^2}{\omega_0^2}\right)^2 + \frac{3}{N^2}\frac{\omega^6}{\omega_0^6}} \qquad [22]$$

At very low frequency, $\beta = 0$ approximately and

$$c' = \frac{c}{\sqrt{1 + fN^2}} \qquad [23]$$

Since, as in Equation [1], $T_0 \propto R_0$, the quantity N is in reality independent of the size of the bubbles. For air in water at atmospheric pressure, where $c = 58{,}000$ inches per second and by Equation [2a], $\omega_0 = 2\pi/T_0 = 2\pi \times 129/R_0$, $N = 58{,}000\sqrt{3}/258\pi = 124$.

The value of N is so large that at very low frequencies, in the absence of all resonance effects, a small amount of air causes a large decrease in the wave velocity. Thus if f = 0.1 per cent, $c' = c/\sqrt{1 + 124 \times 0.124} = 0.25\ c$; if f = 1 per cent, $c' = 0.08\ c$.

The coefficient of reflection, or fraction of the incident energy that is reflected, is given by Equation [70] or

$$K = \frac{\left(1 - \frac{c}{c'}\right)^2 + \beta^2}{\left(1 + \frac{c}{c'}\right)^2 + \beta^2} \qquad [24]$$

At very low frequencies this becomes, approximately,

$$K = \left[\frac{1 - \frac{c}{c'}}{1 + \frac{c}{c'}}\right]^2 = \left[\frac{\sqrt{1 + fN^2} - 1}{\sqrt{1 + fN^2} + 1}\right]^2 \qquad [25]$$

from Equation [23], a formula that is easily obtained from a much simpler calculation. The latter formula gives, for f = 0.1 per cent of air,

$$K = \left(\frac{3}{5}\right)^2 = 0.36$$

and for 1 per cent of air,

$$K = \frac{11.4^2}{13.4^2} = 0.72$$

Curves are shown in Figures 6 and 7 for 0.1 per cent of air in water, or for N = 124 and f = 0.001. In Figure 6 the ratio of velocities

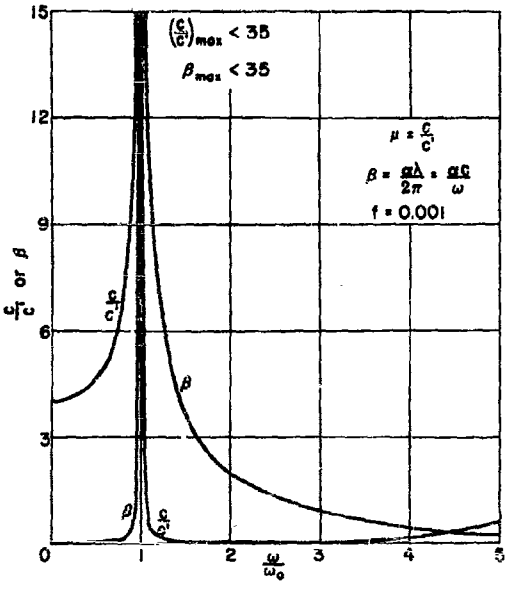

Figure 6 - Refractive Index relative to Homogeneous Water, c/c', and Extinction Coefficient β for Sinusoidal Waves in Water containing 0.1 per cent of Air in Fine Bubbles

c' = wave speed

c = wave speed in homogeneous water

$\omega = 2\pi$ times wave frequency

$\omega_0 = 2\pi$ times natural frequency of radial oscillation of the bubbles

β = extinction coefficient

Pressure decreases by factor $e^{-2\pi\beta}$ as wave progresses a distance $\lambda = 2\pi c/\omega$.

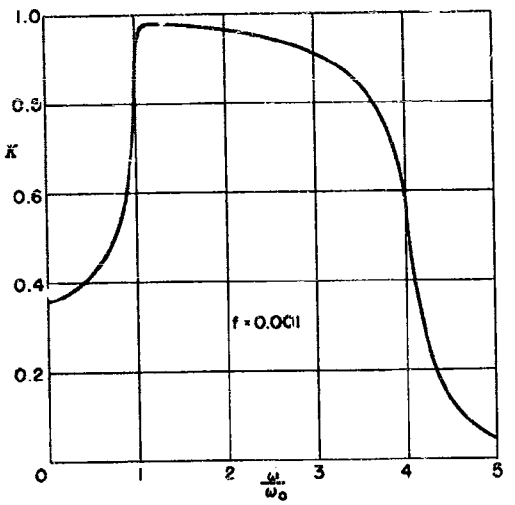

Figure 7 - Reflection Coefficient K

K is the fraction of the incident energy that is reflected, for the bubbly water to which Figure 6 refers.

c/c', or refractive index of bubbly water relative to homogeneous water, and the quantity β are plotted against ω/ω_0, which represents the ratio of the wave frequency to the natural frequency of the bubbles. In Figure 7 is plotted the reflection coefficient K of the bubbly water. The curves are valid for any bubble size that is not too large; the size of the bubbles determines ω_0.

A strong resonance effect is brought into evidence by these curves. Especially striking is the persistence of this effect as ω increases above ω_0. The decrease in wave speed c' that is caused by the bubbles at low frequencies is replaced, as ω begins appreciably to exceed ω_0, by an increase in wave speed; for $f = 0.001$ and $\omega = 2.5\omega_0$, $c' = 22\,c$, and even at $\omega = 5\omega_0$, $c' = 1.7\,c$. Furthermore, the scattering, which is proportional to β, shows a strong persistence at values of ω/ω_0 up to 2 or 3. As a consequence, there is a strong band of nearly total reflection from $\omega = \omega_0$ to $\omega = 3\omega_0$. Above $\omega = 5\omega_0$, on the other hand, reflection becomes inappreciable; at such frequencies, the inertia of the bubbles prevents them from following the vibrations of the incident wave to any considerable degree.

If ω is increased to very high values, however, a point is ultimately reached at which the assumptions underlying the analysis no longer apply, because the incident wave length is no longer large as compared with the spacing of the bubbles.

Observations have been reported on the scattering of sound by bubbly water, but they do not seem to lend themselves to a test of these equations. The analytical results may be employed, however, to throw some light upon the effect to be expected when a shock wave enters bubbly water. A photograph of this phenomenon is shown in Figure 8.

If the effective length of the shock wave is relatively great, or at least not less than a third as great as the wave length corresponding to the average natural frequency of the bubbles ($\omega/\omega_0 < 3$), then it may be concluded with safety that the reflection will exceed the value given by

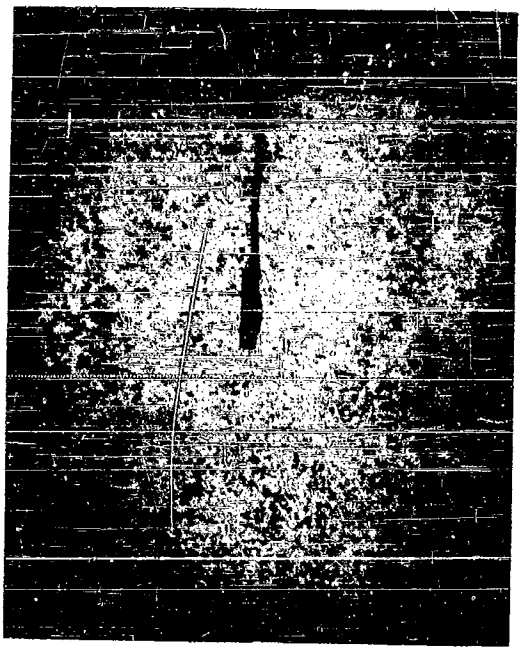

Figure 8a - Before the Explosion

Figure 8b - After the Explosion

Figure 8 - Photographs showing a Shock Wave forming in Bubbly Water

Equation [25]. In this statement, the wave length as it exists in homogeneous water is meant. If the effective length of the shock wave is actually comparable with the bubble wave length, the reflection should be materially increased by resonance effects, and at the same time the wave in the bubbly water should be heavily damped, in consequence of the scattering of the incident wave. If the length of the shock wave is progressively decreased, however, until it becomes several times smaller than the bubble wave length, the reflection should fall off rapidly, and as the shock wave is further shortened both reflection and scattering should tend toward small values.

The statements regarding high reflection are conditioned by the assumption that cavitation does not occur. As stated in the previous section, cavitation occurring in the homogeneous water lying next to the bubbly layer may decrease the reflection or markedly alter its character.

The part of the incident energy that is not reflected but enters the bubbly water is gradually scattered by the bubbles as the waves progress; this process accounts for the progressive weakening of the waves. In reality there will be also a certain dissipation of energy due to friction and heat conduction, but estimates indicate that this dissipation ought to be comparatively small.

The scattered waves are hard to treat analytically because they are themselves subject to continual re-scattering. It may be of interest, however, to consider for comparison the scattering by a single bubble. It is found that the bubble should scatter as much energy as is transported in the incident waves across a certain area A, which may be called the *scattering cross section* of the bubble. The value of A for waves much longer than the diameter of the bubble, as given in Equation [75], is

$$A = \frac{4}{\left(1 - \frac{\omega_0^2}{\omega^2}\right)^2 + \frac{3}{N^2}\frac{\omega^2}{\omega_0^2}} \pi R_0^2$$

At $\omega = 0$, $A = 0$; from $\omega = 0.6\omega_0$ well up toward such high frequencies that the validity of the formula becomes doubtful, A exceeds πR_0^2, the actual cross-sectional area of the bubble itself. For air in water, $N = 124$. For such bubbles, A approximates $4\pi R_0^2$, the superficial area of the bubble, when ω lies within the range

$$4\omega_0 < \omega < 20\omega_0$$

An extremely sharp resonance effect occurs. At $\omega = \omega_0$, $A = 20{,}500\pi R_0^2$; the bubble scatters more than 20,000 times as much energy as would fall on it directly. If ω differs from ω_0 by 2 per cent, however, the scattering is only a ninth of its maximum value. The half-value width, or width of the resonance peak between points on the curve at which A has half of its maximum value, is $0.014\omega_0$.

The energy scattered by a group of bubbles should be just the sum of the energies scattered by the individual bubbles, provided the bubbles are distributed at random, and provided differences in the intensity of the incident waves may be neglected. If the bubbles are not distributed at random, however, interference effects may occur. The reflected beam from a bubbly region of water having a sharp boundary arises from constructive interference of the waves scattered by the individual bubbles, and it is for this reason that the resonance peak in reflection is so much broader than the peak in the scattering curve for a single bubble. If there is no sharp boundary but the density of bubbles varies gradually, the reflection will be weaker; if the density is nearly uniform within any distance equal to one wave length of the incident waves, the process becomes essentially one of scattering with little resemblance to regular reflection.

REFERENCES

(1) "Underwater Explosions. Time Interval between Successive Explosions," by Willis, February 1941, Volume II of this compendium.

(2) "Theory of the Pulsations of the Gas Bubble Produced by an Underwater Explosion," by Conyers Herring. Volume II of this compendium.

(3) "Stability of Air Bubbles in the Sea," by P. Epstein. NDRC Report C4-sr 30-027, September 1941.

(4) "Report on Underwater Explosions," by E.H. Kennard, Volume I of this compendium.

APPENDIX

MATHEMATICAL THEORY OF RADIAL MOTION AROUND GAS SPHERES IN WATER

Consider a sphere of gas behaving adiabatically, so that, if p_g and V are its pressure and volume respectively, or R its radius, and if V_0 and R_0 denote values under the hydrostatic pressure p_0, then

$$p_g V^\gamma = p_0 V_0^\gamma$$

$$p_g \left(\frac{4}{3}\pi R^3\right)^\gamma = p_0 \left(\frac{4}{3}\pi R_0^3\right)^\gamma$$

whence

$$p_g = p_0 \left(\frac{R_0}{R}\right)^{3\gamma} \qquad [26]$$

Here γ is the ratio of the specific heat of the gas at constant pressure to its specific heat at constant volume. The energy of such a gas is

$$W = \frac{pV}{\gamma - 1} = \frac{4\pi}{3(\gamma - 1)}\, p_0 R_0^3 \left(\frac{R_0}{R}\right)^{3\gamma - 3} \qquad [27]$$

or, if $\gamma = 4/3$,

$$W = 4\pi p_0 \frac{R_0^4}{R} \qquad [27a]$$

THE RADIAL MOTION

By inserting the value of W from Equation [27] and also $r_g = R$ in Equation [14] on page 46 of TMB Report 480 (4), the fundamental equation of radial motion for the sphere of gas in incompressible water under steady hydrostatic pressure p_0 is obtained in the form

$$\left(\frac{dR}{dt}\right)^2 = \frac{C_1}{R^3} - \frac{2}{3}\,\frac{1}{\gamma - 1}\,\frac{p_0}{\rho}\left(\frac{R_0}{R}\right)^{3\gamma} - \frac{2}{3}\,\frac{p_0}{\rho} \qquad [28]$$

where ρ denotes the density of water and C_1 a constant whose value depends upon initial conditions.

The maximum and minimum radii of the oscillating sphere, R_2 and R_1 respectively, occur when $dR/dt = 0$ and hence are those values of R which make the right-hand member of Equation [28] vanish. Hence R_1 and R_2 are connected with each other and with C_1 as follows:

$$C_1 = \frac{2}{3}\,\frac{p_0}{\rho}\, R_1^3\left[1 + \frac{1}{\gamma - 1}\left(\frac{R_0}{R_1}\right)^{3\gamma}\right] = \frac{2}{3}\,\frac{p_0}{\rho}\, R_2^3\left[1 + \frac{1}{\gamma - 1}\left(\frac{R_0}{R_2}\right)^{3\gamma}\right] \qquad [29]$$

whence, after dividing by $2p_0R_0^3/3\rho$,

$$\left(\frac{R_1}{R_0}\right)^3 + \frac{1}{\gamma-1}\left(\frac{R_0}{R_1}\right)^{3(\gamma-1)} = \left(\frac{R_2}{R_0}\right)^3 + \frac{1}{\gamma-1}\left(\frac{R_0}{R_2}\right)^{3(\gamma-1)} \qquad [30]$$

The relation between the radius and the time t may be found by solving Equation [28] for dt and integrating:

$$t = \int dt = \int\left[\frac{C_1}{R^3} - \frac{2}{3}\frac{1}{\gamma-1}\frac{p_0}{\rho}\left(\frac{R_0}{R}\right)^{3\gamma} - \frac{2}{3}\frac{p_0}{\rho}\right]^{-\frac{1}{2}} dR$$

or, in terms of

$$x = \frac{R}{R_0},\quad C = \frac{3\rho}{2p_0}\frac{C_1}{R_0^3} \qquad [31a, b]$$

$$t = \sqrt{\frac{3\rho}{2p_0}}\,R_0\int x^2 dx\left[Cx - x^4 - \frac{1}{\gamma-1}x^{4-3\gamma}\right]^{-\frac{1}{2}} \qquad [32]$$

For infinitesimal amplitudes of oscillation about $R = R_0$ or $x = 1$, the integration is easily effected by writing

$$x = 1 + w,\quad C = 1 + \frac{1}{\gamma-1} + b$$

where b is a small positive constant, expanding powers of $(1 + w)$ by the binomial theorem, and dropping all terms whose effect on t becomes negligibly small as $b \to 0$. Then Equation [32] becomes

$$t = \sqrt{\frac{3\rho}{2p_0}}\,R_0\int\left(b + bw - \frac{9}{2}\gamma w^2\right)^{-\frac{1}{2}} dw = \qquad [33]$$

$$\sqrt{\frac{3\rho}{2p_0}}\,R_0\sqrt{\frac{2}{9\gamma}}\,\sin^{-1}\left(\frac{9\gamma w - b}{\sqrt{b^2 + 18\gamma b}}\right)$$

For a half oscillation, the limits for w are the roots of the quantity in parentheses in the integral; these roots give to the sine of the angle the values +1 and -1, respectively, as is easily verified. Thus for a complete oscillation the $\sin^{-1}$ contributes a factor 2π, and the period is

$$T_0 = \sqrt{\frac{3\rho}{2p_0}}\,R_0\sqrt{\frac{2}{9\gamma}}\,2\pi = 2\pi R_0\sqrt{\frac{\rho}{3\gamma p_0}} \qquad [34]$$

or, for $\gamma = 4/3$,

$$T_0 = \pi R_0\sqrt{\frac{\rho}{p_0}} \qquad [34a]$$

For larger amplitudes numerical integration is necessary. This is simplest when $\gamma = 4/3$, so that Equation [32] becomes

$$t = \sqrt{\frac{3\rho}{2p_0}}\, R_0 \int \frac{x^2\,dx}{(Cx - x^4 - 3)^{\frac{1}{2}}} \qquad [35]$$

and

$$C = x_1^3 + \frac{3}{x_1} = x_2^3 + \frac{3}{x_2} \qquad [36]$$

in terms of the minimum or maximum values of x, x_1 or x_2. For purposes of numerical calculation, the substitution, $x = x_1(1 + u^2)$ is useful near x_1, and $x = x_2(1 - v^2)$ near x_2.

When the amplitude of oscillation is large, a useful analytical approximation for t can be obtained which is valid near the time t_1 at which the radius R takes on its minimum value R_1. When R is near R_1, x^4 is relatively small and can be dropped without much error; if x_1^3 is similarly dropped in Equation [36], so that $C = 3/x_1$, the integral in Equation [35], taken between the limits x_1 and x, becomes

$$\int_{x_1}^{x} \sqrt{\frac{x_1}{3}}\, \frac{x^2\,dx}{(x - x_1)^{\frac{1}{2}}} = \frac{x_1^{\frac{5}{2}}}{\sqrt{3}}\, (x - x_1)^{\frac{1}{2}} \left(\frac{16}{15} + \frac{8}{15}\frac{x}{x_1} + \frac{2}{5}\frac{x^2}{x_1^2}\right)$$

It is convenient, also, to eliminate ρ and p_0 by means of T_0 as given by Equation [34a]. Then Equation [35] gives, since $x_1 = R_1/R_0$,

$$t - t_1 = \frac{\sqrt{2}}{\pi}\, T_0 \left(\frac{R_1}{R_0}\right)^3 \sqrt{\frac{R}{R_1} - 1} \left(\frac{8}{15} + \frac{4}{15}\frac{R}{R_1} + \frac{1}{5}\frac{R^2}{R_1^2}\right) \qquad [37]$$

This formula should hold well so long as x^4 is small as compared to 3, perhaps up to $R = R_0/2$.

PRESSURE IN THE WATER

The pressure in incompressible water around a sphere of gas executing radial oscillations is given by Equation [8] on page 46 of TMB Report 480 (4), provided r_g is replaced by R and u_g by dR/dt. This gives, with u replaced by v for the particle velocity of the water,

$$p = \frac{R}{r}\left[p_g + \frac{1}{2}\rho\left(\frac{dR}{dt}\right)^2 - p_0\right] - \frac{1}{2}\rho v^2 + p_0 \qquad [38]$$

for the pressure p at a distance r from the center of the bubble. Here ρ is the density of water and p_0 is the hydrostatic pressure. Or, if substitution is made for p_g from Equation [26], for dR/dt from Equation [28], and for C_1 from Equation [29],

$$p = \frac{p_0}{3}\frac{R}{r}\left\{\left[1 + \frac{1}{\gamma - 1}\left(\frac{R_0}{R_1}\right)^{3\gamma}\right]\left(\frac{R_1}{R}\right)^3 - 4 + \left(3 - \frac{1}{\gamma - 1}\right)\left(\frac{R_0}{R}\right)^{3\gamma}\right\} - \frac{1}{2}\rho v^2 + p_0 \qquad [39]$$

and for $\gamma = 4/3$,

$$p = p_0 \frac{R}{r}\left\{\left[\left(\frac{R_0}{R_1}\right)^4 + \frac{1}{3}\right]\left(\frac{R_1}{R}\right)^3 - \frac{4}{3}\right\} - \frac{1}{2}\rho v^2 + p_0 \qquad [39a]$$

The maximum pressure, occurring at the instant at which $R = R_1$ and the water comes to rest, is, if $\gamma = 4/3$,

$$p_{max} = p_0 \frac{R_1}{r}\left[\left(\frac{R_0}{R_1}\right)^4 - 1\right] + p_0 \qquad [40]$$

If R_1/R_0 is small, only the terms in $(R_0/R_1)^4$ need be kept. Then, approximately, for $\gamma = 4/3$,

$$p_{max} = p_0 \frac{R_0}{r}\left(\frac{R_0}{R_1}\right)^3 + p_0 \qquad [41]$$

$$p = p_0 \frac{R_0}{r}\left(\frac{R_0}{R_1}\right)^3\left(\frac{R_1}{R}\right)^2 - \frac{1}{2}\rho v^2 + p_0 \qquad [42]$$

or

$$p = (p_{max} - p_0)\left(\frac{R_1}{R}\right)^2 - \frac{1}{2}\rho v^2 + p_0 \qquad [43]$$

An examination of Equation [39a] shows that for any $R < R_0/2$, which implies that $R_1 < R_0/2$ also, the error in Equations [42] and [43] is not over 7 per cent.

The effective *impulse*, $\int (p - p_0)dt$, may be found by direct integration, but it is most easily found by using Equation [9] on page 46 of TMB Report 480 (4)

$$\int (p - p_0)\, dt = \frac{\rho}{r}\Delta\left(R^2 \frac{dR}{dt}\right) - \frac{1}{2}\rho \int v^2 dt$$

where R and v replace r_g and u in the original. If t_1, the instant of minimum radius, is taken as the lower limit, at which $dR/dt = 0$, $\Delta(R^2\, dR/dt)$ becomes simply the value of $R^2 dR/dt$ at the upper limit t. Hence, from Equations [28] and [31b]

$$I = \int_{t_1}^{t} (p - p_0)\, dt = \sqrt{\frac{2}{3}\rho p_0}\,\frac{1}{r}\left[\frac{3\rho}{2p_0} C_1 R - \frac{R^4}{\gamma - 1}\left(\frac{R_0}{R}\right)^{3\gamma} - R^4\right]^{\frac{1}{2}} - \frac{1}{2}\rho \int v^2\, dt$$

or, using Equation [29] and eliminating ρ by means of Equation [34a],

$$I = \frac{1}{\pi}\sqrt{\frac{2}{3}}\, p_0 T_0 \frac{R_0}{r}\left\{\left[\left(\frac{R_{1,2}}{R_0}\right)^3 + \frac{1}{\gamma-1}\left(\frac{R_0}{R_{1,2}}\right)^{3\gamma-3}\right]\frac{R}{R_0} - \left(\frac{R}{R_0}\right)^4 - \frac{1}{\gamma-1}\left(\frac{R_0}{R}\right)^{3\gamma-4}\right\}^{\frac{1}{2}} - \frac{1}{2}\rho\int v^2\,dt \qquad [44]$$

in which $R_{1,2}$ indicates that R_1 may be inserted in both places, or R_2 may be employed instead of R_1. For $\gamma = 4/3$,

$$I = \frac{\sqrt{2}}{\pi}\, p_0 T_0 \frac{R_0}{r}\left\{\left[\frac{R_0}{R_{1,2}} + \frac{1}{3}\left(\frac{R_{1,2}}{R_0}\right)^3\right]\frac{R}{R_0} - \frac{1}{3}\left(\frac{R}{R_0}\right)^4 - 1\right\}^{\frac{1}{2}} - \frac{1}{2}\rho\int v^2\,dt \qquad [44a]$$

As R varies from R_1 to R_2, I as given by Equation [44] or [44a] rises to a maximum and returns to zero. Its maximum value represents the contribution of positive pressures and may be denoted by I_+; this value occurs when $p - p_0 = dI/dt = 0$. If the Bernouilli term $\rho v^2/2$ may be neglected, Equation [39a] gives

$$p - p_0 = 0 = p_0 \frac{R}{r}\left\{\left[\left(\frac{R_0}{R_1}\right)^4 + \frac{1}{3}\right]\left(\frac{R_1}{R}\right)^3 - \frac{4}{3}\right\}$$

and elimination of R between this equation and Equation [44a] with $R_{1,2} = R_1$ gives, for $\gamma = 4/3$,

$$I_+ = \frac{\sqrt{2}}{\pi}\, p_0 T_0 \frac{R_0}{r}\left\{\left(\frac{3}{4}\right)^{\frac{4}{3}}\left[\frac{R_0}{R_1} + \frac{1}{3}\left(\frac{R_1}{R_0}\right)^3\right]^{\frac{4}{3}} - 1\right\}^{\frac{1}{2}} \qquad [45]$$

RADIATION OF ENERGY

As stated on page 9 the pressure field at a distance from the gas sphere is essentially an acoustic field and involves the usual radiation of energy to infinity. The intensity of a sound wave, or the energy conveyed across unit area per second, is $(p - p_0)^2/\rho c$; the amount conveyed per second across a large sphere of radius r concentric with the bubble is, therefore,

$$4\pi r^2 \frac{(p - p_0)^2}{\rho c}$$

since p is uniform over such a sphere, and the total energy emitted will be

$$\Omega = \int 4\pi r^2 \frac{(p - p_0)^2}{\rho c}\, dt$$

In this integration the lag in time caused by the finite rate of propagation of sound waves can be ignored.

Because the energy depends on the square of the quantity $p - p_0$, radiation will occur almost exclusively near the peak of the wave, provided the amplitude of oscillation is large. At large distances, furthermore, the term $\rho v^2/2$ may be dropped. Hence, for $\gamma = 4/3$, Equation [42] may be employed for p, or, in terms of $x = R/R_0$, $x_1 = R_1/R_0$,

$$p - p_0 = p_0 \frac{R_0}{r} \frac{1}{x_1 x^2}$$

From Equation [35]

$$dt = \sqrt{\frac{3\rho}{2p_0}} R_0 \frac{x^2 dx}{(Cx - x^4 - 3)^{\frac{1}{2}}}$$

Hence, approximately, for $\gamma = 4/3$,

$$\Omega = \frac{2\pi}{c} \sqrt{\frac{6}{\rho}} p_0^{\frac{3}{2}} \frac{R_0^3}{x_1^2} \int \frac{dx}{x^2 (Cx - x^4 - 3)^{\frac{1}{2}}} \qquad [46]$$

in which C is given by Equation [36].

If the amplitude is large, x^4 may be dropped and C may be replaced by $3/x_1$, as in obtaining Equation [37]. In integrating up to a large x, furthermore, the limit can be replaced by ∞ without much error, because of the rapid decrease in the integrand. Hence, if $\gamma = 4/3$ and the amplitude of oscillation is large, the energy emitted during a compression and subsequent re-expansion has the approximate value

$$\Omega_1 = \frac{2\pi}{c} \sqrt{\frac{2}{\rho}} p_0^{\frac{3}{2}} \frac{R_0^3}{x_1^{\frac{3}{2}}} 2 \int_{x_1}^{\infty} \frac{dx}{x^2 (x - x_1)^{\frac{1}{2}}}$$

The integral equals $\pi/(2x_1^{3/2})$. Hence

$$\Omega_1 = \frac{2\sqrt{2}\,\pi^2}{c} \rho^{-\frac{1}{2}} p_0^{\frac{3}{2}} R_0^3 \left(\frac{R_0}{R_1}\right)^3 \qquad [47]$$

or, if we also eliminate ρ by means of Equation [34a],

$$\Omega_1 = 2\sqrt{2}\,\pi^3 \frac{p_0 R_0^4}{c T_0} \left(\frac{R_0}{R_1}\right)^3 \qquad [48]$$

For comparison, the total energy of oscillation E is equal to the kinetic energy in the water at the instant at which the radius $R = R_0$, since, if the water were suddenly arrested at this instant, the sphere would remain in equilibrium. As R decreases to its minimum value, R_1, this energy, together with the work done by hydrostatic pressure as the radius decreases, becomes expended in work done in compressing the gas. Hence, by Equation [27]

$$E + \frac{4}{3}\pi p_0 (R_0^3 - R_1^3) = \frac{4\pi}{3(\gamma - 1)} p_0 R_0^3 \left[\left(\frac{R_0}{R_1}\right)^{3\gamma - 3} - 1\right]$$

whence

$$E = \frac{4}{3}\pi p_0 R_0^3 \left[\frac{1}{\gamma - 1}\left(\frac{R_0}{R_1}\right)^{3(\gamma - 1)} + \left(\frac{R_1}{R_0}\right)^3 - \frac{\gamma}{\gamma - 1}\right] \qquad [49]$$

in which, according to Equation [30], R_2 might be substituted for R_1; or, if $\gamma = 4/3$,

$$E = 4\pi p_0 R_0^3 \left[\frac{R_0}{R_1} + \frac{1}{3}\left(\frac{R_1}{R_0}\right)^3 - \frac{4}{3}\right] = 4\pi p_0 R_0^3 \left[\frac{R_0}{R_2} + \frac{1}{3}\left(\frac{R_2}{R_0}\right)^3 - \frac{4}{3}\right] \qquad [49a]$$

BUBBLE UNDER VARIABLE EXTERNAL PRESSURE

Up to this point the hydrostatic pressure p_0 has been assumed to be constant. Let it now be assumed to vary with the time. Such variation may be caused by the action of a piston upon the water; if compression of the water is negligible, this pressure will be transmitted instantly to all parts of the water. The theory developed for this case should also hold approximately for the action of a shock wave upon a bubble, provided the bubble is much smaller than the effective length of the shock wave in the water.

Examination of the deduction of Equations [1] to [10] on pages 45 and 46 of TMB Report 480 (4) shows that all of these equations remain valid if p_0 varies with the time t. If in Equation [10] on page 46, R is written for r_g, the radius of a spherical gas bubble, the equation becomes

$$p_g = \rho\left[\frac{3}{2}\left(\frac{dR}{dt}\right)^2 + R\frac{d^2R}{dt^2}\right] + p_0$$

or

$$p_g = \frac{\rho}{R^{\frac{1}{2}}}\frac{d}{dt}\left(R^{\frac{3}{2}}\frac{dR}{dt}\right) + p_0$$

Only the simple case of an impulsive variation of p_0 will be treated here. Let p_0 take on large values during a very short time t_1. Integrating the last equation during this interval,

$$\int p_g\, dt = \rho\int \frac{1}{R^{\frac{1}{2}}}\frac{d}{dt}\left(R^{\frac{3}{2}}\frac{dR}{dt}\right) dt + \int p_0\, dt$$

Now p_g is nearly constant during the short time t_1, hence $\int p_g\, dt$ is very small and may be dropped in comparison with $\int p_0\, dt$. In the second integral, R is nearly constant, whereas dR/dt may undergo considerable change; hence, approximately,

$$\int \frac{1}{R^{\frac{1}{2}}} \frac{d}{dt}\left(R^{\frac{3}{2}} \frac{dR}{dt}\right) dt = \frac{1}{R^{\frac{1}{2}}} \int \frac{d}{dt}\left(R^{\frac{3}{2}} \frac{dR}{dt}\right) dt = \frac{1}{R^{\frac{1}{2}}} \Delta\left(R^{\frac{3}{2}} \frac{dR}{dt}\right) = R \Delta \frac{dR}{dt}$$

where Δ denotes the change of a quantity during the time t_1. Thus

$$\Delta \frac{dR}{dt} = -\frac{1}{\rho R} \int p_0 \, dt \qquad [50]$$

If $dR/dt = 0$ initially, the velocity produced by the impulsive variation of p_0 is, therefore,

$$\frac{dR}{dt} = -\frac{1}{\rho R} \int p_0 \, dt \qquad [51]$$

EFFECT OF MANY SMALL BUBBLES ON LONG PLANE SINUSOIDAL WAVES OF A SMALL AMPLITUDE

In order to deal accurately with the effect of bubbles upon waves of pressure, it is necessary to make full allowance for the compressibility of the water. The analysis then becomes very difficult unless it is restricted to very small variations of pressure, so that acoustic theory can be employed. This restriction will now be made. Even so, only the case of sinusoidal waves can be handled readily; waves of other forms may then be treated if necessary, with the help of Fourier analysis.

It will be assumed that the spacing of the bubbles, although large relatively to their diameter, is small relatively to the wave length of the wave, either in the bubbly water or in homogeneous water. This assumption will be taken to imply, in particular, that the average pressure in the water at any instant is sensibly the same as the pressure at points midway between the bubbles, and also that the local pressure field around each bubble is sensibly the same as it would be if this field were exactly spherically symmetrical and had a value at infinity equal to the actual mean pressure between the bubbles.

Let there be n bubbles per unit volume, all having radius R_0 when in equilibrium under the hydrostatic pressure p_0. Let x denote distance in the direction of propagation of the waves.

The equations of propagation are easily obtained in the usual way, by considering an element of volume having the form of a cylinder of length dx and of unit cross-sectional area. Let v denote the average particle velocity of the water in the direction of x. Then the volume of the mixture of bubbles and water that is in the element at any instant increases during the next interval dt by

$$\frac{\partial v}{\partial x} \, dx \, dt$$

This change in volume is supplied partly by a change in the volume of the water itself, partly by a change in the volume of the bubbles. As the elasticity of water is equal to ρc^2, where ρ is its density and c the speed of sound in it, the increase in volume of the water is

$$\frac{1}{\rho c^2}\left(-\frac{\partial p}{\partial t}\,dt\right)dx$$

where p denotes the average pressure in the water surrounding the bubbles. The increase in volume of the $n\,dx$ bubbles in the element is

$$n\,dx\,\frac{\partial}{\partial t}\left(\frac{4}{3}\pi R^3\right)dt = 4\pi n R^2\,\frac{dR}{dt}\,dx\,dt$$

Hence

$$\frac{\partial v}{\partial x}\,dx\,dt = -\frac{1}{\rho c^2}\,\frac{\partial p}{\partial t}\,dx\,dt + 4\pi n R^2\,\frac{dR}{dt}\,dx\,dt$$

$$\frac{\partial p}{\partial t} = -\rho c^2\,\frac{\partial v}{\partial x} + 4\pi n \rho c^2 R^2\,\frac{dR}{dt} \qquad [52]$$

During the same time the momentum in the layer has been changed by

$$\rho\left(\frac{\partial v}{\partial t}\,dt\right)dx = -\frac{\partial p}{\partial x}\,dx\,dt$$

since $dx(-\partial p/\partial x)$ represents the net force on the element, whence

$$\frac{\partial v}{\partial t} = -\frac{1}{\rho}\,\frac{\partial p}{\partial x} \qquad [53]$$

If Equation [52] is differentiated with respect to t and Equation [53] with respect to x, and if $\partial^2 v/\partial t\,\partial x$ is then eliminated between the two equations, the equation of propagation for p is obtained

$$\frac{\partial^2 p}{\partial t^2} = c^2\,\frac{\partial^2 p}{\partial x^2} + 4\pi n \rho c^2 R^2\,\frac{d^2 R}{dt^2} \qquad [54]$$

Here a term in $(dR/dt)^2$ has been dropped as being of the second order. In the same way ρ was treated as constant in deducing Equation [53]; and the decrease in mass due to the presence of bubbles was also ignored as being very small.

Equation [54] is unusual in form among wave equations in that it contains two dependent variables, p and R. A second equation is, therefore, necessary, and it may be obtained by analyzing the motion of the bubbles.

This motion can be handled conveniently with the help of the principle of superposition. If the bubbles did not change in radius, the incident wave, according to the assumptions made, would cause the pressure p near

a bubble to vary in time without the occurrence of marked inequalities of pressure. The effect of a radial motion of the bubble will then be to superpose upon this incident pressure field an emitted train of spherical waves. If p_e is the pressure due to these waves, the local pressure at any point near the bubble will be $p + p_e$.

The average pressure in the water can be written

$$p = p_1 e^{-\alpha x} \cos \omega \left(t - \frac{x}{c'} \right) + p_0 \qquad [55]$$

where p_1, ω and α are constants and c' is the speed of propagation of the waves through the bubbly water. The factor $e^{-\alpha x}$ is introduced to allow for damping due to the scattering action of the bubbles. The corresponding particle velocity, obtained by calculating $\partial p/\partial x$, substituting in Equation [53], and integrating with respect to t, is

$$v = \frac{p_1}{\rho c'} e^{-\alpha x} \left[\cos \omega \left(t - \frac{x}{c'} \right) + \frac{\alpha c'}{\omega} \sin \omega \left(t - \frac{x}{c'} \right) \right] \qquad [56]$$

The mean pressure near a bubble at $x = 0$ will then be

$$p = p_1 \cos \omega t + p_0 \qquad [57]$$

Under the influence of this pressure, the bubble will execute forced harmonic vibrations. Because of this vibratory motion, it will emit a train of spherical waves which, according to our assumptions are to be regarded as superposed upon the average pressure represented by Equation [55]. The pressure in the emitted waves at a distance r from the center of the bubble can be written

$$p_e = \frac{R_0}{r} p_2 \cos \omega \left[t' - \frac{r - R_0}{c} \right], \quad t' = t + b$$

in which R_0 is the radius of the bubble when undisturbed, c is the speed of sound in water, and p_2, ω and b are constants. The corresponding particle velocity, taken positive outward, is

$$v_e = \frac{R_0}{\rho c r} p_2 \left[\cos \omega \left(t' - \frac{r - R_0}{c} \right) + \frac{c}{\omega r} \sin \omega \left(t' - \frac{r - R_0}{c} \right) \right]$$

as can be verified from Equation [3] on page 38 of TMB Report 480 (4). At the surface of the bubble, where r can be set equal to R_0 in constructing a first-order theory,

$$p_e = p_2 \cos \omega t'$$

$$v_e = \frac{dR}{dt} = \frac{p_2}{\rho c} \left(\cos \omega t' + \frac{c}{\omega R_0} \sin \omega t' \right)$$

and the displacement and acceleration of the surface of the bubble are, respectively,

$$R - R_0 = \int \frac{dR}{dt}\, dt = \frac{p_2}{\rho c \omega}\left(-\frac{c}{\omega R_0}\cos\omega t' + \sin\omega t'\right)$$

$$\frac{d^2R}{dt^2} = \frac{p_2}{\rho c}\left(\frac{c}{R_0}\cos\omega t' - \omega \sin\omega t'\right)$$

It is easily verified from these equations that the value of p_e at the surface of the bubble can be written in terms of R as follows

$$p_e = \frac{\rho R_0 \frac{d^2R}{dt^2} + \frac{\rho}{c}\omega^2 R_0^2 \frac{dR}{dt}}{1 + \frac{\omega^2 R_0^2}{c^2}} \qquad [58]$$

Here ω has reference to the incident waves, so that if λ is their wave length in homogeneous water,

$$\frac{\omega}{c} = \frac{2\pi}{\lambda}, \quad \frac{\omega R_0}{c} = 2\pi \frac{R_0}{\lambda}$$

But according to our assumptions, R_0/λ must be small. Hence the term $\omega^2 R_0^2/c^2$ can be dropped and Equation [58] can be written

$$p_e = \rho R_0 \frac{d^2R}{dt^2} + \frac{\rho}{c}\omega^2 R_0^2 \frac{dR}{dt} \qquad [59]$$

The total pressure is now the sum, $p + p_e$; and at the bubble this must equal the pressure of the gas. The volume strain of the bubbles is $\delta V/V = \delta(R^3)/R^3 = 3\delta R/R = 3(R - R_0)/R_0$. Hence, if E' is the elasticity of the gas, the pressure of the gas is

$$p_0 - 3E' \frac{R - R_0}{R_0}$$

Hence

$$p + p_e = \frac{-3E'(R - R_0)}{R_0} + p_0$$

and by Equations [57] and [59],

$$\rho R_0 \frac{d^2R}{dt^2} + \frac{\rho}{c}\omega^2 R_0^2 \frac{dR}{dt} + \frac{3E'}{R_0}(R - R_0) = -p_1 \cos\omega t$$

The corresponding equation for non-compressive theory is obtained by letting c become infinite. If p_1 is also replaced by zero, the usual equation for free oscillation is obtained, namely,

$$\frac{d^2R}{dt^2} + \frac{3E'}{\rho R_0^2}(R - R_0) = 0$$

Thus

$$\omega_0^2 = \frac{3E'}{\rho R_0^2} \qquad [60]$$

where $\omega_0/2\pi$ is the frequency of free undamped oscillation as deduced from non-compressive theory. Hence the preceding equation can be written

$$\frac{d^2R}{dt^2} + \frac{\omega^2}{c} R_0 \frac{dR}{dt} + \omega_0^2 (R - R_0) = -\frac{p_1}{\rho R_0} \cos \omega t \qquad [61]$$

A particular solution of the last equation is easily verified to be

$$R - R_0 = -\frac{p_1}{\rho R_0 \left[(\omega_0^2 - \omega^2)^2 + R_0^2 \frac{\omega^6}{c^2}\right]} \left[(\omega_0^2 - \omega^2)\cos\omega t + \frac{R_0 \omega^3}{c} \sin \omega t\right] \qquad [62]$$

This solution represents steady forced oscillations of the bubble.

The occurrence of sin ωt in Equation [62], or of dR/dt in Equation [61], represents the effect of radiation damping or of scattering of the incident wave by the bubble. The complementary solution obtained by solving Equation [61] with $p_1 = 0$, represents a superposed damped free oscillation that soon dies out.

Values of the derivatives that occur in Equation [54] may now be calculated and inserted from Equations [62] and [55], with x set equal to 0. Furthermore, R may be replaced by R_0 for a first-order theory. Since the equation must hold at all times, the cosine terms must balance independently of the sine terms on the two sides of the equation. Thus are obtained two equations for the determination of c' and α

$$\omega^2 \frac{c^2}{c'^2} - c^2\alpha^2 = \omega^2 + \frac{4\pi n c^2 R_0 \omega^2 (\omega_0^2 - \omega^2)}{(\omega_0^2 - \omega^2)^2 + \frac{R_0^2 \omega^6}{c^2}}$$

$$2\omega \frac{\alpha}{c'} = \frac{1}{c} \frac{4\pi n R_0^2 \omega^5}{(\omega_0^2 - \omega^2)^2 + \frac{R_0^2 \omega^6}{c^2}}$$

A more interesting form is obtained, however, by introducing, first, the fraction of the space that is occupied by gas, or

$$f = \frac{4}{3} n \pi R_0^3 \qquad [63]$$

second, the ratio of the elasticity of water to the elasticity of the gas, which will be denoted by N^2, where

$$N^2 = \frac{\rho c^2}{E'} = \frac{3c^2}{R_0^2 \omega_0^2} \qquad [64]$$

y Equation [60], and, lastly, the "extinction coefficient"

$$\beta = \frac{\alpha c}{\omega} = \frac{\alpha \lambda}{2\pi} \qquad [65]$$

here λ is the wave length of the incident waves in homogeneous water. Then

$$\frac{c^2}{c'^2} - \beta^2 = 1 + fN^2 \frac{1 - \frac{\omega^2}{\omega_0^2}}{\left(1 - \frac{\omega^2}{\omega_0^2}\right)^2 + \frac{3}{N^2}\frac{\omega^6}{\omega_0^6}} = X \qquad [66]$$

$$2\beta \frac{c}{c'} = \sqrt{3}\, fN \frac{\frac{\omega^3}{\omega_0^3}}{\left(1 - \frac{\omega^2}{\omega_0^2}\right)^2 + \frac{3}{N^2}\frac{\omega^6}{\omega_0^6}} = Y \qquad [67]$$

The values of c' and of β can also be written separately in terms of the quantities denoted by X and Y as

$$c' = c\left(\frac{1}{2}X + \frac{1}{2}\sqrt{X^2 + Y^2}\right)^{-\frac{1}{2}} \qquad [68]$$

$$\beta = \frac{Y}{2}\left(\frac{1}{2}X + \frac{1}{2}\sqrt{X^2 + Y^2}\right)^{-\frac{1}{2}} \qquad [69]$$

COEFFICIENT OF REFLECTION

Suppose that, under the conditions specified in the foregoing, a train of plane sinusoidal waves in homogeneous water falls at normal incidence upon the plane face of a layer of uniformly bubbly water. Then there will be a reflected train of waves in the homogeneous water and a transmitted train in the bubbly water; see Figure 9. The pressures and particle velocities in these three trains may be written as follows, in the notation just employed:

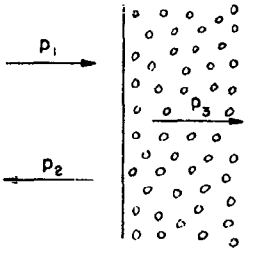

Figure 9 - Sketch illustrating the Reflection of a Wave from Bubbly Water

Incident: $p = p_1 \cos\omega\left(t - \frac{x}{c}\right)$ $\qquad v = \frac{p}{\rho c}$

Reflected: $p = p_2 \cos\omega\left(t + \frac{x}{c} + \tau\right)$ $\qquad v = -\frac{p}{\rho c}$

Transmitted: $p = p_3\, e^{-\alpha x} \cos\omega\left(t - \frac{x}{c'} + \tau'\right)$

$$v = \frac{p_3}{\rho c'}\, e^{-\alpha x}\left[\cos\omega\left(t - \frac{x}{c'} + \tau'\right) + \frac{\alpha c'}{\omega}\sin\omega\left(t - \frac{x}{c'} + \tau'\right)\right]$$

The last two of these equations are adapted from Equations [55] and [56]. In writing the pressures, hydrostatic pressure is omitted.

In these equations p_1 may be regarded as given, whereas p_2, p_3 and the phase shifts τ and τ' are determined by the boundary conditions. At the interface, at which $x = 0$, the pressure and the particle velocity must be continuous. By writing down the two equations that express these conditions, and putting in them, first, $t = 0$, then $\omega t = \pi/2$, four equations are obtained. From these equations p_2, p_3, τ', τ can be found. It will suffice to write down the following formula, obtained by eliminating all unknowns but p_2 from the four equations:

$$\left[\left(1 - \frac{c}{c'}\right)^2 + \frac{\alpha^2 c^2}{\omega^2}\right] p_1^2 = \left[\left(1 + \frac{c}{c'}\right)^2 + \frac{\alpha^2 c^2}{\omega^2}\right] p_2^2$$

The coefficient of reflection K, or fraction of the incident energy that is reflected, is equal to p_2^2/p_1^2, since reflected and incident waves travel in the same medium and their intensity is, therefore, proportional to p^2. Hence

$$K = \frac{\left(1 - \frac{c}{c'}\right)^2 + \frac{\alpha^2 c^2}{\omega^2}}{\left(1 + \frac{c}{c'}\right)^2 + \frac{\alpha^2 c^2}{\omega^2}} = \frac{\left(1 - \frac{c}{c'}\right)^2 + \beta^2}{\left(1 + \frac{c}{c'}\right)^2 + \beta^2} \qquad [70]$$

in view of Equation [65].

SCATTERING BY A SINGLE BUBBLE

The amplitude of pressure at a distance r in the waves scattered by an isolated bubble is $p_2 R_0/r$ in terms of the amplitude p_2 at the surface of the bubble, whose radius is R_0. Where r is large, the waves are sensibly plane, and the average energy transmitted by them across unit area per second, if they are sinusoidal, is

$$\frac{1}{2\rho c}\left(\frac{p_2 R_0}{r}\right)^2 \qquad [71]$$

in which the factor 1/2 represents the effect of averaging over the square of a sinusoidal function of the time; see TMB Report 480 (4), page 39, Equation [5]. The total energy scattered to infinity per second by the bubble is thus

$$\Omega = \frac{1}{2\rho c}\left(\frac{p_2 R_0}{r}\right)^2 4\pi r^2 = \frac{2\pi R_0^2}{\rho c} p_2^2 \qquad [72]$$

Now upon substituting derivatives from Equation [62] in Equation [59] and combining the resulting terms into a single sinusoidal term, it is found that

$$p_e = \left[\frac{1 + R_0^2 \frac{\omega^2}{c^2}}{(\omega_0^2 - \omega^2)^2 + R_0^2 \frac{\omega^6}{c^2}}\right]^{\frac{1}{2}} \omega^2 p_1 \sin(\omega t + \gamma)$$

where γ is a phase angle of no present importance. The coefficient of $\sin(\omega t + \gamma)$ represents p_2, the amplitude of p_e; in this coefficient the term $R_0^2\omega^2/c^2$ can again be dropped in comparison with unity. With the value of p_2 thus obtained, Equation [72] becomes

$$\Omega = \frac{2\pi R_0^2}{\rho c} \frac{\omega^4 p_1^2}{(\omega_0^2 - \omega^2)^2 + R_0^2 \frac{\omega^6}{c^2}} \qquad [73]$$

It is more useful, however, to express Ω in terms of the intensity of the incident waves, or the energy transported by them across unit area per second, which is, in analogy with Equation [71],

$$I = \frac{p_1^2}{2\rho c} \qquad [74]$$

In terms of N as defined in Equation [64],

$$\Omega = AI$$

where

$$A = \frac{4}{\left(1 - \frac{\omega_0^2}{\omega^2}\right)^2 + \frac{3}{N^2}\frac{\omega^2}{\omega_0^2}} \pi R_0^2 \qquad [75]$$

Thus the bubble scatters as much energy as falls on an area A placed perpendicularly to the direction of propagation of the incident waves.

THE MOTION AND SHAPE OF THE HOLLOW PRODUCED BY AN EXPLOSION IN A LIQUID

G. I. Taylor and R. M. Davies
Cambridge University

British Contribution

February 1943

THE MOTION AND SHAPE OF THE HOLLOW PRODUCED BY AN EXPLOSION IN A LIQUID

G. I. Taylor and R. M. Davies

February 1943

* * * * * * * * *

Summary.

It is shown in a previous paper by one of us that the gas-filled hollows produced by explosions in water cannot be reproduced on a small scale unless the pressure above the water is correspondingly reduced. In the experiments here described, which are on a very small scale, bubbles were produced by sparking under a liquid contained in an evacuated vessel. In this way it seems that we can reproduce, on a very small scale, the changes in form and motion of the gas bubble produced by a large explosion. It is worth noticing that, in small-scale explosions at atmospheric pressure, the effect of the free surface is so great that the bubble hardly rises at all, even when it gets to 3 feet diameter, yet these bubbles of 6 cm. maximum diameter showed the rise under gravity which is expected in large-scale explosions.

One of the objects of these experiments was to see how far the assumption that the explosion gas bubble is spherical is justified. This assumption has been made to facilitate calculation of the rate of rise of the bubble, and our experiments show that it is correct over the greater part of the first pulsation of the bubble. The photographs also verify the theoretical conclusion that the surface of the bubble should be smooth and stable during the first expansion and the early part of the first contraction, but should become unstable when the bubble has contracted to near its minimum volume.

1. *Introduction.*

In Report (*Vertical motion of a spherical bubble and the pressure surrounding it*), hereafter called Report A, the effect of gravity on a bubble is calculated, assuming that the bubble is maintained spherical by internal constraints which do no work on the surrounding fluid apart from that which is done by the gas contained in it during the expansion and contraction of its volume. This assumption imposes a severe limitation on the accuracy with which the calculated results may be expected to apply to real explosion gas bubbles. On the other hand it does enable calculations to be made which may be expected to be reasonably significant in cases where analysis in which the whole motion is taken as a small perturbation of a pulsating bubble referred to a fixed centre cannot be used.

In the calculation of Report A the effect of the free surface or of a horizontal rigid surface on the motion of the bubble was not considered though, as Conyers Herring* showed, it may in some cases be comparable or even greater than that of gravity. Photographs, taken by Edgerton ♯ at the Taylor Model Basin, of the bubble produced by exploding a detonator cap at a small depth below a free surface do in fact show that during its first period, at any rate, the effect of the free surface is greater than that of gravity, so that the bubble sinks instead of rising. This is, qualitatively at any rate, in accordance with the theoretical prediction of Herring.

In Report A it is shown that large upward displacements of the bubble, due to gravity, may be expected when its maximum diameter is comparable with the head of water necessary to produce the hydrostatic pressure at the level of its centre. This condition occurs when an explosion produces in water a bubble

whose .....

* U.S. Report No. CM-sr 20-010, "The theory of the pulsations of the gas bubble produced by an underwater explosion", October 1941.

♯ U.S. Report. "A photographic study of underwater explosions", October 1941

whose diameter is comparable with 33 feet, but not when a detonator cap produces a bubble only 10 inches diameter. A small-scale explosion under water with a free surface at atmospheric pressure cannot therefore represent dynamically the events accompanying a full-scale explosion, but if the explosion could be made under water with a free surface at reduced pressure similarity in this respect would be obtained. Experiments, in which bubbles were produced by sparking under water and other liquids in an evacuated vessel, were therefore undertaken with a view to seeing, on a small scale, what may be expected to happen to the bubble in large-scale explosions. Photographs of a series of similar bubbles at successive stages of their development were first taken on stationary plates, but later a revolving drum camera enabled the history of a single bubble to be traced. A preliminary report on these experiments is given below.

2. *The similarity relationships.*

With ideal fluids, free from viscosity, the conditions that two bubbles whose linear scales are in the ratio 1:N shall be similar, are:-

(1) $h_1 = Nh_2$

where h_1 is the depth of the large-scale charge below the surface and h_2 is that of the small one.

(2) $P_1/\rho_1 = NP_2/\rho_2$

where P_1 and P_2 are the pressures of the air above the surfaces in the two cases, and ρ_1 and ρ_2 the densities of the fluids.

(3) $W_1/\rho_1 = N^4 W_2/\rho_2$

where W_1 and W_2 are the energies which the explosives give up when the products of combustion expand adiabatically to infinity.

(4) $G(a_1)/\rho_1 = N^4 G(a_2)/\rho_2$

where G(a) represents the work which would be done by the gas in expanding adiabatically from radius a to infinity.

If the liquids considered in the two experiments are viscous, their viscosities μ_1, μ_2 must be related by

(5) $\mu_1/\rho_1 = N^{3}/_{2}\, \mu_2/\rho_2$

This condition ensures that the Reynold's numbers of the two bubbles shall be the same at any stage.

In the cases where the pressure in the bubble falls below the saturation vapour pressure (S.V.P.) at the temperature of the liquid, it is necessary, in order that both liquids may boil at the same stage of the expansion, that

(6) (S.V.P. of liquid 1)$/\rho_1$ = N. (S.V.P. of liquid 2)$/\rho_2$

3. *Limitation to applicability of scale relationships.*

It is unlikely that it would ever be possible to satisfy all the six above relationships simultaneously. Some of them, however, are of little importance compared with others.

After fixing arbitrarily a value for N, (1) can be satisfied by setting the charge at the correct depth and (2) by exhausting the air in the chamber where the model experiment is to be carried out; (3) can can be satisfied by varying the energy of the explosive charge or the spark which produces the bubble.

Condition .....

Condition (4) is more difficult to satisfy. It could be satisfied if (a) the model and full-scale bubbles were both produced by explosion of gases contained in thin spherical envelopes such as rubber balloons, provided the initial pressures of the unexploded gases in the two cases were the same as (or any given multiple of) those of the surrounding fluids, and (b) the densities of the two fluids are the same, i.e., $\rho_1 = \rho_2$. Such experimental conditions would ensure that conditions (3) and (4) were both satisfied, but it would be difficult to devise a model experiment so that (4) was satisfied when the full-scale bubble is due to the explosion of a solid explosive and the small bubble to a spark. Fortunately, however, there is not much difference between the bubble produced by releasing all the energy at a very small radius and that produced by releasing most of it at very small radius and the rest during the expansion. Dr. Comrie's curves showing the radius a as a function of time are very insensitive to the constant "C" which determines the value of G(a)/W.

The value of G(a)/M for the bubble produced by a mass M of a given explosive depends only on the absolute preesure in the bubble. If similarity of bubbles on two scales is obtained by choosing the atmospheric pressure, weight of explosive and depth so that conditions (1), (2) and (3) are satisfied, G(a)/M will be less at a given stage of the expansion in the small-scale experiment than in the large-scale explosion, owing to the fact that the pressure is less. It seems that, in comparing large-scale underwater explosions with small-scale sparks in a liquid under reduced pressure, one is comparing bubbles in which the constant C in Comrie's calculation varies from 0.06 up to 0.1 with the case where C is so small as to be negligible. The difference between the two cases is not great.

4. *The effect of viscosity.*

To satisfy condition (5) in a small-scale experiment designed to represent a bubble in water would require a liquid whose viscosity is very much less than that of water. No such liquid is available. Fortunately, however, it is not necessary to satisfy this condition, because the loss of energy due to the viscous forces opposing the expansion or contraction of the bubble is very small compared with the whole energy of the bubble, even when a liquid of much greater viscosity than water is used.

The rate of dissipation of energy owing to viscosity is

$$F = \tfrac{1}{2}\mu \iint \left[\frac{\partial q^2}{\partial r}\right]_{r=a} dS \qquad (7)$$

the integral being taken over the surface of the sphere, and q being the radial velocity of the fluid.

Since $q = \dot{a}a^2/r^2$, equation (7) gives

$$F = 8\pi\mu a\dot{a}^2$$

and the total energy, W_μ, dissipated during time t is

$$W_\mu = 8\pi\mu \int_0^t a\dot{a}^2\, dt = 8\pi\mu \int_{a_0}^{a} a\dot{a}\, da.$$

Equation (2) of Report A is now modified to the form

$$\tfrac{4}{3}\pi\rho a^3 gz + 2\pi\rho a^3 \dot{a}^2 + \tfrac{1}{3}\pi\rho a^3 \dot{z}^2 + 8\pi\mu \int_{a_0}^{a} a\dot{a}\, da = W - G(a) \qquad (8)$$

Reducing to the non-dimensional form of equation (5) of Report A equation (8) becomes

$$\left(\frac{da'}{dt'}\right)^2 = \frac{1}{2\pi a'^3}\left\{1 - \frac{G(a)}{W} - \delta\right\} - \frac{1}{6}\left(\frac{dz'}{dt'}\right)^2 - \frac{2}{3}z' \qquad (9)$$

where

$$\delta = \frac{8\pi\mu}{(\rho^5 W^3 g)^{\frac{1}{8}}} \int_0^{t'} a'\left(\frac{da'}{dt'}\right)^2 dt' \qquad (10)$$

If .....

If δ is small the relationship between a' and t' will be little altered by viscosity, so that the value of the integral in equation (10) can be estimated using the values calculated when $\mu = 0$. In the case calculated in Report A, where $z'_0 = 2$, the value of $\int_0^{t'} a' \left(\frac{da'}{dt'}\right)^2 dt'$, taken over the whole of the first period of the bubble is 0.6, so that the value of δ at the end of the first period is

$$\delta = \frac{4.8\,\pi\,\mu}{(\rho^5 w^3 g)^{\frac{1}{6}}} \qquad (11)$$

In some of our experiments, in which transformer oil of viscosity 0.3 poises and density 0.875 gm./cc. was used, z'_0 was of the order of 2; the value of δ calculated from equation (11) was 0.006, so that less than one per cent of the energy of the bubble is dissipated by viscous forces during the first period, if the bubble remains spherical.

5. *The choice of operating liquid.*

With explosions in open water the pressure at points far distant from the bubble is never less than 1 atmos; the minimum pressure in the bubble, though considerably less than 1 atmos., does not fall as low as the saturation vapour pressure (S.V.P.) of water. In experiments with water under a surface pressure which is low compared with normal atmospheric pressure but well above the S.V.P. the minimum pressure near the surface of the bubble may be less than the S.V.P. The water then boils near the bubble.

Figure 1 shows two superposed photographs, on the same plate, of a bubble made by a spark under water at surface pressure rather greater than the S.V.P., (1) at an early stage of the expansion, when it is smooth and spherical, and (2) at a later stage, when the small vapour bubbles due to boiling have had time to develop. It will be seen that the surface has become pitted by the boiling.

In order to avoid boiling when experimenting at low pressures it is necessary to use a liquid with a low S.V.P. For this reason transformer oil was used. Though the viscosity of this liquid is about 30 times that of water, it has been shown that the expansion of the gas bubble is not likely to be materially different from what it would be in water, at any rate while it is approximately spherical.

6. *Description of the apparatus.*

The airtight vessel in which the bubbles are produced is shown in elevation in Figure 2; it consists of a vertical glass cylinder, A, 12 inches diameter, ¼ inch wall, 15 inches high, cemented between two horizontal steel end-plates, B and C, 18 inches diameter, ½ inch thick. This vessel is filled with water or oil to a depth of about 11 inches, and it is connected to a vacuum pump and a pressure gauge through the tube D.

A bubble is produced in the liquid by the discharge of a condenser, charged to a potential difference of 4,000 volts, across a gap of about 10/1000th inches between the rounded ends of the horizontal brass rods E and F, $\frac{1}{8}$th inch diameter and 3 inches long. The electrode E is connected electrically to the upper steel plate B, which is earthed; the electrode F is insulated and is connected to the condenser and the timing pendulum by a lead passing through the insulated bush, G. The electrodes are fixed to the brass frameworks shown in the diagram so that they can be moved independently, without admitting air to the vessel, by means of a brass push tube and two brass push rods passing through stuffing boxes fixed to the upper steel plate.

The framework supporting the electrode F can be moved vertically or rotated by means of the push rod passing through the right stuffing box shown in the diagram. A hinge H_1 allows the electrode to fly back during an explosion, whilst the horizontal member of the framework is supported and is prevented from moving at right angles to the plane of the diagram by a wire staple J_1 fixed to a block of insulating material attached to the push rod.

The framework supporting the electrode E is connected through the hinged joint H_2 to the push tube passing through the lower stuffing box, shown on the left in the diagram; a push rod passes through this tube and through the upper stuffing box and carries at its lower end a horizontal brass bar to which

is fixed .....

is fixed a knife-edge K and a wire staple J_2 passing over the brass bar attached to H_2. When the upper stuffing box is tight and the lower one is slightly slackened the framework can be moved vertically as a whole or rotated. When the upper stuffing box is tight and the lower one is slightly slackened the framework can be moved vertically as a whole or rotated. When the upper stuffing box is slackened and the lower one is tight the central push rod can be moved up or down relative to the push tube, thus raising or lowering the knife-edge K and increasing or decreasing the gap between the ends of E and F.

When photographing the bubble, it is essential to correct the optical distortion caused by the cylindrical form of the bubble tank. For this purpose, two parallelizing tanks, L, consisting of plate glass plates cemented to metal frames which in turn are cemented to the outside of the tank, are placed opposite one another so that the glass plates are vertical and parallel; water or oil is poured into the parallelizing tanks so that the level of the liquid is the same on the two sides of the glass cylinder.

The inset in Figure 2 shows the non-adjustable spark gap which was used in the early experiments with water; this gap was attached to a rod passing through a stuffing box in the lower steel plate, C, and it is seen in the photograph of Figure 1. It was discarded because it offers too large an obstruction near the spark and because the gap was not adjustable.

The general layout of the apparatus is shown in Figure 3. In this diagram, A represents the bubble tank in plan (with the end plates, etc., omitted), E and F the electrodes forming the under-liquid spark gap and L the glass-fronted tanks for correcting the distortion due to the cylindrical form of the bubble tank. M represents the illuminating spark gap with electrodes set about 20/1000th inches apart; in experiments with water, the electrodes were made of magnesium, which gives an intense spark with most of the energy in the blue region of the spectrum, and blue-sensitive ("ordinary") photographic plates or films were used. In experiments with our oil, which transmits only the green and yellow regions of the spectrum, zinc electrodes were used in conjunction with fast orthochromatic plates or films.

The spark gap M is placed at the focus of a condenser lens, N, 6 inches diameter and 6 inches focal length. The light from the illuminating spark thus passes through the bubble tank as a parallel beam; after emerging from the vessel, it passes through a second lens P of high optical quality, which is set so as to bring the light to a focus on the centre of the camera objective, Q. The camera can be used either as a stationary plate camera, or, as shown in the diagram, as a revolving drum camera. The camera lens is adjusted so that the under-liquid spark gap is sharply focussed on the photographic plate or film.

Figure 3 also shows the timing pendulum and the electrical circuits used to produce the explosion and illuminating sparks. The pendulum, whose period is one second, consists of a steel rod fixed to a horizontal rod mounted between accurately machined centres; at its lower end, the pendulum carries an extension shaped as shown in the diagram. This extension swings above a number of brass screws with rounded upper ends, the gap between the screws and the pendulum being adjusted to 4/1000th inches; these screws are mounted on an arc of insulating material and they are spaced so that the pendulum takes 5 milliseconds to pass from any one screw to the next when the pendulum is released from the horizontal. The first screw, labelled 0 in the diagram, determines the discharge of the condenser C_e used to produce the under-liquid spark; the remaining screws, labelled 1, 2, 3,... in the diagram, determine the discharge of the condenser C_i (of which only four are shown and only one labelled) used to produce the sequence of illuminating sparks for photographing the bubble.

As the diagram shows, these condensers are connected in series with resistances across a large reservoir condenser C_r, charged through a valve rectifier to a potential difference of 4000 volts; the junctions of the condensers and the series resistances are each connected to an electrode screw.

When the pendulum swings over the screw 0, the gap between the screw and the pendulum is momentarily in series with the under-liquid spark gap; the two gaps break down and the condenser C_e discharges across them. Similarly, the first condenser C_1 discharges across the illuminating gap and the gap between the pendulum and the screw 1 when the pendulum moves over this screw, and so on. The 5 megohm resistances in series with C_e in effect isolate this condenser and prevent more than one spark under the liquid during the course of an experiment. The resistances R_i are such that the time-constants R_iC_i and R_iC_r are large enough to prevent the reservoir condenser C_r and the later C_i's from discharging completely during the early illuminating sparks and, at the same time, small enough to allow a certain amount of charge to flow into the condensers C_i from C_r.

7.....

7. *Experiments under vacuum.*

Though experiments under a vacuum do not represent any possible full-scale explosion in open water, they are of interest for two reasons:-

(1) with a given value of the non-dimensional parameter z'_0*, the effect of the free surface on the motion of the bubble is as small as it can be, so that comparison with the formulae of Report A is as justifiable as it can be;

(2) The instability of the free surface, which occurs when it is accelerated downwards under the action of external pressure, is absent.

Before the revolving drum camera had been constructed, a number of single photographs were taken of the bubbles produced by sparks in oil using a 0.4 μ F. condenser charged to 4000 volts. These photographs were timed to occur at times t = 5, 10, 15, 20 .... up to 120 milliseconds after the initiating spark. Figure 4 shows the bubble at t = 0.025 seconds. It will be seen that it is a very smooth and perfect sphere. It remains spherical during its expansion, but during its contraction its vertical dimension decreases more rapidly than its transverse diameter so that it becomes flattened. This flattening is more pronounced on the under side than the upper side. Figure 5 shows the bubble at t = 0.05 seconds. The flattening is here very apparent.

As the bubble decreases in diameter the flattening becomes more and more accentuated, till the underside becomes concave and the bubble assumes the shape of a mushroom. Figure 6 shows the bubble at t = 0.08 seconds. This is somewhere near the minimum size at the end of the first period of pulsation.

Figure 7 shows the radius, a, and the rise, $z_0 - z$, of the centre of the bubble at times up to 80 milliseconds after its formation. To compare these with calculations based on the assumption that the bubble remains spherical, it is necessary to assume a value for the energy, W, which the spark gives to the oil. It will be seen that, in Figure 7, if a smooth curve is drawn through the points representing the radius of the bubble its maximum value, a_{max}, will be about 3.7 cm., and since the total depth z_0 of the liquid from the level where the pressure is zero is 6.05 cm., $a_{max}/z_0 = 3.7/6.05 = 0.61$.

In Comrie's calculated curves in Report A for C = 0, i.e , with no gas inside the bubble, it will be found that $a_{max}/z_0 = 0.63$ for $z'_0 = 1.0$, 0.25 for $z'_0 = 2.0$, 0.14 for $z'_0 = 3.0$ and 0.098 for $z'_0 = 4.0$. It appears therefore that the bubbles represented in Figure 7 correspond very closely with the condition $z'_0 = 1.0$. When $z'_0 = 1.0$, the scale-length, L, is the same as the depth z_0 of the explosion below the level of zero pressure, so that L = 6.05 cm. This corresponds with energy $W = g\rho L^4 = 1.16 \times 10^6$ ergs. when $\rho = 0.875$ gm./cm.^{3}

The non-dimensional time scale t' in which the calculations are expressed is related to the true time scale t by the relation $t = t'\sqrt{(L/g)} = 0.0786\ t'$ seconds, when L = 6.05 cm. Multiplying the ordinates of Comrie's curve for $z'_0 = 1.0$ by 6.05, and the abscissae by 0.0786, the calculated relationships between a, $(z_0 - z)$ and t are found. These have been plotted in Figure 7. It will be seen that, until the top of the bubble is very near the free surface, its observed radius and rise are close to what was calculated theoretically.

8. *Experiments under surface pressure of 6.5 cm. of oil.*

The depth of the spark was 6.05 cm. so that experiments in which the surface pressure was that due to 6.5 cm. of oil are equivalent to explosions at a depth of $(33 \times 6.05)/6.5 = 30.8$ feet in open water.

In one .....

* $z'_0 = z_0/L$ where $z_0 = p/\rho g$, p is the pressure at the level of the explosion and L is the scale length defined by the equation (3) of Report A, namely $L = (W/g\rho)^{\frac{1}{4}}$

In one set of experiments under these conditions the drum camera was used and the bubbles were produced by discharging a 0.4 μ F. condenser charged to 4050 volts. Two films, due to two separate sparks, were taken and together they covered the period t = 0 to t = 120 milliseconds. The first film, covering the period t = 0 to t = 60 milliseconds, is shown in Figures 8a and 8b; the numbers to the left of each photograph are (1) the number (v. Figure 3) of the particular contact of the timing pendulum which is operative in the photograph; and (2) the value of t, calculated from the seperation of the photographs on the film. The dark band, lying on the right-hand side of the photographs, is due to one of the leads to the under-oil spark gap; the faulty reproduction of photograph No. 2 is due to the fact that it lies on the join of the two ends of the film on the camera drum. The second film covered the period t = 60 milliseconds to t = 120 milliseconds and photographs No. 17 to No. 22 are reproduced in Figure 8c. The values of t are not exactly spaced at intervals of 5 milliseconds owing to the fact that the timing pendulum was not always in exactly the same position relatively to the lower point of the gap when the spark went off. Some of the sparks were as much as 1 millisecond late and one of them was nearly 1.5 milliseconds late.

Owing to optical difficulties the field of view was not large enough to take in the bottom of the bubble in its early stages. The radius was, however, taken as half the horizontal diameter, and the rise of the centre above the spark gap was taken as (the height of the top of the bubble above the spark gap) minus (half the horizontal diameter). Figure 9 shows the radii (indicated by points surrounded by triangles) and the heights of rise (indicated by crosses) obtained in this way. The points are numbered 1, 2, ... on the same system as the photographs of Figure 8, and the points given by the second spark are distinguished from those given by the first by the letter 'a'. The points 12 and 12a do not coincide, showing that the energy of the spark was different in the two cases. It will be noticed that the two sets of points lie very well on smooth curves.*

The maximum radius of the bubble was 3.15 cm., and since $z_0 = 6.5 + 6.05 = 12.55$ cm., $a_{max}/z_0 = 0.25$. It has already been mentioned that this happens to be the value which corresponds with $z'_0 = 2.0$, so that $L = z_0/z'_0 = 12.55/2 = 6.27$ cm. The corresponding value of W is $W = 981 \times 0.875 \times 6.27^4 = 1.32 \times 10^6$ ergs. The factors by which Comrie's calculated values for $z'_0 = 2.0$ must be multiplied are given by the equations $a = 6.27\ a'$ and $t = 0.080\ t'$.

For $z'_0 = 2.0$, Comrie gives the first minimum contraction at $t' = 0.67$ which corresponds with 0.0535 seconds. This is considerably larger than the observed value shown in Figure 9, namely 0.045 seconds. The difference may largely be explained by taking account of the effect of the free surface. According to Herring, the period is reduced by the proximity of the free surface in the ratio $\left(1 - \frac{\bar{a}}{4h}\right) : 1$, where $\bar{a}$ is the mean value of a during the pulsation and h is the depth of the explosion below the free surface. Taking $\bar{a}$ as 2.7 cm. (v. Figure 9) h = 6.05 cm., the predicted period of the bubble is $0.0535\ (1 - 2.7/24.2) = 0.0475$ seconds, which is close to the observed period of 0.045 seconds.

9. *Comparison of rate of rise with theoretical estimate.*

The calculation of the rate of rise, neglecting the effect of the free surface, cannot usefully be compared with the observations because the critical point at which the minimum radius and consequent rapid rise occurs is, as has been seen, 0.009 seconds earlier than that predicted by the simple theory. To take account of the effect of the free surface, using the equations given in the Appendix, involves a great deal of laborious calculation. Two simpler methods can be used. One is to take Comrie's calculated values of $z'_0 - z'$ for observed values of a, rather than for the values of t'; another is to calculate $U = -dz/dt$ directly from the observed values of a and t, using equation (1) of Report A, and then finding z by integration. The values obtained by these methods are indistinguishable in the range shown in Figure 9. It will be seen that until the bubble begins to contract the observed rise is not very far from the calculated rise, but that the observed rate of rise becomes less than that calculated shortly after this. When the radius begins to contract rapidly at t = 0.035 seconds the bubble begins to rise rapidly, but the rate of rise is much less than that calculated on the theory which assumes that the bubble remains spherical. The probable reason for this seems to be that the bubble ceases to be even approximately spherical as it gets near its minumum radius. It flattens on the underside and even becomes hollow there before reaching the minimum, as Figures 5, 6 and photographs No. 7 to 10 of Figure 8b show.

The .....

* Comparing Figures 7 and 9 it will be seen that the scatter of the points in Figure 7 is a true measure of the variability of the energy of the bubbles produced by successive sparks.

The hollow which appears in photograph No. 9 of Figure 8b subsequently disappears as the bubble expands a second time but reappears on its second contraction. Photograph No. 19 of Figure 8c appears to have a flat undersurface but the fact that it is really only a thin hollow shell will be seen in No. 20, where the bubble is at its second minimum (see Figure 9) and the shell has contracted to vanishing thickness over a large part of its area.

The very rapid rise near the minimum radius, which is so characteristic a feature of the simple theory, depends on the fact that the virtual momentum of a spherical hollow is $\frac{2}{3}\pi\rho\, a^3 U = \frac{1}{2} U$ (mass of liquid displaced), so that a decrease in a corresponds with a rapid increase in U. If the bubble becomes flattened, the virtual inertia rapidly increases if it flattens without changing radius. The virtual inertia of an infinitely thin disk is actually rather greater than that of a sphere of the same diameter. Thus if the "radius" of the bubble is taken as $\frac{1}{2}$ (the horizontal diameter) instead of $\frac{1}{2}$ (horizontal diameter + vertical diameter), the measured curve will not reach such a low minimum and the calculated vertical velocity will be reduced. Figure 9 shows both methods of estimating a near the minimum; the points calculated by the former method are surrounded with a triangle, and by the latter with a circle.

Even making this assumption as to a, the theoretical calculation predicts a larger rise of the bubble than is observed in this experiment. Some, but not all, of this can be accounted for as being due to the effect of the free surface. It seems probable that a wake is formed behind the bubble shortly after it begins to contract and that this greatly decreases the vertical velocity, so that at the time the contraction of radius becomes very rapid the bubble has far less virtual inertia in a form in which it can be concentrated by the contraction than it has according to theory. It may be that the effect is accentuated by the high viscosity of the oil used in these experiments. Further light is thrown on this by experiments made with a smaller bubble.

10. *Experiments with a smaller bubble.*

Another set of measurements was made with the pressure at the surface equivalent to 6.5 cm. of oil and the spark at 6.05 cm. below the surface, but with a spark of smaller energy, namely that given by the discharge of a 0.2 μ F. condenser charged to a potential difference of 4000 volts. The stationary plate camera was used, giving a set of single photographs of the bubbles produced by the different sparks. The results are shown in Figure 10. It will be seen that $a_{max} = 2.1$ cm., so that $a_{max}/z_0 = 2.1/(6.5 + 6.05) = 0.167$. This lies between the value 0.14 for $z'_0 = 3.0$ and 0.25 for $z'_0 = 2.0$. By interpolation the value of z'_0 corresponding with $a_{max}/z_0 = 0.167$ is $z'_0 = 2.8$. For this value of z'_0 interpolation from Comrie's curves gives $a_{max}/L = 0.44$ so that $L = 2.1/0.44 = 4.76$ cm. For this value of L the time scale is given by $t/t' = \sqrt{(4.76/981)} = 0.070$. The duration of the first period of oscillation for $z'_0 = 2.8$ is given by interpolation as $t' = 0.51$, so that $t = 0.51 \times 0.070 = 0.035$ seconds. This is larger than what is observed, namely about 0.030 seconds. The effect of the surface, however, is to decrease the period in the ratio $\left(1 - \frac{\bar{a}}{4h}\right)$: 1 and taking $\bar{a} = 1.9$ cm. this ratio is 0.92, so that the calculated period would be 0.0325 seconds. No better agreement with observation could have been expected in view of the fact that each point in this series refers to a different bubble.

Referring to Figure 10 it will be seen that, after the bubble has ceased to rise at the rate calculated on the assumption that it remains spherical while pulsating, the rate of rise fluctuates with the pulsations but attains roughly constant mean velocity of about 80 cm./sec. If the resistance of the bubble is expressed in the form $R = k\pi a^2 (\frac{1}{2}\rho U^2)$ where k is a drag co-efficient, R is equal to the buoyancy, so that $\frac{4}{3}\pi a^3\rho g = k\pi a^2 (\frac{1}{2}\rho U^2)$ or $k = 8ag/3U^2$, and since the mean radius during the period while the bubble is rising approximately uniformly is 1 cm., $k = (8 \times 1 \times 981) \div (3 \times 80^2) = 0.41$. This is of the order of magnitude that might be expected. The drag co-efficient of a solid sphere at the same value of Reynold's number is 0.56.

It is worth noticing that the drag co-efficient of a spherical bubble, for the small values of Reynold's numbers in the region where Stokes' Law holds, is two-thirds the drag co-efficient of a solid sphere of the same radius. If this relationship holds at the larger value of Reynold's number appropriate to our rising bubble, the drag co-efficient would be 0.374.

11.....

11. *The stability of the surface of the bubble near the position of minimum contraction.*

When the bubble contains gas the radius contracts at increasing rate until the volume decreases sufficiently to raise the internal pressure above the undisturbed hydrostatic pressure at the level of the centre. The radial velocity then decreases and reverses sign at the minimum radius. The curvature of the (a, t) curve is concave towards the axis of t during the greater part of the first oscillation so that the acceleration of the surface is directed from the liquid inwards towards the gas. During this part of the pulsation small disturbances of the surface should be stable. When the pressure of the gas rises the radial velocity decreases and the (a, t) curve becomes convex to the t axis, the surface being accelerated outwards from the gas towards the liquid. Under this condition the surface may be expected to be unstable in the same way that a horizontal liquid surface is unstable when the liquid is above and the air below, so that gravity acts from the liquid toward the air.

These conclusions are borne out by the photographs of a bubble taken near its minimum radius. For example, in the photographs shown in Figure 8b, it will be seen that up to photograph No. 8 the surface of the bubble is very smooth, indicating stability of small disturbances, and Figure 9 shows that when photograph No. 8 was taken, the surface had not begun to accelerate outwards. The part of the (a, t) curve of Figure 9 which is convex downwards occurs just before photograph No. 9 was taken, so that instability might be expected to show itself in the photograph. It will be seen that in photograph No. 9 the surface has in fact become ragged owing to the instability.

It will be noticed in photographs Nos. 9, 10, 11 and 12 of Figure 8b that the instability which has appeared in No. 9 seems to disappear very rapidly on the lower part of the bubble but continues and increases at the top.

12. *The appearance of the free surface.*

In the photographs of Figures 8a, b and c, the free surface appears rather out of focus above the bubble; in photographs Nos. 1 to 12, the free surface has moved very little, but in Nos. 17 to 22, it has risen to a considerable height.

13. *Appendix. The effect of a free or rigid surface on the motion of a spherical bubble.*

In order to compare the results of these experiments with calculation of the observed rate of rise and pulsations of the bubble, it became necessary to extend the calculations of Report A so as to include terms representing the effect of the free surface. The condition which enables the rise of the bubble under gravity in one pulsation to be comparable with its maximum diameter necessarily involves a free surface effect which is comparable with the gravity effect.

Herring gave a formula for the effect of a distant free or rigid surface on the position of the centre of a bubble. If U is the velocity towards the surface his formula is

$$\frac{1}{a^2}\frac{d}{dt}\left(a^3\frac{dR_2^{\omega}}{dt}\right) = \mp\frac{3}{4}\frac{d}{dt}\left(a^3\frac{da}{dt}\right) \qquad (A.1)$$

where

a = the radius of the bubble at time t,

h = the depth of the explosion,

$U = \frac{1}{h^2}\frac{dR_2^{\omega}}{dt}$ and R_2^{ω} is defined in Herring's paper,

and the upper sign refers to a rigid surface while the lower refers to a free surface. Since only terms of order $1/h^2$ are retained it seems that equation (A.1) may be written

$$\frac{d}{dt}(a^3 U) = \mp\frac{3a^2}{4h^2}\frac{d}{dt}\left(a^3\frac{da}{dt}\right) \qquad (A.2)$$

The .....

The formula (A.1) was given by Herring as applicable only to cases when U is small compared with da/dt but it applies equally well when U is comparable with da/dt provided it is assumed that the bubble is constrained to remain spherical and terms containing powers of 1/h higher than $1/h^2$ are neglected. With these assumptions the velocity potential of the flow is

$$\phi = \frac{a^2\dot{a}}{r} + \frac{Ua^3\cos\theta}{2r^2} \pm \left\{\frac{a^2\dot{a}}{r'} + \frac{Ua^3\cos\theta'}{2r'^2} + \frac{a^2\dot{a}}{4h^2}\left(\frac{a^2\cos\theta}{2r^2}\right)\right\} \qquad (A.3)$$

where r' and θ' are the co-ordinates of any point referred to the image centre as origin and the line joining the centre of the sphere with its image as $\theta' = 0$. The upper sign refers to a rigid plane and the lower to a free surface.

Near the sphere ϕ may be written

$$\phi = \frac{a^2\dot{a}}{r} + \frac{Ua^3\cos\theta}{2r^2} \pm \left\{\frac{a^2\dot{a}}{2h} + \frac{a^2\dot{a}r\cos\theta}{4h^2} + \frac{Ua^3}{8h^2} + \frac{a^5\dot{a}\cos\theta}{8h^2r^2}\right\} \qquad (A.4)$$

The kinetic energy T of the whole motion is one-half the kinetic energy of the flow surrounding the sphere and its image so that $\frac{2T}{\rho} = -\iint\phi\left(\frac{\partial\phi}{\partial r}\right)dS$, the integral being taken over the sphere only.

Substituting ϕ and $\partial\phi/\partial r$ from equation (A.4)

$$\frac{T}{\rho} = 2\pi a^3\dot{a}^2\left(1 \pm \frac{a}{2h}\right) + \frac{\pi a^3U^3}{3} \pm \frac{\pi a^3\dot{a}U}{2}\left(\frac{a^2}{h^2}\right) \qquad (A.5)$$

The energy equation is therefore

$$\frac{4}{3}\pi\rho a^3 gz + 2\pi\rho a^3\dot{a}^2\left(1 \pm \frac{a}{2h}\right) + \frac{\pi}{3}\rho a^3U^2 \pm \frac{\pi\rho a^3}{2}\cdot\frac{a^2}{h^2}\dot{a}U = W - G(a) \qquad (A.6)$$

where W and G(a) have the same meaning as in Section 2 above.

The condition that no resultant external force acts on the sphere implies that the co-efficient of $\cos\theta$ in the expression for the pressure at the surface of the sphere shall vanish.

$$\frac{p}{\rho} = \left[\frac{d\phi}{dt}\right]_{\text{fixed point}} - \tfrac{1}{2}q^2 + gz - gr\cos\theta \qquad (A.7)$$

where z is the depth of the centre below the level where the pressure is zero. Also if $\partial\phi/\partial t$ represents the rate of variation of ϕ at a point which moves vertically at the same velocity as the centre of the sphere

$$\left[\frac{d\phi}{dt}\right]_{\text{fixed point}} = \frac{\partial\phi}{\partial t} - U\left\{\frac{\partial\phi}{\partial r}\cos\theta - \frac{1}{r}\sin\theta\frac{\partial\phi}{\partial\theta}\right\} \qquad (A.8)$$

Substituting from equation (A.3) in equations (A.8 and 7) the term containing $\cos\theta$ in p/ρ is found to be

$$\left\{\frac{1}{2}a\dot{U} + \frac{3}{2}\dot{a}U - ga \pm \frac{1}{4h^2}\left(\frac{3}{2}a^3\ddot{a} + \frac{9}{2}a^2\dot{a}^2\right)\right\}\cos\theta$$

Multiplying this by $2a^2$ and equating to zero it is found that

$$\frac{1}{dt}(a^3U) - 2ga^3 \pm \frac{3a^2}{4h^2}\frac{d}{dt}\left(a^2\frac{da}{dt}\right) = 0 \qquad (A.9)$$

This .....

This is identical with Herring's equation (2) except that a term has been added to allow for the effect of gravity. Equations (A.6) and (A.9) together with the equation

$$U = -\frac{dz}{dt} \tag{A.10}$$

may be used as in Report A to find the motion of the bubble using step-by-step methods of numerical integration. For this purpose it is convenient to transform equations (A.6) and (A.9) into non-dimensional forms by substituting

$$L = \left(\frac{W}{g\rho}\right)^{\frac{1}{3}}; \quad z = Lz'; \quad a = La'; \quad t = \sqrt{\frac{L}{g}}\, t'$$

Equation (A.6) then assumes the form

$$\left[1 \pm \frac{a}{2(z' - h'_0)}\right]\left(\frac{da'}{dt'}\right)^2 \pm \frac{a'^2}{4(z' - h'_0)^2}\left(\frac{da'}{dt'}\right) U' - \frac{1}{2\pi a'^3}\left\{1 - \frac{G(a)}{W}\right\} + \frac{U'^2}{6} + \frac{2z'}{3} = 0 \tag{A.11}$$

where $U' = dz'/dt'$, $h'_0 = Lh_0$ and h_0 is the value of z at the liquid surface, so that the depth of the explosion below the surface is $z_0 - h_0 = L(z'_0 - h'_0)$. Equation (A.9) assumes the form

$$\frac{d}{dt'}(a'^3 U') = 2a'^3 \mp \frac{3a'^2}{4(z' - h'_0)^2}\frac{d}{dt'}\left(a'^3 \frac{da'}{dt'}\right) \tag{A.12}$$

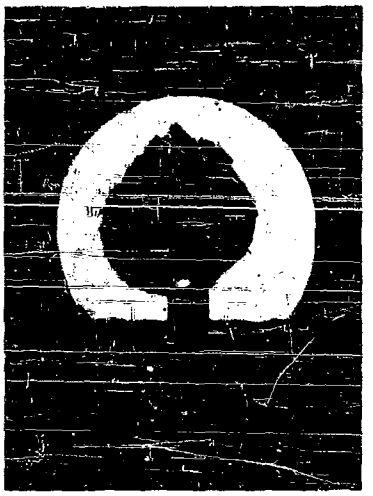

FIG. 1.

Two photographs of the same bubble in water under low surface pressure.

(1) at an early stage, when it is smooth and spherical;
(2) at a later stage, when the bubble has become pitted by boiling near the surface.

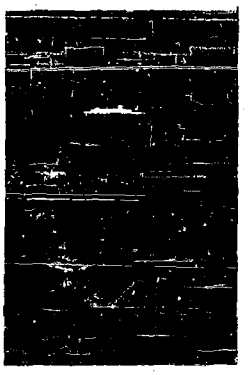

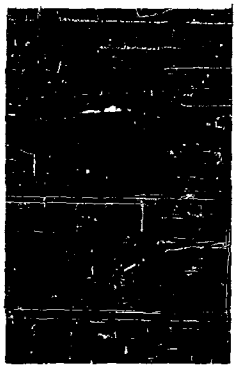

FIG. 4. FIG. 5. FIG. 6.

Photographs of bubbles in oil under vacuum, showing how the bubble becomes distorted as its age increases.

Fig. 4. Spherical bubble, age 25 millisec.

Fig. 5. Bubble with pronounced flattening on underside, age 50 millisec.

Fig. 6. Mushroom-shaped bubble, age 80 millisec.

FIG. 2. THE BUBBLE TANK.

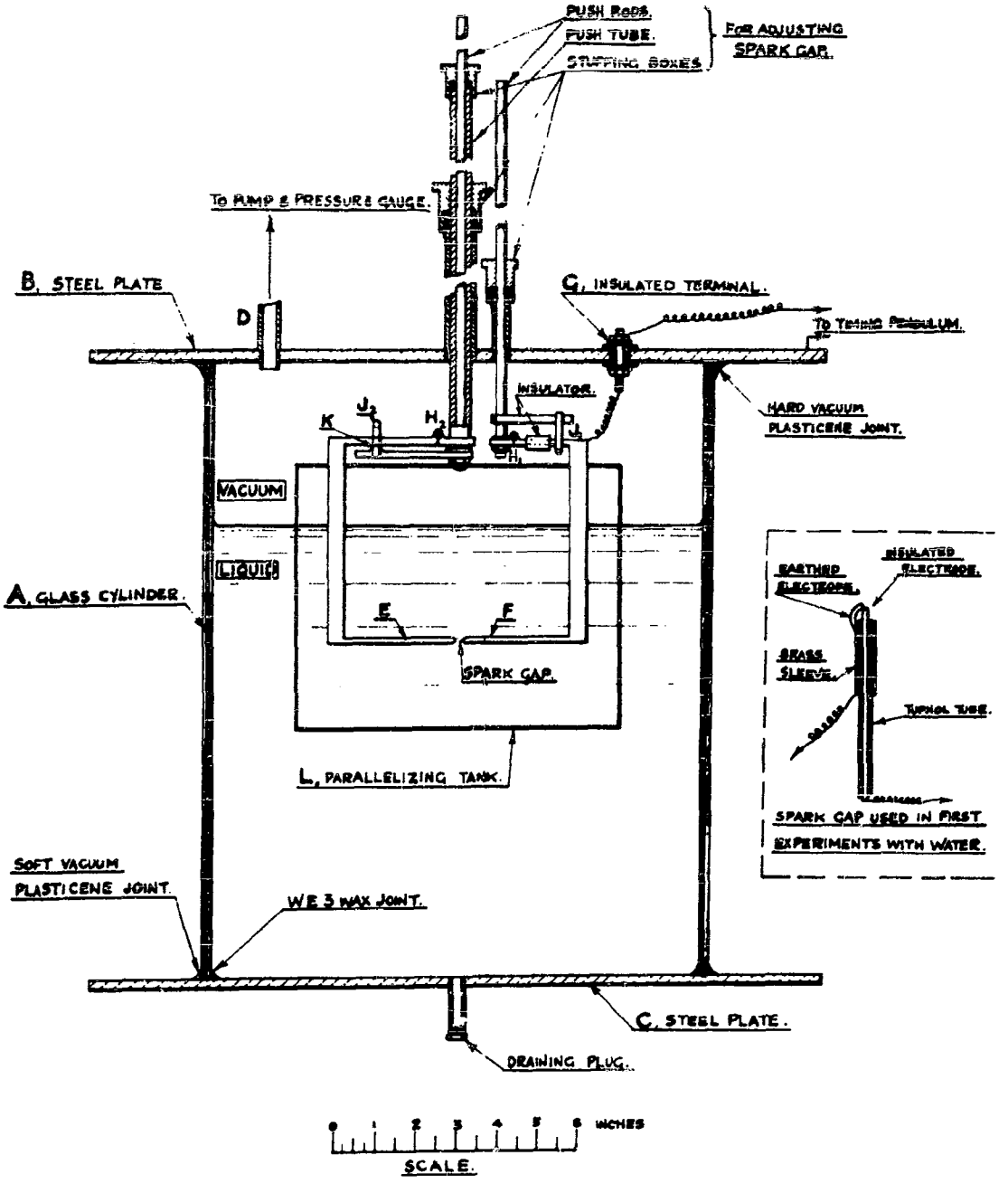

FIG. 3. SCHEMATIC DIAGRAM OF APPARATUS AND ELECTRICAL CONNECTIONS.

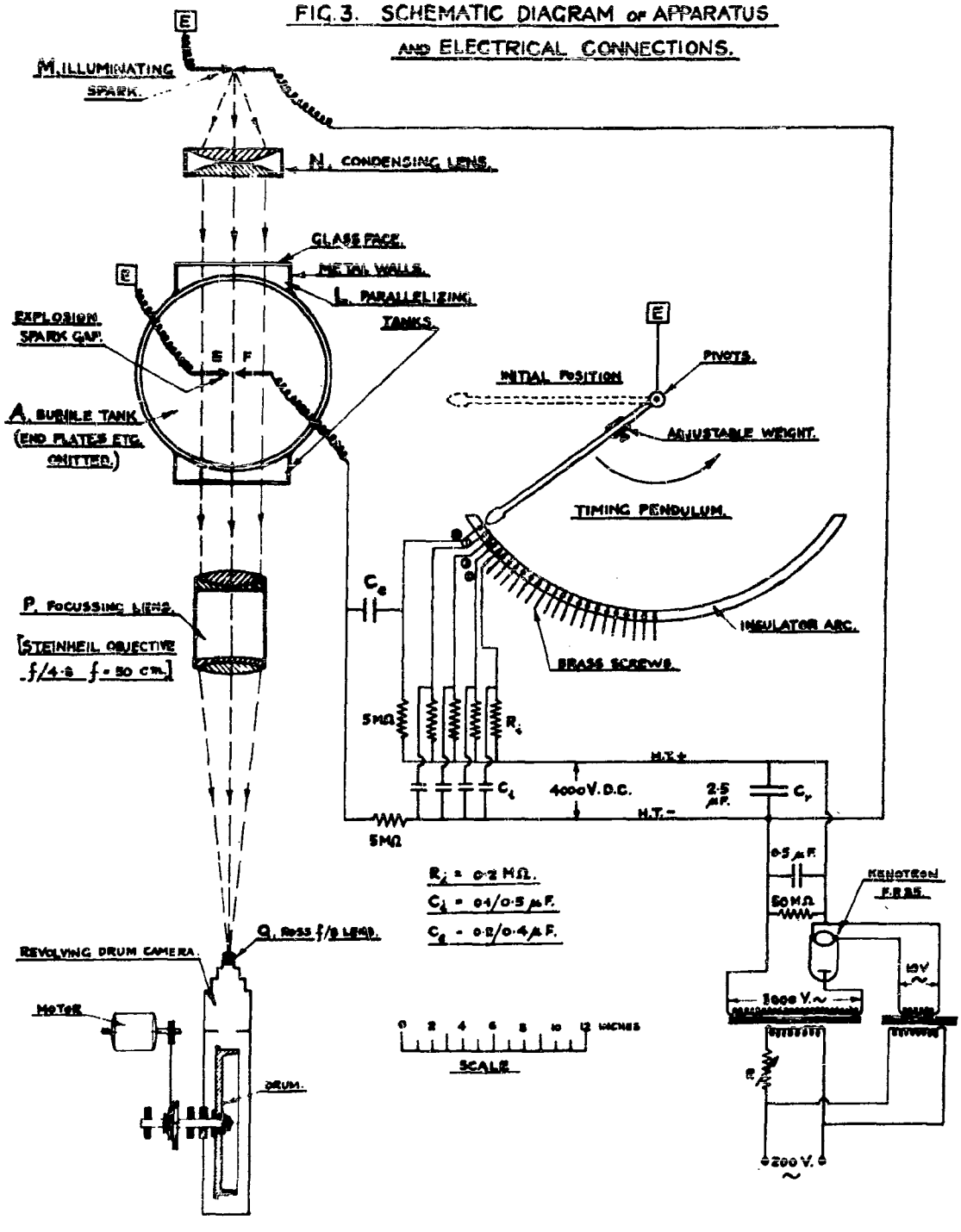

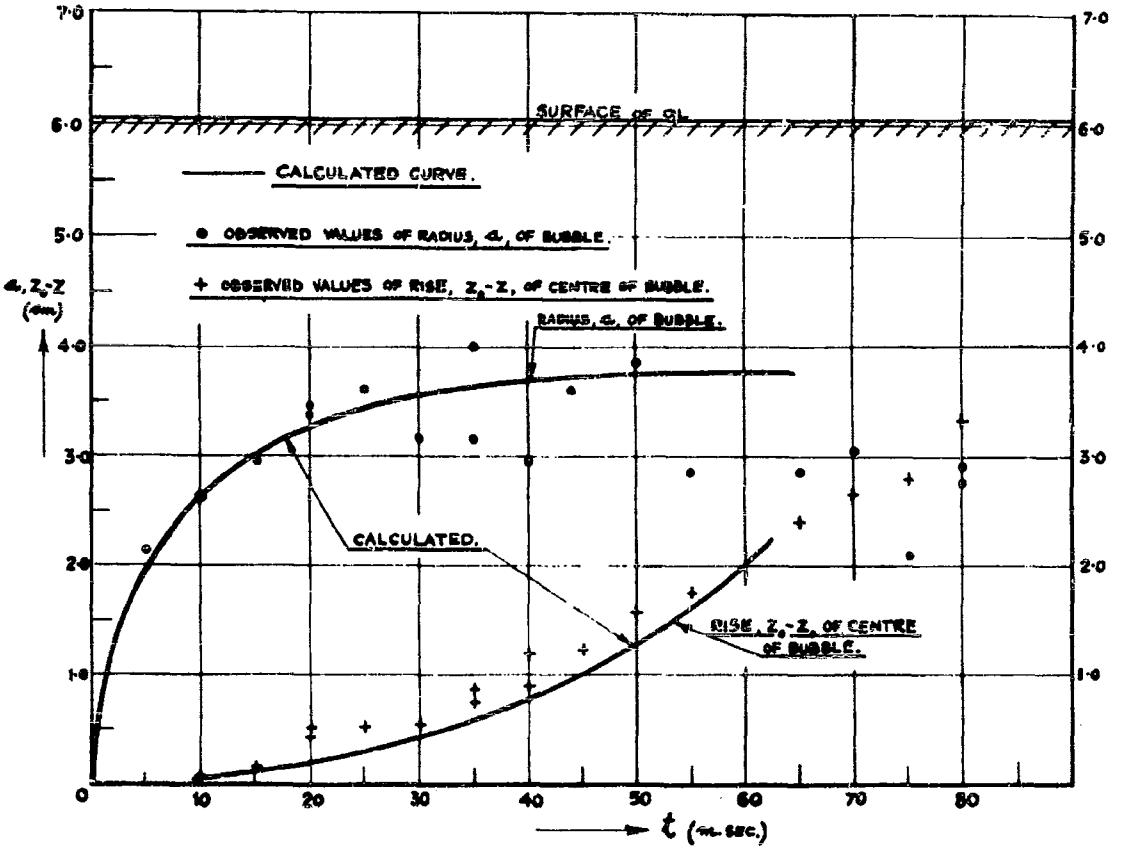

SURFACE PRESSURE = 0. DEPTH OF SPARK = 6·05 cm.

$W = 1{\cdot}15 \times 10^6$ ERGS; $Z_0' = 1$; $L = 6{\cdot}05$ cm.

OBSERVED AND CALCULATED RELATIONSHIPS FOR BUBBLE IN OIL.

FIG. 7.

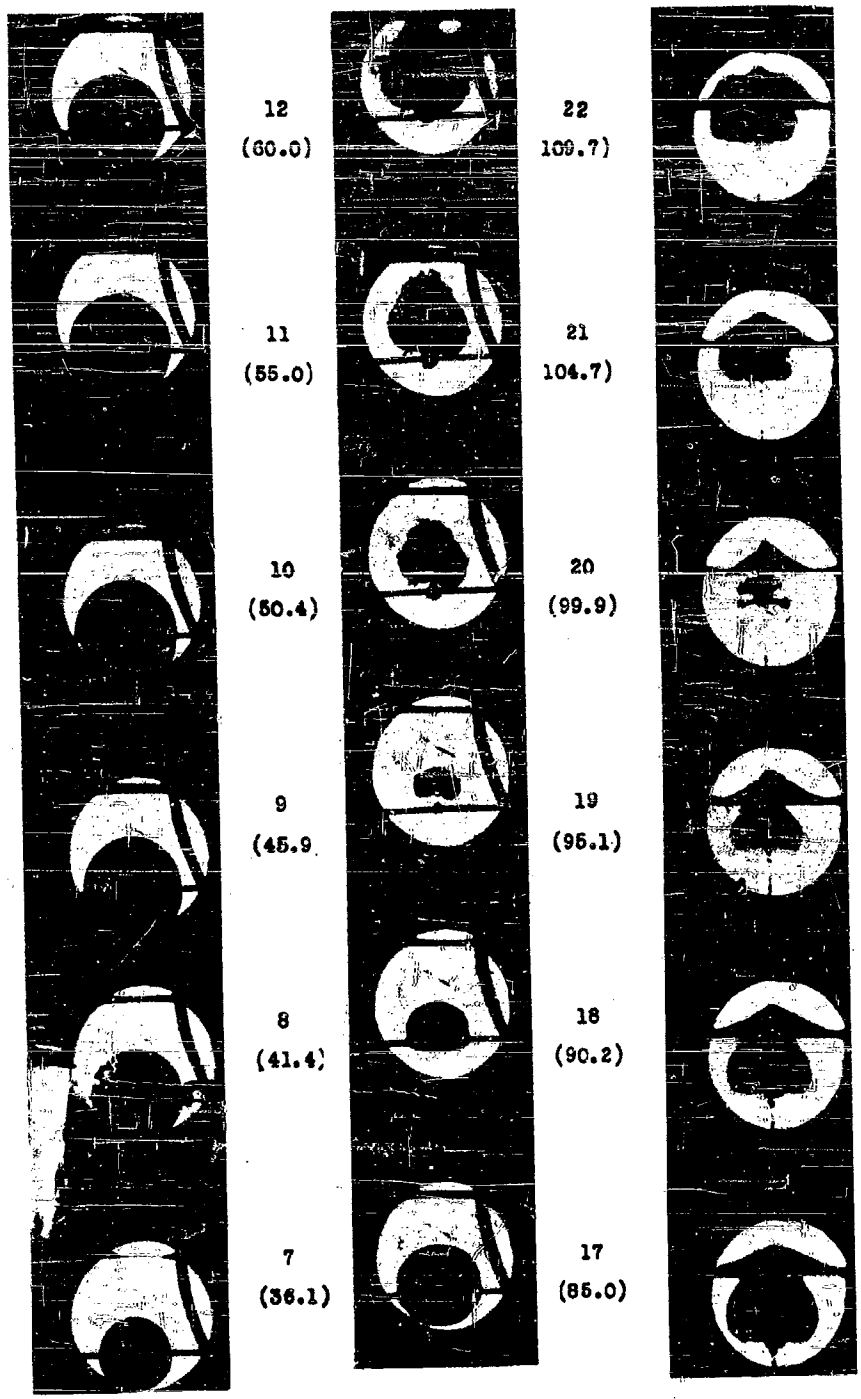

Figs. 8a. 8b. 8c.

Photographs of bubble in oil taken with a revolving drum camera.

Upper number - identification number of photograph.
Lower number (in brackets) - age of bubble (in milliseconds).

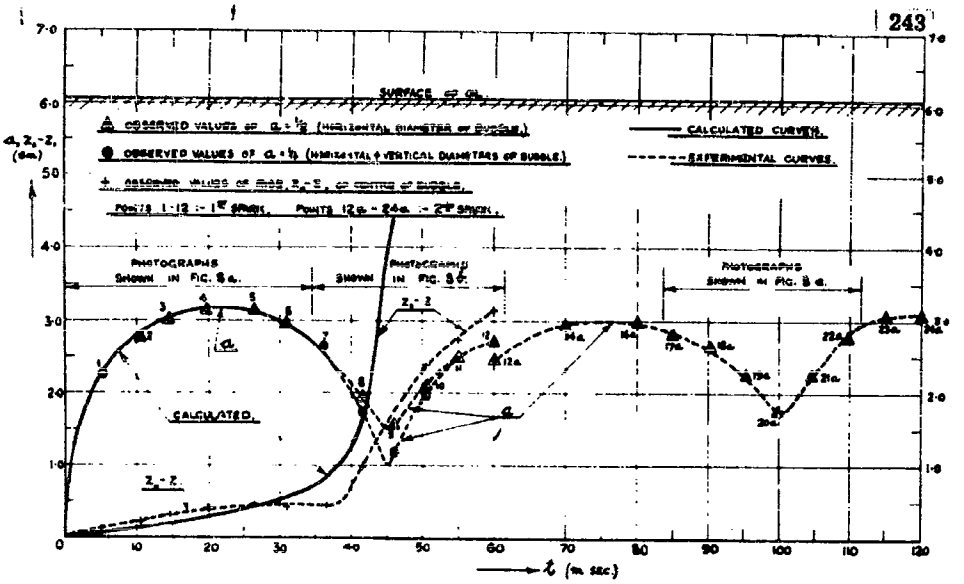

SURFACE PRESSURE = 6·5 cm. of oil. DEPTH OF SPARK = 6·06 cm.

W = 1·32 × 10^6 ERGS; Z'_0 = 2; L = 6·27 cm.

OBSERVED & CALCULATED RELATIONSHIPS FOR BUBBLE IN OIL.

FIG. 9.

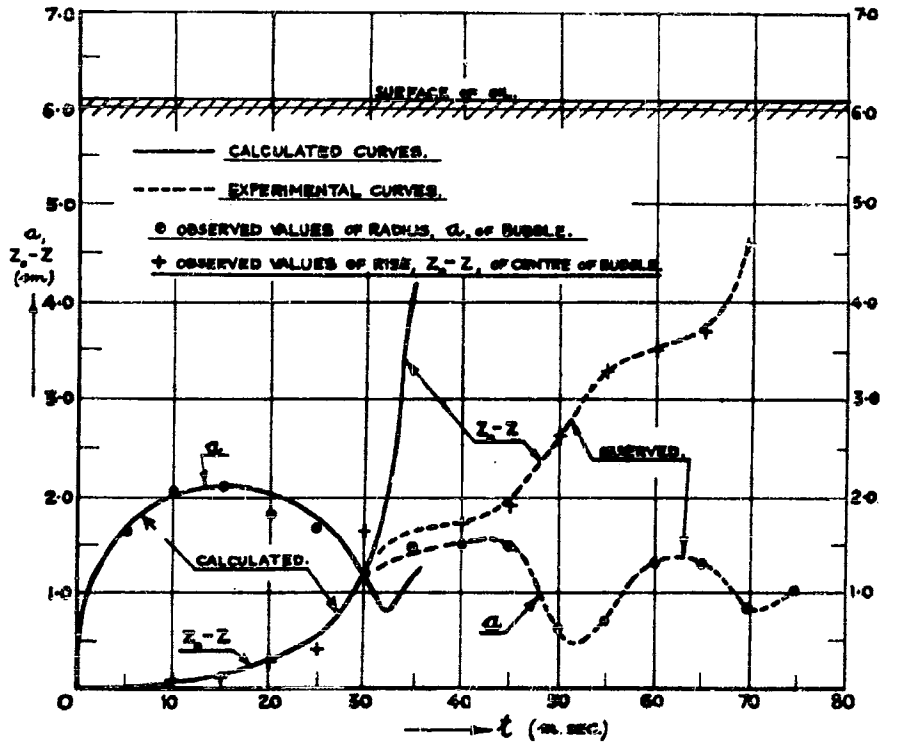

SURFACE PRESSURE = 6·5 cm. of oil. DEPTH OF SPARK = 6·05 cm.

W = 0·44 × 10^6 ERGS; Z'_0 = 2·8; L = 4·76 cm.

OBSERVED & CALCULATED RELATIONSHIPS FOR BUBBLE IN OIL.

FIG. 10.

STUDIES ON THE GAS BUBBLE RESULTING FROM UNDERWATER EXPLOSIONS

ON THE BEST LOCATION OF A MINE NEAR THE SEA BED

M. Shiffman and B. Friedman
Institute for Mathematics and Mechanics
New York University

American Contribution

May 1944

TABLE OF CONTENTS

		Page
Introduction		1
Part I. Discussion of the Results.		
1.	Preliminary remarks	6
2.	The principle of stabilization	7
3.	The location of the mine	8
4.	An example	10
Part II. Mathematical Study of the Secondary Pressure Pulse.		
1.	Introduction	11
2.	The energy equation	12
3.	Non-dimensional variables	14
4.	The scaling factors and the internal energy of the gas for T.N.T.	15
5.	The equations of motion for small values of the radius a	17
6.	The minimum radius	18
7.	The pressure pulse	19
8.	The optimum peak pressure	22
9.	The impulse	23
Part III. The Mechanism of Stabilization by Gravity and the Sea Bed.		
1.	The exact equations of motion	26
2.	The approximate evaluation of the period and the momentum	29
3.	The stabilized position	32
4.	The migration of the bubble	34
5.	The correction due to the free surface	35
Appendix I.		
The Numerical Integration of the Differential Equations.		38

Page

Appendix II.

The Velocity Potential for a Pulsating Sphere Moving Perpendicularly to a Wall.

1. Statement of the problem 41
2. Some theorems on images 42
3. The construction of Φ_0 44
4. The construction of Φ_1 49
5. The kinetic energy of the water 51
6. Approximate theory for a sphere pulsating between a rigid wall and a free surface 54

Appendix III.

Numerical Evaluation of Some Definite Integrals. 57

TABLE OF GRAPHS

Figure 1. Scaling factor L 61
Figure 2. Distance from bottom to produce maximum pressure 63
Figure 3. Pressure factor for mine of 1500 lbs. of T.N.T. in water 150 ft. deep 65
Figure 4. Pressure factor at sea level for mine of 1500 lbs. of T. N. T. in water 150 ft. deep 67
Figure 5. Dependence of internal energy ($\bar{u}$) on momentum ($\bar{s}$) 69
Figure 6. Dependence of pressure factor (q) on momentum ($\bar{u}$) 71
Figure 7. The displacement of the bubble 73
Figure 8. Radius of bubble; case 7 75
Figure 9. Position of bubble; case 1 77
Figure 10. Position of bubble; case 3 79
Figure 11. Position of bubble; case 4 81

Summary of Formulas 83

Bibliography 85

Studies on the Gas Bubble Resulting From Underwater Explosions

ON THE BEST LOCATION OF A MINE NEAR THE SEA BED

At the request of the David Taylor Model Basin of the Bureau of Ships and of Division Re 2 of the Bureau of Ordnance, a series of investigations has been undertaken by the New York University Group of the Applied Mathematics Panel of the N.D.R.C. with the object of analyzing the phenomena associated with the gas bubble produced by an underwater explosion.

The present study, carried out by Dr. Max Shiffman and Dr. Bernard Friedman, with the cooperation of the Mathematical Tables Project in the extensive numerical work, is concerned with the following problem: If a mine of given weight of explosive is to be placed near the sea bed, what position should it have to cause maximum damage to a target at the surface?

It seems appropriate to make a few introductory remarks about the broader research program of which this report is a part. Often the destructive effect of an underwater explosion is not wholly due to the high pressure shock of the explosion. After the initial shock wave has passed with enormous speed, a comparatively slow pulsation of the gas bubble (consisting of the burned gases) takes place. In the second and sometimes even third pulse of this motion of the bubble, a pressure pulse of considerable strength is emitted. While the peak of the shock pressure from the explosion is far above that of the later pulses (in typical cases, six to ten times the pressure of the second pulse), the duration of these later pulses is much longer (about twenty times as

long); so that the momentum imparted and the destruction caused may be comparable to that of the first shock. The importance of the second pulse has been confirmed more and more not only by model experiments, but also by analysis of actual damage to allied ships by mines [1], [2].*

Just as significant as the long duration of the second pressure pulse, is the migration of the gas bubble during the pulsation. The migration can increase the effect of the second pressure pulse because, under suitable conditions, the center of this pulse might be much closer to the target than the explosion. Factors influencing the motion of the bubble are: rigid walls such as the hull of a ship or the sea bed, which attract the bubble; the free surface of the water, which has a repulsive effect; and the buoyant force of gravity, which causes the bubble to rise towards the surface.

Understanding and controlling the complicated interplay of these effects is of sufficient practical importance to warrant comprehensive research. Unfortunately, a great variety of experiments with full size charges is hardly feasible, and experiments with small charges cannot easily be reinterpreted for large charges. Such difficulties call for theoretical investigation as a guide to experiment.

Historically, the earliest theoretical problem, satisfactorily analyzed in older studies, is that of a single spherical gas bubble immersed in an infinite body of water; in particular, the pressure as a function of time and distance, and the period of pulsation of the bubble can be explicitly determined.

For the past few years an extensive research program on underwater explosions has been pursued by G. I. Taylor

---

* Bracket references refer to the bibliography.

and his associates in England. In this country, theoretical work was started by C. Herring (Division 6, N.D.R.C.) and is being carried on at the David Taylor Model Basin (in particular by Captain W. P. Roop, E. H. Kennard, G. E. Hudson) and by the N.Y.U.Group of the A.M.P. at the request of the Model Basin and of the Bureau of Ordnance; considerable experimental research is being done at the Underwater Sound Laboratory of Division 8, N.D.R.C.

Taylor [3] and others have determined the upward motion of the bubble under the buoyant force of gravity, a motion taking place in jerks. Herring [4] and others have studied the manner in which rigid walls attract the bubble, assuming that the bubble is rather far from the wall. Shiffman [5] has developed an improved method which permits numerical analysis of the motion when the bubble is close to the wall, and even when it touches the wall. The influence of non-rigid walls and the repulsive effect of the free surface of the water on the bubble have also been studied. Much of the material is condensed and supplemented in the comprehensive work by Kennard[6].

A very important aspect of the problem is concerned with plastic-elastic deformations of the target in interaction with the motion of the water. The process of damage can be understood only by a careful analysis of this interaction. Extended research by J. G. Kirkwood [7] has established that the damage to a structure depends on the ratio of the duration time of the incoming pressure pulse to the "time constant" of the structure, i.e., the span of time during which the structure is "receptive" to the impinging pressure effects. If this ratio is small, the impulse is the more important factor for damage, while if it is large, the peak pressure is more important.

Another problem that should be mentioned is that of

the change in the shape of the gas bubble. The migrating gas bubble does not retain its spherical shape, but flattens out in a plane perpendicular to the direction of the motion. The result is a deceleration of the bubble and, as a consequence, an intensification of the pressure pulse. Preliminary studies of this effect have been carried out independently in England and at N.Y.U. by Dr. Shiffman [8].

Finally, the still unsolved problems presented by the striking phenomena occurring at the water surface must be mentioned. A proper interpretation of the "domes" and "plumes" rising into the air above the explosion should yield much information concerning the process taking place under water.

The effect of gravity in moving the bubble closer to the target is not the only factor which leads to increased damage by the second pulse. Another element of major importance, emphasized by Shiffman and Friedman, is that the peak pressure of the second pulse depends greatly on the state of motion of the bubble at the moment of the first contraction. It is shown that the peak pressure of the second pulse possesses a decided maximum if the gas bubble is stationary at the moment of contraction. For depths of water and weights of explosives actually used, it is indeed possible to keep the bubble stationary by counterbalancing the gravitational force with the attractive force of the sea bed and the repulsive force of the water surface.

This principle of stabilization forms the main point of the following report. It is assumed that the mine is to be placed fairly close to the sea bed, but not necessarily directly on it, and it is then found (roughly stated) that for mines of about 500 to 2000 lbs. of explosive in water about 70 to 150 ft. deep, the optimal position is about one

maximum bubble radius above the sea bed; this means that the mines should be moored approximately 20 ft. above the sea bed. More precisely, for water of given depth and for a mine of given weight of explosive, there is a definite optimum location for the detonation, that location being given by the principle of stabilization.

Of course, such a statement makes sense only if, at the outset, the position of the mine is restricted to a place deep under water, i.e., fairly distant from the target.

Similar problems concerning the optimal position of an explosion also occur for charges nearer the surface, and for charges dropped from fast flying planes and thus having an initial horizontal and vertical momentum at the instant of the detonation. The discussion of such questions is planned for later reports.

Richard Courant
Contractor's Technical Representative

Part 1. Discussion of the Results

1. Preliminary Remarks.

The present report is concerned with the following problem: what is the best location of a mine near the bottom of the sea so that during the secondary pulse the peak pressure is a maximum? The result obtained is: for weights of 500 to 2000 lbs. of T.N.T., in water of depth 100 to 150 ft., the mine should be placed about 20 ft. above the sea bed. More exact locations are contained in table 1, p. 9.

It is significant to compare different mine positions as to their effects on the secondary pulse. This report demonstrates that, during the secondary pulse, the highest possible peak pressure at the surface is obtained when the mine is placed in a definite "best" position. The theory indicates that if the mine is placed even a few feet away from its best location, the peak pressure might be as little as one-half of that corresponding to the "best" location.* Furthermore, when the mine is placed directly on the sea bed, experimental evidence is available showing that the secondary pulse is weak and erratic.[9]

Another point of interest is that the "best" position also increases the effectiveness of the shock wave compared with a location on the sea bed itself. In the latter case, some experiments indicate that the presence of the sea bed has no effect on the shock wave, and others, that it results in an increase of about 12 percent in the peak pressure and

---

* See the example discussed in section 4 below.

impulse.* On the other hand, when a mine is at the "best" location (about 20 ft. above the sea bed for a depth, say, of 100 ft.), then the shock wave peak pressure at the surface is increased about 25 percent over that of the sea bed position since the pressure at the surface is inversely proportional to the distance from the explosion.

2. The principle of stabilization.

The best location of the mine is determined by the following Principle of Stabilization: For a given mass of explosive, the maximum peak pressure in the secondary pulse is obtained if the gas bubble produced by the explosion is kept motionless at the time of its minimum size. This stabilization can be attained for mines by suitably balancing the upward buoyant force on the bubble against the downward attractive force due to the sea bed. In other cases, the repulsive force of the surface, as well as additional factors, could be utilized.

In part II, a mathematical demonstration of the principle of stabilization is given. The following plausible argument also points to the same result. In general, the total energy of the bubble and water is divided into two parts, namely, the kinetic energy of the water surrounding the bubble, and the internal energy of the gas inside the bubble. If the bubble is moving at the time of its minimum size, then some of the total energy is diverted into kinetic energy of the water and thus less is available for the internal energy

---

* [9] reports no change in the shock wave for a mud bottom. Experiments in Woods Hole for a sand bottom show an increase of 12 percent, according to an oral discussion. Theoretically, if the sea bed were perfectly rigid, the peak pressure would be multiplied by the factor $\sqrt[3]{2}$, which means an increase of 26 percent. Actually, however, the explosion tears a hole in the sea bed and also transmits a shock into it.

of the gas. This would reduce the pressure inside the gas and also the pressure in the water. To obtain the optimum pressure, therefore, this bubble must be motionless at the time of its minimum size.*

For an appraisal of the value of stabilization, the damage due to the secondary pulse must be studied. All theories of damage show that for a pressure pulse which lasts long relative to the time constant of the structure to be damaged, the damage is approximately proportional to the peak pressure and not to the impulse or energy. Since the duration of the secondary pulse is approximately twenty times that of the shock wave, it would seem that maximizing the peak pressure of the secondary pulse increases the damage.

3. The location of the mine.

Let W be the weight of the explosive in pounds, (the numerical values refer to T.N.T. for which the characteristic constants were available to the authors), D the distance in feet from the bottom of the sea to a point 33 feet above sea level (allowing for the pressure of the atmosphere), and B_o the distance in feet from the center of the mine to the sea bed. The problem is to determine the best value for B_o if W and D are given. This is more easily expressed in terms of the non-dimensional quantities which are used in part II. For the unit of length select

$$L = 13.2\left(\frac{W}{D}\right)^{1/3} \text{ ft.}, \tag{1.1}$$

which represents (approximately) the maximum radius of the

* This argument is not completely rigorous since contributions to the pressure in the water occur from the motion of the water as well as from the gas pressure inside the bubble. The fact that the gas pressure is the more important contribution arises from the mathematical analysis of the interplay of the two effects.

gas bubble at the first expansion. Set

$$(1.2) \qquad d = \frac{D}{L}\ ,\ b_o = \frac{B_c}{L}\ ,$$

so that d and b_o represent the distance D and B_o measured in "bubble radii".

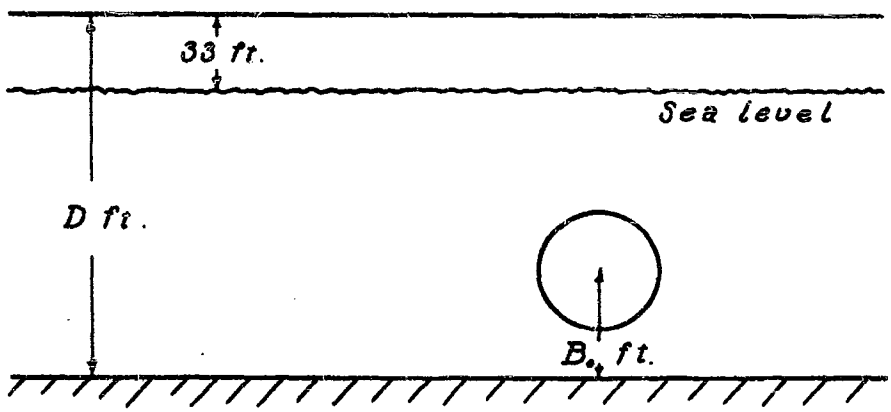

The best position of the mine is determined approximately from the equation

$$(1.3) \qquad d = 6.2b_o^2 + 3.3b_o + .4\ .$$

(See derivation in part III). Graphs of (1.1) and (1.3) are drawn in figures 1, 2 at the end.

On the basis of (1.1) and (1.3), the following table can be constructed showing the best location:

Table 1

Weight of T.N.T. (in lbs.)	Depth of Sea Bed From Sea Level (in ft.)	Best Location of Mine from Sea Bed (in ft.)
1500	150	21.0
1000	150	20.2
1000	100	17.0
500	100	15.5

The following limitations and qualifications should be noted. First, the effect of the free surface has been ignored, so that these results are valid if the mine is sufficiently far from the sea level, say, more than 3.5 L ft.* Second, it is assumed that the bubble does not meet the sea bed in the course of its motion. This is approximately equivalent to $B_0 > .8L$. Third, the sea bed is assumed to act like a rigid wall.

The validity of this last assumption should be tested by experiment. But there are plausible reasons for supposing that as far as the balancing phenomenon is concerned, the sea bed does act very much like a rigid wall. During the largest part of the time of pulsation of the bubble, the bubble is large and the pressure in the water is low; therefore, a sand bottom could be considered as rigid. The balancing effect is determined in the main by this portion of the period of pulsation.

4. An example.

Consider a mine with 1500 lbs. of T.N.T, in water of depth 150 ft. Figure 3 is a graph showing the relative magnitudes of the peak pressure in the secondary pulse when the mine is placed at varying distances from the bottom of the sea. The best location of the mine is 21.0 ft. from the bottom; the resulting peak pressure at any point in the water, as computed in part II, is 2015/R atmospheres, where R is the distance in feet from the point to the center of the contracted bubble. If the mine is initially placed at any other distance from the bottom, this value for the peak pressure is to be multiplied by the factor whose graph is drawn in figure 3.

This graph demonstrates a remarkable sharpness** in the peak pressure curve as a function of the distance of the

---

* The correction due to the free surface is treated in part III, section 5.

** In reality the graph will not be quite as sharp because of deviations from the assumptions listed on page 12.

mine from the bottom. For example, if the mine is placed either 17 ft. or 29 ft. from the bottom, the peak pressure is only one-half of the maximum.

If one is interested in the damage to objects on the surface of the water, it is necessary to take into account the migration of the gas bubble. Again considering the above example, the peak pressure at the surface directly overhead is 15.6 atmospheres (excluding the reflection from the bottom) when the mine is placed 21.0 ft. from the bottom. For any other location of the mine, this value is to be multiplied by the factor whose graph is drawn in figure 4. The graph still exhibits a considerable sharpness, but if one places the mine somewhat higher than 21.0 ft. from the sea bed, the effect on the surface would be improved slightly. This is due to the upward migration of the bubble. Note, however, that if the mine is placed too high, say 27 ft. from the bottom, the favorable effect of the upward migration is sharply counterbalanced by the resulting weakness of the secondary pulse.

Part II. Mathematical Study of the Secondary Pressure Pulse

1. Introduction.

High pressure pulses are produced only when the size of the gas bubble is near its minimum. During this time, the buoyant force due to gravity is small. Likewise, the proximity of rigid walls or free surfaces will not materially affect the motion, since their influence depends on the ratio of the bubble radius to the distance from the bubble, and is small if this ratio is small. Therefore, during the stage of minimum size, the bubble can be considered as immersed in an infinite body of water and subject to no outside forces. The pressure pulse produced by the bubble under these

circumstances will be investigated.

On the other hand, all these outside influences do affect the bubble in the stage when it is not small. Consequently, in contracting to its minimum size, the bubble and surrounding water have a linear momentum which remains practically constant while the bubble passes through the minimum size stage when the outside influences can be neglected. The pressure pulse produced by the bubble depends on the linear momentum acquired by the bubble. The dependence of the peak pressure on this linear momentum is the main objective of this investigation and is represented in figure 6.

For the derivation of this result, the following assumptions are made:

1. The water is an ideal incompressible fluid.
2. The bubble remains spherical in shape.
3. The gas inside the bubble is in thermal equilibrium at each instant and follows the adiabatic law.

These assumptions are reasonable for the major portion of the period of pulsation, and are violated only in the very short time interval when the radius of the bubble is small. The violations are in the nature of corrections to the theory, and will not materially affect the principle of stabilization. We shall not enter into a discussion of the assumptions, but merely refer to [4].

2. The Energy Equation.

Let A be the radius of the bubble at any time, B the vertical distance of its center from some horizontal level, and P_o the hydrostatic pressure of the water at the center of the bubble. The motion of the bubble is described by specifying A, B as functions of the time T.

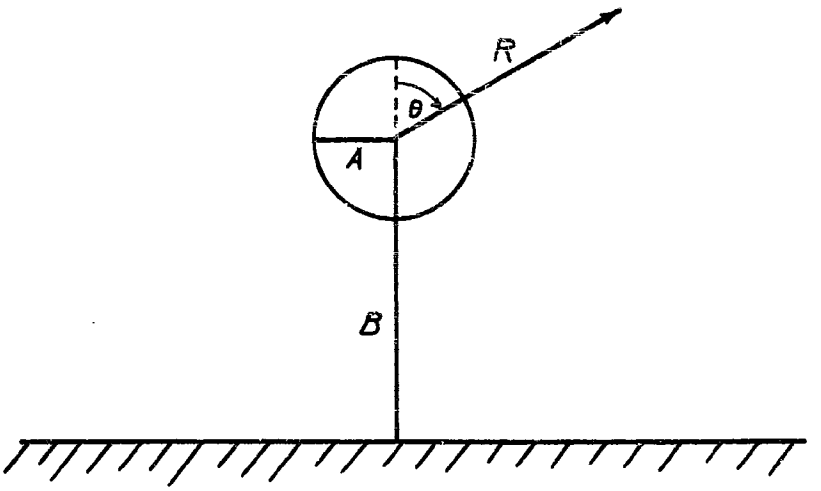

The velocity potential Φ describing the flow around a moving, pulsating sphere in an infinite body of water is easily obtained from classical hydrodynamics. It is

$$\Phi = \frac{A^2 A'}{R} + \frac{A^3 B'}{2} \frac{\cos\theta}{R^2} \,, \tag{2.1}$$

where R,θ are coordinates as indicated in the diagram above, and the "prime" denotes a time derivative. The kinetic energy $\mathcal{T}$ of the water is then

$$\mathcal{T} = 2\pi\rho A^3 [A'^2 + \tfrac{1}{6} B'^2] \tag{2.2}$$

where ρ is the density of the water. For these classical results, see, for example, [3] or Appendix II.

The potential energy $\mathcal{U}$ of the system of gas bubble and water is

$$\mathcal{U} = \tfrac{4}{3}\pi A^3 P_o + G(A) \tag{2.3}$$

where the first term is the gravitational potential energy

of the bubble due to the absence of water and the second term G(A) is the internal energy of the gas. If the gas obeys the adiabatic law, the internal energy is

$$G(A) = \frac{K M^{\gamma}}{A^{3(\gamma - 1)}}$$

where γ is the adiabatic exponent, K is a constant depending on the explosive, and M is the mass of the explosive used.

The energy equation is

(2.4) $$\mathcal{T} + \mathcal{U} = E$$

where E is the constant total energy in the system (after the passage of the initial shock wave due to the explosion).

3. Non-dimensional variables.

A considerable simplification in the writing of the equations is obtained by introducing non-dimensional quantities with appropriate scaling factors. Likewise, in part III, it is even more important to introduce non-dimensional quantities. For the purpose of comparing the formulas developed in this part with those in part III, we shall use the scaling factors convenient for part III. It should be mentioned that these are not the most convenient factors to use if the results of part II were the sole objective.

Set

(2.5) $$A = La, \quad B = Lb, \quad T = Ct,$$

where L,C are scaling factors with the dimensions of length, time, respectively, and a, b, t are non-dimensional variables. (Henceforth, capital letters will indicate dimensional quantities and small letters non-dimensional quantities.) The scaling factors

which we shall use are

$$(2.6) \qquad \begin{cases} L = \sqrt[3]{\dfrac{3E}{4\pi P_o}} \\ C = L\sqrt{\dfrac{3\rho}{2P_o}} \end{cases}$$

where P_o is the hydrostatic pressure at the center of the explosion, and ρ is the density of water.* These scaling factors are advantageous because they have a simple physical interpretation intimately connected with the motion of the bubble. It will be seen in part III that L is the maximum radius of the bubble if the internal energy of the gas could be neglected. Actually the maximum radius is approximately .92L. Also, it will be shown in part III that the time scaling factor C represents 2/3 of the period of pulsation of the bubble if no outside influences such as rigid walls or free surfaces are present.

The energy equation in terms of the non-dimensional variables becomes

$$(2.7) \qquad a^3\left[\dot{a}^2 + \frac{1}{6}\dot{b}^2\right] + a^3 + \frac{G(A)}{E} = 1,$$

where the "dot " denotes differentiation with respect to the non-dimensional time t.

4. The scaling factors and the internal energy of the gas for T. N. T.

It is desirable to express the scaling factors L,C in terms of the mass of explosive and the depth of the explosion.

---

* These scaling factors differ from those used by G. I. Taylor in [3].

Let D_o be the distance of the center of the explosion from a point 33 ft. above sea level, so that $P_o = \rho g D_o$. It is still necessary to express the energy constant E in terms of the mass of explosive. For the case of T. N. T., experimental results indicate that E is approximately one-half of the total chemical energy released by the explosion. See [4]. Slight changes in E will not materially affect the results since E appears in the form $\sqrt[3]{E}$. Using the values given by G. I. Taylor in [3], p. 4, and converting to the English system of measurements, one finds that

$$(2.8) \qquad \begin{cases} L = 13.2 \sqrt[3]{\dfrac{W}{D_o}} \text{ feet}, \\ C = 2.85 \dfrac{W^{1/3}}{D_o^{5/6}} \text{ seconds}, \end{cases}$$

where W is the weight of T. N. T. in pounds, and D_o is the distance in feet of the center of the explosion from a point 33 ft. above sea level.

Likewise, making use of the experimental values given by G. I. Taylor in [3], p. 4, the quantity $\frac{G(A)}{}$ for T. N. T. is, in m

where M
non-dime

(2.9)

where k

Changing to English units and using (2.8), one finds that

$$k = .0307\, D_o^{1/4} \quad , \tag{2.10}$$

where D_o has the same meaning as in (2.8). Equations (2.9) and (2.10) are the desired expressions of the internal energy for T.N.T.

5. The equations of motion for small values of the radius

The secondary high pressure pulse is emitted when the bubble is near its minimum size, and henceforth small consider the case when the radius is small. additive term a^3 in the energy equation (2.7) is when negligible compared with the number 1, and the energy equation becomes

$$a^3(\dot{a}^2 + \frac{1}{6}\dot{b}^2) + \frac{k}{a^{3/4}} = 1. \tag{2.11}$$

The Lagrangean equations of motion are

$$\frac{d}{dt}\frac{\partial \mathcal{L}}{\partial \dot{a}} - \frac{\partial \mathcal{L}}{\partial a} = 0 \tag{2.12}$$

$$\frac{d}{dt}\frac{\partial \mathcal{L}}{\partial \dot{b}} - \frac{\partial \mathcal{L}}{\partial b} = 0 \tag{2.13}$$

where $\mathcal{L} = \mathcal{T} - \mathcal{U}$. They become

$$\frac{d}{dt}(2\, a^3 \dot{a}) = 3a^2(\dot{a}^2 + \frac{1}{6}\dot{b}^2) + \frac{3}{4}\frac{k}{a^{7/4}} \quad , \tag{2.14}$$

$$\frac{d}{dt}(\frac{1}{3}\, a^3\, \dot{b}) = 0. \tag{2.15}$$

264

...n (2.15) shows that when the bubble is near its minimum ... The ... size, the linear momentum $\frac{1}{3} a^3 \dot{b}$ remains constant. Denote ... constant value by $\bar{s}$. Then

$$\dot{b} = \frac{3\bar{s}}{a^3} \quad , \tag{2.16}$$

and the energy equation (2.11) yields

$$\dot{a}^2 = \frac{1}{a^3} - \frac{k}{a^{15/4}} + \frac{3\bar{s}^2}{2a^5} \quad . \tag{2.17}$$

The equations (2.16), (2.17) completely determine, in terms of $\bar{s}$, the motion of the bubble during its most interesting phase when the radius a is small. An integration of (2.17) and then of (2.16), yields a, b as functions of t.

Equation (2.14) gives an expression for the quantity $(a^2\dot{a})^{\cdot}$, which is important for the determination of the pressure:

$$(a^2\dot{a})^{\cdot} = a\left(\frac{1}{2}\dot{a}^2 + \frac{1}{4}\dot{b}^2 + \frac{3}{8}\frac{k}{a^{15/4}}\right) \quad . \tag{2.18}$$

Substituting (2.16), (2.17) in (2.18), we obtain

$$(a^2\dot{a})^{\cdot} = \frac{1}{2a^2} + \frac{3\bar{s}^2}{2a^5} - \frac{k}{8a^{11/4}} \quad . \tag{2.19}$$

6. The minimum radius.

The value of a quantity q at the time when the bubble is exactly at its minimum size will be denoted by $\bar{q}$. The minimum radius $\bar{a}$ of the bubble is obtained by setting $\dot{a} = 0$ in (2.17). The resulting equation is simplified by introducing, in place of $\bar{a}$, the (non-dimensional) internal energy

$\bar{u}$ of the gas, defined by

$$(2.20) \qquad \bar{u} = \frac{k}{\bar{a}^{3/4}} \text{ , or } \bar{a} = \left(\frac{k}{\bar{u}}\right)^{4/3} .$$

The quantity $\bar{u}$ represents the portion of the total energy of the system which exists as internal energy of the gas at the time of minimum size. From (2.17), we get the following equation which determines $\bar{u}$:

$$(2.21) \qquad \frac{1 - \bar{u}}{\bar{u}^4} = \frac{3}{2}\left(\frac{\bar{s}}{k^2}\right)^2 , \text{ (Graphed in Fig. 5).}$$

The values of various other quantities at the time of minimum size of the bubble are of interest. From (2.16) we have

$$(2.22) \qquad \bar{\dot{b}} = \frac{3\bar{s}}{\bar{a}^3} = \frac{3\bar{s}}{k^4}\bar{u}^4 ,$$

and (2.19) yields

$$(2.23) \qquad \overline{(a^2\dot{a})^{\cdot}} = \frac{3}{8k^{8/3}}\bar{u}^{8/3}(4 - 3\bar{u}) .$$

Thus, given $\bar{s}$, the internal energy $\bar{u}$ at minimum size is obtained from equation (2.21). All the other quantities $\bar{a}$, $\bar{\dot{b}}$, $\overline{(a^2\dot{a})^{\cdot}}$ can then be found from (2.20), (2.22), (2.23).

7. The pressure pulse.

Sections 5 and 6 give a complete description of the motion of the bubble when it is near its minimum size. We shall now investigate the pressure pulse delivered to the surrounding water.

The potential function Φ for the flow of the surrounding water has been constructed in equation (2.1). The pressure in the water can be obtained from Bernoulli's equation as follows:

$$(2.24) \qquad \frac{P}{\rho} + \frac{1}{2}(\text{grad } \Phi)^2 - \left(\frac{\partial \Phi}{\partial T} - B' \frac{\partial \Phi}{\partial Z}\right) = 0,$$

where P is the excess over hydrostatic pressure, $Z = R \cos \theta$, and the term $B' \frac{\partial \Phi}{\partial Z}$ appears because of the moving coordinate system. A substitution of (2.1) in (2.24) yields

$$(2.25) \qquad \frac{P}{\rho} = \frac{(A^2 A')'}{R} + \text{terms in higher powers of } \frac{1}{R}.$$

For points in water not too near the bubble, the first term on the right hand side of (2.25) is dominant and the other terms may be dropped. Introducing non-dimensional variables, we obtain

$$(2.26) \qquad P = \frac{L^3}{C^2} \frac{(a^2 \dot{a})^\cdot}{R} = \frac{2P_0}{3} \cdot \frac{L}{R}(a^2 \dot{a})^\cdot.$$

The pressure in the water, therefore, depends essentially on the quantity $(a^2 \dot{a})^\cdot$.

The formula (2.18) for $(a^2 \dot{a})^\cdot$ can be given an interesting interpretation. The last term $\frac{3}{8} \frac{k}{a^{15/4}}$ represents the (non-dimensional) pressure of the gas inside the bubble, and (2.26) then shows that the pressure at any point in the water is composed of two parts: the internal pressure of the gas, and the dynamic pressure due to the motion of the water. This is more clearly seen if equations (2.26), (2.18) are rewritten in terms of the original dimensional variables. The

result is

$$(2.27) \qquad P = \frac{A}{R}\left(\frac{1}{2}\rho A'^2 + \frac{1}{4}\rho B'^2 + p(A)\right) ,$$

where $p(A)$ is the pressure of the gas inside the bubble when its radius is A.

The principle of stabilization asserts that the most important term in the expression (2.27) is the gas pressure term $p(A)$. To obtain the maximum possible effect, one should maximize $p(A)$ even at the expense of complete elimination of the dynamic terms $\frac{1}{2}\rho A'^2 + \frac{1}{4}\rho B'^2$. This is not obvious and requires a mathematical proof.

Returning now to the expression (2.26) for P, we wish to determine the time when the pressure pulse reaches a peak value. It is to be expected that the peak pressure occurs when the bubble is of minimum size. Although this is not obvious from the expression (2.18) for $(a^2\dot{a})^{\cdot}$, it is a simple consequence of the equation (2.19). By differentiating (2.19) with respect to a and by using (2.17), we have

$$\frac{d}{da}(a^2\dot{a})^{\cdot} = -\frac{1}{a^3} - \frac{15}{2}\frac{\bar{s}^2}{a^6} + \frac{11}{32}\frac{k}{a^{15/4}} = -\dot{a}^2 - \frac{9\bar{s}^2}{a^6} - \frac{21}{32}\frac{k}{a^{15/4}} .$$

This shows that $\frac{d}{da}(a^2\dot{a})^{\cdot}$ is negative and therefore attains its maximum at the smallest possible value of a. Hence the peak pressure occurs at the time of the minimum size of the bubble.

The value of the peak pressure $\bar{P}$ can now be obtained by substituting (2.23) in (2.26); the resulting expression is

$$(2.28) \qquad \bar{P} = \frac{1}{R} \cdot \frac{P_o L}{4k^{8/3}} \cdot \bar{u}^{-8/3}(4 - 3\bar{u}) .$$

This indicates the dependence of the peak pressure $\bar{P}$ on the internal energy $\bar{u}$ at the time of minimum size, and through (2.21), on the linear momentum $\bar{s}$.

The quantity $\bar{u}^{8/3}(4 - 3\bar{u})$ will be called the "pressure factor" and will be denoted by the symbol $\bar{q}$:

$$\bar{q} = \bar{u}^{8/3}(4 - 3\bar{u}) . \tag{2.29}$$

It depends on $\bar{s}$ by virtue of (2.21).

8. The optimum peak pressure.

We are now in a position to find that linear momentum $\bar{s}$ which produces the maximum peak pressure. The peak pressure $\bar{P}$, by (2.28), is proportional to the pressure factor $\bar{q}$ in (2.29), which in turn depends on $\bar{s}$ by virtue of (2.21). A graph of $\bar{q}$ as a function of $\frac{\bar{s}}{k^2}$ is drawn in figure 6, and demonstrates the very significant fact that $\bar{q}$ is largest when $\bar{s}$ is practically 0 (or $\bar{u}$ practically 1). Actually, by (2.29), $\bar{q}$ is a maximum when $\bar{u} = \frac{32}{33}$, or by (2.21), when $\bar{s} = .151\ k^2$. But since k is small, this differs so little from $\bar{s} = 0$ that it can be neglected. See figure 6.

Thus, the following general Principle of Stabilization has been demonstrated: <u>For a given mass of explosive, the optimum peak pressure in the secondary pulse is obtained by keeping the bubble motionless at the time of its minimum size.</u>

The value of the optimum peak pressure $\bar{P}_{opt.}$ can be obtained from (2.28) by setting $\bar{u} = 1$, with the result

$$\bar{P}_{opt.} = \frac{1}{R} \cdot \frac{P_o L}{4k^{8/3}} .$$

Using (2.7) and (2.10), and expressing P_o in atmospheres by means of $P_o = D_o/33$ atmospheres, where D_o is the distance in feet of the center of the explosion from a point

33 ft. above sea level, we have

$$(2.30) \qquad P_{opt.} = 176 \frac{W^{1/3}}{R} \text{ atmospheres}$$

where W is the weight of T. N. T. in pounds and R is the distance from the center of the bubble in feet.

This may be compared with the peak pressure of the primary shock wave, whose value, experimentally obtained, is*

$$P_{shock} = 1160 \frac{W^{1/3}}{R} \text{ atmospheres.}$$

The optimum peak pressure of the secondary pulse is approximately 15 percent of the shock wave peak pressure, but the duration is much longer, as will be seen in the next section.

9. The impulse.

The impulse I per unit area, carried by the secondary pulse, is the time integral of the pressure,

$$I = \int P dT = C \int P dt,$$

where the limits of integration are the times when $P = 0$.** By (2.26),

$$I = \frac{2P_o C}{3} \cdot \frac{L}{R} \int (a^2 \dot{a})^{\cdot} dt,$$

where the limits of integration are the times when $(a^2\dot{a})^{\cdot} = 0$. Using the fact that the motion is approximately symmetric about

---

* See [3] page 13, where this experimental result is quoted in metric units.

** The significance of this value of the impulse will be discussed later.

the time of the minimum size of the bubble, the above integral becomes

$$I = \frac{4P_o C}{3} \cdot \frac{L}{R} \cdot [a^{2\cdot}\dot{a}], \tag{2.31}$$

where $[a^{2\cdot}\dot{a}]$ is to be evaluated at the time when $(a^{2\cdot}\dot{a})^{\cdot} = 0$, or $a^{2\cdot}\dot{a}$ is a maximum.

Equations (2.8), (2.9) and (2.16) yield

$$a^{4\cdot}\dot{a}^2 = a - ka^{1/4} - \frac{3\bar{s}^2}{2a^2} - a^4$$

and

$$\frac{d}{da}(a^{4\cdot}\dot{a}^2) = 1 - \frac{k}{4a^{3/4}} + \frac{3\bar{s}^2}{a^3} - 4a^3 .$$

Setting the last expression equal to zero in order to find the maximum of $(a^{2\cdot}\dot{a})^2$, we obtain an equation for a. If both k and $\bar{s}$ were equal to zero, the solution of this equation would be $a = .63$. In a more realistic case when $k = .2$, $\bar{s} = .06$, one obtains $a = .61$. This illustrates that the value of a when $a^{2\cdot}\dot{a}$ is a maximum is not very sensitive to changes in the momentum $\bar{s}$, since $\bar{s}$ is generally quite small in actual cases.* Using $a = .61$ and $k = .2$, the value of $[a^{2\cdot}\dot{a}]$ is .55.

By (2.7), equation (2.31) becomes

$$I = .73 \frac{P_o CL}{R} = \frac{.83}{D_o^{1/6}} \frac{W^{2/3}}{R} \text{ atmosphere-seconds.}$$

Taking a typical case of a depth of 100 ft., so that $D_o = 133$, we find that

$$I = .37 \frac{W^{2/3}}{R} \text{ atmosphere-seconds.} \tag{2.32}$$

---

* See Part III.

We have shown that the impulse carried by the secondary pulse is practically independent of the linear momentum $\bar{s}$ of the bubble, and is given by (2.32).

The impulse carried by the primary shock wave is experimentally measured to be*

$$I_{shock} = .12 \frac{W^{2/3}}{R} \quad \text{atmosphere-seconds.}$$

A comparison with (2.32) indicates that the impulse carried by the secondary pulse is three times the impulse carried by the shock wave.

This conclusion can be stated in an approximate manner in terms of the durations of the pulses. Using the relation between the peak pressures obtained at the end of the last section, one can state that the secondary pulse lasts about eighteen times as long as the shock wave.

This result, and formula (2.32), should not be taken too literally but merely as order of magnitude statements. The reason for this is that the impulse carried by the secondary pulse was computed between the times when the pressure is zero. This includes a relatively long period of time during which the pressure is low, and the resulting contribution to the impulse will not be experimentally noticed and will not have much effect in damaging structures.

---

* [3], p.13

Part III. The Mechanism of Stabilization by Gravity and the Sea Bed.

1. The exact equations of motion.

In this part, the effects of gravity and of a rigid wall upon the motion of the bubble are considered. The linear momentum $\bar{s}$ produced by these factors in the course of one complete pulsation of the bubble is calculated. As was shown in part II, it is $\bar{s}$ which determines the peak pressure produced by the bubble at the time of its minimum size. An equation for determining the best location of the mine can be obtained by setting the momentum $\bar{s}$ equal to zero.

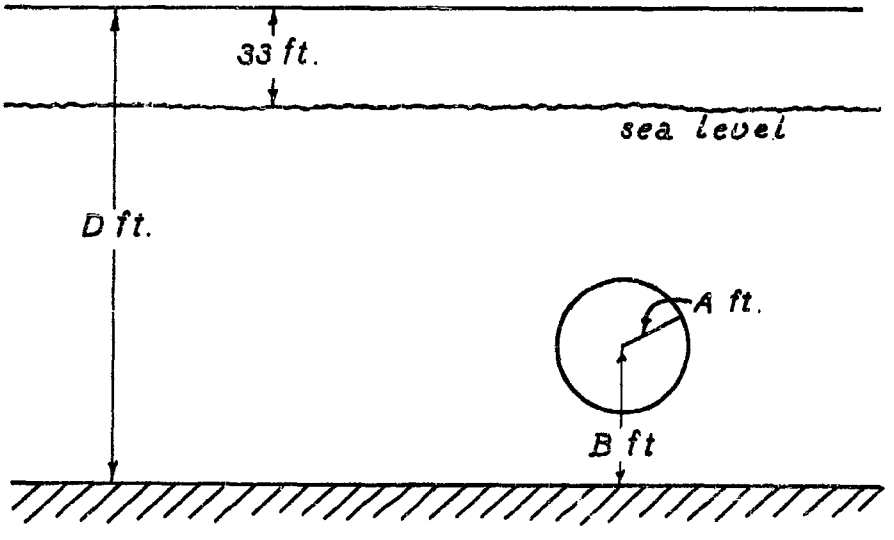

Use the same variables A,B as in part II and let D stand for the (fixed) distance of the sea bed from a point 33 ft. above sea level. In place of the equations (2.2), (2.3), (2.4), we have*

$$(3.1)\qquad 2\pi\rho A^3\left[(1+f_o)\dot{A}^2 - 2f_1\dot{A}\dot{B} + (\tfrac{1}{6}+f_2)\dot{B}^2\right]$$

$$+\frac{4}{3}\pi A^3\rho g(D-B) + G(A) = E,$$

where f_o, f_1, f_2 are functions of the ratio A/B which represent the influence of the rigid wall on the motion of the bubble, $\frac{4}{3}\pi A^3\rho g(D-B)$ represents the gravitational potential energy due to the lack of water in the space occupied by the bubble, and g is the acceleration due to gravity. Explicit expressions for f_o, f_1, f_2 are derived in [5], and will be reproduced in appendix II of this report.

Introduce non-dimensional quantities as in equations (2.5), (2.6) of part II, sections 3 and 4. The energy equation becomes

$$(3.2)\qquad a^3[(1+f_o)\dot{a}^2 - 2f_1\dot{a}\dot{b} + (\tfrac{1}{6}+f_2)\dot{b}^2]$$

$$+\frac{d-b}{d-b_o}a^3 + \frac{k}{a^{3/4}} = 1,$$

where $d = \frac{D}{L}$, $b_o = \frac{B_o}{L}$ and B_o is the initial distance of the bubble from the sea bed.

The motion of the bubble is determined from (3.2) and one of the Lagrangean equations (2.12), (2.13). Using

---

* See appendix II for details.

the b-equation (2.13), we obtain

$$(3.3)\qquad \frac{d}{dt}\left[2a^3\left(\frac{1}{6}+f_2\right)\dot{b} - 2a^3 f_1 \dot{a}\right]$$

$$= -\frac{a^4}{2b^2}\left[\frac{df_0}{d\alpha}\dot{a}^2 - 2\frac{df_1}{d\alpha}\dot{a}\dot{b} + \frac{df_2}{d\alpha}\dot{b}^2\right] + \frac{1}{d-b_0}a^3,$$

where

$$(3.4)\qquad \alpha = \frac{a}{2b},$$

and the quantities f_0, f_1, f_2 are functions of α only.

The differential equations (3.2), (3.3) are to be integrated, subject to the following initial condition:

$$\text{at } t = 0, \quad a = a_0, \ \dot{a} = 0$$

$$b = b_0, \ \dot{b} = 0,$$

where a_0 is the smallest root (near $k^{4/3}$) of $a^3 + \frac{k}{a^{3/4}} = 1$. Of course, these initial conditions are not exactly realistic, since at the very beginning a shock wave is formed by the explosion. But the time interval required for incompressible flow to set in is relatively minute and may be ignored.*

The quantity in the brackets on the left-hand side of (3.3) is the linear momentum s of the system. The first term on the right-hand side of (3.3) is due to the presence of the rigid wall, and the second term is due to gravity.

By integrating equation (3.3) we obtain the momentum $\bar{s}$ at the end of the period of pulsation of the bubble:

---

* See [4].

$$(3.5)\quad \bar{s} = -\int_0^{\bar{t}} \frac{a^4}{2b^2}\left[\frac{df_0}{d\alpha}\dot{a}^2 - 2\frac{df_1}{d\alpha}\dot{a}\dot{b} + \frac{df_2}{d\alpha}\dot{b}^2\right]dt$$

$$+ \frac{1}{d-b_0}\int_0^{\bar{t}} a^3 dt\ ,$$

where the integration is extended over the full period $\bar{t}$ of the pulsation, from the explosion to the time of minimum size.

2. <u>The approximate evaluation of the period and the momentum.</u>

The results of a numerical integration of equations (3.2), (3.3) are tabulated for special cases in appendix II. They serve as a check on the approximations which will now be made to evaluate the period $\bar{t}$ and the momentum $\bar{s}$.

The bubble expands to a maximum size before contracting again. Indicate the value of a quantity at the time of maximum size by a subscript 1. Thus t_1 is the time of maximum size, s_1 is the linear momentum, etc. We shall introduce the following approximations which are especially accurate when the bubble is in its balanced position:

1. The time $\bar{t}$ and linear momentum $\bar{s}$ at the minimum size of the bubble is twice the corresponding quantity at the maximum size; i. e., $\bar{t} = 2t_1$, $\bar{s} = 2s_1$. This assumption agrees very closely with the numerical integration of the equations. It means that the motion is approximately symmetric about the time t_1 of maximum size. This would be exactly correct if the b-coordinate did not vary.

2. During the first half of the period of pulsation, until time t_1, $\dot{b}$ is small and can be taken as zero, so that b remains equal to b_0. This agrees satisfactorily with the numerical integration, as well as with experimental evidence.

Substituting $b = b_o$ in (3.2), we get

$$\ddot{a} = \frac{\sqrt{1 - a^3 - k a^{-3/4}}}{a^{3/2}\sqrt{1 + f_o}} \quad . \tag{3.6}$$

The solution of (3.6) is immediately obtained by integration, with the following result for the half-period t_1:

$$t_1 = \int_0^{t_1} dt = \int_{a_o}^{a_1} \frac{a^{3/2}\sqrt{1 + f_o}}{\sqrt{1 - a^3 - k a^{-3/4}}}\, da \tag{3.7}$$

where a_o is the smallest and a_1 the largest root of

$$1 - a^3 - k\, a^{-3/4} = 0. \tag{3.8}$$

To evaluate the integral (3.7) it is necessary to have a specific value for k. The value of k is given by (2.10) and depends on the distance D_o of the explosion from a point 33 ft. above sea level. The following table is calculated from (2.10):

D_o	33	83	133	183
k	.146	.183	.206	.223

Selecting a depth of water of about 100 ft. as typical, the value of k is approximately .2. We shall select this value of k throughout the remaining calculations. A different value for k will change the formulas slightly.

For $k = .2$, the roots a_o, a_1 of (3.8) are

$$a_o = .118, \qquad a_1 = .924. \tag{3.9}$$

The last equation (3.9) is noteworthy, since a_1 represents the non-dimensional maximum radius of the bubble. The actual maximum radius A_1 is thus

$$A_1 = .924\ L.$$

If the internal energy $\frac{k}{a^{3/4}}$ of the gas were neglected, the maximum radius would be exactly L.

The quantity $\sqrt{1 + f_o}$ in the integral (3.7) is very closely equal to $1 + \frac{\alpha}{2} = 1 + \frac{a}{4b_o}$ as is shown in appendix II. Making this approximation, we can evaluate the integral (3.7) numerically. This numerical evaluation is discussed in appendix III, the result being

$$t_1 = .735 + \frac{.136}{b_o}\ .$$

The total (non-dimensional) period $\bar{t}$ of the pulsation is therefore

$$(3.10) \qquad \bar{t} = 2t_1 = 1.47 + \frac{.272}{b_o} = 1.47\left(1 + \frac{.185}{b_o}\right)\ .$$

Formula (3.10) shows that if no rigid walls are present $(b_o = \infty)$, the actual period $\bar{T}$ in seconds would be

$$\bar{T} = 1.47\ C,$$

or about 3/2 times C . This provides the physical interpretation of the scaling factor C mentioned in section 3 of part II.

Substituting $b = b_o$, $\dot{b} = 0$ in (3.5), we obtain for

the half-momentum s_1,

$$s_1 = - \int_0^{t_1} \frac{a^4}{2b_o^2} \frac{df_o}{d\alpha} \dot{a}^2 dt + \frac{1}{d-b_o} \int_0^{t_1} a^3 dt,$$

or

$$(3.11)\quad s_1 = - \frac{1}{2b_o^2} \int_{a_o}^{a_1} \frac{a^{5/2} \sqrt{1 - a^3 - ka^{-3/4}} \cdot \frac{df_o}{d\alpha}}{\sqrt{1 + f_o}} da$$

$$+ \frac{1}{d-b_o} \int_{a_o}^{a_1} \frac{a^{9/2} \sqrt{1 + f_o}}{\sqrt{1 - a^3 - ka^{-3/4}}} da ,$$

using (3.6). The first term on the right hand side of (3.11) is the downward momentum due to the rigid wall, and the second term is the upward momentum due to gravity.

Again taking $k = .2$, using the approximation $\sqrt{1 + f_o} = 1 + \frac{a}{4b_o}$, $\frac{df_o/d\alpha}{\sqrt{1 + f_o}} = 1 - \frac{a}{4b_o}$, and evaluating these integrals numerically, we get the following expression for the full momentum $\bar{s}$:

$$(3.12)\quad \bar{s} = - \left(\frac{.113}{b_o^2} - \frac{.019}{b_o^3} \right) + \frac{1}{d-b_o} \left(.704 + \frac{.148}{b_o} \right).$$

See appendix III for the numerical evaluations.

3. The stabilized position.

By the principle of stabilization, the maximum peak

pressure is obtained by setting $\tilde{s} = 0$, with the result

$$d - b_o \approx \frac{.704 + \frac{.148}{b_o}}{\frac{.113}{b_o^2} - \frac{.019}{b_o^3}} .$$

Expressing d in descending powers of b_o, we get

$$(3.13) \qquad d = 6.2\, b_o^2 + 3.3\, b_o + .4 .$$

A graph of equation (3.13) is drawn in figure 2.

More generally, the peak pressure, as a function of the distance b_o of the mine from the sea bottom, is obtained by combining equation (2.28), (2.29), figure 6, and equation (3.12). As a typical example of this dependence, consider the case discussed in section 3, part I, of a mine containing 1500 lbs. of T. N. T. in water of depth 150 ft. The scaling factor L, as obtained from figure 1, is

$$L = 27.6 \text{ ft.}$$

The depth D of the sea bed from a point 33 ft. above sea level is 183 ft., so that

$$d = \frac{D}{L} = 6.63.$$

The best location of the mine according to figure 2 is $b_o = .76$, or

$$B_o = Lb_o = 21 \text{ ft.}$$

above the sea bed.

If the mine is located at various other distances B_o, the pressure factor $\bar{q}$ can be obtained from figure 6 by first determining $\bar{s}$ from equation (3.12). The results are tabulated below, and the graph is drawn in figure 3.

b_o	.6	.7	.76	.8	.9	1.0	1.1	1.2
$\bar{s}$	-.066	-.020	+.003	.015	.039	.059	.074	.087
$\bar{q}$	.51	.92	1.0	.96	.72	.55	.47	.42

As stated in section 3, part I, figure 3 shows a remarkable sharpness in the peak pressure curve as a function of the distance from the bottom.

4. The migration of the bubble.

A formula for the distance travelled by the bubble in the course of its pulsation is difficult to obtain because it involves a complicated repeated integration. But by combining a theoretical argument with the results of numerical integration, an empirical formula can be developed.

It seems reasonable to suppose that the displacement $\Delta b = \bar{b} - b_o$ of the bubble is an odd function of $\bar{s}$. It can therefore be represented by the beginning terms of a Taylor expansion,

$$\Delta b = c_1 \bar{s} + c_2 \bar{s}^3 ,$$

where c_1, c_2 are appropriate constants. In fact, a theoretical justification of this can be given on the basis of the differential equations (3.2), (3.3), but this will be omitted here.

We can determine the constants c_1, c_2 empirically by using the results of the numerical integration tabulated in

appendix I. The least squares solution yields the following formula:

$$\Delta b = 19\bar{s}\,(1 - 62\bar{s}^2). \tag{3.14}$$

A graph of (3.14) is drawn in figure 7, and is compared with the tabulated values. The formula (3.14) is seen to be very close to the tabulations.

5. The correction due to the free surface.

For the sake of completeness, we shall include some remarks concerning the effect of the free water surface. The latter exerts a repellent force on the bubble, aiding the downward force of the sea bed. A complete discussion would require a knowledge of the potential function Φ and of the corresponding values for f_o, f_1 and f_2. A careful examination of the previous argument, however, shows that only the first terms in the expansions of f_o and $\frac{\partial f_o}{\partial b}$ in powers of a were used. In appendix II these first terms are obtained by successive reflections. The results are as follows:

If C is the depth of the bubble below the free surface, and x is set equal to $\frac{C-B}{C+B}$, then the expansion of f_o begins with

$$\frac{a}{2b} F(x)$$

and the expansion of $\frac{\partial f_o}{\partial b}$ begins with

$$-\frac{a}{2b^2} G(x)$$

where the formulas for $F(x)$ and $G(x)$ are given in appendix II. A short table of their values follows:

x	1	.9	.8	.7	.6	.5	.4	.3	.2	.1	0
F(x)	1	.86	.72	.58	.43	.28	.11	-.06	-.25	-.46	-.69
G(x)	1	1.00	1.00	1.01	1.03	1.07	1.10	1.22	1.33	1.54	1.86

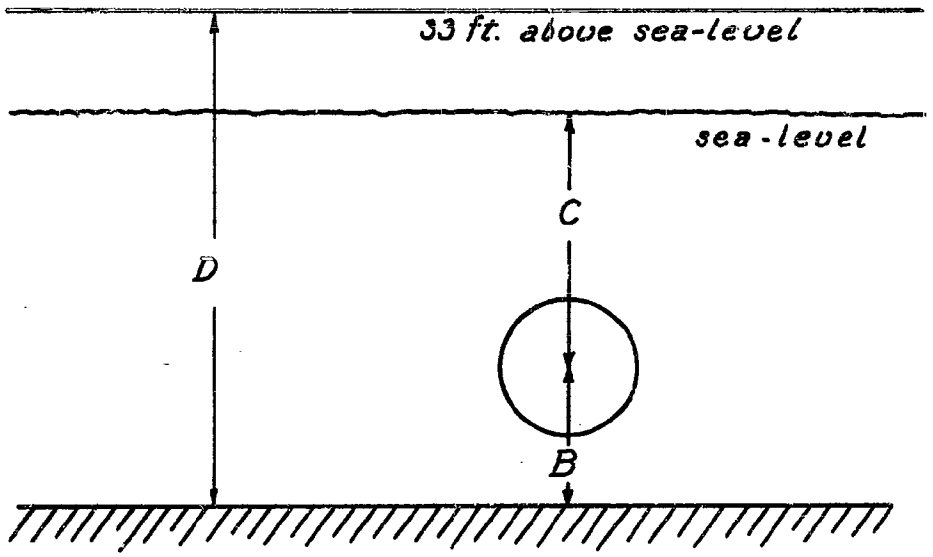

When these expansions are used, formulas (3.10) and (3.12) for $\bar{t}$ and $\bar{s}$ are modified, as follows:

$$\bar{t} = 1.47\left(1 + \frac{.185\ F(x)}{b_o}\right) \tag{3.15}$$

$$\bar{s} = -\frac{G(x)}{b_o^2}\left(.113 - \frac{.019\ F(x)}{b_o}\right) + \frac{1}{d-b_o}\left(.704 + \frac{.148\ F(x)}{b_o}\right) . \tag{3.16}$$

It is to be noted that $x = 1$ corresponds to no free surface ($c = \infty$), while $x = 0$ corresponds to a point midway between the free surface and the rigid bottom.

An interesting result is that $F(x) = 0$ when $x = 1/3$, so that the influence of the free surface on the period of the bubble cancels the influence of the rigid bottom.

Appendix I. The Numerical Integration of the Differential Equations.

To test the validity of the approximations made in part III, the exact differential equations (3.2), (3.3) were integrated numerically. The coefficients f_0, f_1, f_2 and their derivatives with respect to α, are tabulated in table 4, appendix II. The numerical integration was carried out by the Mathematical Tables Project operating under the Applied Mathematics Panel.*

In this report we have not reproduced the complete tables, but have included the graphs drawn in figures 8 - 11, which are based on these tables. Here we shall set down only the most interesting items in these calculations, namely, the behavior at the beginning, at the time of maximum size, and at the time of minimum size.** The following table shows the results:

---

* In particular, Dr. G. Blanche, Dr. C. Lanczos and Dr. A. N. Lowan helped overcome the considerable difficulties in the numerical integration.

** Details of the computation can be obtained from an extensive report by the Mathematical Tables Project prepared for the Applied Mathematics Panel.

Table 2. The results of numerical integration

	t	a	$\dot{a}$	b	$\dot{b}$	s	$\dot{s}$
I. d = 11.17 b_o = 1.5	0	.1172	0	1.5	0	0	.00017
	.8289	.925	0	1.565	.066	.0189	.079
	1.657	.192	0	2.11	16.0	.0378	.0006
2. d = 11.17 b_o = 1.17	0	.1172	0	1.17	0	0	.00016
	.8505	.926	0	1.243	.0231	.00716	.0794
	1.6993	.138	0	1.49	15.8	.0139	.0
3. d = 11.17 b_o = 1.08	0	.1172	0	1.08	0	0	0
	.8576	.926	0	1.156	.006	.00205	.0791
	1.7146	.120	0	1.19	6.9	.00393	0
4. d = 11.17 b_o = .9	0	.1172	0	.9	0	0	0
	.8753	.926	0	.986	-.041	-.0154	.0769
	1.7574	.167	0	.352	-16.9	-.0270	-.076
5. d = ∞* b_o = 2.0	0	.117	0	2.0	0	0	0
	.8043	.922	0	2.01	-.0470	-.0127	-.0001
	1.610	.163	0	1.58	-17.4	-.0251	-.00236
6. d = ∞* b_o = 1.5	0	.117	0	1.5	0	0	0
	.8204	.923	0	1.52	- .0769	-.0219	-.0002
	1.6504	.202	0	.808	-15.4	-.0426	-.007
7. d = ∞* b_o = 1.2	0	.117	0	1.2	0	0	0
	.8266	.922	0	1.23	- .111	-.0339	-.0004
	1.699	.237	0	.282	-12.6	-.0645	-.58

* This case corresponds to a rigid wall alone, with gravity ignored.

The period $\bar{t}$ and the momentum $\bar{s}$ for the cases listed above were computed from the formulas developed in part III. They are collected in the following table, and compared with the numerical values given in the preceding table. The agreement is excellent.

TABLE 3.

	$\bar{t}$		$\bar{s}$	
	Calculated from (3.10)	Numerical (Table 2)	Calculated from (3.12)	Numerical (Table 2)
1. $d = 11.17$, $b_o = 1.5$	1.65	1.66	+.039	+.038
2. $d = 11.17$, $b_o = 1.17$	1.70	1.70	+.012	+.014
3. $d = 11.17$, $b_o = 1.08$	1.72	1.71	+.002	+.004
4. $d = 11.17$, $b_o = .9$	1.77	1.76	-.030	-.027
5. $d = \infty$, $b_o = 2.0$	1.61	1.61	-.026	-.025
6. $d = \infty$, $b_o = 1.5$	1.65	1.65	-.044	-.043
7. $d = \infty$, $b_o = 1.2$	1.70	1.70	-.067	-.065

Appendix II. The Velocity Potential for a Pulsating Sphere Moving Perpendicularly to a Wall.

1. Statement of the problem.

An ideal incompressible fluid is bounded by a plane infinite rigid wall,* and has a pulsating and moving sphere immersed in it. It is required to find the velocity potential describing the (irrotational) flow, and to obtain the kinetic energy of the liquid. The case of a moving sphere is classical and can be found in the standard books on Hydrodynamics. The pulsating sphere, however, does not seem to be generally known and has certain features of interest. The treatment here follows [5].

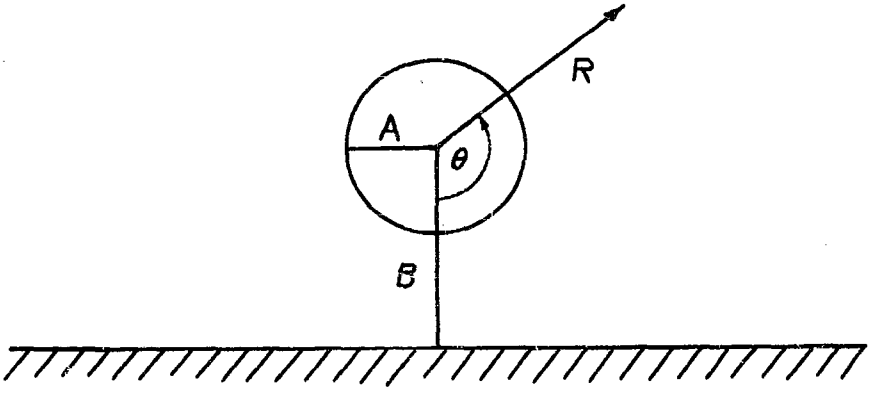

Let A be the radius of the sphere at any time T, and B the distance of its center from the rigid wall. The velocity potential Φ describing the flow of the liquid satisfies the potential equation

$$\Delta\Phi = \Phi_{xx} + \Phi_{yy} + \Phi_{zz} = 0$$

---

* The method used here can also be applied to a spherical wall.

and has the following boundary conditions:

$$(1)\qquad \begin{cases} -\dfrac{\partial \Phi}{\partial n} = A' - B' \cos\theta & \text{on the sphere} \\ -\dfrac{\partial \Phi}{\partial n} = 0 & \text{on the plane,} \end{cases}$$

where n is the normal direction pointing into the liquid and the "prime" denotes a time derivative.

The construction of Φ can be decomposed into two simpler problems by setting

$$(2)\qquad \Phi = A' \Phi_0 - B' \Phi_1$$

where Φ_0, Φ_1 are potential functions satisfying the following boundary conditions:

$$(3)\quad -\frac{\partial \Phi_0}{\partial n} = 1 \quad \text{on the sphere,} \quad -\frac{\partial \Phi_0}{\partial n} = 0 \quad \text{on the plane}$$

$$(4)\quad -\frac{\partial \Phi_1}{\partial n} = \cos\theta \quad \text{on the sphere,} \quad -\frac{\partial \Phi_1}{\partial n} = 0 \quad \text{on the plane.}$$

Physically, Φ_0 represents the potential function for a sphere of fixed center and radius expanding with unit velocity, while Φ_1 is the function associated with a rigid sphere moving away from the wall at unit velocity. The functions Φ_0, Φ_1 will be constructed by means of the method of images.

2. Some theorems on images.

The theorems that follow supplement well known theorems on images. See Milne-Thomson, Theoretical Hydrodynamics, Chapter 15.

We wish to find a potential function Φ, defined outside a given sphere, with a given distribution of sources outside the sphere and vanishing normal derivative, $\frac{\partial \Phi}{\partial n} = 0$, on the boundary. A standard method for constructing Φ is to place a suitable arrangement of sources inside the sphere, called the image of the original distribution.

The image of a point source and a radial dipole are well known, and will be found in Milne-Thomson, pp. 420,421. Here we consider the image of a line source.

Theorem 1. Consider a sphere with center 0 and radius a. The image of a uniform line source of strength μ per unit length stretching from Q_1 to Q_2 is the following: a uniform line source of strength $\mu \frac{\overline{OQ_2}}{a}$ per unit length, stretching between the points Q_1', Q_2' inverse to Q_1, Q_2, and a uniform line sink of strength $\mu \frac{\overline{Q_1Q_2}}{a}$ per unit length extending from 0 to Q_1'.

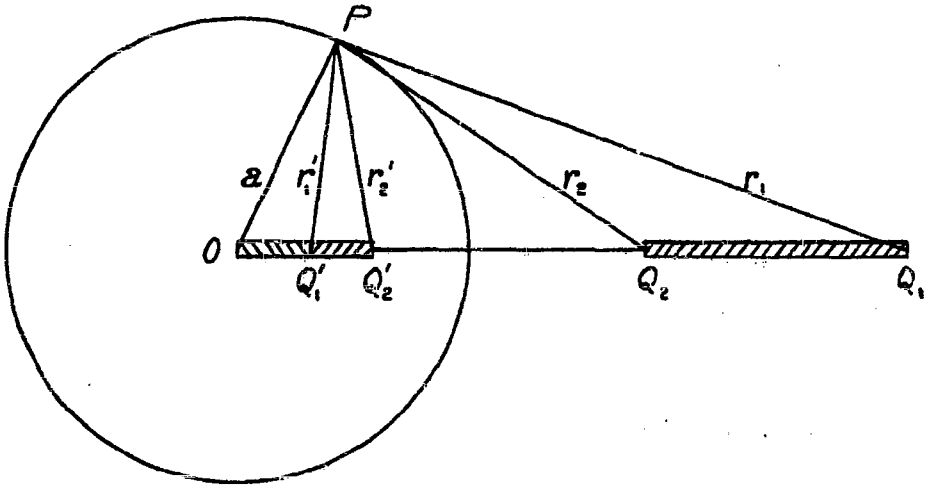

Proof. If P is any point, the Stokes stream function Ψ (see Milne-Thomson, Chapter 15, esp. pp. 420, 421) is

$$\Psi = -\mu \frac{\overline{Q_1Q_2}}{a}(r-r_1') + \mu \frac{\overline{OQ_2}}{a}(r_1'-r_2') + \mu(r_2-r_1) .$$

If P is on the sphere, we have $r_1' = \frac{a}{\overline{OQ_1}} r_1$, $r_2' = \frac{a}{\overline{OQ_2}} r_2$ (a property of inverse points, due to the similarity of triangles OPQ_1', OQ_1P), and consequently $\Psi = -\mu \frac{\overline{Q_1Q_2}}{a} = \text{const.}$ Therefore $\frac{\partial \Phi}{\partial n} = 0$ on the sphere.

Combining this result with the known image of a point source (Milne-Thomson, pp. 420,421), we obtain the following:

Theorem 2. The image of a point source of strength m situated at the point Q_2, together with a uniform line sink of strength μ per unit length extending from Q_1 to Q_2, where $m = \mu\overline{Q_1Q_2}$ (so that the total strength is zero), is the following: a point source of strength $m\frac{a}{\overline{OQ_2}}$ at the point Q_2' and a uniform line sink of strength $\mu\frac{\overline{OQ_1}}{a}$ per unit length extending between Q_1', Q_2'.

3. The construction of Φ_0.

The function Φ_0 is required to satisfy the boundary conditions (3). If the plane were not present, Φ_0 would be $\frac{A^2}{R}$, which represents a source of strength A^2 placed at O. The presence of the plane, however, causes the boundary condition (3) on the plane to be violated. To satisfy it, introduce the image of the source relative to the plane, which is a source of equal strength at the reflected point Q_1. But the boundary condition on the sphere is now violated, and to

remedy it, introduce the image of the point source at Q_1 relative to the sphere. This image is a point source of strength $A^2\frac{A}{\overline{OQ}_1}$ at the inverse point Q_1' and a uniform line sink of strength $A^2\frac{1}{A}$ per unit length extending from 0 to Q_1'; this process continues and requires the use of theorem 2 for the images relative to the sphere. The successive images fit very neatly together, as indicated in the diagram.

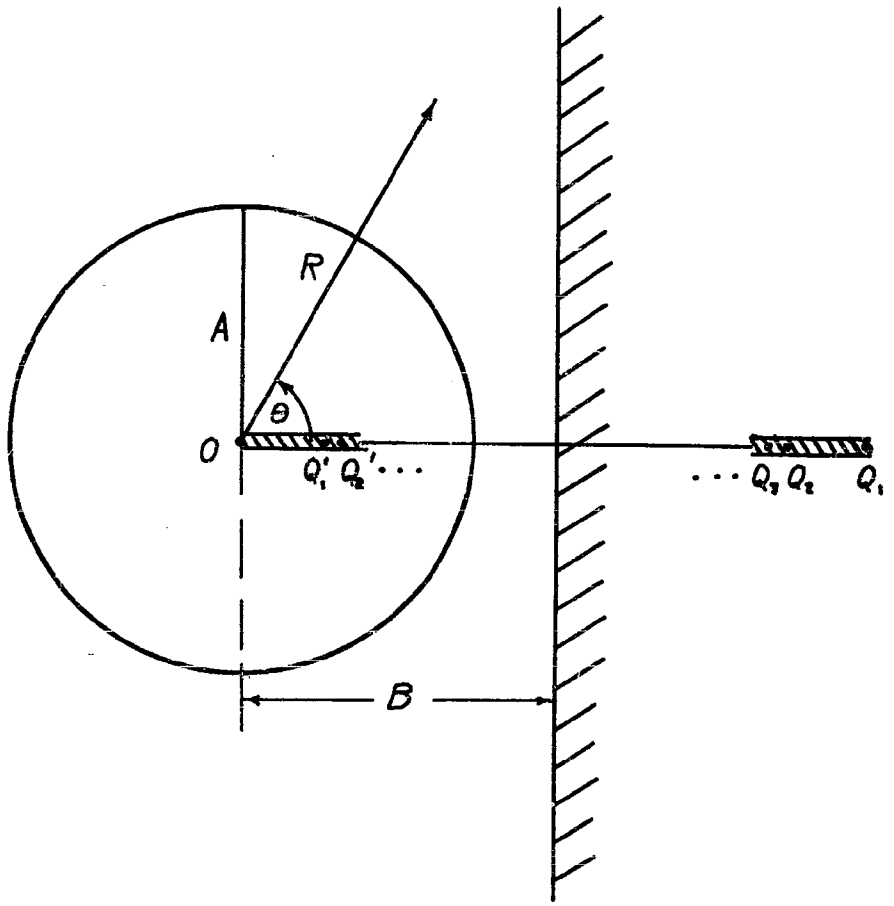

The successive reflections are described in the following table:

Strength of point source	Situation of point source	Strength per unit length of uniform line sink	Situation of uniform line sink
A^2	0		
A^2	Q_1		
$A^2\frac{A}{\overline{OQ}_1}$	Q_1'	A	OQ_1'
$A^2\frac{A}{\overline{OQ}_1}$	Q_2	A	Q_1Q_2
$A^2\frac{A}{\overline{OQ}_1}\frac{A}{\overline{OQ}_2}$	Q_2'	$\frac{\overline{OQ}_1}{A}A$	$Q_1'Q_2'$

etc.

Set

$$d_n = \frac{A}{\overline{OQ}_n} \tag{5}$$

and

$$D_n = d_1 \cdot d_2 \cdot \cdots \cdot d_n \ . \tag{6}$$

By the inversion, d_n is also equal to $\frac{\overline{OQ}_n'}{A}$. The general expressions for the strengths of the sources are:

(7) A point source of strength AD_n at Q_n' and Q_{n+1}; a uniform line sink of strength $\frac{A}{D_n}$ per unit length along $Q_n'Q_{n+1}'$ and $Q_{n+1}Q_{n+2}$.

Introduce the quantity

$$\alpha = \frac{A}{2B} \quad . \tag{8}$$

The quantities d_n can be expressed in terms of α. We have

$$d_{n+1} = \frac{A}{\overline{OQ}_{n+1}} = \frac{A}{2B - \overline{OQ}_n'} = \frac{1}{\frac{2B}{A} - d_n} \quad .$$

Thus

$$d_1 = \alpha, \ldots, \; d_{n+1} = \frac{1}{\frac{1}{\alpha} - d_n} \; , \ldots \; , \tag{9}$$

so that the d's are convergents to a continued fraction.

The quantities D_n can be obtained as functions of α from the definition (6). They can also be obtained by solving a second order linear difference equation with constant coefficients for the quantity $\frac{1}{D_n}$, obtained from the recursion formula (9).

It is convenient to expand Φ_o in the neighborhood of the surface of the sphere in terms of spherical harmonics. The expansion of a unit point source lying outside the sphere at a distance X from the center is

$$\frac{1}{X} + \frac{R}{X^2} P_1(\cos\theta) + \frac{R^2}{X^3} P_2(\cos\theta) + \ldots \; , \tag{10}$$

while a point source lying inside the sphere has an expansion

$$\frac{1}{R} + \frac{X}{R^2} P_1(\cos\theta) + \frac{X^2}{R^3} P_2(\cos\theta) + \ldots \; , \tag{11}$$

where $\{P_n(\cos\theta)\}$ are the Legendre polynomials of $\cos\theta$. (See diagram on page 41). Integration with respect to X yields the expansion of a uniform line source. The expansion of Φ_o is then easily obtained by using the distribution of sources and sinks given in (7).

For the present purpose it suffices to know merely the value of $\frac{1}{4\pi A^2}\int_K \Phi_o dS$, the mean value of Φ_o over the surface K of the sphere. The integral of a unit point source over the surface of the sphere is, by (10) and (11),

(12) $$\frac{1}{Y} \quad \text{or} \quad \frac{1}{A},$$

according as the source lies outside or inside the sphere. The first of these is to be expected from the mean value theorem for potential functions, while the second is a constant, independent of the position of the sources inside the sphere.

The value of $\frac{1}{4\pi A^2}\int_K \Phi_o dS$ can now be obtained by using the distribution of sources and line sinks (7). The contribution of the distribution <u>inside</u> the sphere reduces to $A^2\frac{1}{A}$ due to the source of strength A^2 at the center. This follows from the second result in (12) and the fact that the successive images, each consisting of a source and a line sink, have a total strength zero. The contribution due to the source A^2D_n at Q_{n+1} and the line sink of strength $\frac{A}{D_{n-1}}$ per unit length along Q_nQ_{n+1} (see equation (7)) is

$$A^2D_n\frac{1}{\overline{OQ}_{n+1}} - \frac{A}{D_{n-1}}\log\frac{\overline{OQ}_n}{\overline{OQ}_{n+1}},$$

or

$$A\,D_{n+1} - \frac{A}{D_{n-1}}\log\frac{d_{n+1}}{d_n},$$

by (5) and (6). Thus we obtain the final result

$$(13)\qquad \int_K \Phi_c \, dS = 4\pi A^3 \left[1 + D_1 + \sum_{n=1}^{\infty} \left(D_{n+1} - \frac{1}{D_{n-1}} \log \frac{d_{n+1}}{d_n} \right) \right].$$

The term D_1 is due to the point source A^2 at Q_1.

4. The construction of Φ_1.

The function Φ_1 is required to satisfy the boundary conditions (4). If the plane were not present, Φ_1 would be the velocity potential due to a dipole of strength $\frac{A^3}{2}$ placed at O, namely, $\frac{A^3}{2} \frac{\cos\theta}{R^2}$. The boundary condition on the plane, however, is violated and to satisfy it, introduce the image radial dipole of strength $-\frac{A^3}{2}$ situated at the reflected point Q_1 (see the diagram on page 45). To remedy this boundary condition on the sphere, which has now been violated, introduce the image of this radial dipole relative to the sphere. This image is another radial dipole of strength $\frac{A^3}{2} \frac{A^3}{OQ_1^3}$ at the inverse point Q_1'. (See Milne-Thomson, p. 421). Etc.

The successive reflections are described in the following table:

Strength of Dipole	Situation of Dipole
$\frac{A^3}{2}$	O
$-\frac{A^3}{2}$	Q_1
$\frac{A^3}{2} \frac{A^3}{OQ_1^3}$	Q_1'
$-\frac{A^3}{2} \frac{A^3}{OQ_1^3}$	Q_2
$\frac{A^3}{2} \frac{A^3}{OQ_1^3} \frac{A^3}{OQ_2^3}$	Q_2'

etc.

The general expressions for the strengths of the dipoles are:

$$(14)\quad \begin{cases} \text{at } Q_n' \text{ , there is a radial dipole of strength } \frac{A^3}{2} D_n^3 \text{ ;} \\ \text{at } Q_{n+1}, \quad " \quad " \quad " \quad " \quad " \quad " \quad " - \frac{A^3}{2} D_n^3 \text{ .} \end{cases}$$

The expansion of a unit radial dipole lying outside a sphere at a distance X from the center is

$$(15)\qquad -\frac{1}{X^2} - \frac{2R}{X^3} P_1(\cos\theta) - \frac{3R^2}{X^4} P_2(\cos\theta) - \cdots\cdots ,$$

while a radial dipole inside the sphere has an expansion

$$(16)\qquad \frac{1}{R^2} P_1(\cos\theta) + \frac{2X}{R^3} P_2(\cos\theta) + \cdots\cdots .$$

These are obtained from (10), (11) by differentiation with respect to X. See Milne-Thomson, pp. 442,443.

For the present purpose we are interested in the expansion of Φ_1 only up to terms involving $P_1(\cos\theta)$.

Using (14), (15), (16), we obtain

$$(17)\qquad \Phi_1 = \frac{A^3}{2} \sum_{n=0}^{\infty} \frac{D_n^3}{\overline{OQ}_{n+1}^2} + A^3 \sum_{n=0}^{\infty} \frac{D_n^3}{\overline{OQ}_{n+1}^3} R\, P_1(\cos\theta)$$

$$+ \frac{A^3}{2} \sum_{n=0}^{\infty} D_n^3 \frac{P_1(\cos\theta)}{R^2} + \text{terms in higher Legendre polynomials.}$$

It is convenient to evaluate $\int_K \Phi_1 dS$ and $\int_K \Phi_1 \cos\theta\, dS$.
Using the orthogonality property of Legendre polynomials,

and (17), (5), (6), we have

$$(18)\qquad \int_K \Phi_1 dS = 2\pi A^3 \sum_{n=0}^{\infty} D_n^3 d_{n+1}^2$$

$$(19)\qquad \int_K \Phi_1 \cos\theta dS = \frac{2}{3}\pi A^3 (1 + 3\sum_{n=1}^{\infty} D_n^3) \quad .$$

5. The kinetic energy of the water.

The kinetic energy $\mathcal{T}$ of the water is

$$\mathcal{T} = \frac{1}{2}\rho \int (\text{grad } \Phi)^2 dV = -\frac{1}{2}\rho \int \Phi \frac{\partial \Phi}{\partial n} dS$$

by Green's theorem. By (2), and the Green's theorem

$$\int \Phi_0 \frac{\partial \Phi_1}{\partial n} dS = \int \Phi_1 \frac{\partial \Phi_0}{\partial n} dS,$$

$$\mathcal{T} = -\frac{1}{2}\rho \left[\dot{A}^2 \int \Phi_0 \frac{\partial \Phi_0}{\partial n} dS - 2\dot{A}\dot{B} \int \Phi_1 \frac{\partial \Phi_0}{\partial n} dS + \dot{B}^2 \int \Phi_1 \frac{\partial \Phi_1}{\partial n} dS \right] .$$

The boundary conditions (3), (4) yield

$$(20)\ \mathcal{T} = \frac{1}{2}\rho \left[\dot{A}^2 \int_K \Phi_0 dS - 2\dot{A}\dot{B} \int_K \Phi_1 dS + \dot{B}^2 \int_K \Phi_1 \cos\theta dS \right] .$$

The integrals appearing in (20) have been calculated in the preceding sections. By (13), (18), (19),

$$(21)\ \mathcal{T} = 2\pi\rho A^3 \left[(1+f_0)\dot{A}^2 - 2f_1 \dot{A}\dot{B} + (\tfrac{1}{6}+f_2)\dot{B}^2 \right] ,$$

where the coefficients f_o, f_1, f_2 are the following functions of the quantity $\alpha = \frac{A}{2B}$:

$$(22)\quad \begin{cases} f_o = D_1 + \sum_{n=1}^{\infty} \left[D_{n+1} - \frac{1}{D_{n-1}} \log \frac{d_{n+1}}{d_n} \right] \\ f_1 = \frac{1}{2} \sum_{n=0}^{\infty} D_n^3 \, d_{n+1}^2 \\ f_2 = \frac{1}{2} \sum_{n=1}^{\infty} D_n^3 \quad . \end{cases}$$

The expressions for d_n, D_n as functions of α are given in (9) and (6).

The series for f_o, f_1, f_2 converge for $\alpha \leqq 1/2$ (which means $A \leqq B$). They are tabulated in table 4 below. Expansions in powers of α begin as follows:

$$f_o = \alpha + \tfrac{1}{2}\alpha^4 + \cdots$$

$$f_1 = \tfrac{1}{2}\alpha^2 + \tfrac{1}{2}\alpha^5 + \cdots$$

$$f_2 = \tfrac{1}{2}\alpha^3 + \tfrac{1}{2}\alpha^6 + \cdots$$

The expansions for $\sqrt{1 + f_o}$, $\dfrac{df_o/d\alpha}{\sqrt{1 + f_o}}$ required in part III, begin as follows:

$$(24)\quad \begin{cases} \sqrt{1 + f_o} = 1 + \frac{1}{2}\alpha \\ \dfrac{df_o/d\alpha}{\sqrt{1 + f_o}} = 1 - \frac{1}{2}\alpha + \quad . \end{cases}$$

α	f_0	f_1	f_2	$\frac{df_0}{d\alpha}$	$\frac{df_1}{d\alpha}$	$\frac{df_2}{d\alpha}$
0	0	0	0	1.00	0	0
.02	.020	.000	.000	1.00	.02	.00
04	040	001	000	1.00	04	00
06	060	002	000	1.00	06	01
08	080	003	000	1.00	08	01
.10	.100	.005	.001	1.00	.10	.02
12	120	007	001	1.00	12	02
14	140	010	001	1.01	14	03
16	160	013	002	1.01	16	04
18	181	016	003	1.01	18	05
.20	.201	.020	.004	1.02	.20	.06
22	221	024	005	1.03	23	07
24	242	029	007	1.03	25	09
26	263	035	009	1.04	28	11
28	283	040	011	1.05	30	13
.30	.305	.047	.014	1.08	.33	.15
32	326	053	017	1.09	36	17
34	348	061	021	1.11	39	20
36	371	070	025	1.15	43	23
38	394	078	030	1.18	48	27
.40	.418	.088	.036	1.23	.53	.32
41	430	094	039	1.26	57	35
42	443	100	043	1.29	60	38
43	456	106	047	1.34	65	42
44	470	112	051	1.40	69	46
.45	.484	.120	.056	1.45	.76	.52
46	499	128	062	1.54	84	60
47	515	136	068	1.64	95	70
48	532	147	076	1.81	1.12	86
49	551	159	085	2.26	1.55	1.27
.50	.577	.178	.101	∞	∞	∞

Table 4.

A comparison with the complete table shows that $1 + \frac{\alpha}{2}$ is a very close approximation to $\sqrt{1 + f_o}$ for all $\alpha \leq \frac{1}{2}$, and differs from it by less than 1 percent. On the other hand, $1 - \frac{\alpha}{2}$ is not too good an approximation to $\frac{df_o/d\alpha}{\sqrt{1 + f_o}}$. Further terms in the expansion of $\frac{df_o/d\alpha}{\sqrt{1 + f_o}}$ are not necessary since they produce only small deviations from the formulas (3.12) and (3.11).

6. Approximate theory for a sphere pulsating between a rigid wall and a free surface.

Consider a pulsating bubble at a distance b from a rigid wall and a distance c from a free surface.* For convenience, the free surface will appear vertical in the diagram.

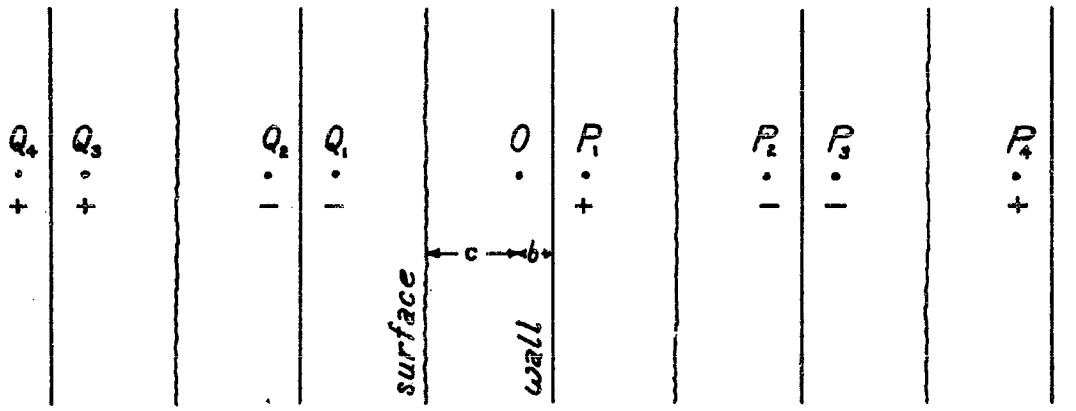

If O is the original position of the center of the sphere, the successive images with respect to the rigid wall and free surface will be at P_1, Q_1; P_2, Q_2; P_3, Q_3; etc. Their distances from O will be given by the following

---

* See [6].

formulas:

$$\overline{OP}_n = 2m(b+c) \quad \text{if} \quad n = 2m$$

$$= 2m(b+c) + 2b \quad \text{if} \quad n = 2m + 1$$

$$\overline{OQ}_n = 2m(b+c) \quad \text{if} \quad n = 2m$$

$$= 2m(b+c) + 2c \quad \text{if} \quad n = 2m + 1$$

The signs of the images are given in the diagram.

Images with respect to the sphere will be neglected.

The first term in the expansion of f_o in powers of a can be obtained by finding the potential at O of the infinite series of images P_1, Q_1, P_2, Q_2, etc. Some simple algebraic transformations lead to the formula

$$f_o = \frac{a}{b+c}(2xf(x) - \log 2)$$

where $x = \frac{c-b}{c+b}$ and

$$f(x) = \frac{1}{1-x^2} - \frac{1}{9-x^2} + \frac{1}{25-x^2} \cdots$$

It is to be noted that

$$\frac{\partial f_o}{\partial b} = -\frac{4a}{(b+c)^2}[f(x) + xf'(x)]$$

To facilitate comparison with previous results,

f_o and $\frac{\partial f_o}{\partial b}$ can be written as follows:

$$f_o = \frac{a}{2b}(1-x)(2xf(x) - \log 2) = \frac{a}{2b}F(x)$$

$$\frac{\partial f_o}{\partial b} = -\frac{a}{2b^2}2(1-x)^2[f(x) + xf'(x)] = -\frac{a}{2b^2}G(x)$$

A short table for $F(x)$ and $G(x)$ is given on page 36.

Appendix III. Numerical Evaluation of Some Definite Integrals

In part III, the problem of evaluating the definite integrals in equations (3.7), (3.11) arose. These integrals have square root singularities at the limits of integration. In this appendix we shall develop a quadrature formula, which was used for this evaluation but does not seem to be as well-known as it should. It is based on Tchebycheff polynomials.

The nth Tchebycheff polynomial $T_n(x)$, $-1 \leq x \leq 1$, is defined by

$$T_n(x) = \cos(n \arccos x),$$

or in other terms, $T_n(x) = \cos n\theta$, where $x = \cos \theta$. The Tchebycheff polynomials are orthogonal with respect to the weight function $\frac{1}{\sqrt{1-x^2}}$, i. e.,

$$\int_{-1}^{1} \frac{T_n(x)\, T_m(x)}{\sqrt{1 - x^2}}\, dx = 0 \qquad \text{if } n \neq m.$$

This follows immediately when we make the transformation $x = \cos \theta$.

By virtue of the orthogonality property, the following theorem can be proved:

Theorem. Let $x_1, x_2, \ldots, x_n$ be the n zeros of $T_n(x)$ in the range $-1 \leq x \leq 1$. Let $f(x)$ be any polynomial of degree at most $2n-1$. Then

$$\frac{1}{\pi} \int_{-1}^{1} \frac{f(x)}{\sqrt{1-x^2}}\, dx = \frac{1}{n} \sum_{i=1}^{n} f(x_i).$$

The proof is similar to the proof of the Gauss quadrature formula. This theorem indicates an exact evaluation of the integral involving $2n$ parameters (a polynomial of degree $2n-1$) in terms of n specially selected points. It is exactly analogous to the more well known Gauss quadrature formula, but it is simpler in two ways: the zeros $x_1,\dots,x_n$ of $T_n(x)$ are easy to obtain, since they are merely the zeros of $\cos n\theta$ where $x = \cos\theta$; and the weight factors multiplying $f(x_i)$ are all equal to $1/n$.

If $f(x)$ is not exactly equal to a polynomial of degree $2n-1$ but can be approximated by one, we can write the approximate quadrature formula

$$\frac{1}{\pi}\int_{-1}^{1}\frac{f(x)}{\sqrt{1-x^2}}\,dx \sim \frac{1}{n}\sum_{i=1}^{n} f(x_i) \quad .$$

The accuracy of this approximate formula depends on the closeness with which $f(x)$ can be approximated by polynomials of degree $2n-1$.

The integrals in question in part III are of the form

$$\int_{a_0}^{a_1}\frac{a^v}{\sqrt{1 - a^3 - \frac{k}{a^{3/4}}}}\,da$$

where v is some exponent, and a_0, a_1 are the two zeros of the expression under the square root sign. This can be written as

$$\int_{a_0}^{a_1} a^v \cdot \frac{\sqrt{(a_1 - a)(a - a_0)}}{\sqrt{1 - a^3 - \frac{k}{a^{3/4}}}} \cdot \frac{da}{\sqrt{(a_1 - a)(a - a_0)}} \quad .$$

where the function $a^{\nu} \cdot \dfrac{\sqrt{(a_1 - a)(a - a_0)}}{\sqrt{1 - a^3 - \dfrac{k}{a^{3/4}}}}$ has no singularities and is rather smooth. The integral can now be evaluated by using the Tchebycheff quadrature formula (changing the range of integration by a linear transformation from a_0, a_1 to -1, 1). The integrals were evaluated in this way by using the 5 zeros of $T_5(x)$, with the results stated in part III. The accuracy depends on the closeness with which the remaining factor $a^{\nu} \cdot \dfrac{\sqrt{(a_1-a)(a-a_0)}}{\sqrt{1 - a^3 - \dfrac{k}{a^{3/4}}}}$ can be approximated by a 9th degree polynomial. It is fortunate that the integrand need be computed only for 5 intermediate points. (Also, the values obtained by using the three zeros of $T_3(x)$ agree within 1 percent with the values quoted.)

It is of interest to see how the momentum $\bar{s}$ depends on the parameter k. If the explosion takes place near the surface, say for a model experiment, the value of k would be approximately .16. For k = .16, the computations yield

$$\bar{s} = -\frac{1}{b_o^2}\left(.127 - \frac{.022}{b_o}\right) + \frac{1}{d-b_o}\left(.760 + \frac{.165}{b_o}\right)$$

in place of (3.12). All the constants have increased, but the alternate additions and substractions tend to cancel these increases. Thus, the new equation for the stabilized position, where $\bar{s} = 0$, is

$$d = 6b_o^2 + 3.32b_o + .4$$

which is practically identical with (3.13). The total period for this case turns out to be

$$\bar{t} = 1.48\left(1 + \frac{.189}{b_o}\right)$$

which is practically identical with (3.10).

Finally, if the internal energy is neglected, i.e., if $k = 0$, the integrals become Beta functions and

$$\bar{s} = -\frac{1}{b_o^2}\left(.182 - \frac{.033}{b_o}\right) + \frac{1}{d-b_o}\left(.934 + \frac{.212}{b_o}\right)$$

$$\bar{t} = 1.49\left(1 + \frac{.203}{b_o}\right).$$

The stabilized position where $\bar{s} = 0$ is

$$d = 5.1b_o^2 + 3.1b_o + .4 .$$

These deviate somewhat from (3.12) and (3.13).

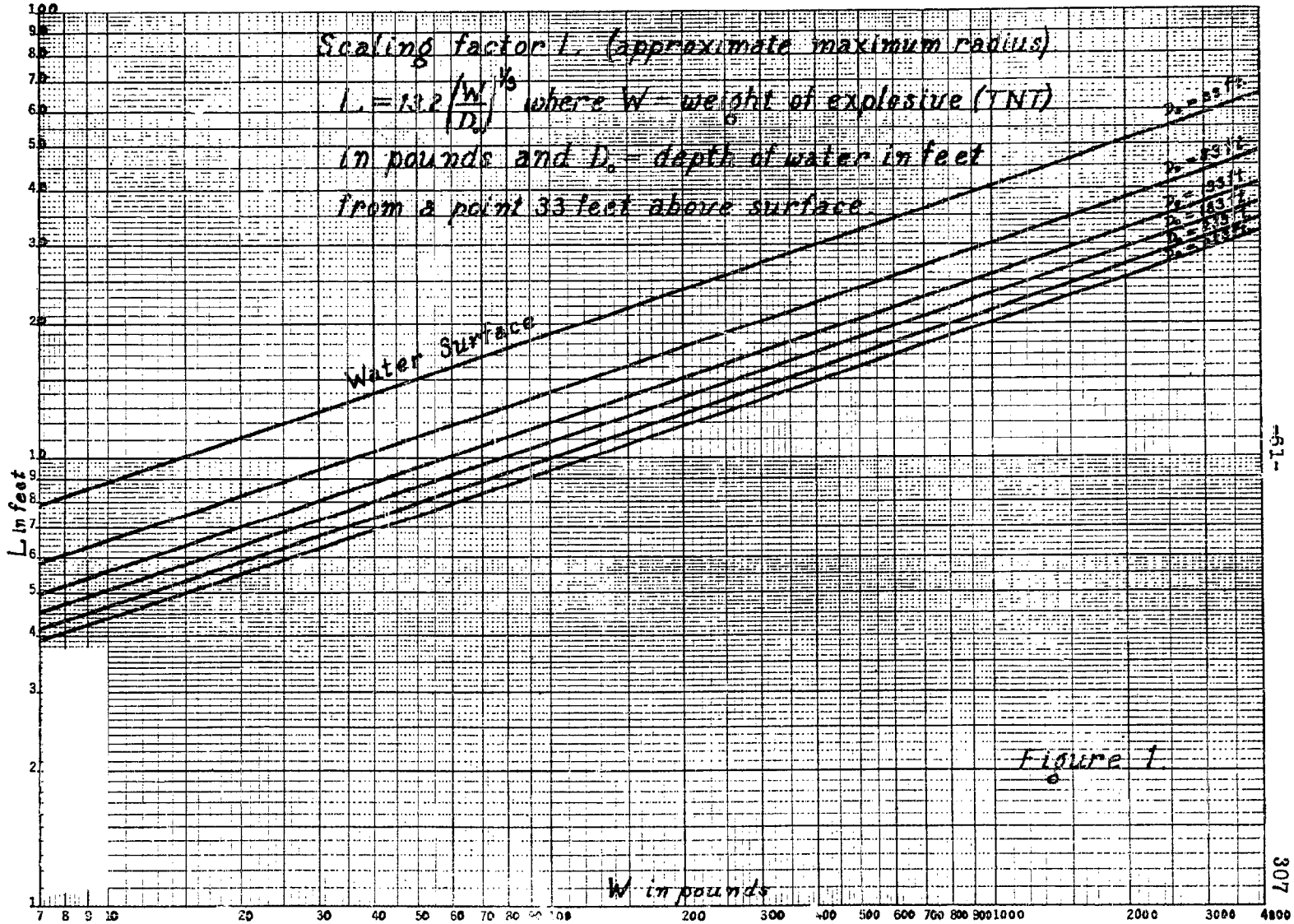
Scaling factor L (approximate maximum radius)
$L = 1.32 \left(\frac{W}{D_o}\right)^{1/3}$ where W = weight of explosive (TNT)
in pounds and D_o = depth of water in feet
from a point 33 feet above surface
Water Surface
L in feet
W in pounds
D_o = 33 ft.
D_o = 43 ft.
D_o = 53 ft.
D_o = 63 ft.
D_o = 73 ft.
D_o = 83 ft.

Figure 1.

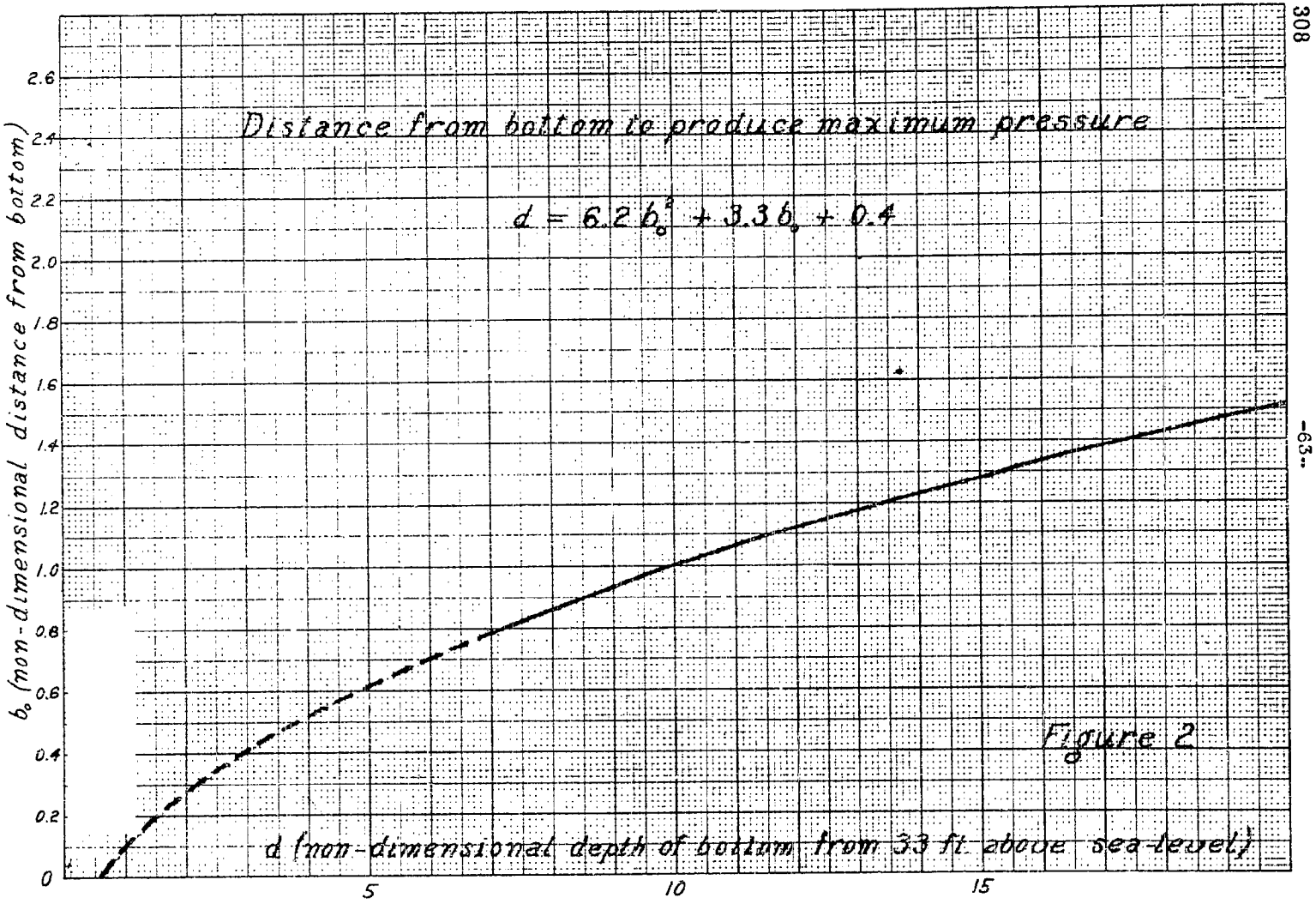
Distance from bottom to produce maximum pressure
$d = 6.2\,b_o^2 + 3.3\,b_o + 0.4$
b_o (non-dimensional distance from bottom)
d (non-dimensional depth of bottom from 33 ft above sea-level)
0
0.2
0.4
0.6
0.8
1.0
1.2
1.4
1.6
1.8
2.0
2.2
2.4
2.6
5
10
15

Figure 2

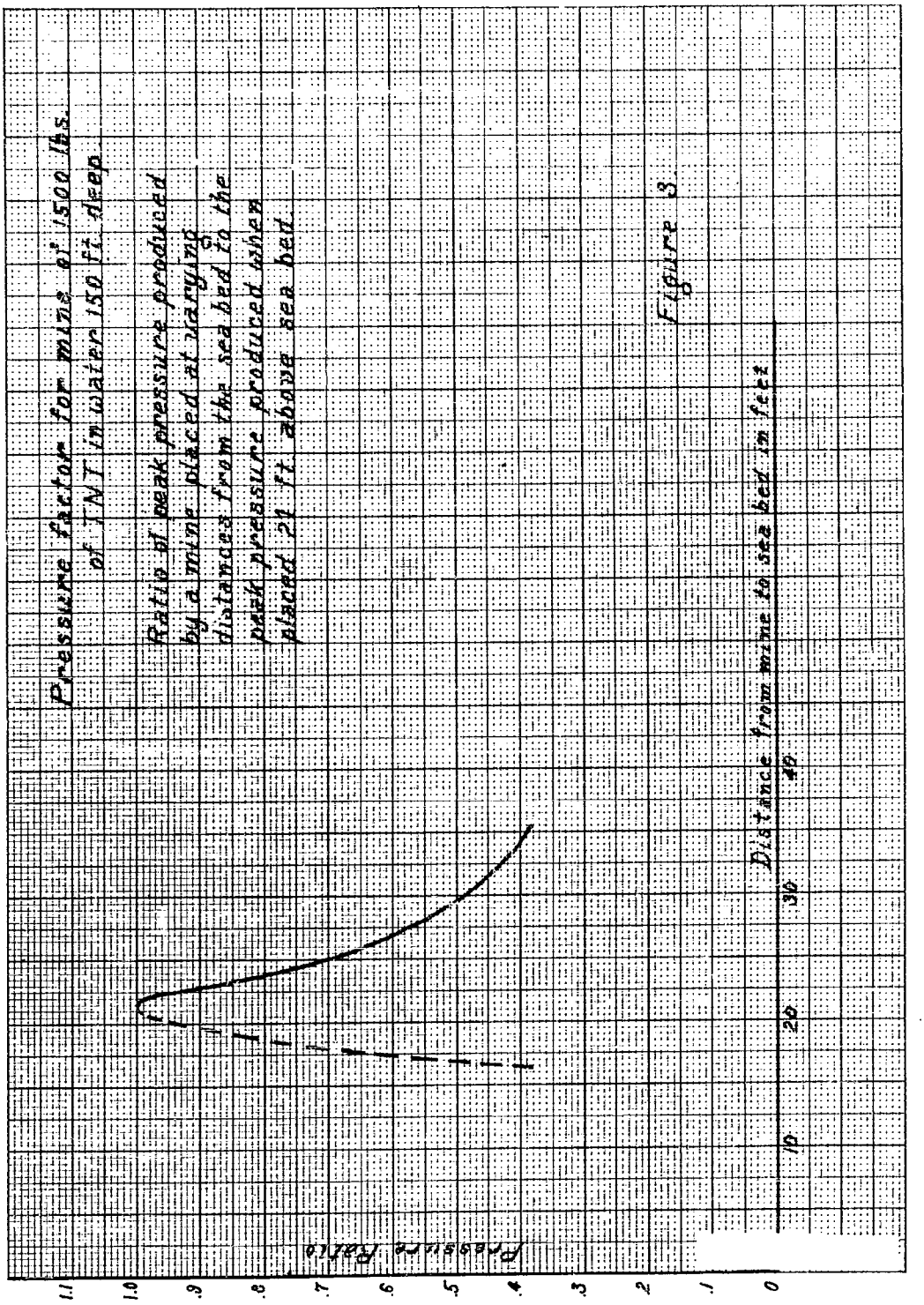
Pressure factor for mine of 1500 lbs.
of TNT in water 150 ft deep.
Ratio of peak pressure produced
by a mine placed at varying
distances from the sea bed to the
peak pressure produced when
placed 21 ft above sea bed.
Pressure Ratio
1.1
1.0
.9
.8
.7
.6
.5
.4
.3
.2
.1
0
10
20
30
40
Distance from mine to sea bed in feet

Figure 3.

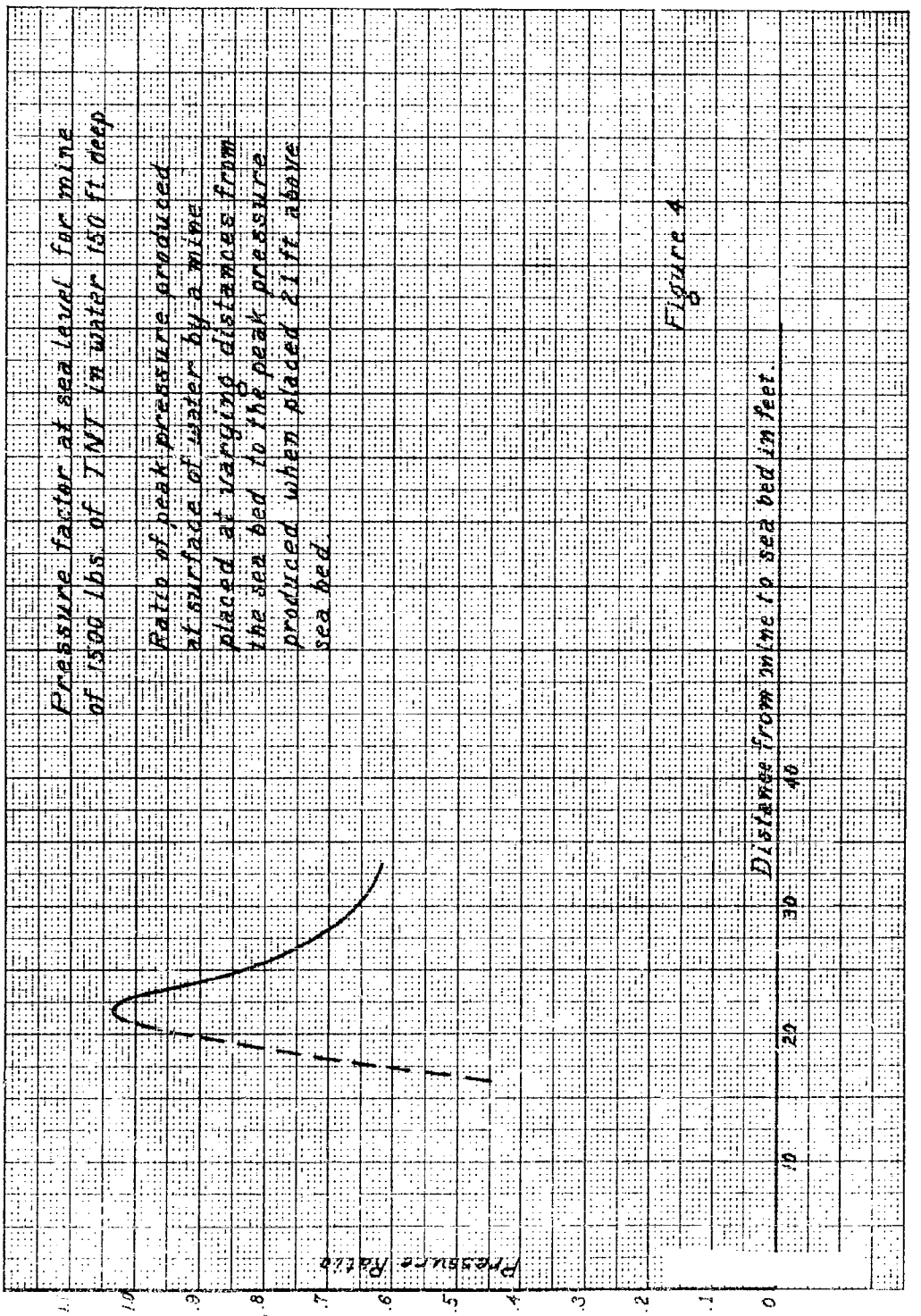
Pressure factor at sea level for mine of 1500 lbs of TNT in water 150 ft deep
Ratio of peak pressure produced at surface of water by a mine placed at varying distances from the sea bed to the peak pressure produced when placed 2.1 ft above sea bed
Pressure Ratio
1.0
.9
.8
.7
.6
.5
.4
.3
.2
.1
0
10
20
30
40
Distance from mine to sea bed in feet.

Figure 4

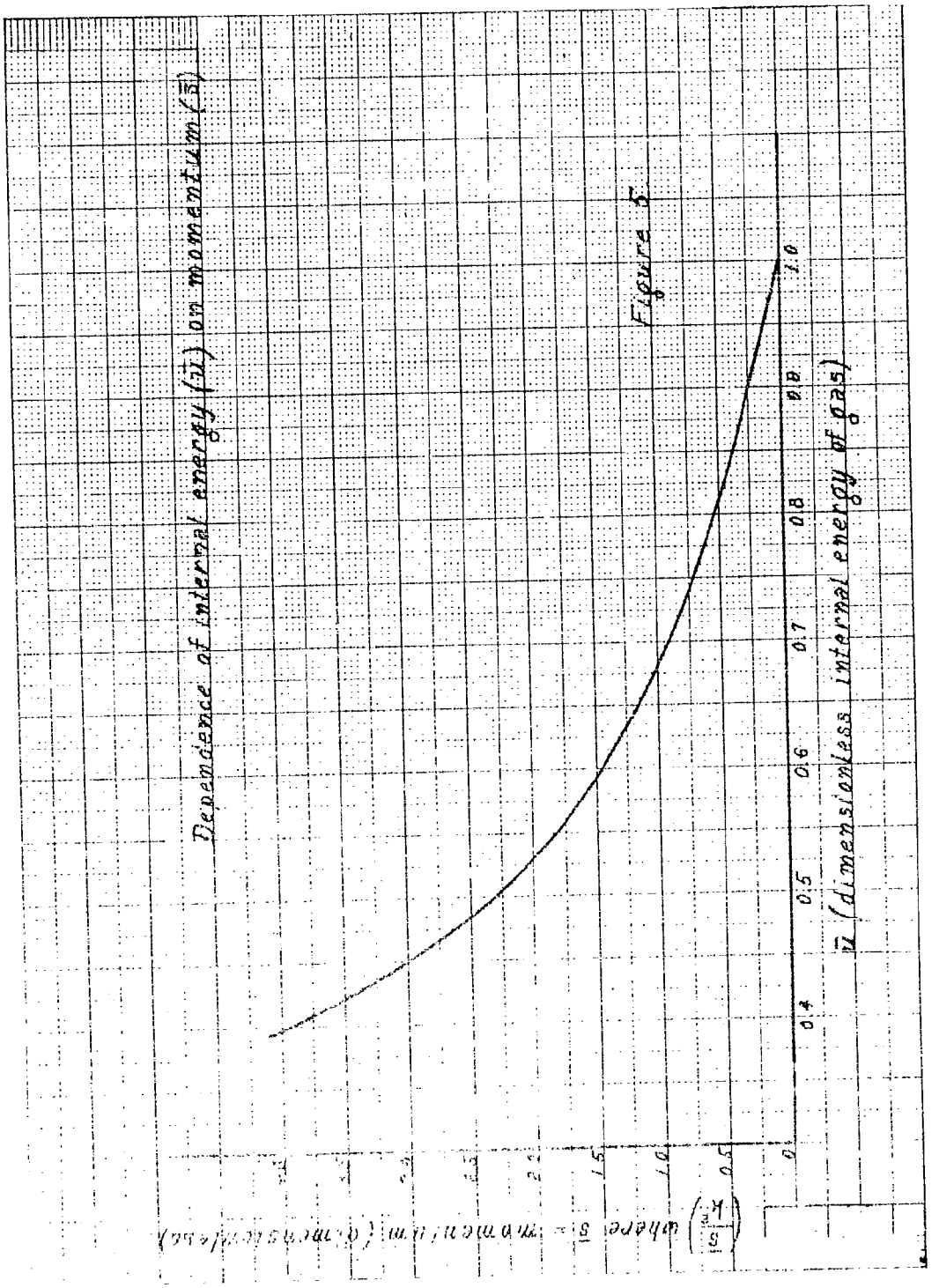
Dependence of internal energy ($\bar{\varepsilon}$) on momentum ($\bar{\pi}$)
$\bar{\varepsilon}$ (dimensionless internal energy of gas)
$\bar{\pi}$ (dimensionless momentum of gas)
0.4
0.5
0.6
0.7
0.8
0.9
1.0

Figure 5

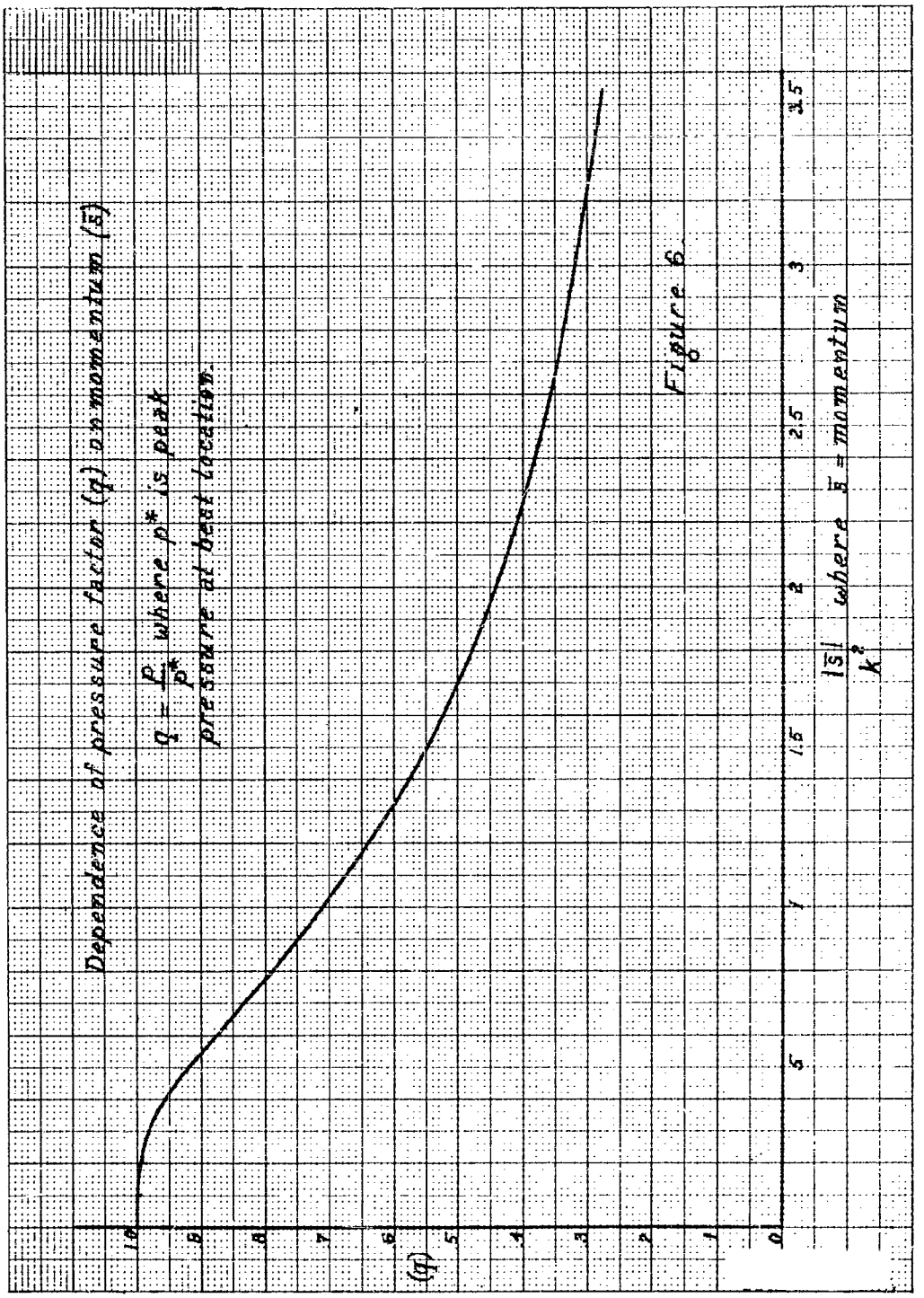
Dependence of pressure factor (q) on momentum (k)
q = p/p* where p* is peak pressure at best location.
(q)
1.0
.9
.8
.7
.6
.5
.4
.3
.2
.1
0
.5
1
1.5
2
2.5
3
3.5
|k| where k = momentum

Figure 6

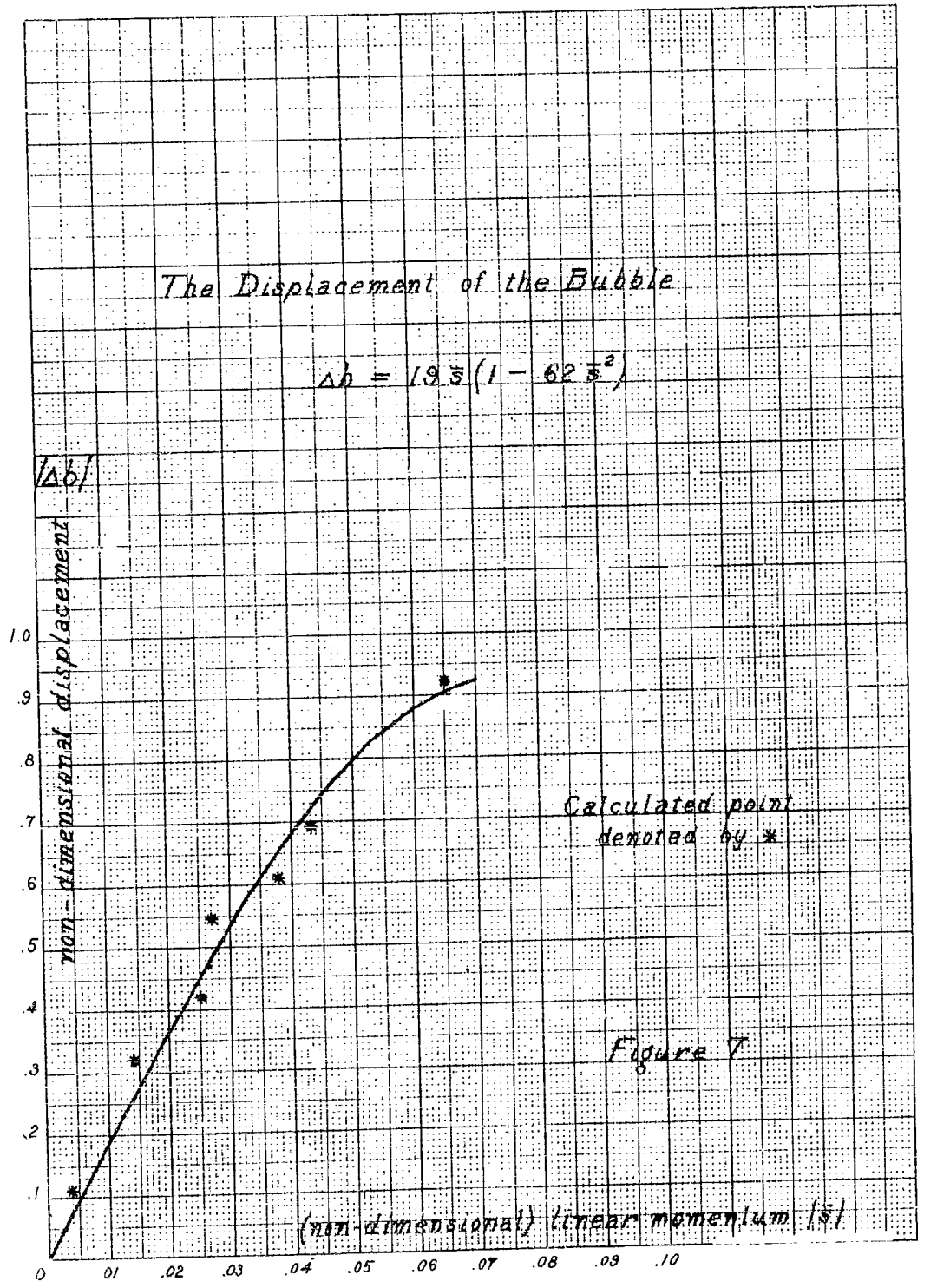
The Displacement of the Bubble
$\Delta b = 1.9\bar{s}(1 - .62\bar{s}^2)$
$|\Delta b|$
non-dimensional displacement
1.0
.9
.8
.7
.6
.5
.4
.3
.2
.1
0
.01
.02
.03
.04
.05
.06
.07
.08
.09
.10
Calculated point denoted by *
(non-dimensional) linear momentum $|\bar{s}|$

Figure 7

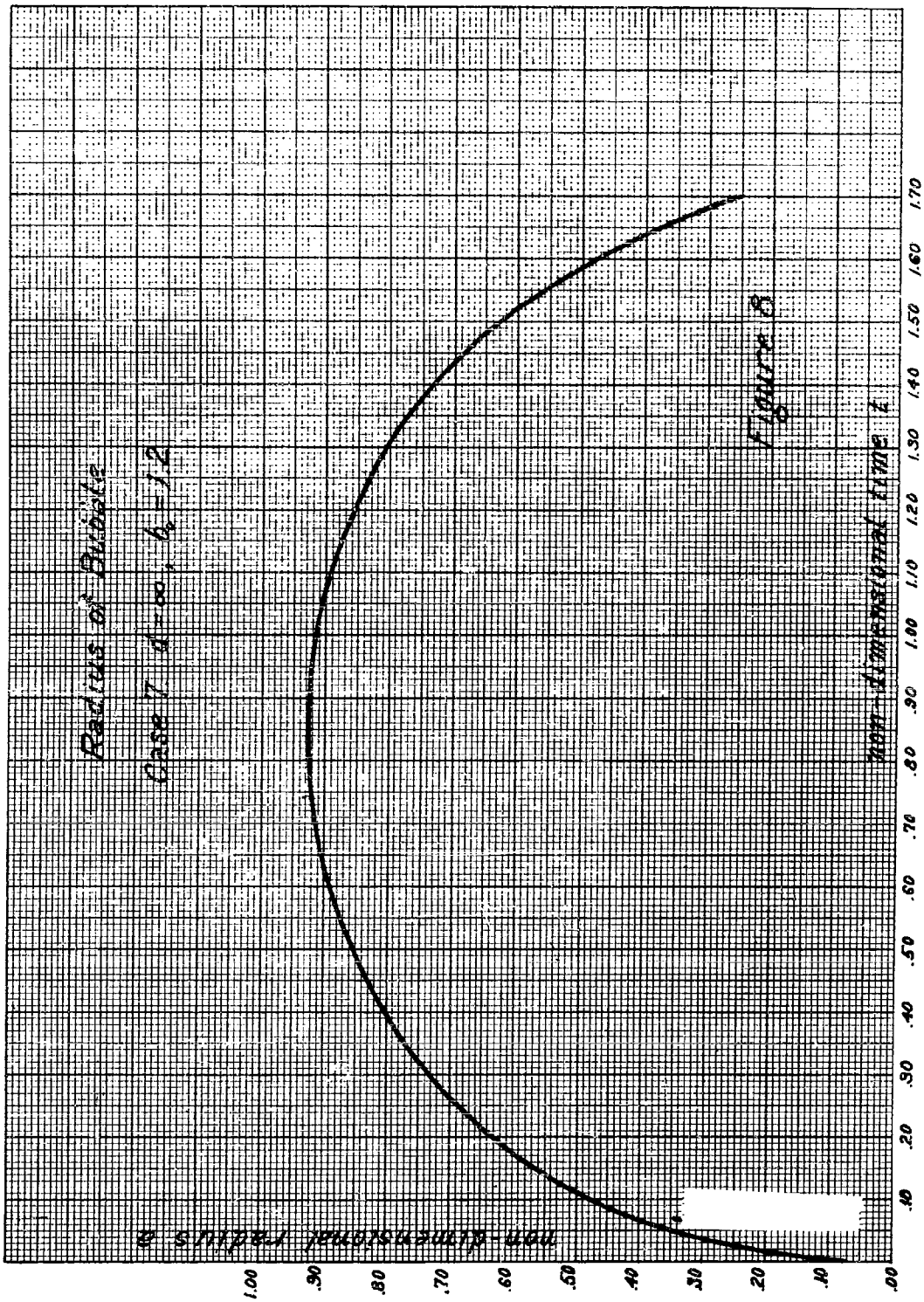
Radius of Bubble
Case 17 d=∞, b=1.2
Figure 8
Non-dimensional time t
Non-dimensional radius R

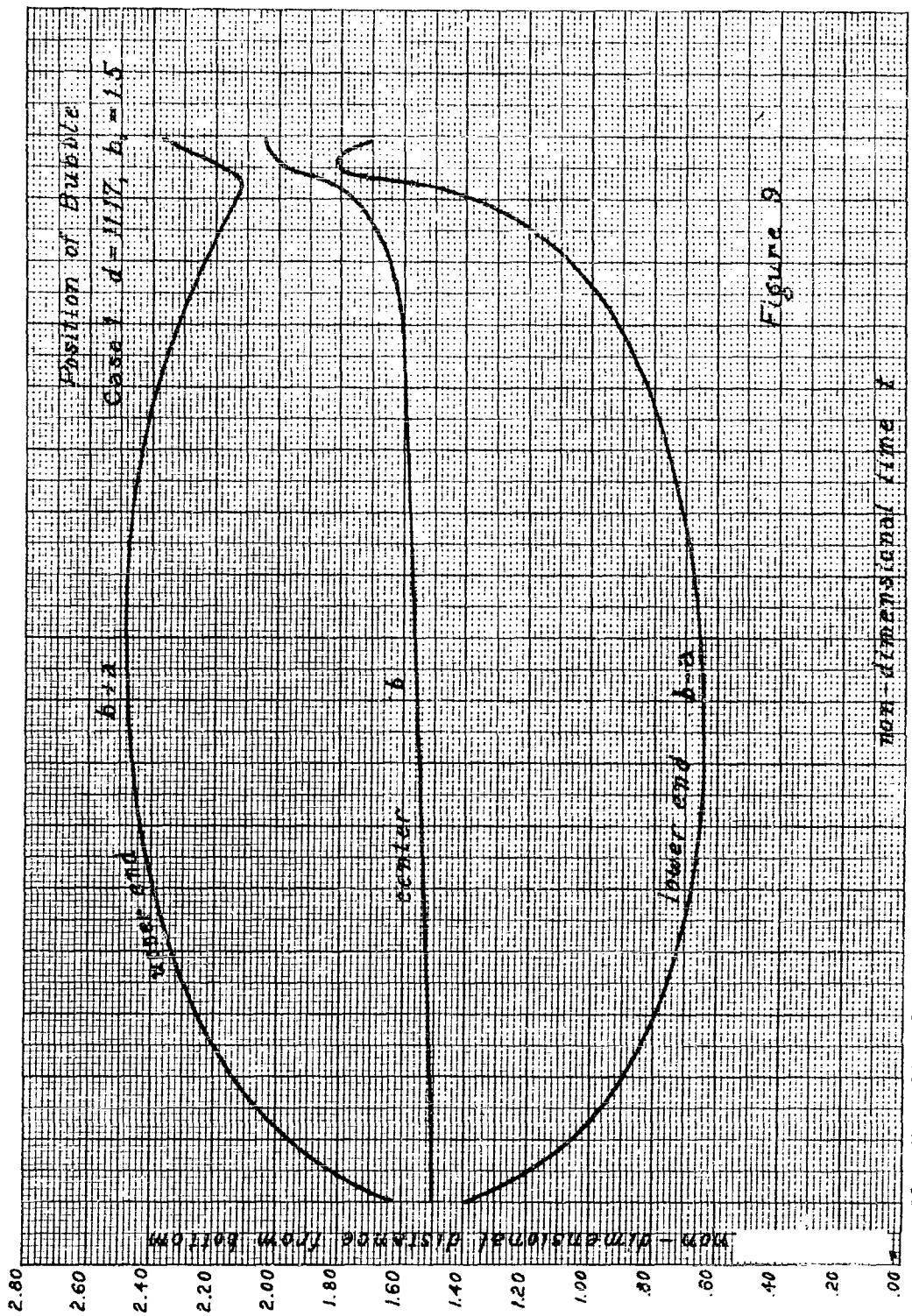
Position of Bubble
Case I d = 11.17, h₁ = 1.5
h/2
upper end
center
lower end h-a
non-dimensional time t
non-dimensional distance from bottom
.00
.10
.20
.30
.40
.50
.60
.70
.80
.90
1.00
1.10
1.20
1.30
1.40
1.50
1.60
1.70
2.80
2.60
2.40
2.20
2.00
1.80
1.60
1.40
1.20
1.00
.80
.60
.40
.20
.00

Figure 9

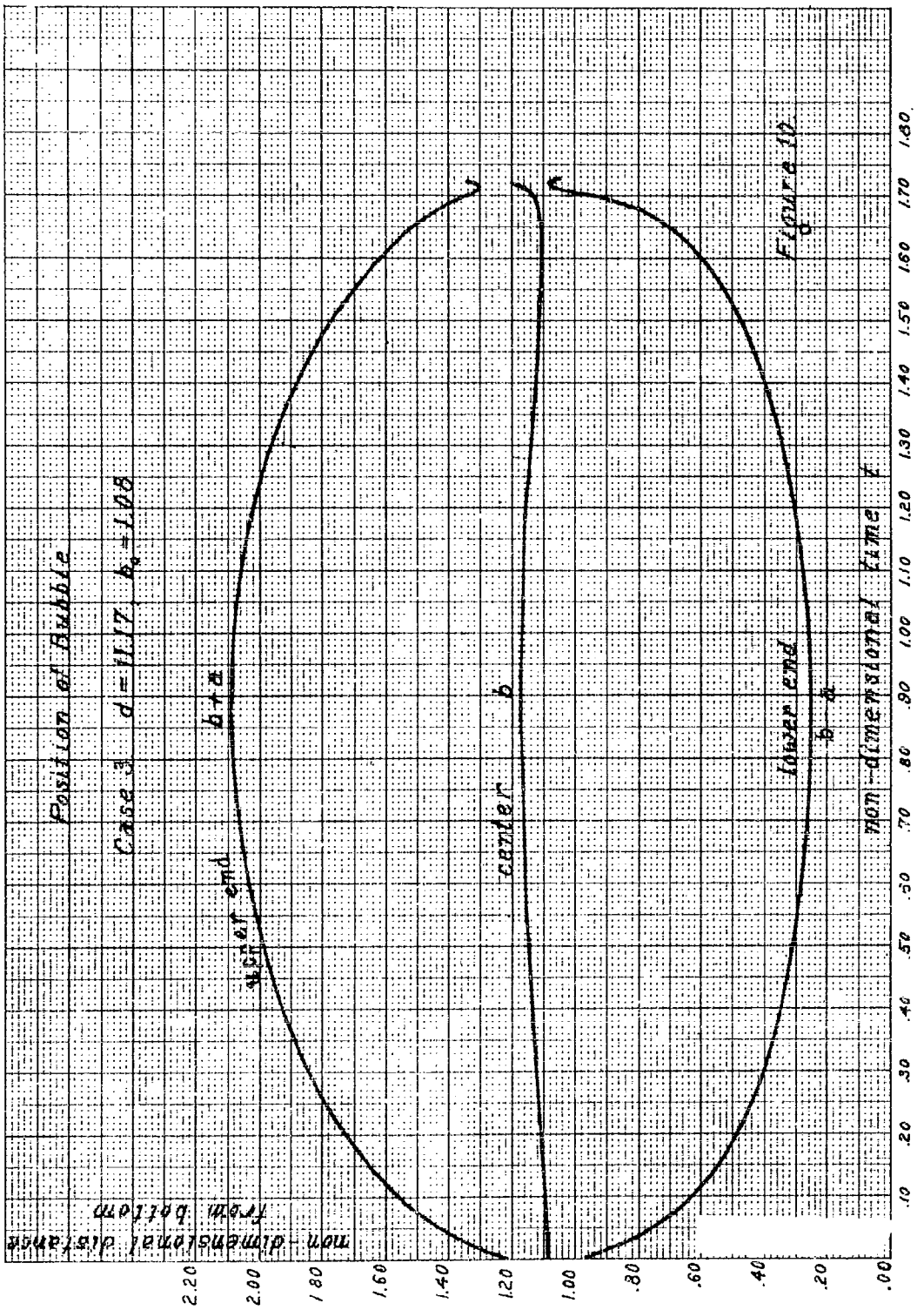
Position of Bubble
Case 3 d=1.17, h_o=1.08
b+x
upper end
center b
lower end
b
x
non-dimensional time t
non-dimensional distance from bottom
.00
.20
.40
.60
.80
1.00
1.20
1.40
1.60
1.80
2.00
2.20
.10
.20
.30
.40
.50
.60
.70
.80
.90
1.00
1.10
1.20
1.30
1.40
1.50
1.60
1.70
1.80

Figure 10

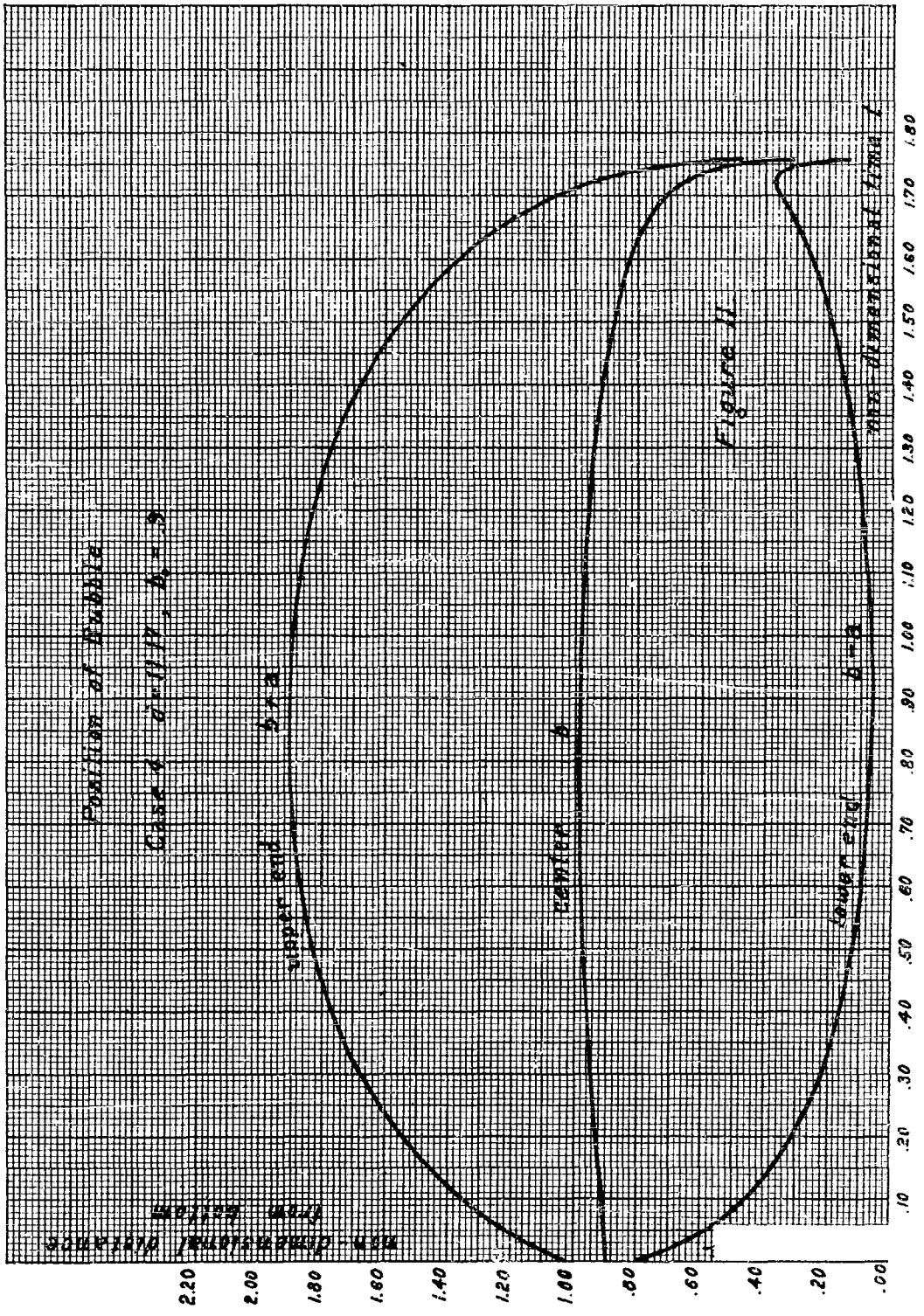
Positions of Rabbits
Case 4 Trial 2
Upper end
Center
Lower end
Figure 11
Non-dimensional distance
Non-dimensional time

SUMMARY OF FORMULAS

1. Scaling factors (for T. N. T.):

$$L = 13.2 \left(\frac{W}{D}\right)^{1/3} \text{ ft.}$$

$$C = 2.85 \frac{W^{1/3}}{D_o^{5/6}} \text{ sec.}$$

where W = weight of T. N. T. in lbs., D_o = distance, in feet, of the explosion from a point 33 ft. above sea level.

2. Period of pulsation:

$$\bar{T} = 1.47C = 4.19 \frac{W^{1/3}}{D_o^{5/6}} \text{ sec.}$$

in the absence of outside influences; if the bubble is at a distance b_o from a rigid wall, this is to be multiplied by

$$\left(1 + \frac{.185}{b_o}\right)$$

3. Maximum radius:

If the internal energy of the gas is neglected, the maximum radius of the bubble is L. If the internal energy is allowed for, the maximum radius is $a_1 L$, where a_1 is the largest root of $a^3 + \frac{k}{a^{3/4}} = 1$, and k is given by the formula $k = .0607\ D_o^{1/4}$.

4. Non-dimensional momentum at time of minimum size:

The momentum due to gravity and a rigid bottom is

$$\bar{s} = -\frac{1}{b_o^2}\left(.113 - \frac{.019}{b_o}\right) + \frac{1}{d-b_o}\left(.704 + \frac{.148}{b_o}\right) .$$

5. Peak pressure for the secondary pulse:

The peak pressure is

$$176\,\frac{W^{1/3}}{R}\,q \text{ atmospheres}$$

where R is the distance in feet from the center of the bubble and q is a factor whose graph is drawn in figure 6.

BIBLIOGRAPHY

[1] G. E. Hudson - "Early and Ultimate Damage due to an Underwater Explosion against 10-inch Diaphragms". Taylor Model Basin Report 509, Aug. 1943.

[2] D. E. J. Offord - Admiralty Naval Construction Dept., WA-669-7, Undex 23, May 1943.

[3] G. I. Taylor - "Vertical Motion of a Spherical Bubble and the Pressure Surrounding It". Taylor Model Basin Report 510, Feb. 1943.

[4] C. Herring - "Theory of the Pulsations of the Gas Bubble Produced by an Underwater Explosion". Division C, NDRC Report C4-sr20-010, OSRD 236, Oct. 1941.

[5] M. Shiffman - AMP Memo 37.1; AMG-NYU, No. 7, July 1943.

[6] E. H. Kennard - "Migration of Underwater Gas Globes due to Gravity and Neighboring Surfaces". Taylor Model Basin Report R-182, Dec. 1943.

[7] J. G. Kirkwood - "Memorandum on the Plastic Deformation of Marine Structures by an Underwater Explosion Wave". OSRD No. 788, Aug. 1942.

[8] M. Shiffman - "The Effect of Non-Spherical Shape on the Motion of a Rising Underwater Bubble". AMP Memo 37.5; AMG-NYU, No. 23, Sept. 1943.

[9] H. F. Willis and M. I. Willis - "Underwater Explosions Near the Sea-Bed". HMA/SEE Internal Report No. 142; OSRD No. WA-1078-4, Sept. 1943.

THE BEHAVIOUR OF AN UNDERWATER EXPLOSION BUBBLE
FURTHER APPROXIMATIONS

A. R. Bryant
Road Research Laboratory, London

British Contribution

March 1945

THE BEHAVIOUR OF AN UNDERWATER EXPLOSION BUBBLE
FURTHER APPROXIMATIONS

A. R. Bryant

March 1945

* * * * * * * * *

Summary.

A number of approximate formulae relating to the behaviour of an underwater explosion bubble are presented here as a supplement to the report "The behaviour of an underwater explosion bubble", hereafter called Report A, Taylor's non-dimensional units are used throughout.

The equations and graphs given make possible the calculation of the displacement and momentum of the bubble towards a number of rigid surfaces, viz. an infinite plane, an infinite cylinder, a sphere and a disc. In the case of the infinite plane the equations are based on the work of Schiffman, and on O.S.R.D. Report No. 3841, and are valid right up to the case where the bubble touches the plane at its maximum radius.

For completeness two equations, based on graphs given in Bureau of Ships (U.S. Navy) Report 1944 – 1, are included whereby the minimum radius and the peak pressure in the pulse emitted by the collapsing bubble can be calculated in the case where all surfaces are absent.

Introduction.

This note is an extension of Report A in which equations and graphs were given enabling some of the principal quantities associated with the underwater explosion bubble to be determined approximately. The equations were based on G.I. Taylor's theory of the motion of the bubble together with Conyers Herring's theory of the influence of plane free or rigid surfaces.

The equations of motion of the bubble near an infinite rigid plane have been extended by Schiffman(1), beyond the approximation given by Herring, right up to the case where the bubble touches the plane at its maximum radius. The integration of his equations to give an approximate formula for the momentum and displacement, and a comparison with some exact integrations of the equations have been given in a recent paper(2). In the present note these approximations have been converted into the more familiar non-dimensional units given by Taylor, and slightly modified to make them of more general application.

A number of other approximate formulae relating to the motion of the explosion bubble are added here, some extracted from the report "A simplified theory of the effect of surfaces on the motion of an explosion bubble", hereafter called Report B, in order to bring the collection of approximations in Report A up to date. As in that note, the equations are collected together in Part I for ease of reference, with their derivations omitted. Their derivations are given in Part II.

Notation.

The notation employed is that given in the previous paper. Taylor non-dimensional units are used throughout and denoted by small letters, i.e. all lengths in feet are divided by the length scale factor $L = 10M^{\frac{1}{3}}$, where M is the weight in lb. of T.N.T. having the same total energy as the bubble under consideration. All times are divided by the time factor $(L/g)^{\frac{1}{2}}$, where g is the acceleration due to gravity. As before, all non-dimensional equations will be labelled as such.

Part I .....

PART I.

Summary of Approximation Formulae

The momentum constant m in the presence of an infinite rigid surface.

If the rigid plane is at a distance d below the bubble and is horizontal, the momentum constant m (positive upwards) is

$$m = \frac{0.122}{z_o^{11/6}} - \frac{0.0107\ (z_o - 1)^{2/3}}{d^2 z_o^{11/6}} \qquad \text{(non-dimensional)} \qquad (2)$$

This equation is valid right up to the point where the bubble touches the plane at its maximum radius; the equation differs from the results of full numerical integration by, at most, 5% of the larger values of m, over the range z_o = 1.5 to 16.

If the plane is not horizontal the momentum $\frac{0.0107\ (z_o - 1)^{2/3}}{d^2 z_o^{11/6}}$ directed towards the plane, is to be added vectorially to the momentum $\frac{0.122}{z_o^{11/6}}$ upwards due to gravity.

The Momentum Constant m in the presence of other rigid surfaces.

$$m = \text{(attraction coefficient of surface)}\ (1.11\ a_m^6 z_o) \qquad \text{(non-dimensional)} \qquad (4)$$

or $$m = \text{(attraction coefficient of surface)} \left[\frac{0.0422}{z_o}\right] \qquad \text{(non-dimensional)} \qquad (4a)$$

The attraction coefficient is a geometrical factor tabulated in Report B for a number of surfaces and plotted in Figure 2 for the cylinder, disc and sphere.

Equations (4) and (4a) are only valid when the maximum bubble radius is small compared to the distance between bubble centre and surface.

Relation between momentum constant m and displacement of bubble at end of first oscillation.

Displacement h^1 and momentum constant m have the same direction and are related numerically by

$$h^1 = 3.57\ (m^{\frac{1}{2}} - 0.008) \qquad \text{(non-dimensional)} \qquad (3)$$

or more accurately by the curve in Figure 1. In equation (3) h^1 and m are the numerical values without regard to sign.

Minimum radius a_1 when no surfaces are present.

$$a_1 = 0.446\ z_o^{-11/9} + 0.198\ c \qquad \text{(non-dimensional)} \qquad (5)$$

This equation agrees with 3 or 4 per cent with the values given in Figure 3 of report A. If surfaces are present then equation (7) of that paper must be used.

Peak Pressure in Pulse emitted by Collapsing Bubble.

When no surfaces are present

$$RP_m = 250\ M^{4/9}\ [\ z_o - z_o^{-1/9}] \qquad (6)$$

where .....

where P_m is the peak pressure in lb/square inches, R the distance of the bubble centre in feet, and W the equivalent weight of T.N.T. in lb.; z_o is the non-dimensional depth of the charge. When surfaces are present equations (7) and (8) and Report A must be used.

PART II.

The Attraction of an Explosion Bubble to an Infinite Rigid Plane

Schiffmann's equations for the motion of a bubble close to a rigid plane wall have been integrated in paper O.S.R.O. 3841 for the special case where the wall is horizontal and below the bubble - i.e. the case considered is that of a charge at a distance d non-dimensional units above a rigid sea bed. Their approximate equation is found to agree very closely with the results of their full numerical integration, and, when put in Taylor units, gives

$$m = \frac{1}{z_o^{11/6}} \left\{ - \frac{0.0120}{d^2} + \frac{0.00123}{d^3 z_o^{17/3}} + \frac{0.1218}{z_o^{2/3}} + \frac{0.0157}{d z_o} \right\}$$

(non-dimensional) (1)

Here m is the "momentum constant", which at any instant near to the occurrence of the *minimum bubble radius*, equals $\frac{a^3 v}{z}$, where a is the radius of the bubble and v its linear velocity.

It may be noted that when the rigid plane is infinitely remote - i.e. when $d = \infty$, the formula becomes

$$m = \frac{0.1218}{z_o^{11/6}}$$ (non-dimensional)

This agrees, within 10 to 15 per cent, with the results of exact numerical integration given in previous reports.

Equation (1) is somewhat cumbersome, and accordingly values of m were plotted against $1/d^2$ for a wide range of values of z_o. The following empirical formula has been found to fit the values given by (1) over a very wide range - the error does not exceed 5% of the larger values of m, over the range $z_o = 1.5$ to 16, and $d = \infty$ to 0.3.

$$m = \frac{0.122}{z_o^{11/6}} - \frac{0.0107 \ (z_o - 1)^{2/3}}{d^2 z_o^{11/6}}$$ (non-dimensional) (2)

Here the momentum is positive upwards - i.e. away from the plane.

It is interesting to compare this equation with that given in Report A, based on Conyers Herring's first order theory. This gave

$$m = \frac{0.7 \ a_m^3}{z_o^{5/6}} \left(1 - \frac{0.52 \ a_m^3 \ z_o^{5/3}}{d^2} \right)$$ (non-dimensional)

Now $a_m^3 z_o = 0.195$ - an approximation found to be true within about 4% over the range $z_o = 2$ to $z_o = 8$. Inserting this in the above equation gives

$$m = \frac{0.136}{z_o^{11/6}} - \frac{0.0138 \ z_o^{2/3}}{d^2 z_o^{11/6}}$$ (non-dimensional)

From this it appears that the simple first order theory, valid strictly only for values of d large compared to the maximum bubble radius, is in fact a fair approximation right up to the point where the bubble touches the plane at its *maximum radius*.

If the plane is not horizontal then it is necessary to add the momentum $\frac{0.0107 \ (z_o - 1)^{2/3}}{d^2 z_o^{11/6}}$ directed towards the plane, vectorially to the momentum $\frac{0.122}{z_o^{11/6}}$ upwards due to gravity.

The .....

The Relation between the Momentum Constant m and the Displacement at the End of the First Oscillation.

In order to calculate the displacement of a bubble it is desirable to have some relation between displacement at the end of the first period and the momentum constant m. The method adopted by Conyers Herring, and in Reports A and B, was to assume that in any given case the displacement with the surface present bore the same ratio to the free displacement under gravity of a bubble at the same depth (with surfaces absent) as the momentum bore to that acquired freely under gravity with surfaces absent. This in fact presupposes a linear relation between displacement and momentum at constant depth z_o.

The values of m and displacement h^1 at the end of the first period, as determined from all available full integrations of the equations of motion of the bubble have been collected together in the following table.

TABLE 1.

Relation between Momentum Constant m and Bubble Displacement h^1 (non-dimensional units throughout)

z_o	c	d	m x 10^3	h^1
2	0.08	∞	41.55	0.69
	0.09		41.16	0.69
	0.10		39.95	0.68
	0.11		38.95	0.68
3	0.08	∞	18.85	0.47
	0.09		18.32	0.46
	0.10		17.75	0.45
	0.11		17.5	0.45
4	0.08	∞	10.92	0.345
	0.09		10.70	0.342
	0.10		10.20	0.338
	0.11		10.00	0.328
7.8	0.063	∞	3.46	0.180
7.2	0.063	.6	-1.33	-0.090
7.8	0.063	1.2	2.055	0.117
16.3	0.05	∞	0.82	0.070
16.3	0.05	1.3	0.435	0.042
3.80	0.0975	0.59	5.47	0.240
3.89	0.0975	0.46	1.98	0.125
3.92	0.0975	0.42	0.569	0.0429
3.97	0.0975	0.35	-3.83	-0.212

NOTE: In the last four entries, taken from O.S.R.D. 3841, d is the non-dimensional distance above a rigid surface. In all other entries d is the distance below a free surface. Negative values of m and h^1 mean that the bubble is moving downwards.

It was shown that when the bubble is near its minimum radius the differential equation of radial motion contains only the parameters c and m. Since also the linear velocity of the bubble is a function only of m and the radius a, it seems likely that the displacement will be a function of m and c only. On plotting h^1 against $m^{1/2}$, as in Figure 1, it is seen that all the points lie on the same curve. Thus h^1 is practically independent of c (which varies as the $\frac{1}{16}$th power of the charge weight). Moreover h^1 is independent of the manner in which the momentum is

acquired .....

acquired, since points representing cases in which gravity alone acts lie on the same curve as those in which a free or rigid surface contributes appreciably to the total momentum.

From Figure 1 it follows that the relation

$$h^1 = 3.57\,(m^{1/2} - 0.008) \qquad \text{(non-dimensional)} \qquad (3)$$

agrees very closely with the results of numerical integration down to values of h^1 of 0.015. In equation (3) only the numerical value of h^1 and m are to be taken; clearly the displacement and moemtum will always have the same direction.(3).

The Attraction of the Bubble to Various Surfaces.

It is seen from the foregoing that the general procedure in calculating the displacement of a bubble at the end of its first oscillation falls into two parts, viz: (i) the calculation of the momentum acquired by the bubble towards or away from the surface (to which must be added vectorially the momentum due to gravity), and (ii) the determination of the displacement h^1 from equation (3) or from Figure 1.

In the neighbourhood of an infinite rigid plane the momentum may be calculated from equations (1) and (2), while if the surface is a free plane surface, equations (5) and (5a) of Report A must be used. Similar "approximate" equations have been obtained for a number of surfaces, in particular the sphere(4), infinite cylinder(4) and disc(5). In Report B it was shown that the momentum acquired at the end of the first oscillation towards a rigid surface can be written

$$m = (\text{attraction coefficient of surface})\ (1.11 a_m^{\,6} z_o) \qquad (4)$$

where a_m is the non-dimensional maximum bubble radius. This may be simplified still further by using the approximation $a_m^{\,3} z_o = 0.195$, discussed above, giving

$$m = (\text{attraction coefficient of surface}) \left[\frac{0.0422}{z_o}\right] \qquad (4a)$$

This attraction coefficient, which is a purely geometrical factor, has been multiplied by $4\pi \times (\text{distance})^2$, and plotted in Figure 2, for the sphere, cylinder and disc. In the case of the cylinder the attraction coefficient used is only an approximate expression for a certain integral, and is not valid when the distance of the bubble from the cylinder axis approaches the value of the radius of the cylinder. Over this region the curve is drawn with a broken line; it has been put in by eye since it is known that the curve must tend to the value unity when the distance of the bubble from the cylinder's surface is very small.

When the maximum bubble radius approaches the value of the distance between bubble and surface these equations are no longer strictly valid. Since there are as yet no equations for these surfaces in which still higher order terms are considered, in such cases the approximate equations will be the best estimate. In this connection it is worth noticing that in the one case where such an "exact" theory is available – viz. the infinite rigid plane as treated by Schiffmann – the approximate theory is not much in error even up to the point where the bubble touches the plane.

Formulae for Minimum Radius and Peak Pressure in Pressure Pulse due to Bubble Collapse when Surfaces are Absent.

In Report A equations were given for a_1, the minimum bubble radius, and P_m, the peak pressure in the pulse emitted by the collapsing bubble. The equations were transcendental and required graphical solution. Two alternative equations have been put forward by the U.S. Bureau of Ships(6) to represent the results of solving these transcendental equations. These alternative formulae are thus more convenient for numerical work, and are given here for completeness.

$$a_1 = 0.446\, z_o^{-11/9} + 0.198c \qquad \text{(non-dimensional)} \qquad (5)$$

in .....

In equation (5) the coefficients given by Bureau of Ships have been increased by about 19 per cent to bring them into better accord with the graphs of Report A and with the data obtained from the full numerical integration of the equations of motion.

The Bureau of Ships formula for P_m, is

$$RP_m = 250\, M^{4/9} \left(z_o - z_o^{-1/9}\right) \qquad (6)$$

where the quantities in the brackets are non-dimensional and where R is the distance from the charge in feet, and M the weight in lb. of T.N.T. having the same bubble energy as the actual charge; P_m is in lb/square inch. Equations (5) and (6) agree within about 5 per cent with the curves in Report A and with the results of the full numerical integration of the equations of motion. It is to be noted that since both RP_m and a_1 are functions of the momentum m equations (5) and (6) can only be used when surfaces are absent. If any surfaces are present which cause an appreciable alteration of the momentum m then the original equations in Report A must be used.

References.

(1) The Effect of a Rigid Wall on the Motion of an Underwater Gas Bubble. M. Schiffman. A.M.P. Memo 37:1; AMG-NYU, No. 7. July, 1943.

(2) On the Best Location of a Mine Near the Sea Bed. A.M.P. Rep. 37:1R. AMG-NYU, No. 49. O.S.R.D. 3841. May, 1944.

(3) In O.S.R.D. 3841 a relation between the displacement and momenium is given which becomes, in Taylor units,

$$h^1 z_o^{1/3} = 41.25\,(m z_o^{1/2})\ [\ 1 - 776\,(m z_o^{1/2})^2\ ]$$

This relation agrees quite well with the points obtained from their numerical integration but deviates markedly for higher values of $h^1 z_o^{1/3}$ from the data in Table I. Equation (3) above is therefore to be preferred.

(4) The results are collected in Report B. These equations are called "approximate" since, in contrast to Schiffmann's treatment of the infinite rigid plane, they are obtained by neglecting terms of the order of a_m^3/d^3 and higher powers, d being the distance of the bubble centre from the surface.

(5) "The Attraction of an Underwater Explosion Bubble to a Rigid Disc".

(6) Buships 1944-1.

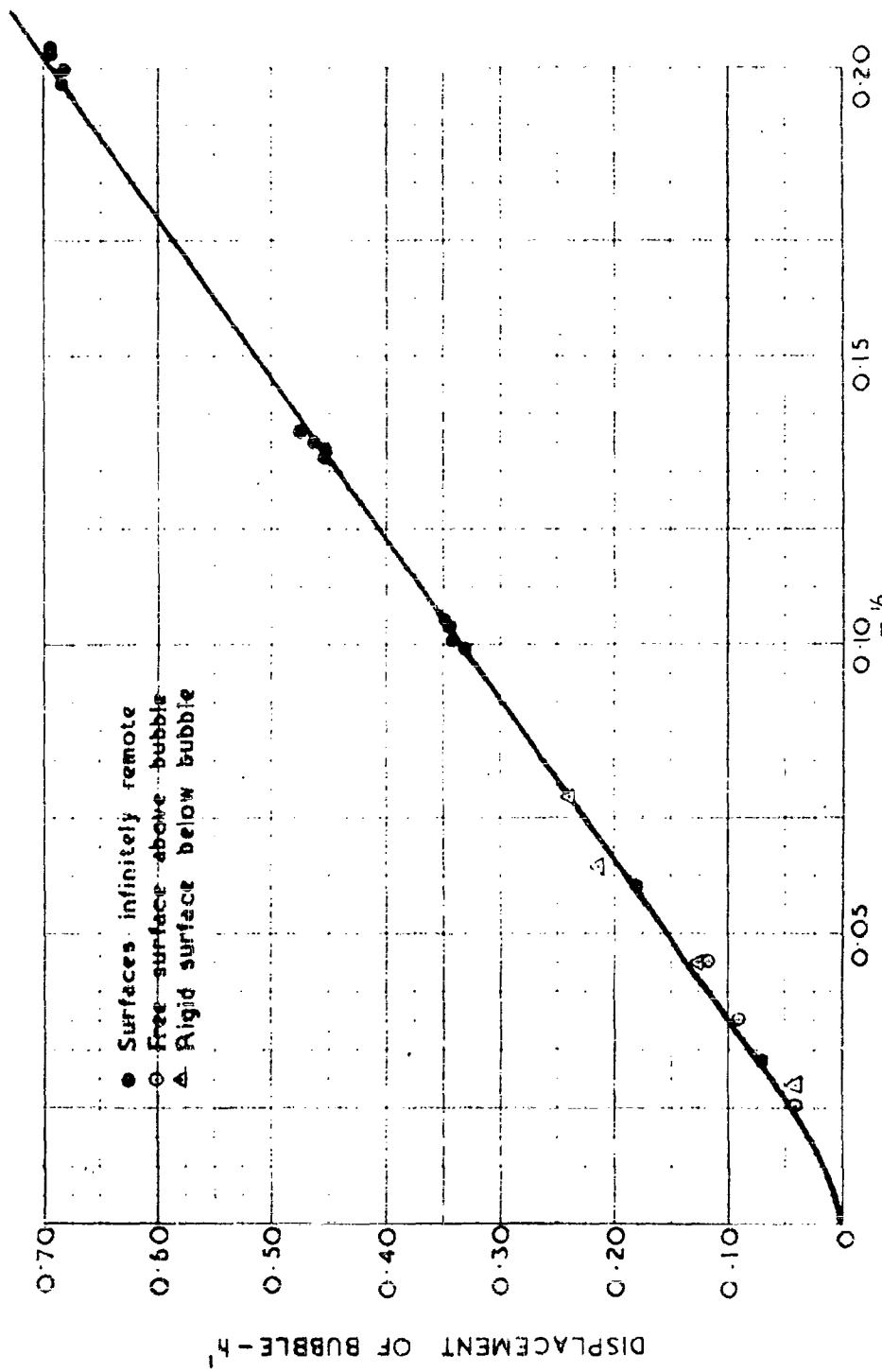

Fig. 1. RELATION BETWEEN BUBBLE DISPLACEMENT AFTER ONE OSCILLATION AND "MOMENTUM CONSTANT" m

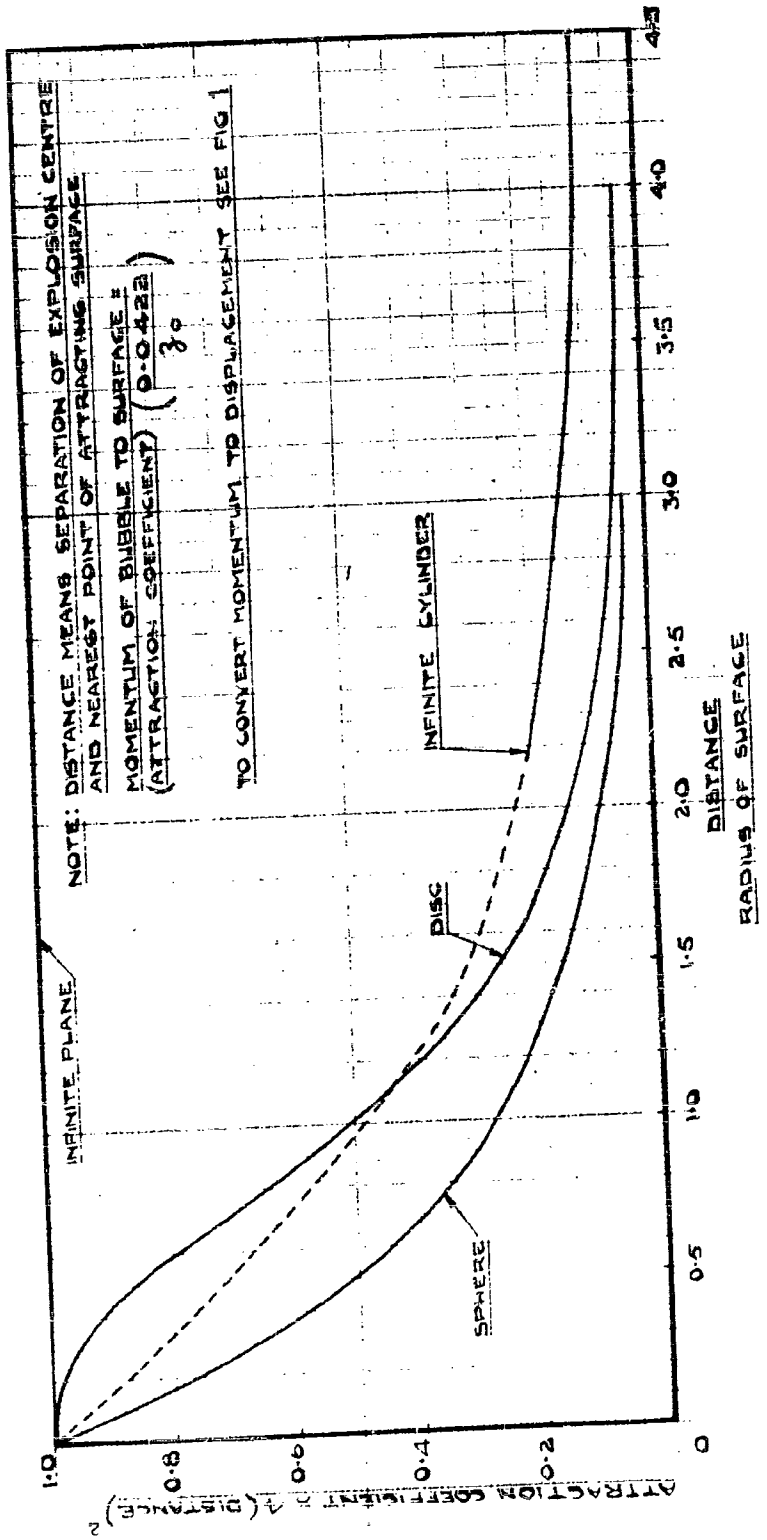
NOTE: DISTANCE MEANS SEPARATION OF EXPLOSION CENTRE AND NEAREST POINT OF ATTRACTING SURFACE
MOMENTUM OF BUBBLE TO SURFACE = (0·0422 / 3ρ) (ATTRACTION COEFFICIENT)
TO CONVERT MOMENTUM TO DISPLACEMENT SEE FIG 1
INFINITE PLANE
INFINITE CYLINDER
DISC
SPHERE
ATTRACTION COEFFICIENT = 4 (DISTANCE)²
DISTANCE
RADIUS OF SURFACE
1·0
0·8
0·6
0·4
0·2
0
0·5
1·0
1·5
2·0
2·5
3·0
3·5
4·0
4·5

FIG 2

THEORY OF UNDERWATER EXPLOSION BUBBLES

B. Friedman
Institute for Mathematics and Mechanics
New York University

American Contribution

September 1947

TABLE OF CONTENTS

	Page
Preface	ii
Introduction	1
Outline	2
Section I: Summary of Formulas	6
Section II: Analysis of Experimental Data . . .	13
Table 1: First Bubble Periods versus Depth .	14
Table 2: $\varphi_1 Z_o^{-1/3}$ versus $\pi Z_o^{5/6}$	15
Section III: Derivation of Formulas	18
Momentum of the Bubble	21
Migration of the Bubble	23
Radius of the Bubble	24
Peak Pressure	24
Section IV: The Electrostatic Problem	27
Potential Function	31
Appendix:	
Tables of f(x) and $\mathcal{F}(x)$	33
Graphs	35-63

THEORY OF UNDERWATER EXPLOSION BUBBLES

Introduction

The theory of the behavior of a gas bubble produced by an underwater explosion has reached such a state of completeness that it seems desirable to give a unified account of some of the main results. When an explosive is detonated under water, a shock wave is first emitted and then the gaseous products of the explosion expand under the influence of their high internal pressure. Because of its inertia, the gas bubble overexpands to a very low pressure and then the hydrostatic pressure of the water recompresses the bubble to nearly its original size. At this stage the bubble starts expanding again and a pressure pulse is emitted. This process of expansion and contraction may occur five or six times before the bubble breaks up and dissolves or escapes from the water.

The behavior of the bubble is affected by the presence of surfaces, such as the bottom of the water, the walls of a tank, the target or the air-water surface. Normally, the bubble would tend to move upward since it is lighter than the surrounding water. However, the free surface of the water repels the bubble while a rigid surface of any kind such as a wall or a bottom attracts it. In some cases these effects may be so strong that the bubble actually moves downward.

Besides influencing the motion of the bubble, the surfaces also change the period of oscillation and modify the size of the peak pressures produced. The theory

presented here explains these effects and gives a quantitative estimate of their size. The values predicted for the period show excellent agreement with those obtained experimentally, while the values predicted for the peak pressure and the distance moved by the bubble show only fair agreement.

An important application of the theory is the determination of the amount of energy left in the bubble after the shock wave has passed. Also the energy in successive bubble oscillations can be found. There is a large amount of energy dissipated in the transition from shock wave stage to bubble motion and also between successive bubble oscillations, which cannot be explained on the basis of the energy radiated by the pressure pulse. The explanation of this large energy dissipation is still unknown.

Outline

As developed in this paper the theory is an extension of that given in AMP Report 37.1R, Studies on the Gas Bubble Resulting from Underwater Explosions: On the Best Location of a Mine Near the Sea Bed. There, the motion of the bubble in the presence of a rigid bottom was investigated and it was shown that the exact theory could be successfully approximated by the addition of a term to the kinetic energy. In this paper we show that the effects of surface, bottom, walls, targets, etc., can all be approximated in the same way by the addition of a suitable term to the kinetic energy. The evaluation of this term depends upon the solution of an "electrostatic problem." In Section IV we work out in detail the case of a bubble between a free surface and a bottom. Other cases can be treated in the same way.

Section I presents a collection of formulas and a summary of methods which can be used to predict the period of oscillation of the bubble, the distance its

center moves during the first oscillation, the maximum and minimum radius of the bubble and, finally, the peak pressure emitted by the bubble. The formulas are given in terms of certain integrals which can be evaluated by the method given in Report 37.1R. Numerical integration of the differential equations of motion of the bubble is completely unnecessary. For convenience Figures 1-6 contain graphs of these integrals for the most frequently occurring values of the parameters.

Section III contains a discussion of these formulas and a short indication of their proof. A careful analysis is made of the dependence of the parameters in the bubble motion upon the properties of the explosive. It is shown that, by a study of the periods of bubbles placed at different depths, it is possible to determine the amount of energy left in the bubble after the shock wave has passed and also to determine the exponent in the equation for the adiabatic expansion of the explosive. This seems to be one of the very few methods by which this exponent can be found.

A similar procedure can be used to determine the amount of energy left in the second bubble oscillation. The experiments indicate that only about 16 percent of the original energy of the explosive remains. Calculations show that the energy radiated by the pressure pulse emitted by the bubble at minimum size is not large enough to explain the energy loss. The explanation of this high dissipation of energy is one of the major unsolved problems of the theory.

As was mentioned before, Section IV contains a solution of the "electrostatic problem" equivalent to the problem of a bubble placed between a rigid bottom and a free surface.

In Section II the theory is applied to the analysis of some experimental data obtained at Woods Hole by Arons

and his co-workers. Three hundred grams of Tetryl were detonated at varying depths below the surface in water 23.5 feet deep. The period of oscillation, the peak pressure and the distance the bubble moved were measured. The agreement between theory and experiment as regards periods is excellent; as regards pressure and distance the bubble moves, the agreement is only fair.

Since the agreement as regards periods is one of the outstanding successes of the theory, it seems worthwhile elaborating on it. Let $\bar{T}$ be the period of oscillation of the bubble at a depth H feet beneath the surface. In Section II it is shown that $\bar{T}(H + 33)^{5/6}$ varies linearly with $\varphi_1(H + 33)^{-1/3}$ where φ_1 is a complicated function of H, so that we have

$$\bar{T}(H + 33)^{5/6} = \alpha + \beta\varphi_1(H + 33)^{-1/3}$$

where α and β are constants independent of H. It is also shown that $\alpha = C_1E^{1/3}$ and $\beta = C_2E^{2/3}$ where E is the amount of energy left in the bubble after the shock wave has passed and C_1 and C_2 are two constants depending upon the exponent in the equation for the adiabatic expansion of the explosive.

From the experimental data, $\bar{T}(H + 33)^{5/6}$ and $\varphi_1(H + 33)^{-1/3}$ are calculated and then the constants α and β are determined by the method of least squares. From the values of α and β the amount of energy left in the bubble and the adiabatic constant can be determined. In the particular case considered in Section II it is found that about 48 percent of the original energy of the explosive is left in the bubble.

Assumptions

As in Report 37.1R we shall idealize the problem by making the following assumptions:

1. The water is an ideal incompressible fluid.
2. The bubble remains spherical in shape.
3. The gas inside the bubble expends adiabatically.

Section I

Summary of Formulas

Units of Length and Time

Let A be the radius of the bubble at time T, B the distance of its center from the bottom, and H the distance from the surface. We put $Z = H + Z^*$, where Z^* is the height of the water column whose pressure equals atmospheric pressure, so that the hydrostatic pressure at

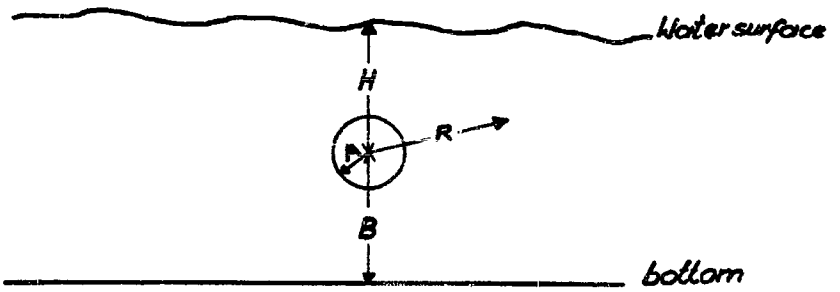

the center of the bubble is $\rho g Z$.

Let E be the amount of energy left in the bubble after the shock wave has passed and let M be the mass of the explosive. We write $E = rQM$ so that rQ is the amount of energy per unit mass of explosive left in the bubble after the shock wave has passed.

All the formulas will be given in dimensionless terms. The unit of length is

$$L = (3E/4\pi\rho g Z_o)^{1/3} \tag{1.1}$$

where Z_o is the value of Z at the time of detonation. The unit of time is

(1.2) $$C = L(2gZ_o/3)^{-1/2}.$$

Note that the unit of velocity is proportional to the square root of Z_o, for

(1.3) $$L/C = (2gZ_o/3)^{1/2}.$$

Parameters in the Bubble Motion

If the pressure and volume of a unit mass of the gas formed by the explosive are connected by the adiabatic relation:

(1.4) $$PV^{\gamma} = K,$$

then the internal energy of the bubble when expressed in non-dimensional terms will depend upon a parameter k which is defined as follows:

(1.5) $$k = K(E/M)^{-\gamma}(\rho g Z_o)^{\gamma-1}/(\gamma - 1).$$

Since $\gamma - 1$ is very close to zero, the value of k will hardly change when Z_o varies slightly. In most cases, therefore, we shall be able to treat k as constant independent of Z_o.

The effects of free surface, gravity and bottom are expressed with the help of a function φ_1. We put

(1.6) $$\varphi_1 = -[f(x) + \log 2]/(H + B) = -\mathcal{F}(x)/H$$

where

(1.7) $$x = \frac{B - H}{B + H}$$

and

(1.8) $$f(x) = 2x \sum_{0}^{\infty} \frac{(-)^n}{(2n + 1)^2 - x^2}$$

and

$$(1.9)\quad \mathcal{F}(x) = \frac{x}{1+x} + (1-x)\left[\sum_{1}^{\infty} \frac{x(-)^n}{(2n+1)^2 - x^2} + \frac{\log 2}{2}\right].$$

Tables and graphs of the functions $f(x)$ and $\mathcal{F}(x)$ are given in the appendix (see Figures 13, 14 and 15 and Tables 3 and 4). Note that if the water is infinitely deep, $B = \infty$ so that from (1.7), (1.9) and (1.6) we have

$$(1.10)\qquad x = 1, \quad \mathcal{F}(x) = 1/2, \quad \varphi_1 = -1/2H.$$

Bubble Quantities at Time of Maximum Size

Small letters, a, b, h, etc., will be used to represent the non-dimensional values of the quantities represented by the corresponding capital letters. The subscript zero attached to these quantities will indicate their value at the beginning of the bubble motion, the subscript one their value at the time of maximum size, and a bar attached to them will indicate their value at the time of recompression when the bubble size is a minimum.

The non-dimensional time from the beginning of the bubble motion to the stage of maximum size is

$$(1.11)\qquad t_1 = I_1 + \frac{1}{2} I_2 L\varphi_1,$$

where

$$(1.12)\qquad I_1 = \int_{a_o}^{a_1} \frac{a^{3/2}\, da}{\sqrt{1 - a^3 - ka^{-3(\gamma-1)}}}$$

and

$$(1.13)\qquad I_2 = \int_{a_o}^{a_1} \frac{a^{5/2}\, da}{\sqrt{1 - a^3 - ka^{-3(\gamma-1)}}}\,.$$

Here, a_o and a_1 denote the smallest and largest roots, respectively, of the denominator. Graphs of I_1 and I_2 for the most frequently occurring values of k and γ are given in Figures 1 and 2.

The vertical momentum at the time of maximum size is

$$(1.14) \quad s_1 = L \frac{\partial \varphi_1}{\partial B}(I_3 - \tfrac{1}{2} L\varphi_1 I_4) + z_o^{-1}(I_5 + \tfrac{1}{2} L\varphi_1 I_6)$$

where

$$(1.15) \quad I_3 = \int_{a_o}^{a_1} a^{5/2}\sqrt{1 - a^3 - ka^{-3(\gamma-1)}}\, da,$$

$$(1.16) \quad I_4 = \int_{a_o}^{a_1} a^{7/2}\sqrt{1 - a^3 - ka^{-3(\gamma-1)}}\, da,$$

$$(1.17) \quad I_5 = \int_{a_o}^{a_1} \frac{a^{9/2}\, da}{\sqrt{1 - a^3 - ka^{-3(\gamma-1)}}},$$

$$(1.18) \quad I_6 = \int_{a_o}^{a_1} \frac{a^{11/2}\, da}{\sqrt{1 - a^3 - ka^{-3(\gamma-1)}}}.$$

The maximum radius of the bubble, a_1, is the root near 1 of the equation:

$$(1.19) \quad a^3 + ka^{-3(\gamma-1)} + 3s_1^2/2a^3 = 1.$$

A good approximation to a_1 is given by the formula:

$$(1.20) \quad a_1 = 1 - \frac{k}{3} - (\frac{\gamma - 1}{3} + \frac{1}{9})k^2 - \frac{3}{2} s_1^2.$$

Bubble Quantities at Time of Minimum Size

The time, $\bar{t}$, from the beginning of the bubble motion to the stage of minimum size is twice the time to the stage of maximum size, that is,

$$(1.21) \quad \bar{t} = 2t_1.$$

The vertical momentum, $\bar{s}$, at the time of minimum size is twice the vertical momentum at the time of maximum size, that is,

$$\bar{s} = 2s_1. \tag{1.22}$$

The minimum radius of the bubble, $\bar{a}$, is the root near zero of the equation:

$$a^3 + ka^{-3(\gamma-1)} + 3\bar{s}^2/2a^3 = 1. \tag{1.23}$$

If we put

$$\xi = k^{1/(\gamma-1)}, \quad \varepsilon = 3\bar{s}^2/2\xi \tag{1.24}$$

and

$$\bar{a}^3 = \xi u, \tag{1.25}$$

then u is the root of the equation:

$$u = u^{2-\gamma} + \varepsilon. \tag{1.26}$$

A graph of u for various values of ε and γ is given in Figure 7.

The non-dimensional distance the bubble moves downward is given approximately by the formula:

$$\Delta b = 3\bar{s}(I_\gamma + \tfrac{1}{2} L\varphi_1 I_\beta) \tag{1.27}$$

where

$$I_\gamma = \int_{\bar{a}}^{a_1} \frac{a^{-3/2}\, da}{\sqrt{1 - a^3 - ka^{-3(\gamma-1)} - 3\bar{s}^2/2a^3}} \tag{1.28}$$

and

$$I_\beta = \int_{\bar{a}}^{a_1} \frac{a^{-1/2}\, da}{\sqrt{1 - a^3 - ka^{-3(\gamma-1)} - 3\bar{s}^2/2a^3}}. \tag{1.29}$$

The non-dimensional peak pressure at the time of minimum size is

$$(1.30)\quad (a^2\dot{a})^{\cdot} = \xi^{-2/3}\, u^{-5/3}\left[\xi^{\frac{3\varepsilon}{2}} + \frac{3(\gamma-1)}{2}\, u^{2-\gamma}\right][1 + \bar{a}L\varphi_1]^{-1}$$

where

$$(1.31)\qquad u = \bar{a}^3\, \xi^{-1}.$$

Actual Values of Bubble Quantities

If $\bar{T}$ is the actual period from the beginning of the bubble motion to the time of minimum size, then

$$\bar{T} = ct$$

or using (1.21), (1.11), (1.1) and (1.2) we find that

$$(1.32)\qquad \bar{T} = \alpha Z_o^{-5/6} + \beta\varphi_1 Z_o^{-7/6}$$

where

$$(1.33)\qquad \alpha = 2I_1(2g/3)^{-5/3}\,(2\pi\rho)^{-1/3}\,E^{1/3},$$

$$(1.34)\qquad \beta = I_2(2g/3)^{-7/6}\,(2\pi\rho)^{-2/3}\,E^{2/3}.$$

Note that

$$(1.35)\qquad \bar{T}Z_o^{5/6} = \alpha + \beta\varphi_1 Z_o^{-1/3},$$

so that $\bar{T}Z_o^{5/6}$ is a linear function of $\varphi_1 Z_o^{-1/3}$. In a later section we shall use this formula to find α and β and then the value of E.

The maximum and minimum radii are found from formulas (1.20) and (1.23) after multiplication by the unit of length, L, given in (1.1).

The peak pressure of the bubble at a distance R from the center of the bubble is

(1.36) $$P = \frac{2}{3}\rho g Z_0 \cdot \frac{L}{R}(a^2\dot{a})^{\cdot}$$

where the value of $(a^2\dot{a})^{\cdot}$ is given by formula (1.30).

At the time of maximum size the pressure in the bubble is

(1.37) $$P_1 = \frac{2}{3}\rho g Z_0 \frac{3(1 - 5a_1^3)}{8a_1^2}$$

Section II

Analysis of Experimental Data

In this section some experimental data obtained by A. Arons and his co-workers at Woods Hole Oceanographic Institution will be analyzed. It will be shown that the theoretical values of the period agree very well with the experimental data while the values for pressure and migration do not agree as well.

The experiments consisted of exploding three hundred grams Tetryl at various depths beneath the surface in water 23.5 feet deep. Table 1 shows the values observed for the period of bubble oscillation.

Before these data can be compared with the theoretical results, the value of E must be known. We shall find E by fitting a straight line to the points obtained when $\bar{T}Z_o^{5/6}$ is plotted against $\varphi_1 Z_o^{-1/3}$. Table 2 gives the values of $\bar{T}Z_o^{5/6}$ and the corresponding values of $\varphi_1 Z_o^{-1/3}$.

A straight line is fitted to these values by the method of least squares. The equation obtained is

$$\bar{T}Z_o^{5/6} = 3.876 - 16.96\, \varphi_1 Z_o^{-1/3}. \tag{2.1}$$

Figure 8 shows how closely the straight line fits the data. This closeness of fit is a confirmation of the theory.

When equation (2.1) is compared with (1.35), we find that

$$\alpha = 3.876, \quad \beta = 16.96. \tag{2.2}$$

Table 1

H (feet)	T (seconds)	H (feet)	T (seconds)
3.5	.1576, .1577, .1582	16.4	.1509
4.0	.1590, .1598, .1602, .1610	17.3	.1516
4.5	.1605, .1608, .1613	18.5	.1475
5.0	.1619, .1621, .1624	18.8	.1480
5.5	.1632, .1637, .1641	19.0	.1455, .1480
6.0	.1625, .1628, .1630	19.1	.1496
6.5	.1643, .1648, .1650	19.2	.1474
7.0	.1629, .1643, .1646, .1651	19.6	.1444
8.0	.1619, .1638, .1640, .1646	19.7	.1456, .1468, .1531
10.0	.1602, .1604, .1609, .1614, .1615	19.8	.1437, .1450, .1456
12.0	.1560, .1564, .1566, .1570, .1591	20.2	.1491
14.0	.1531, .1534, .1543	20.4	.1521
15.4	.1511		

Table 2

H	$TZ_o^{5/6}$	$\varphi_1 Z_o^{-1/3}$	H	$TZ_o^{5/6}$	$\varphi_1 Z_o^{-1/3}$	H	$TZ_o^{5/6}$	$\varphi_1 Z_o^{-1/3}$
3.5	3.158	.0428	7.0	3.524	.0198	15.4	3.830	.000620
	3.160			3.554				
	3.170			3.560		16.4	3.893	-.00210
				3.571				
4.0	3.223	.0372				17.3	3.969	-.00525
	3.239		8.0	3.575	.0166			
	3.247			3.617		18.5	3.938	-.0108
	3.263			3.621				
				3.634		18.8	3.971	-.0122
4.5	3.290	.0332						
	3.296		10.0	3.680	.0121	19.0	3.915	-.0140
	3.307			3.684			3.983	
				3.696		19.1	4.032	-.0148
5.0	3.353	.0292		3.707				
	3.357			3.710		19.2	3.980	-.0157
	3.363							
			12.0	3.722	.00710	19.6	3.923	-.0188
5.5	3.419	.0262		3.732				
	3.430			3.736		19.7	3.963	-.0197
	3.438			3.746			3.996	
				3.796			4.167	
6.0	3.442	.0238				19.8	3.917	-.0204
	3.448		14.0	3.788	.00385		3.953	
	3.452			3.795			3.969	
				3.817				
6.5	3.516	.0216				20.2	4.091	-.0264
	3.527							
	3.531					20.4	4.174	-.0288

Formulas (1.33) and (1.34) show that α and β depend on the value of E and of I_1 and I_2. If we consider the ratio α^2/β we have

$$(2.3)\quad \frac{\alpha^2}{\beta} = 4I_1^2 I_2^{-1}(2g/3)^{-1/2} \quad \text{or} \quad \frac{I_1^2}{I_2} = 1.155\,\frac{\alpha^2}{\beta}$$

which is independent of E. A graph of I_1^2/I_2 for different values of k and γ is given in Figure 9.

Three physical quantities are needed to fully describe the bubble motion--the values of K, γ and E. Since we have only two constants α and β determined, we must assume the value of one of the three quantities. We shall assume that $\gamma = 1.25$, the value proposed by Jones for T.N.T., and then by the use of Figure 9 we find that $k = .23$. From this value of k, using Figures 1 and 2 and formulas (1.33) and (1.34), we find that $rQ = 500$ calories/gram. Since the detonation energy of Tetryl is 1060 calories/gram, this value for rQ is another confirmation of the theory.

Since we know the value of $E = rQM$, we can use (1.1) and get

$$(2.4)\qquad L = 13.88\,(W/Z_o)^{1/3}$$

where L is in feet, W in pounds and Z_o in feet, and

$$C = 2.997\,W^{1/3}Z_o^{-5/6}.$$

Since k varies with depth as $Z_o^{\gamma-1}$, the value, $k = .23$, is really an average value over the range $Z_o = 33$ to $Z_o = 56.5$. If we assume that this value of k corresponds to a depth halfway between the bottom and the surface of the water, we find that k varies from .213 to .244. This change in k can be neglected in the calculation of the period, momentum and migration. However, in the calculation of the peak pressure it must be taken into account since the pressure varies as $k^{-2/3(\gamma-1)}$.

Figure 10 shows how the periods calculated from the equation (2.1) compare with the observed results. The agreement is excellent.

Using k = .23 and formulas (1.27) and (1.28) the migration was found by numerical integration of I_γ for each value Z_o. The calculated results are compared with the observed values in Figure 11. The agreement seems to be fair.

The peak pressure is calculated from formulas (1.36) and (1.30). If we use the values of k and γ determined by the period measurements, the calculated pressures are about one-half the observed pressure. Theoretically, it would be possible to use one experimentally determined value of pressure with the two constants α and β to solve for the three quantities rQ, k and γ. This was done but it did not lead to consistent results. It seems likely that the value of γ at the time of minimum size may be different from the value of γ during the time of expansion and contraction.

Despite this difficulty with the magnitude of the pressure, the variation of pressure with depth is given approximately by formula (1.30). If we multiply the calculated pressures by a constant chosen so that the calculated pressure agrees with that experimentally observed at the depth of 18.5 feet, we get Figure 12.

Section III

Derivation of Formulas

Consider the motion of a gas bubble in water of finite depth, taking into account the effects of the bottom, the free surface and gravity. As before, we let A be the radius of the bubble at the time T, B the distance of its center from the bottom, and H the distance from the surface. We put $Z = H + Z^*$ where Z^* is the height of the

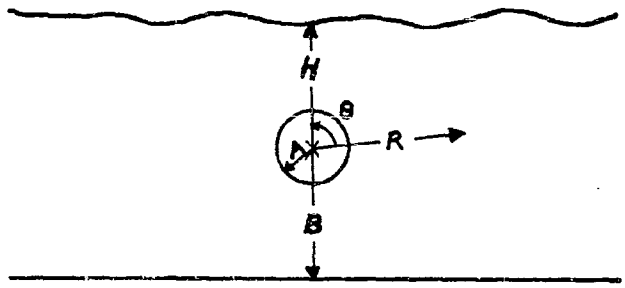

water column whose pressure equals atmospheric pressure, so that the pressure at the center of the bubble is $\rho g Z$.

Just as in Report 37.1R we find that if we use coordinates R and θ to describe the motion of the water, the velocity potential describing the flow is

$$\Phi = \frac{A^2 A'}{R} + \frac{A^3 B'}{2} \frac{\cos\theta}{R^2} + \Phi_1 \tag{3.1}$$

where Φ_1 is the "image" potential necessary to satisfy the boundary conditions on the bottom and on the surface. The primes indicate time derivatives.

By classical hydrodynamics we can show (see Report 37.1R) that the kinetic energy of the water is given by

$$(3.2)\quad 2\pi\rho A^3[A'^2(1 + A\varphi_1) - 2A^2\varphi_2 A'B' + \frac{1}{6}B'^2(1 + A^3\varphi_3)]$$

where φ_1, φ_2 and φ_3 are functions of A, B and H which represent the effect of the surface and the bottom. Note that φ_1, φ_2, φ_3 are of the dimensions $(\text{length})^{-1}$, $(\text{length})^{-2}$, $(\text{length})^{-3}$ respectively.

The potential energy of the displaced water is equal to the volume of the bubble multiplied by the hydrostatic pressure at the center of the bubble, that is, to $4\pi A^3\rho gZ/3$.

Assume the pressure and volume of one unit mass of the gas in the bubble under an adiabatic change are connected by the relation

$$(3.3)\qquad PV^\gamma = K.$$

If M is the mass of the explosive, then for the actual bubble

$$PV^\gamma = KM^\gamma$$

and the internal energy of the gas when the bubble has radius A is

$$(3.4)\qquad \begin{aligned} G(A) &= \int P\,dV = KM^\gamma V^{1-\gamma}/(\gamma - 1) \\ &= KM^\gamma(\tfrac{4}{3}\pi A^3)^{1-\gamma}/(\gamma - 1). \end{aligned}$$

By our assumption the total energy, E, left in the bubble after the shock wave has passed is equal to the sum of the kinetic energy of the water and the potential energy of the displaced water and the internal energy of the gas. We have, then

$$(3.5)\qquad \begin{aligned} &2\pi\rho A^3[A'^2(1 + A\varphi_1) - 2A^2\varphi_2 A'B' + \tfrac{1}{6}B'^2(1 + A^3\varphi_3)] \\ &\qquad + \tfrac{4}{3}\pi A^3\rho gZ + G(A) = E. \end{aligned}$$

If we use L and C defined in (1.1) and (1.2) as units, equation (3.5) can be written in terms of non-dimensional quantities as follows:

$$a^3[\dot{a}^2(1 + aL\varphi_1) - 2\dot{a}\dot{b}a^2L^2\varphi_2 + \frac{1}{6}\dot{b}^2(1 + a^3L^3\varphi_3)] + a^3zz_o^{-1} + ka^{-3(\gamma-1)} = 1, \tag{3.6}$$

where $ka^{-3(\gamma-1)}$ is the internal energy of the gas expressed in non-dimensional quantities. k is defined in equation (1.5).

It was shown in Report 37.1R that the period can be found by assuming b is constant so that $\dot{b} = 0$. Equation (3.6) reduces to

$$a^3\dot{a}^2(1 + aL\varphi_1) + a^3 + ka^{-3(\gamma-1)} = 1. \tag{3.7}$$

If we approximate $(1 + aL\varphi_1)^{1/2}$ by $1 + aL\varphi_1/2$, equation (3.7) can be solved for $\dot{a}$ and we get

$$\frac{a^{3/2}(1 + aL\varphi_1/2)da}{\sqrt{1 - a^3 - ka^{-3(\gamma-1)}}} = dt. \tag{3.8}$$

Let

$$I_1 = \int_{a_o}^{a_1} \frac{a^{3/2}\,da}{\sqrt{1 - a^3 - ka^{-3(\gamma-1)}}}, \tag{3.9}$$

$$I_2 = \int_{a_o}^{a_1} \frac{a^{5/2}\,da}{\sqrt{1 - a^3 - ka^{-3(\gamma-1)}}}, \tag{3.10}$$

where a_o and a_1 are respectively the smallest and largest zeros of the denominator. We find then that the time from beginning to maximum is

$$t_1 = I_1 + \frac{1}{2} I_2 L\varphi_1, \tag{3.11}$$

which is formula (1.11). The total period from beginning to minimum will be twice t_1.

Momentum of the Bubble

The vertical momentum, s, of the bubble is equal to $a^3\dot{b}/3$. Using the Lagrangian equation associated with the b coordinate, we find that

$$\frac{d}{dt}(a^3\dot{b}/3) = a^4\dot{a}^2 L \frac{\partial \varphi_1}{\partial b} + a^3 z_o^{-1}. \tag{3.12}$$

Integration gives the value of s at the maximum as

$$s_1 t = 2\left[\int_{t_o}^{t_1} a^4\dot{a}^2 L \frac{\partial \varphi_1}{\partial b}\, dt + z_o^{-1} \int_{t_o}^{t_1} a^3 dt\right].$$

Using equations (3.7) and (3.8) and the fact that

$$\dot{a}dt = da$$

we express s_1 as integrals over a. We have

$$\begin{aligned} s_1 &= L \frac{\partial \varphi_1}{\partial b} \int_{a_o}^{a_1} a^{5/2}(1+aL\varphi_1)^{-1/2}\sqrt{1-a^3-ka^{-3(\gamma-1)}}\, da \\ &\quad + z_o^{-1} \int_{a_o}^{a_1} \frac{a^{9/2}(1 + aL\varphi_1/2)da}{\sqrt{1 - a^3 - ka^{-3(\gamma-1)}}} \qquad (3.13) \\ &= L \frac{\partial \varphi_1}{\partial b}(I_3 - \tfrac{1}{2} L\varphi_1 I_4) + z_o^{-1}(I_5 + \tfrac{1}{2} L\varphi_1 I_6) \end{aligned}$$

where

$$I_3 = \int_{a_o}^{a_1} a^{5/2}\sqrt{1 - a^3 - ka^{-3(\gamma-1)}}\, da,$$

$$I_4 = \int_{a_o}^{a_1} a^{7/2}\sqrt{1 - a^3 - ka^{-3(\gamma-1)}}\, da,$$

(3.14)

$$I_5 = \int_{a_o}^{a_1} \frac{a^{9/2}\, da}{\sqrt{1 - a^3 - ka^{-3(\gamma-1)}}},$$

$$I_6 = \int_{a_o}^{a_1} \frac{a^{11/2}\, da}{\sqrt{1 - a^3 - ka^{-3(\gamma-1)}}}.$$

These equations are the same as (1.14)-(1.18).

The momentum can be used to give us an approximation to the energy equation (3.6) which takes into account the fact that b does change. We shall neglect the terms $a^2L^2\varphi_2$ and $a^3L^3\varphi_3$ which are of second and third order, respectively, as compared to the first order term $aL\varphi_1$. Now, since

$$\dot{b} = 3s/a^3,$$

equation (3.6) becomes

(3.15) $$a^3\dot{a}^2(1 + aL\varphi_1) + a^3 + ka^{-3(\gamma-1)} + 3s^2/2a^3 = 1.$$

If s were known as a function of a, this could be integrated:

(3.16) $$\int \frac{a^{3/2}(1 + aL\varphi_1/2)da}{\sqrt{1 - a^3 - ka^{-3(\gamma-1)} - 3s^2/2a^3}} = t.$$

The vertical distance the bubble moves can be found from this formula since

$$\dot{b} = 3s/a^3$$

so that

$$(3.17)\quad \Delta b = 3\int s\,dt/a^3 = 3\int \frac{s a^{-3/2}(1 + aL\varphi_1/2)\,da}{\sqrt{1 - a^3 - ka^{-3(\gamma-1)} - 3s^2/2a^3}}\,.$$

Since s is given as the indefinite integral of the right side of (3.12), Δb is really a double integral but we can change it to a single integral by the following argument:

During the first part of the bubble motion, that is, until the bubble reaches its maximum size, s increases from zero to s_1. During the second part of the motion, from the bubble maximum to the bubble minimum, s increases from s_1 to $\bar{s} = 2s_1$. The momentum at any time during the second half of the motion is $\bar{s}$ minus the momentum developed as the bubble contracts from its given size to its minimum size. Because of the symmetry of the bubble motion, this minus momentum is the same as the momentum developed when the bubble increases from its initial size to the given size. We may then conclude that the distance moved during the bubble expansion just balances the distance which would be produced by the minus momentum so that the total distance moved is given by one term

$$(3.18)\quad \begin{aligned}\Delta b &= 3\bar{s}\int_{a_1}^{\bar{a}} \frac{a^{-3/2}(1 + aL\varphi_1/2)\,da}{\sqrt{1 - a^3 - ka^{-3(\gamma-1)} - 3\bar{s}^2/2a^3}} \\ &= 3\bar{s}(I_\gamma + \tfrac{1}{2} L\varphi_1 I_8),\end{aligned}$$

$$(3.19)\quad I_\gamma = \int_{a_1}^{\bar{a}} \frac{a^{-3/2}\,da}{\sqrt{1 - a^3 - ka^{-3(\gamma-1)} - 3\bar{s}^2/2a^3}}\,,$$

$$(3.20)\quad I_8 = \int_{a_1}^{\bar{a}} \frac{a^{-1/2}\,da}{\sqrt{1 - a^3 - ka^{-3(\gamma-1)} - 3\bar{s}^2/2a^3}}\,.$$

This proves (1.27).

Radius of the Bubble

The maximum radius of the bubble is found by putting $\dot{a} = 0$ in equation (3.15) and solving

$$a^3 + ka^{-3(\gamma-1)} + 3s_1^2/2a^3 = 1 \tag{3.21}$$

for the root near one. If we expand a in powers of k and solve (3.21) we find that

$$a_1 = 1 - \frac{k}{3} - (\frac{\gamma - 1}{3} + \frac{1}{9})k^2 - \frac{3s_1^2}{2}. \tag{3.22}$$

This is the same as formula (1.20).

To find the minimum radius of the bubble we put $\dot{a} = 0$ in equation (3.15) and consider it at the time of minimum size. The equation reduces to

$$a^3 + ka^{-3(\gamma-1)} + 3\bar{s}^2/2a^3 = 1 \tag{3.23}$$

and the root near zero is the minimum radius. Note that (3.23) is the same as (3.21) except for the value of the momentum. The equation simplifies if we put

$$\xi = k^{1/(\gamma-1)}, \quad \bar{a}^3 = \xi u, \quad \varepsilon = 3\bar{s}^2/2\xi \tag{3.24}$$

and neglect that a^3 term, since a is near zero. We have

$$u^{-(\gamma-1)} + \varepsilon u^{-1} = 1$$

or

$$u = u^{2-\gamma} + \varepsilon. \tag{3.25}$$

Peak Pressure

The pressure in the water is given by Bernoulli's Law as

$$\frac{p}{\rho} = \frac{\partial \bar{\Phi}}{\partial t} - \frac{1}{2}(\nabla \bar{\Phi})^2.$$

The second term can be neglected compared to the first. Using (3.1) we find that

$$\frac{P}{\rho} = \frac{(A^2A')'}{R} + \frac{(A^3B')'\cos\theta}{2R^2} + \cdots .$$

For moderate distances from the bubble only the first term is important, so that

$$\frac{P}{\rho} = \frac{L^3}{C^2}\frac{(a^2\dot{a})^{\cdot}}{R} . \tag{3.26}$$

The value of $(a^2\dot{a})^{\cdot}$ can be found by multiplying (3.15) by a and then differentiating. This gives

$$2a^2\dot{a}(a^2\dot{a})^{\cdot}(1 + aL\varphi_1) + a^4\dot{a}^2\dot{a}L\varphi_1 + 4a^3\dot{a}$$
$$+ k(4 - 3\gamma)a^{3-3\gamma}\dot{a} - 3s^2a^{-3}\dot{a} = \dot{a}.$$

Since the peak pressure will be found at the time of minimum size, we may put $\dot{a} = 0$ and solve for $(a^2\dot{a})^{\cdot}$. The result is

$$(a^2\dot{a})^{\cdot} = \frac{\frac{1}{2\bar{a}^2} + \frac{3\bar{s}^2}{2\bar{a}^5} - \frac{k(4 - 3\gamma)}{2}\bar{a}^{1-3\gamma}}{1 + \bar{a}L\varphi_1}$$

$$= \frac{\frac{9\bar{s}^2}{4\bar{a}^5} + \frac{3k(\gamma - 1)}{2}\bar{a}^{1-3\gamma}}{1 + \bar{a}L\varphi_1} \tag{3.27}$$

if we make use of equation (3.23). Using the notation of (3.24) equation (3.27) becomes

$$(a^2\dot{a})^{\cdot} = \frac{1}{\bar{a}^2}\left[\frac{3\varepsilon}{2u} + \frac{3(\gamma - 1)}{2}u^{1-\gamma}\right]$$

$$= \frac{3(\gamma - 1)}{2\xi^{2/3}u^{2/3}}\left[\frac{\varepsilon}{(\gamma - 1)u} + u^{1-\gamma}\right]. \tag{3.28}$$

Notice that since u is near one the bracket does not change much as k changes.

We may write formula (3.26) for the pressure in a more convenient form as follows:

$$P = \frac{L^2}{c^2}\frac{L}{R}(a^2\dot{a})^{\cdot} = \frac{2}{3}\rho g Z_o \cdot \frac{L}{R}(a^2\dot{a})^{\cdot}$$

(3.29)

$$= \frac{(\gamma - 1)\rho g Z_o}{\xi^{2/3}\, u^{2/3}}\left[\frac{\varepsilon}{(\gamma - 1)u} + u^{1-\gamma}\right]\frac{L}{R}$$

by formulas (1.3) and (3.28).

Replace L by its value given in (1.1); then

$$(3.30)\quad P = \frac{(\gamma - 1)\rho g Z_o}{\xi^{2/3}\, u^{2/3}\, R}\left[\frac{\varepsilon}{(\gamma - 1)u} + u^{1-\gamma}\right]\left(\frac{3E}{4\pi\rho g Z_o}\right)^{1/3}.$$

This formula can be combined with the formulas (1.33) and (1.34) for α and β to solve for the three parameters of the bubble motion: rQ, K and γ.

Suppose, for example, that we know P when the momentum, s, is zero. This means that $\varepsilon = 0$ and $u = 1$. Consider the ratio P/α. We have

$$(3.31)\qquad \frac{P}{\alpha} = \frac{(\gamma - 1)\rho g\left(\frac{2g}{3}\right)^{1/2} Z_o^{2/3}}{2I_1\, R\, \xi^{2/3}}$$

and the right side depends only on k and γ. Combining this with the formula for α^2/β, which also depends only on k and γ, we will be able to solve for these quantities.

Section IV

The Electrostatic Problem

In Section III functions φ_1, φ_2 and φ_3 were introduced into the energy equation to take account of the presence of free and rigid surfaces. However, the results obtained depended only on the function φ_1. This function φ_1 can be evaluated, to a first approximation, by finding the kinetic energy of water motion due to a fixed expanding bubble. Consider the velocity potential for a fixed expanding bubble, assumed spherical, located at a distance H beneath the surface in water whose depth is D feet. If we take spherical coordinates, R, θ, Ψ

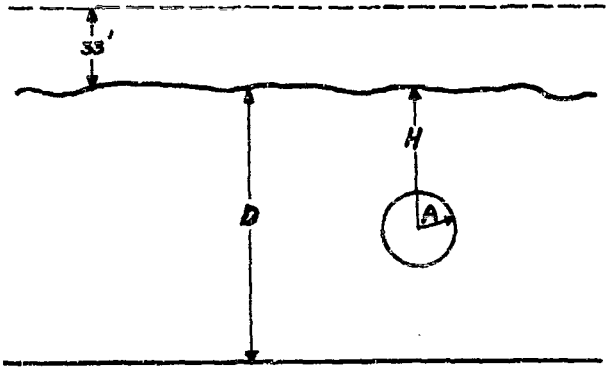

with pole at the center of the bubble, the problem can be formulated mathematically as follows:

Find a potential function $\Phi(R,\theta)$ such that

(4.1) $\quad \frac{\partial \Phi}{\partial R} = \dot{A}$ on the sphere,

(4.2) $\quad \frac{\partial \Phi}{\partial n} = 0$ on bottom,

(4.3) $\quad \Phi = 0$ on surface.

The last condition is obtained by taking Bernoulli's equation on the surface, assuming that gravity can be neglected, and then neglecting square terms.

Equation (4.1) is satisfied by taking

$$\Phi = \frac{A^2\dot{A}}{R} .$$

This is equivalent to assuming a source of strength $A^2\dot{A}$ at the center of the sphere. We can then satisfy equations (4.2) and (4.3) by reflecting this source in the bottom and in the free surface. It turns out that the image with respect to one boundary must be reflected in the other boundary and this process carried out on the successive images leads to an infinite sequence of images: Let

$$\Phi = A^2\dot{A}\left(\frac{1}{R} + \Phi'\right) \tag{4.4}$$

where Φ' is the potential due to the images. It can be evaluated by a method similar to that in Report 37.1R.

After Φ has been found we get the kinetic energy of the water by evaluating

$$\frac{1}{2}\rho \int \Phi \frac{\partial \Phi}{\partial n}\, dS$$

over all boundaries. Because of conditions (4.2) and (4.3) this reduces to the integral over the sphere.

Using equation (4.1) we have that

$$E = \frac{1}{2}\rho \int_{\text{sphere}} \Phi \frac{\partial \Phi}{\partial n}\, dS = \dot{A} \int \Phi A^2 d\omega = A^2\dot{A} \int \Phi d\omega \tag{4.5}$$

where $d\omega$ is the element of solid angle so that $dS = A^2 d\omega$. By the Mean Value theorem

$$\frac{1}{4\pi} \int \Phi'\, d\omega = \Phi'(0)$$

where $\Phi'(0)$ is the value of the potential Φ' at the center

of the sphere. From equation (4.4) and this result we find that

$$E = 2\pi\rho A^4\dot{A}^2\left(\frac{1}{A} + \Phi'(0)\right)$$

$$= 2\pi\rho A^3\dot{A}^2(1 + A\Phi'(0)) \tag{4.6}$$

so that $\varphi_1 = \Phi'(0)$.

Solution of the Electrostatic Problem

This shows that we need the value of Φ only at the center of the sphere. It will be found by considering the infinite set of images produced by reflecting the original source at the center and its images in the bottom and free surface.

For convenience of representation we shall draw the surfaces vertically. The situation is as follows:

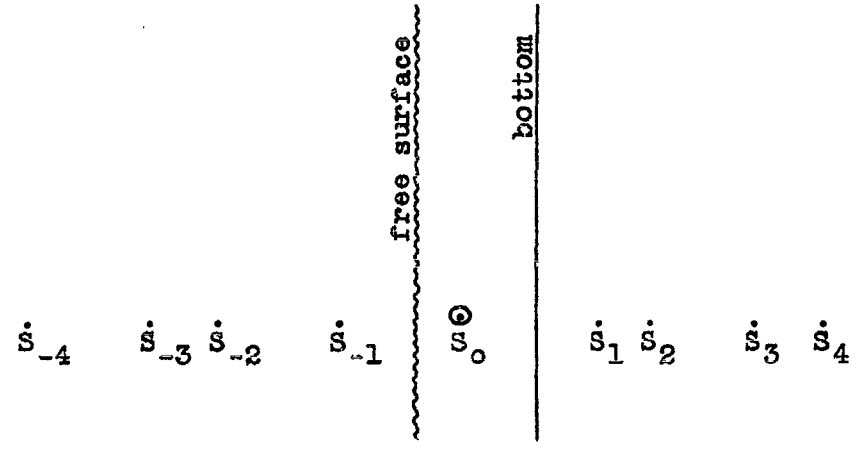

Here, S_o is the source of strength one at the center of the bubble. S_1, S_{-1}, S_2, S_{-2}, $\cdots$ denote the image sources and sinks. They are obtained as follows:

S_1 is the reflection of S_o in the bottom

S_{-1} is the reflection of S_o in the surface

S_{n+1} is the reflection of S_{-n} in the bottom

S_{-n} is the reflection of S_{n-1} in the surface.

Note that a reflection in the bottom, to satisfy equation (4.2), gives an image of the same strength, while a reflection in the free surface to satisfy equation (4.3) gives an image of the same strength with the opposite sign. (A source of negative strength is to be considered a sink.) We find that

the strength of S_{2n} is $(-)^n$ at a distance $2nD$ from S_o

the strength of S_{2n-1} is $(-)^{n+1}$ at a distance $2nD-2B$ from S_o

the strength of S_{-2n} is $(-)^n$ at a distance $2nD$ from S_o

the strength of S_{-2n-1} is $(-)^{n+1}$ at a distance $2nD+2B$ from S_o.

$\Phi'(0)$, the potential at the center of the bubble due to this collection of sources and sinks can be obtained by combining the effects of S_n and S_{-n}.

The potential at S_o due to S_{2n} and S_{-2n} is

$$\frac{(-)^n}{nD}$$

while that due to S_{2n+1} and S_{-2n-1} is

$$(4.7)\quad (-)^n\left[\frac{1}{(2n+2)D-2B} - \frac{1}{2nD+2B}\right] = \frac{(-)^n\,(4B-2D)}{[(2n+1)D+D-2B][(2n+1)D-(D-2B)]}$$

The total potential due to all the image sources and sinks is, therefore,

$$(4.8)\quad \sum_1^\infty \frac{(-)^n}{nD} + \frac{1}{D}\left(\frac{4B}{D} - 2\right) \sum_0^\infty \frac{(-)^n}{(2n+1)^2 - \left(1 - \frac{2B}{D}\right)^2}$$

or, if we let $\frac{2B}{D} - 1 = x$, this can be written as

$$(4.9) \qquad -\frac{\log 2}{D} + \frac{2x}{D} \sum_{0}^{\infty} \frac{(-)^n}{(2n+1)^2 - x^2} .$$

The series on the right can be expressed in terms of tabulated functions as follows:

$$(4.10) \qquad \begin{aligned} f(x) &= 2 \sum_{0}^{\infty} \frac{(-)^n x}{(2n+1)^2 - x^2} \\ &= 2 \frac{d}{dx}\left[\log \Gamma\left(\frac{1+x}{4}\right) + \Gamma\left(\frac{1-x}{4}\right)\right] - \frac{\pi}{2} \tan \frac{\pi x}{2} \end{aligned}$$

and we have

$$(4.11) \qquad \begin{aligned} \Phi'(0) &= -\frac{1}{D}(f(x) + \log 2) \\ &= -\frac{1}{2B} F(x) = -\frac{1}{2Lb_o} F(x). \end{aligned}$$

Note, that if $D \to \infty$, $\Phi'(0) = -\frac{1}{2B}$. By differentiation we find that

$$(4.12) \qquad \frac{\partial \Phi'}{\partial b} = -\frac{1}{D} f'(x) \frac{\partial x}{\partial b} = -\frac{2}{D^2} f'(x).$$

Appendix

Table 3

x	f(x)
0	0
.05	.09184
.10	.1852
.15	.2816
.20	.3829
.25	.4910
.30	.6081
.35	.7379
.40	.8840
.45	1.051
.50	1.246
.55	1.481
.60	1.769
.65	2.136
.70	2.619
.75	3.292
.80	4.298
.85	5.968
.90	9.305
.95	19.31
1.00	∞

Table 4

x	$\mathcal{F}(x)$	x	$\mathcal{F}(x)$
0	.3466		
.05	.3729	-.05	.3157
.10	.3952	-.10	.2794
.15	.4143	-.15	.2366
.20	.4304	-.20	.1862
.25	.4440	-.25	.1264
.30	.4554	-.30	.05528
.35	.4651	-.35	-.03021
.40	.4731	-.40	-.1336
.45	.4796	-.45	-.2593
.50	.4849	-.50	-.4150
.55	.4891	-.55	-.6104
.60	.4924	-.60	-.8608
.65	.4950	-.65	-1.190
.70	.4969	-.70	-1.637
.75	.4982	-.75	-2.274
.80	.4991	-.80	-3.244
.85	.4996	-.85	-4.880
.90	.4999	-.90	-8.181
.95	.49998	-.95	-18.15
1.00	.5	-1.00	$-\infty$

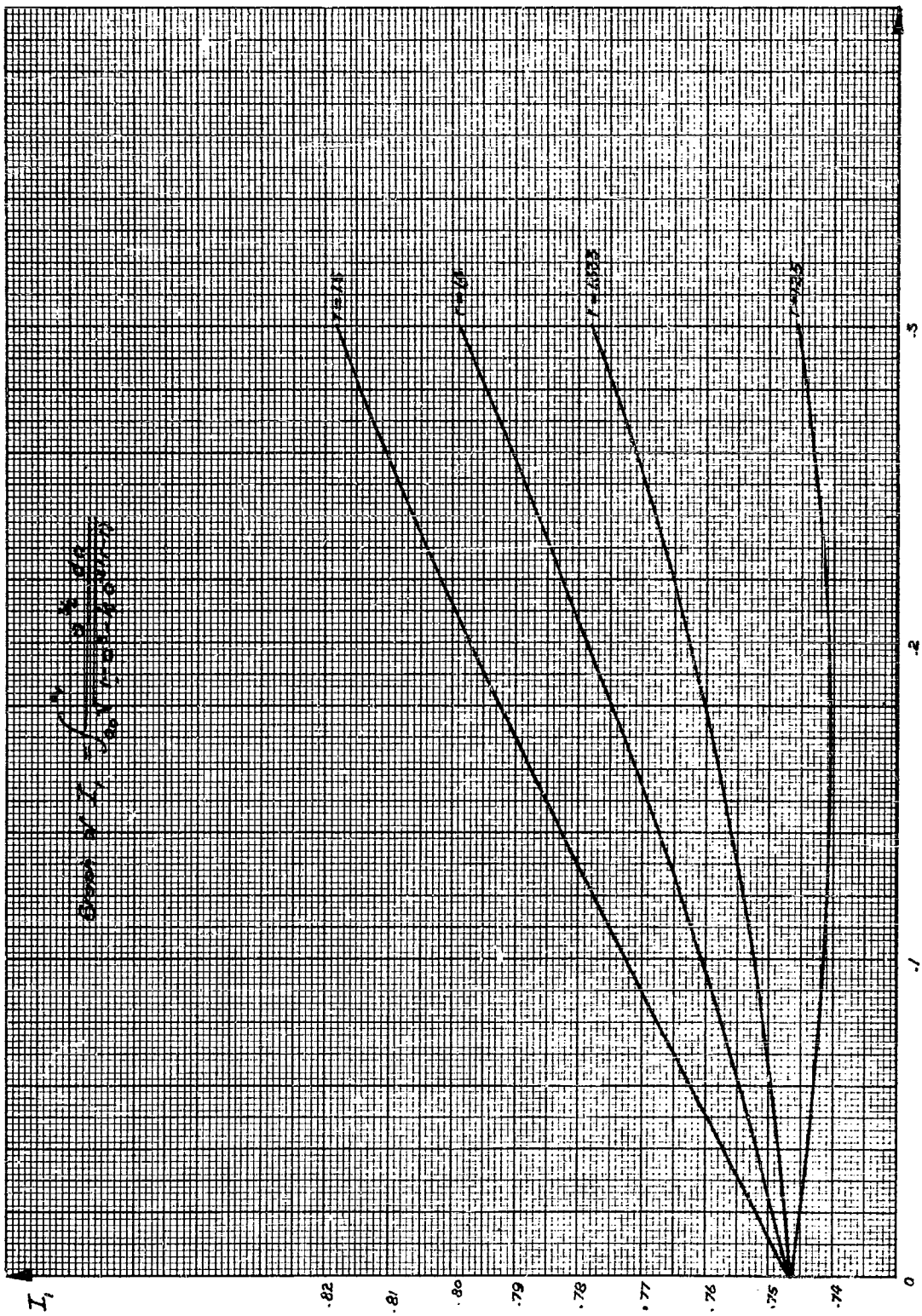

Figure 1

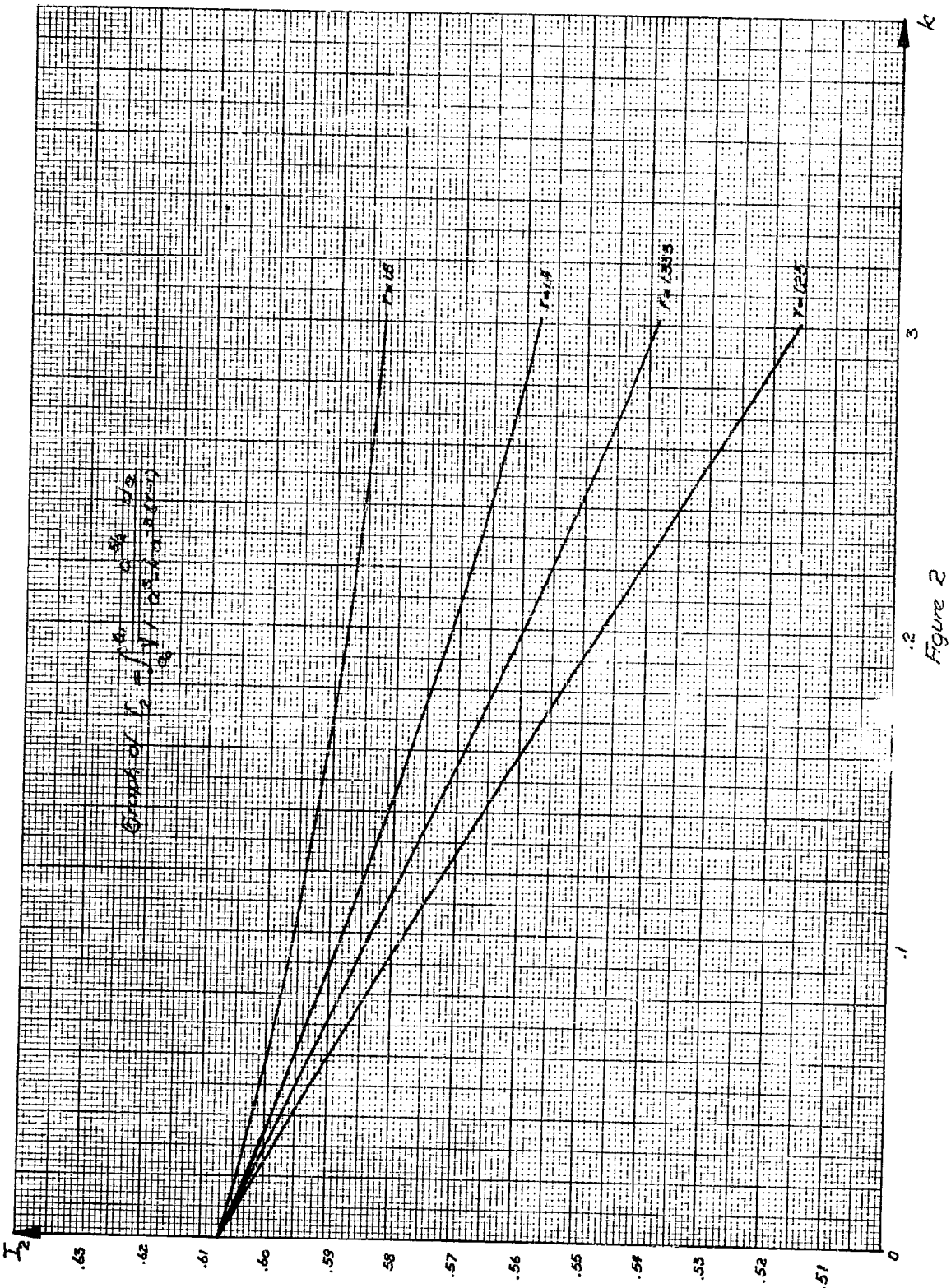
I_2
.63
.62
.61
.60
.59
.58
.57
.56
.55
.54
.53
.52
.51
0
.1
.2
3
k
r=1.68
r=1.414
r=1.333
r=1.25
Graph of $I_2 = \int_{\theta_0}^{\theta_1} \sqrt{1-k^2\sin^2\theta}\, d\theta$

Figure 2

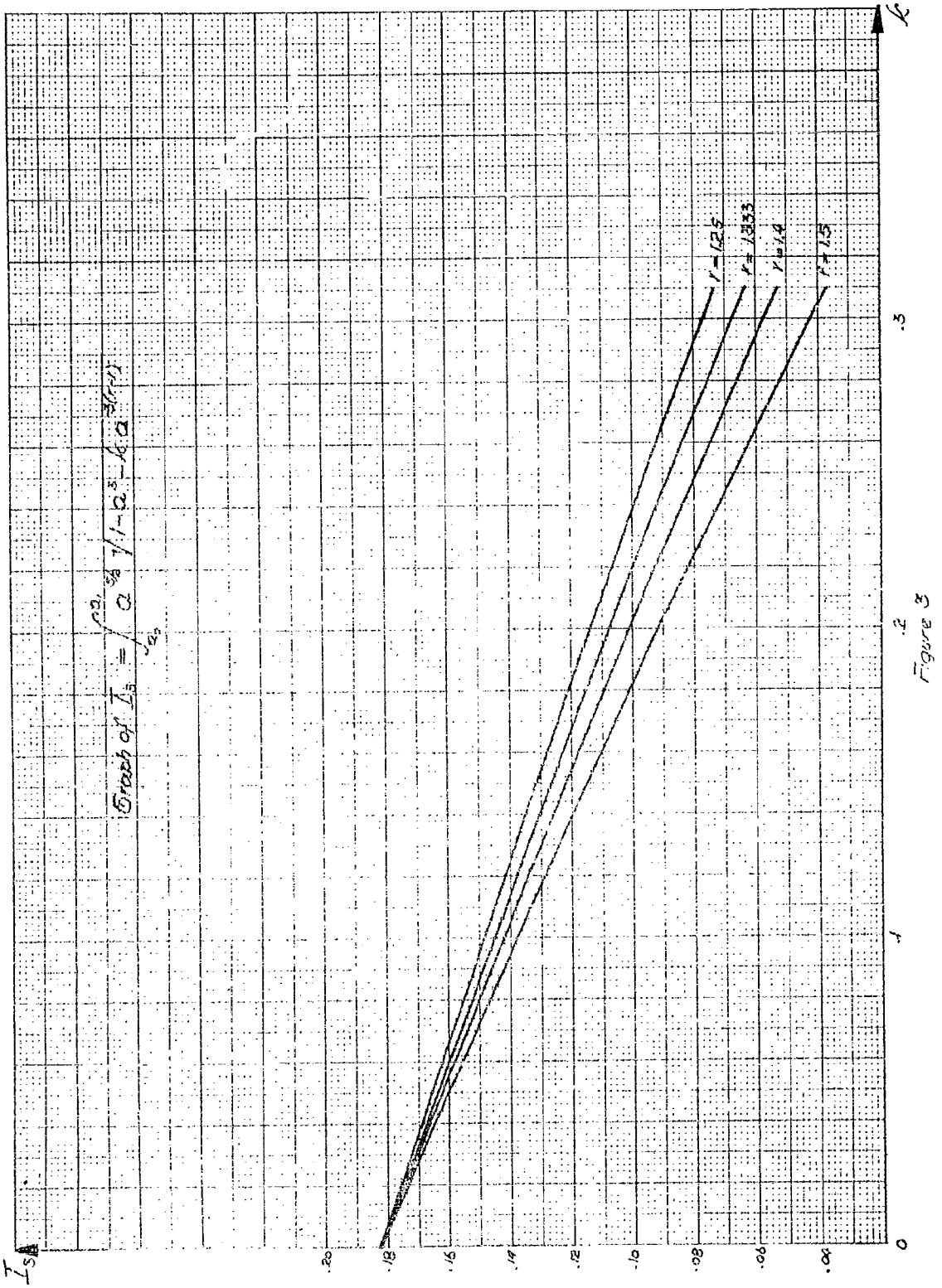
Graph of $I_s = \int_{\varepsilon_2}^{\varepsilon_1} \frac{r^2 a^{3/2}\sqrt{1-a^3}}{1-a^3} da$
r = 1.25
r = 1.333
r = 1.4
r = 1.5
I_s
ε
.20
.18
.16
.14
.12
.10
.08
.06
.04
0
.1
.2
.3

Figure 3

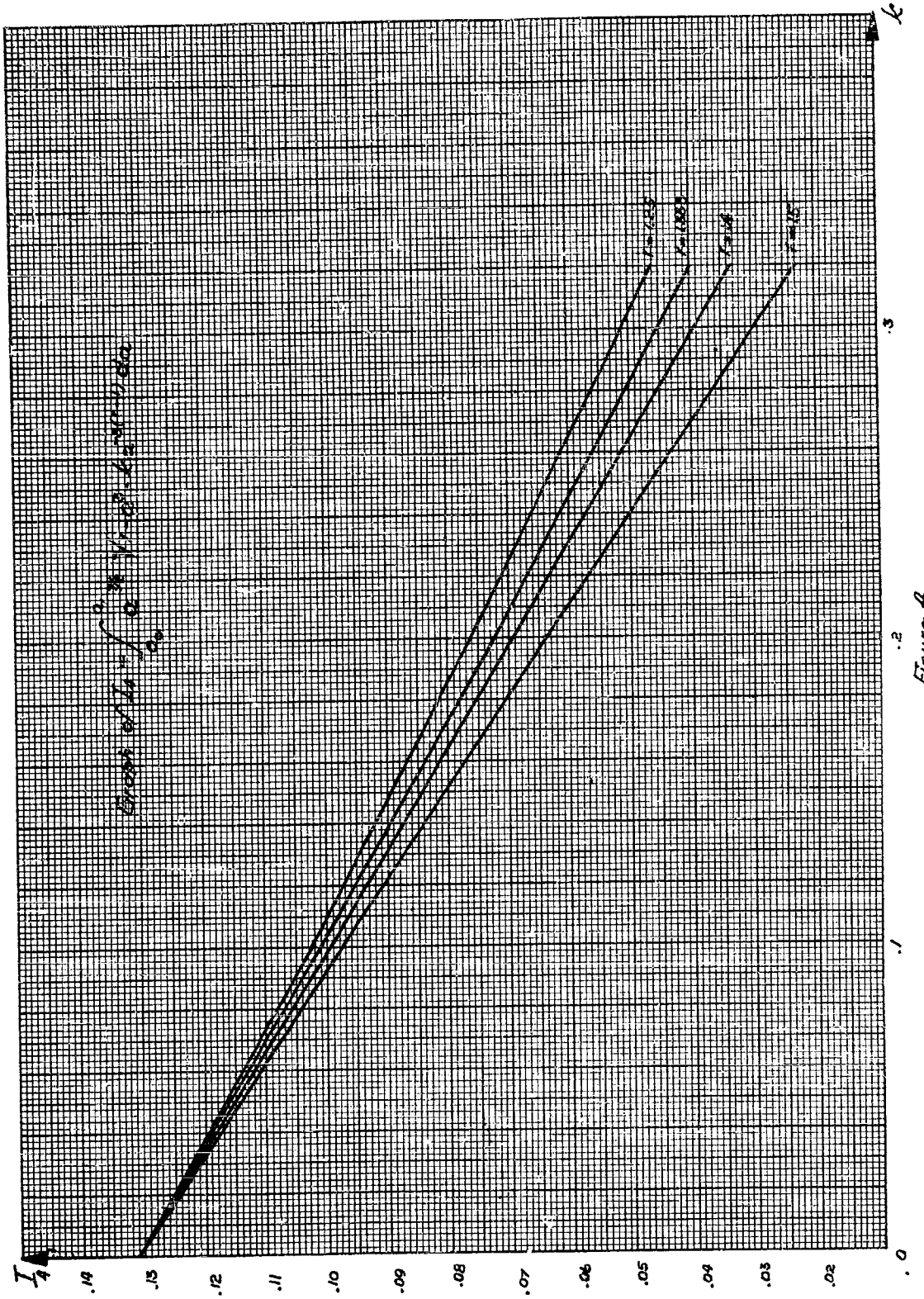

Figure 4

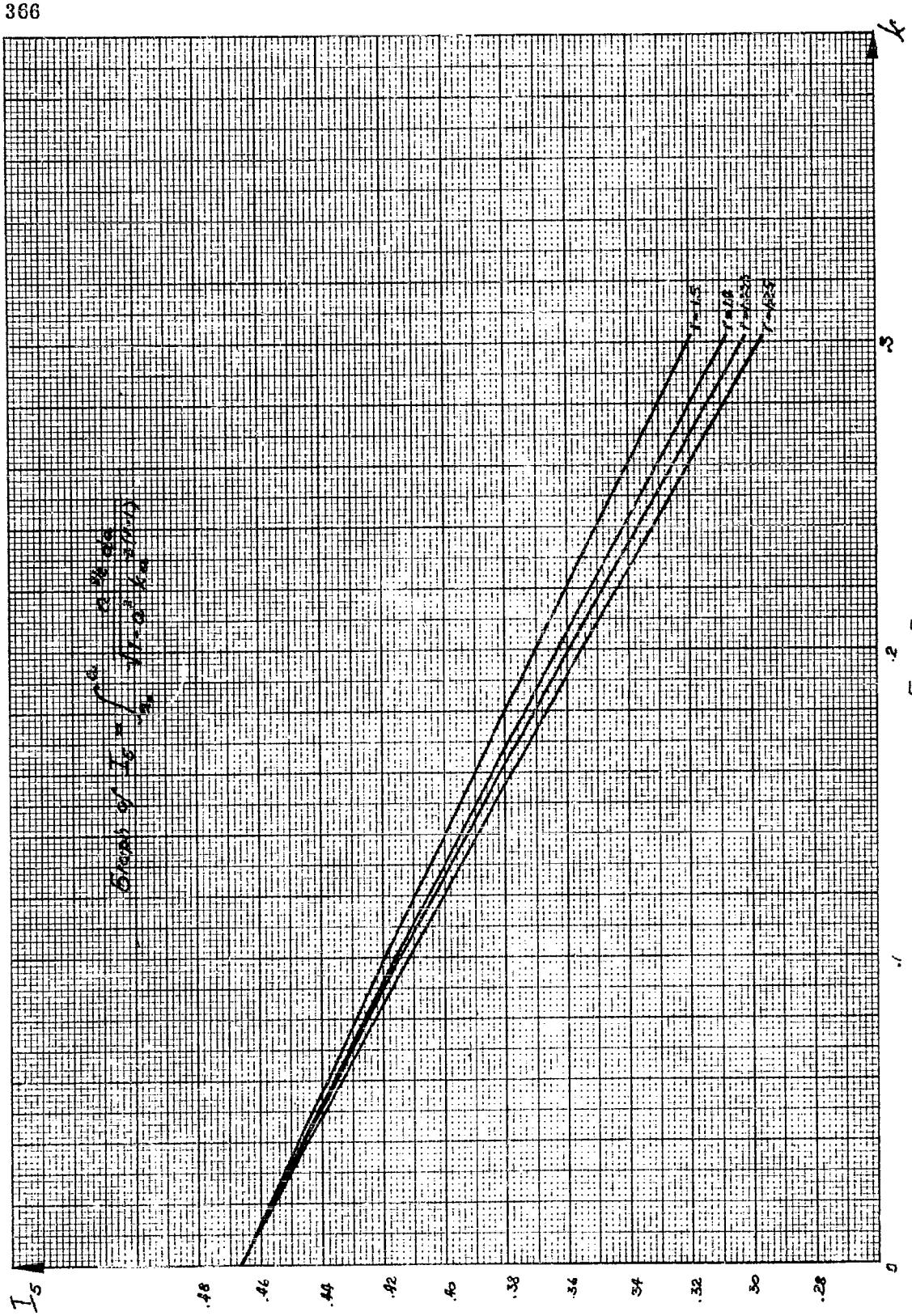
I_5
.48
.46
.44
.42
.40
.38
.36
.34
.32
.30
.28
0
.1
.2
.3
$\gamma = 1.5$
$\gamma = 1.4$
$\gamma = 1.3$
$\gamma = 1.2$

Figure 5

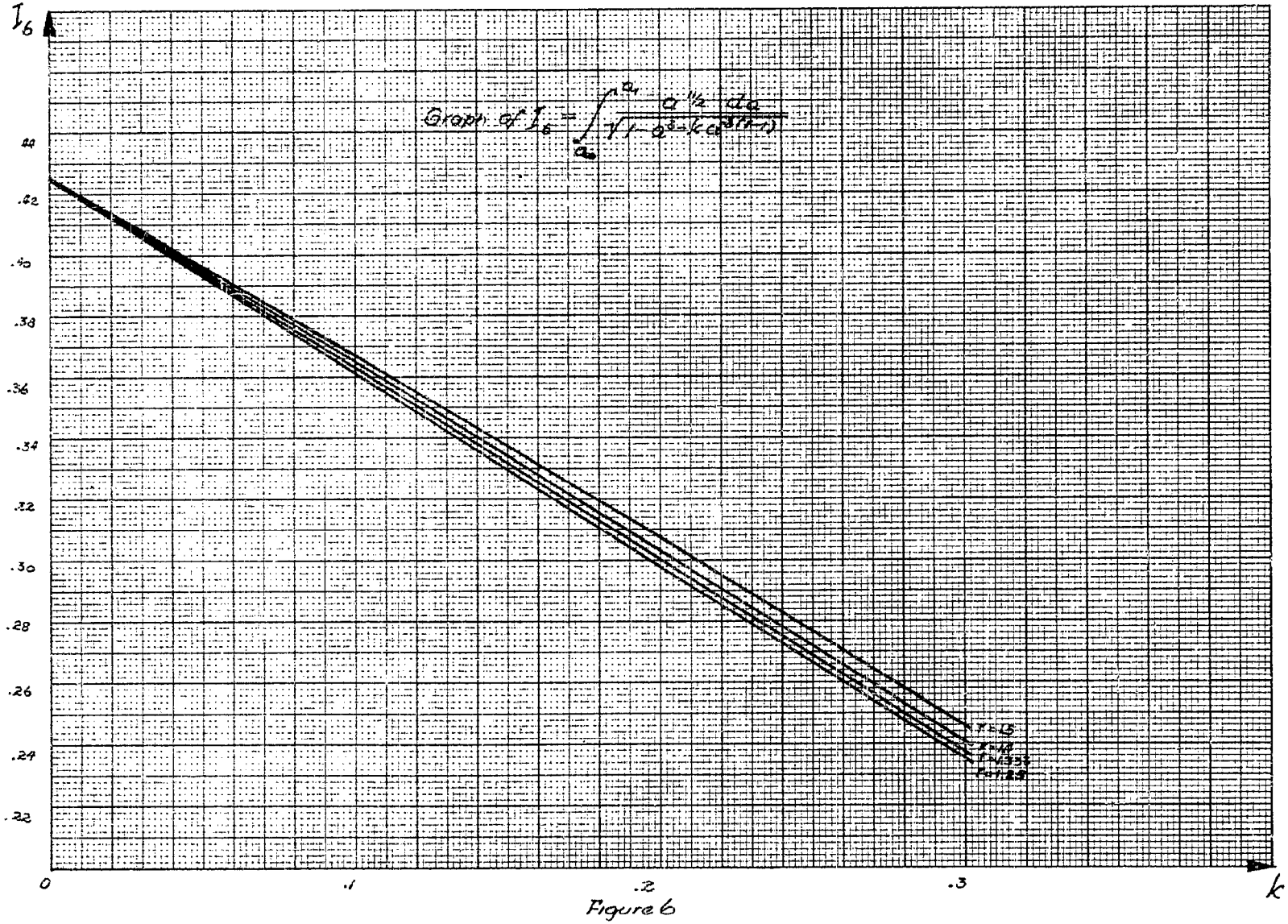
I_6
Graph of $I_6 = \int_{a_0}^{a_1} \frac{a^{1/2}\,da}{\sqrt{1-a^3-k\,a^{3/2}}}$
.44
.42
.40
.38
.36
.34
.32
.30
.28
.26
.24
.22
0
.1
.2
.3
k
n=1.5
n=1.4
n=1.333
n=1.25

Figure 6

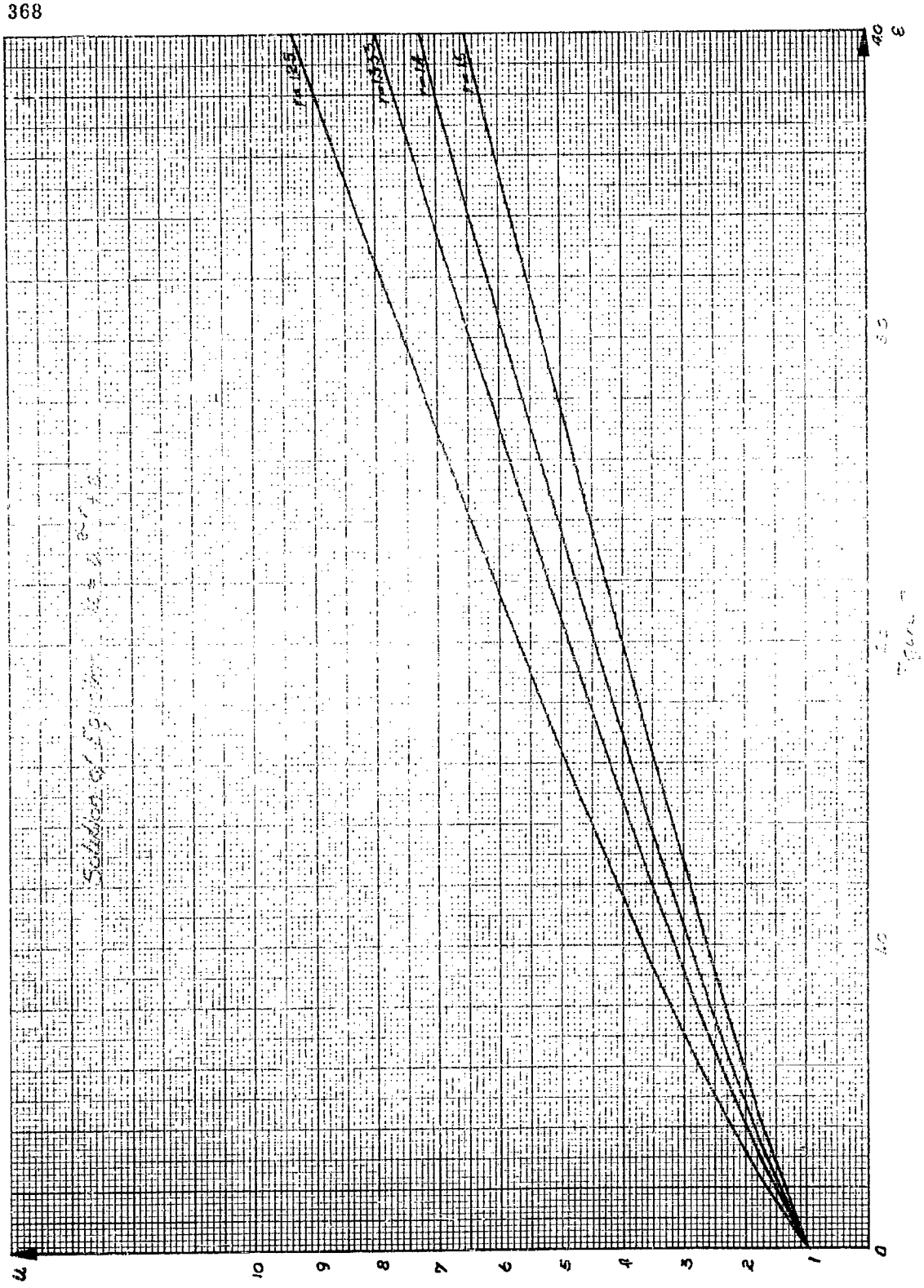
ε
40
35
0
u
10
9
8
7
6
5
4
3
2
1

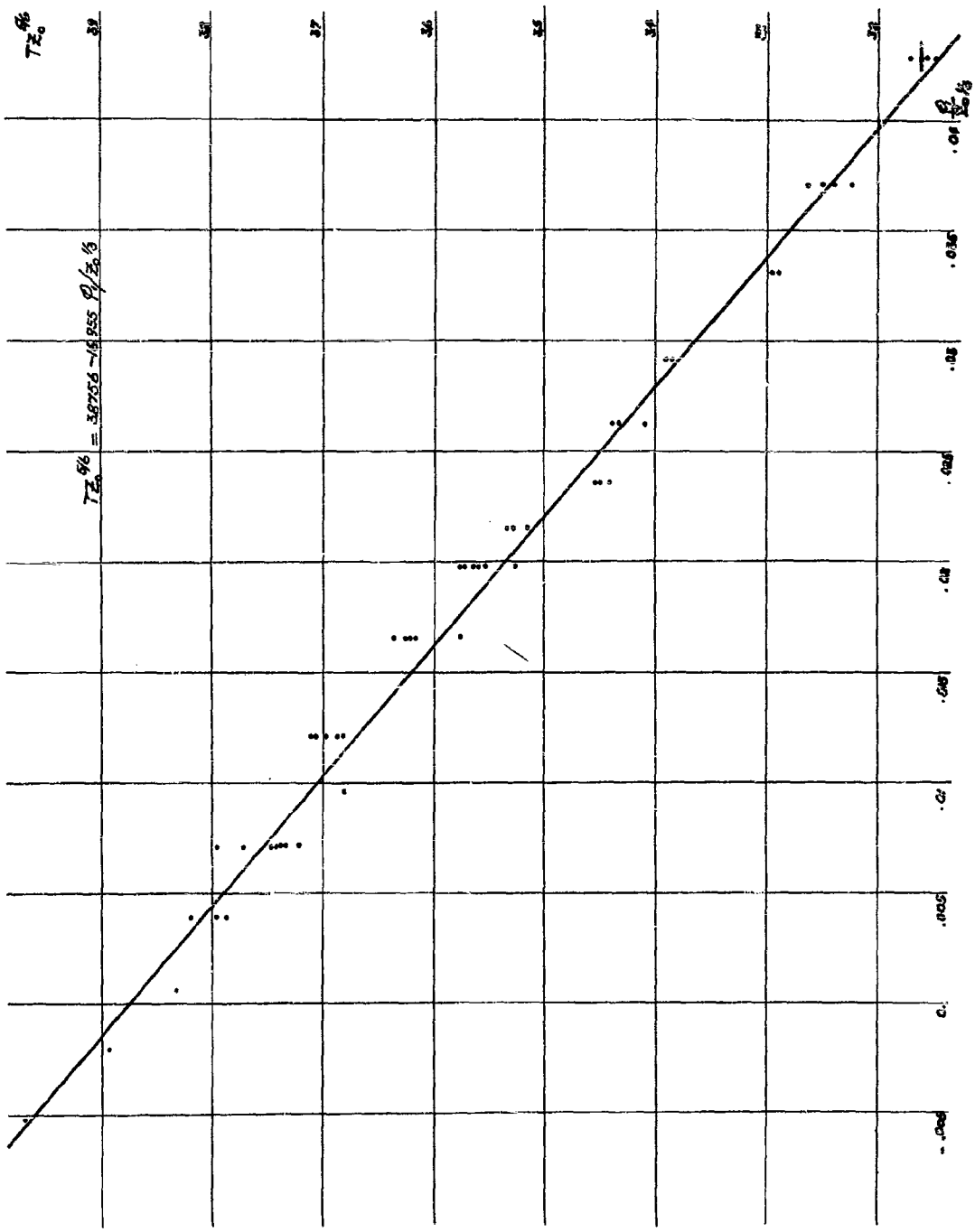

Figure 8

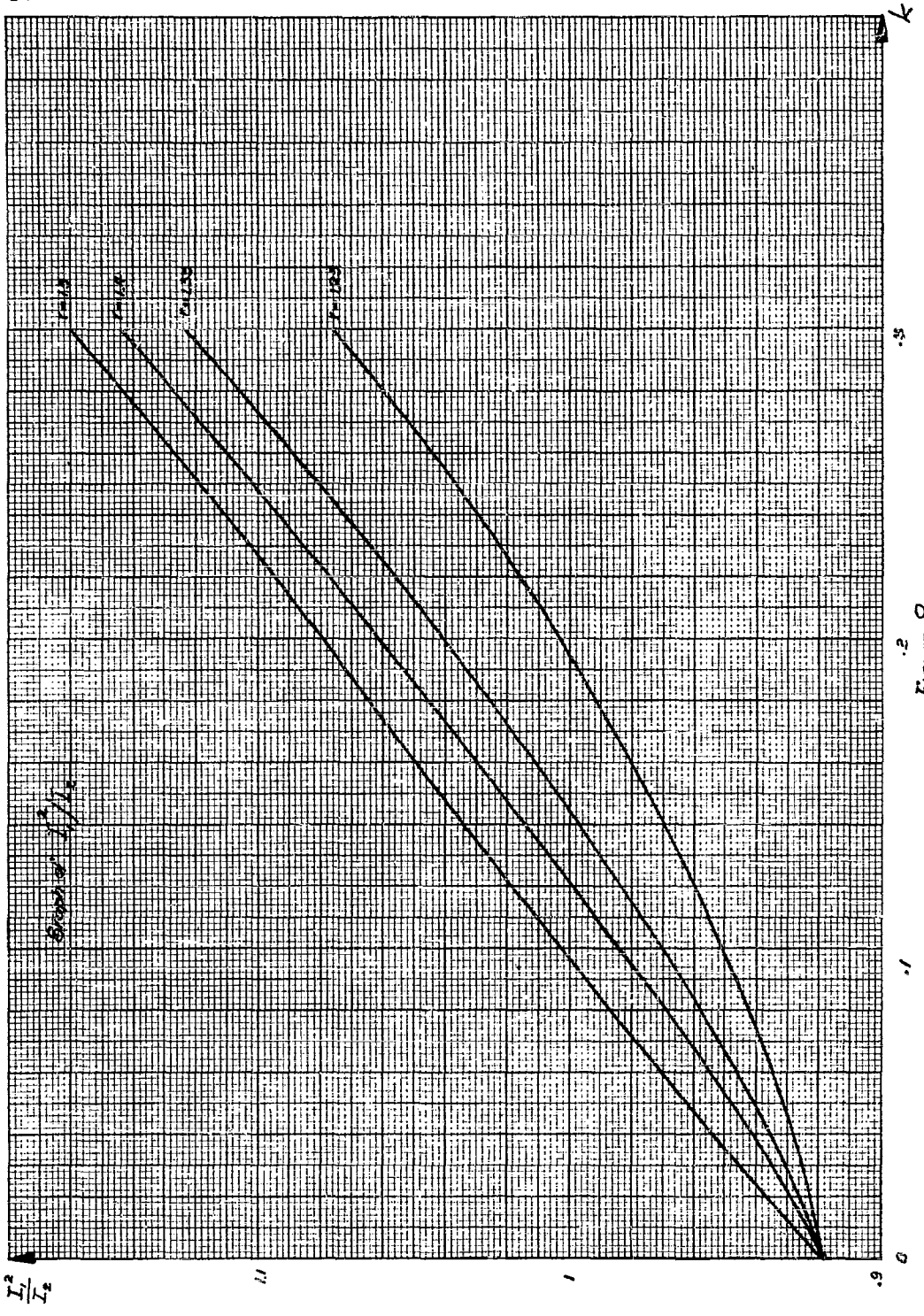

Figure 9

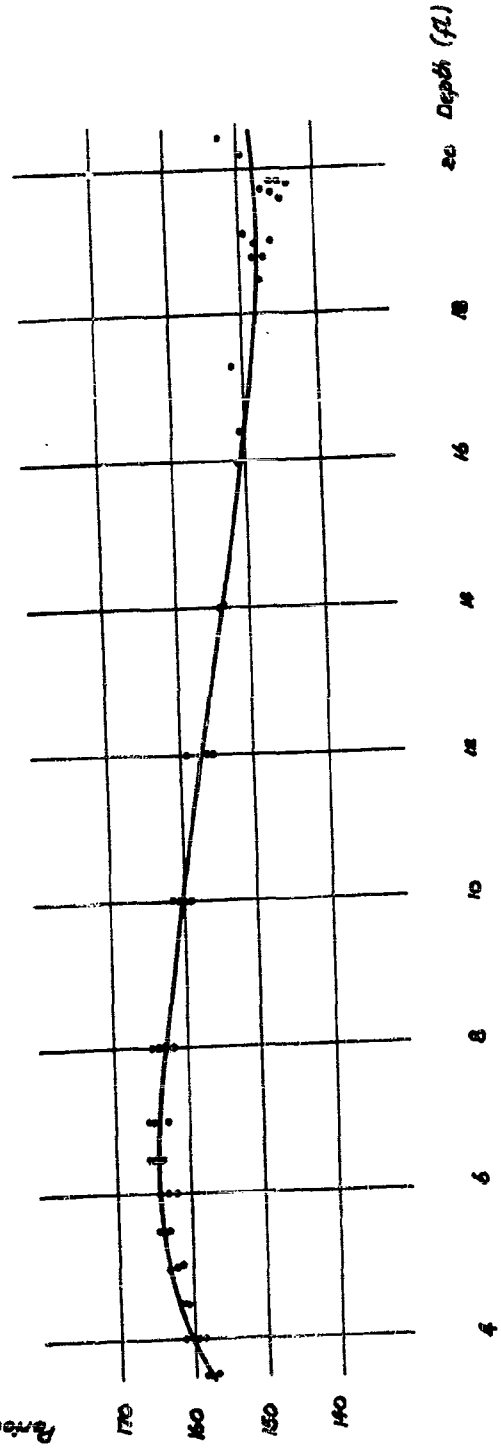

First bubble periods versus depth for 300 grams tetryl.

Figure 10

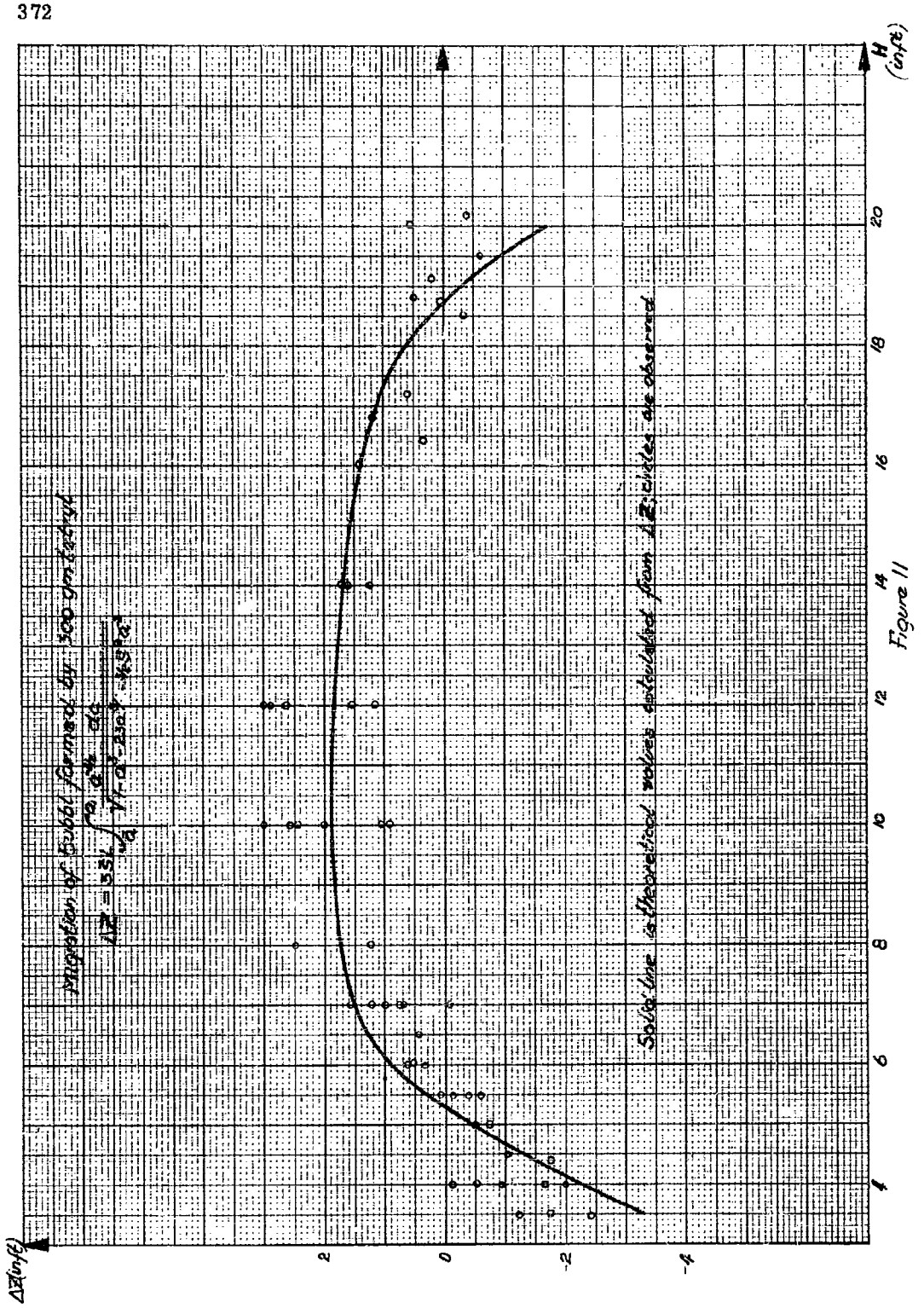
ΔZ (in ft)
H (in ft)
2
0
-2
-4
4
6
8
10
12
14
16
18
20
Solid line is theoretical values calculated from ΔZ-cycles observed
Integration of Dubbel formula by 100 gradient
ΔZ = 55k ∫ (a²b da / √(r-a²-Δa²-k²a²))

Figure 11

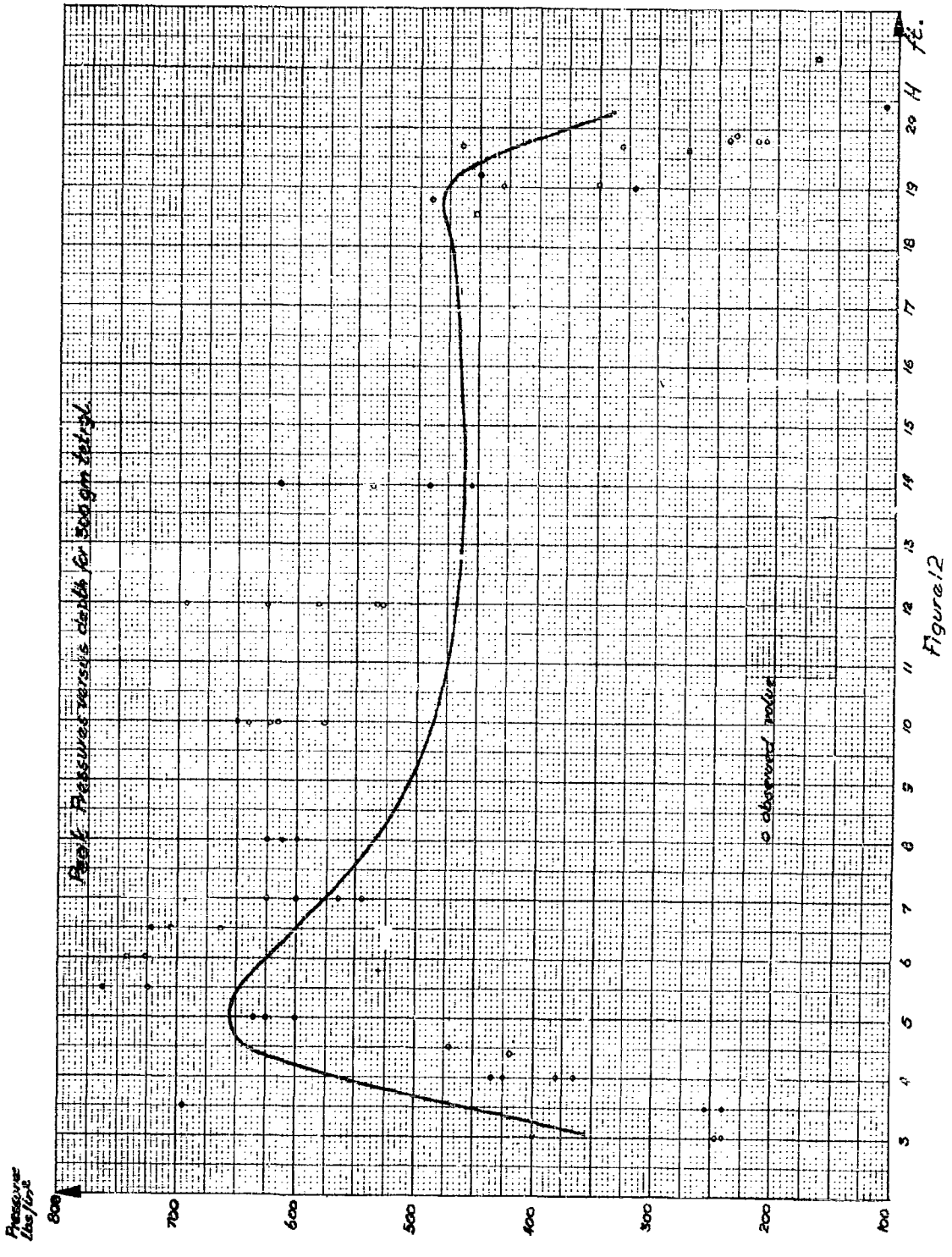
Peak Pressures versus depth for 500 gm Petryl.
Pressure lbs/in²
800
700
600
500
400
300
200
100
3
4
5
6
7
8
9
10
11
12
13
14
15
16
17
18
19
20
H ft.
observed points

Figure 12

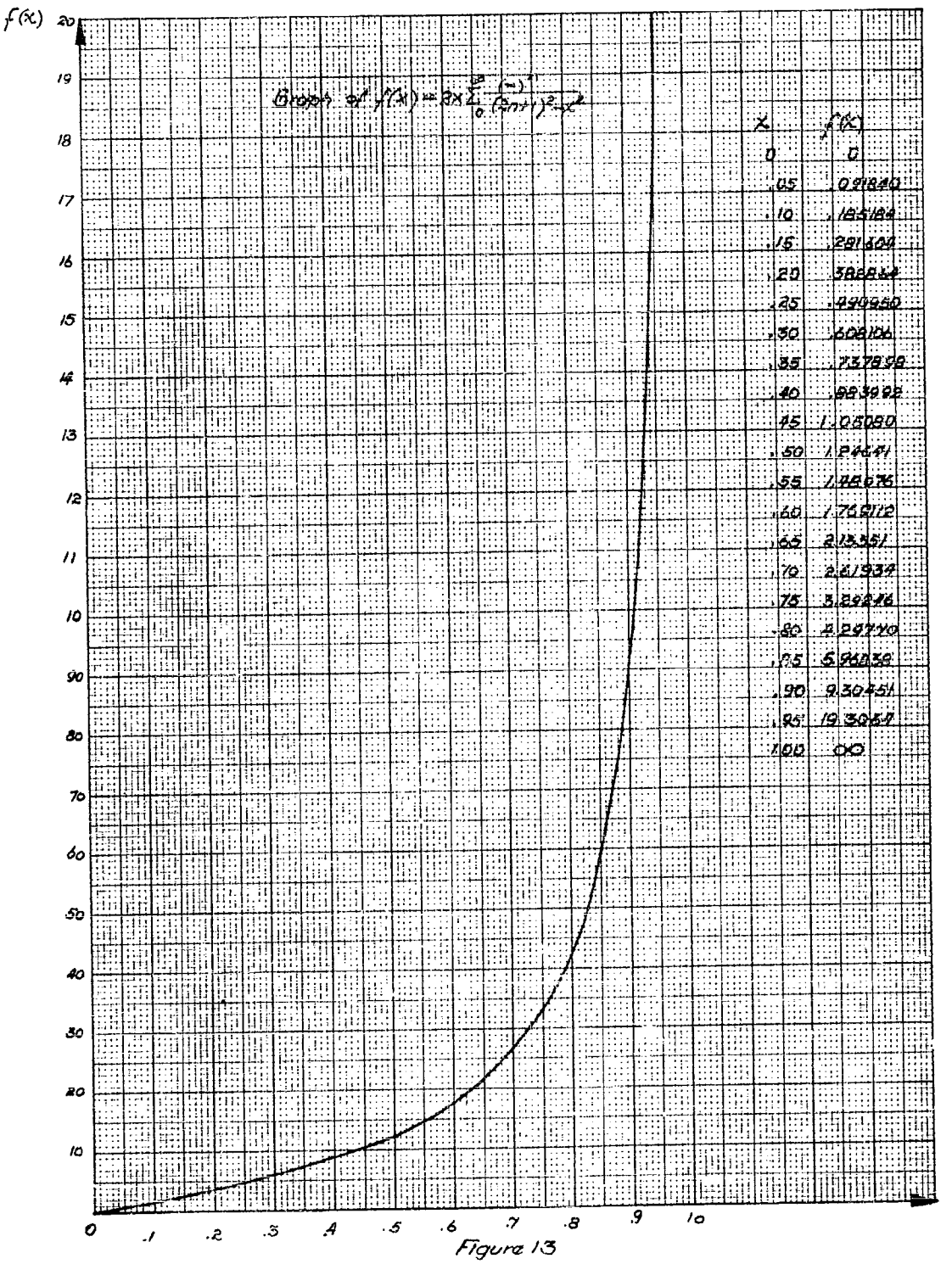
f(x)
Proof of $f(x) = 3x \sum_{0}^{\infty} \frac{(-)^n}{(2n+1)^2} x^{2n}$
x f(x)
0 0
.05 .091840
.10 .184184
.15 .281600
.20 .388854
.25 .490950
.30 .608106
.35 .737859
.40 .893992
.45 1.05080
.50 1.24641
.55 1.48676
.60 1.76512
.65 2.13351
.70 2.61939
.75 3.29246
.80 4.29770
.85 5.96238
.90 9.30451
.95 19.3064
1.00 ∞

Figure 13

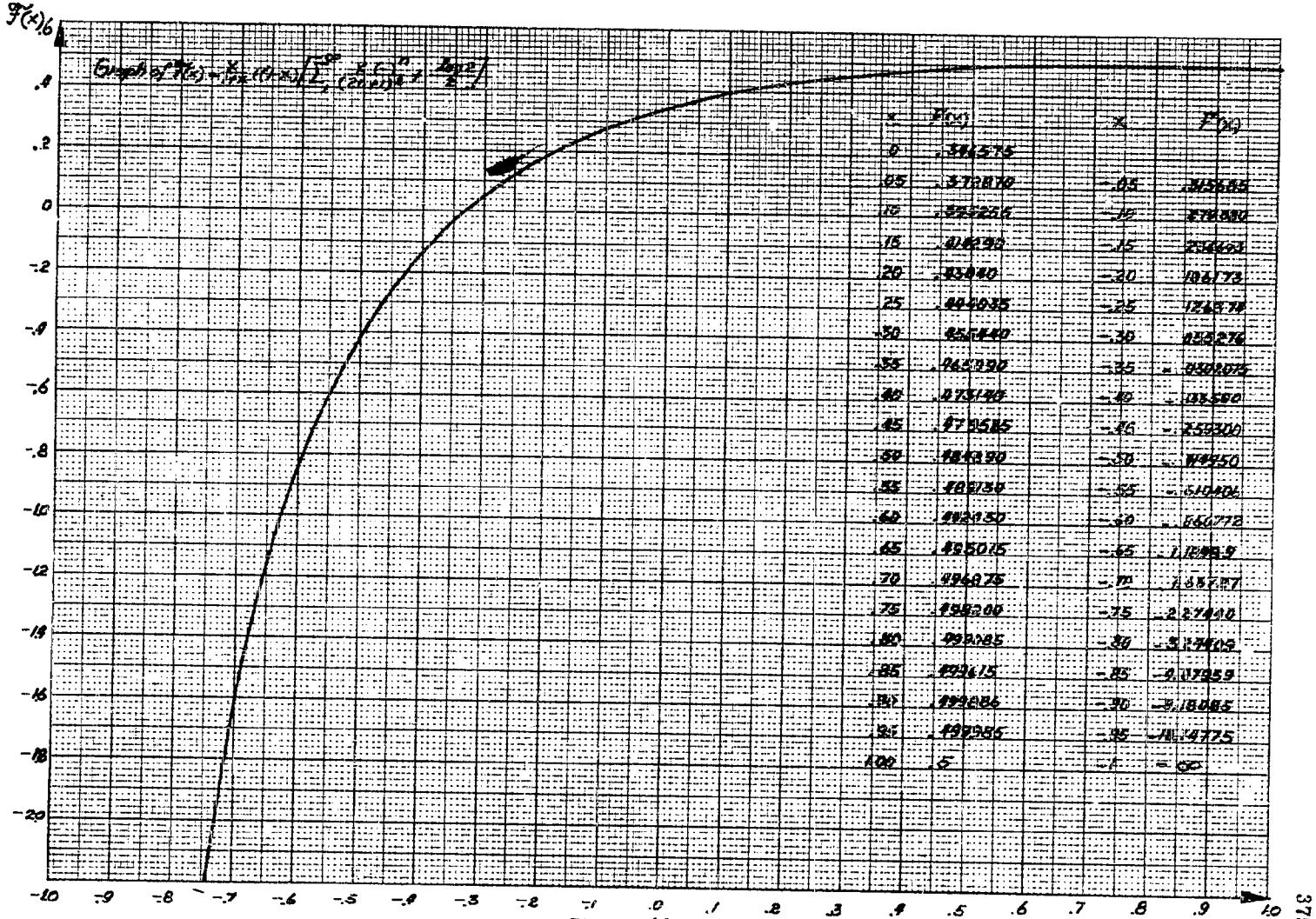

x	F(x)
0	.386575
.05	.378870
.10	.372256
.15	.366392
.20	.361040
.25	.356035
.30	.351240
.35	.346530
.40	.341780
.45	.336885
.50	.331690
.55	.326130
.60	.320150
.65	.313615
.70	.306470
.75	.298200
.80	.289085
.85	.279615
.90	.269086
.95	.257955
1.00	.5

x	F(x)
-.05	.395685
-.10	.404880
-.15	.414463
-.20	.424473
-.25	.434978
-.30	.446276
-.35	-.458075
-.40	-.470560
-.45	-.483300
-.50	-.496550
-.55	-.510404
-.60	-.524772
-.65	-.539899
-.70	-.555787
-.75	-.572410
-.80	-.589759
-.85	-.607959
-.90	-.626985
-.95	-.646775
-1.	= ∞

Figure 14

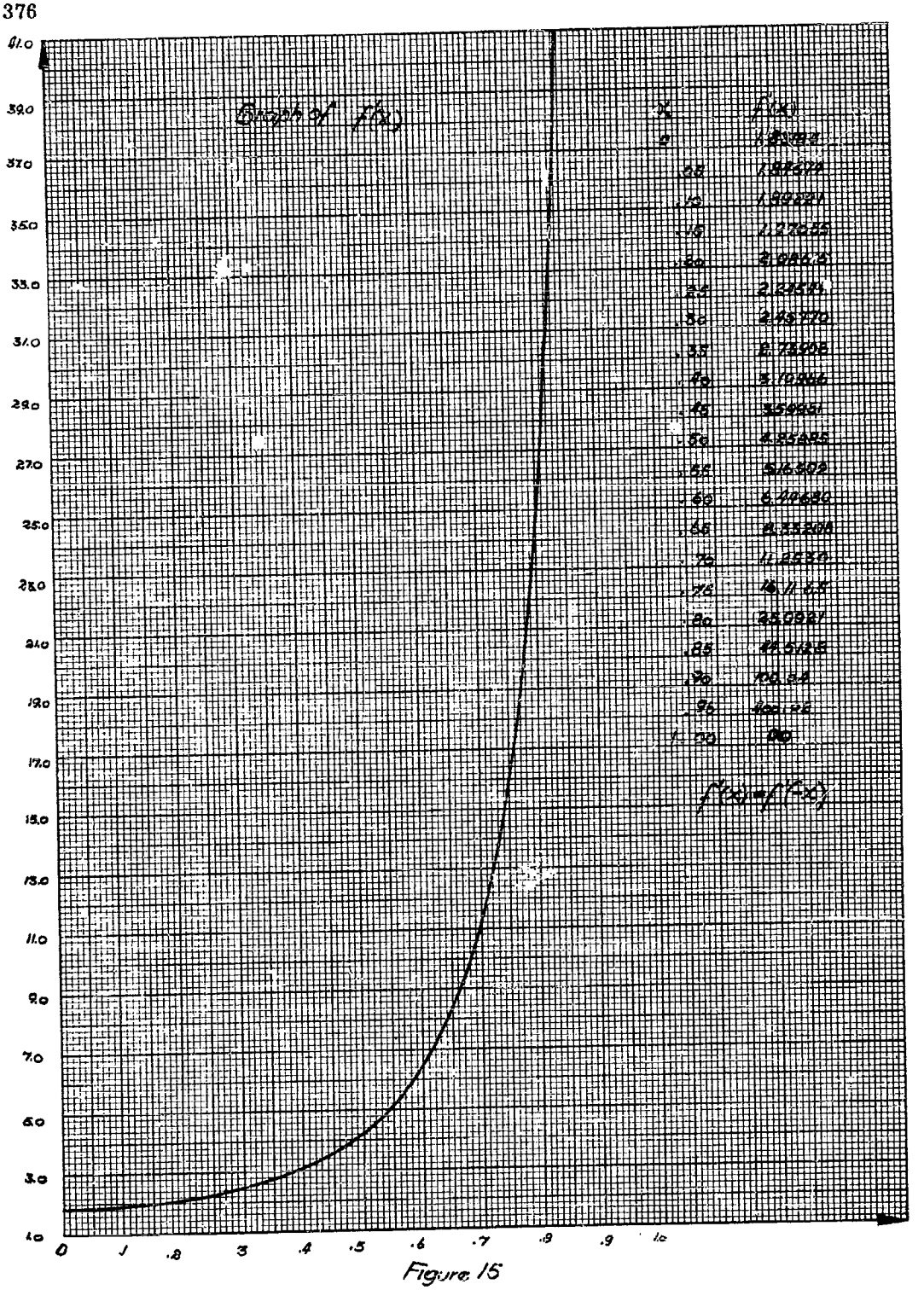
41.0
39.0
37.0
35.0
33.0
31.0
29.0
27.0
25.0
23.0
21.0
19.0
17.0
15.0
13.0
11.0
9.0
7.0
5.0
3.0
1.0
0
.1
.2
.3
.4
.5
.6
.7
.8
.9
1.0

Figure 15

MIGRATION OF UNDERWATER GAS GLOBES DUE TO GRAVITY AND NEIGHBORING SURFACES

E. H. Kennard
David W. Taylor Model Basin

American Contribution

December 1943

NOTATION

c_X, c_Y, c_Z	Cosines of the angles between the upward vertical and the X, Y, Z axes, respectively
D	Depth of water
D'	Hydrostatic pressure, including atmospheric pressure, expressed as an equivalent depth of water
g	Acceleration due to gravity
g_X, g_Y, g_Z	Components of the acceleration due to gravity in the directions of the X, Y, Z axes; $g_X = -gc_X$, $g_Y = -gc_Y$, $g_Z = -gc_Z$
H	Vertical component of Q
I	Impulse per unit area or $\int p\,dt$
$I_{0.2}$	Impulse per unit area due to the peak of pressure included between the instants at which p has one-fifth of its intervening maximum value
M, N_X, N_Y, N_Z	Functions of the distances from certain surfaces, varying from case to case
p	Pressure in the water
p_0	Hydrostatic pressure, including atmospheric pressure, at the level at which a charge is detonated
p_A	Hydrostatic pressure p_0 expressed in atmospheres
p_g	Pressure of the gas in a gas globe
Q	Linear displacement of the center of the gas globe from the time of detonation until the time of the first peak recompression
R	Radius of the gas globe
R_0	Radius of gas globe when its pressure equals hydrostatic pressure at the level of its center
R_2	Maximum radius of the gas globe
r	Distance from the center of the gas globe to a point in the water
S	Horizontal component of Q
T_1	Period of first oscillation, up to first peak recompression
T_{10}	Value of T_1 at the same level if no bounding surface is near
t	Time
W	Weight of charge
X, Y, Z	Coordinates of the center of the gas globe
X_0, Y_0, Z_0	Values of X, Y, Z at instant of detonation of charge
z_0	A dimensionless coefficient referring to depth below the surface and occurring only in Figure 5
γ	Ratio of the specific heat of the gas in the gas globe at constant pressure to its specific heat at constant volume

DIGEST*

The gas globe formed by an underwater explosion not only pulsates in size but also usually changes position as each pulsation occurs (1).** This migration may be of importance because the first recompression or contraction of the globe thereby comes to be centered at a point different from that of the initial detonation, and the location of the point of recompression influences the damage that may be done by the associated secondary pulse of pressure.

Accurate solution of the general equations of the motion of the gas globe set up by Herring (4) in this country and by G.I. Taylor and others (5) (6) (7) (8) in England is, in general, possible only by numerical solution of the differential equations; it has not yet been found possible to embark on such an enterprise in this country because of the labor involved. For purposes of analysis, calculations of the motion of the gas globe have been made by an approximate method. The assumptions underlying this method are set forth in the first part of the report, together with a discussion of the apparently conflicting and paradoxical motions of the gas globe under various conditions.

For example, in free water of unlimited extent the gas globe rises because of its buoyancy. Near a rigid boundary such as a vertical wall, the globe is attracted toward the boundary, as shown in Figure 2. Near the surface of the water, the gas globe is repelled from the free surface. However, although the action of gravity is always present to cause the globe to rise through the water by virtue of its buoyancy, the attraction of a rigid bottom in shallow water, or the repulsion from the free surface of the water, may decrease the

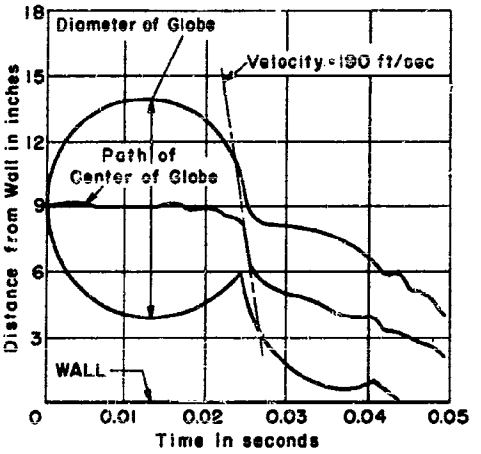

Figure 2 - Curves of Size and Position of a Gas Globe near a Vertical Wall

The charge was fired 9 inches from a rigid vertical wall. Note that the velocity of the center of the globe is greatest during the compression phases.

---

* This digest is a condensation of the text of the report, containing a description of all essential features and giving the principal results. It is prepared and included for the benefit of those who cannot spare the time to read the whole report.

** Numbers in parentheses indicate references on page 33 of this report.

rise due to gravity; in certain cases, they may actually produce a downward motion of the globe.

The results found by acceptance of the assumptions given and by use of the approximations are summarized in a series of formulas and curves. Many of the results are stated in terms of the radius R_2 of the globe at maximum expansion. For tetryl or TNT, this is estimated from observation as

$$R_2 = 4.1\left(\frac{W}{p_A}\right)^{\frac{1}{3}} \qquad [18]$$

where R_2 is in feet,

W is the charge weight in pounds, and

p_A is the total pressure, including atmospheric, expressed in atmospheres.

Figure 4 presents this information graphically.

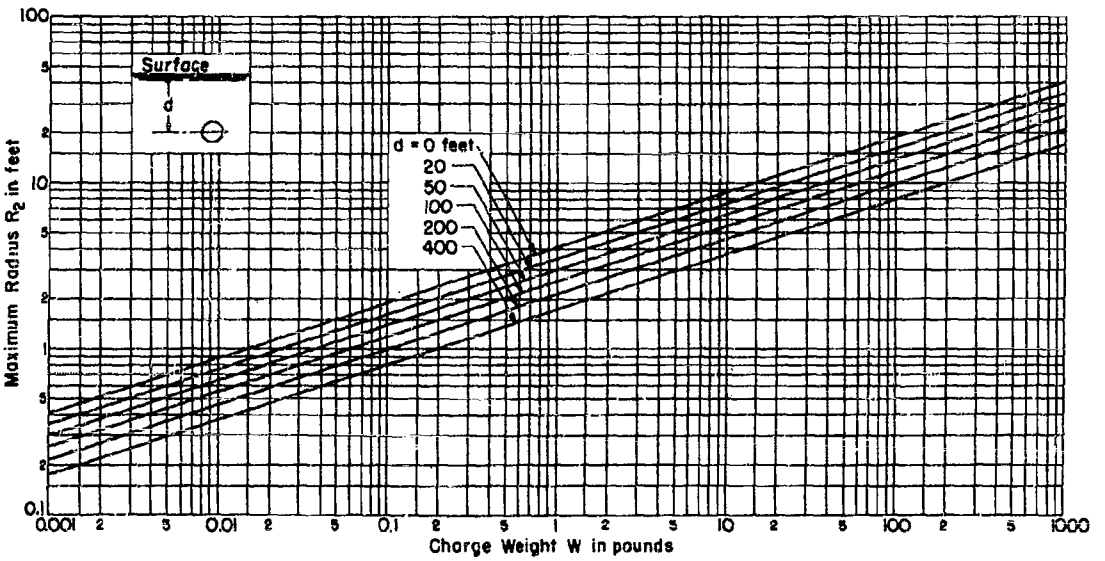

Figure 4 - Maximum Radius R_2 on First Expansion of the Gas Globe Produced by a Charge of W Pounds of Tetryl or TNT

The center of the globe is d feet below the surface of the sea; lines are drawn for several values of d; see Equation [18] at top of page.

Vertical migration due to gravity alone is a special case treated first by the approximate method. By neglecting the action of the gas in the globe, it becomes possible to express the solution in dimensionless terms, and this is done for four depths in Figure 5 on page 13, and in Table 1 on page 13. The minimum depth below the surface at which recompression will

occur is assumed to be equal to the sum of the maximum radius and the rise to the time of the first peak. The results are shown in Figure 6.

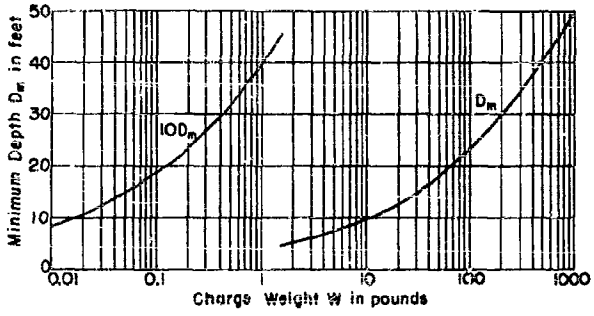

Figure 6 - Curve Giving a Rough Estimate of the Minimum Depth D_m below the Surface at which a Charge W may be Detonated without Blowing through the Surface before Undergoing Recompression

The migration caused by the proximity of a surface, in the absence of gravity, is shown in Figure 7 on page 16, expressed as a fraction of R_2. The combined effect of gravity and a vertical wall for a single small charge is shown in Figures 9 and 10. Curves for estimating the rise of the gas globe under a free surface and above a rigid horizontal bottom are given in Figure 11 and 12 respectively, page 20, for a wide range of charges.

In Figures 15 and 16 on page 26, the two components of migration, vertical and horizontal, are given for the combined effect of gravitation, a free surface, and a vertical wall. As the weight of the charge increases, the gravitational effect is shown to predominate; thus the downward motion of the globe from a small charge is reversed with an increasing charge in the

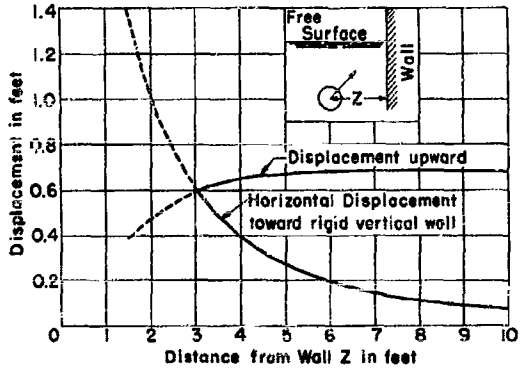

Figure 9 - Upward and Horizontal Components of Displacement of the Gas Globe from 3/4 Ounce of Tetryl or TNT

The charge is assumed to be detonated 10 feet below the surface of the water, far above the bottom, and Z feet from a rigid vertical wall. The curves show the displacement from the point of detonation up to the point of greatest recompression, according to approximate calculations.

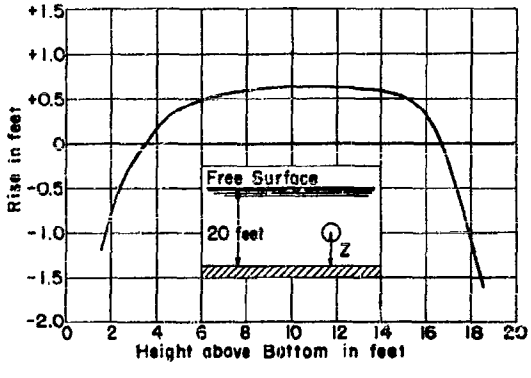

Figure 10 - Displacement of the Center of the Gas Globe from 3/4 Ounce of Tetryl or TNT, up to the Instant of Maximum Recompression

Detonation is assumed to occur at the height shown above a rigid horizontal bottom in water 20 feet deep. Positive ordinates represent a rise, negative ones a descent. The curve is based on approximate calculations.

cases studied, and the motion is upward for all charges over 1/2 pound. The horizontal motion diminishes with an increasing size of charge in the cases studied at all charges over 1/2 pound.

Finally, a rough estimate is made of the effect of the migration upon the pressure that is generated in the water by the recompression of the gas globe; curves are shown in Figure 17 on page 28. A migratory displacement equal to one-third of the maximum radius R_2 decreases the peak pressure by about one-third, whereas a displacement equal to R_2 reduces the peak pressure to one-tenth of its value for zero migration. The impulse, however, is much less affected by the migration.

Important cases remain to be taken up, in particular those in which the distance from the wall is less than $2R_2$, and in which the charge lies between two rigid surfaces, like the ground and a ship's bottom.

The conditions for exact similitude with respect to migration can not be reconciled with those governing the flow of destructive energy from a charge to a target, as applied in the nominal theory of TMB Report 492 (11). The application of model tests of migration effects to the prediction of full-scale phenomena is therefore subject to correction for scale effect and any direct expansion from a very small scale to full scale, without full knowledge of the scale effects, may lead to erroneous conclusions. The exact formulation of the scale effect corrections will form the subject of further work.

MIGRATION OF UNDERWATER GAS GLOBES DUE TO GRAVITY AND NEIGHBORING SURFACES

ABSTRACT

Approximate formulas are assembled, and illustrated by curves, for the migration of gas globes under water due to the action of gravity and of neighboring surfaces. In addition to the effect of a single surface, rigid or free, consideration is given to the combination of a free surface with a rigid bottom or a vertical wall. The general analytical procedure by which the formulas were obtained is described but most of the details are omitted.

INTRODUCTION

The gas globe formed by an underwater explosion not only pulsates in size but also usually changes position as each pulsation occurs (1).* This migration may be of importance because the first recompression or contraction of the globe thereby comes to be centered at a point different from that of the initial detonation, and the location of the point of recompression influences the damage that may be done by the associated secondary pulse of pressure. Measurements of the migration will be reported separately but a number of analytical results have been obtained, and these results will be assembled here for convenience of reference. Deductions of the formulas may be found elsewhere (2).

The motion of the water around the pulsating gas globe is sufficiently slow so that compression of the water can be neglected. Furthermore, good experimental support exists for the assumption that the globe remains approximately spherical during the larger part of the first cycle at least. For these reasons certain aspects of the migration are adequately covered by old investigations on the motion of spheres, which are summarized in Lamb's Hydrodynamics, Section 100 (3).

A thorough survey of the problem has been given recently by Herring (4) and numerical studies have been made, especially of the gravitational displacement, by Taylor and others in England (5) (6) (7) (8). Calculations by an approximate method have been made under the author's supervision at the David Taylor Model Basin. More extended calculations are in progress under the direction of Professor R. Courant of New York University; these will be described in a later report.

---

* Numbers in parentheses indicate references on page 33 of this report.

GENERAL FEATURES OF THE MIGRATION OF A GAS GLOBE

The migration results from the action of gravity and from the effects of bounding surfaces such as a rigid wall or bottom or the free surface of the water; see Figure 1. These various actions are not simply superposed upon each other, because the extent of the migration is greatly increased by the periodic compression of the gas globe and the degree of compression is itself materially decreased when the rapidity of the migration becomes large. The migratory motion implies the existence of kinetic energy of translation in the surrounding water; this energy is abstracted from the energy of the radial motion, with the result that the inward motion of contraction ceases sooner than it would in the absence of the migration.

If the gas globe were fixed in size and far removed from all boundaries, it would simply rise with an acceleration of $2g$, or twice the ordinary acceleration due to gravity; for the water surrounding the gas globe is acted on by a buoyant force equal to the weight of the displaced water, and the effective mass of the water is only half of the mass of the displaced water for the type of motion that results in the upward displacement of the globe (3).

The effects of a bounding surface or wall in the neighborhood of the globe can be regarded as arising in the following manner: While the gas globe is compressed, the pressure in the water is positive, and this pressure is increased owing to the blocking effect of the wall. The pressure increase due to the wall is greatest between the gas globe and the wall, and the inequality of pressure thus produced has somewhat the same effect as if it were due to a gravitational field acting toward the wall. The gas globe then floats away from the wall in accelerated motion. During the expanded phase, on the other hand, the pressure is less than hydrostatic, and the deficit of pressure is greater on the side toward the wall, as it is relieved less on that side by the inflow of water. Thus during the expansion phase motion of the water is developed that acts to carry the gas globe toward the wall. The action on the globe throughout one cycle can be regarded as equivalent to a sort of buoyant force acting alternately away from the wall and toward it.

The action during the expansion phase predominates, however, both because this phase lasts longer than the compression phase, and because the buoyant action on a large globe is much greater than that on a small one. Since the first phase after detonation is one of positive pressure, the initial effect will be a slight displacement of the globe away from the wall; but thereafter the distribution of momentum in the water will always be such that the gas globe moves toward the wall, the momentum increasing in magnitude during each expansion phase and losing only a little during each compression. The actual velocity of the gas globe, however, will be greatest

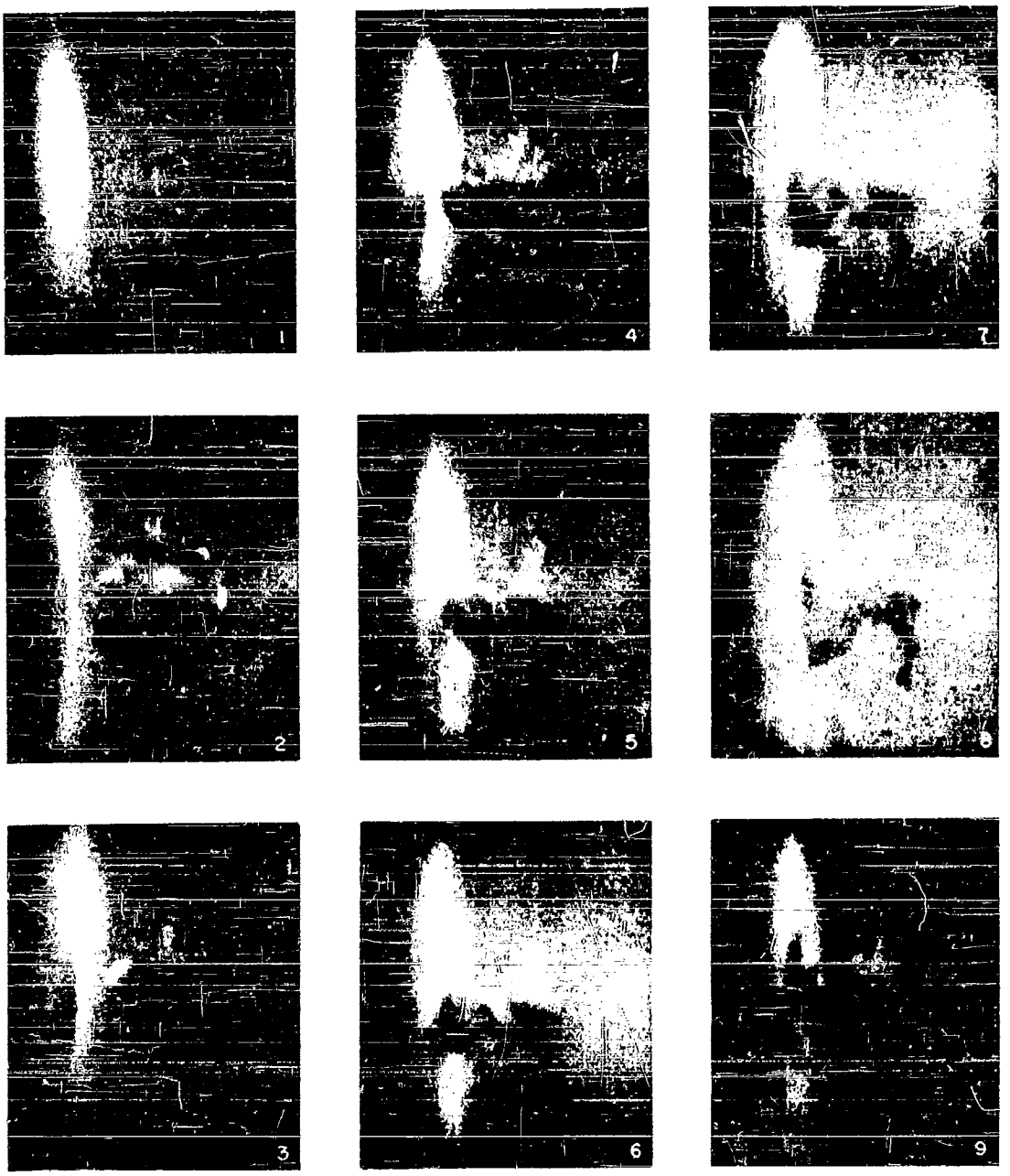

Figure 1 - High-Speed Photographs of a Gas Globe from a Charge Fired near a Wall

The charge was fired 6 inches from a rigid vertical wall shown at the left of the photographs. In Photograph 3 the globe begins to move toward the wall. Photograph 4 shows the peak of compression at the end of the first cycle. After reaching the wall, the globe continues to pulsate on it, as shown by Photographs 5 to 9.

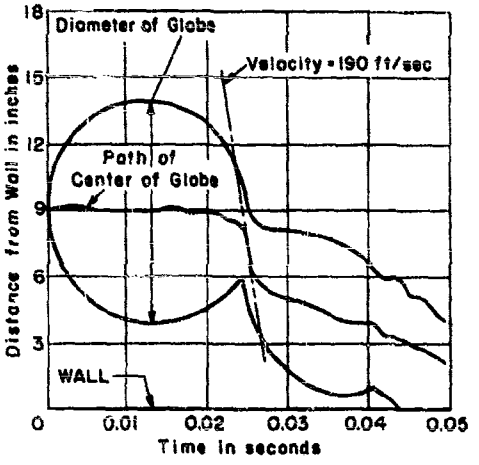

Figure 2 - Curves of Size and Position of a Gas Globe near a Vertical Wall

The charge was fired 9 inches from a rigid vertical wall. Note that the velocity of the center of the globe is greatest during the compression phases.

during the compression phase, when the momentum becomes concentrated into a comparatively small volume of water surrounding the globe. Thus the center of the gas globe moves continually toward the wall but advances chiefly in spurts during the compression phases, as shown in Figure 2.

The effect of a free surface, when the gas globe is not near enough to the surface to break through, is approximately opposite to that of a rigid surface. The initial expansion of the gas globe accelerates the water above it upward and that below it downward. While the globe is expanded, the pressure near it is very low, and this deficit of pressure acts so as to check and then reverse the radial motion. Because the pressure remains constant on the free surface, the deficit is less, or the pressure is greater, near the surface than it would be if there were additional water instead of air above the surface; and because of this relative excess of pressure, the water lying either above or below the gas globe is given an excess of momentum downward. During the next compression phase this momentum becomes concentrated in a much smaller volume of water and, provided the effect is not canceled by the simultaneous and opposed action of gravity, the globe is carried downward. Arguments from momentum in the water are dangerous, however; some further remarks on this subject are introduced at the end of this report.

By this action, the gas globe is attracted toward a rigid boundary but repelled from the free surface of the water. Although the action of gravity is always present, to cause the globe to rise through the water by virtue of its buoyant nature, attraction by the bottom in shallow water or repulsion from the free surface of the water may merely decrease the rise due to gravity, or it may actually produce a downward displacement of the globe.

The effect of a boundary should increase as the gas globe approaches the boundary. Under certain circumstances, however, observation shows that marked departures from sphericity of the globe may occur. Near a free surface, for example, part of the gas may blow through the surface while the remainder migrates down into the water; see Figure 3. Furthermore, a gas globe

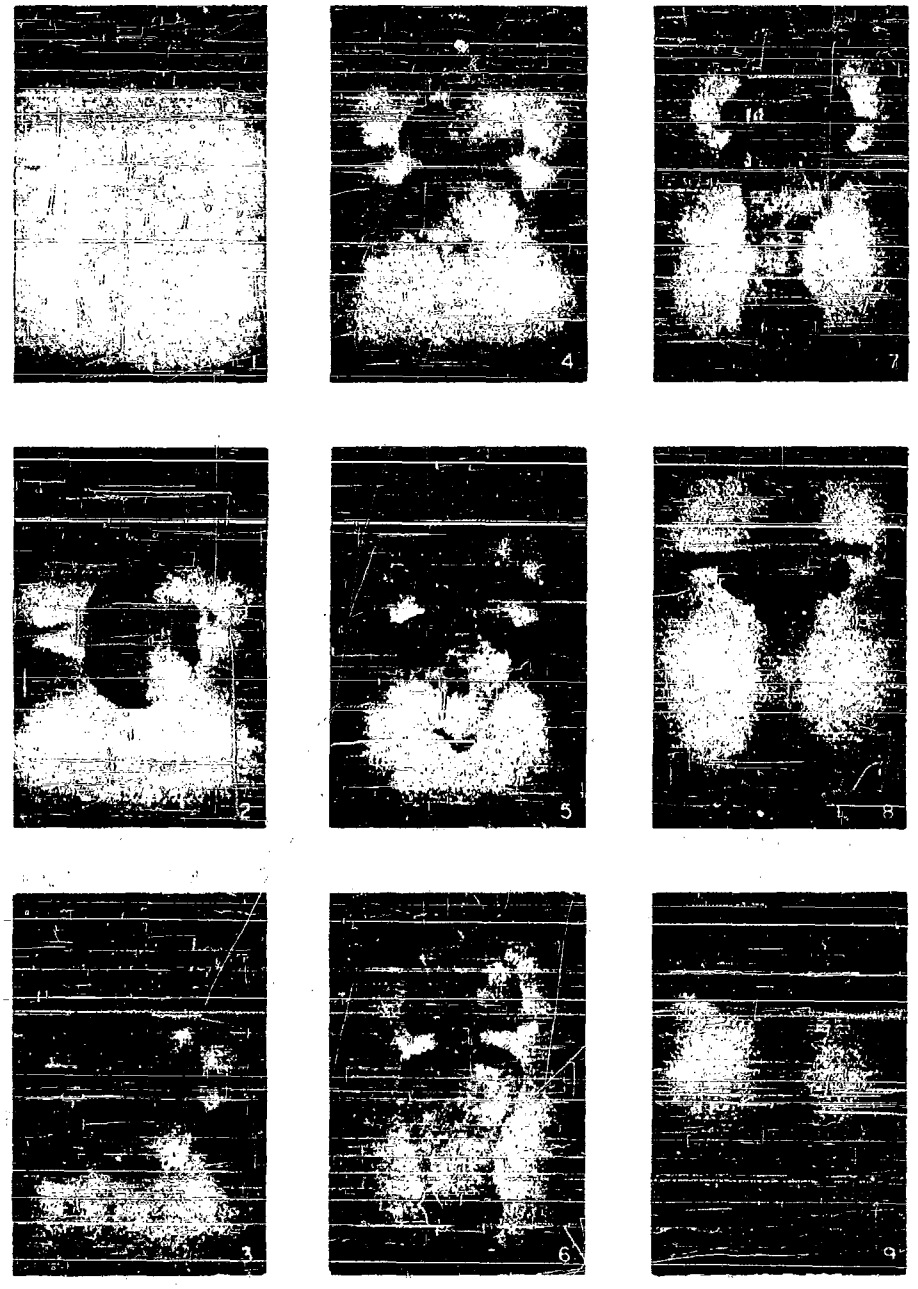

Figure 3 - High-Speed Photographs of a Gas Globe from a Charge Fired Just under the Free Water Surface

The charge was fired 1 inch under the surface of the water. In Photograph 2 part of the gas has vented through the water surface. In Photographs 4 to 9 the lower part of the globe is moving downward. More gas appears to be venting through the surface on the second expansion shown in Photograph 7.

midway between two rigid boundaries may break in two, one half migrating each way (1). Such features can only be handled by a more complete analysis in which the shape of the globe is not limited by assumption but is left to the control of the hydrodynamic action.

DESCRIPTION OF THE MATHEMATICAL METHOD FOR DETERMINING MIGRATION

Provided the gas globe remains spherical, the effect of gravity alone is easily found. The analysis can be extended to include the effect of plane boundaries by using the method of images that is familiar in electrostatic theory, and by expanding in negative powers of the distances from the surfaces, as in Herring's report (4) The entire analysis, including a special method of approximation for the first oscillation, has been completed (2) but is not given here.

If the solution is required to satisfy the boundary conditions only as far as the inverse second powers of the distances from the boundaries, differential equations of the following type are obtained:

$$\dot{R}^2 = \frac{1}{1+\frac{MR}{2}}\left\{\frac{C}{R^3} + \frac{2}{\rho R^3}\int (p_g - p_0)\,R^2\,dR - \frac{1}{6}\left(\dot{X}^2+\dot{Y}^2+\dot{Z}^2\right)\right. \qquad [1]$$

$$\left. + \frac{1}{4}R^2\dot{R}\left(N_X\dot{X}+N_Y\dot{Y}+N_Z\dot{Z}\right) - \frac{2}{3}\left[g_X(X-X_0)+g_Y(Y-Y_0)+g_Z(Z-Z_0)\right]\right\}$$

$$\dot{X} = \frac{3}{4}N_X R^2\dot{R} - \frac{3}{2}\frac{N_X}{R^3}\int_0^t R^4\dot{R}^2\,dt - \frac{2g_X}{R^3}\int_0^t R^3\,dt \qquad [2]$$

$$\dot{Y} = \frac{3}{4}N_Y R^2\dot{R} - \frac{3}{2}\frac{N_Y}{R^3}\int_0^t R^4\dot{R}^2\,dt - \frac{2g_Y}{R^3}\int_0^t R^3\,dt \qquad [3]$$

$$\dot{Z} = \frac{3}{4}N_Z R^2\dot{R} - \frac{3}{2}\frac{N_Z}{R^3}\int_0^t R^4\dot{R}^2\,dt - \frac{2g_Z}{R^3}\int_0^t R^3\,dt \qquad [4]$$

Here
- R is the radius of the bubble,
- X, Y, Z are the cartesian coordinates of its center,
- t is the time,
- $\dot{R}, \dot{X}, \dot{Y}, \dot{Z}$ stand for dR/dt, dX/dt, dY/dt, dZ/dt, respectively,
- X_0, Y_0, Z_0 denote values at $t = 0$,
- ρ is the density of the water,
- p_0 is the total hydrostatic pressure including atmospheric pressure, at the point X_0, Y_0, Z_0,
- p_g is the pressure of the gas in the globe, supposed to be a known function of R,

g_X, g_Y, g_Z are components in the X, Y, Z directions of the gravitational acceleration g,

C is a constant depending on the initial conditions, and

M, N_X, N_Y, N_Z stand for simple functions of X, Y, and Z, depending upon the choice of axes and upon the nature and location of the boundaries.

An accurate solution of these equations can be effected only by numerical integration. This method has the disadvantage that many repetitions of the entire calculation are required to obtain results covering a wide variety of conditions.

For the first oscillation of the globe, on the other hand, formulas can be obtained which, although less accurate, are widely applicable. These formulas give the position of the gas globe at the peak of the first recompression, which is particularly important because it is the point of origin of the first secondary pulse of pressure.

The method of approximation is based upon the observation that, as the time t advances, the integrals in Equations [2], [3], and [4] grow chiefly while R is large, whereas, because of the factor $1/R^3$ preceding the integrals, they are effective in causing displacement of the gas globe chiefly while R is small. Approximate values for the displacement during the first recompression can be obtained, therefore, by substituting for these integrals in Equations [2], [3], and [4] constants equal to the values of the integrals at the instant of greatest compression. In calculating these values, on the other hand, an approximate value of dR/dt, obtained by neglecting certain terms in Equation [1], is sufficiently accurate. The same expression for dR/dt leads to a corrected value of the period.

The first period is thus found to be

$$T_1 = T_{10}(1 + 0.20\,MR_2) \qquad [5]$$

where T_{10} is the period when no bounding surfaces are near. Here M is the coefficient that occurs in Equation [1], and R_2 is the maximum radius of the gas globe during the first expansion; see Equation [18].

The approximate formulas obtained for the displacement of the center of the gas globe from the position of detonation X_0, Y_0, Z_0 to the point X_1, Y_1, Z_1 at which the next minimum radius occurs, may be written

$$X_1 - X_0 = \sqrt{6}\,B_X R_2 U \qquad [6a]$$

$$Y_1 - Y_0 = \sqrt{6}\,B_Y R_2 U \qquad [6b]$$

$$Z_1 - Z_0 = \sqrt{6}\,B_Z R_2 U \qquad [6c]$$

where

$$B_X = -\frac{1}{\sqrt{6}}\left(\frac{6\rho}{p_0}\, g_X Q R_2 + 3PN_X R_2^2\right) \qquad [7a]$$

$$B_Y = -\frac{1}{\sqrt{6}}\left(\frac{6\rho}{p_0}\, g_Y Q R_2 + 3PN_Y R_2^2\right) \qquad [7b]$$

$$B_Z = -\frac{1}{\sqrt{6}}\left(\frac{6\rho}{p_0}\, g_Z Q R_2 + 3PN_Z R_2^2\right) \qquad [7c]$$

Here N_X, N_Y, and N_Z are to be evaluated at the point X_0, Y_0, Z_0, and P, Q, and U represent the three integrals defined as follows:

$$P = \int_{y_1}^{1} y^4\left(1 + \frac{1}{2}MR_2 y\right)^{-\frac{1}{2}}\left[\frac{C'}{y^3} - \frac{1}{\gamma - 1}\left(\frac{R_0}{R_2}\, y\right)^{3\gamma} - 1\right]^{\frac{1}{2}} dy \qquad [8]$$

$$Q = \int_{y_1}^{1} y^3\left(1 + \frac{1}{2}MR_2 y\right)^{\frac{1}{2}}\left[\frac{C'}{y^3} - \frac{1}{\gamma - 1}\left(\frac{R_0}{R_2}\, y\right)^{3\gamma} - 1\right]^{-\frac{1}{2}} dy \qquad [9]$$

$$U = \int_{y_1'}^{1} \left(1 + \frac{1}{2}MR_2 y\right)^{\frac{1}{2}}\left[C'' y^3 - \frac{1}{\gamma - 1}\left(\frac{R_0}{R_2}\right)^{3\gamma} y^{6-3\gamma} - y^6 - B^2\right]^{-\frac{1}{2}} dy \qquad [10]$$

in which

$$B^2 = B_X^2 + B_Y^2 + B_Z^2 \qquad [11]$$

R_0 is the radius of the gas globe when the pressure of the gas equals the hydrostatic pressure at the level of its center, and C' and C'' have such values that the roots of the quantity in square brackets are in each case the same as the limits of integration, that is 1 and y_1 or y_1'. The gas is assumed to behave as an adiabatic ideal gas, in which the ratio of its specific heats is γ.

For gas globes due to underwater explosions, R_2/R_0 exceeds 2.5 and the term in γ has only a small influence upon the values of P and Q; this term represents the effect of the gas upon the motion during the expansion phase. If this term is dropped, P and Q are easily obtained as series in powers of MR_2:

$$P = 0.182(1 - 0.18\, MR_2 \cdots) \qquad [12a]$$

$$Q = 0.467(1 + 0.23\, MR_2 \cdots) \qquad [12b]$$

A curve for the integral U, defined in Equation [10], as a function of B^2 has been constructed by numerical integration, on the simplifying

assumption that $\gamma = 4/3$. As B^2 increases, U decreases; the conversion of the energy of oscillation into translatory kinetic energy, as a result of gravity or of the presence of boundaries, checks the inward motion and thereby diminishes the extent of the compression, with a resulting decrease in U. For $R_2/R_0 = 2.65$, which seems to be within reason as an estimate for actual gas globes, the curve is represented closely by the formula

$$U = \frac{1.06}{\sqrt{B + \dfrac{0.009}{1 + 4000B^2}}} \qquad [13]$$

With the introduction of these approximate values of the integrals, Equations [6a, b, c], [7a, b, c], and [11] become, for sea water of specific gravity $\rho = 1.026$, if W is in pounds,

$$X_1 - X_0 = FB_X, \quad Y_1 - Y_0 = FB_Y, \quad Z_1 - Z_0 = FB_Z \qquad [14a, b, c]$$

where

$$F = \frac{2.60\ R_2}{\sqrt{B + \dfrac{0.009}{1 + 4000\,B^2}}} \qquad [15]$$

$$B = +\sqrt{B_X^2 + B_Y^2 + B_Z^2} \qquad [16]$$

$$B_X = 0.0346\,(1 + 0.23\,MR_2)\,c_X\,\frac{R_2}{p_A} - 0.223\,(1 - 0.18\,MR_2)\,N_X R_2^2 \qquad [17]$$

with two other sets of equations similar to Equations [15], [16], and [17], in which X is changed to Y or to Z, respectively. Here in the products MR_2, $N_X R_2^2$, $N_Y R_2^2$, $N_Z R_2^2$ it is sufficient to use the same unit of length in both factors, but elsewhere R_2 has been assumed to be expressed in feet; p_A is the hydrostatic pressure at the initial level of the center of the gas globe measured in atmospheres; and c_X, c_Y and c_Z are the cosines of the angles between the upward vertical and the X, Y and Z axes, respectively, so that $g_X = -gc_X$, $g_Y = -gc_Y$, $g_Z = -gc_Z$.

Here R_2, the maximum radius, may be assumed to vary as $(W/p_A)^{\frac{1}{3}}$. For tetryl or TNT a fair estimate seems to be

$$R_2 = 4.1\left(\frac{W}{p_A}\right)^{\frac{1}{3}} \text{ feet} \qquad [18]$$

where W is the weight of the charge in pounds and p_A is the total pressure in atmospheres. For tetryl the best experimental evidence available would replace 4.1 by 4.2, whereas for TNT, Figure 2 in Reference (7) gives 3.95. Equation [18] is plotted for several values of p_A in Figure 4; p_A is specified by

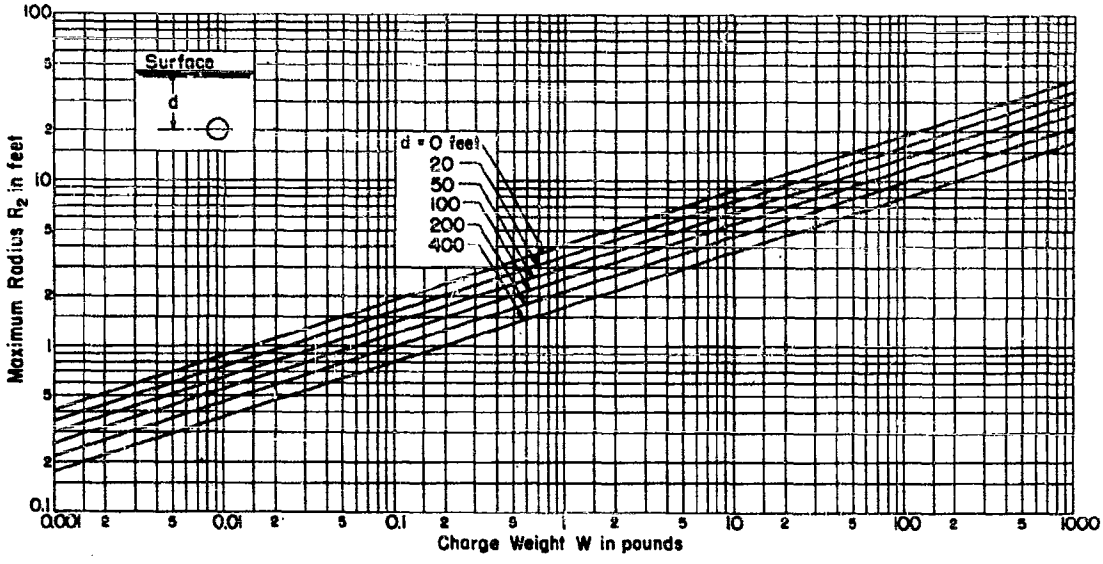

Figure 4 - Maximum Radius R_2 on First Expansion of the Gas Globe Produced by a Charge of W Pounds of Tetryl or TNT

The center of the globe is d feet below the surface of the sea; lines are drawn for several values of d; see Equation [18].

giving the equivalent depth d in feet below the surface of the sea, so that $p_A = 1 + d/33$.

With this value of R_2 and with M, N_X, N_Y, N_Z now expressed in terms of feet, Equations [15] and [17] become

$$F = \frac{10.7 \left(\frac{W}{p_A}\right)^{\frac{1}{3}}}{\sqrt{B + \frac{0.009}{1 + 4000\,B^2}}} \qquad [19]$$

$$B_X = 0.142\left[1 + 0.94\,M\left(\frac{W}{p_A}\right)^{\frac{1}{3}}\right] c_X \frac{W^{\frac{1}{3}}}{p_A^{\frac{4}{3}}} - 3.75\left[1 - 0.74\,M\left(\frac{W}{p_A}\right)^{\frac{1}{3}}\right] N_X \left(\frac{W}{p_A}\right)^{\frac{2}{3}} \qquad [20]$$

or, if the small term in M is dropped, approximately,

$$B_X = 0.142\,c_X \frac{W^{\frac{1}{3}}}{p_A^{\frac{4}{3}}} - 3.75\,N_X \left(\frac{W}{p_A}\right)^{\frac{2}{3}} \qquad [21]$$

with similar equations in Y and Z.

The accuracy of these approximate formulas is hard to estimate. Serious doubts arise as to their validity when the center of the gas globe comes closer to any bounding surface than $2R_2$ or twice its maximum radius. No correction has been made for the change in hydrostatic pressure as the

gas globe rises or sinks. Furthermore, effects due to compressibility of the water, associated with the emission of acoustic radiation, have been neglected.

MIGRATION DUE TO GRAVITY ALONE

If X is taken vertically upward, Equations [1] and [2] become, when no boundary is near,

$$\dot{R}^2 = \frac{C}{R^3} + \frac{2}{\rho R^3}\int (p_g - p_0) R^2 dR - \frac{1}{6}\dot{X}^2 + \frac{2}{3} g (X - X_0) \qquad [22]$$

$$\dot{X} = \frac{2g}{R^3}\int_0^t R^3 dt \qquad [23]$$

Here g is the acceleration due to gravity.

Numerical integrations of these equations have been given by Taylor (5) and others (6) (7) (8) The effect of the gas, as represented by the occurrence of p_g in Equation [22], is usually not large; its smallness arises from the fact that, in practical cases of motion due to gravity alone, the inward motion of the water during each compression phase is arrested chiefly not by the gas but as a consequence of the conversion of radial kinetic energy of the water into kinetic energy of translational motion. That is, when the center of the gas globe is nearly stationary, the radial kinetic energy of the inrushing water becomes converted, at the instant of peak compression, entirely into energy of compression of the gas; but if translational motion of the gas globe occurs, part of the kinetic energy remains in the water in association with the translational motion. For this reason the inward radial motion is checked at a larger radius than when the globe is stationary. In migration due to gravity alone, nearly all of the energy usually thus remains in the water, and the motion during the compression phase is nearly the same as if no gas at all were present. Because of this conversion of the energy, the radial oscillations gradually die out, as the velocity of rise increases, especially if the hydrostatic pressure is very low or if the gas globe was produced by a large charge.

In UNDEX 10 (7), Figures 1 and 8, two plots are given, based upon numerical integrations, from which estimates of the rise due to gravity can be made for a wide range of charge weights and depths. These estimates agree within 8 per cent with values calculated from the convenient approximate formula

$$H = 4\frac{\sqrt{W}}{p_A} \qquad [24]$$

where W is the weight of the charge in pounds,

p_A is the total hydrostatic pressure, including atmospheric pressure, expressed in atmospheres, and

H is the rise in feet from the point of detonation to the location of the next peak compression.

The total rise during the first compression and the re-expansion should be about $2H$. The charge may vary from 1 ounce to 1000 pounds, and the depth may be as much as 300 feet for the larger charges.

In using this formula it must be remembered that if the point of detonation is too close to the surface, the gases will blow through the surface, at least in large part, and no typical recompression can occur. This ought almost certainly to be the case if the point of detonation is closer to the surface than the maximum radius attained by the gas globe in its first expansion.

The formula for H as given by the approximate calculations of the present report may be found by putting $B_Y = B_Z = 0$, $c_X = 1$, $N_X = 0$ and dropping the term in B^2 in Equation [19], which turns out to be negligible in all interesting cases of purely gravitational action. Then Equations [14a], [16], [19], and [21] give $H = X_1 - X_0 = 4.0\sqrt[3]{W}/p_A$, in exact agreement with Equation [24].

It will be noted that the rise H up to the first peak compression increases as the weight of the charge increases, and also as the hydrostatic pressure decreases. The increase results partly from the greater buoyant force on a larger gas globe and partly from an increase in the time occupied by the oscillation.

An interesting plot given in Reference (8) is reproduced in Figure 5. It shows the radius of the gas globe and the upward displacement of its center as functions of the time, for four different values of the initial hydrostatic pressure, as found by numerical integration. The plot applies approximately to any charge at suitable depths; small errors will remain owing to the fact that in the calculations no allowance was made for the gas pressure. It is interesting that at the smallest depth, $z_0 = 1$, the gravitational effect is so large that the radial motion is almost deadbeat, so that no succeeding pulses occur.

The scales in Figure 5 vary with W, the weight of the charge in pounds. Unity on the axis of ordinates represents L feet, and unity on the axis of abscissas represents T seconds, where L and T are given by the formulas

$$L = 10\,W^{\frac{1}{3}} \text{ feet}$$

$$T = 0.55\,W^{\frac{1}{3}} \text{ seconds}$$

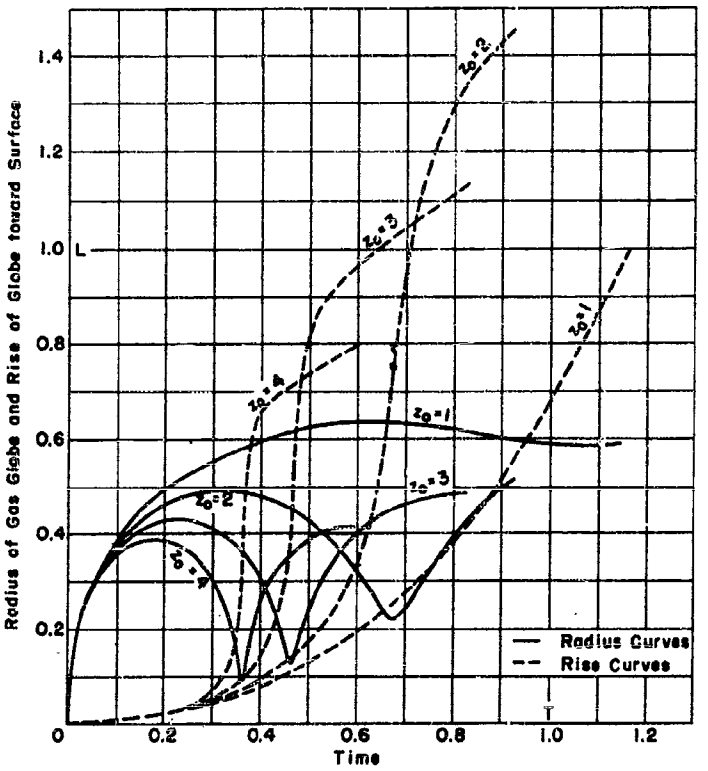

Figure 5 - Curves, Obtained by Numerical Integration, Showing Variation with Time of the Radius of the Gas Globe and the Rise of the Globe toward the Surface

For notation and units, see the text. This figure is copied from Reference (8).

TABLE 1

Values of the Coordinate Units for Figure 5

Charge pounds	L feet	T seconds	$z_0 L$*			
			$z_0 = 1$	$z_0 = 2$	$z_0 = 3$	$z_0 = 4$
1/16	5	0.39	5	10	15	20
1	10	0.55	10	20	30	40
50	26.6	0.90	27	53	80	106
100	31.6	0.98	32	63	95	126
300	41.6	1.12	42	83	125	166
1000	56.2	1.30	56	112	168	225

* Here $z_0 L$ is the total hydrostatic pressure in equivalent feet of sea water, where 33 feet = 1 atmosphere.

The four pairs of curves refer to an initial hydrostatic pressure, including atmospheric pressure, at the center of the globe equivalent to $z_0 L$ feet of sea water, or to L, $2L$, $3L$, and $4L$ feet, respectively. Some values are given in Table 1.

A question of interest in practice concerns the depth at which the globe from a given charge may be

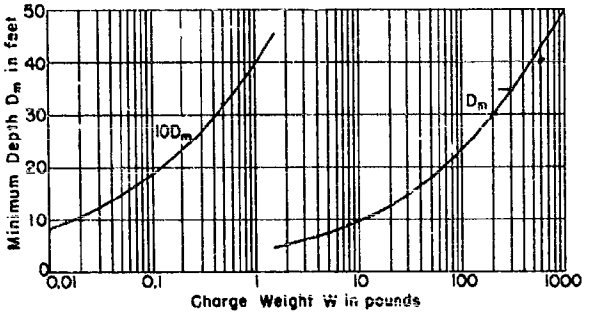

Figure 6 - Curve Giving a Rough Estimate of the Minimum Depth D_m below the Surface at which a Charge W may be Detonated without Blowing through the Surface before Undergoing Recompression

expected to execute a complete oscillation and emit a secondary pressure pulse during a first phase of recompression. If the charge is too near the surface, at least part of the gas will blow through the surface and no recompression of the full globe can occur, as illustrated in Figure 3 on page 5. The proper criterion is uncertain. It may be assumed tentatively as plausible, and as supported somewhat by experiment, that recompression will occur only when the depth exceeds both the maximum radius as calculated for a spherical gas globe and the calculated gravitational rise to the first peak compression.* The minimum depth D_m determined in this way is plotted on a basis of charge weight W in Figure 6. If the depth of detonation exceeds D_m, recompression of the gas globe should occur, although the emitted pulse of pressure may not be very effective if, because of the gravitational rise, the recompression occurs very near to the surface of the water.

GENERAL EFFECT OF SURFACES

A nearby surface limiting the body of water attracts or repels the gas globe. In a rough way this effect is superposed upon that of gravity, as is evident from the linear combination of the two terms in B_X, B_Y, B_Z, as in Equations [7a, b, c], [17], [20], [21]. Some interaction of the two effects arises, however, from the fact that the integral U in Equation [6a, b, c], or the quantity B defined by Equation [16], depends upon both effects.

Comparisons for charges of different weights are most easily made at distances from the limiting surface in proportion to the maximum radius R_2. Then at corresponding distances the factors N_X, N_Y, N_Z in Equations [7a, b, c], [17], [20], [21] actually vary as $1/R_2^2$, so that the corresponding surface terms in B_X, B_Y, B_Z do not vary at all, whereas under fixed hydrostatic pressure the gravity terms vary as R_2 or as $W^{\frac{1}{3}}$, where W is the weight of the charge. For this reason it turns out that, at distances of the order of $2R_2$

* For small charges, where the rise is decreased or even made negative by an effect of the free surface, D_m is determined by the maximum radius.

from the surface and at ordinary depths below the surface of the water, the effect of a bounding surface should predominate for small charges like detonators; for charges of a few ounces the two effects should be comparable in magnitude, and for charges of 100 pounds or more the gravity effect should usually predominate.

MIGRATION DUE TO A SURFACE IN THE ABSENCE OF GRAVITY

If Z denotes the distance from the surface, $N_X = N_Y = 0$, and it is found that

$$M = \pm \frac{1}{Z}, \quad N_Z = \pm \frac{1}{Z^2} \qquad [25a, b]$$

where the upper sign refers to a rigid surface and the lower sign to a free surface.

The period of the first oscillation will be approximately, from Equation [5]

$$T_1 = T_{10}\left(1 \pm 0.20 \frac{R_2}{Z}\right) \qquad [26]$$

in terms of the period T_{10} for $Z = \infty$ and the first maximum radius R_2. Thus a rigid boundary lengthens the period, a free surface decreases it. For $Z = 2R_2$, however, the change in the period is only 10 per cent.

If the gravitational effect is neglected, as is justifiable for the gas globe produced by a detonator under ordinary pressures, from Equations [14c], [15], [16], and the Z analog of Equation [17],

$$\frac{Z_1 - Z_0}{R_2} = \mp \frac{2.60\,B}{\sqrt{B + \dfrac{0.009}{1 + 4000\,B^2}}} \qquad [27]$$

$$B = 0.223\left(1 \mp 0.18 \frac{R_2}{Z}\right)\left(\frac{R_2}{Z}\right)^2 \qquad [28]$$

Here $Z_1 - Z_0$ represents the displacement of the gas globe, from the point of detonation up to the first peak recompression, measured positively away from the surface.

For R_2/Z near 1/2, approximately

$$\frac{Z_1 - Z_0}{R_2} = \mp 1.23 \frac{R_2}{Z} \qquad [28a]$$

whereas at very small R_2/Z, approximately

$$\frac{Z_1 - Z_0}{R_2} = \mp 6.1 \frac{R_2^2}{Z^2} \qquad [28b]$$

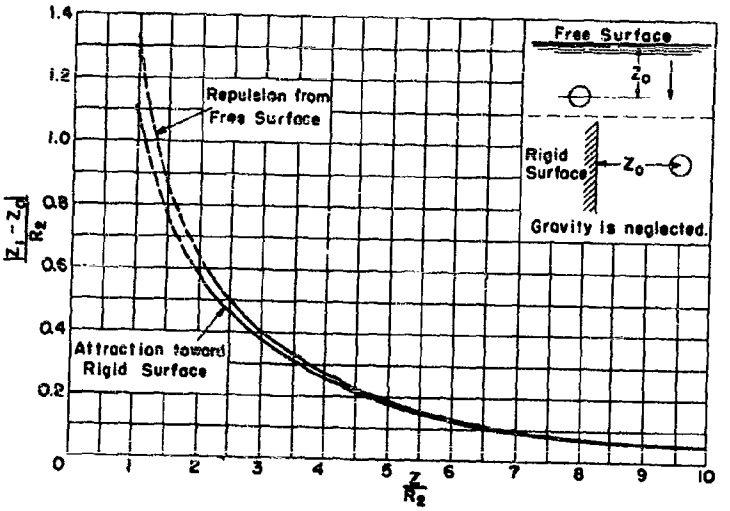

Figure 7 - Effect of a Single Surface on a Gas Globe when Gravity is Neglected

$|Z_1 - Z_0|$ denotes the displacement of the center during the interval until the first peak compression, Z_0 the distance of the point of detonation from the surface, R_2 the maximum radius during the first expansion.

Thus the effect of the surface should fall off with increasing distance Z at first nearly as $1/Z$, then more rapidly and ultimately as $1/Z^2$.

The sign indicates that a rigid surface (upper signs) should attract the gas globe, whereas a free surface (lower signs) should repel it, in agreement with observation. The two effects are nearly equal in magnitude, but the repulsion is a little greater.

Equation [27] is plotted in Figure 7. In using these formulas it must be remembered that R_2 varies with the hydrostatic pressure, as indicated in Equation [18]. The formulas probably become unreliable when $Z < 2R_2$; the corresponding parts of the curves are shown broken in Figure 7.

MIGRATION DUE TO GRAVITY AND A SI

Assume that the surface
the gas globe, make an angle θ wi
tance of the center of the gas gl
coordinate of the center measured
upward in a vertical plane; see Fi
are Equations [14a, c], [15], [16]
sin θ, $c_Y = 0$, $c_Z = \cos\theta$; and the

$$M =$$

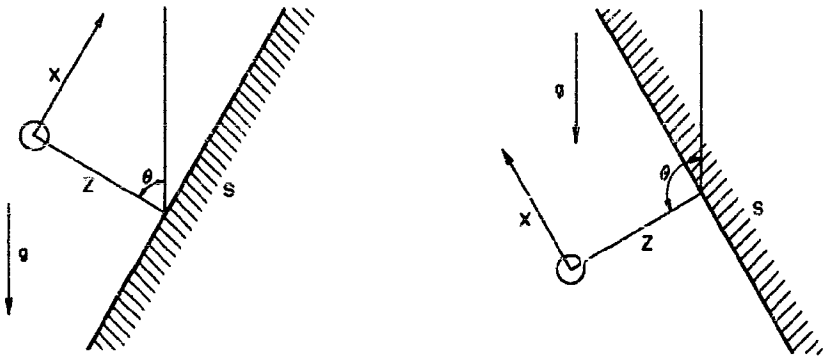

Figure 8 - Diagram Illustrating a Gas Globe under the Simultaneous Influence of Gravity and a Neighboring Rigid Surface S

The circle represents a globe of gas surrounded by water; the mass of water is bounded on one side by a rigid wall.

while $N_X = N_Y = 0$. Hence, for the displacement of the globe to the first peak recompression

$$X_1 - X_0 = FB_X, \quad Z_1 - Z_0 = FB_Z \qquad [30a, b]$$

$$F = \frac{2.60\, R_2}{\sqrt{B + \dfrac{0.009}{1 + 4000\, B^2}}} \qquad [31a]$$

$$B = \sqrt{B_X^2 + B_Z^2} \qquad [31b]$$

$$B_X = 0.0346 \left[1 + 0.23 \frac{R_2}{Z}\right] \frac{R_2}{p_A} \sin\theta \qquad [32]$$

$$B_Z = 0.0346 \left[1 + 0.23 \frac{R_2}{Z}\right] \frac{R_2}{p_A} \cos\theta - 0.223 \left[1 - 0.18 \frac{R_2}{Z}\right] \left(\frac{R_2}{Z}\right)^2 \qquad [33]$$

or, to a good approximation,

$$B_X = 0.0346 \frac{R_2}{p_A} \sin\theta \qquad [34a]$$

$$B_Z = 0.0346 \frac{R_2}{p_A} \cos\theta - 0.223 \left(\frac{R_2}{Z}\right)^2 \qquad [34b]$$

Here $X_1 - X_0$ and $Z_1 - Z_0$ represent components of the displacement measured positively in the direction of increasing X or Z.

The first period, from Equation [5], is

$$T_1 = T_{10} \left[1 + 0.20 \frac{R_2}{Z}\right] \qquad [35]$$

In the formulas, values of W are in pounds and all values of X and Z in feet; p_A is the total hydrostatic pressure in atmospheres.

The case, $\theta = 0$, applies to a rigid horizontal bottom. The formulas for $\theta = \pi$, on the other hand, are found to apply to a free surface, with Z measured away from the surface and hence downward, provided changes are made corresponding to the assumption that, for the free surface,

$$M = -\frac{1}{Z}, \quad N_Z = -\frac{1}{Z^2} \qquad [36a, b]$$

in place of Equations [29a, b]. Hence for a rigid horizontal bottom and for the free surface of the water, the formulas can conveniently be written together as follows:

$$Z_1 - Z_0 = \frac{2.60\, B_Z R_2}{\sqrt{|B_Z| + \dfrac{0.009}{1 + 4000\, B_Z^2}}} \qquad [37]$$

$$B_Z = \pm\left\{0.0346\left[1 \pm 0.23\,\frac{R_2}{Z}\right]\frac{R_2}{p_A} - 0.223\left[1 \mp 0.18\,\frac{R_2}{Z}\right]\left(\frac{R_2}{Z}\right)^2\right\} \qquad [38]$$

or, to a good approximation

$$B_Z = \pm\left[0.0346\,\frac{R_2}{p_A} - 0.223\left(\frac{R_2}{Z}\right)^2\right] \qquad [38a]$$

The upper sign refers to the rigid bottom and the lower sign to the free surface. The symbol $|B_Z|$ denotes the numerical value of B_Z taken without regard to sign; and $Z_1 - Z_0$ represents in each case the displacement measured positively away from the surface.

The first period is

$$T_1 = T_{10}\left[1 \pm 0.20\,\frac{R_2}{Z}\right] \qquad [39]$$

These formulas probably become unreliable when

$$Z < 2R_2 = 8\left(\frac{W}{p_A}\right)^{\frac{1}{3}}$$

Because of the negative sign between the two parts of B_Z, the gravitational effect and the effect of the surface oppose each other in the case of a free surface or a rigid surface below the charge, whereas the two effects are in the same direction when a rigid surface lies above the charge. The gas globe from a *small* charge near the surface of the water sinks instead of rising.

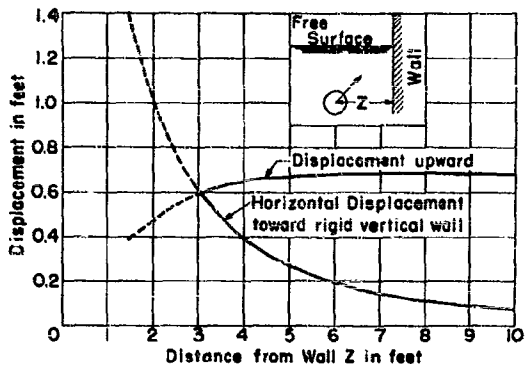

Figure 9 - Upward and Horizontal Components of Displacement of the Gas Globe from 3/4 Ounce of Tetryl or TNT

The charge is assumed to be detonated 10 feet below the surface of the water, far above the bottom, and Z feet from a rigid vertical wall. The curves show the displacement from the point of detonation up to the point of greatest recompression, according to approximate calculations.

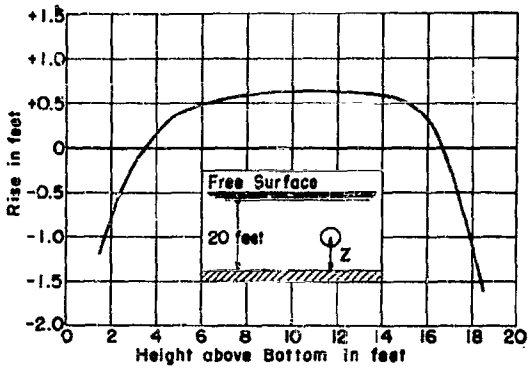

Figure 10 - Displacement of the Center of the Gas Globe from 3/4 Ounce of Tetryl or TNT, up to the Instant of Maximum Recompression

Detonation is assumed to occur at the height shown above a rigid horizontal bottom in water 20 feet deep. Positive ordinates represent a rise, negative ones a descent. The curve is based on approximate calculations.

The effects due to gravity and to the surface are almost additive but not entirely so, because of the occurrence of B or $|B_g|$ in F. When gravity and the surface produce opposite effects, as in the case of a rigid bottom or a free surface, the net displacement is a little greater than the numerical difference of the values that the two displacements would have if they occurred singly. In such cases the gas globe contracts to a smaller radius than it would if only one effect occurred, and this decrease in the minimum radius increases the displacement. Otherwise, as in the case of a rigid wall located to one side of the globe or the rigid bottom of a boat above it, the two displacements are slightly decreased by their coexistence.

The formulas are illustrated in Figures 9 and 10, which refer to a 3/4-ounce charge of tetryl or TNT detonated at Z feet from a surface. In Figure 9 the surface is assumed to be a rigid vertical wall, the charge is detonated 10 feet below the surface of the water, and the bottom is assumed to lie much deeper. The vertical rise of the center of the gas globe and its horizontal displacement toward the wall, up to the point of maximum compression, are shown by curves. In Figure 10 curves are shown for the same charge Z feet above a horizontal rigid bottom in water 20 feet deep. It will be noted that the gas globe descends if formed less than about 3.5 feet from either the bottom or the free surface.

The formulas for a free surface and for a rigid bottom are plotted in general terms in Figures 11 and 12, as explained under the figures.

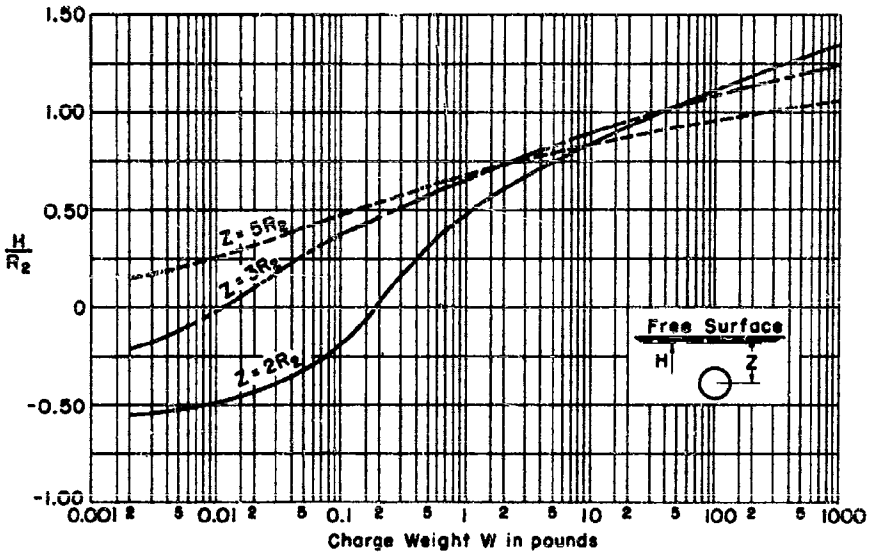

Figure 11 - Rise H of the Gas Globe Formed by W Pounds of Tetryl or TNT Detonated at a Depth Z below the Surface of the Sea of Infinite Depth

H is the rise of the center of the globe from the time of detonation up to the time of the first peak recompression; both H and Z are expressed in terms of R_2, the intervening maximum radius. Curves are shown for three values of Z. For R_2 see Figure 4 or Equation [18].

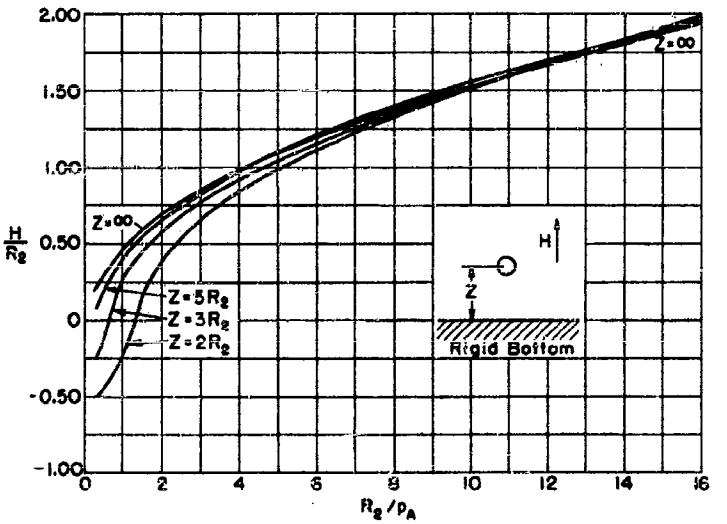

Figure 12 - Curves for Estimating the Rise H of a Gas Globe at a Distance Z above the Bottom of the Sea

The rise is from the time of detonation up to the time of the next peak recompression. R_2 is the intervening maximum radius in feet; p_A is the total hydrostatic pressure in atmospheres or $1 + d/33$ where d is the depth of water in feet at the point of detonation. Curves are shown for four values of Z/R_2. For R_2 see Figure 4 or Equation [18]. The curves are drawn on the assumption of infinite depth; they are fairly accurate if the gas globe is at least $5R_2$ below the surface.

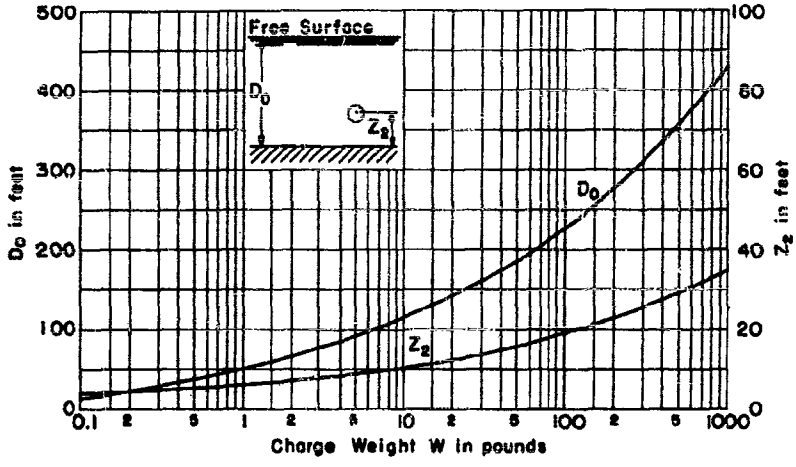

Figure 13 - Plot of the Critical Depth D_0 for Migration near the Bottom of the Sea

In sea water of depth less than D_0 feet, the gas globe should rise during the first recompression if detonation occurs at a distance $Z > Z_2$ above the bottom, where $Z_2 = 2R_2$; Z_2 is plotted in terms of a larger scale shown at the right. In water of depth greater than D_0, the globe should sink toward the bottom if $Z = Z_2$. For fair accuracy the gas globe should be at least $5R_2$ below the surface of the sea.

From Figure 11 it is seen that migration downward can be produced by a free surface only if the charge is less than 0.2 pound, provided detonation occurs at a depth at least as great as $2R_2$ below the surface. In the absence of more exact calculations, it may reasonably be surmised that the globe from 1 pound or more of TNT or tetryl should migrate upward, however close to the surface it may be formed.

The effect of the bottom is more complicated because the total hydrostatic pressure, as influenced by the depth of the water, enters as a new variable. In order to illustrate more concretely the implications of Figure 12, there is plotted on a basis of W in Figure 13 the depth of sea water D_0 at which $R_2/p_A = 1.33$; the value of Z when $Z = 2R_2$ in water of this depth is shown, on a different scale, as Z_2.

The formulas for D_0 and Z_2 are

$$D_0 = 33\left[\frac{107}{99}\left(\frac{3}{4}\,4.1\right)^{\frac{3}{4}} W^{\frac{1}{4}} - 1\right], \quad Z_2 = 8.2\left(\frac{3}{4}\,4.1\right)^{-\frac{1}{4}} W^{\frac{1}{4}}$$

In water shallower than D_0, the gas globe should rise if formed at a distance Z_2 or greater above the bottom; in water deeper than D_0, it should sink when it is formed at a distance equal to Z_2, and also at progressively greater distances as the depth of water is increased.

Unfortunately the approximate formulas become unreliable at those short distances which are of greatest practical interest; they should be fairly accurate if $Z \geq 2R_2$.

It is particularly unfortunate that calculations do not exist for charges detonated on the bottom. They are made difficult by the inevitable distortion of the gas globe. As Z is diminished below $2R_2$, the attractive effect of the bottom should probably increase and then decrease again. This conclusion is based on the following ideal case. The water flow around a hemispherical charge lying with its flat face on a rigid bottom and detonated at its center should resemble half of the flow around a spherical charge of the same radius detonated in open water; gravity should, therefore, cause the gas globe from the hemisphere to rise. From the analytical results it may reasonably be surmised that the gas globe from 10 pounds or over, detonated on the bottom under any depth of water of practical interest, will probably rise during the first recompression.

MIGRATION OF A GAS GLOBE IN SHALLOW WATER

The combined effect of the free surface and of a parallel rigid bottom can be obtained by extending the method of images. If Z is taken to stand for the distance of the center of the gas globe above the bottom, it is found that only those changes need to be made in the formulas, as obtained for a rigid bottom alone, which correspond to the assumption, instead of [29a, b]

$$M = T_1 - \frac{1.39}{D}, \quad N_Z = S_2 \qquad [40a, b]$$

where D is the total depth of the water, 1.39 represents 2 log 2, and T_1 and S_2 stand for the series

$$T_1 = \frac{1}{Z} - \frac{1}{D-Z} - \frac{1}{D+Z} + \frac{1}{2D-Z} + \frac{1}{2D+Z} - \frac{1}{3D-Z} - \cdots$$

$$S_2 = \frac{1}{Z^2} + \frac{1}{(D-Z)^2} - \frac{1}{(D+Z)^2} - \frac{1}{(2D-Z)^2} + \frac{1}{(2D+Z)^2} + \cdots$$

Hence the displacement of the gas globe measured upward, during the first expansion and recompression, is

$$Z_1 - Z_0 = \frac{2.60\, B_Z R_2}{\sqrt{|B_Z| + \frac{0.009}{1 + 40 B_Z^2}}} \qquad [41]$$

$$B_Z = 0.0346 \left[1 + 0.23 \left(T_1 - \frac{1.39}{D}\right) R_2\right] \frac{R_2}{p_A}$$

$$- 0.223 \left[1 - 0.18 \left(T_1 - \frac{1.39}{D}\right) R_2\right] S_2 R_2^2 \qquad [42]$$

or, very nearly

$$B_Z = 0.0346 \frac{R_2}{p_A} - 0.223 S_2 R_2^2 \qquad [42a]$$

The first period, from Equation [5], is

$$T_1 = T_{10}\left[1 + 0.20\left(T_1 - \frac{1.39}{D}\right) R_2\right] \qquad [43]$$

Here distances are to be measured throughout in feet. The formulas become questionable if either boundary is closer than $2R_2$ or $8(W/p_A)^{\frac{1}{3}}$.

These formulas are the same as those obtained for the bottom alone except that $1/Z$ is replaced by $T_1 - 1.39/D$ and $1/Z^2$ is replaced by S_2. If the small term containing T_1 and D is omitted, it is clear that the displacement is the same as that due to a single surface at a distance Z_s such that $1/Z_s^2 = S_2$ or

$$Z_s = \frac{1}{\sqrt{S_2}}$$

In S_2 the effects of the bottom and of the free surface are added in a sort of quadratic fashion. If $Z = D/2$, so that the charge lies midway between the surface and the bottom,

$$T_1 = 0, \quad S_2 = \frac{2}{Z^2}\left(1 - \frac{1}{3^2} + \frac{1}{5^2} \cdots\right) = \frac{1.83}{Z^2}$$

Thus

$$Z_s = 0.74 Z$$

so that the displacement is roughly the same as that when either surface alone is present at about three-fourths of the actual distance to either top or bottom. As the charge is moved toward either surface, however, the effect of the other surface rapidly decreases. Thus if $Z = 0.35 D$ or $0.65 D$, the effect is about the same as that due to the nearer surface acting alone at a distance 0.91 times its actual distance.

The effect of the free surface on the period somewhat exceeds that of the bottom. Hence when the charge is detonated midway between the two the period is shortened. The first period is

$$T_1 = T_{10}\left(1 - 0.28 \frac{R_2}{D}\right)$$

EFFECT OF PROXIMITY TO A FREE SURFACE AND A VERTICAL WALL

The wall is supposed to be plane and rigid and to extend from the surface to a great depth. Let X denote the distance of the center of the

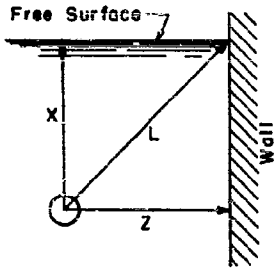

Figure 14 - Diagram Illustrating a Gas Globe near the Surface of the Water and also near a Vertical Rigid Wall

globe below the surface, measured downward, and Z its distance from the wall; see Figure 14. Then, in Equations [14a, c], [15], [16], [17] and its Z analog, clearly $c_X = -1$, $c_Y = c_Z = 0$. The analysis gives

$$M = \frac{1}{Z} - \frac{1}{X} - \frac{1}{L} \qquad [44a]$$

$$N_X = -\left(1 + \frac{X^3}{L^3}\right)\frac{1}{X^2} \qquad [44b]$$

$$N_Z = \left(1 - \frac{Z^3}{L^3}\right)\frac{1}{Z^2} \qquad [44c]$$

where $L = \sqrt{X^2 + Z^2}$, and $N_Y = 0$. Thus, for the displacement from the point of detonation to the point of peak compression,

$$X_1 - X_0 = \frac{2.60\left(\frac{W}{p_A}\right)^{\frac{1}{3}} B_X R_2}{\sqrt{B + \frac{0.009}{1 + 4000\,B^2}}} \qquad [45]$$

$$Z_1 - Z_0 = \frac{2.60\left(\frac{W}{p_A}\right)^{\frac{1}{3}} B_Z R_2}{\sqrt{B + \frac{0.009}{1 + 4000\,B^2}}} \qquad [46]$$

$$B = \sqrt{B_X^2 + B_Z^2} \qquad [47]$$

$$B_X = -0.0346\left[1 + 0.23\,MR_2\right]\frac{R_2}{p_A} + 0.223\left(1 + \frac{X^3}{L^3}\right)\left[1 - 0.18\,MR_2\right]\left(\frac{R_2}{X}\right)^2 \qquad [48]$$

$$B_Z = -0.223\left[1 - 0.18\,MR_2\right]\left(1 - \frac{Z^3}{L^3}\right)\left(\frac{R_2}{Z}\right)^2 \qquad [49]$$

or, very nearly,

$$B_X = -0.0346\,\frac{R_2}{p_A} + 0.223\left(1 + \frac{X^3}{L^3}\right)\left(\frac{R_2}{X}\right)^2 \qquad [50]$$

$$B_Z = -0.223\left(1 - \frac{Z^3}{L^3}\right)\left(\frac{R_2}{Z}\right)^2 \qquad [51]$$

Here $X_1 - X_0$ is the upward component of the displacement, while $Z_1 - Z_0$ is the horizontal component measured positively away from the wall.

The first period, from Equation [5], is

$$T_1 = T_{10}\left[1 + 0.20\left(\frac{1}{Z} - \frac{1}{X} - \frac{1}{L}\right)R_2\right] \qquad [52]$$

The formulas are probably unreliable when either X or Z is less than $2R_2$ or $8(W/p_A)^{\frac{1}{3}}$.

Here the additional terms containing L represent the principal effect of the interaction between the surfaces. Crudely speaking, the repulsive effect of the surface is increased by a factor $1 + X^2/L^2$, while the attractive action of the wall is decreased by a factor $1 - Z^2/L^2$, as compared to what these effects would be if the other surface were not present. The interaction between the two effects is greatest when $X = Z$. Then $L = \sqrt{2}X$ and the repulsion from the surface is increased in the ratio 1.35, while the attraction toward the wall is decreased in the ratio 0.65. These numbers will be somewhat modified, however, by the concomitant change in B.

On the period, the surface effect again predominates and results in a shortening; the first period is

$$T_1 = T_{10}\left[1 - 0.20\,\frac{R_2}{L}\right]$$

The most interesting feature in this case is the variation of the displacement with weight of charge. As the weight increases, the gravitational effect comes to predominate. In order to illustrate this fact, Figures 15 and 16 show curves of vertical displacement H and the horizontal displacement S toward the wall, for a charge detonated at several distances Z from the wall in combination with several distances X below the surface of the water, plotted against the charge weight W. These figures also serve to indicate qualitatively the relative magnitudes of the two displacements at shorter distances from the surface, where the numerical formulas become unreliable.

This case has some resemblance to that of a floating mine exploding near a ship. For the relatively slow motion involved in the production of migration a ship should function as a rigid obstacle. The ship extends downward, however, only to a limited depth. For this reason the attraction toward the ship should be considerably less, and the rise a little greater, than in the ideal case here considered.

PRESSURE IN THE WATER AS INFLUENCED BY THE MIGRATION

The pressure generated in the water by the recompression of the gas globe may be greatly altered by the migration. The general effect is complicated, as is illustrated by G.I. Taylor (5). The pressure will probably be further modified, however, in consequence of departures from spherical symmetry, so that calculations based upon the assumption of symmetry possess in most cases only a limited interest. For this reason the following rough method of estimating the pressure as modified by the occurrence of migration may be of interest.

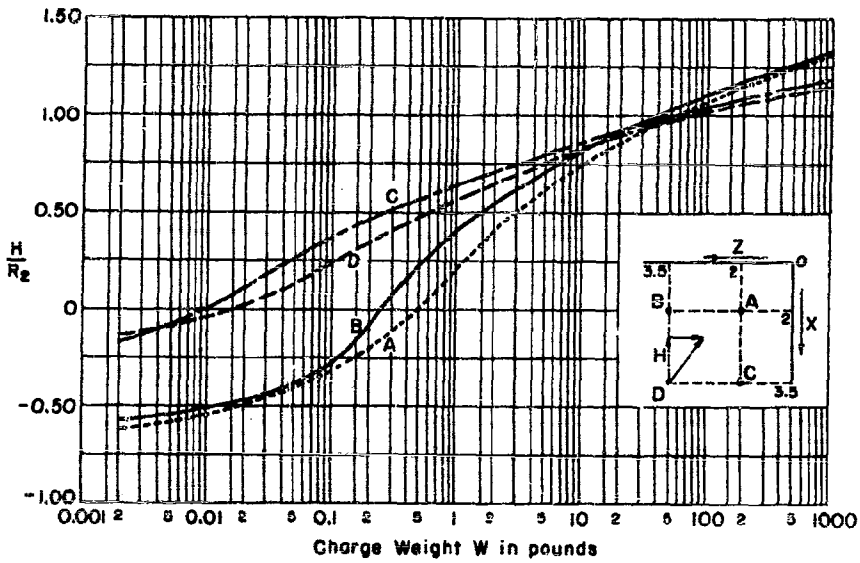

Figure 15 Vertical Rise H of a Gas Globe near the Surface of the Sea and near a Vertical Wall

The rise is from the time of detonation up to the time of the next peak recompression. R_2 is the intervening maximum radius. Curves are shown for 4 positions: (A) $X = Z = 2R_2$; (B) $X = 2R_2$, $Z = 3.5R_2$; (C) $X = 3.5R_2$, $Z = 2R_2$; (D) $X = 3.5R_2$, $Z = 3.5R_2$, where X is the distance of the point of detonation below the surface and Z the distance of this point from the wall. W is the weight of the charge in pounds. For R_2 see Figure 4 or Equation [18].

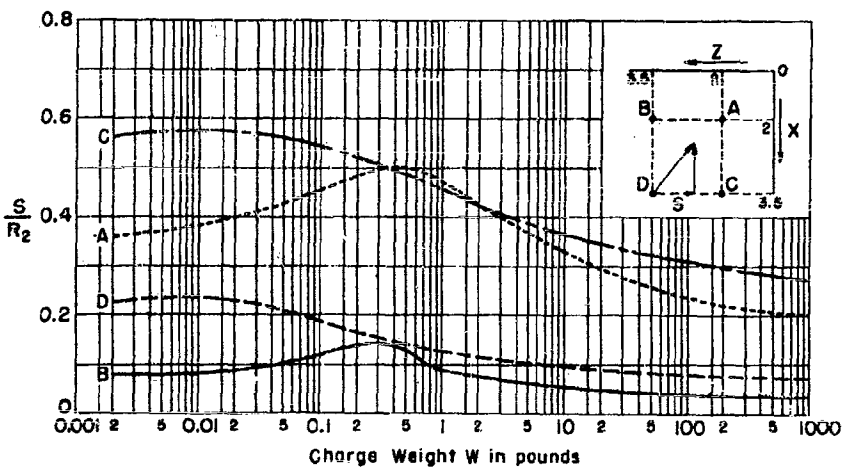

Figure 16 - Horizontal Component of Displacement S of the Gas Globe of Figure 15

The motion of the water can be resolved into three parts superposed upon each other, a spherically symmetrical part associated with the radial oscillations of the gas globe, a part caused by any bounding surfaces that may be present, and a part associated with the motion of migration. The pressure can then be divided into three corresponding parts, provided the Bernoulli term $\rho v^2/2$ is omitted, so that the pressure is simply proportional to the rate of change of the velocity potential. The part of the pressure that is associated directly with the migratory motion is then essentially of dipole character and hence falls off relatively rapidly with distance; it may therefore be dropped in a rough calculation, except near the gas globe. The part due to a bounding surface, if any, is simply the pressure due to the image of the gas globe in the surface and is easily allowed for on this basis. There remains then the part of the pressure that is associated with the radial motion. This part is altered by the migration because the radial motion is altered.

The radial part of the pressure is given by Equations [6] or [7] on page 45 of TMB Report 480 (10) with the omission of u^2; it may not be correctly given by Equation [8] of that report, however, in which the term in u_s^2 is not negligible and is influenced by the migratory motion. The pressure p at a point distant r from the center of the gas globe is thus

$$p = \frac{\rho}{r}\frac{d}{dt}(R^2\dot{R}) + p_0 \qquad [53]$$

where ρ is the density of the water and p_0 denotes the total hydrostatic pressure at the level of the gas globe. Only the phase of intense compression is of interest, hence Equation [1] of the present report can be simplified as before, and even the small term $M\dot{R}/2$ can be omitted for the present purpose. Thus from Equation [1]

$$\dot{R}^2 = \frac{C}{R^3} + \frac{2}{\rho R^3}\int (p_s - p_0)\, R^2\, dR - \frac{(\dot{X}^2 + \dot{Y}^2 + \dot{Z}^2)}{6} \qquad [54]$$

The approximate values employed previously for $\dot{X}$, $\dot{Y}$, $\dot{Z}$ can then be inserted, and they may conveniently be expressed in terms of the linear displacement of the gas globe from the instant of detonation to the instant of peak recompression, which is

$$Q = \sqrt{(X_1 - X_0)^2 + (Y_1 - Y_0)^2 + (Z_1 - Z_0)^2} = \sqrt{H^2 + S^2} \qquad [55]$$

The pressure as thus estimated is found to depend on the ratio Q/R_2, where R_2 is the first maximum radius, and to be proportional to $p_0 R_2/r$. The impulse $I = \int (p - p_0)dt$, is proportional to $R_2^2\sqrt{p_0}/r$. A single graph applicable

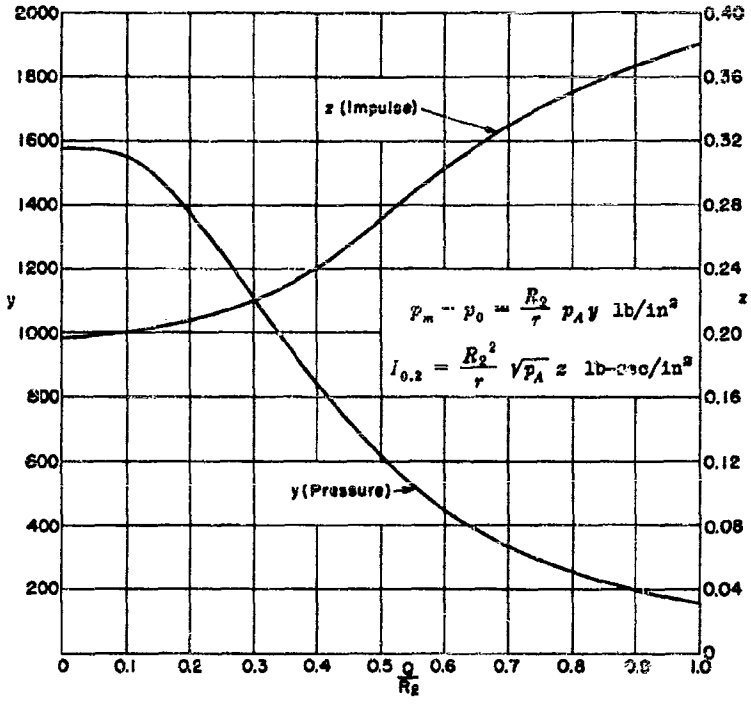

Figure 17 - Curves and Formulas for Estimating Roughly the Effect of Migration on the Pressure in the Water

p_m is the maximum pressure in the water at the instant of greatest recompression of the gas globe in pounds per square inch, p_0 is the total hydrostatic pressure in pounds per square inch and p_A is the same pressure expressed in atmospheres, $I_{0.2}$ is the peak impulse defined as $\int p\,dt$ integrated between points before and after the peak at which $p_m - p_0$ is one-fifth of its value at the peak, r denotes distance in feet from the center of the gas globe at the instant of maximum recompression, R_2 is the first maximum radius of the gas globe in feet, Q is the linear displacement of the gas globe from the point of detonation until the instant of greatest recompression, in feet.

to all migratory cases can be constructed, therefore, by plotting against Q/R_2 values of

$$\frac{p_m r}{p_A R_2}, \quad \frac{r I}{R_2^2 \sqrt{p_A}}$$

where p_A is the total hydrostatic pressure p_0 measured in atmospheres and p_m is the maximum excess of pressure above p_0. This is done in Figure 17. The impulse $I_{0.2}$ is taken between the two instants at which the excess of pressure $p - p_0$ is 1/5 of its intervening maximum value. The values of $I_{0.2}$ thus serve to give an idea of the estimated width of the pressure peak.

To use Figure 17, the value of the displacement Q is first estimated by use of formulas given previously; then values of y and z are read off the curves and p_m and $I_{0.2}$ are calculated from the formulas

$$p_m - p_0 = \frac{R_2}{r} p_A y \text{ pounds per square inch} \qquad [56a]$$

$$I_{0.2} = \frac{R_2^2}{r}\sqrt{p_A}\, z \quad \text{pound-seconds per square inch} \qquad [56b]$$

in which r and R_2 are in feet, p_m in pounds per square inch and $I_{0.2}$ in pound-seconds per square inch.

If there is a plane bounding surface in the neighborhood, a correction is then to be added representing the effect of a phantom gas globe located at the mirror image in the surface of the actual one. The pressure and impulse due to the image are calculated from the same formulas as those due to the actual gas globe, with r made equal to the distance from the image. The total pressure and impulse are then the sum of these respective quantities for the actual globe and the image if the surface is rigid, or the difference if the surface is a free one. At the surface itself, the effect of the image is to double the excess of pressure above hydrostatic pressure on a rigid surface, or to keep the pressure at the hydrostatic level on a free surface.

From Figure 17 it is seen that, as the migration increases, the peak pressure decreases, but the width of the peak increases so that the impulse due to it is about constant. At $Q = R_2/3$, the peak pressure has decreased by about a third; the rate of decrease then becomes greater, so that at $Q = 1$ the peak pressure is only a tenth of what it would be in the absence of migration.

The increase in $I_{0.2}$ at large values of Q/R_2 in the figure arises from the fact that the total range of pressure becomes small and the peak, defined as extending from one-fifth of the maximum to one-fifth on the other side, comes to include almost the entire range of positive pressure. The ratio of $I_{0.2}$ to the total positive impulse increases from about 1/3 at $Q = 0$ to 4/5 at $Q = R_2$.

MIGRATION OF A GAS GLOBE IN A TROUGH OR BOX

The necessary formulas have been written out for a charge detonated inside a rectangular box partly filled with water; this obviously includes as special cases a deep well of rectangular cross section or a trough with parallel vertical sides. The series obtained in these cases are complicated, however, and for this reason no results will be cited here.

MIGRATION AND SIMILITUDE

In considering similitude as it applies to phenomena of migration, it should be noted that physical processes of four different types are involved and each process imposes its own characteristic requirements for similitude. These differing requirements are not entirely reconcilable. Thus, in order that similar motions may occur on different scales:

a. The laws of the non-compressive motion of water require that pressure differences and the squares of velocities shall vary in the same ratio, or

$$\Delta p \propto v^2$$

b. The intervention of gravity requires that all pressure differences shall vary, as do gravity heads, in proportion to the linear dimensions, or

$$\Delta p \propto L$$

where L is any convenient linear dimension.

c. If a confined mass of gas is present, its pressure must usually remain unchanged with scale, on the assumption that the mass of gas present is varied in proportion to the cube of the linear dimensions. Hence, all pressures must remain unchanged.

d. Certain boundary conditions, such as exposure to the atmosphere or the presence of cavitation, may fix the actual value of the pressure at certain points.

The hydrodynamical requirement a. is consistent with many types of similitude. The addition of the gravity requirement b. restricts the choice to one in which $v^2 \propto L$, as in ship model testing. Then, also, $\Delta p \propto v^2 \propto L$.

If the migration effect on a gas globe is large, the gas has little effect on the radial and translatory motion, so that the pressure in the gas globe may be assumed to be zero. The pressure at certain points is then fixed, as in d. To keep $\Delta p \propto L$, the atmospheric pressure must then be adjusted in proportion to L. Furthermore, since the kinetic energy in the water is proportional to $L^3 v^2$ or to L^4, and since this energy may be assumed to be a fixed fraction of the energy released by the charge, and since the latter energy is proportional to the weight of the charge W, it follows that W must be varied in proportion to L^4. Thus linear dimensions and pressures vary in proportion to $W^{\frac{1}{4}}$, and, since $v^2 \propto L$, velocities and times vary in proportion to $W^{\frac{1}{8}}$. The atmospheric pressure must also be varied in proportion to $W^{\frac{1}{4}}$; and the depth of the water must be varied in the same ratio if the depth is significant. In corresponding positions, the maximum radius R_2 and the migratory displacement of the gas globe likewise vary as $W^{\frac{1}{4}}$.

When the migratory displacement is small relative to R_2, the similitude is not exact, because the motion is then appreciably influenced by the pressure of the gas. The partial failure of similitude in this case is not apparent from the approximate equations written in this report, because these equations are based upon a fixed value of R_2/R_0, whereas in reality this ratio will vary somewhat with the hydrostatic pressure.

In any case, similitude of the type described does not extend to the dimensions of the charge nor to the shock wave. These features can be included only if gravitational effects are neglected. If that is done, requirements a, c, and d can be met by keeping all pressures and velocities the same at corresponding points, while linear dimensions and times are changed in proportion to $W^{\frac{1}{3}}$. The effects of the gas pressure are then correctly covered; and the similitude will hold for migration due solely to the presence of bounding surfaces. This is the type of similitude that is familiar in the discussion of underwater explosions with neglect of all gravitational effects.

The various conditions requiring study thus lead to different criteria for similitude, a situation which occurs also in other applications of the ship model testing method. Thus in model tests of ship propulsion it has long been the accepted practice to break down the model resistance into two parts which are stepped up to full-scale values by the use of different laws of similitude.

It is hoped that a similar procedure can eventually be established in the present case, so that migration effects observed on small scale can be made the basis for a correction of the results of direct scaling according to the nominal theory based on the solid angle subtended at the charge by the target, as explained in TMB Report 492 (11).

However, such a procedure is not yet possible. A study of migration from that point of view is being made and the results will be communicated in a later report.

NOTE ON MOMENTUM IN THE WATER

In thinking about the motion of gas globes it is often natural to resort to reasoning based upon the principle of momentum. Much greater care must be used, however, in applying the principle of momentum to the noncompressive motion of liquids than in applying the principle of energy. It is very easy to go astray and arrive at the wrong conclusion. The fundamental reason lies in the fact that the transmission of momentum involves only the pressure itself, whereas the transmission of energy depends upon both pressure and particle velocity; because of this difference, momentum in an incompressible liquid is more readily transmitted to great distances than is energy.

To illustrate the care that must be used in considerations of momentum, consider a sphere of the same mean density as water, so that it will remain suspended without rising or sinking. Let an upward force be applied to it, causing it to rise in accelerated motion. The sphere is thereby

caused to press upward against the water in order to accelerate it; the water loads the sphere, in fact, with an equivalent mass equal to half the mass M of the displaced water, and an upward force $F = Ma/2$ must act on the water where a is the acceleration of the sphere. This force imparts upward momentum $\int F dt$ to the water.

Yet if the total amount of upward momentum is calculated from the usual formulas, for the water lying within any given distance r of the center of the globe, the result is zero. The water around the sides of the gas globe moves downward as that above and below it moves upward, and, as regards the water inside of any spherical surface concentric with the gas globe, the downward momentum on the sides just cancels the upward momentum above and below the sphere. The question thus arises, what has become of the upward momentum imparted to the water by the upward force F?

The paradox is redoubled by the following consideration. Since the sphere moves upward, water must on the whole move downward. The total momentum in the water must, therefore, be directed ***downward***, not upward. It is easily shown that this downward momentum is, in fact, of magnitude $2\int F dt$.

The solution of the paradox is found upon careful consideration to lie in the occurrence of a decrease in the pressure near the bottom. As a result of the motion of the sphere, the upward force of the bottom on the water is decreased by $3F$. One-third of this decrease compensates for the lifting effect of the sphere caused by its upward motion and thereby absorbs the upward momentum given by it to the water; the remaining two-thirds of the decrease allows part of the downward force due to gravity to develop in the water downward momentum of magnitude $2\int F dt$.

These considerations are based, of course, upon the assumption of incompressible water. If the action is so rapid, or the body of water so large, that non-compressive theory is not adequate to describe the motion throughout, then part or all of the upward momentum given to the water will remain in it, although perhaps not in the neighborhood of the sphere.

The motion of the water around a moving spherical gas globe of fixed radius is exactly the same as around a sphere of equal size moving at the same rate, hence the same considerations apply to the motion of the gas globe. The statements made in this report have been carefully worded so as to be correct as they stand; caution must be used if the references to momentum are altered or extended.

REFERENCES

(1) "Motion of a Pulsating Gas Globe Under Water - A Photographic Study," by Lt. D.C. Campbell, USNR, TMB Report 512, May 1943.

(2) Deductions of the formulas are available for inspection in manuscript form at the David Taylor Model Basin.

(3) "Hydrodynamics," by Horace Lamb, M.A., LLD., Sc.D., F.R.S., University Press, Cambridge, 1924.

(4) "Theory of the Pulsations of the Gas Bubble Produced by an Underwater Explosion," by Conyers Herring, Volume II of this compendium.

(5) "The Vertical Motion of a Spherical Bubble and the Pressure Surrounding It (S.W. 19)," by Professor G.I. Taylor, F.R.S., Volume II of this compendium.

(6) "Behaviour of the Gas Bubble from 1 Ounce of TNT Detonated at Depths of 3 and 6 Feet, Including an Approximate Computation of the Effect of the Surface on the Vertical Movement," Department of Scientific and Industrial Research, Road Research Laboratory, Report to the Admiralty, UNDEX 7, Note ADM/86/AJH, December 1942.

(7) "The Behaviour of an Underwater Explosion Bubble - Approximations Based on the Theory of Professor G.I. Taylor," Department of Scientific and Industrial Research, Road Research Laboratory, Report to the Admiralty, UNDEX 10, Note ADM/91/ARB, December 1942.

(8) "Calculations in Connection with S.W. 19" (See Reference 5), by L.J. Comrie and H.O. Hartley. Prepared by the Scientific Computing Service, S.W. 26.

(9) "The Pressure Pulses Produced by the Oscillation of the Underwater Explosion Bubble from 1 Ounce of Polar Ammon Gelegnite," Department of Scientific and Industrial Research, Road Research Laboratory, Report to the Admiralty, UNDEX 16, Note ADM/99/ARB, February 1943.

(10) "Report on Underwater Explosions," by Professor E.H. Kennard, Volume I of this compendium

(11) "The Design of Ship Structures to Resist Underwater Explosion - Nominal Theory," by Captain W.P. Roop, USN, TMB Report 492, August 1943.

THE RATE OF RISE OF LARGE VOLUMES OF GAS IN WATER

G. I. Taylor and R. M. Davies
Cambridge University

British Contribution

June 1944

THE RATE OF RISE OF LARGE VOLUMES OF GAS IN WATER

G. I. Taylor and R. M. Davies

June 1944

* * * * * * * * *

Summary.

The work described in this report is concerned with the rate of rise of bubbles, ranging in volume from 1.5 to 100 cc., produced by the non-explosive release of a volume of air in nitrobenzene or in water.

Measurements of photographs of bubbles formed in nitrobenzene showed that the central portion of the upper surface was spherical in form. A theoretical discussion, based on the assumption that the pressure over the front of the bubble is the same as that in ideal hydrodynamic flow round a sphere, shows that the velocity of rise, U, should be related to the radius of curvature, R, in the region of the vertex, by the equation $U = 2/3\sqrt{gR}$; the agreement between this relationship and the experimental results is excellent.

For geometrically similar bubbles of such a diameter that the drag co-efficient should be independent of Reynolds number, it would be expected that U would be proportional to the sixth root of the volume, V; measurements of about ninety bubbles show considerable scatter in the values of $U/V^{1/6}$ although there is no systematic variation in the value of this ratio with the volume. If U is expressed in cm./sec. and V in c.cs., the experiments give the formula $U = 24.8\ V^{1/6}$. If this formula is applied to the volume of gas given off by the explosion of 300 lbs. of Amatol, the calculated rate of rise is about 17 ft./sec. Although no direct measurements of this velocity have been made, this estimate is not inconsistent with measurements of the time between the appearance of the dome and the plume when depth charges are exploded at great depths.

1. *Introduction and Experimental Method.*

The rise of gas bubbles in liquids has been studied by several workers*, but in all the work so far published, the bubbles have been so small that the results are not applicable to the study of the rise of large volumes of gas, such as those produced in submarine explosions. In the experiments here described, bubbles ranging in volume from 1.5 to 34 c.cs. were formed in nitrobenzene contained in a tank, 2 feet x 2 feet x 2 feet 6 inches filled to a depth of about 2 feet with the liquid. The bubbles were photographed by spark photography at intervals of about 10 milliseconds, using a revolving drum camera in the manner previously described #. In some further experiments, bubbles covering a range of volume from 4.5 to 200 c.cs. were formed in a cylindrical tank, 2 feet 6 inches diameter, filled with water to a depth of 3 feet 6 inches, and their mean velocity of rise over a measured distance was determined. In both sets of experiments, the air volume was determined by collecting the bubble in a graduated glass cylinder.

Considerable difficulty was found in producing single, large bubbles of gas, and the method finally adopted was to pivot an inverted beaker containing air, which was then tilted so that the air was released. In general, the air is released from the beaker in a stream of bubbles of varying sizes, but by adjusting the rate of tilting, it was found possible to arrange that the air was spilled into a single bubble.

Two successive photographs of a typical bubble formed in this way in nitrobenzene are shown in Figure 1, the time-interval between the two photographs being 10.3 millisecs. In addition to the

bubble .....

* Allen, H.S., Phil.Mag., Vol. 50 pp.323 and 519 (1900). Hoefer, K, V.D.I., Vol.57, p.1174 (1913) Miyagi, O, Tohoku Imperial University, Technological Reports, Vol.5, p.135 (1925); Vol.8,p.587 (1929) Phil.Mag., Vol.50, p.112, (1925).

\# Taylor, G.I. and Davies, R.M. "The Motion and Shape of the hollow produced by an explosion in a liquid".

bubble, the photographs show a steel ball, $\frac{1}{4}$ inch diameter, soldered at the lower end of a vertical rod immersed in the liquid; this arrangement was used to find the scale of the photographs and to give a reference mark from which the vertical displacement of the bubble could be measured.

In the original photographs, a region of turbulence is clearly shown behind the large bubble. This is due no doubt to some anisotropic optical property of nitrobenzene when subjected to viscous stresses. That such stresses exist could be inferred from the fact that the largest of the small bubbles in the wake of the large one is not spherical and is rapidly changing in shape. This bubble has a diameter of about 6 mm. Still smaller bubbles are less distorted and one of diameter about 2 mm., seen to the left side of the 6 mm. bubble is distorted so that its length/diameter ratio is about 1.1.

The rate of shear which might be expected to produce a distortion of this amount has been calculated ϕ. In the field of flow represented by the equations

$$u = Cx, \quad v = -Cy, \quad w = 0 \qquad \ldots \quad \ldots \quad \ldots \quad \ldots \quad \ldots \quad \ldots \qquad (1.1)$$

an air-bubble of mean radius a would be pulled out so that

$$\frac{L - B}{L + B} = \frac{2C\mu a}{T} \qquad \ldots \quad \ldots \quad \ldots \quad \ldots \quad \ldots \quad \ldots \qquad (1.2)$$

where L and B are the length and breadth of the bubble and μ and T the viscosity and the surface tension of the liquid. For nitrobenzene, $\mu = 0.018$ poises, $T = 43.9$ dynes/cm., so that for the 2 mm. bubbles, $a = 0.1$ cm., $L/B = 1.1$ and $(L - B)/(L + B) = 0.05$, giving

$$C = \frac{0.05 \times 43.9}{2 \times 0.018 \times 0.1} = 6.1 \times 10^2 \ \text{sec}^{-1}$$

The rate w of dissipation of energy per c.c. in the flow represented by equation (1.1) is

$$W = \mu\left\{\left(\frac{\partial u}{\partial x}\right)^2 + \left(\frac{\partial v}{\partial y}\right)^2\right\} = 2\mu C^2 = 1.34 \times 10^4 \ \text{ergs/c.c./sec.}$$

If the rate of dissipation were constant through the wake and if wake extends over the whole of the region which appears disturbed in Figure 1, namely through a diameter of 5.9 cm., the total rate of dissipation in the wake is

$$\begin{aligned} & 1.34 \times 10^4 \times (\text{volume of wake}) \\ = \ & 1.34 \times 10^4 \times \frac{\pi}{4} (5.9)^2 \times 3.8 \\ = \ & 1.4 \times 10^6 \ \text{ergs/sec.} \end{aligned}$$

The total rate of dissipation would be known if the drag co-efficient, C_D of the large bubble were known. Since the density ρ of nitrobenzene is 1.2 gm/c.c. whilst the velocity of rise, U, of the large bubble in this experiment was 36.7 cm/sec. and its maximum transverse dimension, 2A, was 5.1 cm., the total rate of dissipation was

$$\begin{aligned} & C_D \times \tfrac{1}{2} \rho U^2 \ \pi A^2 \times U \\ = \ & C_D \left\{\tfrac{1}{2} \times 1.20 \times 36.73 \times \pi \times \left(\frac{5.1}{2}\right)^2\right\} \\ = \ & 6.1 \times 10^5 \ C_D \ \text{ergs/sec.} \end{aligned}$$

Since C_D is of the order 1.0 (see Table I) it will be seen that the rate of dissipation which would distort the bubbles by the observed amount is of the same order as that deduced from the rate of rise.

For .....

ϕ G. I. Taylor "Formation of Emulsions in definable fields of flow" Proc. Roy. Soc. Vol. 146 p.501, (1934)

For the largest of the small bubbles in the wake, viscous stresses would produce such a distortion that the formula (1.2) would not be expected to apply.

The uniformity of the velocity of rise of the bubbles, and the order of magnitude of the experimental error in the measurement of the velocity may be judged from Figure 2, in which, time t, and the vertical displacement, X, of the two bubbles are plotted as abscissae and ordinates, respectively. The actual measured values of X and t for the bubble of Figure 1 are indicated by the circular dots in Figure 2, and those for a second, larger bubble by crosses; the straight lines of closest fit drawn through the observed points are denoted by 'A' and 'B' respectively. It will be seen that the scatter of the experimental points is not excessive and that the velocity of rise of the two bubbles is reasonably constant over the interval measured.

The shape of the profile of the bubbles was found by measuring the films on a travelling microscope fitted with two independent motions at right angles to one another. The results for the lower photograph of Figure 1 are shown graphically in Figure 3 where the circular dots represent points on the central, regular portion of the profile of the bubble, deduced from the microscope readings. In Figure 3, the vertical and horizontal axes are parallel to the corresponding axes in the tank and the origin is taken at the uppermost point on the bubble; the dimensions given in Figure 3 refer to the actual size of the bubble. The crosses with vertical axes and with axes at 45° to the vertical in Figure 3 represent points on the profile of the same bubble, obtained from measurements of photographs taken 105.7 and 132.5 milliseconds earlier than the lower photograph of Figure 1. The agreement between the three sets of points shows that the shape of the cap of the bubble undergoes very little variation over the range of time covered by the three photographs.

The curve in Figure 3 is an arc of circle of radius 3.01 cm., drawn to pass through the origin and since the scatter of the observed points around this curve is within the limits of the errors made in measuring the film, the upper part of the bubble is a portion of a sphere within the experimental error. It is worth noticing that the angle subtended at the centre of the circle by the arc in Figure 3 is about 75°, whilst the angular width of the whole bubble in Figure 2 (referred to the centre) is about 90°.

2. *The vertical motion of a gas bubble with a spherical cap.*

Measurements of the pressure over the front part of the surface of a sphere exposed to a wind shows that the distribution of pressure is very similar to that calculated assuming ideal hydrodynamic flow. Similar measurements over a solid spherical cap set with its vertex facing the wind show that the removal of the rear part of the sphere does not greatly affect the pressure distribution over the front except near the rim of the cap.

According to the hydrodynamic theory of ideal fluids, the pressure p at angle ϕ from the stagnation point of vertex of a sphere (see inset in Figure 3) moving with uniform velocity U in a fluid of density ρ is

$$p = p_z + \tfrac{1}{2}\rho U^2 \left(1 - \tfrac{9}{4}\sin^2\phi\right) \qquad \ldots \quad (2.1)$$

where p_z is the pressure at the depth z, of the point concerned, at a great horizontal distance from the sphere.

Thus

$$p_z = p_0 + g\rho z \qquad \ldots \quad (2.2)$$

where p_0 is the atmospheric pressure, and, at angle ϕ, for a sphere of radius R,

$$z = d + R(1 - \cos\phi) \qquad \ldots \quad (2.3)$$

where d is the depth of the vertex.

From equations (2.1), (2.2) and (2.3)

$$p = p_0 + g\rho d + g\rho R(1 - \cos\phi) + \tfrac{1}{2}\rho U^2\left(1 - \tfrac{9}{4}\sin^2\phi\right) \qquad \ldots \quad (2.4)$$

The .....

The condition which must be satisfied over the surface of the bubble is that, apart from surface tension effects which are small when the diameter of the bubble is greater than 2 cm., the pressure inside must be equal to the pressure outside. At the vertex, the pressure is $(p_0 + g\rho d + \frac{1}{2}\rho U^2)$ and this must therefore be the pressure of the air inside the bubble. The expression (2.4) for the pressure is therefore satisfied all over the spherical cap if

$$\frac{9}{8} U^2 \sin^2\phi = gR(1 - \cos\phi) \quad \ldots \quad \ldots \quad \ldots \quad \ldots \quad \ldots \quad \ldots \quad (2,5)$$

This equation is satisfied for small values of ϕ if

$$\frac{U^2}{gR} = \frac{4}{9}$$

$$\text{or} \quad U = \frac{2}{3}\sqrt{gR} \quad \ldots \quad \ldots \quad \ldots \quad \ldots \quad \ldots \quad \ldots \quad (2.6)$$

for, in that case, $\lim_{\phi \to 0}\left(\frac{1 - \cos\phi}{\sin^2\phi}\right) = \frac{1}{2}$

To see how far the theoretical relationship (2.6) is verified experimentally and to obtain further data concerning the rise of bubbles, fourteen bubbles, rising in nitrobenzene, were photographed. The results of the measurement of the films are summarized in Table I, where the first three columns give the volume, V of the bubbles, the radius of curvature, R, near the uppermost point, and the observed velocity of rise, U. The fourth column in the table gives the maximum transverse dimension, 2A of the bubble and the fifth column the angle $\phi_m = \sin^{-1} A/R$. The sixth column gives the drag co-efficient, C_D, of the bubble, calculated from the equation

$$C_D \times \pi A^2 \times \tfrac{1}{2}\rho U^2 = g\rho V \quad \ldots \quad \ldots \quad \ldots \quad \ldots \quad \ldots \quad \ldots \quad (2.7)$$

The last column in the table gives the value of Reynolds number, Re, referred to the radius, A, of the maximum transverse section of the bubble, i.e.,

$$Re = \frac{UA}{\nu} \quad \ldots \quad \ldots \quad \ldots \quad \ldots \quad \ldots \quad \ldots \quad (2.8)$$

where ν is the kinematic viscosity of the liquid. For nitrobenzene, the viscosity is 0.018 poises at 14°C., and the density is 1.20 gm./c.c., hence $\nu = 0.015$ cm^2/sec.

TABLE I.

Bubbles in Nitrobenzene.

Volume V (c.c)	Radius of curvature R	Velocity U (cm./sec.)	Maximum transverse dimension 2A	$\phi_m = \sin^{-1} A/R$	Drag co-efficient C_C	Reynolds number Re
	(cm.)		(cm.)			
1.48	2.41	29.2	2.86	36.4°	0.53	2780
3.50	2.09	29.6	3.14	48.6°	1.02	3090
4.06	2.04	28.9	3.48	58.3°	1.00	3360
4.31	2.17	28.0	3.16	46.8°	1.37	2950
6.40	2.78	35.5	4.98	63.6°	0.52	5900
7.30	2.65	34.2	4.40	56.1°	0.80	5010
8.02	2.67	34.0	4.23	52.5°	0.97	4790
–	3.01	36.7	–	–	–	–
8.80	3.17	37.2	5.26	56.1°	0.58	6520
9.18	2.77	33.0	4.53	55.6°	1.00	5020
18.40	3.30	37.3	5.10	50.7°	1.27	6340
21.25	3.51	38.1	5.85	56.5°	1.07	7440
28.1	4.16	43.0	–	–	–	–
33.9	4.27	42.1	6.19	46.5°	1.25	8700
–	4.84	48.2	–	–	–	–

The accuracy of the relationship (2.6) can be judged from Figure 4, in which the values of U given in table I are plotted against the values of $\sqrt{R}$; it will be seen that the experimental points are, on the whole, reasonably well represented by the straight line given by the relationship $U = 2/3\sqrt{gR}$.

The values of C_D given in table I are very variable and they do not appear to show any consistent variation with respect to either of the variables Φ_m or Re. At an early stage in the experiments it was thought that C_D might be a function of Φ_m and, for comparison, a series of experiments was carried out in a wind-tunnel in order to find how the drag co-efficient of a rigid spherical cap varied with the semi-vertical angle Φ_m. The cap was supported so as to face the wind and its leeward side was closed with a plane metal disc; using pressure orifices connected in turn to a manometer, the pressures at various points on the curved and flat surfaces of the cap were determined and the drag co-efficient calculated in the usual way*. Four bodies, with a radius of 1 inch and with Φ_m equal to 90°, 75°, 55° and 30° respectively were used in the experiments and the values of C_D are given in the second column of table II. In the experiments, the wind speed was kept constant at 1500 cm./sec., and the values of the Reynolds numbers, defined by equation (2.8) are given in the third column of the table.

TABLE II.

Drag co-efficients of a rigid spherical cap.

Φ_m	C_D	Reynolds Number
90°	0.463	25400
75°	0.521	24600
55°	0.647	20800
30°	0.862	12400

These values of C_D plotted against Φ_m, are shown in Figure 5 by the circular dots; this diagram also shows the values of C_D given in table I for bubbles rising in nitrobenzene.

It is clear that, whereas the results of the wind-tunnel experiments lie on a smooth curve, the results of the nitrobenzene experiments show a rather large scatter, and, in addition, the general trend of the curve of closest fit drawn through the points for the bubbles (indicated by the broken line in Figure 5) differs considerably from the curve given by the wind-tunnel experiments.

It is difficult to be certain of the reason for these effects. They may, for example, be due to the variation in Reynolds number, although this is unlikely since the values of C_D for the bubble show no systematic variation with Reynolds number. It is more likely that the effects in question are due to variations in the shape of the bubbles. In this connection, it must be remembered that our photographs show only the projection of a bubble on a vertical plane, so that the lower surface of a bubble is invisible unless it is convex downards. Visual observation shows that the lower surface is, in fact, usually concave downards, its curvature being less than that of the upper surface, and the difference between the observed (C_D, Φ_m) curves for the bubble and for the wind-tunnel experiment may be caused by the difference in the wake in the two experiments, due to the difference in the geometrical forms of the bubble and the flat-bottomed spherical cap.

Similarly, in the case of the bubbles themselves, the scatter of the experimental values of C_D for a given value of Φ_m may be caused by differences in the value of the ratio of the curvatures of the upper and lower surfaces when Φ_m is constant

3.....

* See for example, R. Jones, Phil. Trans. A Vol. 226 p.231, (1927).

3. *The relationship between the volume and the rate of rise of a bubble.*

If all the bubbles were geometrically similar and if the drag co-efficient were independent of Reynolds number, it would be expected that the velocity of rise would be independent of the density of the liquid and would be proportional to $(\text{volume})^{1/6}$. Figures 6 and 7 show the results of experiments, involving 13 bubbles rising in nitrobenzene and about 75 bubbles rising in water, which were carried out to test the truth of this prediction. In Figure 6, the velocity of rise, U, (in cm./sec.) is plotted against the volume, V, (in c.c.) whilst, in Figure 7, the ratio $U/V^{1/6}$ is plotted as a function of $V^{1/3}$. In the diagrams, the results for bubbles in water and in nitrobenzene are plotted as circular dots and crosses surrounded by circles respectively; the two diagrams also show the curves derived from the experimental results of Miyagi and of Hoefer.

Figure 7 shows a considerable scatter of the experimental points around the horizontal straight line of ordinate 24.8 which represents the mean value of $U/V^{1/6}$ derived from the observations; in the same way, the experimental points are widely scattered around the curve $U = 24.8\ V^{1/6}$ in Figure 6. It is worth noticing that in Figure 7, there is no systematic variation of $U/V^{1/6}$ with V, and that the points for bubbles in water and in nitrobenzene can be represented by the same curve; in all probability, the scatter of the points is due to the reason already put forward to account for the discrepancies in Figure 5, namely the lack of geometrical similarity in the bubbles.

4. *The time of rise of gas from a deep submarine explosion.*

Photographs of bubbles produced by a spark* show that such bubbles pulsate violently and rise at a very variable speed during the first few pulsations. The amplitude of these pulsations dies down very greatly after three or four cycles and the rate of rise becomes more nearly constant, and, at the same time, the bubbles assume a mushroom-like form which is rather similar to that shown in Figure 1 for air released non-explosively.

Measurements of the time-interval between the appearance of the spray dome and that of the plume have been made for depth charges filled with 300 lbs. of amatol, fired at different depths. The results show considerable scatter. The mean curve representing these experimental results, is shown in Figure 8 of the present report. It will be seen that the mean rate of rise of gas from the depth charge is very rapid (of order 45 ft./sec.) when the depth of the charge is less than about 90 feet; when the charge is deeper than 90 feet, the mean rate of rise rapidly decreases. From the sound-ranging observations it appears that the plume comes through the surface during the fourth oscillation if the depth is about 90 feet and that bubble oscillations can hardly be distinguished beyond this point.

It is not possible from these observations to deduce the rate of rise of gas after the bubble oscillations have ceased. If, however, the rate of rise during the first four pulsations is assumed to be independent of depth, the slope of the curve of Figure 8 for times greater than 2½ seconds would give the rate of rise after the fourth pulsation. With this assumption, the time for the gas to rise from 90 feet above the charge to 134 feet above it would be 3.0 seconds, corresponding with a mean velocity of 44/3.0 = 14.7 ft./sec. If the time from 110 to 134 feet above the charge were taken from Figure 8 as 2.2 seconds, the corresponding mean velocity is 24/2.2 = 10.9 ft./sec.

Taking the amount of gas released from 1 gm. of amatol, after the water vapour has been condensed, as 650 c.c., the volume released from a 300 lb. depth charge is 8.8×10^7 c.c. The formula $U = 24.8\ V^{1/6}$ deduced from the present experiments would therefore predict that the rate of rise of gas from a 300 lb. depth charge would be

$$U = 24.8 \times (8.8 \times 10^7)^{1/6} = 525 \text{ cm./sec.} = 17.2 \text{ ft./sec.}$$

For comparison with the experimental results, a straight line whose slope corresponds with this velocity is shown in Figure 8. It will be seen that the actual vertical velocity of gas from an explosion, when

pulsation .....

* Taylor, G. I. and Davies, R.M. "The motion and shape of the hollow produced by an explosion in a liquid.

pulsation has died away, is of the same order as that predicted from measurements with bubbles whose volumes are of order one ten-millionth to one millionth of that of the explosion products.

Though the work here discussed is concerned with single bubbles, it may be remarked that if the gas separates into two bubbles, the velocity of each would only be reduced by 12½ per cent if the bubbles rose independently. If it separates into 64 equal bubbles and each rises independently, the rate of rise would be reduced by 50 per cent, but if they co-operate so that each bubble moves in a rising current produced by the others, the rate of rise will not be reduced so much.

Fig. 1. Successive spark photographs of an air-filled bubble rising in nitrobenzene.

Time-interval between photographs = 10.3 millisecs.

Velocity of rise of bubble = 36.7 cm./sec.

Diameter of steel ball shown in upper part of photograph = ½ inch.

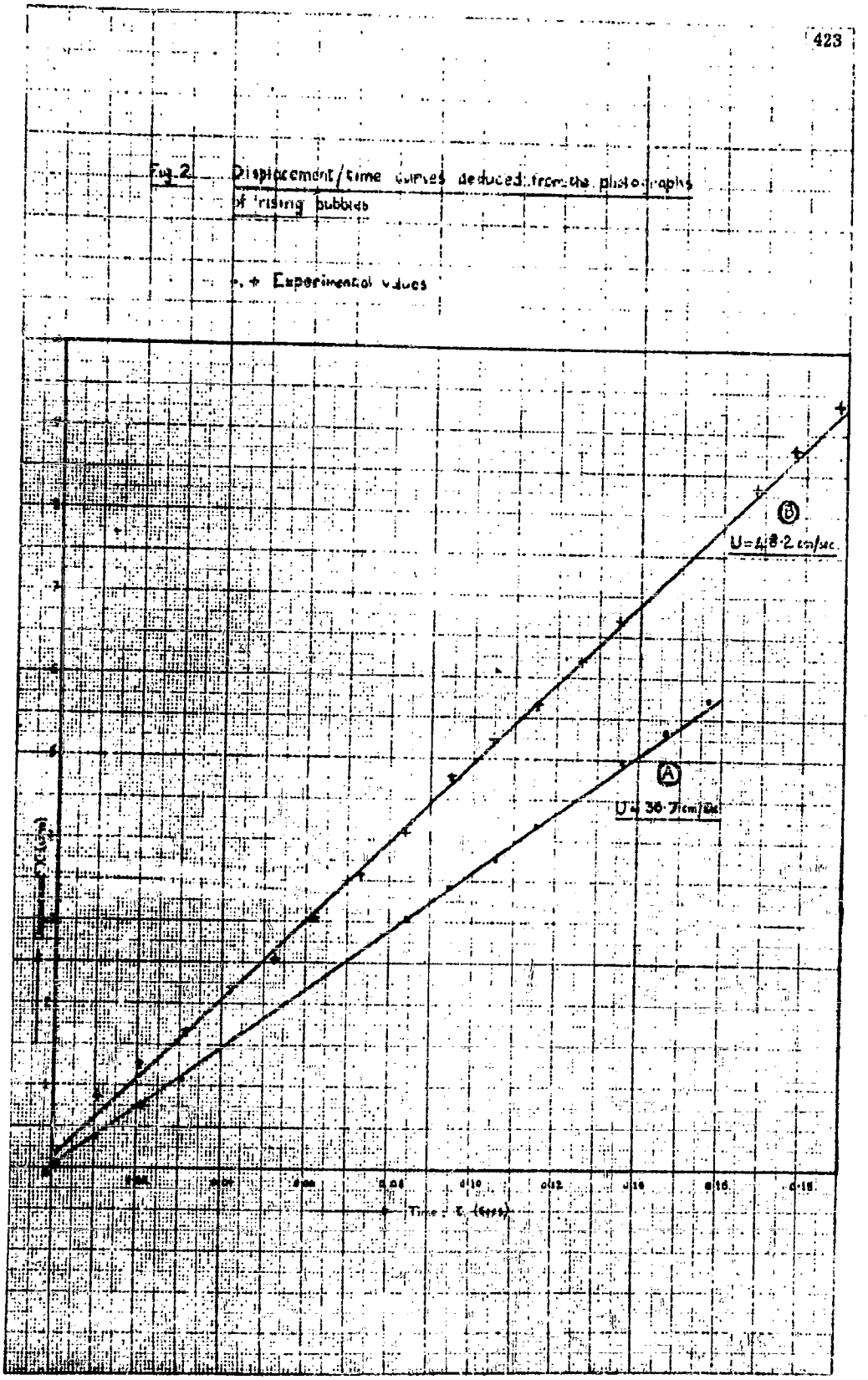
Fig. 2 Displacement/time curves deduced from the photographs of rising bubbles
+ Experimental values
B
U = 4.8·2 cm/sec
A
U = 36·7 cm/sec
Time - t (secs)

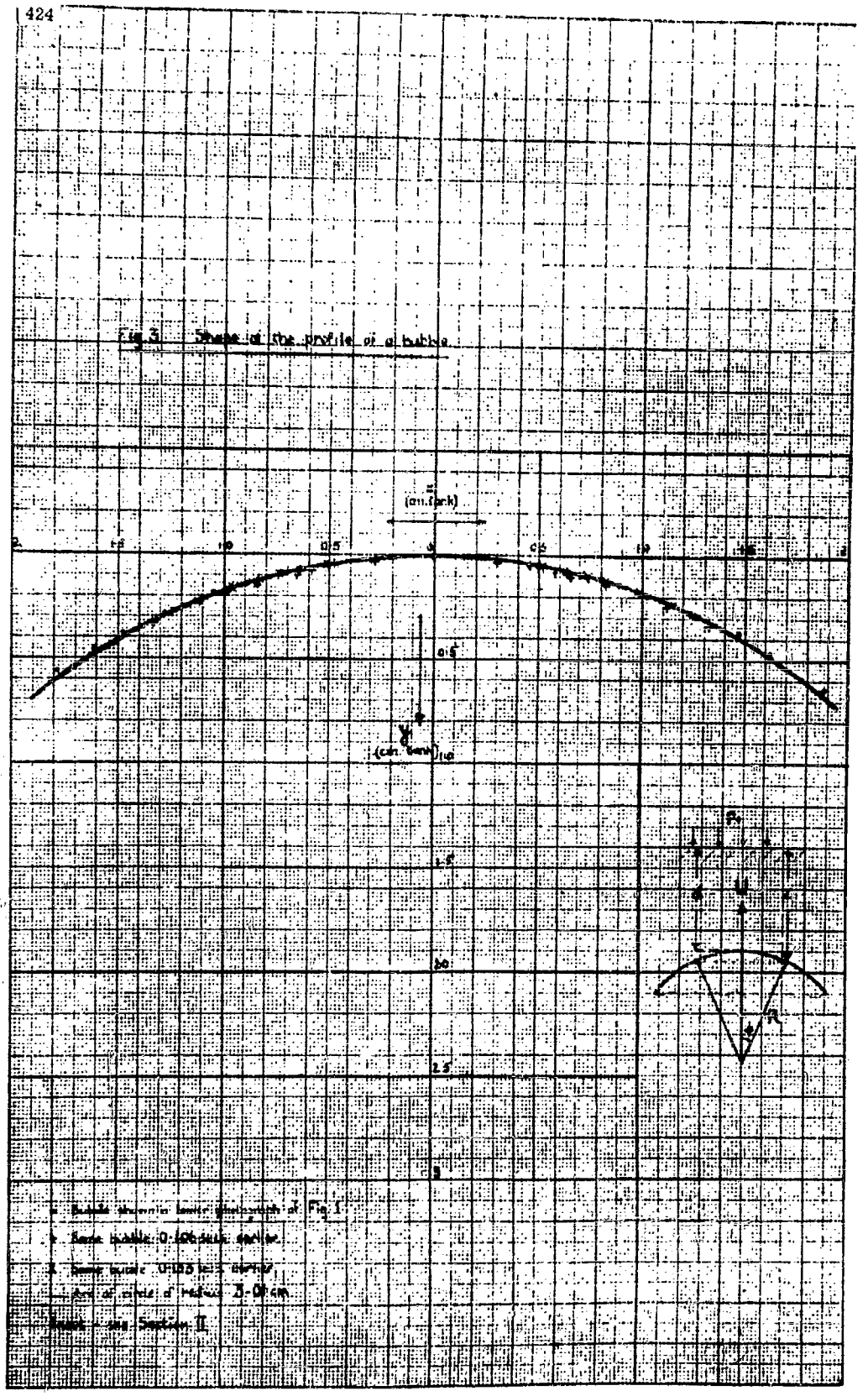

Fig. 3. Shape of the profile of a bubble

a Bubble shown in lower photograph of Fig. 1

b Same bubble 0·106 sec. earlier

c Same bubble 0·185 sec. earlier

R Arc of circle of radius 3·0 cm

Bubble a, see Section II.

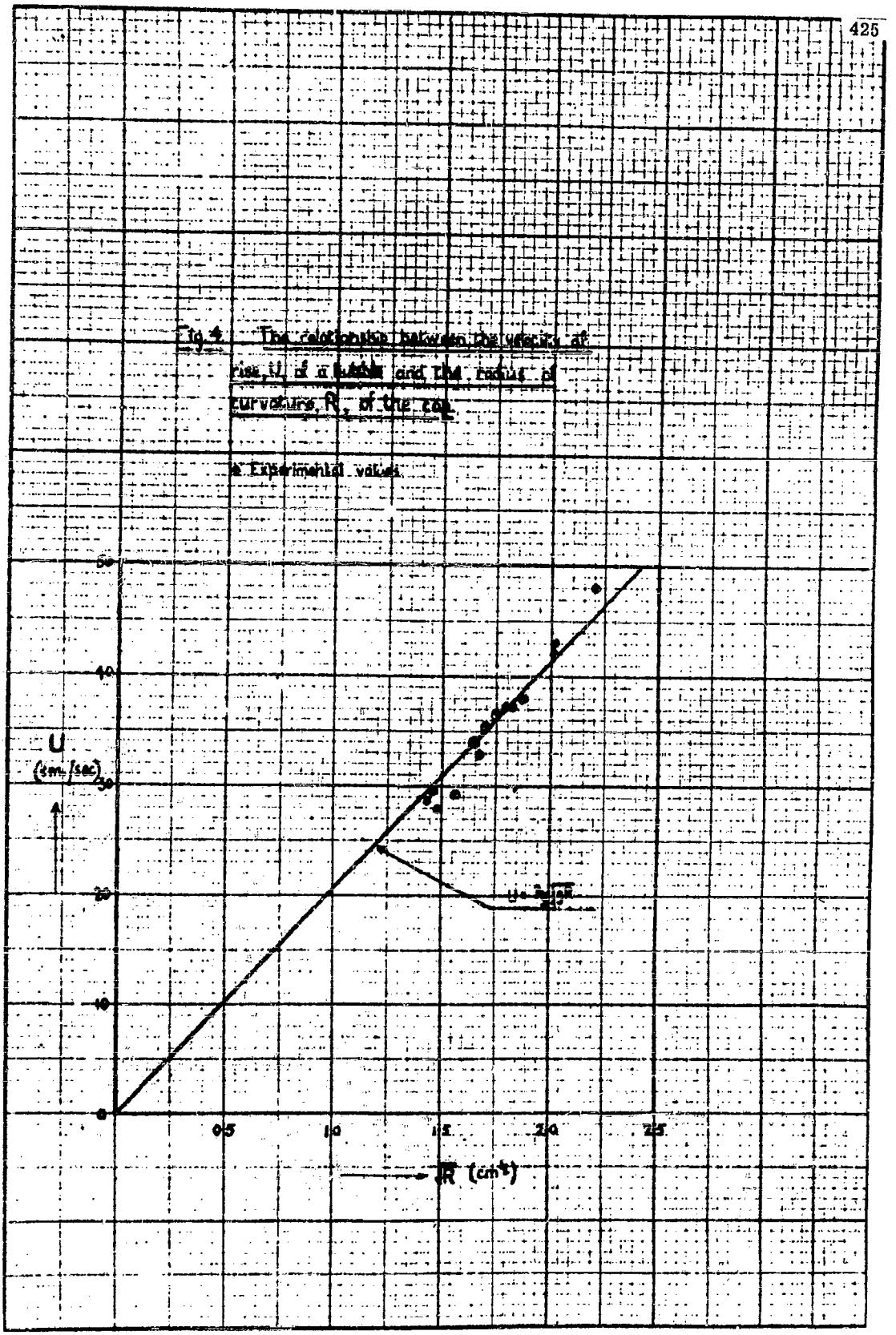
Fig 4. The relationship between the velocity of rise, U, of a bubble and the radius of curvature, R, of the cap.
Experimental values
U (cm./sec)
R (cm)
0
10
20
30
40
0.5
1.0
1.5
2.0
2.5

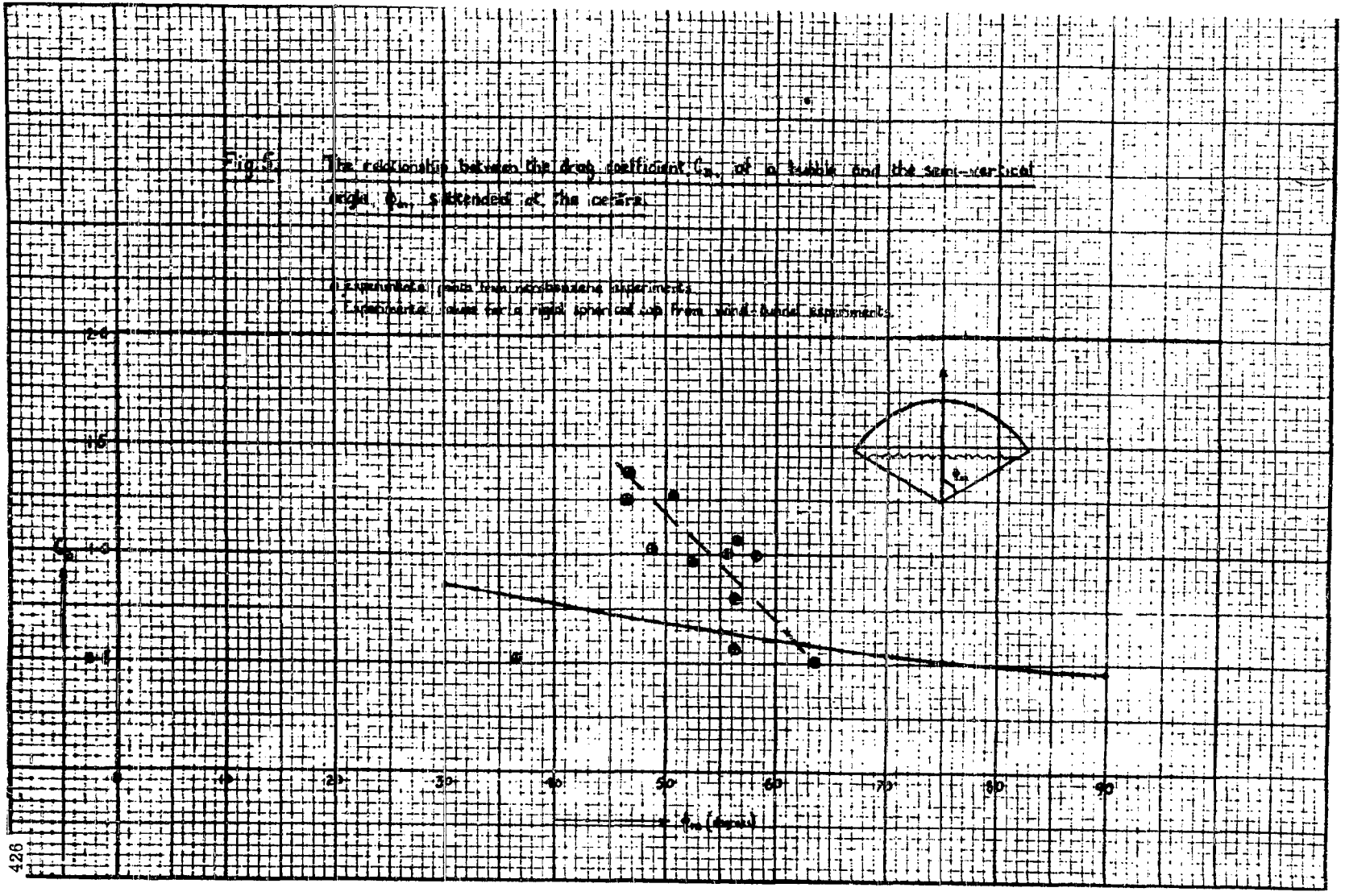
Fig.5. The relationship between the drag coefficient C_D of a bubble and the semi-vertical angle ϕ_m subtended at the centre.
Experimental points from photographic experiments.
Experimental values for a rigid spherical cap from wind-tunnel experiments.
2·0
1·6
1·2
0·8
C_D
0
10°
20°
30°
40°
50°
60°
70°
80°
90°
ϕ_m (degrees)
ϕ_m

Fig. 6. Experimental results for the velocity of rise U of a bubble of volume V.

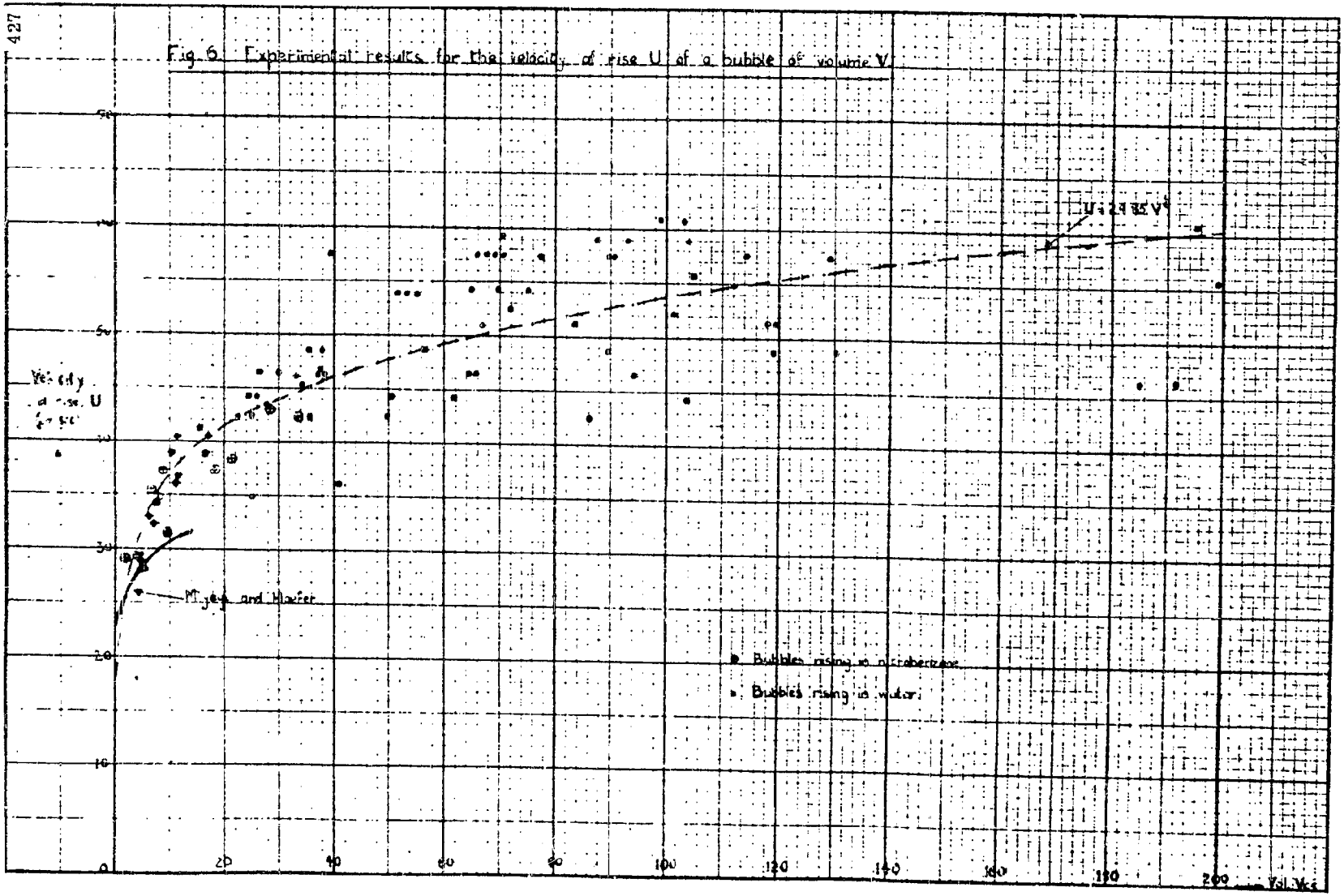

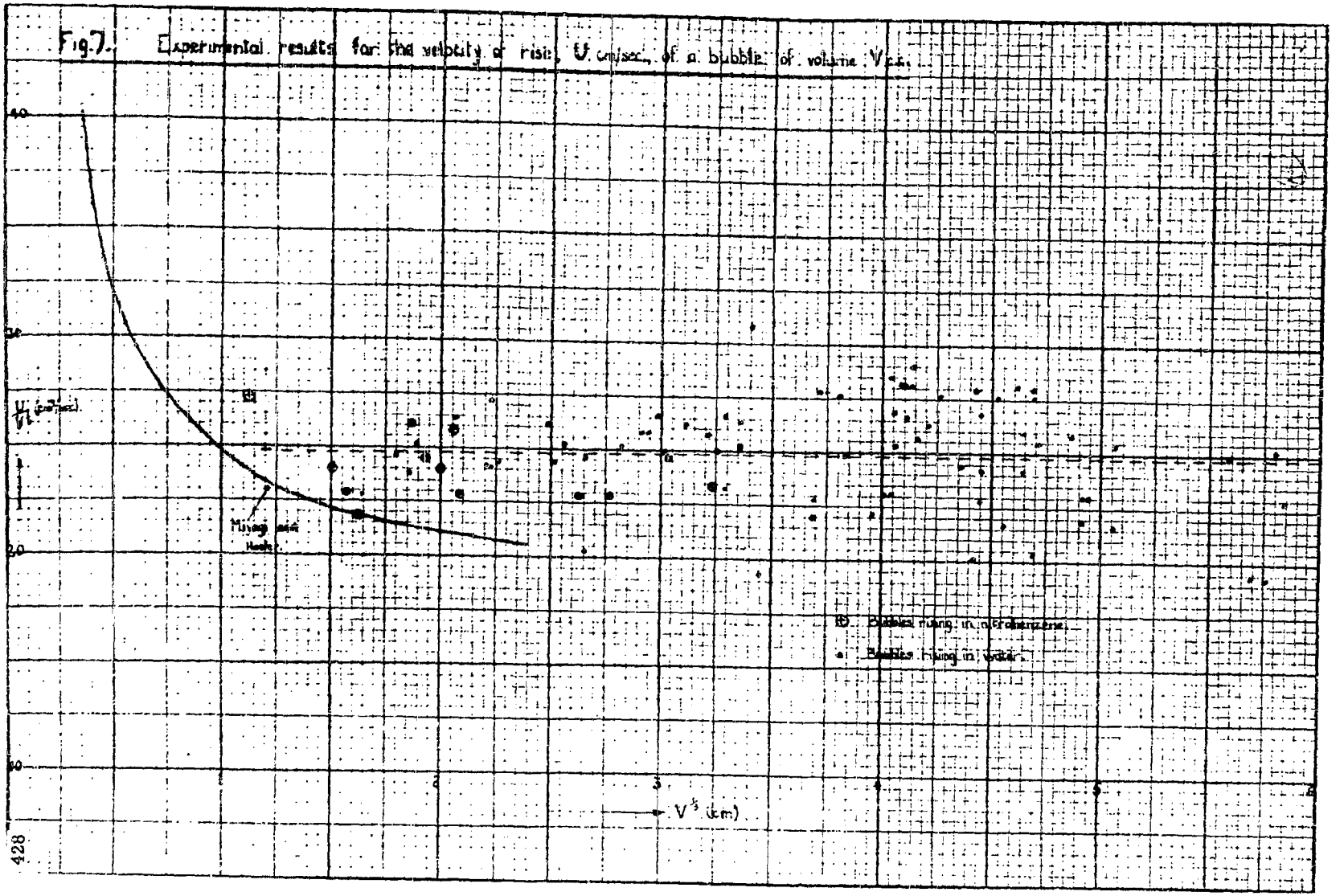
Fig.7. Experimental results for the velocity of rise, U cm/sec., of a bubble of volume V c.c.
40
30
20
10
U (cm/sec)
Rising and Hooks
V^{1/3} (c.m)
Bubbles rising in nitrobenzene.
Bubbles rising in water.

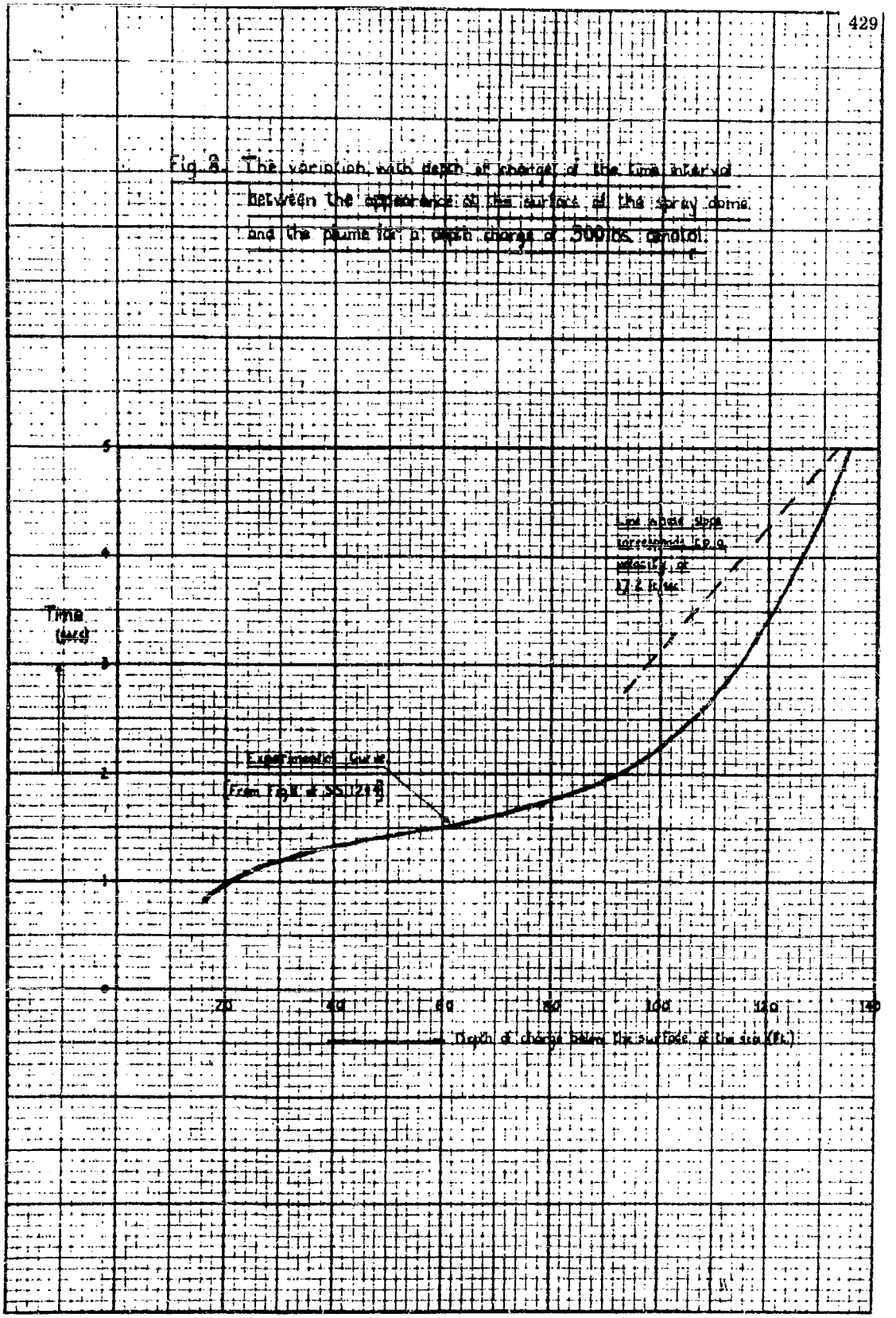

Fig. 8. The variation with depth of charge of the time interval between the appearance at the surface of the spray dome and the plume for a depth charge of 300 lbs. amatol.

A SIMPLIFIED THEORY OF THE EFFECT OF SURFACES ON THE MOTION OF AN EXPLOSION BUBBLE

A. R. Bryant
Road Research Laboratory, London

British Contribution

October 1944

A SIMPLIFIED THEORY OF THE EFFECT OF SURFACES ON THE MOTION OF AN EXPLOSION BUBBLE

A. R. Bryant

October 1944

* * * * * * * * * *

Summary.

A simple physical explanation of the effect of surfaces on the displacement of an explosion bubble is suggested. This explanation leads to the same quantitative expression as the treatments given by Conyers Herring and by Taylor. It is shown that in order to calculate the effect of any given surface it is only necessary to determine the space gradient of the velocity potential due to the "image" sources "induced" by a unit source at the explosion centre. A table of this factor for a number of common surfaces is added for convenience.

Introduction.

The purpose of this note is to suggest a simple physical explanation of the influence of surfaces on an explosion bubble. It will be shown that this explanation leads, with comparatively simple mathematics, to the same quantitative expressions as the treatment given by Conyers Herring (1) and Taylor (2).

For purposes of explanation it will be convenient to consider a simple case first, viz. the influence of an infinite rigid plane on an explosion bubble. The generalization to any arbitrary surface follows at once. For the moment the effect of gravity will be ignored.

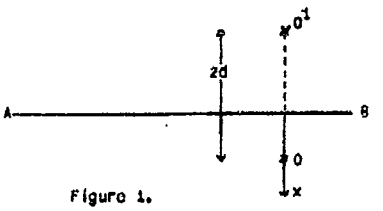

Figure 1.

In Figure 1, O is the centre of an explosion bubble of radius a, assumed small compared to its distance d from the rigid plane AB. The motion of the water outside the bubble due to its pulsation is the same as that produced by a point "source" at O of strength

$$e = 4\pi a^2 \dot{a} \qquad (1)$$

The effect of the plane surface AB is then the same as that produced by a source e at the mirror image point O^1.

The image source e at O^1 will produce a velocity in the water everywhere directed radially away from or to O^1 according as the sign of e is positive or negative, and this velocity is superimposed on the radial flow due to the explosion bubble at O. Hence the water in the neighbourhood of O will have a net velocity U_1 towards O^1 given by

$$U_1 = \left.\frac{\partial \phi^1}{\partial x}\right\}_{\text{at O}} \qquad (2)$$

where ϕ^1 is the velocity potential due to the image source at O^1 the origin of the x co-ordinate being taken at O^1.

In .....

In addition the image source produces a presence p^1 at any point in the water. For points not too close to O^1 the pressure p^1 is simply $\rho \frac{\partial \phi}{\partial t}$. The pressure gradient $\frac{\partial p^1}{\partial x}$ in the neighbourhood of O due to the image source at O^1 is thus.

$$\frac{\partial p^1}{\partial x}\Big] = \rho \frac{\partial}{\partial t}\left[\frac{\partial \phi^1}{\partial x}\right]_{\text{at } O} \qquad (3)$$

Now it is a matter of common experience that a bubble or hollow in a liquid in which there is a pressure gradient due to gravity will move upwards in the direction of the pressure gradient, i.e. from regions of high pressure to regions of low. In the same way the explosion bubble will tend to drift in the direction of the pressure gradient set up by the image source at O^1; this will be away from the surface AB if e is positive.

G.I. Taylor has derived by a simple physical argument an equation for the velocity of the bubble U due to the action of a pressure gradient $g\rho$. The argument runs as follows. The "floating power" of a spherical hollow of radius a due to the pressure gradient $g\rho$ is $\frac{4}{3}\pi a^3 g\rho$, and this is therefore equal to the vertical momentum communicated per second to the water flowing round the spherical hollow. The inertia of the mass of water effectively moving with the bubble is $\frac{2}{3}\pi a^3\rho$ (a well known hydrodynamical result), and its momentum is hence $\frac{2}{3}\pi a^3\rho U$ where U is the velocity of the centre of the bubble. Thus $\frac{d}{dt}(\frac{2}{3}\pi a^3\rho U) = \frac{4}{3}\pi a^3 g\rho$, from which follows equation (4). The same equation is obtained by Conyers Herring by his perturbation method. Using Taylor's equation for U

$$U = \frac{2}{a^3}\int_0^t ga^3 dt \qquad (4)$$

It is clear that any pressure gradient, no matter how produced, will cause a similar drift velocity. Thus a pressure gradient $\rho \frac{\partial}{\partial t}\left[\frac{\partial \phi^1}{\partial x}\right]_{\text{at } O}$ due to the image source will cause the bubble to acquire a velocity U_2 towards O^1, where

$$U_2 = \frac{2}{a^3}\int_0^t \frac{\partial}{\partial t}\left[\frac{\partial \phi^1}{\partial x}\right]_{\text{at } O} a^3 dt \qquad (5)$$

The total drift velocity of the bubble U towards the rigid surface is thus the sum of U_1 and U_2.

In the particular case discussed here it can be seen that $\phi^1 = \frac{a^2\dot{a}}{x}$ and the velocity U of the bubble towards the rigid plane distance d from the bubble

$$U = -\frac{a^2\dot{a}}{4d^2} - \frac{1}{2d^2a^3}\int_0^t a^3 \frac{d}{dt}(a^2\dot{a})\,dt$$

$$= -\frac{2}{4}\frac{a^2\dot{a}}{d^2} + \frac{2}{2d^2a^3}\int_0^t a^4\dot{a}^2 dt \qquad (6)$$

on integrating by parts. Equation (6) is that given by Conyers Herring and by Taylor.

Extension to the General Case.

The argument used above for the simple case of a rigid plane is quite general, and can easily be extended to the general case. The result is simply stated here.

Let there be any set of free or rigid surfaces symmetrical about the axis x of co-ordinates passing through the centre of the explosion bubble O. Assume that a distribution of image sources can be found which satisfies the boundary conditions at the given surfaces when a unit source is placed at O. Let the velocity potential due to these image sources be ϕ. Then the drift velocity U of the bubble in the direction of the x axis towards the origin of co-ordinates is

U = ...

$$U = \left[\frac{\partial \Phi}{\partial x}\right] \text{ at } 0 \left[+ 3a^2\dot{a} - \frac{6}{a^3}\int_0^t a^4\dot{a}^2\,dt \right] \qquad (7)$$

Strictly speaking a dipole source should be added to 0 to allow for the linear motion of the bubble (β), and further multipoles to allow for its change of shape. The effect of "induced" image sources due to these will be second order small quantities if the effect of the primary image distribution is a first order small quantity. Similarly, since the drift is a first order small quantity the error due to assuming the distance from bubble to surfaces to remain constant will be a second order small quantity.

The velocity U_1 is oscillatory and is directed away from rigid surfaces in the first half of the oscillation, and towards rigid surfaces in the second half, its integrated effect over a whole cycle being usually negligible. The velocity U_2 due to the pressure gradient set up by the image sources is directed away from rigid surfaces as long as the pressure is positive, i.e. as long as the bubble is greater than the hydrostatic pressure at the same depth. When the bubble pressure falls below this hydrostatic pressure the pressure gradients are reversed and the velocity U_2 is then towards a rigid surface. Since the force exerted on a hollow vessel is proportional to its volume the bubble acquires most of its momentum when it is large and as the pressure is below the normal hydrostatic pressure when the bubble is large the net effect at the end of one oscillation is a drift towards rigid surfaces. These statements may assist an understanding of the phenomena found by Temperley in calculating the effect of a deformable target plate on the motion of the bubble, and in particular the correlation between the sign of the motion and the sign of the pressure in the bubble.

Approximate Formula for the Displacement of the Bubble.

The integral for the momentum of the bubble towards a surface, and that for the vertical momentum due to gravity both become nearly constant towards the end of the first oscillation. It is in this region that most of the displacement of the bubble occurs. Hence it is a reasonable approximation to assume that the total displacements at the end of the first period due to the surface and to gravity are in the same ratio as the momenta. Denoting these two displacements by S and H respectively we have

$$\frac{S}{H} = -\left[\frac{\partial \Phi}{\partial x}\right] \text{ at } 0 \; \frac{6\int a^4\dot{a}^2 dt}{2\int a^3 dt} \qquad \text{(R.H.S. Non-dimensional)} \qquad (8)$$

Where the integrals are to be taken over the whole period, S is towards the origin of the origin of the co-ordinate x.

In obtaining (8) all lengths and times on the right hand side have been converted to Taylor's non-dimensional units, i.e. all lengths are divided by the standard length $l = (W/g\rho)^{\frac{1}{4}}$, where W is the energy of the motion, ρ the density of water. All times are divided by the standard time $\sqrt{\frac{l}{g}}$. $\frac{\partial \Phi}{\partial x}$ has the dimensions L^{-2}. In addition the small oscillatory term $3a^2\dot{a}$ in the expression (7) has been dropped, since it may be exactly integrated and shown to be very small at the end of a period. In Table 1 the value of these integrals are calculated for a number of cases, and compared with two suggested approximate formulae.

Table 1 .....

TABLE 1.

	z_0	2	2	3	4	7.8
	C	0.11	0.08	0.10	0.10	0.063
	Charge Weight (T.N.T)	475 lb.	2.74 lb.	100 lb.	100 lb.	1 oz.
	$\int a^4\dot{a}^2dt \times 10^3$	6.91	8.03	4.64	3.26	1.86
(1)	$0.30\, a_m^{\,5} z_0^{\,\frac{1}{2}} \times 10^3$	8.55	9.53	5.32	3.68	1.89
	$0.370\, a_m^{\,6} z_0 \times 10^3$	6.83	7.79	4.55	3.28	1.92
	$\int a^3dt \times 10^3$	38.8	41.4	18.07	10.36	3.46
(2)	$\frac{0.70\, a_m^{\,3}}{z_0^{\,5/6}} \times 10^3$	37.8	40.2	17.9	10.36	3.27

(1) Conyers Herring's formulae in non-dimensional form.

(2) Formulae given in the report "The Behaviour of an Underwater Explosion Bubble."

The values of the integrals given in Table 1 were obtained from the numerical integration of Taylor's equations for the motion of an explosion bubble in the absence of all surfaces. It has been assumed that the perturbing effect of the presence of the surface on the radius/time curve of the bubble is small during the time when the bubble is large and the two integrals are growing.

It will be seen that Conyers Herring's formula for $a^4\dot{a}^2dt$ is considerably in error, and an alternative formula viz., $0.37 \times 10^{-3}\, a_m^{\,6} z_0$ obtained empirically, is put forward in the Table which gives reasonable agreement. Inserting this approximation, and the one given in the last line of the Table, in equation (8) now yields

$$\frac{S}{H} = -\left.\frac{\partial \phi}{\partial x}\right]_{\text{at } 0} 1.59\, a_m^{\,3} z_0^{\,11/6} \qquad \text{(R.H.S. Non-dimensional)} \quad (9)$$

To take the approximation one stage further the value of the rise due to gravity obtained, may be inserted. The equation given was

$$\text{Rise due to gravity } h = \frac{1.19}{z_0^{\,5/6}} \qquad \text{(Non-dimensional)} \quad (10)$$

Hence the displacement s of the bubble towards the surface in non-dimensional units becomes

$$s = \left.\frac{\partial \phi}{\partial x}\right]_{\text{at } 0} 1.89\, a_m^{\,3} z_0 \qquad \text{(Non-dimensional)} \quad (11)$$

But $a_m^{\,3} z_0$ is very nearly independent of c, i.e. independent of charge weight and also of z_0 (depth). Replacing it by an average value giving the best fit over the whole range, (11) becomes finally.

$$\text{Non-dimensional displacement towards origin of x co-ordinates in first period} = -\,0.37 \left.\frac{\partial \phi}{\partial x}\right]_{\text{at } 0} \quad \text{(Non-dimensional)} \quad (12)$$

This .....

This simplification agrees with equation (11) within 7% over the range $z_0 = 7.8$, $C = 0.063$ (1 oz. at 6 feet depth) to $z_0 = 2$, $C = 0.11$ (475 lb. at 93 feet).

Comparison with a $W^{1/3}$ Law of Scaling

Let S be the absolute displacement of the bubble at the end of the first period in any particular set up of charge and surfaces. Let S^1 be the bubble displacement in a geometrically similar set up where all dimensions are increased in the ratio λ, the charge weight being increased in the ratio λ^3. Then it follows at once from equation (12) that

$$S^1 = \lambda^{\frac{1}{2}} S \qquad (13)$$

Equation (13) is independent of the depth at which the explosion occurs. If the displacement had scaled according to the $W^{1/3}$ law S^1 would have been equal to λS, so that (13) indicates that the displacement of a large explosion bubble is less than the value obtained by scaling up from a small scale experiment.

Conclusion.

The effect of surfaces on an explosion bubble has been shown to be due to two principal causes, viz., the velocity imparted to the water near the bubble by the image sources, and the pressure gradient set up in the water by the image sources. It is found that to calculate the effect it is necessary only to calculate the space gradient, along the axis of symmetry, of the velocity potential due to the image sources produced by a unit source at the explosion centre. A simple formula, equations (11) or (12), then enables the displacement of the bubble in the first oscillation to be calculated. These displacements are almost independent of depth. A table of values of the coefficient $\frac{\partial \phi}{\partial x}$ in equations (11) and (12) is appended for convenience.

References.

(1) Theory of the Pulsations of the Gas Bubble formed by an Underwater explosion. Report No. C4-sr20-010.

(2) The Motion and Shape of the Hollow Produced by an Explosion in a Liquid. G.I. Taylor and R.M. Davies.

(3) cf. "The motion and shape of the hollow produced by an explosion in a liquid", G.I. Taylor and R.M. Davies, where the bubble is represented by a point source and a dipole and the effect of the images due to each is considered.

(4) This result is also given by Savic.

(5) Calculated from Savic's equation for the potential due to the images by differentiating with respect to d his expression for W.

Appendix .....

APPENDIX.

Table of Coefficient.

Nature of Surface	Dimensions	Distance of Bubble Centre	$\frac{\partial \phi}{\partial x}$ at bubble centre
Rigid Infinite Plane	-	d from bubble to plane	$-\frac{1}{4d^2}$
Rigid Sphere (4)	Radius R	d bubble to sphere centre	$-\frac{R^3}{d\,(d^2-R^2)^2}$
Rigid Sphere with centre in Infinite Free surface	Radius R	d bubble to sphere centre	$\frac{1}{4d^2}-\frac{2R^3(d^4+R^4)}{(d^4-R^4)^2 d}$
Rigid Infinite Cylinder (5)	Radius R	d bubble to cylinder axis	$-\frac{21\pi R^2}{64 d^4}$
Rigid Infinite Cylinder with axis in Infinite Free Surface (5)	Radius R	d bubble to cylinder axis	$\frac{1}{4d^2}-\frac{27\pi R^2}{64 d^4}$

THE RATE OF RISE OF LARGE VOLUMES OF GAS IN WATER

H. N. V. Temperley and Ll. G. Chambers
Admiralty Undex Works, Rosyth, Scotland

British Contribution

January 1945

THE RATE OF RISE OF LARGE VOLUMES OF GAS IN WATER

H. N. V. Temperley and Ll. G. Chambers

January 1945

* * * * * * * * *

Summary.

The work described by Taylor and Davies (1) is extended to volumes of gas of the order of gallons. The necessary large volumes of gas were obtained by overturning a bucket under water and by ½ ounce charges of burning cordite. The resulting bubbles were photographed in the glass-fronted tanks of the M.A.E. Establishment at Glen Fruin. The relation $U = {}^{2}/_{3}\sqrt{ga}$ between velocity and radius, found experimentally and theoretically by Taylor and Davies, was confirmed for bubbles with cap radii of up to 15 cm., and it was concluded that such bubbles are near the limit of stability.

The work appears to be in general agreement with existing knowledge of the behaviour of the gaseous products from very deep explosions. It is concluded that the bubbles from such explosions break up into comparatively small fragments, once the oscillation has ceased.

An attempt is made to improve the theoretical solution of the hydro-dynamic equations found by Taylor and Davies, but it appears that the convergence of the method is rather slow.

1. *Introduction.*

The work described in this report was carried out in continuation of that by Taylor and Davies (1). The largest volume of gas used by them was of the order of 100 cc., and it was desired to extend the work to much larger volumes of gas to gain a more complete idea of what happens in the final stages of an underwater explosion. Thus, the volume of gaseous products released from one gram of Amatol (neglecting water) is given by Taylor and Davies as 650 cc. Thus we conclude that an ounce of explosive will liberate roughly four gallons of gaseous products at atmospheric pressure. In order to deduce what happens during the final stages of an underwater explosion, we wish to know whether such large volumes of gas can exist as coherent bubbles, or, if not, what is the volume of the largest bubble that can exist and rise through the water without breaking up.

2. *Methods of carrying out the Trial.*

The relative fragility of the glass windows in the Glen Fruin tanks precluded the use of any form of high explosives and therefore two alternative methods were employed.

(a) The method described by Taylor and Davies (1) was tried on a larger scale. A bucket (capacity 2½ gallons) was lowered upside down to the bottom of the tank, a sinker being attached to the handle. A small out-of-balance weight (4 lbs.) was attached to the end of a short lever pivoted at the bottom of the bucket. While the bucket was being lowered this lever was supported by a string, and the bucket remained inverted with the air trapped underneath it. When the string was released the lever fell to a horizontal position and the out-of-balance weight tipped the bucket upwards "emptying out" the air.

(b) ½ ounce burning cordite charges were ignited electrically by means of a "puffer". Two types of container were used, a "pill-box" type of bakelite container which broke easily when the charge was fired, and a stout brass cartridge-case the only exit from which was a hole of 1" diameter.

The .....

The resulting bubbles were photographed by cine-camera (16 frames/second nominal speed) distances being determined by comparison with the edges of the panes of glass (2½ feet), and the mesh of the protective wire-netting inside the tank (3 inches). The time-scale was established by photographing dials driven by a phonic motor controlled by a tuning fork.

3. *Description of Bubbles.*

The out-of-balance couple on the bucket had been adjusted in preliminary experiments near the surface of the water, so that all the air was "poured out" simultaneously. If the couple is too small, the air escapes in the form of small bubbles, while if it is too large the bucket goes beyond the vertical before all the air can escape. When the weight was properly adjusted, the air "poured out" caused a considerable upheaval and "whitening" of the water, similar to the "plume" from a deep explosion. When the bucket was 10 feet or more below the water surface, it was found that the air came up as about 4 - 10 large bubbles and a large number of smaller ones. The disturbance produced at the surface was very slight. It was concluded that the original large bubble had broken up. When the experiments proper were begun in the glass-fronted tank it was found that the large bubble broke up almost immediately into a small number of large bubbles and a multitude of very small ones. All the large bubbles were of the characteristic "mushroom" shape described by Taylor and Davies (1) and rose at speeds of the order of 2 feet per second. Some were observed to break up as they floated upwards and it was also thought that some were colliding and coalescing, but the latter impression provided, on examination of the films, to be a mistake. Two bubbles sometimes settled down into an apparently stable configuration, one below the other, but with axes of symmetry offset, and rose together. No larger complexes were seen.

The bubbles produced by the burning cordite were very similar to the air-bubbles, and the general sequence of events seemed to be very much the same. It did not appear to make any difference to the general nature of the phenomena whether the cordite was fired in the easily breakable pill-box or the strong cartridge-case. Indeed, one of the largest bubbles obtained in the trial was obtained in the latter circumstances, which one would think were the most unfavourable. Some close-up photographs were taken in the smaller tank at Glen Fruin in order to get the earlier stages of bubble formation in more detail, but the earlier stages were obscured by what appeared to be a cloud of small bubbles. A few photographs were taken from above of a bubble "breaking surface" but exhibited no feature of interest. The surface phenomena were confined to slight ripples (Figure 1(b)).

Two features noticed by Taylor and Davies (1) were apparent in the records. First, the bubbles are often "lop-sided," i.e. not perfectly symmetrical about an axis, the "lopsidedness", when it exists, often persisting throughout the life of the bubble; secondly, in many of the records, there is an indication of a wake lying approximately in the sphere of which the bubble is a cap, similar to the effect shown by Taylor and Davies (1) in Figure 1 of their report. In our case the existence of a wake is suggested by clouds of small bubbles following each large one (Figure 1(a)).

4. *Analysis of the Records.*

The trajectories of 31 bubbles of various sizes were plotted. Within the errors of the experiment the velocities were all constant in time, in spite of the fact that the depth of water was 33 feet so that the bubbles must have expanded to twice their volume during the rise. A few of the trajectories showed indications of a slight oscillation (too small to measure) about a mean velocity, but there was no definite upward or downward curvature. The images of the bubbles were somewhat blurred, but in some cases it was possible to estimate the radius of curvature of the upper cap of the bubble, in order to check up the relation $U = {}^{2}/_{3}\sqrt{ga}$ found by Taylor and Davies (1) for their small bubbles. The blurring of our images may be due to the condensation mist on the glass panes of the tank, which was difficult to remove completely.

The radius of curvature was measured by projecting a magnified image of the bubble on to squared paper and estimating the radius from the length of the chord and the distance from the chord to the top of the bubble. Owing to the blurring it was not possible to say how nearly the bubbles are to parts of spheres, but it appeared that the departure was not great, and that the estimates of the radii should be accurate to 20%. The radius was measured at several different points on each

trajectory .....

trajectory and a mean taken. The results are plotted in Figure 2, together with Taylor and Davies' points. In one film the time-scale was uncertain, and the points obtained from it are shown separately on an arbitrary velocity scale. They have been included because one of these points was from a double bubble of the kind described above. The results indicate that its upward velocity is definitely less than that of a single one of the same mean radius (Figure 3).

Leaving this doubtful film out of account it will be seen that the remaining 11 points agree with Taylor and Davies' relation within the experimental error. Taylor and Davies' values for the radii of the caps of the bubbles extended from 2 cm. to 6 cm., while ours extend from 4 cm. to 15 cm. The question of the stability of bubbles of various sizes was examined by measuring the velocities of 9 bubbles that ultimately split up, but no correlation between velocity and stability could be traced, the bubbles appearing to split at all velocities in the range studied. This seems to indicate that we are near the limit of stability, which is perhaps fixed by the relative importance of surface tension and hydrodynamical forces. By tending to keep the surface small, surface tension would act as a stabilising influence, but would become less important for larger bubbles. Taylor and Davies (1) mention that conditions had to be adjusted carefully to obtain their bubbles. This agrees with what we have found with our rather larger ones.

If this interpretation of the results is correct, it would seem that the final upward velocity of the products of an explosion, after the oscillations have ceased, and the bubble has broken up into small ones, is of the order of 2 - 3 feet per second, compared with 17.2 feet per second inferred by Taylor and Davies for a 300 lb. charge on the assumption that the explosion products remain as one bubble.

It is perhaps worth mentioning that the rate of rise of bubbles of exhaust gas from a torpedo is known to be of the order of 2 feet per second (again of the same order of magnitude).

5. *Theoretical Considerations.*

Although it is clear from Taylor and Davies' and our photographs that these bubbles have a wake, the motion of the remainder of the water is probably irrotational and it is of interest to examine whether there are any solutions of the hydrodynamical equations which enable the velocity and pressure conditions to be satisfied along a cap of a sphere of limited angle. A start on this problem is made by Taylor and Davies (1), who show that the ordinary solution for a sphere in a uniform stream satisfies the conditions for continuity of pressure as well as velocity as far as terms involving θ^2 (where θ is the polar angle referred to an axis through the cap of the bubble) provided that velocity and radius are connected by the relation $U = {}^2/_3\sqrt{ga}$ which has been confirmed experimentally. If we take a more general velocity potential of the form

$$\phi = \frac{A_0}{r} + \frac{A_1 \cos\theta}{r^2} + U\, r \cos\theta,$$

representing a combined source and dipole in a uniform stream, it is possible to satisfy the continuity conditions as far as terms involving θ^4, provided that we assume that the profile of the cap is of the form $R = a + b_2\theta^2 + b_4\theta^4$. (It is unnecessary to introduce odd powers of θ). Alternatively, if we assume A_1 zero, so that the bubble behaves as a simple source rather than as a dipole source, we can still satisfy the equations as far as terms of the order θ^2. The various solutions are tabulated in Table 1.

TABLE 1.

	A_0/Ua^2	A_1/Ua^3	b_2/a	b_4/a	$U/\sqrt{ga}$	$U/\sqrt{gD}$	
(1)	0	.50	0	0	.67	.67	Taylor and Davies'
(2)	1.00	0	+ .125	0	1.00	.87	Source in stream
(3)	- 1.23	+ 1.12	- .079	- .019	.50	.54	

The .....

The last column is obtained by putting in the radius of curvature of the cap at its top point instead of a. By the usual formula we have

$$\rho = \frac{a}{1 - \frac{2b_2}{a}}$$

It is evident that the relation between the velocity and the radius of the cap is sensitive to slight departures from the spherical shape of the cap. (It is known that the virtual mass of an ellipsoid of given volume is sensitive to the exact shape of the ellipsoid). It would therefore seem that one would have to go to high powers of θ, and introduce a correspondingly large number of spherical harmonics in the velocity potential in order to determine the exact theoretical shape. It is probable that one could obtain a multiplicity of solutions, and one would then have to determine which are stable by assuming small perturbations. As a matter of fact, substitution of the apparently better solution (3) for (1) would worsen the agreement with experiment.

We have introduced a certain degree of arbitrariness by the fact that the origin of co-ordinates is unspecified. The same profile might be specified in quite different ways (as a function of θ) for different choices of origin. It will, in fact, be noticed that the discrepancies between the various values of $U/\sqrt{g\rho}$ are much smaller than those between the various values of $U/\sqrt{ga}$, so that it may be that the three solutions we have found are all really first approximations to the same actual profile. These points seem well worth further investigation, but it has not been thought advisable to hold up the issue of the report as the investigation would be lengthy. The profiles corresponding to the various solutions are plotted in Figure 4. It might be thought that it would be an easy matter to decide experimentally between them, but even curves 2 and 3 can be brought nearly into coincidence over the relevant range of angles (about 60°) by shifting the origin of co-ordinates, and choosing the scale so that the radii of curvature of the caps are the same.

6. *Conclusions.*

Taylor and Davies' formula relating upward velocity and radius has been confirmed for radii up to 15 cm., which is probably near the limit of stability. The available evidence suggests that, after an underwater explosion bubble has ceased oscillating, it splits up into many small bubbles of about this order of size.

Reference.

(1) The rate of rise of large volumes of gas in water. Taylor and Davies.

TYPICAL PHOTOGRAPHS OF RISING BUBBLES.

FIG. 1 (a).
BUBBLES FROM CORDITE CHARGE SHEWING WAKES.
(SIDE VIEW).

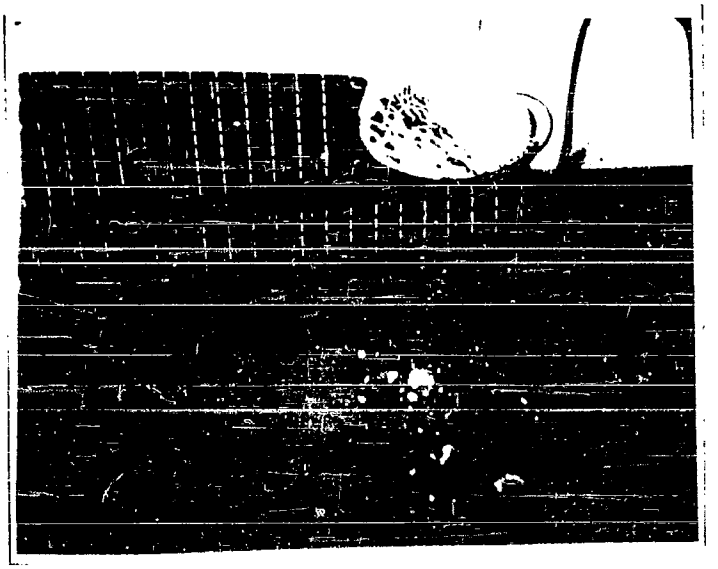

FIG. 1. (b).
BUBBLE FROM CORDITE CHARGE ABOUT TO BREAK SURFACE.
(VIEW FROM ABOVE).

PLATE. I.

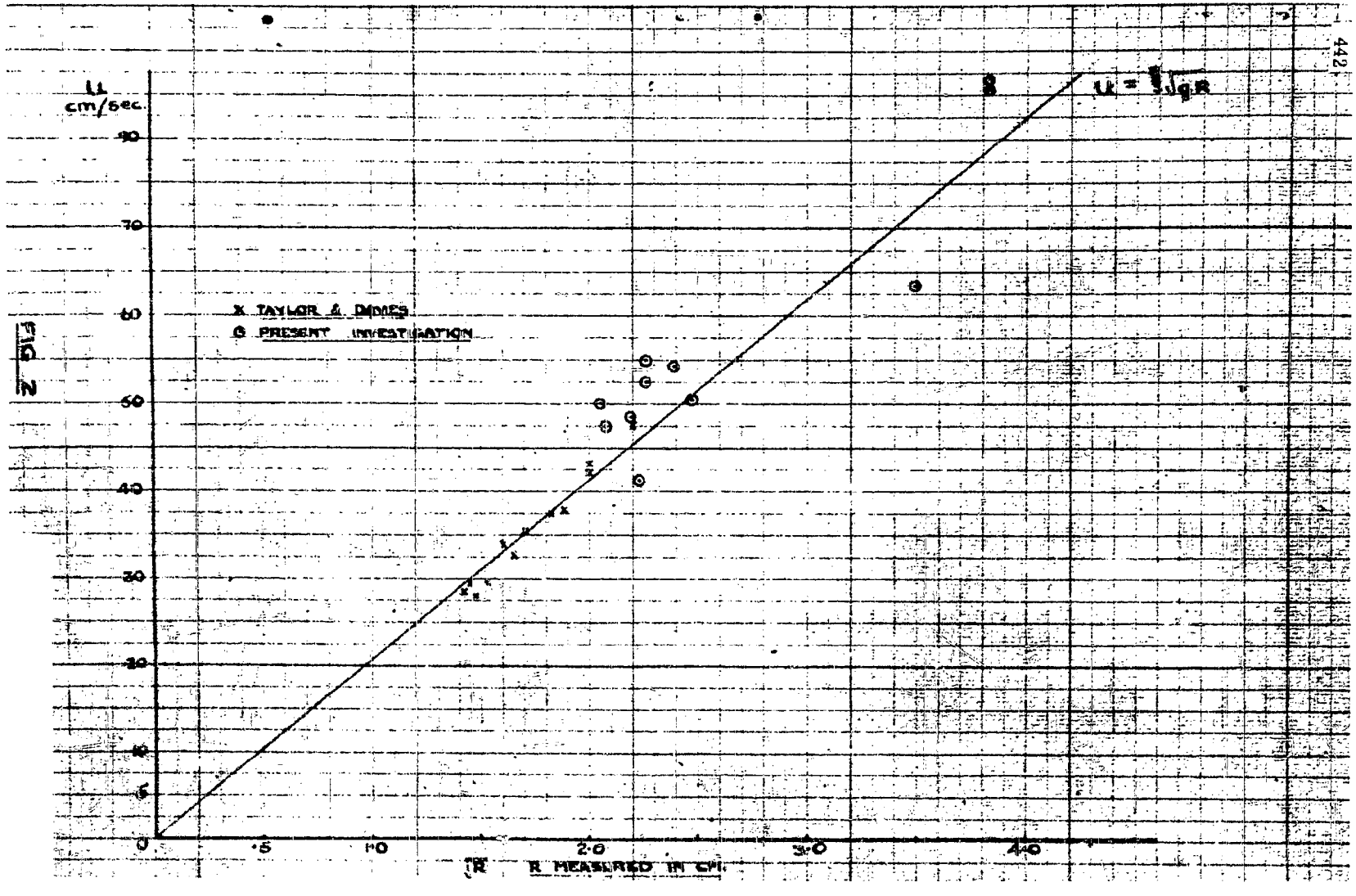
u
cm/sec.
90
70
60
50
40
30
20
10
5
0
·5
1·0
2·0
3·0
4·0
R MEASURED IN CM.
X TAYLOR & DIXIES
O PRESENT INVESTIGATION
u = √gR

FIG 2

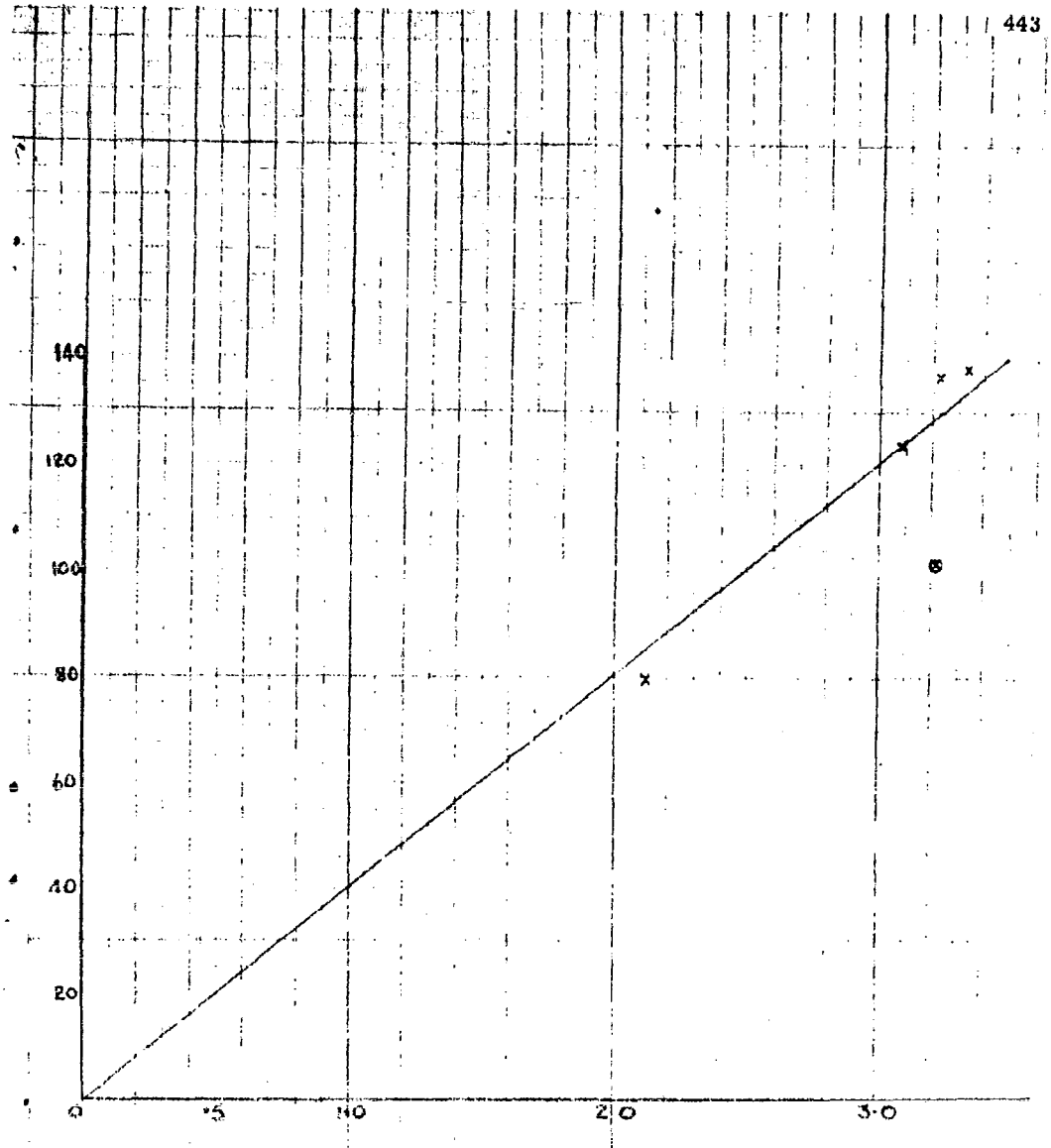

THE ABSCISSA IS $R^{\frac{1}{2}}$, R MEASURED IN KM.
THE ORDINATE IS μ. μ MEASURED IN UNKNOWN UNITS.
THE LINE IS THE LINE OF BEST FIT TO THE FOUR POINTS X.
THE POINT MARKED ⊗ CORRESPONDS TO A DOUBLE BUBBLE.

FIG.

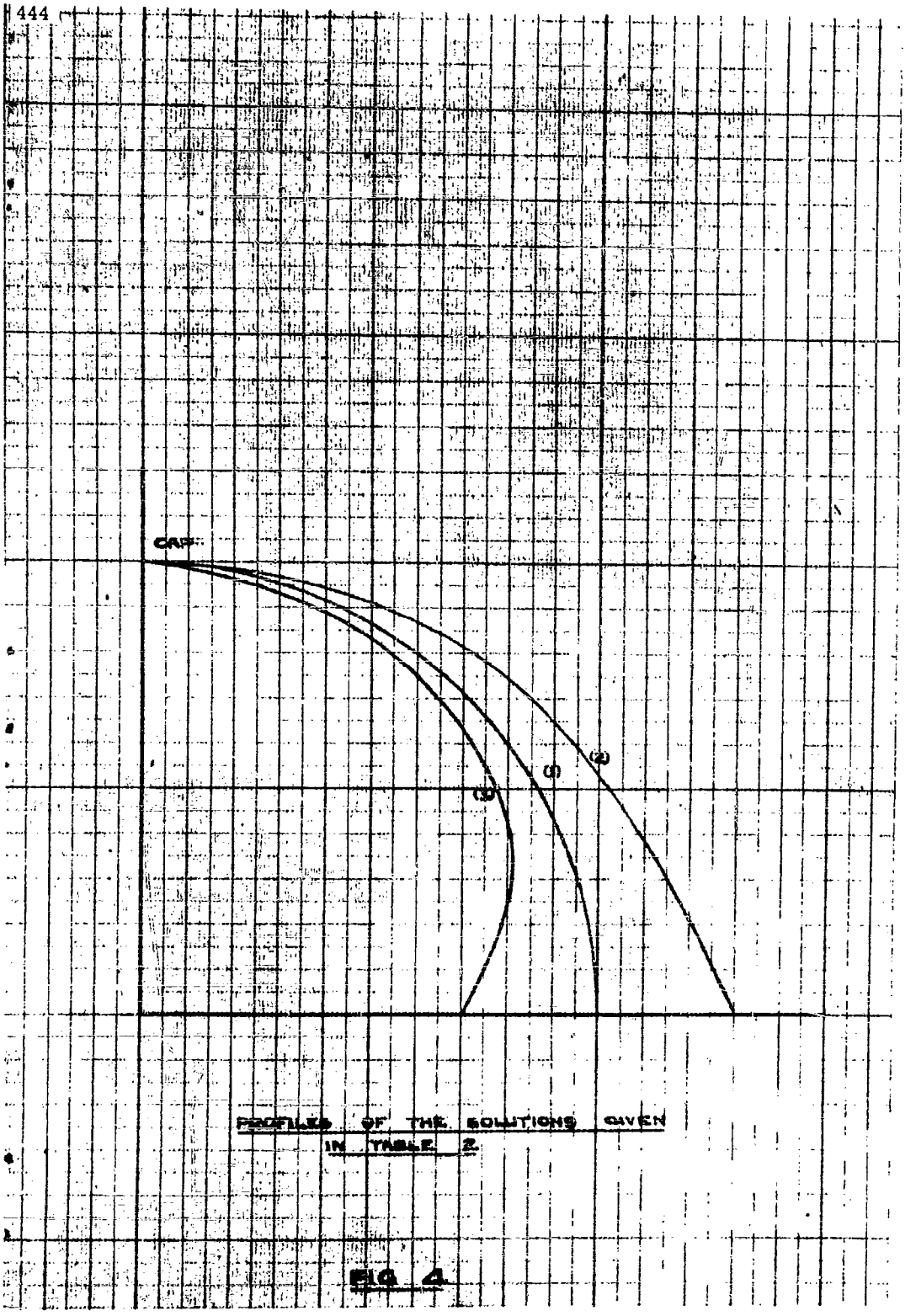

PROFILES OF THE SOLUTIONS GIVEN IN TABLE 2.

FIG 4.

THE ATTRACTION OF AN UNDERWATER EXPLOSION BUBBLE TO A RIGID DISC

A. R. Bryant
Road Research Laboratory, London

British Contribution

February 1945

THE ATTRACTION OF AN UNDERWATER EXPLOSION BUBBLE TO A RIGID DISC

A. R. Bryant

February 1945.

* * * * * * * *

Summary.

The attraction of an explosion bubble towards a rigid disc has been calculated for two important cases, viz. (1) the disc fixed, (2) the disc moving along the line joining disc and explosion centre. The case in which only part of the disc is moving has been treated in an Appendix.

For the fixed disc the attraction falls off more rapidly with distance than the attraction of an infinite rigid plane. At one disc radius the attraction is one half that of the infinite rigid plane at the same distance. At one disc diameter the attraction is one seventh that of the infinite rigid plane.

The attraction of the moving disc depends on both its velocity and acceleration. That part of the attraction which is due to its motion falls off more rapidly with increasing distance than the part due to its rigidity.

It is suggested that the attraction of a bubble to a rigid disc is a reasonable approximation to the practical case of a target like a Box Model. It is pointed out that the motion of the Box Model as a whole due to the explosion pressures may have an appreciable influence on the displacement of the bubble.

Introduction.

In considering the damage to finite targets caused by underwater explosions it is desirable to calculate, at least approximately, the displacement of the bubble towards or away from the target. So far the only finite rigid surface whose attraction has been calculated is the sphere. For targets like the D.N.C. box model, or the "drum" model used in the U.S.A., where a target plate is surrounded by a rigid "skirt" or baffle of finite extent, it is suggested that the attraction of an explosion bubble to a rigid disc would be a better approximation to the experimental conditions than the attraction to a sphere. The problem of a rigid disc is treated in the following note.

The following assumptions have been made:-

(1) The bubble remains spherical throughout its motion.

(2) The maximum radius of the bubble is small compared to its distance from the disc.

(3) The velocity of displacement of the bubble is small and its contribution to the attractive forces is neglected.

The Attraction of an Explosion Bubble to a Fixed Rigid Disc.

The method of calculating the attraction of a fixed rigid disc is as follows. A point source of unit strength is placed at the explosion centre. A potential φ_2 is found which, when added to the potential ϕ_1 due to the point source, gives the correct boundary condition over the surface of the disc. This potential may be regarded as due to image sources "induced" by the original point source. The required "attraction coefficient" is then the value at the explosion centre of the space gradient $\frac{\partial \phi_2}{\partial x}$, where x is positive in a direction away from the disc along the axis of symmetry. It was shown in an earlier paper* that the velocity of the bubble towards the surface at any time is the product

of two .....

* "A Simplified theory of the Effect of Surfaces on the Motion of an Explosion Bubble."

of two factors, one the "attraction coefficient" $\frac{\partial \phi_2}{\partial x}$, which is a geometrical factor, and the other an integral expression involving the radial motion of the bubble and independent of the geometry of the surfaces.

The Velocity Potential Equations.

The most suitable co-ordinates in which to solve the problem are oblate spheroidal co-ordinates r, s, ψ, as shown in Figure 1. AB is the disc, radius c, and A, B, are the foci of the confocal oblate spheroids, r = constant and the hyperboloids of one sheet s = constant. OP is the axis of symmetry, and the explosion centre is at X on this axis, distance d from the disc. It is convenient to choose $o \leqslant r \leqslant \infty$, so that s varies between - 1 and + 1. This choice makes the s co-ordinate continuous in the region of the field. It is to be noted that s changes sign on passing through the disc.

The relationship between the spheroidal co-ordinates r, s, and cylindrical co-ordinates x, ρ, origin at o and the x co-ordinate positve in the direction of OX, is

$$x = c\, r\, s \qquad (1)$$

$$\rho = c\,[(1 + r^2)(1 - s^2)]^{\frac{1}{2}} \qquad (2)$$

Since the problem is entirely symmetrical with regard to ψ it will not appear in the equations.

The disc AB is thus the surface r = o. Denoting the potential due to the point charge at X ($r = r_b$, $s = 1$, $\psi = o$) by ϕ_1 we have*

$$\phi_1 = \frac{i}{c} \sum_{n=o}^{\infty} (2_n + 1)\, Q_n (ir_o)\, P_n (ir)\, P_n (s) \qquad r < r_o \qquad (3a)$$

$$\phi_1 = \frac{i}{c} \sum_{n=o}^{\infty} (2_n + 1)\, P_n (ir_o)\, Q_n (ir)\, P_n (s) \qquad r > r_o \qquad (3b)$$

Where P_n and Q_n are the Legendre functions of the first and second kind, and $i = \sqrt{-1}$.

To this must be added a potential ϕ_2 which satisfies Laplace's equation, vanishes at infinity, and has no singularities in the region of the field. Thus

$$\phi_2 = \sum_{n=o}^{\infty} A_n P_n (s)\, Q_n (ir) \qquad (4)$$

The potential $\phi = \phi_1 + \phi_2$ has to satisfy the condition that at the disc, i.e. the surface r = o, its gradient normal to the surface is zero, since the disc is both rigid and fixed. This gives an equation from which the coefficients A_n may be determined. Thus

$$\sum_{n=o}^{\infty} \{A_n\, Q_n^1 (i.r) + \frac{i}{c} \cdot (2n + 1)\, Q_n (ir_o)\, P_n^1 (ir)\}\, P_n (s) = o \qquad (5)$$

for r = o

whence

$$A_n = -\frac{2}{\pi c} (2n + 1)\, Q_n (ir_o) \qquad n \text{ odd}$$

$$= o \qquad n \text{ even.}$$

(It is .....

* Static and Dynamic Electricity. Smythe, McGraw Hill 1939, p.165. It may be verified that the potentials given in (3a) and (3b) satisfy Laplace's equation in these co-ordinates, and reduce to Heine's expansion of $\frac{1}{c(r_o - r)}$, or $\frac{1}{c(r - r_o)}$ respectively, along the axis of symmetry s = 1 (see Whittaker and Watson, 4th Edition p.322).

(It is to be noted that the function Q_n has a branch line along the real axis between -1 and +1, and that the value of $Q_n^1(ir)$ at $r = o$ is really the limit of $Q_n^1(i\delta)$, as δ tends to zero through positive values).

The desired potential due to the "induced" images is therefore

$$\phi_2 = \frac{2}{\pi c} \sum_{m=o}^{\infty} (4m + 3)\, Q_{2m+1}(ir_o)\, Q_{2m+1}(ir)\, P_{2m+1}(s) \qquad (6)$$

The "attraction coefficient" of the disc is $\frac{\partial \phi_2}{\partial x} = \frac{1}{c} \frac{\partial \phi_2}{\partial r}$ at $s = 1$ and $r = r_o = \frac{d}{c}$, i.e. at the explosion centre X.

$$\left(\frac{\partial \phi_2}{\partial x}\right)_{\text{at X}} = \frac{2i}{\pi c^2} \sum_{m=o}^{\infty} (4m + 3)\, Q_{2m+1}(ir_o)\, Q^1_{2m+1}(ir_o) \qquad (7)$$

Equation (7) may be put in finite form as follows. Heine's development of $1/t-z$ is: (Whittaker and Watson, p.321)

$$\frac{1}{t-z} = \sum_{n=o}^{\infty} (2n + 1)\, P_n(z)\, Q_n(t) \qquad (8)$$

The series in (8) is valid for all points z lying inside an ellipse in the complex plane passing through t and with foci at ± 1. Changing the sign of z throughout and subtracting this new expression from (8) gives

$$\sum_{m=o}^{\infty} (4m + 3)\, P_{2m+1}(z)\, Q_{2m+1}(t) = \frac{z}{(t^2 - z^2)}$$

Dividing both sides by $-2\,(t - z)^2$, and integrating both sides with respect to z from -1 to +1, yields

$$\sum_{m=o}^{\infty} (4m + 3)\, Q_{2m+1}(t)\, Q^1_{2m+1}(t) = -\frac{1}{2} \int_{-1}^{1} \frac{z\,dz}{(t^2 - z^2)(t - z)^2}$$

$$= -\frac{1}{8t^2} \log\left(\frac{t - 1}{t + 1}\right) - \frac{1}{4t} \frac{(1 + t^2)}{(1 - t^2)^2} \qquad (9)$$

Since the reversal of the order of integrating and summing may be justified for all values of t not on the branch line of the Q functions, i.e. the portion of the real axis between -1 and +1.

Finally, replacing t in (9) by (ir_o), and taking only the principal value of the complex logarithm in (9) as necessitated by the boundary condition at the surface of the disc, equation (7) for the "attraction coefficient" of the fixed rigid disc becomes

$$\left(\frac{\partial \phi_2}{\partial x}\right)_{\text{at X}} = \frac{1}{\pi c^2}\left\{\frac{\tan^{-1} r_o}{2r_o^2} - \frac{\pi}{4r_o^2} - \frac{1 - r_o^2}{2r_o(1 + r_o^2)^2}\right\} \qquad (10)$$

where $r_o = d/c$

It may be verified that as d tends to zero, the attraction coefficient in (10) tends to $-1/4d^2$, the attraction coefficient for an infinite rigid plane. Recapitulating the result obtained in R.R.L. Note ADM/210/ARB, the velocity U of the bubble towards the disc is therefore

$$U = \left(\frac{\partial \phi_2}{\partial x}\right)_{\text{at X}} \left\{3a^2\dot{a} - \frac{6}{a^3} \int_o^t a^4 \dot{a}^2\, dt\right\} \qquad (11)$$

Where a is the radius of the bubble at time t, and $\partial \phi_2 / \partial x$ is given by (10).

Comparison .....

Comparison of Fixed Rigid Disc with Infinite Rigid Plane.

In Figure 2 the "attraction coefficient" (10) for a fixed rigid disc has been divided by $-1/4d^2$, the value for an infinite rigid plane, and plotted against $r_o = d/c$. It will be seen that the attraction of the disc is always less than that of the plane and falls off quite rapidly with increasing distance. Thus, for an explosion bubble at a distance of one disc radius the attraction is only half that for the infinite plane at the same distance, while the fraction is one seventh at a distance of one disc diameter.

The Attraction of a Moving Rigid Disc.

The extension of the foregoing to the case of a rigid disc moving with velocity v along the axis of symmetry, i.e. towards or away from the explosion centre, will now be made. The co-ordinate system is fixed in space and the surface r = o is made coincident with the disc at the instant considered.

The velocity potential due to a disc of radius a moving along its axis with velocity v away from the explosion centre at $r_o = d/c$ is

$$\phi_3 = \frac{2cv}{\pi} Q^1 (ir)\, s \qquad (12)$$

If this is added to $\phi = \phi_1 + \phi_2$ the complete velocity potential for a moving rigid disc and a unit point source is obtained. Since this added potential is independent of the strength of the source the analysis given in R.R.L. Note ADM/210/ARB must be modified slightly. Pressure gradients and velocities along the axis of symmetry will be additive so that the drift velocity or displacement of the bubble due to the motion of the disc may be calculated separately and added to that due to a fixed rigid disc - equation (11).

Following the physical arguments of the above mentioned paper the effect of this added velocity potential is two fold. First, the motion of the disc imparts a drift velocity $\partial\phi_3/\partial x$ towards the disc to the water in the neighbourhood of the explosion centre. Second, a pressure gradient

$$\rho \frac{\partial}{\partial x}\left(\frac{\partial \phi_3}{\partial t}\right)$$

is set up in the water in the neighbourhood of the explosion centre and this gives the bubble a drift velocity towards the disc

$$\frac{2}{a^3}\int_o^t \frac{\partial}{\partial x}\left(\frac{\partial \phi_3}{\partial t}\right) a^3\, dt$$

Adding these two drift velocities, separating out the geometrical factor, and inserting the value of ϕ_3 from (12) gives for the drift velocity U^1 of the bubble towards the disc due to the disc's motion.

$$U^1 = \left[1 - \frac{2}{\pi}\tan^{-1} r_o - \frac{2}{\pi}\frac{r_o}{1+r_o^2}\right]\left[v + \frac{2}{a^3}\int_o^t a^3 \frac{dv}{dt}\, dt\right] \qquad (13)$$

where $r_o = d/c$ =

since $\frac{\partial \phi_3}{\partial x} = \frac{1}{cs}\frac{\partial \phi_3}{\partial r}$ along the line s = 1, i.e. along the axis of symmetry.

For convenience of use the geometrical factor in the first bracket in (13) has been plotted in Figure 3. It will be seen that the influence of the motion of the disc falls off more rapidly with increasing distance than the attraction due to the disc's rigidity.

If the acceleration dv/dt is a constant independent of time it may be removed from the integral in (13). This integral is now the same as that occurring in the equations of motion of the bubble under the influence of gravity and in the absence of surfaces; in fact the velocity and displacement of the bubble due to the acceleration of the disc are a constant fraction k of the velocity and displacement of the bubble under gravity, where

k = ...

$$k = \frac{\alpha}{g}\frac{dv}{dt}$$

α is the factor in the first bracket in (13) which has been plotted in Figure 3.

Application to Box Model Experiments.

In Box Model and similar experiments where the target is slung in such a way that it is free to move as a whole under the influence of the explosion pressures acting on it, the effect of such movement on the displacement of the bubble may be estimated by means of equation (13). The following approximate numerical example suggests that this effect may be of real importance.

The area of the target plate and "skirt" of the R.R.L. box model is 5 square feet, i.e. for the purposes of using equation (13) the equivalent disc would have a radius of 1.25 feet. Consider the case of a 1 oz. charge, 3 feet deep, fired at a distance of 1.5 feet from the target plate. It will be supposed that the effect of the explosion pressures on the box model as a whole is to give it an initial velocity away from the explosion centre which is rapidly reduced to zero by the drag forces in the water.

It is not practicable with present knowledge to calculate the initial velocity and the deceleration, but in order to estimate the importance of the effect arbitrary values will be assumed. Let it be assumed that the box model is brought to rest by the drag forces with a uniform deceleration of 4g, and that it comes to rest in 50 milliseconds. This corresponds to an initial velocity of 6.4 feet/second and a total displacement of the box of 1.9 inches. These two latter figures do not seem unreasonable for a box model slung at the same horizontal level as the charge.

The displacement of the bubble due to the motion of the box model alone may be calculated from (13). The overall displacement is away from the box and is found to be approximately one half the rise of the bubble under the influence of gravity at the end of the first oscillation, i.e. it is displaced about 5 inches.

Strictly speaking equation (13) only holds for cases where the maximum bubble radius is small compared to the distance from the disc, and this condition is considerably exceeded in the numerical example above. The example does, however, suggest the desirability, either of measuring the overall movement of the box model so that this effect may be estimated, or of fixing the box model so rigidly that the effect becomes negligible.

Conclusions.

(1) The attraction of a fixed rigid disc for an explosion bubble has been calculated and is found to decrease rapidly with distance. If the explosion centre is one radius distance from the disc the attraction is one half that of an infinite rigid wall at the same distance. At a distance of one disc diameter the attraction is only one seventh of that due to an infinite wall at the same distance.

(2) The attraction of a rigid disc moving towards or away from the explosion centre has been calculated. The effects due to the motion of the disc fall off with increasing distance more rapidly than the attraction from a stationary rigid disc. Both the velocity and the acceleration of the disc give terms in the equation for the velocity of the explosion bubble towards the disc.

(3) It is pointed out that in experiments with box models or similar targets with flat plates surrounded by rigid flanges the foregoing analysis is relevant. In particular the motion of the box model as a whole due to the explosion may have an appreciable influence on the displacement of the explosion bubble.

Appendix .....

APPENDIX.

The Attraction of a Rigid Disc of which Part is Moving.

The attraction of a rigid disc of which the centre portion moves with a given velocity while the outer annulus remains fixed is of some practical interest as being rather like the case of a fixed rigid box model with a rigid "skirt" in which the target plates moves as a result of the pressure in the water. This case will now be solved formally, though it has not been found possible to reduce the solution to a simple finite form suitable for computation. The case where the rigid "skirt" extends to infinity has been treated by Temperley.

Let the velocity of any point of the disc be v. Only the case of radial symmetry is considered and over the surface of the disc r = o, the other spheroidal co-ordinate s is a function only of the radial distance ρ of the point from the axis. The relation is

$$\rho = c\,[1 - s^2]^{\frac{1}{2}}$$

Hence if v is a given function of ρ it may be written as a function of s and, with the usual restrictions on the form of the function, may be expanded in a series as follows.

$$sv = sf(s) = \sum_{n=o}^{\infty} a_n P_n(s) \qquad (14)$$

$$\text{where } a_n = \frac{2n+1}{2} \int_{-1}^{1} t\, f(t)\, P_n(t)\, dt \qquad (15)$$

The potential ϕ_4 fits the boundary condition that the normal velocity over the surface r = o is everywhere equal to v is

$$\phi_4 = -ic \sum_{n=o}^{\infty} \frac{a_n Q_n(ir)\, P_n(s)}{Q_n^1(i,o)} \qquad (16)$$

This potential is to be added to $\phi = \phi_1 + \phi_2$ to give the complete potential for the disc and the unit point source. The "attraction coefficient" in equation (13), i.e. the term in the first bracket, is replaced in this case by

$$\left(\frac{\partial \phi}{\partial x}\right)_{\text{at } X} = \frac{1}{c}\left(\frac{\partial \phi}{\partial r}\right)_{\text{at } r = d/c = r_o,\quad s = 1}$$

$$= \sum_{n=o}^{\infty} \frac{a_n Q_n^1(ir_o)}{Q_n^1(io)} \qquad (17)$$

The special case of a piston of radius R moving with velocity v in a fixed finite circular baffle of radius c is given by

$$f(s) = v \qquad \lambda < |s| < 1$$

$$= o \qquad o < |s| < \lambda$$

$$\text{where } \lambda = \left(1 - \frac{R^2}{c^2}\right)^{\frac{1}{2}}$$

In this case the coefficients a_n to be inserted in equation (17) are

$$\left.\begin{aligned} a_n &= o \qquad n \text{ even} \\ a_1 &= (1 - \lambda^2)v \\ a_n &= -v\left\{\frac{n+1}{2n+3} P_{n+2}(\lambda) + \frac{2n+1}{(2n-1)(2n+3)} P_n(\lambda) - \frac{n}{(2n-1)} P_{n-2}(\lambda)\right\} \end{aligned}\right\} \qquad (18)$$

for n = 3, 5, 7, ——— etc.

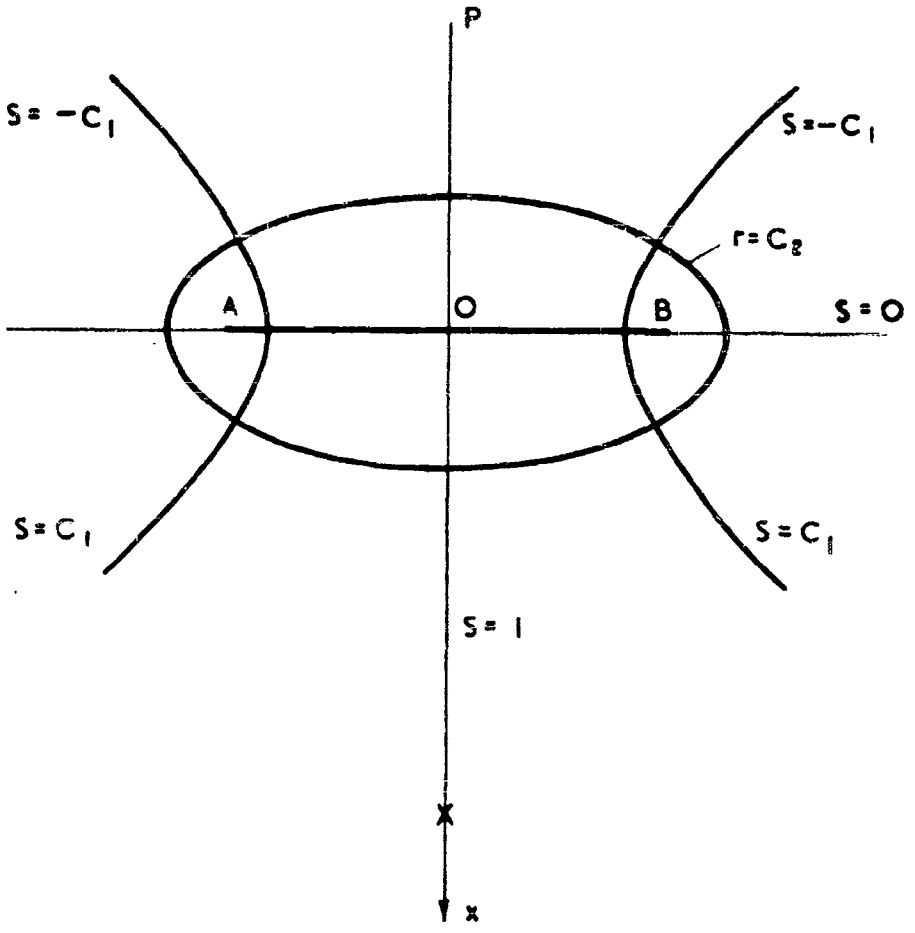

Fig.1. SPHEROIDAL CO-ORDINATES

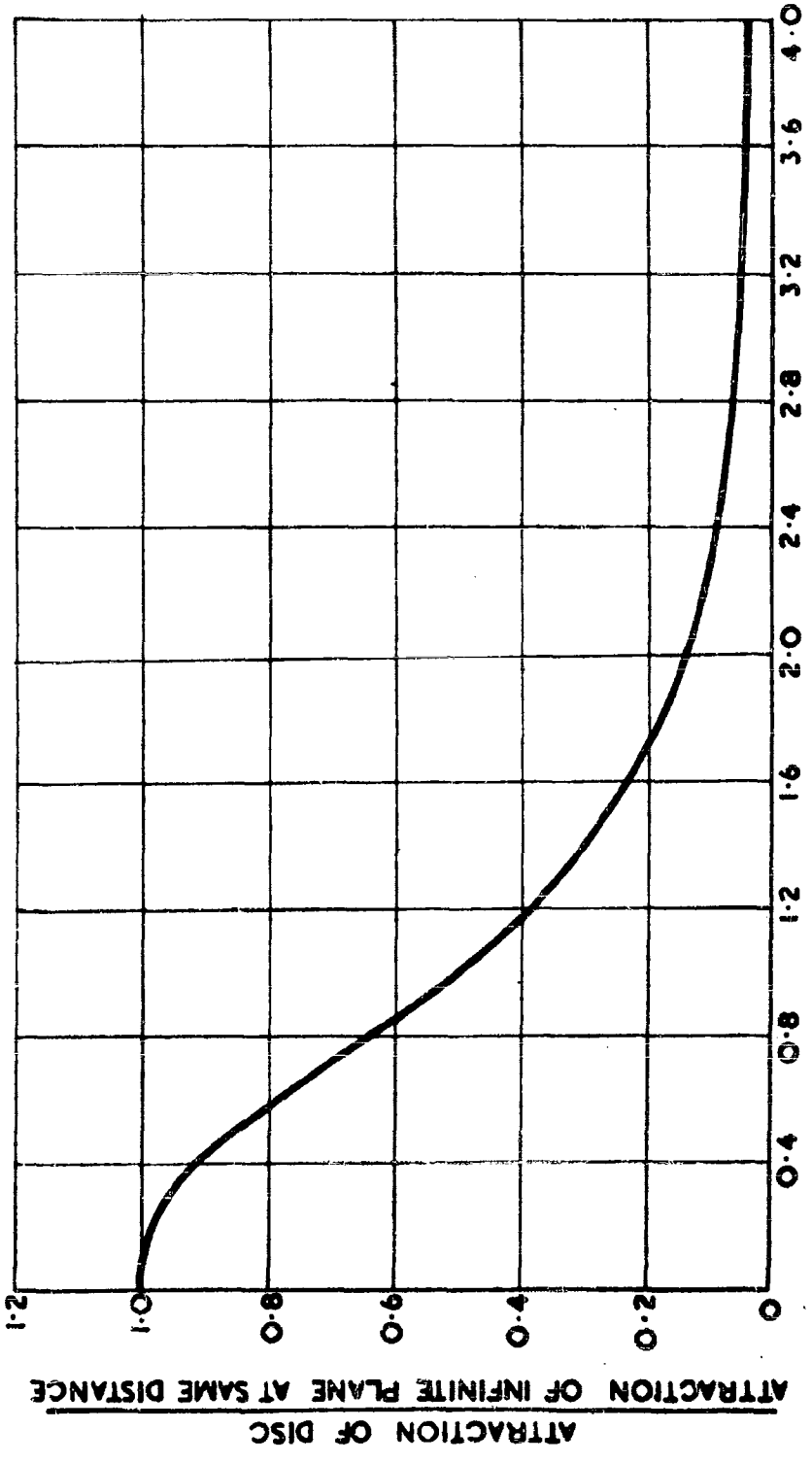

Fig. 2. THE RATIO OF THE ATTRACTION COEFFICIENT OF A FIXED RIGID DISC TO THAT OF AN INFINITE RIGID PLANE AT THE SAME DISTANCE

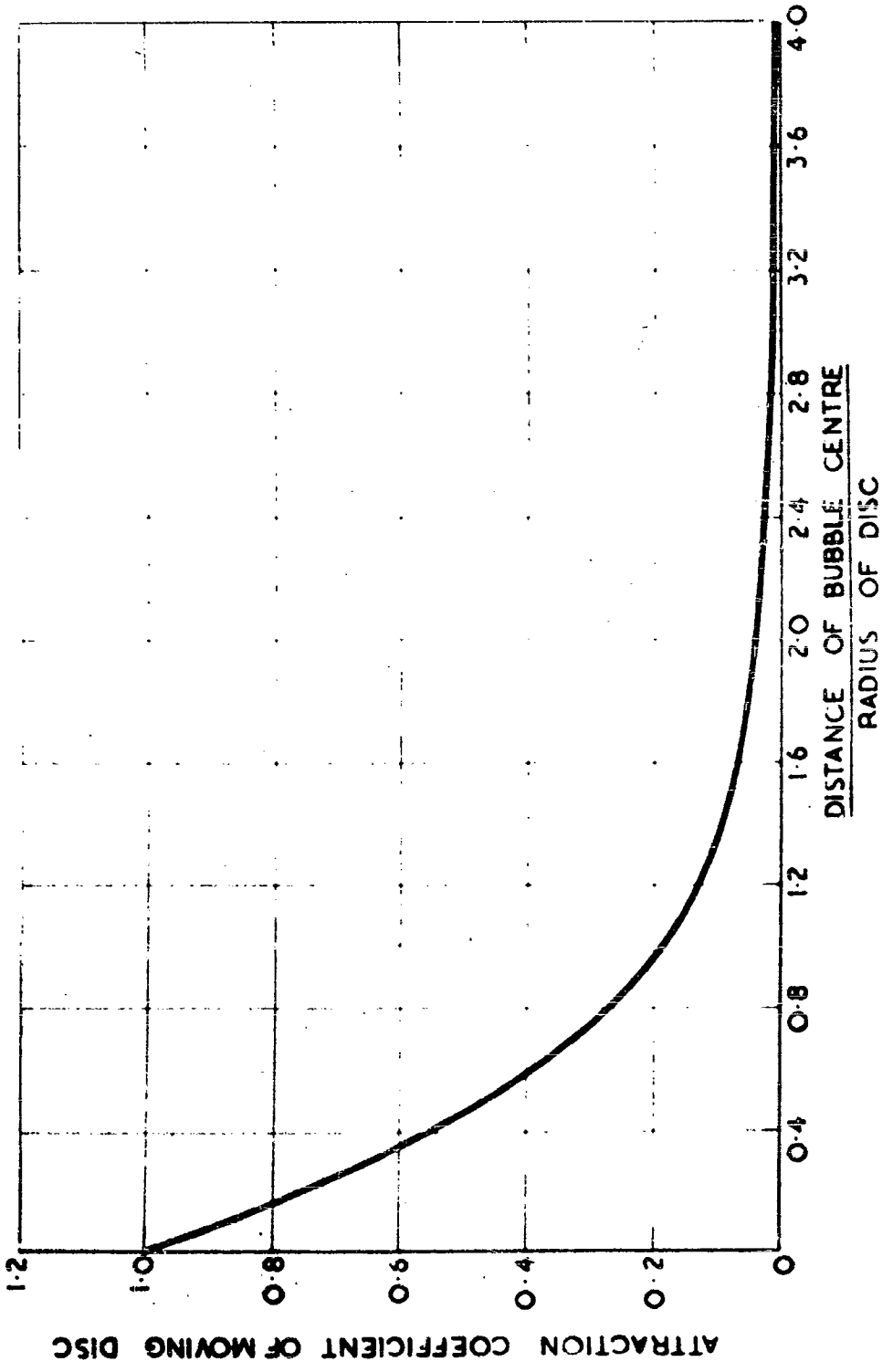

Fig. 3. THE ATTRACTION COEFFICIENT OF A RIGID DISC MOVING ALONG ITS AXIS

THE EFFECT OF AN ADJACENT DEFORMING TARGET UPON THE BUBBLE DUE TO A SUBMARINE EXPLOSION

Ll. G. Chambers
Admiralty Undex Works, Rosyth, Scotland

British Contribution

November 1946

THE EFFECT OF AN ADJACENT DEFORMING TARGET UPON THE BUBBLE DUE TO A SUBMARINE EXPLOSION

Lt. G. Chambers

November 1946

* * * * * * * *

Summary.

Reference is made to previous work on the subject. An alternative theory is put forward to account for discrepancies which have arisen in Box Model work and calculations are described based on certain Box Model shots and discussed. It is concluded that the effect of the rigidity of the target on the bubble is small and may, in general, be neglected.

Notation and Symbols used.

The suffix 0 indicates values at t = 0. The quantities are non-dimensional, being defined in terms of the units introduced by G. I. Taylor in the report "Vertical motion of a spherical bubble and the pressure surrounding it"

a = radius of bubble, assumed to remain spherical.
b = equivalent radius of plate.
c = an explosive parameter.
d = depth of centre of bubble below target.
h = central deflection of target.
k = a constant of integration, chosen to satisfy the initial conditions.
t = time.
u = velocity of bubble $= -\frac{dz}{dt}$
v = upward velocity of centre of plate.
z = depth of bubble below virtual surface.

Introduction.

It is well known that the mechanism of damage due to an underwater explosion is extremely complex, even in the comparatively simple case of a single plate rigidly clamped at its edges, and that the phenomena involved are many - for example, the elastic properties of the steel, the occurrence of cavitation either at or away from the steel-water interface, and lastly the effect of the motion of the gas bubble. It is with this last phenomenon that this report is mainly concerned.

It has been shown by Conyers Herring and by others, that the bubble is liable to migrate, the nature of this migration depending on the nature of adjacent surfaces. On the whole, the bubble is attracted by a rigid surface and repelled by a free surface, although there is initially a repulsion away from a rigid surface. Thus, for a given charge and distance, there may be a particular strength of plate such that the bubble migration is negligible during the very important first oscillation of the bubble.

If the plate was weaker than this, the net effect would be a repulsion, so that the first minimum of the bubble would occur farther from the plate than the original explosion. If the plate is stronger, the net effect would be an attraction, which increases rapidly as the distance from the plate decreases, so that the first minimum of the bubble would occur very near to, or even in contact with, the plate, and might thus give a large contribution to damage, while the contribution in the repulsive case would be negligible.

It was found that in certain Box Model shots inconsistencies arose and this was thought to be due to some intrinsic instability in the dependence of the bubble movement on the movement of the plate. Thus in considering the attraction of the bubble towards the target, it is desirable to know whether the motion of the target plate in the baffle effects the bubble or whether we can assume with sufficient accuracy the target plate to be rigid.

A.....

A difficulty is encountered as water is compressible. This question was attacked by first considering the plate to start at rest and secondly by considering the plate to be given an impulsive velocity equivalent to the experimentally measured impulse per unit area due to 1½ lb. of T.N.T. In this case the motion of the Box Model plate was subject to the following assumptions:-

(a) The "skirt" of the Box Model was assumed to be an infinite wall.

(b) The tension of the plate, during the process of stretching, was assumed to be constant at the yield point, the plate being represented as a piston backed by a spring closing hole in an infinite wall. This representation was deemed to hold after the stretching when elastic recovery makes the plate move out again.

It was concluded by Temperley that a deformable structure may act either as a free surface or as a rigid surface, and also that the nature of the effect may be reversed during the interval of the experiment. The valid objection has been made against this treatment that effectively the whole infinite baffle is moving. An alternative derivation of the equations of motion, due to Temperley is presented here, together with a discussion of the results of integrating the equations in two cases.

Theory.

The target is treated as a fixed rigid plate and the motion of the target plate is allowed for by introducing at its centre a simple source whose strength is chosen so that the flow through a hemisphere with centre at the source is equal to the volume actually swept out by the target.

The conditions of continuity of pressure and velocity at the gas-water interface give, on equating terms independent of $\cos\theta$, and terms in $\cos\theta$, respectively.

$$\frac{2c}{16\pi}\, a^{-\frac{15}{4}} - z = a\ddot{a} + \frac{3}{2}\dot{a}^2 - \frac{1}{4}U^2 + \frac{a^2\dot{a} + 2a\dot{a}^2}{2d}$$

$$(1) \qquad + \frac{1}{2}\frac{a^2}{d^2}\dot{a} + \frac{a^3}{8d^2}\dot{U} - \frac{b^2}{2d}\frac{dV}{dt} + U\frac{Vb^2}{4d^2}$$

and $$2a = 3\dot{a}U + a\dot{U} + \frac{9}{4}\frac{a^2\dot{a}^2}{d^2} + \frac{3}{4}\frac{a^3\ddot{a}}{d^2}$$

$$(2) \qquad - \frac{3}{2}\frac{b^2}{d^2}(a\dot{V} + \dot{a}V)$$

where Taylor's units are used throughout.

To aid in the computation we form a pseudo-energy equation. This is derived by multiplying (1) by $4\pi a^2\dot{a}$, and (2) by $\frac{4}{3}\pi a^2 z$, substracting and integrating the resulting equation with respect to time. We obtain

$$2\pi a^3\dot{a}^2\left(1 + \frac{a}{2d}\right) + \frac{\pi a^3\dot{z}^2}{3} + \frac{4\pi a^3 z}{3} - \frac{\pi a^5}{2d^2}\dot{a}\dot{z}$$

$$(\alpha) \qquad + 4\pi b^2\int_0^t \dot{V}\left(\frac{a^3 z}{8d^2} - \frac{a^2\dot{a}}{4d}\right)dt = k - ca^{-3}$$

We may note in passing that (α) presents several interesting features. It is, in fact, similar to equation (2) of the report "Vertical motion of a spherical bubble and the pressure surrounding it". The radial kinetic energy is increased by a factor $(1 + \frac{a}{2d})$ due to the rigid surface as pointed out by Conyers Herring. The cross product $\dot{a}\dot{z}$ does not occur in equation (2) of above mentioned report which is a true energy integral. k is not equal to unity, being analogous to the total energy of the system, which includes an unknown amount of energy in the moving target plate system.

Putting .....

Putting (2) in the form

$$(\beta) \qquad 2a^3 = -\frac{d}{dt}(a^3 z) + \frac{3a^2}{4d^2}\frac{d}{dt}(a^3\dot{a}) - \frac{3a^2b^2}{2d^2}\frac{d}{dt}(aV)$$

we note that putting the left hand side of (β) equal to zero gives the case of zero gravity.

Also we have

$$\frac{d}{dt}(d - z) = V.$$

This assumes that d is measured from the centre of the bubble to the centre of gravity of target plate. It might be more consistent with the other assumptions to measure d from the initial position of the plate, in which case $\frac{d}{dt}(d - z) = 0$. The values of d obtained from the two assumptions only differ by $\int_0^t V\,dt$ which is never more than a few inches, and since the other two equations only involve d itself, and not its derivatives, the difference between the two assumptions is small.

Experimental Data.

Fortunately there became available records of the Box Model shots detailed below. The diagrammatic set-up is as shown in Figure 3. In the actual calculations the set-up was simplified to the case of Figure 4. It was assumed that the mutual effects of the target and bubble would be the same whether the target was above the charge or to its side. The conditions of the experiments were:-

Test 48:	Depth of charge	=	5 feet.
	Stand-off	=	2 feet.
	Charge	=	1 oz. of T.N.T.
Test 50:	Depth of charge	=	5 feet.
	Stand-off	=	2½ feet.
	Charge	=	1 oz. of T.N.T.

In both cases the equivalent radius of the plate was 8.25 inches. For this charge the Taylor unit of length is 5 feet, and the Taylor unit of time is 0.394 seconds.

Description of Tables.

The integration of the equations derived in paragraph 3 were carried out under the following conditions:-

$$a_o = 0.016$$
$$z_o = 7.6$$
$$\left(\frac{da}{dt}\right)_o = \left(\frac{dz}{dt}\right)_o = 0$$
$$c = .063$$
$$b = .133$$
$$k = 1.4006$$

There were four cases.

Table 1:	d_o = .40	α)	v = 0
		β)	v from Test 48
Table 2:	d_o = .50	α)	v = 0
		β)	v from Test 50

The values of v used in cases 1β and 2β were derived from smoothed graphs of the deflection time curves.

For .....

For the purpose of computation, a variable x was introduced, defined by:-

$$x = 10 \int_0^t \frac{dt}{a^{3/2}}$$

In fact, in the Tables the quantities involved are defined in terms of equal intervals of x, which obviously increases continuously with values of t, although the corresponding values of t are given. The computations were carried out to the point where the equations ceased to have any physical meaning owing to the radius of the bubble becoming greater than the distance from the model. (In the case of test 50, this happened just before the first minimum of the bubble and the equations would have broken down in any case). As regards the accuracy of the solutions, the following should be noted:-

(a) A warning must be given about the interpretation of the computed figures. In some cases more figures than are justified have been retained in order to keep a fixed number of decimals. The computer is fully aware of this and precautions have been taken accordingly.

(b) It is realised that 4 decimals in a and z are meaningless but it is essential to keep this number of figures in order to comprehend the full behaviour of the solution and to understand the structure of the differential equations. No great pains have been taken to maintain this accuracy, though owing to the inherent stability of the equation for a, the last figure should be reasonably good, even to the end.

The tables give - for the rigid case a, t, z, and - for the case where there assumed to be a source a, t, z, h, v.

Discussion of Results.

It will be seen by reference to Tables 1 and 2 and Figures 1 and 2 that the actual effect of the plate motion on the bubble appears to be fairly small. In fact from Figure 1 it appears that the effect of the mobility of the plate has not appreciably affected the depth of the centre of the bubble. This may be due to the fact that over the greater part of the period under consideration, i.e. from t = .02 to t = .17, the motion of the plate is comparatively small, the bubble being fairly large over this time. As is well known, the bubble acquires momentum, chiefly when large, and at this time the plate is practically stationary. The motion of the plate has little effect on the radius. The maxima occur as far as can be seen practically at the same time and the maximum radius is diminished by about 2% by the plate being assumed to be non-rigid.

In both cases the bubble begins to flatten itself against the target before the minimum is approached although at this time the approximations cease to be valid in any case.

Considering Table 2 and its graphical representation Figure 2, it may be seen that, although the plate has sprung back, and has even come back beyond its original position, the effect on the bubble is somewhat the same as in the case where the plate remained dished inward.

The differences between the rigid case and the moving plate are very slight, as regards the movement of the bubble, and less than the probably accuracy of the theory. This might be expected as the subsequent movement towards the plate is governed mainly by the momentum constant. This agrees with photographic observations of the bubble moving towards the box model when a rigid plate theory gave excellent results for both $\frac{1}{10}$ inch and $\frac{1}{16}$ inch plate.

It should be noted that in the actual experiments the Box Model and charge are at the same depth, where gravity is approximately cancelled out by free surface and bottom.

Conclusions .....

Conclusions and suggested further work.

It is concluded on the whole that the bubble is not very sensitive to the motion of the target plate, there being a slight tendency for the bubble to follow the motion of the target plate, and for the bubble not to expand quite as much as it would if the target were rigid. It is intended to determine by photography or otherwise the behaviour of the bubble in two experiments, the conditions of which are identical except that the two target plates are of widely varying strength, the motion of the plates being recorded and correlated with the behaviour of the bubble.

Acknowledgements.

The theory on which this report is based is due to Mr. H.N.V. Temperley.

TABLE 1.

(Test 48. $d_o = 0.40$)

x	RIGID PLATE			NON RIGID PLATE				
	a	t_{10}^{-5}	z	a	t_{10}^{-5}	z	h	$\frac{dh}{dt} = V_{10}^{-3}$
0	.0160	0	7.6000	.0160	0	7.6000	.0000	1908
1	.0353	36	7.6000	.0352	36	7.6000	.0010	1243
2	.0698	156	7.6003	.0697	156	7.6002	.0038	927
3	.1073	421	7.6009	.1074	420	7.6006	.0110	1966
4	.1450	870	7.6021	.1449	870	7.6018	.0181	-237
5	.1816	1532	7.6039	.1805	1528	7.6041	.0145	-181
6	.2162	2421	7.6062	.2143	2407	7.6066	.0138	17
7	.2479	3541	7.6087	.2454	3511	7.6092	.0150	0
8	.2760	4884	7.6110	.2729	4834	7.6115	.0137	-28
9	.2997	6432	7.6123	.2961	6355	7.6129	.0135	-17
10	.3184	8155	7.6120	.3143	8045	7.6127	.0128	-11
11	.3314	10011	7.6091	.3270	9865	7.6101	.0127	6
12	.3384	11954	7.6030	.3338	11769	7.6045	.0131	6
13	.3391	13931	7.5929	.3345	13705	7.5953	.0131	0
14	.3335	15886	7.5783	.3290	15620	7.5820	.0131	0
15	.3219	17766	7.5591	.3177	17463	7.5644	.0131	40
16	.3050	19524	7.5352	.3011	19188	7.5424	.0159	79
17	.2823	21122	7.5065	.2799	20757	7.5160	.0184	11
18	.2577	22532	7.4727	.2548	22142	7.4851	.0167	-6
19	.2290	23734	7.4333	.2266	23325	7.4493	.0180	11
20				.1963	24299	7.4078	.0173	-51
21				.1650	25068	7.3593	.0161	-28

TABLE 2.

(Test 50, d = 0.50)

x	RIGID PLATE			NON RIGID PLATE				
	a	t_{10}^{-5}	z	a	t_{10}^{-5}	z	h	$\frac{dh}{dt} = V_{10}^{-3}$
0	.0160	0	7.6000	.0160	0	7.6000	.0000	1638
1	.0353	36	7.6000	.0351	36	7.6000	.0008	1090
2	.0698	156	7.6002	.0698	156	7.6001	.0030	763
3	.1077	422	7.6006	.1078	422	7.6004	.0102	1915
4	.1460	875	7.6014	.1459	876	7.6013	.0168	-299
5	.1832	1545	7.6026	.1823	1542	7.6030	.0125	-226
6	.2183	2447	7.6041	.2169	2436	7.6048	.0110	-90
7	.2505	3584	7.6057	.2485	3561	7.6065	.0100	56
8	.2789	4949	7.6070	.2764	4909	7.6078	.0118	-17
9	.3026	6520	7.6075	.2997	6459	7.6084	.0096	-107
10	.3210	8265	7.6066	.3177	8178	7.6078	.0044	-169
11	.3333	10141	7.6037	.3300	10025	7.6052	-.0011	-107
12	.3395	12096	7.5984	.3360	11952	7.5999	-.0034	0
13	.3395	14078	7.5902	.3354	13901	7.5915	-.0020	0
14	.3333	16033	7.5790	.3284	15817	7.5799	-.0025	51
15	.3210	17909	7.5644	.3152	17646	7.5651	-.0019	-11
16	.3032	19656	7.5463	.2967	19342	7.5470	-.0002	45
17	.2800	21234	7.5247	.2734	20867	7.5252	.0020	339
18	.2530	22613	7.4992	.2461	22193	7.4987	.0223	339
19	.2228	23776	7.4691	.2159	23305	7.4684	.0192	-34
20	.1906	24717	7.4330	.1840	24201	7.4319	.0196	96
21	.1579	25445	7.3882	.1518	24889	7.3861	.0211	45
21.5	.1420	25735	7.3612	.1364	25162	7.3584	.0211	-6
22	.1269	25981	7.3301	.1220	25394	7.3265	.0210	-23
22.5	.1133	26189	7.2944	.1093	25590	7.2897	.0209	-45
23	.1019	26365	7.2534	.0991	25758	7.2477	.0207	-62
23.5	.0931	26517	7.2075	.0918	25905	7.2014	.0205	-56

TABLE 2.

(Test 50, d = 0.50)

x	RIGID PLATE			NON RIGID PLATE				
	a	t_{10}^{-5}	z	a	t_{10}^{-5}	z	h	$\frac{dh}{dt} = V_{10}^{-3}$
0	.0160	0	7.6000	.0160	0	7.6000	.0000	1638
1	.0353	36	7.6000	.0351	36	7.6000	.0008	1090
2	.0698	156	7.6002	.0698	156	7.6001	.0030	763
3	.1077	422	7.6006	.1078	422	7.6004	.0102	1915
4	.1460	875	7.6014	.1459	876	7.6013	.0168	-299
5	.1832	1545	7.6026	.1823	1542	7.6030	.0125	-226
6	.2183	2447	7.6041	.2169	2436	7.6048	.0110	-90
7	.2505	3584	7.6057	.2485	3561	7.6065	.0100	56
8	.2789	4949	7.6070	.2764	4909	7.6078	.0118	-17
9	.3026	6520	7.6075	.2997	6459	7.6084	.0096	-107
10	.3210	8265	7.6066	.3177	8178	7.6078	.0044	-169
11	.3333	10141	7.6037	.3300	10025	7.6052	-.0011	-107
12	.3395	12096	7.5984	.3360	11952	7.5999	-.0034	0
13	.3395	14078	7.5902	.3354	13901	7.5915	-.0020	0
14	.3333	16033	7.5790	.3284	15817	7.5799	-.0025	51
15	.3210	17909	7.5644	.3152	17646	7.5651	-.0019	-11
16	.3032	19656	7.5463	.2967	19342	7.5470	-.0002	45
17	.2800	21234	7.5247	.2734	20867	7.5252	.0020	339
18	.2530	22613	7.4992	.2461	22193	7.4987	.0223	339
19	.2228	23776	7.4691	.2159	23305	7.4684	.0192	-34
20	.1906	24717	7.4330	.1840	24201	7.4319	.0196	96
21	.1579	25445	7.3882	.1518	24889	7.3861	.0211	45
21.5	.1420	25735	7.3612	.1364	25162	7.3584	.0211	-6
22	.1269	25981	7.3301	.1220	25394	7.3265	.0210	-23
22.5	.1133	26189	7.2944	.1093	25590	7.2897	.0209	-45
23	.1019	26365	7.2534	.0991	25758	7.2477	.0207	-62
23.5	.0931	26517	7.2075	.0918	25905	7.2014	.0205	-56

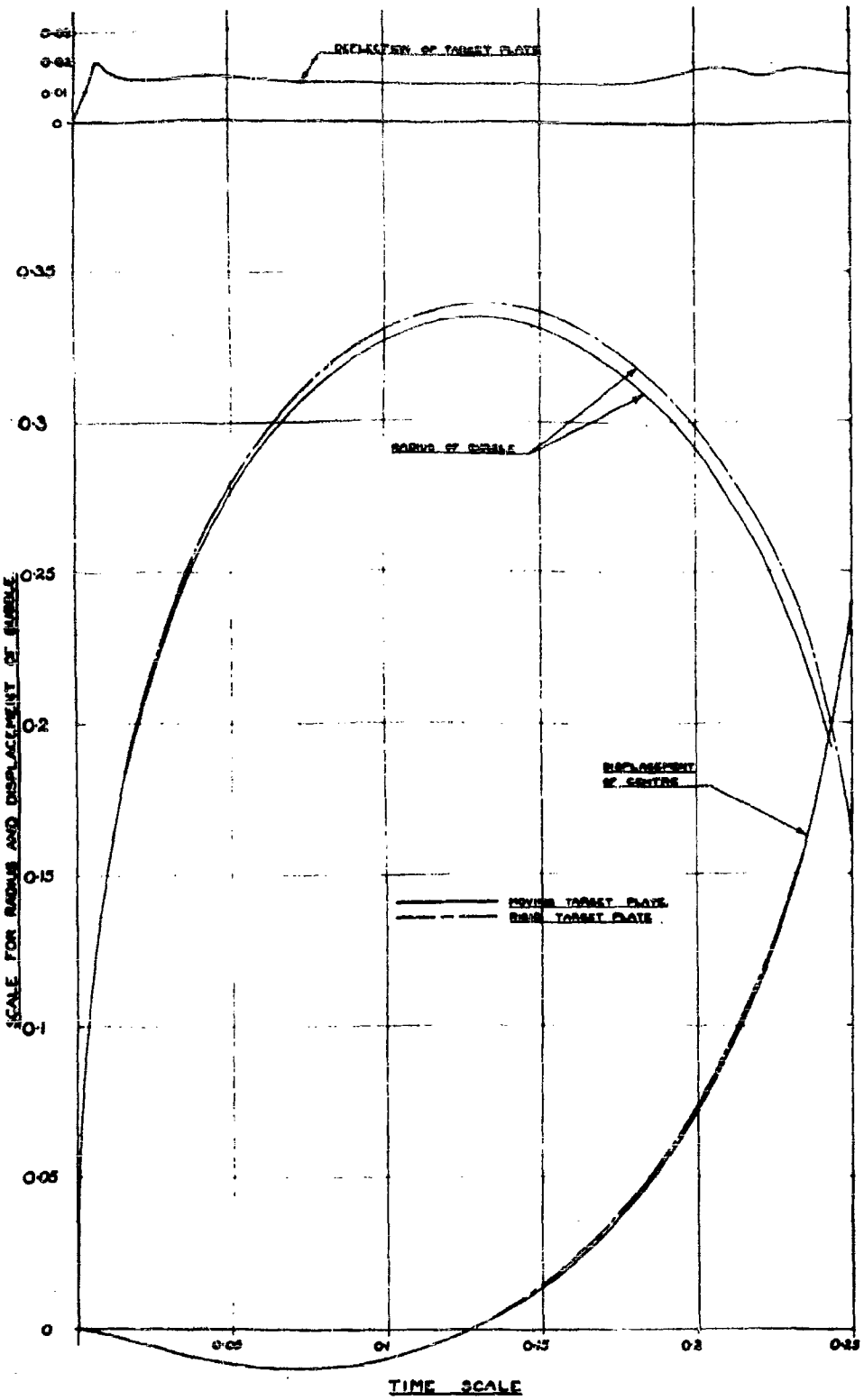

Fig. 1. Test 48. 1 oz. charge 2 ft. from Box Model.

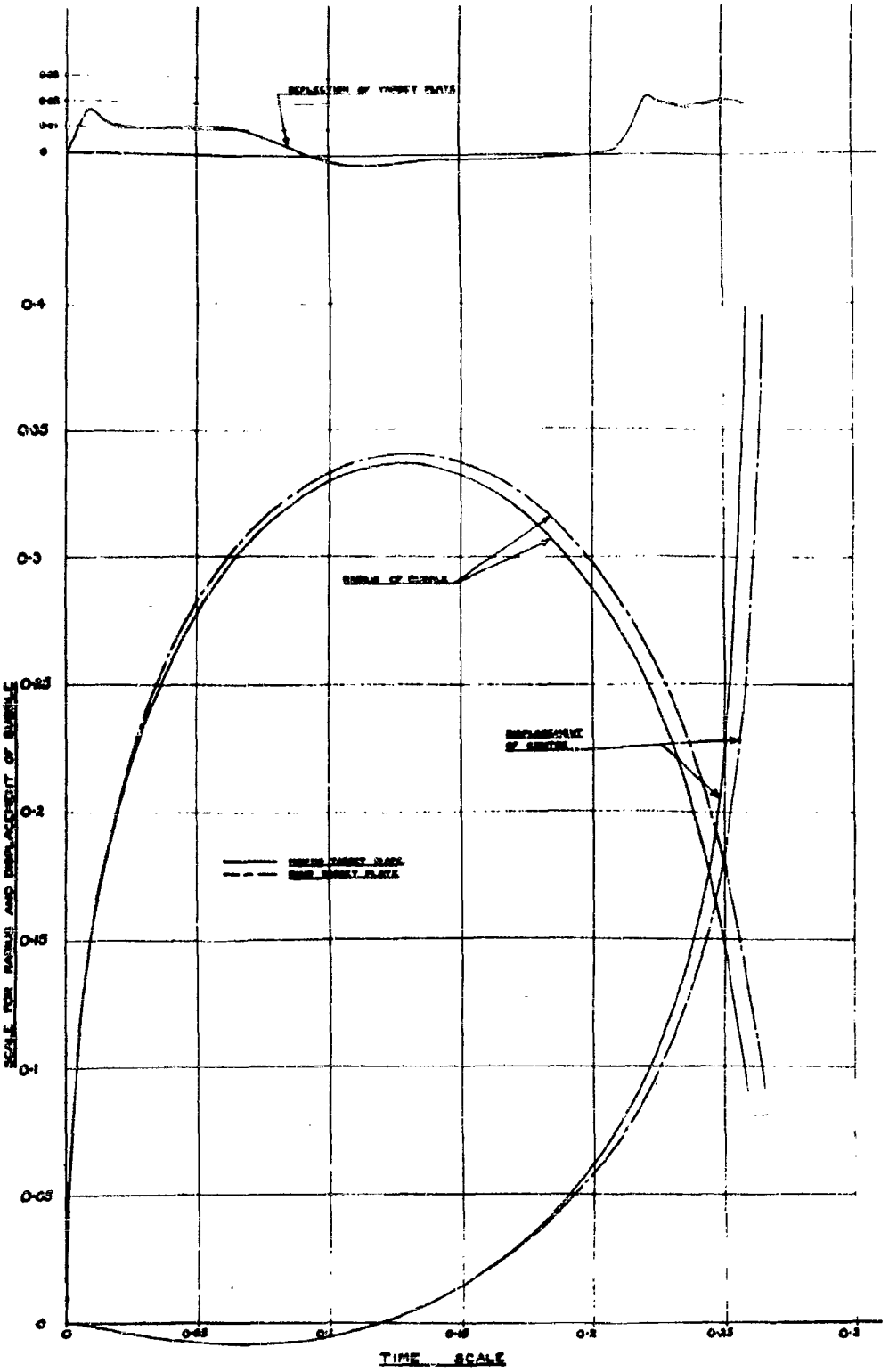

Fig. 2. Test 50. 1 on. chain 2'6" from Box Model.

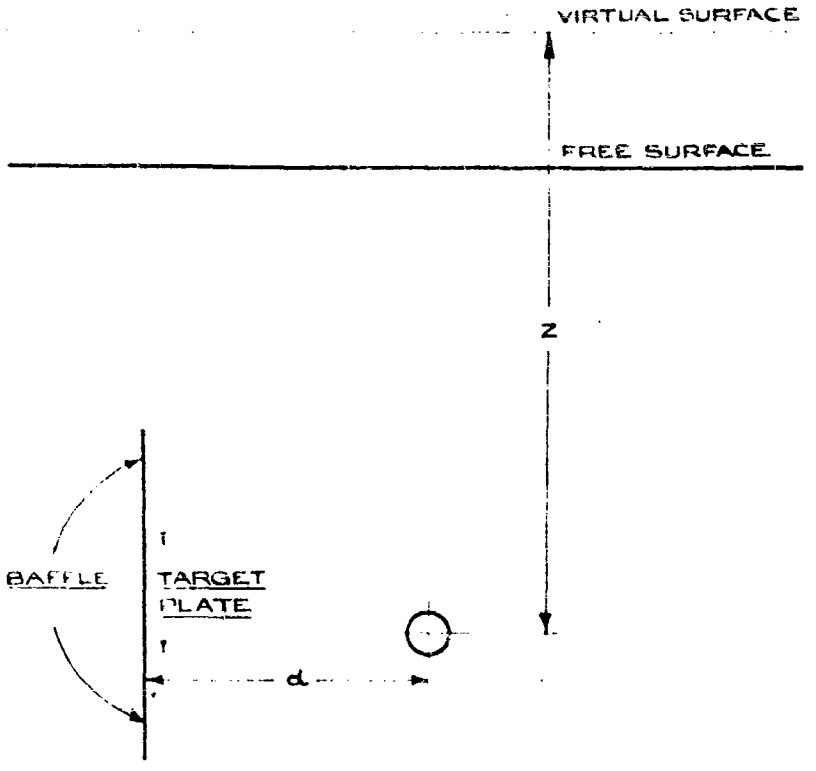

SET UP OF BOX MODEL FOR RRL SHOTS.

FIG. 3

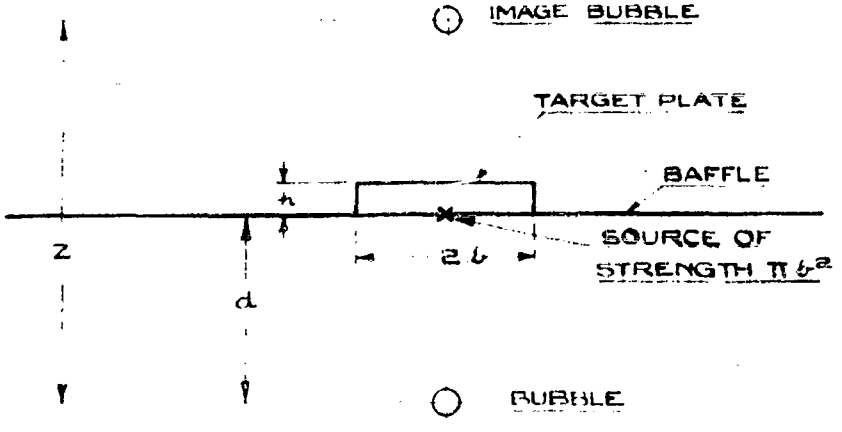

EXPERIMENTAL SET UP AS MODIFIED FOR CALCULATIONS

FIG. 4

THE PRESSURES PRODUCED BY EXPLOSIONS UNDERWATER OF SMALL CHARGES NEAR A RIGID BOTTOM

G. Charlesworth
Road Research Laboratory, London

British Contribution

December 1943

THE PRESSURES PRODUCED BY EXPLOSIONS UNDERWATER OF SMALL CHARGES NEAR A RIGID BOTTOM

G. Charlesworth

December 1943

* * * * * * * * *

Summary.

Pressure-time curves have been obtained, by means of piezo-electric gauges, at points 2, 3, 4 and 5 feet above 1 oz. charges of P.A.G. fired underwater at distances from 0 to 3 feet from a rigid bottom. The results have been compared with those observed previously with a gravel bottom.

The shock wave tail was not reduced so much for the charge near the rigid bottom as when it was fired near the gravel bottom. As before, it was found that lower intensity pulses of unknown origin occurred some 4 to 7 milliseconds after both the shock waves and bubble waves, their occurrence, but not their form, being independent of the presence of the bottom.

The forms of the bubble waves with a rigid bottom were similar to those obtained with a gravel bottom, but with the charge near the rigid bottom were more intense and of shorter duration. At a given distance from the charge the pressures and impulses in both the 1st and 2nd bubble waves, when plotted against the distance of the charge from the rigid bottom, had maxima for some value of this distance between 0 and 2 feet. With the gravel bottom this effect was only observed for the 1st bubble wave impulses. Whereas for the gravel bottom no second bubble-wave was detected when the charge was 1 foot 6 inches or less from the bottom the corresponding distance from the rigid bottom was 6 inches.

The 1st bubble period increased as the charge approached the rigid bottom; with the gravel bottom the period decreased.

Introduction.

The object of the tests was to termine the underwater pressures produced by exploding charges near to a rigid bottom and to compare the results with those previously obtained near a gravel bottom.

Experimental.

Site:- The tests were made in a concrete tank in a depth of 9 feet 6 inches of water. The bottom of the tank was flat and the "rigid bottom" used in the tests consisted of a steel plate 3 feet square and 1½ inches thick placed flat on the bottom of the tank.

Charges:- As before, 1 oz. charges of P.A.G. were used, detonated by No. 8 A.S.A. detonators. The charges were cylindrical in shape with height equal to diameter. They were placed with their axes vertical and detonated from the top.

Pressure measurement:- Pressures were measured by means of piezo-electric gauges recording photographically using cathode-ray oscillographs.

Arrangement of tests:- The gauges were suspended vertically above the charge at distances of 2, 3, 4 and 5 feet from it. Tests were made with the charge at distances from 0 to 3 feet from the bottom.

Results .....

Results.

The forms of the pressure-time curves recorded at a point 5 feet above the charge, for various distances of the charge from the bottom are shown in Figures 1 and 2; the shock-wave peaks have not been recorded and portions of the records between the pulses have been omitted. The records exhibit the same general features as those obtained in earlier work where charges were fired near a gravel bottom though there are certain differenves as mentioned below.

Shock waves:- The recorded parts of the shock waves were similar in form to those obtained previously except that with the charge very near to the bottom the reduction in the tail was not so pronounced. A few measurements were made of the magnitude of the peak shock wave pressures produced with the charge on the bottom. The results indicated that there was an increase in peak pressure above the 'open water' value. Further investigations are required to determine more precisely the action of the bottom in this case (e.g. to determine whether the charge plus bottom acts as a single charge of greater weight or as two separate charges).

Waves of unknown origin:- Pulses similar in form and magnitude to those observed in the earlier tests were recorded some 4 to 7 milliseconds after both the shock wave and bubble waves. This is further evidence against these waves being produced by reflections from a denser substrata since the two sets of tests were made at different sites.

Bubble waves:- In most cases two bubble waves were observed. In the previous tests, only one bubble wave was observed for charge distances of 1 foot 6 inches or less from the bottom, whereas here two pulses were recorded at 1 foot from the bottom. At distances of 1 foot 6 inches or less, there was a difference in wave form in the two cases, e.g. with the charge fired on the rigid bottom, the bubble wave was more intense and of shorter duration than when fired on the gravel bottom.

The maximum pressures and impulses in the 1st and 2nd bubble waves at points 2, 3, 4 and 5 feet above the charge are shown in Figures 3, 4, 5 and 6 for various distances of the charge from the bottom.

The pressures and impulses in the 1st bubble waves with the charge 3 feet from the bottom are about the same as observed before. The present results, however, show an increase in both pressure and impulse with the charge about 6 inches from the bottom. This effect was not previously observed for the pressures, but was observed to some extent for the impulses.

The variations of pressure and impulse in the 2nd bubble waves with distance of the charge from the rigid bottom were appreciably different from those with the gravel bottom. Thus Figure 5 shows that the pressure has a maximum value for the charge about 2 feet from the bottom and Figure 6 shows that the impulse has a maximum for the charge about 1 foot from the bottom whereas previously both pressure and impulse decreased with distance of the charge from the gravel bottom.

No measurements were made of the rise or fall of the bubble. It is proposed to make these measurements using the underwater camera, which will also give information on the shape of the bubble.

Bubble periods:- The periods of the 1st and 2nd bubble oscillations are shown in Figure 7 as functions of the distance of the charge from the bottom. Also shown in Figure 7 is the theoretical curve for the 1st oscillation of 1 oz. of T.N.T. neglecting the effects of the free and rigid surfaces. It is seen that the 1st period increases as the charge approaches the bottom, until the charge is 6 inches from the bottom where the period is a maximum. This increase is expected theoretically if the bottom behaves as a rigid surface. With the gravel bottom no such increase in period was observed. The bubble periods observed here are greater than those obtained in the gravel pit. This may be due to the proximity of the sides of the tank to the explosion

Conclusions.

The principle effects observed with the rigid and gravel bottoms are summerised below for charge distances of 3 feet or less from the bottom.

Rigid .....

	Rigid bottom	Gravel bottom
Shock wave	Some reduction in tail with charge near the bottom.	As for rigid bottom but effect more marked.
Wave of unknown origin	Occurs at 4 - 7 milliseconds after shock wave and bubble waves regardless of proximity to bottom.	As for rigid bottom.
1st bubble wave	Pressure a maximum for the charge about 6 inches from the bottom. Impulse a maximum for the charge about 6 inches from the bottom.	No maximum. Pressure decreases as charge is brought nearer to the bottom. Indications of maximum impulse for the charge about 6 inches from the bottom.
2nd bubble wave	Pressure a maximum for the charge about 2 feet from the bottom. Impulse a maximum for the charge about 1 foot from the bottom. No bubble wave for the charge 6 inches or less from the bottom.	No maximum for either pressure or impulse, both of which decrease as the charge is brought nearer to the bottom. No bubble wave for the charge 1 foot 6 inches or less from the bottom.
Period	1st bubble period increases with decreasing distance from the bottom until the charge is 6 inches from the bottom where the period is a maximum.	1st period decreases as distance from the bottom decreased.

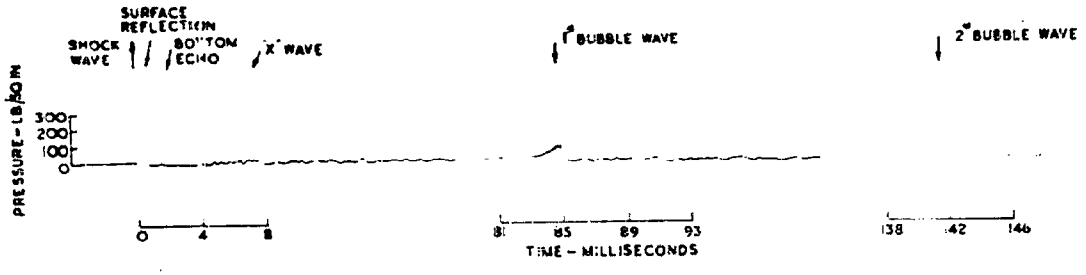

(a) Charge 3ft from the bottom

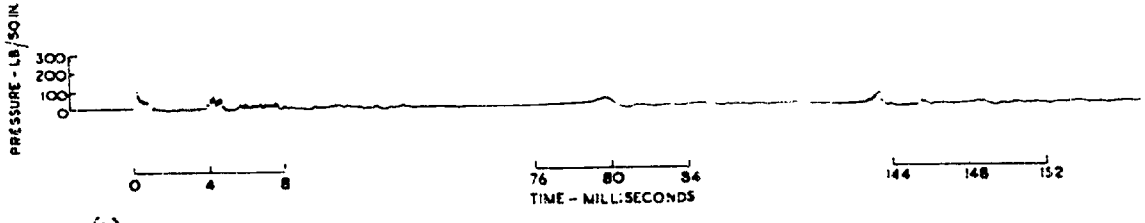

(b) Charge 2ft. from the bottom

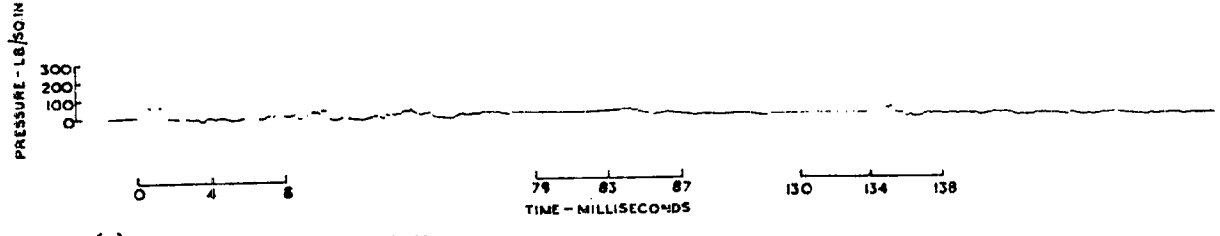

(c) Charge 1ft. 6in from the bottom

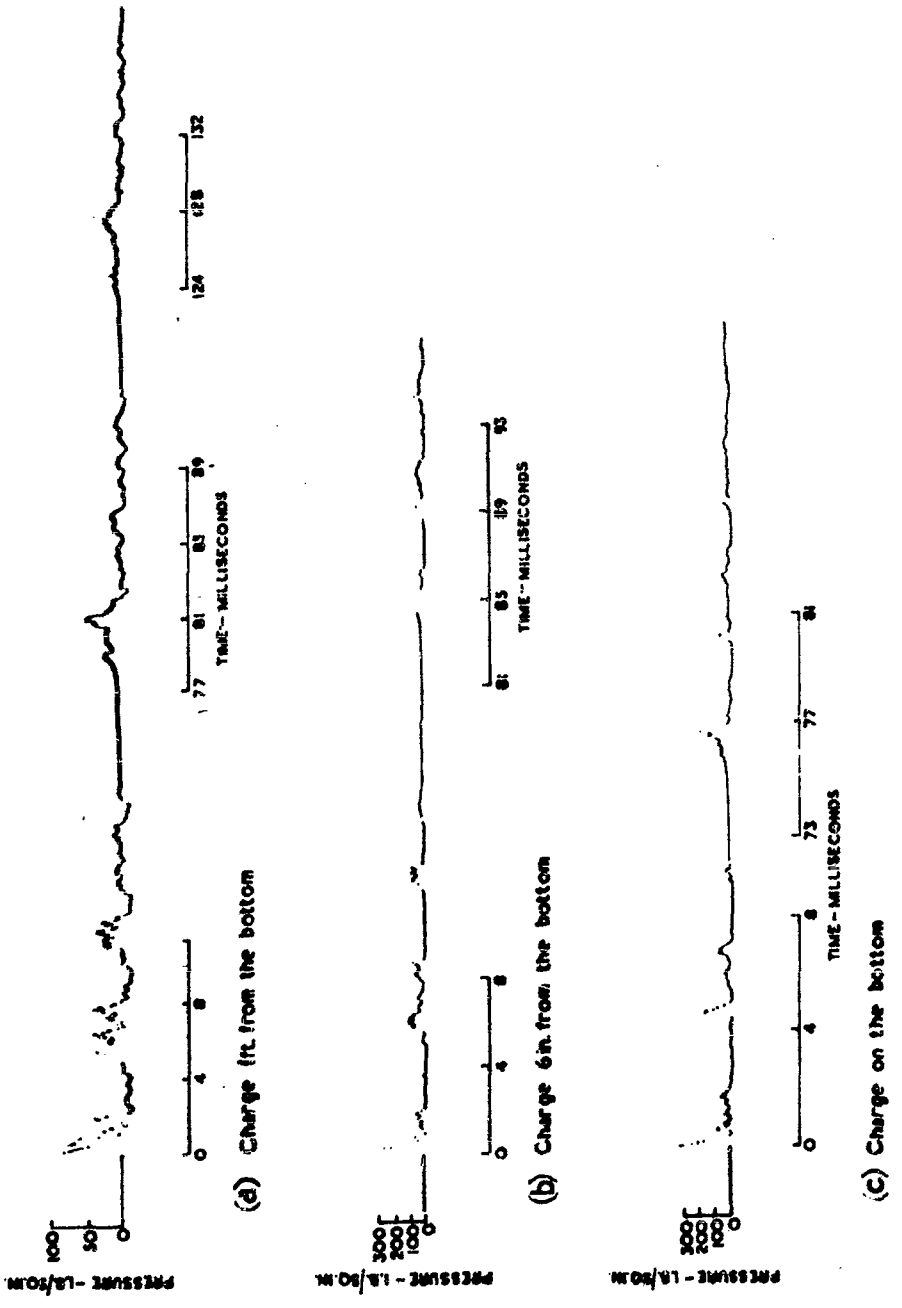
PRESSURE - LB/SQ.IN.
TIME - MILLISECONDS
(a) Charge fit from the bottom
(b) Charge 6 in. from the bottom
(c) Charge on the bottom

FIG. 2

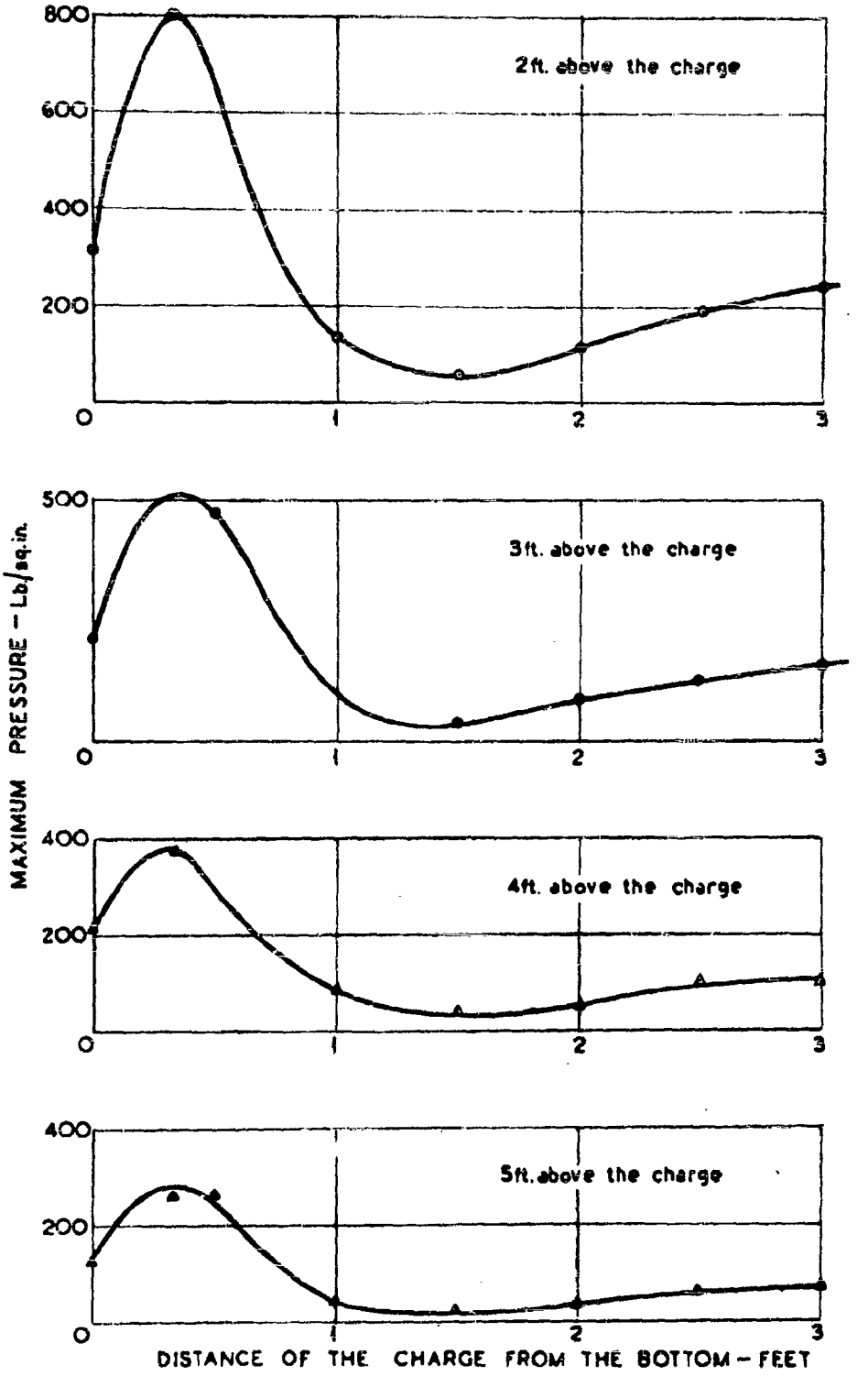

Fig.3. MAXIMUM PRESSURES IN THE 1st BUBBLE WAVES AT POINTS 2, 3, 4, AND 5 ft. ABOVE THE CHARGE FOR VARIOUS DISTANCES OF THE CHARGE FROM THE BOTTOM

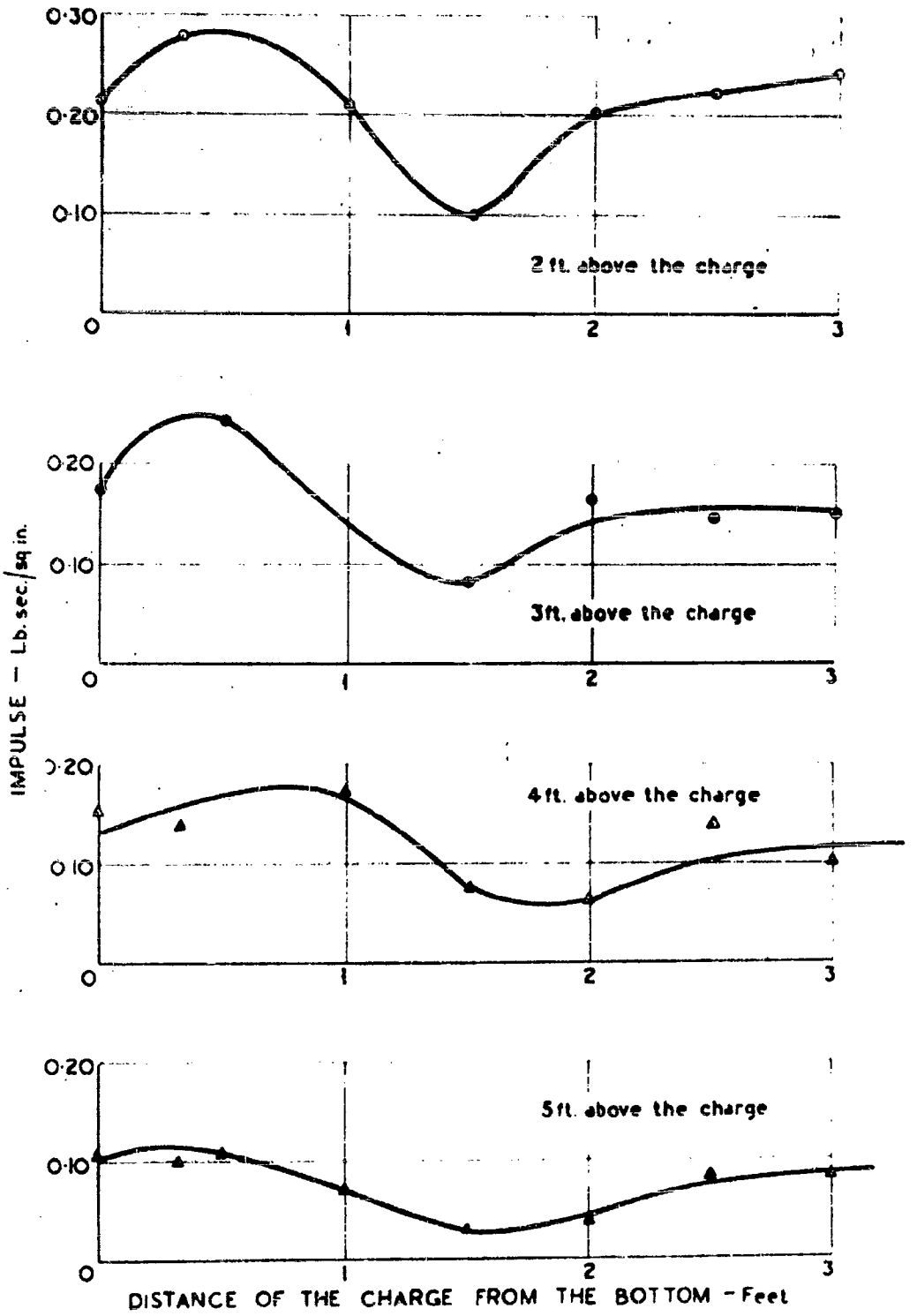

Fig. 4. IMPULSES IN THE 1st BUBBLE WAVES AT POINTS 2, 3, 4, AND 5 ft. ABOVE THE CHARGE FOR VARIOUS DISTANCES OF THE CHARGE FROM THE BOTTOM

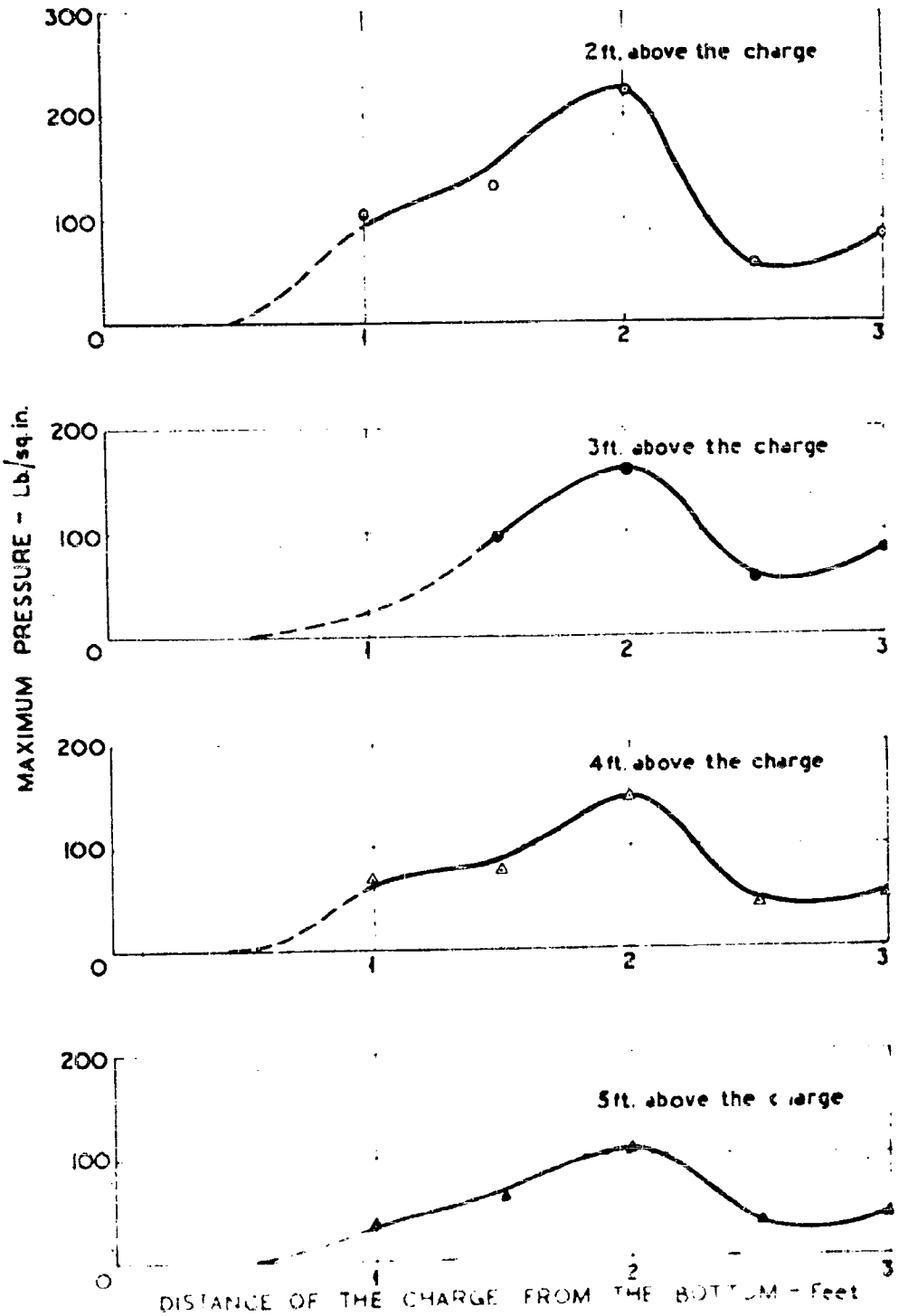

Fig 5 MAXIMUM PRESSURES IN THE 2ND BUBBLE WAVES AT POINTS 2 3 4 AND 5ft ABOVE THE CHARGE FOR VARIOUS DISTANCES OF THE CHARGE FROM THE BOTTOM

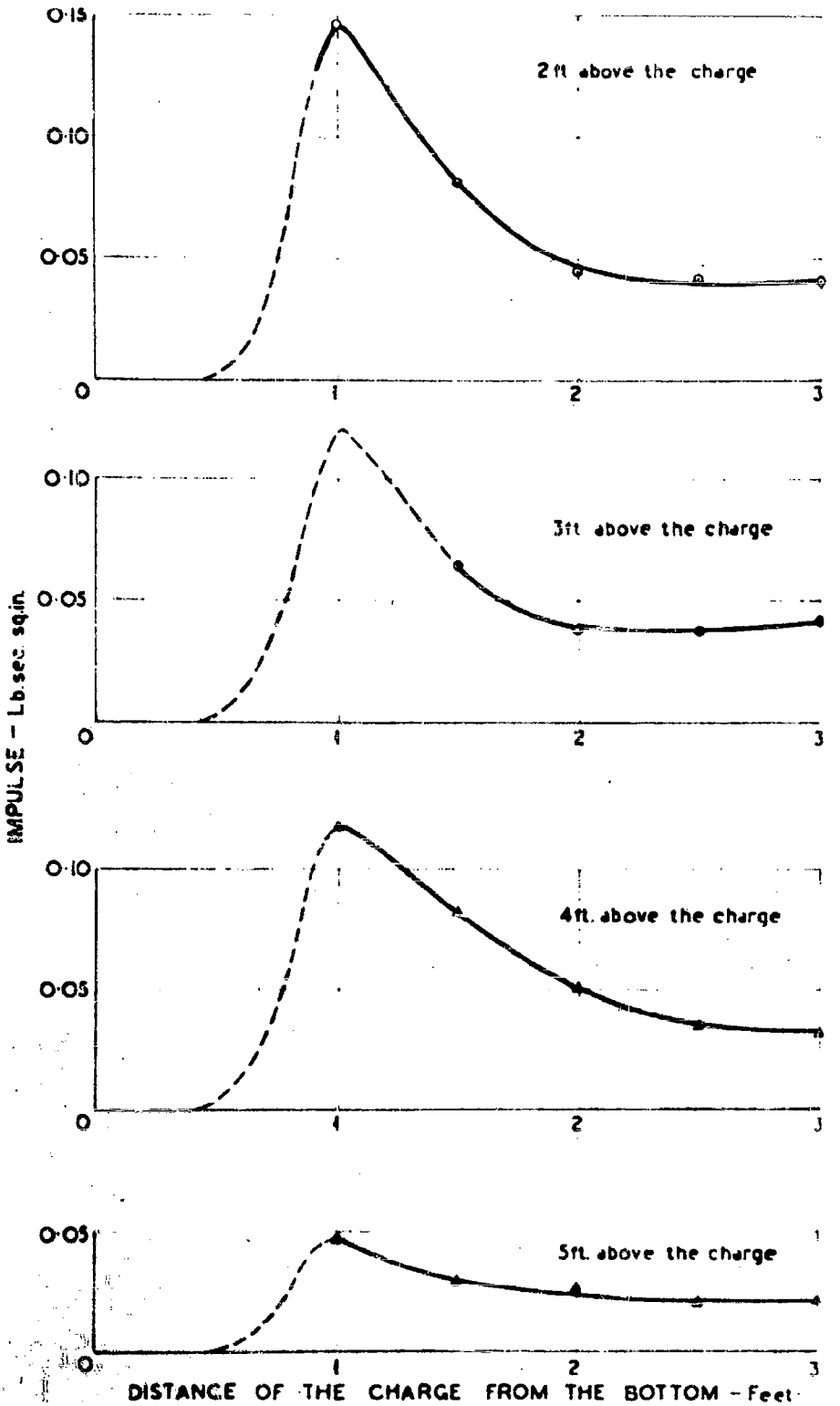

Fig.6. IMPULSES IN THE 2nd BUBBLE WAVES AT POINTS 2,3,4 AND 5ft ABOVE THE CHARGE FOR VARIOUS DISTANCES OF THE CHARGE FROM THE BOTTOM

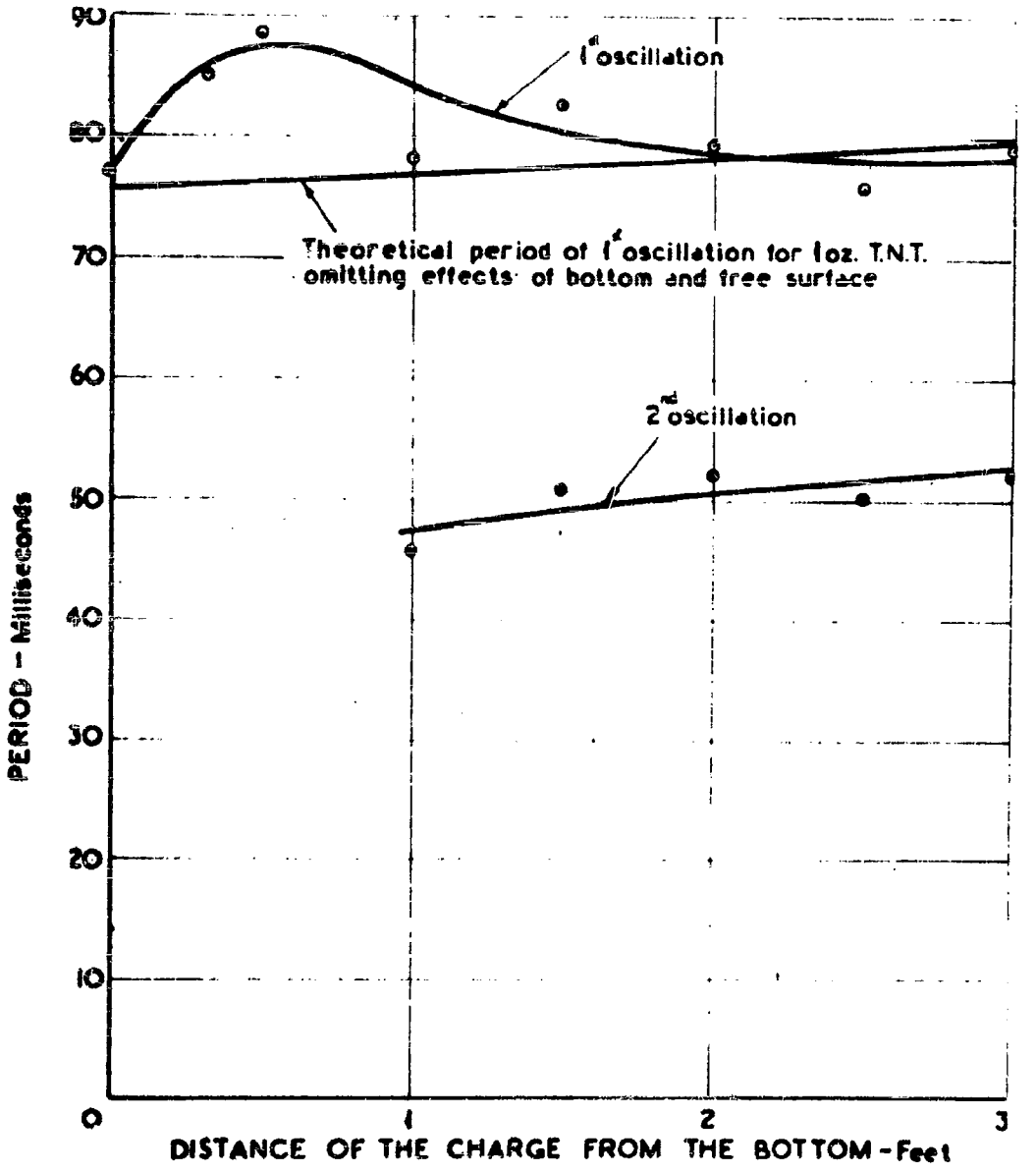

Fig. 7. OBSERVED PERIODS OF THE 1st AND 2nd OSCILLATIONS OF THE BUBBLE PRODUCED BY FIRING 1oz. CHARGES OF P.A.G. AT VARIOUS DISTANCES FROM THE BOTTOM

SECONDARY PRESSURE PULSES DUE TO GAS GLOBE OSCILLATION IN UNDERWATER EXPLOSIONS
I. EXPERIMENTAL DATA

A. B. Arons, J. P. Slifko, and A. Carter
Underwater Explosives Research Laboratory
Woods Hole Oceanographic Institution

American Contribution

January 13, 1948

Reprinted from THE JOURNAL OF THE ACOUSTICAL SOCIETY OF AMERICA,
Vol. 20, No. 3, pp. 271-276, May 1948

THE JOURNAL OF THE ACOUSTICAL SOCIETY OF AMERICA VOLUME 20, NUMBER 3 MAY, 1948

Secondary Pressure Pulses Due to Gas Globe Oscillation in Underwater Explosions. I. Experimental Data*†

A. B. ARONS,** J. P. SLIFKO,*** AND A. CARTER
Underwater Explosives Research Laboratory, Woods Hole Oceanographic Institution, Woods Hole, Massachusetts

(Received January 13, 1948)

Pressure waves emitted by the oscillating gas globe in underwater explosions of T.N.T. have been recorded at depths great enough to render small the perturbation effects due to migration of the bubbles under the influence of gravity. The first eight periods of oscillation have been measured and the pressure-time curves analyzed in order to obtain peak pressure, positive impulse, and energy flux resulting from the first two pulses. The scaling of pressure pulse parameters with charge size is examined.

I. INTRODUCTION

1.1. The detonation of an explosive charge results in the conversion of the initial solid material into a globe of gaseous products at exceedingly high temperature and pressure. This is followed by expansion of the gas globe and propagation of a strong shock wave through the fluid medium surrounding the charge.

In underwater explosions, the succeeding phenomena are associated with the oscillation of the gas globe, which expands to a maximum radius and then collapses under the influence of the hydrostatic pressure. A pressure pulse (called the first bubble pulse) is emitted while the bubble is near minimum size, and second, third, etc. bubble pulses are emitted as the bubble proceeds with successive oscillations. A typical pressure-time curve for the entire phenomenon is reproduced in Fig. 1.

1.2. The gas globe produced in an underwater explosion tends to migrate vertically upwards under the influence of gravity, the migration being most pronounced in the interval when the bubble is near its minimum radius. In the process of migration, some of the potential energy is converted into kinetic energy of vertically moving water. This energy is not restored to the bubble as it collapses, and hence the amplitude of the emitted pressure wave is less than it would have been had no migration occurred. This effect does not scale with charge size in the same way as other parameters because of the constancy of the acceleration of gravity, g.

From the foregoing, it is evident that the pressure pulse will be at a maximum under conditions which make the bubble migration negligible or cause the bubble to be in a "rest position." It is known that for relatively small charges a rest position occurs at a certain critical depth below the water surface owing to the balancing of gravitational effects by the repulsion from the free surface.[1] However, accurate pressure-time measurements under these circumstances are not possible because proximity to the free surface causes serious interference from the surface reflection of the pressure wave.

Since migration decreases with increasing depth of detonation, it is possible, by performing experiments at sufficiently great depths, to make the migration effects relatively small, or in some cases completely negligible, and thus determine the parameters of the bubble pulse unperturbed by the effects of nearby surfaces and bubble migrations.

1.3. The object of the present investigation was to obtain such unperturbed measurements in order to test the scaling of bubble pulse parameters with charge size and to obtain better impulse and energy flux data than have hitherto been available for the stationary bubble.

Cast T.N.T. was used in three charge sizes: 0.505 lb., 2.507 lb., and 12.01 lb. Measurements

* This work was performed under contract NOrd 9500 with the Navy Department, Bureau of Ordnance.
† Contribution from the Woods Hole Oceanographic Institution No. 430.
** Present address: Department of Physics, Stevens Institute of Technology, Hoboken, New Jersey.
*** Present address: Naval Ordnance Laboratory, Washington, D. C.

[1] B. Friedman, "Theory of underwater explosion bubbles," Report IMM-NYU 166, Institute for Mathematics and Mechanics, New York University, September 1947.

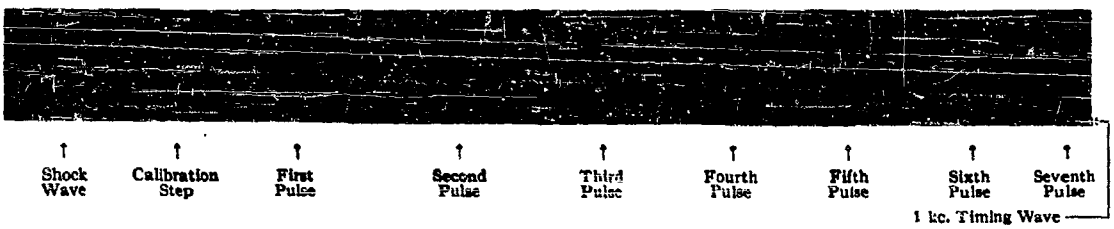

FIG. 1. Pressure-time record showing shock wave and bubble pulses. Charge: 0.505 lb. T.N.T.; Gauge dist.: 2.25 ft. Depth: 500 ft.

were made at a depth of 500 ft. in water having an over-all depth in excess of 650 ft. (For comparison several 0.505- and 2.507-lb. charges were fired at 250 ft.) Under these conditions, surface and bottom effects were negligible. The half-pound charge is deemed to be the smallest T.N.T. charge which can be reliably detonated under these circumstances. The twelve-pound charge is the largest that could be tolerated at a distance of 500 ft. below the vessel performing the experiments; thus, the range of charge size was the widest attainable with the available experimental equipment and with T.N.T. as the explosive.

All pressure-time measurements were made at a distance from the charge such that the value of $W^{\frac{1}{3}}/R$ was constant and equal to 0.352, W being the charge weight in pounds and R the charge to gauge distance in feet. A typical pressure-time record is reproduced in Fig. 1. Periods of pulsation have been measured to the seventh and, in some cases, to the eighth bubble pulse. Peak pressures, impulse, and energy flux have been obtained for the first and second pulses.

II. PERIODS OF OSCILLATION

2.1. Theoretical analysis shows[1] that to a first approximation the period of oscillation of a gas globe is given by

$$T = KW^{1/3}/Z_0^{5/6}, \qquad (1)$$

where K = constant of proportionality, W = charge weight, and Z_0 = absolute hydrostatic depth.

If the energy associated with the oscillation were constant (i.e., if there were no dissipation or acoustic radiation), the period would also remain constant. However, appreciable energy is lost, principally in the neighborhood of the bubble minimum owing to the emission of the pressure wave and other dissipative effects and, consequently, the period of successive oscillations decreases. A summary of the experimental results is given in Table I in terms of the proportionality constant, K, defined by Eq. (1).

2.2. It will be noted in Table I that the values of K_1 for the 2.5- and 12-lb. charges are significantly lower than those for the 0.5-lb. charges. The reproducibility of the period measurements and the fact that charge sizes were alternated in a definite sequence during the shooting program make it very unlikely that the difference is due to systematic experimental error in the measurement of T or Z. The discrepancy can be interpreted only as a slight but significant departure from the ideal cube root law of variation of period with charge weight. (Although correction has been made for the effect of the tetryl booster present in each charge, one cannot be certain of the accuracy of the correction, and it is therefore possible that the observed discrepancy may be due to the relatively larger proportion of booster in the half pound charges.)

Examination of K_n as a function of n shows that the period drops off sharply during the first three oscillations and then decreases slowly but steadily in such a way that the results do not yield a value of K which could be regarded as an accurate limiting value, applicable to the ultimate small amplitude oscillations of the gas globe.

III. PEAK PRESSURE: FIRST AND SECOND PULSES

3.1. Peak pressures of the first and second bubble pulses are summarized in Table II.

As will be indicated in Section V, the cylindrical charges were oriented with their axes in a horizontal plane. Pairs of gauges were placed above, below, and to the side of the charge in positions denoted by $G1$, $G4$, and $G2,3$, respec-

TABLE I. Summary of period constants for T.N.T. $T_n = K_n W^{1/3}/Z_0^{5/6}$, T_n = period of nth oscillation (sec.), W = charge weight (lb.), Z = depth of charge below surface (ft.), Z_0 = absolute hydrostatic depth = $Z + 33$ (ft.).

W (lb.)	Z (ft.)	Period constant, K_n							
		K_1	K_2	K_3	K_4	K_5	K_6	K_7	K_8
0.505	250	4.36±.01*	3.14±.03	2.56±.02	2.38±.03	2.16±.04	2.08±.04	1.96±0.1	—
0.505	500	4.36± 01	3.06±.01	2.51±.01	2.32±.01	2.15±.02	1.97±.02	1.90±.02	1.9±.1
2.507	250	4.27**	3.11	2.53	2.35	2.25	2.02	1.94	—
2.507	500	4.26±.01	3.06±.01	2.48±.01	2.31±.01	2.17±.01	2.02±.01	—	—
12.01	500	4.29±.01	3.19±.01	2.56±.01	2.39±.01	2.16±.01	2.04±.01	1.94±.02	1.73±.05

* The stated error is the standard deviation of the mean.
** The error is not indicated since only two shots were made under these conditions. Results of the two shots agreed very closely.

tively, all the gauges being positioned off the cylindrical surface of the charge. It was assumed that the difference between the average pressures at *G*1 and *G*4 was due only to displacement of the bubble toward *G*1, and the pressure was assumed to vary inversely as the gauge to bubble distance. This treatment neglects any effects resulting from possible asymmetry of the pressure field, but it appears to be justified by the fact that when pressures at *G*1 and *G*4 are corrected to the same distance as the *G*2,3 position, all the values agree within experimental scatter.

The values given in Table II are the averages of pressures measured at all three positions and corrected (by means of the apparent migration result) to the given distance from the center of the bubble, $R = W^{\frac{1}{3}}/0.352$ ft.

Because of uncertainty as to the exact location of the true base-line of zero excess pressure on the individual photographic records, the records were read with respect to an arbitrary base-line and were then adjusted to the theoretical baseline value calculated by means of the theory summarized by Friedman.[1] This is based on a calculation of the negative pressure (below surrounding hydrostatic level) existing at the time of the first bubble maximum, and for the conditions represented in Table II the values are −80 and −120 lb./in.^{2} at depths of 250 and 500 ft., respectively.

3.2. Ideal scaling would require that all the peak pressure values at a given ratio of $W^{\frac{1}{3}}/R$ be equal regardless of charge size. Examination of Table II shows that this is not the case. The principal cause of the observed variation is undoubtedly the migration of the bubble. Theoretical calculation of the influence of migration on peak pressure[1] predicts very much less effect than is observed, the expected decrease in peak pressure for the worst case (2.5 lb. at 250 ft.) being less than 1 percent, whereas Table II indicates 15 percent, if ΔP for the half-pound charges at 500 ft. is used as a basis of comparison. Further discussion of this result will be found below in Section IV.

3.3. The results summarized in Table II indicated that the pressure field was cylindrically symmetrical with respect to the axis of the charge. A number of shots were fired with the charge so placed that gauges in position *G*2 faced the cap end while gauges at *G*3 faced the butt end of the charge. Gauges at *G*1 and *G*4 were still above and below the charge, respectively. In Table III the pressures at *G*2 and *G*3 are compared with the pressure at *G*2,3 (off the cylindrical surface) given in Table II. It will be noted that a marked degree of asymmetry exists, particularly in the case of the small charges, with the pressure from the cap end being significantly higher than the pressure from the butt end.

IV. POSITIVE IMPULSE AND ENERGY PULSE

4.1. For convenience in describing and working with various portions of the continuous

TABLE II. Apparent bubble migration and corrected peak pressures. ΔP_n = excess peak pressure of nth pulse (lb./in.^{2}), R = distance from bubble center of point where ΔP_n is measured; $R = W^{\frac{1}{3}}/0.352$ (ft.), W = charge weight (lb. T.N.T.), Z = depth of charge below surface (ft.), Δh_n = vertical displacement of center of bubble from initial charge position at time of nth bubble minimum (ft.).

W (lb.)	Z (ft.)	ΔP_1 (lb./in.^{2})	Δh_1 (ft.)	ΔP_2 (lb./in.^{2})	Δh_2 (ft.)
0.505	250	1120±16*	0.32	225±5	0.51
2.507	250	1020±10	0.80	215±5	1.12
0.505	500	1210±10	0.11	250±5	0.16
2.507	500	1160±10	0.32	245±5	0.47
12.01	500	1140±10	0.86	260±5	0.79

* Stated error is standard deviation of the mean.

TABLE III. Bubble pulse peak pressures for various charge orientations. Notation for position of measurement: $G2,3$—gauge facing cylindrical surface of charge, $G2$—gauge facing cap end of charge, $G3$—gauge facing butt end of charge. Gauge distance from center of bubble: $R=W^{1/3}/0.352$ (ft.), W=charge weight (lb. T.N.T.), ΔP_n =excess peak pressure of nth pulse (lb./in.^{2}).

W (lb.)	Z (ft.)	ΔP_1(lb./in.^{2})			ΔP_2(lb./in.^{2})		
		$G2$	$G2,3$	$G3$	$G2$	$G2,3$	$G3$
0.505	500	1365	1210	1095	285	250	230
2.507	500	1200	1160	1150	280	245	240
12.01	500	1200	1140	1120	295	260	250

pressure-time curve illustrated in Fig. 1, an arbitrary subdivision has been adopted. The shock wave is defined as that portion of the curve lying between the shock front (where the time, $t=0$) and the point of first bubble maximum ($t=T_1/2$). Similarly, the first bubble pulse is the portion between first and second bubble maxima, i.e., $T_1/2<t<T_2/2$, etc.

4.2. The impulse delivered by the pressure wave during a fixed interval of time is defined:

$$I=\int_{t_a}^{t_b}\Delta p\,dt. \tag{2}$$

During a bubble pulse, the pressure is initially negative, becomes positive, and then again negative. It can be shown from acoustic theory that the integral in Eq. (2) taken over the entire pulse as defined above must be very nearly equal to zero. (Actually, there is a small negative residual.) Of principal interest, however, is the magnitude of the positive impulse, the integral being taken only over the region of positive pressure. A summary of average positive impulse values is given in Table IV.

4.3. Impulses measured at $G1$ vertically above the charge are systematically high and those at $G4$ below the charge are systematically low, as would be expected on the basis of the migration results given in Table II. As with the peak pressure (Table III), the impulse is higher at points off the cap end and lower off the butt end than off the cylindrical surface of the charge.

Using the $G2,3$ position (off the cylindrical surface) as being representative of the unperturbed impulse, it is seen that at each depth the impulse scales according to the ideal similarity law within the experimental precision which is

TABLE IV. Positive impulse: First and second bubble pulses (no correction applied for bubble migration). Distance of point of measurement from center of initial charge position: $R=W^{1/3}/0.352$ ft., W=charge weight (lb. T.N.T.), Z=depth of charge below surface (ft.).

W (lb.)	Z (ft.)	Reduced positive impulse, $I/W^{\frac{1}{3}}$ (lb. sec./in.^{2} lb.$^{\frac{1}{3}}$)									
		First pulse					Second pulse				
		$G1$*	$G2$	$G2,3$	$G3$	$G4$	$G1$	$G2$	$G2,3$	$G3$	$G4$
0.505	250	1.39	—	1.34	—	1.32	0.66	—	0.51	—	0.46
2.507	250	1.43	—	1.33	—	1.22	0.71	—	0.57	—	0.47
0.505	500	1.10	1.22	1.16	1.12	1.15	0.45	0.48	0.44	0.40	0.39
2.507	500	1.11	1.17	1.12	1.04	1.07	0.44	0.46	0.43	0.44	0.40
12.01	500	1.15	1.16	1.17	1.06	1.11	0.51	0.49	0.47	0.46	0.46

* See Section 3.3 and Table III for key to position notation.

of the order of 4 percent. This agreement indicates that the pressure differences noted in Table II are confined to a very narrow region in the immediate vicinity of the peak of the pulse and do not affect the remainder of the pressure-time curve appreciably.

Thus, the effect of migration on peak pressure is more than would have been expected on the basis of the theoretical predictions, but the other parameters of the pressure-time curve remain virtually unaffected. Since the impulse obeys the ideal scaling law, it is presumed that the peak pressure also would if the effect of migration could be reduced still further, but this is not conclusively demonstrated and further measurements would be necessary to test the presumption.

4.4. Theoretical analysis[1] shows that to a first approximation the positive impulse in a bubble pulse would be expected to vary as the inverse sixth root of the absolute hydrostatic pressure at the depth at which the bubble is located. A test of this prediction is given in Table V. Since the quantity $IZ_0^{1/3}/W^{1/3}$ is essentially constant with depth, it is seen that the prediction is confirmed within the available experimental accuracy.

4.5. Integrations of the pressure-time curves were also performed for the purpose of determining the irreversible energy flux which is given by acoustic theory as:

$$F=\frac{1}{\rho_0 c_0}\int_{t_a}^{t_b}(\Delta p)^2 dt,$$

where Δp=excess pressure (lb./in.^{2}), t=time (sec.), $\rho_0 c_0$=acoustic impedance of water (slug ft./in.^{3} sec.), and F=energy flux (in. lb./in.^{2}).

The integration was made over the entire bubble pulse as defined in Section 4.1, including both the positive and negative phases, and the averaged results are summarized in Table VI.

4.6. Energy flux measured at *G*1 vertically above the charge is systematically high and that at *G*4 below the charge systematically low, as would be expected on the basis of the migration indicated in Table II. As with the peak pressure (Table III), the energy flux is higher at points off the cap end (*G*2) and lower off the butt end (*G*3) than off the cylindrical surface (*G*2,3).

First pulse energy flux measured in the horizontal plane off the cylindrical surface (*G*2,3) is appreciably decreased by migration losses only in the most severe case—that of the 2.5-lb. charge at 250 ft. The remaining scatter in this column of Table VI is probably due to experimental error.

4.7. From the successive period measurements given in Table I, it is possible to compute the total energy lost by the bubble during the intervals defining the first and second pulses:

$$(B_n - B_{n+1}) = B_n\left[1-\left(\frac{T_{n+1}}{T_n}\right)^3\right] \qquad (4)$$

where B_n = total energy associated with the nth oscillation; T_n = period on nth oscillation.

Taking B_1 as 490 cal./g. of charge and using the values given in Table I, it is found that the total energy lost by the bubble during the first pulse is 300 cal./g. and during the second pulse 85 cal./g. Assuming spherical symmetry about the center of the charge, the *G*2,3 results of Table VI were converted to obtain the total acoustic energy flowing through a spherical surface having a radius equal to the value of R as defined in that table. The resulting energies for the first two pulses are 120 and 15 cal./g., respectively.

It is evident that the measured acoustic radiation accounts for only a fraction of the total energy loss sustained by the bubble in each case. At this time there exists no concrete evidence pointing to the cause of the unaccounted energy loss, although various speculations have been advanced regarding the role of turbulence, chemical reactions among detonation products, etc.

TABLE V. Variation of positive impulse of first bubble pulse with depth of detonation. Z = depth below surface (ft.), $Z_0 = Z + 33$ (ft.), $I/W^{\frac{1}{3}}$ = reduced impulse at $R = W^{\frac{1}{3}}/0.352$, W = charge weight (lb. T.N.T.).

Z_0 (ft.)	$I/W^{1/3}$ (lb. sec./in.^{2} lb.$^{1/3}$)	$IZ_0^{1/3}/W^{1/3}$
40	1.66*	3.1
283	1.34	3.4
533	1.15	3.3

* Obtained at rest position for 300-g T.N.T.-charge near surface and corrected for surface reflection. This value would be expected to be systematically low.

V. EXPERIMENTAL TECHNIQUES

5.1. The charges used were cylinders of cast T.N.T. boostered with pressed tetryl pellets. The weight of tetryl was converted to an equivalent weight of T.N.T. by multiplying by 1.03 as suggested by the results of various period measurements made at this laboratory. One gram was added to the charge weight to account for the explosive in the engineers special blasting caps which were used to detonate the charges.

5.2. Tourmaline piezoelectric gauges[2, 3] were used as the pressure sensitive element. The gauges were $\frac{7}{8}$ inch in diameter and had an average sensitivity of 24 micro-microcoulombs per lb./in.^{2}.

5.3. Eight piezoelectric gauges were mounted on $\frac{3}{16}$-in. steel cable in the plane of a 15-ft. diameter steel ring. The ring was suspended in a vertical plane and the charge was mounted at its center. Pairs of gauges were placed at equal

TABLE VI. Acoustic energy flux: First and second bubble pulses (no correction applied for bubble migration). Distance of point of measurement from center of initial charge position: $R = W^{\frac{1}{3}}/0.352$, W = charge weight (lb. T.N.T.), Z = depth of charge below surface (ft.).

W (lb.)	Z (ft.)	Reduced energy flux; $F/W^{\frac{1}{3}}$ (in. lb./in.^{2} lb.$^{\frac{1}{3}}$)									
		First pulse					Second pulse				
		*G*1*	*G*2	*G*2,3	*G*3	*G*4	*G*1	*G*2	*G*2,3	*G*3	*G*4
0.568	250	161	—	141	—	122	23	—	15	—	11
2.507	250	154	—	125	—	101	28	—	16	—	11
0.505	500	140	164	141	135	136	17	20	17	14	14
2.507	500	138	145	134	131	121	19	20	16	16	13
12.01	500	150	150	142	128	120	24	21	22	17	19

* See Section 3.3 and Table III for key to position notation.

[2] Clifford Frondel, "Construction of tourmaline gauges for piezoelectric measurement of explosion pressure waves," OSRD Report No. 6256; NDRC Report No. A-378.

[3] A. B. Arons and C. W. Tait, "Design and use of tourmaline gauges for piezoelectric measurement of air blast," OSRD Report No. 6250; NDRC Report No. A-372.

distances vertically above, vertically below, and horizontally on each side of the charge.

The center of the charge was in the plane of the ring, and two charge orientations were used: (a) axis of cylinder perpendicular to the plane of the ring, (b) axis of cylinder horizontally oriented in the plane of the plane of the ring.

Dimensions were so chosen that the wire structure supporting the gauges did not come in contact with the bubble and was never damaged or appreciably loosened by the forces of the explosion. This insured against uncertainty in gauge position owing to displacement of gauges by the shock wave.

5.4. The over-all depth of water was measured by means of a fathometer, and all experiments were performed in such depths that the charge was always at least 150 ft. away from the bottom. The depth of the charge was determined by the measured length of suspension cable supporting the ring, the method being very reliable since experiments were performed in a region of negligible tidal currents, and the suspension always hung vertically downward. This is confirmed by the reproducibility of the period measurements given in Table I.

5.5. Continuous 600 ft.-lengths of Simplex (F.O. 5879) signal free coaxial cable were used between the gauges and oscilloscopes, thus avoiding occurrence of spurious cable signal for an interval sufficiently long to allow faithful recording of the first two bubble pulses. Cable effects were further minimized by the relatively high sensitivity of the gauges. The polythene core of the cable rendered negligible any low frequency distortion due to dielectric dispersion. The cables were compensated in accordance with principles discussed elsewhere.[4]

5.6. Recording equipment consisted of eight oscilloscope channels[5] on the schooner "Reliance." In order to avoid low frequency distortion, it was necessary to increase the input impedance of the oscilloscopes by using cathode follower preamplifiers. The final over-all time constant of the recording circuits was about 500 millisec.

A 110-v d.c. motor with variable armature voltage was used to drive the rotating drum cameras. Writing speeds were varied from 125 to 400 millisec. per revolution of the 10-inch circumference drums.

---

[4] R. H. Cole, "The use of electrical cables with piezoelectric gauges," OSRD Report No. 4561; NDRC Report No. A-306.

[5] R. H. Cole, D. Stacey, and R. M. Brown, "Electrical instruments for the study of underwater explosions and other transient phenomena," OSRD Report No. 6238; NDRC Report No. A-360.

SECONDARY PRESSURE PULSES DUE TO GAS GLOBE OSCILLATION IN UNDERWATER EXPLOSIONS
II. SELECTION OF ADIABATIC PARAMETERS IN THE THEORY OF OSCILLATION

A. B. Arons
Stevens Institute of Technology
Hoboken, N. J.

American Contribution

January 13, 1948

Reprinted from THE JOURNAL OF THE ACOUSTICAL SOCIETY OF AMERICA,
Vol. 20, No. 3, pp. 277-282, May 1948

THE JOURNAL OF THE ACOUSTICAL SOCIETY OF AMERICA VOLUME 20, NUMBER 3 MAY, 1948

Secondary Pressure Pulses Due to Gas Globe Oscillation in Underwater Explosions. II. Selection of Adiabatic Parameters in the Theory of Oscillation*

A. B. Arons
Department of Physics, Stevens Institute of Technology, Hoboken, New Jersey
(Received January 13, 1948)

A summary is given of the theory of pulsation of a stationary gas globe in an infinite incompressible fluid. If three parameters appearing in the formulation are selected by fitting the equations to three independent experimental results, it is shown that the theory fits the remaining experimental results and can be used to predict bubble pulse properties over wide ranges of the independent variables.

I. INTRODUCTION

1.1. The theory of the pulsation of gas globes formed in underwater explosions has been treated by several investigators during the past few years and has been summarized by Friedman in a recent report of the New York University Institute for Mathematics and Mechanics.[1] The theory in this formulation depends upon three parameters which cannot be accurately determined by means of *a priori* calculations, and recourse must be had to experimental information regarding certain properties of the bubble pulsation.

Experimental results obtained in deep water at the Woods Hole Oceanographic Institution[2] afford the necessary information, and it is the purpose of this report to discuss the selection of parameters which make it possible to fit the theory to the experimental results over a wide range of the primary variables.

II. FORMULATION OF THE THEORY

2.1. The theory referred to above[1] has been set up to treat the general case in which the gas bubble migrates as a result of the combined effects of gravity and the presence of neighboring free and rigid surfaces. A brief summary of the formulation will be given here, modified for application to the special case of the stationary bubble (i.e., negligible migration).

Consider a perfect sphere of radius A expanding at radial velocity A' in an infinite incompressive liquid of density ρ. The total kinetic energy of the fluid external to radius A is given by

$$\mathrm{T}=\int_A^\infty 4\pi R^2\frac{\rho(R')^2}{2}dR=2\pi\rho A^3(A')^2, \quad (1)$$

where the primes denote time derivatives.

The potential energy of the system is

$$U=(4/3)\pi A^3P_0+G(A), \quad (2)$$

where the first term represents energy stored against hydrostatic pressure (P_0 being the absolute hydrostatic pressure at the depth of the bubble center), and the second term represents the internal energy of the gas in the bubble. The zero of internal energy is defined as the infinite limit of adiabatic expansion, thus:

$$G(A)=\int_A^\infty pdV, \quad (3)$$

where the line integral is taken along an adiabatic and V represents the total volume of gas.

It is assumed that the gas approximates ideal behavior:

$$pv^\gamma=k_1, \quad (4)$$

where v is specific volume, k_1 is a constant, and γ is the ratio of heat capacities.

Combining Eqs. (3) and (4),

$$G(A)=k_1M^\gamma\int_{V_A}^\infty\frac{dV}{V^\gamma}=\frac{k_1M^\gamma}{(\gamma-1)A^{3(\gamma-1)}(4\pi/3)^{\gamma-1}}, \quad (5)$$

where M is the mass of gas.

Denoting the total energy associated with the oscillation by E,

$$E=2\pi\rho A^3(A')^2+(4/3)\pi A^3P_0+G(A). \quad (6)$$

* Contribution of the Woods Hole Oceanographic Institution No. 431.

[1] Bernard Friedman, "Theory of underwater explosion bubbles," Institute of Mathematics and Mechanics, New York University, Report No. IMM-NYU 166.

[2] A. B. Arons, J. P. Slifko, and A. Carter, "Secondary pressure pulses due to gas globe oscillation in underwater explosions. I. Experimental data," this Journal.

Following the convention adopted by Friedman,[1] it is convenient to transform to dimensionless variables by using the following scale factors for length and time, respectively:

$$L=(3E/4\pi P_0)^{\frac{1}{3}}, \tag{7}$$

$$C=L(3\rho/2P_0)^{\frac{1}{2}}. \tag{8}$$

Combining Eqs. (5), (6), (7), and (8),

$$a^3\dot{a}^2+a^3+ka^{-3(\gamma-1)}=1, \tag{9}$$

where $a=A/L$, the dot denotes derivative with respect to non-dimensional time, and k is given by

$$k=\frac{k_1P_0^{\gamma-1}}{(\gamma-1)\epsilon^\gamma}; \tag{10}$$

ϵ is the bubble energy per unit mass of gas (or original explosive charge).

It will be noted that throughout the following analysis the total energy for a cycle of the oscillation will be considered constant. This is a very close approximation for most of the parameters since appreciable quantities of energy are lost by the bubble only during the very short intervals of time in the neighborhood of the bubble minima. The treatment of the peak pressure of the pulse, however, may be appreciably in error because of this approximation.

2.2. Since the bubble is at maximum or minimum when $\dot{a}=0$, the corresponding maximum and minimum bubble radii are given by the roots of the equation,

$$a^3+ka^{-3(\gamma-1)}-1=0. \tag{11}$$

The non-dimensional maximum radius is the root near unity of the above equation, i.e.,

$$a_M=[1-ka_M^{-3(\gamma-1)}]^{\frac{1}{3}}. \tag{12}$$

The actual maximum radius is given by $A_M=La_M$.

The non-dimensional minimum radius is

$$a_m\cong k^{1/3(\gamma-1)}. \tag{13}$$

2.3. Assuming the radius-time curve to be symmetrical about the time of bubble maximum, integration of Eq. (9) gives the non-dimensional period of oscillation,

$$t=2\int_{a_m}^{a_M}\frac{a^3}{[1-a^3-ka^{-3(\gamma-1)}]^{\frac{1}{2}}}da. \tag{14}$$

The actual period of oscillation is given by $T=Ct$.

Shiffman and Friedman have given a method of obtaining this integral[1] with a high degree of precision. Figure 1 shows a family of curves giving t as a function of k for various values of γ.

2.4. Bernoulli's equation affords a relationship for the excess pressure at points in fluid:

$$\Delta p/\rho=(\partial\varphi/\partial\tau)-\tfrac{1}{2}(\nabla\varphi)^2. \tag{15}$$

Here τ is dimensional time and φ the velocity potential which, in the case of spherically symmetrical incompressive flow, is given by

$$\varphi=A^2A'/R. \tag{16}$$

The second term in Eq. (15) is negligibly small compared with the first. Neglecting this term, the excess pressure is given by

$$\Delta p=\rho(A^2A')'/R=2P_0L(a^2\dot{a})^{\cdot}/3R. \tag{17}$$

An expression for $(a^2\dot{a})^{\cdot}$ can be obtained from the equations of motion; the most convenient method is the application of the Lagrange equation to the energy relation of Eq. (6). The result is substituted into Eq. (17), yielding

$$\Delta p=\frac{P_0L}{R}\left[\frac{a^2\dot{a}}{3}-a+\frac{(\gamma-1)k}{a^{3\gamma-1}}\right], \tag{18}$$

since

$$2(a^2\dot{a})^{\cdot}=a\dot{a}^2-3a+3(\gamma-1)ka^{-3\gamma+1}. \tag{19}$$

When a is at a maximum or minimum, $\dot{a}$ is zero. The excess pressure at bubble maximum becomes

$$\Delta P_M=-\frac{P_0L}{R}\left[a_M-\frac{(\gamma-1)k}{a_M^{3\gamma-1}}\right]. \tag{20}$$

Using Eq. (13), the excess pressure at bubble minimum is given by

$$\Delta P_m=\frac{P_0L}{R}\frac{(\gamma-1)}{k^{2/3(\gamma-1)}}\left[1-\frac{k^{1/(\gamma-1)}}{(\gamma-1)}\right]. \tag{21}$$

In Eq. (20) it will be noted that (since γ is of the order of 1.3, k of the order of 0.2, and a_M about 0.9) the first term predominates, the second term representing a relatively small cor-

rection for the internal energy of the gas. Thus the minimum excess pressure is negative relative to the original hydrostatic level, as would be expected, and is not critically dependent upon the equation of state of the gas.

Because of the base line uncertainties in the measurements described in the preceding paper,[2] calculations based on Eq. (20) were used to select a baseline to which the pressure-time records were subsequently referred.

2.5. It is seen from Eq. (17) that the non-dimensional bubble radius a_0 at which Δp is zero is determined by the condition that $(a^2\dot{a})\cdot$ be zero. Applying this condition and eliminating $\dot{a}$ from Eqs. (9) and (19), one obtains

$$4a_0^3 = 1-(4-3\gamma)ka_0^{-3(\gamma-1)}. \tag{22}$$

2.6. The positive impulse I delivered by the pressure wave is defined by

$$I=\int_{a_{01}}^{a_{02}} \Delta p\dot{a}\,d\tau, \tag{23}$$

where the integration is performed over the region lying between the point at which Δp rises to zero during the collapsing phase and the point at which it again falls to zero on the expanding phase, i.e., between points where the non-dimensional bubble radii are denoted by a_{01} and a_{02}, respectively.

Because of the radiation of acoustic energy, the pressure-time curve is not symmetrical about the peak pressure ordinate. For convenience, therefore, the integral of Eq. (23) will be separated into two parts,

$$I=\int_{a_{01}}^{a_m} \Delta p\dot{a}\,d\tau+\int_{a_m}^{a_{02}} \Delta p\dot{a}\,d\tau, \tag{24}$$

where a_m is the non-dimensional minimum bubble radius, i.e., the radius when Δp is a maximum.

Elimination of Δp between Eqs. (17) and (24) and conversion of dimensional time τ to non-dimensional time gives

$$I=\frac{2P_0L_1C_1}{3R}\int_{a_{01}}^{a_m} d(a^2\dot{a}) + \frac{2P_0L_2C_2}{3R}\int_{a_m}^{a_{02}} d(a^2\dot{a}), \tag{25}$$

where L_1 and C_1 are the scale factors of the first and L_2 and C_2 the scale factors of the second bubble oscillation.

Since $\dot{a}$ is zero at the instant of bubble minimum, Eq. (25) becomes

$$I=\frac{2P_0}{3R}[L_1C_1(a^2\dot{a})_{01}+L_2C_2(a^2\dot{a})_{02}]. \tag{26}$$

(In Eq. (26), $\dot{a}$ is understood to represent only the magnitude of the quantity, whereas in Eq. (25) the symbol has an associated algebraic sign.)

The appropriate expression for $(a^2\dot{a})_0$ can be obtained from Eq. (19) by setting $(a^2\dot{a})\cdot$ equal to zero; the result is

$$(a^2\dot{a})_0=1.732a_0^2\left[1-\frac{(\gamma-1)k}{a_0^{3\gamma}}\right]^{\frac{1}{2}}. \tag{26a}$$

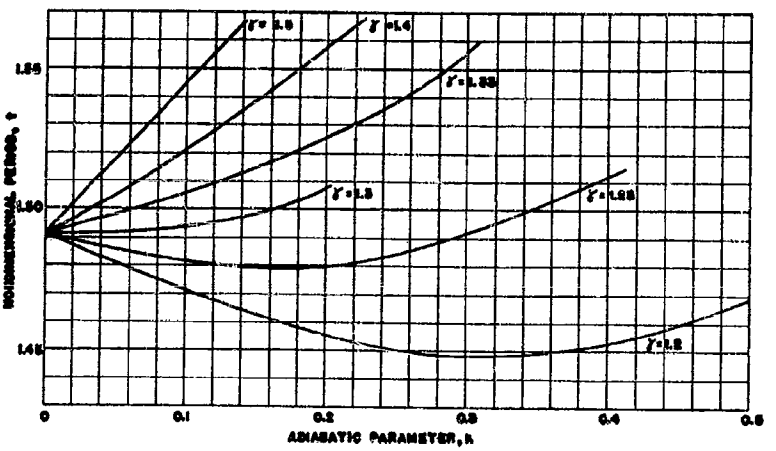

FIG. 1. Non-dimensional bubble period, t, *versus* parameter k for various values of γ.

TABLE I. Comparison of experimental impulse values with calculations based on Eq. (36).

Z_0 (ft.)	$I/W^{\frac{1}{3}}$ (lb. sec./in.^{2} lb.$^{\frac{1}{3}}$) Experimental	From Eq. (36)
40	1.7*	2.0
283	1.33	1.31
533	1.15	1.12

* This value is known to be systematically low because complete correction could not be made for surface reflection effects.

III. SELECTION OF PARAMETERS

3.1. The theory developed in the preceding chapter contains three parameters related to the properties of the gas in the bubble. These are the adiabatic parameters γ and k_1 and the total energy ϵ per unit mass. Although the values of γ, k_1, and ϵ can be estimated roughly on the basis of *a priori* considerations relating to the properties and behavior of the detonation products, such estimates do not lead directly to results of sufficient accuracy to make the theory a means of calculating reliable values of the bubble pulse parameters over reasonably wide ranges of the independent variables.

In order to obtain an empirical fit accomplishing the latter purpose for T.N.T., recourse must be had to the experimental results reported in the preceding paper[2] and to radius-time curves obtained from high speed motion pictures by Dr. J. C. Decius and his co-workers at Woods Hole.

3.2. In general, it is seen from Eq. (14) that the non-dimensional period of oscillation depends on γ and k. Since the latter parameter is a function of the hydrostatic pressure, as given by Eq. (10), one would expect the actual bubble period ($T=Ct$) to deviate from the ideal inverse 5/6 power dependence upon the depth of detonation. Experimental results over a wide range of depth (*ca.* 10 to 500 ft.) indicate that no such deviation is observable within the precision of experimental measurements.

Reference to Fig. 1 shows that the theory would be quite consistent with the above result if the value of γ is taken to be in the neighborhood of 1.25,* since along this curve a wide variation in the value of k has very little effect on the non-dimensional bubble period t. This is equivalent to making t nearly independent of depth and allowing T to vary as $P_0^{-5/6}$ as given by the scale factor C.

3.3. Substitution of the appropriate values in Eqs. (7) and (8) gives the following expressions for the scale factors:

$$L=1.733\epsilon^{\frac{1}{3}}(W/Z_0)^{\frac{1}{3}}, \tag{27}$$

$$C=0.373\epsilon^{\frac{1}{3}}(W^{\frac{1}{3}}/Z_0^{5/6}), \tag{28}$$

where L is in ft., C in sec., ϵ in cal./g, W is charge weight in lb., and Z_0 is absolute hydrostatic depth in ft. If Z is the depth of the charge below the surface, $Z_0=Z+33$.

The experimental data for the first period of oscillation of the T.N.T., bubble is represented by

$$T=4.36W^{\frac{1}{3}}/Z_0^{5/6}. \tag{29}$$

Since $T=Ct$, combination of Eqs. (28) and (29) gives

$$\epsilon^{\frac{1}{3}}t=11.7. \tag{30}$$

It will be seen below that, for the depth range which has so far been accessible, k lies between 0.1 and 0.3. From Fig. 1, t in this range has an average value of 1.483 along the $\gamma=1.25$ curve. Putting this value of t into Eq. (30) gives $\epsilon=490$ cal./g.

3.4. There still remains the problem of selecting the third parameter, k_1. Fitting it to the peak pressure data is the most sensitive method. Expressing P_0 in terms of the hydrostatic depth Z_0, setting $\gamma=1.25$, $\epsilon=490$, and combining Eqs. (7), (10), and (21),

$$\Delta P_m=\frac{3.55(10^7)}{\beta^{2.67}}\frac{W^{\frac{1}{3}}}{R}(1-4k^4), \tag{31}$$

where ΔP_m = excess peak pressure, lb./in.^{2}, W = charge weight, lb., ϵ = bubble energy, cal./g, $k=\beta Z_0^{\gamma-1}/(\gamma-1)\epsilon^{\gamma}$, Z_0 = absolute hydrostatic depth, ft., R = radial distance from bubble center, ft.

The term $(1-4k^4)$ in Eq. (31) represents a correction factor which differs from unity by only three percent at depths as great as 1000 ft. It can therefore be disregarded for all practical purposes. The parameter β represents a numerical factor in the general expression for k, and β must be selected in such a way as to provide a fit to the experimental peak pressure data.

* This value is identical with the one obtained by Jones in Britain as a result of the theoretical study of the composition of the detonation products and their equilibrium during the early stages of the bubble expansion.

Measurements of ΔP_m for the first bubble pulse in deep water under conditions of very small bubble migration give values[2] of about 1200 lb./in.^{2} at $W^{\frac{1}{3}}/R=0.352$. Using this result in Eq. (31) gives $\beta=31.8$, and the general expression for the peak pressure becomes

$$\Delta P_m=3450\frac{W^{\frac{1}{3}}}{R}(1-4k^4), \tag{32}$$

and k is given by

$$k=0.0552Z_0^{\gamma-1}. \tag{33}$$

IV. APPLICATION TO OTHER MEASUREMENTS

4.1. In the preceding section, experimental period and peak pressure results were used to determine the values of the three arbitrary parameters appearing in the theory. It is now necessary to ascertain whether the same parameters will also fit the rest of the available experimental data, consisting of (a) the maximum bubble radius, (b) the time and corresponding bubble radius at which $\Delta p=0$, and (c) the positive impulse in the first bubble pulse.

4.2. High speed motion picture measurements of T.N.T. bubbles give the maximum bubble radius as

$$A_M=12.6(W/Z_0)^{\frac{1}{3}}, \tag{34}$$

where A_M is expressed in ft. This represents the average of a large number of measurements over a wide range of depths (*ca.* 100 to 600 ft.). The accuracy of the measurement is believed to be about ± 2 percent, and within this scatter there seems to be no systematic variation with depth of the numerical constant 12.6 in Eq. (34). The experimental non-dimensional maximum bubble radius, a_M, is therefore constant and equal to 0.92 if ϵ is taken as 490 cal./g in calculating the scale factor.

The theoretical values of a_M obtained from Eq. (12) vary from 0.94 to 0.90 for the range of depths cited above. This predicted variation is not confirmed experimentally, but since it is small and of the order of the magnitude of the experimental error, the agreement between experiment and the theoretical fit can be considered quite satisfactory.

4.3. The pressure-time curves[2] which yielded the value of ΔP_m used in the preceding section, also provided measurements of the time (measured from the shock front) at which the excess pressure dropped to zero during the initial bubble expansion and the time at which it returned to zero from the negative phase as the bubble proceeded to collapse. When compared with radius-time curves obtained from high speed motion pictures, these data show the non-dimensional bubble radius a_0 to be 0.62 when $\Delta p=0$. Within the precision of measurement, this value appears to be independent of charge size and depth of detonation.

The corresponding theoretical value of a_0 is obtained by solving Eq. (22) using $\gamma=1.25$ and k as given by Eq. (33). It is found that a_0 is very insensitive to variation in the depth and has values of 0.62 to 0.61 over the range $Z_0=83$ to 533 ft. This is in excellent agreement with the experimental observation of 0.62.

4.4. The positive impulse delivered in the first bubble pulse can be computed from Eqs. (26) and (26a), providing an adequate assumption can be made concerning the magnitude of the scale factors L_2 and C_2. Both of these factors depend upon $\epsilon_2^{\frac{1}{3}}$, and ϵ_2 is known to be less than ϵ_1, owing to the radiation of acoustic energy associated with the emission of the bubble pulse. If period measurements are adopted as the criterion, one would expect as a first approximation that

$$(\epsilon_2/\epsilon_1)^{\frac{1}{3}}=T_2/T_1. \tag{35}$$

Experimental results give $T_2/T_1=0.72$ as an average.

Thus Eq. (26) can be rewritten

$$I/W^{\frac{1}{3}}=11.9Z_0^{-1/6}(W^{\frac{1}{3}}/R)(1-1.59k)^{\frac{1}{3}}, \tag{36}$$

γ having been set equal to 1.25 and a_0 to its average value of 0.615 as determined above; the assumption is made that to a first approximation $(a^2\dot{a})_{01}$ is equal to $(a^2\dot{a})_{02}$.

In Eq. (36), $I/W^{\frac{1}{3}}$ = reduced positive impulse (lb. sec./in.^{2} lb.$^{\frac{1}{3}}$), Z_0 = absolute hydrostatic depth (ft.), W = charge weight (lb.), R = radial distance from bubble center (ft.), and $k=0.0552Z_0^{\gamma-1}$.

A comparison of experimental values[2] of $I/W^{\frac{1}{3}}$ with those calculated from Eq. (36) is given in Table I for various depths Z_0. It will be noted that the agreement is quite satisfactory.

4.5. From Eq. (13) it is also possible to make a theoretical prediction concerning the minimum

bubble radius. Combining Eq. (13) with the expression for k, the non-dimensional minimum radius becomes

$$a_m = 0.0210 Z_0^{\frac{1}{3}}, \tag{37}$$

and the dimensional minimum radius,

$$A_m = 0.286 W^{\frac{1}{3}}, \tag{38}$$

where Z_0 = absolute hydrostatic depth (ft.), A_m = minimum radius (ft.), and W = charge weight (lb.).

Unfortunately there is no direct experimental evidence available to check Eq. (38), since the bubble minimum cannot be measured on the high speed motion pictures owing to obscuration by carbon particles, etc. left behind in the water.

V. SUMMARY

5.1. It has been demonstrated in the preceding sections that if the parameters γ, ϵ, and k are set equal to 1.25, 490 cal./g, and $0.0552 Z_0^{\gamma-1}$, respectively, the theoretical equations provide a satisfactory fit to all the available experimental data. This fact increases the utility of the theory in that it should now be possible to make reasonably accurate predictions of stationary bubble behavior under various circumstances, and the same parameters should apply to Friedman's more general theory[1] which includes effects resulting from migration and the influence of neighboring surfaces.

It should be emphasized, however, that any detailed physical interpretation of the parameters γ and k is tenuous at best. It is somewhat surprising that so satisfactory a fit to the peak pressure and impulse data can be obtained with the same parameters which fit the maximum bubble radius and period data. One would expect, for example, the true pressure-volume relationship to deviate appreciably from the ideal gas adiabatic which was used in the theoretical formulation, and the deviation would be most pronounced during the high pressure, high temperatures phase in the neighborhood of the bubble minimum.

In view of the multitude of approximations and assumptions involved, it would appear to be more rational to regard the numerical values of γ and k as parameters affording a useful fit of simplified theory to experimental results rather than as actual physical properties of the detonation products. The distinction may appear to be subtle, but it is probably significant.

VI. ACKNOWLEDGMENTS

6.1. The author wishes to express his gratitude to Dr. J. C. Decius and Dr. B. Friedman for permission to reproduce the curves of Fig. 1 and to the Underwater Explosive Research Laboratory, Woods Hole Oceanographic Institution, Woods Hole, Massachusetts where all the experimental data quoted in this report were obtained.

THE THEORETICAL SHAPE OF THE PRESSURE PULSE PRODUCED BY AN UNDERWATER EXPLOSION BUBBLE

A. R. Bryant and Ll. G. Chambers
Naval Construction Research Establishment
Rosyth, Scotland

British Contribution

1950

THE THEORETICAL SHAPE OF THE PRESSURE PULSE PRODUCED BY AN UNDERWATER EXPLOSION BUBBLE.

A. R. Bryant and Ll. G. Chambers

Naval Construction Research Establishment

1950

* * * * * * * * *

Summary.

This report presents a method whereby the actual shape of the pressure pulse produced by an underwater explosion bubble may be delineated with little labour. It is shown that a single universal curve may, with appropriate adjustments of the pressure and time scales, be made to fit reasonably closely the theoretical curves obtained by lengthy numerical integrations for a wide range of charge weights and depths. A formula for the peak pressure in the pulse and curves for the minimum bubble radius and the half-period of the pulse are given.

Introduction.

The theory developed by Taylor (reference 1) describes the oscillation and the rise of the bubble produced by an underwater explosion in terms of two simultaneous non-linear differential equations which so far have only been integrated for a very limited number of cases. In reference 2, a number of approximate solutions were developed for certain maximum and minimum values of the variables. It was found possible for instance, to derive an analytic expression for the peak pressure in the pulse produced when the bubble passes through its minimum size. The present paper extends this work by presenting an approximate method for calculating with little effort the actual shape of the pressure pulse. For convenience in actual use, the important formulae and the use of the graphs is summarised with an example, in the last section.

Theory.

If a is the non-dimensional radius of the bubble at time t, and z is its depth relative to an origin 33 feet above sea-level, the differential equations derived by Taylor are

$$\frac{4}{3}\pi a^3 z + 2\pi a^3 \dot{a}^2 + \frac{\pi}{3} a^3 \dot{z}^2 = 1 - \frac{G}{W} \qquad (1)$$

and

$$\dot{z} = -\frac{2}{a^3}\int_0^t a^3\,dt \qquad (2)$$

In these equations non-dimensional lengths are used, derived from real lengths in feet by dividing by the length scale factor $L = 10\ M^{\frac{1}{3}}$ where M is the charge weight in lb. T.N.T. (or equivalent weight of T.N.T. on an energy basis if some other explosive is considered). Non-dimensional times are converted to real times by multiplying by the unit of time $\sqrt{(L/g)}$.

In equation (1) the quantity G/W is the ratio of the energy left in the gas to the total energy of the motion and for T.N.T. it can be written.

$$G/W = ca^{-1} \qquad (3)$$

where

$$c = 0.075\ M^{\frac{1}{18}} \qquad (4)$$

Two assumptions are now made which reduce equation (1) to an equation with only one dependent variable. It is assumed first that for times fairly close to the instant when the bubble reaches its minimum size the integral in (2) may be regarded as sensibly constant at a value m which has been called the "momentum constant" since, apart from a numerical factor, it is equal to the momentum of the water in a vertical direction associated with the moving bubble.

The .....

The reason for this assumption is that near the time of the minimum radius the integrand is very small compared to its value during the large part of the oscillation when the bubble is large. Accordingly equation (2) is replaced near the time of the minimum radius by

$$\dot{z} = -\frac{2m}{a^3} \qquad (5)$$

Methods of computing m in the presence of various surfaces or in open water are described in references 2, 3, and 4. It should be realised that in what follows it does not matter whether this momentum arises solely as the result of the buoyancy forces acting on the bubble or from the attraction or repulsion exerted by rigid or free surfaces.

The second assumption made is that the term containing z in equation (1) is negligible compared to the other terms during the short period near the minimum radius when the pressure pulse is mainly produced. The reasonableness of both these assumptions is best demonstrated by comparison of the results arising from this approximate treatment with the results calculated by numerical integration of the full differential equations. This comparison will be made below.

With these two assumptions equation (1) reduces to

$$\dot{a} = \left[\frac{1}{2\pi a^3}\left(1 - ca^{-4} - \frac{4\pi m^2}{3a^3}\right)\right]^{\frac{1}{2}} \qquad (6)$$

The minimum radius a_1 follows at once from (6) by setting the quantity under the square root equal to zero, giving

$$\frac{3}{4\pi} a_1^3 \left(1 - ca_1^{-4}\right) = m^2 \qquad (7)$$

Equation (7) is not easily solved by successive approximations. Moreover, since it contains the parameter c which depends on charge weight, and the momentum constant m it is not easy to portray it graphically. However it is shown in Appendix 1 that by a suitable change of variables a universal minimum radius curve may be plotted. Such a curve has been plotted in Figure 1.

The pressure pulse.

In the Bernoulli equation for the excess pressure p in the water the term falling off as the inverse first power of the distance will predominate over other terms with higher inverse powers except quite close to the bubble. At a distance r from the centre of the bubble this term is

$$p = \frac{1}{r}\frac{d}{dt}\left(a^2\dot{a}\right)$$

Using (6) in this expression, and after some reduction, we get

$$rp = \frac{1}{4\pi a^2}\left[1 - \tfrac{1}{2}ca^{-4} + \frac{8\pi m^2}{3a^3}\right] \qquad (8)$$

Thus p is given by equation (8) in terms of the radius a with c and m as parameters. As it stands (8) is of little use since we have no analytic expression for a in terms of the time t. However, it may be shown that the maximum pressure arises at the instant of the minimum radius and by substituting from (7) into (8) we get the following expression for the maximum pressure p_m.

$$rp_m = \frac{1}{4\pi a_1^2}\left(1 - \tfrac{1}{4}ca_1^{-4}\right) \qquad (9)$$

(It is convenient to have the pressure expressed in lb./in.^{2} and the distance in feet and this will result if the quantity on the right hand side of (9) is multiplied by $43.4\ M^{\frac{1}{3}}$).

The above formulae were derived in reference 2 and are repeated here for convenience.

In order to make use of (8) to obtain the shape of the pressure pulse as well as its peak value it is necessary to obtain the radius a as a function of time t, i.e., it is necessary to integrate (6) in the neighbourhood of the minimum radius. There seems no simple way, either of integrating (6) by expansion in series, or of plotting or tabulating the resulting solutions

over .....

over a large enough range of the two parameters to enable interpolation to be carried out. However a lucky guess showed that the variety of pressure - time curves resulting from (6) and (8) could be reduced with fair approximation to a single universal curve by suitable adjustments of pressure and time scales. The process by which this is achieved is described below.

A value of c = 0.10 corresponding to a charge of 100 lb. was selected as a useful starting point. Equation (6) was then integrated numerically, as described in Appendix 2, for the following values of m, viz., $10^{n}m$ = 0, 25, 64, 100, 225 and 400. For each of these values of m the pressure function given by the expression on the right of (8) was computed from the values of a and plotted against time. Inspection of these pressure time curves showed that whereas for small values of m the curves were narrow with large values of the peak pressure, for large values of m the curves were broad with low values of peak pressure. Nevertheless the curves all had a certain similarity. The experiment was therefore tried of adjusting the pressure scales in each to give the same numerical value for the peak pressure, while the time scales were adjusted to make the family of curves coincident at the point where the pressure had fallen to half its maximum value.

Thus for each of the values of the momentum constant m the quantity p/p_m was plotted against the quantity $t/t_{\frac{1}{2}}$ (the origin of the time scale being taken at the instant of minimum radius) where $t_{\frac{1}{2}}$ is the time taken by the pressure to fall from its maximum to half its peak value. It may be called conveniently the "half-period". Two such curves for the extreme cases m = 0, and m = 0.04 have been plotted in Figure 2. It was found that in the region where p/p_m is greater than about 0.2 these curves fitted each other very closely. In fact the closeness of fit is probably better than it is reasonable to expect as between pressure-time curves obtained from exact solution of equations (1) and (2), and from actual experiments. Accordingly it seems quite adequate for all practical purposes to take any one of these pressure-time curves, expressed in this manner, as a universal pressure time curve - as regards shape - for the pulse produced by the collapse and re-expansion of the explosion bubble*.

So far we have only considered one specific value of the parameter c depending on the charge weight. In Appendix 1 it is shown that these solutions may be converted into solutions for any other desired value of the charge weight by a simple linear transformation of the length and time scales and for a corresponding altered value of the momentum constant m. Since, as stated above, and demonstrated in Figure 2, change in m makes an almost negligible difference to the shape of the pressure time curve when expressed in terms of the peak pressure and the half period it follows that all solutions for other values of c and m (within reasonable limits) will lie very close to the two curves in Figure 2.

Also plotted on Figure 2 are points obtained from the full integration of Taylor's equations for four cases ranging from 1 gram 3 feet deep to 460 lb. at a depth of 60 feet. It will be observed that the approximations used in this report have not resulted in errors of more than about five per cent of the peak pressure. The agreement will become progressively worse at times longer than two and one half times the half period due to the neglect of the term in z in equation (1) which becomes more important the larger the radius. Nevertheless the differences of the order of five per cent arising due to the approximations made are a small price to pay to be able to delineate the shape of the main part of the pressure time curve for a very wide range of charge weights and depths without recourse to the very laborious integration of the full equations.

In order that Figure 2 may yield a pressure-time curve in real units it is necessary to be able to calculate the peak pressure p_m and the half period $t_{\frac{1}{2}}$ - preferably in real units. By using Figure 1 to get a_1 and inserting in equation (9) the peak pressure may be easily obtained. The values of $t_{\frac{1}{2}}$ obtained from the numerical integrations mentioned above have been collected and plotted as a function of the momentum constant m. As explained in Appendix 1 this curve may now be made applicable to all values of the parameter c (and hence to all values of the charge weight) by relabelling the abscissa $m/100c^2$ and by relabelling the ordinates $t_{\frac{1}{2}}/(10c)^{\frac{10}{3}}$. However, this latter quantity can be converted to real times by multiplying $t_{\frac{1}{2}}$ by the time scale factor $\sqrt{(10\,M^{\frac{1}{3}}/g)}$. Thus the ordinates of this graph may also be labelled $4.67\ T_{\frac{1}{2}}/M^{1/3}$. These values of the half period have been plotted in Figure 3 (after a further change of scale length to remove the numerical factor 4.67) using open circles. Also plotted are four values obtained from the full integration of Taylor's equations. It will be seen that except for large values of m the agreement between the more exact values and those obtained by the approximations of this report are very close. Accordingly the curve drawn in Figure 3 may be regarded as a universal curve for obtaining the half period of the bubble pressure pulse.

The .....

* Since the equation of radial motion (8) is symetrical with regard to the time of minimum radius the resulting pressure time curve is also symetrical and only one half of it is given in Figure 2.

Large values of m only arise in general for large shallow charges when large vertical migration of the bubble occurs, with considerable departure of the bubble from sphericity, and the pressure pulses produced are relatively feeble and unimportant.

The calculation of a bubble pressure pulse - Summary of formulae.

For convenience in use the relevant equations and directions for the use of the graphs in obtaining the pressure pulse to be expected from a given charge at a given depth are collected here together with a numerical example.

(i) The two parameters c and m must first be calculated. For T.N.T. and approximately for equivalent weights of other explosives on an energy basis, $c = 0.075\ M^{1/16}$ where M is the charge weight in lb. The momentum constant may be calculated from formulae in references 2, 3 and 4 for the case of a charge in open water or near various surfaces. In open water an approximate expression for m is

$$m = \frac{0.167}{z_0^{\frac{1}{2}}} \left(1 - 1.43\ c\ z_0^{\frac{1}{2}}\right)$$

where z_0 is the initial depth below a point 33 feet above sea-level, in non-dimensional units. To convert to these non-dimensional units divide all lengths by $L = 10\ M^{\frac{1}{3}}$ and all times by the unit of time $(L/g)^{\frac{1}{2}}$.

(ii) The minimum radius a_1 in non-dimensional units and its value A_1 in feet may be read off the curve in Figure 1 for the calculated value of the parameters c (or M) and m.

(iii) The peak pressure p_m in non-dimensional units is next calculated from

$$rp_m = \frac{3}{4\pi a_1^2} \left(1 - \tfrac{1}{2} c\ a_1^{-2}\right)$$

where r is the non-dimensional distance from the point to the centre of the bubble. If the distance is required in feet and the pressure in lb./sq.in. the right hand side of this expression should be multiplied by $43.4\ M^{\frac{1}{3}}$.

(iv) The half period $T_{\frac{1}{2}}$, defined as the time for the pressure to drop from its maximum to one half its maximum value, is read off the curve in Figure 3 for the particular value of the parameters c and m.

(v) Finally either of the two curves in Figure 2 may be taken as giving the pressure time curve (or strictly as half the pressure time curve since the curve is theoretically symmetrical about the time of the peak pressure). By multiplying the numerical values of the ordinates of the curve by the value of the peak pressure calculated in (iii) above and the values of the abscissae by the half period $T_{\frac{1}{2}}$ calculated in (iv) above this curve becomes the theoretical pressure time curve in absolute units.

As an example consider a charge of 200 lb. T.N.T. at 200 feet depth. The length scale factor L = 37.5 feet and c = 0.1046. The non-dimensional depth is thus 233/37.5 = 6.21 = z_0. From (i) above the value of m for open water (i.e. in the absence of surfaces) is 0.00454. The factor $100\ c^2 = 1.094$ so that $m/100\ c^2 = 0.00415$. From Figure 1 the minimum radius $a_1 = 0.067\ (10c)^{4/3}$ so that $a_1 = 0.3713$ and the minimum radius in feet is 2.67. Inserting this value of a_1 in the formula for the peak pressure the quantity rp_m is evaluated to be 20.35. The value of $43.4\ M^{\frac{1}{3}}$ is 613 so that in feet and lb./sq.in. units the quantity rp_m is 12490. This means for example that at a distance of 20 feet the peak pressure in the pulse is approximately 624 lb./sq.in. Finally from Figure 3 the value of $T_{\frac{1}{2}}/M^{1/3}$ is seen to be 0.68 for this value of m and c, which gives $T_{\frac{1}{2}} = 4.0$ milliseconds. The shape of either half of the pressure time curve is given by Figure 2.

References.

(1) Sir Geoffrey Taylor. "The vertical motion of a spherical bubble and the pressure surrounding it".

(2) A.R. Bryant. "The behaviour of an underwater explosion bubble. Approximations based on the theory of Professor G.I. Taylor".

(3) A.R. Bryant. "A simplified theory of the effect of surfaces on the motion of the explosion bubble".

(4) A.R. Bryant. "The behaviour of an underwater explosion bubble. Further approximations".

APPENDIX A.

INTEGRATION OF EQUATION (6) FOR ALL CHARGE WEIGHTS

Let us suppose that we have integrated (6) for a specific value of the parameter c, say c = 0.10, corresponding to M = 100 lb. and for any specific value of m, say m = $\bar{m}$. Let the solution be denoted by the suffix zero, i.e., a_0, t_0 satisfy.

$$\frac{da_0}{dt_0} = \left[\frac{1}{2\pi a_0^3}\left(1 - 0.1\, a_0^{-1} - \frac{4\pi \bar{m}^{-2}}{3\, a_0^3}\right)\right]^{\frac{1}{2}} \qquad (I)$$

Now let

$$a = (10\,c)^{\frac{4}{3}}\, a_0$$
$$t = (10\,c)^{\frac{10}{3}}\, t_0 \qquad (II)$$

Then after substitution of these new variables in (I) we get

$$\frac{da}{dt} = \left[\frac{1}{2\pi a^3}\left(1 - ca^{-1} - \frac{4\pi}{3a^3}\,(100\, c^2\bar{m})^2\right)\right]^{\frac{1}{2}} \qquad (III)$$

It follows then that any solution a_0, t_0, of equation (6) for c = 0.10 is transformed by the relations (II) into a solution a, t, of equation (6) with any selected value of the parameter c but for a value of the momentum constant m = $(100\, c^2)\,\bar{m}$. It is therefore only necessary to integrate (6) for one value of c and for a range of values of m.

For example equation (7) for the minimum radius has been solved by tabulating and plotting m for a range of values of a_1 and for c = 0.10. By relabelling the ordinates $a_1/(10\,c)^{4/3}$ and the abscissae $m/100\,c^2$ the curve becomes universally applicable for all values of c and hence all values of charge weight. Since the minimum radius is more often required in feet, a further change may be made by writing $a_1 = A_1/10\,M^{\frac{1}{3}}$ where A_1 is the minumum radius in feet. Making use of the relation (4) between c and M we find that

$$\frac{a_1}{(10\,c)^{\frac{4}{3}}} = \frac{0.147\, A_1}{M^{\frac{1}{3}}}$$

so that the ordinates in Figure 1 may be also labelled with this alternative expression.

In the same way, after calculating the value of the half period $t_{\frac{1}{2}}$ for a range of values of m and for c = 0.10 it is only necessary to relabel the ordinates $t_{\frac{1}{2}}/(10\,c)^{10/3}$ and to relabel the abscissae $m/100\,c^2$ to have a curve giving $t_{\frac{1}{2}}$ against m for all values of the parameter c and charge weight. The non-dimensional half period $t_{\frac{1}{2}}$ may be converted to real units by using the time scale factor $(10\,M^{\frac{1}{3}}/g)^{\frac{1}{2}}$ so that the ordinates of such a curve may also be labelled $4.67\, T_{\frac{1}{2}}/M^{1/3}$. In plotting the curve in Figure 3 the values of $t_{\frac{1}{2}}$ have been multiplied by 1000/4.67 so as to remove the numerical factor and give $T_{\frac{1}{2}}$ in milliseconds.

It may be remarked that in Figures 1 and 3 real lengths and times have been divided by the quantity $M^{1/3}$. This result would have been expected if the usual system of non-dimensional units employed in dealing with explosive phenomena had been introduced at the start instead of the special non-dimensional units introduced by Taylor. In general the non-dimensional system usually employed in dealing with shock-wave phenomena is inapplicable to the motion and behaviour of the bubble owing to the role of gravity. However, when dealing with phenomena near the time of the minimum radius, when the internal gas pressure is the dominant factor the approximating assumptions used above remove any explicit connection with gravity effects so that this system of non-dimensional units can be effectively employed. The effect of gravity, or in other words the non-dimensional parameter z_0, is nevertheless present since it largely determines the parameter m.

APPENDIX 2.

METHOD OF NUMERICAL INTEGRATION OF THE EQUATIONS OF MOTION

Inspection of equation (6) shows that while the dependent and independent variables can easily be separated, making solution by numerical quadrature possible, the right hand side has a zero at the start of the integration (the origin of time is chosen at the instant of minimum radius). The integrand in the quadrature process is therefore infinite at the start, and the singularity is not easily removed. Accordingly the following process of numerical integration was adopted.

The first five or six values of a at equal intervals of t were computed by writing down the first few terms of a Taylor series for a near the minimum value a_1. The first and third derivatives of a with respect to t vanish at the origin. The second and fourth derivatives were calculated by repeated differentiation of the right hand side of (6), making use of the condition (7) to remove the parameter m. The following values were obtained:

$$\left.\frac{d^2a}{dt^2}\right]_{t=0} = \frac{3}{4}\, a_1^{-4}\,(1 - \tfrac{4}{7}\, c a_1^{-\frac{1}{2}})$$

$$\left.\frac{d^4a}{dt^4}\right]_{t=0} = \frac{45}{8}\, a_1^{-9}\,(1 - \tfrac{4}{7}\, c a_1^{-\frac{1}{2}})\left(1 - \frac{129}{160}\, c a_1^{-\frac{1}{2}}\right)$$

The time interval for each step was chosen so that after about six steps the term in t^4 was still small. The Taylor series was also differentiated and the resultant series evaluated at the last time interval. This value was then compared with the value of da/dt calculated directly from equation (6) with the appropriate value of a inserted to verify that neglect of higher terms in the Taylor series had caused no appreciable error.

With these starting values for a, and the corresponding values of da/dt calculated from (6) the process described on page 942 of "Interpolation and Allied Tables" for integration of differential equations of first order was carried out*. The fourth differences of da/dt were watched but at no stage was their contribution to the integration appreciable.

*"Interpolation and Allied Tables" published by H.M. Stationery Office on behalf of H.M. Nautical Almanac Office.

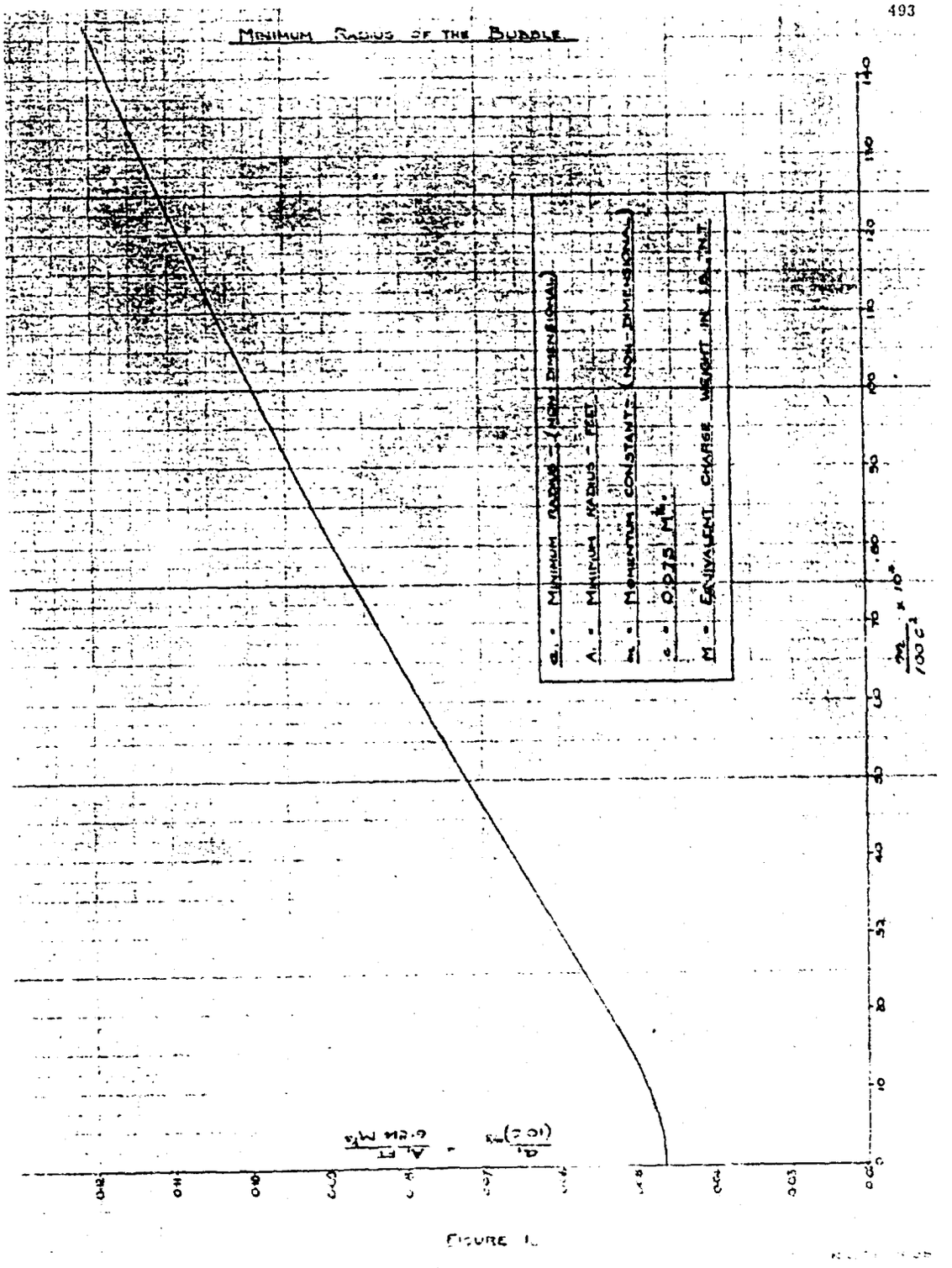
MINIMUM RADIUS OF THE BUBBLE
a. = MINIMUM RADIUS = (NON-DIMENSIONAL)
A. = MINIMUM RADIUS - FEET
n. = NEWMARK CONSTANT = (NON-DIMENSIONAL)
= 0.975 M.
M. = EQUIVALENT CHARGE WEIGHT IN LB. TNT

FIGURE 1.

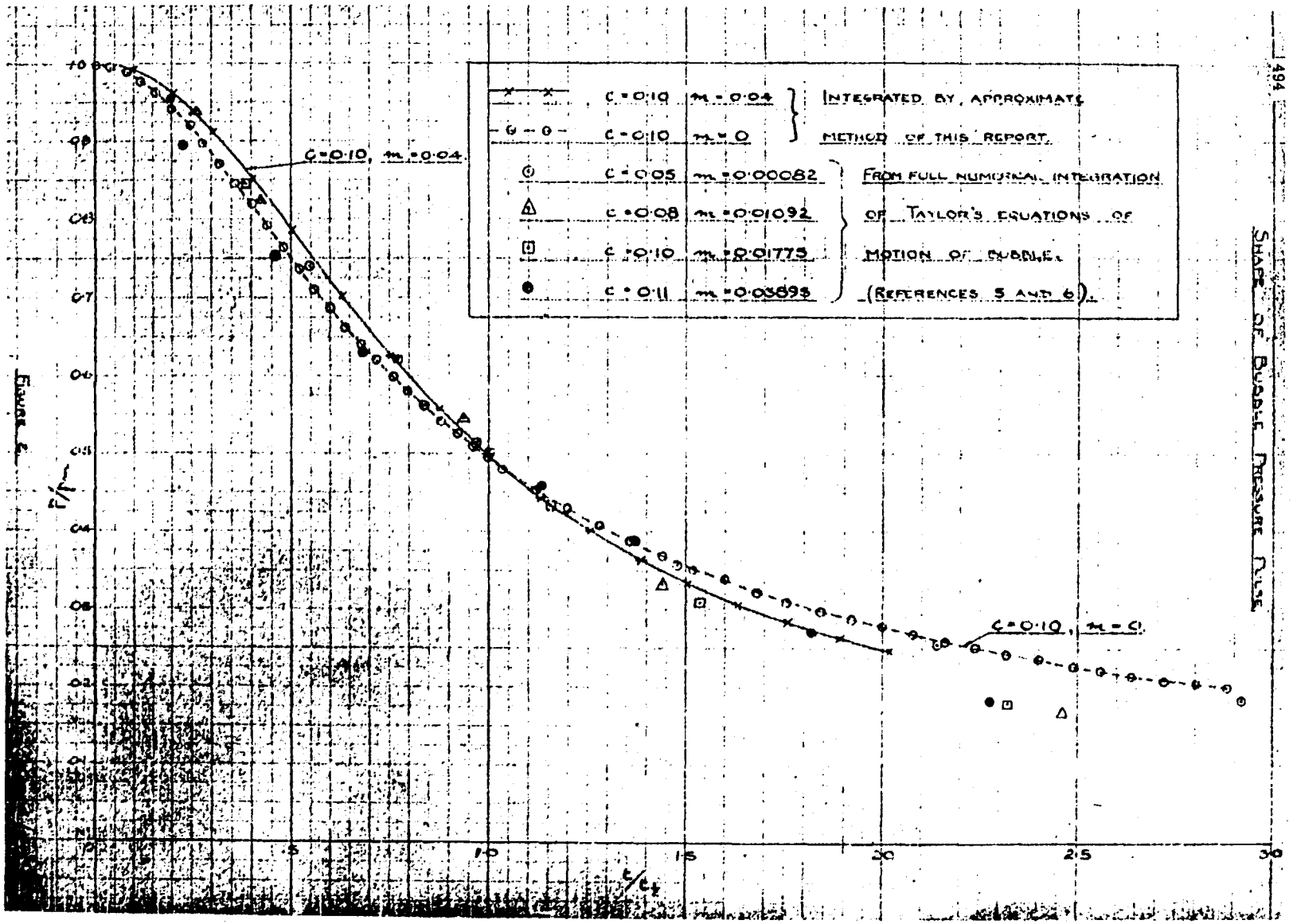

Figure 6

SHAPE OF BUBBLE PRESSURE PULSE

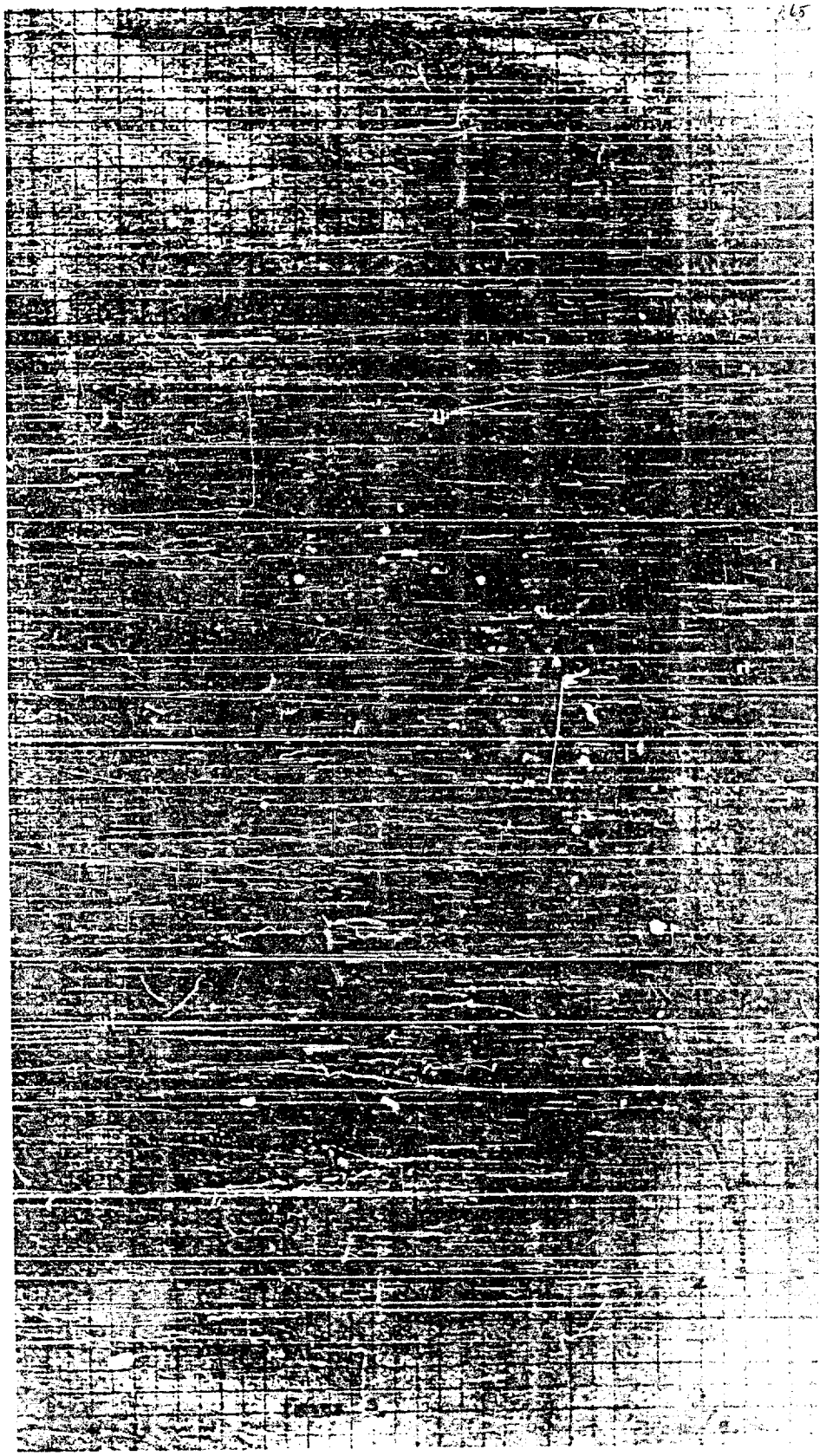

THE OSCILLATION OF THE GAS-BUBBLE FORMED BY A DETONATOR EXPLODING UNDERWATER
DETAILED COMPARISON OF THEORY WITH EXPERIMENT

H. N. V. Temperley
Admiralty Undex Works, Rosyth, Scotland

British Contribution

March 1944

THE OSCILLATION OF THE GAS-BUBBLE FORMED BY A DETONATOR EXPLODING UNDERWATER. DETAILED COMPARISON OF THEORY WITH EXPERIMENT

H. N. V. Temperley

March 1944

* * * * * * * * *

Summary.

The discussion of the behaviour of gas-bubbles from large charges has been extended to detonators, for which we possess the much more detailed evidence given by actual photographs of the bubbles. Calculations have therefore been made for the representative case of a gram charge of T.N.T. 3 feet below the surface of the water, and the results have been compared both with experiment and also with the approximate formulae developed by Herring and Bryant. The agreement of the exact calculations with the approximate formulae is found to be such that, with one exception, the latter can be applied to detonators even though quite a high value of Taylor's non-dimensional parameter z_0 is involved. The following quantities are compared with experiment:-

(a) The radius-time curve for the bubble: Agreement is already known to be satisfactory, except near the minima where energy is being lost in various ways.

(b) The trajectory of the centre of the bubble: Both under gravity and in the presence of a single free or rigid surface. Agreement is at any rate qualitative up to the first minimum.

(c) The shape of the bubble: Agreement is satisfactory.

(d) The behaviour of the bubble from a charge fired in contact with a steel plate: Agreement is only rough, two serious discrepancies (which may be different aspects of the fact that a steel plate can hardly be regarded as rigid for a contact charge) have been found.

(e) The behaviour of the bubble from a charge fired between two steel plates: Agreement is as good as one could reasonably expect.

Taken as a whole, the position seems to be very similar to that found for large charges. Phenomena which depend on the behaviour of the bubble near its minimum radius, (such as the minimum radius itself, or the secondary pressure-pulses) cannot be predicted, while phenomena such as the period of the bubble, and the rise or fall of its centre up to first minimum can be predicted fairly accurately.

1. *Introduction.*

Up to the present time, practically all underwater photography of the gas-bubble has been of charges not larger than a detonator. Now it is known that, unless the pressure of the atmosphere above the surface of the water can be reduced, such experiments give an indication of the behaviour to be expected if full-scale charges are fired at depths of the order of 500 feet, whereas we are most interested from a practical point of view in charges fired at depths of up to 200 feet. By working under a partial vacuum, Taylor and Davies have obtained scale models of the bubbles from charges fired at depths of this order, but the remaining work with detonators seems to lack direct application to the problem of damage to ships by explosions underneath them, and to be more of the nature of fundamental research. Up to the present time also, theory has concerned itself mostly with the behaviour of the bubble at these relatively shallow depths, which can only be inferred experimentally from a very long scaling-up of Taylor and Davies' results, or indirectly from pressure-gauge measurements on the full scale. The rather anomalous position has thus arisen that the more recent developments in the theory have not been applied

to that .....

to that region for which experimental knowledge is the most detailed, and the calculations reported upon here were put in hand in order to fill up this gap.

2. *Details of the Calculations.*

The theory used in substantially that developed by Herring N.D.R.C. Report CU - SP20 - 010) and Taylor ("Vertical motion of a spherical bubble and the pressure surround it"), who both developed formulae to allow for the effect of gravity, and of the proximity of free and rigid surfaces. The effect of dropping the assumption that the bubble remains spherical has been investigated by Shiffmann (Applied Mathematics Panel Memo. 37-5) and, in more detail, by Temperley. The theory of the bubble formed by an explosion in contact with a rigid surface was also given by Temperley. The theory of the behaviour of the bubble from a charge fired between two rigid surfaces is now published for the first time.

The calculations were all made for a detonator equivalent to one gram of T.N.T., and a total pressure of 36 feet of water, i.e., the detonator 3 feet below the surface of the water at atmospherical pressure. In Taylor's non-dimensional units, which we shall use henceforward, the values of the relevant quantities are as follows:-

Factor to convert non-dimensional lengths to feet (L) = 2.2 feet

Factor to convert non-dimensional times to seconds (T) = .261 second

Non-dimensional total external pressure (z_o) = 16.3

Non-dimensional initial depth below free surface (d_o) = 1.3

3. *Comparison of the Calculations with approximate theory.*

These conditions were chosen because they were thought to be fairly representative, but they do not exactly correspond with any of the previous experiments. Wright, Campbell and Senior used a No. 6 detonator, which corresponds almost exactly to 1 gram of explosive, but the depth was only 1.5 feet and not 3 feet. Lieutenant Campbell's experiments included work at 3 feet, but he used a No. 8 detonator, which is stated by him to contain about 0.7 gram of explosive. The best that we can do appears to be to compare the results of this calculation with the approximate formulae developed by Herring and Bryant. If the approximations prove satisfactory for the two cases calculated (conditions as above, effect of free surface first neglected then taken into account) we can then apply them to other cases with confidence. Without these calculations by Nautical Almanac Office we should have to extrapolate the formulae from the range z_o = 1.5 to 7.8 (over which they have been checked against the results of direct solution of the hydrodynamic equations) to the region z_o = 16, an undesirably long extrapolation. The following table accordingly gives the results of this comparison:-

Table I. .....

Table I. Comparison of N.A.O. calculations with formulae due to Herring and Bryant.

1 gram of T.N.T. at a depth of 3 feet.	Free Surface absent.		Free Surface present.	
	N.A.O.	Approximations	N.A.O.	Approximations
Period of 1st Oscillation	28.4	28.6	27.4	27.5 millisec.
Radius at first Maximum	.508	.509	.508	.509 feet
Radius at first Minimum	.055	.055	.046	.05' feet
Maximum Vertical Velocity	+ 900	+ 930	+ 820	+ 690 feet/ sec.
Rise of Bubble up to first Minimum	+.159	+.255	+.090	+.141 feet
Vertical "momentum constant" m	+ 82	+ 85	+ 43.5	+ 51 x 10^{-5}
"Pr" (max.) lbs./ sq. in. foot	+ 326	+ 325	+ 370	+ 335
I Impulse (lbs./ sq. in. foot sec.)	.134	.124	.139	.124

It will be seen that the comparison is quite satisfactory except that the figures for the rise of the bubble are not correct, the approximate formula for the rise of the bubble giving too high a result. Subject to this correction, it seems that the use of the approximate formulae in this region is quite satisfactory, as a basis of comparison with experiment. The approximate formula for the rise was arrived at empirically, and the fact that it is incorrect in no way affects the validity of the remaining approximations, which can now be used with confidence.

4. *Comparison of theory with experiment.*

The following quantities suggest themselves for this purpose:-

4.1 The radius of the bubble as a function of time: Careful comparisons have been made by Herring, (using photographs obtained by Edgerton), and by Lieutenant Campbell. Agreement is good except in the region near the minimum radius where there is reason to believe that the simple incompressible theory breaks down, due to radiation of acoustic energy and possibly to other causes also. The maximum radius and period between explosion and first minimum have also been compared with experiment by Wright, Campbell and Senior, who find excellent agreement. The minimum value of the radius is hard to obtain from the photographs, owing to the fact that motion is very fast in that neighbourhood, and also owing to the obscuring effect of debris in the water. The further history of the bubble, after the first minimum can also be accounted for satisfactorily, provided that it is assumed that there is a loss of energy at each minimum.

4.2 .....

4.2 The trajectory of the centre of the bubble: A detailed comparison is difficult unless a calculation is made in detail for each separate case. Lieutenant Campbell does not give any figures for the trajectory of the bubble in the presence of the free surface only. Wright, Campbell and Senior give a detailed trajectory, but in their work the effect of the bottom of the tank must have been appreciable, it being only about 2½ feet below the charge, (the free surface being 1½ feet above it). They find that during the first expansion phase, there is (as predicted by theory) a definite attraction of the bubble towards the free surface, repulsion setting in during the contracting stage. Using the Road Research Laboratory formulae and considering the effect of the free surface only, they find good agreement for both the total depression of the centre of the bubble up to the first minimum but not for the velocity of the centre of the bubble at this point. We have seen that the formulae used would give a numerically too large value for the rise or fall of the centre, and the close agreement actually found may be due to the mutual cancellation of this error with the fact that the effect of the bottom was neglected. The situation regarding the vertical velocity at minimum is not so clear, the agreement being very poor. Wright, Campbell and Senior give in error a theoretical maximum velocity of 64.5 feet per second compared with an observed value of 64 feet per second, the correct theoretical figure being 645 feet/second. The explanation of this large discrepancy is probably similar to that of similar disagreements found by Lieutenant Campbell discussed below.

A comparison can also be made with Lieutenant Campbell's results on the bubble near a vertical wall. The horizontal motion due to this will then be approximately independent of the vertical motion due to gravity plus the effect of the free surface and bottom. We use the data in his Table 2 and Figures 20 and 21. We need first of all an estimate of the energy given to the water by a No. 8 cap (apart from the energy appearing as a shock wave). This is best obtained from the maximum radius of the bubble, which is given by him as 5.05 inches (average) which corresponds almost exactly to the figure to be expected for 0.6 gram of T.N.T. In the cases where the wall is so near that the bubble touches it before reaching its maximum radius, the maximum volume is considerably less, than in the cases where it forms a complete sphere. The reason for this is not very clear, but it is possible that energy is carried away as a compressional wave in the steel of the wall, to a greater extent than it is in the water. Anyway, theory cannot at present be applied to these cases where the bubble actually touches the walls except to the limiting one where the charge is fired in actual contact with the wall. This case will be discussed later on. We make the calculations for 0.6 gram of T.N.T. on the basis of the approximate formulae, dividing the figures for the rise of the bubble under gravity by a factor of 1.6 in order to bring the approximate formulae into line with the detailed calculations. The remaining approximations are used as they stand.

Table II. Comparison of Lieutenant Campbell's results with theory.

0.6 gram of T.N.T. 30 inches below free surface, and at various distances from rigid wall.

Distance from Wall (Inches)	Period of Oscillation (Milliseconds)		Displacement towards wall after one oscillation (Inches)		Maximum velocity of centre of bubble (feet/sec.)		Minimum radius of bubble (Inches)	
	Calculated	Observed	Calculated	Observed	Calculated	Observed	Calculated	Observed
24	24.8	25	0.7	0.5	420	40	.57	1.5
18	25.2	26	0.9	1	750	30	.68	2:0
12	25.9	26	1.3	1.5	760	70	.74	1.5
9	26.3	27	1.7	2	590	190	.97	-
6	27.9	27	2.6	3	350	140	1.53	-

It is .....

It is clear from these results that the discrepancies are due to the fact that the bubble never closes up as much as incompressible theory indicates, owing presumably to the losses of energy that seem to occur near the minimum. If the observed values for minimum radius are used instead of the calculated ones in the calculation of the maximum velocity, much better agreement is obtained. The values obtained thus are shown in brackets, but they are only very rough, as they are inversely proportional to the cube of the minimum radius, which is not known accurately.

4.3. The shape of the bubble: This can be dealt with very shortly. The calculations made by Nautical Almanac Office applying the theory developed by Temperley shows that (contrary to what was at first expected) large departures from the spherical shape might be expected to occur even for the case of a detonator 3 feet below the water. This would not occur (even if the incompressible theory were valid right up to the minimum) until a few hundredths of a millisecond before the minimum, so that it would be extremely difficult to detect experimentally. It may therefore be said that the fact that the photographs show the bubble staying very nearly spherical for several oscillations is not in disagreement with theory.

4.4. The behaviour of the bubble from a charge fired in contact with a steel plate: Photographs of the bubble from a detonator fired under these conditions were also obtained by Lieutenant Campbell. The effect of gravity on a bubble in this case was investigated theoretically by Temperley, who found that, for a bubble above a horizontal steel plate the effect of gravity should be to make the bubble become pointed during the early stage of its oscillation, and then to flatten itself against the plate just before it reaches its minimum. The photographs show that, although the bubble certainly does flatten itself against the plate, this process is fairly gradual and is spread over a considerable proportion of the oscillation, in contradiction with the theory. This discrepancy may be connected with the one already noted, that a charge fired in contact with a steel plate does not produce so large a bubble as a similar charge in mid-water. This matter seems worth further investigation, as it may have some bearing on the behaviour of a "contact" charge.

4.5. A charge fired between two steel plates, ("the bubble that splits in half"): Lieutenant Campbell investigated the effect of firing a detonator exactly mid-way between two vertical steel plates. Although the bubble rushed towards one or other of the plates unless the detonator was fairly accurately centred, it was possible to obtain two other types of behaviour. If the plates were fairly far apart, the bubble behaved very much as if they were not there at all. If they were fairly close together, the bubble divided just before the minimum into two equal halves, one of which moved rapidly towards each plate, and flattened itself against it. For the No. 8 cap, the critical distance between the plates was found to lie between 12 and 18 inches. It was decided to investigate this phenomenon mathematically, as it seemed to afford a very good opportunity of making a fairly stringent check on the whole theory of the distortion of the bubble.

We consider a bubble with its centre mid-way between two vertical rigid surfaces. We neglect the effect of gravity and of the surface of the water. A motion of a few inches parallel to the plates would not affect otion in a perpendicular direction very much. (At the time this theory was developed it was imagined that the effect of gravity in distorting the bubble would not be very large, at any rate until the first minimum is reached. As stated above, this is not quite true, but it is sufficiently nearly true for the present investigation to be valid). The method used is a modification of the original image theory due to Herring. We use spherical polar co-ordinates, and take as the θ axis the line through the centre of the bubble perpendicular to the plates. We take the profile of the bubble to be:-

$$R = a + b_2 P_2(\cos\theta) + b_4 P_4(\cos\theta) \qquad (1)$$

The odd harmonics will be absent owing to symmetry considerations.

Allowing for possible departures from the spherical shape, we assume the velocity potential expanded as a series of axial harmonics. In order that the boundary conditions at the rigid surfaces should be satisfied, we introduce an infinite series of images exactly equivalent to the compound source that represents the bubble in an infinite sea. If this proceeding were permissible, the velocity potential would take the form:-

$$\phi = \frac{A_0}{r} + \frac{A_2 P_2(\cos\theta)}{r^3} + A_0 \sum_{n=2}^{\infty} \frac{1}{(r^2 + n^2d^2 + 2nd\, r\cos\theta)^{\frac{1}{2}}} + \frac{1}{(r^2 + n^2d^2 - 2nd\, r\cos\theta)^{\frac{1}{2}}}$$

$$+ \text{ similar series for } A_2, A_4 \text{ etc.} \qquad (2)$$

Where .....

where 2d is the distance between the surfaces.

Such a velocity potential satisfied Laplace's equation and the boundary conditions at both surfaces, but is not physically permissible because it diverges. This difficulty was pointed out by Herring. It can, however, be overcome as follows:-

If we consider the region in which $r < d$, we may transform the image terms (involving spherical harmonics about the origins $\pm n d$) to series of spherical harmonics about the centre of the bubble. We then get, by well-known formulae:-

$$\phi = \frac{A_0}{r} + \frac{A_2 P_2 (\cos\theta)}{r^3} - \frac{2A_0}{d} \sum_2^\infty \frac{(1)}{(n)} + \frac{2A_0 r^2 P_2 (\cos\theta)}{d^3} \sum_2^\infty \frac{(1)}{(n^3)}$$

+ similar series.

We now strike out the terms which vary with the time only, such as $\frac{A_0}{d}$, $\frac{A_2}{d^3}$ etc., as we can always subtract any term depending on the time only from a velocity potential without altering its physical meaning. In particular, the new velocity potential will now be finite everywhere (owing to the disappearance of the terms making up the series $\Sigma \frac{1}{n}$) and will still satisfy both Laplace's equation, and the boundary condition at the rigid surfaces. This velocity potential must therefore be the appropriate one for our problem. We treat this velocity potential by writing down the conditions that the pressure and normal velocity should be continuous at the surface of the bubble $R = a + b_2 P_2 (\cos\theta) + \ldots\ldots$

The final form of the velocity potential is

$$\phi = \frac{A_0}{r} + \frac{A_2 P_2 (\cos\theta)}{r^3} + \frac{2A_0 r^2 P_2 (\cos\theta)}{d^3} \sum_2^\infty \frac{(1)}{(n^3)} + O\frac{(1)}{(d^5)} \qquad (3)$$

We notice that the perturbing term is of the order of $\frac{1}{d^3}$, so will be fairly sensitive to the distance apart of the plates. If we regard $\frac{1}{d^3}$ and b_2 as small quantities, and neglect their powers and products, we get:-

$$A_0 = a^2 \dot{a}, \frac{3A_2}{a^4} = \dot{b} + 2a b_2 + \frac{.808}{d^3} a^3 \dot{a} \qquad (4)$$

From the equation for continuity of normal velocity. Substituting these values in the expression for the pressure, we obtain finally:-

$$Pg - gz = a \ddot{a} + \frac{3}{2} \dot{a}^2 \qquad (5)$$

(We have neglected the higher order perturbing terms).

$$a \ddot{b}_2 + 3\dot{a} \dot{b}_2 - \tfrac{4}{a} b_2 + \frac{2.02}{d^3} \frac{d}{dt}\left\{a^4 \frac{da}{dt}\right\} = 0 \qquad (6)$$

Where Pg is the pressure in the bubble, and egz the total pressure in the water outside. Equation (5) is of exactly the same form as the equation for a charge in an infinite sea, showing that, to a first approximation, neither the period nor the energy of the bubble will be affected by the presence of the two rigid surfaces. (This result is due to the absence of terms involving Legendre co-efficients of odd order). We know that the effect of a single rigid surface is both to attract the bubble and to increase the period, whereas the introduction of a second rigid surface seems to cancel both effects. Indeed, we see from Lieutenant Campbell's results that for a bubble 12 inches from a single rigid surface the first oscillation takes 26 milliseconds, whereas for a bubble midway between two rigid surfaces 24 inches apart, the first oscillation takes only 23 milliseconds in agreement both with theory and with the period of a bubble right away from rigid surfaces.

Equations .....

Equations (5) and (6) have been integrated by the Nautical Almanac Office for a 1 gram charge of T.N.T. between rigid walls 18 inches and 12 inches apart. It is found that b_2 first rises to a positive maximum then diminishes and changes sign and becomes numerically large. A positive value of b_2 becoming comparable with the radius of the bubble would imply that it splits in half. The results can only be qualitatively correct, both because for such small values of d we cannot neglect the higher order perturbing terms, and also because a No. 8 cap seems to correspond more closely to a 0.6 gram charge than to a 1 gram charge. Some specimen results are as follows:-

Table III. Distortion of Bubble due to rigid walls alone compared with that due to gravity alone. 1 gram of T.N.T. 3 feet below surface.

Time (Milli-seconds)	4.9	9.7	15.4	20.9	25.2	27.7	28.3	28.6	28.7	28.8
Mean Radius of Bubble (inches)	4.78	5.83	6.11	5.54	4.27	2.63	1.80	1.03	.52	.49 minimum
b_2 (inches) due to gravity alone	-	-	-	-	- .005	- .026	- .074	- .309	Breakdown	
b_2 (inches) due to rigid walls 18" apart	- .005	- .013	0	+ .076	+ .180	+ .272	+ .282	+ .190	- .182	Break-down
b_2 (inches) due to rigid walls 12" apart	- .024	- .048	+ .037	+ .304	+ .647	+ .937	+ .948	+ .591	Breakdown	

Experimental facts. Period of Bubble in open water 23 milliseconds.

Between plates 18" apart period = 22 - 23 milliseconds. Bubble does not divide.

Between plates 12" apart bubble divides after 21 milliseconds.

Maximum radius of bubble 5.1"

As already stated, the discrepancies in period and maximum radius are due to assuming too large a value for the energy of the No. 8 caps. It will be seen that for the plates 12" apart, b_2 becomes positive and comparable with a, corresponding to splitting of the bubble, one half going to each plate, whereas for the plates 18" apart, b_2 eventually becomes negative and comparable with a, corresponding to a flattening of the bubble along the plane midway between the plates. In the actual experiment gravity acts in a direction perpendicular to the line we have taken as the θ axis, so that, by itself, it would tend to flatten the bubble along a horizontal plane perpendicular to the plates, and would thus tend to assist the splitting effect due to the plates. By the use of tesseral instead of axial harmonics one could take account of the effect of gravity and the rigid walls simultaneously, but this refinement seems hardly worth while, as we have already shown that the theory of this phenomena is in qualitative agreement with experiment.

5. *Conclusions.*

The comparison of phenomena on the detonator scale with experiment reveals very much the same sort of situation as exists for large charges. The simple theory, assuming that the bubble remains spherical

throughout .....

throughout, enables one to predict with confidance such quantities as the maximum radius, period of oscillation, and the trajectory of the centre of the bubble up to first minimum. Owing to a variety of causes, such as flattening of the bubble and dissipation of energy in various ways, phenomena which depends on the behaviour of the bubble near its minimum radius, such as the actual minimum volume and the pressure-time curve due to the oscillations of the bubble, cannot be satisfactorily predicted theoretically.

PHOTOGRAPHIC MEASUREMENTS OF THE SIZE, SHAPE AND MOVEMENT OF THE BUBBLE PRODUCED BY 1-OZ. CHARGES OF POLAR AMMON GELIGNITE DETONATED UNDERWATER AT A DEPTH OF 3 FEET

A. R. Bryant
Road Research Laboratory, London

British Contribution

June 1944

PHOTOGRAPHIC MEASUREMENTS OF THE SIZE, SHAPE AND MOVEMENT OF THE BUBBLE PRODUCED BY 1-OZ. CHARGES OF POLAR AMMON GELIGNITE DETONATED UNDERWATER AT A DEPTH OF 3 FEET

A. R. Bryant

June 1944

* * * * * * * * *

Summary.

Measurements of the size, shape and movement of the bubble produced by 1 oz. of Polar Ammon gelignite detonated at a depth of 3 feet have been obtained photographically. The measurements cover the first oscillation in detail and a number of typical photographs is included. The results are compared with calculations based on the theory of Professor G. I. Taylor, in which the effect of the free surface is also considered.

The theoretical radius-time curve agrees quite well with the observed mean radius up to the first oscillation, although owing to large energy losses the minimum radius observed is somewhat larger than the predicted value. The downward velocity of the bubble is of the same order as that calculated except very near the minimum when the very high calculated values are not attained. The bubble commences to flatten much earlier than according to the theory of Temperley, and at the minimum is roughly hemispherical with a slightly concave upper surface and a spherical lower surface, like an inverted mushroom.

The failure of the bubble to attain the predicted maximum velocity is attributed, at least in part, to the flattening of the bubble. It is shown that the vertical momentum in the water is approximately conserved if the effective mass of water moving with the bubble is taken to be a half of that displaced by a sphere whose radius equals the greatest horizontal radius of the actual bubble.

Introduction.

The purpose of the tests described here was to extend the single flash photographic technique previously used with detonators to 1-oz. charges. It was desired to compare the behaviour of the 1-oz. bubble with theoretical predictions and to provide data which would assist in interpreting experiments on damage produced by 1-oz. charges.

Experimental Method.

Single photographs of the bubble taken on stationary film were obtained at a series of times throughout the history of the bubble. The bubble appeared silhouetted against a white painted metal reflector which was illumined by a very bright flash of short duration. The flash was produced by detonating a 2 feet length of Cordtex in a glass tube filled with argon.

When photographs near the minimum were required the light flash detonator was fired by an electronic switch operated by the pressure pulse produced by the collapsing bubble, suitable time delays being obtained electrically when desired. For other photographs a rotary switch with adjustable pre-set contacts fired the main charge, tripped the camera shutter, and fired the light flash at any desired time intervals. In all cases a piezi-electric pressure gauge in the water near the bubble gave a record on a cathode-ray oscillograph from which the timing of the light flash could be measured with an accuracy of about 0.05 milliseconds. All experiments were carried out after dark and the shutter

remained .....

remained open for about 1 second.

Location of the Charge.

The charge was suspended, detonator underneath, at a depth of 9 feet in a total depth of water of 9 feet 6 inches. In most cases a rigid steel rod framework was fixed in the plane of the charge; this served as a reference framework in the photographs giving both a length scale and a fixed reference point from which the movement of the bubble could be determined as well as its size and shape.

In order to obtain a satisfactorily large image of the bubble when near its minimum, it was necessary for the camera to be about 5 feet from the charge. At this distance the field of view was a circle of about 30 inches diameter; accordingly the reference framework had to be well within the volume occupied by the bubble when large. The framework was therefore made of small enough section to produce a negligible disturbance of the bubble motion. A number of photographs were taken with no framework present, and the bubble shape and size were exactly the same as when a framework was used.

For photographs of the bubble near its maximum size the camera was 8 feet away, and the field of view about 4 feet diameter so that a more rigid framework with its members further from the centre of the bubble could be used.

Method of Measuring the Photographs.

(a) Volume of the Bubble:- It was assumed that, apart from small protuberances and needle-like projections, the bubble was symmetrical about a vertical axis through its centre. The horizontal diameter of the profile of the bubble was measured at a number of equally spaced levels along this axis of symmetry - any small asymmetrical bumps on the profile being ignored as containing a negligible volume. The squares of these diameters were then summed, the intervals being small enough to justify this.

It will be observed later that when the bubble is very close to its minimum its upper surface appears to be actually concave. This "mushrooming" of the bubble has been observed by Taylor with his "micro-scale" spark bubbles". The profile of the bubble no longer coincides with the cross-section - the profile shows only the rim of the "saucer"-like depression at the top of the bubble. However, the bubble is not completely opaque and it is thought that the upper boundary of the "splash" of light coming through the centre of the bubble, which has been seen on some previous photographs, marks the lower edge of this hollow depression in the bubble. Hence an a proximate shape to the cross-section of the bubble may be sketched in and its volume computed.

The apparent diameter of a sphere viewed at a finite distance is always less than its true diameter. This difference can be allowed for quite simply from geometrical considerations and in the present experiments only amounts to 2% for the largest bubble diameters.

(b) The position of the "Centre of Gravity" of the Bubble:- The position of the "centre of gravity" of the volume occupied by the bubble was calculated by taking moments of the squares of the horizontal diameters about any convenient horizontal line. The chief error involved in determining the total displacement of the bubble lies in uncertainty as to the absolute position, relative to other objects in the photograph, of the point where the charge was detonated. Errors in setting the depth of the charge were of the order of ¼ inch and a random error of this order is inherent in every measurement of the displacement of the bubble.

(c) .....

The motion and shape of the hollow produced by an explosion in a liquid.
G. I. Taylor and R. M. Davies.

(c) The Shape Co-efficients of the Bubble:- If R be the radius vector from a point on the axis of a bubble to its surface, then a bubble of any given shape (assuming axial symmetry) may be represented by an infinite set of "shape co-efficients" as follows:-

$$R = a + b_1 P_1 (\cos\theta) + b_2 P_2 (\cos\theta) + \ldots\ldots \text{ etc.}$$

where $b_2 b_3$ etc. are here called the "shape co-efficients"

θ is the angle between the radius vector and the axis of symmetry; $\theta = 0$ is taken downward. Pn is the Legendre Polynomial of the nth order.

To a first order in small quantities, b_1 will be zero if the origin of the co-ordinates is taken at the centre of gravity. Since it was desired to compare the observed shape co-efficients with those calculated theoretically in which the origin is usually chosen so as to make b_1 always zero, the centre of gravity was chosen as the origin for measurements.

The method of measuring the co-efficients a, b_2, b_3 etc. for a given bubble outline is considered in detail in an Appendix. Briefly, the method assumes that no co-efficients higher than b_6 are necessary to express the shape observed. Radii vectores are measured for seven equally spaced values of θ, and the resulting simultaneous equations are solved for the seven co-efficients. It is sufficient justification of the method, here, to say that when the full outline given by the seven co-efficients thus calculated is drawn out it agrees with the observed outline with an error less than the uncertainty in delineating the observed outline of the bubble, even for extreme cases so far found.

(d) Accuracy of Measurement:- Length measurements can be made on the photographs within about 2 or 3%, but absolute values of the position of the bubble are probably only accurate to within about ¼ inch. Values of the velocity of displacement of the bubble are therefore subject to rather large inaccuracies, though this is somewhat reduced by drawing a smooth curve through a number of observations.

Experimental Results.

The experimental results are plotted in Figures 1 to 5. The timing of all observations near a minimum was measured in milliseconds before or after the minimum rather than in milliseconds after detonation since there was considerable variation in the value of the first period. The period varied between 74 and 80 milliseconds with an average of 77 milliseconds, and this value has been used in plotting the data in Figure 1.

The data for the second oscillation are scanty and have been put in a table which follows.

TABLE 1.

Average Second Period	Second Minimum Radius (mean)	Displacement downward at second minimum
56 milliseconds	3.8 inches	16.5 inches

Description of the Photographs.

In Figures 7, 8 and 9 a number of typical photographs of the bubble are given in each of which the bubble appears silhouetted against a white reflector. The explosive, being of a type which gives rise to no free carbon in the explosion products, resulted in a bubble which was fairly transparent so that in most photographs a splash of light appeared at the centre of the bubble where the gas-water

interface .....

interface was approximately normal to the light path between source and camera. In Figure 7a, however, it was necessary to open the camera shutter before firing the charge so that the image of the detonated charge is found as a very bright patch at the centre of the bubble.

The bubble remains very nearly spherical, apart from small excrescences on its surface, until about 10 milliseconds before the first minimum (Figure 7d). As the bubble collapses further it becomes flattened, but in such a way that the lower half of the bubble remains very roughly hemispherical (Figures 7e, f, 8a, b, c). In Figure 8b the bubble is nearly hemispherical with a flat top, while in 8c the flat top has become concave so that the bubble resembles an inverted mushroom. During the later stages of collapse the needle-like projections have become more accentuated relative to the bubble as a whole, and appear to be slightly more marked on the lower surface. The shape of the bubble at the minimum is somewhat obscure, perhaps owing to the relatively large duration of the light flash - about 100 microseconds. The asymmetrical lobe on the left of the bubble in Figures 8d and e is probably due to a perturbation of the bubble when large since in these cases the charge was fired to the left of the centre of the framework. The framework in these was relatively stiff, and was made of channel iron; the bubble when large enveloped the left hand member of the framework. In all other photographs at the minimum no asymmetry was found.

That the bubble is moving downwards may be inferred from the shape of the horizontal cross wires nearest to the bubble seen in Figures 8d and e. These wires were terminated by stretched springs designed to keep them taut when the inward rush of water pilled in the sides of the framework. In practice the transverse pressure exerted on the wires by the moving water displaced them very considerably. The actual shape of the wires is determined by the past history of the water velocity in its neighbourhood, and it is clear from their shape in Figures 8d and e that the motion has been mainly radially inward, but with a velocity vertically downwards superimposed on this flow in the immediate neighbourhood of the bubble.

In all the photographs near the minimum there appears to be a region just above the bubble where the water scatters the light rather than transmitting it in the normal manner. In Figure 8e, for example, the intensely bright line of light produced by the detonated Cordtex appears to be interrupted by this region; the wire in Figure 8e becomes almost, if not quite, invisible when passing through this region. It is suggested that this is evidence of a "wake" in the rear of the moving bubble. Perhaps this region is filled with many small eddies and fine bubbles.

After the minimum the bubble expands somewhat irregularly - Figures 8f, 9a, b and c. Its lower surface shows small protuberances, but not the long needles which are such a prominent feature of the lower surface before the minimum. The upper surface of the bubble, however, shows a very marked array of approximately radial streamers or "whiskers" which appear to be long trials of bubbles. The length of these "whiskers" is of considerable interest; in Figure 9a they occupy water on either side of the bubble which in Figure 8e was quite clear and free from such bubbles. It seems somewhat unlikely that these "whiskers" have actually been pushed out so far in advance of the main surface of the bubble. These streamers may be composed of fine bubbles of gas, actually left behind in the water by the collapsing bubble which were compressed and rendered practically invisible by the very high pressure existing in the water round the bubble when near its minimum.

The curious radial streaks of light in Figure 7e are thought to have nothing to do with the bubble. It is thought that they are produced by small white hot particles - perhaps pieces of aluminium from the detonator - projected outward at detonation. Although the solenoid which operated the camera shutter was not energized until some 15 milliseconds after detonation, it is probable that in this case the impact of the shockwave operated the rather delicately set shutter trigger. This would account for the absence of the actual flash of the detonating charge, and for the absence of any streaks near the centre of detonation. The increased intensity of these streaks towards the end of their path would be due to the increase of light-gathering power of the lens as the shutter opened. This same phenomenon has been observed on several occasions when the timing of the main light flash and thus of the actual bubble photograph differed very considerably.

Discussion .....

Discussion - Comparison with Theory.

(a) Radius - Time Curves:- In Figures 1 and 2 the mean radius of the bubble - defined as the radius of a sphere having the same volume as the bubble - is plotted against time. For comparison with experimental data, values of the radius as calculated by the Nautical Almanac Office have been plotted in Figures 1 and 2. These calculations refer to a non-dimensional depth $z_o = 7.2$, the bubble being assumed to remain spherical, and account has been taken of the presence of a free surface 0.6 units above the charge. These correspond to a 1-oz. charge with a bubble energy of 440 calories/gm. at a depth of 3 feet. The standard length for this case is 5 feet and the standard time 0.394 seconds yielding a value of 77 milliseconds for the period. This period is so close to the observed average period that the theoretical results have been plotted without any adjustments of scale.

It appears from Figure 1 that there is a discrepancy somewhere in that the periods agree while the observed maximum radius exceeds the theoretical value by about 8%. If the energy of the motion be calculated from the observed maximum radius, (assuming that the fraction of the energy left in the gas, amounting to about 15%, is the same as in the theoretical case) a figure of 550 calories/gm. is obtained. The energy calculated from the period assuming the correctness of the theory, is only 440 calories/gm.

In assessing the cause of this discrepancy it does not seem likely that the maximum radius measurement is more than 2% in error, while the measurement of the average period might be as much as 3% in error. These two might conceivably contribute an error of 15% in the energy, in the worst case where the errors act in the same direction.

It is possible that the theory of the effect of the free surface is somewhat in error for a bubble as close to the surface as this, since the theory is only an approximation which neglects cubes and higher powers of the reciprocal of the distance of the free surface. According to the approximate theory used the presence of the free surface reduces the period from 86 to 77 milliseconds in this case; a large correction which if itself in error might account for some of the discrepancy. It has also to be remembered that the effect of the rigid bottom at a distance of 6 feet 6 inches from the bubble has been neglected in the theoretical calculations. This, however, would raise the theoretical period to about 81 milliseconds and increase the size of the discrepancy.

It is further just possible that there is a considerable energy loss during the contraction stage, though most of this would have to occur while the bubble is large in order to reduce the period to such an extent. It is estimated from the ratio of the first to the second period that about 60% of the bubble energy is lost between the first and second oscillation, but it seems more likely that most of this loss occurs near the minimum when the bubble is moving most rapidly in a vertical direction. The data plotted in Figure 2 bring out the quite sharp energy loss as indicated by the much slower expansion after the minimum, than contraction before the minimum.

(b) The Minimum-Radius:- Energy Considerations:- According to the theory of a spherical bubble the minimum radius should be 2.01 inches when the energy in the gas is 81% of the total, the remaining 19% being kinetic energy in the vertical motion of the water. The observed mean radius at the minimum, based on the volume, is 2.7 inches. This puts the energy in the gas at 64%, assuming that the gas adiabatic is substantially that of the theory. If one assumes that the effective volume of water moving with the bubble is half the volume displaced (as is true for a spherical bubble and streamline motion) the kinetic energy of vertical motion works out at 1.9% of the total - taking the observed maximum velocity as about 185 ft./sec.

However, the shape of the bubble at the minimum is more nearly hemispherical with a radius of 3.9 inches (see Figure 8d). If one thus assumes that the effective volume of the water moving vertically is one half that displaced by a sphere of radius 3.9 inches the kinetic energy at the minimum works out at 5.6% of the total. (In fact the effective volume of water moving may be even greater since a hemisphere moving rapdily through water is likely to drag with it a volume of dead water lying immediately behind its flat surface in addition to the water circulating round it). This brings the energy in these two phases to about 70% of the total. It is not unreasonable to suppose, therefore, that of the observed loss of energy between the two cycles of about 60% (based on the ratio of the first and second periods) half is lost just before the minimum, the other half just after the minimum when the vertical velocity is high.

In a .....

In a recent paper G. I. Taylor and Davies ϕ have shown that a small bubble rising steadily through water tends to assume the shape of the cap of a sphere with a turbulent wake in its rear, and with a drag co-efficient of between 0.5 and 1.2. Using, thus, a drag co-efficient of 1 the energy loss by turbulence of the 1-oz. explosion bubble has been calculated up to the first minimum. The observed value of the velocity is given in Figure 5, and the maximum horizontal radius of the bubble in Table 2 below. It is found that 62% of the energy loss occurs in the last ½ millisecond before the minimum, 86% of the loss occurring in the last millisecond. The total loss, however, only amounts to about 500 calories, i.e. to about 3.7% of the total bubble energy. Since the velocity enters as the cube in this calculation, if the actual bubble velocity were double the assumed figure for the last half or one millisecond the energy loss would be about 25% of the total bubble energy. It is also possible that the drag co-efficient of the bubble is somewhat higher than unity, perhaps owing to the needle-like projections from its surface.

(c) Velocity-Time Curve. Momentum Considerations:- An attempt has been made to estimate the velocity of the bubble from the displacement-time curve, Figure 3. As was remarked above, this velocity data is only very approximate. The estimated value has been plotted in Figure 5, together with the theoretical curve.

The failure of the bubble to reach anything like the theoretical maximum velocity is very probably due to turbulence, but also in part to the change of shape of the bubble. In Table 2 are tabulated for a few times the observed values of the velocity U, the mean radius a, and the maximum horizontal radius a^1 of the actual bubble. The vertical momentum factor $2m = Ua^3$ has been tabulated in columns 5 and 6 calculated in two ways. In the fifth column the effective volume of water moving with the bubble is assumed to be half that actually displaced by the bubble; in the sixth column the volume of water moving is assumed to be half that displaced by a sphere of radius equal to the greatest horizontal radius a^1 of the bubble.

It will be seen that in the first case the calculated momentum of the water decreases rapidly as the minimum is approached, whereas in the second method of calculation (i.e. assuming the volume of water moving is half that displaced by a sphere of radius equal to the greatest horizontal radius of the bubble) the momentum appears to remain more nearly constant, as in fact it should.

TABLE 2

Vertical Velocity and Momentum Data.

Time msecs. before minimum	Vertical Velocity U (ft./sec.)	Mean Radius a (ft.)	Maximum Horizontal Radius a^1 (ft.)	Vertical Momentum Factor Ua^3	Vertical Momentum Factor $U(a^1)^3$
2.60	33	0.635	0.675	8.5	10.2
1.94	41	0.555	0.595	7.0	8.6
1.34	56	0.477	0.574	6.1	10.5
0.87	87	0.406	0.466	5.8	8.8
0.50	140	0.339	0.440	4.7	11.9
0	185	0.225	0.325	2.0	6.3

(d)

ϕ The Rate of Rise of Large Volumes of Gas in Water. G. I. Taylor and R. M. Davies.

(d) Shape Change of the Bubble:- In Figure 4 the second harmonic shape co-efficient b_2 has been plotted as a fraction of the co-efficient of zero order a up to just before the minimum. The following table includes figures for the higher order co-efficients also. It will be seen that b_1 is always small; the small shift of origin which would have to be made to make it vanish exactly should not affect the other co-efficients appreciably.

TABLE 3.

Harmonic Shape Co-efficients during Contracting Phase.

Milliseconds before first minimum	a (in.)	b_1/a	b_2/a	b_3/a	b_4/a
9.89	19.88	+.025	-.025	+.014	-.019
5.66	11.2	+.004	-.057	+.036	-.032
2.60	7.5	-.080	-.136	+.097	+.002
1.94	6.58	+.020	-.182	+.110	0
1.35	6.13	+.047	-.220	+.165	+.006
0.87	4.69	+.008	-.345	+.187	+.068
0.50	4.30	+.065	-.423	+.300	-.068
0.50	4.10	-.093	-.455	+.488	-.151.

For comparison with the observed measurements of the second harmonic shape co-efficient b_2, the value calculated by the Nautical Almanac Office using Temperley's equation has been plotted in Figure 4. Temperley's equation contains various time derivatives of the first co-efficient a, and the linear velocity U of the bubble. These values were taken from the earlier calculation in which the bubble was assumed to remain spherical; i.e. it was assumed that a and U are not perturbed by the growth of the higher shape co-efficients b_2 etc.

It will be seen that though the general form of the $b_{2/a}$ versus time curve is roughly the same experimentally as is given by the N.A.O. calculation, $b_{2/a}$ attains appreciable magnitude much earlier than in the theory. It seemed possible that this was due to actual linear velocity U being greater than the theoretical one in the early stages of collapse of the bubble. Accordingly Temperley's equation was reintegrated, using the observed value of the velocity U together with the theoretical values of the mean radius a and its derivatives. This result has also been plotted in Figure 4. It will be seen that this $b_{2/a}$ curve is now somewhat nearer the observed curve, but there is still a considerable difference. It is thought that most of this discrepancy could be due to error in the velocity-time curve used. A final check of the correctness of Temperley's equation must therefore await a more accurate determination of the velocity-time curve for the bubble.

Conclusions.

(1) During most of the first oscillation the bubble remains very nearly spherical and agrees reasonably well with Taylor's theory when allowance is made for the presence of the free surface.

(2) During the last five milliseconds before the first minimum the bubble flattens, its vertical diameter shortening, and the upper surface becomes flatter while the lower surface remains approximately hemispherical. Close to the minimum the upper surface becomes concave and the bubble resembles an inverted mushroom.

(3) .....

(3) The sign of the shape change agrees with that predicted by Temperley's theory, but the change takes place considerably earlier than in the theory. A reintegration of Temperley's equation using the observed velocity-time curve reduces this discrepancy somewhat.

(4) The downward displacement agrees reasonably well with the theory, but is somewhat less at the first minimum than the predicted value. The observed maximum velocity of 185 ft./sec. falls considerably short of the theoretical value of 890 ft./sec.

(5) This failure to reach the high velocity predicted may be partly due to turbulence, but may also be due to the flattening of the bubble.

(6) The vertical momentum in the water appears to be approximately conserved up to the minimum if it is assumed that the effective mass of water moving with the bubble is one half that displaced by a sphere of radius equal to the maximum horizontal radius of the flattened bubble.

(7) The vertical kinetic energy in the water at the minimum is estimated to be about 6% of the total energy of the motion, in contrast to the theoretical value of 19%.

(8) The energy in the gas at the minimum is estimated at 64% of the total initial energy of the motion.

(9) There is an indication of a "wake" or region of disturbed water in the rear of the downward moving bubble when near its minimum size.

(10) The bubble remains coherent for at least two complete oscillations.

Appendix .....

APPENDIX

Harmonic Analysis of Bubble Shapes.

The silhouette photographs of the bubble give profiles which in general have the shape of a cross-section through the axis of symmetry. It was desired to determine the co-efficients in the series.

$$R = a + b_1 P_1 (\cos\theta) + b_2 P_2 (\cos\theta) + \ldots\ldots \text{ etc.} \qquad (1)$$

in which R is the radius vector to the surface of the bubble from a given origin on the axis, θ the angle included between the radius vector and the axis.

As a first attempt it was decided to determine that curve in which only the first seven co-efficients were non-zero, and which fitted the observed section at seven equally spaced values of the angle θ, viz. 0°, 30°, 60°, 90°, 120°, 150° and 180°. The radii vectors R_0 ..... R_6 at these angles were measured giving seven simultaneous equations, of which a typical one is:-

$$R_n = a + b_1 P_1 (\cos\theta_n) + b_2 P_2 (\cos\theta_n) + \ldots\ldots + b_6 P_6 (\cos\theta_n)$$

$$\theta_n = n\pi/6 \qquad (2)$$

These equations were solved once and for all for the seven co-efficients in terms of the radii R_0 to R_6. The solution is given here for reference.

$$\left.\begin{aligned}
a &= .034\, r_0 + .243\, r_1 + .467\, r_2 + .256\, r_3 \\
b_1 &= .086\, r_4 + .660\, r_5 + .687\, r_6 \\
b_2 &= .152\, r_0 + .776\, r_1 - .267\, r_2 - .661\, r_3 \\
b_3 &= .237\, r_4 + .513\, r_5 - 1.364\, r_6 \\
b_4 &= .442\, r_0 - .274\, r_1 - .945\, r_2 + .777\, r_3 \\
b_5 &= .677\, r_4 - 1.173\, r_5 + .677\, r_6 \\
b_6 &= .372\, r_0 - .745\, r_1 + .745\, r_2 - .372\, r_3
\end{aligned}\right\} \qquad (3)$$

where $r_0 = \dfrac{R_0 + R_6}{2}$, $r_1 = \dfrac{R_1 + R_5}{2}$, $r_2 = \dfrac{R_2 + R_4}{2}$

$$r_3 = R_3$$

$$r_4 = \frac{R_0 - R_6}{2}, \quad r_5 = \frac{R_1 - R_5}{2}, \quad r_6 = \frac{R_2 - R_4}{2}$$

A fairly extreme example is illustrated in Figure 6. The full line is the observed cross-section of a bubble, the broken line is the curve given by the seven co-efficients as calculated by the above method. The agreement between the two curves is well within the limits imposed by the actual photographs. The above method which is the simplest that could be devised, was accordingly used in analysing all the photographs obtained.

Analytically, the ideal method of calculating any given co-efficient in the series (1) say b_n is to use the known relation

$$b_n = \frac{2n + 1}{2} \int_{\theta = 0}^{\theta = 180} R\, P_n (\cos\theta).d(\cos\theta) \qquad (4)$$

To use.....

To use this R has to be measured at a number of angles giving equally spaced values of $\cos\theta$, and the product $RP_n(\cos\theta)$ then integrated numerically. This method has the advantage that any co-efficient is given without assuming that any of the others are zero. The main disadvantage is that because of the fluctuations of $P_n(\cos\theta)$ over the range the number of radii which must be measured to give any reasonable accuracy in the numerical integration is rather large. This point is brought out in the following table in which the result of analysing the shape shown in Figure 6 by the two methods is compared. Simpson's rule was used for the numerical integration, and 9, 11 and 21 ordinates were measured.

Comparison of Methods of Shape Analysis

Co-efficient	Method			
	Equation (3)	Equation (4)		
	7 Radii	9 Radii	11 Radii	21 Radii
a	+ 4.30	+ 4.24	+ 4.24	+ 4.27
b_1	+ 0.28	+ 0.34	+ 0.35	+ 0.30
b_2	- 1.82	- 1.70	- 1.76	- 1.73
b_3	+ 1.29	+ 1.00	+ 1.13	+ 1.17
b_4	- 0.29	- 0.02	- 0.10	- 0.23
b_5	- 0.61	- 0.28	- 0.51	- 0.40
b_6	+ 0.51	+ 0.85	+ 0.9	+ 0.56

The table shows that the 7 ordinate method using equation (3) is quite adequate, at least up to b_4, and clearly involves only a third of the labour of the method using equation (4) and 21 radii vectores.

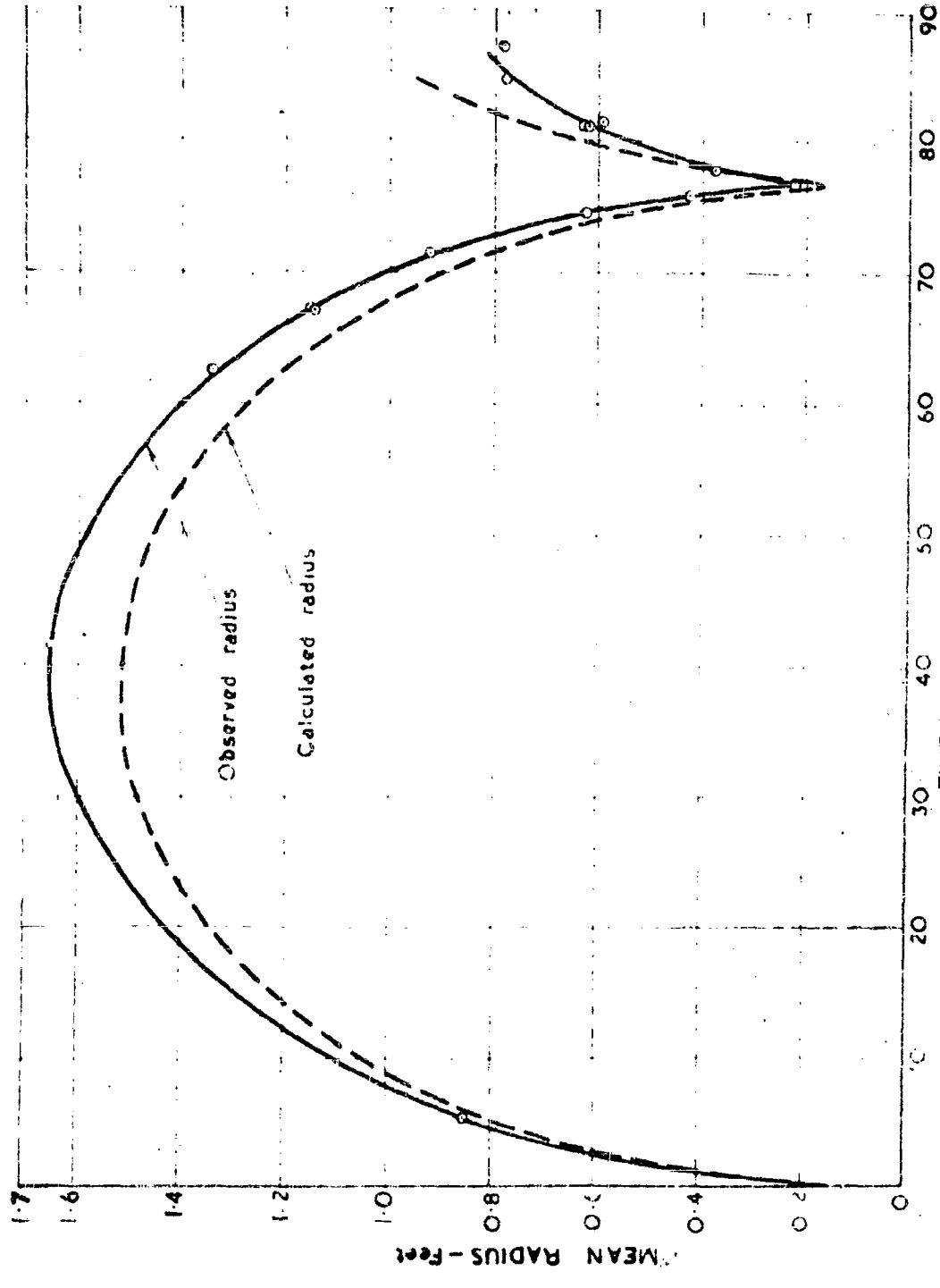

Fig. 1. RADIUS–TIME CURVE FOR BUBBLE PRODUCED BY 1oz. P.A.G. 3ft. DEEP

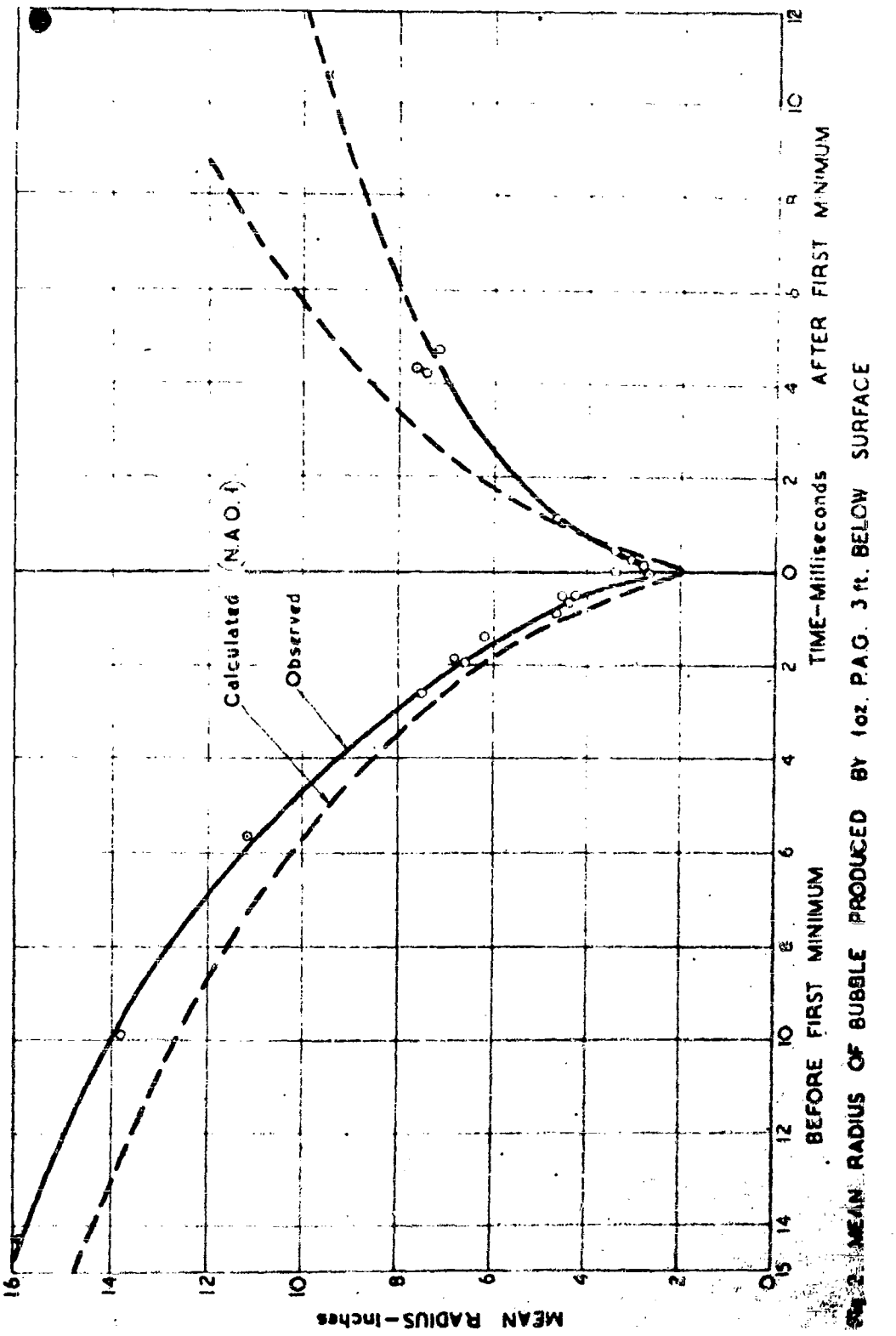

Fig. 2. MEAN RADIUS OF BUBBLE PRODUCED BY 1oz. P.A.G. 3 ft. BELOW SURFACE

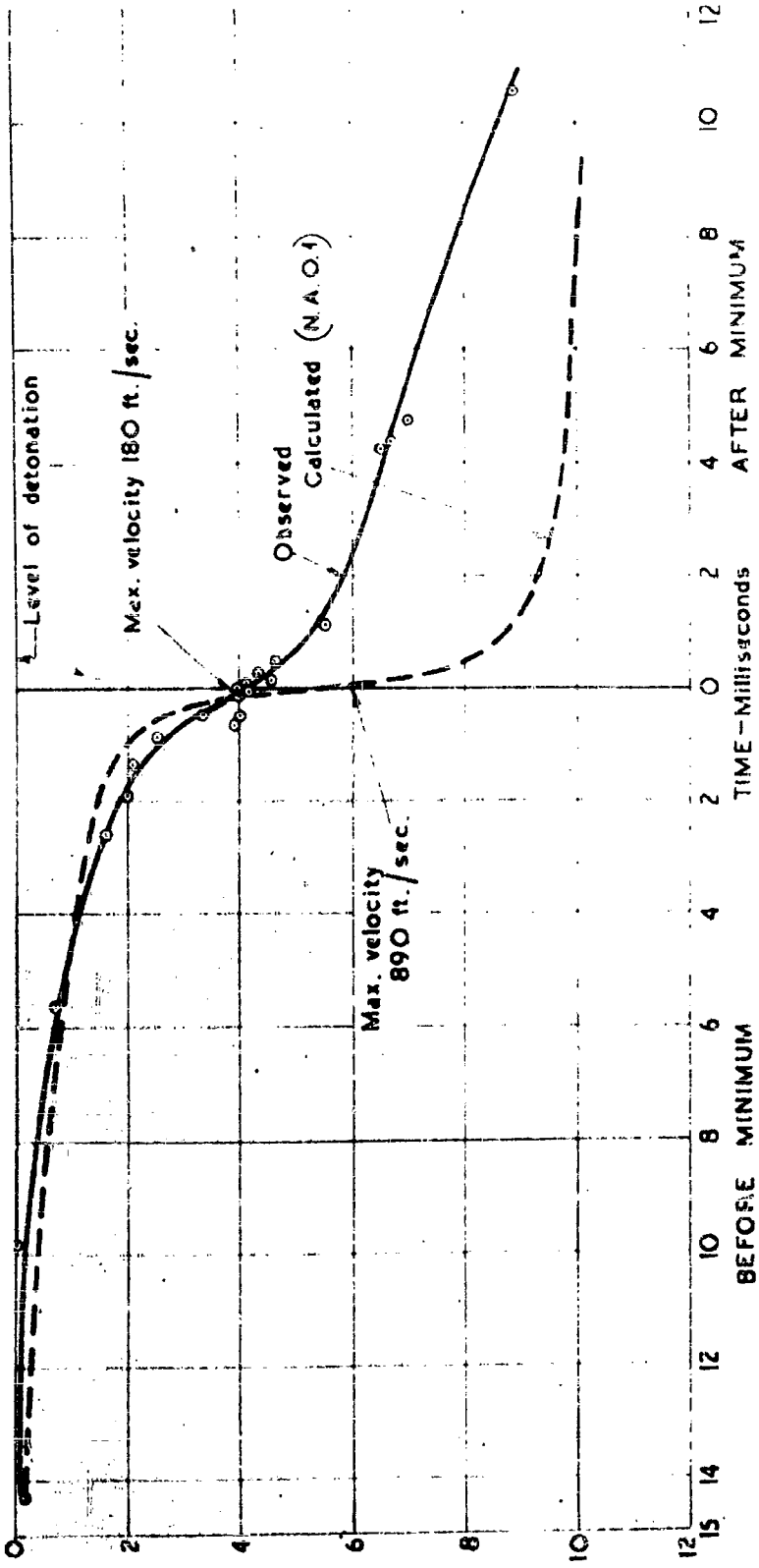

Fig. 3. VERTICAL DISPLACEMENT OF CENTRE OF GRAVITY OF BUBBLE PRODUCED BY 1oz P.A.G. DETONATED AT 3ft. DEPTH

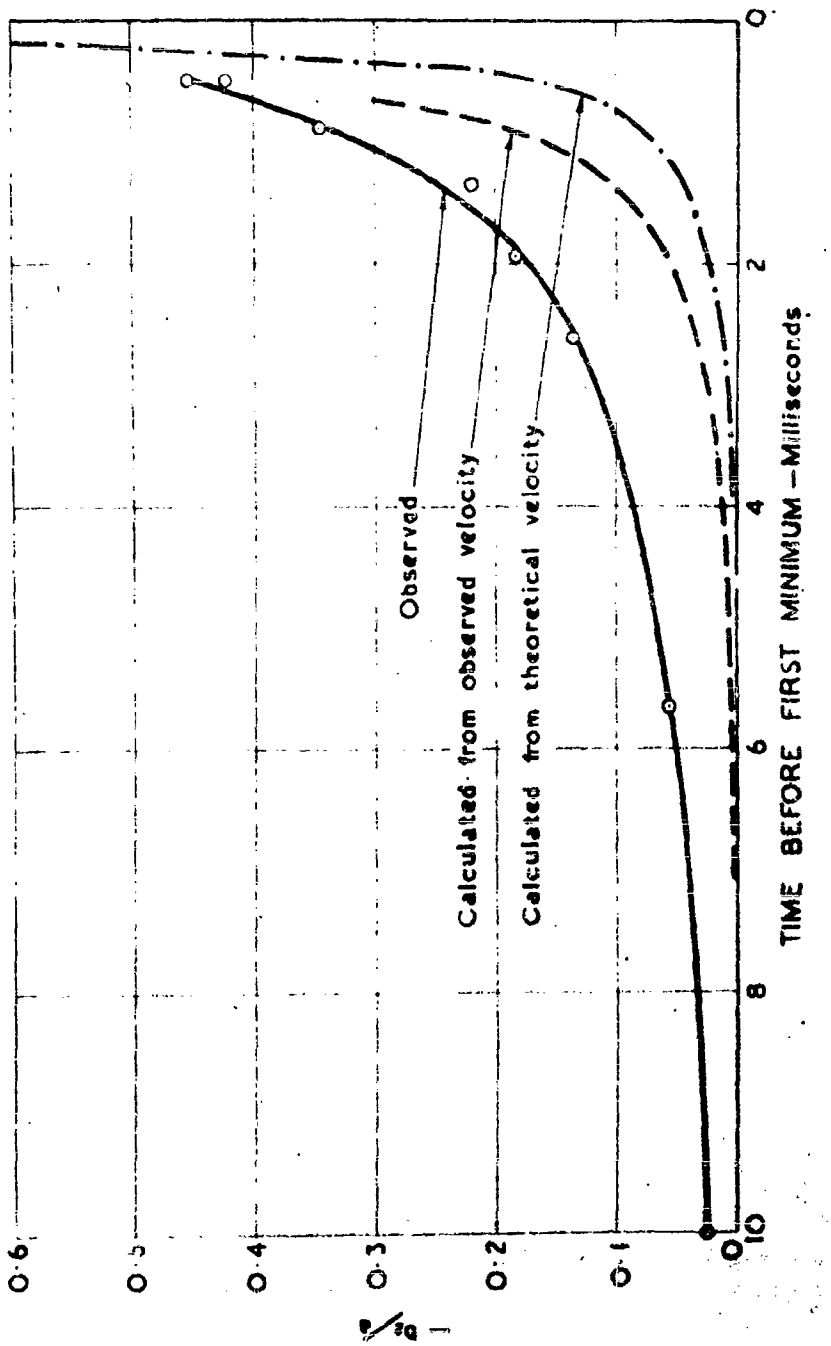

Fig. 4. OBSERVED AND CALCULATED SECOND HARMONIC SHAPE COEFFICIENT—
4oz. P.A.G. AT 3 ft. DEPTH

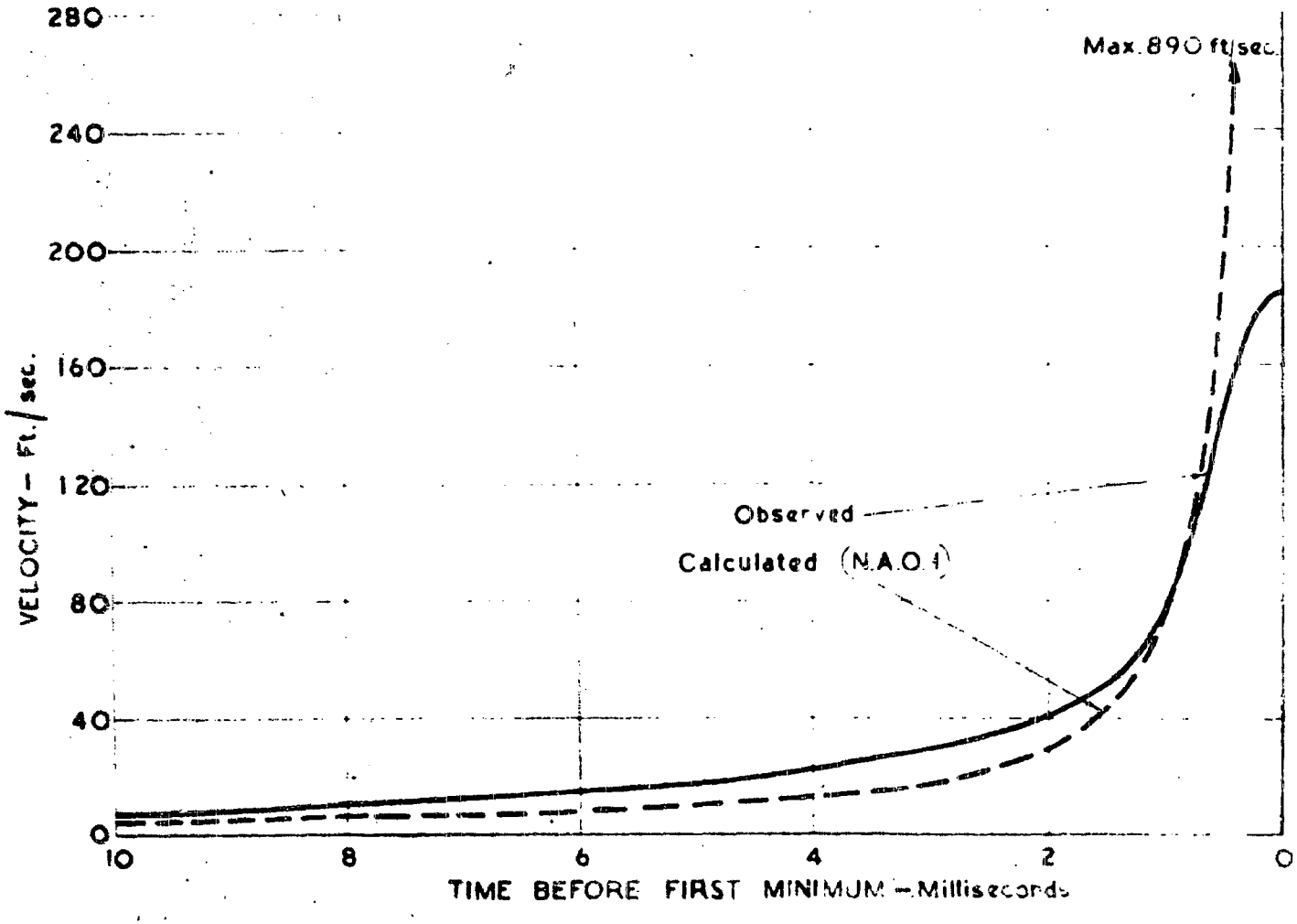

Fig. 5. VELOCITY DOWNWARDS OF BUBBLE FROM 1oz. P.A.G. AT 3 ft.

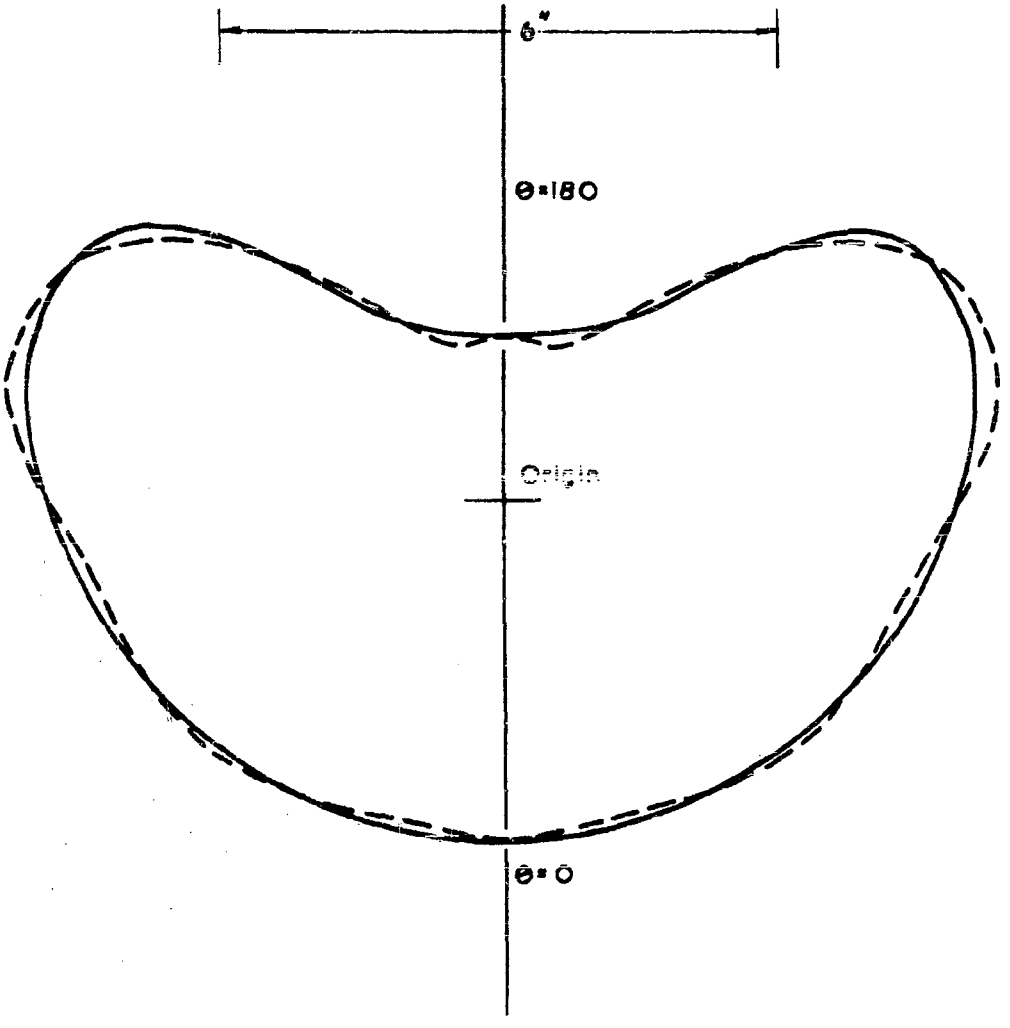

——— Observed shape — — Shape using 7 harmonic coefficients only

$$R = 4{\cdot}30 + 0{\cdot}28\ P_1(\cos\theta) - 1{\cdot}82\ P_2(\cos\theta) + 1{\cdot}29\ P_3(\cos\theta) - 0{\cdot}29\ P_4(\cos\theta) - 0{\cdot}61\ P_5(\cos\theta) + 0{\cdot}51\ P_6(\cos\theta)$$

Fig. 6. COMPARISON OF OBSERVED BUBBLE SHAPE AND BEST FITTING CURVE USING 7 HARMONIC COEFFICIENTS ONLY

(7a) 5·45 MILLISECONDS AFTER DETONATION

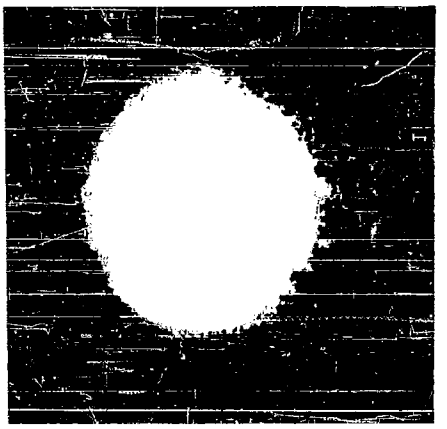

(7b) 41·50 MILLISECONDS AFTER DETONATION

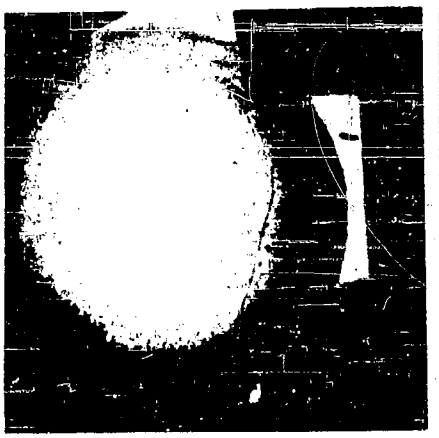

(7c) 14·30 MILLISECONDS BEFORE FIRST MINIMUM

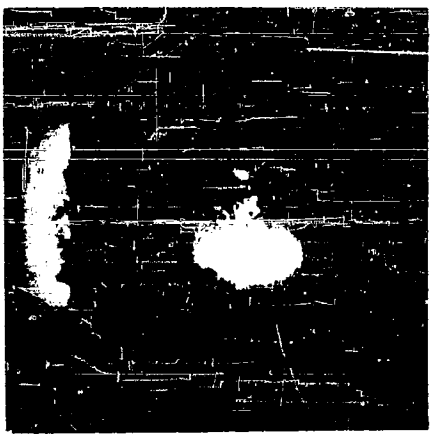

(7d) 9·90 MILLISECONDS BEFORE FIRST MINIMUM

(7e) 5·65 MILLISECONDS BEFORE FIRST MINIMUM

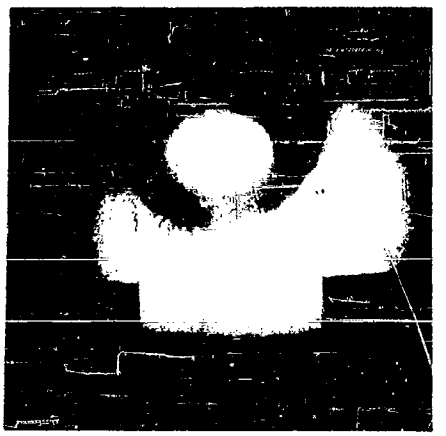

(7f) 2·60 MILLISECONDS BEFORE FIRST MINIMUM

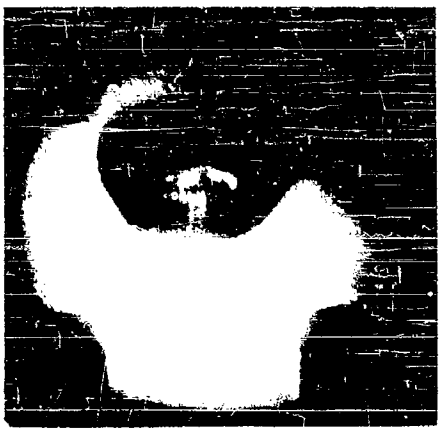

(8 a) 1·95 MILLISECONDS BEFORE FIRST MINIMUM

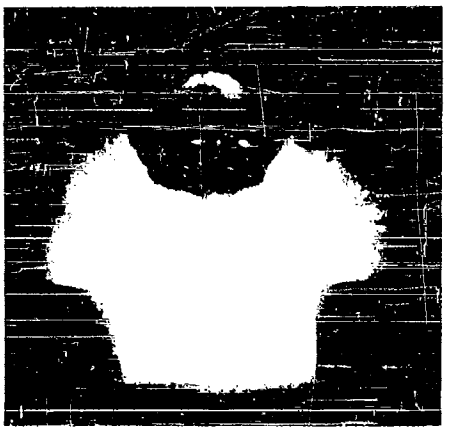

(8 b) 0·85 MILLISECONDS BEFORE FIRST MINIMUM

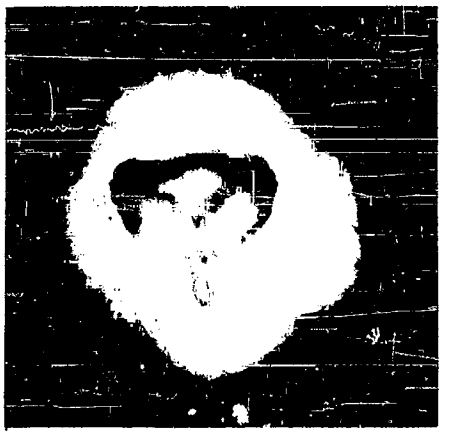

(8 c) 0·50 MILLISECONDS BEFORE FIRST MINIMUM

(8 d) AT FIRST MINIMUM

(8 e) 0·25 MILLISECONDS AFTER FIRST MINIMUM

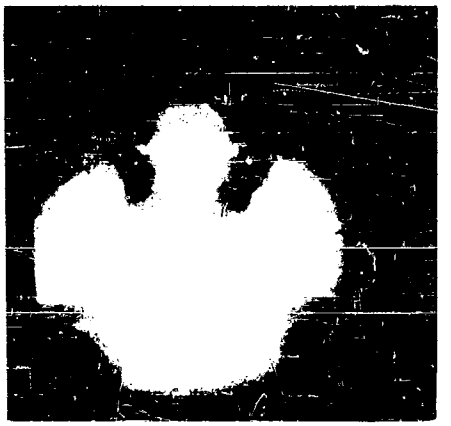

(8 f) 0·80 MILLISECONDS AFTER FIRST MINIMUM

(9a) 1·15 MILLISECONDS AFTER FIRST MINIMUM

(9b) [illegible] MILLISECONDS AFTER [illegible]

(9c) 10·60 MILLISECONDS AFTER FIRST MINIMUM

(9d) 0·15 MILLISECONDS AFTER SECOND MINIMUM

A TECHNIQUE FOR MULTIFLASH PHOTOGRAPHY OF UNDERWATER EXPLOSION PHENOMENA

A. R. Bryant and K. J. Bobin
Road Research Laboratory, London

British Contribution

August 1945

A TECHNIQUE FOR MULTIFLASH PHOTOGRAPHY OF UNDERWATER EXPLOSION PHENOMENA

A. R. Bryant and K. J. Bobin

August 1945

* * * * * * * * *

Summary.

A method is described which enables a number of photographs to be taken at one millisecond intervals of explosion bubbles produced by the detonation underwater of charges weighing about 1 oz. A total of forty to fifty pictures in two groups may be taken, the two groups being usually timed to cover the period when the bubble is near its first and second minima respectively.

Light from an Arditron discharge lamp is focused by a large metal reflector placed underwater on to the lenses of a twin drum camera housed in a watertight casing situated at the same level as the charge, thus producing a bright field of light against which the bubble appears silhouetted.

The electrical gear producing the discharges in the Arditron is housed in a laboratory near the experimental tank and connected by 80 feet of cable to the Arditron which is situated just above the water.

A description of the electrical circuits and the underwater camera is given together with a set of photographs from a typical shot.

Introduction.

In two previous papers (1) a method has been described for obtaining single flash photographs of an underwater explosion bubble produced by small charges. In order to determine the behaviour of the bubble in the neighbourhood of targets such as the box-model, however, it was necessary to devise some method of taking a succession of pictures during the course of a single explosion. This note describes apparatus developed for this purpose.

General Arrangement.

Figure 1 shows diagrammatically the experimental arrangements. A rotating twin-drum camera housed in a watertight casing, and with all controls electrically operated, is bolted on to a rigid steel framework which is lowered by crane on to the sloping side of the experimental tank and clamped in position with the camera at the required depth. Light from an Arditron discharge lamp in a housing just above the water's surface, illuminates a large curved metal reflector and is focused on to the camera lens as shown, so that the reflector appears in the photograph as a bright ground more than filling the field of view. The charge and the target are suitably placed to appear silhouetted against this reflector.

The Arditron lamp is operated stroboscopically by electrical equipment housed in a nearby laboratory, the lamp being connected to the equipment by high voltage concentric cable. Since most of the bubble shape changes and displacements occur when the bubble is small, and since these are the times when the bubble causes damage, it was decided to restrict photographs to two periods near the first and second minima respectively. The apparatus has therefore been arranged to take a total of forty to fifty pictures in two groups, one on each camera drum, the pictures in each group being spread at 1 millisecond intervals.

Multiflashing .....

Multiflashing Equipment.

The electrical equipment for producing the light flashes in the Arditron lamp is housed in the laboratory for reasons of bulk and general convenience of servicing. This has necessitated the use of a transmission line 80 feet long to connect the equipment to the lamp. It has been necessary to devise an electrical circuit which would minimise the undesirable effects on the efficient operation of the Arditron due to the total inductance of the transmission line. The circuit adopted is shown in Figure 2 and its operation is as follows:-

The reservoir condenser, which serves as the power supply, consists of 28 $\frac{1}{2}$-microfarad condensers connected in parallel and trickle charged to 8,000 volts by a neon-sign transformer and ten H176 Westinghouse rectifiers in series.

A seven-inch diameter Tufnol disc, rotating at 3,000 r.p.m., carries 20 short lengths of 4 B.A. brass studding screwed through the disc at equally spaced intervals round a circle concentric with the axis of rotation. The disc is mounted so that these lengths of studding pass in succession between two pairs of fixed points, S_1 and S_2 the clearance being about 6/1,000 inch. Thus every millisecond one of the twenty studs passes between the points S_1 and S_2. These fixed points are so arranged that there is half a millisecond interval between studs passing between them, i.e. if a stud is in line with S_1 at a certain instant then half a millisecond later a stud will pass S_2 and vice versa.

With the relay R closed, when one of the studs passes between the points S_1, the gaps at S_1 break down and the intermediate condenser, capacity 0.5 microfarad, is charged up to the voltage of the reservoir. The 8-ohm resistance limits the current in this charging stroke.

Half a millisecond later, when there is no conducting path at S_1, a stud passes between the points S_2. This gap breaks down and the intermediate condenser discharges down the concentric cable thus charging up the final condenser, capacity 0.2 microfarad. After a time of the order of 10 to 12 microseconds, when the final condenser is nearly fully charged, the voltage applied to the grid of the Arditron reaches its breakdown voltage and triggers the tube which breaks down and a discharge passes between anode and cathode.

The main requirement of the lamp is that it should produce a high intensity light flash of short duration, and it is therefore necessary that the current pulse in the lamp should be of great intensity and short duration. The final condenser is therefore housed in the lamp housing as close to the Arditron as possible, thus keeping the inductance and resistance of the discharge circuit as low as possible. It is estimated that the peak current in this discharge is from 3,000 to 5,000 amperes, and the pulse lasts for about a microsecond. This is followed by a much longer discharge due to the intermediate condenser discharging down the cable and the lamp. The 30-ohm. resistance, however, limits the current in this part of the discharge to a maximum value of 200 amperes, which decreases with a time constant of the order of 15 microseconds. Thus the pulse of current in the lamp is conjectured to be somewhat as in Figure 3.

By suitable adjustment of the lens aperture and the speed of the film it is possible to arrange that the intensity of light falling on the moving film due to the long "tail" of the current-time curve shall be less than the threshold value for the film, so that only the short peak of the light pulse registers photographically. However, in high lights, where the level of the illumination is locally very much higher than that over most of the picture, it is impossible to prevent some of this later portion of the discharge registering photographically. This causes a short "trail" of light, extending in the direction of motion of the film, on each of the high lights. The pictures obtained by this circuit are nevertheless much sharper than those obtained by discharging a condenser of the same capacity as the final condenser down the 80 feet of cable with the lamp at its far end.

The rotary spark gap isolates the lamp from the intermediate and reservoir condensers during the recharging stroke. This two-stage process is repeated every millisecond until the relay R is opened or until the voltage of the reservoir falls below a critical value. In normal operation two groups of flashes are produced, each consisting of 20 to 25 flashes, and these groups must be timed relative to the firing of the explosion with an accuracy of three or four milliseconds, so that the relay R must operate quickly and repeatedly. To this end a Post Office high speed relay has been

adapted .....

adapted, a light Tufnol arm being attached to the moving armature. 4 BA brass studs on the moving arm and on a fixed Tufnol arm serve as contacts. A gap of just over $\frac{1}{8}$th inch in the open position has been found sufficient when working at 8,000 volts to prevent the train of sparks passing across the points of the rotary gap. The total time of operation of this relay is about 10 milliseconds, although the contacts are only moving for about 3 milliseconds.

The Camera.

The underwater camera is shown diagrammatically in Figure 4; Figure 5 is a photograph of the camera removed from its watertight housing. It is, in effect, two separate drum cameras mounted side by side. This enables a sufficient number of pictures to be taken without having an abnormally large drum. It also permits the two groups of flashes to be timed solely with regard to the phenomena to be observed and without regard to the relative position of the two sets of pictures on the film.

The two 7 inch diameter duralumin drums A carrying 35 m.m. film are mounted side by side on a common spindle and driven at speeds up to 3,000 r.p.m. by a belt drive B from a 12 volt car dynamo C used as a motor. The ball races D in which runs the drum spindle are housed in a pair of brackets formed by angle iron members E welded rigidly to the bed plate F. This design combines lightness with great rigidity.

The two lenses G are Taylor Hobson "Speed Panchro" lenses with an aperture of $f/_2$ and a focal length of 58 m.ms. Between the lens and the film a single duralumin vane H, 6/1,000 inch thick, acts as a shutter and is activated by a solenoid and lever system I. The arrangement was the simplest which could be put in the available space. On the application of about 18 volts to the solenoid the shutter opens in about 15 milliseconds; on removal of the voltage the shutter closes in a similar time. Under present conditions of use this gives ample time for one shutter to close and the other to open in the intervals between the two groups of light flashes. Approximately 25 pictures 1 inch in diameter may be obtained on each drum.

Each lens and shutter is mounted separately on a shaped brass base J which may be moved through an arc of about 5° round the periphery of the drum. Thus one lens may be tilted upwards while the other may be tilted downwards. In Figure 5 the right hand lens is shown tilted downards, while the brass dust cover has been removed to show the solenoid which operates the shutter. This arrangement of tilting lenses enables two different fields of view, one above the other, to be covered, a feature which may be used to advantage when the bubble is known to be moving either upwards or downwards.

The film is held in position by simple spring clips L. The camera unit is made light-tight by a light cover K.

The camera proper is contained in a strong watertight housing which is made in two pieces. The bed plate F of the camera bolts on to a heavy rigid plate M which in turn is bolted on to the external framework holding the camera under water. The front portion of the watertight housing N is welded on to the plate M. This portion has a compartment containing the motor C and a plate glass window O, 1 inch thick, is bolted between rubber gaskets to the front of N. This window has been found to withstand the explosive effects of a 1 oz. charge detonated at distances greater than 2 feet 6 inches from it. The rear portion of the housing consists of the watertight cover P which is also bolted on to the plate M to complete the seal.

Lamp Housing.

The Arditron lamp is mounted in a large car headlamp reflector in such a way that the beam of light is concentrated roughly into a cone of about 50° semiangle. The 0.2-microfarad condenser is mounted just behind the reflector and the whole is mounted in a wooden box held just above the water surface. It has not been found necessary to use a glass plate in the water surface to prevent scattering of light by ripples.

Underwater Reflector.

The construction of the curved metal reflector in Figure 1, is shown in greater detail in Figure 6. The basic framework consists of three rows of upright angle irons A welded to three cross-

braced.....

braced longitudinal angle iron members B. To the uprights are bolted nine pieces of ¼ inch thick plywood cut to a calculated curvature and bevelled. Narrow strips of 16 gauge duralumin plating are screwed on to the plywood sections, the strips having been cut and fitted by trial.

Ideally the reflector should form part of an ellipsoid of revolution, with the lamp and camera at the two foci. This requires that the position of both lamp and camera should always be fixed in relation to the reflector, and that the lamp should operate underwater. Owing to the shape of the experimental tank these conditions are not easily satisfied over a range of operating depths. As a compromise, the present reflector has been made with sections calculated for a paraboloid of revolution with axis horizontal the lamp being operated just above the water surface. Owing to the finite size of the car headlamp reflector in which the Arditron is housed, this optical system produces a satisfactory bright background for a range of operating depths down to 5 feet, as may be seen from typical photographs in Figure 8. It will be seen from these photographs that the illumination tends to be patchy; this is due to the anticlastic curvature of the strips of duralumin which form the reflecting surface. The reflector will withstand repeated explosions of a 1 oz. charge 3 or 4 feet away.

Timing Controls.

The firing of the two groups of sparks, the opening and closing of the two shutters in the underwater camera, and the firing of the charge are performed in their correct sequence by a rotary switch carrying 6 brass sectors mounted in adjustable rotating ebonite discs. The period of the bubble motion being determined by previous oscillographic records, or by calculation, the sectors of the rotary switch are each preset to operate at the correct time, allowance being made for the known time lags in the spark relay and the shutter mechanisms.

The rotating spark gap is driven by an induction motor working off the 50-cycle mains. As the motor is practically on "no load" its speed is always very close to 3,000 r.p.m. (this has been verified by a tachometer). The speed of the drums in the underwater camera has to be adjusted to give proper spacing to the photographs, and for this purpose a remote reading electrical revolution counter has been devized whose operation is shown diagrammatically in Figures 7a and 7b.

In Figure 7a, B is the spindle whose rotational speed is required. The brass disc A carries five small equally spaced soft iron inserts C which pass in turn between the poles of a permanent magnet D causing a series of voltage pulses to be induced in the solenoid E. This pulse consists of a positive and an identical negative portion and lasts for about one twentieth of the interval between successive pulses.

Figure 7b shows the electrical circuit used to indicate the frequency of arrival of the voltage pulses produced by the solenoid on the camera. Valves V_1 and V_2 form a straight forward "flip flop" circuit in which there is normally no current flowing in the anode circuit of V_2. The arrival of a negative pulse of sufficient magnitude from the camera solenoid causes a square pulse of current to flow in the anode circuit of V_2, the duration and magnitude of this pulse being governed solely by the circuit constants and not by the shape or magnitude of the triggering pulse. At normal drum speeds the needle of the milliammeter in the anode circuit of V_2 cannot follow the individual pulses it receives but gives a deflection equal to the time average of the current passing through it. The deflection is therefore directly proportional to the frequency of the triggering pulses. The circuit shown has a response of 1 milliamp per 1,000 r.p.m. of the camera drum, linear from 500 r.p.m. up to at least 3,500 r.p.m.

V_3 is a thyratron and the associated circuit produces a very short negative pulse at the frequency of the A.C. mains, thus enabling the overall current-frequency sensitivity of the "flip-flop" circuit to be standardized just before use.

Typical Photographs.

In Figures 8 and 9 are shown some typical photographs obtained from the explosion of a single 1 oz. charge of Polar ammon gelignite at a depth of 9 feet. The interval between pictures is 1 millisecond. The group shown in Figure 8 was recorded on one drum of film and was timed to include the first bubble minimum; the pictures in Figure 9 include the second minimum. The general appearance of the bubble

is similar ....

is similar to that shown by "single-shot" photographs on stationary film given in a previous paper (1) it is clear from the present photographs that the bubble is self-luminous for a period of the order of a millisecond near its first minimum, the gas at the centre of the bubble being the first to become hot enough to glow. It now seems probable that the patch of light seen in the centre of the bubble in the "single-shot" photographs of the above mentioned paper (Figures 7d, e, f, - 8a, b, c, d, e, f, - 9a, b, c) is not light from the illuminating source passing through the bubble as suggested in that paper, but the flash produced by the self-luminous bubble at its minimum, since in obtaining these photographs the shutter was opened for a period including the first minimum.

Reference.

(1) Photographic measurements of the size, shape and movement of the bubble produced by 1 oz. charges of Polar Ammon gelignite detonated underwater at a depth of 3 feet.

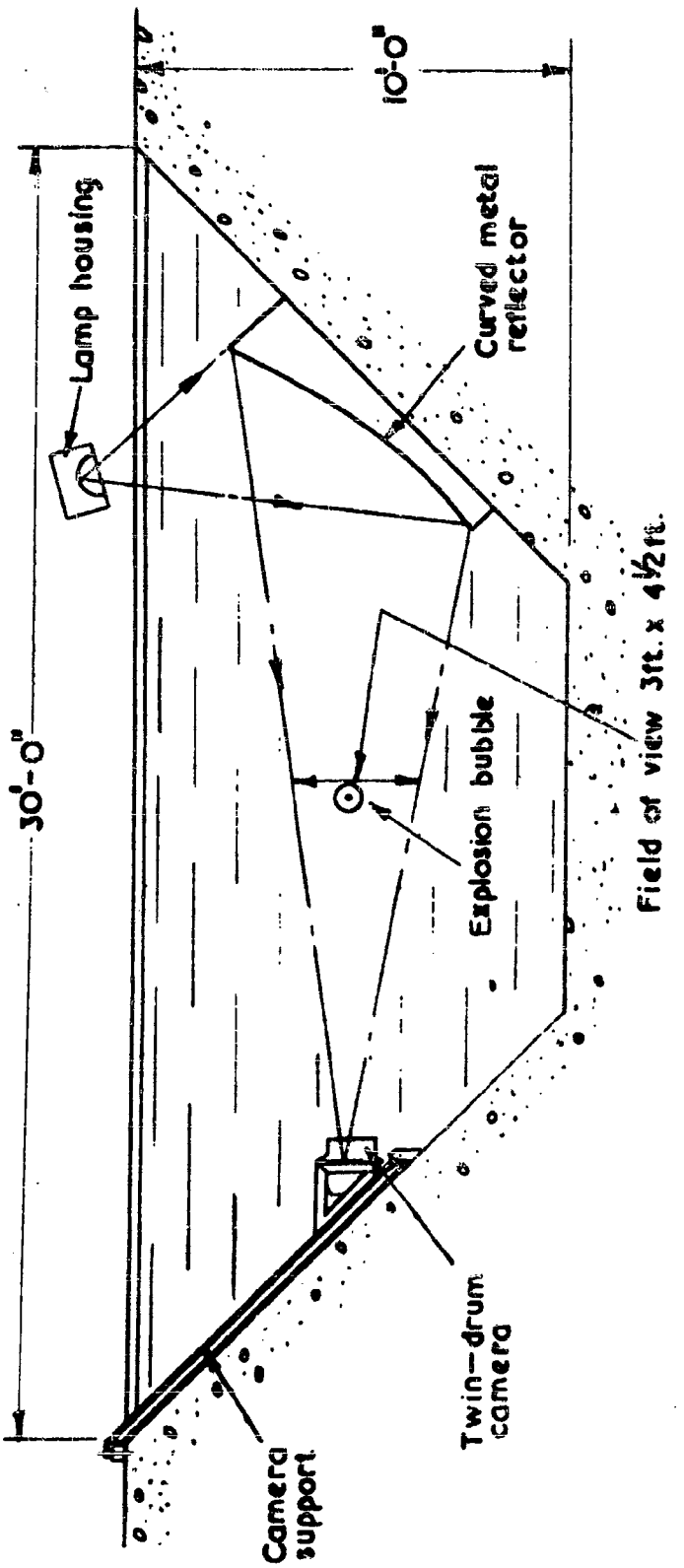

Fig1. ARRANGEMENT OF PHOTOGRAPHIC GEAR IN EXPERIMENTAL TANK

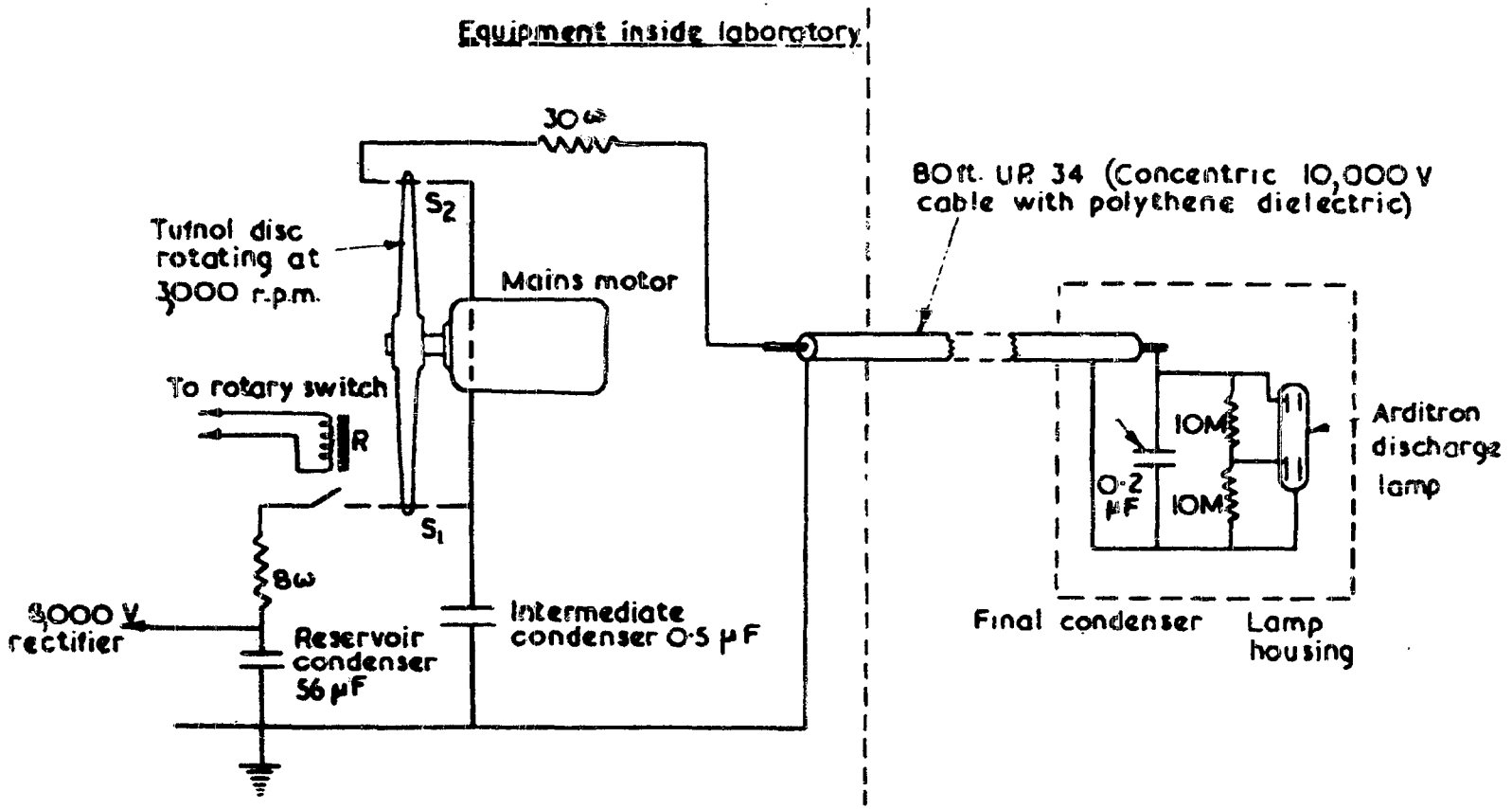

Fig. 2 "MULTIFLASHING" CIRCUIT

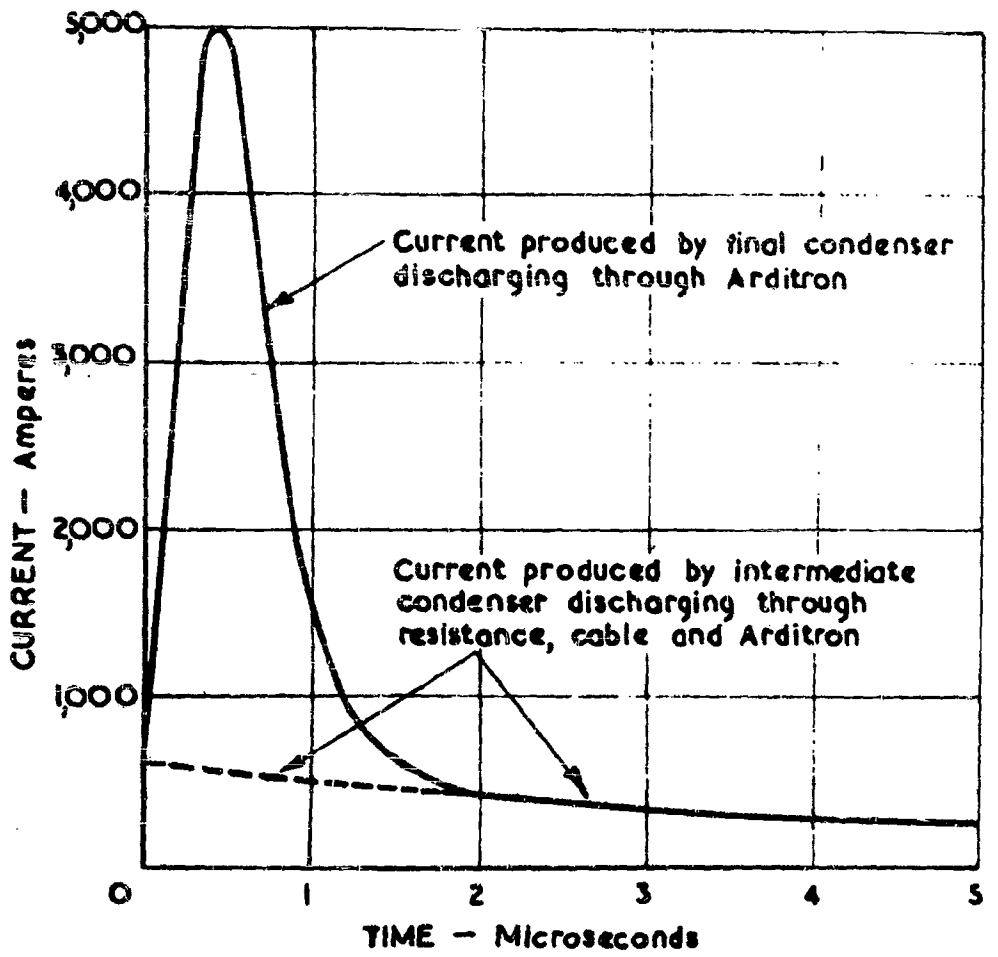

Fig.3. CONJECTURED CURRENT — TIME CURVE IN ARDITRON LAMP WITH CIRCUIT OF Fig. 2.

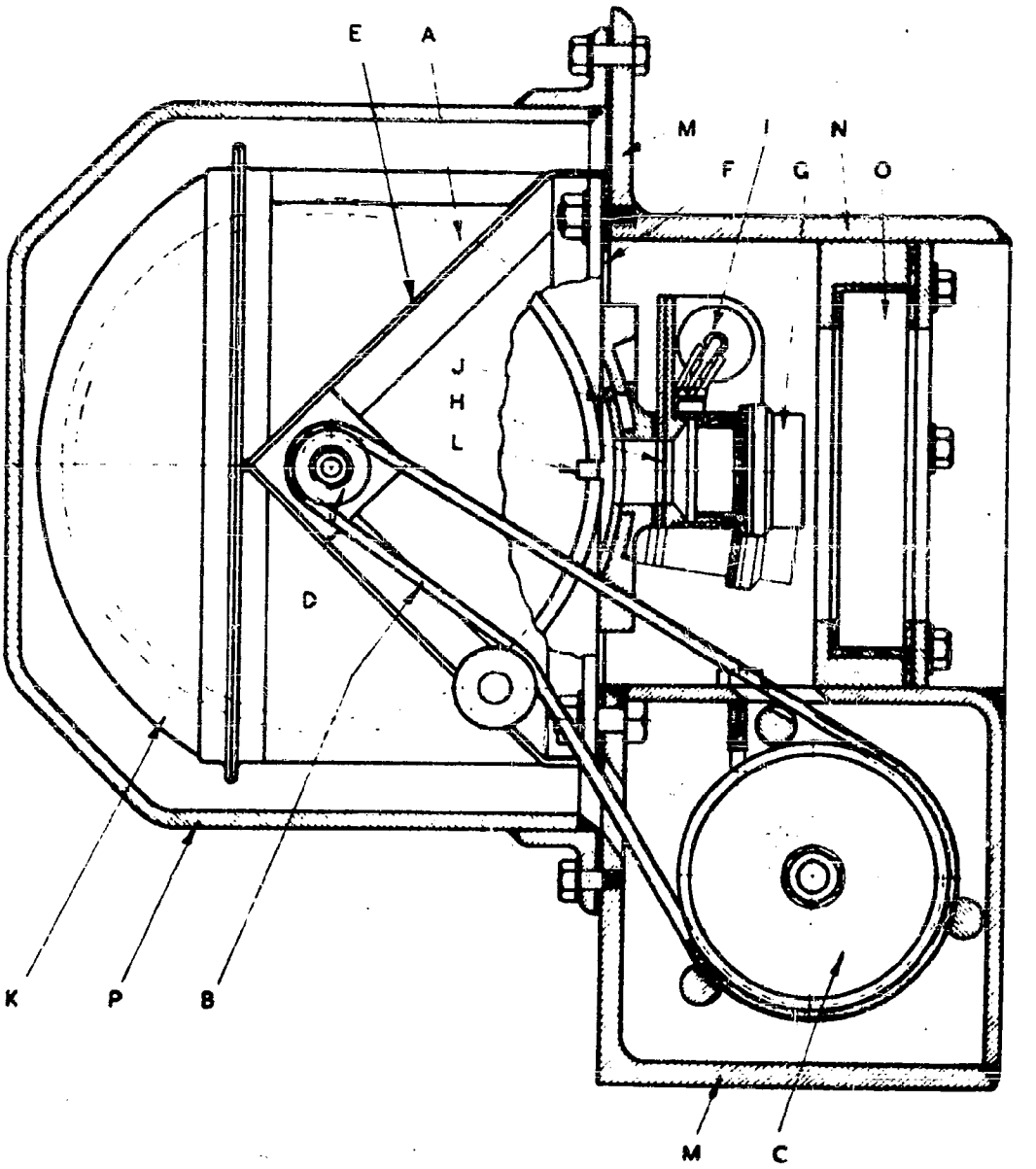

Fig.4. ARRANGEMENT OF TWIN-DRUM UNDERWATER CAMERA

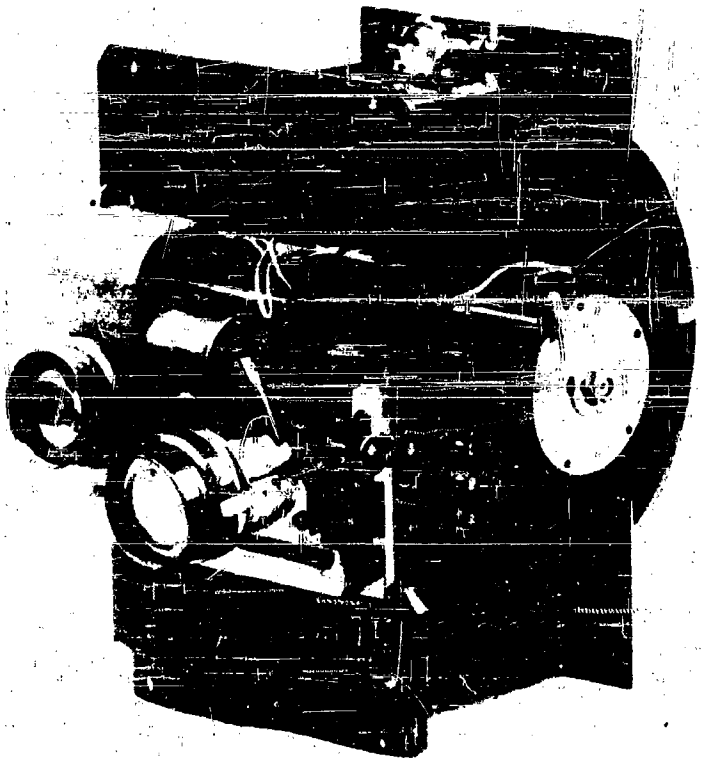

FIG. 5

Underwater Camera

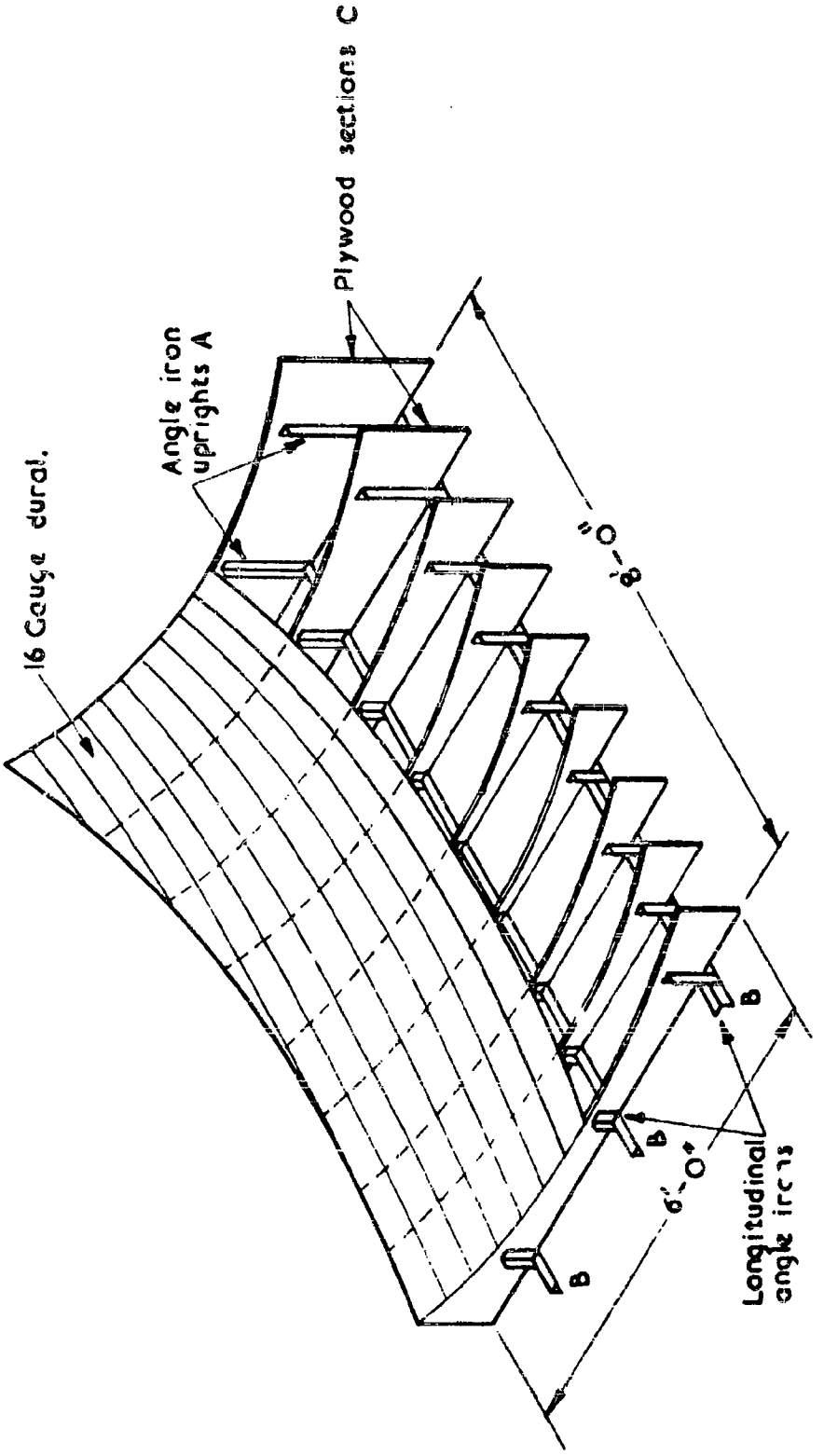

Fig.6 CONSTRUCTION OF UNDERWATER REFLECTOR

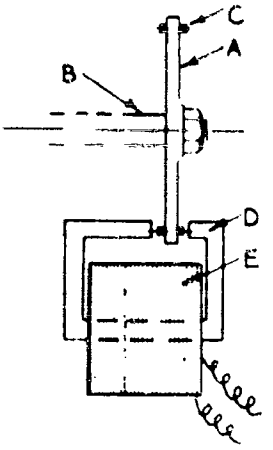

Fig 7a DRUM SPEED TIMING DEVICE

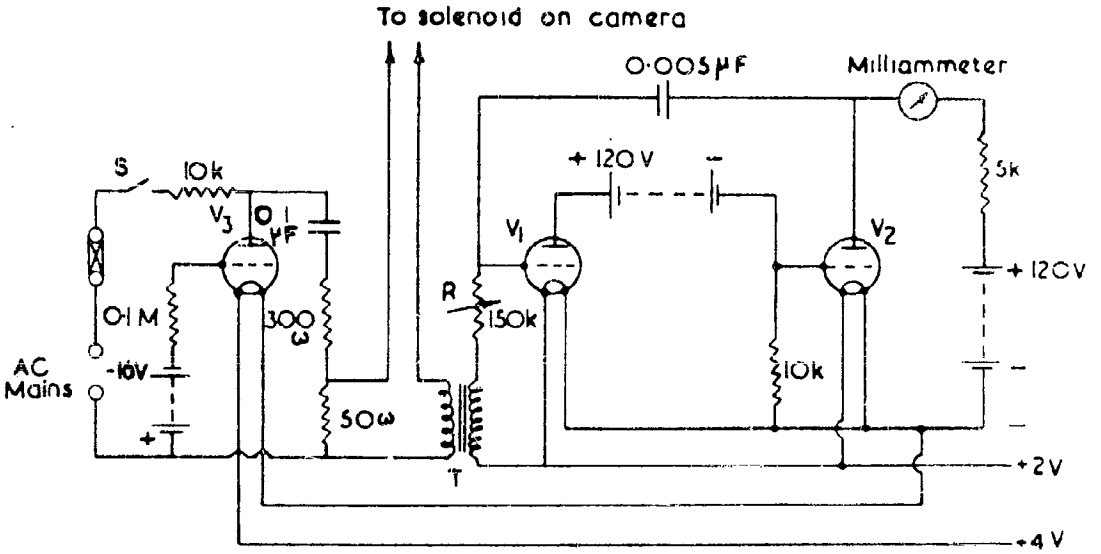

Fig 7b ELECTRICAL CIRCUIT FOR INDICATING FREQUENCY OF VOLTAGE PULSES

Fig.8. THE BUBBLE PRODUCED BY 1oz. GELIGNITE AT 3ft. DEPTH CONSECUTIVE FRAMES AT 1 MILLISECOND INTERVALS NEAR FIRST MINIMUM

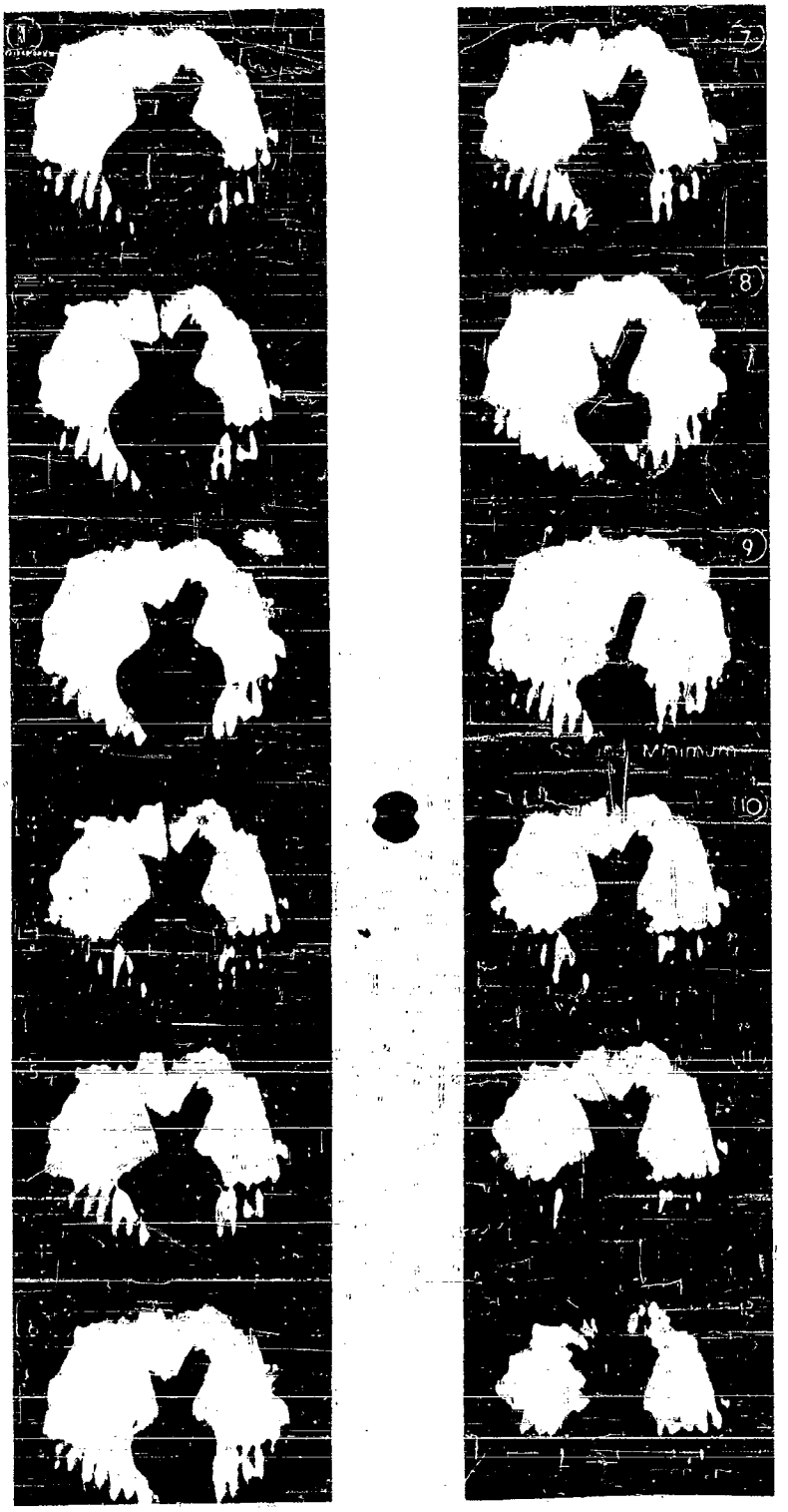

THE BUBBLE PRODUCED BY 1 oz. GELIGNITE AT 3ft. DEPTH CONSECUTIVE FRAMES AT 1 MILLISECOND INTERVALS NEAR SECOND MINIMUM

PHOTOGRAPHIC MEASUREMENTS OF THE ATTRACTION OF AN UNDERWATER EXPLOSION BUBBLE TO A BOX MODEL TARGET

A. R. Bryant
Road Research Laboratory, London

British Contribution

April 1946

PHOTOGRAPHIC MEASUREMENTS OF THE ATTRACTION OF AN UNDERWATER EXPLOSION BUBBLE TO A BOX MODEL TARGET

A. R. Bryant

April 1946

* * * * * * * *

Summary

Stroboscopic photographs at 1 millisecond intervals have been taken of the bubble produced when 1 oz. charges of polar Ammon-gelignite were fired at various distances from the target plate of the R.R.L. Box Model. The photographs show that the bubble was strongly attracted to the target. For a charge distance of about 19¼ inches the bubble made contact with the target plate at the time of its first minimum radius. Graphs of the radius and displacement of the bubble when near its minimum are given as functions of the time for various charge distances

The displacement of the bubble at the minimum was in reasonable agreement with values calculated on the assumption that the flat target plate and rigid surrounding flange may be treated as a rigid disc of equal area. This agreement is regarded as indicating that the theory provides a good estimate of the linear momentum associated with the moving bubble, except perhaps during a short time near the minimum. The observed minimum radii were considerably larger than the predicted values, and the maximum velocities correspondingly lower than the predicted values, throughout the range of charge distances considered.

Introduction.

In early measurements of the deflection of the R.R.L. Box Model target plate it was apparent that the explosion bubble was contributing appreciably to the damage (1). The following experiments were designed to determine photographically the movement of the bubble towards the target in order to assist in an analysis of the damage and to confirm the theory of reference (2), with regard to the bubble's displacement.

Experimental Method.

The R.R.L. Box Model was rigidly held with its target plate vertical at a depth of 5 feet in R.R.L. tank, and 1 oz. charges of polar Ammon-gelignite were fired at distances ranging from 30 to 18 inches from the centre of the target plate. The method of mounting the box model may be assumed to hold the box absolutely rigid. Photographs at one millisecond intervals were taken of the bubble by a camera situated about 10 feet from and at the same depth as the charge. The Arditron equipment described in reference (3) was used to provide the stroboscopic light flash, and the bubble appeared as a silhouette against a bright background. A simple rod framework attached to the rigid flange of box model served to hold the charge in position and to provide reference marks in the photographs. A plan and elevation of the camera and target positions are shown in figure 1. Target plates of both $\frac{1}{16}$ inch and $\frac{1}{10}$ inch thickness were used.

In each shot a group of about 20 pictures was taken near the time of the first bubble minimum. In a few cases a further group were taken near the expected time of the second minimum, but the pictures were of no interest as the bubble was then in all cases an irregular mass of gas clinging to the surface of the target plate and with little observable tendency to expand or contract.

The .....

The depth of charge and target plate centre was kept throughout the series at five feet as at this depth the effect of free surface and rigid bottom almost exactly cancel the influence of gravity during the first oscillation. The migration of the bubble up to its first minimum was thus almost entirely due to the attractive effect of the rigid box model.

Measurement of Photographs.

From the silhouettes of the bubbles, volumes and positions of the centres of gravity of the bubbles were estimated by the method described in reference (4). As the effect of gravity approximately cancelled the free surface and rigid bottom effects the bubbles were assumed to be symmetrical about a horizontal axis normal to and through the centre of the target plate. The actual appearance of the bubbles up to their first minima suggested that this was a reasonable assumption, but immediately after the minimum the bubbles became considerably distorted and quite clearly had no axis of symmetry. The measurement of volumes and positions of centre of gravity of the bubbles is thus subject to considerable error after the minimum size has been passed.

Results.

Typical photographs are shown in Figures 2, 3 and 4 in which the following features may be noted. Before the minimum the bubble is relatively smooth, apart from thin needle like streamers at the surface, and is elongated in a direction normal to the target plate. On reaching the minimum size the bubble moves quickly in towards the target plate, becomes very distorted in general shape and shows a very irregular uneven surface. A short time before the minimum the surface of the bubble farthest from the target plate develops a very marked "plume-like" structure, most clearly seen in Figure 4, which is left behind as the bubble moves in towards the plate. This plume appears to be related to the wake behind the moving bubble. It is not certain whether it consists of a trail of particles of dirt or unburnt carbon, or whether it is a stream of fine bubbles. The plume does not oscillate appreciably in size and remains more or less stationary after the bubble has spread itself out over the target plate. This same plume has been observed in other photographs of the bubble produced by 1 oz. charges in the absence of a target where appreciable movement of the bubble occurred, and was always situated in the rear of the moving bubble.

In all shots where the charge was 23 inches or more from the target plate the bubble was self-luminous for a short time near its minimum size, and this "flash" produced a bright streak on the moving film, which may be seen in Figure 2. The production of this flash was noted in reference (3), and is discussed below.

The quantitative measurements from the photographs are depicted in Figures 5, 6 and 7, and numerical values set out in Tables, I, II and III. Table I contains a summary of the principal quantities determined for each shot.

Radius-Time Curves.

In Figure 5 the mean radius of the bubble, defined as the radius of a sphere having the same volume as the bubble, has been plotted against time for a range of values of the initial charge distance. The zero of time is chosen arbitrarily to exhibit the curves in relation to each other to the best advantage. For the larger charge distances the curves are similar to those for a charge in open water away from any target. When the charge was initially 22 inches or less from the target plate the bubble and water acquired a great deal of kinetic energy due to the bubble's motion toward the target; in consequence, the collapse of the bubble was somewhat inhibited, the potential energy in the gas being less in these cases and the corresponding minimum radii greater. Moreover, the subsequent expansion of the bubble also seemed to be less rapid for these closer shots, which may in part have been the result of losing a considerable amount of energy to the target plate, in addition to the probable loss of energy as the result of turbulence.

The observed values of minimum radius are set out in Table II, together with those calculated from equation (7), reference (5) relating the minimum radius to the "momentum constant" m. This momentum constant m is a non-dimensional constant proportional to the linear momentum acquired by the

bubble .....

bubble during the first oscillation, and has been calculated in a manner to be discussed presently. It will br observed that in every case the observed minimum radius is considerably greater than the calculated value.

Because of the observed luminosity of the bubble gases it seemed of interest tc attempt some calculation of the gas temperature at the instant of maximum compression. As data for the adiabatic of the explosion products of polar Ammon-gelignite were not available the adiabatic for the explosion products of T.N.T. given by Jones (6) has been used to calculate the temperatures given in Table II. These temperatures are rather low in view of the very great intensity of the "flash" produced by the smallest bubbles - e.g. shot 124. It is noticeable that the region of luminosity only occupied a fraction of the volume of the bubble, and in the shots which produced rather weak "flashes" this luminous region was very small compared to the total volume. It might be argued that contrary to the assumption in the usual bubble theories the pressure throughout the gas is not uniform, and this could lead to some increase in pressure in parts of the bubble. Since, however, the temperature (absolute) varies approximately as the one fifth power of the pressure, it does not appear likely that the maximum temperature will be much above the figures given in the Table.

Displacement - Time Curves.

The displacement of the centre of gravity of the bubble towards the target is plotted as a function of time before and after the occurrence of the minimum radius in Figure 6 for a range of values of the charge distance. As may be seen from Figure 5 this time is not very clearly defined in the close shots. For the more distant shots the deflection time curve is roughly symmetrical about the time of minimum radius. In the nearer shots the bubble approached very close to the target plate, making contact with it soon after the minimum, so that a marked asymmetry of the displacement-time curve is to be expected.

Comparison of Observed Displacement with Theory.

In calculating the attractive effect of the box model it has been assumed that the flat target plate surrounded by its rigid flat flange may be approximated by a rigid fixed disc of equal area. Accordingly the "momentum constant" m, defined as one half the cube of the non-dimensional minimum radius multiplied by the maximum non-dimensional velocity, has been calculated using the formula for the attraction co-efficient for a rigid disc given in reference (2). The displacement at the minimum was then calculated. This curve was obtained by plotting the results of all available full integrations of the equations of bubble motion. The displacement thus calculated has been plotted in Figure 7 together with the observed values for all the photographic shots. The results for both $\frac{1}{16}$ inch and $\frac{1}{10}$ inch plating do not appear to lie on separate curves, and in plotting them in Figure 7 no distinction has been made. This is to be expected since the target plate is practically motionless, and therefore effectively rigid, during the period when the bubble is large, i.e. when it acquires most of its momentum.

The agreement between the observed and predicted displacement of the bubble shown in Figure 7 requires to be interpreted with caution. In common with most experimental observations of the bubble's behaviour near its minimum, there are rather wide discrepancies between theory and observation in regard to quantities such as minimum radius or maximum linear velocity. Since, however, a considerable proportion of the resultant displacement takes place some little time before the minimum, at least for the closer shots, the agreement in observed and calculated displacements might still be expected, provided that the discrepancies arose only very close to the time of minimum radius. It is thus reasonable to regard the observed agreement as indicating that the theory provides a good estimate of the linear momentum of the bubble, except possibly during a very short time near the occurrence of the minimum radius. Moreover, it should be remembered that the theory given in (2) was derived on the assumption that the radius of the bubble when large is small compared to its distance from the target. For a one ounce charge the maximum radius is about 18 inches so that the theory is here being used well beyond the region of validity of this assumption.

Having .....

Having regard to the relatively long interval between flashes, the difficulty of measuring the volume accurately, and the uncertainty concerning the correct value to be assumed for the "virtual mass" of the water moving with the bubble very little accuracy is possible in a direct measurement of the momentum from the photographs. An attempt has, however, been made to estimate the linear momentum at a time near the minimum radius from the photographs and the values of the "momentum constant" are given in Table III together with the corresponding calculated values (the actual momentum in non-dimensional units is $4\frac{\pi}{3}$ m, where m is the quantity denoted as the "momentum constant"). The observed momenta are at any rate of the same order of magnitude as those calculated.

This confirms the deduction made from displacement results.

Conclusions.

(1) The displacement of the bubble towards the target plate at the first minimum is in reasonable agreement with values calculated from the theory of the attraction of an explosion bubble towards a rigid disc.

(2) The observed agreement is regarded as indicating that the theory provides a correct estimate of the linear momentum of the bubble, except possibly during a very short time near the occurrence of the minimum radius.

(3) There is considerable discrepancy in the predicted and observed values of the minimum radius and the maximum velocity. This discrepancy in radius and velocity may, however, only occur for a small interval near the time of minimum radius.

References.

(1) Deflection-Time Curves at the centre of Box-model plates, resulting from Underwater Explosions.

(2) The Attraction of an Underwater Explosion Bubble to a rigid disc.

(3) A Technique for Multiflash Photography of Underwater Explosion Phenomena.

(4) Photographic Measurements of the size, shape and movement of the Bubble produced by 1 oz. charges of Polar Ammon Gelignite detonated Underwater at a depth of 3 feet.

(5) The Behaviour of an Underwater Explosion Bubble.

(6) The Behaviour of an Underwater Explosion Bubble further approximations.

TABLE I.

Summary of Measurements of Photographs

Shot No.	Distance of charge from Target	Plate Thickness	Displacement of C.G. of Bubble at First Minimum	Minimum Radius of Bubble	Maximum Velocity of Bubble	Displacement of flash
124	30.5 in.	1/16"	4.3 in.	2.9 in.	250 ft/sec.	3.4 in.
121	27.5	1/16"	4.6	2.85	310	3.9
120	24.5	1/16"	7.5	2.9	310	6.4
105	23.5	1/16"	8.6	3.1	250	7.8
114	23.5	1/10"	8.8	3.2	310	7.5
126	22.5	1/16"	9.2	3.9	200	8.8
110	21.5	-	-	-	-	9.9
107	21.5	1/16"	10.6	-	-	9.5
108	20.5	1/16"	13.6	4.80	210	No flash
111	20.5	1/10"	14.3	5.0	200	No flash
112	19.5	1/10"	14.0	-	180	No flash
125	19.5	1/16"	13	4.75	200	No flash
130	18.5	1/16"	16.6	4.75	180	No flash
103	24.5	1/16"	-	-	240	6.8

TABLE II.

Minimum Radius and Gas Temperature in Bubble.

Shot No.	Distance of Charge from Target Plate	Calculated Minimum Radius	Observed Minimum Radius	Maximum Gas Temperature	Nature of "Flash"
124	30.5 in.	1.74 in.	2.9 in.	365°C	Strong
121	27.5	1.97	2.85	380	Strong
120	24.5	2.30	2.9	365	Strong
105	23.5	2.46	3.1	335	Very faint
114	23.5	2.46	3.2	320	Medium
126	22.5	2.65	3.9	240	Very faint
108	20.5	3.15	4.8	180	No flash
111	20.5	3.15	5.0	150	No flash
125	19.5	3.46	4.75	160	No flash
130	18.5	3.85	4.75	160	No flash

TABLE III.

Observed and Calculated Momentum of Bubble at Minimum.

Shot No.	Distance of Charge from Target Plate	Observed Maximum Velocity	Bubble Radius at time of Maximum Velocity	Observed "Momentum Constant"	Calculated "Momentum Constant"	Calculated Maximum Velocity
124	30.5 in.	260 ft/sec.	2.9 in.	1.13×10^{-3}	0.25×10^{-3}	780 ft/sec.
121	27.5	310	2.9	1.38	1.22	805
120	24.5	310	3.0	1.54	1.91	864
105	23.5	250	3.6	2.12	2.25	830
114	23.5	310	3.6	2.64	2.25	830
126	22.5	200	4.25	2.80	2.68	788
108	20.5	210	5.25	5.42	3.83	673
111	20.5	200	5.12	4.90	3.83	673
112	19.5	180	5.55	5.63	4.62	609
125	19.5	200	5.05	4.71	4.62	609
130	18.5	180	5.35	4.95	5.62	539

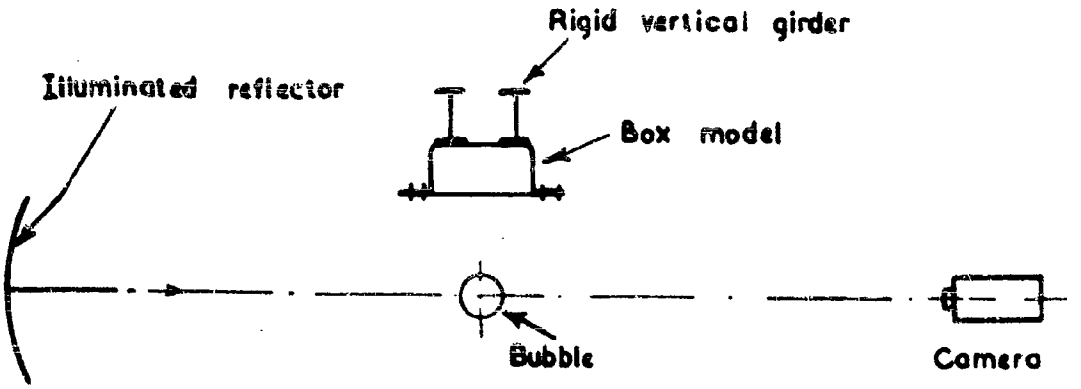

Plan View of Box Model and Camera

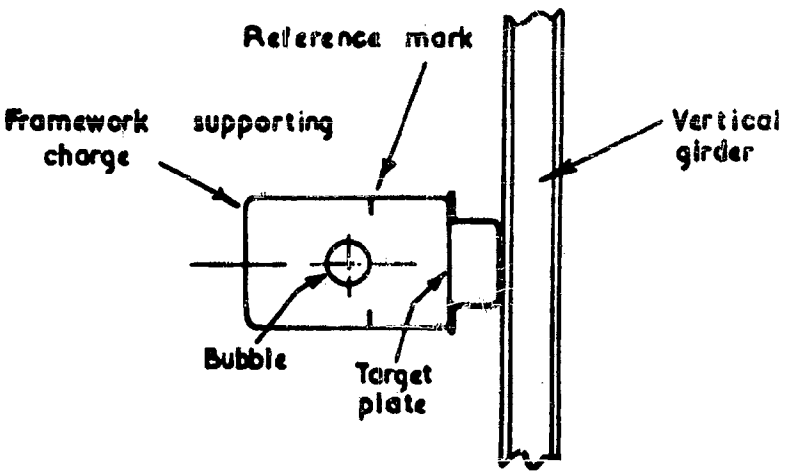

Elevation of Box Model Viewed from Camera

Fig.1 PLAN AND ELEVATION OF BOX MODEL AND CAMERA ADJUSTMENT

Fig. 2. Charge 2½ in. from 1/16-in. target Plate
Pictures at 1 msec. intervals.

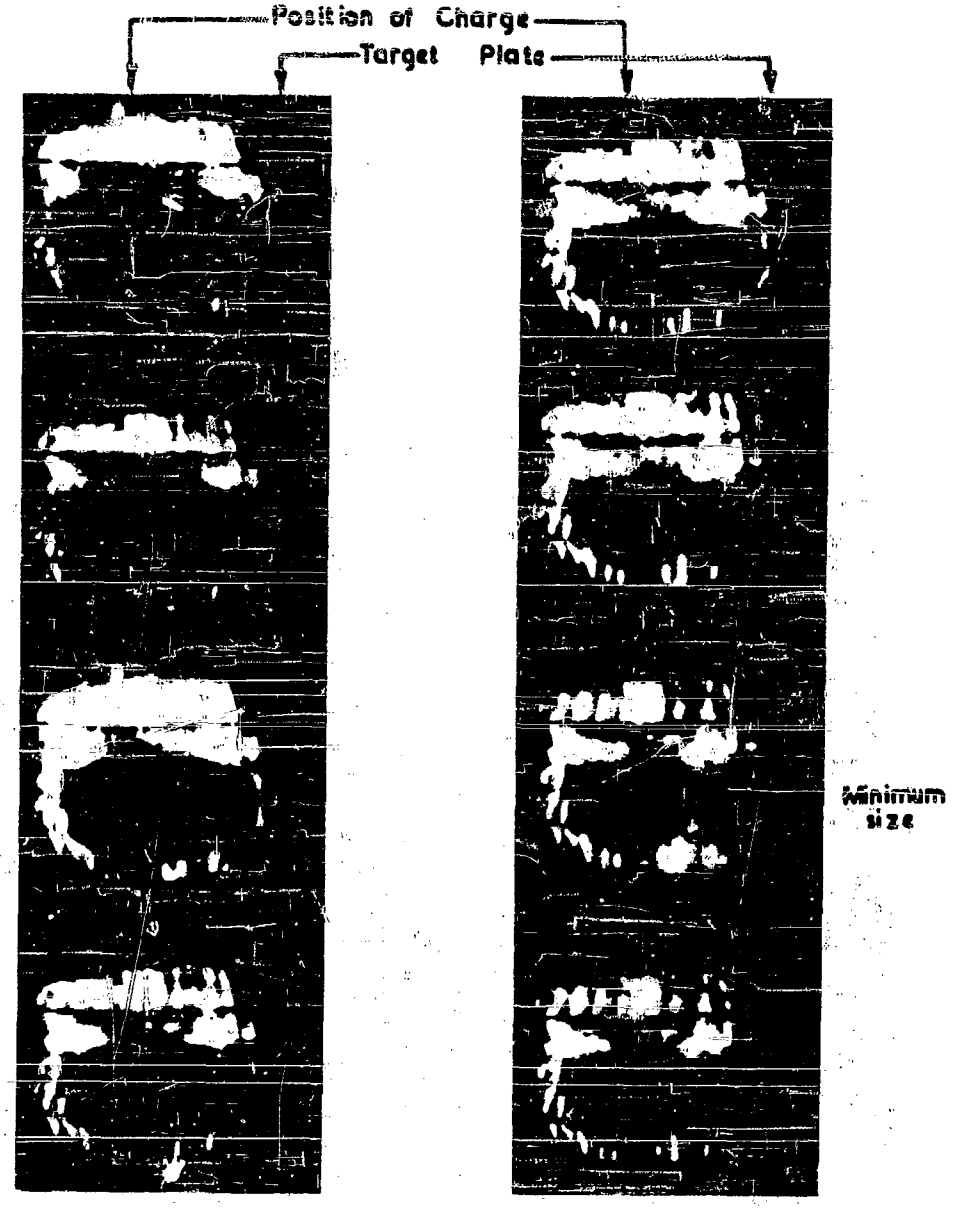

Fig.3. Charge 20 in. from 1/16th-in. target plate
Pictures at 1 msec intervals.

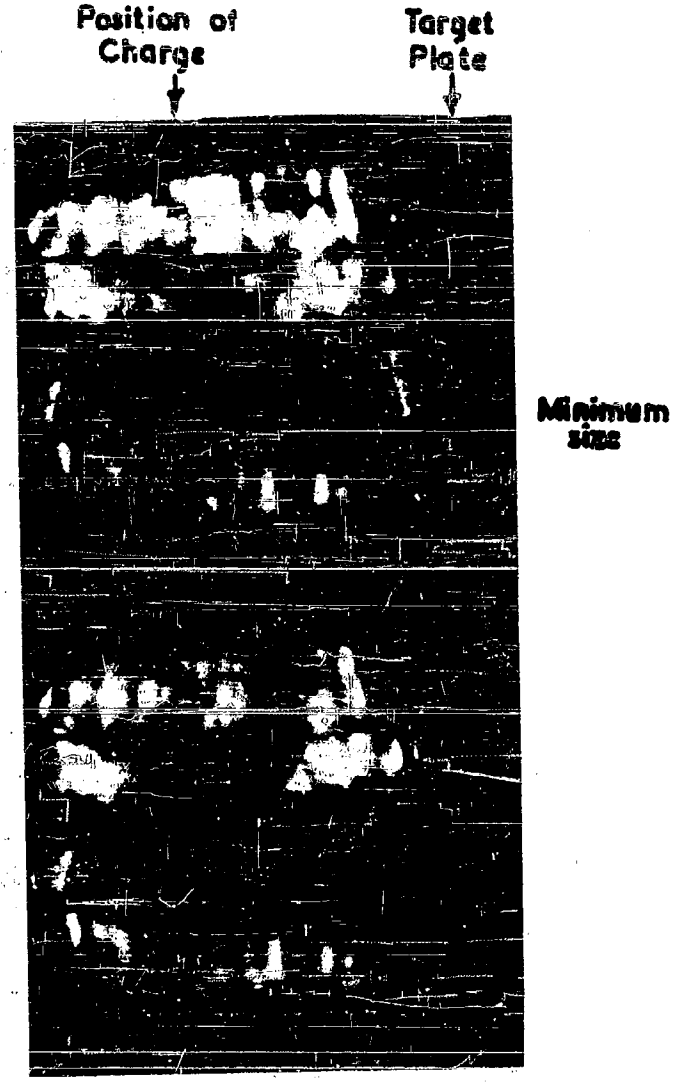

Fig. 4. Charge 21 in. from 1/16th-in. target plate
Pictures at 1 msec. intervals.

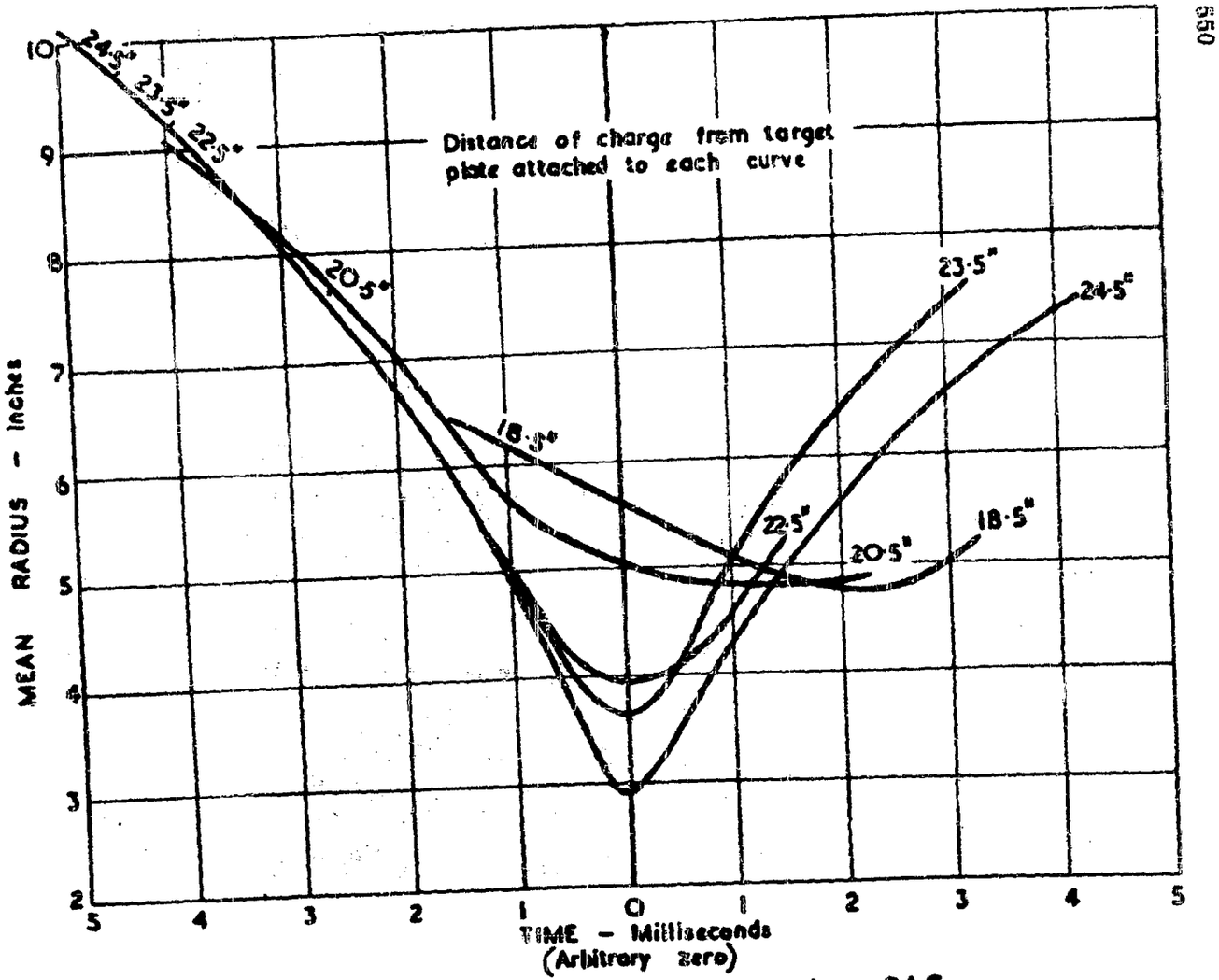

Fig.5. MEAN RADIUS OF BUBBLE FROM 1oz. P.A.C.

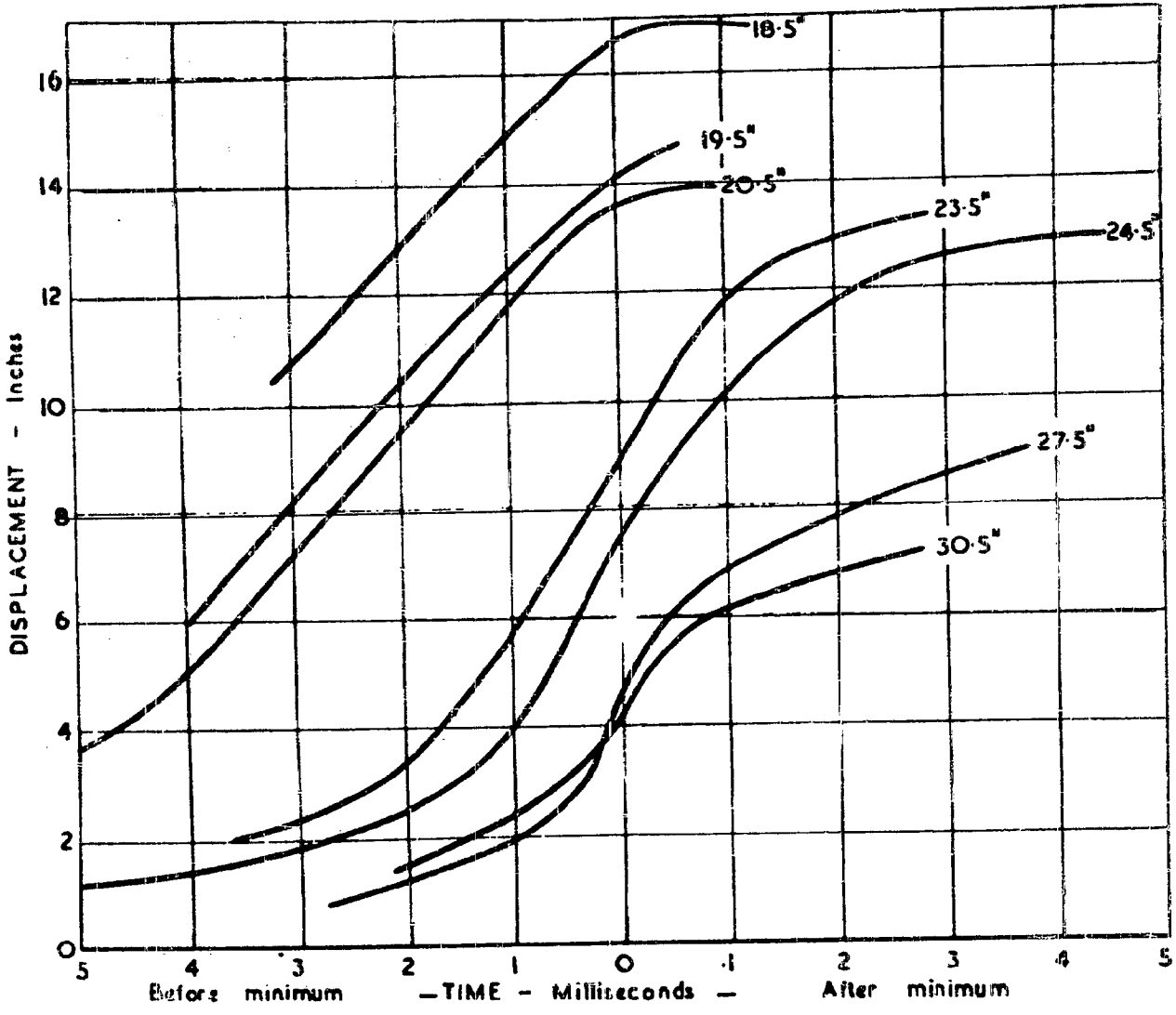

Fig.6. DISPLACEMENT OF C.C. OF BUBBLE TOWARDS TARGET PLATE

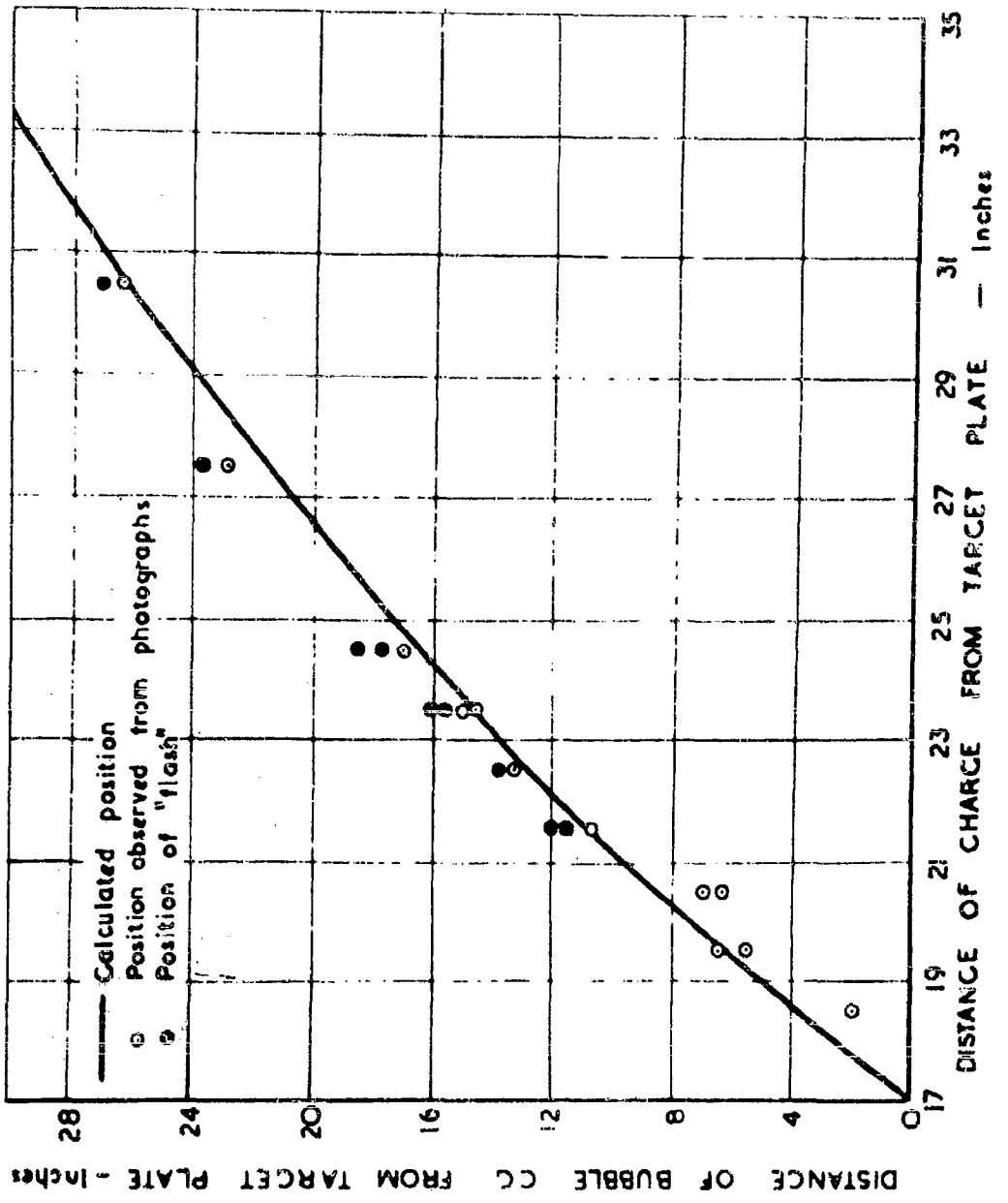

Fig.7 POSITION OF BUBBLE AT FIRST MINIMUM

MEASUREMENT OF BUBBLE PULSE PHENOMENA, III
RADIUS AND PERIOD STUDIES

E. Swift, Jr. and J. C. Decius
Underwater Explosives Research Laboratory
Woods Hole Oceanographic Institution

American Contribution

11 September 1947

CONTENTS

		Page
ABSTRACT		
LIST OF SYMBOLS		
I.	INTRODUCTION	1
II.	EXPERIMENTAL METHODS	1
	1. Bubble Periods	1
	2. Depth	2
	3. Charge Weight	2
	4. Radius Measurements	2
III.	RESULTS	3
	5. First Bubble Period in Free Water	3
	6. Second and Third Bubble Periods in Free Water	11
	7. First Bubble Periods Close to a Free Surface	11
	8. Maximum Bubble Radii	15
	A. Free Water	15
	B. Radii Close to a Free Surface	18
	C. Radii for Second and Third Periods in Free Water	20
IV.	COMPARISON OF EXPERIMENTAL RESULTS WITH THEORY	20
	9. Resume of the Theory: The Role of the Adiabatic Parameters	20
	10. Determination of the Bubble Energy	26
APPENDIX I		32
LIST OF REFERENCES		42

LIST OF FIGURES

Figure		Page
1	Radius-Time Curve for 300 gm of TNT Depth of 300 ft	16
2	Non-Dimensional Period vs Parameter k for Various γ (Ratio of Specific Heats)	25
3	Period/Maximum Radius (Non-Dimensional) vs Parameter k for Various γ	27
4	Composite, Non-Dimensional Radius-Time Curve for TNT - 300 ft Depth	33
5	Composite, Non-Dimensional Radius-Time Curve for TNT - 550 ft Depth	34
6	Composite, Non-Dimensional Radius-Time Curve for Tetryl - 300 ft Depth	35
7	Composite, Non-Dimensional Radius-Time Curve for Tetryl - 600 ft Depth	36
8	Composite, Non-Dimensional Radius-Time Curve for Torpex-2 - 600 ft Depth	37
9	Composite, Non-Dimensional Radius-Time Curve for Blasting Gelatin - 500 ft Depth	38

ABSTRACT

This report presents measurements of the periods of oscillation and the radii at maximum size of bubbles of product gases from underwater explosions. The significance of these measurements is discussed as it pertains to the energy of the bubble. No attempt is made to relate this energy to the energy emitted by the bubble in the form of a pressure wave or "bubble pulse" at the time of the bubble minimum.

A large number of piezoelectrically recorded period measurements are reported for charges weighing from 1 oz to 1/2 lb. Maximum radii obtained from simultaneous photographic records are also shown. The charges were fired at depths ranging from 2 to 700 ft.

An analysis of the data is made, based on the theory as developed by Shiffman and Friedman. Their numerical integrations of the period have been extended to include a wider range of the parameters which describe the internal energy of the product gases. By making reasonable assumptions in the calculations, the energy of the bubble is computed to be about 50% of the total energy released by the detonation. It is shown that there is some uncertainty in these calculations due to the limited range of the experiments and the lack of definite knowledge as to the state of the gases in the bubble.

LIST OF SYMBOLS

A	radius of gas bubble
a	non-dimensional radius of gas bubble
A_{Mn}, a_{Mn}	maximum radius of gas bubble for n-th oscillation
A_{mn}, a_{mn}	minimum radius of gas bubble for n-th oscillation
α	adiabatic constant
C	time scaling factor
D	total depth of water
E	total energy of bubble
g	acceleration of gravity
H	depth to the charge
J_n	radius constant for n-th oscillation
K_n	period constant for n-th oscillation
k	parameter in energy equation
L	length scaling factor
m,n	arbitrary constants in equation of curtate cycloid
p_o	hydrostatic pressure at depth of detonation
p_g	pressure inside the gas bubble
Q	detonation energy
q	ratio of A_{m1} to A_{M1}
r	fraction of detonation energy left in bubble
t_n	non-dimensional period of n-th bubble oscillation
T_n	period of n-th bubble oscillation
W	weight of charge
Z_o	depth of detonation + 33 ft
γ	ratio of specific heats
ρ	density of sea water
Φ (y)	see Ref. (5)
ε	curve fitting parameter for empirical radius-time curve
ϕ	parameter in empirical radius-time curve

MEASUREMENT OF BUBBLE PULSE PHENOMENA, III

RADIUS AND PERIOD STUDIES

I. INTRODUCTION

In any study of the mechanism and energetics of an underwater explosion, one is inevitably led to a realization of the very considerable amounts of energy inherent in the bubble of explosion product gases. Since the total damage done by an underwater explosion is caused by both the shock wave and the subsequent bubble pulses, these effects must be separated for a proper understanding of the mechanisms involved. To determine the exact quantities of energy present at various stages of the explosion and to find the amount of useful energy is a task of great magnitude. In this report are presented data which were gathered in an attempt to evaluate the energy in the bubble.

One of the easiest measurements to make is the measurement of the periods of oscillation of the bubble, that is, the time intervals between successive minima in the bubble radius. These are referred to as the first bubble period, second bubble period, and so on. The length of the bubble period is related to the energy left after the passage of the shock wave by the equations discussed below. In general, it may be said that the longer the period, the greater the energy. However, it is necessary to have additional information -- specifically, the equation of state of the product gases -- before an exact calculation of the total energy can be made.

A second measure of the energy may be obtained from a study of the maximum and minimum radii of the bubble. Photographs of the bubble at various stages of its oscillation show that the outline of the bubble is rather clearly delineated up to the first maximum, but that it is somewhat less clear at subsequent maxima, and is completely obscured by carbon streamers in the water at the minima. Since the bubble radii at the minima have not been measured, it is not possible to obtain a good value of the energy from radius measurements alone. By a combination of radius and period measurements, however, an attack can be made on a more precise calculation of the energy in the bubble.

This report presents a compilation of data obtained in a rather extensive program of bubble period and radius measurements.[1,2] These appear to be the most complete and accurate data of this sort available at the present time. Using these measurements, calculations of energy and other parameters appearing in the bubble equations have been carried out.

II. EXPERIMENTAL METHODS

1. Bubble Periods

Periods were measured[1] by recording oscillographically the signal from a piezoelectric gauge exposed to the shock wave and bubble pulses. The pressure changes were recorded on moving film simultaneously with a 1 kc timing wave.

The precision of measurement of the periods depended on the precision with which the film record could be read. This is estimated to be about 0.5%. Much greater precision is not very likely to be attained by this method because of the finite width of the trace on the film and because of the difficulty of locating the exact position of the bubble pulse maximum on the film.

2. Depth

Depths were found from measured lengths of cable, or, in the deeper shots, from readings of a Bourdon depth gauge. From the various data collected, it is estimated that the precision of measurement is about 1% and may be as poor as 2% in the worst cases. Less reliance can be placed on those shots where the cable angle was great, i.e., greater than 20° from the vertical, and where no depth gauge was used.

Since the radius of the bubble depends upon the cube root of the depth, it is not very sensitive to errors in the latter. However, the period depends upon the 5/6 power of the depth, so only slightly more precision is attainable in the period than is inherent in the depth measurement.

3. Charge Weight

The half-pound charges used were weighed to the nearest gram, the 1 oz charges to 0.1 gm. Since charge weight appears in the equations as a cube root, the error made here is quite negligible.

A correction had to be made for the booster in each case. This correction was made by reducing (or increasing) the weight of booster used in the calculation to an equivalent weight of the explosive being studied. The factor employed was found from the ratios of bubble period constants, by successive approximations if necessary. Any error made in this correction will introduce a negligible error in the final weight, since the weight of booster is only a small fraction of the total.

4. Radius Measurements

Because of the relatively narrow angle of view of the high-speed cameras used, the bubble at maximum size ordinarily came very close to the edges of the photograph. In the very shallow shots using 25 gm charges, the narrower dimension of the picture was too small to include an entire bubble diameter.

The possibility of optical distortion due to the lens was first investigated. Photographs of a grid taken with the Fastax camera showed no appreciable distortion ($\leq 2\%$) over the whole usable field. Calculation[2] of the distortion introduced by the glass-air interface before the lens showed that in the worst case the correction would be entirely negligible.

Measurements of the radius of the bubble were made on photographic prints. Diameters were measured in at least three directions and averaged. Care was taken to avoid including irregularities outside what was believed to be the true surface of the bubble of gases. As the minimum is approached, the bubble is progressively obscured by opaque streamers of explosion products,

so that close to the minimum measurements were not at all reliable. The overall precision of the bubble radius measurement is estimated to be about 2%. Some improvement in these measurements could have been made by providing standards of length of nearly the same size as the bubble diameter, and by very sharp focussing.

III. RESULTS

5. First Bubble Periods in Free Water

These results constitute what are believed to be reliable measurements of the first bubble periods for TNT, tetryl, and torpex-2 [25], in the absence of any interfering surfaces, and at such depths that migration effects can be considered negligible. All charges were in the form of cylinders of height slightly greater than the diameter. A few values are given for pentolite and blasting gelatin, but these cannot be considered as giving a definitive value of the period. Some of the results included are for shots made in water of such depth that the surface corrections would be small, but not negligible.

Table I shows the results at several depths for cast TNT charges of density 1.5. Depths were measured by a Bourdon depth gauge[1], but in a few cases the meter wheel reading of the length of cable let out was used. Periods were read from piezoelectric records.* The period constant K_n was defined by the equation[3]

$$T_n = K_n \frac{W^{1/3}}{Z_o^{5/6}} \qquad (5.1)$$

where T_n = the period (sec)
Z_o = H+33, where H is the initial charge depth (ft)
W = charge weight (lb)
n = refers to the first, second, or third bubble period.

The TNT in each charge weighed slightly more than a half-pound; to that weight was added the TNT equivalent of the 44 gm tetryl booster and 1 gm for the detonator. As far as bubble energies go, pressed tetryl appears to be about 3% more energetic than TNT, so the weight of tetryl used was converted to the equivalent weight of TNT by multiplying by 1.03.

The average value for the period constant for cast TNT obtained in this way is 4.36. The standard deviation of the mean is shown together with the average in the table.

---

* In a few cases, indicated in Table I, when piezoelectric records were not available, the periods were read from radius-time curves plotted from the Fastax pictures of the bubble cycle. These values are probably accurate to 2% or better, as indicated by the correlation when both measurements were available.

Two other values have been obtained under carefully controlled conditions. Slichter, Schneider, and Cole[4] report a value of 4.36 for 295 lb TNT charges in relatively shallow water, after correcting their period measurements for the effects of surfaces[5]. Borden and Arons[6] have similarly corrected the period values for 1/2 lb charges in shallow water found by Arons, Borden, and Stiller[7] and from their results the constant appears to be 4.32. These authors, however, have assumed a slightly higher energy factor for the tetryl booster. If the factor of 1.03 used in this report is applied to their data, their TNT period constant becomes 4.35. Other values may be found in Table X.

TABLE I

FIRST PERIOD CONSTANTS FOR CAST TNT IN FREE WATER

Shot No.	Charge Weight (lb)	Depth H (ft)	Period T_1 (msec)	K_1
G1F	0.651	343	27.4	4.43
G2F	.660	304	29.8	4.38
G4F	.660	304	30.0 *	4.41
G5F	.662	305	29.89	4.40
G6F	.658	304	29.92	4.41
G7F	.669	298	30.23*	4.36
G8F	.663	304	29.82*	4.38
G9F	.651	304	29.64*	4.38
G17F	.660	305	29.62*	4.38
G18F	.660	302	29.61*	4.32
G20F	.660	538	19.64*	4.47
G21F	.651	593	19.10*	4.73
G23F	.658	567	18.14*	4.32
G70F	.660	503	19.9	4.30
G71F	.658	463	21.0 **	4.26
G72F	.660	586	17.85	4.36
G73F	.655	576	18.16*	4.38
G74F	.660	556	18.1 **	4.24
G76F	.660	587	17.7	4.33
Average (excluding G21F)				4.36±0.014

* Period from pictures agrees to ± 2%.
** Period from pictures--no piezoelectric record.

Table II presents the data obtained for torpex-2 charges. The depth measurement in this case is perhaps slightly less reliable than for the TNT, since it was found from meter wheel readings alone in four of the eight shots. Three of the eight periods were read from radius-time curves made from the pictures. Since in the other five cases the difference between this period and the electronic measurement was at worst 1.3%, this may be considered sufficiently good. The booster correction was made by multiplying the weight of tetryl (44 gm) by 0.65.

The resulting period constant, K_1 = 5.065, may be compared with the value 5.10, obtained by Borden and Arons (references indicated under the discussion of TNT).

More recently a series of 280 gm torpex-2 charges fired at this laboratory within 5 ft of the surface gives an average value of 5.08 for K_1 after correcting for the effects of surfaces[8].

TABLE II

FIRST PERIOD CONSTANTS FOR TORPEX-2 IN FREE WATER***

Shot No.	Charge Weight W (lb)	Depth H (ft)	Period T_1 (msec)	K_1
G119F	0.582	597*	19.5 **	5.017
G120F	.578	600*	19.46	5.046
G121F	.620	603*	19.9 **	5.065
G122F	.602	611	19.65	5.096
G123F	.602	611	19.8 **	5.135
G124F	.576	603*	19.34	5.044
G125F	.574	598	19.38	5.017
G126F	.572	603	19.51	5.100
Average				5.065±0.015

* Depth from meter wheel
** Period calculated from film
***See Ref. 25 for composition of torpex-2.

Table III gives the results obtained for 1/2 lb pressed tetryl charges, density 1.5, in free water. The shots labelled "GC" were recorded when the charge was in the vicinity of a small steel cylinder[9]; however, a critical comparison of these shots with the rest showed no systematic discrepancy. This seems reasonable because of the relatively small size of the cylinder. Occasionally a large discrepancy in the period appeared, as in shot GC40E where the deviation from the mean is about 30%*. This error was occasioned by the electronic gear, and was not a scatter in the property being measured, as indirect evidence from the collapse of the cylinder, discussed in Ref. (9), shows the period to be actually about 20 msec in this case, resulting in a period constant consistent with the other values.

An entirely independent series of shots is shown in Table IV. These were carried out with a different set of equipment and in water sufficiently

* See also G21F in Table I.

TABLE III

FIRST PERIOD CONSTANTS FOR PRESSED TETRYL IN FREE WATER

Charge Weight: 0.500 lb

Shot No.	Depth H (ft)	Period T_1 (msec)	K_1
G11F	300	27.73*	4.41
G12F	300	27.52*	4.38
G13F	302	27.62*	4.42
G14F	303	27.53*	4.42
G15F	305	27.16*	4.38
G16F	302	27.4 **	4.38
G22F	607	16.02*	4.40
G31F	547	17.31*	4.38
GC39E	712	14.30	4.45
GC40E	471	24.55	5.68
GC41E	471	19.52	4.38
GC42E	237	32.92	4.40
GC43E	232	32.57	4.27
GC47E	474	19.40	4.39
GC49E	481	19.47	4.47
GC79F	704	14.21	4.39
GC80F	695	14.22	4.36
GC101F	695	14.21*	4.35
GC102F	493	19.24*	4.49
GC103F	230	33.06*	4.34
GC106E	689	14.35	4.36
GC107E	240	32.83	4.44
GC108E	462	19.76	4.39
Average (excluding GC40E)			4.39±0.01

* Period from pictures agrees to ± 2%
** Period obtained from pictures--no piezoelectric record.

TABLE IV

FIRST PERIOD CONSTANTS FOR PRESSED TETRYL
Charge Weight: 0.500 lb
H = 39 ft

Shot No.	Total Water Depth (ft)	Period T_1 (msec)	K_1
RE462	72	99.4	4.40
RE466	108	98.6	4.41
RE470	117	98.1	4.41
RE472	117	99.3	4.47
RE474	117	97.9	4.41
RE476	89	97.9	4.40
RE478	84	97.5	4.38
Average			4.41±0.01

deep that the correction which was made for surfaces amounted to only about 1%.* The averaged result for K_1, 4.41, is in good agreement with the value of Table III, 4.39.

Further results of work with pressed tetryl charges are shown in Tables V and VI. These charges weighed slightly less than an ounce, and may be considered as being in free water (surface correction much less than 1%). Note that both series of shots give a value of the period constant which averages about 1% lower than that for the 1/2 lb charges.

The results of a slightly less reliable series of measurements in free water are shown in Table VII. The depth in this case was measured from the known length of cable let out, multiplied by the cosine of the angle the cable made with the vertical at the surface. As long as the angle is small, this gives a good measure of the depth; however, since the angle in this series ranged up to 32°, the uncertainty in the depth may be as much as 5%. The period constant is, as a result, somewhat less precisely known in this series, the standard deviation of a single observation being about 2%. The average value, 4.31, is also in this case found to be lower than that for the 1/2 lb charges.

TABLE V

FIRST PERIOD CONSTANTS FOR PRESSED TETRYL IN FREE WATER

Charge Weight: 0.0558 lb
Total Depth of Water: 85-100 ft
H = 55 ft

Shot Number	Period T_1 (msec)	K_1
EDG 1	39.52	4.32
2	39.94	4.36
3	39.89	4.36
4	39.90	4.36
5	40.07	4.37
6	39.81	4.35
Average		4.354±0.007

* The correction for surfaces was made by using the equation in Ref. (5), page 5. For convenience, this was transformed to:

$$K = \frac{T\, Z_0^{5/6}}{W^{1/3}} \left(\frac{1}{1 - \frac{1.179\, K\, W^{1/3}\, \Phi(y)}{D\, Z_0^{1/3}}} \right)$$

by using the relationship $5.78\, K^3 = rQ$ where K is the value of the period constant. A value of K is put into the correction term as a first approximation, and if the value of K found by solving the equation differs greatly from this, a second approximation should be made. The values of K reported in Tables IV, VIII, and IX were found by this method. The numerical constant 5.78 is not a universal constant, but may be used in all cases considered here without incurring much error.

TABLE VI

FIRST PERIOD CONSTANTS FOR PRESSED TETRYL

Charge Weight: 0.0558 lb
Total Depth of Water 85-100 ft
H = 39 ft

Shot No.	Charge Weight W (gm)	Total Water Depth (ft)	Period T_1 (msec)	K_1
RE463	25.3	68	47.3	4.32
RE465	25.3	106	47.1	4.30
RE467	25.5	109	47.5	4.33
RE473	25.5	114	47.2	4.35
RE475	25.5	93	47.0	4.33
RE477	25.6	88	47.1	4.33
RE480	25.6	80	47.2	4.35
RE481	25.8	81	46.9	4.30
RE482	25.7	82	46.9	4.31
Average				4.324±0.006

TABLE VII

FIRST PERIOD CONSTANTS FOR PRESSED TETRYL IN FREE WATER

Charge Weight: 0.0558 lb

Shot No.	Period T_1 (msec)	Depth H (ft)	K_1
E15	10.80	380	4.27
E16	10.79	380	4.26
E17	17.90	196	4.34
E18	12.45	334	4.47
E19	11.55	344	4.24
E20	11.22	347	4.16
E22	17.45	205	4.37
E23	17.49	207	4.40
E39	7.20	661	4.39
E41	7.50	585	4.15
E42	7.05	672	4.36
E43	8.08	545	4.24
E45	7.96	578	4.37
E46	10.86	380	4.31
Average			4.31±0.025

No data were obtained for loose tetryl charges in free water but a few shots were made with 1/2 lb charges in water deep enough so that the surface correction amounted to only about 1%. These values are given in Table VIII. It will be noted that the value of the period constant is about 3% higher than for the pressed charges. Borden and Arons[6] also found a higher value for loose tetryl charges of various sizes than the value reported here for pressed tetryl.

Because of the accuracy of the experimental methods and the confirmation of the results under differing conditions, it is felt that this difference between loose and pressed tetryl is a real one. There also may be a real discrepancy between the 1 oz and 1/2 lb pressed charges, although the evidence is not entirely conclusive.

TABLE VIII

FIRST PERIOD CONSTANTS FOR LOOSE TETRYL

Charge Weight: 0.552 lb
H = 39 ft

Shot Number	Total Water Depth (ft)	Period T_1 (msec)	K_1
RE452	72	104.2	4.52
RE453	68	105.0	4.55
RE454	69	104.0	4.51
RE456	69	104.2	4.52
RE458	69	103.8	4.50
RE460*	64	105.6	4.58
Average			4.53±0.012

* Depth not accurately known due to rough seas.

Table IX gives the results of several shots made with various 1/2 lb pentolite charges. These values were obtained incidentally to other studies, and the experimental conditions are not strictly comparable. The data are not sufficient in number to give a final value for the period constant, nor is it felt that they are as accurate as the scatter would indicate. The average falls between the averages for the TNT and pressed tetryl charges of comparable weight. It may be significant that the periods for the two long cylindrical charges are somewhat lower than for the other charges.

Finally, for comparison, a number of period constants calculated from period values available in the literature are given in Table X.

TABLE IX

FIRST PERIOD CONSTANTS FOR 50-50 PENTOLITE

Shot Number	Charge Weight W (lb)	Depth H (ft)	Bottom Depth (ft)	Period T_1 (msec)	K_1
G19F	0.552	335	3600	26.07	4.36
G32F	.566	404	4800	22.9 [d]	4.39
G33F [a]	.550	396	4700	22.4 [d]	4.26
G75F [b]	.551	380	6700	23.47	4.32
RE485	.655[c]	39	106	108	4.43[e]
RE488	.671[c]	39	87	108	4.42[e]
RE490	.658[c]	39	----	108	4.43[e]
Average					4.37±0.023

a. Long cylinder - 6 in. by 1.5 in.
b. Lower half cased in brass, same shape as G33F
c. 44 gm tetryl booster used. Weight added directly to weight of pentolite and total reported here.
d. Period from pictures - no piezoelectric measurement
e. Correction made for surfaces.

TABLE X

MISCELLANEOUS VALUES OF PERIOD CONSTANT

Explosive	K_1	Reference	Remarks
Cast TNT	4.28	10	Correction for surface made
Cast TNT	4.36	4	Correction for surface made
Cast TNT	4.35*	6	Correction for surface made
Cast TNT	4.36	**	Free water
Pressed Tetryl	4.7	11	Extrapolated value. 1 oz charges
Pressed Tetryl	4.31	**	1 oz charges; Free water
Pressed Tetryl	4.39	**	1/2 lb charges; Free water
Loose Tetryl	4.48	6	120 gm; Correction for surface made
Loose Tetryl	4.43	6	300 gm; Correction for surface made
Loose Tetryl	4.53	**	250 gm; Correction for surface made
Torpex-2	5.10	6	Correction for surface made
Torpex-2	5.065	**	Free water
Minol	4.6	12	Correction for surface made
Minol	4.91	4	Free water
100% Blasting Gelatin	4.9	**	Free water
100% Blasting Gelatin	4.74	13	Depth uncertain
50-50 Pentolite	4.37	**	Conditions variable

* See comments in Sec. 5
** Values from this report.

6. Second and Third Bubble Periods in Free Water

No piezoelectric records of the bubble pulses after the first were obtained; however, it was found possible to get a period record from the motion pictures taken of the bubble in free water. The values were obtained from radius-time curves which are probably not as precise as piezoelectric records. Comparisons between piezoelectric and photographic records of the first period show differences of 1-2%; the later periods are more difficult to measure and somewhat greater discrepancies would be expected.

The results for second period measurements are shown in Table XI. The period constant for torpex-2 is about 8% higher than that for TNT, and those for tetryl and pentolite about 1-2% higher. This order is essentially the same as for the first period. The ratios T_2/T_1 were also calculated and in Table XII are compared with values obtained from other sources. It might be noted that the aluminized explosives show a smaller value of this ratio in each series.

Table XIII gives the values obtained for the third bubble periods from measurements on the photographs. The bubble period constants calculated from these values show greater scatter. This would be anticipated because of the difficulty of discerning the outline of the bubble after the first maximum.

7. First Bubble Periods Close to a Free Surface

As part of a study of the interaction of bubbles with the surface, the explosions of a number of 25 gm tetryl charges were photographed very close to the surface[1]. Charge depths ranged from 15 in. to 5 ft, which distances correspond approximately to 0.75 and 3 bubble radii. Thus in the shallowest case, the bubble always vented; at intermediate depths, the behavior was not exactly reproducible, presumably because of uncontrolled variations in the surface or in the depth. At 21 in. -- a distance only very slightly greater than venting depth -- the bubble appeared to drag in air from the atmosphere as it collapsed. This resulted in an increase in the apparent minimum size and a damping of the oscillation. As a result, no piezoelectric record of the bubble pulse was obtained in these cases.

The periods were measured on the high-speed photographs by counting the number of 1000 cycle timing marks between the frame showing detonation and that showing the minimum. Such an estimation of the period is based on a subjective judgment as to the times of detonation and of the minimum relative to the frames and the timing marks. The error incurred may easily amount to as much as a millisecond, and is probably more at the 21 in. depth where the minimum is indefinite. The values of the periods so obtained are shown in Table XIV, the values for loose and pressed tetryl being shown separately.

To obtain period constants comparable to the values obtained in free water, corrections for the effect of the free surface of the ocean and for the bottom must be applied. This was done by the method indicated in the

TABLE XI

SECOND PERIOD CONSTANTS IN FREE WATER

Explosive	Shot No.	Charge Weight W (lb)	Depth H (ft)	Period T_2 (msec)	T_2/T_1	K_2
Cast TNT	G7F	0.669	298	22.6	0.75	3.26
	G8F	.663	304	22.7	.76	3.33
	G9F	.651	304	22.3	.75	3.30
	G17F	.660	305	23.0	.78	3.40
	G18F	.660	302	21.6	.73	3.16
	G20F	.660	538	13.9	.71	3.16
	G21F	.651	593	14.1	.74	3.49
	G23F	.658	567	13.3	.73	3.17
	G71F	.658	463	14.9	.71	3.01
	G72F	.660	586	13.0	.73	3.17
	G76F	.660	587	12.2	.69	2.94
Average					0.73	3.22±0.05
Torpex-2	G118F	0.589	595		0.67*	
	G119F	.582	597	13.5	.69	3.47
	G120F	.578	600	13.9	.71	3.60
	G121F	.620	603	13.6	.68	3.46
	G122F	.602	611	13.7	.70	3.51
	G123F	.602	611	13.4	.68	3.48
	G124F	.576	603	13.3	.69	3.47
	G125F	.574	598	13.2	.68	3.42
	G126F	.572	603	13.3	.68	3.48
Average					0.69	3.47±0.02
Pressed Tetryl	G14F	0.500	303	21.4	0.78	3.43
	G15F	.500	305	20.2	.74	3.26
	G16F	.500	302	21.0	.77	3.36
	G22F	.500	607	11.8	.74	3.24
	G31F	.500	547	12.8	.74	3.24
	GC101F	.500	695	10.2	.72	3.13
	GC102F	.500	493	14.0	.73	3.26
	GC103F	.500	230	24.7	.75	3.23
Average					0.75	3.27±0.03
Pentolite 50-50	G19F	0.551	335	19.6	0.75	3.28
	G33F	.548	396	17.1	.76	3.25

* No timing; from film, assuming constant film speed.

TABLE XII

SUMMARY OF VALUES OF T_2/T_1

Explosive	This Report	Ref. (7)*	Ref. (4)
TNT	0.73	0.77	--
Pressed Tetryl	0.73	--	--
Loose Tetryl	--	0.77	--
Pentolite	0.75	--	--
Torpex-2	0.69	0.72	--
Minol	--	--	0.70

* Data obtained near surfaces.

TABLE XIII

THIRD PERIOD CONSTANTS IN FREE WATER

Charge Weight: $\sim \frac{1}{2}$ lb

Shot Number	Explosive	Period T_3 (msec)	T_3/T_2	K_3
G15F	TNT	19.0	0.88	2.77
G21F		11.9	0.85	2.94
G23F		10.7	0.80	2.54
Average				2.75±0.11
G15F	Pressed Tetryl	16.9	0.84	2.72
G16F		17.4	0.83	2.78
G22F		10.2	0.87	2.81
GC101F		8.6	0.84	2.63
GC102F		11.8	0.84	2.76
Average				2.72±0.03
G19F	Pentolite	14.0	0.71	2.34
G119F	Torpex-2	11.9	0.88	3.06
G121F		11.5	0.85	2.93
G123F		10.6	0.79	2.75
G124F		9.9	0.75	2.58
G125F		10.2	0.77	2.64
Average				2.79±0.09

footnote on page 7 of this report, the corrections amounting to as much as 15%. The total water depth was 20 ft. The corrected period constants are given in the last column of Table XIV.

Excluding the values at 1.75 ft (21 in.) for the reasons indicated above, the average value of the period constant for pressed tetryl is 4.44, and for loose tetryl is 4.57. These values show only a slight scatter and are only about 1% higher than the corresponding ones in free water* (see Tables III and VIII). This higher result would indicate some effect of the surface, not taken into account in the theory, which becomes of importance when the bubble is within 2-3 radii of the surface. However, considering that the total correction for the surface may be as much as 15%, the agreement is remarkably good.

Note also that the difference between loose and pressed tetryl found in the deeper shots is preserved here almost quantitatively.

TABLE XIV

FIRST PERIOD CONSTANTS FOR 25 GM TETRYL CHARGES CLOSE TO THE SURFACE

	Shot No.	Depth H (ft)	Period T_1 (msec)	K_1**
Pressed Tetryl	G99F	5	77.8	4.47
	G135F	5	77.5	4.45
	G134F	3	77.5	4.45
	G133F	2	74	4.42
	G136F	2	73.5	4.39
	GG139F	2	74.7	4.46
	G132F	1.75	74.5	4.55
Average				4.46±0.02
Loose Tetryl	GG150F	5	79.8	4.59
	G147F	5	79.4	4.57
	G146F	3	80.2	4.60
	G145F	2.5	79	4.58
	G144F	2	75	4.50
	G148F	1.75	75	4.61
	G151F	1.75	78	4.80
Average				4.61±0.04

* Corrected for the effect of surface and bottom.

** The values for 1/2 lb charges. Those for 25 gm charges in free water appear to be lower, but the evidence is not conclusive.

8. Maximum Bubble Radii

A. Free Water. The high-speed motion pictures[1] of the bubble were used for these measurements.* The actual size of the bubble was calculated from measurements of its apparent diameter and of the apparent length of a known scale on each print. This was checked by calculating the size of the bubble from the image size on the film and the known optical characteristics of the system (see Ref. (2), Appendix I). Object sizes calculated by the two methods agree to about 2%. Since the scale comparison was less laborious, this method was used to find the bubble radii reported here.

In the case of the 25 gm charges (Table XVI) the area in the picture covered by the bubble was found by planimetering, and the radius was then calculated from the area. No checks were made in this series.

The precision of the radius measurement appears to be about 2%. This degree of precision is possible, however, only up to the first maximum. After this point, as the bubble collapses, its outline is obscured by the streamers in the water. This makes an exact measurement of the size of the bubble very difficult, and at the minimum the measurements may be considerably in error. Some attempt to compensate for the masking of the bubble was made by measuring the radius of the sphere at the base of the streamers, assuming that the streamers themselves contained none of the gas. This cannot be done very well at the minimum, since there they form a compact blur completely masking the bubble.

After the first minimum, the bubble, while nearly spherical, is never as smooth as during the first expansion. It is thus apparent that the difficulty of estimating the position of its outline becomes greater in the second and succeeding cycles, and the validity of conclusions based on the estimated radii becomes more doubtful.

From the measured radii, smoothed radius-time curves were drawn for each charge photographed, in some cases through the third minimum. As can be seen in Fig. 1, a typical curve is extremely steep right after detonation and near the minima. Little reliance can be put on the values in these regions; however, near the first maximum, the radius can be estimated rather accurately because of the flatness of the curve. As a consequence, the calculations carried out were based on the maximum radii, and no attempt was made to use the observed minimum radii other than as upper limits.

Tables XV and XVI show the results obtained for the first maximum. The shot numbers refer to the same charges discussed under bubble periods and the exact weight of each charge can be found there. From the values of the measured radii were calculated values of the proportionality constant in the equation

---

* It should be noted that the standard procedure was to photograph the cylindrical charge with its axis normal to the optical axis of the recording system. Any exceptions to this charge orientation will be specifically pointed out.

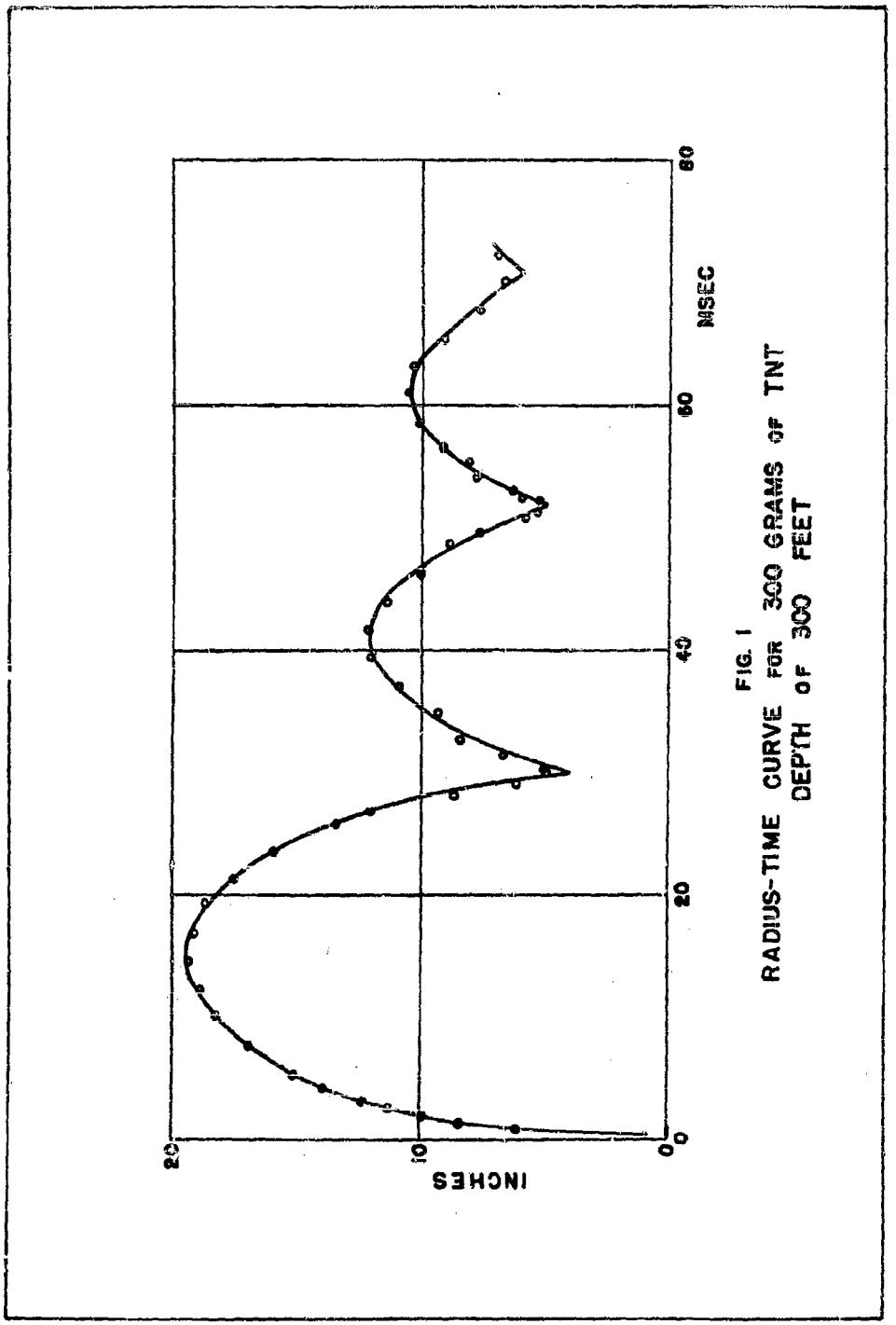

FIG. 1
RADIUS-TIME CURVE FOR 300 GRAMS OF TNT
DEPTH OF 300 FEET

TABLE XV

FIRST MAXIMUM BUBBLE RADIUS

Charge Weight: ~ 1/2 lb

Explosive	Shot Number	Depth H (ft)	A_{M1} (in.)	J_1
Cast TNT	G2F	304	18.8	12.5
	G4F	304	18.8	12.5
	G5F	305	18.8	12.5
	G6F	304	18.8	12.5
	G7F	298	18.9	12.4
	G8F	304	18.9	12.5
	G9F	304	18.7	12.5
	G17F	305	19.4	12.9
	G18F	302	19.4	12.8
	G20F	530	15.9	12.6
	G21F	593	15.7	12.9
	G23F	567	15.6	12.6
	G71F	463	16.6	12.6
	G72F	586	15.4	12.5
	G73F	576	15.6	12.7
	G74F	556	15.7	12.6
	G76F	587	15.1	12.3
Average				12.6±0.04
Pressed Tetryl	G11F	300	17.3	12.6
	G12F	300	17.2	12.5
	G13F	302	17.3	12.6
	G14F	303	17.5	12.8
	G15F	305	17.4	12.7
	G16F	302	17.8	13.0
	G22F	607	14.3	12.9
	G31F	547	14.9	13.0
Average				12.8±0.07
Torpex-2	G119F	597	16.9	14.5
	G120F	600	16.9	14.5
	G121F	603	17.1	14.4
	G122F	611	17.1	14.6
	G123F	611	16.8	14.3
	G124F	603	17.1	14.7
	G125F	598	16.6	14.2
	G126F	603	16.7	14.4
Average				14.5±0.07
Pentolite	G19F	335	17.5	12.7
	G33F	396	15.9*	12.1

* Average of two radii of the slightly elliptical bubble.

$$A_{Mn} = J_n \left(\frac{W}{Z_o}\right)^{1/3} \qquad (8.1)$$

where A_{Mn} = maximum radius for n-th oscillation (ft)
W = charge weight (lb)
Z_o = H + 33, where H is the depth of the charge in ft.

The values of J_1 are shown in the last column of the tables.

TABLE XVI

FIRST MAXIMUM BUBBLE RADIUS, PRESSED TETRYL

Charge Weight: 0.0558 lb

Shot Number	Depth H (ft)	A_{M1} (in.)	J_1
E15	380	7.75	12.6
E16	380	7.3	11.9
E17	196	8.7	11.6
E18	334	8.7	13.6
E19	344	8.35	13.2
E20	347	8.2	12.9
E22	205	9.6	13.0
E23	207	9.8	13.3
Average			12.8±0.25

B. Radii Close to a Free Surface. Photographs of the bubbles from 25 gm tetryl charges described under period measurements (Sec. 5) were measured, and radius-time curves drawn. The resulting maximum radii are given in Table XVII together with the values of J_1.

The precision of measurement is less for these shots than for the previous ones despite the superior definition of the bubble surface occasioned by back lighting in this instance. The scale used was a 12 in. transparent ruler, with the 1 in. squares on the ends blackened. This was rather indistinct in the photographs, and checks of the 12 in. against the 10 in. distance often disagreed by as much as 2-4%. Another indication of possible errors appeared when a check of the bubble radius was made from the optical characteristics of the system and differed from the above measurement by 2-3%. The overall accuracy in the radius measurement is probably no better than 3-4%. The greatest difficulty comes from the fact that only part of the circumference of the bubble is visible in

the photographs*. Since the bubble may very well be ovoid when so close to the surface, the nearly vertical radii (which were the only ones that could be measured) may not accurately represent the radius of the equivalent spherical volume.

TABLE XVII

FIRST MAXIMUM BUBBLE RADIUS FOR TETRYL CHARGES CLOSE TO THE SURFACE

Charge Weight: 0.0558 lb

Charge	Shot No.	Depth H (ft)	A_{M1} (in.)	J_1
Pressed Tetryl	G132F	1.75	19.9	14.0
	G97F	2	21.0	14.8
	G133F	2	19.7	13.9
	G136F	2	20.0	14.1
	GC139F	2	20.0	14.1
	G98F	3	19.7	14.2
	G134F	3	19.4	13.9
	G99F	5	19.3	14.2
	G135F	5	19.7	14.4
	G137F	5	18.6	13.7
Average				14.1 ± 0.13
Loose Tetryl	G148F	1.75	20.6	14.5
	G151F	1.75	20.8	14.7
	G144F	2	20.4	14.4
	G145F	2.5	20.2	14.3
	G146F	3	20.5	14.8
	GC150F	5	20.5	15.0
	G147F	5	19.7	14.4
Average				14.6 ± 0.08

It will be noted that the average value of J_1 for loose tetryl is about 3.5% above that for the pressed tetryl. The period constant for loose tetryl was also found to be about this same percentage higher than that for pressed tetryl, not only in free water (1/2 lb charges, Sec. 5) but also in this same series of shallow shots (Sec. 7). Since both J_1 and K_1 (the period constant) are directly related to the energy of the bubble, the fact that the difference between loose and pressed charges is maintained here seems significant, since equal systematic errors in the measurement of J and K are exceedingly unlikely. The results are most plausibly interpreted as indicating a real difference in bubble energy, due either to variation of

*. See Ref. (1), Figs. 36-39.

detonation energy with density of loading or to a difference in the partition of a given amount of detonation energy between the shock wave and bubble phenomena for the two types of charge.

The values of the proportionality constant, J_1, are higher here than for the shots in free water. The values of K_1 (Table XIV) are similarly higher than the free water values. This would argue that there may well be a systematic difference between the deep and shallow shots. (See Sec. 10.)

In Table XVIII are shown for comparison some results from an earlier report[2] on larger charges. The first charge was within 3 bubble radii of the surface and is thus roughly comparable to the 25 gm charges at 5 ft. The other two are relatively deeper. The values of J_1 are slightly higher than for the 1/2 lb charges in free water (Table XV), but this is within the limits of error of Table XVIII and may not be significant.

TABLE XVIII

MAXIMUM BUBBLE RADIUS, LARGE TNT CHARGES

Shot No.	Weight W (lb)	Depth H (ft)*	A_{M1} (ft)	J_1
G112J	56	36	12.3	13.2
G114J	56	83	10.0	12.7
G117J	295	95	17.5	13.3
Average				13.1±0.2

* Calculated from period.

C. Radii for Second and Third Periods in Free Water. These were found as described above and are summarized in Table XIX. No values for the very shallow shots were measured because of the uncertainty in the depth after the first oscillation. The scatter in J is an indication of the decrease in precision of these values as compared to the first bubble cycle.

One value for a 56 lb charge is included. The exterior of the bubble appeared to be very rough during the second oscillation and the radius cannot be estimated at all precisely. To calculate J_2 in this case, the bubble was assumed to migrate upwards 15 ft between the first and second bubble maxima.

IV. COMPARISON OF EXPERIMENTAL RESULTS WITH THEORY

9. Resume of the Theory: The Role of the Adiabatic Parameters

The theory of the oscillating motion of the bubble of gases produced by an underwater explosion has been developed in recent years principally by Döring[14], Zoller[15], Hermes[16], Keil and Wunderlich[17] in Germany; Taylor[18]

TABLE XIX

SECOND AND THIRD MAXIMUM BUBBLE RADII IN FREE WATER

Charge Weight: ~ 1/2 lb

Explosive	Shot Number	A_{M2} (in.)	J_2	A_{M3} (in.)	J_3
TNT	G6F	13.2	8.8		
	G7F	12.7	8.4		
	G8F	12.8	8.5		
	G9F	11.4	7.6	10.0	6.7
	G17F	13.4	8.9		
	G18F	12.1	8.0	10.6	7.0
	G20F	10.6	8.4	8.2	6.5
	G21F	9.9	8.1	7.9	6.5
	G23F	9.9	8.0	7.8	6.3
	G71F	11.0	8.3		
	G72F	11.6	9.5		
	G76F	11.6	9.5		
Average			8.5±0.2		6.6±0.1
Pressed Tetryl	G14F	12.1	8.8		
	G15F	11.8	8.6	9.1	6.7
	G16F	12.2	8.9	9.5	6.9
	G22F	9.0	8.1	7.1	6.4
Average			8.6±0.2		6.7±0.15
Torpex-2	G118F	10.2	8.7		
	G119F	10.9	9.3	8.2	7.0
	G120F	10.5	9.0		
	G121F	10.8	9.0	8.6	7.2
	G122F	11.1	9.5		
	G123F	10.7	9.1	8.1	6.9
	G124F	11.1	9.6	8.3	7.2
	G125F	10.4	8.9	8.8	7.6
	G126F	10.2	8.8	8.3	7.2
Average			9.1±0.1		7.2±0.1
Pentolite	G19F	12.7	9.3		
	G33F	10.9	8.4		
56 lb TNT	G109J	9.3 ft	9.1		

Temperley[19] in Great Britain, and Herring[3], Kennard[20], Shiffman and Friedman[21] in the United States. In this section, the experimental results described previously in this report will be compared with the theory subject to the following assumptions:

i. the liquid is regarded as an inviscid, incompressible medium of unlimited extent,
ii. the vertical motion of the center of gravity of the bubble is considered to be negligible,
iii. the kinetic energy of the gas is neglected,
iv. the expansion and contraction of the gas is assumed to be adiabatic and to follow the equation

$$pV^{\gamma} = c \tag{9.1}$$

appropriate for an ideal gas.

Under these conditions, it is convenient to introduce non-dimensional definitions of the radius and time, in accordance with Ref. (21), which have the form:

$$A = La \tag{9.2}$$

$$T = Ct \tag{9.3}$$

in which A and T are the actual radius and time respectively, a and t are the non-dimensional radius and time respectively, and the length and time scaling factors are defined by the following equations:

$$L = \left(\frac{3rQW}{4\ p_o}\right)^{1/3} = 1.729\ (rQ)^{1/3}\ \frac{W}{Z_o}^{1/3} \tag{9.4}$$

$$C = \left(\frac{3\rho}{2p_o}\right)^{1/2} L = 0.374\ (rQ)^{1/3}\ \frac{W^{1/3}}{Z_o^{5/6}} \tag{9.5}$$

where W is the weight of the charge, Q the detonation energy per unit weight, r the fraction of the detonation energy remaining in the bubble motion after passage of the shock wave, p_o the initial, hydrostatic pressure at the depth Z_o (which includes the equivalent depth of the atmosphere) where the bubble is formed, and ρ the density of the liquid medium; the numerical factors in the third members of Eqs. (9.4) and (9.5) are appropriate for L and Z_o in feet, C in seconds, rQ in calories per gram, W in pounds, with $\rho = 1.025$ (sea water).

The use of the non-dimensional variables thus defined allows the expression for the conservation of energy to be written in the form:

$$a^3 (\dot{a}^2 + 1) + k\, a^{3(1-\gamma)} = 1 \qquad (9.6)$$

in which the dot signifies differentiation with respect to non-dimensional time. The parameter k is defined by the expression:

$$k = \frac{c\, p_0^{\gamma-1}}{(rQ)^{\gamma}\ (\gamma-1)} = \frac{c(\rho g)^{\gamma-1} Z_0^{\gamma-1}}{(rQ)^{\gamma}\ (\gamma-1)} \qquad (9.7)$$

The following considerations give the theoretical relation between the observed period and maximum radius and the value of rQ, under different assumptions regarding the parameters k and γ in Eq. (9.6): At maximum or minimum radius, $\dot{a}$ vanishes in Eq. (9.6) leading to an equation

$$a^3 + k\, a^{3(1-\gamma)} = 1 \qquad (9.8)$$

whose greatest and least roots should be the non-dimensional maximum and minimum radii; note that if k vanishes (internal energy negligible) the maximum radius becomes simply $a_M = 1$ or $A_M = L$. The roots for various values of γ and k appear in Table XX, where a_M is the non-dimensional maximum radius and a_m the non-dimensional minimum radius.

The time for one oscillation is computed by obtaining twice the time between minimum and maximum radii.* In the case where k is neglected, Eq. (9.6) can be integrated in terms of the incomplete beta function[3] and the numerical result is 1.492. On the other hand, when k is not neglected, Shiffman and Friedman[21] have shown that the period can be approximated very accurately by means of a quadrature formula involving the Tchebycheff polynomials. Such calculations were performed by Shiffman and Friedman for a few values of γ and k using fifth-order Tchebycheff polynomials; those authors remark that the fifth-order approximation agrees within 1% with the third-order approximation. In the present report Shiffman's and Friedman's calculations have been extended to include a wider range of values of the parameters γ and k for reasons described below. A sample calculation was also performed comparing the fifth- and seventh-order approximations which were found to agree within 0.025%. The results are reported in Table XXI, and are also exhibited graphically in Fig. 2.

* Examination of experimental radius-time curves reveals that they are essentially symmetrical about the maximum radius.

TABLE XX

MAXIMUM AND MINIMUM NON-DIMENSIONAL RADII FOR VARIOUS γ AND k VALUES

γ	k	a_M	a_m
1.2	0.1	0.9647	0.02154
	0.2	0.9246	0.06844
	0.3	0.8774	0.1350
	0.4	0.8188	0.2211
	0.5	0.7363	0.3359
1.25	0.1	0.9645	0.04642
	0.2	0.9235	0.1172
	0.3	0.8742	0.2031
	0.4	0.8100	0.3064
1.3	0.1	0.9643	0.07747
	0.2	0.9225	0.1681
1.4	0.05	0.9827	0.08242
	0.1	0.9639	0.1472
	0.2	0.9201	0.2657
---	0	1.0	- - -

TABLE XXI

NON-DIMENSIONAL PERIOD OF BUBBLE OSCILLATION FOR VARIOUS γ AND k VALUES

γ	k	t	γ	k	t
1.2	0.1	1.4713	1.3	0.1	1.4943
	0.2	1.4549		0.2	1.5084
	0.3	1.4484			
	0.4	1.4531	1.4	0.05	1.5052
	0.5	1.4689		0.1	1.5210
				0.2	1.5578
1.25	0.1	1.4621			
	0.2	1.4804	---	0	1.492
	0.3	1.4918			
	0.4	1.5120			

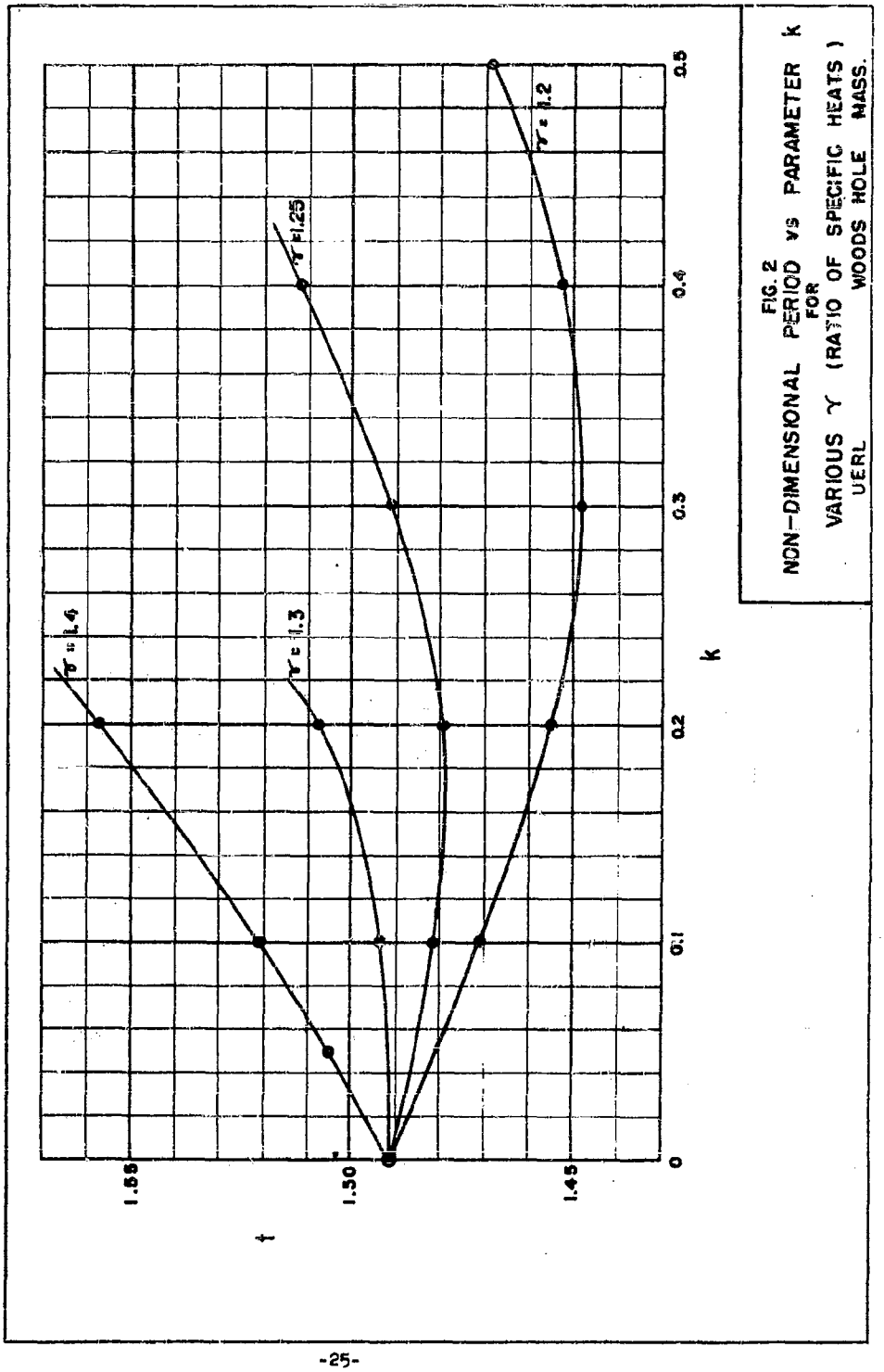

FIG. 2
NON-DIMENSONAL PERIOD vs PARAMETER k
FOR
VARIOUS γ (RATIO OF SPECIFIC HEATS)
UERL WOODS HOLE MASS.

10. Determination of the Bubble Energy

Combination of Eqs. (5.1), (9.3), and (9.5) gives an equation for rQ in terms of the experimental period constant

$$rQ = 19.2 \left(\frac{K}{t}\right)^3 \tag{10.1}$$

while a similar combination of Eqs. (8.1), (9.2), and (9.4) gives an equation for rQ in terms of the experimental radius constant

$$rQ = 0.194 \left(\frac{J}{a_M}\right)^3 \tag{10.2}$$

Making the natural assumption that rQ is independent of the depth and noting that t and a_M are slightly depth dependent through the parameter k, it is expected that the proportionality "constants" J and K will vary directly with a_M and t. If such variation of J and K with depth had been measurable with sufficient precision over a wide enough range, it would have been possible, in principle, to determine uniquely the parameters γ and k as well as rQ. Since, however, such variation was masked by the experimental error in J and K for the small range of depths actually observed*, it has not proved feasible to make a unique calculation of these parameters. Therefore the two Eqs. (10.1) and (10.2) were first used to eliminate rQ with the result

$$\frac{t}{a_M} = 4.62 \frac{K}{J} \tag{10.3}$$

The observed values of the period and radius proportionality constants were used to compute the apparent value of t/a_M. Reference to Fig. 3 (which was obtained from the figures in Tables XX and XXI) then allows the determination of k for an arbitrarily chosen γ. The non-dimensional period and radius then become determinate, and a value of rQ may be obtained which is consistent with both the radius and period data. In Table XXII, these energy values are given for the first period of oscillation of several of the explosives described previously in this report.

---

* Although the depths varied by about two-fold, k depends upon depth to the 1/2 power or less, and a_M and t are not very sensitive to k.

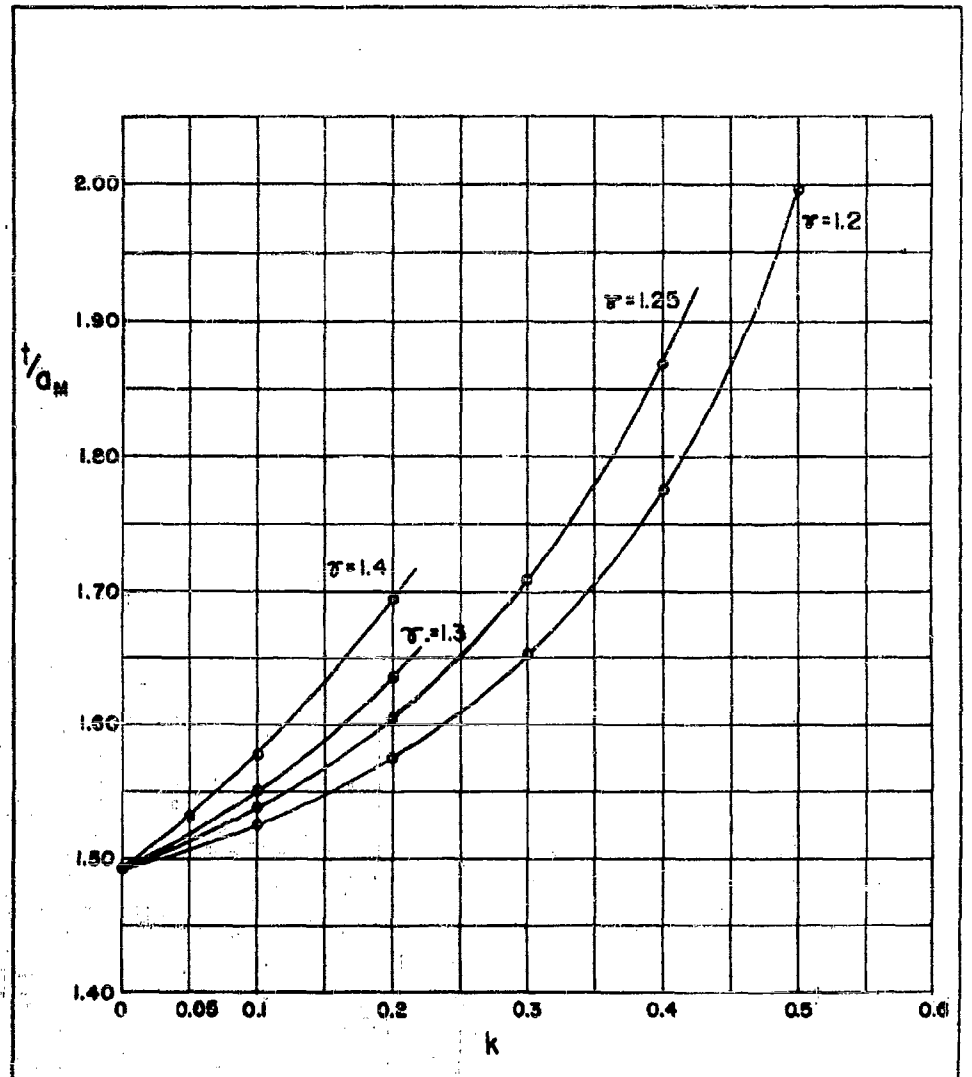

FIG. 3

PERIOD / MAXIMUM RADIUS (NON-DIMENSIONAL) VS PARAMETER k FOR VARIOUS γ

UERL WOODS HOLE, MASS.

TABLE XXII

FIRST PERIOD ENERGY CALCULATIONS FOR VARIOUS ADIABATIC PARAMETERS

Explosive	Remarks	J_1	K_1	t/a_M	$(rQ)_1$(cal/gm)				
					k = 0		k ≠ 0		
					Value from Radius	Value from Period	$\gamma = 1.2$	$\gamma = 1.3$	$\gamma = 1.4$
TNT	½ lb charges at 300 - 600 ft	12.6	4.36	1.60	388	477	517	467	443
TNT	55-300 lb charges at 50-100 ft	13.1	4.36	1.54	437	477	500	473	461
Tetryl	½ lb pressed charges at 300 - 600 ft	12.8	4.39	1.59	407	486	523	482	455
Tetryl	1/18 lb pressed charges at 300-600 ft	12.8	4.31	1.56	407	459	438	455	488
Tetryl	1/18 lb pressed charges 2-5 ft	14.1	4.46	1.46[a]	542	508	---	---	---
Tetryl	1/18 lb loose charges 2-5 ft	14.6	4.61	1.46[a]	603	564	---	---	---
Torpex-2		14.5	5.07	1.61	592	744	805	728	690
Blasting Gelatin		13.1	4.9	1.73	437	673	735	626	582

a. Since this value is lower than any appearing in Fig. 3, no calculation of the energy can be made for which the radius and period constants give a consistent result.

In each case the value of the bubble energy is also given neglecting the internal energy of the gas ($k = 0$), which fixes the values $a_M = 1$ and $t = 1.492$. Here it is to be expected that the radius calculation will give a lower value than that obtained from the period constant, since t is relatively insensitive to k, whereas a_M, when the internal energy is taken into account, may decrease 10% by comparison with its value for no internal energy. This is found to be true in all cases except the two involving tetryl charges very near the surface. Consistent calculations of the energy cannot be made in these two cases, since the energy calculated from the maximum radius is apparently higher than that obtained from the period of oscillation (this leads to values of t/a_M lower than any found in Fig. 3).

No complete explanation of this anomaly can be given at present. However, it is interesting to see what the theory predicts for a case in which the adiabatic law, Eq. (9.1), is replaced by the simple assumption that the gas pressure is a constant, p_g. This assumption may be a rough representation of the facts, if, during a large part of the motion, the condition of the gas is largely determined by the condensation of water vapor, a condition which might be true when the explosion occurs at the shallowest depths described in this report.

The resultant expressions for non-dimensional radius and period are, respectively:

$$a_M = \left(1 - \frac{p_g}{p_o}\right)^{-1/3} \tag{10.4}$$

$$t = 1.492 \left(1 - \frac{p_g}{p_o}\right)^{-5/6} \tag{10.5}$$

Although the ratio t/a_M is never less than 1.492 for positive pressure ratios, p_g/p_o, and thus cannot explain the low value $t/a_M = 1.46$ found experimentally, it seems noteworthy that both the radius and period constants should be larger on the basis of Eqs. (10.4) and (10.5) than in the case where the adiabatic law holds and that the observed constants are indeed found to be larger near the surface than at greater depths.

Calculations for the second period of bubble oscillation are given in Table XXIII.

From this discussion it is seen that suitable data are not available at present to determine the most appropriate value of the specific heat ratio. It should be mentioned that the theoretical calculations of Jones[22] indicate an effective value of $\gamma = 1.25$ for TNT of the density used in these experiments.

TABLE XXIII

SECOND PERIOD ENERGY CALCULATIONS FOR VARIOUS ADIABATIC PARAMETERS

Explosive	Remarks	J_2	K_2	t/a_M	$(rQ)_2$(cal/gm)				
					k = 0		k ≠ 0		
					Value from Radius	Value from Period	$\gamma = 1.2$	$\gamma = 1.3$	$\gamma = 1.4$
TNT	300-600 ft	8.5	3.22	1.75	119	191	207	178	164
Pressed Tetryl	300-600 ft	8.6	3.27	1.76	123	201	218	184	171
Torpex-2	600 ft	9.1	3.47	1.77	146	239	260	218	204

Using the data shown above, it is now possible to propose a partition of the energy released in the explosion. This is shown in Table XXIV. For the bubble energy, a value of $\gamma = 1.30$ was assumed. The values for the total energy are obtained from Ref. (23). They were calculated by assuming that the oxygen was consumed in the following sequence:

i. $H_2 + \frac{1}{2} O_2 \rightarrow H_2O$

ii. $C + \frac{1}{2} O_2 \rightarrow CO$

iii. $CO + \frac{1}{2} O_2 \rightarrow CO_2$

The shock-wave energy values have been computed from empirical equations for the energy flux as determined experimentally at the Underwater Explosives Research Laboratory.

TABLE XXIV

ENERGY PARTITION IN UNDERWATER EXPLOSIONS

Explosive	Total Energy Q (cal/gm)	Shock-Wave Energy (cal/gm)	Bubble Energy (First Period) (cal/gm)
TNT	977[a]	244[b]	467
Pressed Tetryl	1035[a]	263[c]	500
Blasting Gelatin	1509[a]	331[c]	626
Torpex-2	--	349[c]	728

a. See Ref. (23), "Assumption II"
b. See Ref. (24)
c. See Ref. (13).

While these values seem reasonable, it must be emphasized that there are uncertainties and assumptions in all of the calculations involved and that further refinements in calculation and measurement in the future will necessitate some revision.

APPENDIX I

EMPIRICAL RADIUS-TIME CURVE FOR OSCILLATING GAS BUBBLES IN FREE WATER

by

M. Arsove

In any study of the phenomena associated with the bubble formed by the gaseous products of an underwater explosion, it is essential that one know the size and shape of the bubble as a function of time. Assuming that the bubble is always spherical in shape, the bubble phenomena are completely determined if the bubble radius is known as a function of time. High-speed motion pictures of the bubble formed by charges which are not greatly elongated show that this is a good approximation for at least the first bubble oscillation.

To date it has been necessary to integrate numerically the theoretical equations of motion derived by Herring[3], Shiffman and Friedman[21], Taylor[18], and others in order to obtain a radius-time curve. If one has an analytic expression for the radius as a function of time, one can avoid the laborious numerical integrations required in order to predict such phenomena as migration, bubble-pulse, etc.

The purpose of this appendix is to find an analytic expression for the experimentally determined radius-time curves in free water and to indicate possible uses for this expression.

In attempting to find such an analytic expression, it is convenient to reduce the experimental data (for the radius as a function of time) to non-dimensional form. The units of time and length used in this appendix are the first bubble period (T_1) and the first maximum bubble radius (A_{m1}), respectively. These units of time and length were chosen because they can be computed from the equations in the body of this report* and because they reduce the data to a form which is easily analyzed.

The radius-time curves used in this analysis are those mentioned in Sec. 8 of this report. The composite curves (Figs. 4-9) in which A/A_{m1} has been plotted against T/T_1 for TNT at depths of 300 and 550 ft; tetryl at 300 and 600 ft; torpex-2 at 600 ft; blasting gelatin at 500 ft contain 7, 7, 9, 4, 8, and 3 individual radius-time curves respectively. Figures 4, 5, 7, 8, and 9 show that there is relatively little scatter in the data from shot to shot when a given weight and type of explosive is observed with the standard charge orientation. There is, however, considerable scatter in the neighborhood of the minimum due to the difficulties mentioned previously in Sec. 8. The data for blasting gelatin (Fig. 9) are of particular interest since they clearly indicate the non-sphericity present in the early stages of the oscillation of a bubble formed by a cylindrical charge whose length and diameter are approximately equal. There is considerable doubt as to the values of the radius for the contracting phase of the oscillation since the bubble was unstable and apparently formed four

* It should be pointed out that in preparing the composite curves the observed values of A_{m1} and T_1 were used to reduce each record to non-dimensional form.

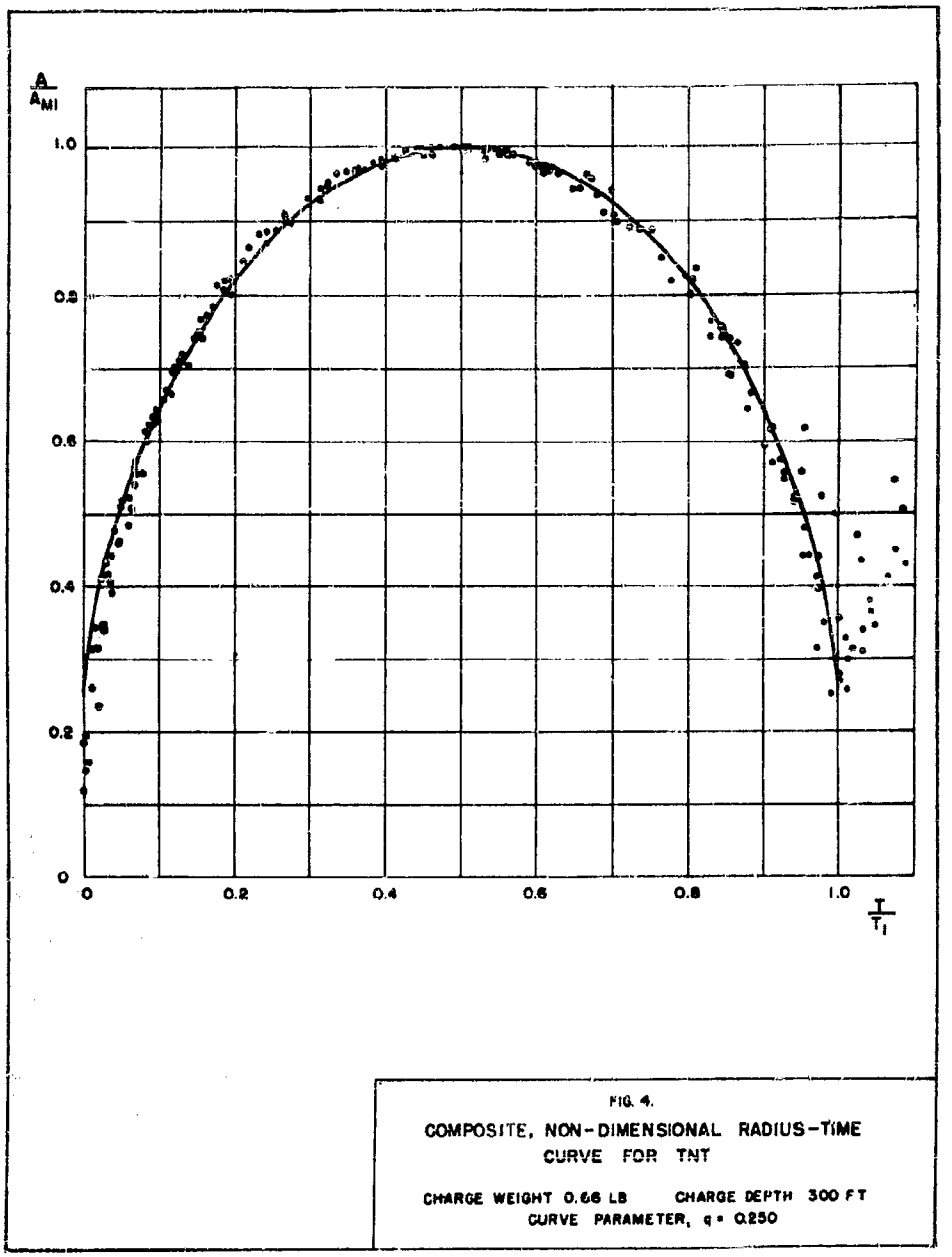

FIG. 4.

COMPOSITE, NON-DIMENSIONAL RADIUS-TIME CURVE FOR TNT

CHARGE WEIGHT 0.66 LB CHARGE DEPTH 300 FT
CURVE PARAMETER, q = 0.250

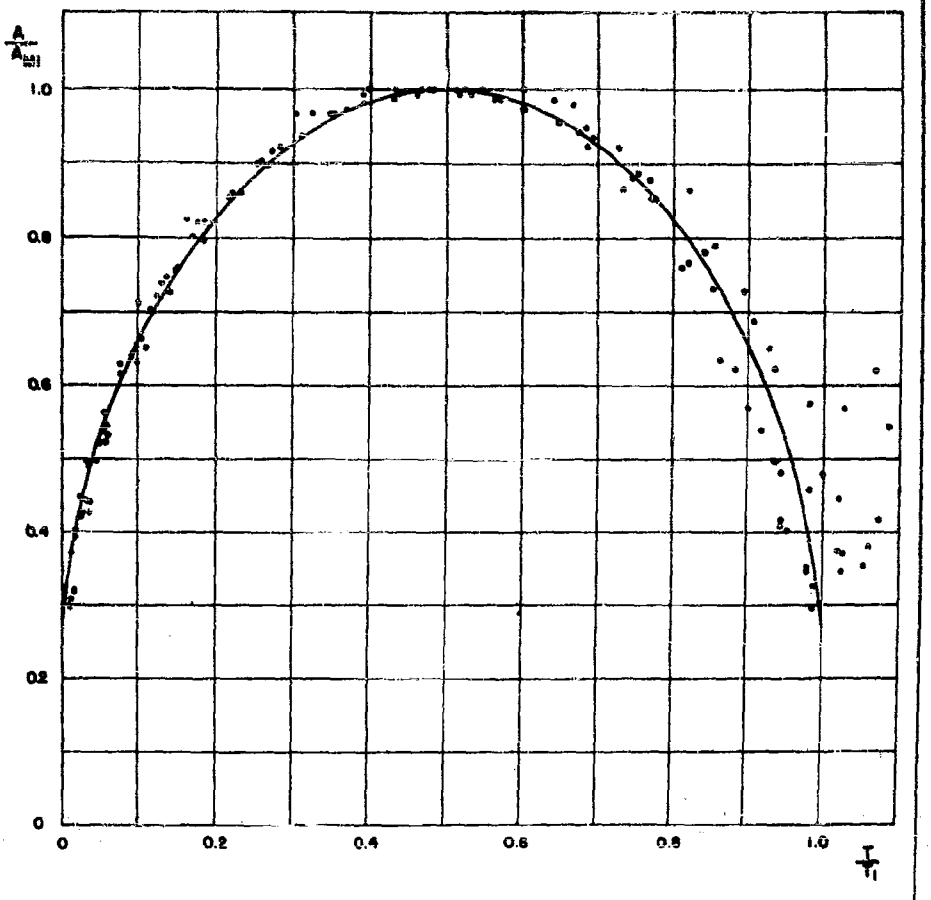

FIG. 5

COMPOSITE, NON-DIMENSIONAL RADIUS-TIME CURVE FOR TNT

CHARGE WEIGHT: 0.66 LB CHARGE DEPTH: 550 FT
CURVE PARAMETER, q = 0.275

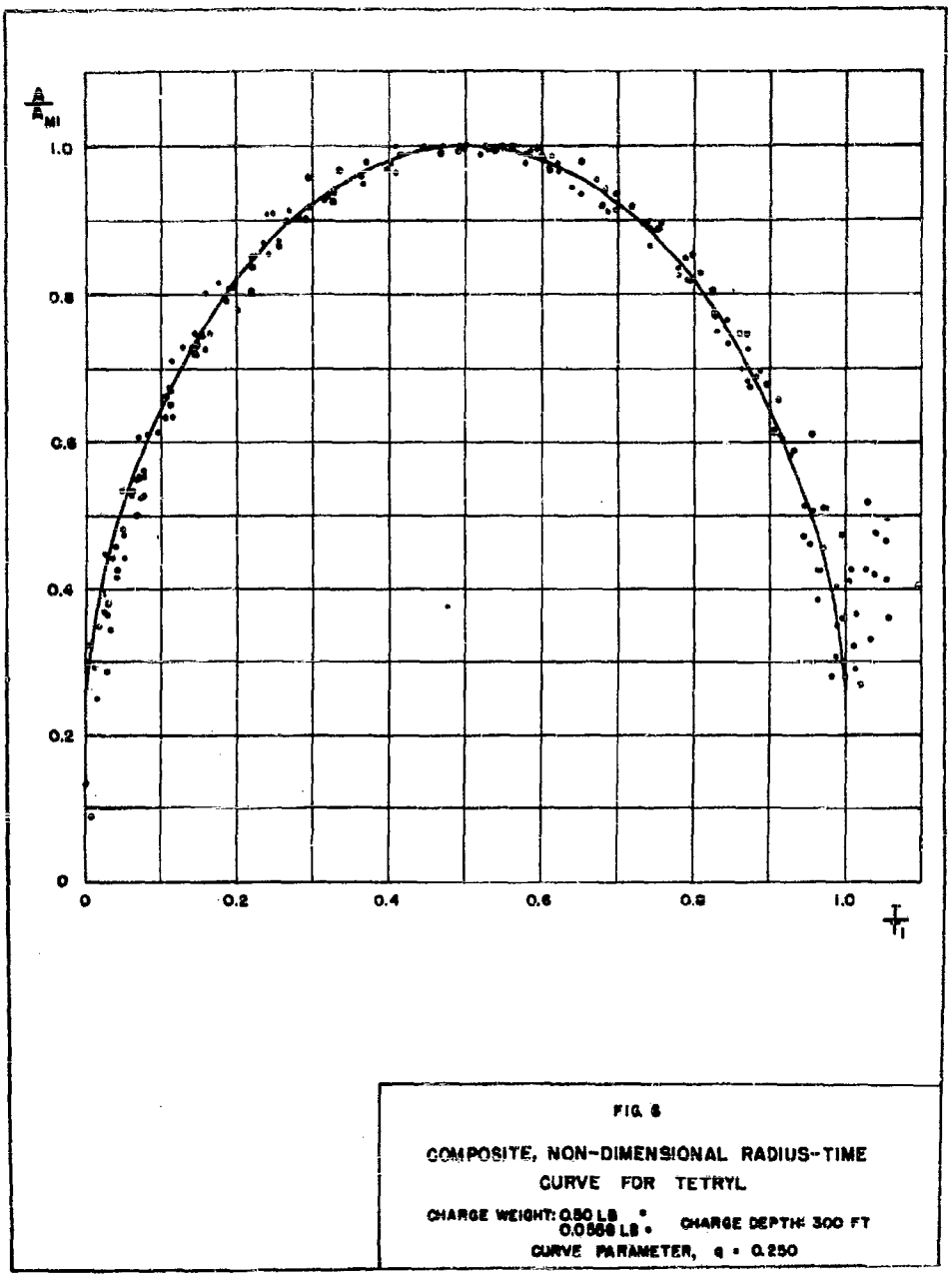

FIG. 8

COMPOSITE, NON-DIMENSIONAL RADIUS-TIME CURVE FOR TETRYL

CHARGE WEIGHT: 0.50 LB • 0.0566 LB • CHARGE DEPTH: 300 FT

CURVE PARAMETER, q = 0.250

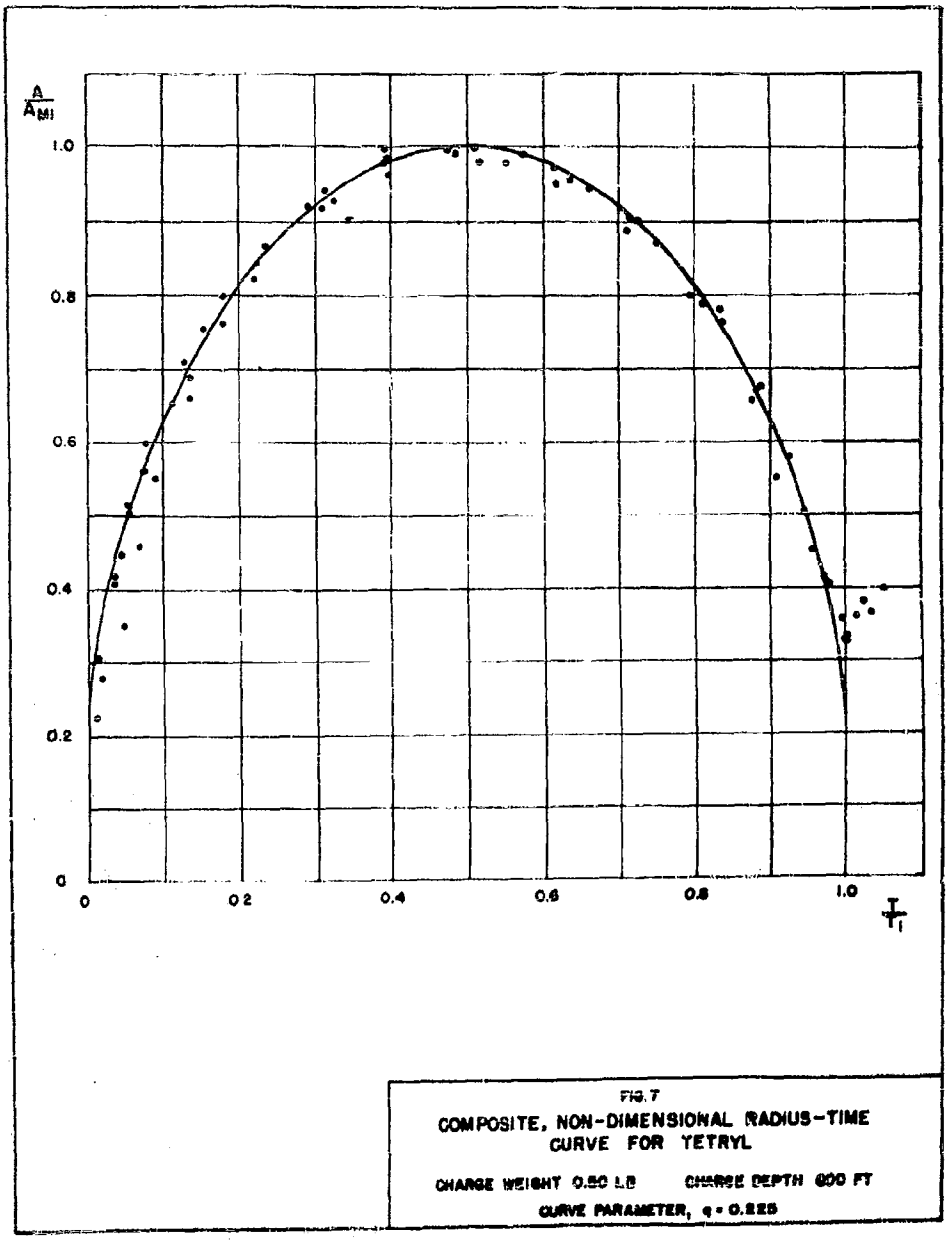

FIG. 7

COMPOSITE, NON-DIMENSIONAL RADIUS-TIME CURVE FOR TETRYL

CHARGE WEIGHT 0.50 LB CHARGE DEPTH 600 FT

CURVE PARAMETER, q = 0.225

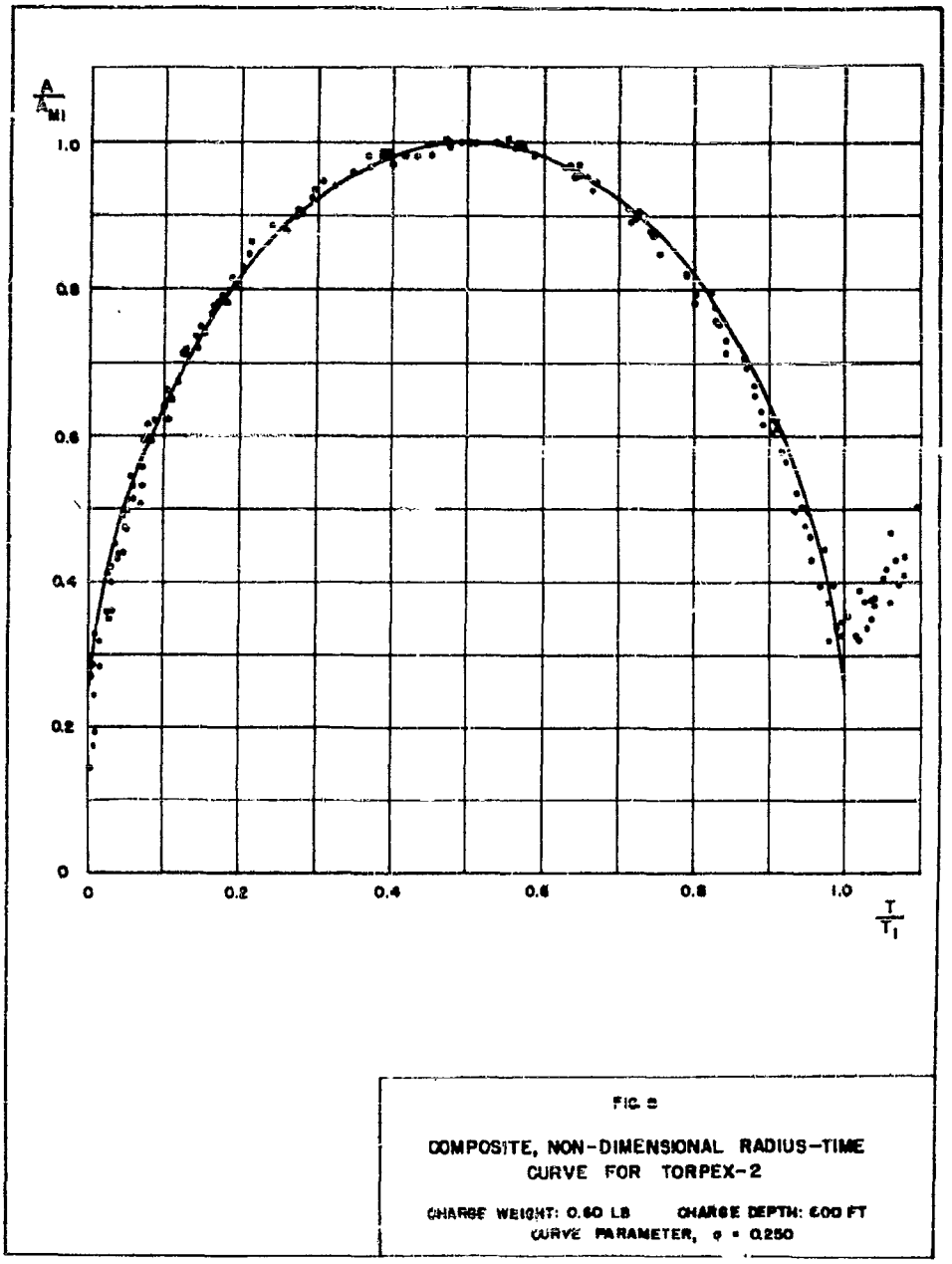

FIG 8

COMPOSITE, NON-DIMENSIONAL RADIUS-TIME CURVE FOR TORPEX-2

CHARGE WEIGHT: 0.60 LB CHARGE DEPTH: 6.00 FT
CURVE PARAMETER, φ = 0.250

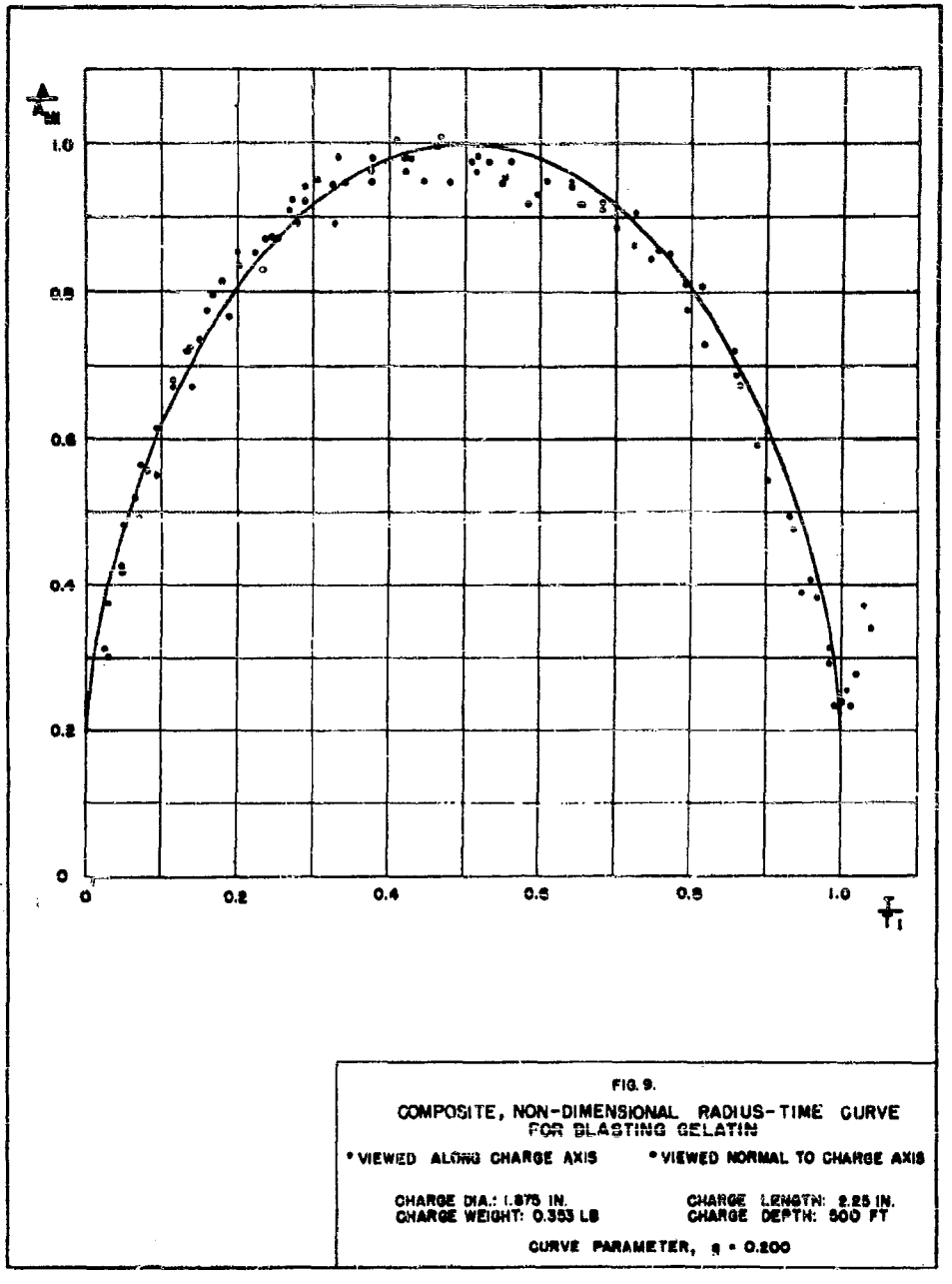

FIG. 9.

COMPOSITE, NON-DIMENSIONAL RADIUS-TIME CURVE FOR BLASTING GELATIN

* VIEWED ALONG CHARGE AXIS * VIEWED NORMAL TO CHARGE AXIS

CHARGE DIA.: 1.875 IN.
CHARGE WEIGHT: 0.353 LB
CHARGE LENGTH: 2.25 IN.
CHARGE DEPTH: 500 FT

CURVE PARAMETER, q = 0.200

small bubbles at the minimum. The radius values used in Fig. 9 were obtained by estimating the total volume of gas present at any instant and then computing the radius of an equivalent sphere. Figure 6, which includes data from two sizes of charge, shows that for a scale range of approximately 2:1 it is possible to represent the radius-time curve for a given explosive at a fixed depth in non-dimensional form. Although data from a wide range of explosive weights at a given depth were not available, it is believed that these non-dimensional curves will represent any size of charge in free water.

The shape of the composite curves resembles that of a curtate cycloid* (the curve traced out by a point on the spoke of a wheel which is rolling along a straight line in a plane). The equation of a curtate cycloid in rectangular, parametric form is:

$$A = m - n \cos \varphi$$

$$T = m\varphi - n \sin \varphi. \qquad m > n > 0 \qquad \text{(I-1)}$$

The constants m and n in this equation must be chosen so that $A = A_{M1}$ and $T = T_1$ for φ equal to π and 2π respectively, and so that A/A_{M1} fits the composite curves at φ equal to 2π. It should be noted that for φ equal to 2π, A/A_{M1} is identically A_{m1}/A_{M1}. If this ratio is represented by the symbol q, Eq. (I-1) becomes:

$$\frac{A}{A_{M1}} = \left(\frac{1+q}{2}\right)\left[1 - \left(\frac{1-q}{1+q}\right)\cos \varphi\right]$$

$$\frac{T}{T_1} = \frac{1}{2\pi}\left[\varphi - \left(\frac{1-q}{1+q}\right)\sin \varphi\right]. \quad 0 \leq q \leq 1 \qquad \text{(I-2)}$$

If one plots Eq. (I-2) with q taken as 0.25 along with the composite curve for TNT at 300 ft, it can be seen that the equation has been made to fit the data at φ equal to π and 2π, but that it predicts a value of A/A_{M1} which is too low for intermediate values of φ. This situation can be remedied if one writes the equations in the form:

---

* Various authorities disagree as to the distinction between a prolate and a curtate cycloid. The author prefers the definition given above.

$$\frac{A}{A_{M1}} = \left(\frac{1+q}{2}\right) \left[1 - \left(\frac{1-q}{1+q}\right) \cos \varphi\right]$$

$$\frac{T}{T_1} = \frac{1}{2\pi} \left[\varphi - \left(\frac{1-q}{1+q} + \varepsilon\right) \sin \varphi\right] \qquad \text{(I-3)}$$

where ε is a constant which in general should depend on q. If Eq. (I-3) is to supply physically admissable radius-time curves, (1-q/1+q) + ε must not exceed unity. The best fit is obtained, however, when:

$$\frac{1-q}{1+q} + \varepsilon = 1. \qquad \text{(I-4)}$$

Assuming that Eq. (I-4) is generally valid, the parametric form of the empirical radius-time curve becomes:

$$\frac{A}{A_{M1}} = \left(\frac{1+q}{2}\right) \left[1 - \left(\frac{1-q}{1+q}\right) \cos \varphi\right]$$

$$\frac{T}{T_1} = \frac{1}{2\pi} \left[\varphi - \sin \varphi\right] \qquad \text{(I-5)}$$

Figures 4-9 show the data mentioned previously along with curves calculated from Eq. (I-5). These curves show that, with a suitable choice of q, Eq. (I-5) give a good analytic representation of the radius-time curve for the portions of the bubble oscillation which are of interest; namely, for values of T/T_1 greater than 0.05. This follows from the fact that bubble phenomena such as the migration to the time of the first minimum in the radius (A_{m1}), the pressure pulse emitted by the bubble, etc., are independent of the exact shape of the radius-time curve in the early stages of the period.

It should be noted that the empirical radius-time curve in the form of equation (I-5) involves only one arbitrary parameter, q, which has a direct physical significance, as has been pointed out previously. Hence there are two main uses to which the equations developed above can be put. One can

compute q on the basis of the existing theory provided one has a knowledge of the physical properties of the gas in the bubble. Using this value of q, one can compare the predicted radius-time curve with the known experimental radius-time curve as a check on theory. In this connection it should be mentioned that the experimental data probably provide an upper limit to q, since the bubble is obscured at the time of the minimum by a mass of material which is more likely solid than gaseous. This difficulty has been discussed in detail in Sec. 8 of the present report. The other line of attack would be to use the value of q necessary to give a good fit with experimental radius-time curves as an aid in arriving at suitable values for the average physical properties of the gas in the bubble.

Another of the uses to which the empirical radius-time curve has been put is the following: Using the bubble theories mentioned previously, one can compute the radius of the bubble for the case of a zero excess pressure field surrounding the bubble. Expressing this radius as a fraction of the maximum radius of the bubble, one can determine, from the empirical radius-time curve, the fraction of the periodic time at which the excess pressure vanishes. It is found that this time agrees excellently with similar times determined from piezoelectric gauge measurements of the pressure field surrounding the bubble[26].

Due to the paucity of photographic data for charges fired at small non-dimensional depths, no attempt has been made to develop an empirical representation of the radius-time curve for this very important case. However, it can be stated with assurance that Eq. (I-5) does not hold when the presence of free or rigid surfaces becomes important.

LIST OF REFERENCES

1. Photography of Underwater Explosions, II: High Speed Photographs of Bubble Phenomena, by E. Swift, Jr., P. M. Fye, J. C. Decius, and R. S. Price, NavOrd 95-46, December 1946.

2. Photography of Underwater Explosions, III: Service Weapons, by J. C. Decius, P. M. Fye, R. S. Price, W. S. Shultz, and E. Swift, Jr., NavOrd 96-46, February 1947.

3. Theory of the Pulsation of the Gas Bubble Produced by an Underwater Explosion, Conyers Herring, NDRC C4-sr20-010, October 1941.

4. Measurement of Bubble-Pulse Phenomena, I: Mark 6 Depth Charges TNT Loaded, by C. P. Slichter, W. G. Schneider, and R. H. Cole, OSRD 6242, NDRC A-364, March 1946.

5. Private Communication, B. Friedman, Applied Mathematics Group, New York University.

6. Private Communication, A. Borden, Taylor Model Basin.

7. Measurement of Bubble Pulse Phenomena, II: Small Charges, by A. Arons, A. Borden, and B. Stiller, OSRD 6578, NDRC A-470, March 1946.

8. Measurement of Bubble Pulse Phenomena, V: Studies of the Anomalous Pulse Using Small Charges, by E. Swift, Jr., W. M. Flook, and R. S. Price, NavOrd 409, (not yet published).

9. Damage to Thin Steel Cylindrical Shells by Underwater Explosions, II, by J. C. Decius and G. Gever, NavOrd 106-46, November 1946.

10. Measurements of Growth and Oscillation of the Bubble Formed by an Underwater Explosion, by Mine Design Department, Scientific Section, Undex 35, May 1943.

11. Vertical Displacements of the Gas Bubble Formed by an Underwater Explosion, by H. F. Willis and R. T. Ackroyd, May 1943.

12. The Experimental Evidence on the Behavior of the Gas Bubble Due to the Explosion of a Mk VII Depth Charge, by Mine Design Department, September 1943.

13. Comparison of Underwater Explosives Having Varying Oxygen Balance, by C. R. Niffenegger, J. P. Slifko, E. A. Christian, A. H. Carter, and J. S. Coles, NavOrd 402, June 1947.

14. Die Schwingungen der bei einer Unterwassersprengung enstehenden Gasblase und die Druckverteilung in iher Umgebung, W. Döring, Institut für theoretisch Physik der Universität Göttingen, January 1943.

15. Adiabatisch pulsierende Gaskugel in unendlich ausgedehnter Flüssigkeit, K. Zoller, Forschungsanstalt Graf Zeppelin.

16. Bemerkugen zum Gasblasenaufsteig, by Hermes, CPVA G187/44.

17. Oscillation of Gas Globes in Underwater Explosions, by A. Keil and W. Wunderlich, TMB Translation 209, February 1946.

18. Vertical Motion of a Spherical Bubble and the Pressure Surrounding It, by G. I. Taylor, S. W. 19.

19. Critical Survey of Bubble Phenomena based on Information Available up to August 1943, by H. N. V. Temperley, Undex 64, November 1943.

20. Migration of Underwater Gas Globes Due to Gravity and Neighboring Surfaces, by E. H. Kennard, TMB R-182, 1943.

21. Studies on the Gas Bubble Resulting from Underwater Explosions: On the Best Location of a Mine Near the Sea Bed, by M. Shiffman and B. Friedman, AMP 37.1R.

22. The Pressure Volume Relations and the Chemical Constitution of the Products of Detonation in TNT during Adiabatic Expansion, by H. Jones, R. C. 212, July 1941.

23. Report on Study of Pure Explosive Compounds, II: Correlation of Thermal Quantities with Explosive Properties, by Arthur D. Little, Inc., Report to Office of the Chief of Ordnance (Contract W-19-020-ORD-6436).

24. NDRC Div. 2 Interim Report on Underwater Explosives and Explosions, UE-23, p. 20, June 15-July 15, 1944.

25. Preparation of Charges for the Study of Explosion Phenomena at the Underwater Explosives Research Laboratory, by P. Newmark and E. L. Patterson, OSRD 6259, NDRC A-381.

26. Energy Partition in Underwater Explosion Phenomena, by A. B. Arons and D. R. Yennie, NavOrd Report 406.

ANALYSIS OF THE SPRAY DOME

G. W. Walker
Mine Design Department, Admiralty

British Contribution

1919

ANALYSIS OF THE SPRAY DOME

G. W. Walker

Mine Design Department,
Admiralty

1919

* * * * *

Object.

The object of this research is to provide sufficient data from which it will be possible to form an accurate estimate of the amount and distribution of explosive material required to produce destruction of a given structure at a given range of distance.

The research might proceed on entirely empirical lines. Apart from the enormous cost of material and time involved, such a method is not in accordance with scientific method, which aims at co-ordinating information in such a way that a reasonable estimate may be formed of the effect of varying any particular set of circumstances.

Thus the research will follow two main lines:-

(1) Full scale sea experiments in which the damage done on certain known structures by given explosions is quantitatively determined.

(2) The determination of those physical quantities in an explosion which determine damage.

A ship is damaged as the result of the pressures exerted on it, and which are propagated through the water as a result of the explosion. Thus a complete knowledge of the time development of pressure in the water at any distance from a given mine is a vital link in the chain which connects the explosion with the damage done.

It will probably be some time before an accurate solution of this difficult problem is obtained, so that meanwhile we proceed to an account of an investigation of part of the problem which has been carried out in Mining School during the past year, and which has thrown considerable light on the matter.

The explosion of a mine in water, is followed by an upheaval of water, gas and stones. General Abbot "Submarine Mines" discusses the question of a study of the phenomena as a means of quantitative measurement. His view, expressed page 42, is that the phenomena are too variable to give results of great value.

Now the phenomena observed occur in distinct phases of which there are two or possibly three depending on circumstances. It appears that General Abbot is thinking about the very fine spectacular effect of the discharge of gas etc., and that he had not observed or had not considered the remarkably sharp spray phenomenon phase (1) which almost immediately follows the firing of the mine and precedes the upheaval of gas, etc.

This spray rises almost instantaneously in the form of a dome as shown in Plate 1. The outer edge is very sharply divided from the still water surface and every part of the dome seems to rise vertically.

Numerous experiments have been made and show that the spray phenomenon is a definite one and that it leads to important conclusions as to the nature of the explosive wave propagated from the mine.

Assumptions have to be made before we can interpret the spray phenomenon and the justification for the assumptions consists in the manner in which the conclusions agree with the experiments.

The .....

The assumptions are:-

(1) That the explosive pressures are propagated with the normal velocity 'C' of sound waves in water. That velocity is 1450 metres per second, and in round numbers we shall call it 1500 metres per second. Measurements of the compressibility of water show that except within a few feet of the explosion there is no reason to expect any serious departure from the above speed.

(2) That the wave is spherically symmetrical about the source.

From this it follows that the pressure at any point while dependent on time varies inversely as the distance r from the source, that the velocity of displacement is entirely radial and if

ρ_0 = density of water

C = speed of propagation

p = pressure of any point

v = radial velocity at same point

then $p = \rho_0 C v$

with very great accuracy.

We may now explain the spray phenomenon in general terms.

Let X Y be the free water surface of deep water.

M a submerged mine at depth d

M^1 an image mine at the optical image of M in X Y.

The whole effect at any point P is due to the primary effect from M combined with the effect reflected from the surface X Y. (See Figure 1).

Now the surface is a free water surface and thus the resultant pressure there must be permanently zero. This can be secured and the effect of the reflection at any point in the water is represented by an imaginary explosion at M^1 of equal magnitude but in opposite sign to that at M and starting at the same instant.

This secures that at any point Q on the surface the pressure is permanently zero, but the resultant velocity at Q is compounded of two equal effects arriving at precisely the same instant, one directed from M to Q and the other from Q to M^1. The resultant is no horizontal component but a purely vertical velocity. Calculation shows that this velocity

$$v_Q = \frac{2 p_0}{\rho_0 C} \cos\theta$$

Now p_0 is varying with time and we can further show that if the negative pressure which the water will support is negligible then each point of the water surface in succession must part company with the general body of water at the instant when p_0 attains a maximum, and proceeds upwards with the corresponding initial velocity. In particular at O vertically above the mine the initial velocity of the spray $v_0 = 2 p_0/\rho_0 C$ where p_0 is the maximum pressure developed at distance d. Conversely if we can measure the initial velocity we can calculate $p = \frac{1}{2} \rho_0 C v$ the maximum pressure developed at distance d. Possible corrections to this simple result will be considered later.

The spray phenomenon is so rapid that a kinema record is required to show its development and enable us to estimate the initial velocity of projection of the spray.

Our kinema normally takes from 16 to 20 pictures per second. The times are at present determined by including at the corner of each picture a photograph of the rapidly moving hand of a chronograph fixed in front of the camera. This hand moves through 120° in 1 second.

The distance scale is determined by including the photograph of a measured base line of 60 feet marked at one end by an empty mine case from which the mine proper is suspended and at the other end by a fisherman's blob.

We thus .....

We thus obtain a series of pictures which are measured so as to give the height attained by the spray at a series of known times, and from these the initial velocity is obtained by analysis.

It appeared at the very outset that the spray particles were not proceeding with a retardation equal to gravity, but with a considerably greater retardation. The natural inference was that the spray particles were so small that considerable viscous resistance was in play.

Accordingly instead of the equation of motion of the particles being

$$\frac{d^2s}{dt^2} = -g$$

where S is the height at time t, and g is the acceleration of gravity, it is assumed that the equation is

$$\frac{d^2s}{dt^2} + k\frac{ds}{dt} = -g .$$

where k is the unknown viscous constant.

The solution is

$$S = \left[\frac{v_o}{k} + \frac{g}{k^2}\right]\left[1 - e^{-kt}\right] - \frac{g}{k}t$$

v_o being the initial velocity.

Our measurements give a series of values of S at certain times. The initial time is, however, unknown, and we have to determine three unknown quantities v_o, k and the initial time from the observations.

Three observations are theoretically sufficient but to reduce casual error we take 6 points and combine in pairs so as to get average values.

A specimen record is reproduced, Plate 2. It shows the explosion of a Torpedo War Head 500 lbs. of T.N.T.

The following is a copy of the measurements and the analysis.

17th September, 1919.

Torpedo War Head 500 lbs. T.N.T. at depth 50 feet
in Water 100 foot deep.
Distance between Blobs = 60 feet
On picture = 6.0 mm.
Hence scale is 1 mm. = 10 feet = 305 cms.
Time scale 1 second = 120°

Picture No.	Angle of Index Hand.	Time in seconds	Measured height of spray at centre in mms.
1			.05
2	4.8	.0400	.4
3	5.2	.0833	.7
4	5.1	.1258	1.0
5	5.3	.1700	1.3
6	5.3	.2142	1.6
7	5.4	.2508	1.7

From these observations drawn on squared paper the following smoothed values are taken as the basis of calculation

	t	S	Calculated by Formula
(1)	t_1	.05	.05
(2)	.05	.47	.47
(3)	.10	.83	.83
(4)	.15	1.16	1.16
(5)	.20	1.46	1.45

From .....

From (1), (2), (3) and (4) we get $k = 1.82$
From (3), (4), (5) and (6) we get $k = 2.06$

mean $k = 1.94$

	Seconds	H.ms/second on picture.
From (1) and (4) we get t_1	= .0057	= 8.901
(2) and (5) we get t_1	= .0059	= 8.954
(3) and (6) we get t_1	= .0054	= 8.888
t_1	= .0057	= 8.914

Hence absolute value of V_0 = 8.914 x 305
= 2720 cms. per second.

Thus taking $\rho_0 = 1$; C = 15×10^4 cms. per second.

We get p max = $\frac{1}{2} \rho_0 Cv$ = 204 atmos. = 3000 lbs. /square inch
= 1.34 tons per square inch.

as the maximum pressure produced by 500 lbs. T.N.T. at distance of 50 feet.

From the deduced values for V_0, k and t_1 the values of S are calculated and entered above. The comparative results are shown in the adjoining diagram Figure 2.

If Stokes viscous law is applicable the above value of k would lead to the conclusion that the particles are about 0.4 mm. in diameter.

A number of experiments have been made with mines, depth charges, and war heads. The explosive, the weight used, the depth, the primer, have all been varied. The method of experimenting has been gradually improved where experience showed the necessity. Discrepancies occur from time to time, so that until the reason for these has been fully investigated, it is not considered desirable to give final results. At the same time it is possible to say with reasonable certainty that the results so far obtained confirm the view that for the same weight of explosive the maximum pressure is inversely proportional to the distance, while for the same distance the maximum pressure appears to be nearly proportional to the square root of the weight of the explosive. The difference between different explosives such as pure T.N.T. and different grades of Amatol do not appear very definite as far as maximum pressure is concerned, but a final decision must wait for further experiments. As regards magnitude it appears that a 300 lb. depth charge of 50/50 Amatol primed with 3 pisco of C.E. gives a maximum pressure of 1.15 tons per square inch at a distance of 50 feet.

The maximum pressures obtained by this method are in themselves very useful, but the method gives no information as to the time element in the explosive wave for which a very different method of procedure is now being investigated. But the known speed of detonation, say 5000 metres per second, in round numbers, and the general dimensions of the mine, say ½ metre, suggest that the order of magnitude of the time from initiation to maximum pressure is of order 10^{-4} seconds. It will vary of course, with the explosive, the amount of it, and the manner of detonation, but this figure and the known value of the maximum pressure are most useful as a guide in the design of the apparatus for measuring the time pressure sequence.

The comparatively simply character of the primary wave from the explosion, as outlined, may appear to be at variance with the observed fact that the damage to a vessel depends greatly on the position relative to the charge and to the surface.

Let us revert to Figure 1 and consider the effects at a point P in the water.

The disturbance from the image mine is opposite in sign to the direct effect, is less in the proportion r_1 and r_2 and arrives later by the time taken to traverse the distance $(r_2 - r_1)$ at the rate 1500 metres per second (the speed of the wave in water). Now at any point the primary and the reflected disturbances each rise to their maximum in a very short time, which we have seen is of order 1/10,000 th of a second. If then $r_2 - r_1$ is 1 metre or say 3 feet, the interval between the two maxima would be 1/1,500th of a second and the two effects are practically separated. But if $r_2 - r_1$ is as small as 3 cm., the interval is only 1/50,000th of a second and thus small compared with 1/10,000th of a second as above. The two effects would thus tend to cancel each other, and we thus see how to reconcile the apparent paradox that the resultant action may be small near the surface, while at some depth there are two separate large shocks.

It may ...

It may be shown that at 200 yards horizontal distance from a mine 50 feet deep, $r_2 = r_1$ would be equal to 1 metre at a depth of 16 feet beneath the surface, and equal to 3 cms. at a depth of 6 inches beneath the surface.

This is shown diagrammatically in Figures 3 and 4.

In the same way Figure 1 shows how reducing the depth of the mine tends to lower its damaging efficiency sideways. r_2 tends to become more nearly equal to r_1 as the mine approaches the surface, so that the opposing actions are more nearly equal in magnitude, and more nearly equal as regards time of arrival, and hence they tend to neutralise each other.

These inferences are in agreement with direct observation. For if we observe at say 200 yards from an explosion only a very slight shock is experienced in a rowing boat or a shallow draught motor launch, whereas in a deep draught trawler the shock is very marked.

In order to preserve simplicity in the preceding argument, we have not referred to a modifying circumstance which must now be considered.

The original surface layer breaks away from the lower water, but successive layers follow as the reflected wave spreads so that a saucer shaped depression should rapidly develop downwards. Between this saucer surface and the dome above there will be a continuous succession of spray, moving however with smaller speed, so that it does not break through, and we can learn nothing about it by direct observation.

The developing saucer boundary forms at each instant the effective reflecting surface for the primary wave and thus the reflected negative wave undergoes distortion in its later stages without affecting anything that occurred earlier. The net result is that a body in the water will experience the primary crushing pressure, which will be followed at the appropriate time by the creation of a vacuum on the side nearest the image mine and which will spread to the remote side. The destructive effect of this on a submarine already crumpled by the primary wave may be very important.

Although the primary velocity acquired by the water at some depth may be very high, e.g. 11 metres per second in the case of a 300 lb. charge at 50 feet yet the time is so short that the water does not move more than about ¼ cm.

Although we have discussed only the reflection from the surface, the effect of the bottom may also be examined by the method of images. If e.g. the bottom is rigid rock the corresponding image would have the same sign as the true mine since the condition is now zero resultant normal velocity instead of zero resultant pressure. Probably, however, the bottom is soft and yields at first and at greater depth becomes rigid so that the composite action may not be nearly so simple as that of a free water surface. Experiments are, however, in progress and further discussion of the effect of the bottom is reserved until these have been analysed.

We have now to consider possible corrections to the simple formula $p_o = \frac{1}{2} \rho_o C v$ for the maximum pressure.

(1) We have neglected a term involving the square of v_o. It is of order v_o/C compared with the main term. At 50 feet from a 300 lb. charge v_o is about 23 metres per second, while C is 1500 metres per second. Thus the correction is of order 1% in this case and may be neglected. For larger charges and shorter distances the effect might rise to a few per cent and would have to be allowed for if the measurements ever attain such a degree of accuracy. The correction is negative in sign.

(2) We have assumed that the water cannot support negative pressure.

Now Osborne Reynolds found that air-free water might in favourable conditions support a negative pressure of 72 lbs. per square inch. Since sea water has plenty of air dissolved in it, it would seem doubtful if it could support anything like this amount. On the other hand certain features in the spray phenomenon, e.g. the sharp boundary suggest that the water may support negative pressure as much as a ton per square inch without breaking. The evidence is, however, still ambiguous, but will be examined later.

If it should prove that the negative pressure must exceed say P tons per square inch before rupture takes place, then the maximum pressure p_o as calculated above is an under estimate of the correct value of $\frac{1}{2}$ P approximately. The result of a finite value of P is that the spray

Instead .....

instead of breaking off continuously in indefinitely thin layers would not break immediately but the first layer would have a finite but small thickness. Thus taking the 300 lb. depth charge at 50 feet, if $p = 0.2$ tons per square inch the thickness of this layer would probably be about 6 cms. and the corrected maximum pressure would be 0.1 tons more. At present, however, this is quite speculative.

As already stated an apparatus for the direct recording of the time pressure sequence is being constructed in Mining School.

Experiments to this have been in progress elsewhere. So far as is known these are:-

(1) Hopkinson's Pressure Bar method in use at Woolwich Arsenal.

(2) Hillier's experiments at Troon by means of crusher gauges.

(3) A method devised by Sir J.J. Thomson which makes use of the piezo electric properties of quartz.

It is hoped that in course of time the different methods may be compared, as the problem is such a difficult and delicate one that it would be most unwise to trust to any one method entirely until satisfactory agreement of two independent methods can be established.

FIG. 1.

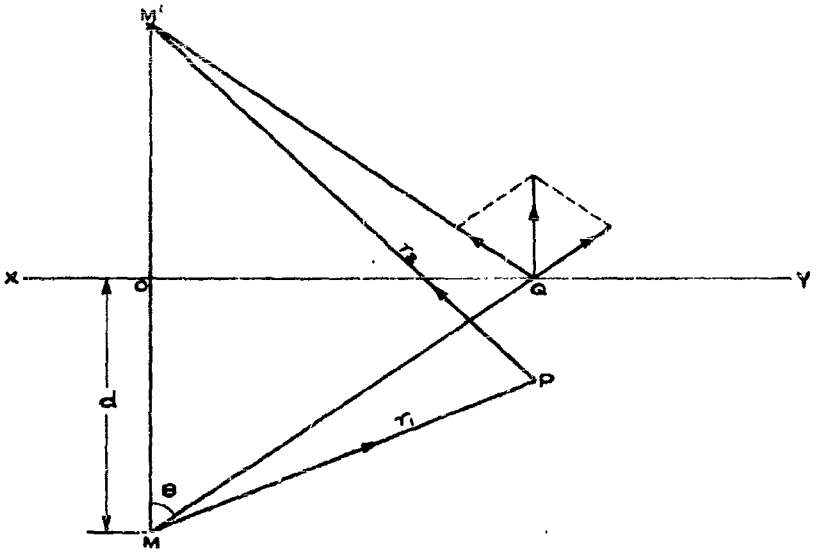

FIG. 2.

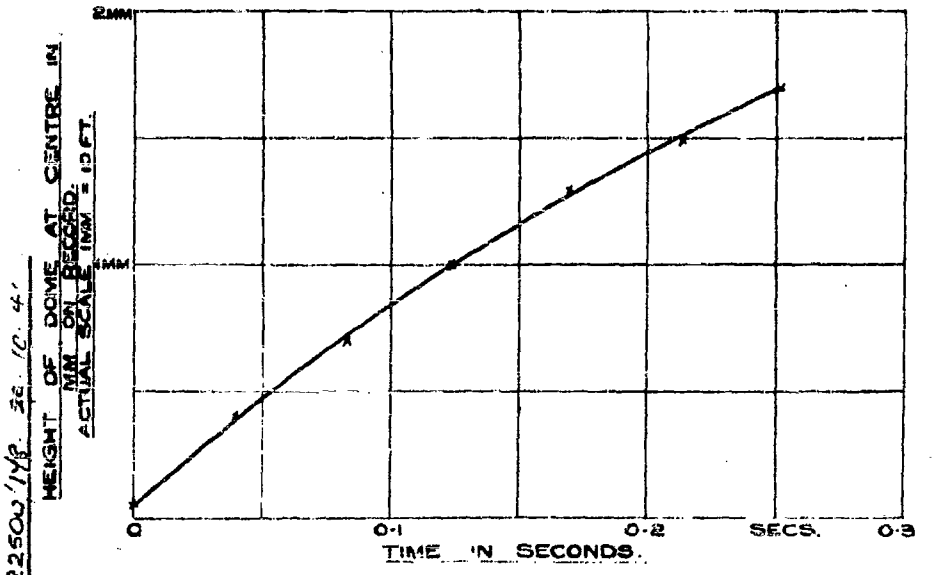

M.D. SK. 22500/148 Sc. 10. 41.

RISE OF SPRAY DOME FROM 500 LBS. T.N.T. AT A DEPTH OF 50 FT. (FROM CINEMA RECORD).

DIAGRAM TO ILLUSTRATE RESULTANT ACTION OF A SUBMERGED MINE

DR WALKER

FIG. 3

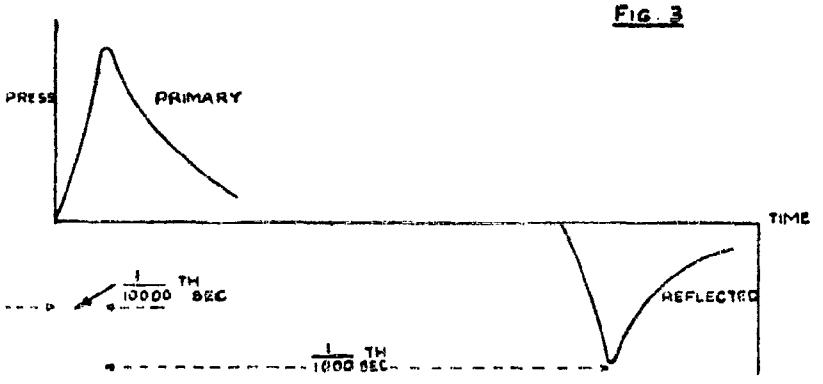

DIAGRAM TO ILLUSTRATE RESULTANT ACTION OF A SUBMERGED MINE

DR WALKER

FIG. 4

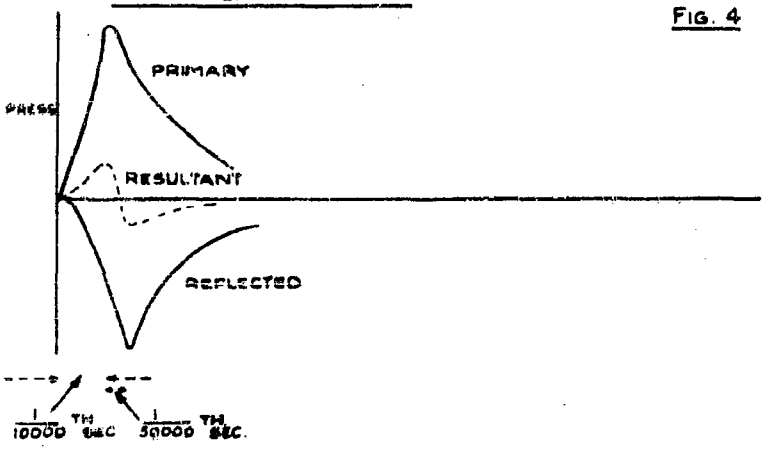

MD.SK. 22502/192 21.7.44.

PLATE 1

4 x ENLARGEMENT OF FRAME AT TOP OF 2ND COLUMN OF PLATE 2

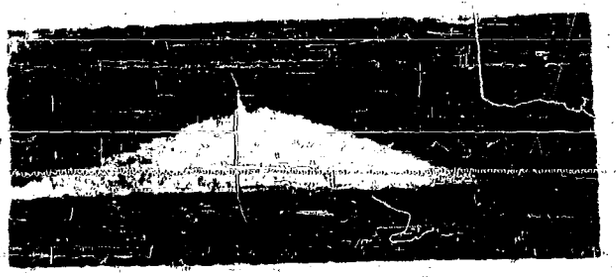

TORPEDO WARHEAD

500 LBS TNT - DEPTH 50 FT.

INSTANTANEOUS PHOTOGRAPH

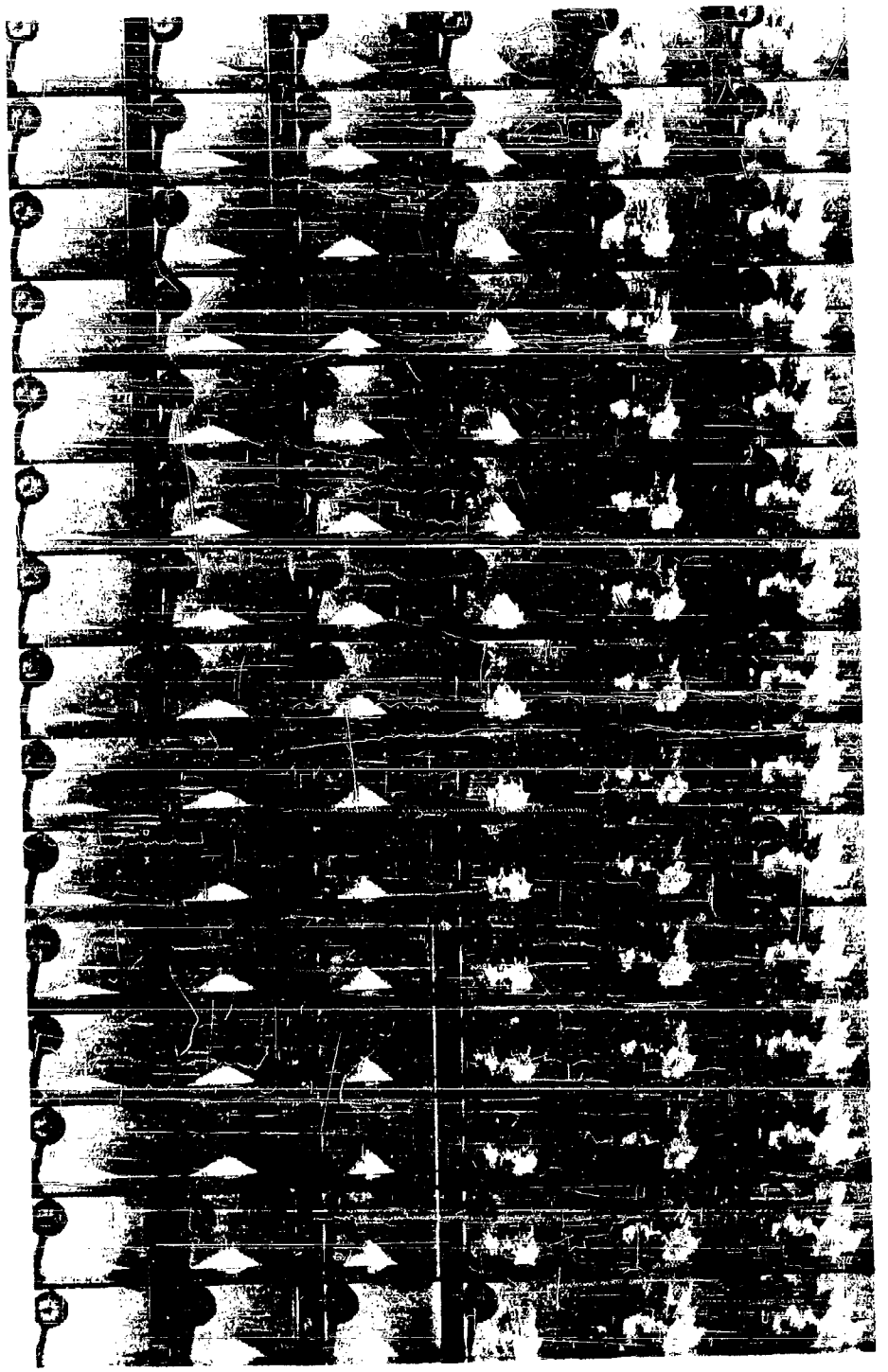

TORPEDO WARHEAD

500 LBS. TNT - DEPTH 50 FT

KINEMA RECORD

A METHOD OF DETERMINING THE DEPTH OF UNDERWATER EXPLOSIONS

R. A. Shaw
Marine Aircraft Experimental Establishment
Scotland

British Contribution

December 1941

A METHOD OF DETERMINING THE DEPTH OF UNDERWATER EXPLOSIONS

R. A. Shaw

Marine Aircraft Experimental Establishment
Scotland

December 1941

* * * * * * * *

Summary.

A method of determining the depth of detonation of a bomb exploding under water from measurements of the distribution of velocity in the spray dome is described. The method is based on the assumption that the detonation wave approximates to a sound wave. This leads to the relationship that the initial velocity at each point in the dome is inversely proportional to the square of its distance from the centre of detonation, so that the depth of detonation can be found from the ratios of the initial velocities at different radii. The method has been applied to the analysis of tests with depth charges, and reasonably consistent results obtained.

Introduction.

When bombs are intended to be dropped into water, it is important to know at what depth detonation takes place.

A method of obtaining the depth is described which depends on an analysis of the velocity distribution in the spray dome which appears on the surface of the water above the exploding charge immediately after detonation.

The method depends on an approximation, which will have to be justified by results, but as a method it has several marked advantages: standard bombs are used, the tests can be done anywhere provided calm deep water is available, and the only equipment necessary is a cine camera operated from a surface craft.

Method.

A typical example of the spray dome is shown in Figure 1 which is made up of enlargements from the cine film of a test with a depth charge. The growth of the same dome is shown graphically in Figure 2, which gives the height of the dome at various radii, plotted on a common time base.

The assumption made in the method is that, to a sufficient approximation, the initial velocity of the spray at any point in the dome is inversely proportional to the square of the distance of that point from the centre of detonation. This is equivalent to saying that

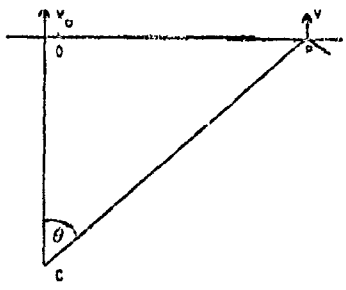

$$v = v_0 \cos^2\theta$$

when v = initial velocity at P

v_0 = " " at O

and since the depth of detonation,

d, is given by

$$d = OP \cot\theta,$$

the ratio v/v_0 indicates the depth in terms of the radius OP, at which the measurements have been taken. In practice, the depth is calculated by taking the average from several radii

chosen .....

chosen generally between 10% and 60% of the maximum radius of the dome. The fact that the dome is limited in diameter is itself an indication that the variation of velocity assumed is only approximate.

Notes on the practical details of the method are given in the Appendix.

Basis of method.

The basic assumption in the method is that the detonation wave except in the immediate neighbourhood of the explosion, behaves approximately as a spherical sound wave. For a spherical sound wave the strain energy in the wave is constant, i.e.

$$4\pi \int_{r}^{r+e} \frac{p^2 r^2 dr}{2K} = \text{constant}$$

It follows that where the wave length, e is constant and small compared with the radius r

$$p^2 r^2 = \text{constant}$$

and the pressure is therefore inversely proportional to the radius.

At the surface the detonation pressure wave is reflected as a suction wave and the particle velocity at the surface which is assumed to be the initial velocity of the spray is given by

$$\rho v c = 2p \cos\theta \quad \text{at } \theta,$$

$$\rho v_0 c = 2p_0 \quad \text{at } 0,$$

where ρ is the density and c is the velocity of sound in sea water.

It follows that $\frac{v}{v_0} = \frac{p \cos\theta}{p_0}$

$$\frac{p}{p_0} = \frac{OC}{OB} = \cos\theta$$

$$\frac{v}{v_0} = \cos^2\theta$$

Results obtained so far with the method.

The method has been applied to the analysis of results obtained with depth charges in tests during September, 1941. The depth charges were dropped from aircraft in a wide range of height and speed conditions.

Particulars of these tests and the results of the analysis are given in Table 1. There is no direct check on the calculated depths of detonation, but some indication of their accuracy can be obtained. In Figures 3 and 4 the calculated depth is plotted against two time intervals which are related to the depth and yet are measured quite independently of the depth calculation.

It will be seen that with one exception the depths obtained are all within 10 feet of a mean curve and the majority are within 5 feet. Both of the time scales used are influenced by other factors which cannot be allowed for with any certainty. The time underwater before detonation (see Figure 3) must depend on the impact conditions which vary widely and the time from detonation to the appearance of the plume (in Figure 4) is bound to be somewhat erratic if only on account of the irregularity of the plume itself. It will be seen, however, that in Figure 4 in which the time base is least dependent on the external conditions of the test, there is the closest grouping of the points. There is one point in Figure 3 which may be noted. In one drop the depth charge bounced on impact so that by the second impact it had lost the greater part of its initial velocity. The time underwater from the second impact to detonation was 5.7 seconds and the calculated depth was 57 feet. This corresponds to a mean sinking speed of 10 f.p.s. which is the accepted figure for these depth charges.

It is reasonable to suppose therefore, that the variations shown in Figure 3 and 4 are real variations in the depth of detonation and that the method in practice gives the depth to within a very few feet. For conclusive proof control tests with depth charges detonated at known depths are required.

It has .....

It has been suggested that for a given weight of charge the product of the initial velocity at the centre of the dome and the depth of detonation is constant. For a 300 lb. weight of charge, a value of $v_o d$ of 1,500 square feet/second based on results obtained by Hilliar was used to decide the depth of detonation of 500 lb. A/S bombs. The results of the present analysis give variations of $v_o d$ from 2000 to 6000 with an average of 4000 square feet/second. There is evidence to support variations of this order from tests with mines so that the assumption of a constant value does not appear to be justified. It will be seen that to assume $v_o d$ is constant for a given charge weight is equivalent to assuming that the maximum pressure in the detonation wave is constant at a given distance from the charge. Since it is known that the detonation wave is characterized by its maximum pressure being reached suddenly in a sharp front, it does not seem likely that the maximum pressure will itself be constant. It would be expected to vary with temperature and with manufacturing conditions, and in this regard it is interesting to note that the variations in the value of $v_o d$ on individual days (in table 1) are rather smaller than they are in general.

There is one other point in the analysis to which reference should be made. Within the dome area the surface water is shattered by the suction developed in the reflected wave, but at the boundary, where no spray appears, it must be assumed that the water is capable of withstanding the suddenly applied suction. This boundary suction has been calculated in terms of the velocity at the centre of the dome as

$$p_s = \frac{\rho v_o c \cos \theta_m}{2}$$

$$= -34 v_o \cos \theta_m \text{ lb./sq.in.}$$

where θ_m is the angle subtended by the dome boundary, i.e.

$$\tan \theta_m = \frac{D}{2d}$$

The values obtained for this suction vary from 700 to 1,800 lb./sq.in. but the greater number are in the neighbourhood of 1,000 lb./sq.in.

Conclusions.

So far as can be judged the proposed method of deriving the depth of detonation from the distribution of velocity in the dome gives the depth accurately to within a few feet.

The accuracy obtained can only be decided with certainty from control tests in which depth charges are detonated at known depths.

Sufficient reliance can be placed on the method of analysis to show that the velocity at the centre of the dome is not by itself a reliable indication of the depth.

TABLE 1.

TESTS WITH DEPTH CHARGES.

PISTOL SETTING feet	AIRCRAFT		TIME INTERVALS			h feet	DOME D feet	v_o f.p.s.	DOME BOUNDARY		CALCULATED DEPTH OF DETONATION D ft.	$v_o d$ sq.ft/sec.
	Height feet	Speed knots	t_w secs.	t_m secs.	t_p secs.				θ_m degrees	Ps lb/sq.in.		
24	1115	136	2.7	-	0.27	-	230	128	77.7	930	25.0	3200
24	980	162	3.4	-	0.78	-	255	128	78.0	900	27.0	3460
24	90	210	4.8	0.91	1.13	26.6	180	114	63.9	1760	44.0	5000
24	60	205	5.6	-	1.22	-	185	140	67.1	1830	39.0	5470
24	60	195	5.8	-	1.14	-	220	128	67.6	1650	45.5	5830
50	40	145	5.7	0.87	1.30	24.2	280	85	67.7	1085	57.0	4850
50	40	144	6.2	1.12	1.54	26.0	315	64	63.9	950	77.0	4920
50	290	146	7.4	1.02	1.30	22.0	184	56	61.5	905	50.0	2800
50	240	163	7.1	0.98	1.40	20.0	266	66	69.4	780	50.0	3300
50	220	177	7.8	0.93	1.40	19.2	258	58	67.2	885	54.0	3670
50	230	191	6.2	1.15	1.46	25.5	230	75	62.6	1170	59.5	4460
50	290	134	6.5	1.04	1.50	24.5	226	72	61.0	1180	63.0	4520
50	290	148	6.9	1.29	-	18.0	194	49	66.1	670	43.0	2110

t_w = time under water before detonation.
t_p = time from detonation to appearance of plume.
D = maximum dome diameter.
t_m = time to reach maximum dome height at centre.
h = maximum dome height at centre.
v_o = initial velocity at centre.

APPENDIX

NOTES ON PRACTICAL DETAILS OF METHOD

1. A standard 35 m.m. Sinclair or Vinton camera has been used in the tests at an average film speed of 25 frames/second. As large a dome as possible is required for satisfactory analysis so a proper choice of lens and distance is important. With a 6 inch lens, the camera should be about 700 to 1,000 yards from the impact, for a dome diameter of 200 to 300 feet.

2. The scale of the dome has to be obtained from the scale of the aeroplane. Corrections have to be applied for the different positions of the aeroplane and the impact, and for high drops, when the aeroplane is out of the picture some time before impact occurs, these corrections are important. To keep the corrections small, it is advisable to use as long a focal length lens as possible, as this will enable the ground distance to be as large as possible by comparison with the height and forward travel during the fall of the bomb.

3. The measured dome heights are corrected for obliquity. This correction is: $\frac{x}{2y} D$ at the centre of the dome, where D is the dome diameter, x is the height of the camera above water level, and y is the distance between camera and dome. The correction is proportionately less at radii away from the centre.

4. Both sides of the dome are measured and the mean is taken in the depth calculations. From Figure 2 it will be seen that the variations are at times considerable.

5. The table of reduction used to obtain the depth from the measurements is shown in Figure 5. The example worked out in the table is the same as that shown in Figures 1 and 2. In practice instead of taking the ratios of the initial velocities at the various radii it has been found more convenient to take the ratios of the dome heights corrected for the gravity fall. Equating these height and velocity ratios is only strictly justified when the time intervals are small and the deceleration of the spray is proportional to its velocity. The approximation amounts to neglecting terms involving t^3 and higher powers, where t is the time interval from detonation. It is realised that the deceleration of the spray is more nearly proportional to the square of its velocity, but the effect of both approximations has been found to be negligible in practice. The analysis of the two drops which gave the shallowest detonation has been repeated using velocity ratios in place of the corrected height ratios; agreement was obtained within less than 0.5 feet.

Frame
No.1.
t = 0.037 secs.
from first
appearance of dome

No.2.

t = 0.074 secs.

No.3.

t = 0.111 secs.

No.5.

t = 0.185 secs.

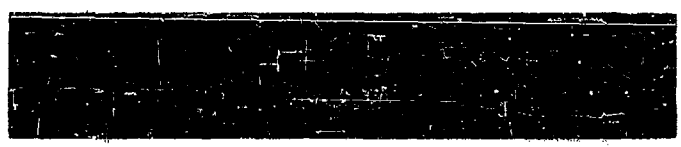

No.7.

t = 0.26 secs.

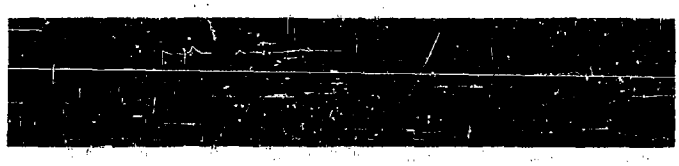

No.15.

t = 0.55 secs.

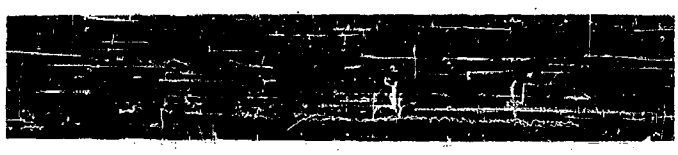

No.25.

t = 0.93 secs.

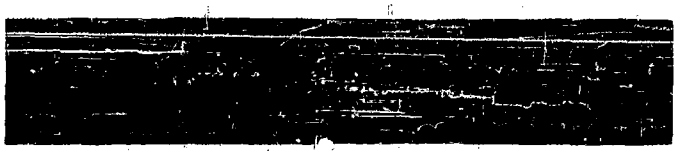

Scale 0 50 100 150 200 ft.

FIG 1 TYPICAL SPRAY DOME
CALCULATED DEPTH OF DETONATION, 24 FEET.

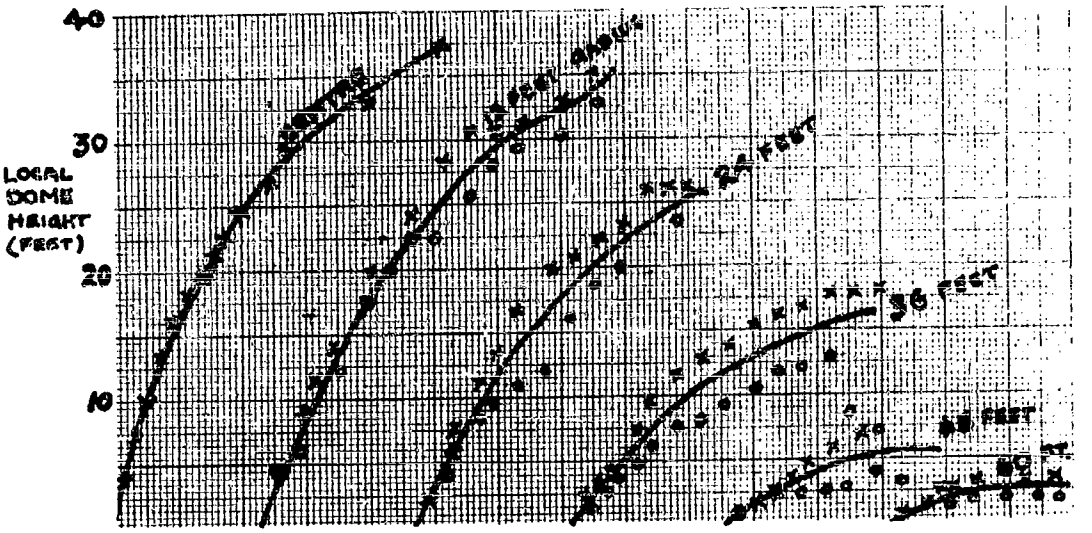

FIG. 2. DOME HEIGHT WITH TIME. 2 mm PER FRAME
FRAME SPEED :- 24 FRAMES / SEC.

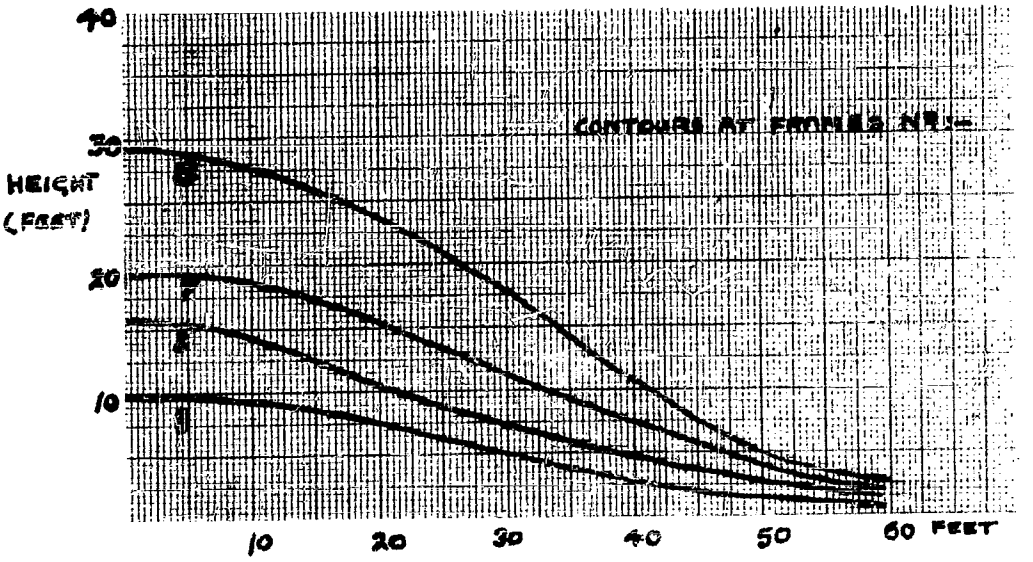

FIG. 3. CHANGE OF DOME CONTOUR WITH TIME.

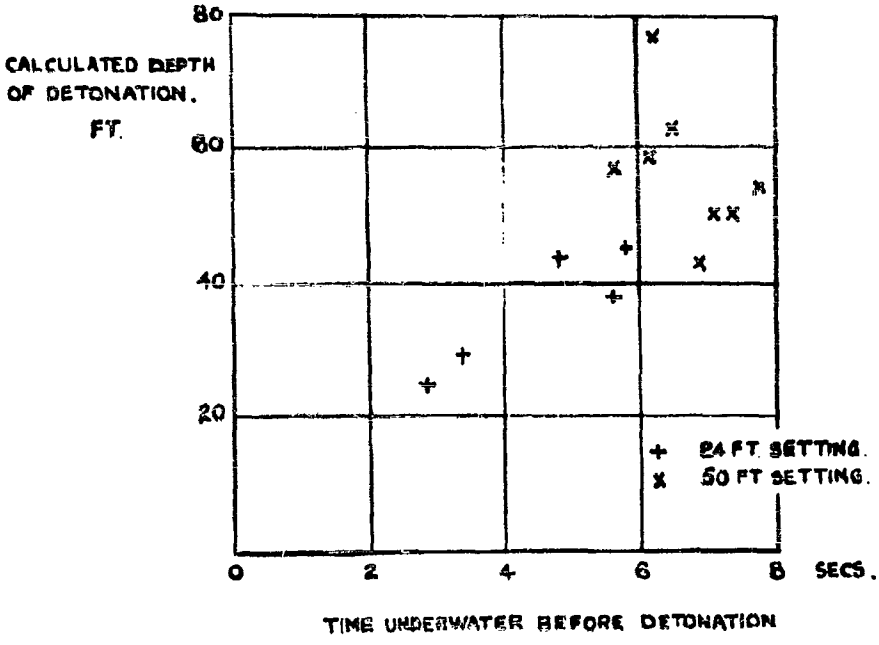

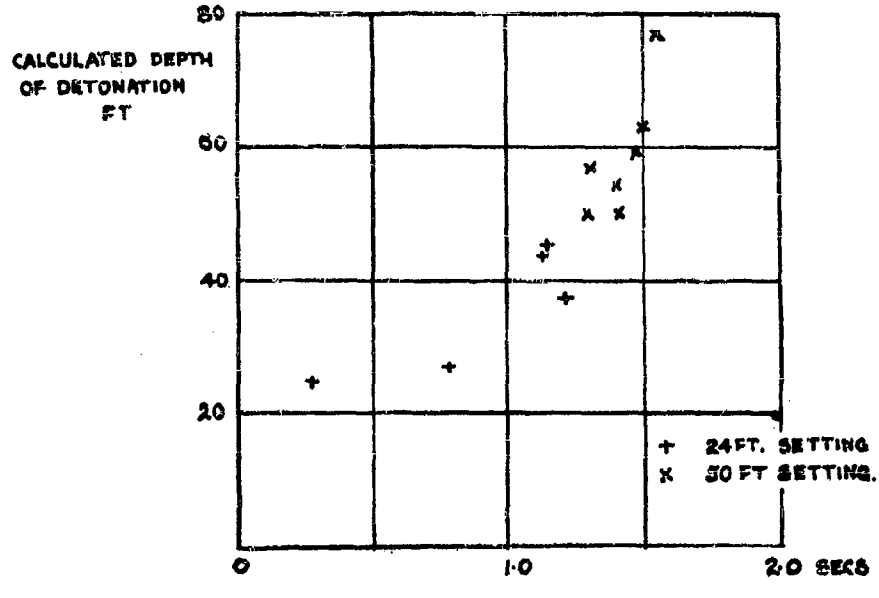

FIG 4. EXPERIMENTAL RESULTS.

Radius, Ft.	0	12	24	36	48	60	
Frame 3. t = 0·11 Sec:							
Local dome height, h ft.	11·15	8·72	6·33	4·00	2·09	1·21	
add $\frac{1}{2}gt^2$ = 0·20 ft.	11·35	8·92	6·73	4·20	2·29	1·41	
$\lambda = \sqrt{(h+\frac{1}{2}gt^2)^2+(\frac{1}{2}ut)^2}$		0·887	0·770	0·603	0·450	0·353	
$\sin^{-1}\lambda = 90-\theta$		62·5	50·4	37·5	26·7	20·6	
Calculated depth $d = r\tan(90-\theta)$		25·1	29·0	27·6	24·3	22·5	25·5 ft mean.
Frame 5. t = 0·185 Sec:							
h	10·0	12·53	10·05	6·2	3·11	1·99	
add $\frac{1}{2}gt^2$ = 0·55 ft	10·55	13·10	10·60	6·75	3·66	2·54	
λ		0·805	0·820	0·639	0·470	0·398	
$90-\theta$		62·5	55·2	39·7	28·1	23·1	
d		25·1	32·0	30·0	25·6	25·6	27·5 ft mean.
Frame 7. t = 0·26 Sec:							
h	10·1	12·13	10·60	6·80	3·66	2·54	
add $\frac{1}{2}gt^2$ = 1·08 ft.	9·78	7·26	5·73	3·11	1·07	0·57	
λ		0·912	0·815	0·653	0·428	0·414	
$90-\theta$		65·8	54·4	41·5	29·2	24·4	
d		23·7	33·5	32·0	29·7	27·1	29·2 ft mean.

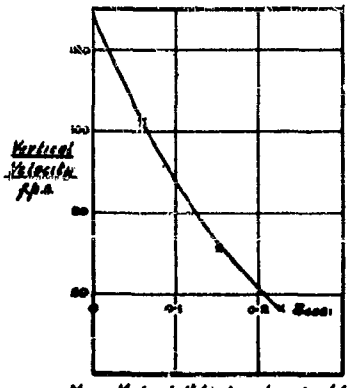

Mean Vertical Velocity at centre / 0·1 Sec. Secs.

Mean calculated depth of detonation ..... 27 Ft.

Initial Velocity at centre ..... 128 F.P.S. (from graph)

FIG. 5. TYPICAL ANALYSIS.

A FURTHER INVESTIGATION INTO THE DOME ANALYSIS METHOD OF DETERMINING THE DEPTH OF UNDERWATER EXPLOSIONS

R. A. Shaw
Marine Aircraft Experimental Establishment
Scotland

British Contribution

April 1942

A FURTHER INVESTIGATON INTO THE DOME ANALYSIS METHOD OF DETERMINING THE DEPTH OF UNDERWATER EXPLOSIONS

R. A. Shaw

Marine Aircraft Experimental Establishment
Scotland

April 1942

* * * * * * * * * *

Summary.

The dome analysis method of depth determination has been checked by the analysis of records obtained with charges at known depths. It has been found in applying the method that while the calculated depth is generally in fair agreement with the true depth, the agreement is improved if allowance is made for the dome shape and the initial plume characteristic of the particular explosion. When a correction for these factors is applied, the depth determined by the dome analysis method should not be in error by more than 10% and will generally be very much closer to the true depth. The relation which has been found between dome and plume suggests that the formation of both is dependent on the characteristics of the pressure pulse set up by the explosion. This should appear in the pressure records and an attempt will be made to relate the pressure results to the dome and plume characteristics.

Introduction.

A method of determining the depth of a charge exploding underwater from an analysis of the spray dome which appears on the surface over the exploding charge was described in a previous report. The method has now been checked by an analysis of some cine records of underwater explosions at known depths. Very close agreement is found between the calculated and the known depth in many instances but a few examples where the method is as much as 20 – 25% in error have occurred.

It was observed in the first report on the method that very large variations in initial dome velocity could be obtained under apparently similar conditions. This is confirmed by the present results but it has now been observed also that these variations are associated with variations in the initial velocity of the plume. Further, the dome itself, even in calm water, is not so regular in form as was at first thought. Some domes are found to be higher at the centre, and some higher at the rim than would follow if they were generated in strict proportion to the $(\cos\alpha)^2$ law used in the dome analysis method.

It has now been found that when the original dome analysis method is in error in calculating the depth, the error can be related to the surface phenomena as a whole. This has been done by assigning dome and plume factors in each instance. The dome factor is the gradient of the calculated depth along the dome radius, and the plume factor is simply the ratio of the mean initial velocity of the dome at its centre. A correction involving these two factors has been found and when this is applied to the depth calculated by the original dome analysis method, very close agreement with the known depths is obtained.

The effect of this is that when the true depth is unknown the depth can be calculated with fair accuracy by the dome analysis method if a correction in terms of these factors is applied.

The overall range of charge weight in the results considered is from 160 to 1,000 lb. and of depth from 15 to 100 feet. The tests include some in which the charges were fired on the sea bottom.

The symbols used in the text are defined below:–

(i) Charge

Weight	W lb.
Depth at detonation	d ft.
Depth calculated by original dome analysis method	d_{c_o} ft.
Calculated depth after correction for dome and plume factors	dc ft.

(ii) .....

(ii) Dome

Initial velocity at centre	v_o ft./sec.
Dome factor	n%

When the dome analysis method is applied the depth is calculated by taking the dome height at different dome radii and proportioning them to the dome height at the centre. This is done at three small time intervals from the first appearance of the dome. It is found that the calculated depth varies both along the radius and with time. The variation is an indication of the distortion of the dome and as a measure of this the dome factor, n, has been defined as:-

$$n = \frac{100}{d_{c_o}} \left(\text{mean depth calculated at a dome radius equal to } 3/2\, d_{c_o} - \text{mean depth calculated at a dome radius equal to } \tfrac{1}{2} d_{c_o} \right)$$

In practice it is found that the part of the dome between radii equal to 0.5 and 1.5 x the depth of detonation is the most satisfactory for measurement and calculation.

The factor n has a positive value when the calculated depth tends to increase outwards from the centre and is associated with a dome which is relatively high at the rim. When n is negative the greatest depths are calculated at the inner radii and the dome is relatively high near the centre.

(iii) Plume

Time from detonation to first appearance of the plume through the dome	t_p seconds
Height of dome when plume appears	h feet
Mean initial velocity of the plume	$\bar{V} = \frac{h + d_o}{t_p}$ ft./second.

Discussion of results.

The results obtained from the analysis of the cine records are given in Table 1. The range of depths covered in the results examined is equivalent to a variation of from just over 10 to nearly 70 feet with a 300 lb. charge if the depths are corrected in proportion to $\sqrt[3]{\text{charge weight}}$.

On the same basis of a 300 lb. charge the variations found in v_o are from under 2,000 to 6,000 square feet per second for charges in deep water and from 4,000 to 8,000 square feet per second for charges on the bottom.

The broad relation found between dome velocity and plume velocity which was the first result in this latest analysis is shown in Figure 1. Included in this figure are Mark VII depth charge results described in the original report on the dome analysis method. It will be seen at once that for all weights and depths of charges, and for charges both on and off the bottom there is a general tendency for v_o and $\bar{V}$ to increase together. In the range considered $\bar{V}$ is on the average equal to 0.75 v_o although the scattering of the points is equal to a ± 30% variation on this. Despite the wide variation there is clear evidence from the figure that a relation exists between the dome and the plume.

The next step in the analysis was to discover if the error found in the depth determination were also related to the plume characteristics. The percentage error in the depth calculation was plotted on the basis of the plume-dome velocity ratio $\bar{V}/v_o$, but the points were found to be widely scattered and no relationship was apparent. This suggested that if a relation existed it involved a second factor. It has been observed that the domes were not always uniform in shape and that in some instances large variations occurred in the depth calculated at different dome radii. It seemed possible that these variations would themselves influence the accuracy of the mean depth figure. Examples of the variation in depth calculated across the dome radius are shown in Figure 2. The three results illustrated are those which give the highest positive and negative values of the dome factor which were obtained in these tests and a zero value.

In Figure 3a the percentage error in the depth calculated by the original dome analysis method is plotted on the basis of the plume factor $\bar{V}/v_o$ and each result is labelled with the value of the dome factor n found in its calculation. It will be seen that without the dome factor n there is no relationship apparent but that with the dome factors shown the results at once align themselves in bands across the figure. This is emphasised by the cross lines which have been drawn in the figure to correspond to the average relation between percentage error, n and $\bar{V}/v_o$ shown by the results.

This .....

This relationship between the error in depth calculated by the original dome analysis method and the values of n and $\bar{V}/v_0$ has been reduced to a formula for a correction factor, μ, where

$$\text{true depth} = \frac{d\,c_0}{\mu}$$

and $$\mu = 0.5 + 0.78\,\bar{V}/v_0 + 0.012\,n - 0.000\,12\,n^2$$

The value of μ has been calculated for each of the results shown in Figure 3a and a revised figure for the calculated depth,

$$dc = \frac{d\,c_0}{\mu}$$

obtained in each instance. The error in dc has then been plotted in Figure 3b and it will be seen at once that when allowance for the dome and plume factors is made in this way, very good agreement between the calculated and the true depths is obtained. The majority of the results are within ± 5% of the true depth and no result is more than 10% in error. When it is realised that all the results at known depths available to date have been analysed and are shown in this figure and that the results include charges both on and off the bottom it will be seen that the method promises to provide a reliable means of determining the depth of charges exploding under water. How far the method can be relied upon outside the range covered by the results examined will be uncertain until further tests are done. The range already covered (from little more than 10 feet to over 60 feet for a 300 lb. charge) is wide enough for most practical purposes.

Some difficulty may arise in practice with bombs fitted with a pistol or fuze which detonates at shallow depths. With these the cavity which the bomb forms at entry may not be closed when the bomb explodes, a condition not represented in static tests. If the plume factor in these conditions is based on the plume which appears prematurely through the still open cavity the factor will be too high. If it is based on the plume which appears later through the unbroken water it may be too low because the force of the plume will have been spent in the open cavity. A method of correcting the calculated depth in these conditions could be based on tests with air launched charges dropped in shallow water of known depth. The bombs would only require to be fitted with impact fuzes so as to detonate on the bottom. Pending the results of such tests it will probably be best to neglect the present correction in applying the dome analysis method to shallow firing bombs when the records show that the cavity is still open*. The depths associated with these conditions will be of the order of 10 – 15 feet and since the uncorrected dome analysis method may be expected to give such depths in general within two feet or less, it will probably be sufficiently accurate.

The relationship between dome and plume.

Although the foregoing analysis has provided a practical method of determining the depth of detonation it does not explain the relationships which have been found.

It has generally been assumed that the spray forming the dome is produced by the action of the detonation pressure pulse. Records obtained with piezo electric pressure gauges have indicated that the detonation pressure pulse is very uniform in the horizontal plane at the level of the charge. That this does not appear to conform with the large variations which occur in the spray velocity would be explained if similar variations in the pressure pulse were found to occur in the region above the charge. This region does not appear to have been explored so far with pressure gauges.

The value of $v_0 c$ for a 300 lb. charge which would be calculated from the peak pressure in the detonation pulse based on the results of tests in the plane of the charge is 3,000 square feet per second. In general therefore (see Table 1) the spray velocity is higher than would be expected from the effect of the detonation pulse found in the horizontal plane although it is less in some instances.

The present analysis shows that the dome velocity is related to the plume velocity. As might have been expected there is also evidence that the dome shape, i.e. the initial distribution of velocity across the dome, is related to the initial plume shape. The growth of the plume for each of the present results is shown in Figure 4. The results have been arranged in order from the highest positive to the lowest negative value of the dome factor, n, irrespective of the other conditions of the test. It will be seen at once that there is a marked tendency for positive

values .....

* See also Note 1 in Appendix.

values of n to be associated with plumes which fork and break out strongly on either side of the centre while negative values of n are found when the plume develops as a central column.

A more solid basis for the comparison than the general outline of the plume will be found by observing in each example the directions in which the plume velocity is highest, particularly in the early stages of development. It will be seen then that positive values of n are associated with plumes which thrust out most strongly to either side and are relatively weak at the centre. Values of n near zero are found with plumes which develop evenly in all directions, negative values of n with plumes which thrust upwards most strongly at the centre.

Some exceptions seem to occur but these may be explained by the fact that the surface phenomena are three-dimensional and the plume outlines drawn in Figure 4 may not be in one plane. Two views at right angles are really required to place the plume contours relative to the dome.

It has been remarked already that positive values of n are found with domes which are relatively high at the rim and negative values for domes which are relatively high near the centre. It seems clear then that the initial plume is very closely related to the initial dome shape. The dome velocity tends to be increased in the areas where the plume, which appears later, is most concentrated. It is not intended to suggest by this, that the dome velocity is simply reinforced by the added plume velocity. The dome velocity is imparted to the spray within a few milliseconds of detonation and the distribution of velocity which is used in the depth calculation is determined from photographs taken within the next one or two tenths of a second. Generally the plume does not appear until more than a second later.

To explain the relation between the dome and plume it seems necessary to find that a pressure pulse associated with the early development of the plume horns is superimposed on the general detonation pulse. If this is found to be true it will indicate that the gas bubble may be far from spherical in its early stages and that its initial irregularities tend to persist right up to the time of the appearance of the plume. It seems probable that the irregularities in the gas bubble will be much more marked above the charge; any instability in this direction would be encouraged by the hydrostatic pressure gradient. As a corollary to this it appears to follow that the destructive effect of an explosion may be most marked above the charge.

Conclusions.

Cine records obtained in tests with charges exploded at known depths have been analysed and have shown that the original dome analysis method of depth determination will give the depth fairly closely in most instances, but that examples when the method is 25% in error may occur.

It has been found, however, that the errors introduced in the dome analysis method are related to the shape of the dome and to the early behaviour of the plume. By introducing factors into the dome analysis to allow for dome shape and plume behaviour the depth of detonation can be determined with confidence to within ± 10% and will in general be much closer than this.

Some difficulty in applying the correction factor may arise in practice with bombs which are detonated at small depths while the cavity formed at entry is still open. Special tests would be required to investigate this condition but at the shallow depths involved the uncorrected dome analysis method may be expected to give the depths sufficiently accurately for most purposes.

The broad relation of dome and plume velocity and the relation between dome and plume shape which have been found in the analysis suggest that variations must occur in the pressure pulse which influence both the dome and the plume.

APPENDIX

NOTES ON THE APPLICATION OF THE REVISED DOME ANALYSIS METHOD

The stages of the method are:-

1. Determine the approximate depth, d_{c_o}, by the original dome analysis method.

2. Calculate the initial dome velocity at the centre v_o ft./second.

3. Plot the calculated depth on the basis of dome radius (as in Figure 2 in this report) and determine the dome factor n. This is the mean value of the depth gradient between a radius equal to $\frac{1}{2} d_{c_o}$ and $3/2\ d_{c_o}$, expressed as a percentage.

4. Note the time t_o from detonation to the first appearance of the plume and the height, h, of the dome, at the same instant.

From this calculate $\bar{V} = \dfrac{h + d_{c_o}}{t_o}$

5. Evaluate the correction factor μ where

$$\mu = 0.50 + 0.78\ \bar{V}/v_o + 0.012\ n - 0.00012\ n^2.$$

6. Obtain the corrected depth d_c as

$$d_c = \frac{d_{c_o}}{\mu}$$

Notes which may be helpful at the different stages are given below.

1. It is found best to work with dome measurements taken at the centre and approximately between radii equal to $\frac{1}{2} d_{c_o}$ and $3/2\ d_{c_o}$ on either side of the centre. Measurements at four or five radii are sufficient. For bombs which detonate after only a short time delay (say one second or less) the cavity formed at entry will still be open. In these circumstances it has been found satisfactory to base the depth calculation on dome measurements taken only on the side away from the cavity. The other side of the dome tends to be distorted by the cavity and is obscured by the splash from the impact of the bomb.

2. In obtaining the initial velocity, v_o, from the dome height it is important to use the time from the first appearance of the spray. This may be between two frames of the cine film but the exact instant can usually be decided by plotting the curve of dome height for successive frames and noting where it cuts the axis.

3. In general this method of obtaining n will be found to give a fair measure of the mean depth gradient. If there should be any sudden distortion in the depth calculated close to the measuring points this may be disregarded and the mean gradient taken through the remaining points. In the present analysis this was only found necessary in one example.

4. Experience in the analysis has shown that it is the appearance of the main plume that must be looked for in determining t_o and that the fine spouts which sometimes precede the plume can be disregarded.

TABLE 1.

Charge Weight	Dome and Plume particulars							Depths (ft.)			$d\sqrt[3]{\frac{200}{W}}$	$v_o d\sqrt[3]{\frac{200}{W}}$
	v_o	h	t_o	$\bar{v}$	n	$\bar{v}/v_o$	μ	d	d_{c_o}	dc		
500 lb. Amatol	94	36	1.34	.66	- 4	0.70	1.06	50 in. 100	52.7 (1.05)	50.0 (1.00)	42.1	3980
250 lb. Amatol	60	11	1.04	70	-22	1.17	1.09	60 in. 100	61.8 (1.03)	56.5 (0.94)	63.8	3820
300 lb. Amatol	120	28	1.26	68	+29	0.56	1.18	50 in. 100	57.9 (1.16)	49.0 (0.98)	50.0	6000
300 lb.	92	26	1.20	63	+ 2	0.68	1.00	60 in. 60	62.3 (1.04)	62.3 (1.04)	60.0	5500
1,000 lb.	112	48	1.43	76	+ 6	0.68	1.17	58 in. 58	60.9 (1.05)	55.2 (0.95)	38.7	4330
1,000 lb. T.N.T.	122	64	1.62	76	- 8	0.62	0.88	60 in. 60	51.8 (0.87)	59.2 (0.98)	40.0	4930
1,000 lb. T.N.T.	120	22			Films incomplete			98 in. 98	104.7 (1.07)		65.2	7878
1,000 lb. T.N.T.	94	22			No plume shown			97 in. 97	98.3 (1.01)		64.7	6100
1,000 lb. T.N.T.	120	23						99 in. 99	97.2 (0.985)		66.1	8000
The following tests were all in 200 feet of water.												
171 lb. Amatol	70	23	0.97	55	-10	0.78	0.98	30	30.3 (1.01)	31.1 (1.04)	36.1	2530
161 lb. Minol	50	24	1.00	51	-26	1.03	0.91	30	27.9 (0.93)	30.7 (1.02)	34.8	1050
388 lb. T.N.T.	140	71	1.30	78	+ 2	0.56	0.96	30	30.0 (1.00)	31.3 (1.04)	27.8	3866
161 lb. Amatol	84	27	0.83	61	-21	0.73	0.75	30	23.7 (0.79)	31.7 (1.06)	36.8	3110
296 lb. T.N.T.	90	30	1.26	65	0	0.50	0.89	30	26.7 (0.89)	30.0 (1.00)	30.2	2700
290 lb. Amatol	88	43	1.11	65	-14	0.74	0.89	30	29.1 (0.97)	32.6 (1.09)	30.3	2730
161 lb. Minol	110	45	0.97	75	-10	0.68	0.90	30	27.3 (0.91)	30.3 (1.01)	36.8	2060
475 lb.	140	80	1.34	81	+ 5	0.58	1.00	30	27.7 (0.92)	27.7 (0.92)	25.7	10
500 lb.	130	86	1.18	90	+18	0.69	1.21	18	20.1 (1.11)	16.7 (0.93)	15.2	1980
500 lb.	200	51	0.28	248	-18	1.24	1.21	15	18.7 (1.24)	15.4 (1.03)	12.7	2540

The bracketed figures in the depth column are the ratios of the calculated depth to the true depth.

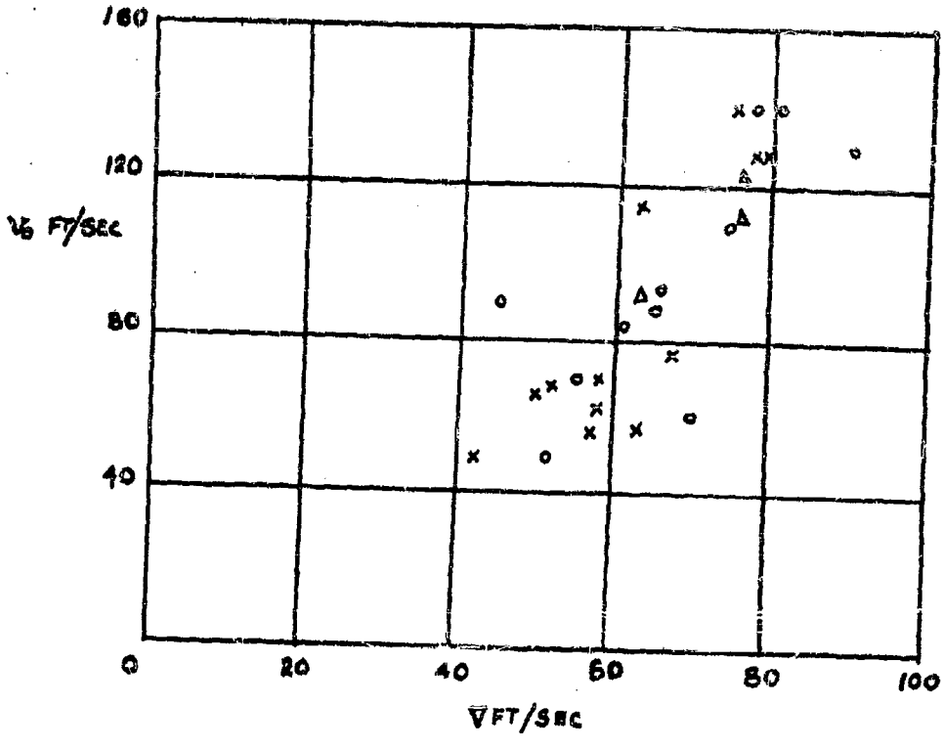

FIG. 1. VARIATION OF INITIAL DOME VELOCITY (V_0) WITH INITIAL PLUME VELOCITY ($\overline{V}$)

× CHARGES DROPPED FROM AIRCRAFT.

o CHARGES FIRED STATICALLY AT KNOWN DEPTHS

Δ CHARGES ON BOTTOM.

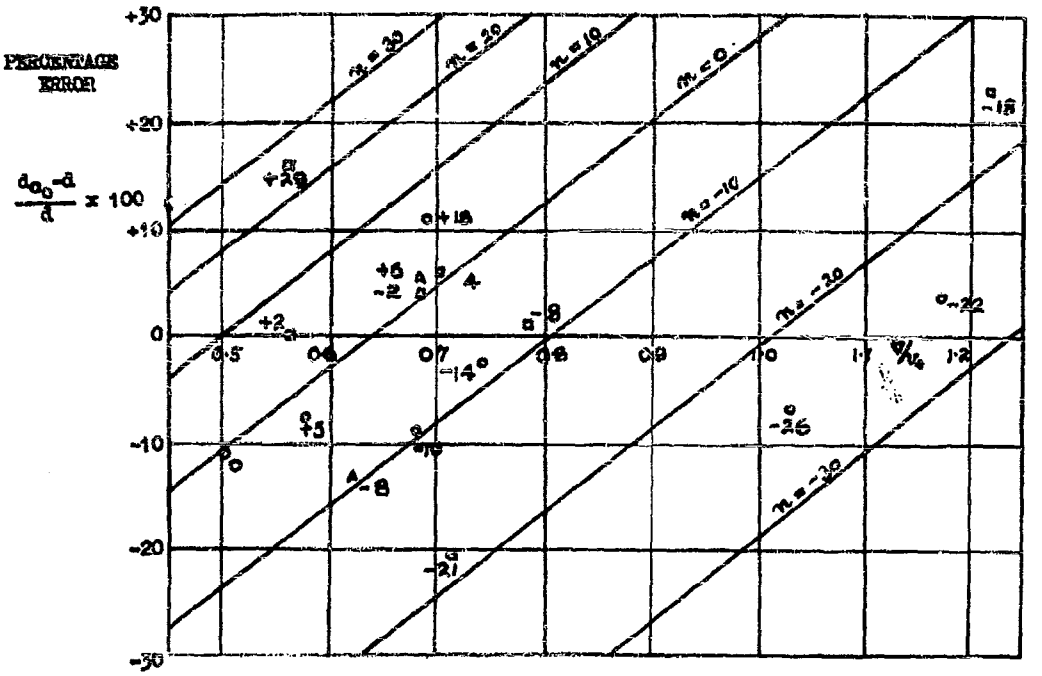

PERCENTAGE ERROR IN DEPTH CALCULATED BY ORIGINAL METHOD

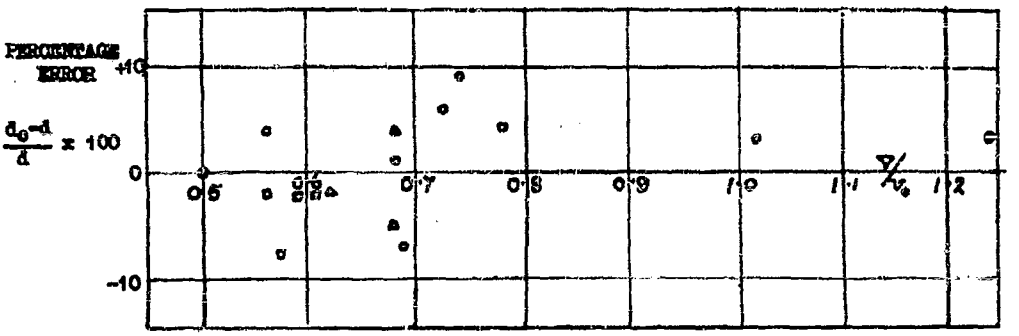

PERCENTAGE ERROR IN DEPTH CALCULATED BY THE REVISED METHOD IN WHICH A CORREATION IS MADE FOR DOME AND PLUME FACTORS

IN BOTH FIGURES THE DEPTH ERRORS ARE PLOTTED ON THE BASIS OF THE PLUME FACTOR $\bar{V}/v_o$. IN THE UPPER FIGURE EACH RESULT IS LABELLED WITH THE DOME FACTOR n FOUND IN ITS CALCULATION. THE CROSS LINES SHOW THE ALIGNMENT OF THESE UNCORRECTED RESULTS WITH n AND $\bar{V}/v_o$. THE FORMULA BASED ON THIS ALIGNMENT IS:-

$$d_o = \frac{d_{o_o}}{\mu} = \frac{d_{o_o}}{0.5 + 0.78\,\bar{V}/v_o + 0.012\,n - 0.00012\,n^2}$$

AND THE SAME RESULTS CORRECTED IN THIS WAY ARE SHOWN IN THE LOWER FIGURE.

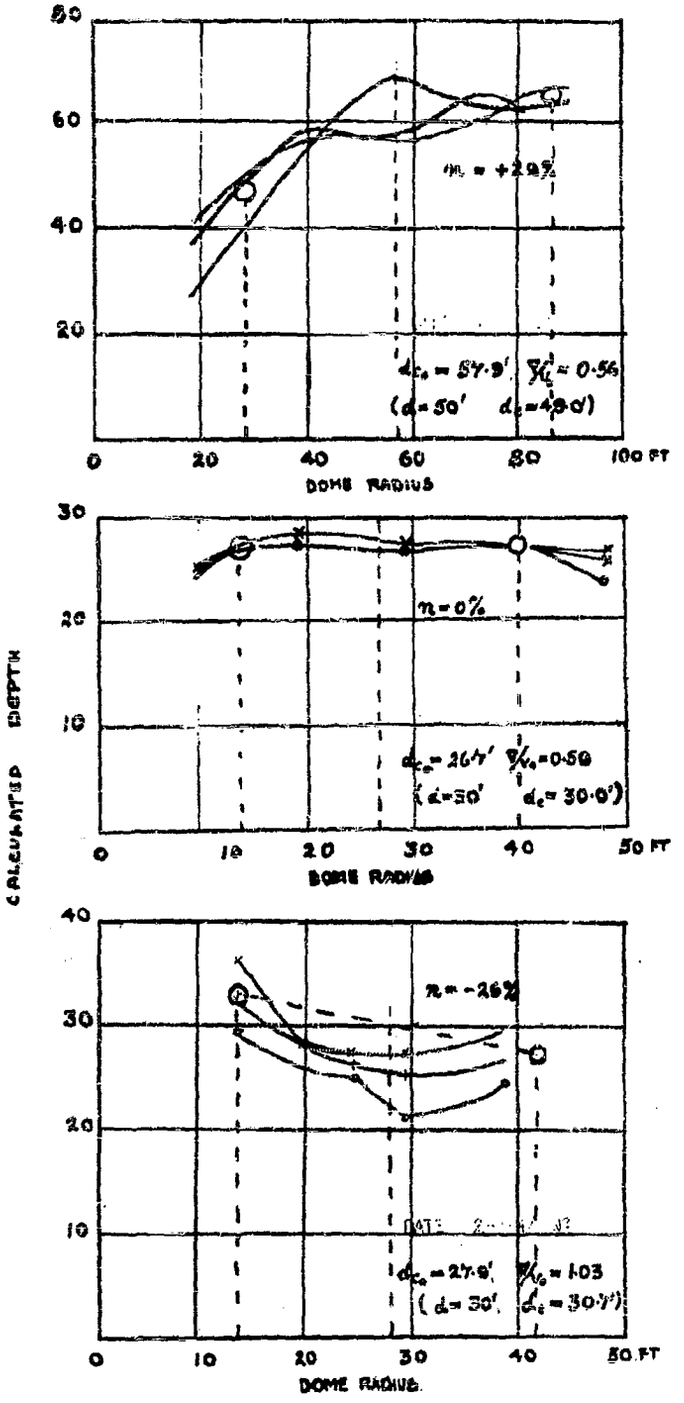
50
60
40
20
n = +29%
d_{c_0} = 57.9' $\frac{d_c}{d_0}$ = 0.56
(d = 50' d_c = 49.0')
0
20
40
60
80
100 FT
DOME RADIUS
30
20
10
n = 0%
d_{c_0} = 26.7' $\frac{d_c}{d_0}$ = 0.58
(d = 30' d_c = 30.0')
0
10
20
30
40
50 FT
DOME RADIUS
CALCULATED DEPTH
40
30
20
10
n = -26%
d_{c_0} = 27.9' $\frac{d_c}{d_0}$ = 1.03
(d = 30' d_c = 30.7')
0
10
20
30
40
50 FT
DOME RADIUS.

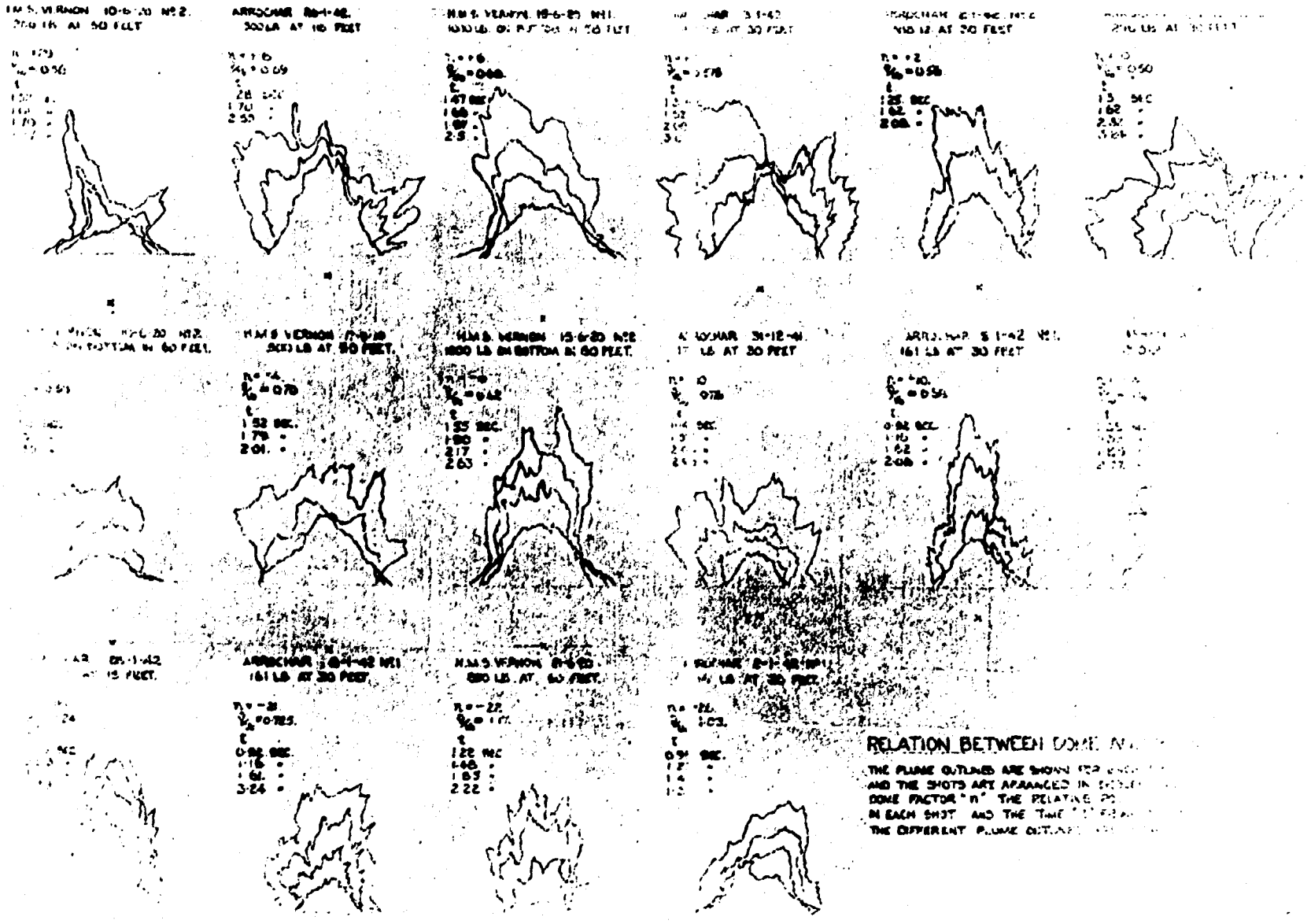

RELATION BETWEEN DOME N

THE RELATION BETWEEN THE APPEARANCE OF THE PLUMES AND THE GAS GLOBE BEHAVIOR IN UNDERWATER EXPLOSIONS

G. K. Hartmann
Naval Ordnance Laboratory

American Contribution

1947

"The Relation Between the Appearance of the Plumes and the Gas Globe Behavior in Underwater Explosions" *

G. K. Hartmann
U. S. Naval Ordnance Laboratory

The appearance of the water surface above an underwater explosion changes after the explosion in what seems to be an irregular fashion as time goes on. Although the initial velocity of the water surface and the resultant shape of the dome in its early stages are extremely reproducible, the later stages of the water motion seem to occur in a random manner. The purpose of this note is to show that the later appearance of the surface and in particular the rather arbitrary behavior of the plumes are related in a fairly quantitative way to the oscillation and migration of the gas globe. The period of oscillation and the amount of migration are of course determined by the weight of charge of a given kind and by the depth of the charge.

The phenomena under consideration will now be described in more detail.

Observation of the water surface reveals that for an explosion at a moderate depth, say 300 lbs. at 30 ft., the water is broken into white spray over a delimited area (outside of which there is a distinctly dark region) and that this spray moves upward vertically with greatest velocity over the charge and decreasing velocities at greater distances. This spray dome, which can be shown to be caused by the reflection of the shock wave at the free surface, is actually freely falling water and moves upward under the influence of gravity and air drag until it reaches its maximum central height whereupon it falls back into the surface, continuously changing its shape as it does so. At some stage in this process other fingers or jets of spray and often explosion gases, identified by their carbon black, break through the dome with various velocities. Sometimes these plumes appear traveling radially from some point near the surface and sometimes they are limited to single high speed vertical jets. The character of these plumes and the times at which they appear are related to the oscillation and migration of the explosion gas globe.

* This note is taken from material presented by the author at the Washington meeting of the American Physical Society in the spring of 1947.

Figure 1 made up from data taken at Woods Hole shows the time of appearance of the plumes as a function of the charge depth, taking the zero of time as the first appearance of the spray dome which is the same as the detonation time, save for the negligible travel time of the shock to the surface. The charges used were the equivalent of 400 lbs. of TNT. The blacked-in points represent the more pronounced velocity change in the case of two charges. The period, T_1, of the first oscillation is calculated taking account of the influence of the surface, and the period of the second oscillation, T_2, is taken, for these depths, as equal to that of the first. In this depth range the decrease in period due to loss of energy is roughly compensated by the increase in period due to the rise of the gas globe. At the end of the first oscillation, at time $t = T_1$, the gas globe is small, compressed, and moving rapidly upward. It is probable therefore, that for charges originally at depths of 25 to 30 feet the columnar upheaval through the spray dome at about one second is caused by the gas globe reaching the water surface in a state of high pressure and high velocity. The known facts concerning upward migration are wholly consistent with this view. The spray dome at this time may be 30 or 40 feet high and the columnar plume will require at least a tenth of a second to emerge from it traveling at a typical velocity of 250 feet per second. The initial velocity for the spray dome due to the shock wave reflection will be about 120 feet per second for a 400 lb. charge at 25 feet. This indicates that the velocity of the plume is a mass motion of water driven by the gas globe and is not analogous to a spray dome of tiny droplets. Hence, the potentiality of this plume for damaging a ship is probably high.

For charges at greater depths the plume emerges at later times with respect to the period of oscillation. There are two reasons for this: First the gas globe has further to travel and second, its velocity is less in the less compressed phases. The blacked-in points in Figure 1 for the depth region from 35 to 45 feet show that the gas globe reaches the surface in the early stages of expansion after the first collapse. The additional points to the right along the $T_1 + T_2$ curve correspond to the expansion after the second collapse of the gas globe. This second collapse is necessary if the globe is at all large when it nears the surface. According to this view, there will be no surface events at the time the gas globe nears the surface if this happens at its maximum size. In this case there will be a delay of about one half period until the collapse and consequent rapid upward velocity occur which will result again in a columnar display as indicated by the heavy points on the $T_1 + T_2$ curve. For charges of this size at depths less than 25 feet the dome and plume phenomena merge together. However, radial plumes associated with radial expansion of the gas globe are observed at about 20 feet whereas for very shallow explosions, in say 5 to 10 feet of water again a columnar formation is observed.

Figure 2 is taken from a report by Schlichter, Schneider and Cole on the Measurement of Bubble-Pulse Phenomena. It shows the appearance of the dome, radial plumes and columnar plumes at different times and for different initial charge depths. The charge weight used is 290 lbs. for this series of shots.

One of the difficulties in interpreting pictures of the type shown in Figure 2 is the fact that the top of the dome is used as a reference point rather than the water surface which is necessarily obscured. If, however, the height of the plume is plotted against time, it is easy to extrapolate this to zero height and thus find the time of emergence of the plume from the surface, called the plume time in Figure 3. Similarly, surface velocities can be found by extrapolating differentiated height vs. time curves. The results have been plotted by the above mentioned authors and are shown in Figure 3. It is seen that vertical plume velocities are high for charges at depths for which the plume time coincides with the gas globe period, or sum of periods. This shows that high plume velocities occur when the gas globe reaches the water surface in a collapsed state. Furthermore, the jog in the plume time curve corresponds with the maximum expansion and the subsequent contracting phase of the gas globe. This means that for charges at these depths it is necessary to wait about an additional half period for the plumes to appear.

It is seen, therefore, that a reasonably satisfactory account of some of the visible surface phenomena can be given by referring them to the behavior of the gas globe, and that plumes of a similar appearance occur if the explosion bubble breaks surface in the same phase of its oscillation after one or two or even three complete periods. Thus the occasional observation of a high columnar plume characteristic of a shallow explosion occurring in the case of a relatively deep explosion is explained by the critical combination of circumstances which permits the gas globe to oscillate through two or three periods and arrive at a depth near the surface in the same phase as if the charge were statically detonated at that point.

It is also clear from Figure 1 that the time of appearance of the plumes is not very sensitive to the charge depth and jumps discontinuously from short times to longer times as the depth is increased. Observation of these times therefore does not lead to a good indication of the actual depth of explosion.

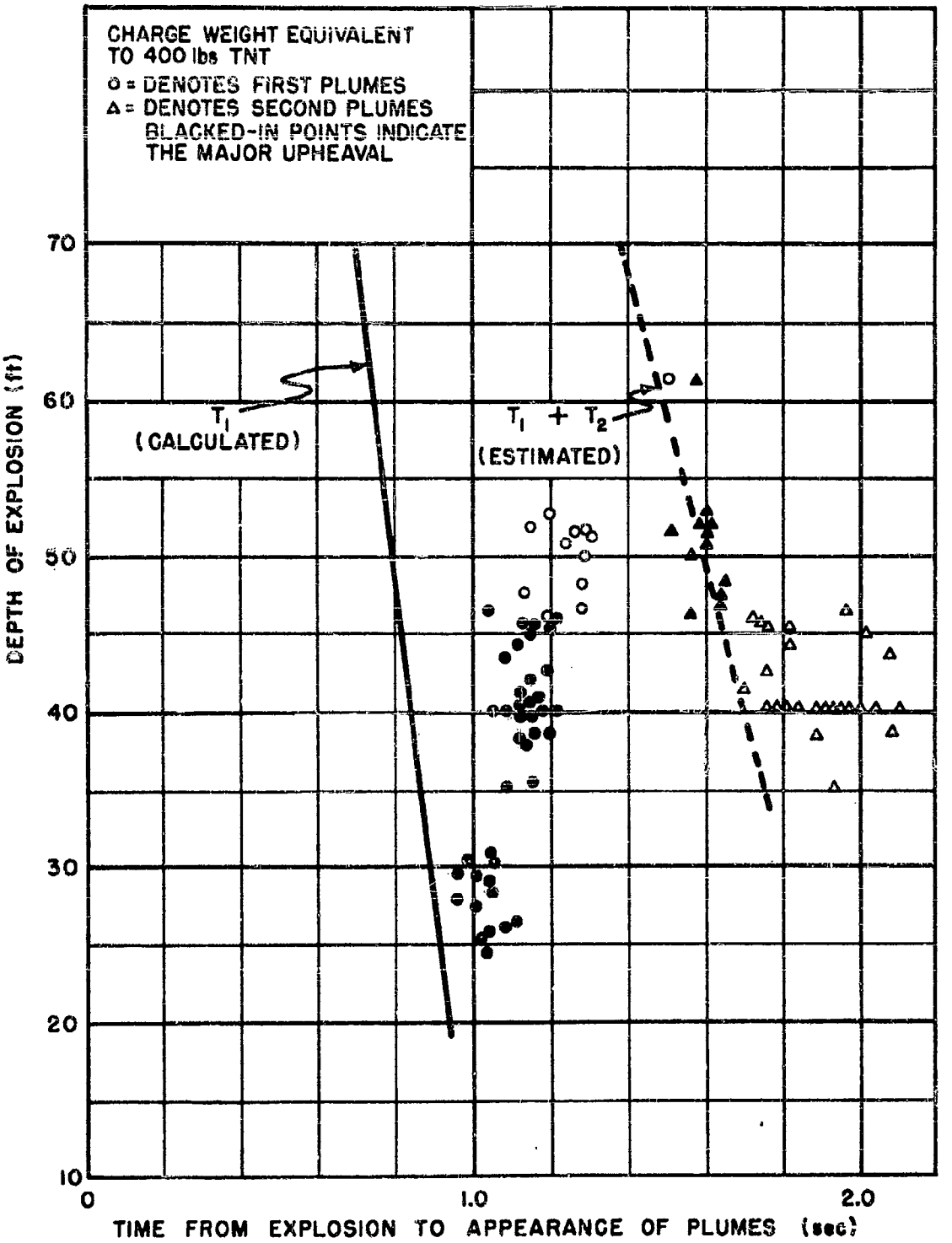

FIG. 1 TIME OF APPEARANCE OF PLUMES AS A FUNCTION OF CHARGE DEPTH

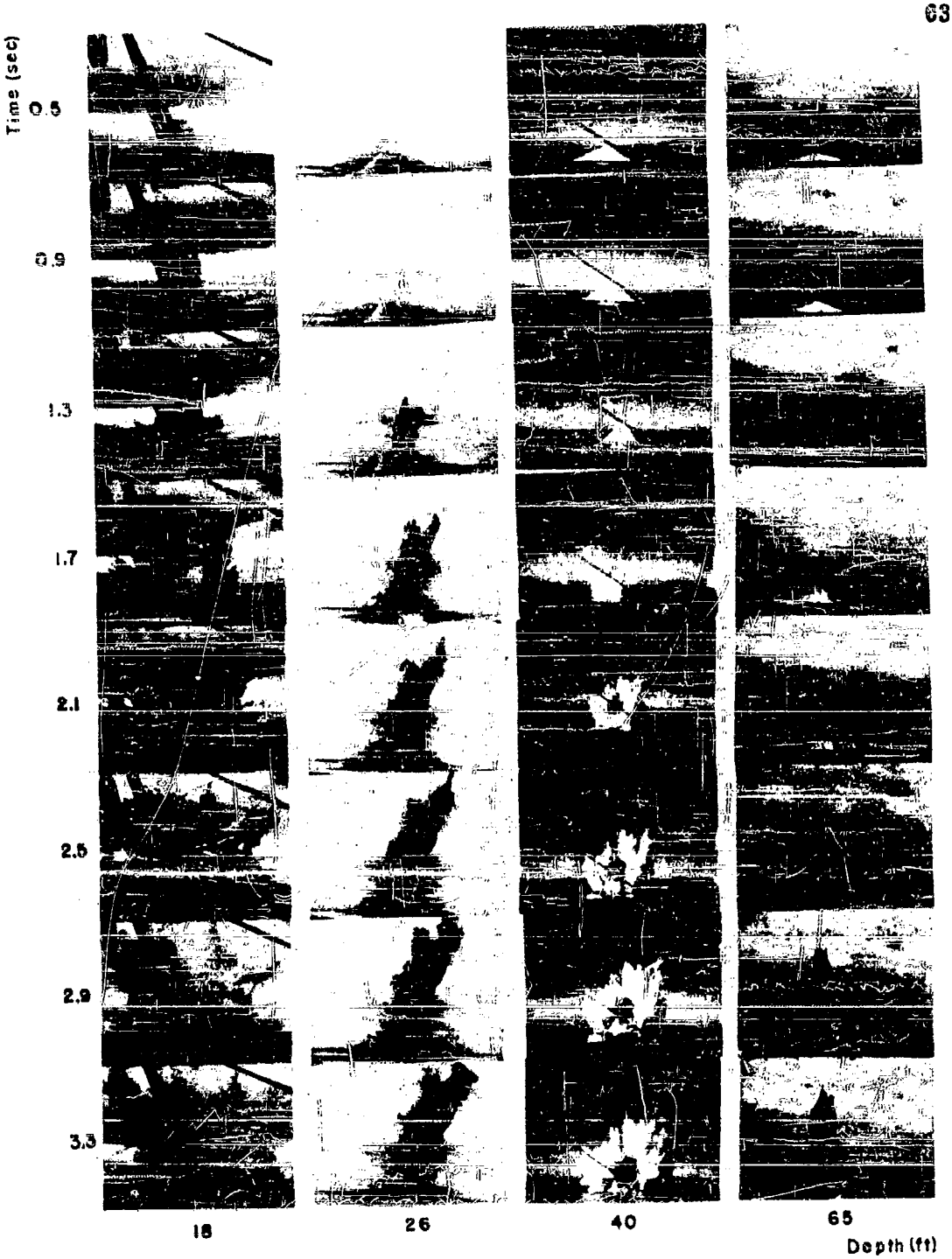

Fig. 12 Development of surface plumes of 290 lb TNT at charge depths of 18, 26, 40, and 65 ft.

The photographs are reduced to the same time scale but the breadth and height scale varies for photographs of different charge depths.

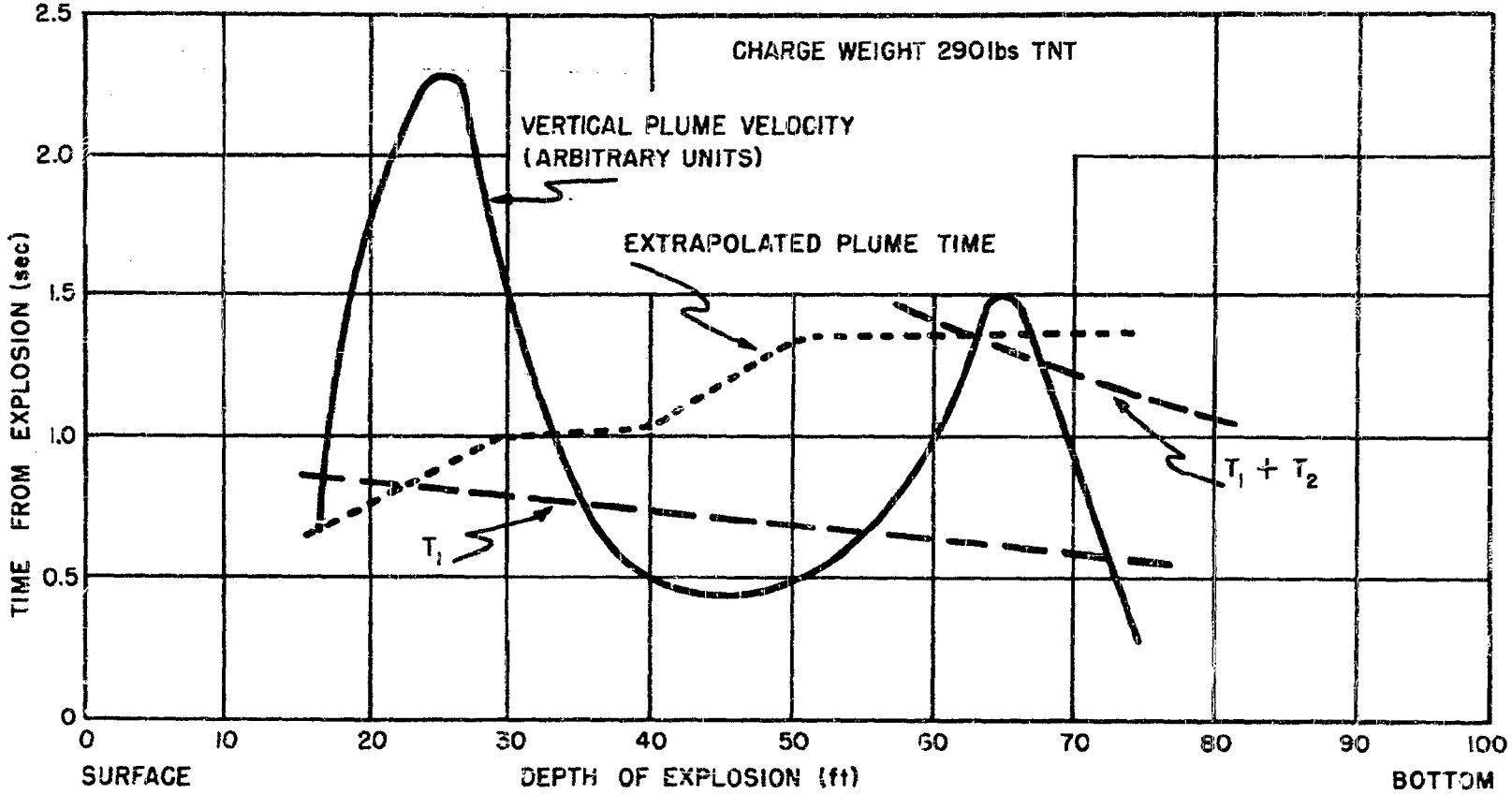

FIG. 3 SURFACE PLUME MEASUREMENTS AS A FUNCTION OF CHARGE DEPTH

THE DETERMINATION OF PEAK PRESSURE OF AN UNDERWATER EXPLOSION FROM A STUDY OF THE INITIAL DOME VELOCITY

D. A. Wilson, B. A. Cotter, and R. S. Price
Underwater Explosives Research Laboratory
Woods Hole Oceanographic Institution

American Contribution

26 May 1947

CONTENTS

		Page
Abstract		1
I.	INTRODUCTION	2
II.	EXPERIMENTAL	2
	1. Pond Work	3
	2. Tank Experiments	5
	3. Critical Depth Experiments	5
III.	EXPERIMENTAL RESULTS	5
	4. Methods of Computation	6
	5. Nonomassett Pond Results	8
	6. Tank Results	8
	7. Methods for Calculating T	13
IV.	DISCUSSION	13
	8. Accuracy of the Method	13
	9. Value of the Method for the Determination of the Peak Pressure	14
	10. Value of the Method for Multiple Charge Effects	14
	11. The Surface Tension Lowering Problem	15
	12. The Tensile Strength of Water	16
Appendix		36
List of References		

LIST OF TABLES

TABLE		PAGE
I	Dome Velocity Results for Pentolite -- Pond Series	7
II	Dome Velocity Results for Pressed Tetryl	7
III	Dome Velocity Similarity Curve Results for Single Engineer's Special Caps -- Tank Series	9
IV	Dome Velocity Sympathetic Detonation Results -- Tank Series	9
V	Dome Velocity Surface Tension Lowering Results -- Tank Series	9
VI	Adding 3300 to Each P_m as Calculated for Tank Shots	10
VII	Approximate Value of T Obtained from Critical Depth Estimations	10
VIII	Approximate Value of T Obtained from Dome Periphery Calculation	11
IX	Summary of Estimated Values of T	12
A-I	Charge Data Pond Experiment Pentolite Series	16
A-II	Charge Data Pond Experiment Tetryl Series	17

LIST OF FIGURES

FIGURE		PAGE
1	Experimental Set Up for Dome Velocity Shots Using Small Charges	18
2	Experimental Set Up for Dome Velocity Shots in Steel Tank	19
3	Cap Holder for Tank Shots	20
4	Critical Depth Experiment Using Caps	21
5	Typical Example of Low Dome Velocity	22
6	Influence of Surface Ripples on Dome Appearance	23
7	Typical Examples of High Dome Velocities	24
8	Similarity Curve for Peak Pressure vs. $W^{1/3}/R$ for Pentolite	25
9	Similarity Curve for Peak Pressure vs. $W^{1/3}/R$ for Pressed Tetryl	26
10	Typical Examples of High and Low Dome Velocities	27
11	Effect of Surface Active Agent on Dome Velocity	28
12	Sympathetic Detonation Series	29
13	Dome Velocity Similarity Curve for Peak Pressure vs. $W^{1/3}/R$ for Engineer's Special Detonators	30
13a	Corrected Peak Pressure vs. $W^{1/3}/R$ for Engineer's Special Detonators	31
14	Sympathetic Detonation from Dome Velocity Points Placed on Similarity Curve from Fig. 13	32
15	Dome Velocity Results with Lowered Surface Tension Points Placed on Similarity Curve from Fig. 13	33
15a	Dome Velocity Results with Lowered Surface Tension Points Placed on Similarity Curve from Fig. 13 and Fig. 13a	34
16	Calculation of T from Greatest Dome Diameter	35

GLOSSARY

W	Weight of explosive charge (lb)
R	Distance of center of explosive from surface (ft)
P_m	Peak pressure (lb/in.^{2})
V_o	Dome velocity (ft/sec)
U	Velocity of propagation of shock wave (ft/sec)
ρ_e	Initial density of water (lb/ft^3)
F	Indicates observations on Fastax motion picture camera
S	Indicates observations on General Radio "streak" camera
n	Number of observations in a group
δ_n	Deviation of a single observation from the mean of the group
σ	Standard deviation of a single observation from the mean

$$\sigma = \sqrt{\frac{\sum \delta_n^2}{(n-1)}}$$

σ_m	Standard deviation of the mean of a group of observations

$$\sigma_m = \frac{\sigma}{\sqrt{n}}$$

T	Tension necessary to rupture water (lb/in.^{2})
γ	Surface tension (dynes/cm)
u	Particle velocity (ft/sec)

ABSTRACT

A systematic investigation has been made of the determination of peak pressure from the measured upward rise of the spray dome when an explosive is detonated at varying shallow depths. The experimental work has included a series using small charges of a typical explosive in a small fresh water pond and another series using Engineer's Special Detonators exploded in a three foot cubic tank filled with fresh water. The latter series has been extended to investigate the effect of varying surface tension on the dome velocity. Measurement of this velocity has been made photographically using either a "streak" camera or a high speed motion picture camera operating at about three thousand frames per second with photoflash illumination.

General agreement with theory has been observed. There is a dependence upon surface tension not hitherto reported. There is no evidence of an initial velocity higher than that predicted theoretically. It is possible to arrive at an upper limit for the value of the tension necessary for the rupture of water at its surface. The method provides a satisfactory approach to a measure of the absolute value of the peak pressure from an underwater explosion.

THE DETERMINATION OF PEAK PRESSURE OF AN UNDERWATER EXPLOSION FROM A STUDY OF THE INITIAL DOME VELOCITY

I. INTRODUCTION

When an explosive charge is detonated beneath the surface of water, provided the depth of the explosive is not too great, the resulting shock wave hitting and being reflected from the surface causes a mass of water to become detached and leave the surface. This detached mass of water is projected normal to the surface with an initial velocity exactly twice that of the particle velocity of the shock wave itself. This doubling of the particle velocity at the surface is due to the reflection from the free water-air interface of a rarefaction wave of the same magnitude but opposite in sign to the incident compression wave. The particle velocity in a shock wave is given by the expression[1]*

$$u = \frac{P_m}{\rho_e U}$$

and the initial velocity of the projected spray by twice that, or

$$V_o = \frac{2 P_m}{\rho_e U} \qquad (1)$$

where u is the particle velocity, V_o the initial velocity of the rising spray dome, P_m the peak pressure of the shock wave, ρ_e the initial density of the medium, and U the propagation velocity of the shock wave.

Although the surface effects resulting from an underwater explosion have been intensively studied for various reasons during the war,[2] the velocity of the rising spray dome has not been seriously proposed heretofore as an accurate method for the determination of the peak pressure of the shock wave except by earlier workers, among them, Hilliar.[3] The Underwater Explosives Research Laboratory became interested in this method because the increasing dependence upon the piezoelectric gauge made desirable the development of an independent method for determining absolute peak pressures as a check on the piezoelectric results.

Introducing a finite force T necessary to rupture water at its surface so that a spray dome may be formed, the equation[4]

---

* All such numbers refer to the List of References at the end of this report.

$$V_0 = \frac{2}{\rho_\bullet U}\left(P_m - \frac{T}{2}\right) \qquad (2)$$

which is more realistic than Eq. (1), may easily be deduced. T is exactly equal, of course, to the tensile strength of the water and, under such conditions that V_0 becomes just equal to zero, this equation provides a means of determining the force necessary to rupture water under the conditions of the experiment. Any means of determining T is interesting because a knowledge of this value is very desirable and not easily determined.[5]

Although Eqs. (1) and (2) derive from pure hydrodynamics[1,b] the derivations take no account of possible variations of such fundamental properties as surface tension and viscosity. It would seem desirable to investigate the effect on the dome velocity of varying these properties. This should give us a better insight into the thermodynamic behavior of the liquid medium under such conditions. The present work includes a study of surface tension effects as well as the effect of spreading oil slick on the surface. The limitations of time and film consumption prevented continuing the work into a program to study viscosity variation. It is hoped that this work will be continued.

II. EXPERIMENTAL

1. Pond Work

The experiments were performed in the fresh water pond on Nonamessett Island. The relative position of the various units of the recording equipment is best seen by reference to Fig. 1. For most of the shots, two cameras were used to record the velocity of the rising dome. To record the "streak" type of picture, a General Radio type 651 AE oscillograph recorder using 35 mm film was used on all shots. The camera was mounted on its side (with the film moving horizontally) about a foot above the water surface. A vertical slit 0.1 in. wide was placed in front of the focal plane in order to narrow the field of view and thus produce a more clearly defined record of the edge of the image formed by the rising dome.[2,b] To understand the phenomena better, and to obtain a different sort of record for measurement, a Fastax 35 mm camera was also used for almost all the shots. This camera was also placed on its side so that the rising dome would be photographed along the long dimension of the frame. This introduced another simplification of measurement because lines could be drawn through a succession of frames to establish a common base line and slope of rise velocity. Timing marks were put on the edge of the film in the General Radio camera by means of a spark coil energized by an electronically amplified pulse from a 100 cycle tuning fork. In the Fastax camera, 1000 cycle timing marks were marked on the edge of the film by means of the timer described by Cole, Stacey, and Brown.[19]

To reduce ambiguity in interpretation, the records of all except a few early shots were made with artificial light provided by firing ten photoflash bulbs simultaneously with the shot. The flash bulbs were fired in two specially designed parabolic reflectors each holding five bulbs. Number 21 or 22 bulbs were used for the high velocity shots; number 31 bulbs were used for the low velocity shots to take advantage of the longer duration of the flash from the focal plane type of flash bulb. Illumination from the flash bulbs was sufficiently intense so that variations of natural lighting could be neglected. The increase in illumination also allowed narrowing the vertical collimating slit in the General Radio camera from 0.1 in. to 0.01 in. This greatly increased the definition of the resulting record although it made focussing and aiming a little more difficult.

Synchronization of the photoflash bulbs, detonation of the charge, and remote control of the cameras were obtained by the use of the time delay circuit described in the Underwater Photography II report.[6] Both cameras ran approximately 2.5 sec using 120 volts for the Fastax and 107 volts for the General Radio cameras. These applied voltages caused the General Radio camera to run 50 ft of film through at about 300 in./sec and the Fastax, 100 ft of film at about 3000 frames/sec. When the cameras were started, a switch in the primary of the timing spark coil was closed so that the timers were operating only during the time the cameras were running.

Those parts of the recording mechanism which had to be relatively close to the exploding charge, i.e., the two cameras and the timing mechanism, were protected by being enclosed in a specially constructed reinforced concrete box with a safety plate glass window.

2. Tank Experiments

In order to determine the dependence of dome velocity upon surface tension it was necessary to construct an experiment in which a reasonable amount of water would be involved. Accordingly, a welded tank was constructed of 1/8 in. sheet iron to the dimensions of a 3 ft cube with open top. This tank was supported on a heavy base constructed of angle iron such that the upper edge of the tank was five feet above ground level. This placed the upper edge exactly in line with the optical axis of the lens of an Eastman High Speed camera located inside the laboratory and focussed on the center of the tank through a plate glass window as indicated in Fig. 2. All the equipment was thus protected from the spray resulting from the explosion. With the exception of the camera, all the supplementary equipment was the same as that described under the preceding section. As with the Fastax camera, the High Speed camera was placed on its side so that measurements of successive frames would be greatly simplified. Illumination was again obtained with synchronized flash but, because of the decreased distances involved, only five flash bulbs were used for each shot.

The explosive used for all of the tank shots was the Engineer's Special Cap manufactured by the Hercules Powder Company of Wilmington, Delaware. It comprises a metal tube 1/4 in. in diameter and 3 in. long with the charge located in the end away from the detonator wires. The

composition of the charge, as given by the Hercules Company, is 13.5 grains of pentaerythritol tetranitrate plus 0.41 grams of a 75/25 mixture of diazodinitrophenol/potassium chlorate primer. In the calculation of similarity curves, it was assumed that this corresponded to 1.20 grams of a single explosive compound. It may or may not be correct but since the same lot of caps was used throughout, the actual weight used does not matter because no attempt was made to compare the absolute values of this explosive with those of other explosives.

The depth of the cap in each explosion was accurately located beneath the surface of the water to ± 1/64 in. by means of the support shown in Fig. 3. Orientation of the cap was always the same with the axis of the cap parallel with the axis of the camera and with the wire end towards the camera. Water was allowed to flow slowly into the tank at all times so that the water level was always the same, being regulated by overflow over the edges of the tank. For the determination of the similarity curve for these caps, single caps were fired, six at each of eight depths, 1/4, 1/2, 1, 2, 3, 4, 5, and 6 in.

The sympathetic detonation series was executed in the following manner. One cap (donor) was fired with its center exactly 3/4 in. from the center of a second cap (acceptor), the axes of both caps being parallel with the optical axis of the camera. Six shots were fired with the plane defined by the axes of the caps parallel with the surface of the water (orientation A D and twelve with this plane perpendicular to the surface of the water. Of these twelve, six were fired with the donor charge below (orientation A) and six with the donor charge above the acceptor (orientation D).
D A
The caps were separated 3/4 in. from center to center by taping them together with accurately made 1/2 in. wooden separators and then taping both separator and cap to the cap support. The depth of all these shots was 5 in. to the center of gravity of the two caps which in the case of the vertical orientation placed the center of the upper cap 4 5/8 in. below the surface.

Surface active materials used were of three different types. For the first twelve shots fired at depths of 4 and 8 in., the tank contained a solution made by dissolving 4 lb of a commercial synthetic detergent (marketed by the National Cooperative stores as "Synthetic Suds") in the contents of the tank. This is probably a sulphonated oil derivative similar to "Dreft". Mixed with the approximately 200 gallons of water in the tank, this produced a solution whose surface tension was about 45.5 dynes/cm. The second experiment was with first 5 lb and then 10 lb of Eimer and Amend Company "Aerosol" 10% solution added to the contents of the tank. This gave solutions with surface tensions of about 41 and 35 dynes/cm respectively. To avoid excessive dilution of these solutions, the water supply was not allowed to flow continuously but was only sufficient to replace solution lost with each explosion. Because the surface tension-concentration curves for solutions of this type do not change very rapidly in this concentration range, the change of surface tension with this necessary dilution was slight. Samples were removed for analysis before and after each explosion and surface tensions were measured with a Du Nouy ring tensiometer manufactured by the Central Scientific Company. Caps were fired at depths of 4, 8, and 12 in. for both of these concentrations of "Aerosol".

The third series, with caps fired at depths of 8, 10, and 13½ in., was not an intended experiment but is included because of the deviation of the results from the normal similarity curve. Experiments with some spreading agent such as oleic acid were planned but because oxidized fuel oil was accidently introduced into the tank during the course of the similarity curve determination, it was decided to continue with the shooting to ascertain if the spreading oil had any effect. Fortunately, the oil did spread easily, probably into a monomolecular layer, and when measured on the ring tensiometer (in the absence of an Adam-Langmuir trough) allowed the ring to separate from the surface at a tension of about 52 dynes/cm thus showing a spreading pressure of between 25 and 30 dynes/cm, since the surface tension of pure water at these temperatures, as measured, is about 80 dynes/cm.

3. Critical Depth Experiments

A direct experimental approach to the value of T in Eq. (2) is the determination of the "critical depth" at which the explosive must be placed so that V_o becomes zero. Above this "critical depth" water is forced from the surface and below, it is not. At this depth, where $V_o = 0$, T can be calculated from Eq. (2) if a reliable value of P_m is available. The "critical depth" can be determined by suspending Engineer's Special detonators at various depths below the surface of the water in the harbor and photographing the resulting explosion by means of a 4 x 5 Speed Graphic camera. The detonator was fired by means of the camera's synchronized flash attachment and the shutter speed was maintained at the relatively low value of 1/25 sec in order to catch any surface effects. A typical print is shown in Fig. 4.

III. EXPERIMENTAL RESULTS

4. Methods of Computation

The initial velocity of the rising dome was obtained by the analysis of strip prints made from the Fastax and Streak negatives from the full scale experiments conducted in Nonomessett Pond and from the Eastman High Speed negatives of the tank experiments. Examples of these strip prints appear in Figs. 5, 6, 7, 10, 11, and 12. Figures 6 and 10 have been reproduced photographically.

For the Fastax and Eastman High Speed prints, a straight edge was used to draw a line through the tips of smoothed dome contours on successive frames, starting with the initial appearance of the dome and continuing until the rise was no longer linear with time or until the image left the print area. Since a carpenter's level was used in mounting the cameras to insure horizontal travel of the film, the edge of the sprocket holes could be used as a base line, and it was therefore easy to calculate the slope of the rise line, i.e., dome velocity, in terms of arbitrary units depending upon the film speed and enlargement for each print. This dome velocity, in arbitrary units, is measured from the Streak prints in much the same manner, the rise line being the best straight line which can be drawn through the edge of the image which corresponds to the path of the maximum dome height.

It is necessary to transform the dome velocity from these arbitrary units to feet per second. The linear dimension is obtained from the geometry of the system and/or from a linear scale of some sort appearing on the same print. For a given set of experimental conditions, for example the tank shots, this is a constant factor. The time base is obtained from the timing marks appearing on the edge of the film.

Knowing the dome velocity, in feet per second, it is easy to calculate from Eq. (1) the corresponding peak pressure. Since, usually, six shots were made for each value of $W^{1/3}/R$, the calculation of P_m for each value of $W^{1/3}/R$ was not made for each shot but rather for the arithmetic mean of the dome velocity for each point. The ordinary methods of statistics were applied to each point, the calculations of the standard deviation of a single observation from the mean (σ) and of the standard deviation of the mean of a group of observations (σ_m) being made in the customary manner. During the course of the 350 or so observations made during this program, the only observations eliminated on any basis other than failure of some experimental unit were three which fell outside of the statistical limits for a chance error.[7]

The only other parameter in Eq. (1), the calculation of which needs explanation, is the value of U, the velocity of propagation of the shock wave. This must be obtained for each calculated P_m from a relation such as that given by Arons[8] between c_o, the velocity of sound under the experimental conditions of temperature and salinity,[9] and U for a wide range of P_m. Since P_m is unknown at the beginning of the calculation, the correct value of U and P_m must be obtained by successive approximations. This is not an onerous task since each calculation is very simple.

5. Nonomessett Pond Results

Typical photographs taken with the Fastax and Streak cameras are shown in Figs. 5, 6, and 7. The behavior of two well-known explosives, pentolite and tetryl, was investigated. Values of $W^{1/3}/R$ were selected such that approximately equally spaced points would appear along the similarity curve plotting $W^{1/3}/R$ against P_m on logarithmic paper. The values were also selected to cover as wide a range of peak pressure as seemed reasonable. The weight of the explosive charges varied from 25 grams to 5 lb, the larger charges in general being used for large values of $W^{1/3}/R$ and the smaller charges for small values of $W^{1/3}/R$. However, enough small charges at shallow depths and large charges at deeper depths were included to show that the dome velocity was dependent only on the peak pressure and not on the charge weight - at least in this range. There is some evidence[20] that V_o might depend somewhat on the charge weight. This evidence is found when these results are compared with those from quite large charges at small values of $W^{1/3}/R$.

Calculations of all peak pressures for both pentolite and pressed tetryl are included in Tables I and II together with the calculated values of σ and σ_m. Similarity curves determined by these results are shown in Figs. 8 and 9. The linear equation representing the similarity curve for pentolite is taken from piezoelectric results[10]. The theoretical curves were calculated by the methods of Kirkwood and Brinkley[11].

TABLE I

DOME VELOCITY RESULTS FOR PENTOLITE

POND SERIES

$W^{1/3}/R$* ($lb^{1/3}/ft$)	Camera	n	V_o (ft/sec)	σ of V_o (ft/sec)	P_m ($lb/in.^2$)	σ of P_m ($lb/in.^2$)	σ_m of P_m ($lb/in.^2$)	σ_m of P_m (%)
0.212	S	6	58	3.2	1920	106	43	2.2
	F	4	56	3.2	1865	106	53	2.8
0.382	S	7	224	14.4	7640	490	185	2.4
	F	4	210	12.1	7165	412	206	2.9
0.732	S	5	436	24.4	15440	865	387	2.5
	F	5	440	11.7	15550	415	186	1.2
1.537	S	5	1000	29.5	39250	1154	516	1.3
	F	5	990	15.9	38700	623	279	0.7
2.255	S	4	1800	134.2	80100	5969	2984	3.7
	F	4	1820	193.5	81000	8612	4306	5.3
3.28	S	5	2700	323.3	134400	16092	7197	5.3
	F	4	2615	101.0	130200	5026	2513	1.9

* Individual charge weights and depths making up each of these averaged values of $W^{1/3}/R$ are included in the Appendix.

TABLE II

DOME VELOCITY RESULTS FOR PRESSED TETRYL

POND SERIES

$W^{1/3}/R$* ($lb^{1/3}/ft$)	Camera	n	V_o (ft/sec)	σ of V_o (ft/sec)	P_m ($lb/in.^2$)	σ of P_m ($lb/in.^2$)	σ_m of P_m ($lb/in.^2$)	σ_m of P_m (%)
0.203	S	6	55	8.5	1797	275	113	6.3
	F	5	56	5.4	1800	176	78	4.3
0.393	S	6	150	9.9	4938	326	133	2.7
	F	6	150	14.9	4938	489	201	4.1
0.779	S	6	360	10.4	12300	355	145	1.2
	F	6	354	10.9	12090	371	151	1.2
1.516	S	5	1061	172	40950	6638	2963	7.2
	F	5	1026	149	39630	5754	2569	6.5
2.19	S	7	1628	106	68800	4480	1691	2.5
	F	7	1607	123	68000	5200	1965	2.9
3.38	S	6	3000	435	152000	22050	9000	5.9
	F	6	2950	350	149000	17680	7216	4.8

* Individual charge weights and depths making up each of these averaged values of $W^{1/3}/R$ are included in the Appendix.

6. Tank Results

The results of applying the analytical methods of Sec. 4 to the tank shots are summarized in Tables III, IV, and V. The similarity curve for Engineer's Special Detonators derived from this work appears in Fig. 13. The results of the sympathetic detonation series are superimposed on this similarity curve in Fig. 14 and those obtained in solutions of lowered surface tension are superimposed on the similarity curve in Fig. 15. Typical film records are shown in Figs. 10, 11, and 12. Discussion of these results will be presented in Part IV.

7. Methods for Calculating T

The principle of obtaining T from Eq. (2) is very simple. Any procedure by which V_o can be made equal to zero will allow T to be calculated.

$$V_o = \frac{2}{\rho_o U}\left(P_m - \frac{T}{2}\right) = 0$$

$$P_m - \frac{T}{2} = 0$$

$$T = 2P_m$$

The only requirement is that P_m be known from some other experimental or theoretical evidence.

Four separate methods have been used to obtain values of T. The first method was discussed in Sec. 3. Measurements of the "critical depth" by lowering the detonator until spray was no longer formed were made on two separate occasions, the first at a time when the water surface was smooth and the second when the surface had about 2 - 3 in. ripples. The results obtained on these two days are shown in Table VII. Other estimates of T made from data in the literature also appear in Table VII. No attempt has been made to include in Table VII all estimates of T that might be made from the data in the literature.

A second method is the extrapolation of curves of dome velocity versus depth to $V_o = 0$. Of the dome velocity results in this report, only those in the tank series allow a justifiable extrapolation to $V_o = 0$. For this case, $V_o = 0$ at a depth of about 18 in. or a $W^{1/3}/R$ value of 0.092 corresponding to a peak pressure of 1800 lb/in.^{2} or tension of 3600 lb/in.^{2}. While this method is interesting it can obviously be applied only to a series of dome velocity results which is very complete and subject to little experimental error, especially for low values of $W^{1/3}/R$.

TABLE III

DOME VELOCITY SIMILARITY CURVE RESULTS FOR SINGLE ENGINEER'S SPECIAL CAPS
TANK SERIES

$W^{1/3}/R$ ($lb^{1/3}/ft$)	n	V_o (ft/sec)	σ of V_o (ft/sec)	P_m ($lb/in.^2$)	σ of P_m ($lb/in.^2$)	σ_m of P_m ($lb/in.^2$)	σ_m of P_m (%)
0.278	6	90	3.2	2890	102.7	41.9	1.4
0.333	6	131	11.4	4230	368	150	3.5
0.417	6	184	13.4	5980	437	178	3.0
0.556	6	292	18.7	9720	622	254	2.6
0.832	6	493	21.9	17000	755	308	1.8
1.67	6	1075	69.2	39200	2522	1030	2.6
3.33	6	2082	102.6	92200	4544	1855	2.0
6.68	(1)	~3700		~200000			

TABLE IV

DOME VELOCITY SYMPATHETIC DETONATION RESULTS
TANK SERIES

$W^{1/3}/R$ ($lb^{1/3}/ft$)	Orientation	n	V_o (ft/sec)	σ of V_o (ft/sec)	P_m ($lb/in.^2$)	σ of P_m ($lb/in.^2$)	σ_m of P_m ($lb/in.^2$)	σ_m of P_m (%)
0.418	A D	6	215	12.7	7050	416	170	2.4
0.418	A D	5	236	6.3	7770	207	92	1.2
0.418	D A	6	160	8.7	5190	282	115	2.2

TABLE V

DOME VELOCITY SURFACE TENSION LOWERING RESULTS
TANK SERIES

$W^{1/3}/R$ ($lb^{1/3}/ft$)	Surface Active Agent	γ (dynes/cm)	n	V_o (ft/sec)	σ of V_o (ft/sec)	P_m ($lb/in.^2$)	σ of P_m ($lb/in.^2$)	σ_m of P_m ($lb/in.^2$)	σ_m of P_m (%)
0.417	Synthetic	45.5	6	272	49.4	9020	1635	668	7.4
0.208	Suds	45.5	6	97.5	4.2	3130	135	55	1.8
0.139	Aerosol	41.0	6	42.4	18.4	1350	586	239	17.7
0.208	(5 lb)	42.0	5	75.3	14.2	2410	454	203	8.4
0.417		41.0	6	199	11.6	6520	380	155	2.4
0.139	Aerosol	35.0	3	51.0	25.3	1624	805	465	28.6
0.208	(10 lb)	35.0	6	96.6	15.5	3100	497	203	6.5
0.417		35.0	7	225	23.8	7400	783	295	4.0
0.124	Oxidized	52.0	5	48.6	6.9	1545	219	99	6.4
0.167	Fuel	52.0	6	54.1	4.3	1723	137	56	3.2
0.208	Oil	52.0	6	64.1	4.1	2050	131	53	2.6

TABLE VI

ADDING 3300 TO EACH P_m AS CALCULATED FOR TANK SHOTS

$W^{1/3}/R$ ($lb^{1/3}/ft$)	P_m ($lb/in.^2$)	$P_m + 3300$ ($lb/in.^2$)
0.278	2890	6190
0.333	4230	7530
0.417	5980	9280
0.556	9720	13020
0.832	17000	20300
1.67	39200	42500
3.33	92200	95500
6.68	200000	203300

TABLE VII

APPROXIMATE VALUE OF T OBTAINED FROM CRITICAL DEPTH ESTIMATION

Explosive	$W^{1/3}/R$ ($lb^{1/3}/ft$)	P_m ($lb/in.^2$)	T ($lb/in.^2$)	Remarks
Engineer's Special Detonators	0.0556	1000	2000	Calm
	0.0398	750	1500	Ripples
Amatol (40 lb) (40/60)	0.05	700	1400	Ref. 3
Amatol (300 lb) (40/60)	0.05	700	1400	Ref. 3
TNT (2 lb)	0.035	400	800	Ref. 12
"PE" (1 lb)	0.041	500	1000	Ref. 13

The method of obtaining a value of P_m for $V_o = 0$ which is most universally applicable is the measurement of the greatest periphery attained by any dome from successive high speed photographs of the underwater explosion. It is assumed that at the edge of the dome, the vertical component of the pressure is the critical value, below which water does not leave the surface. The calculation can be readily understood by reference to Fig. 16 and the vector diagram giving T/2 from P_a and the angle α. It is obvious that we need the weight of the charge, the depth R, some means of obtaining a good value of P_a, and a knowledge of the geometry of the system so that we can calculate D, the greatest dome diameter, from the photographic image. Unfortunately, this sort of calculation could not be applied to any of the work presented in this report because the photographs were taken at short distances to obtain the best value of V_o at the center of the dome and hence did not include the complete phenomena. However, many suitable photographs have been taken in this laboratory during the course of other work and this calculation has been made for a representative number of shots. Large charge experiments were used to get an estimate of T from full scale work in the open sea for comparison with the other values presented which were obtained largely from laboratory scale explosions. These calculations are summarized in Table VIII.

TABLE VIII

APPROXIMATE VALUE OF T OBTAINED FROM DOME PERIPHERY CALCULATION*

Shot No.	$W^{1/3}/R$	P_m (lb/in.^{2})	T (lb/in.^{2})
B-1	0.0133	180	360
B-9	0.0178	240	480
B-13	0.0315	440	880
K-1	0.0149	200	400
K-8	0.0140	190	380
K-9	0.0133	180	360
K-10	0.0133	180	360
K-17	0.0153	205	410
L-5	0.0128	170	340
L-13	0.0171	230	460
L-17	0.0166	225	450
L-21	0.0150	200	400
L-22	0.0176	240	480
L-25	0.0185	250	500
PH-3	0.0185	250	500
M-13	0.0124	155	310
M-14	0.0127	160	320
M-31	0.0207	270	540
M-32	0.0171	230	460

* Charge equivalent to 325 lb TNT.

The last method of estimating T to be presented here is that based on a comparison of P_m as obtained from Eq. (1) and dome velocity measurements and P_m obtained for the same values of $W^{1/3}/R$ from piezoelectric measurements. It is well-known that piezoelectric results give a similarity curve which is a straight line when plotted on logarithmic paper. Inspection of Figs. 8 and 9 will show that the values of P_m calculated from Eq. (1) tend to fall below the piezoelectric straight line and/or the theoretical curves for the smaller values of $W^{1/3}/R$. The straight line relationship must be assumed for the case of the tank series (Fig. 13) because piezoelectric results are not available for such small explosions. This departure from a straight line is undoubtedly due to our lack of knowledge of the proper value of T to put in Eq. (2). If T were known for each set of conditions, then P_m as calculated from Eq. (2) would probably be more nearly the same as that obtained from other records. This T correction should also be applied to the higher values of P_m, but P_m is so large for high values of $W^{1/3}/R$ that T is insignificant by comparison.

If the above explanation is correct, one can obtain an approximate value of T by correcting the values of P_m obtained by the dome velocity method so as to bring them more nearly in accord with curves from other sources. This estimation is questionable in the case of pentolite (Fig. 8) but the value of 1500 lb/in.^{2} is necessary to make the first point match the piezoelectric straight line. This assumption would not place the other points unreasonably high. The similarity curve for pressed tetryl charges is not as well known as is probably necessary for this calculation[14] but a comparison with known experimental values shows that a value of about 2000 lb/in.^{2} is necessary for correspondence at the lower values of $W^{1/3}/R$. Since no similarity curve is known for Engineer's Special Detonators it seems reasonable to assume values which would correct the curve of Fig. 13 to the straight line of Fig. 13a. This gives a value of 3300 lb/in.^{2} which corresponds to T = 6600 lb/in.^{2}, the highest value of T obtained by any of the considerations of this section. The value seems reasonable because it allows all of the results obtained with lowered surface tension to be included in the area between the experimental and corrected curves, Fig. 15a. The logic of this statement will be discussed later.

The various estimations of T are summarized in Table IX.

TABLE IX

SUMMARY OF ESTIMATED VALUES OF T

Method of Calculation	T (lb/in.^{2})
Critical Depth	1500 (800 - 2000)
Dome Periphery	450 (300 - 900)
Extrapolation to $V_0 = 0$	3600
Similarity Curve Correction	4500 (3000 - 6600)

IV DISCUSSION

8. Accuracy of the Method

A comparison of the standard deviation of any of the pressures reported here with those obtained from piezoelectric measurements[14] shows that the dome velocity method is of about the same precision. The percentage deviation is about the same for all of the pressures studied except for the highest value of $W^{1/3}/R$ in the tank series. The difficulty in this case can be understood by inspection of Fig. 10. The initial velocity is so great and the retarding influences of friction and gravity appear so early that the camera speed is not sufficient to resolve the phenomenon. The only recourse here is to use the greatest slope observed between the first dome appearance and the preceding frame as the closest possible approach to the correct slope. The recorded result for this point corresponds therefore to the single observation giving the greatest velocity and does not represent an arithmetical mean as do all the others.

There does not appear to be any choice between the three cameras used with regard to attained accuracy. However, the Fastax or Eastman High Speed negatives allow a more detailed study if such is considered desirable.

More scatter is apparent in the surface tension series. Since every other condition was identical with the other tank series, this might very well be due to slight changes of the surface tension from shot to shot even though the measured values of samples in the laboratory were nearly identical. It is known[15] that the surface tension of dilute solutions of surface active materials gradually diminishes with time from the value obtained at a freshly prepared or swept surface. No attempt was made in the course of this experiment to keep the "age" of the surface constant between shots since it was impossible to maintain conditions in accord with the practices of surface chemistry.

9. Value of the Method for the Determination of the Peak Pressure

The precision of the dome velocity method has been established as being as good as that of other accepted methods for the determination of peak pressure. The limitations of the method are

(1) that only peak pressure can be estimated,
(2) that the range of $W^{1/3}/R$ values is limited to greater than about 0.2 because the inaccuracy due to the unsatisfactory knowledge of the tension T in Eq. (2) becomes increasingly important in this region of lower values, and
(3) that only one measurement is obtained from each shot whereas with gauge methods, for example, the number of observations is limited only by the number of gauges and/or recording channels available.

However, the advantages outweigh, at least for some considerations, the disadvantages. They are

(1) that the method can be applied to any size of charge with equal precision,
(2) that the cost of the recording equipment is only a fraction of that needed for piezoelectric measurements, especially where a drum type of camera is used,
(3) that the analysis of the photographs is less onerous than in some other methods, piezoelectric data for example,
(4) that pressures can be determined for very high values of $W^{1/3}/R$. (This is the only experimental method of determining such high pressures with the exception of difficult and costly optical methods), and
(5) that the method rests on sound hydrodynamic theory, giving a more nearly absolute measure than some other methods.

10. Value of the Method for Multiple Charge Effects

It is seen by reference to Table IV that the precision of measuring sympathetic detonation effects is satisfactory. While this application was attempted only in the tank shots where various delay times could not be tried, it would be quite possible to apply the method to full scale charges with delay times between the firing of the two charges regulated by such means as varying lengths of primacord. It is not in the province of the present report to discuss the interpretation of sympathetic detonation and/or multiple charge effects.[16] Nevertheless, it can be shown by a simple calculation for orientation $\frac{A}{D}$ in Table IV, that if the pressure from D is simply added to that from A at the surface, the sum is 7900 lb/in.^{2} which more than accounts for the recorded value of 7770 lb/in.^{2}. It would appear, therefore, that if the multiple charge effect really does give an augmentation as is proposed by some, this can only be proved by a careful study of energy as well as pressure data and cannot be accomplished by the dome velocity method.

11. The Surface Tension Lowering Problem

The derivation of Eq. (2) does not include the surface tension of the medium as a variable. It remains to be explained why V_o and hence the measured value of P_m is elevated in our surface tension experiments. An illuminating fact is observed if one assumes T = 6600 lb/in.^{2} for the tank shots. The surface tension results can then be placed on the corrected and uncorrected curves (Fig. 15a). It will be noted that when plotted on Fig. 15a all the surface tension points fall between the two curves, indicating that the effect of lowering the surface tension is directed towards lowering the value of T.

It is difficult to sort out the role of surface tension from the complex phenomena associated with dome formation. Nevertheless, since the size of droplets formed in a gravity field under essentially static conditions is dependent upon surface tension, it is not too difficult to assume a dependence of the tensile strength T upon surface tension. Unfortunately our experiments could not be performed under sufficiently controlled conditions to point out an experimental relation between these quantities although one undoubtedly exists. If the surface tension results have no other value they at least allow more reliance to be placed on the estimated value of T.

12. The Tensile Strength of Water

The value of the tensile strength for water reported here is quite at variance with the value assumed by Pekeris in his description of the dome velocity problem.[17] His assumption of Reynold's value of 5 atmospheres as an upper limit is unjustified both on the basis of this work and the discussion of Temperley.[5] It is difficult to see how the estimated values of Table IX could be in error by the order of magnitude necessary to bring about correspondence with values estimated from cavitation studies[18] for example. It may be that the experimental conditions are sufficiently different to account for the discrepancy. The extreme dependence of the determined values of T upon the experimental method is well discussed by Temperley and our estimates lie within the range of values reported by him from various sources.

It is interesting that the value of T estimated by this method decreases as the size of the charge increases. This observation would indicate that the value depends upon the time constant of the shock wave or, in other words, upon the length of time during which the necessary pressure is acting upon the surface layer. This is reasonable and, if one is justified in estimating T from dome velocity methods, this may provide a method for determining the energy in the shock wave as well as the peak pressure. Since the time constant of a pressure wave depends not only on the size of the charge but also on the distance from the center of the charge, one must on this basis assume that the apparent value of T will be larger for the higher values of $W^{1/3}/R$ for the same size of charge. There is obviously a need for a great amount of additional work to obtain values with which to test these interesting and fundamental relationships. These problems can only be indicated by the present work because the amount of data, unfortunately, is not sufficient to give the solution.

APPENDIX

TABLE A-I

CHARGE DATA POND EXPERIMENT PENTOLITE SERIES

Shot Number	Weight (lb)	Depth (ft)	Shot Number	Weight (lb)	Depth (ft)
$W^{1/3}/R = 0.212$			$W^{1/3}/R = 0.382$		
NP 11	0.54	3.86	NP 8	4.45	4.29
NP 17	0.054	1.71	NP 28	4.47	4.29
NP 54	0.546	3.90	NP 29	4.40	4.29
NP 55	0.555	3.90	NP 30	4.47	4.29
NP 56	0.553	3.90	NP 33	4.45	4.29
NP 57	0.550	3.90	NP 34	4.42	4.29
			NP 35	4.42	4.29
			NP 36	4.43	4.29
$W^{1/3}/R = 0.732$			$W^{1/3}/R = 1.537$		
NP 48	0.586	1.14	NP 39	0.57	0.54
NP 49	0.579	1.14	NP 41	0.607	0.54
NP 50	0.597	1.14	NP 45	0.558	0.54
NP 51	0.580	1.14	NP 46	0.528	0.54
NP 52	0.572	1.14	NP 47	0.572	0.54
$W^{1/3}/R = 2.255$			$W^{1/3}/R = 3.28$		
NP 42	4.45	0.729	NP 10	4.38	0.50
NP 43	4.43	0.729	NP 60	4.40	0.50
NP 44	4.46	0.729	NP 61	4.47	0.50
NP 53	4.438	0.729	NP 62	4.41	0.50
			NP 63	4.44	0.50

TABLE A-II

CHARGE DATA POND EXPERIMENT TETRYL SERIES

Shot Number	Weight (lb)	Depth (ft)	Shot Number	Weight (lb)	Depth (ft)
$W^{1/3}/R = 0.203$			$W^{1/3}/R = 0.393$		
NP 89	0.055	1.87	NP 64	0.677	2.24
NP 90	0.055	1.87	NP 65	0.678	2.24
NP 91	0.055	1.86	NP 67	0.681	2.24
NP 92	0.054	1.87	NP 68	0.678	2.24
NP 93	0.055	1.87	NP 69	0.678	2.24
NP 94	0.054	1.87	NP 70	0.697	2.24
$W^{1/3}/R = 0.779$			$W^{1/3}/R = 1.516$		
NP 71	0.681	1.13	NP 77	0.668	0.58
NP 72	0.685	1.13	NP 78	0.678	0.58
NP 73	0.701	1.13	NP 79	0.678	0.58
NP 74	0.678	1.13	NP 80	0.681	0.58
NP 75	0.677	1.13	NP 81	0.685	0.58
NP 76	0.678	1.13			
$W^{1/3}/R = 2.19$			$W^{1/3}/R = 3.38$		
NP 82	3.75	0.708	NP 95	4.90	0.503
NP 83	3.75	0.708	NP 96	4.86	0.503
NP 84	3.75	0.708	NP 97	4.89	0.503
NP 85	3.75	0.708	NP 98	4.88	0.503
NP 86	3.75	0.708	NP 99	4.87	0.503
NP 87	3.75	0.708	NP 100	4.89	0.503
NP 88	3.75	0.708			

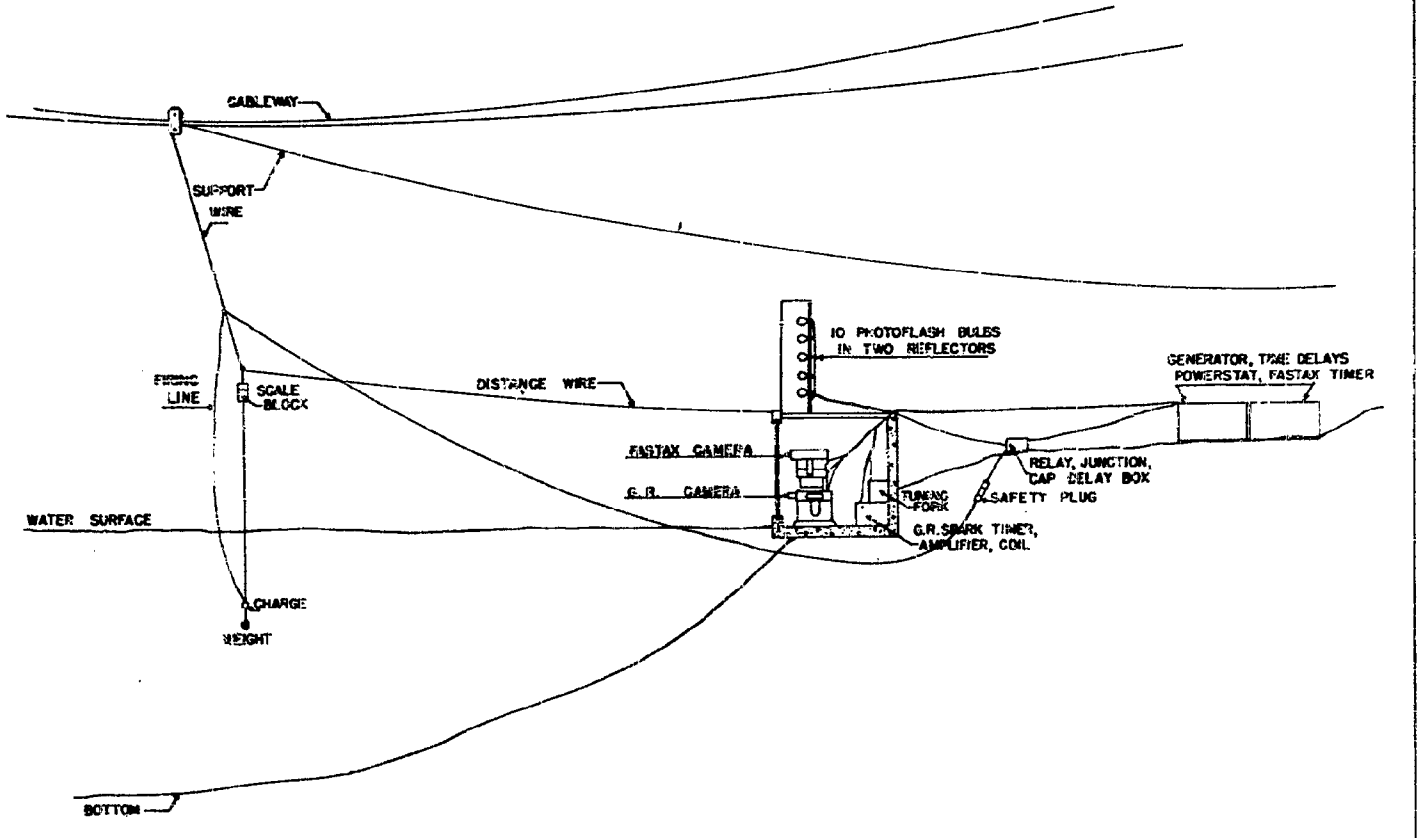

FIG. 1

EXPERIMENTAL SET UP
FOR
DOME VELOCITY SHOTS USING SMALL CHARGES

UERL WOODS HOLE, MASS.

TRACED BY NRC
11-19-46

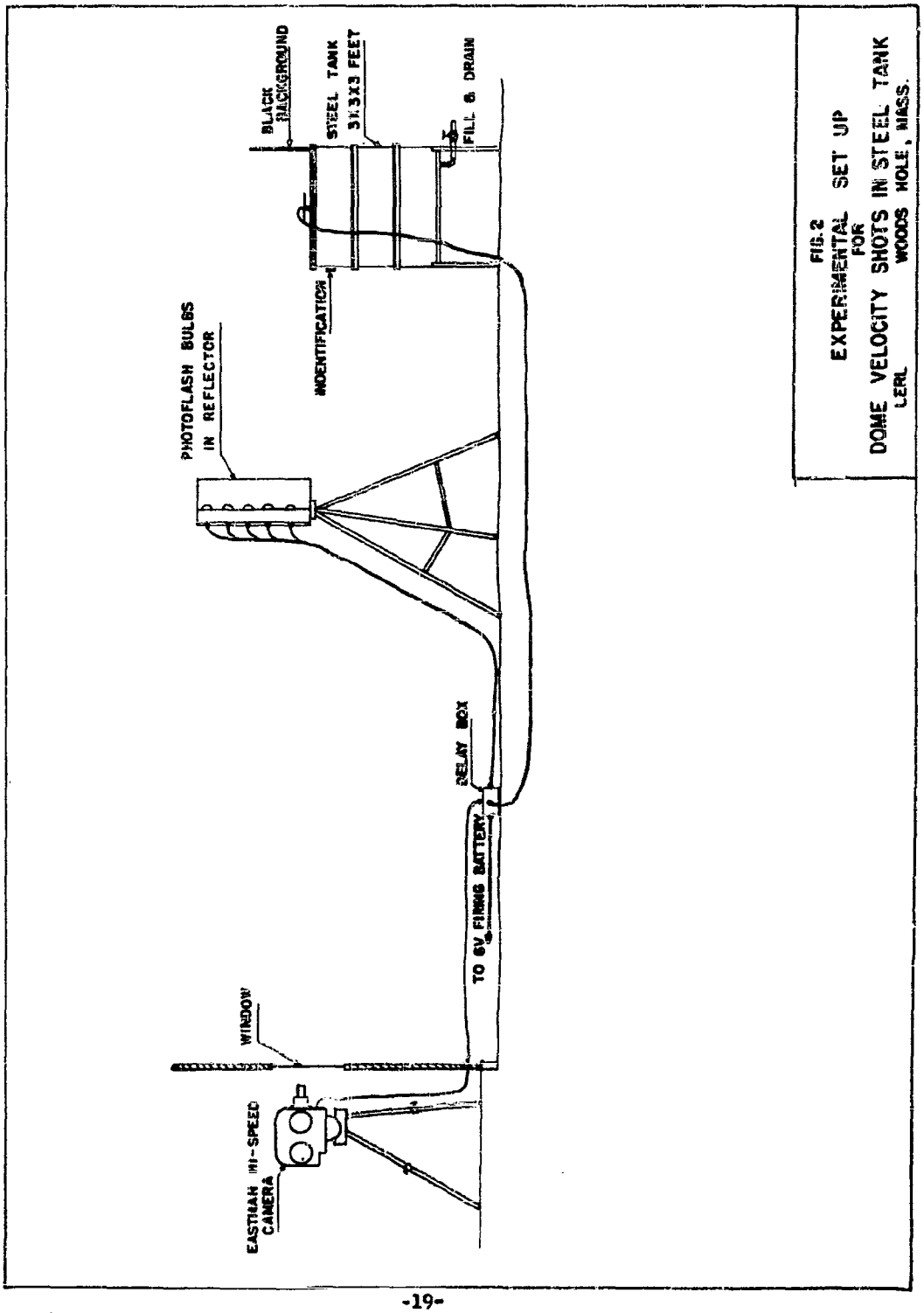

FIG. 2
EXPERIMENTAL SET UP
FOR
DOME VELOCITY SHOTS IN STEEL TANK
LERL WOODS HOLE, MASS.

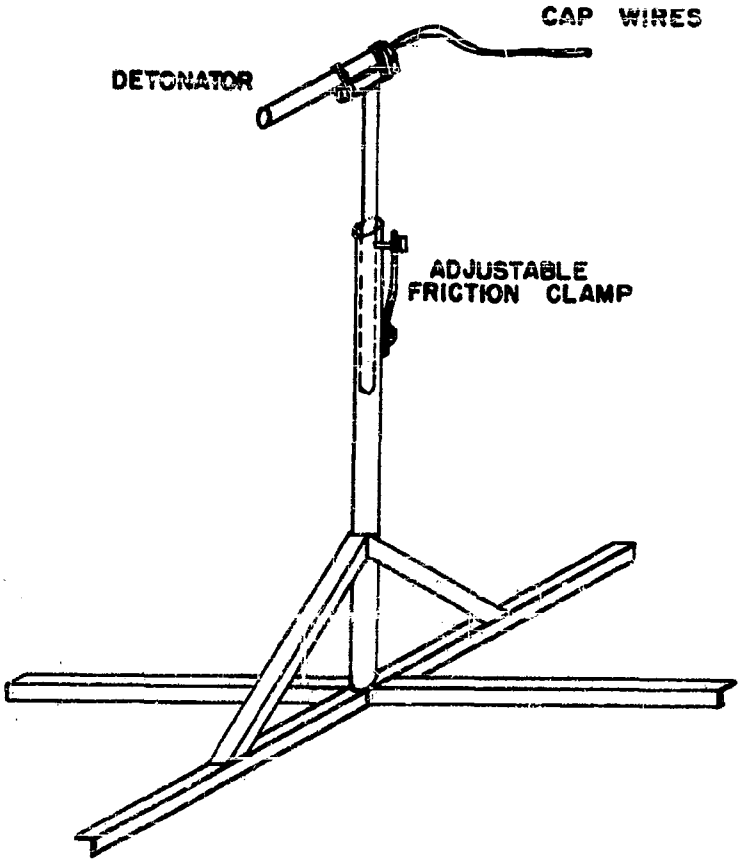

FIG. 3
CAP HOLDER FOR TANK SHOTS
UERL WOODS HOLE, MASS.

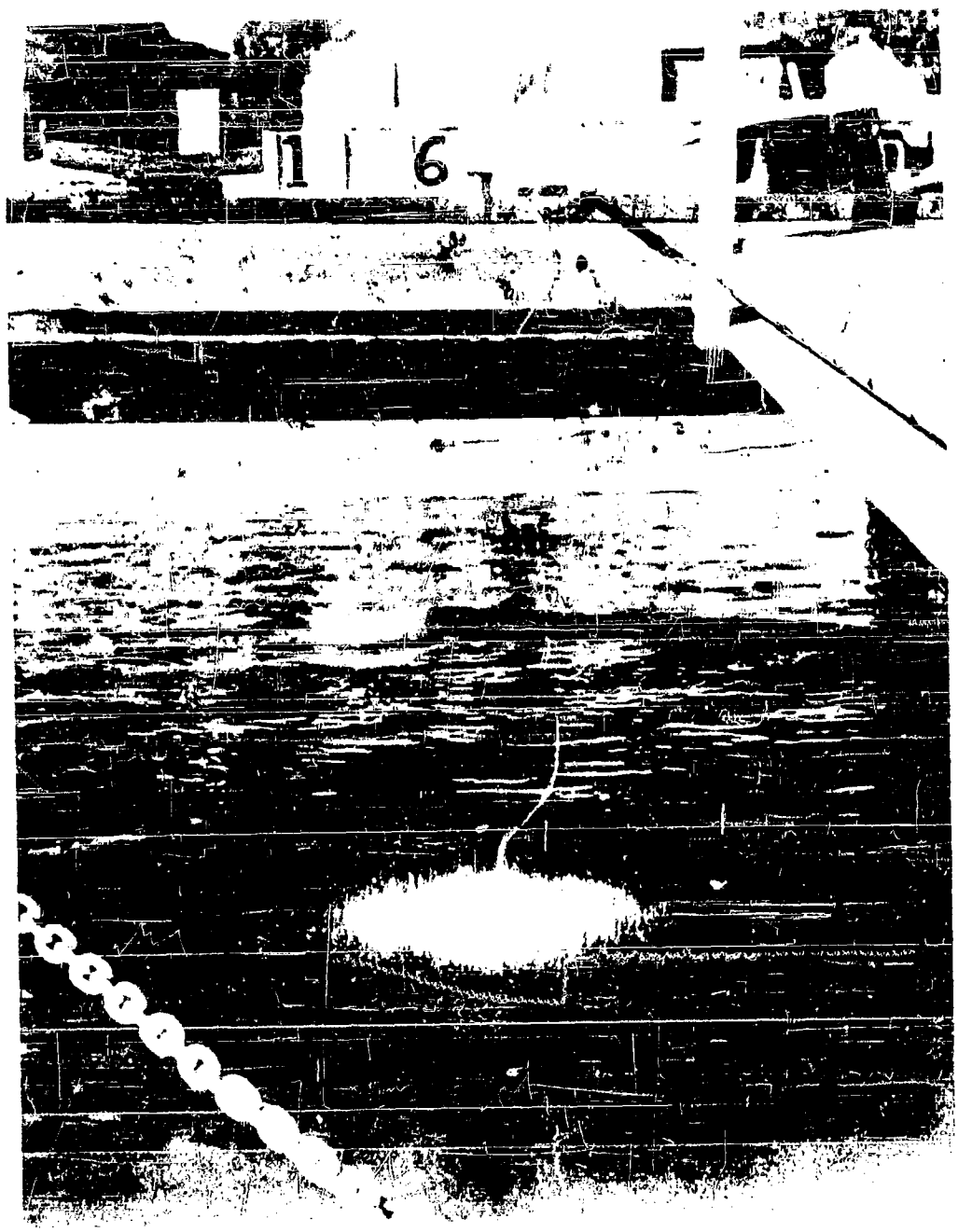

Fig. 4. Critical depth experiment using caps

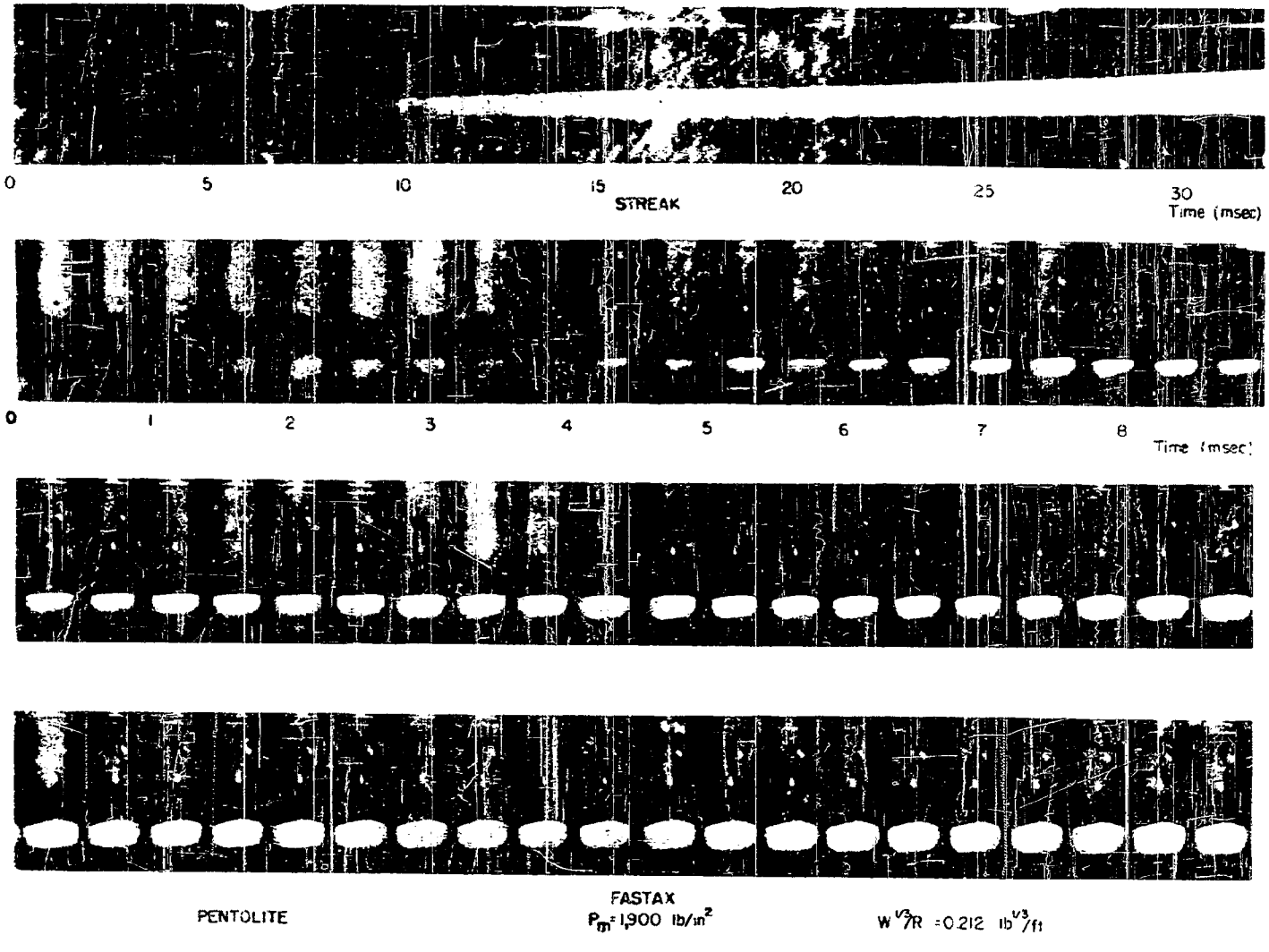

Fig. 5. Typical example of low dome velocity

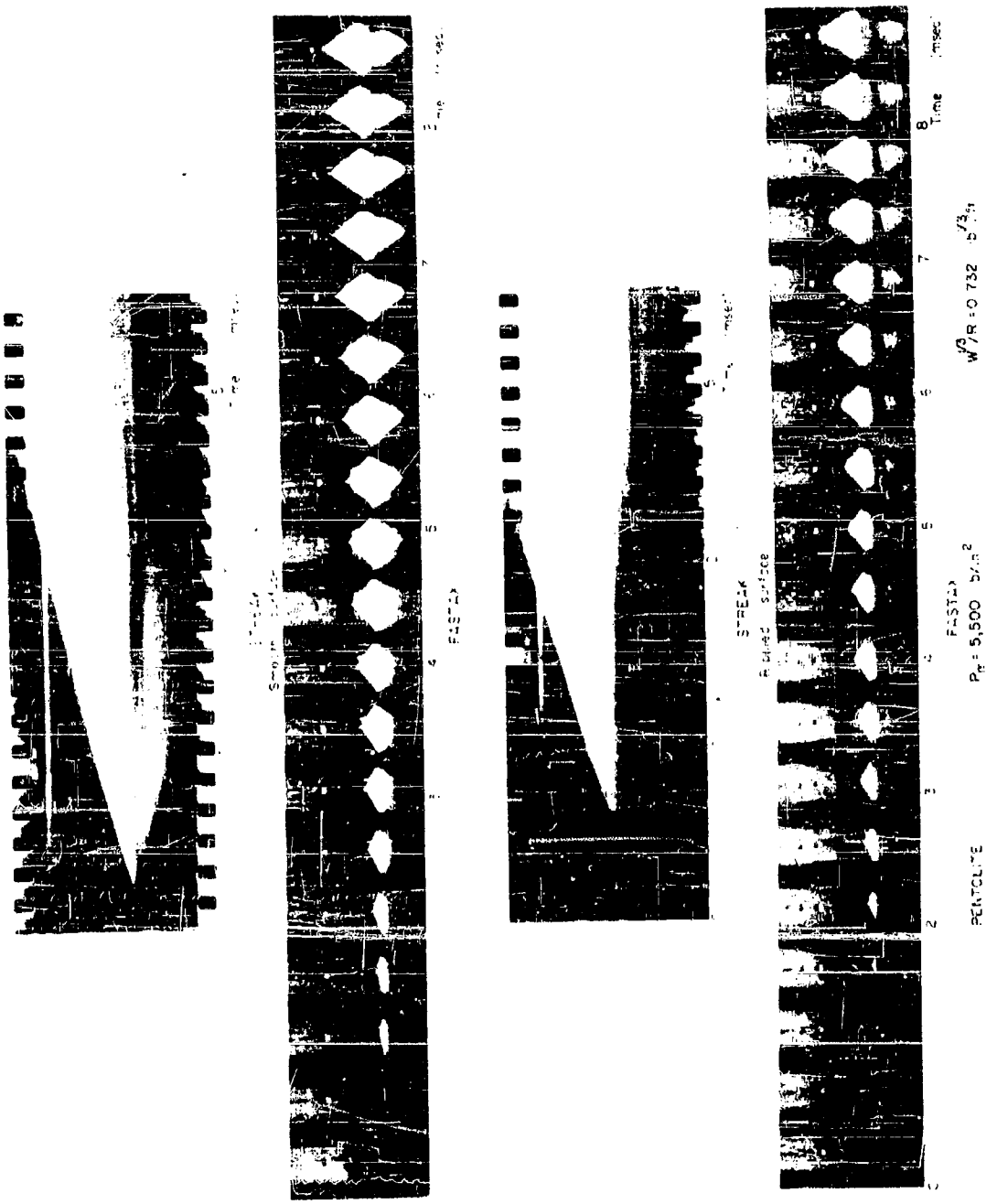

Fig 6 Influence of surface ripples on dome appearance

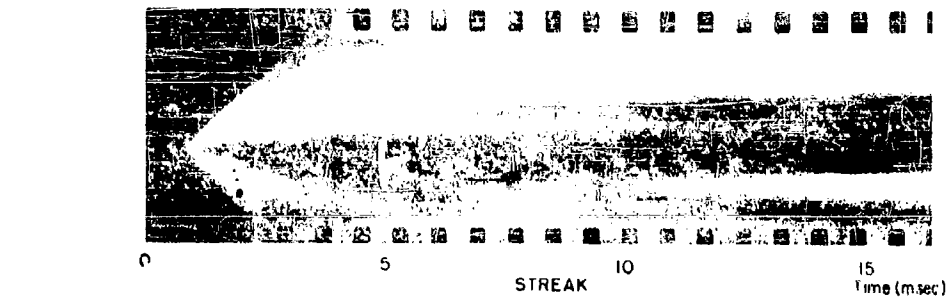

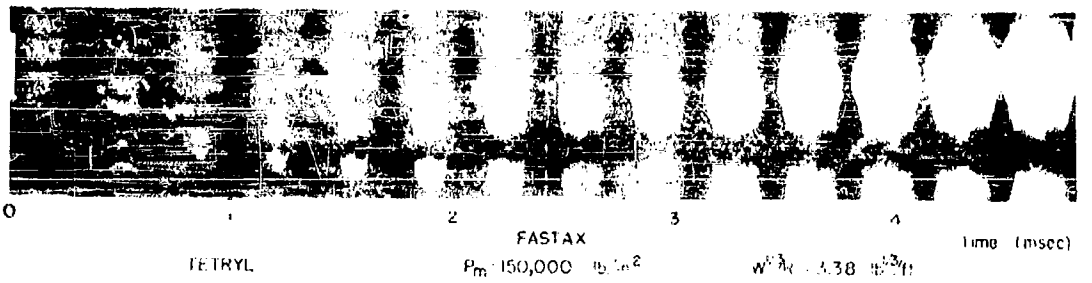

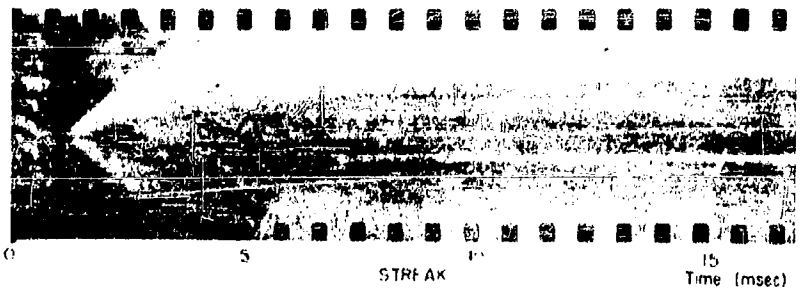

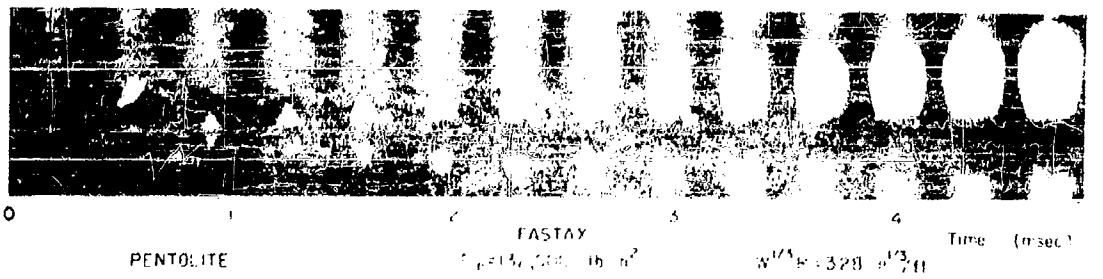

Fig. 7 Typical examples of high-[illegible] records

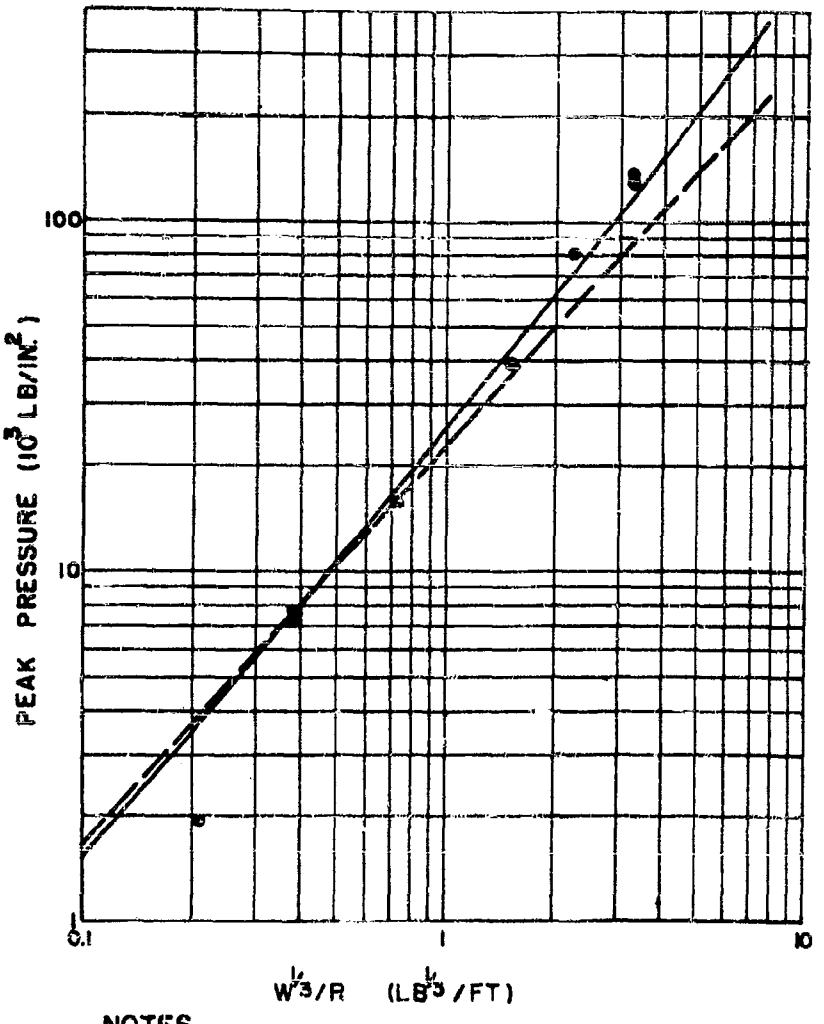

NOTES

o = DOME VELOCITY

——— = THEORETICAL CURVE, (KIRKWOOD AND BRINKLEY, OSRD 5649)

– – – = $P = 2.25 \times 10^4 (W^{1/3}/R)^{1.13}$

FIG. 8
SIMILARITY CURVE
FOR
PEAK PRESSURE VS $W^{1/3}/R$ FOR PENTOLITE
UERL WOODS HOLE, MASS.

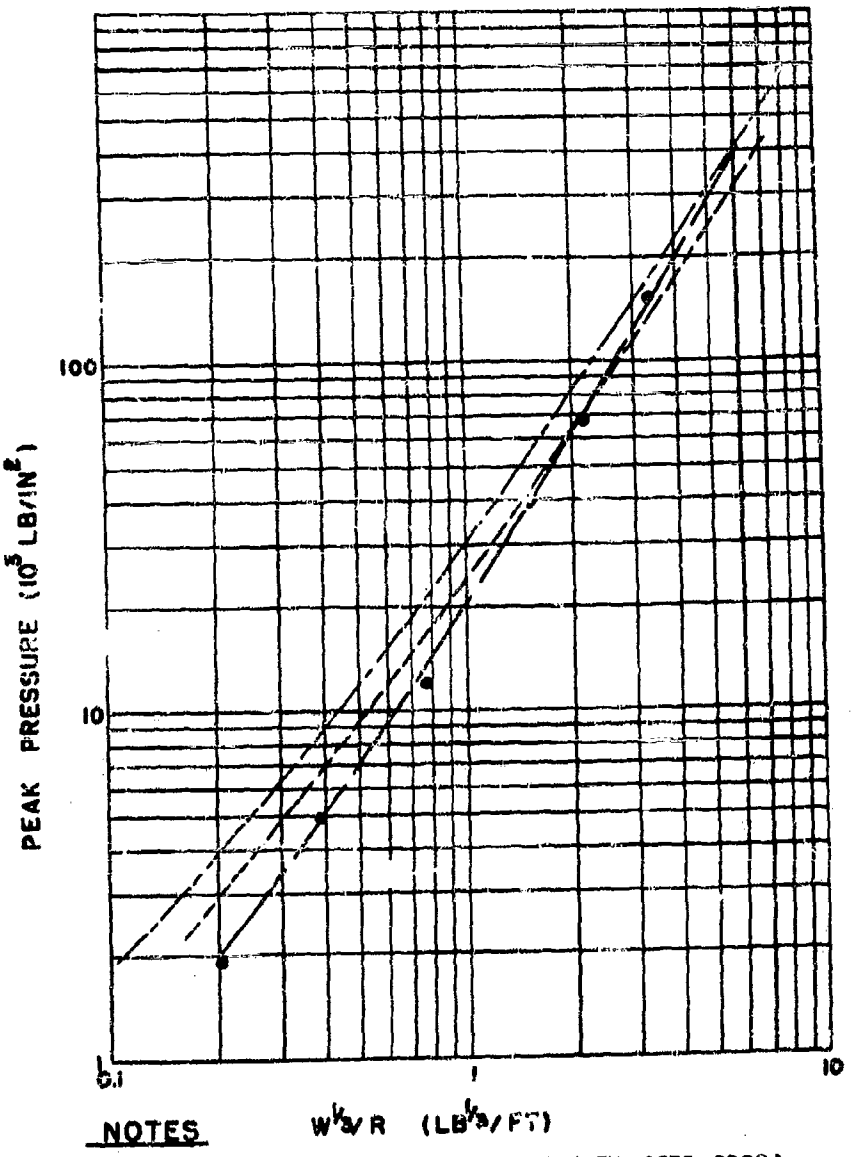

FIG. 9
SIMILARITY CURVE
FOR
PEAK PRESSURE vs $W^{1/3}/R$ FOR PRESSED TETRYL
UERL WOODS HOLE, MASS.

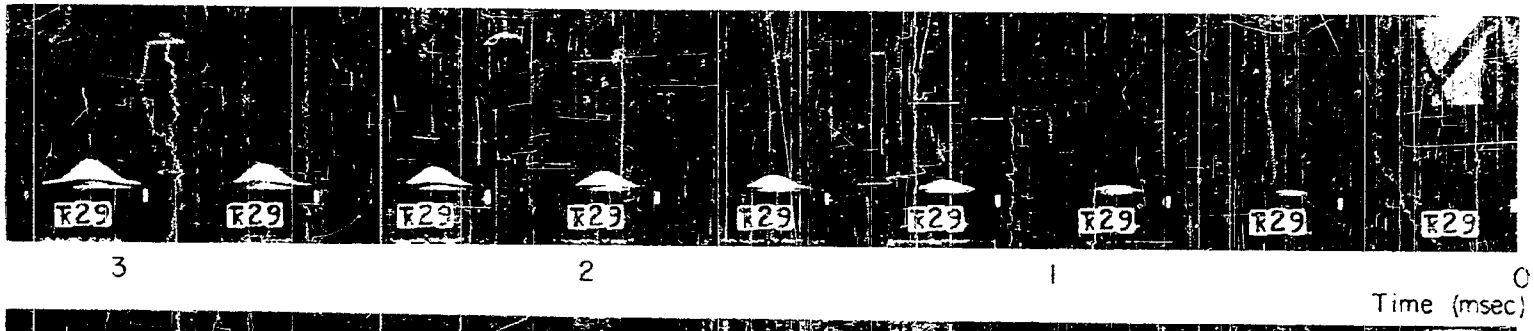

Fig. 10. Typical examples of high and low dome velocities.

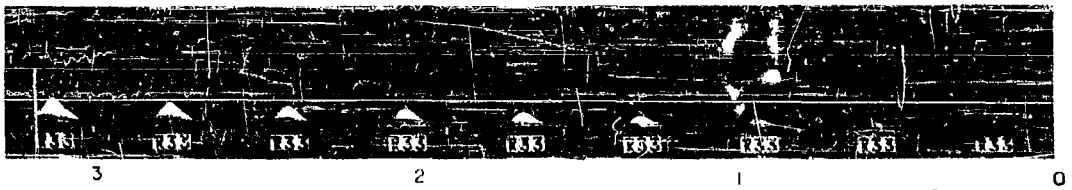

DETONATOR P_{in} = 5980 lb/in^2 $W^{1/3}/R$ = 0.417 lb$^{1/3}$/ft
NO SURFACE AGENT

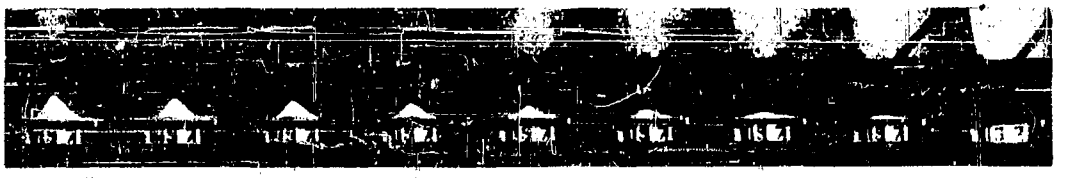

EASTMAN HIGH SPEED
DETONATOR P_m = 6520 lb/in^2 $W^{1/3}/R$ = 0.417 lb$^{1/3}$/ft
5 lb AEROSOL

Fig. 11. Effect of surface active agent on dome velocity

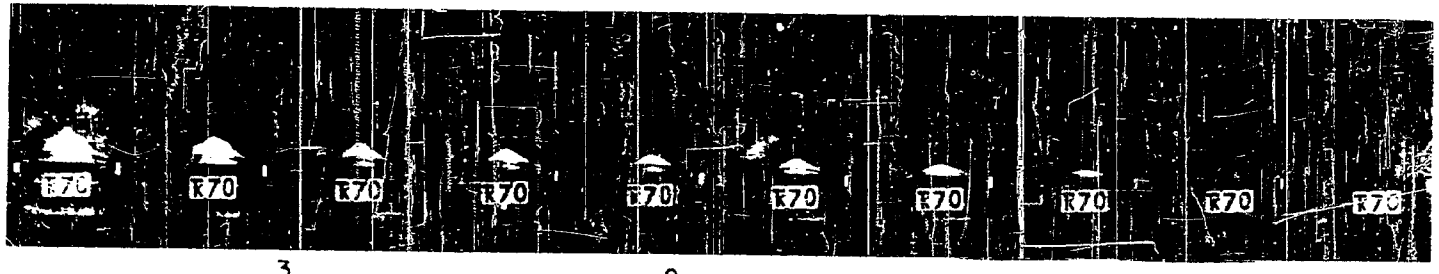

3 2 1 0

2 Detonators, orientation D/A P_m = 5,190 lb/in.^{2} $W^{1/3}/R$ = 0.418 $lb^{1/3}/ft$ Time (msec)

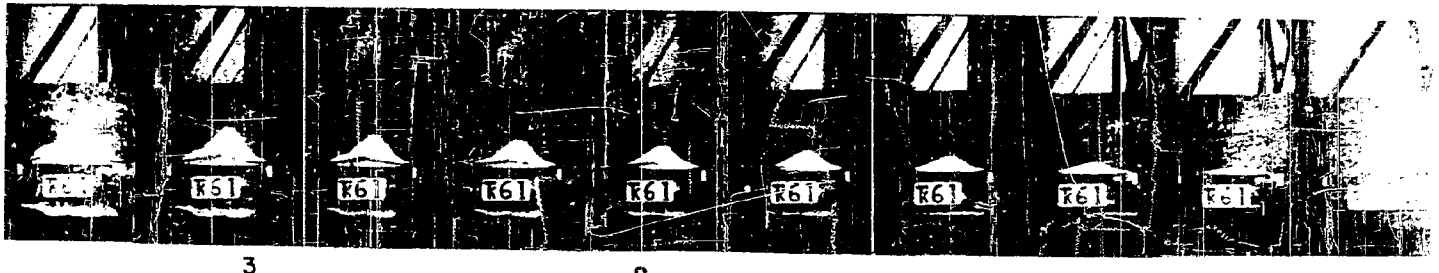

3 2 1

2 Detonators, orientation AD P = 7,050 lb/in.^{2} $W^{1/3}/R$ = 0.418 $lb^{1/3}/ft$ Time (msec)

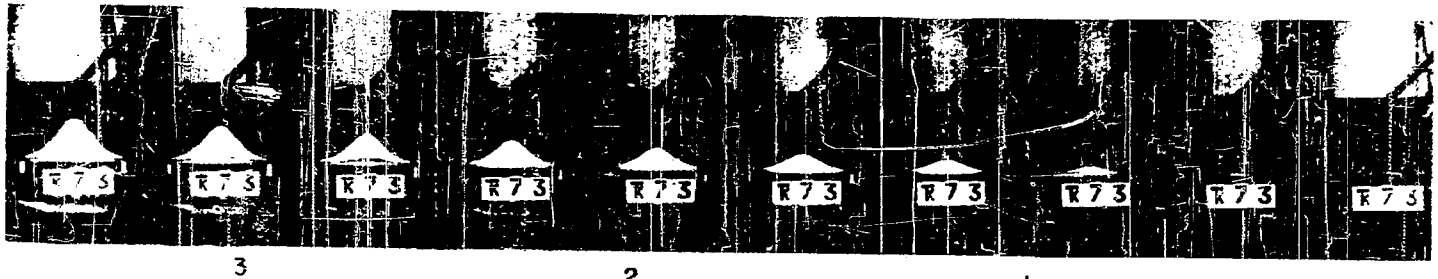

3 2 1 0

2 Detonators, orientation A/D P_m = 7,770 lb/in.^{2} $W^{1/3}/R$ = 0.418 $lb^{1/3}/ft$ Time (msec)

Fig. 12. Sympathetic detonation series.

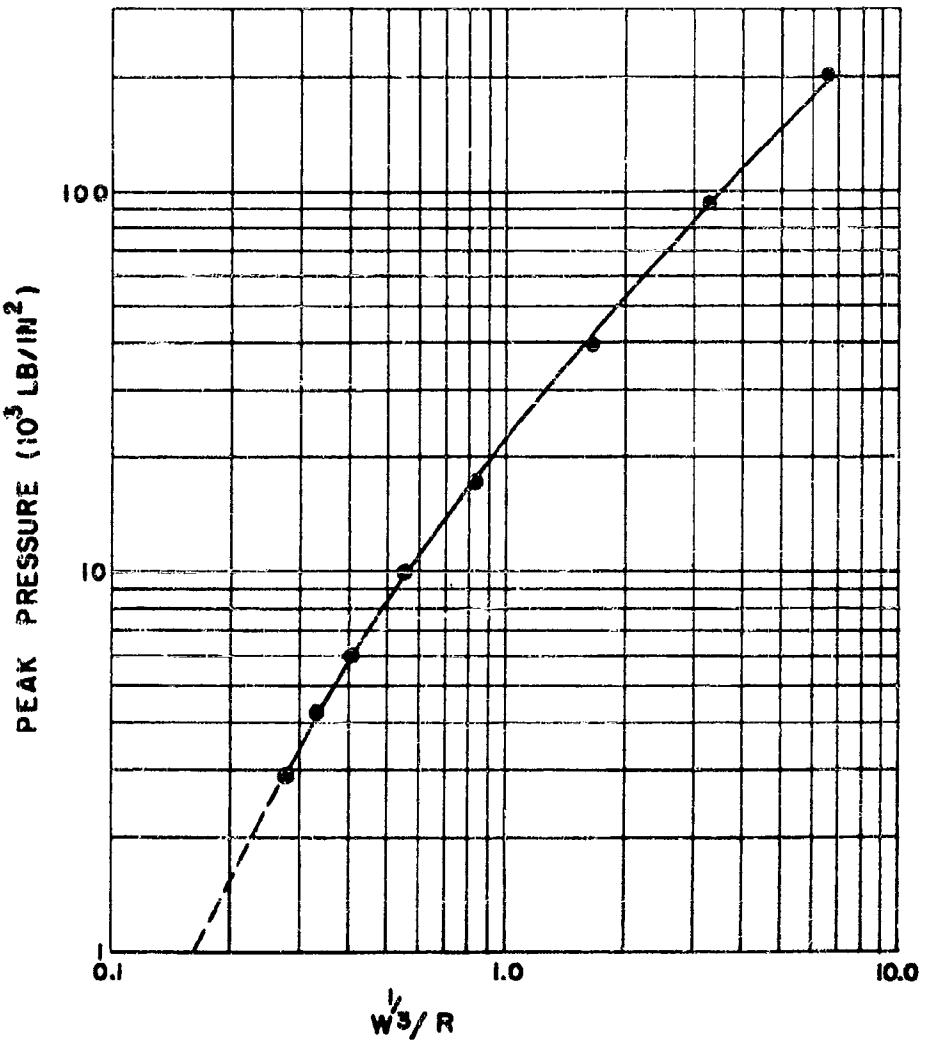

FIG 13
DOME VELOCITY SIMILARITY CURVE
FOR
PEAK PRESSURE vs $W^{1/3}/R$ FOR
ENGINEERS SPECIAL DETONATORS
UERL WOODS HOLE, MASS.

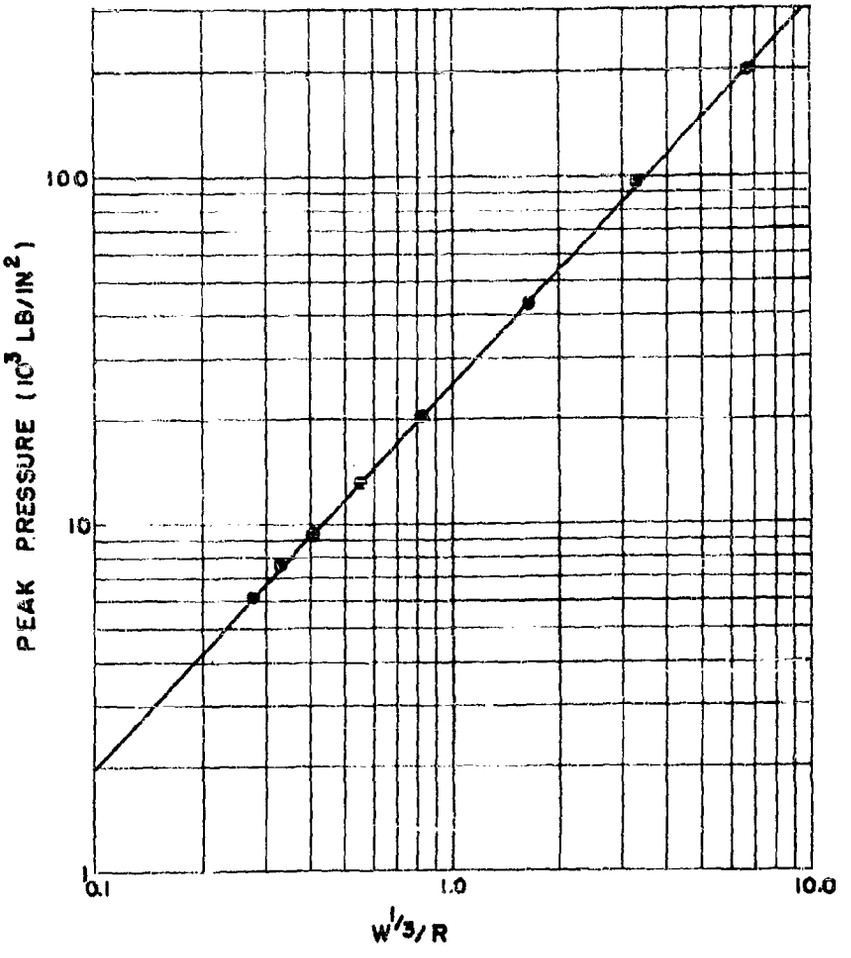

FIG. 13 C
CORRECTED PEAK PRESSURE VS $W^{1/3}/R$ FOR
ENGINEERS SPECIAL DETONATORS
UERL WOODS HOLE, MASS.

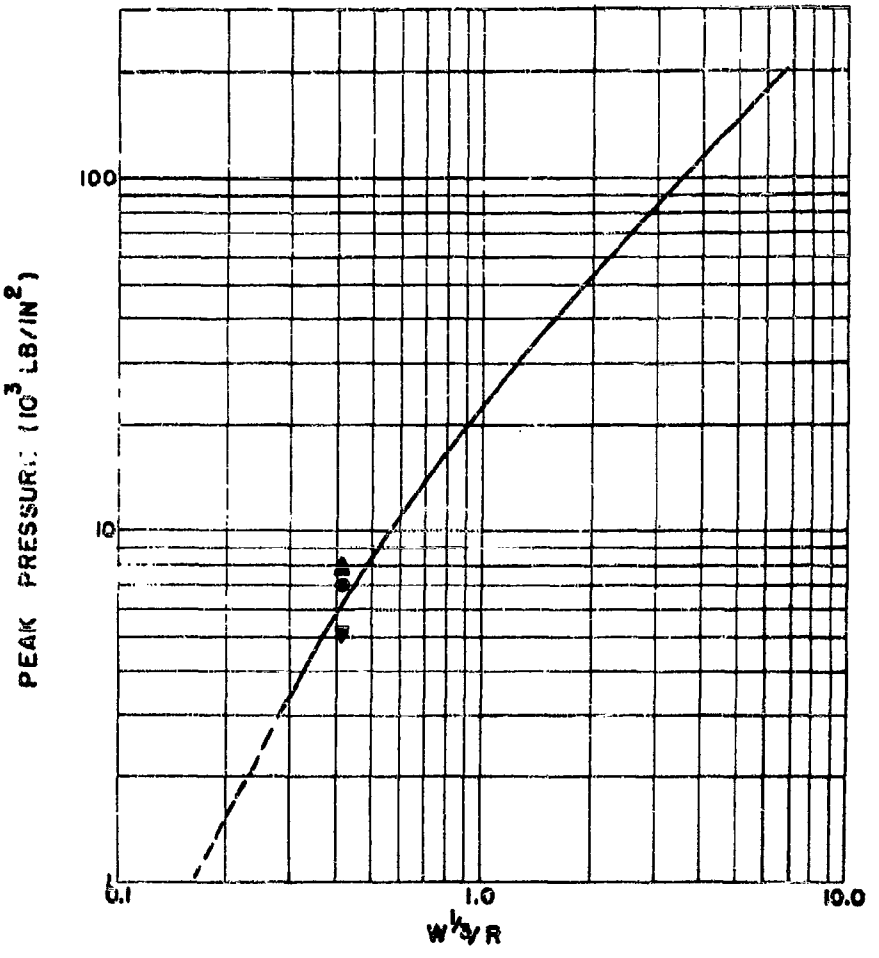

FIG 14

SYMPATHETIC DETONATION FROM DOME VELOCITY POINTS PLACED ON SIMILARITY CURVE FROM FIG. 13

UERL WOODS' HOLE, MASS.

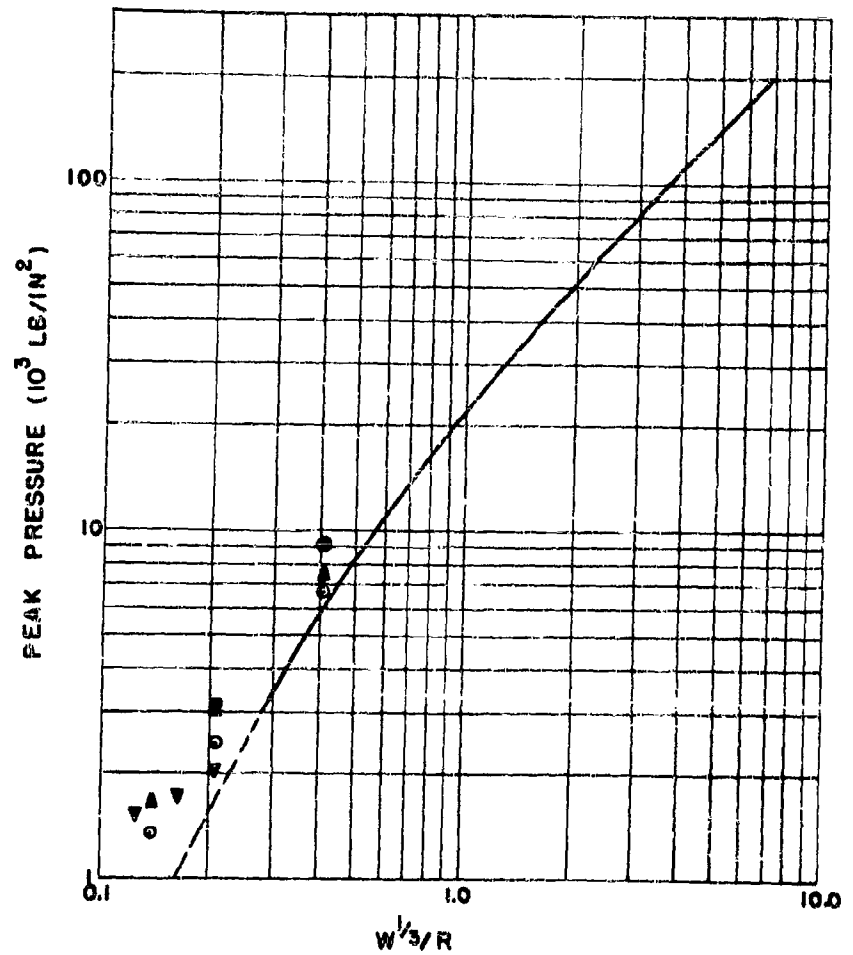

NOTES

- "SYNTHETIC SUDS"
- ⊙ "AEROSOL" 5LB IN TANK
- ▲ "AEROSOL" 10LB IN TANK
- ▼ OXIDIZED FUEL OIL ON SURFACE

FIG. 15

DOME VELOCITY RESULTS WITH LOWERED SURFACE TENSION
POINTS PLACED ON SIMILARITY CURVE FROM FIG. 13
UERL WOODS HOLE, MASS

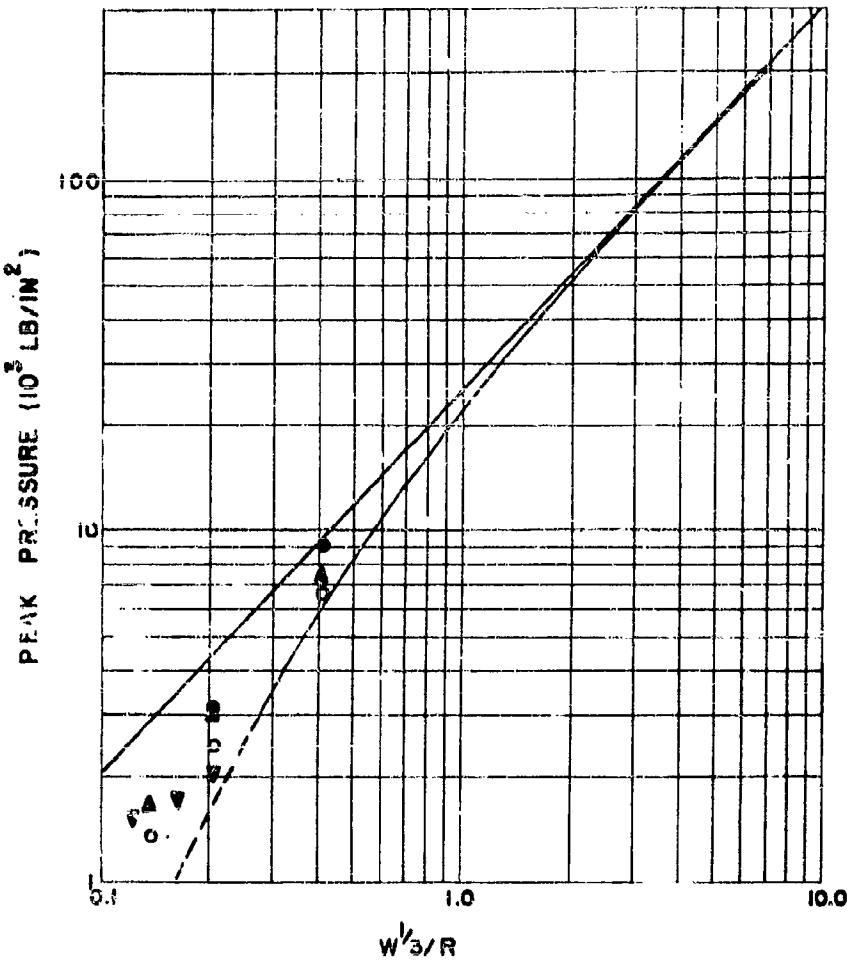

NOTES

- ● "SYNTHETIC SUDS"
- ○ "AEROSOL" 5 LB IN TANK
- ▲ AEROSOL 10 LB IN TANK
- ▼ OXIDIZED FUEL OIL ON SURFACE

FIG. 15 a

DOME VELOCITY RESULTS WITH LOWERED SURFACE TENSION
POINTS PLACED ON SIMILARITY CURVE FROM FIG. 13 AND FIG. 13a
UERL WOODS HOLE, MASS.

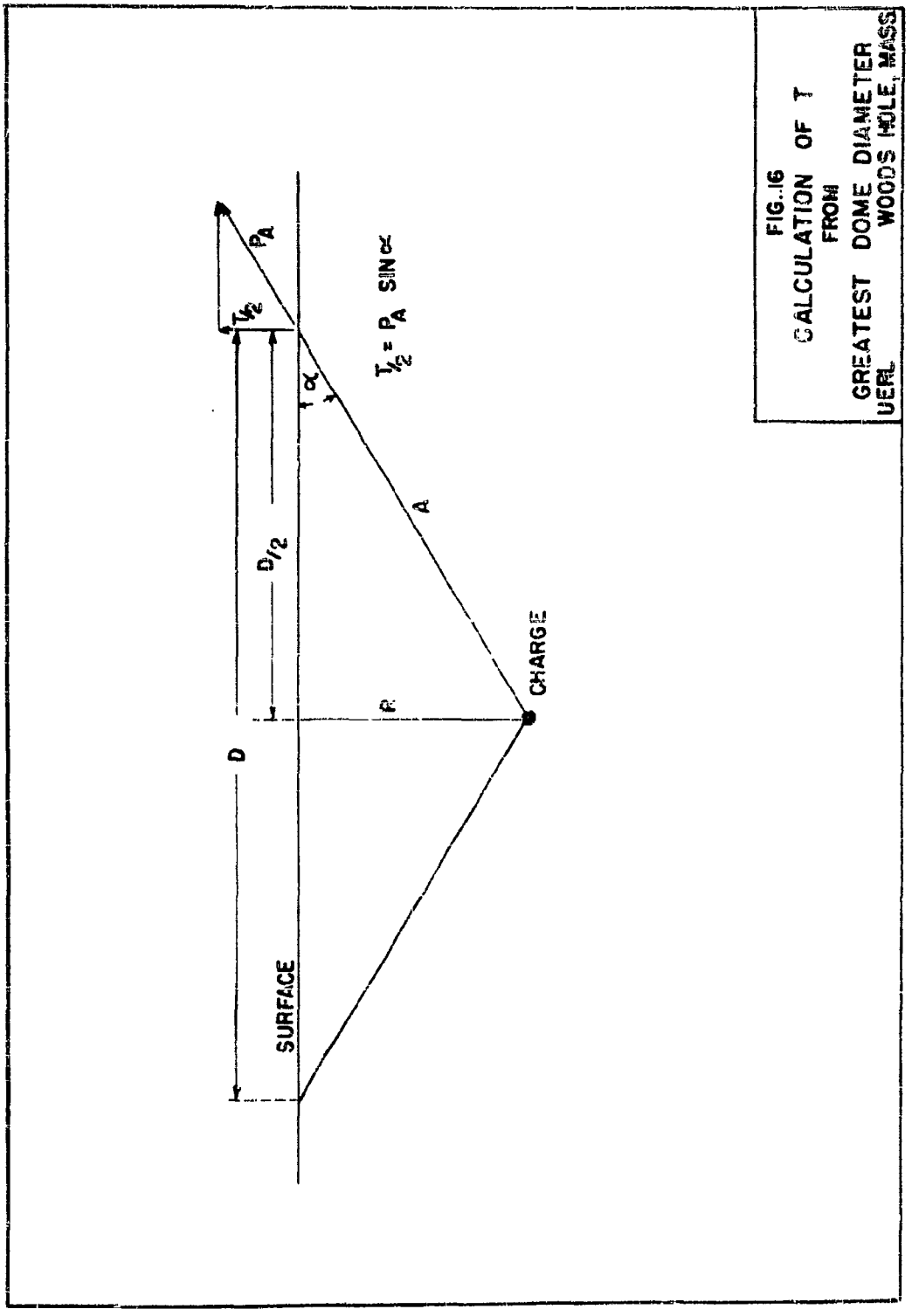

FIG. 16
CALCULATION OF T
FROM
GREATEST DOME DIAMETER
UERL WOODS HOLE, MASS

LIST OF REFERENCES

1. (a) Theory of Sound, Lord Rayleigh, 1st American Ed. Dover Publications, Vol. II, Section 252.

   (b) Hydrodynamics, H. Lamb, 6th Ed., Cambridge University Press, Section 284.

2. (a) A Method of Determining the Depth of Underwater Explosions, R. A. Shaw, Report No. H/Arm/Res. 1, December 10, 1941.

   (b) Measurement of Shock-Wave Peak Pressure by the Dome Velocity Method, Div. 2 Interim Report on Underwater Explosives and Explosions, UE Series Report No. 27, OSRD Report No. 4406, p. 19. October 15, 1944 to November 15, 1944.

3. Experiments on the Pressure Wave Thrown Out by Submarine Explosions, H. W. Hilliar, Dept. of Scientific Research and Experiment, R.E. 142/19, June 14, 1919.

4. Splashes from Underwater Explosions, Part I: Shallow Charges, H. Kolsky, M. T. Sampson, C. I. Snow, A. C. Shearman, Undex 118, Dec. 1. 1944.

5. An Investigation of the Behavior of Water Under Hydrostatic Tension, H. N. V. Temperley, Lt. C. Chambers, Undex 167, September 1945.

6. Photography of Underwater Explosions II: High Speed Photographs of Bubble Phenomena, E. Swift, Jr., P. M. Fye, J. C. Declus, R. S. Price, NavOrd Report 95-46, December 17, 1946.

7. The Mathematics of Physics and Chemistry, H. Margenau and G. M. Murphy, D. Van Nostrand Co., Inc., p. 13.36.

8. Hugoniot Calculations for Sea Water at the Shock Front and Experimental Confirmation of Theoretical Sound Velocities, Division 2 Interim Report on Underwater Explosives and Explosions, UE Series Report No. 27, OSRD Report No. 4406, p. 10, October 15, 1944 to November 15, 1944.

9. Tables of the Velocity of Sound in Pure Water and Sea Water for Use in Echo-Sounding and Sound Ranging, D. J. Matthews, Hydrographic Dept., Admiralty, H.D. 282, 1939.

10. Underwater Shock Wave Measurements of Pressure, Momentum, Energy, and Decay Constant from Spherical Pentolite (50/50) Charges, Division 2 Interim Report on Underwater Explosives and Explosions, UE Series Report No. 32, OSRD Report No. 4874, p. 16, March 15, 1945 to April 15, 1945.

11. (a) The Pressure Wave Produced by an Underwater Explosion, Part V, J. G. Kirkwood, S. R. Brinkley, Jr., and J. M. Richardson, OSRD Report No. 2022, November 13, 1943.

(b) Tables and Graphs of the Theoretical Peak Pressures, Energies, and Impulses of Shock Waves from Explosive Sources in Sea Water, S. R. Brinkley, Jr., and J. G. Kirkwood, OSRD Report No. 5649, NDRC No. A-342, October 1945.

12. Surface Phenomena Following Underwater Explosions, I: Some Preliminary Observations on High Speed Motion Pictures, Division 8 Interim Report on Underwater Explosives and Explosions, UE Series Report No. 20, p. 50, March 1944.

13. Splashes from Underwater Explosions, Part II: Domes from Deep Charges, H. Kolsky, J. P. Lewis, M. T. Sampson, C. I. Snow, Undex 163, October 17, 1945.

14. The Measurement of Small-Charge Shock-Wave Parameters with UERL Type B Underwater Gauges, A. B. Arons and P. F. Smith, NavOrd Report No. 104-46, December 24, 1946.

15. Reversible Adsorption in the Surfaces of Soap Solutions, J. W. McBain and D. A. Wilson, JACS 58, p. 379 (1936).

16. The Multiple Charge Effect, Part I, SS Informal Report No. 1294.
The Multiple Charge Effect, Part II, SS Informal Report No. 1300, Undex 96.
The Multiple Charge Effect, Part III, SS Informal Report No. 1338, Undex 147.

17. Determination of Depth of Explosion of Statically-Fired Depth Bombs from Photographs of the Dome of Spray, C. L. Pekeris, Office of Scientific Research and Development, NDRC Division 6, Section 6.1, June 29, 1944.

18. Photography of Underwater Explosions, I, J. E. Eldridge, P. M. Fye, R. W. Spitzer, OSRD Report No. 6246, NDRC Report No. A-368 (not yet published).

19. Electrical Instruments for Study of Underwater Explosions and Other Transient Phenomena, R. H. Cole, D. Stacey, and R. M. Brown, OSRD Report No. 6238, NDRC No. A-360, November 1945.

20. Depth of Explosion of Aerial Depth Bombs with Some Data on Bomb Trajectories, W. G. Schneider, R. R. Halverson, and P. C. Cross, OSRD Report No. 6258, NDRC No. A-380, March 1946.

GRAVITY WAVES PRODUCED BY SURFACE AND UNDERWATER EXPLOSIONS

W. G. Penney
Imperial College of Science and Technology, London

British Contribution

March 1945

GRAVITY WAVES PRODUCED BY SURFACE AND UNDERWATER EXPLOSIONS

W. G. Penney

March 1945

* * * * * * *

Summary.

The waves produced by explosions above, on or under the surface of the water are considered. General arguments are advanced to show that the greatest waves from an underwater explosion are obtained when the initial depth just equals the radius of the bubble produced. The waves at a distance less than 10–20 times this radius may be regarded as started by the initial inflow of water into a crater. Two thousand tons H.E. exploded at a depth 250–300 feet will give a series of waves at 2300 feet the largest of which is 18 feet high while the following trough is about equally deep. At 8600 feet, the greatest wave and the following trough are each about 6 feet. A similar charge on the surface produces much smaller waves. Using the experimental fact that the waves from a 1 oz. charge appear to be about the same whether the explosion is on the surface, or a foot or two below, it follows from the laws of scaling that the surface explosion of 2000 tons will produce waves about five times smaller than those from the explosion at 285 feet depth.

This report discusses the wave systems produced by explosions above, on or under the surface of water. A reasonably accurate solution is obtained for explosions above or on the surface, and an exact law of scaling is discovered for all depths of water. In the case of underwater explosions, the treatment is only approximate, because of the large number of conflicting factors such as pulsations of the bubble, cavitation near the free surface, instability of the surface leading to spray formation, etc. Laws of scaling are suggested in this case, and they are probably good enough to make fair predictions on a full scale explosion, using information obtained from model small scale charges.

The mechanism proposed for the formation of a wave system from a surface explosion is that at time $t = 0$ the free surface over a certain area receives a downward impulse. This impulse has radial symmetry, and is assumed to be a known function of radius $I(r)$. Unfortunately, no experimental measurements are available for constructing the function $I(r)$. All that is known is that a distances $r \geqslant 30$ charge radii, the positive and negative phases of the pressure pulse are of equal area, within the experimental error. At smaller values of r, of course, the positive phase must exceed the negative phase, and the difference in the two areas is the function $I(r)$. Two cases may be considered

$$I(r) = I_0 \quad \text{if } r \leqslant a, \quad I(r) = 0 \quad \text{if } r > a \qquad \text{(Equation 1a)}$$

$$I(r) = K_0 (1 - r^2/a^2) \quad \text{if } r \leqslant a, \quad I(r) = 0 \quad \text{if } r \geqslant a \qquad \text{(Equation 1b)}$$

The value assumed for a is the radius of the flame zone, say about 30 charge radii.

When an explosion occurs underwater, the gaseous bubble at first increases very rapidly in size. It continues to grow, but less and less quickly, until its radius is 10 – 30 times the initial radius, depending on the depth. During this expanding phase, the centre of the bubble probably rises, but not very much, the exact amount depending on how near the bubble is to the bottom and to the free surface. Provided the bubble reaches its maximum possible size before breaking through the free surface, we have, at the instant of maximum size, a free surface which is shaped in the conventional dome form, while below the dome is the gas bubble. The contracting phase now sets in and the gas bubble begins to rise more rapidly. If the initial depth was chosen correctly, the conditions are now critical, the water film at the top of the bubble breaks, and the free surface has the form of a volcano, the volume of the crater

being .....

being equal roughly to the volume of water above the initial free surface. If the initial depth were greater than this critical depth, then the bubble will break at less than the maximum radius, but the chances of the radius being appreciably different from the maximum are not large because the radial velocity of the bubble is small near the maximum, and very large near the minimum. On the other hand, the velocity of rise is much greater in the contracted phase, and this fact implies that there is not negligible chance that the bubble will break surface in a contracted condition. The occasional "spouts" observed by Hilliar and subsequent observers are interpreted as events of this type. Presumably explosions leading to "spouts" will be particularly ineffective in causing gravity waves, but the probability of obtaining them is small, and we neglect them.

If V is the maximum volume of the bubble, then the equation of the dome on the free surface, before it breaks, may be taken to be

$$\zeta_d (r) = \frac{VH}{(h^2 + r^2)^{3/2}} \qquad (2)$$

where h is the initial depth of the charge. The crater may be taken to be a cylinder, paraboloid or hemisphere. A convenient form, however, is one of the same class as (2) namely,

$$\zeta_c (r) = -3 Vh^3/(h^2 + r^2)^{5/2} \qquad (3)$$

The initial surface ζ_0 is the sum of ζ_d and ζ_c (as shown in figure 1). The volume V of the bubble and dome may be estimated in the following way. Imagine a spherical hole of radius h to be created in a sea of infinite extent, in such a way that the top of the sphere is just below the horizontal free surface. The work done in displacing the water against hydrostatic plus atmospheric pressure is $4\pi h^3 \rho g (h + Z)/3$, where Z is the head of water producing atmospheric pressure. Equate this work to 40% of the chemical energy of the explosion. Thus

$$4\pi h^3 \rho g (h + Z)/3 = 0.40 E \qquad (4)$$

The reason why 40% has been chosen is that the energy of an underwater explosion is known to be partitioned roughly as follows

(a) 30% wasted irreversibly in heating the water.
(b) 40% in the pulsating motion of the bubble.
(c) 30% radiated as a non-returning pressure pulse.

Thus (4) is equivalent to saying that the shock wave and consequent cavitation, disintegration and spray formation are all unimportant as far as the large scale coherent surface waves are concerned.

It will be noticed that the qualitative discussion given above leads to the conclusion that the greatest waves will be obtained from a given weight of charge when the critical depth is roughly equal to h. At greater depths, the bubble is likely to break surface with a volume less than the maximum volume, while at greater depths, the volume of the bubble may again be somewhat restored, it will never equal that given by (4) because the energy of the pulsating motion rapidly diminishes with the order of the pulsation. At very great depths, the bubble has disintegrated by the time it reaches the surface, and our theory does not apply to such cases. Experimental evidence in any case shows that little or no wavey system is started by such explosions.

If the energy released by the charge is 1000 cal/gm., the optimum wave system is obtained with the charge, of weight W lb. exploded at depths D feet shown in the table overleaf.

Table 1.....

TABLE 1.

W lb.	$\frac{1}{16}$	$\frac{1}{4}$	1.0	4	64	300	1000	4000	4×10^6
D feet	1.56	2.45	4.20	5.96	14.1	22.8	31.4	46.5	285

According to the ideas outlined above, the explosion of a charge W at less than the optimum depth D will produce a wave system exactly the same as does a charge of less weight for which the optimum depth is just D provided the charge was not so near to the surface that the explosive gases when they break surface do not deliver an appreciable impulse to the surface. For this to happen, the charge depth is only a few charge radii, and the explosion is then more like a surface explosion.

The Scaling Laws

Referring to Lamb's Hydrodynamics (Sixth Edition, page 430) the fundamental solution of the wave equation for cylindrically expanding infinitesimal gravity waves in water of uniform depth d is seen to be

$$\phi = g \frac{\sin \sigma t}{\sigma} \frac{\cosh k (z + d)}{\cosh kd} J_0 (kr) \tag{5}$$

$$\zeta = \cos \sigma t \quad J_0 (kr) \tag{6}$$

where ϕ is the velocity potential and ζ the surface elevation. The condition that the fluid velocity at the free surface equals the normal velocity of the free surface, leads, in the usual way, to

$$\sigma^2 = g k \tanh kd \tag{7}$$

Generalizing these results by the Fourier double integral theorem, we have that, corresponding with an initial surface elevation -

$$\zeta_0 = F(r) , \qquad \phi_0 = 0$$

$$\phi = g \int_0^\infty \frac{\sin \sigma t}{\sigma} \frac{\cosh k (z + d)}{\cosh kd} J_0 (kr)\, k\,dk \int_0^\infty F(\alpha)\, J_0 (k\alpha)\, \alpha\, d\alpha \tag{8}$$

$$\zeta = \int_0^\infty \cos \sigma t \quad J_0 (kr)\, k\,dk \int_0^\infty F(\alpha)\, J_0 (k\alpha)\, \alpha\, d\alpha \tag{9}$$

Similarly, corresponding with an initial surface impulse

$$\zeta_0 = 0 , \qquad \rho \phi_0 = F(r)$$

$$\phi = \frac{1}{\rho} \int_0^\infty \cos \sigma t \frac{\cosh k (z + d)}{\cosh kd} J_0 (kr)\, k\,dk \int_0^\infty F(\alpha)\, J_0 (k\alpha)\, \alpha\, d\alpha \tag{10}$$

$$\zeta = -\frac{1}{g\rho} \int_0^\infty \sigma \sin \sigma t \quad J_0 (kr)\, k\,dk \int_0^\infty F(\alpha) \quad J_0 (k\alpha)\, \alpha\, d\alpha \tag{11}$$

Case I. Initial Surface Impulse.

We consider the scaling laws in this case first because they are simplest. Imagine a comparison of the wave systems from two charge weights W_2 and W_1 detonated at heights t_2 and t_1 above the water. Write

$$n = (W_2/W_1)^{1/3} \tag{12}$$

The scaling laws are

$$t_2 = n t_1$$

$$a_2/a_1 = r_2/r_1 = d_2/d_1 = k_1/k_2 = \sigma_1^2/\sigma_2^2 = t_2^2/t_1^2 = n$$

$$F_2 (a_2)/F_2 (a_1) = n$$

$$\zeta_2 (nx, t\sqrt{n}) = \sqrt{n}\ \zeta_1 (x, t) \tag{13}$$

These .....

These laws can be verified by substitution in (5), (6), (7), (10) and (11). The velocity of the waves at corresponding points are in the ratio of n:1.

The fact that wave heights at corresponding distances are only in sixth root of the charge ratio implies that only relatively modest waves are to be expected from large surface explosions.

Case II. Initial Crater and Dome.

Writing as before

$$n = (W_2/W_1)^{1/3} \tag{14}$$

we must first solve the equation

$$\frac{h_2^3 (h_2 + Z)}{h_1^3 (h_1 + Z)} = n^3 \tag{15}$$

for the ratio h_2/h_1. Suppose that the solution is

$$h_2/h_1 = m \tag{16}$$

Then the scaling laws are

$$\alpha_2/\alpha_1 = d_2/d_1 = h_1/h_2 = r_2/r_1 = \sigma_1^2/\sigma_2^2 = t_2^2/t_1^2 = m$$

$$f_2(\alpha_2)\ f_2(r_1) = m \tag{17}$$

$$\zeta_2 (m x, \sqrt{m}\, t) = m\ \zeta_1 (x,t)$$

The velocities of the waves at corresponding points are in the ratio $\sqrt{m}$.1.

If a small model experiment is compared with a very large full scale trial we may assume that h_1 is negligible compared with Z and that Z is negligible compared with h_2. Then

$$m = n^{3/4} (Z/h_1)^{1/4}$$

The results to be expected from large explosions therefore scale up with those from those of a given small explosion in the ratio of the fourth root of the charge ratio, the corresponding distances and depths being in the same ratio.

The results to be expected from two small scale experiments may be approximated by assuming that h_1 and h_2 are both negligible compared with Z. Then

$$m = n$$

and the wave heights, distances and depths scale according to the linear dimensions of the charges.

Wave System from a Surface Explosion over Deep Water.

According to the Cauchy–Poisson theory of gravity surface waves (Lamb's Hydrodynamics Sixth Edition page 432), the surface elevation of radius ω and time t caused by the application of unit impulse downward at the origin at time t = 0 is given by

$$\zeta = \frac{t}{2\pi\rho\omega^3}\ G(gt^2/\omega) \tag{18}$$

where

$$G(\theta) = -1 + \frac{1^2\ 3^2}{5!}\theta^2 - \frac{1^2\ 3^2\ 5^2}{9!}\theta^4 + \ldots\ldots \tag{19}$$

if .....

If θ is large, asymptotic formulae for G and ζ are

$$G_A(\theta) = (\theta/4\sqrt{2}) \sin (\theta/4)$$

$$\zeta_A = \frac{gt^3}{2^{1/2}\pi\rho\omega^4} \sin \frac{gt^2}{4\omega} \qquad (20)$$

It is not obvious how good an approximation the asymptotic formula is, and in fact one would not expect even reasonable agreement for the values of θ which are needed to sketch the first two or three waves. Therefore, the function $G(\theta)$ has been computed, and the values compared with $G_A(\theta)$. The values of $G(\theta)$ are given in the table below, where the accuracy is to the last figure given, and a comparison of G with G_A is shown in Figure 2. It appears that the asymptotic formula gives a surprisingly good representation of the function over the whole range, except for values of θ less than about 4. Hence the asymptotic formulas can be used with accuracy at least 10^{-3} over the whole range of θ, except for $\theta \leq 4$, which represents the leading parts of the disturbance, a trough extending to infinity.

TABLE 2.

The Functions $G(\theta)$ and $H(\theta)$.

θ^2	$G(\theta)$	$H(\theta)$	θ^2	$G(\theta)$	$H(\theta)$
1100	5.7175	4.4741	200	-0.0476	4.7580
1050	5.7868	2.2841	150	1.1515	4.2122
1000	5.6274	0.0380	100	1.8385	2.4339
950	5.2398	-2.1515	80	1.8420	1.4625
900	4.6320	-4.1800	60	1.6193	0.4056
850	3.8264	-6.0052	40	1.1150	-0.5784
800	2.8545	-7.4912	20	0.2658	-1.2245
700	0.6001	-9.0155	15	-0.00865	-1.2240
600	-1.6448	-8.4661	10	-0.31026	-1.2051
500	-3.2661	-5.7491	8	-0.43879	-1.1142
400	-3.6533	-1.5151	6	-0.57194	-1.0464
300	-2.4621	2.7371	4	-0.70981	-0.90197

Main Properties of the Wave System.

It appears from (18) that it is not an allowable approximation to assume that the impulse from the surface explosion is concentrated at a point. If this were so, the wave amplitude at any point would increase indefinitely with time.

The wave height at R, t is given by

$$\zeta(R, t) = \int I(r) \zeta(\omega) \, dS, \qquad (21)$$

where ζ is given by (18) or (19) as the case may be, the integration is over the circle of radius a over which the impulse is delivered, and ω is the distance of the surface element dS to the point R.

The First Wave.

From Figure 2, it is seen that the first wave corresponds with a point $\theta \sim 10$. Provided the maximum and minimum distances of the point R to the circle correspond at time t with $4 < \theta < 14$, the surface elevation will be positive, and if the distance to the centre of the circle corresponds with $\theta = 10$, then the surface elevation will be at its greatest value in the first wave. Hence for a fixed value of R such that $R > 3a$, the position of the first crest is given by the first maximum of $\sqrt{\theta}\, G(\theta)$ namely -

gt^2.....

$$gt^2/R = 10$$

or

$$R = 3.2t^2 \qquad (22)$$

$$R = 6.4t = 3.58R^{1/2}$$

It is perhaps worth pointing out that the three equations just given were obtained on the assumption that the waves are infinitesimal. The first wave for $R \leq 3$, will certainly be very large in practice, and may in fact break in this region. Consequently R will be greater than $3.2t^2$.

At $R > 3a$, the amplitude of the first wave decreases steadily like $R^{-5/2}$ and at lesser values of R, the amplitude should be a more slowly varying function of R. Equations (22) should become more and more nearly independent of the finite and even breaking character of the early stages of the wave as time increases and the wave expands.

The Second and Higher Waves.

For simplicity, let us consider the case where the formula (19) applies, and R is much greater than a. Take co-ordinates (x y) with the x axis joining the origin to the point R. Then in the integration in (1a) the dependence of ω on y may be neglected. Hence

$$\zeta\,(R,t) = -\frac{gt^3}{2^{7/2}\,\pi\,\rho\,R^4} \int_{-a}^{a} I(x)\,\left(1 - \frac{4x}{R}\right)\,\sin\,\frac{gt^2}{4R}\,\left(1 - \frac{x}{R}\right)\,dx.$$

where

$$I(x) = 2 \int_{0}^{\sqrt{(a^2 - x^2)}} I(r)\,dy \qquad (23)$$

We have assumed $gt^2/4R$ is large compared with unity, and that a/R is small. Clearly, if the product of these two quantities is also large, there will be much cancelling of positive and negative regions in the integration and the value of the integral will be small. Hence, as R decreases, the value of the integral decreases, but the factor R^{-4} increases. The largest value of ζ will occur at the smallest value of R consistent with a minimum of cancelling in the integral. Neglecting the variation with x of all the slowly varying factors, and thus retaining only the sine term, we see that the maximum values of $\zeta\,(R,t)$ occurs when

$$\frac{gt^2}{4R} = (4n - 3)\,\frac{\pi}{2}, \qquad n > 1 \qquad (24)$$

Hence the velocity of the nth crest at any instant is

$$v_n = gt/n\,(4n - 3) \qquad (25)$$

The nth crest is the greatest crest of all when in addition to (22), the following condition also holds

$$\frac{gt^2}{4R}\,\frac{a}{R} = \frac{\pi}{2} \qquad (26)$$

Thus, counting wave crests from the outside inwards, the nth crest is at position

$$R = gt^2/2\,(4n - 3), \qquad n > 1 \qquad (27)$$

While the nth will be the greatest of all crests when it is at

$$\left.\begin{aligned} R &= (4n - 3)\,a \\ t &= (4n - 3)\,\sqrt{(2\pi\,a/g)} \end{aligned}\right\} \qquad (28)$$

This demonstration is not completely satisfactory because it has yet to be shown that for a given value of time, say t_1, the factor R^{-4} in (23) does not increase as R gets smaller, more rapidly than the integral decreases. Writing the coefficient of the sine term in the integral as P (x) and transforming successively by parts, we have for example after two reductions

ζ .....

$$\zeta\,(R,\,t_1) \;=\; -\frac{gt_1^3}{2^{7/2}\,\pi\,\rho\,R^4}\left\{\frac{4R^2}{gt_1^2}\left[-P(x)\cos\frac{gt_1^2}{4R}\left(1-\frac{x}{R}\right)\right]_{-a}^{a}\right.$$

$$+\frac{16R^4}{g^2t_1^4}\left[P'(x)\sin\frac{gt_1^2}{4R}\left(1-\frac{x}{R}\right)\right]_{-a}^{a}$$

$$\left.-\frac{16R^4}{g^2t_1^4}\int_{-a}^{a}P'(x)\sin\frac{gt_1^2}{4R}\left(1-\frac{x}{R}\right)\,dx\right\}$$

The residue of the first square bracket after the limits have been inserted is zero, because P vanishes at the limits. The residue of the next square bracket is also seen to be zero by using the fact that the crests occur at values of $gt_1^2/4R$ given by equation (22) and also that the coefficient of the "even" terms in P' (x) is zero, and the "odd" terms vanish by symmetry when the limits are inserted. Hence only the integral remains; apart from high order effects, by which are meant residues in the first two square brackets when higher order terms are retained, the surface elevation at time t_1 varies like

$$\zeta \sim R^k, \qquad k > 0$$

the most prominent value of k near the greatest wave being 2.

The velocity of the nth wave, at the epoch when it is the greatest wave is

$$v = \sqrt{(2\,ga/\pi)} \tag{29}$$

a result which is independent of n, R and t. Thus the velocity of the nth wave increases steadily with time, according to (25) and during the period when it is the greatest wave, its velocity is given by (29).

The ratio of the wave height of the mth wave during the period when it is the greatest wave, to the wave height of the nth wave during the period when it is the greatest wave is

$$H_m/H_n = (4n-3)/(4m-3) \qquad m > n > 1 \tag{30}$$

The velocity of the point of greatest wave height, i.e., the group velocity, is one half of v given by (29) i.e.

$$V = \sqrt{(ga/2\pi)} \tag{31}$$

The above argument is easily modified to the discussion of troughs. Thus the pth trough is at its greatest, and is greater at this instant than any other crest or trough, when

$$R = (4p-1)\,a$$

$$t = (4p-1)\,\sqrt{(2\pi\,a/g)}$$

The pth trough is defined as the trough following the pth crest, i.e., the leading edge of the disturbance, an extremely shallow trough extending to infinity, is neglected in counting the number of the trough.

Numerical Examples.

Consider the explosion of a 1 oz. charge on the surface. Then a is about 2 feet. Over the range $0 < R < 6$ feet the first wave is the greatest. At R = 6 feet the magnitudes of the first and second waves as they pass are about equal. The time for the first wave to reach 6 feet is 1.36 seconds. (This may well be an estimate on the high side because the first wave, because of its great height, will travel faster than indicated by equation (2), and may in fact be a broken wave). The second wave is the greatest at R = 10 feet, its velocity is then 6.4 feet/second and the time is 3.14 seconds. The first wave is then at 32 feet. The third wave is the greatest at R = 18 feet, and its height is 5/9 of the height of the second wave at its greatest; its velocity is then 6.4 feet/second, the time is 5.65 seconds, the first crest is at 102 feet, and the second crest is at 32.5 feet. The second crest is 0.095 of the height of the third crest, and the first crest is indetectable.

Consider .....

Consider the explosion of 2000 tons of H.E. on the surface (such as, for example, the explosion of a ship loaded with bombs). The above results on the 1 oz. charge now apply provided the distances are multiplied by 815 times and wave heights by 20.4.

Other examples may be easily constructed from the scaling laws and the figures just given for the 1 oz. charge.

The Wave Heights and Total Impulse:

It will be noticed that the above numerical estimates are only concerned with wave velocities, and with interference phenomena such as the position at which a certain wave is the greatest. To calculate the wave heights requires a knowledge of the total positive impulse delivered to the surface. If I_p is this impulse, then, for example, the height in inches of the second crest at 10 feet from a 1 oz. charge exploded on the surface is approximately

$$H = 11 \times 10^{-3} \; I_p$$

where I_p is in pounds/weight/seconds.

An approximate value of I_p may be obtained from the knowledge that the explosion of a charge in free air may be regarded as the release at the origin of a volume of gas at atmospheric pressure 20,000 times the charge volume. (This factor is made up of 1000 for the gas products and 19,000 for the shock wave heating of the air near the charge). Hence, the pressure wave from a 1 oz. charge on the surface may be very roughly computed by the theory of the sound waves caused by the release at the origin of 25 cubic feet of gas at atmospheric pressure. Then from the theory of sound, the impulse over the water surface should be

$$I_p = Vyp_0/2c = 32 \text{ lb./weight/seconds.}$$

where V is volume of gas (25 feet^3) γ is ratio of specific heat of air (1.4) p_0 is atmospheric pressure (2100 lb./feet^2) and c is the velocity of sound (1180 feet/second). Hence the height of the second wave at 10 feet is one third of an inch. This estimate is almost certainly too low by a factor at least two, but better agreement is hardly to be expected from the theory of sound.

Underwater Explosions.

The wave system from an initial dome and crater of the form shown in Figure 1 is required. However, before evaluating this, it is instructive to repeat the discussion given for the surface impulse to the present case. As before, the group velocity and wave velocities, position of the greatest crest at any time tc., follow simply from the area of the disturbance, and not from the details.

According to the Cauchy-Poisson theory (see Lamb page 430) the wave height at ω, t due to unit volume placed on the surface at 0,0 is

$$\zeta\,(\omega,t) = -\frac{1}{2\pi\omega^2} \; H\,(gt^2/\omega)$$

$$H\,(\theta) = -\frac{1^2}{2!}\theta + \frac{1^2 \cdot 3^2}{6!}\theta^3 - \frac{1^2 \cdot 3^2 \cdot 5^2}{10!}\theta^5 + \ldots\ldots \qquad (32)$$

with the asymptotic formula when gt^2/R is large

$$H_a\,(\theta) = -\frac{\theta}{2^{3/2}} \cos\,(\theta/4)$$

$$\zeta_a = \frac{gt^2}{2^{5/2}\pi\omega^3} \cos\,(gt^2/4\omega) \qquad (33)$$

Numerical values of the function $H\,(\theta)$ are given in Table 2 while a comparison of $H\,(\theta)$ and the asymptotic expression $H_a\,(\theta)$ is shown in Figure 3. It is seen that the asymptotic expression gives numerical values within 10-15% for all $\theta > 8$.

Assuming .....

Assuming that the dimensions of the initial disturbance are h, then the surface elevation at any point R from the centre at time t is

$$\zeta (R,t) = \int f(r)\ \zeta (\omega,t)\ dS \qquad (34)$$

the integration being over the circle of radius r = h, while the initial elevation at radius r is f (r). The convention of sign chosen implies that f (r) is negative near the origin; ω is the distance from the point R to the element dS of the circle of radius h_0 defining an initial crater.

The expanding wave system from the crater is led by a trough, the bottom of which moves according to

$$gt^2/R = 5 \quad \text{or} \quad R = 6.4\ t^2 \qquad (35)$$

The nth crest moves according to

$$R = gt^2/4\ (2n - 1) \qquad (36)$$

so that the velocity of the nth crest is

$$\begin{aligned} R &= gt/2\ (2n - 1) \\ &= \sqrt{\{g\ R/\pi\ (2n - 1)\}} \end{aligned} \qquad (37)$$

Hence the velocity of any crest or trough increases indefinitely with time.

The nth crest is the greatest of all crests or troughs, and is at its greatest size when

$$R = 2\ (2n - 1)\ h \qquad (38)$$

The velocity of the crest at this instant is

$$v = \sqrt{(2\ gh/\pi)} \qquad (39)$$

The group velocity, i.e., the velocity of the region in which the waves are greatest is just half this quantity, namely --

$$v = \sqrt{(gh/2\ \pi)} \qquad (40)$$

The ratio of the greatest height of the mth crest to the greatest height of the nth crest is

$$H_m/H_n = (2n - 1)/(2m - 1) \qquad n > m > 1 \qquad (41)$$

The motion of the pth trough is given by

$$R = gt/8\ \pi\ p \qquad (42)$$

and the trough is at its greatest size when it is at

$$R = 4\ p.h. \qquad (43)$$

Since the length h defining the crater dimensions from a charge W is practically equal to the distance "a" over which the impulse from a surface explosion of W extends, there will be a strong resemblance between the wave systems in the two cases. The main point of difference will be in the wave heights.

Calculation of Wave Heights from an Underwater Explosion.

The wave system caused by an underwater explosion is to be regarded as the interference pattern of the waves produced by a dome and those produced by a hollow or bubble. In view of the difficulties of scaling accurately from very small charges to those of two thousand tons, we have made a direct attempt to estimate the waves from a large explosion. In this case, the time scale of the waves is great enough

to permit .....

to permit the neglect of spray, broken water etc. We assume, as has already been described, that the water system is released from rest at time zero from a configuration,

$$f(r) = \frac{2h^4}{3}\left[\frac{1}{(h^2+r^2)^{3/2}} - \frac{3h^2}{(h^2+r^2)^{5/2}}\right] \qquad (44)$$

Figure 1 shows the shape of such a configuration. An exact solution of this problem can be obtained by the partial differentiation with respect to h, and subsequent simplification, of some formulae given by Terazawa (Proc. Roy. Soc. A42, 57, 1922). The result is -

$$\zeta(r,t) = \frac{2h^4}{3S^2}\sum_1^\infty (-1)^{n-1}\frac{n!}{(2n-2)!}\left(\frac{gt^2}{S}\right)^{n-1}\left[nP_{n-1}(\gamma) - (2n+1)\gamma P_n(\gamma)\right]$$

where

$$S^2 = h^2 + r^2 \quad , \quad \gamma = h/S \qquad (45)$$

There would be no difficulty in computing the first two waves at the interesting times, by using (45) and seven figure tables of Legendre polynomials. Unfortunately no such tables are available to the writer, but some rough calculations have been made with the aid of the four figure tables in Jahnke-Emde. The leading part of the wave system is a trough, and when it is at about 1000 feet, is roughly 30 feet deep. The analysis given earlier, however, enables one to predict the wave heights within 20 or 30% and this is perhaps sufficiently accurate for present purposes. By studying Figure 1 it becomes clear that the waves at 1000-3000 feet are caused mainly by the crater at the centre. Only at very large distances, and possibly at the origin, does the surface elevation outside the crater have much effect compared with the waves from the crater. The volume of the crater may be taken as

$$V_c = \int_0^{h\sqrt{2}} 2\pi r f(r)\, dr = 0.385\, V \qquad (46)$$

At this point, an encouraging conclusion may be reached. Up till now, it has not been clear that the scaling laws proposed for an underwater explosion would be applicable to small charges, because the disintegrated water flung into the air does not fall back again for several seconds, and by this time the waves from the hole are well away from the centre. With a very large explosion, the height reached by the water is only about equal to that reached by a small explosion, and most of the water has returned to the surface before the wave system has had a chance to develop. However, even in the case of a large explosion the big waves near the explosion are due almost entirely to the flow into the crater, which may, as above, be regarded as the difference of the bubble volume and the volume of the dome to radius h. Since the volume of the crater is about 0.4 times the volume of the bubble, we may roughly describe our conclusions by stating that in the case of a small explosion, the big waves are caused entirely by the bubble cavity and that in the case of a large explosion the big waves are caused by a cavity roughly equal to one half of the bubble. Hence we expect that the scaling laws will apply over a wide range ($10^7 : 1$) within a factor of about 50%.

Returning now to the details of the large explosion, we see from (41) and (42) that the pth crest is the largest crest when it is at

$$R = gt^2/6\pi p = 4.p.h. \qquad (47)$$

(Notice that "troughs" and "crests" have been interchanged, since (41) and (42) refer to the troughs from an initial elevation).

Performing the integration (34) with about 10% accuracy, we find that the maximum wave at time t is the pth wave, which is at R, where P, t and p are related by (47) and that the height of the wave is approximately

$$H_p = h/8p \qquad (48)$$

The height of the qth trough is approximately

$$H_q = h/4(2q-1) \qquad (49)$$

when .....

when the qth trough is greatest, namely when

$$R = 2\,(2q-1)\,h$$

$$t = 2\,(2q-1)\sqrt{(2\pi h/g)} \qquad (50)$$

Thus from a 2000 ton explosion at depth 285 feet we have that h = 285 feet (See Table 1). The first wave is greatest at r = 1140 feet, t = 30 seconds, and the height of the wave is 36 feet. The first trough (not counting the one which leads the distance) is greatest at R = 1710 feet, its depth is 24 feet, and t = 45 seconds. At this instant, the first wave has reached 2750 feet and its height is 8 feet. Further details are easily calculated from (47), (48) and (49).

For a 1 oz. charge at 1.56 feet depth the first wave is greatest at t = 1.7 seconds, R = 6.2 feet and the height is 48 inches (probably the wave is broken). The following trough is greatest at 2.6 seconds, R = 9.3 feet and the depth is 3 inches. At this time, the first crest is at 14 feet, and its height is 1 inch.

Motion of the Central Point.

One interesting feature of the motion is that at the centre, and this can be obtained without difficulty from the results of Terazawa (l.c). According to him, if the initial surface elevation at time t = 0 is

$$K(x) = A/\sqrt{(h^2 + r^2)} \qquad (51)$$

the motion of the centre is given by

$$\zeta_0(t) = A\eta/h$$

where

$$\eta = 1 - 2\tau e^{-2\tau^2} \int_0^{\tau} e^{\tau^2}\, d\tau \qquad (52)$$

$$\tau^2 = gt^2/4h$$

Since the initial surface elevation adopted by us, namely that given by equation (44) is related to that of Terazawa by

$$f(r) = \frac{\partial^2 K(r)}{\partial h^2}, \qquad A = 2h^4/3 \qquad (53)$$

the motion of the central point in our case is given by

$$\zeta_0(t) = \frac{\partial^2 \zeta_0}{\partial h^2} \qquad (54)$$

Hence

$$\zeta_0(t) = -\frac{2h}{3}\, L(\tau)$$

where

$$L(\tau) = (2 - \tfrac{3}{2}\tau^2 + \tau^4) - \tau\,(\tfrac{15}{2} - 10\tau^2 + 2\tau^4) e^{-\tau^2} \int_0^{\tau} e^{\tau^2}\, d\tau$$

Figure 4 shows the motion of the centre with a 2000 ton charge of H.E. exploded at depth 285 feet in deep water. Of course, no comparison of Figure 4 with direct measurements would be possible, at least for t < 5 seconds, because what is seen is spray, and this may extend two or three hundred feet above the water surface. In any case, several seconds are required for the surface to become reconstituted.

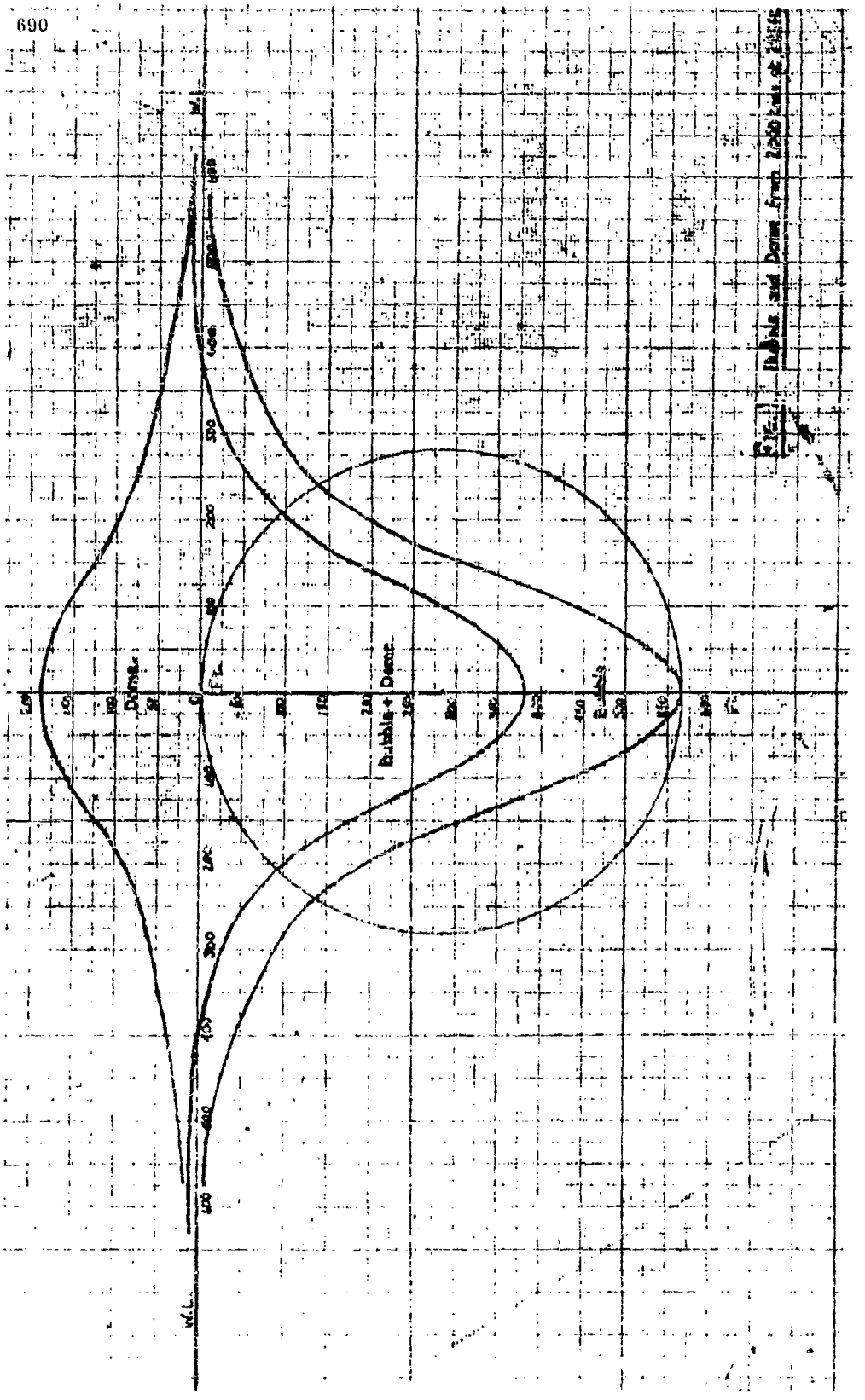
W.L.
Dome
Bubble + Dome
Bubble
W.L.

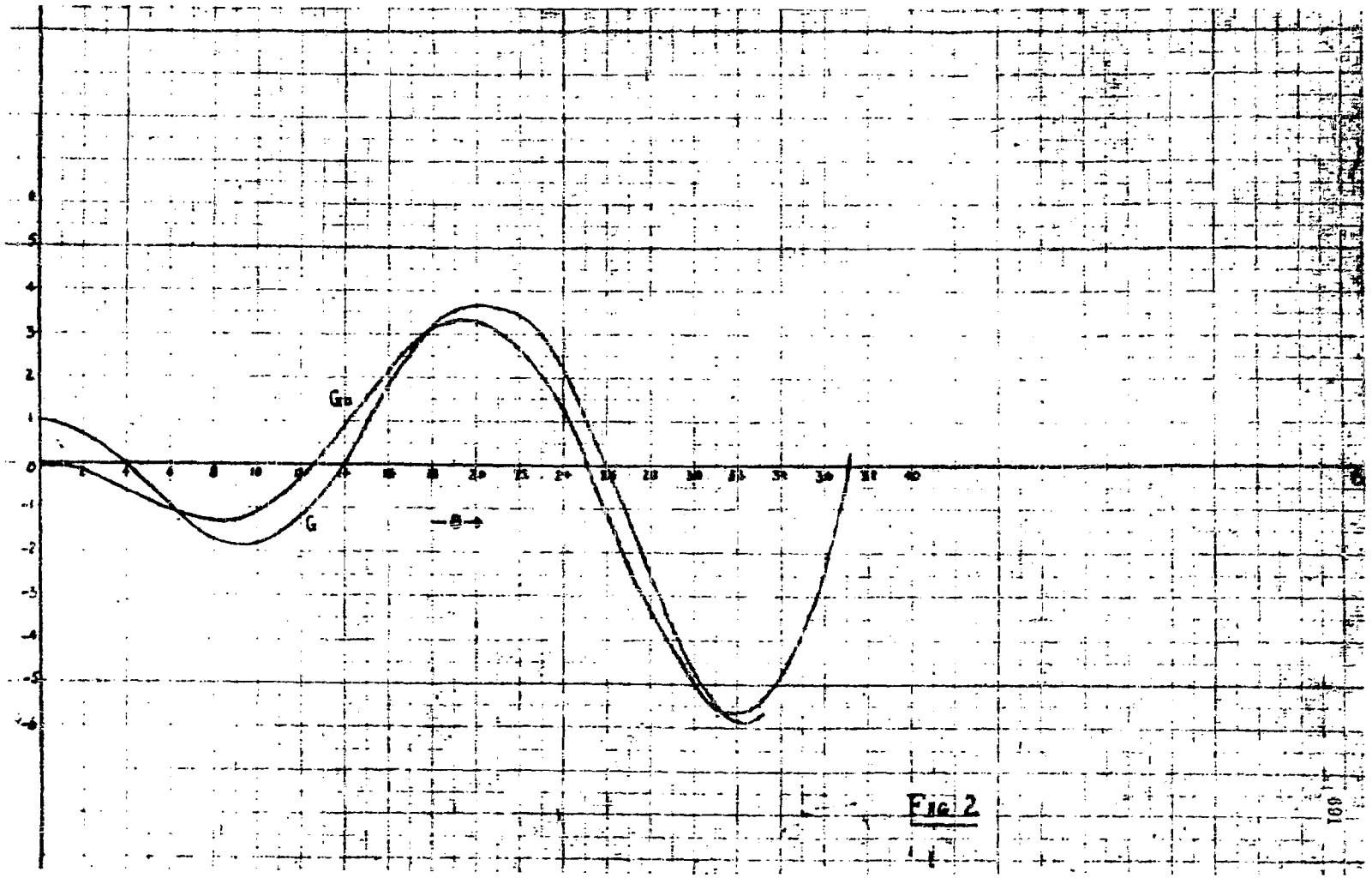

Fig 2

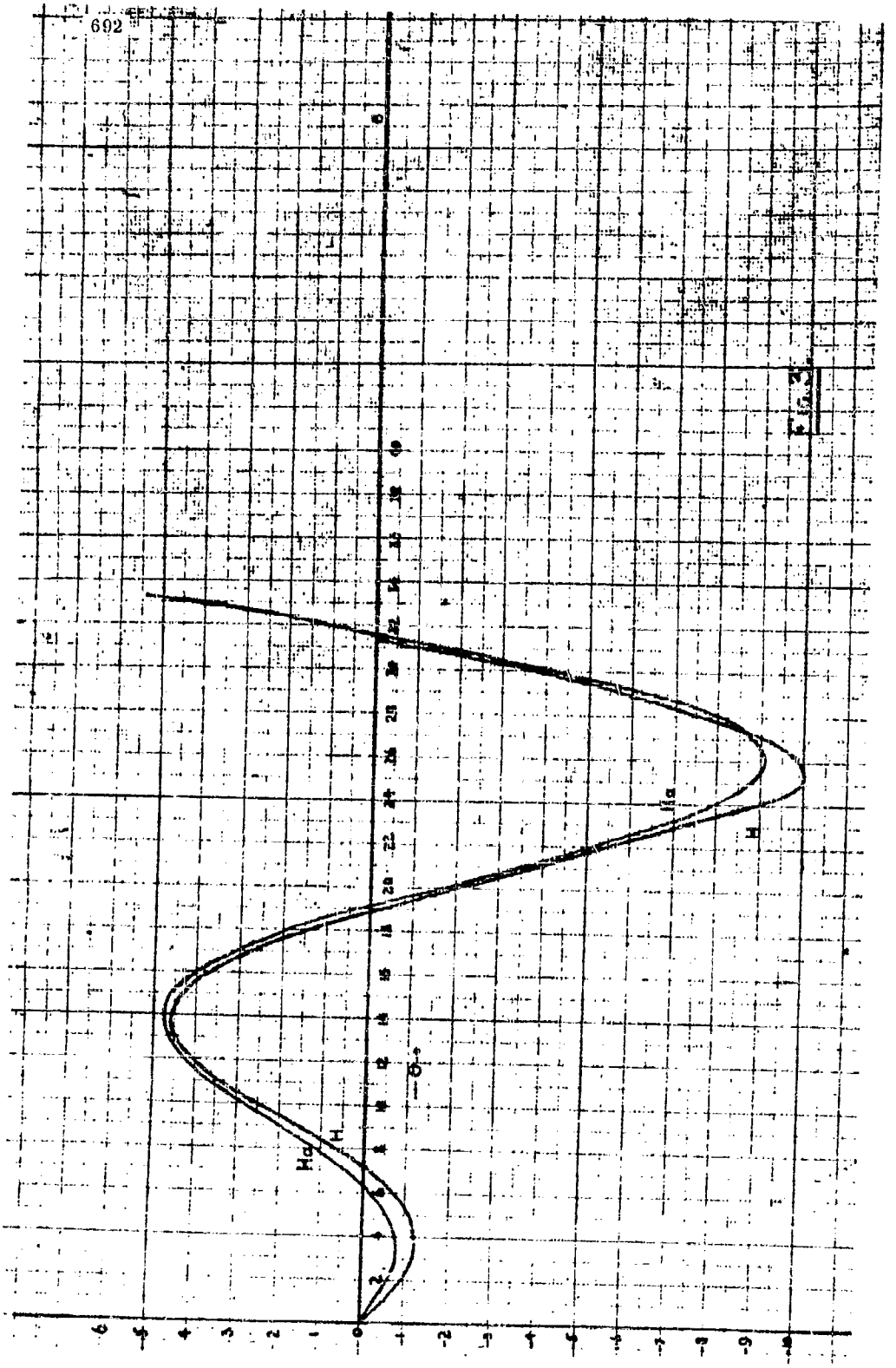
Ha
H
Ha
H
−θ°

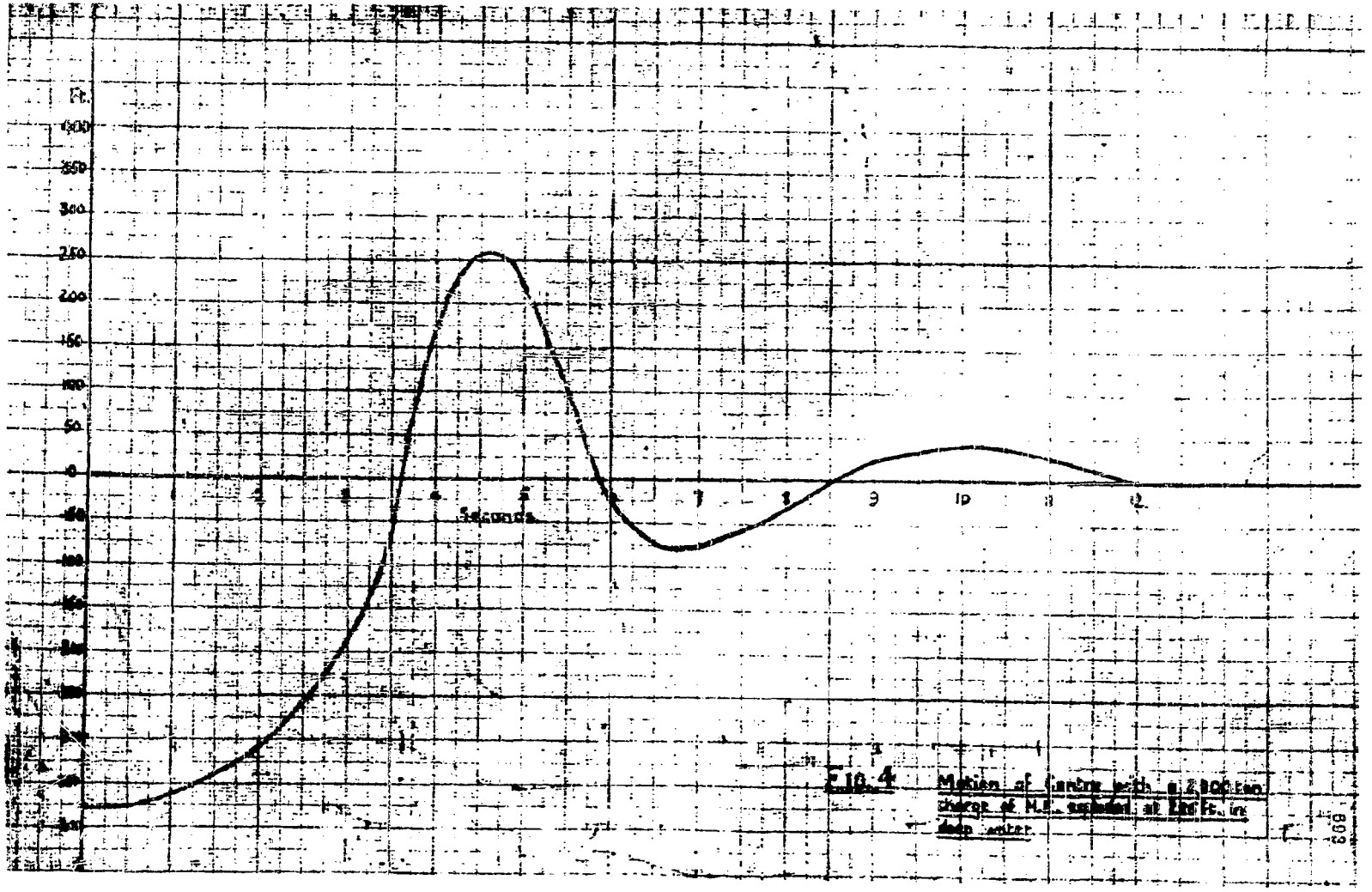

Fig. 4 Motion of centre with a 2,500 ton charge of N.E. exploded at 150 ft. in deep water

SURFACE WAVES PRODUCED BY FIRING UNDERWATER 32-LBS. CHARGES OF POLAR AMMON GELIGNITE AT VARIOUS DEPTHS

G. Charlesworth
Road Research Laboratory, London

British Contribution

February 1945

SURFACE WAVES PRODUCED BY FIRING UNDERWATER 32-lb. CHARGES OF POLAR AMMON GELIGNITE AT VARIOUS DEPTHS

G. Charlesworth

Road Research Laboratory, London

February 1945

* * * * * * * * *

Summary.

The amplitudes of the surface waves produced by firing underwater 32-lb. charges of P.A.G. at various depths in about 15 feet of water have been measured photographically. The waves were photographed by means of a 16-mm. cine camera as they passed along a reference board located in the surface at a horizontal distance of 55 feet from the charge.

In all but one case, the second wave had the largest positive amplitude and the largest negative amplitude was equal to or greater than this. The periodicity of the waves was not very different for all charge depths, the period in the region of the first and second waves being about 2.5 to 3 seconds. The velocity of the waves was estimated at about 8 feet/second and the wavelength about 20 to 25 feet.

Largest positive amplitudes were obtained for charge depths in the region of 0.6 times the maximum bubble radius. Comparison of the results with those obtained from 2-oz. and 2-lb. charges of P.A.G. showed that the positive amplitudes did not scale up as much as expected on a one-fourth power law, suggesting possibly a loss of wave making efficiency as the charge weight was increased from 2 oz. to 32 lb. The 32-lb. charge results, however, agreed quite well with those from 300-lb. T.N.T. depth charges. This may mean that for fairly large charges, there is little change in efficiency as the scale of the model is increased.

Introduction.

The object of the tests was to obtain further experimental data on scale relationships involved in wave making by means of explosives.

Experimental.

Charges.

The charges were of Polar Ammon gelignite, 32 lb. in weight, and were initiated by 4 oz. of G.E.

Measurement of wave amplitude.

Amplitudes were measured by photographing the waves as they passed along a reference board set in the water surface. The board was of tinplate 6 feet long x about 3 feet high. The camera used was a 16-mm. cine camera with a lens of focal length 3 inches and the camera was run at about 16 frames/second.

Site and arrangement of tests.

The tests were made in a gravel pit in about 15 feet of water. The centre of the reference board was placed at a horizontal distance of 55 feet from the charge. The camera was located on the bank at a distance of about 70 feet from the board. A plan view of the layout of the tests is shown in Figure 1.

Experimental .....

Experimental results.

The variation of amplitude with time at points at the front edge and at the centre of the reference board (points at horizontal distances of 52 feet and 55 feet from the charge) are given in Figures 2 and 3.

It is seen that in all cases except with the charge 2 feet deep, the positive amplitude was greatest for the second wave. This was observed previously for 2-oz. and 2-lb. charges. It is also to be noted that the maximum negative amplitude was equal to or greater than the maximum positive amplitude.

The periodicity of the waves was about the same for all charge depths. The period in the region of the first and second waves was between 2.5 and 3 seconds and decreased for the subsequent smaller waves.

The velocity of the waves across the board was about 8 feet/second from which the wave length of the main wave is estimated to be about 20 to 25 feet.

In Figure 4 positive amplitudes of the second waves in feet divided by the fourth root of the charge weight M in lb. are shown as functions of charge depth/(maximum bubble radius). Included in Figure 4 are previous results for 2-oz. and 2-lb. charges of Polar Ammon gelignite and for 300-lb. T.N.T. depth charges. The results confirm previous conclusions that the optimum depth for wave production was of the order of 0.6 times the maximum bubble radius.

In a previous enquiry it was considered that approximate scaling might obtain if the scale of the model were made proportional to the fourth root of the charge weight provided the ratio of depth of charge to maximum bubble radius were kept constant. The Polar Ammon gelignite results in Figure 4 show that the wave amplitudes from the larger charges did not increase as much as expected according to their scale relationship, a result which suggests that the larger charges may not have been so efficient in wave making. It is to be noted, however, that the results using 300-lb. charges were in fair agreement with the present tests. This may mean that provided large enough charges are used, there is not much change in efficiency of wave production as the scale of the model is increased.

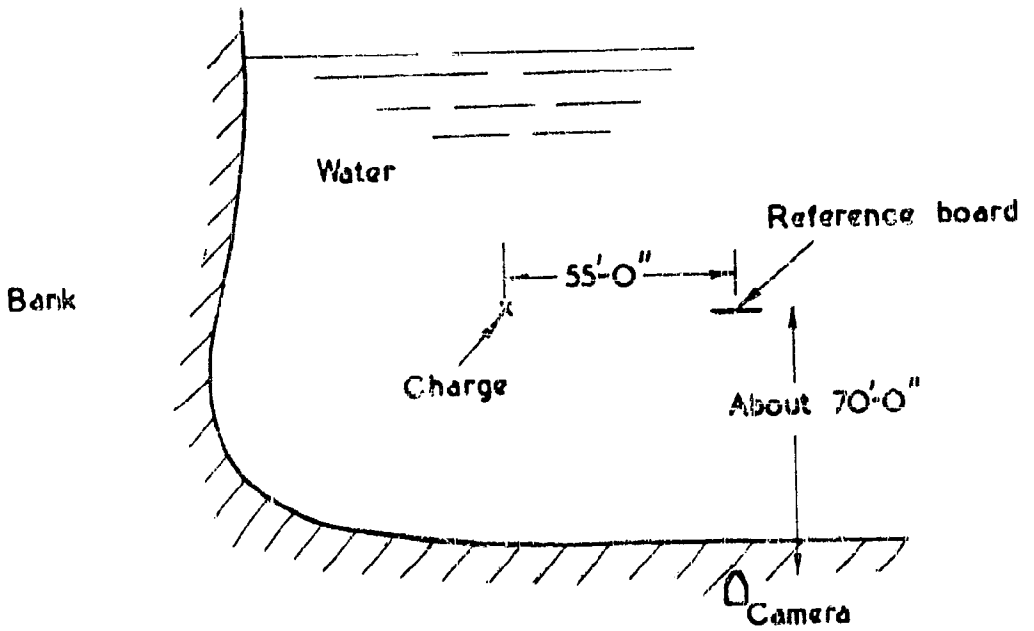

Fig.1. PLAN OF LAYOUT OF TESTS

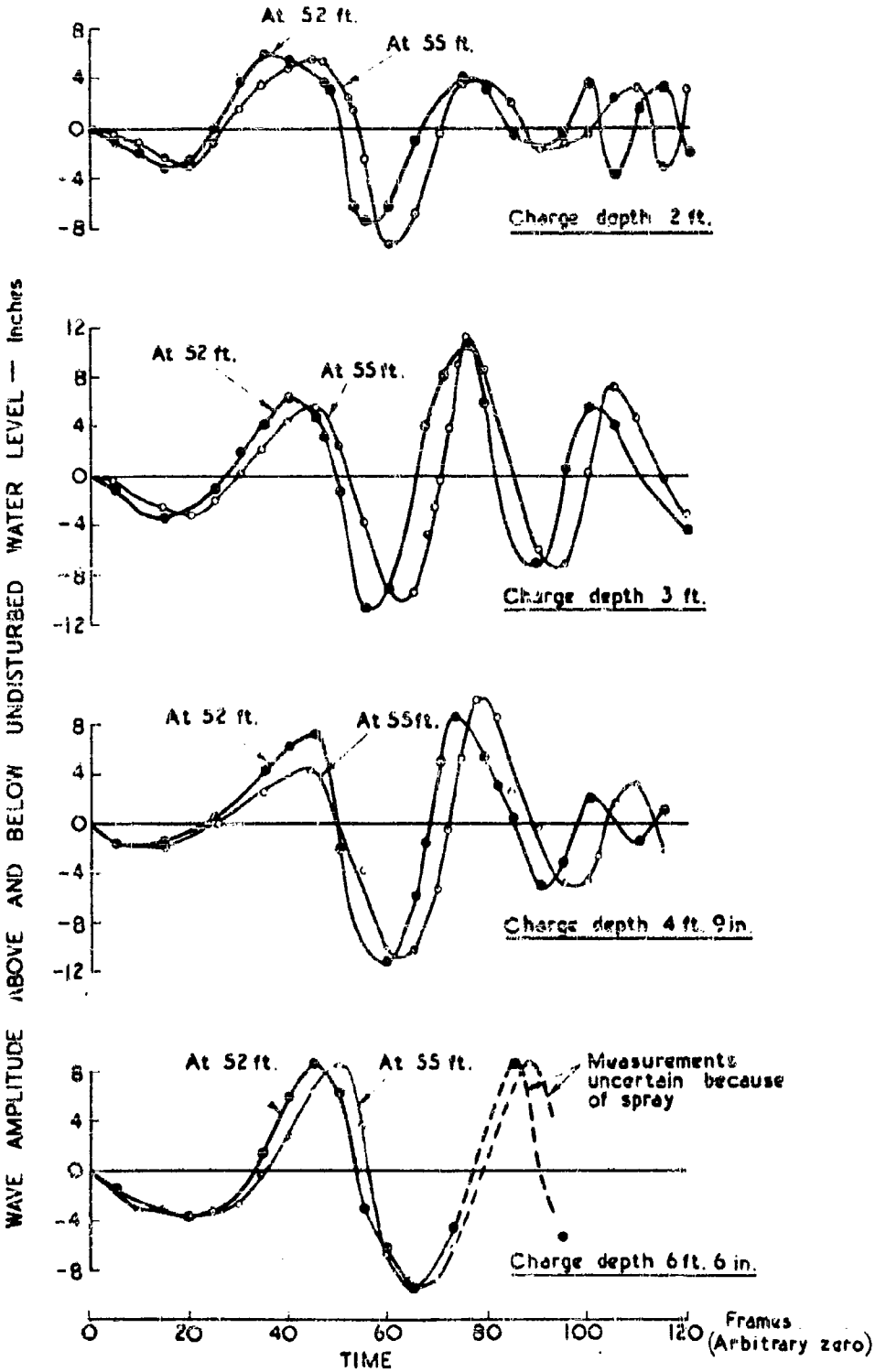

Fig. 2. WAVE AMPLITUDE AS FUNCTION OF TIME AT HORIZONTAL DISTANCES OF 52 ft. AND 55 ft. FROM THE CHARGE. FRAME SPEED 14·5/sec.

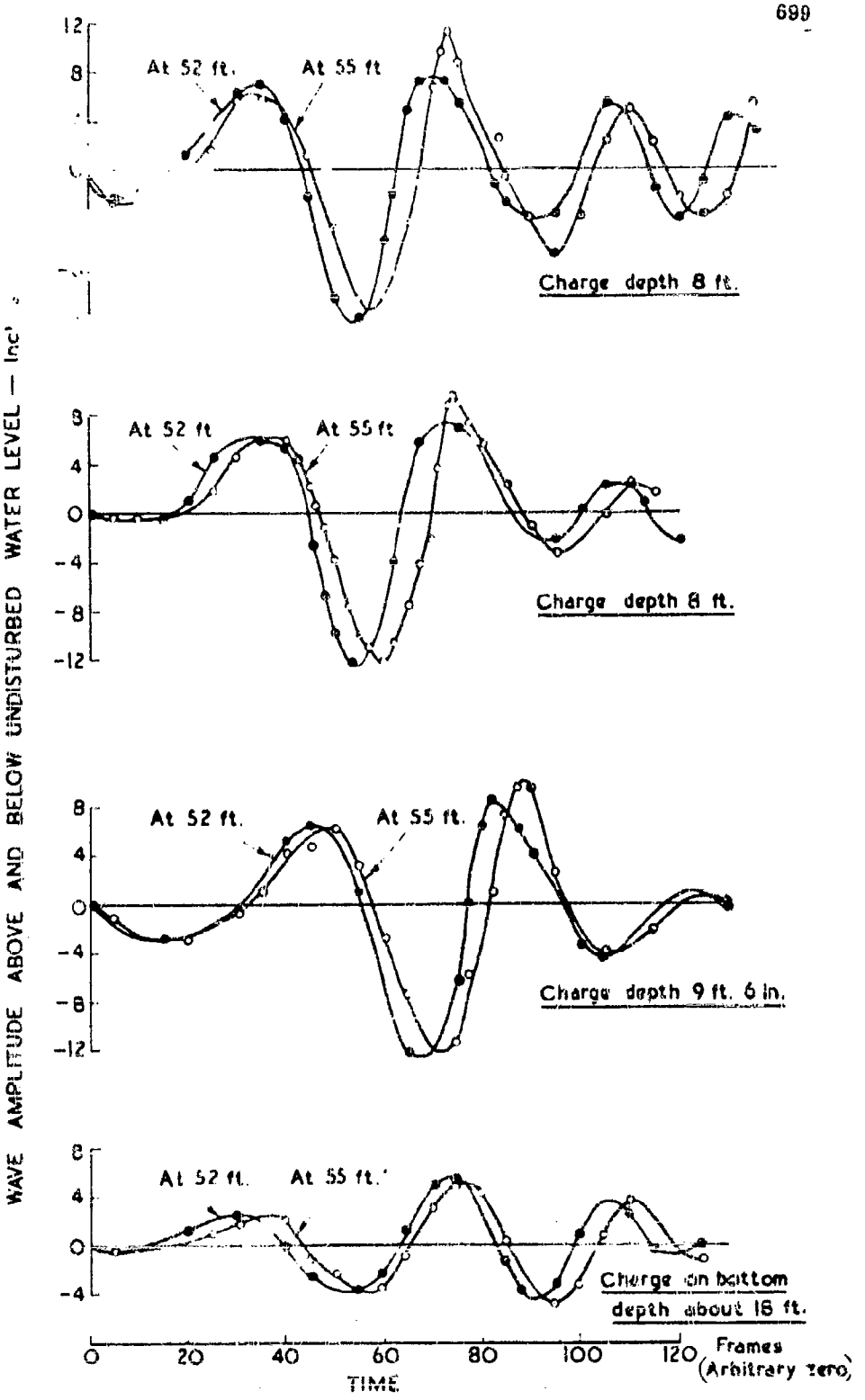

Fig. 3. WAVE AMPLITUDE AS FUNCTION OF TIME AT HORIZONTAL DISTANCES OF 52 ft. AND 55 ft. FROM THE CHARGE. FRAME SPEED 14 5/sec.

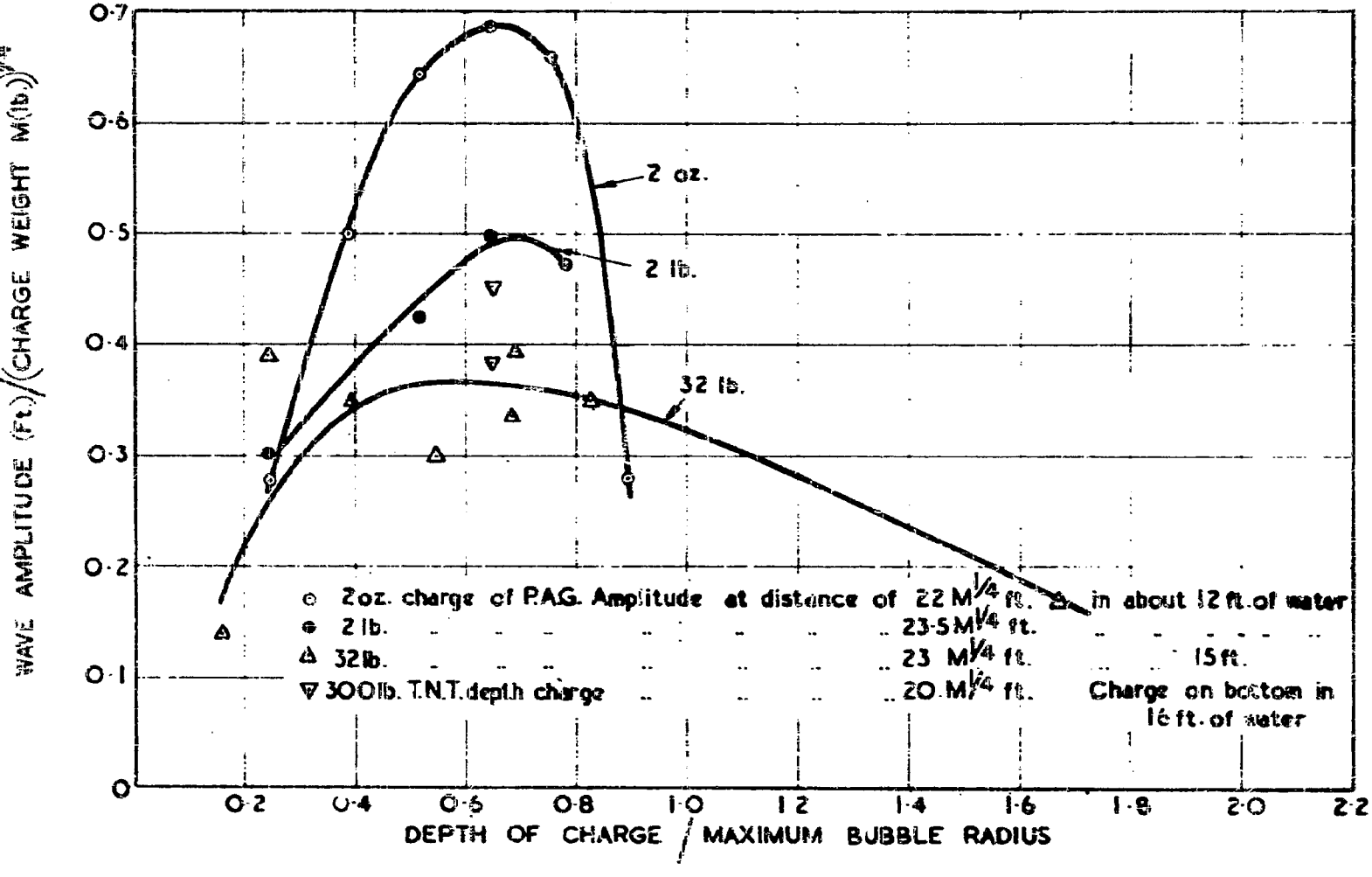

Fig.4. REDUCED WAVE AMPLITUDE AS A FUNCTION OF THE RATIO OF DEPTH OF CHARGE / MAXIMUM BUBBLE RADIUS FOR 2 oz., 2 lb. AND 32 lb. CHARGES OF P.A.G. FIRED UNDERWATER

SURFACE WAVES PRODUCED BY UNDERWATER EXPLOSIONS COMPARISON OF THE THEORY OF W. G. PENNEY WITH EXPERIMENTAL RESULTS FOR A 32-LB. CHARGE

A. R. Bryant
Road Research Laboratory, London

British Contribution

September 1945

SURFACE WAVES PRODUCED BY UNDERWATER EXPLOSIONS COMPARISON OF THE THEORY OF W. G. PENNEY WITH EXPERIMENTAL RESULTS FOR A 32-lb. CHARGE

A. R. Bryant

Road Research Laboratory, London

September 1945

* * * * * * * * *

Summary.

The amplitude of surface waves produced by a 32-lb. charge detonated in water at a depth of 8 feet has been calculated for a point 56.6 feet from the charge by W.G. Penney's theory[1]. Calculations extend as to the third trough.

The results have been compared with experimental observations for a similar charge[2]. Agreement is excellent as to the arrival of the second crest, but the calculated third trough is larger than that observed. Reasonable agreement as to the third trough is obtained if the shape of the initial cavity assumed in Penney's theory is modified to give a shallower cavity of the same total volume.

Equations used.

Penney's theory assumes that the waves are produced by the filling in of an initial cavity, whose shape is given by

$$y_0 = \frac{2h^4}{3}\left[\frac{1}{(h^2+r^2)^{3/2}} - \frac{3h^2}{(h^2+r^2)^{5/2}}\right] \qquad (1)$$

where y_0 is the initial elevation of the free surface above the original undisturbed water level at a point distant r from a vertical axis of symmetry through the charge. It can be shown that this is a reasonable representation of the cavity which might be expected to be produced when a gas bubble at its maximum radius h just touches the top of the "dome" created by the charge. The shape of this cavity is shown in Figure 1.

At any time t later the system of waves produced by this cavity is described by the following relation between surface elevation y and distance r.

$$y = \frac{2h^4}{3s^3}\sum_{n=1}^{\infty}(-1)^{n-1}\frac{n!}{(2n-2)!}\left[\frac{gt^2}{s}\right]^{n-1}\left[n\,P_{n-1}\left(\frac{h}{s}\right) - (2n+1)\left(\frac{h}{s}\right)P_n\left(\frac{h}{s}\right)\right]$$

$$\text{where } s^2 = h^2 + r^2 \qquad (2)$$

and P_n is the nth Legendre polynomial. This formula is only suitable for computation at small values of the time. For later times it is more convenient to use the following approximate integral method given by Penney.

If ω is the distance of a small element in the water surface of area dS from the point at which the wave height y is measured, and if r be the distance of this same area from the vertical axis through the charge, then

$$y = \frac{-1}{2\pi}\int \frac{y_0(r)}{\omega^2}\,H\left[\frac{gt^2}{\omega}\right]dS \qquad (3)$$

where .....

where $H(a) = \frac{1^2}{2!}a + \frac{1^2 3^2}{6!}a^3 - \frac{1^2 3^2 5^2}{10!}a^5 \ldots\ldots$

and y_0 is the initial elevation of the element dS, and is given by equation (1). The integral in (3) is to be taken over the whole of the region occupied by the initial cavity.

In Penney's method of evaluating (3) two approximations are made. Firstly, the integration is restricted to that portion of the cavity shown in Figure 1 where the water surface is initially below the undisturbed level, i.e. r varies from zero to $\sqrt{2}h$. Secondly an approximate expression for ω is used, which is illustrated in Figure 2. Here a plan of the water surface is shown, O being the vertical axis through the charge, and P being the point distant R from O, at which the wave height is to be calculated. The circle of radius $h\sqrt{2}$ represents the area within which the water surface is initially depressed. Then in (3) ω is approximated by the quantity $R - x$ which tends to ω when R is large compared with h. With these two approximations (3) may be reduced to

$$y = \frac{4h}{3^{5/2}\pi}\int_{\sqrt{2}}^{\infty}\frac{F(z)}{(X-z)^{\frac{1}{2}}}\,H\left[\frac{-8z^2}{(X-z)\,h}\right]dz \qquad (4)$$

where $F(z) = \frac{(2-z^2)^{3/2}}{(1+z^2)^2}$

and where $z = \frac{x}{h}$ and $X = \frac{R}{h}$

Numerical values.

It was assumed that the energy in the bubble motion of Polar Amron gelignite was 440 calories per gram, i.e. the same as that used in most calculations of bubble behaviour for T.N.T. This gives for a 32-lb. charge, $h = 31.3$ feet. The maximum bubble radius h is calculated from the formula given in a previous paper[3]. The wave height y was calculated at a distance $R = 5h = 56.5$ feet. Up to $t = 3.75$ seconds equation (2) was used, while for greater times equation (4) was used. In this latter equation the integral was performed numerically by dividing the range of z into twenty equal steps. The integration is estimated to be accurate to at least 5%; for most of the range the errors are probably not more than 2%.

The calculated wave amplitude is shown in Figure 3 by a full curve up to about 9.20 seconds, when the third trough has just reached the point under consideration. The slight discontinuity at $t = 3.75$ seconds in this curve is due to the change from equation (2) to equation (4). Equation (2) takes account of the whole of the cavity while (4) ignores the effects of that portion of the initial disturbance outside a radius of $\sqrt{2}h$, where the water is initially above the undisturbed water level.

Comparison with experimental observations.

Penney's theory applies strictly only when the total depth of the water is very large compared to the bubble radius. In the experiments described[2] the total depth of water was about 15 feet. The wavelengths observed did not exceed 25 feet so that as far as the propagation of waves is concerned the difference between the experiment and the case in which the depth was assumed infinite will be slight. The chief effect of the bottom will be to distort the shape of the cavity though it should not greatly alter its volume.

The case where the charge was fired at 8 feet depth is most nearly [illegible] envisaged by the theory, since at this depth the top of the bubble will just reach the dome the bubble attains its maximum volume. Accordingly the wave amplitudes observed at a distance of [illegible] feet from a 32-lb. charge 8 feet deep have been taken from the experimental paper[2] and plotted in Figure 3 by a broken line. As the zero of time for this curve was not known it has been arbitrarily chosen to give the best fit.

It will be seen that the agreement between theory and experiment is remarkably good, at least up to the second crest. From the calculations it seemed likely that the lack of agreement for times later than about 9 seconds might be due to the actual cavity being shallower than the assumed cavity owing to the presence of the bottom. To test this idea a cavity, having the same volume as, but shallower than, that assumed by Penney was arbitrarily chosen. This is shown by a broken line in Figure 1. A few points, corresponding to two crests and two troughs were recomputed using this modified cavity shape, and are plotted in Figure 3 by circles. These are in better agreement with the observed waves, except for the crest at 8 seconds.

It may .....

It may be concluded that, at least for charges of the order of 32-lb. the theory of Penney is in reasonable agreement with observation, though the initial shape of the cavity produced in the water by the charge may differ somewhat from that assumed.

References.

(1) W.G. Penney. "Gravity waves produced by surface and underwater explosions".

(2) G. Charlesworth. "Surface waves produced by firing underwater 32 lb. charges of polar ammon gelignite at various depths."

(3) A.R. Bryant. "The behaviour of an underwater explosion bubble".

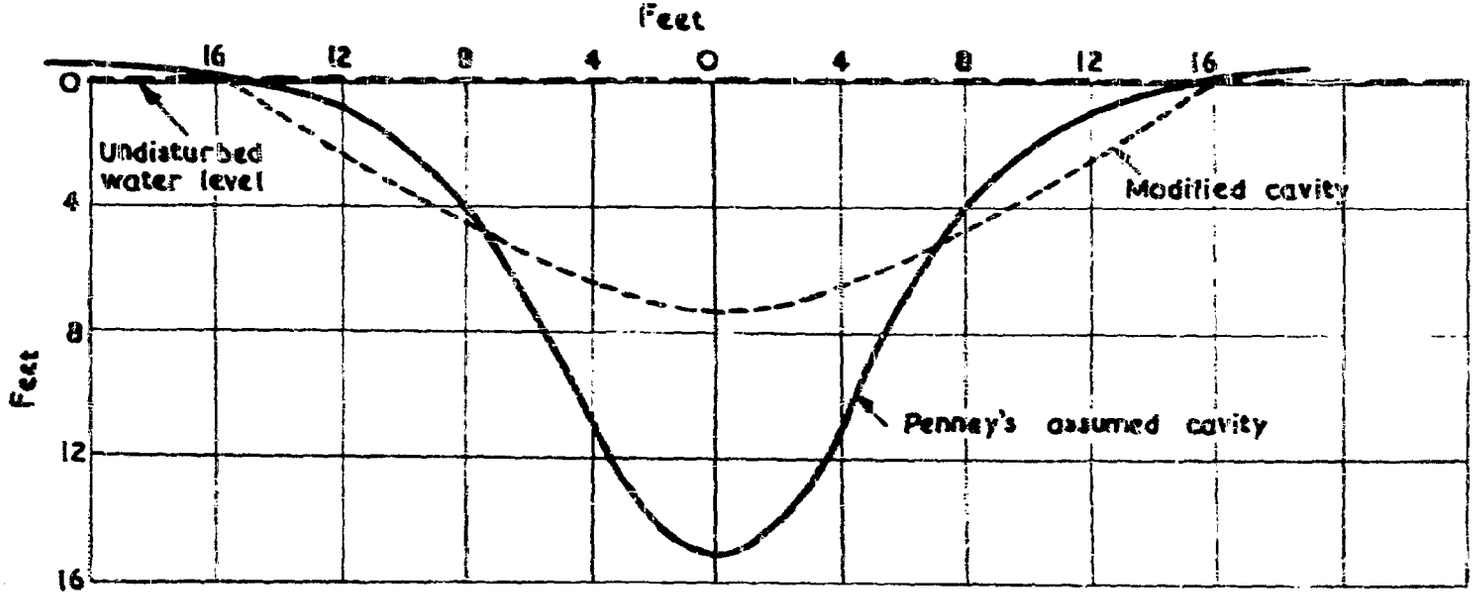

Fig 1. CROSS-SECTION OF INITIAL CAVITY FORMED BY UNDERWATER EXPLOSION

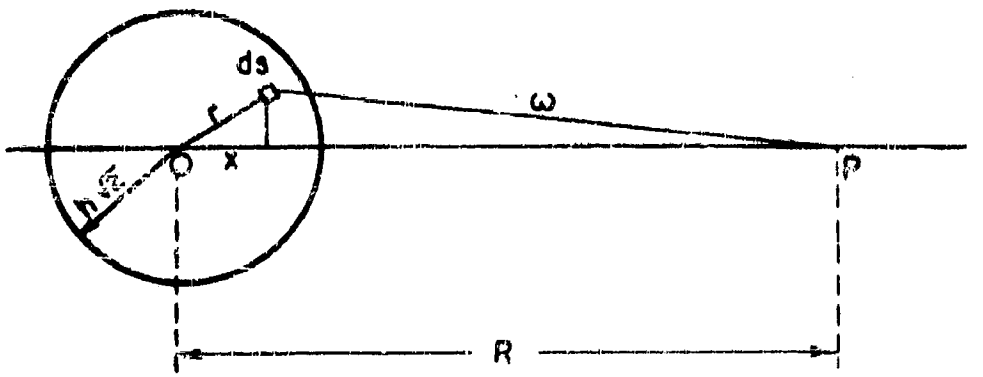

Fig. 2.

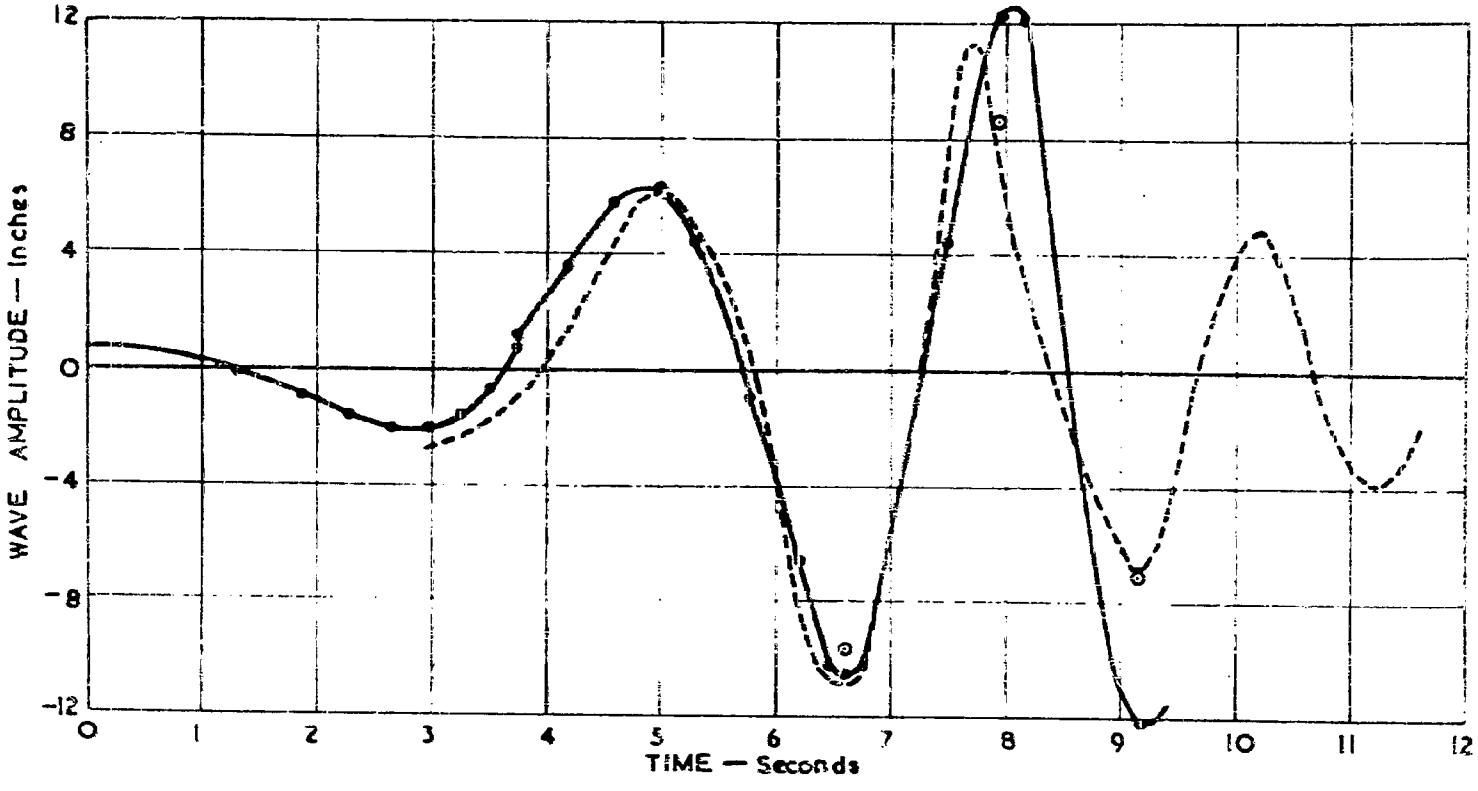

⊙ Peaks calculated using modified cavity shape. Amplitude calculated at 56·5 ft from charge

– – – – Observed wave. 32 lb. at 8ft. depth. Amplitude measured at 55 ft. from charge

—o—o— Wave calculated from Penney's theory — assuming h = 11·3 ft. Amplitude calculated at 56·5 ft. from charge

Fig.3. AMPLITUDES OF WAVES PRODUCED BY A 32-lb. CHARGE FIRED AT A DEPTH OF 8ft.

SURFACE WAVES FROM AN UNDERWATER EXPLOSION

J. G. Kirkwood
Cornell University, N. Y.

and

R. J. Seeger
Naval Ordnance Laboratory

American Contribution

27 May 1947

SURFACE WAVES FROM AN UNDERWATER EXPLOSION

Consider a surface wave generated by an underwater explosion. [1] The effect of the shock wave is assumed to be negligible so that the sole source is the pulsating gas globe, which has an instantaneous volume V(t) at the time t. This gas globe, assumed to be spherically symmetric, as a first approximation, will migrate under the influence of gravity and of the neighboring surfaces. Let $z_B(t)$ designate its instantaneous position above the bottom. It is required to find the flow for infinite water of uniform depth h above a rigid bottom.

Let P be a point (cf. Fig. 1) with cylindrical polar coordinates r, θ, z. Then the conservation of mass requires that the divergence of the material velocity $\underline{q}(r, \theta, z, t)$ of an inviscid, incompressible fluid with uniform density ρ vanish everywhere except at the source (equation of continuity), i.e.,

If the flow is further assumed to be irrotational, then the velocity $q(r, \theta, z, t)$ is the negative gradient of a velocity potential $\Phi(r, \theta, z, t)$ and Laplace's equation results from the above one, i.e.,

$$\nabla^2 \Phi = 0 \qquad (1$$

Fig. 1

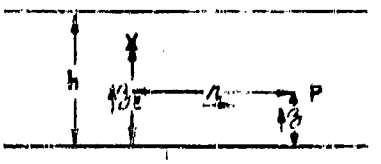

In addition, the function Φ must satisfy two boundary conditions. At the fixed bottom there is no component of the velocity normal to the surface. i.e.,

$$\frac{\partial \Phi}{\partial z} = 0 \quad , \quad z = 0 \qquad (2$$

At the free surface the pressure p_a is uniformly atmospheric. The effect of this condition is seen by a consideration of the Eulerian equation of motion, viz.,

$$\frac{\partial \underline{q}}{\partial t} + \underline{q} \cdot \nabla \underline{q} = - \nabla(gz) - \frac{1}{\rho} \nabla p \quad ,$$

where (gz) is the gravitational potential and $p(r, \theta, z, t)$ is the instantaneous fluid pressure at a point. Integrating with respect to the coordinates and neglecting the square of the speed q , we obtain

$$- \frac{\partial \Phi}{\partial t} + gz + \frac{p}{\rho} = 0 \quad , \qquad (3$$

where an arbitrary integration-function of t has been absorbed in $\frac{\partial \Phi}{\partial t}$. Including in it also the constant p_a/ρ on the surface, we have, to the same order of approximation, for a small disturbance of the free surface

$$-\left(\frac{\partial \Phi}{\partial t}\right)_{z=h} + g z = 0 \quad , \text{ free surface.}$$

Now kinematically the velocity of the fluid normal to the surface must be the same as the normal component of the surface velocity so that approximately (to first order terms)

$$-\left(\frac{\partial \Phi}{\partial z}\right)_{z=h} = \frac{\partial z}{\partial t} \quad , \text{ free surface.}$$

Differentiating the preceding equation with respect to t and substituting for $\frac{\partial z}{\partial t}$, we obtain for our second boundary condition

$$\frac{\partial^2 \Phi}{\partial t^2} + g \frac{\partial \Phi}{\partial z} = 0 \quad , \quad z = h \, . \tag{3}$$

Suppose $\Phi_B(h, z, t)$ is the cylindrically symmetric velocity potential for the case of a bottom only, i.e., no free surface. Then

$$\Phi_B = \frac{1}{4\pi} \frac{dV}{dt} \left\{ \frac{1}{\sqrt{k^2+(z-z_s)^2}} + \frac{1}{\sqrt{k^2+(z+z_s)^2}} \right\} \, , \tag{4a}$$

where $\frac{dV}{dt}$ is the strength of an assumed simple source, i.e., a point source with uniform radial flow. Let $\Phi_S(h, z, t)$ be the additional term required for a free surface to be satisfied also. Thus

$$\Phi = \Phi_B + \Phi_S \tag{4}$$

Inasmuch as Φ_B satisfies Laplace's equation subject to the condition of the fixed bottom, it follows from equations (1) and (2), respectively, that

$$\nabla^2 \Phi_S = 0 \tag{1'}$$

and

$$\frac{\partial \Phi_S}{\partial z} = 0 \quad , \quad z = 0 \tag{2'}$$

Substituting the expression (4) for Φ in equation (3), we have

$$\frac{\partial^2 \Phi_s}{\partial t^2} + g \frac{\partial \Phi_s}{\partial z} = - \frac{\partial^2 \Phi_g}{\partial t^2} - g \frac{\partial \Phi_g}{\partial z}, \quad z = h,$$

or, upon substituting for Φ_s the expression (4a),

$$\left(\frac{\partial^2 \Phi}{\partial t^2}\right)_{z=h} + g \left(\frac{\partial \Phi_s}{\partial z}\right)_{z=h} =$$

$$- \left(\frac{\partial^2 \Phi_g}{\partial t^2}\right)_{z=h} + \frac{g}{4\pi} \frac{dV}{dt} \left\{ \frac{h - z_a}{(h^2 + (h - z_a)^2)^{3/2}} + \frac{h + z_a}{(h^2 + (h + z_a)^2)^{3/2}} \right\} \quad (3')$$

We shall assume a Hankel transform $f(k, z, t)$ for the cylindrically symmetric solution $\Phi_s(r, z, t)$, namely,

$$\Phi_s(r, z, t) = {}_0T_k \left(f(k, z, t) \right), \quad (4b)$$

where $${}_0T_k \left(f(k, z, t) \right) = \int_0^\infty f(k, z, t) J_0(kr) k \, dk$$

and $J_0(kr)$ is the Bessel function of zero order. Substituting this expression for Φ_s in equations (1') and (2') and commuting operators, we obtain, respectively,

$${}_0T_k \left(\frac{\partial^2 f}{\partial z^2} - k^2 f \right) = 0$$

$${}_0T_k \left(\frac{\partial f}{\partial z} \right)_{z=0} = 0$$

Applying the inverse transformation and recalling that iteration of this operator is equivalent to multiplication by unity, we find

$$\frac{\partial^2 f}{\partial z^2} - k^2 f = 0$$

$$\left(\frac{\partial f}{\partial z} \right)_{z=0} = 0$$

These conditions are satisfied by

$$f(k, z, t) = K(k, t) \cosh kz$$

Substituting Φ_s from (4b) also in equation (3') and commuting operators, we have

$$\mathcal{F}_k\left(\frac{\partial^2 \eta}{\partial t^2} + g\frac{\partial \eta}{\partial z}\right)_{z=h} = -\left(\frac{\partial^2 \Phi_B}{\partial t^2}\right)_{z=h} + \frac{g}{4\pi}\frac{dV}{dt}\left\{\frac{h-z_E}{(r^2+(h-z_E)^2)^{1/2}} + \frac{h+z_E}{(r^2+(h+z_E)^2)^{1/2}}\right\} \quad (3')$$

Applying the inverse and noting that

$$\mathcal{F}_k\frac{\mu}{(r^2+\mu^2)^{3/2}} = e^{-k\mu}, \quad \mu > 0,$$

we obtain

$$\frac{\partial^2 K}{\partial t^2}\cosh kh + gkK\sinh kh = -\mathcal{F}_k\left(\frac{\partial^2 \Phi_B}{\partial t^2}\right)_{z=h} + \frac{g}{4\pi}\frac{dV}{dt}\left(e^{-k(h-z_E)} + e^{-k(h+z_E)}\right)$$

Put

$$\omega \equiv \sqrt{gk\tanh kh}$$

Then

$$\frac{\partial^2 K}{\partial t^2} + \omega^2 K = -\frac{1}{\cosh kh}\mathcal{F}_k\left(\frac{\partial^2 \Phi_B}{\partial t^2}\right)_{z=h} + \frac{g\epsilon^{-kh}}{2\pi\cosh kh}\cosh kz_E$$

The real solution of this equation is given by

$$K(k,t) = A(k)\cos(\omega t - \alpha(k)) + \frac{1}{\omega\cosh kh}\int_{t_0}^{t}\left\{-\mathcal{F}_k\left(\frac{\partial^2 \Phi_B}{\partial S^2}\right)_{z=h} + \frac{g}{2\pi}e^{-kh}\frac{dV}{dS}\cosh kz_E\right\}\sin\omega(t-s)\,dS,$$

where t_0 is some time prior to the explosion and $A(k)$, $\alpha(k)$ are arbitrary constants of integration. Let the explosion take place at the time $t = 0$. For all times previous to this instant $\Phi_s(k, z, t)$, and consequently both $K(k,t)$ and $A(k)$, must vanish. Therefore,

$$K(k,t) = \frac{1}{\omega\cosh kh}\int_{t_0}^{t}\left\{-\mathcal{F}_k\left(\frac{\partial^2 \Phi_B}{\partial S^2}\right)_{z=h} + \frac{g}{2\pi}e^{-kh}\frac{dV}{dS}\cosh kz_E\right\}dS$$

If the gas globe is stationary, i.e., z_g constant, then from the expression (4a) for Φ_s

$$k\Gamma_k\left(\frac{\partial^2\Phi_s}{\partial s^2}\right)_{z=h} = \frac{1}{4\pi}\frac{d^3V}{ds^3}\,k\Gamma_k\left\{\frac{1}{\sqrt{h^2+(h-z_g)^2}} + \frac{1}{\sqrt{h^2+(h+z_g)^2}}\right\}$$

Noting that

$$k\Gamma_h\,\frac{1}{(h^2+\mu^2)^{1/2}} = \frac{e^{-k\mu}}{k}\,, \qquad \mu > 0\,,$$

we obtain

$$K(k,t) = \frac{e^{-kh}\cosh kz_g}{2\pi\omega\cosh kh}\int_{t_0}^{t}\left(-\frac{1}{k}\frac{d^3V}{ds^3} + g\frac{dV}{ds}\right)\sin\omega(t-s)\,ds\,.$$

Integrating by parts, we find

$$K(k,t) = \frac{\cosh kz_g}{2\pi\cosh kh}\left\{-\frac{e^{-kh}}{k}\frac{dV}{dt} + \frac{g}{\cosh kh}\int_{t_0}^{t}V(s)\cos\omega(t-s)\,ds\right\}$$

Hence the complete solution Φ is given by

$$\Phi(h,z,t) = \Phi_s(h,z,t) + \frac{1}{2\pi}\,h\Gamma_k\left\{\frac{\cosh kz\cosh kz_g}{\cosh kh}\left(-\frac{e^{-kh}}{k}\frac{dV}{dt}\right.\right.$$
$$\left.\left. + \frac{g}{\cosh kh}\int_{t_0}^{t}V(s)\cos\omega(t-s)\,ds\right)\right\} \qquad (4')$$

The evaluation of the integrals involved in Φ for an actual gas globe is straightforward, but lengthy. It is convenient, therefore, to introduce a simplifying assumption, the value of which must be tested by analysis of experimental data. If the period τ of the first pulsation of the gas globe is much less than the time interval after the explosion, it is reasonable to suppose that

$$V(t) = \bar{V}\,, \qquad 0 \le t \le \tau\,,$$

where the constant $\bar{V}$ is some average volume for the period τ. Thus

$$\Phi(h,z,t) = \frac{g}{2\pi}\,\bar{V}\,h\Gamma_k\,\frac{\cosh kz\cosh kz_g}{\omega\cosh^2 kh}\left\{\sin\omega t - \sin\omega(t-\tau)\right\} \qquad (4'')$$

and from equation (3a)

$$\phi(r,z,t) = -\rho g z + \frac{\rho g}{2\pi} \overline{V} \int_k \frac{\cosh kz \cosh kz_\varepsilon}{\cosh^2 kh} \left\{ \cos\omega t - \cos\omega(t-\tau) \right\} \quad (5$$

For computational purposes it is convenient to introduce dimensionless variables, namely,

$$k' = \frac{k}{\frac{g}{h}} \quad , \quad z' = \frac{z}{\frac{g}{h}} \quad , \quad z'_\varepsilon = \frac{z_\varepsilon}{\frac{g}{h}}$$

and $$t' = t\sqrt{\frac{g}{h}} \quad , \quad \tau' = \tau\sqrt{\frac{g}{h}} \quad , \quad \omega' = \omega\sqrt{\frac{h}{g}}$$

Also put $$\beta = kh$$

then $$\omega' = \sqrt{\beta \tanh \beta}$$

Hence $$\phi_{z'_\varepsilon}(k',z',t') = -\rho g h z' + \frac{\rho g}{2\pi h^2} \overline{V} G_{z'_\varepsilon,\tau'}(k',0,t') \quad (5'$$

where $$G_{z'_\varepsilon,\tau'}(k',z',t') = G_{z'_\varepsilon}(k',z',t') - G_{z'_\varepsilon}(k',z',t'-\tau')$$

and $$G_{z'_\varepsilon}(k',z',t') = \int_0^\infty \frac{\cosh\beta x' \cosh\beta z'_\varepsilon}{\cosh^2\beta} \cos\omega' t' \; J_0(\beta k')\beta \, d\beta$$

A problem of practical interest is the determination of the pressure due to an explosion at the bottom ($z'_\varepsilon = 0$). The function $G_0(k', 0, t')$ has been evaluated[2] numerically for $k' = 5, 10, 15, 25, 50, 500$; its values for the initial disturbance are given in Table 1A. The function $G_0(k', /, t')$ [equal to $G_1(k', 0, t')$] for the pressure at the surface has been evaluated[3] numerically for $k' = 5, 10, 15, 25, 50$; its values for the initial disturbance are given in Table 1B.

The function $G_{z'_\varepsilon}(k', 0, t')$ apparently has alternately positive and negative phases, as is seen in typical representations, $G_0(25, 0, t')$, $G_0(25, 1, t')$, $G_{1/2}(25,0,t')$ in graphs 1a, b, c, respectively. The maximum of $G_0(k', 0, t')$ for the first positive phase and that for the second one are shown for the several values of k' in Graphs $2a_1, a_2$, respectively; likewise, the minima of the first two negative phases are given for corresponding values of k' in Graphs $2b_1$, a_2 (positive) and in Graphs $3b_1$, b_2 (negative). The corresponding values for $G_0(k', /, t')$ are plotted in graphs $2a_1'$, a_2', b_1', $3a_1'$,

TABLE 1A

t'	$G_0(5,0,t')$	t'	$G_0(5,0,t')$	t'	$G_0(5,0,t')$	t'	$G_0(5,0,t')$
0.0	0.0025	4.0	0.0701	8.0	-0.0742	12.0	0.0284
0.1	0.0027	4.1	0.0727	8.1	-0.0796	12.1	0.0263
0.2	0.0029	4.2	0.0751	8.2	-0.0844	12.2	0.0237
0.3	0.0031	4.3	0.0774	8.3	-0.0886	12.3	0.0207
0.4	0.0033	4.4	0.0794	8.4	-0.0921	12.4	0.0172
0.5	0.0036	4.5	0.0812	8.5	-0.0949	12.5	0.0135
0.6	0.0040	4.6	0.0828	8.6	-0.0970	12.6	0.0095
0.7	0.0044	4.7	0.0841	8.7	-0.0982	12.7	0.0054
0.8	0.0048	4.8	0.0850	8.8	-0.0988	12.8	+0.0012
0.9	0.0054	4.9	0.0856	8.9	-0.0985	12.9	-0.0030
1.0	0.0060	5.0	0.0858	9.0	-0.0974	13.0	-0.0070
1.1	0.0068	5.1	0.0856	9.1	-0.0956	13.1	-0.0109
1.2	0.0076	5.2	0.0851	9.2	-0.0930	13.2	-0.0146
1.3	0.0086	5.3	0.0840	9.3	-0.0897	13.3	-0.0180
1.4	0.0096	5.4	0.0826	9.4	-0.0857	13.4	-0.0210
1.5	0.0108	5.5	0.0806	9.5	-0.0811	13.5	-0.0236
1.6	0.0120	5.6	0.0782	9.6	-0.0760	13.6	-0.0258
1.7	0.0134	5.7	0.0753	9.7	-0.0703	13.7	-0.0276
1.8	0.0148	5.8	0.0720	9.8	-0.0642	13.8	-0.0288
1.9	0.0165	5.9	0.0681	9.9	-0.0577	13.9	-0.0295
2.0	0.0182	6.0	0.0638	10.0	-0.0509	14.0	-0.0296
2.1	0.0201	6.1	0.0590	10.1	-0.0440	14.1	-0.0293
2.2	0.0220	6.2	0.0537	10.2	-0.0369	14.2	-0.0286
2.3	0.0241	6.3	0.0480	10.3	-0.0298	14.3	-0.0274
2.4	0.0262	6.4	0.0419	10.4	-0.0227	14.4	-0.0258
2.5	0.0285	6.5	0.0355	10.5	-0.0156	14.5	-0.0239
2.6	0.0309	6.6	0.0286	10.6	-0.0091	14.6	-0.0217
2.7	0.0334	6.7	0.0215	10.7	-0.0027	14.7	-0.0193
2.8	0.0360	6.8	0.0141	10.8	+0.0033	14.8	-0.0167
2.9	0.0386	6.9	+0.0065	10.9	0.0088	14.9	-0.0139
3.0	0.0413	7.0	-0.0013	11.0	0.0139	15.0	-0.0111
3.1	0.0441	7.1	-0.0092	11.1	0.0183	15.1	-0.0084
3.2	0.0469	7.2	-0.0171	11.2	0.0221	15.2	-0.0057
3.3	0.0498	7.3	-0.0250	11.3	0.0253	15.3	-0.0031
3.4	0.0527	7.4	-0.0328	11.4	0.0278	15.4	-0.0007
3.5	0.0556	7.5	-0.0404	11.5	0.0296	15.5	+0.0016
3.6	0.0586	7.6	-0.0479	11.6	0.0307		
3.7	0.0615	7.7	-0.0551	11.7	0.0311		
3.8	0.0644	7.8	-0.0619	11.8	0.0309		
3.9	0.0672	7.9	-0.0683	11.9	0.0300		

Note: The entries are correct to within three units in the fourth decimal place.

TABLE 1A (Continued)

t'	$Q_0(10,0,t')$	t'	$Q_0(10,0,t')$	t'	$Q_0(10,0,t')$	t'	$Q_0(10,0,t')$
3.0	0.0002	8.0	0.0254	13.0	-0.0165	18.0	0.0311
3.1	0.0003	8.1	0.0267	13.1	-0.0207	18.1	0.0315
3.2	0.0003	8.2	0.0280	13.2	-0.0249	18.2	0.0315
3.3	0.0004	8.3	0.0294	13.3	-0.0290	18.3	0.0311
3.4	0.0004	8.4	0.0308	13.4	-0.0331	18.4	0.0303
3.5	0.0005	8.5	0.0322	13.5	-0.0371	18.5	0.0290
3.6	0.0005	8.6	0.0335	13.6	-0.0408	18.6	0.0274
3.7	0.0006	8.7	0.0349	13.7	-0.0443	18.7	0.0254
3.8	0.0007	8.8	0.0363	13.8	-0.0476	18.8	0.0231
3.9	0.0008	8.9	0.0377	13.9	-0.0506	18.9	0.0205
4.0	0.0008	9.0	0.0391	14.0	-0.0534	19.0	0.0176
4.1	0.0010	9.1	0.0404	14.1	-0.0560	19.1	0.0145
4.2	0.0011	9.2	0.0418	14.2	-0.0582	19.2	0.0112
4.3	0.0012	9.3	0.0428	14.3	-0.0601	19.3	0.0078
4.4	0.0013	9.4	0.0439	14.4	-0.0617	19.4	0.0043
4.5	0.0014	9.5	0.0449	14.5	-0.0630	19.5	+0.0007
4.6	0.0016	9.6	0.0459	14.6	-0.0639	19.6	-0.0028
4.7	0.0018	9.7	0.0468	14.7	-0.0644	19.7	-0.0063
4.8	0.0020	9.8	0.0475	14.8	-0.0645	19.8	-0.0097
4.9	0.0022	9.9	0.0482	14.9	-0.0642	19.9	-0.0129
5.0	0.0025	10.0	0.0487	15.0	-0.0636	20.0	-0.0160
5.1	0.0028	10.1	0.0491	15.1	-0.0625	20.1	-0.0188
5.2	0.0031	10.2	0.0494	15.2	-0.0611	20.2	-0.0214
5.3	0.0034	10.3	0.0495	15.3	-0.0593	20.3	-0.0237
5.4	0.0037	10.4	0.0494	15.4	-0.0571	20.4	-0.0257
5.5	0.0041	10.5	0.0492	15.5	-0.0546	20.5	-0.0273
5.6	0.0045	10.6	0.0488	15.6	-0.0518	20.6	-0.0286
5.7	0.0049	10.7	0.0481	15.7	-0.0486	20.7	-0.0295
5.8	0.0054	10.8	0.0473	15.8	-0.0452	20.8	-0.0299
5.9	0.0059	10.9	0.0463	15.9	-0.0415	20.9	-0.0301
6.0	0.0064	11.0	0.0451	16.0	-0.0376	21.0	-0.0298
6.1	0.0069	11.1	0.0437	16.1	-0.0335	21.1	-0.0291
6.2	0.0075	11.2	0.0422	16.2	-0.0292	21.2	-0.0281
6.3	0.0082	11.3	0.0404	16.3	-0.0248	21.3	-0.0267
6.4	0.0089	11.4	0.0384	16.4	-0.0204	21.4	-0.0250
6.5	0.0096	11.5	0.0362	16.5	-0.0158	21.5	-0.0231
6.6	0.0104	11.6	0.0338	16.6	-0.0113	21.6	-0.0209
6.7	0.0112	11.7	0.0311	16.7	-0.0068	21.7	-0.0184
6.8	0.0120	11.8	0.0283	16.8	-0.0024	21.8	-0.0158
6.9	0.0129	11.9	0.0253	16.9	+0.0019	21.9	-0.0130
7.0	0.0139	12.0	0.0221	17.0	0.0061	22.0	-0.0102
7.1	0.0149	12.1	0.0187	17.1	0.0100	22.1	-0.0072
7.2	0.0159	12.2	0.0151	17.2	0.0137	22.2	-0.0042
7.3	0.0169	12.3	0.0114	17.3	0.0170	22.3	-0.0013
7.4	0.0180	12.4	0.0076	17.4	0.0201	22.4	+0.0015
7.5	0.0192	12.5	+0.0036	17.5	0.0229	22.5	0.0042
7.6	0.0204	12.6	-0.0003	17.6	0.0253		
7.7	0.0216	12.7	-0.0043	17.7	0.0273		
7.8	0.0228	12.8	-0.0084	17.8	0.0290		
7.9	0.0241	12.9	-0.0124	17.9	0.0302		

Note: The entries are correct to within three units in the fourth decimal place.

TABLE 1A (Continued)

t'	$G_0(15,0,t')$	t'	$G_0(15,0,t')$	t'	$G_0(15,0,t')$	t'	$G_0(15,0,t')$	t'	$G_0(15,0,t')$
8.0	0.0004	12.5	0.0148	17.0	0.0226	21.5	-0.0357	26.0	-0.0073
8.1	0.0004	12.6	0.0156	17.1	0.0208	21.6	-0.0333	26.1	-0.0099
8.2	0.0005	12.7	0.0164	17.2	0.0189	21.7	-0.0308	26.2	-0.0124
8.3	0.0006	12.8	0.0172	17.3	0.0169	21.8	-0.0280	26.3	-0.0148
8.4	0.0007	12.9	0.0180	17.4	0.0148	21.9	-0.0252	26.4	-0.0170
8.5	0.0007	13.0	0.0189	17.5	0.0126	22.0	-0.0222	26.5	-0.0190
8.6	0.0008	13.1	0.0197	17.6	0.0103	22.1	-0.0192	26.6	-0.0209
8.7	0.0009	13.2	0.0206	17.7	0.0079	22.2	-0.0160	26.7	-0.0224
8.8	0.0010	13.3	0.0214	17.8	0.0055	22.3	-0.0128	26.8	-0.0238
8.9	0.0011	13.4	0.0223	17.9	0.0030	22.4	-0.0096	26.9	-0.0249
9.0	0.0012	13.5	0.0232	18.0	+0.0004	22.5	-0.0064	27.0	-0.0257
9.1	0.0013	13.6	0.0241	18.1	-0.0023	22.6	-0.0032	27.1	-0.0263
9.2	0.0014	13.7	0.0249	18.2	-0.0050	22.7	-0.0001	27.2	-0.0265
9.3	0.0015	13.8	0.0258	18.3	-0.0077	22.8	+0.0030	27.3	-0.0265
9.4	0.0017	13.9	0.0266	18.4	-0.0105	22.9	0.0060	27.4	-0.0262
9.5	0.0018	14.0	0.0275	18.5	-0.0132	23.0	0.0088	27.5	-0.0256
9.6	0.0021	14.1	0.0283	18.6	-0.0160	23.1	0.0115	27.6	-0.0248
9.7	0.0022	14.2	0.0291	18.7	-0.0187	23.2	0.0141	27.7	-0.0237
9.8	0.0024	14.3	0.0298	18.8	-0.0214	23.3	0.0165	27.8	-0.0224
9.9	0.0026	14.4	0.0306	18.9	-0.0240	23.4	0.0187	27.9	-0.0208
10.0	0.0029	14.5	0.0312	19.0	-0.0267	23.5	0.0207	28.0	-0.0190
10.1	0.0031	14.6	0.0319	19.1	-0.0291	23.6	0.0224	28.1	-0.0171
10.2	0.0034	14.7	0.0325	19.2	-0.0315	23.7	0.0239	28.2	-0.0150
10.3	0.0036	14.8	0.0331	19.3	-0.0337	23.8	0.0252	28.3	-0.0127
10.4	0.0039	14.9	0.0335	19.4	-0.0360	23.9	0.0262	28.4	-0.0103
10.5	0.0042	15.0	0.0340	19.5	-0.0379	24.0	0.0269	28.5	-0.0079
10.6	0.0046	15.1	0.0343	19.6	-0.0399	24.1	0.0273	28.6	-0.0054
10.7	0.0049	15.2	0.0346	19.7	-0.0415	24.2	0.0274	28.7	-0.0029
10.8	0.0053	15.3	0.0347	19.8	-0.0431	24.3	0.0272	28.8	-0.0005
10.9	0.0056	15.4	0.0349	19.9	-0.0444	24.4	0.0267	28.9	+0.0019
11.0	0.0060	15.5	0.0349	20.0	-0.0457	24.5	0.0260	29.1	0.0041
11.1	0.0064	15.6	0.0349	20.1	-0.0466	24.6	0.0250		
11.2	0.0069	15.7	0.0347	20.2	-0.0475	24.7	0.0236		
11.3	0.0074	15.8	0.0346	20.3	-0.0479	24.8	0.0220		
11.4	0.0079	15.9	0.0342	20.4	-0.0484	24.9	0.0206		
11.5	0.0084	16.0	0.0338	20.5	-0.0484	25.0	0.0186		
11.6	0.0089	16.1	0.0332	20.6	-0.0483	25.1	0.0165		
11.7	0.0095	16.2	0.0325	20.7	-0.0477	25.2	0.0142		
11.8	0.0101	16.3	0.0316	20.8	-0.0471	25.3	0.0117		
11.9	0.0107	16.4	0.0307	20.9	-0.0460	25.4	0.0091		
12.0	0.0113	16.5	0.0296	21.0	-0.0448	25.5	0.0064		
12.1	0.0120	16.6	0.0285	21.1	-0.0434	25.6	0.0036		
12.2	0.0127	16.7	0.0272	21.2	-0.0418	25.7	+0.0006		
12.3	0.0134	16.8	0.0258	21.3	-0.0400	25.8	-0.0020		
12.4	0.0141	16.9	0.0242	21.4	-0.0379	25.9	-0.0047		

Note: The entries are correct to within three units in the fourth decimal place.

TABLE 1A (Continued)

t'	$Q_0(25,0,t')$	t'	$Q_0(25,0,t')$	t'	$Q_0(25,0,t')$	t'	$Q_0(25,0,t')$	t'	$Q_0(25,0,t')$
18.0	0.0008	23.0	0.0133	28.0	0.0087	33.0	-0.0188	38.0	-0.0083
18.1	0.0008	23.1	0.0136	28.1	0.0074	33.1	-0.0190	38.1	-0.0099
18.2	0.0009	23.2	0.0143	28.2	0.0061	33.2	-0.0152	38.2	-0.0115
18.3	0.0009	23.3	0.0147	28.3	0.0047	33.3	-0.0133	38.3	-0.0130
18.4	0.0009	23.4	0.0152	28.4	0.0033	33.4	-0.0115	38.4	-0.0143
18.5	0.0009	23.5	0.0156	28.5	0.0018	33.5	-0.0095	38.5	-0.0155
18.6	0.0010	23.6	0.0161	28.6	+0.0003	33.6	-0.0076	38.6	-0.0167
18.7	0.0011	23.7	0.0165	28.7	-0.0013	33.7	-0.0055	38.7	-0.0177
18.8	0.0012	23.8	0.0169	28.8	-0.0028	33.8	-0.0035	38.8	-0.0186
18.9	0.0012	23.9	0.0173	28.9	-0.0044	33.9	-0.0015	38.9	-0.0194
19.0	0.0013	24.0	0.0177	29.0	-0.0060	34.0	+0.0005	39.0	-0.0200
19.1	0.0014	24.1	0.0181	29.1	-0.0075	34.1	0.0024	39.1	-0.0204
19.2	0.0016	24.2	0.0185	29.2	-0.0091	34.2	0.0043	39.2	-0.0207
19.3	0.0017	24.3	0.0189	29.3	-0.0107	34.3	0.0060	39.3	-0.0207
19.4	0.0019	24.4	0.0193	29.4	-0.0123	34.4	0.0078	39.4	-0.0206
19.5	0.0020	24.5	0.0196	29.5	-0.0138	34.5	0.0095	39.5	-0.0203
19.6	0.0022	24.6	0.0200	29.6	-0.0153	34.6	0.0112	39.6	-0.0199
19.7	0.0023	24.7	0.0203	29.7	-0.0168	34.7	0.0126	39.7	-0.0193
19.8	0.0025	24.8	0.0207	29.8	-0.0183	34.8	0.0141	39.8	-0.0185
19.9	0.0027	24.9	0.0210	29.9	-0.0197	34.9	0.0153	39.9	-0.0176
20.0	0.0029	25.0	0.0213	30.0	-0.0211	35.0	0.0166	40.0	-0.0166
20.1	0.0031	25.1	0.0215	30.1	-0.0224	35.1	0.0176	40.1	-0.0154
20.2	0.0034	25.2	0.0217	30.2	-0.0237	35.2	0.0185	40.2	-0.0143
20.3	0.0036	25.3	0.0218	30.3	-0.0248	35.3	0.0191	40.3	-0.0127
20.4	0.0038	25.4	0.0219	30.4	-0.0259	35.4	0.0198	40.4	-0.0112
20.5	0.0040	25.5	0.0219	30.5	-0.0269	35.5	0.0202	40.5	-0.0096
20.6	0.0043	25.6	0.0220	30.6	-0.0279	35.6	0.0206	40.6	-0.0079
20.7	0.0045	25.7	0.0220	30.7	-0.0287	35.7	0.0206	40.7	-0.0061
20.8	0.0048	25.8	0.0220	30.8	-0.0296	35.8	0.0207	40.8	-0.0043
20.9	0.0051	25.9	0.0219	30.9	-0.0302	35.9	0.0204	40.9	-0.0025
21.0	0.0054	26.0	0.0218	31.0	-0.0308	36.0	0.0202	41.0	-0.0007
21.1	0.0056	26.1	0.0216	31.1	-0.0312	36.1	0.0196	41.1	+0.0010
21.2	0.0059	26.2	0.0215	31.2	-0.0317	36.2	0.0191	41.2	0.0027
21.3	0.0062	26.3	0.0212	31.3	-0.0319	36.3	0.0182	41.3	0.0044
21.4	0.0065	26.4	0.0210	31.4	-0.0322	36.4	0.0174	41.4	0.0059
21.5	0.0068	26.5	0.0206	31.5	-0.0322	36.5	0.0162	41.5	0.0074
21.6	0.0071	26.6	0.0203	31.6	-0.0322	36.6	0.0151		
21.7	0.0074	26.7	0.0199	31.7	-0.0320	36.7	0.0137		
21.8	0.0077	26.8	0.0195	31.8	-0.0317	36.8	0.0124		
21.9	0.0080	26.9	0.0189	31.9	-0.0312	36.9	0.0108		
22.0	0.0084	27.0	0.0184	32.0	-0.0308	37.0	0.0093		
22.1	0.0088	27.1	0.0177	32.1	-0.0300	37.1	0.0076		
22.2	0.0093	27.2	0.0170	32.2	-0.0293	37.2	0.0059		
22.3	0.0097	27.3	0.0161	32.3	-0.0283	37.3	0.0041		
22.4	0.0102	27.4	0.0153	32.4	-0.0273	37.4	0.0023		
22.5	0.0107	27.5	0.0143	32.5	-0.0261	37.5	+0.0005		
22.6	0.0112	27.6	0.0133	32.6	-0.0249	37.6	-0.0014		
22.7	0.0117	27.7	0.0122	32.7	-0.0234	37.7	-0.0031		
22.8	0.0123	27.8	0.0112	32.8	-0.0220	37.8	-0.0049		
22.9	0.0128	27.9	0.0100	32.9	-0.0204	37.9	-0.0066		

Note: The entries are correct to within three units in the fourth decimal place.

TABLE 1A (Continued)

t'	$G_0(50,0,t')$	t'	$G_0(50,0,t')$	t'	$G_0(50,0,t')$	t'	$G_0(50,0,t')$
40.0	0.0001	44.0	0.0016	48.0	0.0079	52.0	0.0111
40.1	0.0001	44.1	0.0016	48.1	0.0075	52.1	0.0110
40.2	0.0002	44.2	0.0017	48.2	0.0077	52.2	0.0108
40.3	0.0002	44.3	0.0018	48.3	0.0079	52.3	0.0106
40.4	0.0002	44.4	0.0019	48.4	0.0082	52.4	0.0104
40.5	0.0002	44.5	0.0020	48.5	0.0084	52.5	0.0102
40.6	0.0002	44.6	0.0021	48.6	0.0086	52.6	0.0099
40.7	0.0002	44.7	0.0022	48.7	0.0088	52.7	0.0096
40.8	0.0003	44.8	0.0023	48.8	0.0090	52.8	0.0093
40.9	0.0003	44.9	0.0024	48.9	0.0092	52.9	0.0090
41.0	0.0003	45.0	0.0025	49.0	0.0094	53.0	0.0086
41.1	0.0003	45.1	0.0026	49.1	0.0095	53.1	0.0082
41.2	0.0004	45.2	0.0027	49.2	0.0097	53.2	0.0078
41.3	0.0004	45.3	0.0028	49.3	0.0099	53.3	0.0074
41.4	0.0004	45.4	0.0030	49.4	0.0101	53.4	0.0069
41.5	0.0004	45.5	0.0031	49.5	0.0102	53.5	0.0065
41.6	0.0005	45.6	0.0032	49.6	0.0104	53.6	0.0060
41.7	0.0005	45.7	0.0033	49.7	0.0105	53.7	0.0055
41.8	0.0005	45.8	0.0035	49.8	0.0107	53.8	0.0049
41.9	0.0005	45.9	0.0036	49.9	0.0108	53.9	0.0044
42.0	0.0006	46.0	0.0038	50.0	0.0110	54.0	0.0038
42.1	0.0006	46.1	0.0039	50.1	0.0111	54.1	0.0033
42.2	0.0006	46.2	0.0041	50.2	0.0112	54.2	0.0027
42.3	0.0006	46.3	0.0042	50.3	0.0113	54.3	0.0021
42.4	0.0007	46.4	0.0044	50.4	0.0114	54.4	0.0014
42.5	0.0007	46.5	0.0046	50.5	0.0115	54.5	0.0008
42.6	0.0008	46.6	0.0048	50.6	0.0116	54.6	+0.0001
42.7	0.0008	46.7	0.0049	50.7	0.0116	54.7	+0.0006
42.8	0.0008	46.8	0.0051	50.8	0.0117	54.8	+0.0012
42.9	0.0008	46.9	0.0053	50.9	0.0117	54.9	+0.0019
43.0	0.0009	47.0	0.0055	51.0	0.0117	55.0	-0.0026
43.1	0.0009	47.1	0.0056	51.1	0.0117	55.1	-0.0032
43.2	0.0010	47.2	0.0058	51.2	0.0117	55.2	-0.0039
43.3	0.0011	47.3	0.0060	51.3	0.0117	55.3	-0.0046
43.4	0.0012	47.4	0.0062	51.4	0.0117	55.4	-0.0053
43.5	0.0012	47.5	0.0064	51.5	0.0117	55.5	-0.0060
43.6	0.0013	47.6	0.0066	51.6	0.0116	55.6	-0.0067
43.7	0.0013	47.7	0.0067	51.7	0.0115	55.7	-0.0074
43.8	0.0014	47.8	0.0069	51.8	0.0114	55.8	-0.0081
43.9	0.0015	47.9	0.0071	51.9	0.0113	55.9	-0.0087

TABLE 1A (Continued)

t'	$G_0(50,0,t')$	t'	$G_0(50,0,t')$	t'	$G_0(50,0,t')$	t'	$G_0(50,0,t')$
56.0	-0.0094	59.5	-0.0138	63.0	0.0126	66.5	-0.0085
56.1	-0.0100	59.6	-0.0131	63.1	0.0128	66.6	-0.0092
56.2	-0.0107	59.7	-0.0124	63.2	0.0129	66.7	-0.0099
56.3	-0.0113	59.8	-0.0117	63.3	0.0129	66.8	-0.0105
56.4	-0.0120	59.9	-0.0110	63.4	0.0130	66.9	-0.0111
56.5	-0.0126	60.0	-0.0102	63.5	0.0129	67.0	-0.0116
56.6	-0.0132	60.1	-0.0094	63.6	0.0128	67.1	-0.0120
56.7	-0.0137	60.2	-0.0086	63.7	0.0126	67.2	-0.0124
56.8	-0.0142	60.3	-0.0078	63.8	0.0124	67.3	-0.0127
56.9	-0.0147	60.4	-0.0069	63.9	0.0121	67.4	-0.0129
57.0	-0.0152	60.5	-0.0060	64.0	0.0117	67.5	-0.0131
57.1	-0.0156	60.6	-0.0051	64.1	0.0113	67.6	-0.0132
57.2	-0.0161	60.7	-0.0042	64.2	0.0108	67.7	-0.0132
57.3	-0.0165	60.8	-0.0032	64.3	0.0102	67.8	-0.0132
57.4	-0.0168	60.9	-0.0023	64.4	0.0096	67.9	-0.0131
57.5	-0.0171	61.0	-0.0013	64.5	0.0089	68.0	-0.0129
57.6	-0.0174	61.1	-0.0004	64.6	0.0082	68.1	-0.0128
57.7	-0.0176	61.2	+0.0005	64.7	0.0075	68.2	-0.0123
57.8	-0.0178	61.3	0.0014	64.8	0.0067	68.3	-0.0119
57.9	-0.0179	61.4	0.0024	64.9	0.0059	68.4	-0.0114
58.0	-0.0180	61.5	0.0033	65.0	0.0050	68.5	-0.0109
58.1	-0.0180	61.6	0.0041	65.1	0.0041	68.6	-0.0103
58.2	-0.0181	61.7	0.0050	65.2	0.0032	68.7	-0.0096
58.3	-0.0180	61.8	0.0058	65.3	0.0023	68.8	-0.0089
58.4	-0.0179	61.9	0.0066	65.4	+0.0013	68.9	-0.0081
58.5	-0.0178	62.0	0.0074	65.5	0.0004	69.0	-0.0073
58.6	-0.0176	62.1	0.0081	65.6	-0.0006	69.1	-0.0065
58.7	-0.0174	62.2	0.0088	65.7	-0.0015	69.2	-0.0056
58.8	-0.0171	62.3	0.0094	65.8	-0.0025	69.3	-0.0047
58.9	-0.0168	62.4	0.0100	65.9	-0.0034	69.4	-0.0038
59.0	-0.0164	62.5	0.0106	66.0	-0.0043	69.5	-0.0028
59.1	-0.0160	62.6	0.0111	66.1	-0.0052	69.6	-0.0018
59.2	-0.0155	62.7	0.0115	66.2	-0.0061	69.7	-0.0009
59.3	-0.0150	62.8	0.0119	66.3	-0.0069	69.8	+0.0001
59.4	-0.0144	62.9	0.0123	66.4	-0.0077	69.9	0.0011

Note: The entries are correct to within three units in the fourth decimal place.

TABLE 1A (Continued)

t'	$G_0(500,0,t')$	t'	$G_0(500,0,t')$	t'	$G_0(500,0,t')$	t'	$G_0(500,0,t')$
477.0	0.00000	482.0	0.00004	487.0	0.00014	492.0	0.00041
477.1	0.00000	482.1	0.00004	487.1	0.00015	492.1	0.00041
477.2	0.00001	482.2	0.00004	487.2	0.00015	492.2	0.00042
477.3	0.00001	482.3	0.00005	487.3	0.00015	492.3	0.00043
477.4	0.00001	482.4	0.00005	487.4	0.00016	492.4	0.00043
477.5	0.00001	482.5	0.00005	487.5	0.00016	492.5	0.00044
477.6	0.00001	482.6	0.00005	487.6	0.00016	492.6	0.00045
477.7	0.00001	482.7	0.00005	487.7	0.00017	492.7	0.00046
477.8	0.00001	482.8	0.00005	487.8	0.00017	492.8	0.00046
477.9	0.00001	482.9	0.00005	487.9	0.00018	492.9	0.00047
478.0	0.00001	483.0	0.00006	488.0	0.00018	493.0	0.00048
478.1	0.00001	483.1	0.00006	488.1	0.00018	493.1	0.00049
478.2	0.00001	483.2	0.00006	488.2	0.00019	493.2	0.00049
478.3	0.00001	483.3	0.00006	488.3	0.00019	493.3	0.00050
478.4	0.00001	483.4	0.00006	488.4	0.00020	493.4	0.00051
478.5	0.00002	483.5	0.00006	488.5	0.00020	493.5	0.00052
478.6	0.00002	483.6	0.00007	488.6	0.00021	493.6	0.00052
478.7	0.00002	483.7	0.00007	488.7	0.00021	493.7	0.00053
478.8	0.00002	483.8	0.00007	488.8	0.00022	493.8	0.00054
478.9	0.00002	483.9	0.00007	488.9	0.00022	493.9	0.00055
479.0	0.00002	484.0	0.00007	489.0	0.00023	494.0	0.00056
479.1	0.00002	484.1	0.00007	489.1	0.00023	494.1	0.00057
479.2	0.00002	484.2	0.00008	489.2	0.00024	494.2	0.00058
479.3	0.00002	484.3	0.00008	489.3	0.00024	494.3	0.00059
479.4	0.00002	484.4	0.00008	489.4	0.00025	494.4	0.00060
479.5	0.00002	484.5	0.00008	489.5	0.00025	494.5	0.00061
479.6	0.00002	484.6	0.00008	489.6	0.00026	494.6	0.00062
479.7	0.00003	484.7	0.00008	489.7	0.00026	494.7	0.00063
479.8	0.00003	484.8	0.00009	489.8	0.00027	494.8	0.00064
479.9	0.00003	484.9	0.00009	489.9	0.00027	494.9	0.00065
480.0	0.00003	485.0	0.00009	490.0	0.00028	495.0	0.00066
480.1	0.00003	485.1	0.00009	490.1	0.00029	495.1	0.00067
480.2	0.00003	485.2	0.00009	490.2	0.00029	495.2	0.00068
480.3	0.00003	485.3	0.00009	490.3	0.00030	495.3	0.00069
480.4	0.00003	485.4	0.00010	490.4	0.00030	495.4	0.00070
480.5	0.00003	485.5	0.00010	490.5	0.00031	495.5	0.00071
480.6	0.00003	485.6	0.00010	490.6	0.00031	495.6	0.00072
480.7	0.00003	485.7	0.00010	490.7	0.00032	495.7	0.00073
480.8	0.00003	485.8	0.00010	490.8	0.00033	495.8	0.00074
480.9	0.00003	485.9	0.00011	490.9	0.00033	495.9	0.00075
481.0	0.00003	486.0	0.00011	491.0	0.00034	496.0	0.00076
481.1	0.00003	486.1	0.00011	491.1	0.00035	496.1	0.00077
481.2	0.00003	486.2	0.00011	491.2	0.00035	496.2	0.00078
481.3	0.00003	486.3	0.00012	491.3	0.00036	496.3	0.00079
481.4	0.00003	486.4	0.00012	491.4	0.00037	496.4	0.00080
481.5	0.00004	486.5	0.00012	491.5	0.00037	496.5	0.00081
481.6	0.00004	486.6	0.00013	491.6	0.00038	496.6	0.00082
481.7	0.00004	486.7	0.00013	491.7	0.00039	496.7	0.00083
481.8	0.00004	486.8	0.00013	491.8	0.00039	496.8	0.00084
481.9	0.00004	486.9	0.00014	491.9	0.00040	496.9	0.00085

TABLE 1A (Continued)

t'	$\theta_0(500,0,t')$	t'	$\theta_0(500,0,t')$	t'	$\theta_0(500,0,t')$	t'	$\theta_0(500,0,t')$
497.0	0.00086	502.0	0.00126	507.0	0.00089	512.0	-0.00069
497.1	0.00087	502.1	0.00126	507.1	0.00087	512.1	-0.00073
497.2	0.00088	502.2	0.00126	507.2	0.00085	512.2	-0.00077
497.3	0.00090	502.3	0.00126	507.3	0.00083	512.3	-0.00081
497.4	0.00091	502.4	0.00127	507.4	0.00081	512.4	-0.00084
497.5	0.00092	502.5	0.00127	507.5	0.00078	512.5	-0.00088
497.6	0.00093	502.6	0.00127	507.6	0.00076	512.6	-0.00092
497.7	0.00094	502.7	0.00127	507.7	0.00074	512.7	-0.00095
497.8	0.00095	502.8	0.00127	507.8	0.00072	512.8	-0.00099
497.9	0.00096	502.9	0.00127	507.9	0.00069	512.9	-0.00103
498.0	0.00097	503.0	0.00127	508.0	0.00067	513.0	-0.00107
498.1	0.00098	503.1	0.00127	508.1	0.00064	513.1	-0.00110
498.2	0.00099	503.2	0.00128	508.2	0.00062	513.2	-0.00114
498.3	0.00100	503.3	0.00128	508.3	0.00059	513.3	-0.00117
498.4	0.00101	503.4	0.00128	508.4	0.00056	513.4	-0.00121
498.5	0.00102	503.5	0.00127	508.5	0.00053	513.5	-0.00125
498.6	0.00103	503.6	0.00127	508.6	0.00051	513.6	-0.00128
498.7	0.00104	503.7	0.00127	508.7	0.00048	513.7	-0.00132
498.8	0.00105	503.8	0.00127	508.8	0.00045	513.8	-0.00135
498.9	0.00106	503.9	0.00127	508.9	0.00042	513.9	-0.00139
499.0	0.00107	504.0	0.00126	509.0	0.00039	514.0	-0.00142
499.1	0.00108	504.1	0.00126	509.1	0.00036	514.1	-0.00145
499.2	0.00108	504.2	0.00126	509.2	0.00033	514.2	-0.00149
499.3	0.00109	504.3	0.00125	509.3	0.00029	514.3	-0.00152
499.4	0.00110	504.4	0.00125	509.4	0.00026	514.4	-0.00155
499.5	0.00111	504.5	0.00124	509.5	0.00023	514.5	-0.00158
499.6	0.00112	504.6	0.00123	509.6	0.00020	514.6	-0.00161
499.7	0.00112	504.7	0.00123	509.7	0.00017	514.7	-0.00164
499.8	0.00113	504.8	0.00122	509.8	0.00014	514.8	-0.00167
499.9	0.00114	504.9	0.00121	509.9	0.00011	514.9	-0.00170
500.0	0.00115	505.0	0.00120	510.0	0.00007	515.0	-0.00173
500.1	0.00115	505.1	0.00119	510.1	+0.00003	515.1	-0.00176
500.2	0.00116	505.2	0.00118	510.2	-0.00001	515.2	-0.00178
500.3	0.00117	505.3	0.00117	510.3	-0.00004	515.3	-0.00181
500.4	0.00118	505.4	0.00116	510.4	-0.00008	515.4	-0.00184
500.5	0.00118	505.5	0.00114	510.5	-0.00012	515.5	-0.00186
500.6	0.00119	505.6	0.00113	510.6	-0.00016	515.6	-0.00188
500.7	0.00120	505.7	0.00112	510.7	-0.00020	515.7	-0.00191
500.8	0.00120	505.8	0.00110	510.8	-0.00023	515.8	-0.00193
500.9	0.00121	505.9	0.00109	510.9	-0.00027	515.9	-0.00195
501.0	0.00121	506.0	0.00107	511.0	-0.00031	516.0	-0.00197
501.1	0.00122	506.1	0.00106	511.1	-0.00035	516.1	-0.00199
501.2	0.00122	506.2	0.00104	511.2	-0.00038	516.2	-0.00200
501.3	0.00123	506.3	0.00102	511.3	-0.00042	516.3	-0.00202
501.4	0.00123	406.4	0.00101	511.4	-0.00046	516.4	-0.00203
501.5	0.00124	506.5	0.00099	511.5	-0.00050	516.5	-0.00205
501.6	0.00124	506.6	0.00097	511.6	-0.00054	516.6	-0.00206
501.7	0.00125	506.7	0.00095	511.7	-0.00057	516.7	-0.00206
501.8	0.00125	506.8	0.00093	511.8	-0.00061	516.8	-0.00207
501.9	0.00125	506.9	0.00091	511.9	-0.00065	516.9	-0.00208

TABLE 1A (Continued)

t'	$G_Q(500,0,t')$	t'	$G_Q(500,0,t')$	t'	$G_Q(500,0,t')$	t'	$G_Q(500,0,t')$
517.0	-0.00209	521.0	-0.00133	525.0	0.00082	529.0	0.00170
517.1	-0.00209	521.1	-0.00129	525.1	0.00087	529.1	0.00169
517.2	-0.00210	521.2	-0.00124	525.2	0.00092	529.2	0.00167
517.3	-0.00211	521.3	-0.00120	525.3	0.00097	529.3	0.00165
517.4	-0.00211	521.4	-0.00115	525.4	0.00102	529.4	0.00162
517.5	-0.00211	521.5	-0.00110	525.5	0.00107	529.5	0.00160
517.6	-0.00211	521.6	-0.00105	525.6	0.00112	529.6	0.00157
517.7	-0.00211	521.7	-0.00100	525.7	0.00117	529.7	0.00154
517.8	-0.00210	521.8	-0.00095	525.8	0.00121	529.8	0.00151
517.9	-0.00210	521.9	-0.00090	525.9	0.00126	529.9	0.00148
518.0	-0.00209	522.0	-0.00084	526.0	0.00130	530.0	0.00145
518.1	-0.00209	522.1	-0.00079	526.1	0.00134	530.1	0.00141
518.2	-0.00208	522.2	-0.00073	526.2	0.00137	530.2	0.00137
518.3	-0.00207	522.3	-0.00068	526.3	0.00141	530.3	0.00134
518.4	-0.00206	522.4	-0.00062	526.4	0.00145	530.4	0.00130
518.5	-0.00205	522.5	-0.00057	526.5	0.00148	530.5	0.00125
518.6	-0.00204	522.6	-0.00052	526.6	0.00151	530.6	0.00121
518.7	-0.00202	522.7	-0.00046	526.7	0.00154	530.7	0.00116
518.8	-0.00201	522.8	-0.00041	526.8	0.00157	530.8	0.00112
518.9	-0.00199	522.9	-0.00035	526.9	0.00160	530.9	0.00107
519.0	-0.00197	523.0	-0.00030	527.0	0.00162	531.0	0.00102
519.1	-0.00195	523.1	-0.00024	527.1	0.00165	531.1	0.00097
519.2	-0.00193	523.2	-0.00018	527.2	0.00167	531.2	0.00092
519.3	-0.00191	523.3	-0.00012	527.3	0.00169	531.3	0.00086
519.4	-0.00189	523.4	-0.00007	527.4	0.00171	531.4	0.00081
519.5	-0.00186	523.5	-0.00001	527.5	0.00172	531.5	0.00075
519.6	-0.00183	523.6	+0.00005	527.6	0.00173	531.6	0.00069
519.7	-0.00181	523.7	0.00011	527.7	0.00174	531.7	0.00063
519.8	-0.00178	523.8	0.00016	527.8	0.00175	531.8	0.00057
519.9	-0.00175	523.9	0.00022	527.9	0.00176	531.9	0.00051
520.0	-0.00171	524.0	0.00028	528.0	0.00176	532.0	0.00045
520.1	-0.00168	524.1	0.00033	528.1	0.00177	532.1	0.00038
520.2	-0.00165	524.2	0.00039	528.2	0.00177	532.2	0.00032
520.3	-0.00161	524.3	0.00045	528.3	0.00177	532.3	0.00026
520.4	-0.00158	524.4	0.00050	528.4	0.00176	532.4	0.00019
520.5	-0.00154	524.5	0.00056	528.5	0.00176	532.5	0.00013
520.6	-0.00150	524.6	0.00061	528.6	0.00175		
520.7	-0.00146	524.7	0.00066	528.7	0.00174		
520.8	-0.00142	524.8	0.00071	528.8	0.00173		
520.9	-0.00138	524.9	0.00077	528.9	0.00172		

Note: The entries are correct to within three units in the fifth decimal place.

TABLE 19

t'	$G_0(5,1,t')$	t'	$G_0(5,1,t')$	t'	$G_0(5,1,t')$	t'	$G_0(5,1,t')$
0.0	0.0005	4.0	0.0714	8.0	-0.1088	12.0	0.0997
0.1	0.0006	4.1	0.0756	8.1	-0.1200	12.1	0.0908
0.2	0.0006	4.2	0.0798	8.2	-0.1305	12.2	0.0800
0.3	0.0007	4.3	0.0840	8.3	-0.1400	12.3	0.0678
0.4	0.0008	4.4	0.0880	8.4	-0.1483	12.4	0.0542
0.5	0.0010	4.5	0.0919	8.5	-0.1555	12.5	0.0396
0.6	0.0012	4.6	0.0956	8.6	-0.1613	12.6	0.0243
0.7	0.0014	4.7	0.0991	8.7	-0.1658	12.7	+0.0084
0.8	0.0017	4.8	0.1023	8.8	-0.1686	12.8	-0.0075
0.9	0.0021	4.9	0.1052	8.9	-0.1699	12.9	-0.0234
1.0	0.0025	5.0	0.1077	9.0	-0.1696	13.0	-0.0387
1.1	0.0030	5.1	0.1098	9.1	-0.1676	13.1	-0.0532
1.2	0.0035	5.2	0.1114	9.2	-0.1638	13.2	-0.0667
1.3	0.0042	5.3	0.1125	9.3	-0.1584	13.3	-0.0788
1.4	0.0049	5.4	0.1130	9.4	-0.1514	13.4	-0.0892
1.5	0.0057	5.5	0.1129	9.5	-0.1427	13.5	-0.0978
1.6	0.0066	5.6	0.1121	9.6	-0.1325	13.6	-0.1044
1.7	0.0076	5.7	0.1106	9.7	-0.1208	13.7	-0.1088
1.8	0.0087	5.8	0.1084	9.8	-0.1079	13.8	-0.1109
1.9	0.0100	5.9	0.1054	9.9	-0.0939	13.9	-0.1108
2.0	0.0113	6.0	0.1016	10.0	-0.0789	14.0	-0.1083
2.1	0.0128	6.1	0.0970	10.1	-0.0631	14.1	-0.1036
2.2	0.0145	6.2	0.0915	10.2	-0.0467	14.2	-0.0968
2.3	0.0163	6.3	0.0852	10.3	-0.0300	14.3	-0.0880
2.4	0.0182	6.4	0.0780	10.4	-0.0131	14.4	-0.0775
2.5	0.0204	6.5	0.0700	10.5	+0.0037	14.5	-0.0655
2.6	0.0227	6.6	0.0613	10.6	0.0201	14.6	-0.0522
2.7	0.0251	6.7	0.0518	10.7	0.0358	14.7	-0.0381
2.8	0.0278	6.8	0.0415	10.8	0.0508	14.8	-0.0234
2.9	0.0306	6.9	0.0305	10.9	0.0646	14.9	-0.0086
3.0	0.0336	7.0	0.0189	11.0	0.0772	15.0	+0.0062
3.1	0.0368	7.1	+0.0068	11.1	0.0883	15.1	0.0204
3.2	0.0401	7.2	-0.0058	11.2	0.0976	15.2	0.0337
3.3	0.0436	7.3	-0.0186	11.3	0.1052	15.3	0.0458
3.4	0.0472	7.4	-0.0318	11.4	0.1107	15.4	0.0566
3.5	0.0510	7.5	-0.0450	11.5	0.1143		
3.6	0.0549	7.6	-0.0583	11.6	0.1156		
3.7	0.0589	7.7	-0.0714	11.7	0.1148		
3.8	0.0630	7.8	-0.0843	11.8	0.1119		
3.9	0.0672	7.9	-0.0968	11.9	0.1068		

Note: The entries are correct to within three units in the fourth decimal place.

TABLE 1B (Continued)

t'	$G_0(10,1,t')$	t'	$G_0(10,1,t')$	t'	$G_0(10,1,t')$	t'	$G_0(10,1,t')$	t'	$G_0(10,1,t')$
2.5	0.0000	7.0	0.0112	11.5	0.0504	16.0	-0.0560	20.5	-0.0646
2.6	0.0000	7.1	0.0121	11.6	0.0480	16.1	-0.0493	20.6	-0.0678
2.7	0.0001	7.2	0.0131	11.7	0.0452	16.2	-0.0423	20.7	-0.0700
2.8	0.0001	7.3	0.0142	11.8	0.0422	16.3	-0.0349	20.8	-0.0713
2.9	0.0001	7.4	0.0153	11.9	0.0389	16.4	-0.0273	20.9	-0.0715
3.0	0.0001	7.5	0.0164	12.0	0.0353	16.5	-0.0195	21.0	-0.0708
3.1	0.0001	7.6	0.0177	12.1	0.0314	16.6	-0.0116	21.1	-0.0690
3.2	0.0001	7.7	0.0189	12.2	0.0272	16.7	-0.0037	21.2	-0.0663
3.3	0.0002	7.8	0.0203	12.3	0.0227	16.8	+0.0042	21.3	-0.0627
3.4	0.0002	7.9	0.0217	12.4	0.0180	16.9	0.0120	21.4	-0.0581
3.5	0.0002	8.0	0.0231	12.5	0.0131	17.0	0.0196	21.5	-0.0528
3.6	0.0003	8.1	0.0246	12.6	0.0079	17.1	0.0269	21.6	-0.0466
3.7	0.0003	8.2	0.0261	12.7	+0.0026	17.2	0.0339	21.7	-0.0399
3.8	0.0003	8.3	0.0277	12.8	-0.0030	17.3	0.0404	21.8	-0.0325
3.9	0.0004	8.4	0.0293	12.9	-0.0086	17.4	0.0464	21.9	-0.0248
4.0	0.0004	8.5	0.0310	13.0	-0.0144	17.5	0.0519	22.0	-0.0167
4.1	0.0005	8.6	0.0327	13.1	-0.0203	17.6	0.0567	22.1	-0.0084
4.2	0.0006	8.7	0.0344	13.2	-0.0262	17.7	0.0608	22.2	-0.0001
4.3	0.0007	8.8	0.0361	13.3	-0.0321	17.8	0.0642	22.3	+0.0082
4.4	0.0007	8.9	0.0379	13.4	-0.0379	17.9	0.0667	22.4	0.0162
4.5	0.0008	9.0	0.0396	13.5	-0.0437	18.0	0.0685	22.5	0.0239
4.6	0.0010	9.1	0.0414	13.6	-0.0494	18.1	0.0694	22.6	0.0312
4.7	0.0011	9.2	0.0431	13.7	-0.0549	18.2	0.0694	22.7	0.0378
4.8	0.0012	9.3	0.0448	13.8	-0.0602	18.3	0.0686	22.8	0.0438
4.9	0.0014	9.4	0.0465	13.9	-0.0653	18.4	0.0669	22.9	0.0489
5.0	0.0015	9.5	0.0482	14.0	-0.0700	18.5	0.0643	23.0	0.0532
5.1	0.0017	9.6	0.0497	14.1	-0.0744	18.6	0.0609		
5.2	0.0020	9.7	0.0512	14.2	-0.0785	18.7	0.0567		
5.3	0.0022	9.8	0.0527	14.3	-0.0821	18.8	0.0518		
5.4	0.0024	9.9	0.0540	14.4	-0.0853	18.9	0.0462		
5.5	0.0027	10.0	0.0553	14.5	-0.0879	19.0	0.0399		
5.6	0.0030	10.1	0.0563	14.6	-0.0901	19.1	0.0331		
5.7	0.0034	10.2	0.0572	14.7	-0.0916	19.2	0.0259		
5.8	0.0037	10.3	0.0580	14.8	-0.0926	19.3	0.0182		
5.9	0.0041	10.4	0.0586	14.9	-0.0930	19.4	0.0103		
6.0	0.0046	10.5	0.0591	15.0	-0.0928	19.5	+0.0022		
6.1	0.0050	10.6	0.0593	15.1	-0.0919	19.6	-0.0059		
6.2	0.0055	10.7	0.0593	15.2	-0.0903	19.7	-0.0140		
6.3	0.0061	10.8	0.0591	15.3	-0.0882	19.8	-0.0220		
6.4	0.0067	10.9	0.0587	15.4	-0.0853	19.9	-0.0297		
6.5	0.0073	11.0	0.0580	15.5	-0.0819	20.0	-0.0370		
6.6	0.0080	11.1	0.0570	15.6	-0.0778	20.1	-0.0439		
6.7	0.0087	11.2	0.0558	15.7	-0.0732	20.2	-0.0501		
6.8	0.0095	11.3	0.0543	15.8	-0.0680	20.3	-0.0557		
6.9	0.0103	11.4	0.0525	15.9	-0.0622	20.4	-0.0606		

Note: The entries are correct to within three units in the fourth decimal place.

TABLE 1B (Continued)

t'	$G_0(15,1,t')$	t'	$G_0(15,1,t')$	t'	$G_0(15,1,t')$	t'	$G_0(15,1,t')$	t'	$G_0(15,1,t')$
8.0	0.0003	12.5	0.0135	17.0	0.0304	21.5	-0.0498	26.0	-0.0128
8.1	0.0003	12.6	0.0143	17.1	0.0286	21.6	-0.0469	26.1	-0.0179
8.2	0.0004	12.7	0.0151	17.2	0.0266	21.7	-0.0429	26.2	-0.0228
8.3	0.0004	12.8	0.0160	17.3	0.0244	21.8	-0.0390	26.3	-0.0274
8.4	0.0004	12.9	0.0169	17.4	0.0221	21.9	-0.0349	26.4	-0.0318
8.5	0.0005	13.0	0.0178	17.5	0.0196	22.0	-0.0305	26.5	-0.0359
8.6	0.0005	13.1	0.0187	17.6	0.0169	22.1	-0.0260	26.6	-0.0396
8.7	0.0006	13.2	0.0197	17.7	0.0142	22.2	-0.0213	26.7	-0.0429
8.8	0.0007	13.3	0.0207	17.8	0.0113	22.3	-0.0165	26.8	-0.0457
8.9	0.0007	13.4	0.0217	17.9	0.0082	22.4	-0.0116	26.9	-0.0480
9.0	0.0008	13.5	0.0227	18.0	0.0051	22.5	-0.0066	27.0	-0.0498
9.1	0.0009	13.6	0.0237	18.1	+0.0018	22.6	-0.0016	27.1	-0.0511
9.2	0.0010	13.7	0.0247	18.2	-0.0016	22.7	+0.0033	27.2	-0.0518
9.3	0.0011	13.8	0.0258	18.3	-0.0050	22.8	0.0082	27.3	-0.0519
9.4	0.0012	13.9	0.0268	18.4	-0.0085	22.9	0.0130	27.4	-0.0514
9.5	0.0013	14.0	0.0279	18.5	-0.0121	23.0	0.0177	27.5	-0.0503
9.6	0.0015	14.1	0.0289	18.6	-0.0157	23.1	0.0222	27.6	-0.0487
9.7	0.0016	14.2	0.0299	18.7	-0.0193	23.2	0.0264	27.7	-0.0465
9.8	0.0018	14.3	0.0309	18.8	-0.0229	23.3	0.0304	27.8	-0.0439
9.9	0.0019	14.4	0.0319	18.9	-0.0265	23.4	0.0342	27.9	-0.0406
10.0	0.0021	14.5	0.0329	19.0	-0.0300	23.5	0.0375	28.0	-0.0369
10.1	0.0023	14.6	0.0338	19.1	-0.0335	23.6	0.0406	28.1	-0.0328
10.2	0.0025	14.7	0.0347	19.2	-0.0369	23.7	0.0432	28.2	-0.0284
10.3	0.0028	14.8	0.0356	19.3	-0.0402	23.8	0.0454	28.3	-0.0236
10.4	0.0030	14.9	0.0364	19.4	-0.0434	23.9	0.0472	28.4	-0.0185
10.5	0.0033	15.0	0.0372	19.5	-0.0464	24.0	0.0485	28.5	-0.0132
10.6	0.0035	15.1	0.0379	19.6	-0.0493	24.1	0.0493	28.6	-0.0078
10.7	0.0038	15.2	0.0385	19.7	-0.0520	24.2	0.0497	28.7	-0.0024
10.8	0.0042	15.3	0.0390	19.8	-0.0544	24.3	0.0495	28.8	+0.0031
10.9	0.0045	15.4	0.0395	19.9	-0.0567	24.4	0.0489	28.9	0.0085
11.0	0.0049	15.5	0.0399	20.0	-0.0587	24.5	0.0477	29.0	0.0137
11.1	0.0053	15.6	0.0402	20.1	-0.0604	24.6	0.0461	29.1	0.0188
11.2	0.0057	15.7	0.0403	20.2	-0.0618	24.7	0.0440	29.2	0.0235
11.3	0.0061	15.8	0.0404	20.3	-0.0629	24.8	0.0414	29.3	0.0279
11.4	0.0066	15.9	0.0404	20.4	-0.0637	24.9	0.0384	29.4	0.0319
11.5	0.0071	16.0	0.0402	20.5	-0.0642	25.0	0.0350	29.5	0.0355
11.6	0.0076	16.1	0.0399	20.6	-0.0643	25.1	0.0313	29.6	0.0386
11.7	0.0081	16.2	0.0394	20.7	-0.0641	25.2	0.0271	29.7	0.0411
11.8	0.0087	16.3	0.0388	20.8	-0.0636	25.3	0.0227	29.8	0.0430
11.9	0.0093	16.4	0.0381	20.9	-0.0627	25.4	0.0180	29.9	0.0443
12.0	0.0099	16.5	0.0372	21.0	-0.0614	25.5	0.0131	30.0	0.0450
12.1	0.0106	16.6	0.0362	21.1	-0.0598	25.6	0.0080	30.1	0.0450
12.2	0.0113	16.7	0.0350	21.2	-0.0578	25.7	+0.0028	30.2	0.0444
12.3	0.0120	16.8	0.0336	21.3	-0.0554	25.8	-0.0024	30.3	0.0432
12.4	0.0127	16.9	0.0321	21.4	-0.0528	25.9	-0.0076	30.4	0.0413

Note: The entries are correct to within three units in the fourth decimal place.

TABLE IH (Continued)

t'	$G_0(25,1,t')$	t'	$G_0(25,1,t')$	t'	$G_0(25,1,t')$	t'	$G_0(25,1,t')$	t'	$G_0(25,1,t')$
18.0	0.0006	23.0	0.0124	28.0	0.0118	33.0	-0.0239	38.0	-0.0127
18.1	0.0006	23.1	0.0129	28.1	0.0104	33.1	-0.0217	38.1	-0.0155
18.2	0.0007	23.2	0.0134	28.2	0.0090	33.2	-0.0193	38.2	-0.0181
18.3	0.0007	23.3	0.0140	28.3	0.0074	33.3	-0.0169	38.3	-0.0205
18.4	0.0008	23.4	0.0145	28.4	0.0059	33.4	-0.0144	38.4	-0.0228
18.5	0.0008	23.5	0.0150	28.5	0.0042	33.5	-0.0118	38.5	-0.0249
18.6	0.0009	23.6	0.0156	28.6	0.0026	33.6	-0.0091	38.6	-0.0269
18.7	0.0010	23.7	0.0161	28.7	+0.0008	33.7	-0.0065	38.7	-0.0286
18.8	0.0011	23.8	0.0166	28.8	-0.0010	33.8	-0.0038	38.8	-0.0301
18.9	0.0011	23.9	0.0172	28.9	-0.0028	33.9	-0.0010	38.9	-0.0313
19.0	0.0012	24.0	0.0177	29.0	-0.0046	34.0	+0.0017	39.0	-0.0323
19.1	0.0013	24.1	0.0182	29.1	-0.0065	34.1	0.0044	39.1	-0.0330
19.2	0.0014	24.2	0.0188	29.2	-0.0084	34.2	0.0070	39.2	-0.0335
19.3	0.0015	24.3	0.0193	29.3	-0.0103	34.3	0.0096	39.3	-0.0336
19.4	0.0016	24.4	0.0198	29.4	-0.0122	34.4	0.0121	39.4	-0.0335
19.5	0.0018	24.5	0.0203	29.5	-0.0141	34.5	0.0146	39.5	-0.0331
19.6	0.0019	24.6	0.0208	29.6	-0.0161	34.6	0.0169	39.6	-0.0324
19.7	0.0020	24.7	0.0212	29.7	-0.0180	34.7	0.0191	39.7	-0.0315
19.8	0.0022	24.8	0.0217	29.8	-0.0198	34.8	0.0212	39.8	-0.0302
19.9	0.0023	24.9	0.0221	29.9	-0.0217	34.9	0.0231	39.9	-0.0287
20.0	0.0025	25.0	0.0225	30.0	-0.0235	35.0	0.0249	40.0	-0.0270
20.1	0.0026	25.1	0.0229	30.1	-0.0252	35.1	0.0265	40.1	-0.0250
20.2	0.0028	25.2	0.0233	30.2	-0.0269	35.2	0.0279	40.2	-0.0228
20.3	0.0030	25.3	0.0236	30.3	-0.0285	35.3	0.0291	40.3	-0.0204
20.4	0.0032	25.4	0.0239	30.4	-0.0301	35.4	0.0301	40.4	-0.0178
20.5	0.0034	25.5	0.0241	30.5	-0.0316	35.5	0.0309	40.5	-0.0151
20.6	0.0036	25.6	0.0243	30.6	-0.0329	35.6	0.0314	40.6	-0.0122
20.7	0.0038	25.7	0.0245	30.7	-0.0342	35.7	0.0317	40.7	-0.0092
20.8	0.0041	25.8	0.0246	30.8	-0.0354	35.8	0.0318	40.8	-0.0062
20.9	0.0043	25.9	0.0247	30.9	-0.0364	35.9	0.0317	40.9	-0.0031
21.0	0.0046	26.0	0.0247	31.0	-0.0374	36.0	0.0313	41.0	-0.0000
21.1	0.0049	26.1	0.0247	31.1	-0.0382	36.1	0.0307	41.1	+0.0031
21.2	0.0052	26.2	0.0246	31.2	-0.0388	36.2	0.0298	41.2	0.0061
21.3	0.0054	26.3	0.0245	31.3	-0.0394	36.3	0.0287	41.3	0.0091
21.4	0.0058	26.4	0.0243	31.4	-0.0397	36.4	0.0274	41.4	0.0120
21.5	0.0061	26.5	0.0241	31.5	-0.0399	36.5	0.0259	41.5	0.0148
21.6	0.0064	26.6	0.0237	31.6	-0.0400	36.6	0.0242	41.6	0.0174
21.7	0.0068	26.7	0.0233	31.7	-0.0399	36.7	0.0222	41.7	0.0198
21.8	0.0071	26.8	0.0229	31.8	-0.0396	36.8	0.0201	41.8	0.0220
21.9	0.0075	26.9	0.0224	31.9	-0.0392	36.9	0.0178	41.9	0.0239
22.0	0.0079	27.0	0.0218	32.0	-0.0386	37.0	0.0154	42.0	0.0256
22.1	0.0083	27.1	0.0211	32.1	-0.0378	37.1	0.0129	42.1	0.0271
22.2	0.0087	27.2	0.0204	32.2	-0.0369	37.2	0.0102	42.2	0.0282
22.3	0.0091	27.3	0.0196	32.3	-0.0358	37.3	0.0074	42.3	0.0291
22.4	0.0096	27.4	0.0187	32.4	-0.0346	37.4	0.0046	42.4	0.0296
22.5	0.0100	27.5	0.0177	32.5	-0.0331	37.5	+0.0017	42.5	0.0299
22.6	0.0105	27.6	0.0167	32.6	-0.0316	37.6	-0.0012	42.6	0.0298
22.7	0.0109	27.7	0.0156	32.7	-0.0299	37.7	-0.0042	42.7	0.0294
22.8	0.0114	27.8	0.0144	32.8	-0.0280	37.8	-0.0071	42.8	0.0286
22.9	0.0119	27.9	0.0131	32.9	-0.0260	37.9	-0.0099	42.9	0.0276

Note: The entries are correct to within three units in the fourth decimal place.

TABLE 1B (Continued)

t'	$G_0(50,1,t')$	t'	$G_0(50,1,t')$	t'	$G_0(50,1,t')$
43.0	0.0008	48.0	0.0073	53.0	0.0097
43.1	0.0009	48.1	0.0075	53.1	0.0094
43.2	0.0009	48.2	0.0077	53.2	0.0090
43.3	0.0010	48.3	0.0079	53.3	0.0085
43.4	0.0011	48.4	0.0081	53.4	0.0081
43.5	0.0011	48.5	0.0083	53.5	0.0076
43.6	0.0012	48.6	0.0085	53.6	0.0071
43.7	0.0012	48.7	0.0088	53.7	0.0066
43.8	0.0013	48.8	0.0090	53.8	0.0060
43.9	0.0014	48.9	0.0092	53.9	0.0055
44.0	0.0014	49.0	0.0094	54.0	0.0049
44.1	0.0015	49.1	0.0096	54.1	0.0043
44.2	0.0016	49.2	0.0098	54.2	0.0036
44.3	0.0017	49.3	0.0100	54.3	0.0030
44.4	0.0018	49.4	0.0102	54.4	0.0023
44.5	0.0018	49.5	0.0104	54.5	0.0016
44.6	0.0019	49.6	0.0106	54.6	0.0009
44.7	0.0020	49.7	0.0108	54.7	+0.0002
44.8	0.0021	49.8	0.0110	54.8	-0.0006
44.9	0.0022	49.9	0.0112	54.9	-0.0013
45.0	0.0023	50.0	0.0114	55.0	-0.0021
45.1	0.0024	50.1	0.0115	55.1	-0.0028
45.2	0.0025	50.2	0.0117	55.2	-0.0036
45.3	0.0027	50.3	0.0118	55.3	-0.0044
45.4	0.0028	50.4	0.0120	55.4	-0.0052
45.5	0.0029	50.5	0.0121	55.5	-0.0060
45.6	0.0030	50.6	0.0122	55.6	-0.0068
45.7	0.0032	50.7	0.0123	55.7	-0.0076
45.8	0.0033	50.8	0.0124	55.8	-0.0084
45.9	0.0034	50.9	0.0125	55.9	-0.0092
46.0	0.0036	51.0	0.0125	56.0	-0.0100
46.1	0.0037	51.1	0.0126	56.1	-0.0108
46.2	0.0039	51.2	0.0126	56.2	-0.0115
46.3	0.0040	51.3	0.0126	56.3	-0.0123
46.4	0.0042	51.4	0.0126	56.4	-0.0130
46.5	0.0044	51.5	0.0126	56.5	-0.0137
46.6	0.0045	51.6	0.0125	56.6	-0.0144
46.7	0.0047	51.7	0.0125	56.7	-0.0151
46.8	0.0049	51.8	0.0124	56.8	-0.0157
46.9	0.0051	51.9	0.0123	56.9	-0.0163
47.0	0.0052	52.0	0.0122	57.0	-0.0169
47.1	0.0054	52.1	0.0120	57.1	-0.0174
47.2	0.0056	52.2	0.0119	57.2	-0.0179
47.3	0.0058	52.3	0.0117	57.3	-0.0184
47.4	0.0060	52.4	0.0115	57.4	-0.0189
47.5	0.0062	52.5	0.0113	57.5	-0.0192
47.6	0.0064	52.6	0.0110	57.6	-0.0196
47.7	0.0066	52.7	0.0107	57.7	-0.0199
47.8	0.0068	52.8	0.0104	57.8	-0.0202
47.9	0.0070	52.9	0.0101	57.9	-0.0204

TABLE 1B (Continued)

t'	$G_0(50,1,t')$	t'	$G_0(50,1,t')$	t'	$G_0(50,1,t')$
58.0	-0.0205	62.0	0.0095	66.0	-0.0054
58.1	-0.0206	62.1	0.0105	66.1	-0.0067
58.2	-0.0207	62.2	0.0114	66.2	-0.0079
58.3	-0.0207	62.3	0.0122	66.3	-0.0090
58.4	-0.0206	62.4	0.0130	66.4	-0.0101
58.5	-0.0205	62.5	0.0137	66.5	-0.0112
58.6	-0.0203	62.6	0.0143	66.6	-0.0122
58.7	-0.0201	62.7	0.0149	66.7	-0.0132
58.8	-0.0198	62.8	0.0154	66.8	-0.0140
58.9	-0.0195	62.9	0.0159	66.9	-0.0149
59.0	-0.0191	63.0	0.0162	67.0	-0.0156
59.1	-0.0186	63.1	0.0165	67.1	-0.0162
59.2	-0.0181	63.2	0.0167	67.2	-0.0168
59.3	-0.0176	63.3	0.0169	67.3	-0.0172
59.4	-0.0169	63.4	0.0169	67.4	-0.0176
59.5	-0.0163	63.5	0.0169	67.5	-0.0177
59.6	-0.0155	63.6	0.0168	67.6	-0.0180
59.7	-0.0148	63.7	0.0166	67.7	-0.0181
59.8	-0.0139	63.8	0.0163	67.8	-0.0181
59.9	-0.0131	63.9	0.0159	67.9	-0.0179
60.0	-0.0122	64.0	0.0154	68.0	-0.0177
60.1	-0.0112	64.1	0.0149	68.1	-0.0173
60.2	-0.0102	64.2	0.0143	68.2	-0.0169
60.3	-0.0092	64.3	0.0136	68.3	-0.0163
60.4	-0.0082	64.4	0.0129	68.4	-0.0157
60.5	-0.0071	64.5	0.0120	68.5	-0.0150
60.6	-0.0060	64.6	0.0111	68.6	-0.0141
60.7	-0.0049	64.7	0.0102	68.7	-0.0132
60.8	-0.0037	64.8	0.0092	68.8	-0.0122
60.9	-0.0026	64.9	0.0081	68.9	-0.0112
61.0	-0.0014	65.0	0.0070	69.0	-0.0101
61.1	-0.0002	65.1	0.0058	69.1	-0.0089
61.2	+0.0009	65.2	0.0046	69.2	-0.0076
61.3	0.0021	65.3	0.0034	69.3	-0.0064
61.4	0.0032	65.4	0.0022	69.4	-0.0051
61.5	0.0043	65.5	+0.0009	69.5	-0.0037
61.6	0.0054	65.6	-0.0004	69.6	-0.0023
61.7	0.0065	65.7	-0.0016	69.7	-0.0010
61.8	0.0076	65.8	-0.0029	69.8	+0.0004
61.9	0.0086	65.9	-0.0042	69.9	0.0018

Note: The entries are correct to within three units in the fourth decimal place.

a_2', b_1', b_2'. It is to be noted from Graph 4 that the maximum of the first positive phase occurs approximately at a time when a so-called shallow wave will arrive, i.e., $t' = h'$ It is also noteworthy that the maxima, minima, and zeros of corresponding phases of $G_o(h', o, t')$, $G_{\frac{1}{2}}(h', o, t')$, and $G_1(h', o, t')$ all have about the same values of t', wherever computed. (This fact seems to hold also for $G_{z_E', \tau'}(h', 0, t')$, where $0.1 \leq \tau \leq 1.1$.)

In order to evaluate $G_{z_E', \tau'}$, it is necessary to know the period of the gas globe. The first period T can be obtained approximately from the following expression [3] for a spherical globe in an incompressible, inviscid liquid bounded by a rigid sea bed parallel to the free surface, and subject to atmospheric pressure (h_a, in units of length):

$$T = 1.485\, L \sqrt{\frac{3}{2g(h+h_a)}} \left(1 - \frac{0.189 L\, F(x)}{h}\right) \qquad (6$$

where $F(X)$ is a known function of x

and $$x = 1 - 2z_E' \quad ,$$

also $$L = \sqrt[3]{\frac{3E}{4\pi\rho g(h+h_a)}}$$

where E is the amount of residual energy in the gas and the liquid after the shock wave has passed. If E is assumed to be 50% of the adiabatic, constant-volume heat of explosion, which has been computed [4] to be 1060 cal/g for TNT, then L can be expressed as follows in terms of the charge weight W, where W is given in pounds and h in feet.

$$L = 14.0 \sqrt[3]{\frac{W}{h+33}}$$

Some values of L of practical interest are given in Table 2.

Table 2

h(ft) \ W(lb)	300	1200	2100	6600
	L	L	L	L
25	14.21	---		
30	13.55	---	---	---
35	12.96	36.45	---	---
40	22.43	35.50	---	---
45	21.94	34.82	41.96	---
50	21.49	34.11	41.10	---
55	21.07	33.45	40.31	59.04
60	20.68	32.84	39.57	57.96
70	19.99	31.74	38.25	56.02
80	19.39	30.77	37.08	54.32
90	18.84	29.92	36.05	52.81
100	18.36	29.15	35.12	51.45
110	17.92	28.45	34.28	50.22
120	17.52	27.82	33.52	49.10

The expression (6) for the first period of the globe is invalid when the distance of the center of the globe from a bounding surface is less than $1.2\,L$. Nevertheless, in the absence of any other information the value of the first period for $Z_E = 1.2\,L$ will be used heuristically for $Z_E \leq 1.2\,L$. On this basis τ and τ' have been computed for various charge weights of TNT over a range of depths; these values are given in Table 3. The function $G_{Z_E,\tau}(h', 0, t')$ can be readily obtained from the master function $G_{Z_E}(h', 0, t')$; its characteristic properties for different values of h' are represented for $\tau' = 0.1$ and 1.1 on the various graphs, viz., 2, 3, 4.

Table 3

h(ft) \ W(lb)	300		1200		2100		6600	
	τ	τ'	τ	τ'	τ	τ'	τ	τ'
25	0.8741	0.9920						
30	0.8575	0.8883		---		---		---
35	0.8330	0.7990	1.192	1.143		---		---
40	0.8065	0.7236	1.170	1.090				
45	0.7790	0.6590	1.143	0.9666	1.319	1.116		---
50	0.7522	0.6037	1.112	0.9226	1.292	1.037		---
55	0.7262	0.5557	1.081	0.8269	1.259	0.9632	---	---
60	0.7018	0.5141	1.050	0.7694	1.226	0.8984	1.653	1.211
70	0.6571	0.4457	0.9909	0.6721	1.163	0.7885	1.589	1.073
80	0.6168	0.3913	0.9356	0.5936	1.102	0.6991	1.519	0.9639
90	0.5810	0.3477	0.8859	0.5299	1.046	0.6254	1.452	0.8685
100	0.5492	0.3116	0.8414	0.4774	0.9943	0.5642	1.388	0.7878
110	0.5209	0.2818	0.8005	0.4331	0.9479	0.5129	1.329	0.7197
120	0.4954	0.2566	0.7632	0.3953	0.9059	0.4693	1.274	0.6597

One additional quantity is required for the determination of the pressure $p_{Z_E}(h', z', t')$, namely, the average volume of the gas globe. Thus the time average of the volume for the first period is given by

$$\overline{V} = \frac{4}{3}\pi\left[a(t)\right]^3,$$

where $a(t)$ is the instantaneous radius of the bubble at the time t. The dimensionless quantity a/L has been calculated [3] for a globe situated in an infinite liquid with no free surface at a distance of $1.2\,L$ from a rigid wall. Using these values we find the average of $\left[a(t)\right]^3$ over the first period to be 0.4819. Thus we obtain

$$\overline{V} = \frac{4}{3}\pi(0.4819)L^3.$$

If the explosive is on the bottom, its gas globe is about half of an oblate spheroid.

Small-scale experiments [5] indicate that its size is slightly less than that of the complete gas globe at a distance of 1.2 L from the wall. In view of the lack of sufficient quantitative information, however, the actual volume $\bar{V}_B$ on the bottom will be assumed here to be half of $\bar{V}$. (In case of venting at the surface a better approximation is the volume of a cylinder of a height equal to the depth of the water and of a radius slightly less than the maximum spherical globe in an unbounded liquid.)

Thus we obtain finally for the pressure $p_o(h', 0, t')$ on the bottom due to the first pulsation from an explosion originating also on the bottom (cf. expression (5'))

$$p_o(h',0,t') = + \frac{2\rho g}{3h^2}(0.4819)L^3 G_{0,T}(h',0,t')$$

Expressing the pressure as $p_o''(h', 0, t')$ in feet we have for TNT

$$p_o''(h',0,t') = 441 \frac{W G_{0,T}(h',0,t')}{h^2(h+33)}$$

The minimum pressure $p_o''(h', 0, t')$ for the first negative phase is represented as a function of the depth h for various values of the charge weight W in Graphs 5a, b, c, d e, f, corresponding to values of h' equal to 5, 10, 15, 25, 50, 500, respectively.

A comparison of these calculated values with available experimental ones shows satisfactory agreement in consideration of the various approximations that have been made. It will be reported in detail elsewhere.

References

1) The theoretical treatment is an application of the standard procedure for surface waves (cf. H. Lamb's "Hydrodynamics", 6th Ed., Ch. IX). The present report embodies certain suggestions made by R. J. Finkelstein, J. von Neumann, and F. J. Weyl of the Bureau of Ordnance Group on the Theory of Explosives.

2) These integrals have all been evaluated by the Mathematics Tables Project under the Applied Mathematics Panel of the N.D.R.C. The authors are particularly indebted to G. Blanch and A. N. Lowan of that group.

3) "On the Best Location of a Mine Near the Sea Bed" NDRC, AMP Report 37.1R, AMG-NYU No. 49, May (1944) and Appendix on "Bubble Periods" February (1945). Also "On the Solution of the Differential Equations Arising from a Particular Energy Function, Mathematical Tables Project, March and October (1944).

4) J. G. Kirkwood and S. R. Brinkley, Jr. "A New Theory of Shock Wave Propagation with an Application to the Underwater Explosion Wave Produced by TNT" Division 2 Interim Report 24 on "Underwater Explosives and Explosions" (1944).

5) Lt. D. C. Campbell, USNR: "Motions of a Pulsating Gas Globe Under Water", David Taylor Model Basin Report 512, May (1943).

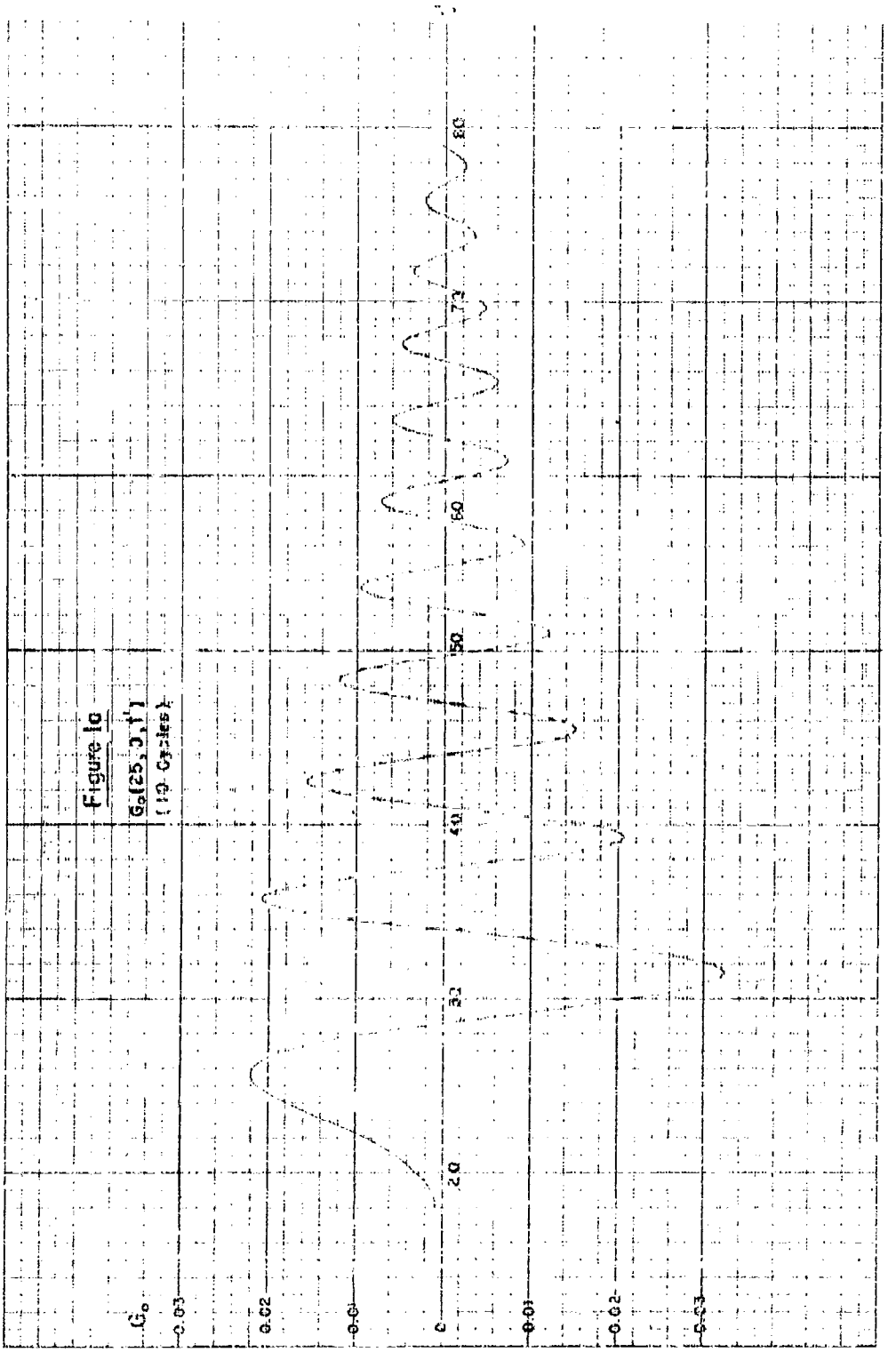
Figure 1a
$G_o(25, 0, f')$
(10 Cycles)
G_o
0.03
0.02
0.01
0
0.01
0.02
0.03
20
30
40
50
60
70
80

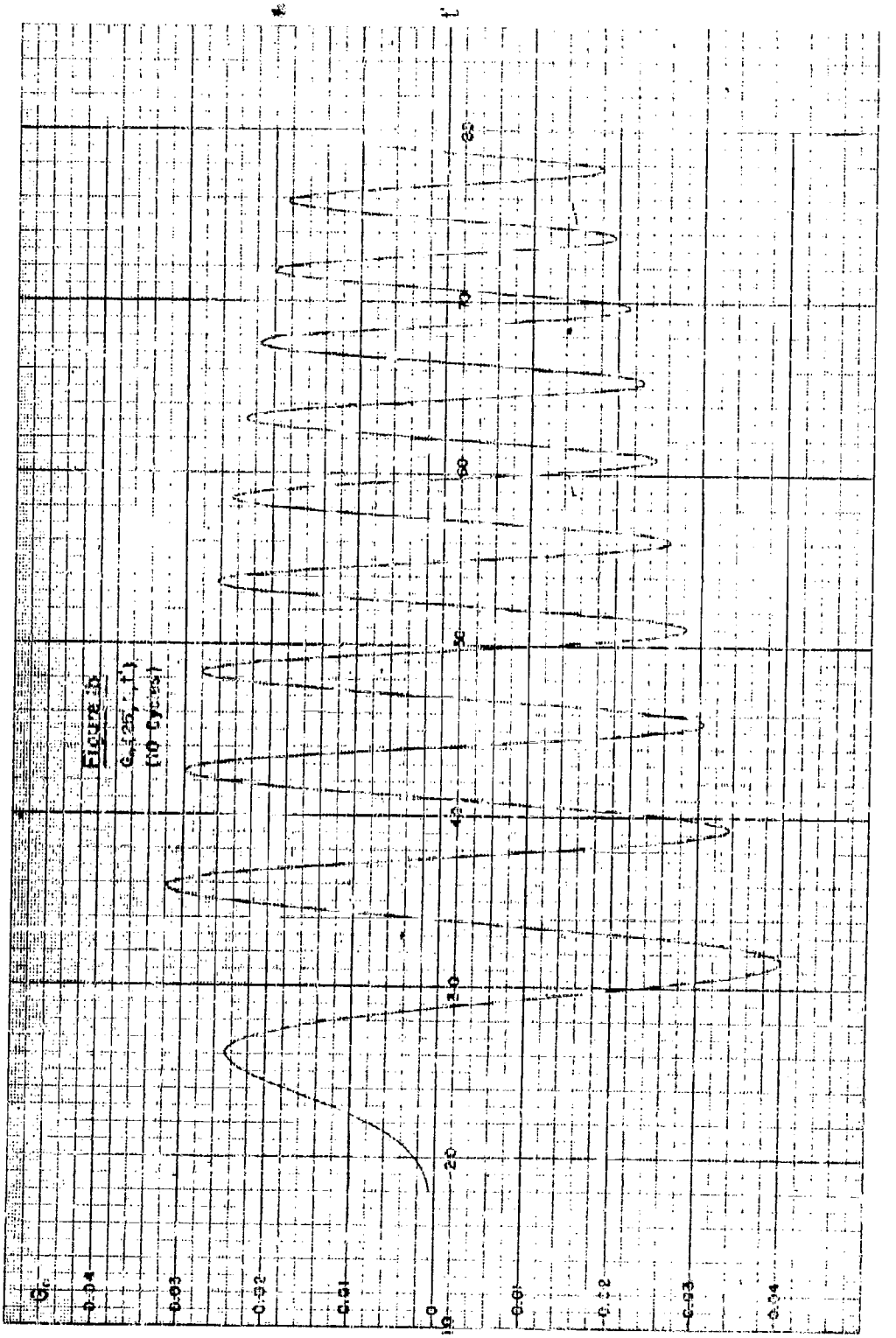
Figure 15
G(.25, t)
(10 cycles)
t'
0
20
40
60
80
100
120
0.04
0.03
0.02
0.01
0
0.01
0.02
0.03
0.04

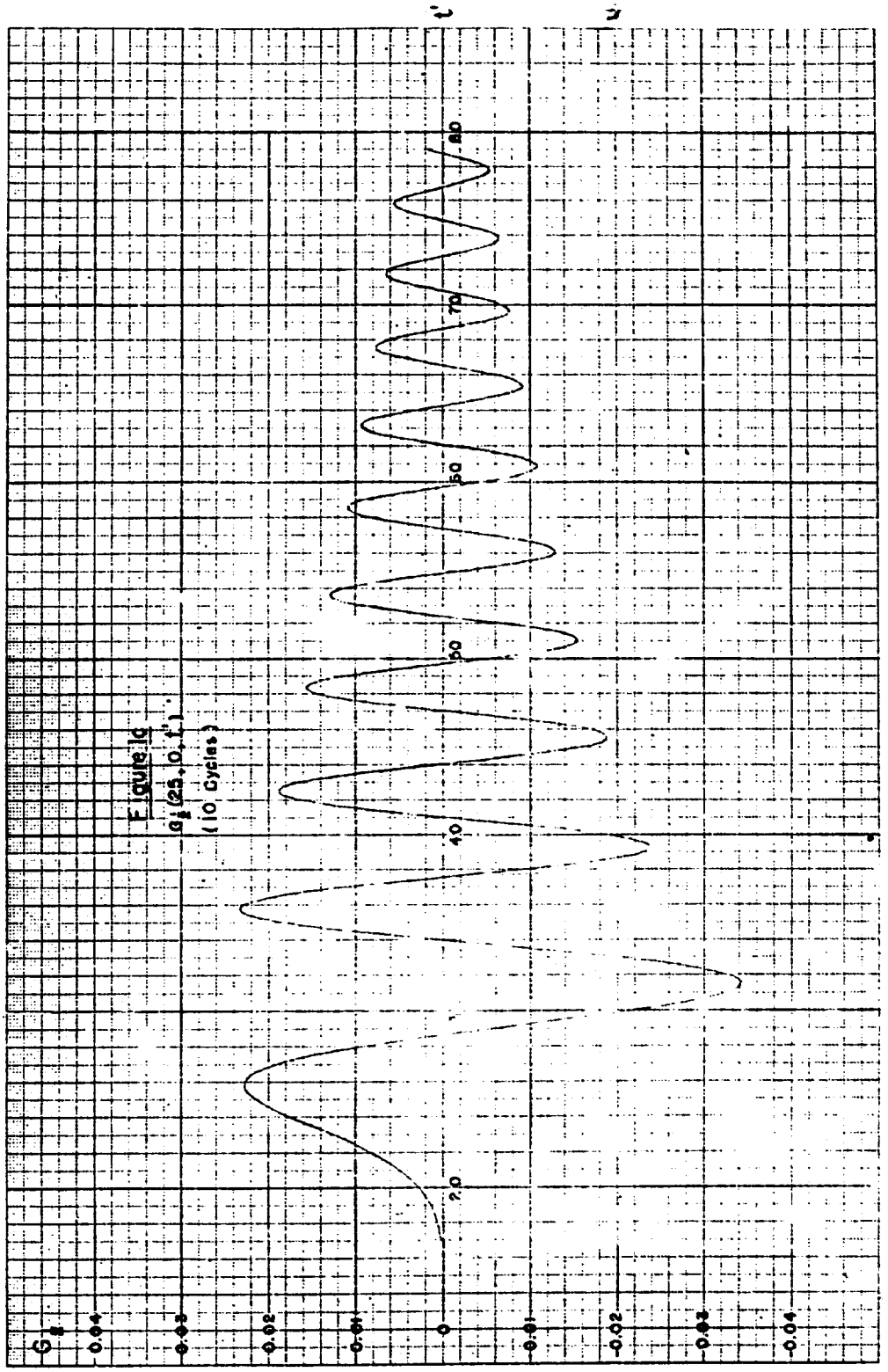

Figure 1c
$g_j(25, 0, t')$
(10 Cycles)

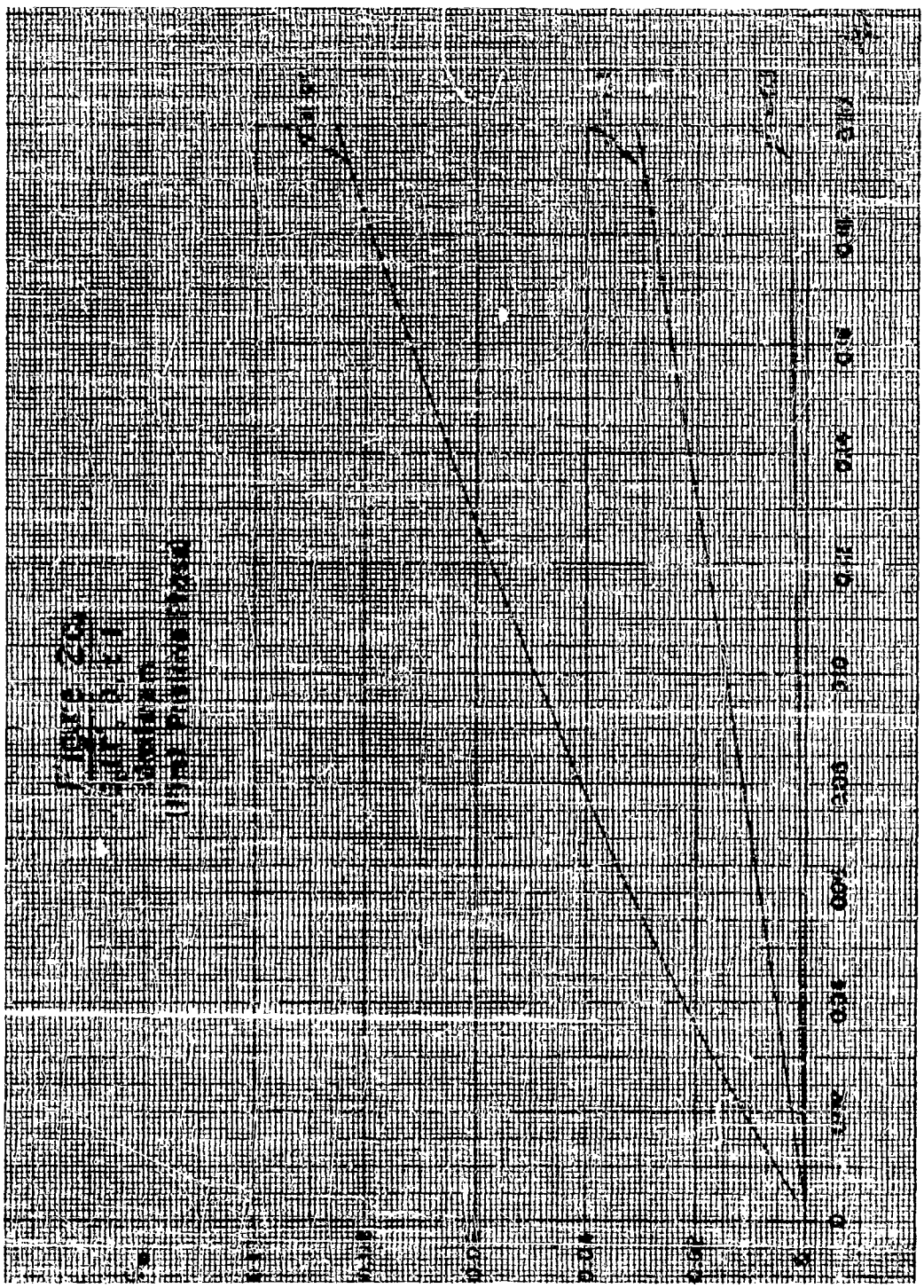

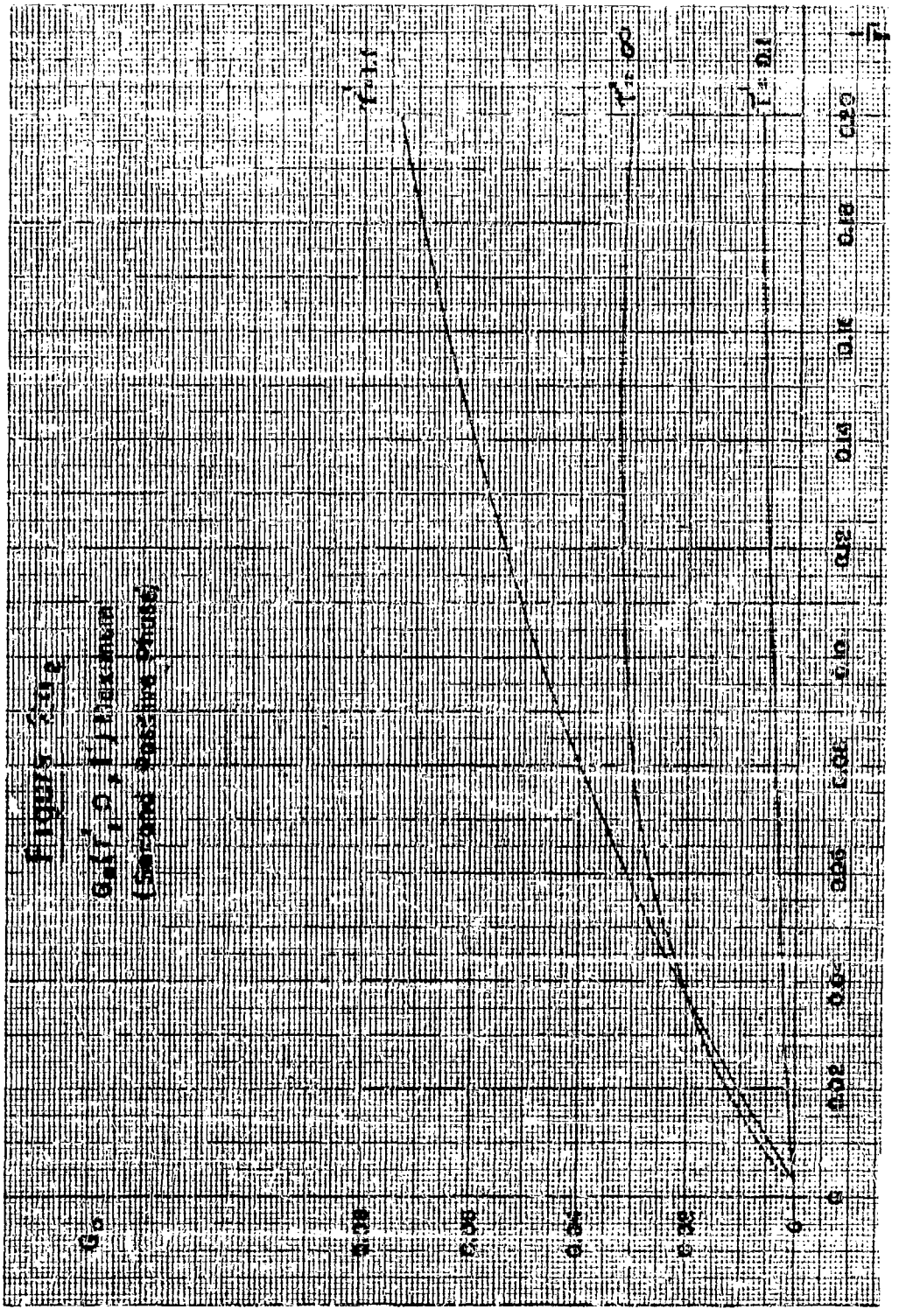
0.30
0.25
0.20
0.15
0.10
0.05
0
0.02
0.06
0.10
0.14
0.18
0.22
1/r

Figure 2b
0.30
0.18
0.12
0.06
0
0.24
0.48
0.36
0.60
0.72
0.84
0.96
1.08
1.20
1.32
1.44
1.56
1.68
1.80
1.92
2.04
2.16
2.28
2.40
2.52
2.64
2.76
2.88
3.00
3.12
3.24
3.36
3.48
3.60
3.72
3.84
3.96
4.08
4.20
4.32
4.44
4.56
4.68
4.80
4.92
5.04
5.16
5.28
5.40
5.52
5.64
5.76
5.88
6.00

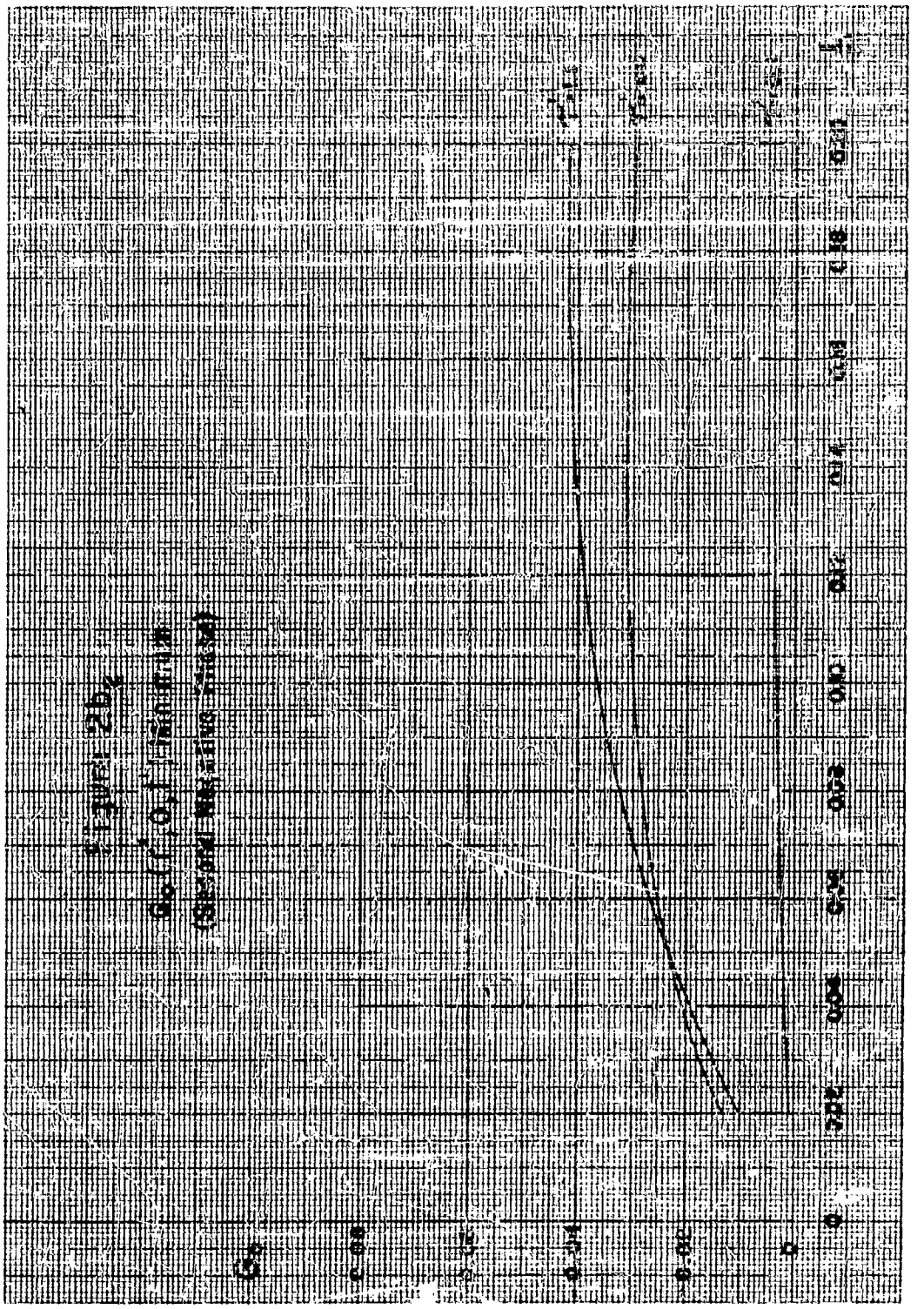

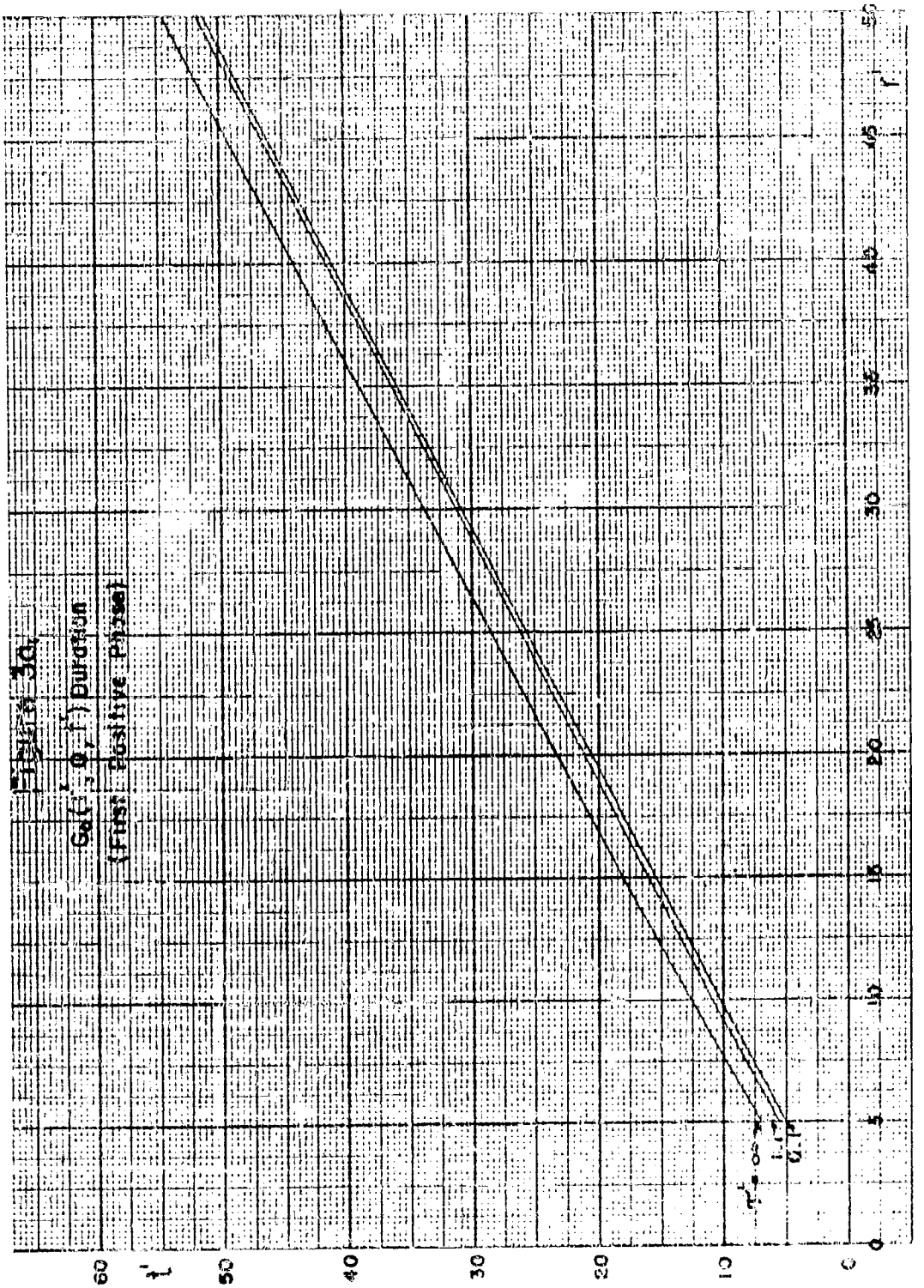
Figure 3(c)
Sol(r_3, θ_r, r^1) Duration
(First Positive Phase)
t'
60
50
40
30
20
10
0
0
5
10
15
20
25
30
35
40
45
50
r'

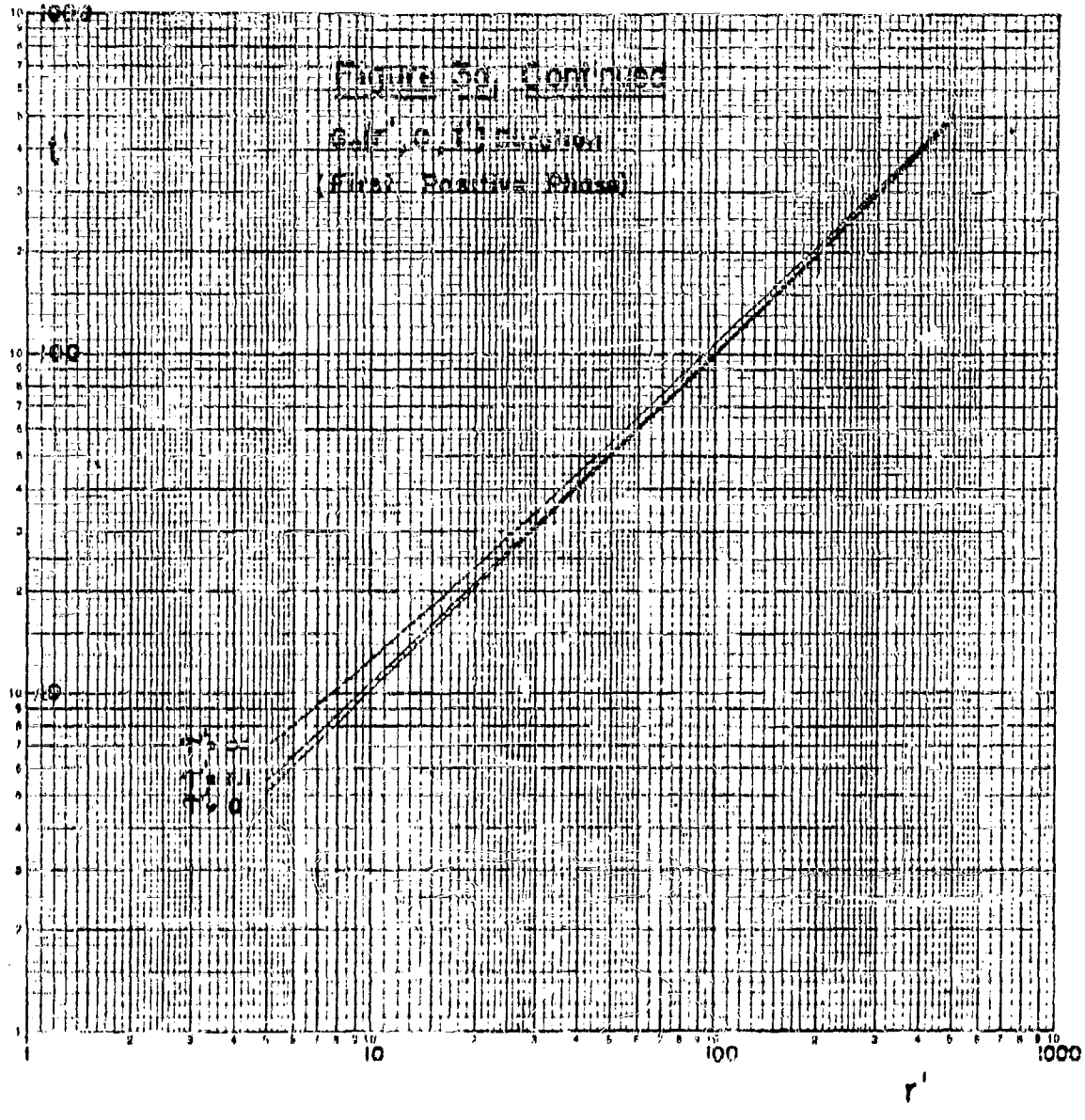
Figure 50. Continued
(First Positive Phase)
100 Å
10
1
10
100
1000
r'

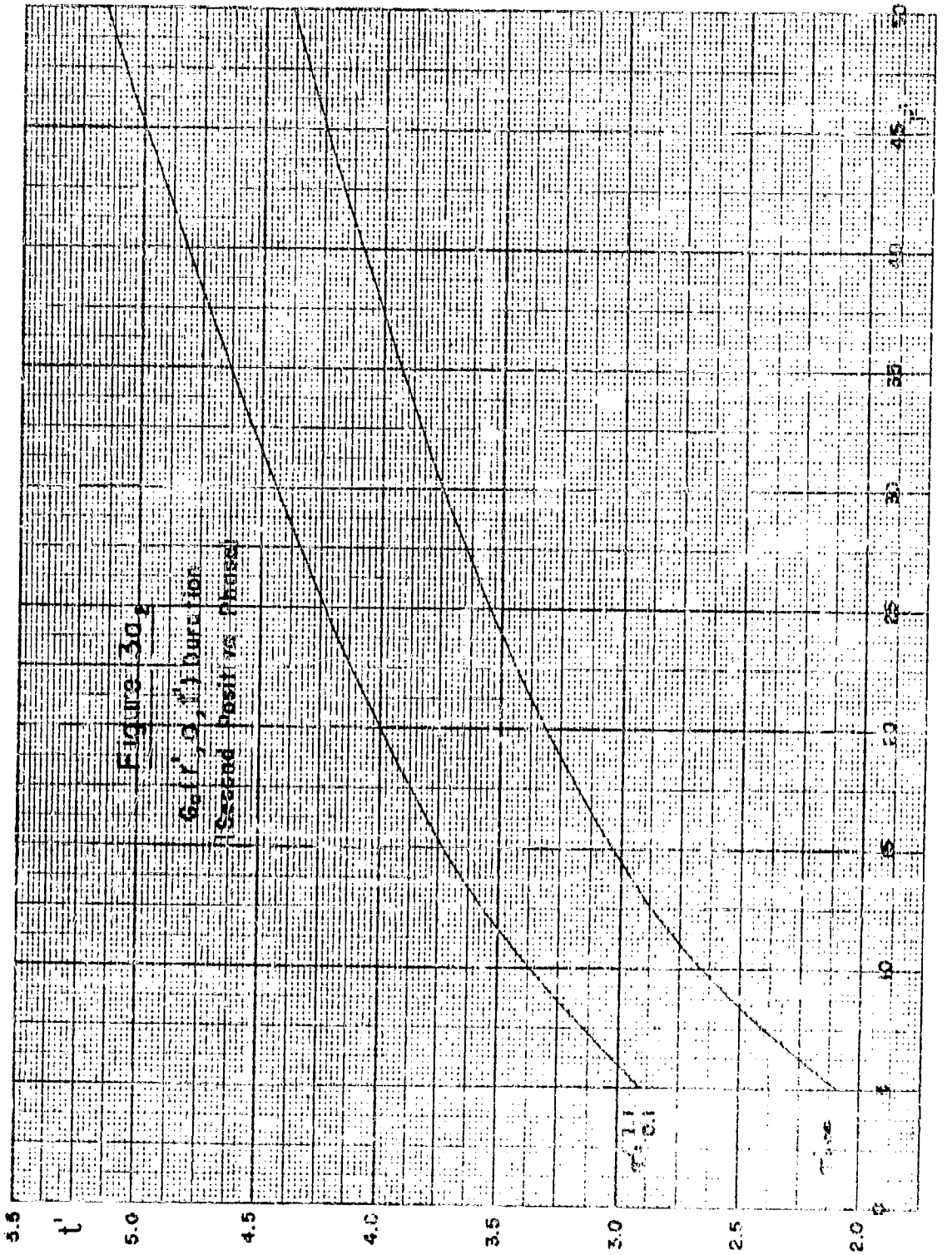

Figure 30-2

Coil 1' 2' 3' 4' 1' Duration
Second Position vs Phase

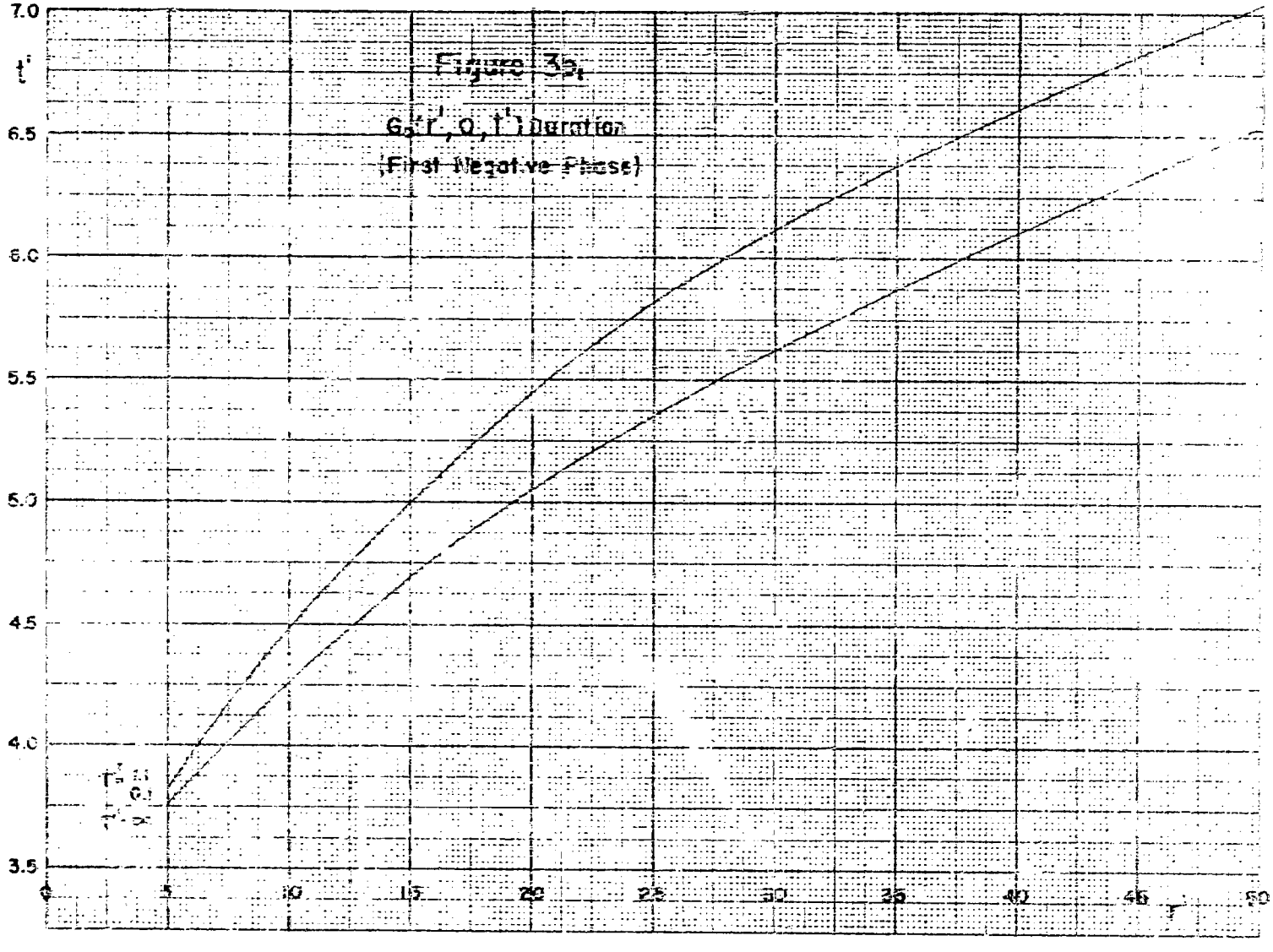
7.0
6.5
6.0
5.5
5.0
4.5
4.0
3.5
0
5
10
15
20
25
30
35
40
45
50
Figure 35
(First Negative Phase)

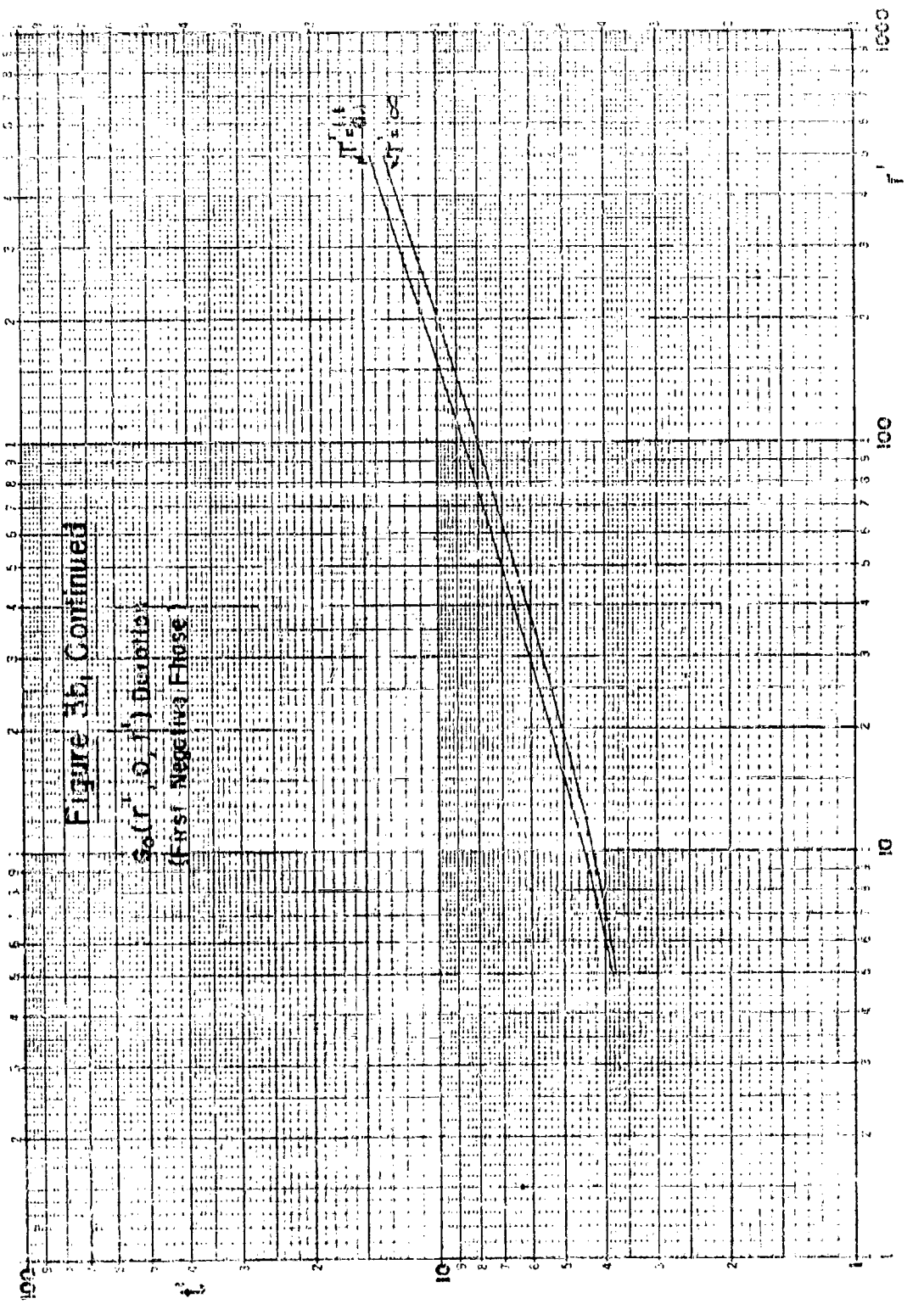

Figure 3b. Continued

$S_0(r', \Omega_z, f')$ Decibels

(First Negative Phase)

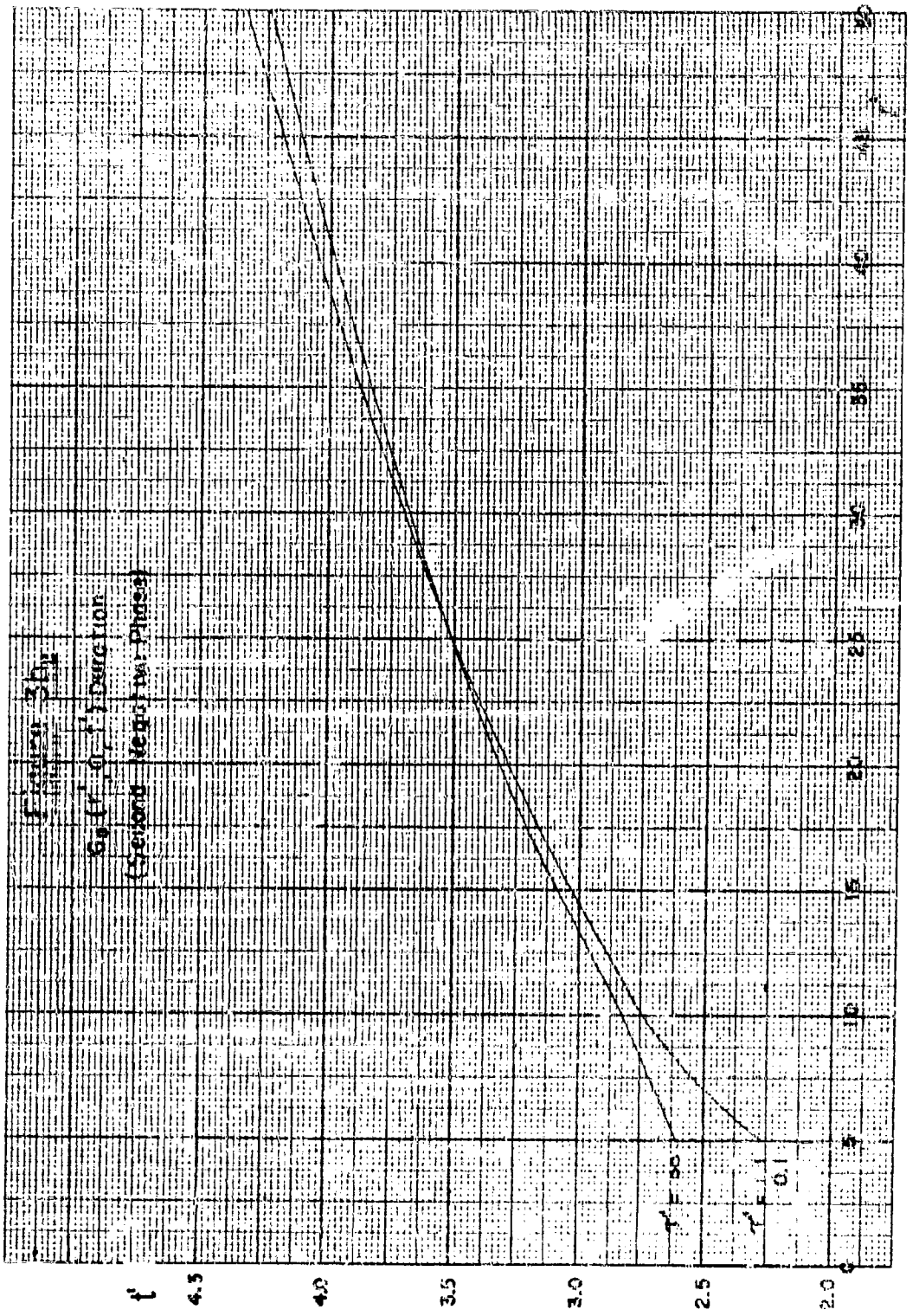
t'
4.5
4.0
3.5
3.0
2.5
2.0
5
10
15
20
25
30
35
40
45
50
F' = 50
F' = 0.1

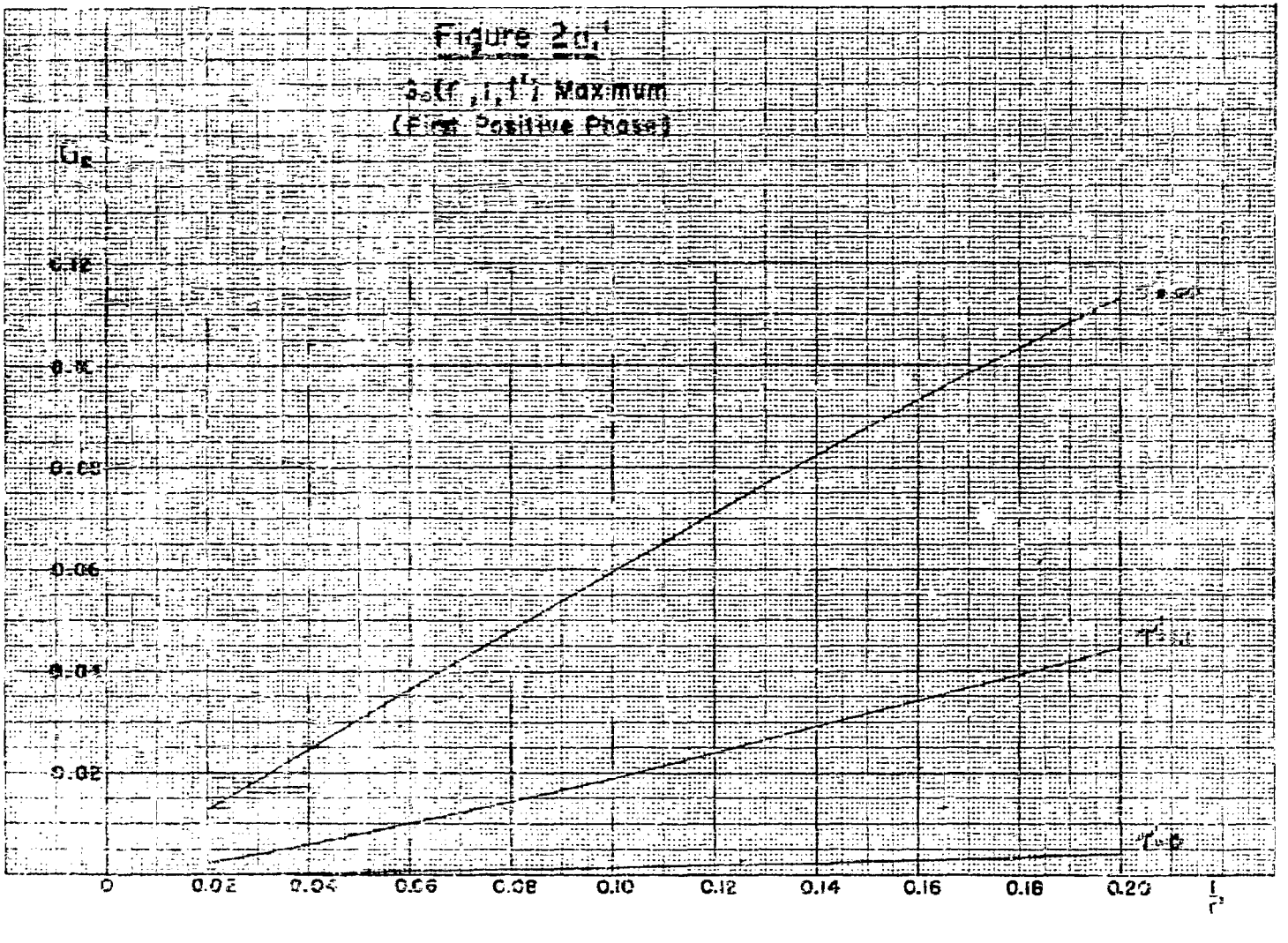
Figure 2a'
$\hat{p}_s(r, i, t')$ Maximum
(First Positive Phase)
$\hat{p}_s$
0.12
0.10
0.08
0.06
0.04
0.02
0
0.02
0.04
0.06
0.08
0.10
0.12
0.14
0.16
0.18
0.20
$\frac{1}{r}$

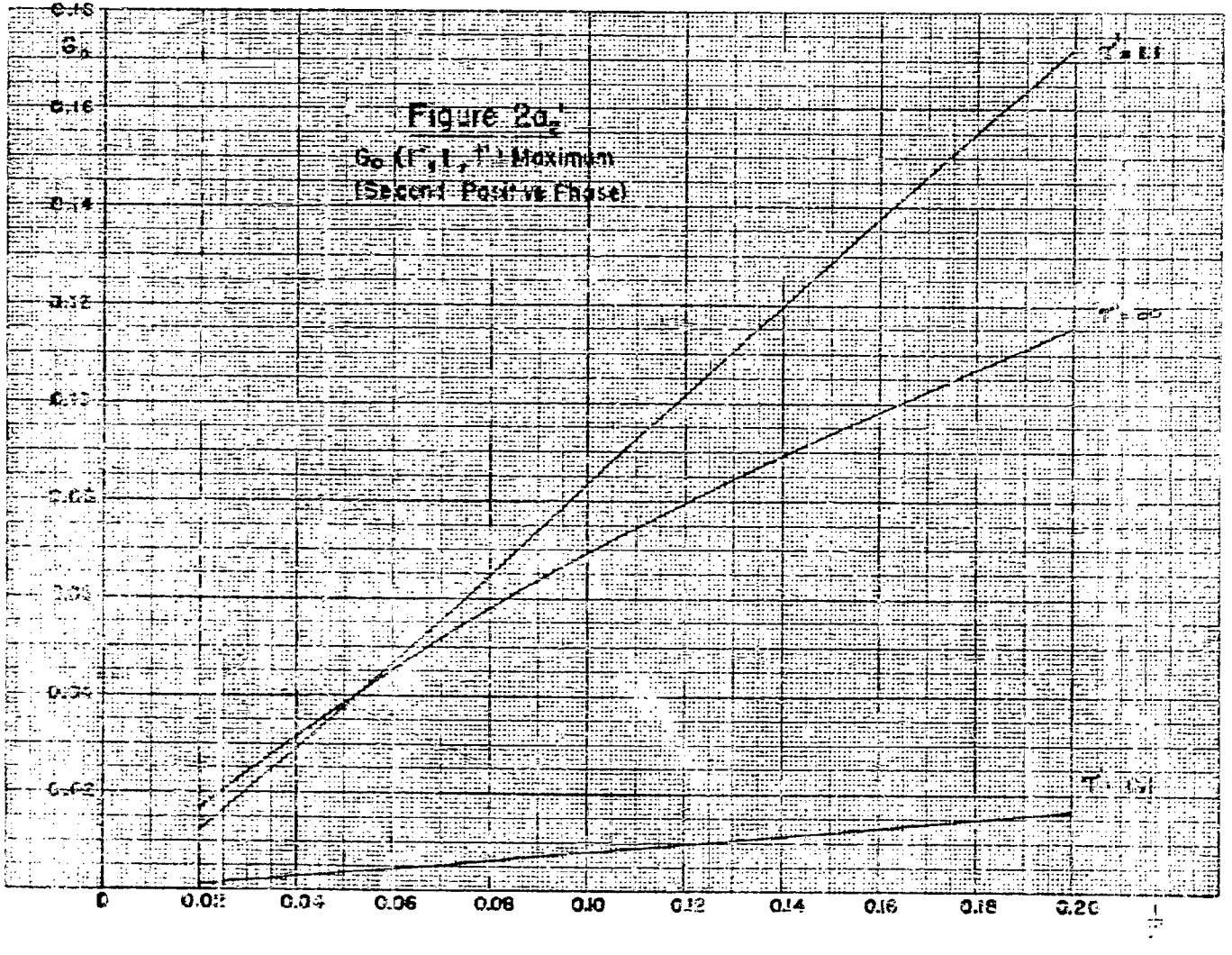
Figure 2a$_2$'
$G_o(\Gamma', t_r, t^1)$ Maximum
(Second Positive Phase)
$\Gamma' = 0.1$
$\Gamma' = 0.0$
0
0.02
0.04
0.06
0.08
0.10
0.12
0.14
0.16
0.18
0.20
$\frac{1}{\Gamma'}$

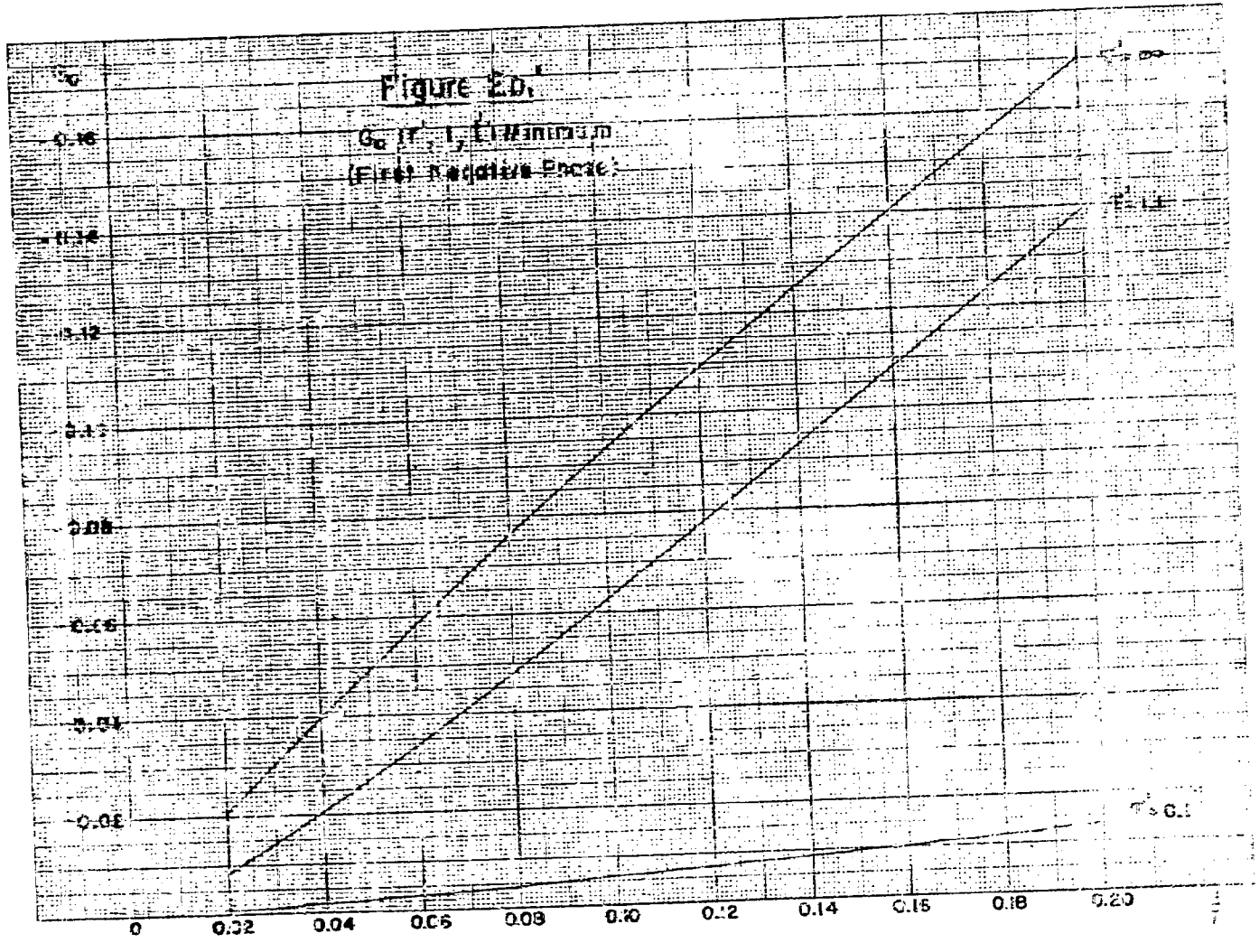
0.16
0.12
0.08
0.04
0
0.02
0.04
0.06
0.08
0.10
0.12
0.14
0.15
0.18
0.20

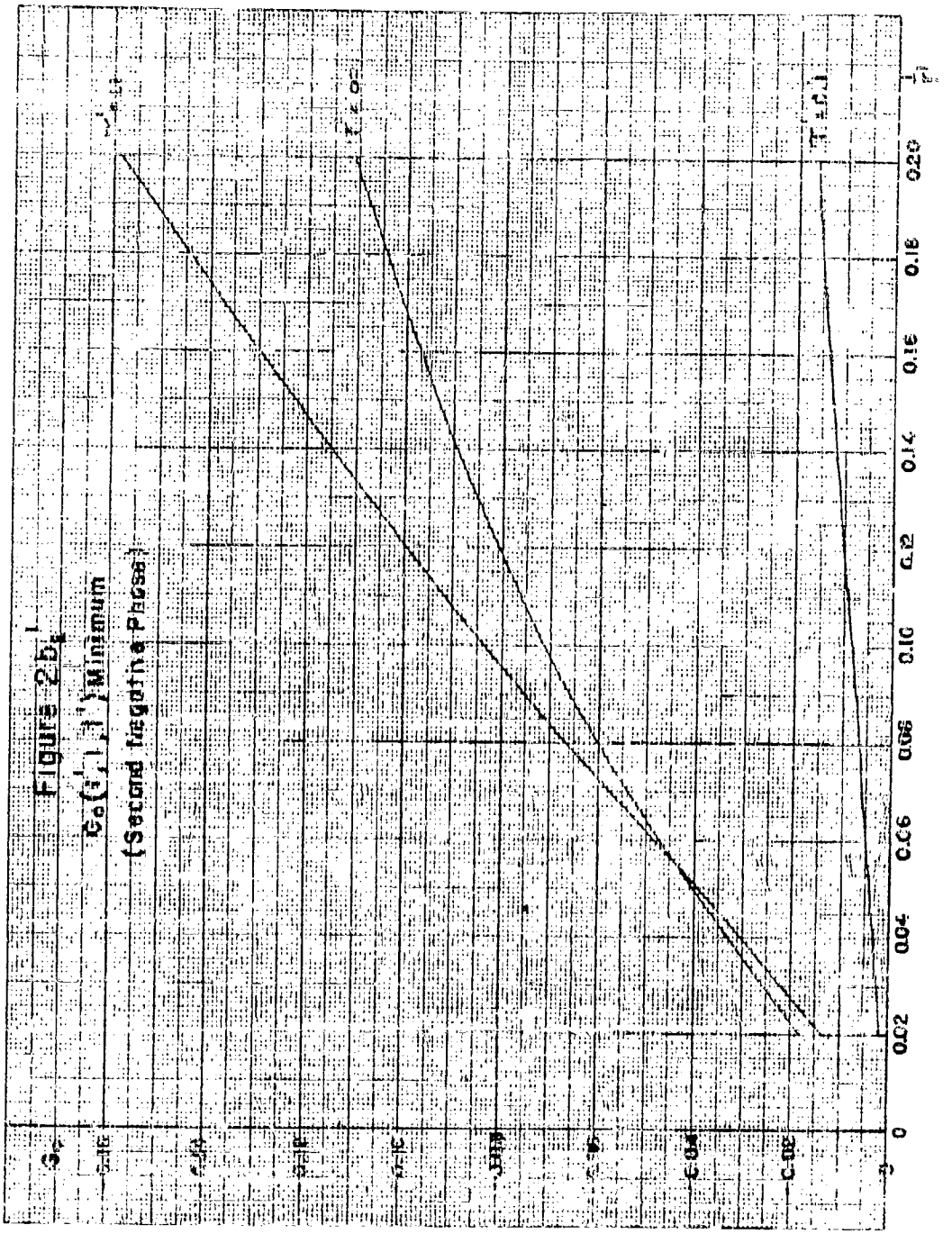
Figure 2b
(Second Negative Phase)
0.16
0.14
0.12
0.10
0.08
0.06
0.04
0.02
0
0.02
0.04
0.06
0.08
0.10
0.12
0.14
0.16
0.18
0.20

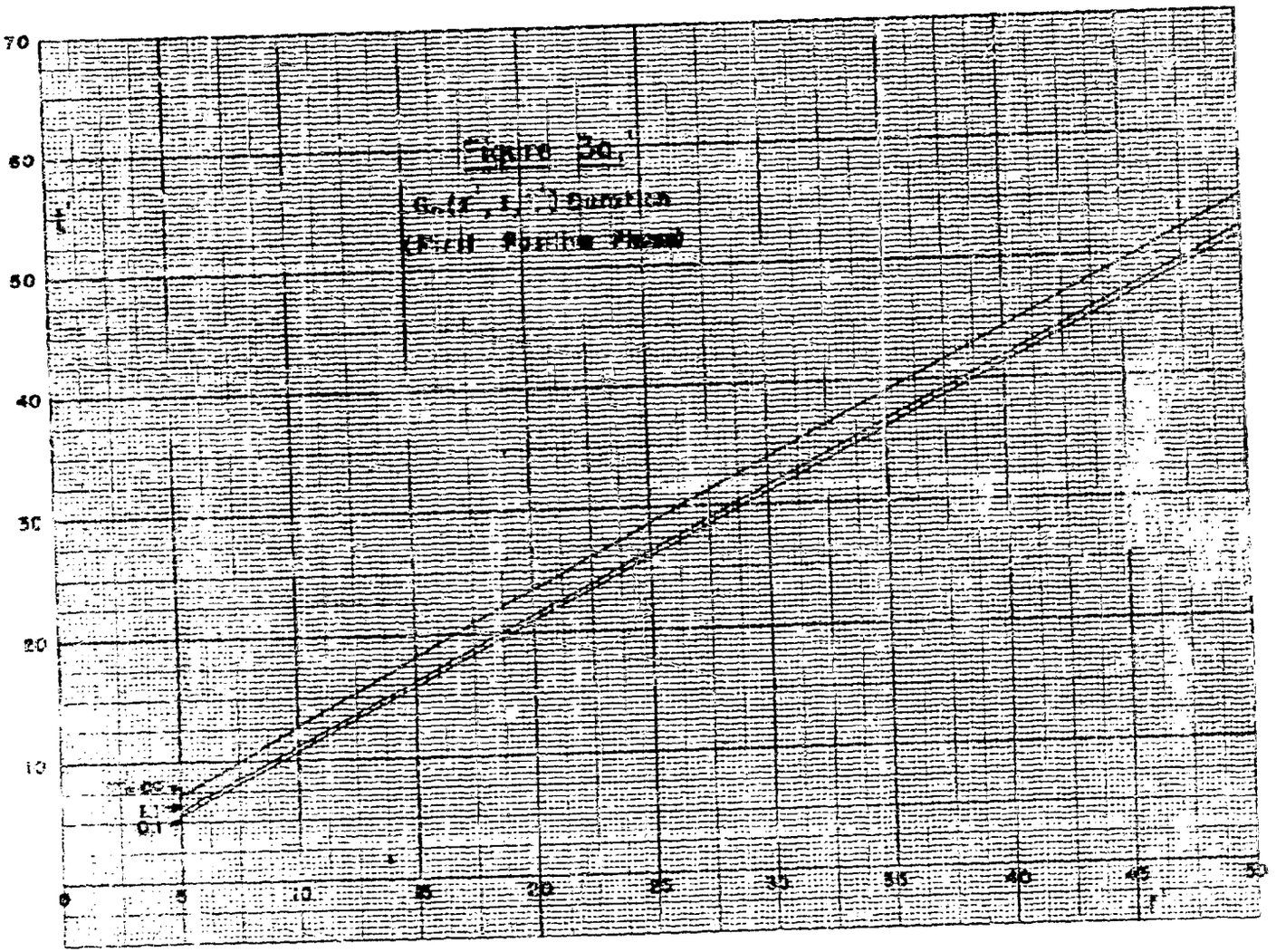

Figure 30.

$G_c(\tau, t_c)$ Duration
Fresh Portland Cement

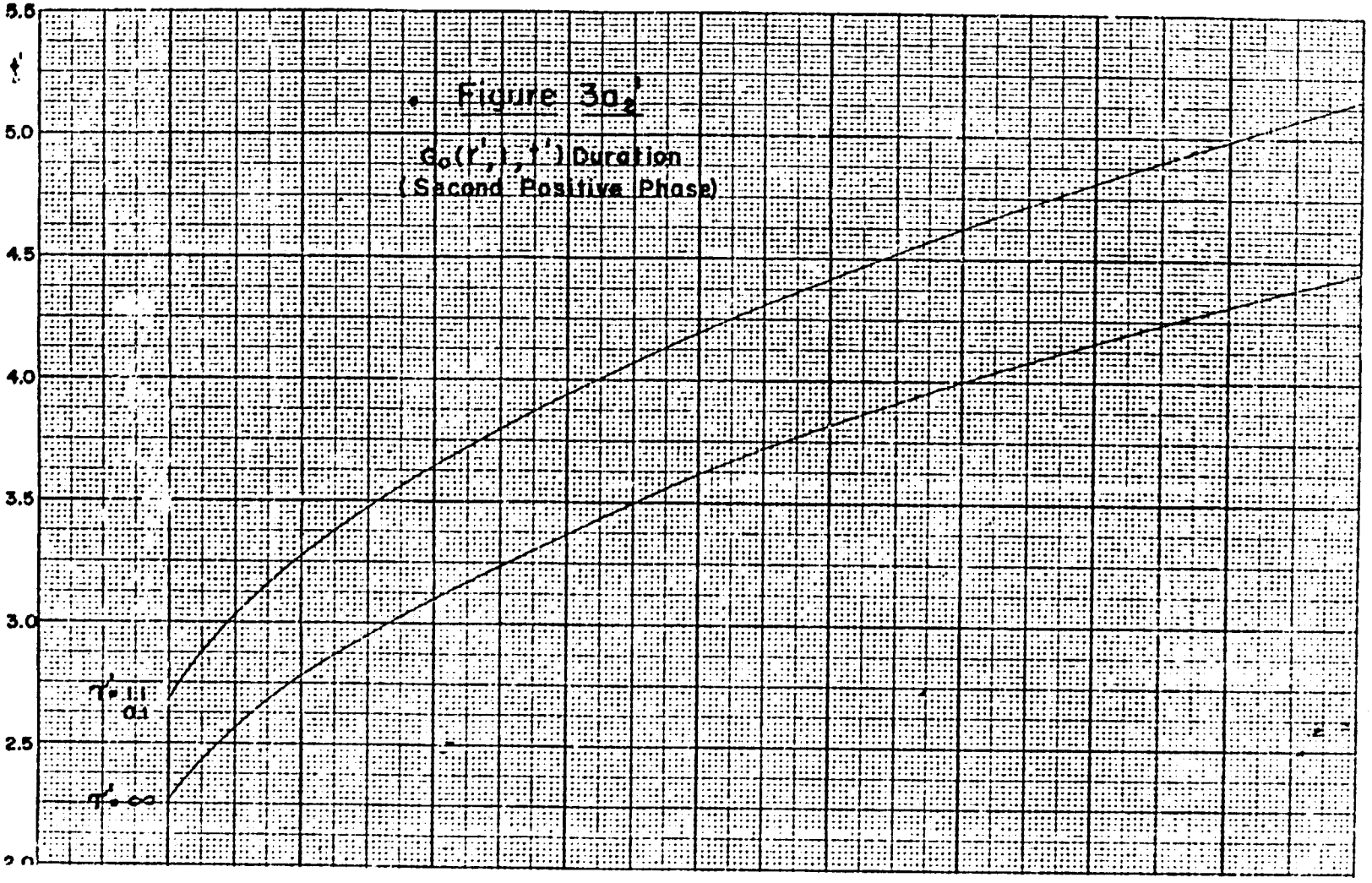

Figure $30_2'$

$G_0(r', \tau', t')$ Duration
(Second Positive Phase)

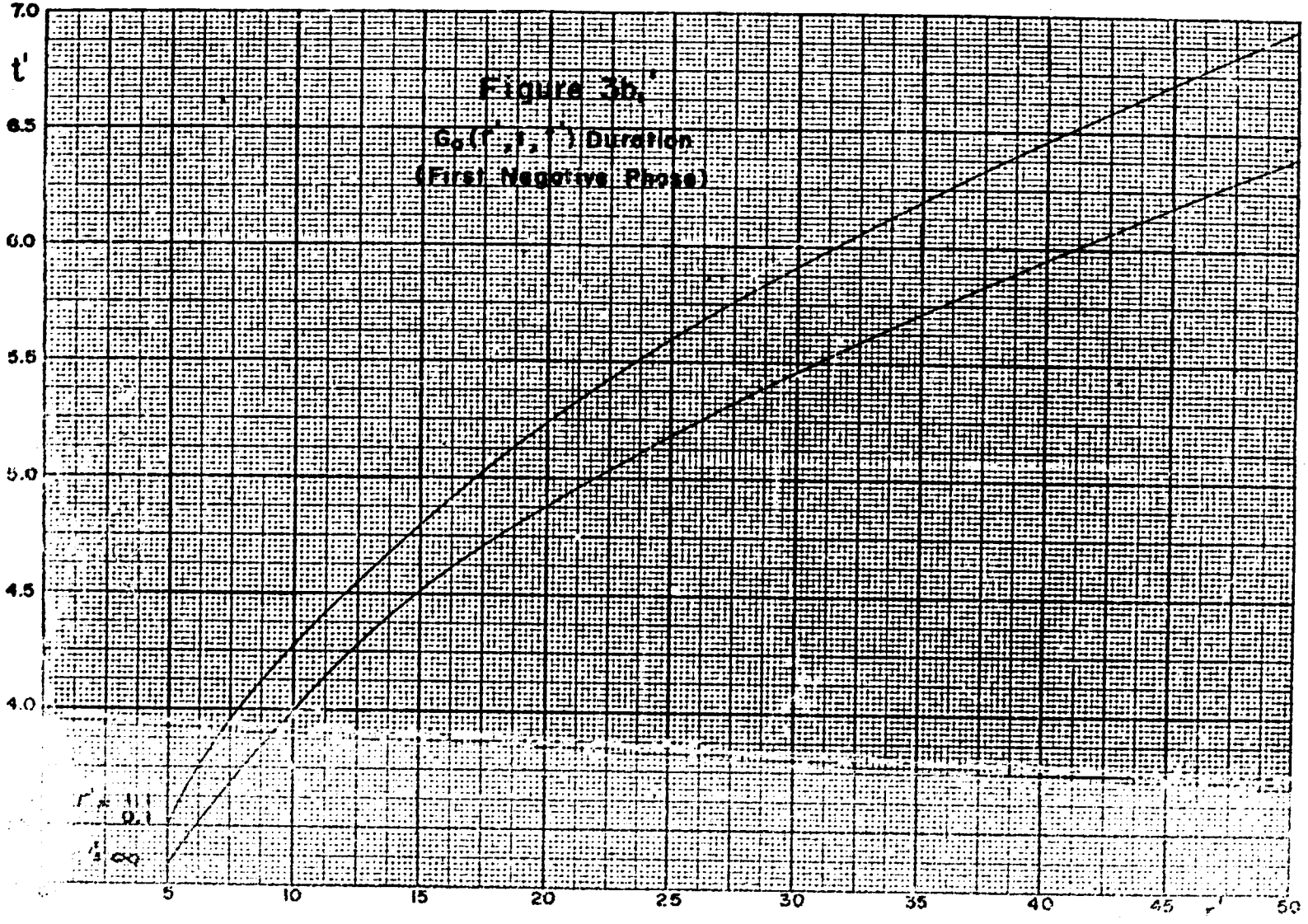
Figure 3b'
$G_0(r', t', \tau')$ Duration
(First Negative Phase)
t'
7.0
6.5
6.0
5.5
5.0
4.5
4.0
5
10
15
20
25
30
35
40
45
50
r'

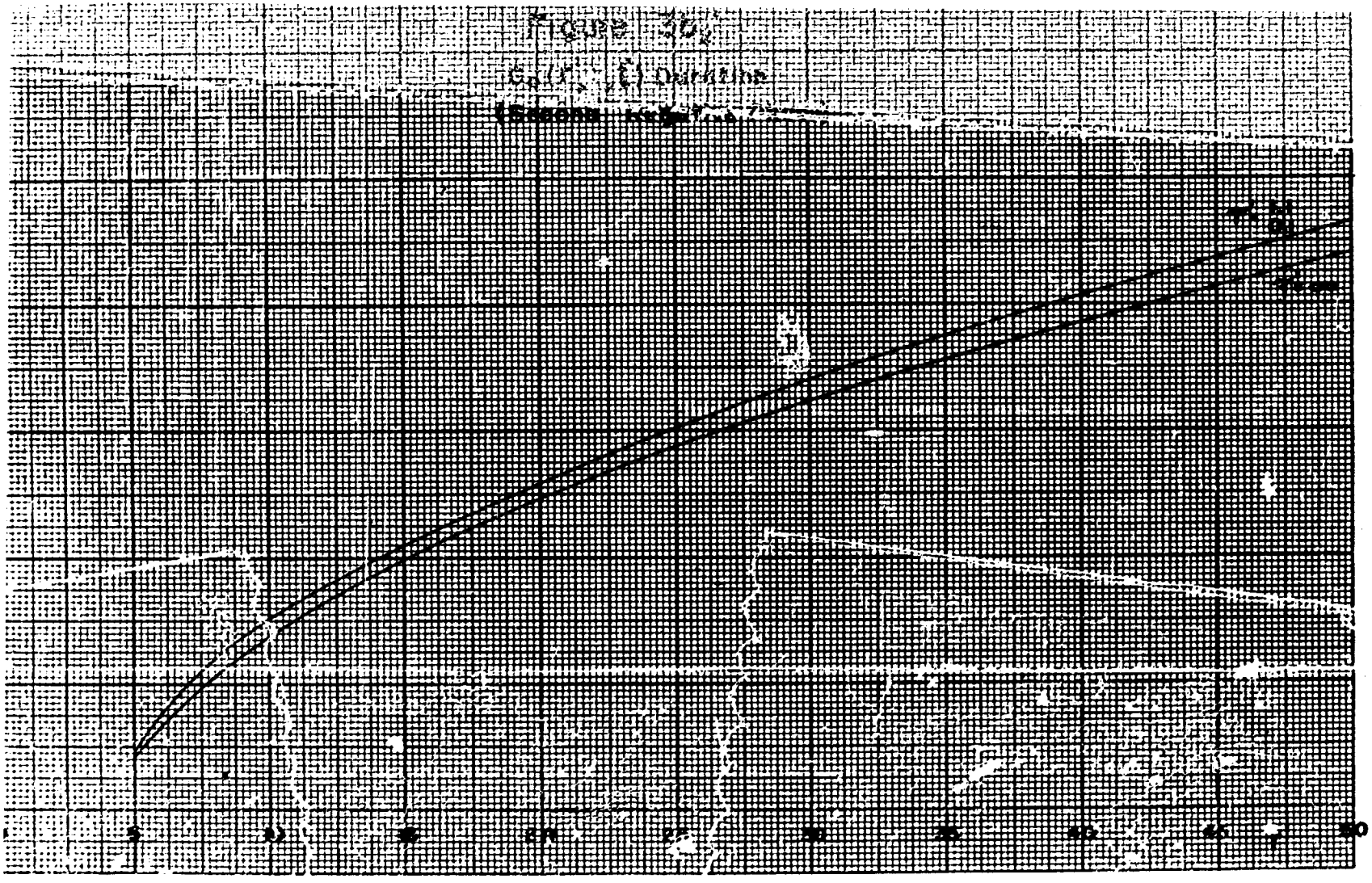

DEPARTMENT OF THE NAVY
OFFICE OF NAVAL RESEARCH
800 NORTH QUINCY STREET
ARLINGTON, VA 22217-5660

IN REPLY REFER TO
5510/6
Ser 43/655
4 Sep 03

From: Chief of Naval Research
To: Commanding Officer, Naval Research Laboratory (NRL 5996.3)

Subj: PUBLIC RELEASE APPROVAL

Ref: (a) Your e-mail to me of 14 Jul 2003

Encl: (1) Underwater Explosion Research, Volume I - The Shock Wave, 1950 (AD 006 841)
(2) Underwater Explosion Research, Volume II - The Gas Globe, 1950 (AD 037 466)
(3) Underwater Explosion Research, Volume III - The Damage Process, 1950 (AD 037 467)

1. In response to reference (a), enclosures (1), (2) and (3) are approved for public release; distribution is unlimited. They are returned for your use.

2. Questions may be directed to the undersigned on (703) 696-4619.

PEGGY LAMBERT
By direction

Copy to:
DTIC-OCQ (Larry Downing)